-PET-Vol.43

ICID
International Centre for Innovation & Development

# Proceedings of Engineering & Technology
# -PET-

## From:

5th International Conference on Automation, Control Engineering and Computer Science (ACECS-2018)

***Hammamet - Tunisia, 19-22 December 2018***

**Editors:**
Dr. Ahmed Rhif (Tunisia)
Dr. Sundarapandian Vaidyanathan (India)

**ISSN: 1737-9334**

ISSN: 1737-9334

# Proceedings of Engineering & Technology

# -PET-

From:

5th International Conference on Automation, Control Engineering and Computer Science

(ACECS-2018)

Hammamet - Tunisia, 19-22December 2018

Editors:

Dr. Ahmed Rhif **(Tunisia)**

Dr. Sundarapandian Vaidyanathan **(India)**

**International Centre for Innovation & Development –ICID –**

# Summary

# Fault Diagnosis by Bond Graph Reduced Observer

Attafi Rim[#1], Zanzouri Nadia[*2]

[#] *University of Tunis El Manar, National Engineering School of Tunis*
*LR11ES20, Analysis Conception and Control of Systems Laboratory (LACS)*
*Box 37, Le Belvedere 1002, Tunis, Tunisia*
[1]rima.attafi@gmail.com

[*] *University of Tunis, Preparatory Engineering Institute of Tunis*
*2, Rue Jawaher Lel Nahrou-Monfleury-1089 Tunis,*
*Tunisia*
[2]*Nadia.Zanzouri@enit.rnu.tn*

***Abstract*—This paper proposes a fault diagnosis method based on reduced observer using the Bond Graph (BG) modeling. Two bank observers structures (BG-DOS) and (BG-GOS) for fault isolation are developed. The effectiveness of the proposed approach is assessed on a real stringing machine.**

***Keywords*—** diagnosis, reduced observer, Bond Graph, stringing machine.

## I. INTRODUCTION

The fault detection and isolation (FDI) technique have been created due to the required high reliability and the complexity of the dynamical systems. The Luenberger observer-based approach [1], is one of the most famous techniques used for residual generation. When we detect the fault, we need for a single residual. However, the fault isolation requires a set of structured residuals. These residuals must be designed to be sensitive to certain faults and robust to others. In the literature for FDI [2], the bank observers based on analytical models are developed. We found the Dedicated Observer Scheme (DOS) which the $i^{th}$ observer is driven by the $i^{th}$ output and all inputs. Other outputs are considered unknown, and Generalized Observer Scheme (GOS) which the $i^{th}$ observer is driven by all outputs and all inputs except the $i^{th}$ output.

Dynamical systems are composed of elements belonging to multiple energy domains (electrical, mechanical, hydraulic, thermal,…). With the causal properties of the Bond Graph (BG) methodology, we can derive the state space form of the system, for fault detection and isolation (FDI) algorithms based on fault indicators generation [3], and design Luenberger and reduced observers for control [4] and state estimation [5] respectively.

Despite all the contribution related to the BG model yet to date, the diagnosis by BG reduced observer, has not been reported. Our contribution is to extend theses observers for fault diagnosis.

This paper is organized as follows: section II proposes a diagnosis by reduced observer using the BG. Section III, an application on the stringing machine is developed and shows the efficiently of the proposed method.

## II. DIAGNOSIS BY REDUCED OBSERVER USING BG APPROACH

### A. Principal of Diagnosis by Reduced Observer

The diagnosis consists on analyzing the residual output estimations $r_x$ and their sensitivity to faults. Using the observer state estimation, the principle of diagnosis is given in Fig. 1.

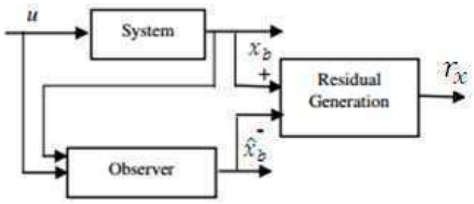


Fig. 1. Diagnosis by reduced observer design

The residual state estimation equation is $r_x = x_b - \hat{x}_b$

### B. BG Modelling

The BG approach was defined in 1961 by [6] and then developed by [7]. This energetic approach serves to point out analogies between different fields of physics. Due to its structure and causal properties, the BG tool is more and more used for modelling and fault diagnosis.

In our work, the BG is used for modelling, state estimation, fault diagnosis and simulation of dynamical system.

### C. Observer Design by BG Modelling

From a BG point of view, we have to check the observability of system, to design the observers. So, according to [8], a BG model is structurally observable if the following two conditions are satisfied:




ISSN 1737-9334

**First condition:** There is at least a causal path linking actuators (respectively sensors) for each dynamic element $I$ or $C$, in the integral causality when we put the bond graph system model in preferred integral causality.

**Second Condition:** All $I$ or $C$ elements derived assuming causality when placed bond graph model in derivative causality, and that the actuators (respectively a sensors) are dualized.

The reduced observer equation using BG variables is shown in eq. (1) :

$$\begin{cases} \dot{\hat{z}} = \bar{M}\hat{z} + \bar{N}u + \bar{P}y \\ \hat{x}_b = \begin{pmatrix} \hat{p}_I \\ \hat{q}_C \end{pmatrix} = \hat{z} + \bar{L}y \end{cases} \quad (1)$$

With $\hat{z}$ is the auxilary variable which avoid the time derivation of the output, $u$ is the input vector, $y$ is the output vector, $\bar{L}$ is the gain of reduced observer to be computed and $\bar{M}$, $\bar{N}$, $\bar{P}$ are constant matrices with appropriate dimension. With

$$\bar{M} = \bar{A}_{bb} - \bar{L}\bar{A}_{ab}, \bar{N} = \bar{B}_b - \bar{L}\bar{B}_a, \quad (2)$$
$$\bar{P} = \bar{A}_{ba} + \bar{A}_{bb}\bar{L} - \bar{L}\bar{A}_{aa} - \bar{L}\bar{A}_{ab}\bar{L}$$

And

$\bar{A}_{aa} = (C_a A_{aa} + C_b A_{ba}){C_a}^{-1}$
$\bar{A}_{ab} = (C_a A_{ab} + C_b A_{bb} - \bar{A}_{aa} C_b),\ \bar{A}_{ba} = A_{ba}{C_a}^{-1}, \bar{A}_{bb} = A_{bb} - A_{ba}{C_a}^{-1}C_b$
, $\bar{B}_a = C_a B_a + C_b B_b,\ \bar{B}_b = B_b$ are the submatrices.

The structure of reduced observer BG model is presented in Fig. 2. For diagnosis, we have to determine the residual output estimate $r_x$.

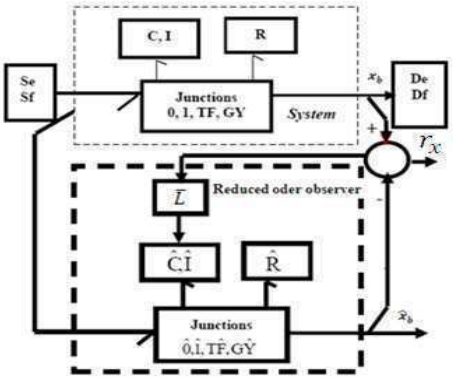


Fig. 2. Structure of reduced observer based on BG

*D. Strategies of Fault Isolation by Reduced Observer*

To isolate the fault by BG approach, we have to extend the bank of observers for FDI sensor modeled by BG approach. Fig. 3 and Fig. 4 represent the BG-DOS and BG-GOS structures needed for fault isolation

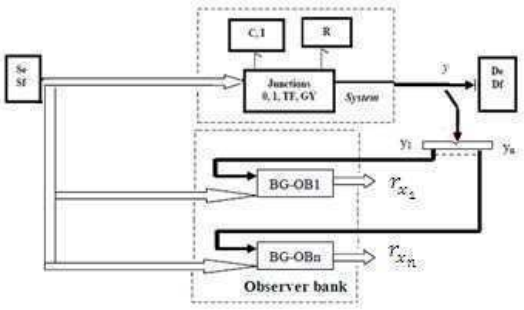


Fig. 3. BG-DOS structure

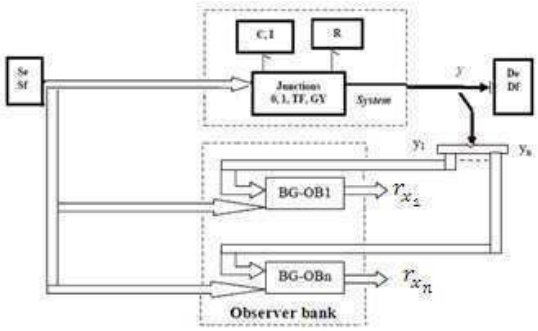


Fig. 4. BG-GOS structure

The obtained residuals deduced from the bank observer are grouped in the FDI table. Its rows and columns correspond to faults and residuals. The table is filled with binary values (fault signature). Zero (0) means that the residual is robust to the fault, and one (1) means that the residual is sensitive.

## III. APPLICATION

*A. Description of System*

We considered here the stringing machine (Fig. 5a). The stringers have used this machine to string rackets for the game professionals (as Roland Garros).

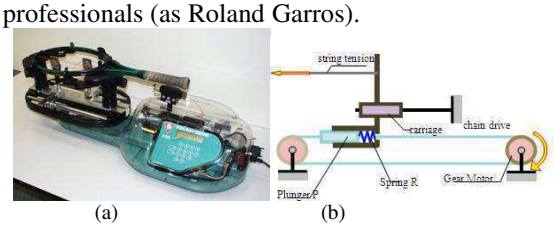


(a) (b)

Fig. 5. (a). Stringing machine, (b). Stringing operator modul

The stringing operator module (Fig .5.b) is composed of a gear motor and chain drive. It ensures the movement of the carriage carrying the drawing jaws. The tensioned chain strand is attached to a plunger (P) supported on the carriage




ISSN 1737-9334

by means of a calibrated spring (R). When the stringing operation, the plunger (P) moves to the right relative to the carriage by crushing the spring (R). This displacement is measured by a linear potentiometer which send a signal, the voltage image in the string, to the electric control unit (ECU). The latter then operates the motor control required to the precise string tension.

The word BG of the stringing operator module in open loop is presented in Fig. 6.

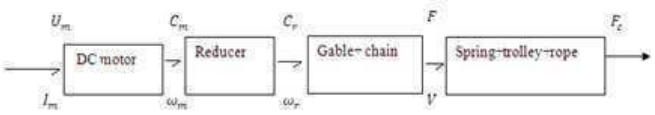


Fig. 6. Word BG of stringing machine

### *B. BG Model of Stringing Machine*

The BG modelling of the stringing machine is presented in Fig. 7. The first junction 1 is used to associate the physical phenomenon or components considered by the induced current $I_m$. Whether, $U_m$ is the induced tension, $R_m$ is the resistance and $L_m$is the inductance.

The second junction 1 is used to associate the physical phenomenon or components considered by the mechanic part which depends of the rotation speed of its axe. Whether $R_1$is the resistive viscous friction, and $J_m$is the moment of the rotor, the shaft and the reducer inertia.

The gyrator element has as $r_1$ constant, transforms the electromotive force in rotation speed of the shaft of reducer. $C_1$ is the coefficient of compressibility.

The transformer element has as $r_2$constant, transforms the rotation movement in translation movement via the rope winding. The mass of the chain is given by the element $I = m$ and the frictions at the gable are negligible.

We consider that the tree is of elastic type (whether $C_2 = \frac{K_r}{1+\frac{K_r}{K_c}}$, the loss resistance is given by $R_2$). The mass of carriage is negligible.

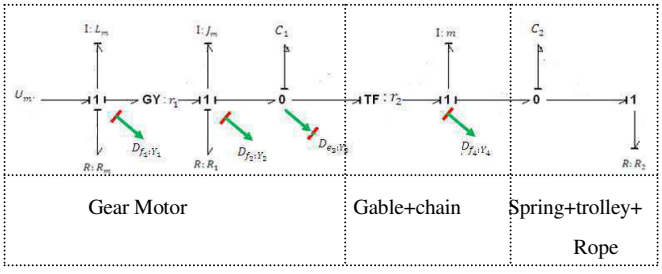


Fig. 7. BG model of stringing machine

From the Fig. 7, we can deduce the state equation [5]:

$$\begin{cases} \begin{bmatrix} \dot{p}_{L_m} \\ \dot{p}_{J_m} \\ \dot{q}_{C_1} \\ \dot{p}_m \\ \dot{q}_{C_2} \end{bmatrix} = \begin{bmatrix} -R_m/L_m & -r_1/J_m & 0 & 0 & 0 \\ r_1/L_m & -R_1/J_m & -1/C_1 & 0 & 0 \\ 0 & 1/J_m & 0 & -1/mr_2 & 0 \\ 0 & 0 & 1/C_1 r_2 & 0 & -1/C_2 \\ 0 & 0 & 0 & 1/m & 0 \end{bmatrix} \begin{bmatrix} p_{L_m} \\ p_{J_m} \\ q_{C_1} \\ p_m \\ q_{C_2} \end{bmatrix} + \begin{bmatrix} 1 \\ 0 \\ 0 \\ 0 \\ 0 \end{bmatrix} Um \\ Y = \begin{bmatrix} y_1(t) \\ y_2(t) \\ y_3(t) \\ y_4(t) \end{bmatrix} = \begin{bmatrix} 1/L_m & 0 & 0 & 0 & 0 \\ 0 & 1/J_m & 0 & 0 & 0 \\ 0 & 0 & 1/C_1 & 0 & 0 \\ 0 & 0 & 0 & 1/m & 0 \end{bmatrix} \begin{bmatrix} P_{L_m} \\ P_{J_m} \\ q_{C_1} \\ P_m \\ q_{C_2} \end{bmatrix} \end{cases} \quad (3)$$

The parameters of stringing machine are presented in TABLE.I.

TABLE I.
PARAMETERS VALUE OF STRINGING MACHINE

| Symbol | Designations | Nominal Values |
|---|---|---|
| $R_m$ | Rotor resistance | 1.1 Ω |
| $L_m$ | Rotor inductance | 1 mH |
| $J_m$ | Moment of geared motor | 0.05 $Kg.m^2$ |
| $R_1$ | Coefficient of viscous | 0.28 N.m/rad/s |
| $r_1$ | Coefficient of torque | 0.0386 N.m/A |
| $r_2$ | Reduction ratio | 0.01 N.m/A |
| m | Chain mass | 0.3 Kg |
| $K_r$ | Spring stiffness | 4 N/mm |
| $K_C$ | Rope stiffness | 32.7 N/mm |
| $C_1$ | Coefficient of compressibility | $10^{-4}$ |
| $C_2$ | Coefficient of compressibility | 0.00028 |
| $R_2$ | Loss resistance | 1000 N.m/rad/s |

### *C. Diagnosis by Reduced Observer using BG Approach*

We have verified the existence conditions of reduced observer design of the stringing machine modeled by BG:

When we put the BG model of the system with preferred integral causality, there is a causal path linking the sensors $Df_1(Y_1), Df_2(Y_2), De_3(Y_3)$ and $Df_4(Y_4)$ for each dynamic elements $L$ and $C$. Also, when the BG model of the system is affected with derivative causality, all the elements $L$ and $C$ have derivative causalities and the sensors $Df_1, Df_2, De_3$ and $Df_4$ are dualized.

Using the bicausality concept used by [9], the reduced observer design is presented by Fig. 8.




ISSN 1737-9334

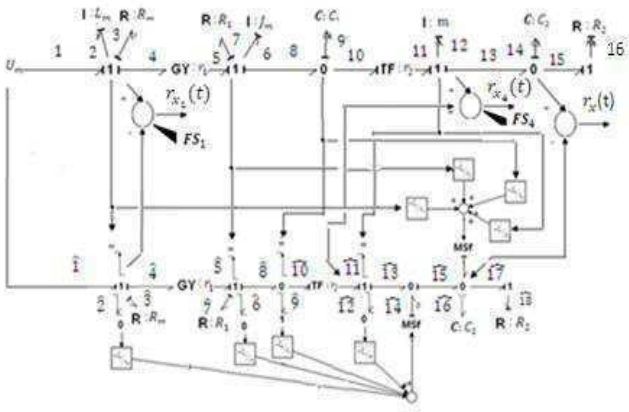

Fig. 8. Reduced observer BG model

We have simulated the system with 20sim. Fig. 9 shows the real and estimated state evolution.

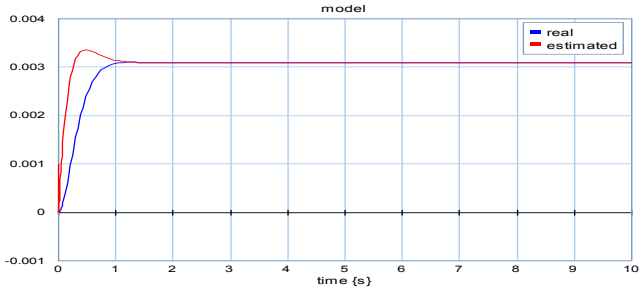


Fig. 9. State variables evolution

*1) Residual generation in normal operation:* From BG model of Fig. 8, we can deduce the residual $r_x(t)$, $r_{x_1}(t)$ and $r_{x_4}(t)$.

- Computing of $r_x(t)$

$$r_x(t) = x_b(t) - \hat{x}_b(t) = e_{14} - \hat{e}_{16} \quad (4)$$

Therefore,

$$r_x(t) = \frac{1}{C_2}\int[Df_4 - \frac{1}{R_2}(\frac{De_3}{r_2} - m\frac{d}{dt}Df_4)]dt - \emptyset \quad (5)$$

with

$$\emptyset = -\bar{L}(\bar{A}_{aa}y + \bar{A}_{ab}(\hat{z} + \bar{L}y) + \bar{B}_a u). \quad (6)$$

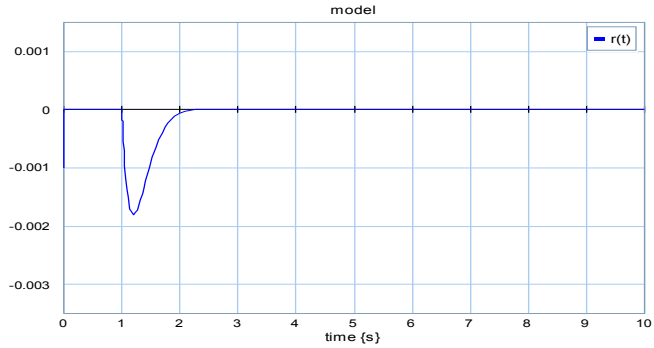


Fig. 10. Residual evolution in normal operation

Fig. 10 shows that the residual converge to zero.

- Computing of $r_{x_1}(t)$

$$r_{x_1}(t) = f_2 - \hat{f}_2 \quad (7)$$

With

$$f_2 = \frac{1}{L_m}\int[U_m - R_m Df_1 - r_1 Df_2]dt \quad (8)$$

And

$$\hat{f}_2 = -\frac{L_1}{m}r_{x_1}(t) \quad (9)$$

- Computing of $r_{x_4}(t)$

$$r_{x_4}(t) = f_{12} - \hat{f}_{12} \quad (10)$$

With

$$f_{12} = \frac{1}{m}\int[\frac{1}{r_2}De_3 - \frac{1}{C_2}\int Df_4]\ dt \quad (11)$$

And

$$\hat{f}_{12} = -\frac{L_4}{m}r_{x_4}(t) \quad (12)$$

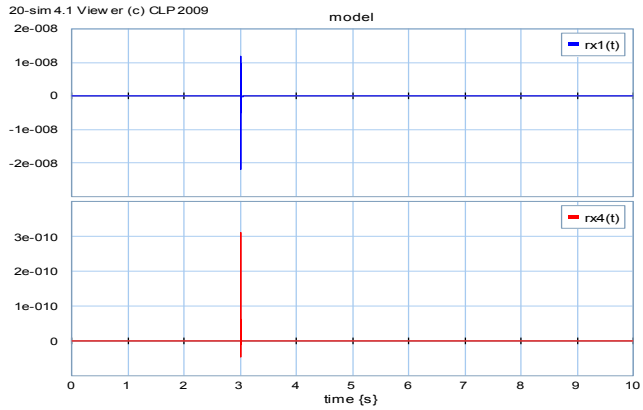


Fig. 11. Residual evolution of $r_{x_1}(t)$ and $r_{x_4}(t)$ in normal operation


ISSN 1737-9334

2) *Residual generation with sensors faults:* The sensors $Df_1, Df_4$ are affected by faults $FS_1$ and $FS_4$ from $t = 4s$ until $t = 5s$ and from $t = 8s$ until $t = 9s$ respectively.

So,

➢

$$r_{x_1}(t) = f_2 - \hat{f}_2 \quad (13)$$

With

$$f_2 = \frac{1}{L_m}\int [U_m - R_m(Df_1 + FS_1) - r_1 Df_2]dt \quad (14)$$

And

$$\hat{f}_2 = -\frac{L_1}{m} r_1(t) \quad (15)$$

➢

$$r_{x_4}(t) = f_{12} - \hat{f}_{12} \quad (16)$$

With

$$f_{12} = \frac{1}{m}\int [\frac{1}{r_2} De_3 - \frac{1}{C_2}\int (Df_4 + FS_4)]\ dt \quad (17)$$

And

$$\hat{f}_{12} = -\frac{L_4}{m} r_4(t) \quad (18)$$

The equations above show that the residuals are sensitive to sensors faults.

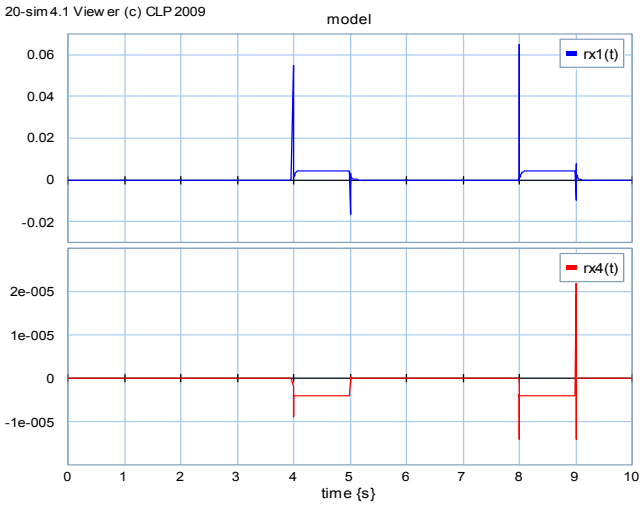


Fig. 12. Residual evolution of $r_{x_1}(t)$ and $r_{x_4}(t)$ in faulty operation

3) *Sensor fault detection and isolation:* Fig. 13 shows the residuals evolution based on BG model with BG-DOS (Fig. 13.a) and BG-GOS (Fig.13.b) structures. The residual $r_{x_1}(t)$ is sensitive to the sensor fault $Df_1$ and the residual $r_{x_4}(t)$ is sensitive to sensor fault $Df_4$. So, the deduced binary signatures can perfectly isolate the fault (TABLE.II).

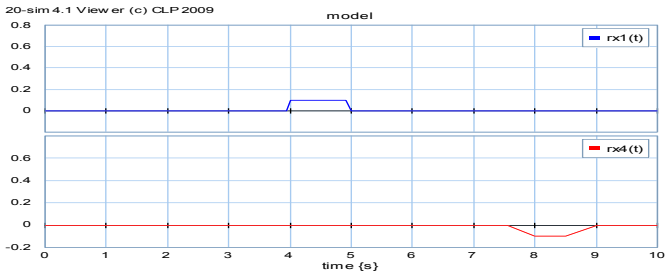


(a)

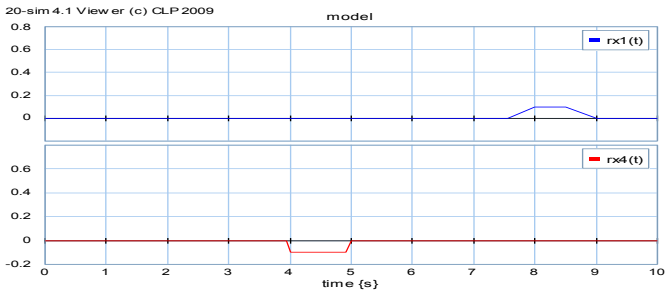


(b)

Fig. 13. Residual evolution with observer bank: (a) BG-DOS, (b) BG-GOS




ISSN 1737-9334

TABLE II. BINARY SIGNATURES

| | $Df_1$ | $Df_4$ |
|---|---|---|
| $r_1$ | 1 | 0 |
| $r_4$ | 0 | 1 |

BG-DOS

| | $Df_1$ | $Df_4$ |
|---|---|---|
| $r_1$ | 0 | 1 |
| $r_4$ | 1 | 0 |

BG-GOS

## IV. CONCLUSIONS

In this paper, a fault detection and isolation (FDI) based on BG reduced observer bank is proposed. Taking into account the advantage of structural properties of the BG model, the observer is designed graphically. The fault indicators are generated in the presence of sensor faults. The BG-DOS and BG-GOS structures are developed in which way the fault is perfectly isolated. At the last, a particular attention will be paid to the study of the fault estimation based on BG reduced observer in the future research works.

## REFERENCES

[1] D. G. Luenberger, *An introduction to observers*, IEEE Transactions on Automatic Control, vol. 16, pp. 596–602, 1971.

[2] R. N. Clark, *Instrument fault detection*, IEEE Trans. Aerospace & Electronic System," EAS-14, pp.558–563, 1978.

[3] B. Ould-Bouamama, A. Samantaray, K. Medjaher, K. Staroswieck, and G. Dauphin-Tanguy, *Model biulder using functional and bond graph tools for FDI desin,* Control Engineering Practice, vol. 13, pp. 875–891, 2005.

[4] R. Attafi, M. Allous, and N. Zanzouri, *Bond graph reduced order observers for active fault tolerant control*, Indian Journal of Science and Technology, vol. 11, no. 18, 2018.

[5] R. Attafi, and N. Zanzouri, *Bond graph modeling and state estimation of stringing machine*, 7th International Conference on Modeling, Identification and Control (ICMIC), Dec 18-20, Sousse, Tunisia, 2015.

[6] H. M. Paynter, *Analysis and design of engineering systems*, M.I.T. Press, 1961.

[7] D. C. Karnopp, and R. C. Rosenberg, *Systems dynamics: a unified approach,* MacGraw Hill, 1983.

[8] C. Sueur, and G. Dauphin-Tanguy, *Structural controllability and observability of linear systems represented by bond graphs*, Journal of Franklin Institute, vol. 326, pp. 869–883, 1989.

[9] C. Pichardo-Almarza, A. Rahmani G. Dauphin-Tanguy and M. Delgado,*Using the bicausality concept to build reduced order observers in linear time invariant systems modelled by bond graphs*, Proceedings of European Control Conference (ECC), 2003.




ISSN 1737-9334

# Self-stabilization on Scale-free Networks

Badreddine Benreguia
*Computer Sciences Department*
*Batna-2 University*
Batna, Algeria
badreddine.benreguia@gmail.com

Hamouma Moumen
*Computer Sciences Department*
*Batna-2 University*
Batna, Algeria
moumenh@gmail.com

***Abstract*—Many of self-stabilizing algorithms have been proposed in literature to deal with fault-tolerance in distributed systems. Most existing works have utilized random graphs (Erdos-Renyi networks) to simulate self-stabilizing algorithms. In the present paper, we propose the use of self-stabilizing algorithms on scale-free graphs (Barabasi-Albert networks) which are more representative for real networks. After that, we test these algorithms under evolutionary dynamic graphs. Performance is evaluated using extensive simulations where three well known self-stabilizing algorithms are tested: nodes coloring, minimal dominating set and maximal independent set.**

***Index Terms*—self-stabilization, scale-free network, dominating set, independent set, nodes coloring, graph evolution**

## I. Introduction

Self-stabilization is a fault-tolerance approach for distributed systems that has been introduced by Djikistra in 1974. A self-stabilizing distributed system is guaranteed to achieve global correct configuration, in a finite time, even with presence of faults inside the system. Suppose a distributed system is in illegitimate configuration after a transient fault, self-stabilization allows to reach a legitimate configuration without any external intervention. Various self-stabilizing distributed algorithms have been proposed in the literature for graph problems such as leader election, nodes coloring, domination problem, independent set identification, construction of spanning tree. A detailed taxonomy of different self-stabilizing algorithms can be found in [1].

Generally, graphs are used to represent networks and complex systems in real-life applications like internet, social networks, network of nerve cells, power grids, systems of transportation, protein particulars, and a lot of other systems that could be found in [2].

Most of the papers have studied self-stabilization on theoretical level using simple undirected graphs and only few of works have used experimental tests on random graphs known as Erdos-Renyi graphs [3]. In fact, it has been proved that most of real networks cannot be represented by the model Erdos-Renyi. Barabasi and Albert have proposed a model known as scale-free network or Barabasi-Albert model [4]. After collecting a set of statistics about real existing networks (like www network, Movie actors, Paper citations) authors study some parameters such as mean distance between two nodes, clustering coefficient, degree distribution [2], [5]. For example in random graphs, degree of the nodes is approximately the same for all the nodes where the degree distribution follows Normal law. This distribution cannot explain the notion of the hubs in the real complex networks where a few of nodes have a very high level of degree. In the proposed model of Barabasi and Albert, the degree is distributed the same manner in real networks following a Power law distribution. Currently, Barabasi-Albert graphs are the most known graphs which are widely used by the community of graph literature.

### A. Contribution

The previous works, proposed in literature, have implemented self-stabilization only for random graphs and static structure of graphs. Although Dolev *et. al.* have indicated that uniform self-stabilizing algorithms can work under dynamic graphs [6], there is no work that simulates self-stabilization in the dynamic context where the graph structure is changing. Our main contributions can be summarized as follows:

(i) We use and test three particular self-stabilizing algorithms under scale-free graphs. The algorithms are: minimal dominating set, maximal independent set and nodes coloring.

(ii) We test self-stabilization under graph growing where at any time, a new node comes to connect the existing graph. We attempt to observe the behavior of the self-stabilizing algorithms under the dynamic structure of the graphs.

### B. Organization of the paper

The remainder of this paper is structured as follows. Section II discusses the concept of self-stabilization. We give particular explanation for three self-stabilizing algorithms $i.e.$ minimal dominating set, maximal independent set and nodes coloring. In section III, scale-free graphs and complex networks are presented. We introduce our version of the algorithm generating scale-free networks in section IV. Section V presents the idea of integrating self-stabilization for evolutionary graphs. Simulation tests and experiments are shown in section VI followed by a conclusion in section VII.

## II. Self-stabilization problem formulation

In a self-stabilizing system, all the nodes have the same collection of rules under the form: **if** $guard$ **then** $statement$ (written generally as: $guard \longrightarrow statement$) and the same local variables that describe the node's $state$, where the guard part is a set of boolean expressions and the statement is an action on the node's state to be committed if the guard is true. The $state$ of every node can be updated by the node itself




ISSN 1737-9334

using its rules. Each node has a partial view of the distributed system ($i.e.\ guard$ which consists of boolean expressions) on its state and the states of the neighbors. A rule is said $enabled$ (or $priviliged$) if the guard is evaluated to be true. A node will be enabled if at least one of its rules is enabled. Executing the statement of the enabled rule by the node is called a $move$. This execution allows updating the state (local variables) of the node in order to be more legitimate with its neighborhood.

We are interesting in this work on *uniform algorithm*, where all nodes in the distributed system execute the same program or check the same set of rules. If there is no enabled rule for all the nodes, the system is in the legitimate global configuration. However, if there is at least one enabled rule (a move) in the overall system, the system is considered not yet stable and it is expected that the network will be in the correct global configuration after executing a finite number of moves. The execution of self-stabilizing algorithms is managed by a daemon (scheduler) that selects the privileged nodes to move from a configuration to another configuration. Two types of daemons are widely used in self-stabilization literature: central and distributed daemons. In the central daemons, one privileged node is selected among all the privileged nodes to be moved. However, in the distributed daemons, a subset of nodes are selected among the set of privileged nodes to make a move simultaneously. Detailed taxonomy introducing various daemons can be found in [7]. In this paper, we discuss particularly three well-known algorithms of self-stabilization: finding maximal independent set, detection of minimal dominating set and nodes coloring.

### A. Maximal Independent Set (MIS)

Let $G = (V, E)$ be a graph, where $V$ is the set of nodes and $E$ is the set of edges. An independent set is a subset of nodes $S \subseteq V$ such that there is no two nodes connected in $S$. The set $S$ is said *maximal* if there is no superset $S'$ of $S$ such that $S'$ is an independent set. Maximal independent set (MIS) is used in many practical applications like head clusters in sensor networks. Shukla *et al.* [8] have proposed a self-stabilizing algorithm to find the MIS. The idea is very simple: a node $v$ joins the set $S$ if $v$ has no neighbor in $S$, and $v$ leaves the set $S$ if at least one of its neighbors is in $S$. Each node $v$ has a local variable called *ind* that takes one value from $\{0, 1\}$. When $v.ind = 1$ that indicates $v$ is in $S$ otherwise $v.ind = 0$. In the legitimate global configuration, the set of nodes $\{v, v.ind = 1\}$ is MIS. Every node $v$ has to check the following two rules:

**Rule 1:** $v.ind = 0 \wedge \forall u \in N(v) : u.ind = 0 \longrightarrow v.ind = 1$
**Rule 2:** $v.ind = 1 \wedge \exists u \in N(v) : u.ind = 1 \longrightarrow v.ind = 0$

Where $N(v)$ is the set of $v$ neighbors. It has been shown that MIS self-stabilizing algorithm converges in $O(n)$ moves under central daemon [8].

### B. Minimal Dominating Set (MDS)

In a graph $G(V, E)$, a set of nodes $S \subseteq V$ is called a dominating set if every node $v \in V$ is either a member of $S$ or is neighbor to a node of $S$. A dominating set $S$ is minimal if no proper subset of $S$ is a dominating set.

Hedetniemi *et al.* [9] has proposed a self-stabilizing algorithm for the minimal dominating set (MDS) problem. Each node has a boolean variable that indicates whether it is in $S$ or not. To find a dominating set, the algorithm is based on the following idea: a node joins the set $S$, if it has no neighbor in S. A node that is a member of $S$, and has a neighbor that is also a member of $S$, will leave the set if all its neighbors are not pointing to it. Thus, after stabilization the set $S$ will be MDS. Although, the algorithm stabilizes in $O(n^2)$ using central daemon, another proposed MDS algorithm [10] converges to the global correct configuration in $O(n)$.

Domination has been widely studied in literature and has been adopted in many real-life applications. Address routing, power management, clustering in ad-hoc networks and influence opinion in social networks are some examples of domination application [11]–[14].

### C. Nodes coloring

Coloring problem consists to assign one color to each node such that no two adjacent nodes could have the same color. Mathematically, for a graph $G(V, E)$, coloring nodes is a function $c : V \rightarrow N$ where $c(i) \neq c(j)$ if $i$ and $j$ are adjacent.

The elements of $N$ are called the available colors. If a graph $G$ may be colored using $k$ colors, we say that is $k-colorable$. The smallest value of $k$ is called the *chromatic number*. Many self-stabilizing algorithms have been proposed in literature. Hedetniemi *et al.* [15] have proposed grundy coloring using at most $(\Delta + 1)$ colors where $\Delta$ is the maximal degree in the graph $i.e.\ k < \Delta$. The drawback of this algorithm is that each node must to know $\Delta$ which is considered as global information. In self-stabilizing systems, it is preferable that nodes know only a partial information about their neighborhood. The algorithm converges to the legitimate global configuration in $O(n)$. Coloring is used generally for channel and frequency assignment in wireless networks.

## III. Complex networks

Erdos and Renyi have proposed in 1959 a first model of graphs based on the concept of randomness where every edge has a probability to exist or to not-exist. The growing interest in complex systems has led to collecting tremendous statistics on real networks. In the past few years, many empirical results showed [2], [5] that the model of Erdos-Renyi is very limited and cannot represent large-scale real networks. For example, the distribution of degree in random graphs, that follows Normal law, cannot explain the notion of *hubs* in the real complex networks where a few of nodes have a very high level of degree.

Thus, Barabasi and Albert [4] have proposed the scale-free model which has two main properties: *graph evolution* and *preferential attachment*. For the first property, authors assume that networks are constructed under time by growing. At any moment, there is a new node that comes to connect the existing graph (born of a new node) with an average of connection called *attachment degree*. The attachment degree




ISSN 1737-9334

**Algorithm 1** Generating Scale-free Graph

**Input:** $n$: graph size
$d$: attachment degree
**Output:** $g$: a scale-free graph

Let $g$ be an initial full-connected subgraph of $d$ nodes where each node has $Deg = d - 1$
**for** $i = d + 1$ to $n$ **do**
  Let $i$ be a new node of $g$ with $Deg_i = 0$
  Let $AttachDeg_i$ be a random integer in $[1, d]$
  **for** $k = 1$ to $AttachDeg_i$ **do**
    $neighbor \leftarrow$ Select an existing node of $g$ proportionally to its degree
    Connect $i$ to $neighbor$
    $deg_{neighbor} \leftarrow deg_{neighbor} + 1$
  **end for**
  $deg_i \leftarrow AttachDeg_i$
**end for**
**return** $g$

is a parameter that indicates the average number of neighbors like the average number of friends in a given social network. The second property, every new node must to connect to the existing nodes using *preferential attachment* law *i.e.* nodes having high degree have more chances to be selected as neighbors by the new node. Thus, each new node connects to existing nodes with probability proportional to their degrees.

Scale-free networks have an important feature that appears under the evolution process. Some nodes will be highly connected and will be more attractive to be neighbors for the new nodes, called $hubs$. This process is known as $rich-get-richer$ [2].

Instead using Erdos-Renyi graphs, we believe that the presence of the $hubs$ in Barabasi-Albert model will give a different behavior for self-stabilizing algorithms. In this sense, we attempt to test self-stabilization under Barabasi-Albert graphs. Firstly, using a set of well-known self-stabilizing algorithms, we try to establish a comparison process of self-stabilization under random graphs and scale-free networks. Secondly, we check the feasibility of self-stabilization under graph evolution. Notice that previous works has supposed that self-stabilization is suitable only for fault-tolerance like dealing with problems of memory corruption.

## IV. Generating scale-free networks

In this section, we present our algorithm used for generating synthetic Barabasi-Albert graphs. Although, there exists tools to generate scale-free graphs like Networkx of Python, the need to integrate the self-stabilizing algorithms under the evolution of the graph leads us to propose our own generator shown in algorithm 1.

The algorithm starts using an initial subgraph of $d$ nodes. In our case, we have used a full-connected graph as an initial subgraph, but it is possible to utilize other structure, like full-disconnected subgraph which is used in Networkx. Note that in reality, $d$ is always less and very small than $n$. In the next step, the graph evolution is represented by the coming of new nodes one-by-one. Each new node connects to the existing graph by preferential attachment where the degree of attachment of the new node is a random value in $[1, d]$. In the case of Networkx, the generator uses a constant attachment degree as $d$. However, in our case we have used a random integer in $[1, d]$ because, in reality, new nodes connect with value close to (not fixed) attachment degree.

Table I illustrates an example of generating three models of graphs. The generated graphs have size of 1000 nodes using an attachment degree of 10 for scale-free graphs and a probability $p = 0.01$ for random graphs $i.e.$ every node has likely 10 neighbors. The degree distribution is shown in table I. It indicates clearly the differences in degree distribution. For random graphs, most of nodes have degree between 1 and 20. Generally the degree distribution fits a Normal law for random graphs (where the mean equals 10 in this example). For the scale-free graphs, the two generators give frequencies that follow the well known power law distribution in Barabasi-Albert model [5]. As for the Networkx generator, it gives values of degree greater or equal to 10. This is due to the manner the generator connects new coming nodes where every node has to attach exactly to 10 neighbors. Thus, no node could have a degree less than 10. This later problem does not appear in our case because we use random values in $[1, d]$ as attachment degree to connect new nodes. It is possible to see that the two algorithms gives hubs having degree greater than 100. Our generator gives 2 hubs while in the second there is 11 hubs, one of them has 177 neighbors. It is worth indicating that we have observed during evolution, the hubs are generally the nodes which are created at the beginning of the evolution. For example in the case of Networkx generator, the hub (of 177 degree) is originally the first node coming directly after constructing the initial subgraph. For our generator, the two hubs are the nodes created during evolution at the moments 2 and 3 respectively. This does not reflect the reality because hubs may be not created at the beginning of evolution in complex networks. For example, in the network of paper citation [2], hubs (papers highly referenced) could be created at the middle of evolution.

TABLE I
Degree distribution on three examples of synthetic graphs

| | Number of nodes | | |
|---|---|---|---|
| Degree | Random generator Erdos-Renyi | Our generator Barabasi-Albert | Networkx generator Barabasi-Albert |
| 1-9 | 468 | 637 | 0 |
| 10-19 | 529 | 262 | 736 |
| 20-29 | 3 | 51 | 134 |
| 30-39 | 0 | 15 | 51 |
| 40-49 | 0 | 11 | 25 |
| 50-59 | 0 | 10 | 15 |
| 60-69 | 0 | 6 | 10 |
| 70-100 | 0 | 6 | 18 |
| 101-177 | 0 | 2 | 11 |




ISSN 1737-9334

## V. SLEF-STABILIZATION UNDER GRAPH EVOLUTION

All the previous works in literature have indicated that self-stabilization is more suitable for fault-tolerance in distributed systems. In this paper, we show that self-stabilization is suitable too for the natural process of evolution that exists in complex networks. The idea of integrating self-stabilization is as follows: suppose at time $t_n$ a graph $G$ is stable (in legitimate configuration) for a given algorithm. At time $t_{n+1}$ a new node $(n+1)$ comes to join the graph $G$. We suppose that at the connection moment, the new node selects a random state for itself. For example, in the MDS problem, the new node selects randomly a value from $\{0,1\}$ to indicate if it is in MDS or not. The connection of the new node with its random state will probably make the graph $G$ in illegitimate configuration. Thus, the process of self-stabilizing must to react in order to move to the global legitimate configuration again. Note that the algorithm re-stabilizes after the addition of just one node.

**Algorithm 2** Self-stabilization Under Evolution

**Input:** $g$: graph in legitimate configuration of $n$ nodes
$d$: attachment degree
$k$: number of nodes will connect $g$
**Output:** $g$: graph in legitimate configuration of $n+k$ nodes

```
for i = 1 to k do
    Let i be a new node with a random state
    g ← Connect i to g with preferential attachment
    Reaction of self-stabilizing algorithm
end for
return g
```

For a long period of evolution $i.e.$ lot of new connecting nodes, the algorithm must to stabilize after adding new one node before the coming of a second new node. It is possible to consider the coming of new node like a fault that occurs on the distributed system which the self-stabilizing algorithm has to deal with it. Generally, it is assumed that the interval between two faults (two new nodes) is so long to allow the system executing its original task during the stable period.

## VI. SIMULATIONS RESULTS

We conduct simulations on three sides: (1) executing self-stabilization on scale-free graphs (2) comparing self-stabilization on random graphs and scale-free graphs (3) and test self-stabilization under graph evolution. Three self-stabilizing algorithms are used in the experiments: maximal independent set [8], [9], minimal dominating set [9] and grundy coloring [15]. To check the efficiency : (i) we calculate the speed of convergence (number of moves needed to achieve legitimate configuration) and calculate a second parameter that depends on the kind of the algorithm. For minimal dominating set, we seek the cardinality of MDS. For maximal independent set, the cardinality of MIS is taken into account. In the coloring problem, the goal is to find the minimal number of colors. Synthetic generated graphs, integration of self-stabilization with evolution process and benchmark tests have been written in Java. However, we have used the Kuszner code [16] to execute the above self-stabilizing algorithms under central daemon. We take the average of calculation after conducting 5 tests in each experiment.

### A. Attachment degree impact on self-stabilization

In this section, we study the behavior of self-stabilizing algorithms under the impact of changing the attachment degree. Curves are plotted using values of attachment degree ranging from 2 to 100. For each algorithm, two sizes of graphs are used: graphs with 1000 nodes and graphs with 5000 nodes.

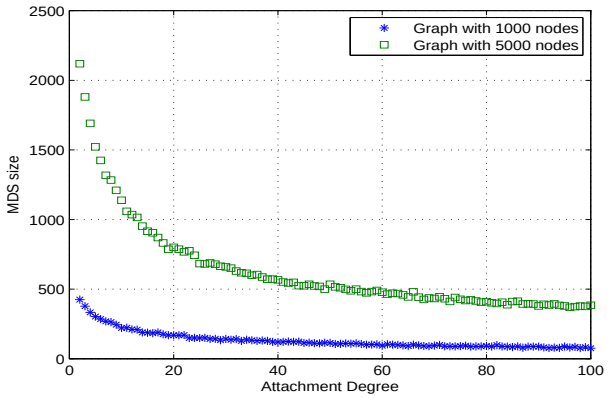


Fig. 1. Size of MDS according attachment degree

*1) MDS:* Figure 1 explains the relation between cardinality of MDS and attachment degree. The MDS size is inversely proportional to the attachment degree $i.e.$ it decreases when the attachment degree grows. This is a rational result because it is expected that the cardinality will decrease when the graph density grows. For example in full-connected graph, the MDS cardinality is 1. It is worth to indicate that the minimal obtained rate of MDS represents 7% of the entire population of nodes (374 nodes in MDS from 5000 when $AttachDeg = 97$).

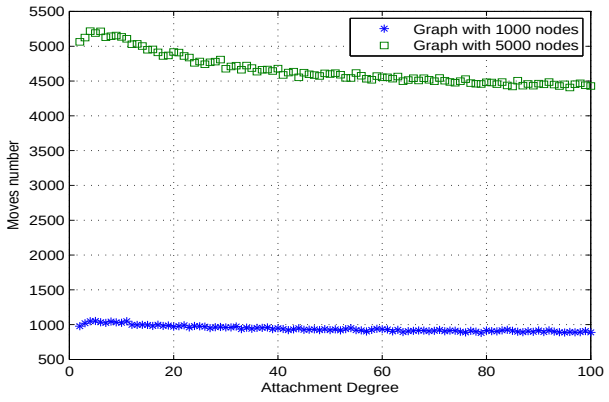


Fig. 2. Time of convergence of MDS according attachment degree

Figure 2 shows the necessary number of moves in order to converge to the legitimate configuration. It illustrates (nearly)




ISSN 1737-9334

a constant plot which means that the time of convergence (number of moves) and graph density (attachment degree) are independent. Observe that the top values of the plots (moves number) are located in the positions of the maximal values of cardinality shown in figure 1. Although Hedetniemi [9] has proved that MDS algorithm stabilizes in $O(n^2)$, simulations show a convergence in $O(n)$. This later complexity has been proved by Turau [10].

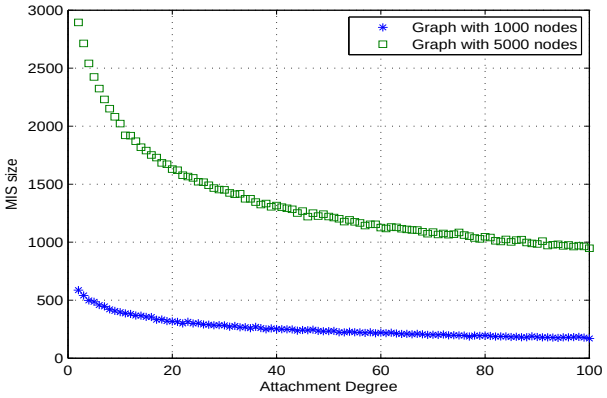


Fig. 3. Size of MIS according attachment degree

*2) MIS:* In figure 3, for graphs of 5000 nodes, the MIS size is in the interval $[950, 2900]$. As for graphs of 1000 nodes, the MIS has size in $[170, 590]$. When the graph density (attachment degree) grows, the cardinality of MIS decreases $i.e.$ size of MIS is inversely proportional to the attachment degree. According figures 1 and 3, MDS sets are always smaller than MIS.

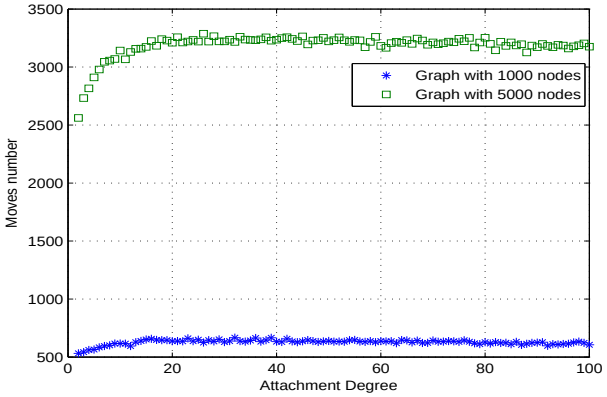


Fig. 4. Time of convergence of MIS according attachment degree

Figure 4 shows the time of convergence for MIS stabilization. When the degree attachment exceeds 10, time of stabilization becomes almost constant. For graphs of 5000, the number of moves is less than 3300 moves, and less than 700 for graphs of 1000 nodes. These results ensure the formal proof that MIS stabilizes in $O(n)$ [8].

*3) Coloring:* Figure 5 illustrates that 7 to 52 colors are needed for coloring scale-free graphs of 1000 nodes. Number of colors is proportional to the graph density (attachment degree). For graphs of 5000, we need a number of colors between 8 and 71. Note that theoretically, the maximal value of colors is $(\Delta+1)$ where $\Delta$ is the maximum degree in the graph [15]. Our tests on scale-free graphs show that values given by simulations does not reflect perfectly theoretical results. In the presence of the hubs, $\Delta$ will be very high whereas the number of colors, given in experiments, is very small comparing to $(\Delta + 1)$. For example, graphs of 5000 nodes (with attachment degree of 100) give easily hubs having more than 900 neighbors whereas the maximal number of colors will not exceed 80. Figure 6 ensures theoretical complexity

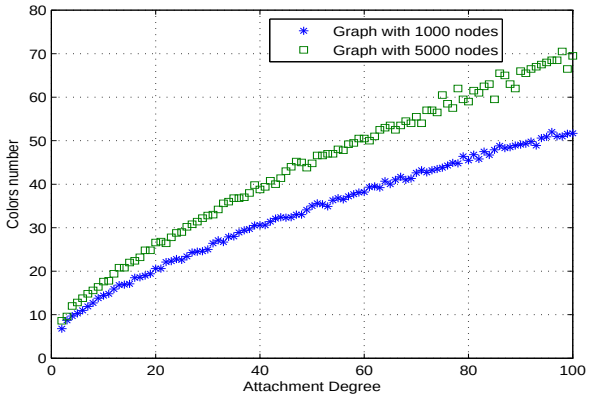


Fig. 5. Number of colors according attachment degree

obtained in [15] that grundy coloring converges in $O(n)$.

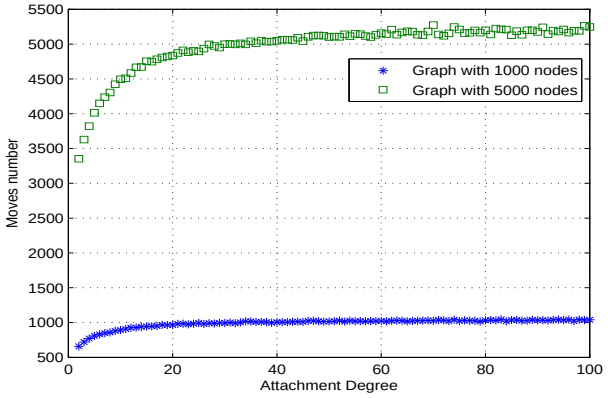


Fig. 6. Time of convergence of nodes coloring according attachment degree

## B. Comparison

In this section, we try to observe the behavior of self-stabilizing algorithms on random graphs and scale-free graphs. We use graphs having sizes of 1000, 2000, ...,10000 nodes. For more accurate results, we generate graphs having nearly the same density (number of edges). For example, the keyword used for curves legend: *Scalefree10* is used for scale-free




ISSN 1737-9334

graphs and *Random10* for random graphs where in both cases, most of nodes have likely 10 neighbors. The same concept is adopted for *Random50* and *Scalefree50* where every node has high probability to be adjacent to 50 neighbors. These values have been chosen according statistics given in previous works [2], [5] where many of real scale-free networkx have an average degree approximated to the taken values.

*1) MDS:* Random graphs give sets smaller than scale-free graphs as shown in figure 7. In fact, up to now, we have no explanation why random graphs give cardinality smaller than scale-free graphs. In other side, plots given in this figure confirm previous results that: more the graphs are dense, smaller MDS are given. However, for the time of convergence,

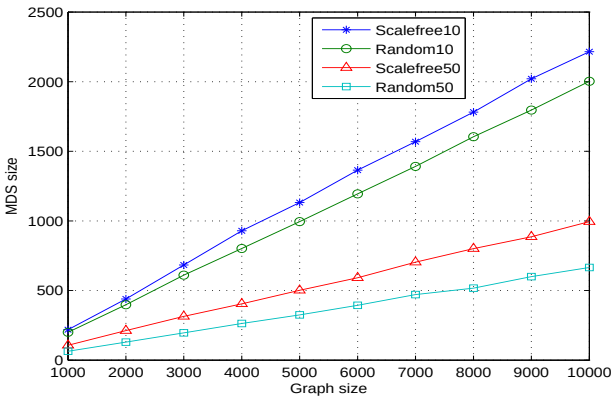


Fig. 7. MDS size in random graphs and scale-free graphs

figure 8 illustrates that calculating MDS in scale-free graph is faster than random graph. This is due to the cardinality where MDS given by random graphs are smaller than scale-free graphs, thus optimal sets need more time to reach legitimate configuration.

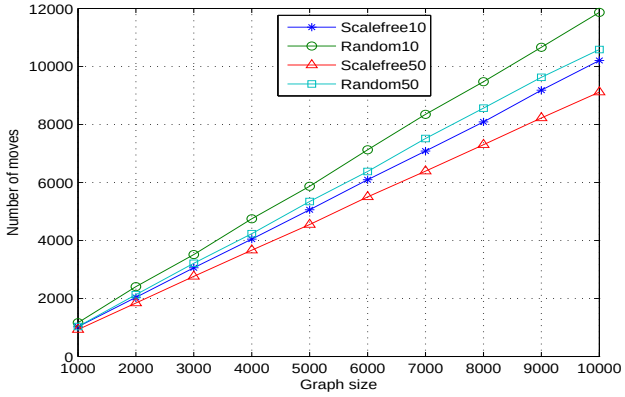


Fig. 8. Time of convergence (MDS) in random graphs and scale-free graphs

*2) MIS:* Recall that in MIS, we aim to maximize the set of independent nodes unlike MDS where the set is minimized. In figure 9, scale-free graphs give MIS sets bigger than random graphs.

Figure 10 shows that MIS of random graphs is found quickly than scale-free graphs. More the MIS is bigger (maximal), self-stabilizing algorithm needs more time to stabilizes. Bigger sets will need an increasing number of moves to be found.

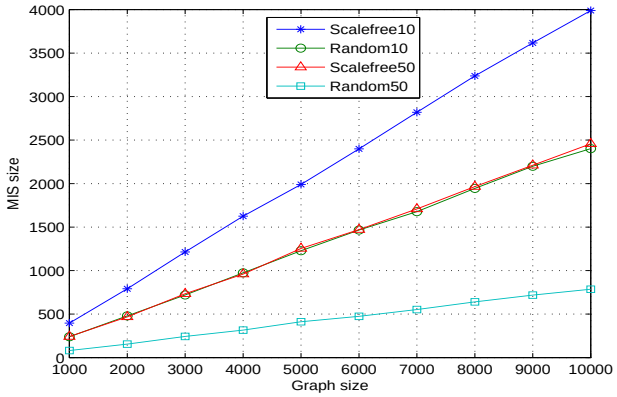


Fig. 9. MIS size in scale-free and random graphs

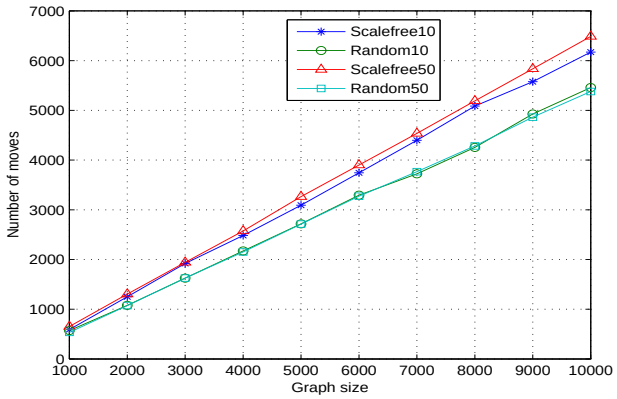


Fig. 10. Time of convergence (MIS) in scale-free and random graphs

*3) Coloring:* The important observation given by figure 11 is the constant number of colors needed in random graphs whatever the size of graphs. The number of colors is independent from graph growing because the average degree remains constant whatever the size of the graphs. It shows that for random graphs with an average degree of 10, we need at most 8 colors and for random graphs with an average degree of 50, we need only 20 colors. For the scale-free graphs, the number of colors is proportional to the attachment degree. It increases slowly when the attachment degree grows. Generally, scale-free graphs with large scale of nodes, contains hubs of high degree. According [15] where the number of colors is dependent to $\Delta$, more the graph grows, hubs will use a greater number of colors.

In figure 12, scale-free graphs find colors quickly than random graphs. It is clear when the interval of choices (colors) is large, it will be easy to find the colors.




ISSN 1737-9334

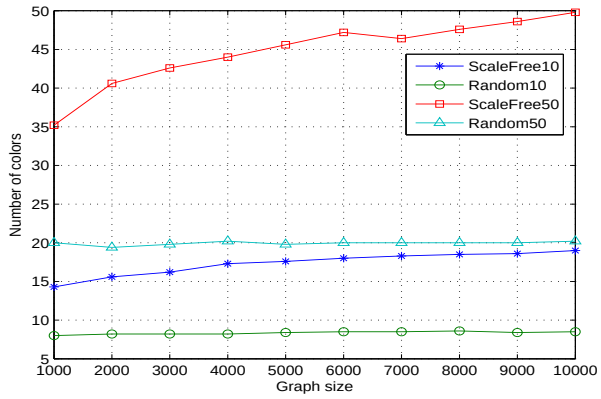


Fig. 11. Colors number in scale-free and random graphs

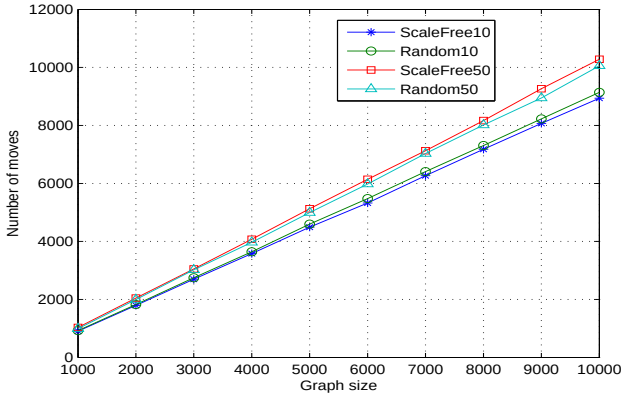


Fig. 12. Coloring convergence in scale-free and random graphs

### C. Evolution

In the previous simulations, graphs are supposed static. Before activating the self-stabilization in static graphs, we assign to each node a random state. After that the algorithm starts until it converges to the legitimate global configuration. However, in this section, we try to show that uniform self-stabilizing algorithms can be integrated easily in Scale-free graphs during the evolution process. The graph is supposed stable (in legitimate configuration) before the attachment of a new node. When the new node joins the existing graph, the self-stabilizing algorithm starts execution in order to move to the legitimate global configuration again.

In the experiments, we have generated a graph of 10000 nodes integrating self-stabilization (using the above three algorithms). According Algorithm 1, after constructing the initial subgraph of 10 nodes (attachment degree=10), the evolution process begins immediately with the coming of $11^{th}$ node. The self-stabilizing process starts at the moment the $11^{th}$ node joins the graph. At this moment, the algorithm has to converge to the correct configuration (the graph is now formed with 11 nodes). Every time there is new node who joins the existing graph, self-stabilizing process is reacting to correct the graph configuration because there is a probability that the new node dis-stabilizes the legitimate configuration. The alternative process, add new node / reaction of self-stabilization, is executed from the joining of the $11^{th}$ node to the $10000^{th}$ node.

Figure 13 shows a partial interval of the alternative process, add node / reaction of self-stabilization, between the coming of nodes 5010 and 5020. Self-stabilizing algorithms give different results. Generally, there is two cases. In the first case , the new node does not influence the global configuration of the graph where there is no executed moves. In this case where the number of moves is not growing, the new node joins the graph selecting a random state without activating its own rules of self-stabilization which means that the new node is in a correct state at least with its neighborhood. In the second case, the number of moves grows when just one new node joins the existing graph. The new node dis-stabilizes the global configuration by executing at least one move which means that the node or one of its neighbors has enabled a rule in order to correct the global configuration. The maximal number of moves executed, for a new node addition, is given by node 5019 in the MDS algorithm where 4 moves are executed for the stabilization of the algorithm (from 9956 to 9960). For 10 added nodes, the coloring problem is the algorithm that needs a greater number of moves for stabilization (18 moves from 7060 to 7078) whereas the MIS algorithms needs 5 moves (smaller number) in the interval of the 10 new nodes. Other

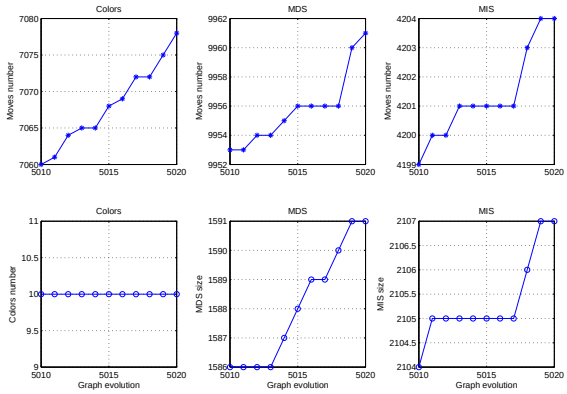


Fig. 13. Self-stabilization for 10 new nodes attaching with degree 10 on scale-free graph of 5010 nodes

results shown by figure 13 are the following. The coloring problem still uses a constant number of colors in this interval. MDS cardinality is increased by including new 5 nodes in the MDS from the 10 possible. The size of MIS grows by adding 3 new nodes in MIS from 10 nodes possible.

Table II gives some results extracted from the entire evolution from the $11^{th}$ node to the $10000^{th}$ node. Although these results are calculated for evolutionary graphs, it will be possible to compare them with static graphs. For the convergence time, static graphs seems faster than evolutionary graphs (according plots $ScaleFree10$ in figures 8, 10 and 12 ). Recall that dynamic graphs stabilizes gradually $i.e.$ a new




ISSN 1737-9334

TABLE II
RESULTS OF SELF-STABILIZING ALGORITHMS DURING GRAPH EVOLUTION

| | MDS | | MIS | | Coloring | |
|---|---|---|---|---|---|---|
| Graph | Moves | Size | Moves | Size | Moves | Colors nbr |
| 11 | 12 | 5 | 1 | 5 | 7 | 3 |
| 1000 | 1912 | 297 | 849 | 418 | 1442 | 9 |
| 2000 | 3989 | 627 | 1733 | 858 | 2852 | 10 |
| 3000 | 6024 | 936 | 2525 | 1280 | 4237 | 10 |
| 4000 | 7958 | 1252 | 3398 | 1698 | 5650 | 10 |
| 5000 | 9924 | 1588 | 4191 | 2097 | 7038 | 10 |
| 6000 | 12043 | 1877 | 5071 | 2499 | 8364 | 10 |
| 7000 | 14138 | 2187 | 5909 | 2889 | 9787 | 10 |
| 8000 | 16235 | 2487 | 6774 | 3305 | 11190 | 10 |
| 9000 | 18332 | 2809 | 7593 | 3721 | 12587 | 10 |
| 10000 | 20317 | 3139 | 8493 | 4144 | 13949 | 10 |

graph with $n$ nodes corrects its configuration knowing that the old graph of $n-1$ is in legitimate configuration. Only the new joining could move to an illegitimate configuration. However in the static graphs, the global legitimate configuration must be achieved after starting from an unknown global random state. Moreover, comparing table II with figures 7, 9 and 11 shows that static graphs gives smaller MDS sets. Whereas dynamic graphs produce maximal sets for MIS and give smaller number of colors for the coloring problem.

## VII. CONCLUSION

In this paper, self-stabilization is tested under scale-free graphs using a set of well-known algorithms. We have illustrated also how self-stabilization works under graph evolution. This later demonstration is important if we know that most of real networks are constructed under evolution. From a point of view application, our work shows that self-stabilization is suitable for distributed systems where the structure is in continuous change according to the evolution process introduced by Barabasi.

Our simulation tests give various results under scale-free graphs, particularly for the problems of: graph coloring, detecting minimal dominating set and finding the maximal independent set.

In the future, we hope to test self-stabilization on graphs with more dynamic structures such as nodes leaving. We will try to interpret some results like the reason random graphs produce smaller sets of MDS and MIS than scale-free graphs.

## ACKNOWLEDGEMENTS

The authors would like to thank N. Guellati, C. Titouna and the referees for their valuable comments in order to improve the paper.

## REFERENCES

[1] N. Guellati and H. Kheddouci, "A survey on self-stabilizing algorithms for independence, domination, coloring, and matching in graphs," *Journal of Parallel and Distributed Computing*, vol. 70, no. 4, pp. 406–415, 2010.
[2] R. Albert and A.-L. Barabási, "Statistical mechanics of complex networks," *Rev. Mod. Phys.*, vol. 74, no. 1, pp. 47–97, 2002.
[3] B. Neggazi, N. Guellati, M. Haddad, and H. Kheddouci, "Efficient self-stabilizing algorithm for independent strong dominating sets in arbitrary graphs," *International Journal of Foundations of Computer Science*, vol. 26, no. 06, pp. 751–768, 2015.
[4] A.-L. Barabasi and R. Albert, "Emergence of scaling in random networks," *Science*, vol. 286, no. 5439, pp. 509–512, 1999.
[5] X. F. Wang and G. Chen, "Complex networks: small-world, scale-free and beyond," *IEEE circuits and systems magazine*, vol. 3, no. 1, pp. 6–20, 2003.
[6] S. Dolev, A. Israeli, and S. Moran, "Self-stabilization of dynamic systems assuming only read/write atomicity," *Distributed Computing*, vol. 7, pp. 3–16, 1993.
[7] S. Dubois and S. Tixeuil, "A taxonomy of daemons in self-stabilization," *CoRR*, vol. abs/1110.0334, 2011.
[8] S. K. Shukla, D. J. Rosenkrantz, and S. S. Ravi, "Observations on self-stabilizing graph algorithms for anonymous networks," in *PROCEEDINGS OF THE SECOND WORKSHOP ON SELF-STABILIZING SYSTEMS*, 1995, pp. 1–7.
[9] S. Hedetniemi, S. Hedetniemi, D. Jacobs, and P. Srimani, "Self-stabilizing algorithms for minimal dominating sets and maximal independent sets," *Computer and Mathematics with Applications*, vol. 46, no. 56, pp. 805–811, 2003.
[10] V. Turau, "Linear self-stabilizing algorithms for the independent and dominating set problems using an unfair distributed scheduler," *Information Processing Letters*, vol. 103, no. 3, pp. 88–93, 2007.
[11] D. Li, L. Liu, and H. Yang, "Minimum connected r-hop k-dominating set in wireless networks," *Discrete Mathematics, Algorithms and Applications*, vol. 1, no. 1, pp. 45–57, 2009.
[12] K. Alzoubi, P.-J. Wan, and O. Frieder, "Maximal independent set, weakly connected dominating set, and induced spanners in wireless ad hoc networks," *International Journal of Foundations of Computer Science*, vol. 14, no. 2, pp. 287–303, 2003.
[13] Y. Ding, J. Z. Wang, and P. K. Srimani, "A linear time self-stabilizing algorithm for minimal weakly connected dominating sets," *International Journal of Parallel Programming*, vol. 44, no. 1, pp. 151–162, 2016.
[14] Y. Ding, J. Wang, and P. Srimani, "Self-stabilizing selection of influential users in social networks," in *17th International Conference on Computational Science and Engineering*. IEEE, 2014, pp. 1558–1565.
[15] S. T. Hedetniemi, D. P.Jacobs, and P. K.Srimani, "Linear time self-stabilizing colorings," *Information Processing Letters*, vol. 87, no. 5, pp. 251–255, 2003.
[16] L. Kuszner, "Tools to develop and test self-stabilizing algorithms," *http://kaims.eti.pg.gda.pl/ kuszner/self-stab/main.html*, 2005.




ISSN 1737-9334

# Cloud Computing in Education: A Survey on the Adoption and the Challenges for the Faculty of IT at the Benghazi University-Libya

Khadiga M. Elnajar [#1], Eiman M. Sahly [*2], Hend M. Farkash [+3], Abdul Ghafar Faraj [&4]

[#] *Dept. of Computer Science, Benghazi University*
*Benghazi, Libya*
[1]Khadiga.Mohamed@uob.edu.Ly
[*]*Dept. of Software Engineering, Benghazi University*
*Benghazi, Libya*
[2]Eiman.sahly@uob.edu.Ly
[+] *The College of Electrical & Electronic Technology*
*Benghazi, Libya*
[3]Hend.mf_ceet@ceet.edu.ly
[&]*Dept. of Statistics, Benghazi University, Faculty of Science*
*Benghazi, Libya*
abdstat@yahoo.com

***Abstract*— Cloud computing provides reliable computing environments and highly scalable resources are accessible to users. Cloud computing in education is the next big trend for efficient e-Learning systems. In fact, educational institutions in developing countries should benefit from the application of cloud technologies to improve the quality of their education. In this paper investigates challenges being encountered in the adoption of cloud computing in University of Benghazi. It implores the use of questionnaire to generate the data. In all, 500 copies of the questionnaire were administered to 303 students, and 80 teachers across to the 6 departments in IT. While 300 copies were returned this represents a respondent rate of 53% student and 30% teachers. The result of the analysis obtained reveals that 66.7% of the teachers and 48.5 % of the students' advowson the use of cloud services in support of curricula in University. The study showed the willingness of both students and teachers to apply cloud computing services in education at the Faculty of Information Technology at Benghazi University.**

***Keywords*— *Cloud computing, Education, Educational institutions, Research Survey, Challenges of Cloud Computing.***

## I. INTRODUCTION

The main goal of any educational institution is the quality of education. However, the cloud computing solves many problems and opens many opportunities to the educational establishments. The main objective of any educational institution is the quality of education. Cloud computing offers a great opportunity for educational institutions in developing countries to improve their education by providing an interactive cloud of lessons and multimedia through the ability to the combination of media.

Cloud Computing is the third revolution after PC and Internet in IT. Specifically, Cloud Computing is the improvement of Distributed Computing, Parallel Computing, Grid Computing and Distributed Databases. In fact, the basic principle of Cloud Computing is making tasks distributed in large numbers of distributed computers but not in local computers or remote servers. The Cloud Computing is capable of integrating large quantities of information and resources stored in personal computers, mobile phones, and other equipment, and putting them on the public cloud for serving users [1]. In other words, cloud computing is Internet-based computing and it provides resources, software, and information to computers and other devices on demand.

The most common definition of cloud computing according to the definition of the National Institute of Standards and Technology (NIST)[2], "Cloud computing is a model for enabling convenient, on-demand network access to a shared pool of configurable computing resources [e.g., networks, servers, storage, applications, and services] that can




ISSN 1737-9334

be rapidly provisioned and released with minimal management effort or service provider interaction".

According to the United Nation's Human Development, Libya has the highest rate of literacy in the ranks of the Arab world that the standard of living, social security, health care and other factors for development .Internet users as of 30-June-2012 stood at 17.0 % of the population. As of 31-Dec-2012, the country had 13.9% Facebook users [3]. There are 108 higher education institutions in Libya, including 12 government universities and another 96 government funded institutes that provide education in the areas of administration and management, technology, creative art, and teacher development. The universities such as Benghazi University, Tripoli University, and Academy of Postgraduate Studies and Economic Research have their basic ICT infrastructure such as computers, Internet access, and a local area network [4].

In fact, the need to adopt new and emerging technologies in higher education is increasingly needed to meet students' educational needs, to provide quality education and to prepare students to meet the challenges of the 21st century. The internet services in Libya provider only by Libya Telecom & Technology LTT is the state-owned company. However, the recent uprising disrupted Libya's telecommunications sector, reconstruction efforts are underway.

Therefore, in this paper, challenges are being investigated in the adoption of cloud computing at Benghazi University. The assessment of trends examines the current level of awareness and adoption of cloud computing in the Faculty of Information Technology at Benghazi University, and the challenges assessed by investigating the problems and limiting factors for successful application and using cloud computing in college. This concludes by suggesting the recommendations of the study the effective adoption and use of cloud computing at Benghazi University.

## II. USING CLOUD COMPUTING IN EDUCATION

Cloud Computing offers universities the possibility of concentrating more on teaching and research activities through a fast IT implementation and complexity can be reduced with Cloud Computing. Many universities recognize the potential and efficiency of using cloud computing in education, which we mention the University of California, the School of Electrical and Computer Science at Washington State University, the higher education institutions of the United Kingdom and Africa, U.S and others [5].

For example on the successful use of cloud in education: in Virginia, many colleges and universities had collaborated at the formation of Virtual Computing Lab. This allowed institutions to reduce IT expenses by reducing licensing requirements and software upgrades. Also, improve IT resources for researches and students. The University of North Carolina has made a significant reduction in expenses with software licensing by including cloud services, and also reducing the number of IT staff on the campus from 15 to 3 employees with the full working schedule [6].

There are several previous studies on cloud computing in education in terms of ease and difficulty as well as how to use and apply them. Masud and Huang [7], proposed the construction of e-learning system based on cloud computing, The infrastructure layer includes physical devices and networks, the software layer contains a unified interaction display for e-learning developers. They recommend that the use of cloud computing technology in e-learning systems to take advantage of the potential and the advantages of this technology. Al-Zoube [8] using library applications through cloud computing to build a virtual and virtual e-learning environment. The proposed environment includes the design and control of educational content, the creation of a system that allows the exchange of educational content and the integration of many educational and learning curricula in the same environment.

Al Shetty[9], was finds that all universities and colleges seek to pursue the rapid technological development in the field of education. Cloud computing is the new and important alternative to educational aspects. The research concluded that the use of cloud computing techniques in e-learning is necessary to give students the opportunity, Students and teachers to quickly access various applications, systems and resources through the Internet, file sharing, documents, exchange of



ISSN 1737-9334

duties, and projects between students. Research has shown that cloud computing technologies help universities and colleges solve many problems Manage and maintain IT resources and improve the learning process. And that cloud computing technologies will help universities and colleges solve many of the problems of managing and maintaining IT resources as well as improving the process of teaching and self-learning.

Matthew[10] presented a study investigates the challenges being encountered in the adoption of cloud computing in Nigerian Universities. It implores the use of a questionnaire to generate the data. Microsoft Excel was used to capture the data while frequency and percentage distributions were used to analyse it. In all, 10, 800 copies of the questionnaire were administered to 54 public universities across the 6 geopolitical zones in Nigeria while represents a respondent rate of 81.1%. The result of the analysis obtained in this research work indicates that 92% of the total respondents are aware of cloud computing in education, 82% of the universities adopt the use of cloud.

## III. Benefits and of Using Cloud Computing in Education

### A. Benefits

There are several benefits of using this technique in education can be summarized as follows:

- Access to applications from anywhere. The use of applications for students and teachers without loading them onto their devices, and also help them to access their files stored from any computer through the Internet.
- Support students learn in new and modern ways to help them manage their projects and duties.
- Ease of communication and interaction between students.
- Software free or pay per use.
- Protection of the environment by using green technologies

### B. Limitations

The difficulties of the use of cloud computing includes the following:

- The main problems are speed/lack of Internet can affect work methods.
- Dissemination politics, intellectual property, protection of intellectual property rights is also one of the problems that raise the concerns of users; there is no guarantee that these rights will not be violated for users.
- Risks related to data protection and security and accounts management and standards adherence.

## IV. Materials and Method

The methodology and approach adopted in this paper are described below. In this section, the research questions are highlighted and research techniques used are discussed.

### C. Research Questions

In this paper we have formulated four research questions to achieve the purpose of this study as follows:

*What is the level of awareness about cloud computing in education?*

*Is there acceptance and willingness to use cloud computing technology in college by both student and professor?*

*What cloud computing services are used to support scientific research?*

*What are the challenges to successful adoption and use of cloud computing at Benghazi University?*

### D. Method and procedures

This study is an empirical research which investigates the level of awareness and adoption of cloud computing at Benghazi University. The data collection tool was questionnaire and an electronic questionnaire[1] titled "The difficulties of employing cloud computing in the Faculty of Information Technology at Benghazi University as seen by teachers and students" in four (4) parts. The first part presents an assessment of the level of awareness about cloud computing, while the second part provides information on assessing the trends of awareness and benefits of using cloud

1 The questionnaire is available on:
https://docs.google.com/forms/d/e/1FAIpQLSdjlsEr0OLSZrk5sKWJSRs31GeWVTGr0R6Q5xRZYyH5EJDleQ/viewform
https://docs.google.com/forms/d/1gXqU2R_77i1W_p3_TFUiU0rQmpVtUjktt7R_5kefAc/edit?ts=5ba23f6f#responses




ISSN 1737-9334

computing at the University. The third part assesses the difficulties of adopting cloud computing by decision makers at Benghazi University while the fourth part investigates the challenges of using cloud computing at Benghazi University.

The study community the Faculty of Information Technology Benghazi University for the academic year 2016-2017:

*1) Students:* It targeted a sample of 303 students out of the size of the community 1288 students as shown in Fig. 1. Actually, we collected 53% of the target sample size.

*Teachers:* It targeted a sample of 80 *Teachers* out of the size of the community 101 Teachers as shown in Fig. 2. Actually, we collected 30% of the target sample size.

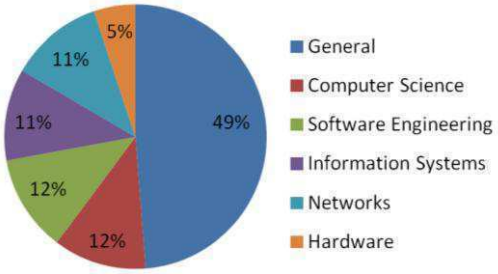


Fig. 1 shows the size of the community, the relative weight and the size of the sample for each department section of the Faculty of Information Technology.

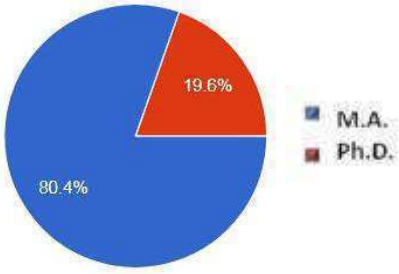


Fig. 2 shows the size of the community, the relative weight and the sample size of a full time faculty member of staff and a part time faculty member of staff.

The questionnaire was validated and tested for reliability using the Pearson Product Moment Correlation. A Cronbach alpha reliability coefficient (α) of 0.882 was obtained, an indication that the instrument was reliable for data collection.

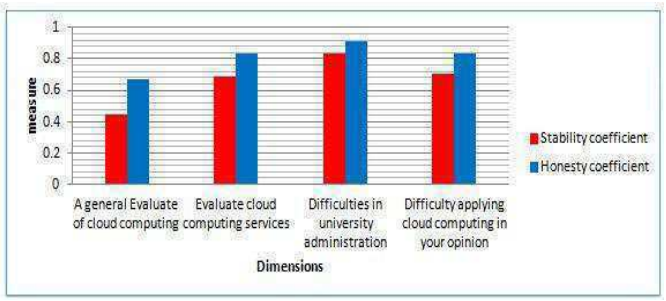


Fig. 3 shows the measurement of honesty and persistence using the alpha-kerobh coefficient of the study variables.

It is clear from the above figure that they are credible and reasonable transactions that reflect the ability of the meter to measure what is designed for it. The stability coefficient for the dimensions as a whole is 77.8%, and the truthfulness coefficients extracted from the square root function is 88.2%. This confirms the validity of the measurements for this study. The dimension is a general estimate for cloud computing. The stability coefficient is 45.5%. It is reasonable and the dimension difficulties in university administration where the stability factor is 83.3 and the honesty factor 91.2%.

## V. RESULTS AND INTERPRETATION

The paper sample was dump on Google forms to capture and analyse the data the descriptive techniques used. The descriptive survey was adopted to obtain the opinion of a representative sample of the target population so as to be able to infer the perception of the entire population.

### *A. Descriptive statistics*

As illustrated in Fig. 4, that most of the respondents hold the degree of assistant lecturer with a total number of 27 by 55.1%. Followed by 11 lecturer with 22.4%, and the lowest number of teachers in the degree of associate professor, where the number reached 2 by 4.1%.




ISSN 1737-9334

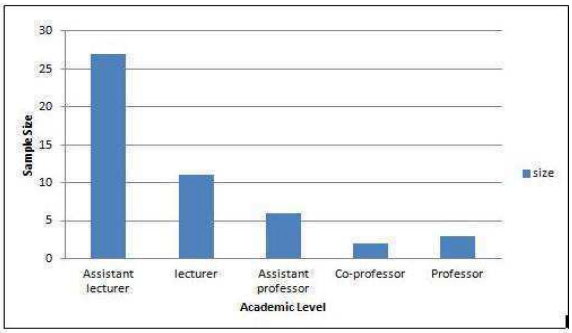


Fig. 4 shows the frequency and percentage of the degree.

The Fig. 5 shows that most of the general department, where the number of 16, by 32.7 followed by the department of Software Engineering, where the number of 8 by 16.3% and the Department of Computer Science, where the number of 8 by 16.3% and less section of the networks, 8.2 The following figure illustrates this.

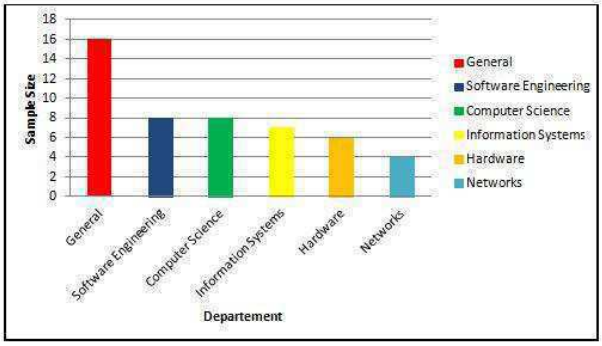


Fig. 5 Shows the frequency of the department of the faculty members.

Fig. 6 shows that most of the students from the fourth grade and graduation were respectively 47 and 45 students with 22% and 21% respectively, followed by students of the sixth grade and above the seventh were respectively 30 and 28% by 14% and 13.1% Respectively for the target sample of the study.

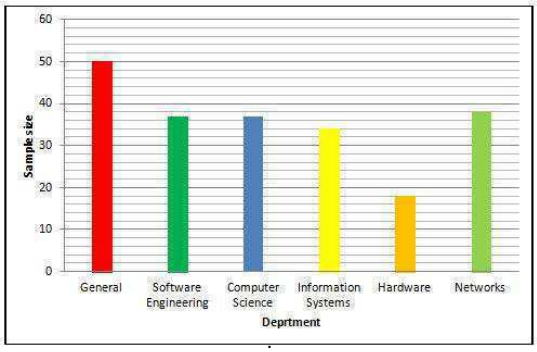


Fig. 6 Shows the frequency of the class for students.

*B. Analytical Statistics*

We used SPSS Statistics to obtain correlation coefficients. Below we present research hypotheses.

- *There is significant difference in a general evaluate of cloud computing*

In Table 1 illustrated that the arithmetic average of the study sample is 3.3317 in the direction of knowledge in the cloud computing assessment of the target sample of the students and the teacher. It is larger than the theoretical computational average of the Likert scale 5 and the standard deviation is 0.8529 in homogeneity on the probability value (0.00), which is less than the significance level (0.05). The difference is significant in the responses of the students and the sample teachers.

TABLE I
A GENERAL EVALUATE OF CLOUD COMPUTING AMONG STUDY MEMBERS

| Probability Value | N | Average | Standard deviation | T | The degree of freedom | Probability value |
|---|---|---|---|---|---|---|
| A general Evaluate of cloud computing | 362 | 3.3317 | 0.8529 | 6.307 | 262 | 0.000 |

- *There is a significant difference in evaluating cloud computing services*

In Table 2 illustrated that the arithmetic average of the study sample is equal to 3.9772. A significant knowledge trend in the evaluation of the cloud computing services in the sample of the target study of the students and the teacher is greater than the theoretical computational average of the Likert scale 5 and the standard deviation of 0.8052 in their homogeneity Based on the probability value (0.00), which is less than the significance level (0.05), the difference is significant in the responses of the students and the sample teacher, the study on their opinions on evaluating cloud services.

TABLE II
A GENERAL EVALUATE OF THE CLOUD COMPUTING SERVICES OF THE STUDY MEMBERS




ISSN 1737-9334

| Probability Value | N | Average | Standard deviation | T | The degree of freedom | Probability value |
|---|---|---|---|---|---|---|
| Evaluate cloud computing services | 362 | 3.9772 | 0.8052 | 19.68 | 262 | 0.000 |

- *There is a significant difference in the extent of difficulties related to university administration*

Table 3 illustrated that the arithmetic average of the study sample is equal to 3.9772. A significant knowledge trend in the evaluation of the cloud computing services in the sample of the target study of the students and the teacher is greater than the theoretical computational average of the Likert scale 5 and the standard deviation of 0.8052 in their homogeneity Based on the probability value (0.00), which is less than the significance level (0.05), the difference is significant in the responses of the students and the sample teacher, the study on their opinions on evaluating cloud services.

TABLE III
THE EXTENT OF THE UNIVERSITY'S DIFFICULTIES WITH THE STUDY MEMBERS

| Probability Value | N | Average | Standard deviation | T | The degree of freedom | Probability value |
|---|---|---|---|---|---|---|
| Difficulties in university administration | 362 | 3.9309 | 0.91321 | 16.532 | 262 | 0.000 |

- *There is a significant difference in the difficulties of implementing cloud computing in your opinion*

In Table 4, illustrated that the sample arithmetic means for a study is 3.7909. A trend in assessing the difficulties of applying cloud computing. In your opinion, individuals in the target study sample of students and the teacher are larger than the theoretical computational average of the Likert scale 5 and the standard deviation is 0.8253 (0.00), which is less than the significance level (0.05). The difference is significant in the answers of the students and the sample professor. The study is based on their opinions on evaluating the difficulties of applying cloud computing in your opinion.

TABLE IV
HOW DIFFICULT IT IS TO APPLY CLOUD COMPUTING TO YOUR SAMPLE

| Probability Value | N | Average | Standard deviation | T | The degree of freedom | Probability value |
|---|---|---|---|---|---|---|
| Difficulty applying cloud computing in your opinion | 362 | 3.7909 | 0.8253 | 15.54 | 262 | 0.000 |

*C. Discussion of research questions*

*1) Awareness of Cloud Computing in education*

On the results of the study, we have acquired 37% of the total respondents of the professors and 11.7% of the students that they are aware of cloud computing in education. The results reveal a readiness to use electronic tests in courses of 37.3% for teachers and 41.1% for students.

*2) Willingness to use cloud computing technology at the University of Benghazi.*

The responses obtained indicated that the responses obtained were 66.7% of the teachers and 41.1% of the students, they are ready to use cloud computing services to support the curriculum in the future. Both students and teachers mentioned the use of a cloud service in one of the previous courses at 25.5 % of the teachers and 30.4% of the students.

*3) Cloud computing services have been used in education*

- Cloud services scientific research tools (Google scholar): 65.9% of the teachers and 36.1% of the students.
- Cloud services presentations and videos (youtube): 60.8% of the teachers and 76.3% of the students.




ISSN 1737-9334

- Cloud social networking services (Facebook): 84.3% of the teachers and 81.3% of the students.
- Cloud storage services (Google Drive): 74.5% of the teachers and 45.2% of the students.
- Cloud services desktop applications (MS office online): 47.3% of the teachers and 21.7% of the students.
- University Mail Service: 47.1% of the teachers and 15.7% of the students.

*4) Challenges facing University adoption Cloud Services in Benghazi*

Based on the analysis of the findings obtained for the research question 4 in this study as presented in Table 5, a number of challenges currently embattling Benghazi University to used cloud services. These factors include: data insecurity, privacy concerns, and fear of downsizing staff positions, reliability challenge and resistance to change in modern technologies in education, and infrastructure problems in the country.

TABLE V
CHALLENGES OF CLOUD COMPUTING ADOPTION IN BENGHAZI UNIVERSITY

| S/N | Challenges of adoption cloud computing in Benghazi university | % of Respondents | |
|---|---|---|---|
| | | Teachers | Students |
| 1 | Data insecurity and privacy concerns | 33.3 | 28.1 |
| 2 | Resistance to renewal and development of the use of modern technologies in education. | 31.4 | 29.8 |
| 3 | Weak Internet currently available. | 68.6 | 38.8 |
| 4 | The lack of support and adequate funding | 62.7 | 37.5 |
| 5 | Lack of awareness of the importance of cloud computing in education. | 54.9 | 36.8 |

## VI. STUDY RECOMMENDATIONS

There are two recommendations limitations of this study:

- Recommendation is on the university administration to equip the infrastructure of the colleges before the application of e-learning, and the processing of the internal network of high speed.
- Teachers publish e-culture among students to achieve maximum interaction with this cloud computing technology of education; it can be used to present curriculum, annotations and examinations.
- Finally Adopting some cloud computing services by the College of Information Technology to provide a model that contributes to the encouragement of the other faculties and departments of the university, then it can make easily by hybrid Cloud between Libyan universities to share sources and cost minimize.

## VII. CONCLUSIONS

Modern education is changing as is an education in the classroom due to the advent of technology. Students expect and require more services from their institutions. The future success of a country depends on the development of the education given to its students. The future world will be a technology-based world so applying the technology in the learning session will help a student to be fully ready for the future world. Therefore, we conducted a study on the extent accepted of cloud computing technology in education. This study aimed to identify the difficulties of employing cloud computing in the Faculty of Information Technology at Benghazi University as seen by teachers and students. The study sample consisted of 250 students, 50 of his professors. The sample of the study community in a random way, and we have built a performance of the study is a questionnaire to measure the difficulties of employing cloud computing at the University of Benghazi. Through the results obtained in this survey, we found that both students and faculty members are ready to use computing technology.

Future work may focus on design an experiment in a subject so that it is divided into two groups. A group is taught using computing and other computing services in the traditional way. Through these two groups, students' educational quality is studied and evaluated.

## REFERENCES

[1] R. Sanchati, and G. Kulkarni, "Cloud Computing in Digital University Libraries," *Global Journal of Computer Science and Technology,* vol. 11, no. 12, pp. 7, 2011.

[2] P. Mell, and T. Grance, *The NIST Definition of Cloud Computing*, Information Technology Laboratory, U.S. Department of Commerce, September 2011.




ISSN 1737-9334

[3] Africa. "http://www.internetworldstats.com/africa.htm#eg.," 22.9.2017, 2012.
[4] A. Hamdy, *Survey of ICT and Education in Africa : Libya Country Report*, Washington, DC, 2007.
[5] N. Sultan, "Cloud Computing for Education: A New Dawn?," *Journal of Information Management,* vol. 30, no. 2, pp. 109-116, April 2010.
[6] D. C. Wyld. "Cloud computing 101: Universities are migrating to the cloud for functionality and savings," 2 November 2017; Available: http://computersight.com/programming/cloud-computing-101-universities-are-migrating-to-the-cloud-forfunctionality-and-savings/.
[7] A. h. Masud, and X. Huang, "An E-learning System Architecture based on Cloud Computing," *World Academy of Science, Engineering and Technology,* vol. 6, no. 1, 2012.
[8] M. Al-Zoube, "E-Learning on the Cloud," *International Arab Journal of Information Technology* vol. 2, no. 1, 2009.
[9] I. M. I. Al Shetty, "The possibility of using cloud computing technology in e-learning at Qassim University."
[10] F. T. Matthew, "Cloud Computing In Education – A Study of Trends, Challenges and an Archetype for Effective Adoption in Nigerian Universities," *Information communication technology (ICT) integration to educational curricula : a new direction for Africa* p. 296: University Press of America, 2015.



ISSN 1737-9334

# Demand Response and Optimal Sizing of Hybrid Renewable Energy Systems

Fatma Zohra Dekhandji, Mouould Bouaraki, Nadhir Zaidi and Abdelmadjid Recioui
Laboratory Signals and Systems, Institute of Electrical and Electronic Engineering,
University M'hamed Bougara of Boumerdes, Avenue de l'indépendance, 35000.
Boumerdes, Algeria.
E-mail: fzdekhandji@yahoo.fr

*Abstract*— **Energy is a vital and essential element of our modern world. Its importance lies in the development process and its close association with sustainable development. This matter stimulated the search need for renewable energy resources, which are environmentally friendly to reduce environmental pollution on one hand, and reduce the pressure on the traditional energy use on the other hand. In this work, a design optimization of a system to illustrate energy management including renewable energy is done using Homer. Next, the system is simulated and tested using LABVIEW. The goal is to verify the adequacy of the designed system and its real life applicability.**

***Keywords-Smart grids;demand response, renewable energies, HOMER, optimization.***

## I. INTRODUCTION

In recent years, there has been an proliferating rise in energy demand due to the economic growth in the industrialized countries, the increase in industry rates and the improvement of the technologies, the development in various fields and the rising oil prices [1-2]. For that, countries have no choice just to look for new energy sources, clean and cheap, especially as concerns over global warming and climate change persist. As a consequence, a considerable growth in using renewable energy resources has been observed [1-16].

Particularly, solar and wind energy are infinite, site-dependent, clean and high potential sources for alternative energy production [1-2]. Hybrid energy systems are the best suited to reduce dependence on fossil fuel using available wind speed and solar radiations [1-16]. The integration of renewable energy sources is not a straightforward operation but it needs a techno-economical analysis and requires the data of the renewable resources [9].

Sizing hybrid systems has been in the last two decades a large research field and many methods have been suggested to solve that problem. Particularly, research is carrying on the modeling accuracy of the component of the hybrid system and the followed power management strategies. The control strategy is the heart beating of any algorithm subjected to optimize a hybrid system, in 1996 Barley and Winn improved the control strategies model of introducing new parameters that have become of great importance in the control strategies of the software tools HYBRID2, HOMER and HOGA [9,16].

HOMER (Hybrid Optimization Model for Electric Renewables), developed by NREL (National Renewable Energy Laboratory in USA), is the most-used optimization software for hybrid systems. It uses a predictive control strategy where the charging of the batteries depends on the prediction of the demand and the energy expected to be generated by means of renewable sources, with this strategy, the energy loss from the renewable energies tends to decrease. Usually, the optimum design is carried out minimizing the Net Present Cost (NPC: investment costs plus the discounted present values of all future costs during the lifetime of the system) or by minimizing the Cost of Energy (COE: total cost of the entire hybrid system divided by the energy supplied by the hybrid system), the results obtained by each used tool will be evaluated by that economic criterion [5].

The goal of this paper is to illustrate the benefits of energy management including the renewable energies. It depicts a design optimization model by Homer software. The simulation and testing of the energy management system including the renewable energy sources is performed in LABVIEW software.

## II. THE DEMAND-RESPONSE CHALLENGE

Demand response provides an opportunity for consumers to play a significant role in the operation of the electric grid by reducing or shifting their electricity usage during peak periods in response to time-based rates or other forms of financial incentives.

Some electric system planners and operators as resource options for balancing supply and demand are using demand response programs that can lower the electricity cost in wholesale markets, and in turn, lead to lower retail rates.
The electric power industry considers DR programs as an increasingly valuable resource option whose capabilities and potential impacts are expanded by grid modernization efforts. For example, sensors can perceive peak load problems and utilize automatic switching to divert or reduce power in strategic places, removing the chance of overload and the resulting power failure. Smart customer systems such as in-home displays or home-area-networks can make it easier for consumers to changes their behavior and reduce peak period consumption from information on their power consumption and costs. These programs also have the potential to help electricity providers save money through reductions in peak demand and the ability to defer construction of new power plants and power delivery systems [17].

Demand Response is a program that helps electricity customers monitor and manage their energy usage by




ISSN 1737-9334

allowing them to participate in electricity markets to respond to price changes through which customers reduce their electricity consumption in response to either high wholesale prices or system reliability risks.

The Federal energy Regulatory Commission (FERC) of the United States defines the term DR as "changes in electric usage by demand side resources from their normal consumption patterns in response to changes in the electricity price over time, or to incentive payments designed to induce lower electricity use at times of high wholesale market prices or when system reliability is jeopardized" [18].

The DR concept is similar to dynamic demand mechanisms that aim to manage customer electricity consumption in response to supply conditions for example, customer's tendency to reduce their electricity consumption at critical times or in response to market prices. However, the difference is that demand response mechanisms meet direct demand and turn off, while dynamic demand devices tend to turn off fully when network pressure is detected.

In addition, the DR may include a reduction in the level of energy actually used or through the initiation of on-site power generation, which may or may not be parallel to the grid.

At the same time, the demand response system is one of the smart energy demand components includes the energy efficiency concept, home and building energy management, distributed renewable resources and the electric vehicles shipment [17].

Understanding and managing electric load is critical to participating in DR programs. Before we can manage the energy use, it is helpful to understand the energy demand (the sum of the various electric loads in our business at any given time) and how we are charged for that energy. Each utility charges its customers for energy amount they consume. In addition, commercial and industrial customers are also frequently billed for their peak demand, the highest rate at which the customer is using energy, generally measured in kilowatts (KW) over a one-hour period.

A load shape (known also as the load profile) is a graphical representation of how a customer uses electricity over the course of a day. The height of the graph at any point shows the customer's peak demand; the area under the load shape is the amount of energy consumed, in kilowatt-hours (kWh), over a given time period.

When customers are billed for energy amount they use, they are often also billed for their demand magnitude, the maximum electricity amount of drawn from the grid at a single moment in time. This demand charge is usually based on the highest amount of demand registered during the billing period (the peak demand). Demand charges to the highest level achieved in preceding period (such as the previous six months). Because a demand ratchet can be a considerable percentage of the bill, C&I customers should peak demand whenever possible to reap the economic benefits.

Consumers, who manage their facility load profiles with a view to reducing their peak demand charges, are effectively undertaking their own DR program. It is entirely possible for consumers to practice their own DR program in response to conventional rate structure while participating in system operator or utility DR programs at the same time [19].

## III. SIZING OF RENEWABLE ENERGY SYSTEMS

The optimal design for hybrid power systems is dependent and closely related to place of application. Therefore, the main objective of the present study is to determine the optimum solar/wind system that can provide the electricity needs in the research center **(CDER)** of Bouzareah, Algeria as average monthly consumptions. The system size and cost optimization is carried out based on the on-site measured data of wind and solar energy characteristics.

Bouzareah is a town located 8 km from the center of Algiers. It is considered as home to several major institutions. Among them, The Center for the Development of Renewable Energies (CDER) which holds world-leading scientific achievements in the field of solar power concentration over the African continent.

### *A. Solar and Wind data*

Solar irradiance data and wind speed historical data were measured for one year by CDER, which belongs to Bouzereah. Table 1 shows the observed wind speed data during 2015 were obtained at 10 meters above ground level with an anemometer. These data were used to investigate the wind power potential of this region.

The highest monthly mean wind speed of 4.795 m/s occurred in April, while the lowest mean wind speed of 3.197 m/s occurred in October. The mean annual wind velocity was 3.839 m/s.

In addition, the table presents the estimated solar PV energy in (kWh/m2 day) of solar irradiance for horizontal surfaces: the highest monthly mean solar irradiation is recorded inJune as 7.200 KWh/ $m^2$ where the lowest is recorded in December as 2.150 KWh/ $m^2$.

Table 1 Monthly average of wind speed, solar irradiation and temperature in CDER of Bouzereah, Algeria. [28]

| Month | Solar irradiation ($KWh/m^2$) | Wind speed (m/s) | Temperature (°C) |
|---|---|---|---|
| Jan. | 2.480 | 3,600 | 10,930 |
| Feb. | 3.380 | 3,890 | 13,420 |
| Ma. | 4.590 | 4,100 | 15,540 |
| Apr. | 5.690 | 4,795 | 19,276 |
| May | 6.490 | 4,300 | 24,646 |
| June | 7.200 | 4,100 | 29,670 |
| July | 7.130 | 3,797 | 32,787 |
| Aug. | 6.440 | 3,496 | 32,554 |
| Sept. | 5.280 | 3,904 | 27,689 |
| Oct. | 3.820 | 3,197 | 21,648 |
| Nov. | 2.630 | 3,398 | 15,131 |
| Dec. | 2.150 | 3,495 | 11,618 |




ISSN 1737-9334

### B. *The load description*

The study area consists of 20 houses each has a living area, kitchen, toilet and laundry area. The study will deal with one, two, three or four bedroom homes that are usually occupied.

The typical relevant electrical loads are lighting, kitchen appliances (electric refrigerator, electric stove with oven and toaster), TV, computer, laptop computer, electric water heating and air conditioning to operate in approximately 8 months per year.

One of the programs that helps to know the technical and economic studies of hybrid systems, which was used in Algeria is Homer's software, which enables the combination of wind turbines, PV arrays, run-of-river hydro power, biomass power, internal combustion engine generators, micro turbines, batteries, and hydrogen storage, serving both electric and thermal loads.

The best feature of this program is the sensitivity analysis in addition to allowing guessing all costs such as initial capital and maintenance costs including pollution penalties. The optimization aims is to assess the economic and technical feasibility of a large technology options number, taking into account differences in technology costs and the energy resources availability.

### C. *The considered system*

The system under consideration is a PV/Wind/Gasoline generator hybrid system as shown in Fig. 1. It consist of:

- Three (03) wind turbines from generic type that has a rated power of 3 KW AC. Each one has a 20 years lifetime with a 25 m as hub height. The typical power curve of these turbinesis shown in **Fig III.3**. The capital cost for one turbine is at 3900$ with the replacement assumed at the same price and the operation/maintenance costs at 100$/year.
- The Gasoline generator is a 2.61kW with a capital cost of 500$ and a lifetime of 5000 operating hours.

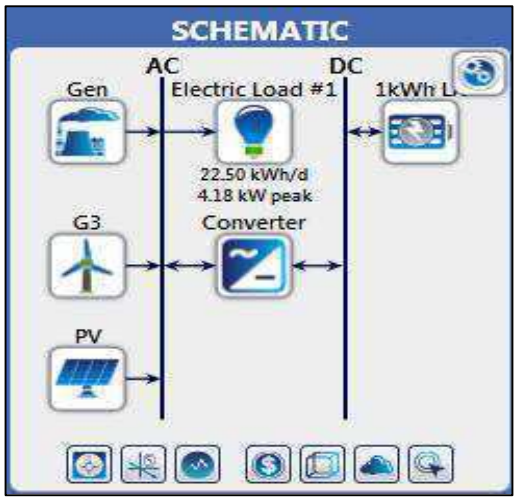


Fig. 1 The hybrid system considered for optimization

Again replacement is assumed to be at the same price with the operation/maintenance costs at 0.03$/h. The fuel price is taken to be constant and it is 0.32$/Litter.

Twenty-four (24) batteries from Lead Acid model that has a nominal voltage of 12V and a 1KWh as capacity. Their capital cost and replacement cost is considered fixe at 300$ and operating/maintenance cost of 10$/year.

For DC/AC or AC/DC conversion, up to 5 items of 1kW converter is used. The capital cost of such a converter is fixed at 300$ and the same replacement price and no operating/maintenance costs. These have 15year lifetime and 90% efficiency.

Two (02) PV panel from flat plate model that has a rated power of 200 KW AC. One has a capital cost of 3000$ with the replacement assumed at the same price and the operation/maintenance costs at 10$/year, and the second one has a capital cost of 5000$ with the replacement price of 4500$and the operation/maintenance costs at 20$/year.

The load demand considered is for home consumption profile. The seasonal profile, which is presentedin Fig. 2, shows a relatively constant power demand over all the year.

The Fig. 3 represents the daily consumption. The chart shows that consumption increases during the day especially in the early morning, noon and night beginning when it starts to decline and negligible at night.

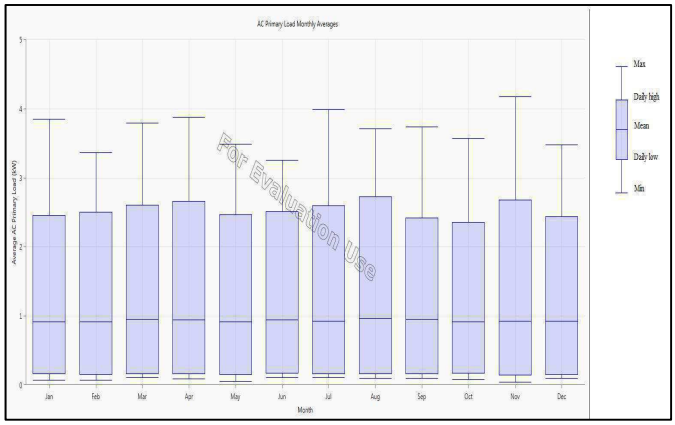


Fig. 2 the seasonal profile of the considered load.

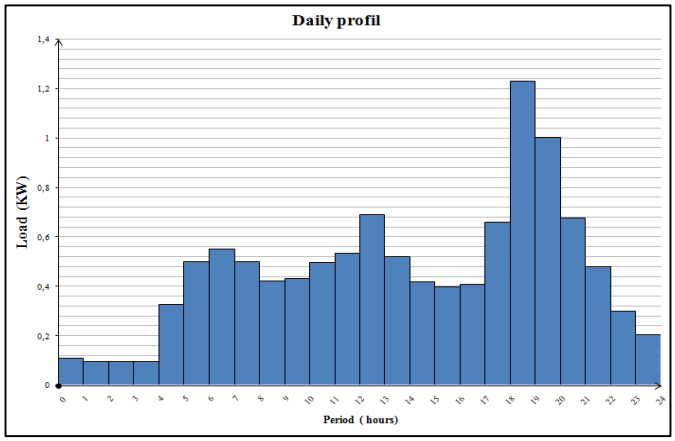


Fig. 3 The daily consumption of the considered load.




ISSN 1737-9334

Export...

Optimization Results

Left Double Click on a particular system to see its detailed Simulation Results.

Categorized Over

| Architecture | | | | | | | | | Cost | | | | System | Gen | | | | | |
|---|---|---|---|---|---|---|---|---|---|---|---|---|---|---|---|---|---|---|---|
| | PV (kW) | G3 | Gen (kW) | 1kWh LA | Converter (kW) | Dispatch | COE ($) | NPC ($) | Operating cost ($) | Initial capital ($) | Ren Frac (%) | Hours | Production (kWh) | Fuel (l) | O&M Cost ($) | Fuel Cost ($) | Capital Cost ($) |
| | 2.31 | 2 | 4.60 | 10 | 50.0 | CC | $0.340 | $75,824 | $1,849 | $25,652 | 49 | 1,546 | 4,211 | 1,461 | 213 | 467 | 5,627 |
| | | 6 | 4.60 | 10 | 50.0 | CC | $0.375 | $83,620 | $2,152 | $25,225 | 42 | 1,688 | 4,742 | 1,631 | 233 | 522 | |
| | 4.68 | | 4.60 | 10 | 50.0 | CC | $0.386 | $86,003 | $2,145 | $27,788 | 35 | 1,939 | 5,337 | 1,846 | 268 | 591 | 10,363 |
| | | | 4.60 | 10 | 50.0 | CC | $0.517 | $115,234 | $3,604 | $17,425 | 0.0 | 3,509 | 10,455 | 3,541 | 484 | 1,133 | |
| | 5.41 | 8 | 4.60 | | | CC | $0.588 | $131,057 | $3,926 | $24,515 | 31 | 4,621 | 5,686 | 2,632 | 638 | 842 | 11,815 |
| | 9.10 | | 4.60 | | | CC | $0.648 | $144,344 | $4,527 | $21,495 | 9.4 | 5,780 | 7,438 | 3,374 | 798 | 1,080 | 19,195 |
| | | 11 | 4.60 | | | CC | $0.696 | $155,174 | $5,107 | $16,600 | 10 | 6,035 | 7,380 | 3,426 | 833 | 1,096 | |
| | | | 4.60 | | | CC | $0.835 | $186,043 | $6,771 | $2,300 | 0.0 | 8,760 | 11,278 | 5,116 | 1,209 | 1,637 | |
| | 31.1 | 38 | | 10 | 50.0 | CC | $0.909 | $194,332 | $2,457 | $127,651 | 100 | | | | | | 63,126 |

Fig. 4 the optimization results with the optimum systems ranked.

### *D. Sizing results*

Once the specification described above is set in HOMER, it performs calculations to determine the best combination that meets the technical and economic requirements as shown in Fig. 4. In the system we simulated, Homer shows us that the optimal system is to combine PV panels with wind turbines and gasoline generators together with the battery bank and the converter.

## IV. SYSTEM TESTING THROUGH SIMULATION

The application is about energy management including renewable energies, which means the grid will compensate the lack in energy in the peak load reduction when the energy demand exceeds the available energy by enabling the renewable energy sources.

As a small and simple presentation of the virtual life and virtual components, which will be integrated in the smart grid, we have represented that the grid contains five (05) houses, each house has its own used equipment that increases the energy consumption.

The results of the test being performed are presented using figures, which display the LABVIEW front panel of the developed system. We have tested five different cases:

**Case one :** The energy consumption is ordinary ( Less than 40KWh). The green LED indicates normal consumption.

**Case two :** The energy consumption is medium ( between 40KWh and 65KWh). The orange LED indicates that the consumption is increase and approaches the power getting from the Gasoline power station.

**Case three :** The energy consumption is high (between 70KWh and 80KWh). The red LED indicates that the consumption is greater that the power getting from the Gasoline power station and the blue LED indicates that the first stage of the Solar wind farm is activated.

**Case four :**The energy consumption is high (between 80KWh and 90 KWh). When the consumption is still rising, the blue LEDs indicate that the first and the second stages of the Solar wind farm are activated.

**Case five:** The energy consumption is high (Greater than 90 KWh). When the third stage of the Solar wind farm is activate, all LEDs are glowing in blue in order to compensate the peak load reduction.

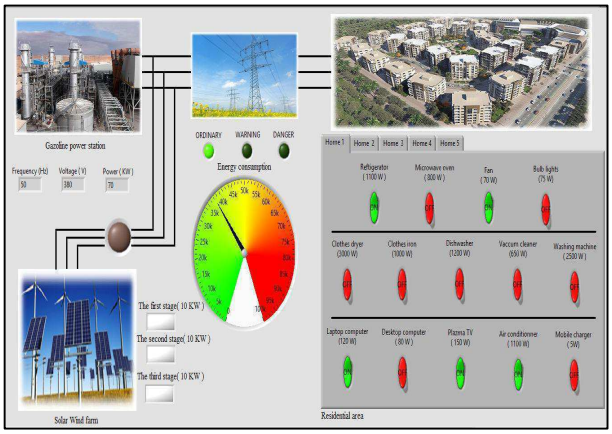


Fig. 5 the energy consumption is ordinary (Less than 40 kWh)

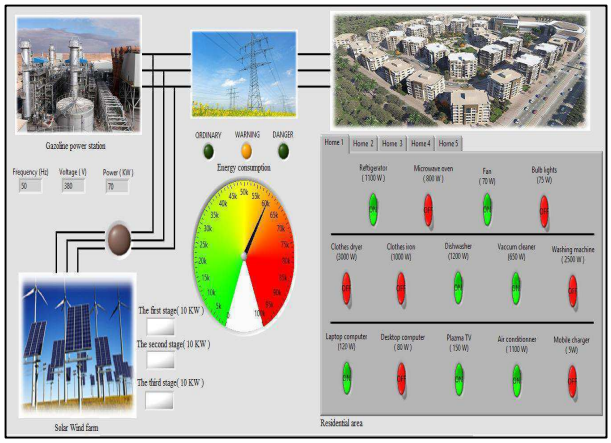


Fig . 6 the energy consumption is medium (between 40KWh and 65KWh)




ISSN 1737-9334

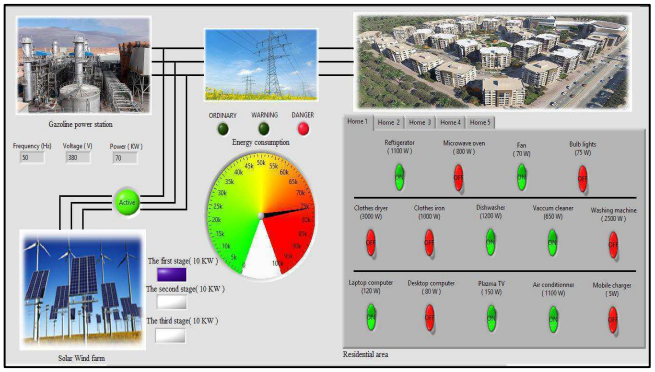


Fig. 7 the energy consumption is high (between 70KWh and 80KWh)

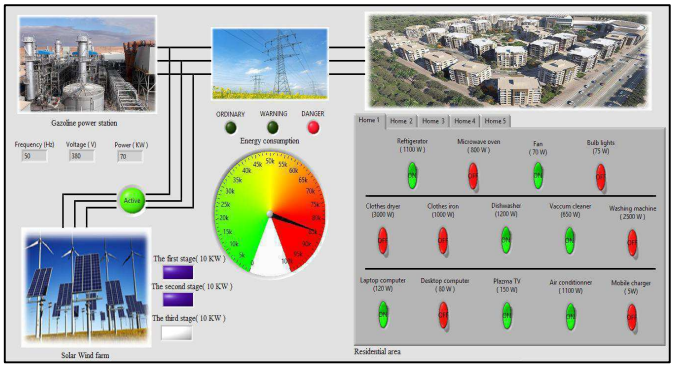


Fig. 8 the energy consumption is high (between 80KWh and 90 KWh)

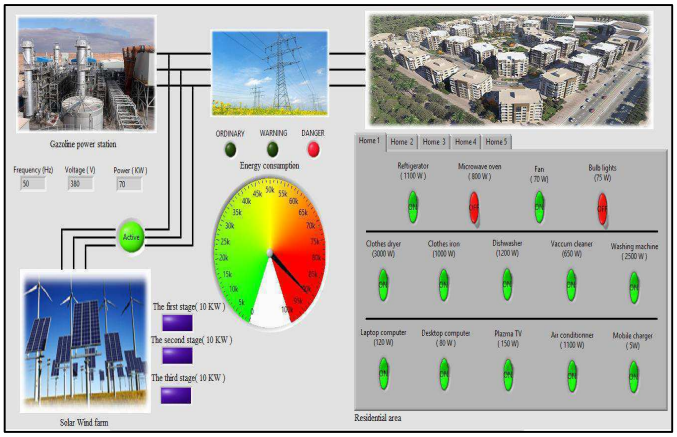


Fig. 9 he energy consumption is high (Greater than 90 KWh)

The following points may be mentioned about the testing results:

- In the displayed figures, the gageis represented the energy consumption of controlled five houses and the three LEDs (ORDINARY – WARNING – DANGER)will indicate the occurrence of thepower on the grid, which is coming from the Gasoline power station and compared with the houses energy consumptions.
- We suppose that the Gasoline power station has a frequency of 50Hz, a peak voltage of 380 V and peak power of 70 KW.
- When the energy consumption is exceeded the power coming from the Gasoline power station, the Solar wind farm stages will active automatically and immediately to compensate this reduction.
- By testing the behavior of the developed system under different conditions (increase of the energy demand), the Solar wind farm was able to recognize the appropriate incompletion.
- When the Solar wind farm stages active, the LEDs indicators has the ability of indicating the correct stage of operation in all cases.
- The Solar wind farm energy increases when the energy consumptions is higherthan the Gasoline power.

## V. CONCLUSIONS

In this paper, we have shown how renewable energies integrated to the grid can maintain the electric system in balance and how this integration is useful for both customers and utilities. We have divided our design of a hybrid system used solar and wind power energies in two parts: Homer software gave us the possible optimization and costing to our system and the second part which has been successfully developed based on LABVIEW software to test the demand response program.

By testing the behavior of the developed system under different conditions, the hybrid system has been able to satisfy the consumption. Finally, after the test, it can be noticed that the obtained results demonstrate the principle of integrating the renewable energies within the smart grid. Moreover, it can be concluded that this proposed scheme has the following advantages:

- Increasing the supply of renewable energy would allow us to replace carbon intensive energy sources andsignificantly reduce global warming emissions.
- In addition to jobs and economics benefits, the used of renewable energy make stable energy prices.

In the light of the results and observations obtained, one can make recommendations in a manner that deals with the promotion of the economics of renewable energies and appreciates their developmental role in rationalizing the context of economic growth, social stability and environmental balance.

## REFERENCES

[1] Recioui A, Bentarzi H, Chellali F, Stand-alone system optimization and assessment of wind energy potential of a remote area in Algeria, International Symposium on Environment Friendly Energies in Electrical Applications, 2-4 November 2010.
[2] Farouk Chellali, Adballah Khellaf , Adel Belouchrani , Abdelmadjid Recioui ,"A contribution in the actualization of wind map of Algeria", Elsevier, Renewable and Sustainable Energy Reviews 15 (2011) 993–1002
[3] Rusawasatt Lutato, Minimising Excess energy in Sizing of Hybrid Renewable Power Systems, SCIE Journals, 2012.
[4] Kashefi Kaviani, et al ,Soft Computing in Green and Renewable Energy Systems, Springer, 2009
[5] HOMER energy modeling software. National Renewable energy laboratory. Available from: http://en.openei.org/wiki/HOMER.




ISSN 1737-9334

[6] Pei Yi Lim, Power Management Strategies for Off-Grid Hybrid Power Systems, Doctor of Philosophy of Curtin University, October 2011.
[7] Mohammadi M, Hosseinian SH, Gharehpetian GB, GA-based optimal sizing of microgrid and DG units under pool and hybrid electricity markets. Int J Elect Power Energy Syst 2012;35(1):83e92.
[8] Hanieh Borhanazad a, Saad Mekhilef a, Velappa Gounder Ganapathy b, Mostafa Modiri-Delshad, Ali Mirtaheri, "Optimization of micro-grid system using MOPSO Renewable Energy", 71 (2014) 295e306
[9] Erdinc O, Uzunoglu M. Optimum design of hybrid renewable energy systems: overview of different approaches. Renew Sustain Energy Rev 2012;16(3): 1412e25.
[10] Luna-Rubio R, Trejo-Perea M, Vargas-V azquez D, Ríos-Moreno GJ. Optimal sizing of renewable hybrids energy systems: a review of methodologies. Sol Energy 2012;86(4) 1077e88.
[11] Bogdan, S. B. and Salameh, Z. M. Methodology for optimally sizing the combination of a battery bank and PV array in a wind/PV hybrid system. IEEE Transactions on Energy Conv. 11(2), 367-375, 1996
[12] Bin, A., Hongxing, Y., Shen, H., Xianbo, L, Computer aided design for PV/Wind hybrid system. Renewable Energy 28,1491-1512, 2003
[13]J. F. Manwell and J. G. McGowan, Lead acid battery storage model for hybrid energy systems, Solar Energy,(1993) Vol. 50, pp. 399–405.
[14] Said Diaf, Djamila Diaf, Mayouf Belhamel, Mourad Haddadi, Alain Louche, A methodology for optimal sizing of autonomous hybrid PV/wind system. Energy Policy, Elsevier, 2007, 35,pp.5708-5718.
[15] Kaabeche A, Belhamel M, Ibtiouen R. Techno-economic valuation and optimization of integrated photovoltaic/wind energy conversion system. Sol Energy 2011;85(10):2407e20.
[16] Deshmukh MK, Deshmukh SS. Modeling of hybrid renewable energy systems. Renew Sustain Energy Rev 2008;12(1):235e49.
[17] Clark W. Gellings, "Smart grid enabling energy efficiency and demand response", August 21, 2009 by CRC Press Reference - 250 Pages ISBN 9781439815748 - CAT# N1011.
[18] Johanne Mose Entwistle, Kurt Nielsen and Tseganesh Wubale Tamirat, Designing a Market Solution for Rapid Demand Response in Kenya, A report from the EURO star project UMEME 24/7.
[19]DEMAND RESPONSE for Small to Midsize Business Customers, Reference guide, 2010 CEATI International.



| Your Name | Title* | Affiliation | Research Field | Personal website |
|---|---|---|---|---|
| Fatma Zohra Dekhandji | Dr. | University of Boumerdes, Algeria | Power quality, machines | |
| Mouloud Bouaraki | Mr. | University of Boumerdes, Algeria | Renewable energies | |
| Nadhir Zaidi | Mr. | University of Boumerdes, Algeria | Master in Power engineering | |
| Abdelmadjid Recioui | Dr. | University of Boumerdes, Algeria | Telecommunications, optimization, smart grids | |






ISSN 1737-9334

# Experimental Study of Inverter Open-Circuit Fault Diagnosis using Stator Current Spectrogram

Bilal Djamal Eddine CHERIF[#1], Azeddine BENDIABDELLAH[#2], Mokhtar BENDJEBBAR[#3]

[#]*Diagnostic Group, Laboratory LDEE, Electrical Engineering Faculty, University of Sciences and Technology of Oran BP 1505 El-Mnaouer Oran 31000, Algeria*

[1]bilal.cherif@univ-usto.dz

[2]bendiazz@yahoo.fr

[3]bendjebb_dz@yahoo.fr

*Abstract*— **Three-phase static converters with voltage structure are widely used in many industrial systems. In order to prevent the propagation of the fault to other components of the system and ensure continuity of service in the event of a failure of the converter, efficient and rapid methods of detection and localization must be implemented. This paper work addresses a diagnostic technique based on the time-frequency representation called Short Time Fourier Transform or Spectrogram (STFT), for the detection of an inverter IGBT open-circuit switch fault. To illustrate the merits of the technique and validate the results, experimental tests are conducted using a built three-phase voltage inverter fed induction motor.**

***Keywords***— **Inverter, diagnostic, detection, open-circuit, STFT, spectrum**

## I. Introduction

Three-phase static converters voltage structures are widely used in many power applications. Continuity of service of these systems and their safety, reliability and performance are of major concerns today. Indeed, the failure of the inverter can lead to loss of control of the phase currents resulting in serious system malfunction or even a complete stop. To prevent the spread of the fault to other system components and ensure continuity of service in all circumstances, upon failure of the inverter, the converter topologies fault tolerant associated with effective and rapid methods of detection and localization failure must be implemented.

Several researchers have carried out their investigation in relation to the field of detection and localization of faults in static converters and more particularly those related to three phase power inverters [1]. The treated fault is mainly concerned with the open-circuit fault of an inverter IGBT switch [2]. Most published papers are based on Park's current vectors approach [3]. This approach is based on the trajectory tracking of the phase current vector. In fact, for the case of a healthy state condition of the inverter, the trajectory of these current vectors in the (d-q) frame is a circle. It was found that the circle becomes a semicircle under an open-circuit IGBT switch fault in one of the legs of the inverter. The position of this semicircle in the (d-q) frame makes it possible to identify the faulty IGBT switch [4]. Another paper used the mean value of the phase currents in Park's frame for the extraction of the open-circuit fault angle of each IGBT switch [3], [4], unfortunately this method presents an inconvenient as it depends on the load. To overcome the problem some authors suggested the normalized DC current method which is fundamentally based on the dc component of the current and the first order harmonic coefficients of the ac-currents [5]. Some detection techniques mentioned above are briefly discussed in reference [6], [7].To overcome this constraint, it is necessary to use a time-frequency representation. Indeed, the Gabor works in the 40s have led to the foundations of a new type of analysis called Short Time Fourier Transform (STFT) or spectrogram. He was the first to imagine a local Fourier transform based on a windowing signal analysis to observe changes in frequency with time. This transformation requires the division of the signal in consecutive short segments and then calculates the Fourier transform of each segment. The idea is to introduce the local frequency parameter so that the Fourier transform is applied to the signal through a sliding window on which the signal is approximately stationary. This method represents the results into three dimensions; the description of the signal is carried out in the time-frequency plan composed of spectral characteristics as a function of time [8].

This paper presents an approach using the technique based on the spectral analysis (STFT) to investigate the detection of the harmonic characterizing the IGBT switch open-circuit fault and localization. This approach addresses the STFT technique to extract the information related to the harmonic characterizing the open-circuit IGBT switch and presents the various experimental results and their interpretations.

## II. Voltage Source Inverter Structure

Fig 1 shows the structure of a three-phase two-level voltage source inverter feeding an induction motor.

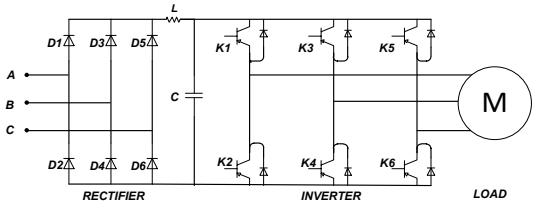


Fig. 1. Structure of a three-phase two-level inverter




ISSN 1737-9334

Experimental tests are conducted to study the effect of the inverter open-circuit faults on the induction motor behavior. The experimental test-rig used, includes a three-phase induction squirrel-cage motor fed by a three-phase two-level voltage source inverter. The detailed characteristics of the motor are given in the appendix. Furthermore, the motor is mechanically coupled to a dc generator supplying resistors, which allows varying the load torque. In addition, the measuring system includes three current Hall Effect sensors and three voltage sensors and a DSPACE 1104 acquisition card to generate pulses for triggering the *IGBTs* gates. The whole set is connected to a computer for visualizing the processed sensed signal as shown in the photo of Fig. 2.The acquisition time is taken as $T_{acq} = 5s$ and the sampling frequency $F_e = 1500Hz$.


Fig.2. Photo of the experimental test-rig

At this stage, it should be noted that all the experimental results which are obtained and presented in this paper work are carried out using the test-rig below built by the 'Diagnostic Group' at the LDEE laboratory University of Sciences and Technology of Oran (USTO-MB).

The following Fig. 3 depicts the phase current waveforms of the induction motor for both a healthy state and an *IGBT* open-circuit faulty inverter.

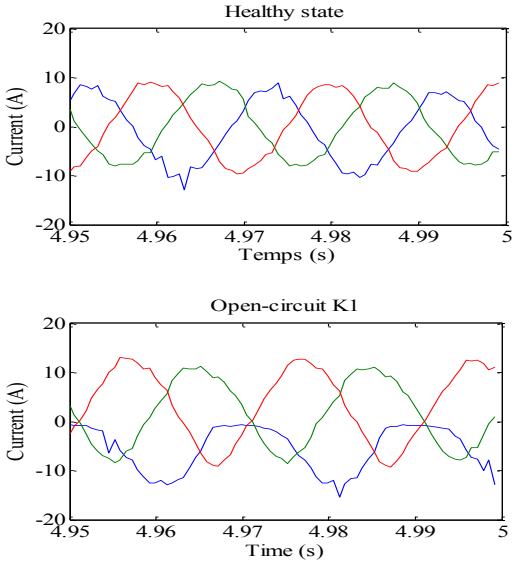


Fig.3 Currents waveforms of an induction motor for healthy case and open-circuit switch at $K_1$

Induction motor is controlled in speed. Following an IGBT open-circuit fault $K_1$ of the inverter leg, the phase current connected to this leg can no longer be controlled as it can only be negative or zero. The sum of the currents of the other two healthy phases is zero which may make it impossible to start the motor.

## III. TIME FREQUENCY ANALYSIS

The Fourier transform is expressed by the following equation:

$$FT_X(f) = \int_{-\infty}^{\infty} x(t)e^{-j2\pi ft}dt \quad (1)$$

We define the power spectral density or PSD as the square modulus of the Fourier transform, which is thus independent of the signal phase. Therefore, any information on the frequency changes with time variation is lost in the PSD. The time-frequency distribution, known as Short Time Fourier Transform or STFT is defined by:

$$STFT_X(t,f) = \int_{-\infty}^{+\infty} x(\tau)h(\tau - t)e^{-j2\pi f\tau}d\tau \quad (2)$$

$$STFT_X(t,f) = \int X(\theta + f)H(\theta)e^{-j2\pi\theta t}d\theta_R \quad (3)$$

The second expression of the STFT xi s obtained from the classical properties of the FT: conservation of the scalar product, shift properties and transformation of a normal product into a convolution one.

The STFT is constituted by the FT of $x(\tau)h(\tau - t)$ obtained by weighting $x(\tau)$ by the window $h(\tau - t)$ which is a short time analysis window localized around t and that shifts by varying the parameter *t*. Join to $h(\tau)$, the family of functions depending on two parameters *t* and *f*, defined by [8]:

$$h_{t,f}(\tau) = h(\tau - t)e^{j2\pi f\tau} \quad , \ (t,f)\epsilon\Re^2 \quad (4)$$

The numbers $STFT_X(t,f)$ are commonly called projections of $x(\tau)$ on the function's system $h_{t,f}$. If $h$ is the rectangle window of T support, the STFT consists in taking the FT of a sequence of signals equal to x on the support and zero elsewhere. We begin by the discrete-time signal $[x_n = x(nT)]$, $T>0$. Let $h_n = h(nT)$ and $N$ is the number of samples in the analysis window. Finally, a discretisation of the frequency variable $f$ is introduced. The STFT is then defined by the entire numbers $X_{k,n}$ calculated as follows [8]:

$$X_{k,n} = \sum_{\ell}^{N-1} x_{\ell+k}h_\ell e^{-j2\pi\ell T\frac{n}{N}}, \ k \in n = 1,2,\ldots. \quad (5)$$

As for the FT, the zero-padding technique allows the improvement of the frequency resolution. The principle of this method is to complete by M zeros a set of *N* samples so that M+ N is a power of 2 and thereafter can perform calculations using the Fast FT algorithm using the N + M points. When M= N, the method use the Discrete FT


ISSN 1737-9334

algorithms that are being made to calculate 2N points from the spectrum, from only N points of the signal.

### *A. Heisenberg-gabor uncertainty principle*

The uncertainty principle, also called time-frequency inequality is based on the uncertainty relationships established by Werner Heisenberg in quantum mechanics. The analogy with the work of Heisenberg for the Fourier transform was made by Dennis Gabor in 1946. Let us consider the finite energy signal $x(t)$ centered in time and frequency around zero. Gabor defines the duration $\Delta t$ and the spectral band $\Delta f$ as follows:

$$\Delta t = \frac{1}{E_x} \int_{-\infty}^{+\infty} |x(t)|^2 dt \quad (6)$$

$$\Delta f = \frac{1}{E_x} \int_{-\infty}^{+\infty} f^2 |X(f)|^2 df \quad (7)$$

Where $Ex$ is the energy of the signal given by the Parceval relationship:

$$E_x = \int_{-\infty}^{+\infty} |x(t)|^2 dt = \int_{-\infty}^{+\infty} |X(f)|^2 df \quad (8)$$

Therefore, the time-frequency inequality is defined by [9]:

$$\Delta t . \Delta f \geq \frac{1}{4\pi} \quad (9)$$

It expresses the fact that the duration-band product of a signal is lower bounded for a $\Delta t$ duration and a $\Delta f$ spectral band. In other words, the greater the accuracy in frequency localization is, the lower the accuracy in time localization and vice versa. The spectrogram is subject to the uncertainty principle due to the use of Fourier transform. This issue requires the search for the right time-frequency compromise suitable to the case considered in determining the correct window width. Gaussian window has the best time-frequency localization. Indeed, it verifies the following equality [10]:

$$\Delta t . \Delta f = \frac{1}{4\pi} \quad (10)$$

Finally, the choice of the window is important because it represents another compromise (comparable to the time-frequency compromise) between the main lobe width and the amplitude of the sideband in the frequency domain.

### *B. Experimental results and discussion*

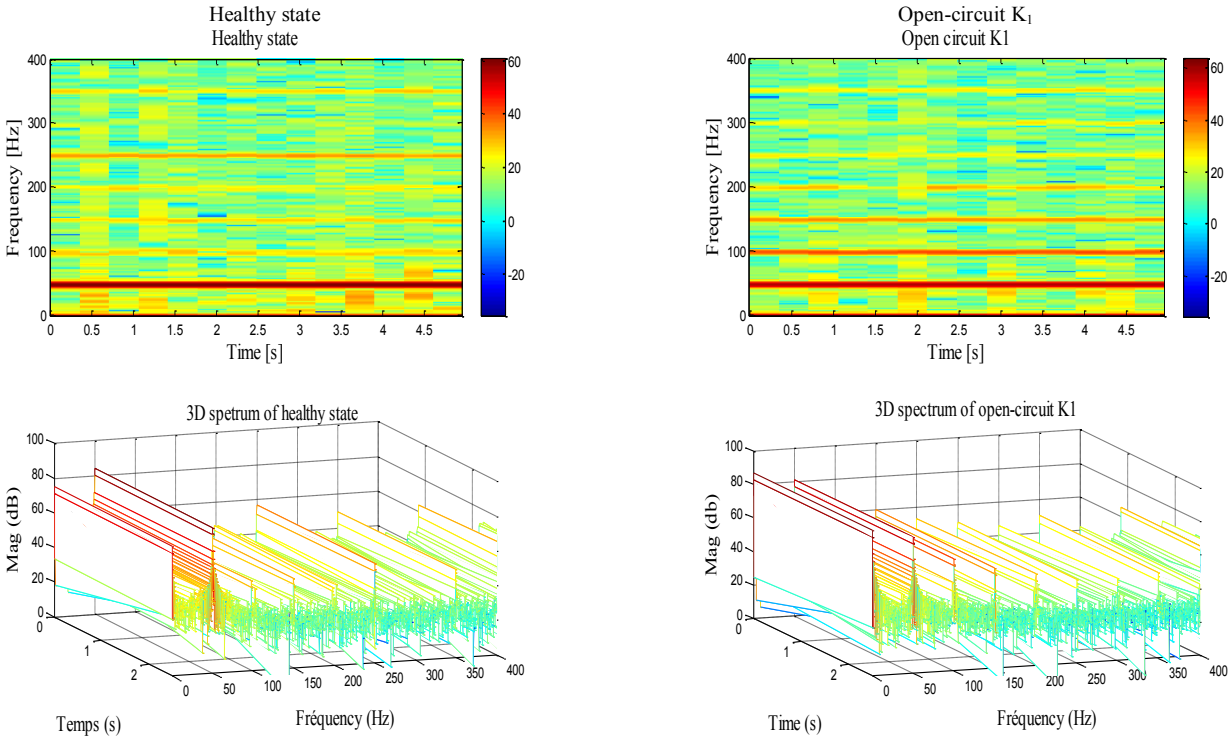


Fig.4 Spectrogram of stator current case healthy state and case open-circuit fault




ISSN 1737-9334

By comparing the spectrogram of the stator current $i_{as}$ of the healthy state and faulty case open-circuit IGBT, it is noted the presence of a red band at the level frequency *0Hz* and *100Hz*.

In the presence of an open-circuit switch fault at $K_1$, the experimental result in Fig. 4 depicts in addition to the fundamental harmonic, a DC component for each phase. It can be noted that the dc component in the faulty phase A is *h* lower than the fundamental harmonic but it is higher compared to the two other DC components in phases B and C. One can also notice that the two healthy phases *B* and *C* have the same dc component value.

Open circuit fault detection based on the presence of the harmonic *100Hz*:

$$f_{o-c} = 2f_s \tag{11}$$

The following Table I, summarizes the calculation of the various fault angles related to the various corresponding faulty switches. The fault angle computation is obtained based on the following equation:

$$\varphi_{h0} = \arccos\left(\frac{h_0}{h_{50}}\right) \tag{12}$$

TABLE I
OPEN-CIRCUIT FAULT CHARACTERISTICS OF THE INVERTER

| | The zero-order harmonic of the three phases | | |
|---|---|---|---|
| Faults Types | Phase A | Phase B | Phase C |
| Healthy case | $\|h_0\|=\varepsilon_{h0}$ | $\|h_0\|=\varepsilon_{h0}$ | $\|h_0\|=\varepsilon_{h0}$ |
| Open-circuit $K_1$ | $\varepsilon_{h0}<\|h_0\|<\|h_{50}\|$ $\varphi_{h0}=270°$ | $\varepsilon_{h0}<\|h_0\|<\|h_{50}\|$ $\varphi_{h0}=90°$ | $\varepsilon_{h0}<\|h_0\|<\|h_{50}\|$ $\varphi_{h0}=90°$ |
| Open-circuit $K_2$ | $\varepsilon_{h0}<\|h_0\|<\|h_{50}\|$ $\varphi_{h0}=90°$ | $\varepsilon_{h0}<\|h_0\|<\|h_{50}\|$ $\varphi_{h0}=270°$ | $\varepsilon_{h0}<\|h_0\|<\|h_{50}\|$ $\varphi_{h0}=270°$ |
| Open-circuit $K_3$ | $\varepsilon_{h0}<\|h_0\|<\|h_{50}\|$ $\varphi_{h0}=90°$ | $\varepsilon_{h0}<\|h_0\|<\|h_{50}\|$ $\varphi_{h0}=270°$ | $\varepsilon_{h0}<\|h_0\|<\|h_{50}\|$ $\varphi_{h0}=90°$ |
| Open-circuit $K_4$ | $\varepsilon_{h0}<\|h_0\|<\|h_{50}\|$ $\varphi_{h0}=270°$ | $\varepsilon_{h0}<\|h_0\|<\|h_{50}\|$ $\varphi_{h0}=90°$ | $\varepsilon_{h0}<\|h_0\|<\|h_{50}\|$ $\varphi_{h0}=270°$ |
| Open-circuit $K_5$ | $\varepsilon_{h0}<\|h_0\|<\|h_{50}\|$ $\varphi_{h0}=90°$ | $\varepsilon_{h0}<\|h_0\|<\|h_{50}\|$ $\varphi_{h0}=90°$ | $\varepsilon_{h0}<\|h_0\|<\|h_{50}\|$ $\varphi_{h0}=270°$ |
| Open-circuit $K_6$ | $\varepsilon_{h0}<\|h_0\|<\|h_{50}\|$ $\varphi_{h0}=270°$ | $\varepsilon_{h0}<\|h_0\|<\|h_{50}\|$ $\varphi_{h0}=270°$ | $\varepsilon_{h0}<\|h_0\|<\|h_{50}\|$ $\varphi_{h0}=90°$ |

The analysis of the first tow harmonics shows that the difference between the healthy state and the case of open-circuit fault state lies at the zero-order harmonics which means the presence of the DC component in the signal. The argument of zero harmonic relative to the fundamental enables us to know the type of fault. On the other hand, the argument of this harmonic enables us also to know the faulty switch either the upper one or the lower one.

From the result of Table I below, we note that the phase which contains the open-circuit fault has its dc component equals to the sum of the dc component of the two other phases and is expressed by the following relations as:

- If the fault is at *phase A*, then: $h_{0A}=h_{0B}+h_{0C}$
- If the fault is at *phase B*, then: $h_{0B}=h_{0A}+h_{0C}$
- If the fault is at *phase C*, then: $h_{0C}=h_{0A}+h_{0B}$

Where $h_{0A}$ is the zero-order harmonic of phase A, $h_{0B}$ the zero-order harmonic of phase B and $h_{0C}$the zero-order harmonic of phase C. From the three above relations, we conclude that: one can detect if there is an open-circuit fault or not in the inverter and from this detection, one can localize which is the faulty switch.

## IV. CONCLUSIONS

In this paper, first, the inverter IGBT switch open-circuit fault impact on the induction motor is presented. Thereafter, a technique is presented and discussed in order to detect and localize voltage inverter switch faults. The proposed technique uses the stator current spectrum analysis of the short time Fourier transforms (STFT). To illustrate the merits of the proposed technique and validate the results, experimental tests are conducted using a built three-phase voltage inverter fed induction motor.

## APPENDIX

| | |
|---|---|
| Rated Power | 3 KW |
| Supply frequency | 50 Hz |
| Rated voltage | 380 V |
| Rated current | 7A |
| Rotor speed | 1440 rev/min |
| Number of rotor bars | 28 |
| Number of stator slots | 36 |
| Power factor | 0.83 |
| Number of pair of poles | 2 |

## REFERENCES

[1] R.Rao.Errabelli, P.Mutschler, "*Fault Tolerant Voltage Source Inverter for Permanent Magnet Drives*", 2011 IEEE.

[2] T. Orlowska-Kowalska, P. Sobanski,"*Simple sensorless diagnosis method for open-switch faults in SVM-VSI-fed induction motor drive*", in: IEEE 39th Ann. Conf. of Ind. Electron. Soc., 2013, pp. 8210–8215.

[3] Won-Sang Im, Jang-Sik Kim, Jang-Mok Kim†, Dong-Choon Lee, and Kyo-Beum Lee, "*Diagnosis Methods for IGBT Open Switch Fault Applied to 3-Phase AC/DC PWM Converter*", Journal of Power Electronics, Vol, 12, No. 1, January 2012.




ISSN 1737-9334

[4] I. Jlassi, S. Khojet, E. Khil, "*A MRAS-Luenberger observer based fault tolerant control of PMSM drive*", J. Electr, Syst, 10 (1) ,2014, pp: 48–62.

[5] W. Zhang, D. Xu, P.N. Enjeti, H. Li, J.T. Hawke, H.S."*Krishnamoorthy, Survey on fault tolerant techniques for power electronic converters*", IEEE Trans. Power Electron. 29, 2014, 6319–6331.

[6] T. Orlowska-Kowalskaand P. Sobanski. *"Simple diagnostic technique of a single IGBT open-circuit faults for a SVM-VSI vector controlled induction motor drive*", bulletin of the polish academy of sciences technical sciences, vol. 63, no. 1, 2015doi: 10.1515/bpasts-2015-0032.

[7] Bilal Djamal Eddine Cherif, Azeddine Bendiabdellah, Mohamed Amine Khelif, *"Detection of Open-Circuit Fault in a Three-Phase Voltage Inverter Fed Induction Motor "*, International Review of Automatic Control (I.RE.A.CO.), Vol. 9, n. 6.(2016).pp.374-382.

[8] A. F. Aimer, A. H. Boudinar, N. Benouzza and A. Bendiabdellah, "*Simulation and experimental study of induction motor broken rotor bars fault diagnosis using stator current spectrogram*," 2015 3rd International Conference on Control, Engineering & Information Technology (CEIT), Tlemcen, 2015, pp. 1-7.doi: 10.1109/CEIT.2015.7233037.

[9] P. Flandrin, Time-Frequency, Hermes Science. 1998

[10] T. Ameid, A. Menacer, H. Talhaoui, and I. Harzelli, "*Broken rotor bar fault diagnosis using fast Fourier transform applied to field-oriented control induction machine: simulation and experimental study*," Int. J. Adv. Manuf. Technol., vol. 92, no. 1–4, pp. 917–928, Sep. 2017.




ISSN 1737-9334

# Spectrum Analysis and Statistical Parameters Based Two Stage Support Vector Machine for Fault Severity Diagnosis of Roller Bearing

T. Thelaidjia, S. Chenikher, A. Moussaoui

***Abstract*—bearings are frequently applied components in the vast majority of rotating machines. The breakdown of one of their constitutive parts can stop processes and cause losses in terms of time and money. In this paper a two stage Support Vector Machine (SVM) approach is proposed for severity fault diagnosis in bearing , The method consists of two stages. Firstly, Frequency domain featues from the demodulated signal followed by support vector machine (SVM) is performed to detect different faults. At the second stage, statistical parameters are used as un input of four SVMs to classify faults severity for each class. To improve the classification accuracy for bearing fault prediction, Particle Swarm Optimisation (PSO) is employed to simultaneously optimize the SVMs parameter's. the proposed condition monitoring scheme is verified and demonstrated by the testing results.**

***Index Terms*—Condition monitoring; Fault Diagnosis; Machine learning; Particle Swarm Optimisation; Roller Bearing; Rotating machines; Spectral analysis; Statistical parameters; Support Vector Machine; Vibration measurement.**

## I. INTRODUCTION

In the context of the diagnosis of electrical systems, rotating machines occupy a predominant place. Statistical studies have shown that failures due to bearings are paramount regardless of the machines power range. Hence, the necessity of their monitoring and diagnosis in order to increase the service quality [1], [2]. Therefore, many important researches had been done in the advanced field of bearing fault diagnosis [1], [3], [4]. Using the vibration signals of rolling bearings and components to monitor and diagnose their working state, is the common used method in the study of bearing fault diagnosis [1], [5]. The key step of pattern classification and recognition is feature extraction from the vibration signal.

Frequency and Time-domain features are simple and effective features without heavy computations which especially are suitable for condition monitoring systems [6], [7], [8].

Several applications used the wavelet analysis as a powerful filtering tools [1], [5], [9], the discrete version , still called multiresolution analysis consists to double filtering the signal by a filter bank called wavelet. It allows a clear visualization of each part of the signal with a resolution adapted to its scale [10].

Support Vector Machine is a relatively new computational supervised learning method which was introduced by Vapnik. It uses structural risk minimization (SRM) principle to minimize an upper bound on the expected risk whereas in ANN, The error is minimized using empirical risk minimization (ERM) [11], [5]. They have been shown better generalization performance than artificial neural network (ANN), for this reason, the algorithms used for SVM started emerging with greater availability of computing power [12], [13] [14], [15]. The results give the evidence that the technique is not only quite satisfying from a theoretical point of view, but also can lead to high performance in practical applications [16], [17].

Parameter optimization is the key to perform SVM. At present, the widely used methods of parameter optimization for SVM are network search method, K-order cross-validation method, Leave-one-out method, etc. These algorithms have the disadvantage of huge amount of computation, and the calculated parameters are not always the best. In recent years, a series of intelligent bionic algorithms are proposed based on the biological behavior study in the natural, such as genetic algorithm (GA) and particle swarm optimization (PSO) [14], [18], [19].

PSO was proposed by Kennedy and Eberhart [20], [21]. And it is inspired by the social behavior of bird flocking, fish schooling and swarm theory, etc. The theoretical framework of PSO is very simple, and PSO possesses the properties of easy implementation and fast convergence [14], [22].

The proposed algorithm for automatic bearing condition classification has several steps. The first step is the digital processing of acquired data. Section 3 describes support vector machine.The PSO algorithm is discussed in section 4. The next section addresses the experimental setup . In section 6 the proposed methodology is discussed, The experimental results are presented in Section 7.

## II. FEATURE EXTRACTION

The fault diagnosis is essentially a problem of pattern recognition, of which, an important step is feature extraction. The step of feature extraction is shown as follows:

- Firstly, the original signal is estimated by frequency domain features.
- Secondly, seven statistical feature parameters are extracted.

### A. Frequency domain features

the frequency spectrum is extracted using the method proposed in [6], this approach consists on three steps:

This work was supported by Laboratory of Electrical Engineering, LABGET, Tebessa University, Algeria.

T. Thelaidjia is with Laboratory of Electrical Engineering, LABGET, Larbi Tebessi University, Tebessa, 12002, Algeria (bilel.toufik@yahoo.fr).

S. Chenikher is with with Laboratory of Electrical Engineering, LABGET, Larbi Tebessi University, Tebessa, 12002, Algeria (s.chenikher@mail.univ-tebessa.dz).

A. Moussaoui is with Department of Electrical Engineering, Guelma University, Guelma, Algeria .


ISSN 1737-9334

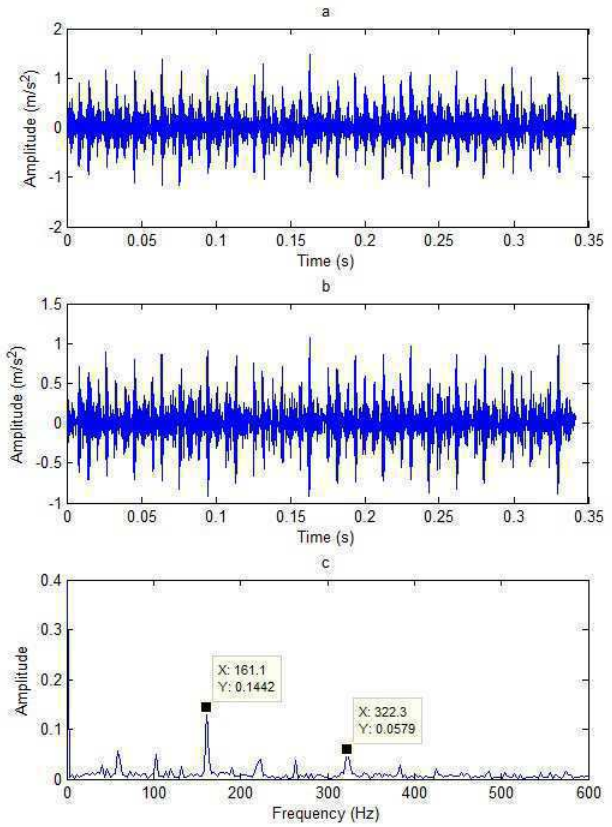


Fig. 1. **a** Measured signal, **b** Reconstructed signal and **c** Its envelope spectrum. Bearing with inner race defect.

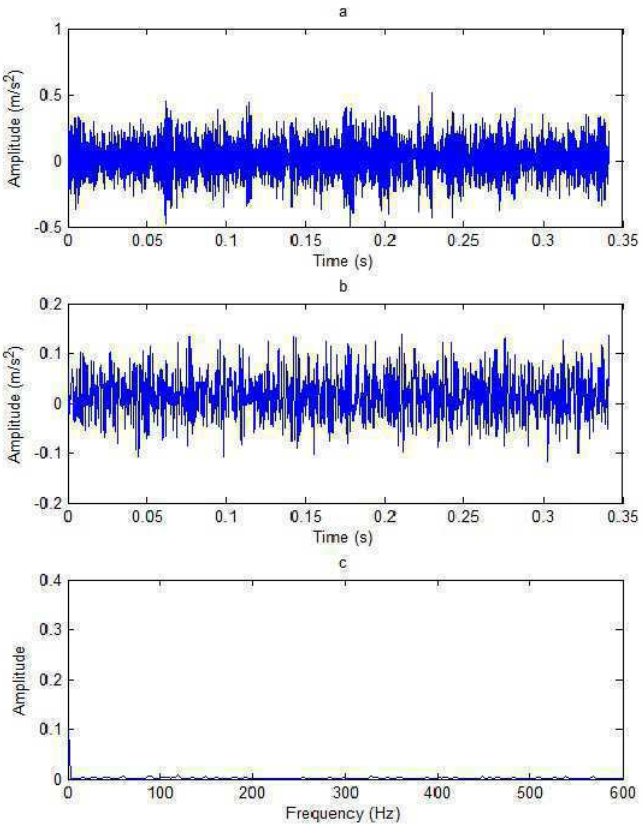


Fig. 2. **a** Measured signal, **b** Reconstructed signal and **c** Its envelope spectrum. Bearing with ball defect.

- **Step 1** Filtering the vibration signals using discrete wavelet transform.
- **Step 2** Extracting the envelope using Hilbert transform.
- **Step 3** Applied the Fourier transform to calculate the envelope spectrum.

After the obtaining of the frequency spectrum, it will be diveded into eight bands.
then we apply the energy at each band as an input variable for SVM classification. The Measured signals, their reconstructed signals and their envelope spectrums are presented in Fig.1, Fig.2, Fig.3 and Fig.4.

### *B. Features in the time domain*

To describe the vibration signal in the time domain, 4 statistical quantities were used: mean value, root mean square value, skewness and kurtosis.

1) The Mean:

$$M = mean(x) \tag{1}$$

2) The standard deviation :

$$SD = \sqrt{\frac{1}{N}\sum_{i=1}^{N}(x(i)-\overline{x})^2} \tag{2}$$

3) The impulse factor :

$$IMF = \frac{PV}{\frac{1}{N}\sum_{i=1}^{N}x(i)} \tag{3}$$

4) The kurtosis:

$$x_{kur} = \frac{\frac{1}{N}\sum_{i=1}^{N}(x(i)-\bar{x})^4}{\left[\frac{1}{N}\sum_{i=1}^{N}(x(i)-\bar{x})^2\right]^2} \tag{4}$$

## III. Support Vector Machine

The basic idea of SVM is to transform the input to a higher dimensional feature space.Then the SVM solves binary problem in which an hyperplane separate data.The hyperplane is defined through the use of support vectors [23].
Support vector machine (SVM) based on statical learning theory is proposed according to optimal hyperplane in the case of linear separable [1].
If all samples are correctly separated by an hyperplane, it must satisfy the following condition [4]:

$$y_k(\langle w;x\rangle - \lambda_0) \geq +1, \forall k \in \{1,...,n\} \tag{5}$$

The following function should be minimized In order to find the optimal hyperplane [4].

$$\varphi(w) = \frac{1}{2}\|w\|^2 \tag{6}$$

Saddles of Lagrange function give solution of the optimal problem as below:

$$L(w,\lambda_0,\alpha) = \frac{\|w\|^2}{2} - \sum_{k=1}^{n}\alpha_k\left[y_k(\langle w;x\rangle - \lambda_0) - 1\right] \tag{7}$$




ISSN 1737-9334

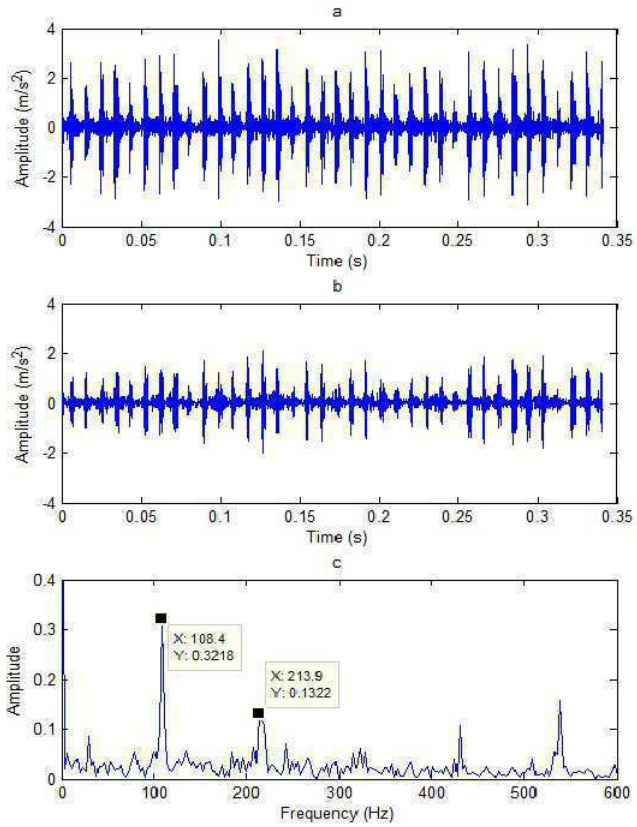


Fig. 3. **a** Measured signal, **b** Reconstructed signal and **c** Its envelope spectrum. Bearing with outer race defect.

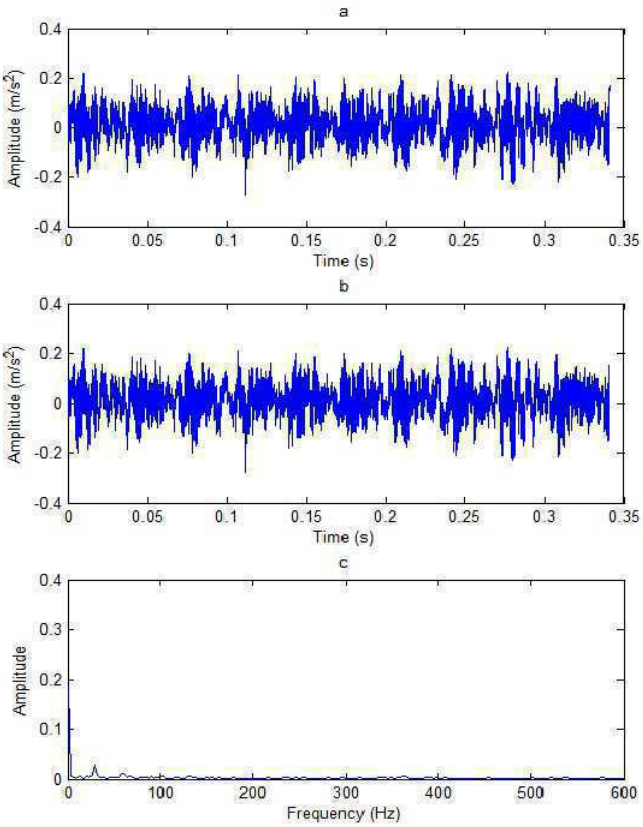


Fig. 4. **a** Measured signal, **b** Reconstructed signal and **c** Its envelope spectrum. Normal Bearing .

where $\alpha = (\alpha_1 ... \alpha_n)$ is the Lagrange coefficient;$\alpha_i \geq 0, \forall i$ The dual problem can be obtained as below :

$$\left\{ W(\alpha) = \sum_{k=1}^{n} \alpha_k - \frac{1}{2} \sum_{k,k'=1}^{n} \alpha_k \alpha_{k'} y_k y_{k'} \left\langle x_k ; x_{k'} \right\rangle , \right\} \tag{8}$$

subject to:

$$\sum_{k=1}^{n} \alpha_k y_k = 0 \text{ et } \alpha_k \geq 0.$$

If $\alpha^*$ is the optimal solution, then

$$\langle w^* ; x \rangle = \sum_{k=1}^{n} \alpha_k^* y_k \langle x_k ; x \rangle \tag{9}$$

According to the $Kuhn - Tucker$ condition, the solution must satisfy

$$\alpha_k^* \left[ y_k (\langle w^* ; x_k \rangle - \lambda_0^*) - 1 \right] = 0. \tag{10}$$

were $\lambda_0^*$ is given by

$$\lambda_0^* = \frac{1}{N_{sv}} \sum_{s=1}^{N_{sv}} (y_s - x_s^T w^*), s = 1 : N_{sv} \tag{11}$$

The decision function is given by:

$$D(x) = sgn \left[ \sum_{k \in S} \alpha_k^* y_k x_i^T x - \lambda_0^* \right] \tag{12}$$

soft-margin SVM solved The nonseparable problem [15], [17], [23].

If we used the inner $\kappa(x_k, x)$ to perform the transformation of original feature space into higher dimensional feature space, the dual problem can be formulated as below:

$$W(\alpha) = \sum_{k=1}^{n} \alpha_k - \frac{1}{2} \sum_{k,k'=1}^{n} \alpha_k \alpha_{k'} y_k y_{k'} \kappa(x_k, x_{k'})$$

subject to:
$\sum_{k=1}^{n} \alpha_k y_k = 0$ et $0 \leq \alpha_k \leq c$
The decision function is written as below:

$$D(x) = sgn \left[ \sum_{k \in S} \alpha_k^* y_k \kappa(x_i^T x) - \lambda_0^* \right] \tag{13}$$

here, $\kappa(x_k, x)$ is called kernel function.
Some kernel functions can be expressed as below [12], [23]:
**Polynomial:**

$$\kappa(x_1, x_2) = (1 + \langle x_1 ; x_2 \rangle)^q \tag{14}$$

where parameter q is the degree of the polynomial.
**Radial basis function (RBF):**

$$\kappa(x_1, x_2) = exp(- \left\| x_1 - x_2 \right\|^2 / 2\sigma^2) \tag{15}$$

where parameter $\sigma^2$ is the variance of the Gaussian function.
**Sigmoid:**

$$\kappa(x_1, x_2) = tanh(\alpha_0 \langle x_1 ; x_2 \rangle + \beta_0) \tag{16}$$

where $\alpha_0$ and $\beta_0$ are the parameters of kernel function.
Support Vector Machines are binary classifiers. However Most of cases in practical, usually more than two classes.




ISSN 1737-9334

In order to overcome this particularity of SVMs, different multiclass strategies have been proposed [12], [24], [25]. Three techniques affect The classification performance of SVM : the selecting of the kernel, the choosing of the kernel parameters, and the choosing of the regularization parameter c [4].
As presented in different works, the SVM generalization performance heavily depends on the right setting of "c" and "$\sigma$", these two parameters need to be set properly by the user.
According to the experience from numerical experiments [26], [27], c and $\sigma$ exhibit a (strong) interaction. As a consequence, they should be optimized simultaneously, rather than separately.

## IV. The Particle Swarm Optimization

The particle swarm optimization (PSO) consists of a swarm of particles flying through the search space. Each particle is treated as a point in a D-dimensional space. The i-th particle is represented $Z_i = (Z_{i1}, Z_{i2}, ..., Z_{id}, ..., Z_{iD})$. The best previous position of any particle is recorded and represented as $P_i = (P_{i1}, P_{i2}, ..., P_{id}, ..., P_{iD})$. The index of the best particle among all the particles in the population is represented by the symbol G. The rate of the position change (velocity) for the i-th particle is represented as $V_i = (V_{i1}, V_{i2}, ..., V_{id}, ..., V_{iD})$. The updated velocity and position of the i-th particle at the k-th iteration are [18]:

$$V_{id}^k = \omega.V_{id}^{k-1} + c_1.r_1.(P_{id} - Z_{id}^{k-1}) + c_2.r_2.(P_{Gd} - Z_{id}^{k-1}) \quad (17)$$

$$Z_{id}^k = Z_{id}^{k-1} + V_{id}^k \quad (18)$$

Where $c_1$ and $c_2$ are constants knows as the cognitive and social acceleration coefficients, respectively, $\omega$ is the inertia weight, $r_1$ and $r_2$ are random numbers between 0 and 1.
The first part of (17) represents the previous velocity, which provides the necessary momentum for particles to fly across the search space. The second part is the "cognition" part, which represents the private thinking of the particle itself.. The third part is known as the "social" component, which represents the collaboration among the particles. In addition, the implementation of PSO also requires placing a limit on the particle velocity, and the limit, i.e. the maximum allowed velocity $V_{max}$, determines the searching granularity of space. The inertia weight $\omega$ plays the role of balancing the global search and local search, and it can be a positive constant or even a positive linear or nonlinear function of time.
The classification performance of SVM are affected by two techniques, the choosing of the kernel parameters, and the choosing of the regularization parameter c [5].
The proposed approaches for SVM parameter optimization with PSO, is as follows:
**Step 1**. *Particle initialization and PSO parameters setting*: Set the PSO parameters including: $c_1$, $c_2$, position of each particle, velocity of each particle, number of particles, number of iterations and velocity limitation .
**Step 2**. *Fitness evaluation*: Perform SVM on each particle in population and compute the prediction accuracy.
**Step 3**. Update the global and personal best ($P_i$ and $P_G$) according to the fitness evaluation results.
**Step 4**. *Particle manipulations*: Each particle moves to its next position using formula (17) and (18).

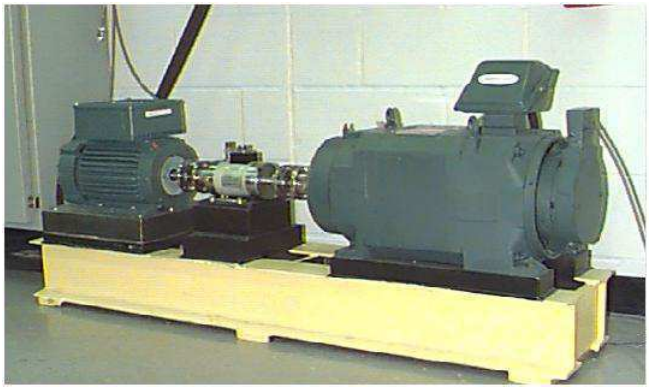

Fig. 5. The test apparatus of bearing

**Step 5**. *Stop condition checking*: If stopping criteria (maximum iterations predefined) are not met, go to **step 2**, otherwise, go to the next step.
**Step 6**. End the training and testing procedure and save optimal c , $\sigma$ for SVM.

In order to select the optimal values of the PSO parameters, a series of experiments had been carried out by varying the values of these parameters.

The swarm size is set to 20 particles. The searching ranges for c and $\sigma$ are as follows: $c \in [0, 10]$, and $\sigma \in [0, 10]$. Preliminary experiments also let this study set the personal and social learning factors (c1, c2) = (1.3, 1.3) that achieves better classification accuracy.
The inertia weight is set to the following equation:

$$\omega(k) = \omega_{max} - \frac{(\omega_{max} - \omega_{min})}{k_{max}}.k \quad (19)$$

where $\omega_{max}$ is the initial weight, $\omega_{min}$ is the final weight, $k_{max}$ is the maximum number of iterations or generation, and k is the current iteration number. The predefined maximum iteration is 10. When the maximum iteration is reached, the accuracy of test set is calculated by the predicted output of the trained SVM classifier.

## V. Experimental Setup and Vibration Data

The vibration data used in this paper have been obtained from the ball bearing test data set of the Western Reserve University Bearing Data Center Website [28]. As shown in Fig. 5, the test stand consists of a 2hp Reliance Electric motor (left), a torque transducer/encoder (center), a dynamometer (right), and control electronics (notshown) [29]. The data is sampled at a rate of 12 kHz, Each signal is 4096 samples long. Data was gathered for four different conditions: (i) inner race fault (IF) ; (ii) ball fault (BF); (iii) outer race fault (OF); (iv) normal (H) . Faults were introduced into the drive end bearing by using electro-discharge machining.

The bearing monitored is a deep groove ball bearing. it is a $6205 - 2RSJEM$ bearing with a FI, a BF and a FO frequency equal to 5.4152, 4.7135 and 3.5848 times the shaft frequency, respectively.
Theoretical estimations of the FI, BF and FO frequencies are presented at Table I.



ISSN 1737-9334

TABLE I
THEORETICAL ESTIMATIONS OF CHARACTERISTIC FAULT FREQUENCIES

| FI | BF | FO |
|---|---|---|
| 162.1852 | 141.1693 | 107.3647 |

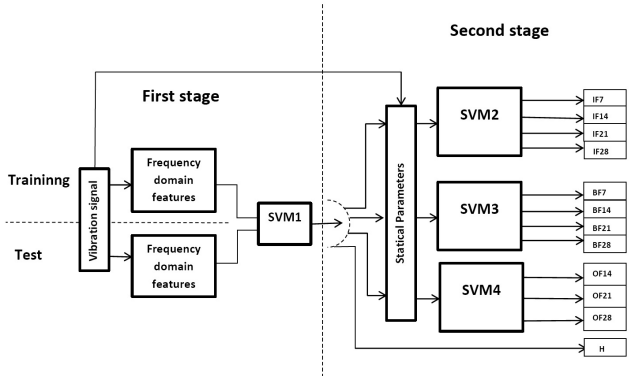


Fig. 6. Proposed diagnosis methodology scheme including feature Extraction and classification.

## VI. Classification strategy

The complete methodology is represented in Fig 6. A a two stage Support Vector Machine (SVM) approach is adapted. First, five Support Vector Machines are trained.The first SVM(SVM1) is trained in order to detect the type of fault (Normal (H), outer race (OF), inner race (OF) or ball fault (BF)). For this reason, the energie of the frequency spectum features are used. When the test signal represents a normal bearing condition, the classification process is over. Otherwise, the fault diagnosisis is transferred to the second stage, where SVM2, SVM3, SVM4 are used to identify the quality of fault one for each fault scenario.

The bearing fault conditions of data are shown in table II

TABLE II
THE DATABASE

| Bearing condition | Fault specifications | | class |
|---|---|---|---|
| | Diameter (inches) | Depth (inches) | |
| Healthy | - | - | H |
| Inner race fault | 0.007 | 0.0011 | IF7 |
| | 0.014 | 0.0011 | IF14 |
| | 0.021 | 0.0011 | IF21 |
| | 0.028 | 0.0011 | IF28 |
| Outer race fault | 0.014 | 0.0011 | OF14 |
| | 0.021 | 0.0011 | OF21 |
| | 0.028 | 0.0011 | OF28 |
| Ball fault | 0.007 | 0.0011 | BF7 |
| | 0.014 | 0.0011 | BF14 |
| | 0.021 | 0.0011 | BF21 |
| | 0.028 | 0.0011 | BF28 |

The leave-one-out ”LOO” validation technique is adapted to guarantee valid results for making predictions regarding new data.

## VII. Analysis of Experimentation Results

To identify the mechanical failure of roller bearing, the feature extraction procedure was performed using the proposed technique.
the the one-against-the-rest SVM classification method is used. Once the data dimension was reduced, The leaving-one-out method is applied by excluding a certain sample from the set of known patterns, and the classifier is designed without it; afterward, the classifier is tested precisely on this pattern. The procedure is repeated for all patterns from both classes.
Two remarks can be extracted:

- The input vector varies depending on the input signal. for healthy bearing kurtosis is around 3 this parameter is increased in the case of defect rolling.
- When the state information changes, the energy of spectral bands varies also.

Table III gives the classification result for this bearing fault classification problem.

TABLE III
CLASSIFICATION RESULT OF BEARING FAULT IN VALIDATION AND TEST

| Classifier | Optimal ”c” | Optimal ”$\sigma$” | Validation Rate | Test Rate |
|---|---|---|---|---|
| SVM1 | 33.97 | 0.004 | 100 | 100 |
| SVM2 | 1.056 | 3.838 | 100 | 100 |
| SVM3 | 5.007 | 3.642 | 100 | 100 |
| SVM4 | 1.524 | 5.075 | 100 | 100 |

## VIII. Conclusion

The present paper introduced a new automated diagnosis method for different types of rolling bearing faults. It should be noted that, this scheme is applied here not only to distinguish between ball, inner and outer faults, but also for faults severity detection.
The proposed strategy applied two stage Support Vector Machine(SVM) approach for the automatic diagnosis of defective rolling element bearings condition. For feature extraction, Frequency domain features are used in the first stage, whereas, statistical parameters are utilized in the second stage. Particle Swarm Optimisation (PSO) is employed to simultaneously optimize the SVM kernel function parameter and the penalty parameter.
PSO optimization requires only simple mathematical operators. This algorithm is simple to implement and effective, and is inexpensive in terms of memory and time required.
the good results obtained highlight the effectiveness of the proposed method for bearing fault diagnosis.

## References

[1] T.Thelaidjia, A. Moussaoui and S.Chenikher, “Feature extraction and optimized support vector machine for severity fault diagnosis in ball bearing,” *Engineering Solid Mechanics*, vol. 4, no. 4, pp. 167–176, 2016.
[2] Z. Chen, S. Deng, X. Chen, C. Li, R.V. Sanchez and H. Qin , “Deep neural networks-based rolling bearing fault diagnosis,” *Microelectronics Reliability*, vol. 75, no. 14, pp. 327–333, 2017.
[3] Z. Tong, W. Li, B. Zhang and M. Zhang , “Bearing fault diagnosis based on domain adaptation using transferable features under different working conditions,” *Shock and Vibration*, 2018.
[4] D. Dyer and M. Stewart, “Detection of rolling element bearing damage by statistical vibration analysis,” pp. 229–235, 1978.
[5] G. Xian, “Mechanical failure classification for spherical roller bearing of hydraulic injection moulding machine using dwt-svm,” *ELSEVIER*, August 2010.
[6] D. Dyer and M. Stewart, “Detection of rolling element bearing damage by statistical vibration analysis,” pp. 229–235, 1978.
[7] A. Boulenger and C. Pachaud, “Diagnostic vibratoire en maintenance prventive,” *Dunod, Paris*, p. 1998.




ISSN 1737-9334

[8] R. S. C. Pachaud and C. Fray, "Crest factor and kurtosis contributions to identify defects inducing periodical impulsive forces," *Mech Syst Signal Process*, vol. 11(6), pp. 903–916, 1997.
[9] A. B. Patil , J. A. Gaikwad , J. V. Kulkarni, "Bearing fault diagnosis using discrete wavelet transform and artificial neural network," *IEEE International Conference on Applied and Theoretical Computing and Communication Technology*, 2016.
[10] C. Pachaud, R. Salvetas, C. Fray, "Crest factor and kurtosis contributions to identify defects inducing periodical impulsive forces," *Mech Syst Signal Process*, vol. 11(6), pp. 903–916, 1997.
[11] L. Shuang and L. Meng, "Bearing fault diagnosis based on pca and svm," *IEEE International Conference on Mechatronics and Automation*, August 2007.
[12] V. N. Vapnik, *The Nature of Statistical Learning Theory*. Springer-Verlag, 1995.
[13] ——, *Statistical Learning Theory*. Springer, 1998.
[14] X. Yun-Jie and X. Shu-Dong, "A new and effective method of bearing fault diagnosis using wavelet packet transform combined with support vector machine," *Journal of computers*, vol. 6, no. 11, November 2011.
[15] S. Mallat, "A theory for multiresolution signal decomposition: The wavelet representation," *IEEE Transactions on Pattern Analysis and Machine Intelligence*, vol. 11(7), pp. 674–693, August 1989.
[16] P. K. Kankar, C. S. Satish and S. P. Harsha, "Fault diagnosis of ball bearings using machine learning methods," *ELSEVIER*, 2011.
[17] J. Christopher and C. Burges, "A tutorial on support vector machines for pattern recognition," *Kluwer Academic Publishers, Bell Lab, Lucent Technologies, Boston*, pp. 1–43, 1998.
[18] R. Yuan and B. Guangchen, "Determination of optimal svm parameters by using ga/pso," *Journal of computer*, vol. 5, no. 8, August 2010.
[19] S. ZHANG, F. KUANG, Y. WANG and L. WANG , "A novel svm model with pso on power transformer fault diagnosis," *Journal of Computational Information Systems*, vol. 8, no. 14, 2012.
[20] J. Kennedy and R. C. Eberhart, "Particle swarm optimization," *Proceedings of International Conference on Neural Networks, IEEE*, pp. 1942–1948, 1995.
[21] J Kennedy, R C Eberhart and Y.Shi, "Swarm intelligence," *Morgan Kaufmann Publishers Inc*, 2001.
[22] J. LI, "A combination of pso and svm for road icing forecast," *Journal op computers*, vol. 5, no. 9, p. 2010, September.
[23] L. Wang, *Support Vector Machines: Theory and Applications*. Springer-Verlag Berlin Heidelberg, 2005.
[24] M. XiaoXiao and H. XiYue, "2ptmc classification algorithm based on support vector machines and its application to fault diagnosis," *Control and Decision*, vol. 18(3), pp. 272–276, 2003.
[25] J. Weston and C. Watkins, "Multi-class support vector machines," *European Symposium on Artificial Neural Networks*, pp. 219–224, April 1999.
[26] X. F. Yuan and Y. N. Wang, "Parameter selection of svm for function approximation based on chaos optimization," *Journal of Systems Engineering and Electronics*, vol. 19, pp. 191–197, 2008.
[27] B. Ustun, W. J. Melssen , M. Oudenhuijzen and L. M. C. Buydens, "Determination of optimal support vector regression parameters by genetic algorithms and simplex optimization," *Analytica Chimica Acta*, vol. 54, pp. 292–305, 2005.
[28] K. A. Loparo, "Bearings vibration data set.case western reserve university," */http://www.eecs.case.edu/laboratory/bearing/download.htm*, consulted on september 2012.
[29] http://csegroups.case.edu/bearingdatacenter/pages/apparatus-procedures .




ISSN 1737-9334

# Advantages of Introducing Blended Learning to Libyan University Students

Sumaya Elageli
English Language Department,
University of Tripoli
College of Education
Tripoli - Libya
sumaya.ageli@gmail.com

***Abstract*—** Blended learning is a notion describing a method of teaching where there is a combination of a lecture hall or classroom setting and an online component during an academic course. The amount of the online component used depends on the requirement and aim of the course as well as the students' flexibility when using the online aspect. This paper sheds light on the benefits of applying blended learning methods to Libyan university students and how it can impact their learning strategies in the future. The pilot study carried out in this paper, examines the credibility of the expressed advantages to both, teachers and students while using what was described by Bonk & Graham (2006) as a "course-level" blending method.

***Keywords*—** blended learning, benefits, components, university students, education.

## I. INTRODUCTION

A noticeable trend among Libyan teachers is their divergence from the traditional 'teacher centered' setting to a more relaxed and friendly 'student centered' environment. The positive effects of this transition on the students' outcomes is evident in these classrooms as students are encouraged to take an active part and increase their interaction with their colleagues, and thus, experimenting more with the language in the presence of a teacher in the form of a facilitator. However, the question that arises at this time is how can we as teachers empower students to take 'full control' of their learning.

## II. USING BLENDED LEARNING WITH LIBYAN UNIVERSITY STUDENTS

The majority of Libyan university students are capable of using the internet for educational purposes, whether it be to complete an assignment or to clarify a vague concept addressed in the classroom. Nevertheless, their reliance on the presence of a teacher to comment on their performance or the credibility of a piece of information they had run across, remains necessary.

Taking on our roll as facilitators, we need to guide the students to take more responsibility towards their learning. We need to train them to use the internet to research the questions they are asking us, while at the same time, teach them to analyze and evaluate the information they come across. This could be accomplished through "blended learning".

### A. *What is 'blended learning'?*

Blended learning as Bonk & Graham (2006) explain is a "delivery mechanism" that combines the traditional face-to-face classroom setting with a modern digital online component.

On the other hand, in E-learning, there is no face-to-face classroom setting with direct contact between teachers and students but rather a complete online synchronous or asynchronous interaction between both parts. On a wider context, we can also identify online learning where the internet is the key component. Pop (2017) describes online learning as the learning experience where technological elements and online tools are used to aid the learning process. Thus, within this perspective, online learning is used as an umbrella term for both e-learning and blended learning.

Thompson (2016) identifies 6 models of blended learning on the basis of the extent of the online component. These are identified as: face-to-face driver model, rotation model, the flex model, online lab school model, self-blended model, and the online driver model.

The face-to-face driver and rotation models incorporate the least amount of online usage. These two models can be used as a starting point for the introduction of blended learning with Libyan university students. In the face-to-face driver model[1], the teacher or lectures will rely on the in-class component while uploading activities and tasks in support of the topics discussed. The rotation model[2], alternates between an in-classroom input and online instruction to support the course activities through a fixed schedule (Gragg, n.d).

### B. *Benefits of 'blended learning'*

1- Blended learning will encourage a greater amount of independent study and offers the students the opportunity to research subjects.

[1] Known as "Activity-level Blending" by (Bonk & Graham , 2006)
[2] Known as "Course-level Blending" by (Bonk & Graham , 2006)




ISSN 1737-9334

2- Because blended learning allows for increased independent study, teachers are able to focus their contact hours on individuals in need of extra attention and guidance, to enable them to match the pace of their peers.
3- It increases students' successes in future learning situations. Blended learning gives the learner the confidence to participate in future online, distance, and e-learning situations to develop themselves as learners and future professionals. Their previous experience with blended learning would allow them to take control of their learning experiences, carry out research and analyze the information thoroughly, and crucially, they would be able to manage their time efficiently and effectively.
4- There will be a diminished need for classroom presence. Given the security situation in Libya, and judging from personal experience in the past few years; reaching the university campus is sometimes not possible. The presence of the digital component in the blended learning offers the opportunity to compensate for absences.
5- An additional related advantage is the fact that, due to the imposed travel restrictions, the opportunity for inviting visiting professors and opportunities for enhanced global learning has been largely missing in Libya. Blended learning generally and e-learning in particular compensates for this in a very effective manner and offers both learners and teachers the opportunity to experience enhanced multi-cultural education. Here faculties and departments can arrange joint online programs and learning sessions and they are also able to participate in online courses, webinars and workshops.

## III. METHODOLOGY

This study targeted two groups of thirty to thirty-five male and female Libyan university students aged between 18 and 21. Their language proficiency ranges from an elementary to an intermediate level. They are part of a 'Phonetics 1' course which deals with the distinction, classification and production of consonant and vowel sounds. It also deals with the phonemic transcription of individual word and connected speech. The course is a minimum of twenty-eight hours per semester (two hours per week, fourteen weeks per semester).

### *A. Strategy*

The two groups were subject to the same content, environment and teaching hours. The first group (G1) took the traditional face-to-face lecture hall setting with an occasional assignment to be discussed the following week. The second group (G2) were subjected to 'blended learning'. A 'social study group' was created on 'Facebook' functioning as the online component. Choosing 'Facebook' as a tool to carry out this study instead of 'Google Classroom' or 'Canvas', will ease the students' tension as they are already familiar and comfortable using this application.

In order to meet the aims of this case study and ensure the validity of the outcomes, (Long 2005, p. 9), different strategies were adopted for (G2).

- The face-to-face driver model stage: In this stage, face-to-face lectures were held during fixed hours for the first couple of weeks. Extra support of the lectures was given to the study group in the form of practice activities, audios for sound recognition, and assignments.
- The rotation model stage: This stage was divided into two parts:
  - The first part dealt with the theoretical part of the subject; students were left with specific unanswered questions at the end of the face-to-face lectures, guiders were given to them online, to aid their research of the questions.
  - The second part adopted a 'flipped teaching' technique. The lecture content was delivered a few days before the face-to-face classes online through a 'live feed' where students had the chance to interact with the lecturer, ask and respond to questions. Then during the lecture hours, practice activities and tasks were given to eliminate any remaining confusion concerning the topic in question.

### *B. Results*

Blended learning proved beneficial to both teachers and students.

#### *1) Curriculum coverage*

The outline of the course description (appendix 1) set by the English Language Department contained a mixture of theoretical aspects and a practical side which targeted students' ability to recognized and differentiate between sounds. With G1, the lecturer was only able to cover around two thirds of the assigned topics. While with G2, all topics were covered with a remaining 4 hours, which were dedicated to additional support of the practical side.

#### *2) Compensating lectures*

National holidays and bad weather conditions have decreased the number of contact hours for (G1) and thus, they have been disadvantaged. However, blended and flipped learning methods compensated for the missed lectures in the case of (G2) students.

#### *3) Learner autonomy*

The use of blended learning with G2 encouraged students to increase their independent study hours and set them on the path of autonomous learning. Students were inquiring about the transcription and the difference between sounds in words they came across while studying independently. Others were inquiring about the existence and classification of sounds from their mother tongue.



ISSN 1737-9334

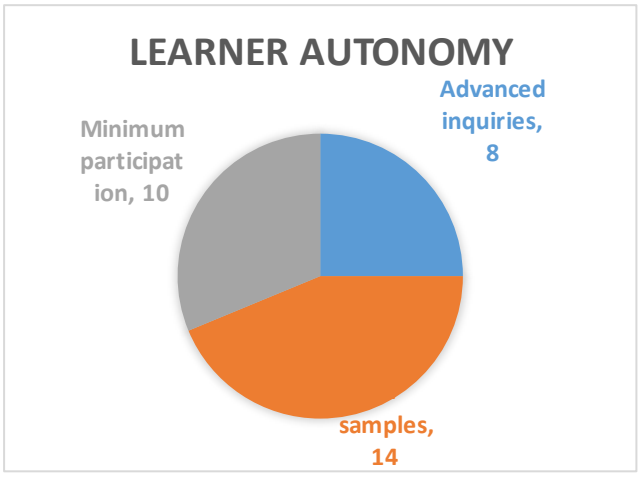


fig.1 'Learner Autonomy'

*4) Extra Support for individuals*

During the contact hours of the practice lessons, students who were in need of extra attention were provided aid from their peers who had a stronger grasp of the subject. This allowed the weaker individuals to be frank in their inquiries and challenged the stronger students to respond.

*5) Praticipation in webinars*

Students from both groups were given a link to participate in an IATEFL webinar titled "Hands on activities to internalize phonetic symbols". Five students from G1 expressed their interest and only 2 actually registered. On the other hand, G2 a good number showed enthusiasm and ten students completed their registration. Furthermore, these students made an effort to acquaint themselves with the subject in preparation of the session.

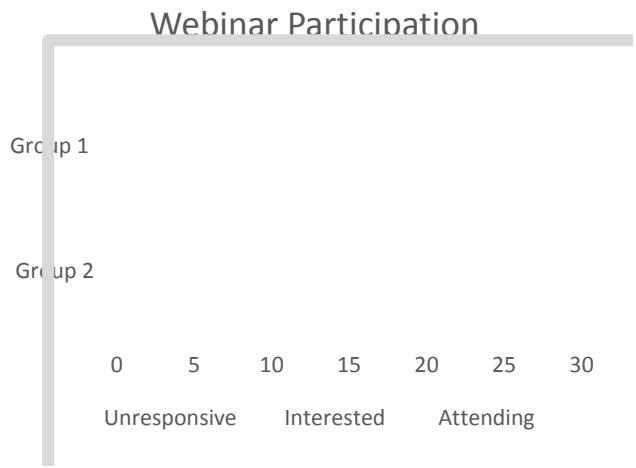


Fig.2 'Webinar Participation'

Nevertheless, a few issues were present while applying blended learning.

The knowledge that most of the material covered in classes and practice activities was provided online, caused some students not to attend the face-to-face meetings. This put them at a disadvantage, as the course was not designed to be fully online. Also, their minimum online activeness did very little to motivate learner autonomy and therefore, they struggled and suffered many misinterpretations of the material and committed a few fossilized errors.

Weak internet connections also impeded the participants on more than one occasion. They were unable to access 'live feed' sessions and sometimes even simple videos. These participants preferred the online component of blended learning to be restricted to the 'face-to-face driver model'.

## IV. Conclusion

Subjecting Libyan university students to blended learning provided them with the preliminary experience and insights on the use of basic technology in education, which hopefully one day they will be able to use with their own students, and hence integrate the use of technology in high school classrooms. Furthermore, applying the first two models of blended learning to Libyan university students, has widened the educational horizons of students and has provided them with unlimited learning opportunities. It will further enable us, as teachers, to train and help prepare students to participate in events that will introduce them to a wider global professional community thus enhance their career opportunities.

## V. References

[1] Bonk, C., & Graham, C. (2006). Handbook of Blended learning: Global Perspectives, Local Designs. San Francisco: CA: Pfeiffer Publishing.

[2] Gragg, M. (n.d). What is Blended learning? Definition and Models. Retrieved from Study.com: https://study.com/academy/lesson/what-is-blended-learning-definition-models.html

[3] Long, M. (2005). Second Language Needs Analysis. Cambridge: Cambridge University Press.

[4] Pop, A. (2017, Sep. 17). Study Portals Online Courses. Retrieved from Distance Learning Portal: https://www.distancelearningportal.com/articles/269/blended-learning-e-learning-and-online-learning-whats-important.html

[5] Thompson, J. (2016, Feb. 12). E-learning Industry. Retrieved from E-learning Industry: https://elearningindustry.com/6-blended-learning-models-blended-learning-successful-students

## VI. Appendix 1

### A. *'Phonetics 1' Course Discription*

Course Code: EL 130 Credits: 2 Hours: 2

Course Prerequisites: none




ISSN 1737-9334

**Course Description:**

After a short introduction to pronunciation problems, the course provides explanations on how the speech organs work. After that students are introduced to the basic sounds and the difference between letters and sounds. Then, the course deals with each sound separately. Learners are provided with both receptive and productive practice. Audio components include cassettes and audio CDs.

**Aims:** The course aims to:

1. Improve students' production of the spoken language.
2. Help students practice some dialogues
3. Direct students with particular pronunciation difficulties

**Course Contents:**

The course covers the following:

1**. Introduction**

The basic sounds
Letters and sounds

**2. What is phonetics?**

**3. What are the branches of phonetics?**

**4. The speech organs**

**5. The descriptions and classification of the English consonants**

Nasal vs. oral sounds
Voiced and voiceless sounds
Places of articulation
Bilabial
Labio-dental
Dental
Alveolar
Post-alveolar
Palato-alveolar
Palatal
Velar
Glottal
Manners of articulation
Friction consonants
Stop consonants
Nasal consonants
Lateral consonants
Gliding consonants

**6. The English vowels**

The descriptions and classification of the English vowels

a. Simple vowels
- Classification of monophthongs
- Position of Jaw
  - Position of tongue
  - Shape of the lips

b. Diphthongs
- The difference between monophthongs and diphthongs
- Forming diphthongs

**7. Word transcription**

**8. Connected speech.**

a. Weak forms
- What are weak forms?
- Weak forms and parts of speech

b. Linking
- Consonant-vowel links
- Linking using /j/, /w/, /r/

c. Elision

d. Assimilation

e. Transcription in connected speech.

**Assessment:**

| Class work + Oral work | First exam | Second exam | Final exam |
|---|---|---|---|
| 40 | | | 60 |

**Course Books:**

1. O'Connor. 1967. Better English Pronunciation. With 2 cassettes. Cambridge University Press.

2. Hancock. 2003. English Pronunciation in Use (Intermediate). Cambridge University Press.

3. Roach, Hartman & Setter (Ed). 2006. English Pronouncing Dictionary. Cambridge University Press.




ISSN 1737-9334

# E-commerce issues and verifying security protocols using AVISPA

1st DAASSA Asma
*Electronics and Microelectronics Laboratory*
*Faculty of Sciences Monastir*
*National Engineering School of Tunis,*
*University of Tunis El Manar*
Tunis, Tunisia
asma.daassa@gmail.com

2nd MACHHOUT Mohsen
*Electronics and Microelectronics*
*Laboratory Faculty of Sciences*
*University of Monastir*
Monastir, Tunisia
machhout@yahoo.fr

3rd AGUILI Taoufik
*SYSCOM Laboratory*
*Department of Information*
*and Communications Technology*
*National Engineering School of Tunis*
Tunis, Tunisia

***Abstract*—Nowadays, customers are still hesitant to make purchases online, because e-commerce suffer from many security issues. Therefore, hackers can have access to sensitive information by exploiting errors in security protocols.**
**Detecting vulnerabilities in e-commerce security protocol remains difficult, because we need to study in depth the protocol and acquire a deep knowledge of it. That is why we will focus on verifying and validating such security protocol especially e-Business Protocols like TLS, SET ...**
**This paper presents e-commerce security issues and the verification of security properties of electronic transaction protocol using AVISPA tool, and finally it highlights several open research problems.**

***Index Terms*—SSL/TLS, SET, security, e-commerce, attacks, AVISPA, mutation testing**

## I. Introduction

The security of e-commerce is necessary due to critical data exchanged during an electronic transaction like bank account management, personal information (credit card number, password...). Therefore, it is very indispensable to protect these assets from unauthorized access, use, alteration, or destruction. In order to ensure the integrity, confidentiality, non-repudiation, authenticity, privacy and availability of these electronic transactions, many security protocols have been developed like SSL/TLS and SET. On the one hand, these protocols need more rigorous and detailed verification than normal communication protocols before their deployment.
On the other hand, ensuring its rigorous analysis and validation is still an open issue. As a result, flaws and attacks are still growing giving the possibilities to hackers to exploit them to access critical data and information.
In order to avoid these attacks, many prevention techniques are being used. Among these techniques, we have the validation and verification of security protocols, which is based upon the abstract formal methods giving analytical rules to indicate if such protocol is secure, or not.
If non-mathematicians use the formal techniques, they will find technical difficulties, that's why they choose to use online validation tools like AVISPA, HERMES which are easy to use and produce outputs assuring if a given cryptographic protocol is secure or not.
This paper investigates the concept of the mutation technique to avoid vulnerabilities in the entire security system of e-commerce transactions.

### Contributions

The contributions of this paper can be summarized as follows:

- We present e-commerce and m-commerce security issues.
- As prevention techniques, we focus on the validation and verification of security protocols using automated tools like AVISPA
- In our case, we aim to test the existence of some attacks in SSL/TLS protocol such as the renegotiation vulnerability, replay attack, triple handshake.
- We discuss countermeasures and we highlight open problems.

### Paper organization

The remainder of the paper is organized as follows. Section 2 reviews related work, section 3 presents e-commerce and m-commerce security issues, section 4 discusses the validation of security protocols using AVISPA tool, security properties and verification assumptions, and finally, we conclude the paper in section 5.

## II. Related Work

Nowadays e-commerce becomes very important for the commercial world. It holds many advantages such as efficiency and convenience. Unfortunately, it has many disadvantages due to the openness of the internet world, especially the security issue of electronic transactions. That is why many articles study in depth the topic of e-commerce security. Thus, it is crucial to improve the security of electronic transactions and to deny the attacker to access highly important information including credit card numbers, personal details etc. Prior work looked at security protocols from the perspective of automated verification using tools such as Proverif [1] [17], Scyther [3] [18], AVISPA [2] [14] [15] [19] [20] [21]. In our previous work [4], we modified the HLPSL model and through AVISPA, we analyzed TLS handshake and we tried to compare results of four back-ends, we noticed from these results that SATMC and TA4SP were useless and OFMC and CLAtSe


ISSN 1737-9334

found attacks and also provided traces. We focused also on the verification of SSL/TLS protocol using the AVISPA tool for automated verification and analyzing security properties. In fact, dedicated modeling and verifying security protocol languages such as HLPSL (High-Level Protocol Specification Language) give researchers the opportunity to verify many security properties such as data secrecy and authentication. However, verifying security protocols is not enough to guarantee the existence of these security properties in the actual implementation of the protocol. That is why few studies [2] [5] [16] introduced a technique that appeared recently called mutation testing.However, the major causes of attacks are the misusing of cryptographic libraries, misunderstanding and misinterpreting of parameters, configurations and options. Therefore, if developers use these libraries incorrectly, they will make many mistakes in their individual applications causing many vulnerabilities and attacks. Mutation testing is very useful. In fact, it consists on injecting faults into models that aim at introducing leaks in the security protocols. These mutations can simulate errors caused by programmers. Then, by using AVISPA tool, we manage to analyze the mutant model to produce an attack trace or a counterexample violating a security property. This technique is useful to detect and prevent logical attacks.

## III. E-COMMERCE AND M-COMMERCE ISSUES

It is very important to identify e-commerce security issues, and to analyze different attacks and vulnerabilities within security protocols, to enhance the security of transactions and customers information. Both m-commerce and e-commerce are based on the same fundamental principles, and aim at making transactions on the internet using computers or laptops for the sake of the web world and using mobile devices for the sake of the mobile world. It has been noticed from a statistical survey research that it is necessary to analyze the security of mobile transactions as well as web transactions. The security of m-commerce is very important nowadays due to the big number of Smartphone users and several research studies noted that e-commerce sales via mobile is still increasing. Over time, it can be assumed that sales done through mobile devices are rapidly growing due to its features compared to e-commerce, such as mobility convenience, connectivity (3G, 4G, and WI-FI), and interactivity. [6] [7] However, m-commerce security is a serious problem and it is a challenge because the service durability is limited to features such as memory, battery storage . . . Therefore, to encourage customers making the purchase of goods and items, we have to improve the security of electronic transactions. That is why researchers study in depth different attacks and propose solutions to these problems. The security of m-commerce is very important especially nowadays over untrusted media (internet).To improve the security of electronic transactions, many protocols are developed. SSL/TLS is the most commonly used, though many dangerous attacks are still found. Many studies confirm that SSL implementations in android applications are actually more prone to vulnerabilities than browsers. Therefore, developers have to ameliorate SSL/TLS to eliminate these attacks and improve security. We choose to highlight the example of Heartbleed because it is the most dangerous attack and especially that it has many attack patterns. The main solution proposed is to update Openssl version, but it is not the best if we talk about Smartphone or tablets. To patch vulnerable server on Android device, we have to update the ROM's phone, and the update cycle is too long. Therefore, some old phones cannot be updated that is why they are still vulnerable. SSL vulnerabilities, especially Heartbleed, have impacts on embedded devices especially Smartphone if they contain a version of Openssl with Heartbleed bug and they have problems with software update. In addition, we can also detect the problem if the mobile browser exposes the vulnerability on the client side. Nowadays many attacks are discovered on SSL/TLS protocol: the logjam attack [**?**], the FREAK attack [**?**] etc. Through Heartbleed, hackers could steal many important information (credit card information, password . . .). As we see, in recent years many vulnerabilities in SSL/TLS have been revealed. So, the security of Smartphones became very exhausting due to its limited features. That is why; many studies analyze the security of mobile transactions and its limited features. [7] [8]

**Countermeasures**

There are several countermeasures to avoid Heartbleed vulnerability and provide security of data, applications and important information of mobile devices. One of the scenarios of attacks on Heartbleed is like MITM but more dangerous, because of a malicious server that exploits revoked certificates.

DNSSEC and OCSP (Online Certificate Status Protocol) are solutions to this problem. On android devices, we recommend the use of SSL certificate pinning, to, securely, exchange important information between server and android banking applications. In fact, users can install unsafe certificates; therefore, the device's trust store can be compromised. SSL pinning ignores these certificates and trusts certificates stored inside the applications. Another important countermeasure is the use of perfect forward secrecy PFS to secure old traffic [9] [10] , but nowadays it is not a good solution due to the discovery of the new attack called the Logjam Attack [**?**].

## IV. VERIFICATION AND VALIDATION

In this paper, we show how existing verification and formal specification tools are revealing very early vulnerabilities that will be difficult to correct at the implementation phase. First-of-all, there are many advantages using automated verification tools. Among these advantages, we can cite; first, using automated verification tools, through which we can find known vulnerabilities. It seems useless to waste time looking for these attacks if they are already known. There are two raisons to do this, to increase the confidence in the tool and to avoid the reappearance of old vulnerabilities. Second, attacks found automatically do not appear in their known form, and this leads us to think differently and to better assess the consequences of attacks. Finally, it is more important to find new vulnerabilities; this is the purpose of many researchers, in fact, automated tools can find unknown attacks and this helps




ISSN 1737-9334

to avoid them in an early phase. There are many techniques to prevent such cryptographic vulnerabilities. In this section, we focus on one of these techniques, which is formal verification of cryptographic protocols. Many mistakes arise when using cryptographic protocol for securing e-commerce transactions. Fuzzing techniques can be applied to the protocols and they can detect vulnerabilities in specific implementations. How to ensure that a new protocol is secure even before its implementations? Nowadays, in view of malicious activity, intrusion attempts and various attacks which computer network suffers from, the verification of security protocols became very important. That is why automated verification tools like AVISPA are effective and efficient ways to test the robustness of cryptographic protocols.

### *A. Verification assumptions*

In the context of modeling security protocols, it is necessary to model the intruder, also define its behavior and limit it. For this, the assumptions used are collected under the name of "Delev-Yao" [11]. This model is based on two assumptions, which are; cryptography is secure and the intruder is the network.
The first assumption is that the intruder cannot decrypt a message without the key; he cannot also guess a secret key or a nonce.
The second assumption is that the intruder has a full control over the internet; in fact, he knows all the public data of such protocols. He can read, store, and block every sent message, he can also compose and decompose messages and he can encrypt and decrypt if he has the key.

### *B. Security properties verification*

E-commerce has additional challenges, in fact, although the properties of secrecy and authentication are still basic, they are not the essential one that we are trying to prove.
Other properties need to be proved for the security of e-commerce transactions. However, Avispa is limited to only two security properties (the authentication goal and the secrecy goal). E-commerce security requires verifying payment properties such as non-replay, non-repudiation...
These properties require working on protocols abstractions that can be verified automatically using automated tools for building and analyzing security protocols.
We also notice another challenging aspect of e-commerce security protocols; these protocols do not include typically two agents or participants (more a server S) for assurance, but instead they include three agents (the buyer, the seller and the bank).
AVISPA tool is essentially used to prove the security properties. Some of these properties are verified as follows.

**Analyzing Attacks on Protocol**

Using AVISPA tool, we try to detect some attacks on the protocol such as Renegotiation attack, replay attack, triple handshake attack, etc.

- Renegotiation attack (CVE-2009-3555)
  The renegotiation attack is a serious flaw made by the renegotiation feature of TLS. It give the possibilities to attacker to inject data into a running connection deprived of destroying the session.
- Replay Attack
  Replay attack is to intercept a communication and send a message already sent in this communication. This can be used to send authentication information copied from those of past communication. SSL pare this attack through the MAC that contains the message sequence number and other parameters specific to the connection. So a forwarded message is detected as not in its place. Either bad sequence number, or bad connection number, etc. In addition, the MAC cannot be modified because it is hashed.

## V. Conclusion

In our paper, we have discussed the problem of validation and verification of e-commerce security protocols using AVISPA tools.
This verification is important to ensure the secrecy and authentication properties in these protocols; but this verification does not guarantee that the implementation of protocol fulfills these properties, also other security properties are difficult to be verified automatically.
As we have seen in this paper, AVISPA is able to verify only secrecy and authentication properties.
The models derived from the Dolev and Yao seem to be the most advanced in what concerns the expressiveness and automation, but they are still relatively abstract. There are still many improvements to add to Dolev-Yao model(Automation, management of various multi-session mode, extension to problems specific to e-commerce) Automatic generation of implementation of cryptographic protocols tested is still an open issue.

## References

[1] Blanchet, B. (2009). Automatic verification of correspondences for security protocols. Journal of Computer Security, 17(4), 363-434.
[2] Dadeau, F., Ham, P. C., & Kheddam, R. (2011, March). Mutation-based test generation from security protocols in HLPSL. In Software Testing, Verification and Validation (ICST), 2011 IEEE Fourth International Conference on (pp. 240-248). IEEE.
[3] The Scyther Tool : Verification, falsification, and analysis of security protocols
[4] Asma, Daassa, Machhout Mohsen, and Aguili Taoufik. "TLS PROTOCOL VERIFICATION FOR SECURING E-COMMERCE WEBSITES." Journal of Internet Banking and Commerce 22.2 (2017).
[5] Maatoug, Ghazi, Frdric Dadeau, and Michael Rusinowitch. "Model-based vulnerability testing of payment protocol implementations." HotSpot'14-2nd Workshop on Hot Issues in Security Principles and Trust, affiliated with ETAPS. 2014.
[6] Sharma, Archana, Vineet Kansal, and R. P. S. Tomar. "Location Based Services in M-Commerce: Customer Trust and Transaction Security Issues." International Journal of Computer Science and Security (IJCSS) 9.2 (2015): 11.
[7] Ngai, Eric WT, and Angappa Gunasekaran. "A review for mobile commerce research and applications." Decision support systems 43.1 (2007): 3-15.




ISSN 1737-9334

[8] Onwuzurike, Lucky, and Emiliano De Cristofaro. "Danger is my middle name: experimenting with SSL vulnerabilities in Android apps." Proceedings of the 8th ACM Conference on Security & Privacy in Wireless and Mobile Networks. ACM, 2015.
[9] pratik guha sarkar, Perfect Forward Security : An Extra Layer Of Security and Privacy, iSEC Partners, Inc 123 Mission Street, Suite 1020 San Francisco, CA 94105, 2014.
[10] Cremers, Cas, and Michele Feltz. One-round strongly secure key exchange with perfect forward secrecy and deniability. ETH Zurich, 2011.
[11] Dolev, Danny, and Andrew Yao. "On the security of public key protocols." IEEE Transactions on information theory 29.2 (83): 198-208.
[12] [AVISPA Team. "HLPSL tutorial the Beginner's guide to modelling and analysing internet security protocols." 2013-01-20]. http://www. avispa-project. org (2006).
[13] Team, T. A. "AVISPA v1. 1 User manual." Information Society Technologies Programme (June 2006), http://avispa-project. org (2006).
[14] Vishesh, Kinchit, and Amandeep Verma. "Formal verification of authenticated AODV protocol using AVISPA." International Journal of Computer Applications 50.19 (2012).
[15] Kasraoui, Mohamed, Adnane Cabani, and Houcine Chafouk. "Formal verification of wireless sensor key exchange protocol using AVISPA." Computer, consumer and control (IS3C), 2014 international symposium on. IEEE, 2014.
[16] Bchler, Matthias, Johan Oudinet, and Alexander Pretschner. "Security mutants for property-based testing." International Conference on Tests and Proofs. Springer, Berlin, Heidelberg, 2011
[17] Shinde, Amol H., and A. J. Umbarkar. "Analysis of Cryptographic Protocols AKI, ARPKI and OPT using ProVerif and AVISPA." International Journal of Computer Network and Information Security 8.3 (2016): 34.
[18] Yang, Huihui, Vladimir A. Oleshchuk, and Andreas Prinz. "Verifying Group Authentication Protocols by Scyther." JoWUA 7.2 (2016): 3-19.
[19] Kurkowski, Mirosaw, Adam Kozakiewicz, and Olga Siedlecka-Lamch. "Some Remarks on Security Protocols Verification Tools." Information Systems Architecture and Technology: Proceedings of 37th International Conference on Information Systems Architecture and TechnologyISAT 2016Part II. Springer, Cham, 2017.
[20] Henzl, Martin, and Petr Hanacek. "A Security Formal Verification Method for Protocols Using Cryptographic Contactless Smart Cards." Radioengineering 25.1 (2016): 132-139.
[21] Islam, Salekul. "Security analysis of LMAP using AVISPA." International journal of security and networks 9.1 (2014): 30-39.




ISSN 1737-9334

# *Performance Evaluation of the ECG Signal Filtering using Averaged Signal Approach*

Hend M. Farkash[1], Mona A. Elzuway[2] and Mohamed Farkash[3]

[1 , 2] College Of Electrical & Electronic Technology/ Benghazi Libya
[1]e mail hend.mf_ceet@ceet.edu.ly [2]e mail mona.elzuway@ceet.edu.ly
[3]Faculty of Medicine Benghazi University Benghazi Libya
Mohamed.farkash@gmx.de

***Abstract ---Electro Cardio Gram*(ECG)-is a heart signal that is used to monitor the health status of heart disease. There adding of such a signal requires an expert that extracts information about the patient omit. The expert taken to write a report about the case under investigation which require sometime ,a very valuable factor for some patients, this paper showing how raw ECG signal used to extract an average , then illustrate the which features of ECG can be extracted from signal average.**

***Index Terms—Electrocardiogram; ECG signal; Signal Filtering Evaluation of the ECG .***

## I. INTRODUCTION

In this work , the heart signal is studied, and a method of finding the average signal for each patient is developed . This average ECG signal carry the information about the condition of the patient . An algorithm is also developed to extract features from the average signal .

This ECGs data records included in the MIT-BIH Arrhythmia Database is a set of over 4000 long-term Holter recordings that were obtained by Harvard-MIT Division of Health Sciences and Technology in Biomedical Engineering Centre[1].

The database contains 48 records (numbered from 100 to 234 inclusive with some numbers missing). Each of the 48 records is slightly over 30 minutes long, The recordings were digitized at 360 samples per second per channel ,this records are the records of ECG taken directly from patient [1].

The heart signal is a periodical signal that repeated based on affixed period . MIT-BIH is a recorded of this repeated signal as series , it is supposing that the received heart signal has the form of MIT-BIH .It is needed to get the average signal from this series of signal . this averaged signal is the characteristics of the patient case and contains the information about him , these information can be extracted in different forms.

In this work to prepare data and extract average signal it was used designed algorithm , but Kania, Fereniec, and Maniewski[8] used cross_corelation method to get average signal.

## II. LITERATURE REVIEW

There are many research works, which deal with the subject of this paper, the first one, is done by von Wagner et al [9] where they present a complete simulation environment for testing ECG classification algorithms under Matlab with Simulink. There are other studies using Fast Wavelet Transform (FWT) for ECG signal processing such as Provazník, and et al [10],which apply the theory of wavelet transform on ECG signals and give promising results, similar to that done by Kania, Fereniec, and Maniewski[8], their aim of this study was to investigate the application of wavelet denoising in noise reduction of multichannel high resolution ECG signals.

## III. AVERAGE SIGNAL APPROACH

In order to get this work done the following steps need to be done in this order :

- Taking and preparing a sample signal.
- Determination of signal period length and average signal.
- Generalization the idea for different patients.
- Feature extraction from the averaged signal

### *A. Taking And Preparing A Sample Signal*

This process is required to cut the first 24000pointsofthepatient signal record and then process it to get the average signal, this process can be summarized in the following steps as shown in Fig. 1.

- Read the whole raw signal of the patient
- Determine length of the sample.
- Cut the required sample from raw signal.




ISSN 1737-9334

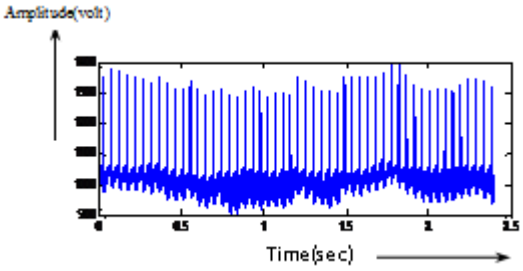


Fig .1 . graphical representation of sample of signal

### B. *Determination Of Signal Periodic Length And Average Signal*

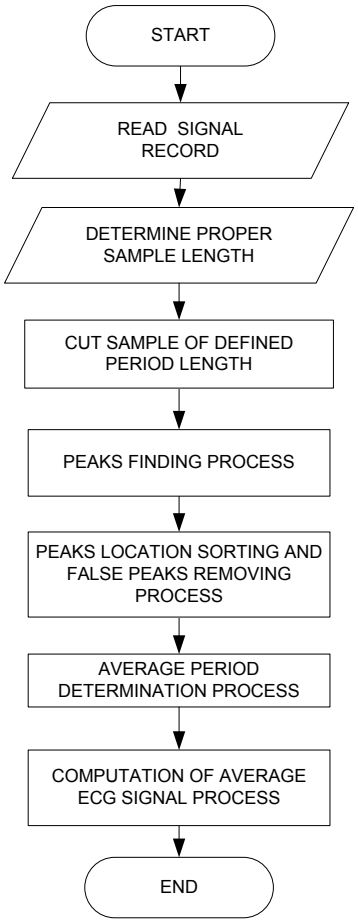


Fig.2. average signal algorithm

This step is collected as complete algorithm to process the sample signal which is shown in Fig .2.This algorithm is named as average signal, Which contain sub process which are:

1. Peaks finding process.
2. Peaks location sorting and false.
   Peaks removing process.
3. Average period determination process.
4. Computation of average ECG signal process.

### C. *Generalizing the idea for different patient*

The approach shown in previous section concerning with using only one recorded of the data collected from the considered source.

The program can be generalized to give the average signal of all recorded signal of different patient by putting the written algorithm program that find the average signal inside a loop as show sin Fig.3. This generalized algorithm works on all signals that represent different patient.

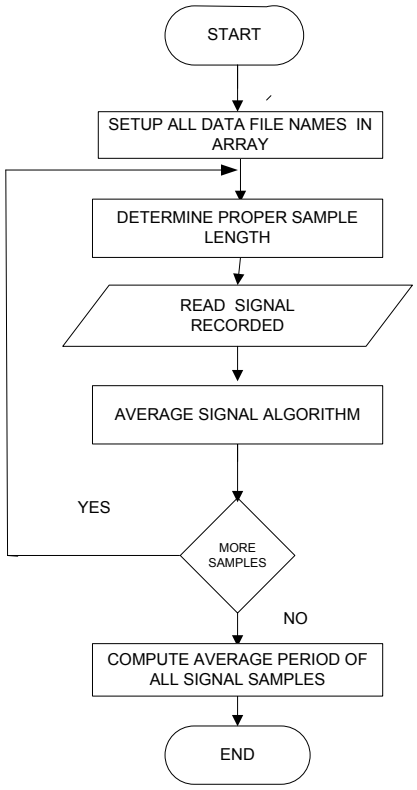


Fig.3. Generalizing the idea for Different patient


ISSN 1737-9334

*D. Feature extraction from the averaged signal*

After getting average of signal from raw data, these features must be extracted from it, these features are represent the parameters of ECG such as :QRS duration ,PR interval ,QT interval, T interval, P interval and others .

- *ECG structure and its components*

As explained before, the normal shape of ECG signal has the following waves and segments[2][3] ,which are shown inFig.4.

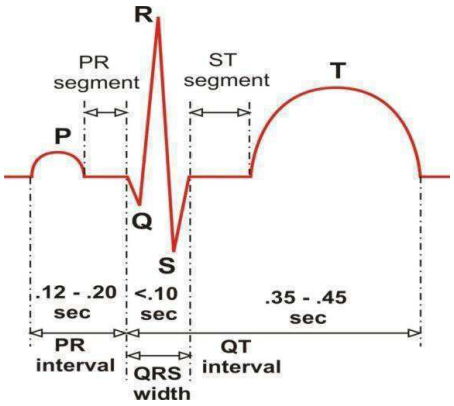


Fig.4.normal shape of ECG signal

- *ECG feature set*

One the average ECG is determined ,features needs to be extracted from it , these features are classified into[4][5].

*Interval features:*

ECG signal contain same of features related to heart beats intervals, which used in second data type ,it can be getting from average ECG signal, these interval are(see Fig.5):

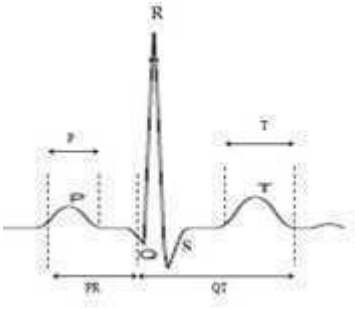

Fig.5.intervalfeatures

PR interval: average duration between onset of p and Q wave.

QT interval: average duration between on set off Q and T wave.

T interval :average duration of T wave.

P interval :average duration of p wave.

*Amplitude features*

This features relative to amplitude of R peak in QRS complex, which are computed by determine amplitude (height)of R peak and compared the difference between it and other waves, this appears same feature srelated to heart rate, similarly to interval feature it can be getting from average ECG signal as following(see Fig .6):

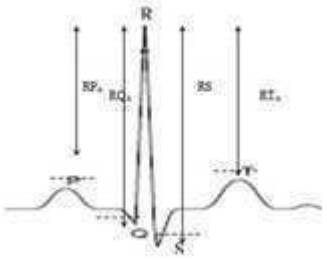

Fig.6.Amplitude features

RQ amplitude: difference amplitude between R wave and Q wave.
RS amplitude: difference amplitude between R wave and S wave.
RT amplitude: difference amplitude between R wave and T wave.
RP amplitude: difference amplitude between R wave and P wave.

*feature extraction* can be performed as a preprocessing step of the average of signal prior to work on [6].Where several methods can be used in the process of extracting appropriate feature by compute importance, for each feature , which provided as input to any supervised learning techniques such as data classification and Pattern Recognition [7] ,




ISSN 1737-9334

## IV. EXPERIMENTS RESULTS

This paper shows the results obtained in this work. MATLAB was used to program the principles of this work, Based on proposed method for computing the average signal from the raw data, this raw data is a train of heart signals that is taken from a single patient and is needed to compute characteristic features of heart signal .

A designed algorithm named average signal algorithm does this procedure, the obtained averaged signal has general features of ECG signal of the patient.

Figure 7 and 8 are represented one of train pulses of normal case and other of train pulses up normal case respectively with obtained average heart signal for different patient:

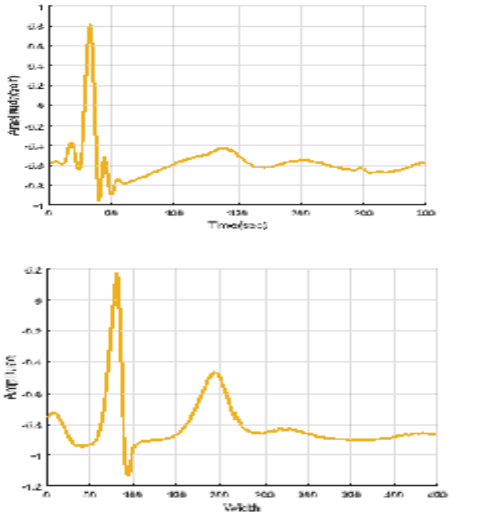

Fig.7 average signals of normal case

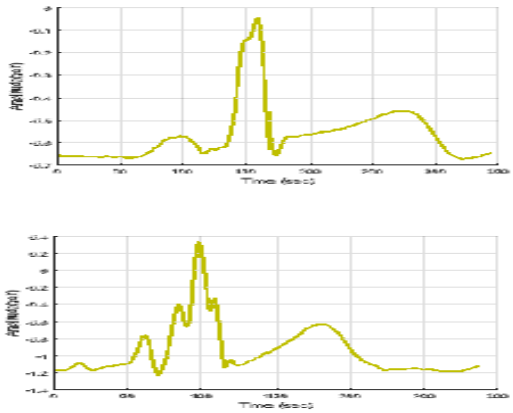

Fig.8 average signals of up normal case

## V. CONCLUSION

In this work , the ECG signal data were collected from data source , which gives a ECG signal that represent the ECG recorded of patient healthy people and Non- healthy people of different heart disease .

In this work, a method was developed to get the average pulse ECG signal of the patient which represent his/ her status and condition . A method were developed to process the signal to get features from the average ECG signal .

## REFERENCES

[1] "Physio : Research resource for Complex Physiologic Signals," http:// www.physionet.org/, Feb. 2018.

[2] A.L. Goldberger, *Clinical Electrocardiography: A Simplified Approach*, Mosby, 1999.

[3] O. polakovic, "Back propagation and his application in ECG classification," University of Ostrava, Institute for Research and Applications of Fuzzy Modeling journal of Electrical Engineering, 2005.

[4] N. Singh and P. Gupta, "ECG to individual identification," Proc. of IEEE 2nd International Conference on Biometrics: Theory, Applications and Systems. Washington DC, USA, IEEE, 2008, pp. 1-8.

[5] J. Hampton, The ECG made easy, USA: Elsevier's Health Sciences, 2003.

[6] A. Al- fahoum and A. Qasaimeh , "ECG Arrhythmia Classification Using Simple Reconstructed Phase Space Approach," Irbid Jorden, computer in cardiology, 2006, pp. 757-760.

[7] A. Babloyantz, V. Ivanov, and P. Zrelov, "New approach to ECG's features recognition involving neural network," Particles and Nuclei 14 Letters, vol. 2, 2001, pp. 41-47.

[8] M. Kania, M. Fereniec, and R. Maniewski, "Wavelet Denoising for Multi-lead High Resolution ECG Signals," Warsaw, Poland. Measurement Science Review, vol. 7, 2007.

[9] G. von Wagner, U. Kunzmann, J. Schöchlin, and A. Bolz, "Simulation methods for the online extraction of ECG parameters under Matlab/Simulink," BiomedizinischeTechnik. Biomedical Engineering, vol. 47 Suppl 1 Pt 2, 2002, pp. 534-537.

[10] I. Provaznik, J. Kozumplik, J. Bardonova, M. Novakova, and Z. Novakova, "Wavelet Transform In ECG Signal Processing," Brno, Czech Republic: Europ Conference Bios.




ISSN 1737-9334

ISSN 1737-9334

ISSN 1737-9334

# Internal Model Control of Fully-actuated Discrete Uncertain Systems

Mouna Mnejja[#1], Raoudha Ben Khaled[*2], Moncef Gasmi[#3]

*Computer Laboratory of industrial systems, INSAT, Carthage university*
*BP 676, 1080, Tunis, Tunisia*

[1]mouna.mnejja92@gmail.com

[2]ben_khaled_raoudha@yahoo.fr

[3]mcf.gsm@gmail.com

***Abstract*— An approach of Internal Model Control (IMC) of linear multivariable (MIMO) sampled Uncertain systems is proposed in this paper. The latter discusses the robustness of such sampled system with parametric uncertainty using Kharitonov's theorem and Jury stability criterion. An application is then presented to show the reliability of the proposed design approach by ensuring stability and rejecting disturbances.**

***Keywords*— Internal Model Control, MIMO systems, Fully actuated systems, Stability, Uncertain systems, Instable zero, Disturbances rejection.**

## I. INTRODUCTION

Industrial systems are very frequently multivariable. They have more than one control input and more than one output. Depending on their number, there are three classes of systems, namely: Fully actuated system (square system is a system having the same number for inputs and outputs), Over-actuated system (non-square system that their number of inputs is superior than that of outputs) and Under-actuated system (a system where the number of inputs is inferior than the number of outputs) [1, 2, 3, 6, 12]. In this work, we are interested in systems having the same number of input-outputs and functionally controllable.

The objective of the control is then to obtain a desirable behaviour of several outputs variables simultaneously, by the manipulation of several inputs. The realization of these control law is based on the modelling of systems.

Nevertheless the model, the regulator are generally and initially given in a continuous time model in the form of a transfer function matrix for multivariable systems, but in some experimental applications, we need to discretise the continuous time model. Then, we distinguish different discretization techniques to convert continuous systems into discrete systems such as impulse invariant method, bilinear transformation (Tustin transformation), state-transition method, … [1, 4, 5]. In this paper, we are interested in the Impulse Invariant Method discretization which produces a discrete time model in such a way that the impulse response is the same (invariant) at the sampling instants.

The calculation of any physical process control requires necessarily a model which can never be a perfect representation of reality: there are always uncertainties of modelling, whose consequence is that the behaviour of a physical system cannot be described exactly by a mathematical model [7, 8]. Indeed, there are different approaches that are proposed for the synthesis of the control law for uncertain multivariable systems such as the control of the internal model that was introduced by Garcia and Morari in 1982 and supplemented by a series of publications by these same authors [9, 10, 11].

The IMC is a powerful controller design strategy for linear systems, using a process model controlled by the same control input applied to the process. It is exploited in the industrial systems by these robustness advantages, the simplicity of construction and the compensation of the errors of modelling.

The objective of this work is the application of the internal model control of a class of multivariable uncertain discrete systems that is an extension of the IMC structure applied in [1]. This paper is organised as follows. Section II is dedicated to the design of the internal model control of multivariable discrete system. Section III presents the notion of uncertain systems and defines the kharitonov theorem that allows us to study the stability of uncertain systems. In Section IV, an application is applied to an uncertain discrete multivariable system to show the robustness and validity of this proposed design which provides stability and preserves system performances despite parametric uncertainties and external disturbances.

## II. IMC OF MULTIVARIABLE DISCRET SYSTEMS

### *A. Proposed IMC Structure for Multivariable Systems*

The Internal Model Control (IMC) takes up the basic principle of the open loop control, which represents a major interest for stability, integrating the advantages of the closed loop allowing the rejection of disturbances and modelling errors.




ISSN 1737-9334

The IMC incorporates a simulation of the process by an internal model in its control structure. Its application mainly concerns the stable systems in open loop. The difference which can exist between the outputs of the process and its model is brought back at the entrance of the control block. The regulator, obtained like reverse approximated of the model, acts simultaneously on the process and its model in order to compensate for this variation [10, 13].

The IMC structure of a multivariate system, having m_inputs - m _outputs can be schematized as shown in Figure 1:

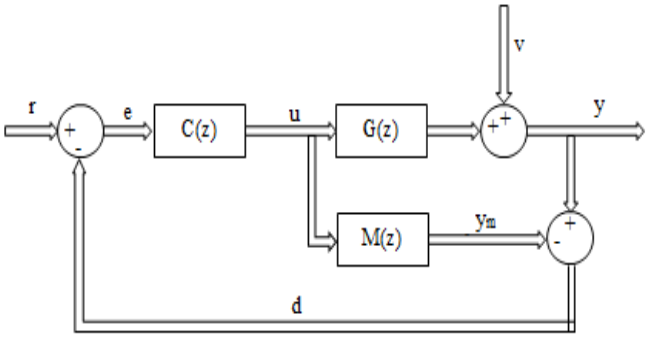


Fig. 1 Basic IMC structure of multivariable system

The configuration of the IMC controller for multivariable systems is represented by:

- G(z) and M(z): are respectively the matrices of transfer of multivariable system and its model of dimension (m x m).
- C(z): the transfer matrix controller of dimension (m x m).
- y and $y_m$: present respectively the output vectors of the process and the model of dimension (m x 1) .
- v: the perturbation vector and of dimension (m x 1).
- d: present the difference between the output and its model.
- r: is the reference vector of dimension (m x 1).

This control structure is defined by the following equations:

$$d = y - y_m = (G - M)u + v \tag{1}$$

$$u = \frac{C}{I_m + C(G - M)}(r - v) \tag{2}$$

$$y = \frac{GC}{I_m + C(G - M)}r + \frac{I_m - CM}{I_m + C(G - M)}v \tag{3}$$

with $I_m$ is the identity matrix.

The synthesis of an IMC corrector that is equal to the direct inverse of the model is essential in order to ensure a perfect follow-up of the reference instructions.
Then, an inversion method has been proposed in [14, 13] to obtain the following IMC regulator:

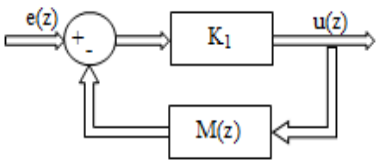


Fig. 2 Blocks of the inversion proposed in the multivariable case

with:

$K_1$ : is a square matrix of inversion of dimension (m x m)

The inversion matrix $K_1$ is an invertible square matrix. It must provide regulator stability. We can choose $K_1$ of the form:

$$K_1 = a \times I_m \tag{4}$$

such as $a \in \mathbb{R}^+$

From Figure 2, the IMC regulator transfer matrix can be expressed by the following expression:

$$C(z) = \frac{u(z)}{e(z)} = \frac{K_1}{I_m + K_1 M(z)} = \frac{1}{K_1^{-1} + M(z)} \tag{5}$$

In order to approximate the controller transfer function C(z) to $M(z)^{-1}$ , we should just select the gain a sufficiently high. So, we obtain:

$$C(z) \simeq M(z)^{-1} \tag{6}$$

The matrix of the static gains of the regulator C(1) can be expressed according to the matrix of the static gains of the system M(1) . It is defined by the equation:

$$C(1) = \frac{K_1}{I_m + K_1 M(1)} = \left(K_1^{-1} + M(1)\right)^{-1} \tag{7}$$

However for certain cases, for example for systems with instable zero or time-delay, the coefficient $K_1$ ensuring the stability of the regulator cannot be chosen sufficiently high. What can involve the degradation of the precision of the system (i.e. the static error is non-null). In order to treat such problem, a second structure CMI can be proposed for this class of dynamic systems by adding a second gain matrix $K_2$ which aims to compensate for the static errors of the multivariable system as shown in figure 3.




ISSN 1737-9334

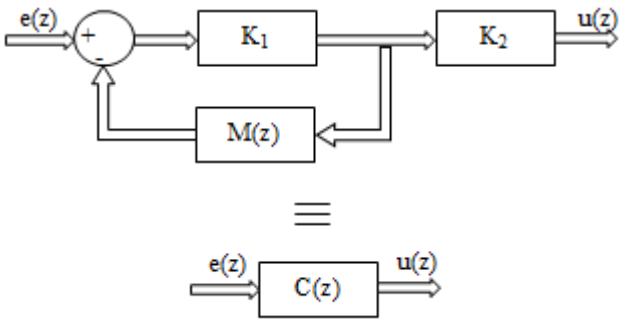


Fig. 3 Generalized multivariable controller structure

$K_2$ can be written in the following form:

$$K_2 = K_1^{-1}(I_m + K_1 M(1)) M(1)^{-1} \quad (8)$$

We can then express the control vector C(z) in the following form:

$$C(z) = K_2(I_m + K_1 M(z))^{-1} K_1 \quad (9)$$

The stability of the proposed controller given in (9) depends on the stability of the model and a best choice of $K_1$.

*B. IMC's Stability*

We can note that the output vector can be written in the following form in order to replace C(z) by its expression given in (9):

$$y(z) = y_r(z)\, r(z) + y_v(z)\, v(z) \quad (10)$$

with:

$$y_r = \frac{GK_2K_1}{I_m(I_m + K_1M) + K_1K_2(G - M)} \quad (10a)$$

$$y_v = \frac{I_m(I_m + K_1M) - K_1K_2M}{I_m(I_m + K_1M) + K_1K_2(G - M)} \quad (10b)$$

The stability of IMC structure depends on the stability of the process to be controlled, its model and the proposed regulator. So, to ensure the stability of the system, it is necessary that each block of the IMC structure is stable in open loop. Given a stable process and model, controller stability only depends on $K_1$.

## III. UNCERTAIN DISCRET SYSTEMS

Generally, uncertainties are grouped into two categories, structured uncertainties and unstructured uncertainties. The first type is often called parametric uncertainty and the second dynamic uncertainty.

The structured uncertainties may be represented by variations of certain physical system parameters over some possible value ranges (complex or real). This type of uncertainties is due to the fact that the parameters could not be accurately modelled or measured. They affect the low-frequency range performance.

Unstructured uncertainties are the ones that affect the system even without having any structural information; this might be due to high frequencies and dynamic uncertainties. Generally, this type of uncertainty can be represented as additive by an unknown transfer function matrix (input multiplicative or output multiplicative). In this work, we are interested of a linear system with parametric uncertainties [7, 8].

We consider in this paper a multivariable linear system given by a transfer function matrix G(z) such as:

$$G(z) = G_{ij}(z)\ ; \begin{cases} i = 1, 2, ..., m \\ j = 1, 2, ..., m \end{cases} \quad (11)$$

If we suppose the presence of parametric uncertainties, $G_{ij}(z)$ is written in the following form:

$$G_{ij}(z) = \frac{N_{ij}(z)}{D_{ij}(z)} = \frac{b_m z^m + b_{m-1} z^{m-1} + ... + b_0}{a_n z^n + a_{n-1} z^{n-1} + ... + a_0} \quad (12)$$

with:

$$n > m;\ \begin{cases} b_m \in [b_m^-, b_m^+] \\ b_{m-1} \in [b_{m-1}^-, b_{m-1}^+] \\ . \\ . \\ b_0 \in [b_0^-, b_0^+] \end{cases} \quad and \quad \begin{cases} a_n \in [a_n^-, a_n^+] \\ a_{n-1} \in [a_{n-1}^-, a_{n-1}^+] \\ . \\ . \\ a_0 \in [a_0^-, a_0^+] \end{cases}$$

*A. Uncertain System's Stability*

There are different methods to study the robust stability of the system depending on the type of transfer function parameters. If the coefficients are time-invariant, we can use the Jury stability criterion to check the discrete system stability. But, if there is uncertainty concerning the parameters of the transfer function, it is necessary to use Kharitonov's theorem to study the linear system stability [7, 15].

*Kharitonov's theorem:*

Kharitonov's theorem allowed characterizing the stability of a system subjected to bounded parametric uncertainties on the transfer function coefficients.

Let the characteristic polynomial P be described by the following equation:

$$P(z) = l_0 + l_1 z + l_2 z^2 + ... + l_n z^n \quad (13)$$


ISSN 1737-9334

Where $l_i \in \mathbb{R}$ are known only in specified ranges such as $l_i^- < l_i < l_i^+$ for i=1; 2 ; … ; n.

The polynomials family P is stable if and only if the following four Kharitonov polynomials ($P_1$ , $P_2$ , $P_3$ and $P_4$) are stable [15]:

$$\begin{cases} P_1(z) = l_0^- + l_1^- z + l_2^+ z^2 + l_3^+ z^3 + l_4^- z^4 + \dots \\ P_2(z) = l_0^- + l_1^+ z + l_2^+ z^2 + l_3^- z^3 + l_4^- z^4 + \dots \\ P_3(z) = l_0^+ + l_1^- z + l_2^- z^2 + l_3^+ z^3 + l_4^+ z^4 + \dots \\ P_4(z) = l_0^+ + l_1^+ z + l_2^- z^2 + l_3^- z^3 + l_4^+ z^4 + \dots \end{cases} \quad (14)$$

We then obtain the Kharitonov polynomials corresponding to D:

$$\begin{cases} D_1(z) = a_0^- + a_1^- z + a_2^+ z^2 + a_3^+ z^3 + a_4^- z^4 + \dots \\ D_2(z) = a_0^- + a_1^+ z + a_2^+ z^2 + a_3^- z^3 + a_4^- z^4 + \dots \\ D_3(z) = a_0^+ + a_1^- z + a_2^- z^2 + a_3^+ z^3 + a_4^+ z^4 + \dots \\ D_4(z) = a_0^+ + a_1^+ z + a_2^- z^2 + a_3^- z^3 + a_4^+ z^4 + \dots \end{cases} \quad (15)$$

### B. *Uncertain System's Control*

The main aim of the robust control for an uncertain system is to guarantee the performances and the stability of a system despite of the risks and fluctuations which can affect the system during its operation.

There exists a difference between the observed behaviour of the real system and its nominal model. The main problem of this type of control is the control law synthesis in closed loop, to guarantee the imposed performance despite model imperfections, uncertainties and external disturbances.

## IV. APPLICATION

Considering the transfer matrix G(z) of the uncertain multivariable process with two inputs-two outputs. Uncertainties occur at the level of the first element of this matrix $G_{11}(z)$ . It is defined by the following transfer matrix:

$$G(z) = Z\left[ B_0(p) \begin{pmatrix} \dfrac{b_1 p + b_0}{p^2 + a_1 p + a_0} & \dfrac{1}{p+2} \\ \dfrac{p+1}{4p^2+3p+2} & \dfrac{3}{p+4} \end{pmatrix} \right] \quad (16)$$

With:

$$b_0 \in [b_{0\min}, b_{0\max}] = [1,4]$$

$$b_1 \in [b_{1\min}, b_{1\max}] = [1,2]$$

$$a_0 \in [a_{0\min}, a_{0\max}] = [1,3]$$

$$a_1 \in [a_{1\min}, a_{1\max}] = [1,4]$$

This uncertain system is represented by the following nominal model:

$$M(z) = Z\left[ B_0(p) \begin{pmatrix} \dfrac{1.5p + 2.5}{p^2 + 2.5p + 2} & \dfrac{1}{p+2} \\ \dfrac{p+1}{4p^2+3p+2} & \dfrac{3}{p+4} \end{pmatrix} \right] \quad (17)$$

### A. *Application of the IMC without $K_2$*

Firstly, let's consider the case characterized by the absence of disturbances.
For a reference vector that is chosen as steps of amplitude 1 applied at t=0s , the simulation results for a gain $K_1$=2 and a sampling time $T_e$=0.1s are given in figures 4 and 5.

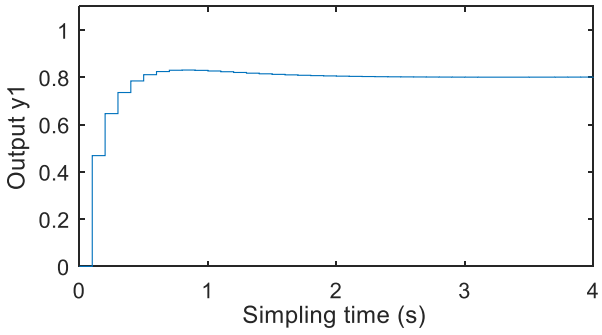


Fig. 4 Output signal $y_1$ without $K_2$

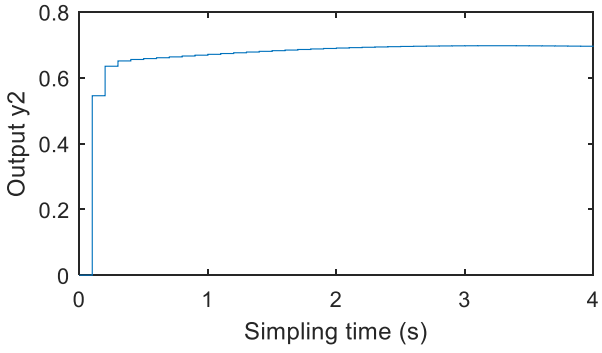


Fig. 5 Output signal $y_2$ without $K_2$

It can be remark from these two figures that the internal model control applied maintains the stability of the chosen discrete multivariable system despite the absence of the gain $K_2$ and the presence of uncertainties. Then, $K_1$ gain is




ISSN 1737-9334

responsible for maintaining stability. But, it is clear that the outputs $y_1$ and $y_2$ do not describe perfectly the reference signals.

### *B. Application of the IMC with $K_2$*

Let's consider now the presence of the gain $K_2$ where $K_2$ defined by (8). For the same reference and a sampling period $T_e$=0.1s and $K_1$=2, the figures 6 and 7 present the simulation results:

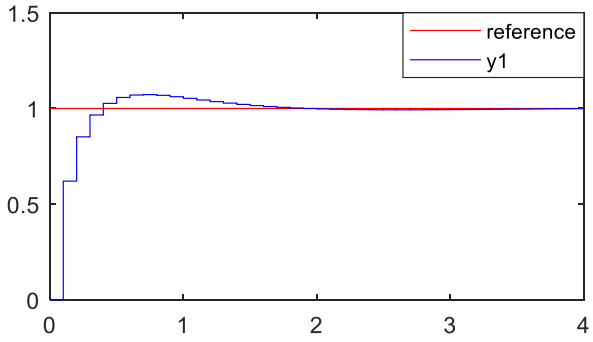


Fig. 6 Output signal $y_1$ with $K_2$

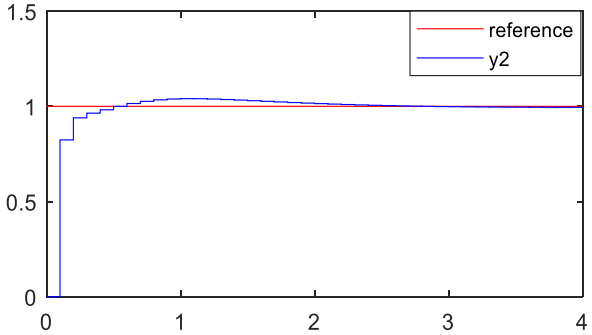


Fig. 7 Output signal $y_2$ with $K_2$

We compare Figures 4 and 5 with Figures 6 and 7, we remark that the outputs of the system perfectly reach the input reference when adding $K_2$; the added gain $K_2$ then is able to compensate for the static error as desired. In this way, we can see that the system remains stable despite the presence of uncertainties.

For the same references and the regulator used previously, we must change the sampling period now.

For $T_e$=0.2s, the simulation results are given in figures 8 and 9.

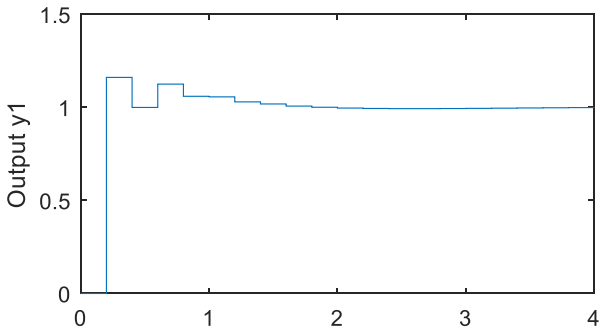


Fig. 8 Output signal $y_1$ for $T_e$=0.2s

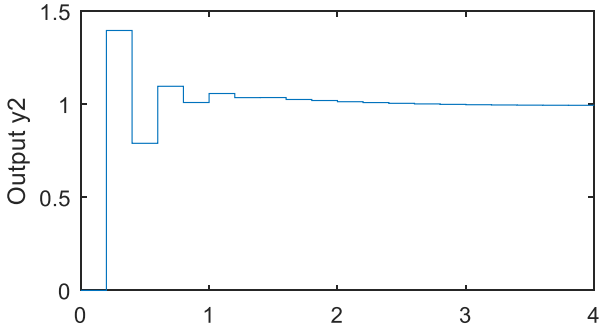


Fig. 9 Output signal $y_2$ for $T_e$=0.2s

For $T_e$=0.3s, the simulation results are given in figures 10 and 11.

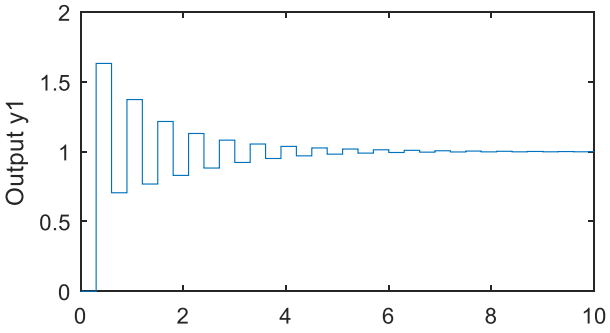


Fig. 10 Output signal $y_1$ for $T_e$=0.3s

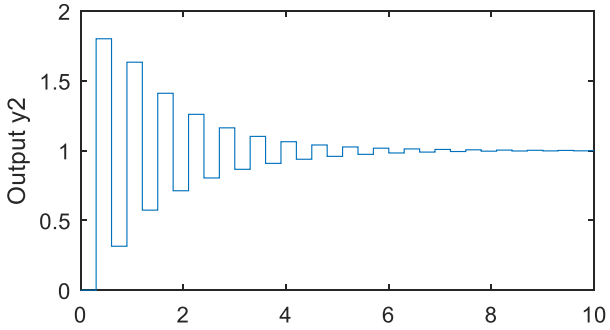


Fig. 11 Output signal $y_2$ for $T_e$=0.3s




ISSN 1737-9334

From Figures 8 - 11, it can be shown that as for the same value of gains $K_1$ and $K_2$ , a high value of the sampling time can result in deterioration of closed loop system performances.

### *C. Application of the IMC with disturbances*

Let's consider now the presence of external disturbances in the form of a unit steps. And, let's show its effect in the case of the internal model control proposed. The simulations results are given by the figures 12 and 13.

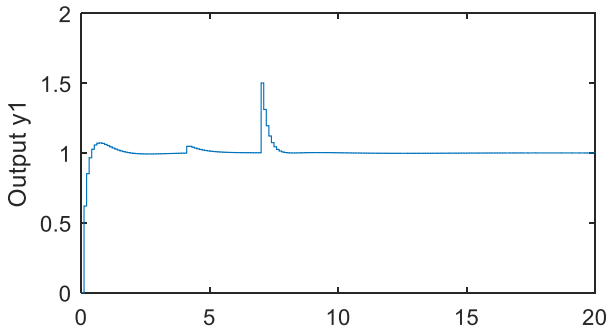


Fig. 12 Output signal $y_1$ with disturbances

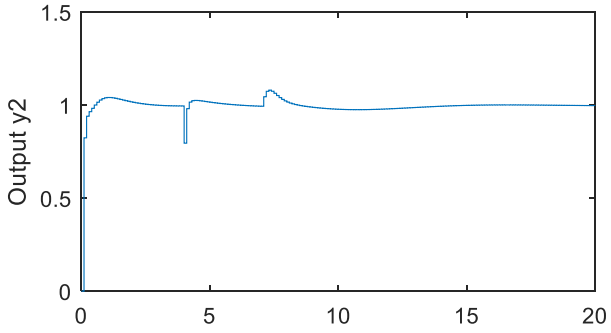


Fig. 13 Output signal $y_2$ with disturbances

Significant peaks of the input signals appear at the moment already chosen for the disturbances, it is clear that the discrete uncertain system controlled by IMC is able to maintain stability despite external disturbances.

The figures show a robust behaviour even on the presence of disturbances directly affecting the outputs of the process.

## V. CONCLUSIONS

In this paper an approach for IMC of linear fully actuated discrete uncertain systems is developed. This approach uses an internal model that is nominal of the uncertain system. The chosen system is a two-input-two-output linear system.

Satisfactory results have been obtained showing the robustness of this approach to maintain stability and reject external disturbances.

## REFERENCES

[1] M. Hannachi and D. Soudani, " I*nternal Model Control of Multivariable Discrete-Time Systems*", IEEE, International Conference on modelling , Identification and Control, ICMIC, Sousse, 2015

[2] A. Dhahri, I. Saidi and D. Soudani, "*A New Internal Model Control Method for MIMO Over-Actuated Systems*". International Journal of Advanced Computer Science and Applications, Vol 7, No. 10, 2016 .

[3] I. Bejaoui, I. Saidi and D. Soudani, "*New Internal Model Controller Design for Discrete Over-Actuated Multivariable System*" IEEE, 4th International Conference on Control Engineering &Information Technology (CEIT-2016), Hammamet.

[4] M. Hannachi, I. Bencheikh Ahmed and D. Soudani, "Discretization of multivariable fully actuated linear systems controlled with Internal Model Control," IEEE 2016.

[5] N. K Sinha and Q. Zhou, "Discrete time approximation of multivariable continuous time systems," IEE Proceeding, vol. 130, Pt.D, May , 1983.

[6] A. Dhahri, I. saidi and D. Soudani, "Internal Model Control for Multivariable Over-Actuated systems with Multiple Time Delays, " 4th International Conference on control Engineering & Information Technology, pp. 623-626, Hammamet, 2016.

[7] M. Naceur, " On the Internal Model Control of Uncertain Systems, ", 978-1-4244-7534-6/10/26.00, IEEE, Juin 2010.

[8] C. Othman, I. Ben Cheikh Ahmed and D. Soudani, " Application of the Internal Model Control Method for the Stability study of uncertain sampled systems, " 978-1-4799-7300-2/14/$31.00 ©2014 IEEE

[9] M. Morari, C. E. Garcia "Internal model control-1- A unifying review and some new results," Ind.Eng. Process Dev, 1982.

[10] C. E. Garcia, M. Morari "Internal Model Control -2- Desing procedure for multivariable systems," Ind. Eng. Chem. Process Des. Dev, 1985.

[11] C. E. Garcia, M. Morari , "Internal Model Control -3-, Multivariable control law computation and tuning guidelines" Ind. Eng. Chem. Process Des. Dev, 1985.

[12] A. Mezzi, D. Soudani and M. Benrejab, "On the Internal Model Control of Multivariable Linear Under actuated systems", Multi-Conference on Compulation Engineering in systems Application, CESA, Marrakech, 2015.

[13] N. Touati, "Sur la commande par modéle interne de systèmes continus multivariables", PhD, ENIT, Tunisia, 2015.

[14] M. Benrejab, M. Naceur and D. Soudani , " On an internal mode controller based on the use of a specific inverse model", ACIDCA 2005, pp. 623-626, Tozeur, 2005.

[15] K. Yeung, S. Nang, "A simple proof of Kharitonov's Theorem ", IEEE Trans. On Automatic Control, Vol. Ac-32, No.9, Sept 1987.




ISSN 1737-9334

# Implementation of Robust Predictive Controller on FPGA device

TELMOUDI BRINI Sirine[1], BOUZOUITA Badreddine[2], BOUANI Faouzi[1]
[1] Tunis El Manar University, National Engineering School of Tunis, Tunisia,
LR11ES20 Laboratory of Analysis Conception and Control of Systems, Tunis, Tunisia.
[2] University of Sousse, National Engineering School of Sousse, Tunisia
Sirinebrini@gmail.com, badreddine.bouzouita@enit.rnu.tn, faouzi.bouani@enit.rnu.tn

*Abstract*— **Implementation of a linear Robust Predictive Controller (RPC) into a FPGA with 20 MHz fixed clock is presented in this work. The design of the controller is based on a single input-single output Auto Regressive Integrated Moving Average (ARIMA) Model. To take into account the uncertain systems behaviour, the parametric polytopic uncertainties are adopted. Supported on worst case strategy, by the resolution of a min-max optimization problem the control law is obtained. Since the performance criterion to be optimized is non-convex, a non-determinist global optimization method based on Genetic Algorithms (GA) is proposed to solve this problem. The efficiency of the proposed approach is demonstrated with the RPC implementation on a Nanoboard 3000XN FPGA platform chip using the Altium Designer such a conception environment.**

***Keywords***— FPGA, Robust Predictive Control, global optimization, Genetic Algorithm, Altium Designer.

## I. INTRODUCTION

Some control technique requires a numerical model intending to predict the future behavior of the system [1]. Thereby, the precision degrees of the considered model cheek a significant role on the controller effectiveness. Therefore, it is necessary to use a controller which ensures the desired performances in the presence of uncertainties [9]. In this case, we talk about robust control. Certainly, predictive control took advantage to exploit systems power of embarked systems on the control processes and also the evolution of the optimization algorithms which became faster [2].

In real-time applications managed using intelligent technology, with the technological advancement in the field of microelectronics, new hardware design solutions such as Field Programmable Gate Array (FPGA), Application Specific Integrated Circuit (ASICs) are available and can be used as digital targets for implementation of the control algorithms in a single component [7], [8]. The advantages of such an implementation are multiple: the reduction of the execution time by adopting parallel processing, the rapid prototyping of the numerical control on FPGA, the confidentiality of the architecture [13], the possibility of applying intelligent commands that have recourse to heavier techniques in terms of computing time and improving the quality of control of industrial process by exploiting the new digital systems technologies [17]. Nowadays, all of these advantages form a need and a necessity for the control of industrial systems characterized by high performance [15]. The concept of robustness has emerged to handle a set of analysis and synthesis problems especially for systems, whose models aren't precisely known [12]. When the structure of the model is uncertain, by adopting the worst case strategy, the calculation of the robust predictive control law amounts to minimizing the maximum of a criterion with respect to the control signal, taking into account all the possible models described by the set of uncertainties such as parametric uncertainties and polytopic uncertainties [5]. Therefore, the control law is obtained by solving a min-max optimization problem [6]. The cost function to be optimized for the robust predictive control is non-convex opposite the uncertainties. Also by using a local optimization technique non optimal control law is obtained. So we proposed global optimization algorithms as genetic algorithms (GA) method [3], [14] which uses stochastic rules and decisions in order to provide the global solution and has known a considerable interest in predictive control.

It is in this spirit that we develop this work which is interested in the synthesis of a robust control law implemented into Nanoboard 3000XN FPGA platform, based on a linear and uncertain ARIMA model which can manipulate unstable open loop systems and decrease the number of model parameters.
The remainder of the paper is organized as follows: section II presents theoretical formulation of RPC. Section III gives the details of RPC algorithm implementation on FPGA. Section IV shows simulation results. The conclusion is provided in section V.

## II. PROBLEM FORMULATION OF RPC

### A. Linear model

In this section, the output predictions are presented by ARIMA model:

$$\Delta y(k) = \frac{B(q^{-1})}{A(q^{-1})}\Delta u(k) \tag{1}$$

where $y(k)$ is the system output and $u(k)$ is the system input. The term $\Delta = 1 - q^{-1}$ is the integral action that allows the cancellation of the static error. $A(q^{-1})$ and $B(q^{-1})$ are polynomials of degrees respectively $na$ and $nb$ in backward shift operator $q^{-1}$ which are bounded and uncertain to take into account the uncertain behavior of the system. These polynomials are given as follows:

$$A\left(q^{-1}\right) = 1 + \sum_{i=1}^{na} a_i q^{-i} \quad , \quad a_i \in \left[\underline{a_i}, \overline{a_i}\right], i = 1,\ldots,n_a \tag{2}$$

$$B(q^{-1}) = \sum_{j=1}^{nb} b_j q^{-j}, b_j \in \left[\underline{b_j}, \overline{b_j}\right], j = 1,\ldots,n_b \tag{3}$$

with $\underline{a}_i$ and $\overline{a}_i$ are respectively the lower and the upper bounds of $a_i$, $\underline{b}_j$ and $\overline{b}_j$ are respectively the lower and the upper bounds of $b_j$.

Therefore, the output prediction $\hat{y}(k+j)$ can be obtained by a multiple recursion using relation (1):


ISSN 1737-9334

$$\hat{y}(k+j) = \sum_{i=1}^{j} g_{j-i+1}\Delta u(k+i-1) + y_l(k+j) \text{ for } j \geq 1 \quad (4)$$

with:

$$\begin{cases} g_1 = b_1 \\ g_j = b_j + \sum_{i=1}^{j-1}(a_{i-1} - a_i)g_{j-i} \end{cases} \quad (5)$$

and:

$$\begin{cases} y_l(k+1) = y(k) - \sum_{i=1}^{na} a_i \Delta y(k+1-i) + \sum_{i=2}^{nb} b_i \Delta u(k+1-i) \\ y_l(k+j) = a_{j-1}y(k) + \sum_{i=j+1}^{nb} b_i \Delta u(k+j-i) + \sum_{i=1}^{min(j-1,na)} (a_{i-1} - a_i)y_l(k+j-i) \end{cases} \quad (6)$$

*B. Control law*

Robust predictive control requires online optimisation of the following min-max optimisation problem:

$$\min_{\Delta U} - \max_{\psi} J \quad (7)$$

where $\Delta U$ is the vector of future optimized control increments, $\psi$ represents the set of uncertainties and $J$ denotes the desired performances and presented by the following Quadratic Problem (QP) [23]:

$$J = \sum_{j=N_i}^{N_y} (y_c(k+j) - \hat{y}(k+j))^2 + \lambda \sum_{j=0}^{N_u-1} \Delta u(k+j)^2 \quad (8)$$

with $\hat{y}(k+j)$: predicted output. $y_c(k+j)$: set point. $\lambda$: weighting on the future increment control. $\Delta$: incremental operator. $u(k)$: the input control. $N_y, N_u$ and $N_i$ denote the output prediction horizon, control horizon and the initial prediction horizon respectively.

We can solve the optimisation problem (7) in two steps; starting by the calculation of the parameters that maximize the cost function $J$, and next, we minimise it facing the input control:

$$\min_{\Delta U} - \max_{\psi} J = \min_{\Delta U} J^*(\Delta U) \quad (9)$$

with

$$J^*(\Delta U) = \max_{\psi} J \quad (10)$$

We can show that the cost function $J$ to be optimized is non-convex opposite the adopted uncertainties. Therefore, the optimization problem (10) is non-convex. The use of a local optimization method such as the gradient algorithm leads to non-optimal control law. In the next section, we propose global optimization algorithm to solve this problem.

*C. Genetic Algorithms*

Genetic algorithms (AG) are stochastic optimization algorithms based on the mechanisms of natural selection and genetics [14]. However, the natural processes to which they refer are much more complex. The individual in a population is represented by a chromosome consisting of genes that contain the hereditary characteristics of the individual. The principles of selection, crossing and mutation are inspired by natural processes of the same name.

To use a genetic algorithm on a particular problem, the following elements must be available:

- *Codification*:

This step consists to describe each individual by a string of alphabet which can be binary, real, symbol or any other [3]. In this work we have chosen the real codification because our parameters are real. This description is called *chromosome* and a set of chromosome presents a *population.*

- *Fitness function:*

The variable to be optimized can be, for example, consumption, yield, transmission factor, profit, cost, development time etc. Thus, an optimization algorithm requires the definition of a function called *fitness function* which allows evaluating of the potential solutions from the variable to be optimized. As a result, the algorithm converges towards an optimum of this function [3].

- *Generation of a new population:*

The initial population $pop_0$ is generated randomly, then for each individual the evaluation function $f_i$ is calculated; from it we obtain the new population using the three genetic steps illustrated as follow:

- *Selection*: the aim of selection is to retain the best individuals to ensure the convergence of the algorithm. Tournament selection is an alternative to proportional selection. This step is described in algorithm 1.

**Algorithm 1: selection step of GA**

1: Evaluation of population individuals: $f_j$

2: Calculate the total sum of population: $F = \sum_{j=1}^{n} f_j$

$n$: number of population chromosomes.

3: Calculate the selection probability: $P_j = \frac{f_j}{F}$

4: Calculate the cumulative probability: $q_j = P_1 + \cdots + P_j$

5: Beginning selection:

- Generate randomly $0 \leq r \leq 1$
- If $r < q_1$ then select the chromosome $P_0$
  - Else
    - for $j$ from *1* to $n$
      - If $q_{j-1} \leq r \leq q_j$
        - then select the chromosome $P_j$
      - End if
    - End for
  - End if

6: End selection

- *Crossover*: the crossing operator is active, with a probability $P_c$, a pair of parent chromosomes $P_1$ and $P_2$ returns a chromosome child $C$ using the arithmetic crossing. The recommended values for the crossover probability parameter are $P_c = 0.95$ from [9] and $P_c \in [0.75, 0.95]$ from [10]. In this step, the population will be divided on two parts, the chromosomes of the first part will be cross two by two, and the chromosome children obtained from each cross will be injected




ISSN 1737-9334

into the second half of the population as it is shown in the algorithm 2. the arithmetic crossing is defined by:

$$C = P_c P_1 + (1 - P_c) P_2 \qquad (11)$$

**Algorithm2: Crossover step of GA**

1: Define the crossover probability parameter $P_c$

- For i from *n/2* to *n* do

$$C(i) = (1 - P_c) P_{n-i+1} + P_c P_{n-i+2}$$

- End for

*Mutation:* in order to furnish genetic diversity, with a probability $P_m$, this step enables the spontaneous transform of an individual, which randomly generates directions that are adaptive with respect to the last successful or unsuccessful generation, is considered. This step is described in algorithm 3.

**Algorithm3: Mutation step of GA**

1: Define the mutation probability parameter $P_m$

2: Generate randomly $0 < r < 1$ :

- For i from 0 to n/2 do

  If $r < P_m$ then

  $POP_{next}(i) = POP_0(0)$

  with $POP_{next}$ is the next population.

  End if

- End for

➢ *Stopping conditions:*

Stopping the algorithm is conditioned by the validation of certain criteria which may be the maximum number of generations or when the individuals of a population don't evolve more rapidly or the maximum time of execution or even a combination of these criteria.

## III. IMPLEMENTATION OF LINEAR RPC ON FPGA

This section presents the method to implement the RPC algorithm on the Map Nanoboard 3000XN supporting Xilinx FPGA.

### A. *Nanoboard 3000XN*

The Nanoboard 3000XN map with a fixed Xilinx Spartan-3AN device (XC3S1400AN-4FGG676C) is crucial for the speedy progression of the systems embedded with the Altium Designer. It is a platform of a reprogrammable design material that exploits the power dedicated to the electronic conception of high capacity, allowing the fast implementation and the debugging of our interactive conceptions [16]. This map is constituted by several material modules which realize miscellaneous tasks according to the designer's needs, such an integrated color TFT LCD panel (240x320), an SVGA interface (24-bits, 80 MHz), a programmable clock (6 to 200 MHz) and a fixed one (20 MHz) both available to FPGA users, a 4-channels 8-bits ADC, and 4-channels 8-bits DAC.

### B. *RPC conception*

Fig. 1 presents the solution for the custom hardware. The predictive algorithm is implemented in C++ and compiled for a Nanoboard 3000XN XC3S1400AN-4FGG676C FPGA. In addition, a TFT screen shows the evolution of the output and control action.

- The first step of the prediction process is for a sample cycle $k$ such that the FPGA calculates the output data $y(k)$ of the system.
- The second step consists to maximize the cost function $J$ to estimate the optimal model parameters $a_{i\,op}$ and $b_{j\,op}$ , using the GA such a non determinist optimized method.
- In the next step, the state observer prepares the data calculating the free responses $y_l$ to feed into the genetic algorithm Min-Max-Problem(Min-Max-P) solver.
- Then the Min-Max-P is solved to give a new sequence of the control action. Only one control signal, $u(k)$ is implemented on the plant while the others are rejected, due to the next sampling instant, $y(k+1)$ is known.
- The LCD screen is used to display the evolutions of output and control action signals.
- The first step is repeated with the updated value and all sequences are brought up to date.

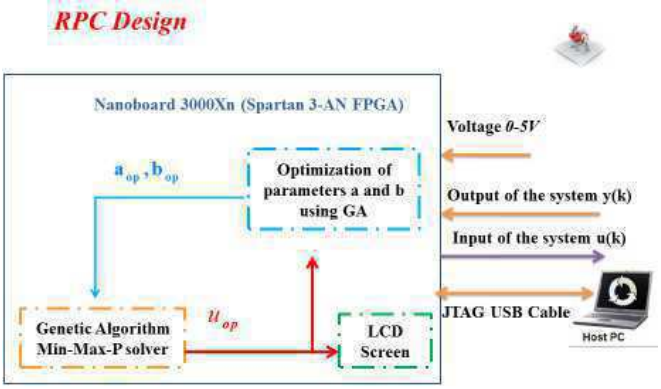


Fig. 1: Structure of the implemented RPC.

### C. *Hardware architecture*

The model given in Fig. 2 approves the designer to construct a processor-based system with a more rational and abstract approach. In this design, a processor TSK3000 is founded to ensure the execution of a software application, which is a 32-bit RISC processor. Most of its instructions are 32 bits wide and run in a single clock cycle. Moreover, there is a memory SRAM to store the data, a controller TFT_VGA to pilot the display of signals on the LCD screen, and two wishbones (one for interconnection and one for arbitration).

### D. *Software architecture*

The important step in the software process is the choice of libraries, as the absence of one library can generate some errors at compilation, so the user must comprehend the utility of each unit before using it [16]. The LCD module of the card Nanoboard 3000XN is utilized where the function name of each library provided by the map shown in Table I is needed.




ISSN 1737-9334

In order to use the RPC controller algorithm, the steps illustrated in the flowchart of Fig. 3 must be followed.

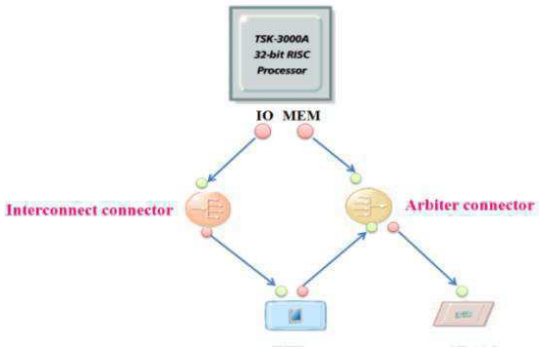


Fig. 2: Hardware architecture for RPC

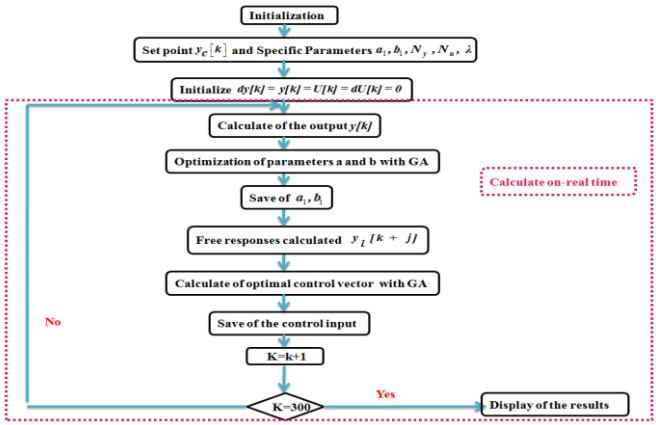


Fig. 3: Flowchart of the robust predictive control algorithm

## IV. SIMULATION RESULTS

In this section, linear robust predictive controller based on ARIMA model proposed in this work is implemented into the map Nanoboard 3000XN which support an FPGA from the Xilinx family. The RPC scheme is designed with the following parameters:

- ARIMA model: $\Delta y(k) = \dfrac{B(q^{-1})}{A(q^{-1})}\Delta u(k)$

  where : $A(q^{-1}) = 1 + a_1 q^{-1}$, $B(q^{-1}) = b_1 q^{-1}$
- Constraints on input signal: $0v \le u(k) \le 5v$
- Constraints onto parameters $a_1$ and $b_1$:

  $-0.99 \le a_1 \le -0.4$ and $0.4 \le b_1 \le 0.8$
- Fitness function: is defined by the cost function to be optimized.
- Population size: is defined by the parameter *n*. A several test are used to determine the optimal size.
- Stopping criteria: is defined by the parameter *num* and it's specified by the maximum number of generations.
- Crossover and mutation probabilities: $P_m = 0.3$ and $P_C = 0.75$

Two cases are envisaged to test the efficient of the GA.

**Case 1:** $a_1$ and $b_1$ are fixed

We suppose that the system is characterized by the following fixed parameters: $a_1 = -0.97, b_1 = 0.6$ for i=1, .., 100

**Case 2:** $a_1$ and $b_1$ are variables

Assume that the system used is characterized by the following parameters:

$a_1 = -0.97, b_1 = 0.6$ for i=1, .., 30

$a_1 = -0.5, b_1 = 0.4$ for i=31, ..., 70

$a_1 = -0.97, b_1 = 0.6$ for i=71, ..., 100

It should be noted that for the two cases even if the parameters $a_1$, $b_1$ and $u$ are multiplied by the crossover probability parameter in the genetic algorithm, their values always remain in the constraint interval and by the consequence children are always feasible with respect to linear constraints and bounds.

### A. *Model parameters estimation*

To solve the optimisation problem (7), calculation of the parameters that maximize the cost function $J$ is required. In this step the genetic algorithm is used as a global optimization method to find, at each iteration, the model parameters. The size of the initial population is $\dim(P_0) = (num, 3)$ and it's defined as follows:

$$P_0 = \begin{pmatrix} a_{11} & b_{11} & u_1 \\ & \cdots & \\ a_{1num} & b_{1num} & u_{num} \end{pmatrix}$$

The first and the second columns are reserved to the model parameters and the third one is dedicated to the control input. For each population individual $ind_i = (a_{1i}, b_{1i}, u_i), i = 1,\ldots,num$, we compute the prediction sequence $\hat{y}(k+j)$, $j = 1 \ldots N_y$ and we evaluate the performance criterion *J* given by (8). Based on the criterion values (fitness), the GA operators (selection, crossover and mutation) are applied in order to find the next population individuals. The procedure will be repeated until a stopping criterion is reached. Then, the parameters of the worst case model are obtained.

For the second optimization problem, we use the following initial population:

$$P_{02} = \begin{pmatrix} u_1 \\ \cdots \\ u_{num} \end{pmatrix}$$

In this case, the size of the initial population is $(num, 1)$ and the model parameters are those obtained in the first optimisation problem. The evolution of the estimated model parameters is illustrated in Fig. 4 (case 1) and Fig.5 (case 2), it can be seen that for the two cases the values of $a_1$ and $b_1$ are always remain in the constraint interval.

TABLE I
FUNCTION NAME OF EACH LIBRARY USED IN PREDICTIVE ALGORITHM

| Function name | Role of peripherals |
|---|---|
| Grapigcs_open | Initialize LCD screen |
| graphics_get_visible_canvas | Get screen active |
| graphics_fill_canvas | Give color to screen background |

### B. *Discussion*




ISSN 1737-9334

The synthesis results of the RPC algorithm implementation on the FPGA are very important for the conception to know the occupation rate concerning the internal resources of the FPGA, such as the number of slices, clocks, etc. Table II summarizes the hardware resources used to implement the RPC algorithm on the FPGA. About 50% of the RAM on the FPGA chip is used, and this value can be considered lightly lower compared to the large number of mathematical operations of the genetic predictive algorithm. Besides, 23% of total LUTs (Look-Up Table) with 4 inputs are used. This is important for envisaging other more complex treatments.

In this study, the influence of the population size parameter $n$, the stopping parameter *num* and the prediction horizon $N_y$ on the performances of the RPC controller are investigated.

- ***Case 1*:** first, it is required to investigate the influence of $N_y$ on the performance of the RPC. Fig. 6 illustrates the evolution of the output $y(k)$ and the input control $u(k)$ for different values of the prediction horizon $N_y$ ($N_y$=3 and $N_y$=7). These results demonstrate that the output reaches the retained set-point. It can be seen that the response time for $N_y$=7 is higher than that noted in the case where $N_y$=3 (Fig. 6). In fact, when $N_y$=3, the response reaches the point of stability after about 10 iterations but for $N_y$=7 the output stabilizes after 20 samples time. In the second experiment, the aim is to test the influence of the population size parameter $n$ and the stopping parameter *num*. Fig. 7 depicts the evolution of the output $y(k)$ and the input control $u(k)$ when $n$ is decreased from 300 to 100. Comparing the paces, it can be seen also that when $n$ is equal to 300 the FPGA-RPC controller will give a better performance. Two tests are done for the influence of the *num* parameter. First, when the population size parameter is important ($n$= *300*), Fig. 8 presents the evolution of system when *num* increases from 10 to 50, it can be noted that between the two pictures there is no big change and it come down to the important value of $n$. Second, when $n$ is quite small ($n$=*100*), Fig. 9 depicts the evolution of the output and the input when the stopping parameter *num* is decreased from 50 to 10, right here the difference is remarkable and it can be seen that the FPGA-RPC controller will produce a better performance when *num* is equal to 50. The choice of the parameter $n$ and *num* is for the two genetic algorithms, and the filling of the first population is done randomly.
- ***Case 2*:** Fig. 11 presents the evolution of the system for n = 300 and num = 50 when the parameters $a_1$ and $b_1$ are variables. In this example, it is remarkable the effectiveness of the algorithm by seeing that the output follows the set-point and the error is almost null. It is noticeable that the average time required for computing the control input $U$ in each sample time is 1*s* for $n$=100 and *num*=50 but also for $n$=300 and *num*=50 is about *3s*. Therefore, it can be concluded that the implementation of the RPC using the GA gives an alternative to control faster systems.

## V. CONCLUSIONS

In this work, linear approach of robust predictive control based on ARIMA model has been implemented into a map Nanoboard 3000XN supported a Xilinx FPGA. To take into account the uncertain dynamic of the process which leads to resolution a non-convex optimization problem, parameters and polytopic uncertainties are considered. A global non-determinist optimization algorithm is proposed to resolve this problem such as the genetic algorithm. The simulation results show that by solving the min-max problem with the proposed optimized approach approve that the output reaches the retained set-point with good performances in terms of pursuit error, rise and response times.

TABLE II
RESOURCES UTILIZATION OF RPC ALGORITHM

| Used Logic | Used | Available | % of use |
|---|---|---|---|
| Number of slice flip flops | 2,262 | 22,528 | 10% |
| Number of slices | 3,074 | 11,264 | 27% |
| Number of LUTs (4 inputs) | 4,942 | 22,528 | 21% |
| Total LUTs (4 inputs) | 5,529 | 22,528 | 23% |
| Number of input /output blocks | 145 | 502 | 28% |
| Number of BUFGMUXs | 2 | 24 | 8% |
| Number of RAMB 16BWEs | 16 | 32 | 50% |

## REFERENCES

[1] B. Stellato, T. Geyer and J. G. Paul, *"High-Speed Finite Control Set Model Predictive Control"*, IEEE Transactions on Power Electronics, Mai, Vol. 32, No. 5, pp. 4007-4020, 2017.

[2] B. Yang, T. Yu, H. Shu, J. Dong and L. Jiang , *"Robust sliding –mode control of wind energy conversion systems for optimal power extraction via nonlinear perturbation observers",* Applied Energy, Vol. 210, pp. 711-723, January 2018.

[3] D. E. Goldberg, *"Genetic Algorithm in Search, Optimisation and Machine Learning"*, Addison- Wesley Pub. Co., 1989.

[4] D. Lamburn, P. Gibbens and S. Dumble, *"Explicit efficient constrained model predictive control"*, International Journal of Automation and Control, Vol. 10, No.14, pp. 329 - 355, 2016.

[5] D. Munoz de la Pena, T. Alamo, D. R. Ramırez, E. F. Camacho , *"Min-Max Model Predictive Control as a Quadratic Program",* IET Control Theory & Applications, Vol. 1, No. 1, pp. 328-333, 2007.

[6] D. R. Ramırez, E. F. Camacho and M. R. Arahal, *"Implementation of min-max MPC using hinging hyperplanes application to a heat exchanger",* Control Engineering Practive, Vol. 12, No. 9, pp. 1197-1205, 2004.

[7] E. N. Hartley, J. L. Jerez, A. Suardi, J. M. Maciejowski, E. Kerrigan and G. Constantinides, *"Predictive control using an FPGA with application to aircraft control"*, IEEE Transactions on Control System Technologic, Vol. 22, No. 3, pp. 1006–1017, 2015.

[8] F. Xu, H. Chen, X. Gong and O. Mei, *"Fast Nonlinear Model Predictive Control on FPGA Using Particle Swarm Optimization"*, IEEE Transactions on Industrial Electronics, Vol. 63, No. 1, pp. 310-321, 2016.

[9] J. B. Rawling and D. Q. Mayne, *"Model Predictive Control: theory and design"*, Nob hill publishing, LlC, 2009.

[10] J. J. Grefensette, *"Optimization of control parameters for genetic algorithms"*, IEEE Transaction on Man and Cybernetics, SMC, Vol.16, No. 1, pp. 122-128, 1986.

[11] J. Shaffer, R. Caruana, L. J. Eshelman and R. Des, *"A Study of Control Parameters Affecting Online Performance of Genetic Algorithms for Functions Optimization"*, 3rd International Conference on Genetic Algorithms, Morgan Kaufman, San Mateo, CA, PP.51-60, 1989.

[12] J. Guo and L. Dong, *"Robust load frequency control for uncertain nonlinear interconnected power systems"*, International Journal of Automation and Control, Vol. 11, No. 3, pp. 239-261, 2017.




ISSN 1737-9334

[13] M. Ricco, P. Manganiello, E. Monmasson, G. Petrone and G. Spagnuolo, *"FPGA-Based Implementation of Dual Kalman Filter for PV MPPT Applications"*, IEEE Transactions on Industrial Informatics, Vol. 13, No. 1, pp. 176-185, 2017.

[14] S. P M. Alinodehi, S. J. Louis, S. Moshfe and M. Nicolescu, *"A Modified Steady State Genetic Algorithm Suitable for Fast Pipelined Hardware"*, IEEE Congress on Evolutionary Computation, 5-6 June, Sain sebastian, Spain, 2017.

[15] S. Lucia, D. Navarro, O. Lucia, P. Zometa and R. Findeisen, *"Optimized FPGA Implementation of Model Predictive Control for Embedded Systems Using High Level Synthesis Tool"*, IEEE Transactions on Industrial Informatics, Vol. 14, No. 1, pp.137-145, 2017.

[16] T. S. Brini, B. Bouzouita and F. Bouani, *"FPGA Implementation of a Model Predictive Control: Application to a control system of water level"*, The 3rd International Conference on Automation, Control Engineering and Computer Science (ACECS), March 20-22, Hammamet, Tunisia, 2016.

[17] X. J. Wu, X. J. Zhu, G.-Y. Cao and H.-Y. Tu, *"Predictive control of sofc based on a ga-rbf neural network model"*, Journal of Power Sources, Vol. 179, No. 1, pp. 232-239, 2007.

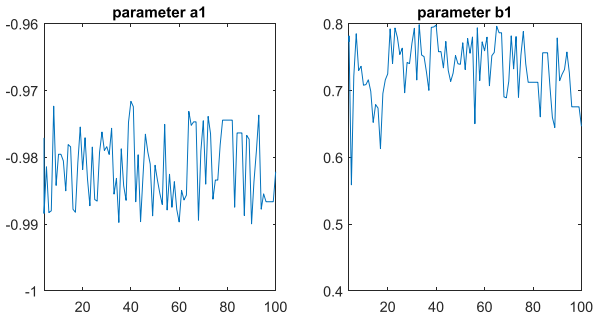


Fig. 4 case 1: Evolution of model estimated parameters

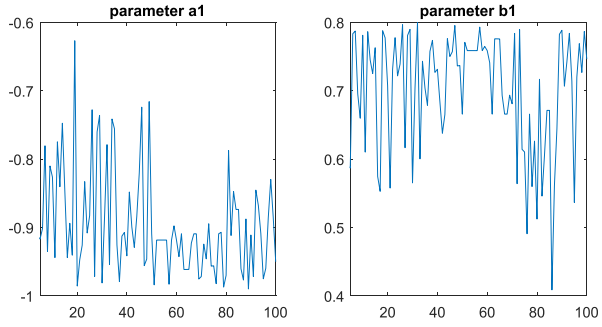


Fig. 5 case 2: Evolution of model estimated parameters

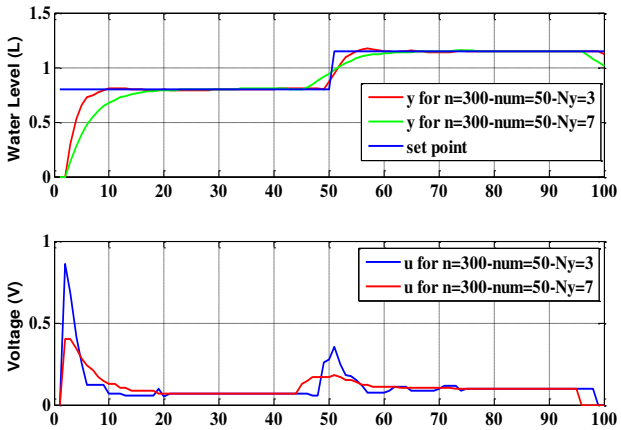


Fig. 6 case 1: Evolution of the output y and the control input u for n=300, num=50, Ny=7 and Ny=3

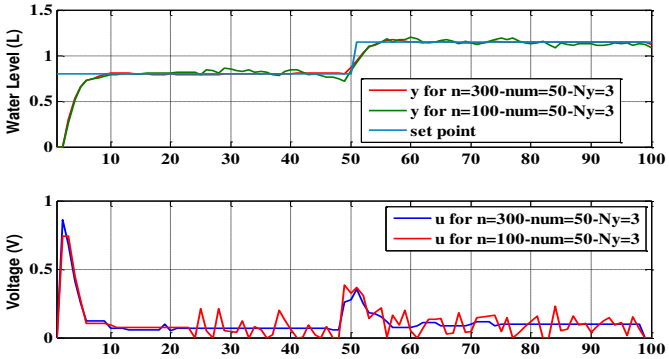


Fig. 7 case 1: Evolution of the output y and the control input u for n=300 and n=100, num=50, Ny=3

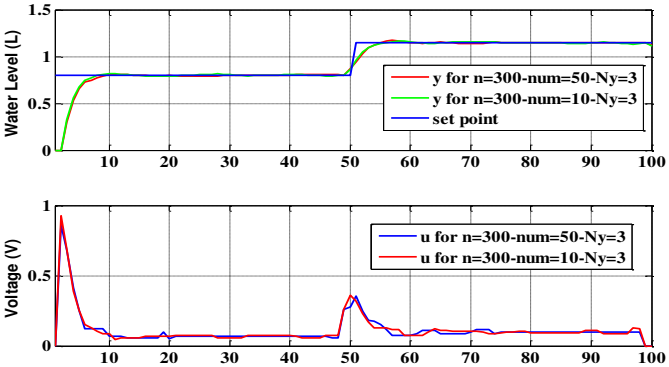


Fig. 8 case 1: Evolution of the output y and the control input u for n=300, num=50 and num=10, Ny=3

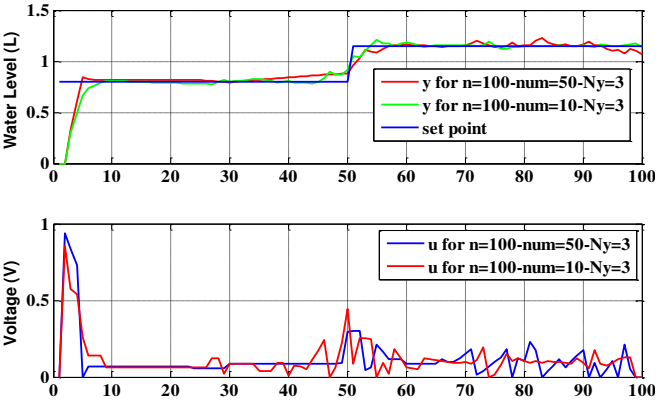


Fig. 9 case 1: Evolution of the output y and the control input u for n=100, num=50 and num=10, Ny=3

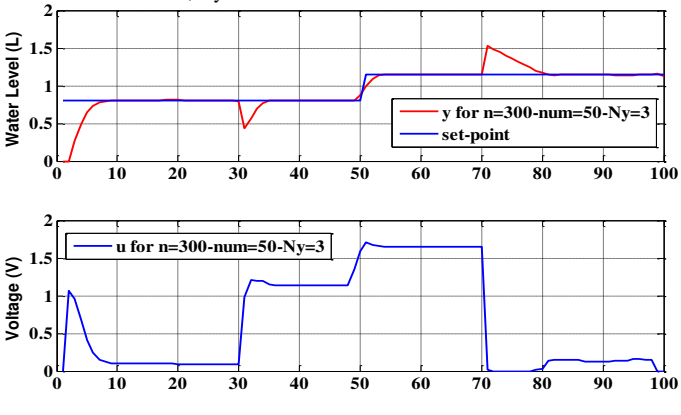


Fig. 10 case 2: Evolution of the output y and the control input u for n=300, num=50, Ny=3




ISSN 1737-9334

# Towards a Knowledge Sharing Mechanism via Digital Networks guided by Communities of Practice and Knowledge Mapping: case of ATM Mobilis

Brahami Menaouer
National Polytechnic School of Oran, Department of Mathematics and Computer Science
Oran, Algeria
mbrahami@gmail.com

Nada Matta
Laboratory ICD/TechCICO, University of Technology of Troyes (UTT)
12 Rue Marie Curie CS 42060/10004, Troyes, France
nada.matta@utt.fr

***Abstract*—with the advent of an economy knowledge-based, the communities of practice (CoPs) constitute for companies interesting structures order to achieve and share their knowledge. Moreover, knowledge / skills mapping (KMap) is seen as a way to improve the sharing and the use of intangible capital, represented especially by the knowledge (tacit and / or explicit), as well as a how to capture best practices in order to foster innovation and help decision making. This paper attempts to understand the knowledge / skills mapping (KMap) which is concretized by an approach to collaboration with the devolvement of communities of practice (CoPs) and devices for knowledge sharing via digital networks, in order to show the actors trades / strategic of organization the interest and importance of this discipline and to describe its possible links to knowledge management. The objective is to trace the best practices and identify devices for sharing knowledge through the digital networks more particularly which are put in place by the operator of the phone mobile ATM Mobilis (Algeria Telecom Mobile Mobilis).**

***Keywords—knowledge management; knowledge mapping; knowledge sharing; digital networks; collaborative networking; system decision support.***

## I. INTRODUCTION

In an economy increasingly based on knowledge, the importance of the production factor "knowledge" increases compared with traditional production factors, we have witnessed the emergence of numerous concepts in order to better manage knowledge (as a central resource) existing at the enterprise level. This knowledge is mainly owned by the actors of the organization and it is necessary to ensure its conservation or at least of prevent errors. Currently, we are strongly interested in the concept of communities of practice because, by definition, they constitute a place to exchange and knowledge sharing more and more useful or even indispensable for companies. Lave and Wenger [13] have defined the CoP as a group of people who come together to share common interests and goals, with the aim of sharing information, developing knowledge and developing themselves both personally and professionally. Furthermore, a CoP is not just a network of connections between people, e.g., a group of people who work in the same building. CoP membership is based on a commitment to the domain of interest and also a shared expertise in that domain.

However, our bibliographic research showed that there are very few works which are dedicated explicitly to the process of knowledge creation within the communities of practice. Communities of Practice (CoPs) [13]; [5]; [6]; [7] are an area of constant study and analysis. Such interest concerns the methods of creation, functioning and management of knowledge in social communities [5]. According to Etty [31], the community of practice is a learning space where both the tacit and explicit dimensions of knowledge are intertwined and developed further. Indeed, Nonaka [12] has developed a framework for knowledge sharing and knowledge creation. New knowledge is created through different modes of knowledge conversion. These modes of conversion are socialization, externalization, combination and internalization and they take place in different forms of interaction across either knowledge management or knowledge mapping.

Proceeding from this observation, we were interested in this paper to bring lighting through of questioning on this emerging concept "community of practice" which constitutes a subject relatively related to knowledge management, which is currently experiencing a resurgence of interest. To this effect, a series of interrogations guided us to lead off our research work: What communities of practice mean? How is realized the process of knowledge sharing in a community of practice? What is meant by knowledge? What does knowledge management and knowledge mapping? What are mechanisms for knowledge sharing via digital networks? Why the communities of practice to ATM Mobilis? With what tools and what methods the company (ATM Mobilis) assures the sharing of practices and knowledge?




ISSN 1737-9334

Our study wishes to bring answer elements to the overall of these questions within the development of collective model knowledge sharing. This analytical model has indeed guided by a grid used during our investigation:

- Studying and show importance and interest of knowledge / skills mapping (kmap) for trades of actors;
- Detect the practices of informative watch and identify devices of knowledge sharing via digital networks and expressed needs;
- Check if the notions of Communities of Practice (CoPs), Knowledge Mapping (kmap) and Knowledge Sharing are genuinely a current preoccupation and well anchored in the professional practices and daily to the ATM Mobilis;
- Studying through a survey carried practices and mechanisms of knowledge sharing via digital networks guided by CoPs and kmap to service of ATM Mobilis.

The overall of study articulates on a willingness for understanding of this new thematic of knowledge sharing guided by communities of practice and by knowledge mapping projected by the revolution in technology of information and communication (ICT) our aim is to improve operational level who these techniques can help for innovation in company. Finally, we conclude summarizing our work and indicating the limits of our approach as well as research prospects.

## II. TEORETICAL FRAMING

This section deals with the main concepts that are employed in this article regarding to context and elements.

### A. *Context and Elements of the management and mapping of knowledge (kmap)*

In the literature, knowledge management is becoming a prime necessity for firms to be competitive in knowledge driven markets. According to Handzic and Durmic [24], Knowledge management (KM) involves collecting, organizing, and distributing knowledge that is accumulated over a period of time for the purposes of improving and increasing a company's competitive edge. On the other side, Knowledge Management (KM) is a cyclic process with a set of activities, techniques and practices that will simplify the process of capturing, creating, storing, distributing and sharing tacit and explicit knowledge [2]. Indeed, tacit/explicit knowledge management is extremely rich and dynamic: It has become necessary to model them. This modeling is to transform large amounts of data, from interviews with experts and searching documents in multiple repositories related to business activities [14], [15]. To this end, a multitude of tools and methods exist for knowledge discovery in data, expert interviews and/or reference materials. These methods are classified into two categories: explicit methods (capitalization) and methods for automatically extracting knowledge [213] (Fig 1)

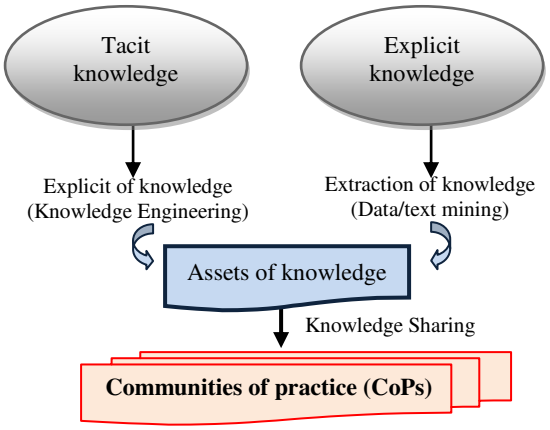


Fig. 1. Explicit and Sharing knowledge

Moreover, knowledge mapping, which is considered as a method of knowledge elicitation, aims to showcase of the trade's critical knowledge of the company [22]. Similarly, it allows for the indication of the importance of knowledge that is at risk of being lost and that must be preserved [23]. Among the problems open from the knowledge mapping, include notably research dynamic of knowledge domains decisional in a knowledge map that is becoming increasingly complex, due to several parameters (number of domains, criteria and degrees of criticality) thereby the evolution of knowledge maps exploiting other sources of enterprise data. Then, it does not allow formalize the data and information in real time. For this, the generalization of the extraction process of knowledge on all available knowledge in the organization (Database, reference documents, enterprise portal) is desirable and possible by the use the data mining techniques [21;22;23].

### B. *Definition and Common Characteristics of Communities of Practice(CoPs)*

Lave and Wenger [13] have defined the CoP as a group of people who come together to share common interests and goals, with the aim of sharing information, developing knowledge and developing themselves both personally and professionally. In addition, Wenger [5] confirmed that community of practice (CoP) defines itself along three dimensions – what it is about, how it functions and what capability it has produced (see table 1).

TABLE I. THREE DIMENSIONS OF A COMMUNITY OF PRACTICE (WENGER 1998)

| Dimension | Description |
|---|---|
| **What it is about** | ***Joint enterprise*** as understood and continually renegotiated by its members |
| **How it functions** | ***Mutual engagement*** that binds members together into a social entity |
| **What capability it has produced** | The ***shared repertoire*** of communal resources (routines, sensibilities, artefacts, vocabulary, styles etc) that members have developed over time |

The joint enterprise, mutual engagement and shared repertoire that Wenger [5] identifies are common across all Communities of Practice. These indicators provide coherent criteria for evaluating communities of practice studies and detecting lack of rigor about a CoP. Furthermore, Preece [16]




ISSN 1737-9334

have described online communities as consisting of people, shared purpose, policies, and computer systems which diminish members' concerns of location and time. CoPs are self-organizing systems whose methods of interaction, rules, issues and lifespan are determined by members, based on the intrinsic value that membership brings [26]. They pursue a shared learning agenda and they create value for their members and stakeholders through developing and spreading new knowledge, practices, capabilities and organizational capacity. They create knowledge networks across professional and hierarchical boundaries, and access the intelligence that is everywhere in the system [10]. Although knowledge within CoPs has gained increasing popularity in managerial literature, the management side of knowledge has been less discussed [7]. According to Joanne [31], the role of communities in the process of learning and knowledge generation has attracted much attention in the context of intra and inter organizational knowledge transfer. Moreover, Communities of practice have become increasingly utilized by organizations as a means of improving performance [8; 36]. In closing, communities of practice can be defined by Al-ghamdia and Al-ghamdib [9] as: "Groups of professionals brought together by shared goals and common concerns regarding participation, exchange, trading, organizing and management of their tacit and explicit knowledge in order to improve their professional performance, as well as the performance of their organizations as a whole. Joshi and Bhardwaj [17] have studied of women involvement in the water and forest management in lesser Himalayan region of Nainital District, India and provides insights into the characteristics of Communities of Practice (CoPs) prevailing in the hill women community for water and forest management of the region.

### *C. Knowledge sharing and knowledge transfer*

In order for that knowledge to create value, it must be shared. The companies may play an important role in process of knowledge generation and transfer, dissemination by establishing necessary collaborative infrastructure to support production development, and collaboration between actors of trades and managers of companies. We have seen in the related work of Knowledge Management that Information and knowledge are critical components of company decision-making, strategic management, regulation, training, innovation and risk management in general. In the early days, knowledge sharing and knowledge transfer were done through passing on of a family secret formula from one generation to another to make unique product. Thus, knowledge can be seen as a source of competitive advantage for many years. For Langley [19], knowledge transfer is embedded in the culture of the effective organizations because they are significantly more likely to value the knowledge transfer processes that are in place.

The author adds that the steps of the Knowledge Transfer Life Cycle [19]:

- Identifying: Determine what knowledge needs to be transferred;
- Capturing: Accumulate the essential knowledge that needs to be transferred ;
- Sharing: Establish methods for transferring the knowledge;
- Applying: Use the knowledge that is transferred;
- Assessing: Evaluate the benefits of the knowledge that is transferred.

According to Järvis and Tint [25], Knowledge transfer focuses on structural capital and the transformation of individual knowledge to group or organizational knowledge, which becomes built into processes, products, and services. Knowledge sharing focuses on human capital and the interaction of individuals. Knowledge transfer includes transfer knowledge at higher level in organization, for instance, group, units, and departments [18].

According to Ryu, Ho and Han [37], knowledge sharing is a people-to people process to exchange knowledge. For an organization, it is very important to have employees, who are willing to share knowledge and are motivated to do this. Christensen [28] determines knowledge sharing as a process of identifying existing knowledge in order to transfer and apply this knowledge to solve common problems in an organization; or a process of creating new knowledge by combining existing knowledge. Cambrera and Cambrera [3] argue that knowledge sharing is a main element in an organization, without it a company could not reach their goals and competitiveness. Likewise, the cost of sharing knowledge is based on a cost of realizing the sharing process (for instance, providing tools, documentation, group meetings etc.).

To summarize, knowledge sharing could be viewed from different perspective, which gives wide understanding of this process. To do an effective knowledge sharing, several factors should be viewed. Likewise, to facilitate knowledge sharing, KM must understand the requirements of the users, as well as the complexities and potential problems with managing knowledge and knowledge sources. Very broadly speaking, the companies must foster a knowledge sharing culture that ensures that these investments are fully utilized.

### *D. Digital Networks*

In the broad sense, a social network refers a set of actors and relationships that they maintain among themselves. Indeed, social networks are playing since long an important role in research on the organizations, especially in the study of professional careers (job search, career, and mobility) [39], of organizational learning [40], of innovation and the access to knowledge or information strategic. According to the great terminological dictionary defines the digital network as a "network in which information, analog or digital, are transmitted by digital links". For the International Telecommunication Union (ITU) has defined ISDN (Integrated Services Digital Network) technology as a network providing digital connectivity from end to end with a wide variety of services.

Furthermore, Reagans and McEvily [33], network structure can affect knowledge transfer independent of the effects of common knowledge and tie strength. Network-based models of social capital emphasize the importance of cohesion



ISSN 1737-9334

and range. The authors have cited that Ingram and Roberts [30] have described how dense friendship networks affected the performance of Sydney hotels. Hotel managers embedded in friendship networks (i.e., managers connected to each other through a dense web of third-party friendship ties) shared customers and best practices, which increased the profitability of their hotels. Reagans and Zuckerman [34] also inferred knowledge transfer from the association between network structure and organizational performance. In their analysis of corporate research and development teams, the authors described how interactions among scientists with non-overlapping networks outside of their team improved productivity. In contrast, Harrison and Hu [1] have cited a approach named Social network analysis of Wasserman and Faust [35] useful for describing the mechanisms through which knowledge is transferred between individuals. A key advantage of using this approach is the ability to examine relationships between individual actors and clusters of actors within a predefined group, like an organization. Bebensee et. Al, [39] argues that online social networks are changing the way individuals share knowledge. These networks, by means of Web 2.0 features, are relevant to processes of knowledge management such as the acquisition, creation and transfer of knowledge [4]. Likewise, digital social networks have the potential to affect significantly the innovative capacity of organizations. Information, knowledge and sources of knowledge troll these networks potentially generating new understanding [4].

En closing, the transfer of knowledge within a network is dependent upon the characteristics of a series of dyadic relationships [1].

## III. Research Methodology

### A. *The method: A case study*

In the framework of the research wearing on a knowledge sharing mechanism via digital networks guided by communities of practice (CoP) and knowledge capitalization, we base our choice on two working methods: the ***content analysis*** and ***the inquiry*** with an ***analysis grid***.

In the content analysis, it's about of a bibliographical study constituted an analytical or critical reading of the reference documents, strategy, quality or the documents on the referential of competences of the ATM Mobilis available in order to identify elements that could help us better understand the problematic and the fundamental concepts of our research work. Moreover, we have completed our methodological approach by researching the web (Intranet and Company Portal) grace to which we have able to structure the literature review in order to draw the history of best practices and lessons learned. This task requires an important analytical capacity. Likewise, the other Information sources include documentation on the organization of its communities of practice that we have collected on the Intranet network (Company Portal, Forum, etc...).

The field survey method has been chosen in order to meet the interlocutors, such as unit managers or the members of the executive committee, faced with the problems the communities of practice and mechanisms of knowledge sharing from day to day; understand the way of which they apprehend and consider the tools and the resources implemented. This survey was consolidated with a few actors of strategy of the ATM Mobilis. It consisted before any into the presentation of knowledge mapping and the communities of practice; are coming afterwards the description of the practice and knowledge networks implemented and finally the analysis of the organization the communities of practice to ATM Mobilis.

It seemed to us useful later to engage in an analysis to the Appendix of the ATM Mobilis of the Oran city through a field survey on the knowledge sharing diagnosis; the needs and practices of the actors of trades and the existing potential in terms of communities of practice and the level of use of computer tools. This has necessitated the preparation of a questionnaire and an analysis structure. The results of this survey are rendered in graphic form, especially in the form a radar diagram (Diagram of Kiviat). A balance sheet of the conclusions concerning on the syntheses carried assorted of the proposals completes the second part of the relative study on the practical application of the capitalization of knowledge to the ATM Mobilis.

In this context, we have proposed a know-how map representation (inspired by Mind map in a process driven logic) and a data collection technique adapted to the interviewees' profile. The data collection was carried out on a period of 5 months from January 2015 to May 2015, based on a series of semi-directive interviews with a number of senior executives of the ATM Mobilis and the Regulatory Authority for Post and Telecommunications, complemented by a thorough exploitation of reference documents which was provided to us.

The data gathered on the ground guided us in the construction of our knowledge mapping, which we briefly describe in two major steps; 1) Building the process Know-how map using the principal of BKMDM (Boolean Knowledge Mapping guided by Data Mining) method and 2) Assessing the process know-how map by interviewing the trade's actors according to the criticality grid defined by the Knowledge Management Club.

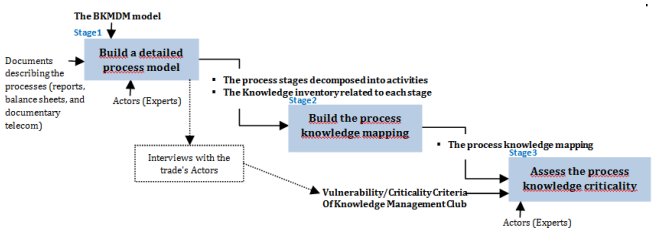


Fig. 2. *The major stages of the critical knowledge modelling approach guided by BKMDM Method*

For this, each criterion is evaluated on a level scale from 1 to 4. The levels of each criterion are carefully described and presented to the interviewee. This systematic approach is certainly useful in facilitating the evaluation exercise. Nevertheless, it requires a high level of professionalization




ISSN 1737-9334

and abstraction on the part of the interviewees, which is a not so obvious condition to satisfy for our case study. For instance, knowledge with high criticality according to the criterion "Difficulty in identifying sources" and "Difficulty using knowledge" advocates expertise localization through the identification of the experts holding this critical knowledge and use of this knowledge at the company level.

Finally, this building of knowledge mapping (See figure 2) helps us to start the second phase of our project which is the diagnosis of information and knowledge sharing, the attitudes to teamwork, and the participation in communities of practice.

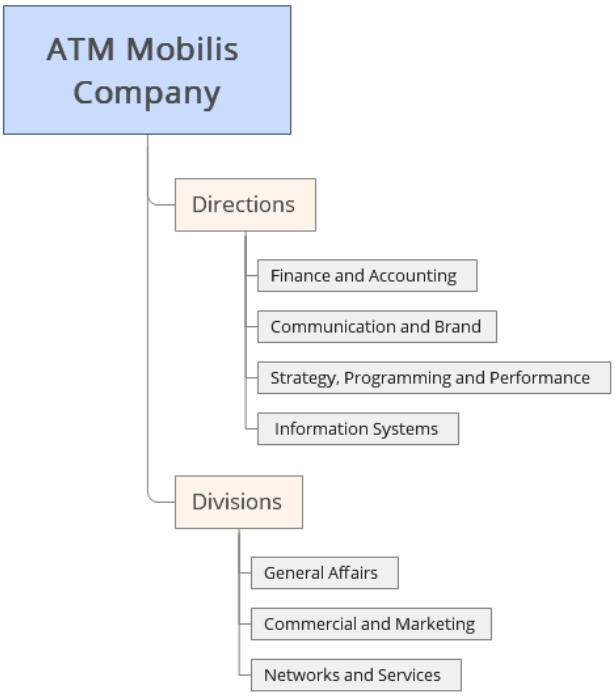


Fig. 3. *The knowledge mapping of the principal divisions and directions to the ATM Mobilis*

We have defined a research protocol approach combining to both qualitative and quantitative [20]. Remember that at this step several tools collection of data has been used.

In qualitative terms, a sample was organized aimed about thirty experts (actors of trades and strategies) of the ATM Mobilis on an effective of the quarantine, is a participation rate of 86.6%. Note that our survey, an analysis grid listing the principal themes to be addressed especially the diagnosis of knowledge sharing, the needs and practices in information of the actors of trades, the existing potential in terms of virtual community and the use of computer tools has been developed in order to able to direct the interviews with respondents.

In quantitative terms, research was based on a grid of 20 surveys of which 10 relate to the diagnosis of the knowledge sharing, 4 on the needs and practices information of the actors of trades and 6 on the existing potential in terms of virtual communities and the level of utilization of the computer tools.

Finally, we found it useful to note that in all of the field survey carried out, the chosen approach is an approach more of the qualitative type than quantitative which aims to draw some findings which will serve to illustrate a certain number of working hypotheses compared to the understanding of the knowledge capitalization and the knowledge transfer mechanisms.

The communities of practice of the ATM Mobilis it possible to ensure the development increased of all thematics responsibilities and operational of the organization and aimed at ensuring that actors of trades be able to build on the capabilities and expertise available within the organization a view to exchanging, sharing of knowledge and experiences, identify practical solutions agreeing to the different situations of the directions.late as follows. The compilation and use of collective experience in terms practices constitute an important part of the implementation of a culture of practice within the ATM Mobilis and the construction of organization based on the knowledge. This process allows the actors of trades to use so as more effectively the knowledge of the organization through access to a knowledge document center at the national scale (in all city of Algeria).

The knowledge / skills map in terms of practice and information sources to this end a tool which has been designed to transfer some attributes of tacit or explicit knowledge in graphic form readily understandable by end users (managers, experts, engineers, etc.). The data collection, the construction of the map and evaluating different knowledge domains (know-how trades) are based on a work of extraction of expert knowledge. At this level, the focus is now placed on substantive capabilities or of the information. This knowledge / skills mapping based on the creation and development of communities of practice to the ATM Mobilis in order to be able to search and identify experts, developers and practitioners possessing internal information sources of being used for different initiatives and also to identify the domains in which the ATM Mobilis intends to strengthen its capabilities. The expected benefits may be, for example, the encouragement of each actors of trades at obtain an appropriate level of information, the knowledge and the experience on the practical and the knowledge share with persons are located on the inside and outside of the ATM Mobilis.

Finally, we present the results of the survey conducted among of the actors of trades of the ATM Mobilis. In the three themes of the survey conducted on field, namely the diagnosis of the knowledge sharing mapped, needs and practices in information of the actors and the existing potential in terms for virtual communities and the level of use of computer tools:

- Develop a pedagogy of digital uses in confidence around a public awareness program to the stakes Faced with the collaboration and exchange of information, we notice through the field survey that over half of the respondents in the directions in the proportion of 66.23% (12 on 20) make appeal more to their immediate colleagues to solve a problem professional in their daily activities being based on the knowledge / skills mapped. In addition, we also find that 61.53% of respondents (10 on 20) believe that they have quite often or always of the time for exchanging information



ISSN 1737-9334

with colleagues. What appears a fact positive 30.76% say they have sometimes or enough often of the time to spend with their colleagues against 7.69% only who declare that they had never or have rarely;

- Faced with the participation in communities of practice, we find that the data related to the knowledge of participants on the existence of communities of practice to the ATM Mobilis show that the set of respondents are aware of their existence either 20 on 20 (100%) but paradoxically little have adhered to at least one of the networks of practice and knowledge either 15 on 20 (42.30%). Note that the evaluation of communities of practice by the participants in these activities was measured by a question very global on the degree of satisfaction related to their participation;

- Faced with the use of permanent manner of computer tools which is one of the highlights of the ATM Mobilis. This is felt to through the results on the question pertaining to the permanent access to a computer and to the Internet. To this effect, we find that all respondents, either 100%, have access to a computer, to the Internet and to the Intranet: This facilitates things for information exchange and knowledge sharing. The respondents have also to pronounce on the tools used to share and exchange information with colleagues. In fact, we remark that a large majority considers the phone, the email, the discussion forums, the company portal and the intranet as the most prized tools successively in the proportion of 96.15% (19 on 20) while the internal information bulletin and video conferencing come in 2nd positions. Consequentially upon our previous objective, we have also wanted to know whether respondents had an adequate training level for the use of computer tools advanced; we find that 92% of respondents (18 on 20) assert to have followed an internal and external training on the use of these tools. Indeed, The ATM Mobilis has organized online training courses for intended all its actors of trades for an upgrade of advanced computer (Soft and Hard) and ICT (see figure 3).

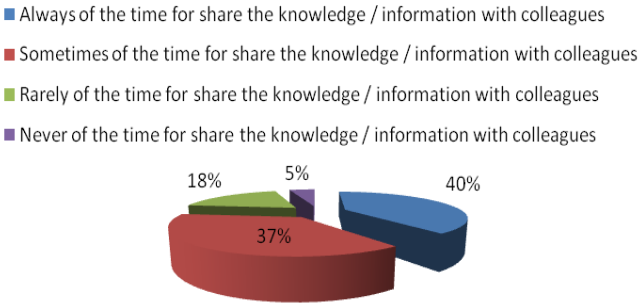


Fig. 4. Attitudes about the cooperation and information exchange

Finally, the risk management of a project requires to capitalize the know-how and the experience gained and to establish rigorous documentation about risks associated with the project (see figure 4).

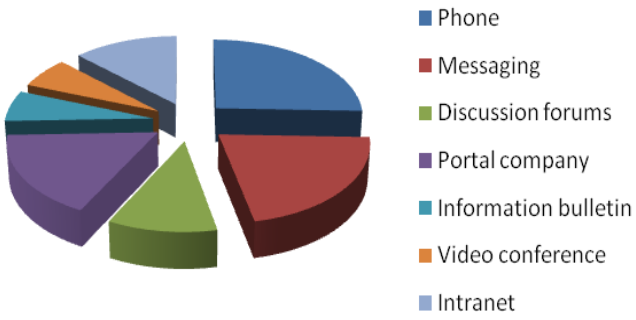


Fig. 5. *Tools used for knowledge sharing*

## IV. Conclusion

This paper is an attempt to comprehension of a new thematic into emerging: knowledge Mapping (kmap) which is concretized in its approach to Collaboration by the establishment the communities of practice (CoPs) and the knowledge sharing devices via digital networks, in order to show to the actors trades of the ATM Mobilis telephony operator in Algeria, interest and importance of this discipline and describes its potential links with knowledge management. Our study has demonstrated clearly that communities of practice (CoPs) and knowledge mapping (kmap) are a veritable environment of sharing and exchange between professionals of a given domain via digital networks. More precise manner, they present the advantage to take over a large share of fixed costs inevitably associated with the need to build and exchange knowledge in conditions of often more effective and less costly than the classic institutional mechanisms.

Finally, our study opens the way on future research such as the creation of an information watch cell, the conception and the organization of a knowledge base across the communities of practice guided by the extraction of new knowledge from data and / or text (data mining & text mining) and the creation of a virtual information center for ATM Mobilis.

### *Acknowledgment*

This project is registered in the context of collaboration between the ATM Mobilis Company, our research team of the laboratory ICD/TechCICO, University of Technology of Troyes (UTT), LIO Laboratory in University of Oran 1, and the National Polytechnic School of Oran (ENPO). The authors also acknowledge the service team of ATM Mobilis for her assistance on to finalize this project.

### *References*

[1] A. Harrison, and Q. Hu, "Knowledge Transfer within Organizations: A Social Network Perspective", 45th Hawaii International Conference on System Sciences, IEEE Computer Society, 2012, pp. 1-10.

[2] A. Mian, P. Helo and T. Kekäle, "Critical factors for knowledge management in project business", Journal of Knowledge Management (JKM), Vol. 14 N°.1, 2010, pp. 156-168.




ISSN 1737-9334

[3] A. Cambrera, and E. Cambrera, "Knowledge-Sharing Dilemmas", Organization Studies, 23(5), 2002, pp. 687-710.

[4] C. Mussi, M. Terezinha Angeloni, and R. Avila Faraco, "Social Networks and Knowledge Transfer in Technological Park Companies in Brazil", Journal of Technology Management & Innovation, Vol. 9, Issue 2, 2014, pp. 172-186.

[5] E. Wenger, Communities of Practice. Learning, Meaning, and Identity. Cambridge: Cambridge University Press, 1998.

[6] E. Wenger, and William M. Snyder, "Communities of Practice: The Organizational Frontier" in Harvard Business Review, January-February 2000.

[7] E. Wenger, "Communities of practice a brief introduction", 2006, Retrieved January, 5, 2015 form http://www.ewenger.com/theory/

[8] E. Wenger, "Communities of practice—A brief introduction". Retrieved February 15, 2007, from http://www.ewenger. com/theory/index.htm

[9] H. Al-ghamdia K., and A. Ali. K. Al-ghamdib, "The Role of Virtual Communities of Practice in Knowledge Management Using Web 2.0", International Conference on Communication, Management and Information Technology (ICCMIT 2015), ScienceDirect, Procedia Computer Science 65 ( 2015 ), pp. 406 – 411.

[10] I-C. Tsai, "Understanding Social Nature of an Online Community of Practice for Learning to Teach", Educational Technology & Society, Vol :15 (2), 2012, pp.271–285.

[11] I. Nonaka, and H. Takeuchi, The Knowledge-Creating Company, Oxford University Press, Oxford, New York, 1995.

[12] I. Nonaka, "A Dynamic Theory of Organizational Knowledge Creation". Organization Science/ Vol. 5, No.1, 1994.

[13] J. Lave, and E. Wenger (1991): Situated Learning: Legitimate Peripheral Participation. Cambridge University Press.

[14] J.L. Ermine, "A Theoretical and formal for Knowledge Management Systems", dans D. Remenyi, 2nd International Conference on Intellectual Capital and Knowledge Management (ICICKM'2005), Dubia, United Arab Emirates (U.A.E), 2005, pp. 187-199.

[15] J.L. Ermine, I. Boughzala, T. Tounkara, "Critical Knowledge Map as a Decision Tool for Knowledge Transfer Actions", The Electronic Journal of Knowledge Management, Vol.4, Issue 2, 2006, Available online : http://www.ejkm.com, pp.129-140.

[16] J. Preece, "Tacit knowledge and social capital: Supporting sociability in online communities of practice", Proceedings of I-KNOW 2003, 3rd International Conference in Knowledge Management. Graz, Australia, July 2-4.*In* K. Tochtermann and H. Maurer, pp.72-78.

[17] K. Joshi, and N. Bhardwaj, "Women And Natural Resource Management: A Study Of 'Communities Of Practice'", Prevailing In Women Farmers' Community for Management of Water and Forests of Lesser Himalayan Region in India, International Journal of Advanced Research (2015), Volume 3, Issue 7, pp.363-374.

[18] L. Argote, and P. Ingram, "Knowledge transfer - a basis for competitive advantage in firms", Organisational Behaviour and Human Decision Processes, 82 (1), 2000, pp. 150-169.

[19] M. A Langley, Capturing the value of project management through knowledge transfer, Project Management Institute, Inc. PMI.org/Pulse, March 2015, PP. 1-32.

[20] M. B, Miles, and A. M, Huberman, Analyse des données qualitatives, Editeur : De Boeck ; Édition : 2ème édition (8 janvier 2003), Collection : Méthodes en sciences humaines, pp.626-632.

[21] M. Brahami, B. Atmani, and N. Matta, "Using rules to enhance evolution of knowledge mapping: Application on Healthcare", International Journal of Computer Science Issues (IJCSI), Vol. 10, Issue 3, May 2013, pp. 261-270.

[22] M. Brahami, B. Atmani, and N. Matta, "Dynamic knowledge mapping guided by data mining: Application on Healthcare", Journal of Information Processing Systems, Vol. 9, N°1, March 2013, pp. 1-30.

[23] M. Brahami, B. Atmani, and N. Matta, "An approach to dynamic fusion of the knowledge maps of an activities process: Application on Healthcare", International Journal of Information Systems in the Service Sector, Vol. 7 Issue 4, October 2015, pp.1-25.

[24] M. Handzic, and N. Durmic, "Knowledge Management, Intellectual Capital and Project Management: Connecting the Dots", The Electronic Journal of Knowledge Management, Vol.13 Issue 1, 2015, pp. 51-61.

[25] M. Järvis and P. Tint, "Knowledge Transfer – Critical Components in Occupational Health and Safety – an Estonian Approach", Symposium Series NO. 154, 2008 IChemE, PP.1-13.

[26] M. Sharratt, and A. Usoro, "Understanding knowledge-sharing in online communities of practice", Electronic Journal on Knowledge Management, 1(2), 2003, pp.187-196.

[27] N. Matta, and J.L. Ermine, "knowledge capitalization with a knowledge engineering approach: the MASK method", IJCAT'2001, knowledge management and organisational memory workshop. International Joint Conference on Artificial Intelligence, seattle, Etats-Unis, 4-10 août 2001.

[28] P. Christensen, "Knowledge Sharing: Moving Away From the Obsession With Best Practices", Journal of Knowledge Management, 11(1), 2007, pp. 36-47.

[29] P. Van Berten, J.L. Ermine, "Applied Knowledge Management: a set of well-tried tools". The Journal of Information and Knowledge Management Systems, vol.36, 4, 2006, pp.423-431.

[30] P. Ingram, and P. Roberts, "Friendships among competitors in the Sydney hotel industry", American Journal of Sociology, 2000, 106: 387-423

[31] R. Etty N., "Organizing for the sharing and creation of knowledge - are we too afraid to kill it?", Conference at the University of Warwick (OLKC 2006), 20th - 22nd March 2006, pp. 1-25.

[32] R. Joanne, "Questioning the Place of Communities of Practice, Durham Business School", Conference at the University of Warwick (OLKC 2006), 20th - 22nd March 2006, pp. 1-25.

[33] R. Reagans, and B. McEvily, "Network Structure and Knowledge Transfer: The Effects of Cohesion and Range Author(s): Source: Administrative Science Quarterly, Vol. 48, No. 2 (Jun., 2003), pp. 240-267.

[34] R. Reagans, and E. Zuckerman, "Networks, diversity and performance: The social capital of R&D units." Organization Science, 12, 2001, pp.502-517.

[35] S. Wasserman and K. Faust, Social network analysis: Methods and applications, Cambridge, UK, Cambridge University Press, 1994.

[36] S. J. Kerno, "Limitations of Communities of Practice A Consideration of Unresolved Issues and Difficulties in the Approach", Journal of Leadership & Organizational Studies Volume 15 Number 1 August 2008, pp. 69-78.

[37] S. Ryu, S. Ho, and I. Han, Knowledge Sharing Behavior of Physicians in Hospitals. Expert Systems with Applications, 25, 2003, pp. 113–122.

[38] S. Ventolini, Quelles explications au réseau de développement professionnel redondant versus non redondant, In Lecoutre M. et Lièvre P. Management et réseaux sociaux : ressource pour l'action ou outil de gestion, ed. Hermès, 2008.

[39] T. Bebensee, Helms, R., and M. Spruit, "Exploring Web 2.0 applications as a means of bolstering up knowledge management", Electronic Journal of Knowledge Management, vol.9, 2011, pp.1-9.

[40] V. Chauvet, La dynamique d'apprentissage dans les PME technologiques : le rôle ambiguë du réseau personnel du dirigeant, In Lecoutre M. et Lièvre P. Management et réseaux sociaux : ressource pour l'action ou outil de gestion, ed. Hermès, 2008.




ISSN 1737-9334

# Optimization the concentration doping of emitter layer for InGaP /GaAs hetero-junction solar cell using the SILVACO ATLAS software

Dennai Benmoussa[*1],Fillali Mostefa[#2],Atouani Toufik [*3]

*Matter Sciences Departement, Faculty of Exact Sciences, Université Tahri Mohammed Béchar
[#]Laboratory of Semiconductor Devices Physics,University of Bechar, Algeria
[1]deennai_benmoussar@yahoo.com
[2]filali_mustapha@yahoo.fr
[3]toufikatouani1972@yahoo.fr

***Abstract*— The photovoltaic power (PV) is obtained by direct conversion of sunlight into electricity by means of PV cell. Performance optimization of InGaP/GaAs heterojunction solar cell can be done by acting on some components and parameters of this cell. The main objective of this work is to optimize the efficiency by varied the concentration doping of emitter layer of this type of solar cell, which is limited by multiple losses in particular those related to photons and carriers. The performances of the chosen model, of this InGaP/GaAs heterojunction, are obtained by using Silvaco-Tcad.**

**The optimisation result shows that the maximum efficiency of 21.68% % has been achieved, with short circuit current density of 32.29mA/cm$^2$, open circuit voltage of 0.82V and fill factor of 0.81%.**

***Keywords*—Performance,Solar cells, heterojunction, InGaP/GaAs. Silvaco-Tcad.**

## I. INTRODUCTION

The use of solar cells is currently one of the best solutions to the energy problems. Solar cell design stared with the simple single junction ones and later moved on to multijunction cells that are used in space applications [1]. There has been considerable interest in recent years in heterojunction device such as the solar cell. At present time, the GaAs /AlGaAs and InGaP/GaAs heterojunction represent a great interest. As shown in Fig.1, This type of cells are made up of materials with different band-gap which are connected back to back and cover a wide range of sun's spectrum.

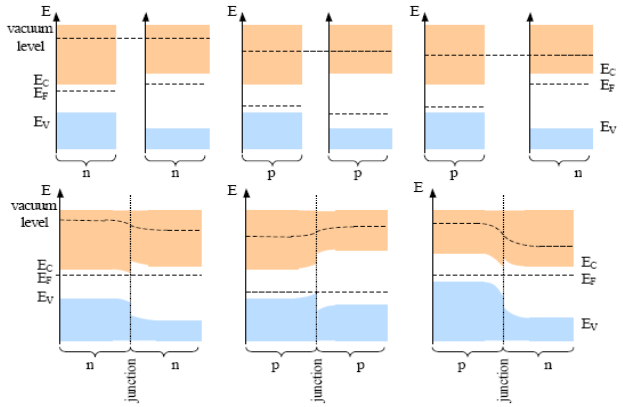


Fig 1 : Band diagram of heterojunction formation[2].

The major goal of heterojunction solar cell design is to maximize the output power for a given solar spectrum. High efficiencies could be obtained by stacking together different absorbers with different band-gaps to maximize the light absorption.[3]

Numerical modelling and simulation help to optimize the solar cell structure in understanding of main physical phenomena, thus decreasing the time and cost for development [4]. The SILVACO ATLAS can be used for the design of III-V heterojunction solar cell. The doping layer concentration of the solar cell is a very important parameter. But the obtaining of the optimal values of the latter, often depends on many complicating factors.

In this work, we report the optimum design of InGaP/GaAs heterojunction solar cell by varying the concentration doping of the emitter layer using the SILVACO ATLAS software. The results obtained show that all output parameters (Isc ,Vco , FF ,$\eta$) are influenced and vary with the concentration doping of the base layer.




ISSN 1737-9334

## II. DEVICE STRUCURE

Figure 1 shows the schematic diagram of the heterojunction solar cell used in the simulation. The device consists of four regions which are ZnO (cathode), n-InGaP (emitter), p-GaAs (base) and Molybdenum (anode). The effects of heterojunction are manifested because the materials used do not have the same parameters as the band gap, the electronic affinity, the density of states and the mobility of the charge carriers. The dominant recombination mechanism in this study is Shockley - Read - Hall and Auger, similar to Si [5].

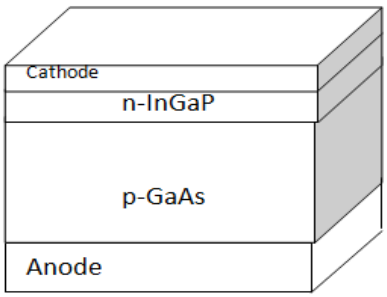


Fig 2 – Schematic representation of the sample structure.

The following table (I) summarizes the parameters of the solar cells used in the simulation [6, 7].

TABLE I
PARAMETERS OF THE INGAP/GAAS HETEROJUNCTION SOLAR CELL

| **layer** | **Cathode** | **emitter** | **base** | **Anode** |
|---|---|---|---|---|
| material | ZnO | GaInP/n | GaAs/p | Molybdenum |
| Thickness( µm) | 0.0001 | 0.5 | 5 | 0.0001 |
| Bandgap Eg (eV) | / | 1.75 | 1.41 | / |
| doping densities ($cm^{-3}$) | / | $1x10^{16}$ to $1x10^{21}$ | $2x10^{16}$ | / |

## III. - MODELING PROCESS

The simulator used works on mathematical models to calculate a solar cell structure; ATLAS solves Poisson's equation, carrier continuity equation, the drift-diffusion transport model and the energy balance transport model [8].

Poisson's equation relates variations in electrostatic potential to local charge densities. The continuity and transport equations describe the way that electron and hole densities evolve as a result of generation, recombination and transport processes [9].

In this work, the models used to optimize the structure are [10]:

**AUGER** specifies Auger recombination;

**CONMOB** specifies that a concentration dependent mobility model be used for silicon and gallium arsenide. This model is a doping versus mobility table valid for 300K only;

**OPTR** selects the optical recombination model. When this parameter is specified, the COPT parameter of the **MATERIAL** statement should be specified;

**SRH** specifies Shockley-Read-Hall recombination using fixed lifetimes;

**FERMIDIRAC** specifies that Fermi-Dirac carrier statistics be used;

**SRH** specifies Shockley-Read-Hall recombination using fixed lifetimes;

The major parameters of the solar cell which are given as [11]:

The total current ($I_{total}$) is calculated by the following equation:

$$I_{tot} = I_0 \left[ exp\left(\frac{qV}{nKT}\right) - 1 \right] - I_l$$

where $I_L$ is the light generated current. The open circuit voltage (Voc) is given by:

$$V_{co} = \frac{nKT}{q} \ln\left(\frac{I_L}{I_0} + 1\right)$$

However the Fill factor (FF) is illustrated by:

$$FF = \frac{V_{oc} - L_n\,(V_{oc} + 0.72)}{V_{oc} + 1}$$

and the conversion efficiency ($\eta$) by:

$$\eta = \frac{V_{oc} I_{sc} FF}{P_{in}}$$

## IV. RESULTS AND DISCUSSIONS

Optimization of the solar cell has gone through two essential steps. The first is the creation of a model of the cell using the appropriate structural and material characteristics. The second step is an iterative routine to adjust the doping concentration of the emitter layer (from $10^{16}$ $cm^{-3}$ to $10^{21}$ $cm^{-3}$).

Figure 3 shows Atlas regions with materials defined:

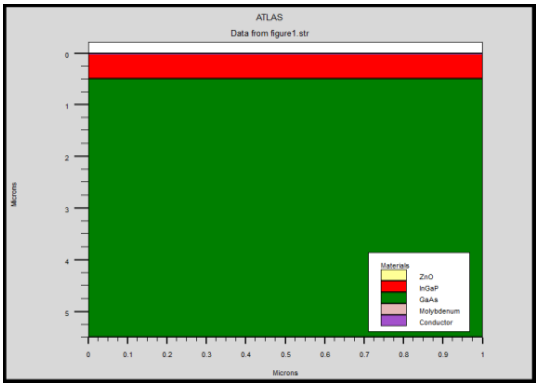


Fig.3. Atlas regions with materials defined

As shown in the figure 4, the first step is specifying the mesh on which the device will be constructed.




ISSN 1737-9334

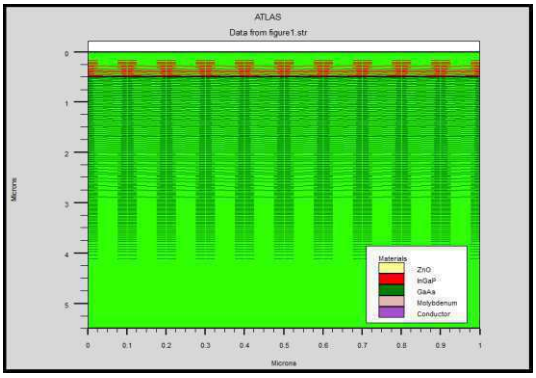


Fig4. Mesh structure of the model.

The physical and optical parameters of the materials used to build the solar cell, were obtained from the SILVACO ATLAS software.

### *A. The effect on short circuit current :*

The effects of the InGaP (n) doping concentration on the short circuit current of the solar cell are shown in Fig.5. The results show the short-circuit current are both increased due to higher the doping concentration but a slight increase by any percentage and this indicates that there is no significant effect to focus on and this due to the increase of the electric field but there is a lack of thickness of space charge area.

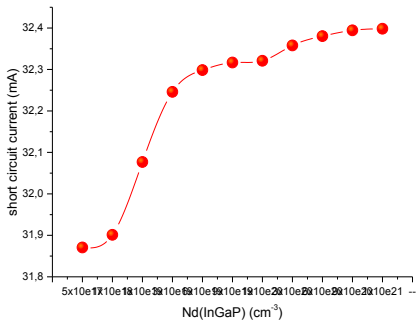


Fig5. Effects of the emitter doping concentration on the short circuit current of the solar cell.

### *B. The effect on open circuit voltage:*

Figure 6 shows the variation the open circuit voltage versusof emitter doping concentration o heterojunction solar cell optimesed.The remarks there are three phases:

- First there is a decrease in open circuit voltage every increasedoping concentration.
- The second phase is an increase open circuit voltagefor each increasedoping concentration.
- The third phase decreasesin open circuit voltage.

This is explained by the great value of Voc= 0.8199 V when Nd=$6x10^{19}cm^{-3}$, If it is Nd<$6x10^{19}cm^{-3}$ less than the electric field is weak and if it is Nd>$6x10^{19}cm^{-3}$ the thickness ofspace charge areais small.

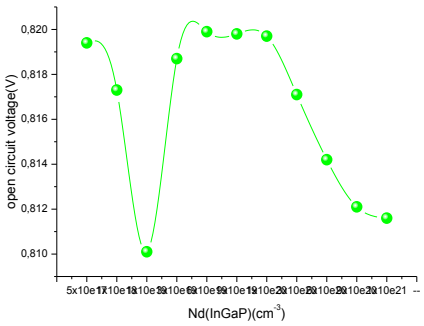


Fig5. Effects of the emitter doping concentration on the open circuit voltage of the solar cell.

### *C. The effect on fill factor:*

The fill factor as a function of the doping concentration of emitter layer is represented in Fig. 6.We observedfor the maximum value of FF=81.88% for Nd= $6x10^{19}cm^{-3}$.

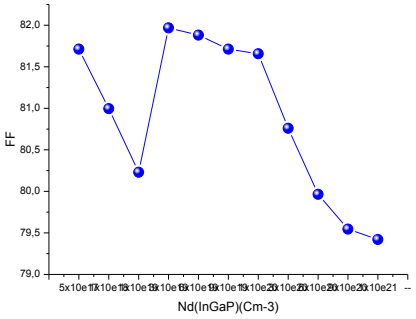


Fig6. Effects of the emitter doping concentration on fill factor

### *D. The effect on efficiency:*

Fig.7 is the efficiency of the solar cell accordingn-type doping concentration. We can distinguish three different behaviours; the first,for Nd<$6x10^{17}cm^{-3}$, where a significant decrease of efficiency is obtained decrease of Voc. The second behaviour is observed for $6x10^{17}$<Nd<$6x10^{19}$ increase of efficiency.The thirdbehaviour is observed for $6x10^{19}$<Nd<$6x10^{21}$decrease of efficiency is obtained decrease of fill factor.


ISSN 1737-9334

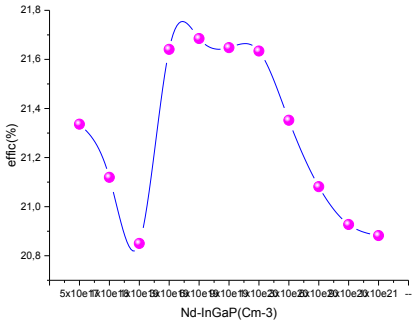


Fig7. Effects of the emitter doping concentration on the efficiency

### *E. Optimal Structure*

From the above results are obtained using the SILVACO ATLAS software.we can determine the best performance of heterojunction solar cell(InGaP/GaAs) which has while giving the doping concentration of emitter layerof the cell.

In Table Ii, we recapitulate the photovoltaic parameters of optimised cells.

TABLE III
OPTIMISED PHOTOVOLTAIC PARAMETERS

| **Doping level ($cm^{-3}$)** | **Isc($mA/cm^{-2}$)** | **Voc(V)** | **FF(%)** | **$\eta$(%)** |
|---|---|---|---|---|
| $6x10^{19}$ | 32.2986 | 0.8199 | 81.8810 | 21.6850 |

The current-voltage characteristics for the device heterojunction solar cell layers with the optimal efficiency for PN structure are shown in Fig. 7,

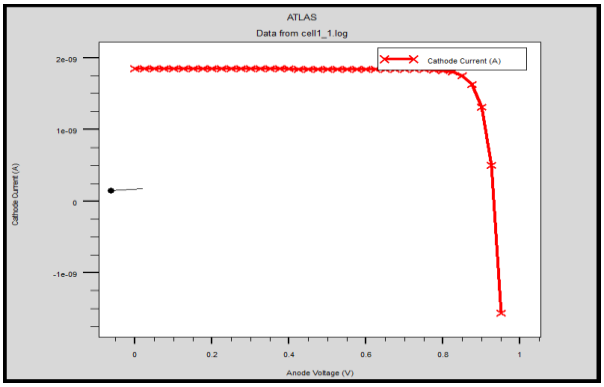


Fig. 7 – I(V) characteristic of the heterojunction solar cell with the optimum performance Silvaco ATLAS simulation

## V. CONCLUSIONS

In this paper, we studied InGaP/GaAsheterojunction solar cell device. Modelling and simulation were performed by using ATLAS-TCAD simulator. Our simulations prove the quality and validity of our model for modelling electronic characteristic of the InGaP/GaAs heterojunction solar cellstudied.

In this design, it has been found that the inclusion of a heterojunction InGaP/GaAs solar cell due. The efficiency has been optimised by changing the doping concentration of the emitter layer.Optimizedemitter material results in Jsc = 32.2986mA/cm$^2$, Voc = 0.82 V with significant enhancement in conversion efficiency up to 21.65% (1sun).

## REFERENCES

[1] B. Dennai et al., "Modeling of Cascade Solar Cell Ga0.5In0.5P /GaAs Using AMPS-1D", Advanced Materials Research, Vol. 685, pp. 174-178, 2013

[2] Panayiotis Michalopoulos, A NOVEL APPROACH FOR THE DEVELOPMENT AND OPTIMIZATION OF STATE-OF-THE-ART PHOTOVOLTAIC DEVICES USING SILVACO, THESIS ser. Lecture Notes in Statistics. NAVAL POSTGRADUATE SCHOOL Monterey, California, 2002,

[3] Fuhs, W., Korte, L., Schmidt, M., 2006. Heterojunctions of hydrogenated amorphous silicon and monocrystalline silicon. Journal of Optoelectrontics and advanced materials 8, 1989-1995.

[4] *ATLAS User's Manual* – Device SimulationSoftware, SILVACO, Santa Clara, USA 2009.

[5] Atanu Bag, "Heterojunction Solar Cells," Computer Aided Design of Micro- and Nanoelectronic DevicesEdition: 1Chapter: 13, Nov. 2016.

[6] ] S.Adachi, "GaAs, AlAs, and Al x Ga1−x As: Material parameters for use in research and device applications", J. Appl. Phys, Vol. 58, pp.R1-R29, 1985..

[7] I. Vurgaftman, J.R. Meyer, L.R. Ram-MohanBand parameters for III–V semiconductors and their alloysJ. Appl. Phys., 89 (2001), p. 5815

[8] ***ATLAS** User's Manual*. Device simulation Software. Volumes I and II. Silvaco International (2002).

[9] S. Selberherr, Analysis and Simulation of Semiconductor Devices, Springer-Verlag, Wien-New York, 1984.

[10] Atlas User's Manual Device Simulation Software ; Silvaco, Inc. 4701 Patrick Henry Drive,Bldg. 2 Santa Clara, CA 95054 October 2, 2013.

[11] Hemmani Abderrahmane, B. Dennai, H. Khachab, A. Helmaoui," Effect of Temperature on the AlGaAs/GaAs Tandem Solar Cell for Concentrator Photovoltaic Performances" J. Nano- Electron. Phys. 8 No1,01015(2016)




ISSN 1737-9334

# A Preformance of Photovoltaic Generator

[1]Eman Abdelsalam Garmoud and [2]Amal Jamal Boukar

Tripoli University, Faculty of Education - Janzour
Tripoli- Libya
[1]E-mail EA.phy2017@gmail.com
[2]E- mail **amal_boukar@yahoo.com**

*Abstract*—Photovoltaic Generators are important generators for the application of renewable energy sources because of the direct conversion of solar energy to electric energy. They have some advantages such as low weight and feasibility of small scales, but they are more expensive compared to other types of energy converters. Therefore, it is important to absorb the output power of the system.

This paper describes a method of modeling and simulation photovoltaic (PV) module that implemented in Simulink/Matlab, using a different DC-AC converter efficiency varying from 80%, 90% and 98% and getting the result of the output AC power, also Solar panels varies during the test to experiment the effect of adding more solar panels while the DC-AC converter efficiency is assumed to be a fixed 98 percent.

***Keywords—DC-AC converter ; Photovoltaic; solar panel; efficiency;***

## I. INTRODUCTION

Solar energy is one type of the renewable energy sources which can be converted easily and directly to the electric energy by Photovoltaic Generators. The process of no movable mechanisms to convert solar energy to electric energy is called photovoltaic phenomena whereas the conversion device is called solar panel [1].

Solar panel convert the energy of light's photons to electric energy with efficiency between 5 to 25 percent without using thermodynamic cycle or active fluid. And it can be light collector directly or can use a light concentrators like mirror or convex lens.

The photovoltaic Generators is a developed energy Generators with the advantages such as: relevant design and installation, silent energy conversion, long life time with less maintenance requirement, easy transportation and light weight. But in compare with other types of energy converters like diesel generator it is more expensive. Therefore, the DC-AC converter efficiency and the number of solar cells are important factors [1,2].

In this paper, an implementations of a photovoltaic generator model that can be used to simulate performance using historical irradiance data. Here the model is tested by varying the DC-AC converter efficiency. Power generation steps immediately following the efficiency change. And the model is also tested by by varying the numbers of solar panels while the DC-AC converter efficiency is assumed to be a fixed 98 percent.

## II. MODELING OF THE PHOTOVOLTAIC SYSTEM

A photovoltaic generator is the whole assembly of solar cells, connections, protective parts, supports etc. In the present modeling, the focus is only on DC-AC converters efficiency, and the number of solar panels.

The components of the Photovoltaic Generator Model

1. The solar panel - The block represents a single solar cell as a parallel combination of a current source, two exponential diodes and a parallel resistor, Rp, that are connected in series with a resistance Rs,Thefollowing figure shows the equivalent circuitdiagram for the solar cell that had been used in this model:[3]

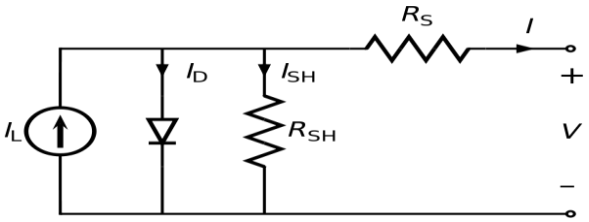


Fig 1 the equivalent circuit of a solar cell




ISSN 1737-9334

The output current I is given by

$$I = I_{ph} - I_s * \left(e^{\frac{V+I*R_s}{N*Vt}} - 1\right) - I_{s2} * \left(e^{\frac{V+I*Rs}{N2*Vt}} - 1\right)$$

$$-(V + I * R_s)/R_p \qquad (1)$$

Where Is and $I_{S2}$ are the diode saturation currents, $V_t$ is the thermal voltage, N and $N_2$ are the quality factors (diode emission coefficients) and $I_{ph}$ is the solar-generated current.

Models of reduced complexity can be specified in the mask. The quality factor varies for amorphous cells, and typically has a value in the range of 1 to 2. The physical signal input Ir is the irradiance (light intensity) in W/m^2 falling on the cell. The solar-generated current $I_{ph}$ is given by $I_r*(I_{ph0}/I_{r0})$ where $I_{ph0}$ is the measured solar-generated current for irradiance $I_{r0}$.

2. The DC-AC Converter - it's a combination of an ideal current sensor which converts current measured in any electrical branch into a physical signal proportional to the current, and also the DC-AC converters consists a controlled voltage source which represents an ideal voltage source that is powerful enough to maintain the specified voltage at its output regardless of the current passing through it. The output voltage is V = Vs, where Vs is the numerical value presented at the physical signal port, and at last the DC-AC PS Gain, This block multiplies the input physical signal by a constant which is the efficiency of the DC-AC Converter.

3. Radiative Heat Transfer - The block represents an energy transfer by radiation between two surfaces. The transfer is governed by the Stefan-Boltzmann law and is directly proportional to the area, the radiation coefficient, and the difference of the forth powers of body temperatures.

The radiation coefficient depends on the configuration properties and emissivity of interacting bodies.

4. Convective Heat Transfer- The block represents an energy transfer by convection between two bodies by means of fluid motion. The transfer is governed by the Newton law of cooling and is directly proportional to the convection heat transfer coefficient, surface area, and the temperature difference.

5. PS Lookup Table (2D) - This block represents a physical signal converter whose input-output relationship is specified by a two-dimensional lookup table. The two table grid vectors define a Cartesian grid in 2D space. Each of the two table grid vectors must be in strictly ascending or strictly descending order, but the spacing can be nonuniform, the optimal operating point of this block is where the power versus voltage curve for current irradiance level and temperature reaches a peak. The tabulated data used here is generated from a polynomial surface fit to data obtained by running the elec_solar_characteristics_callback.m script used by the Solar Cell Power Curve example model.

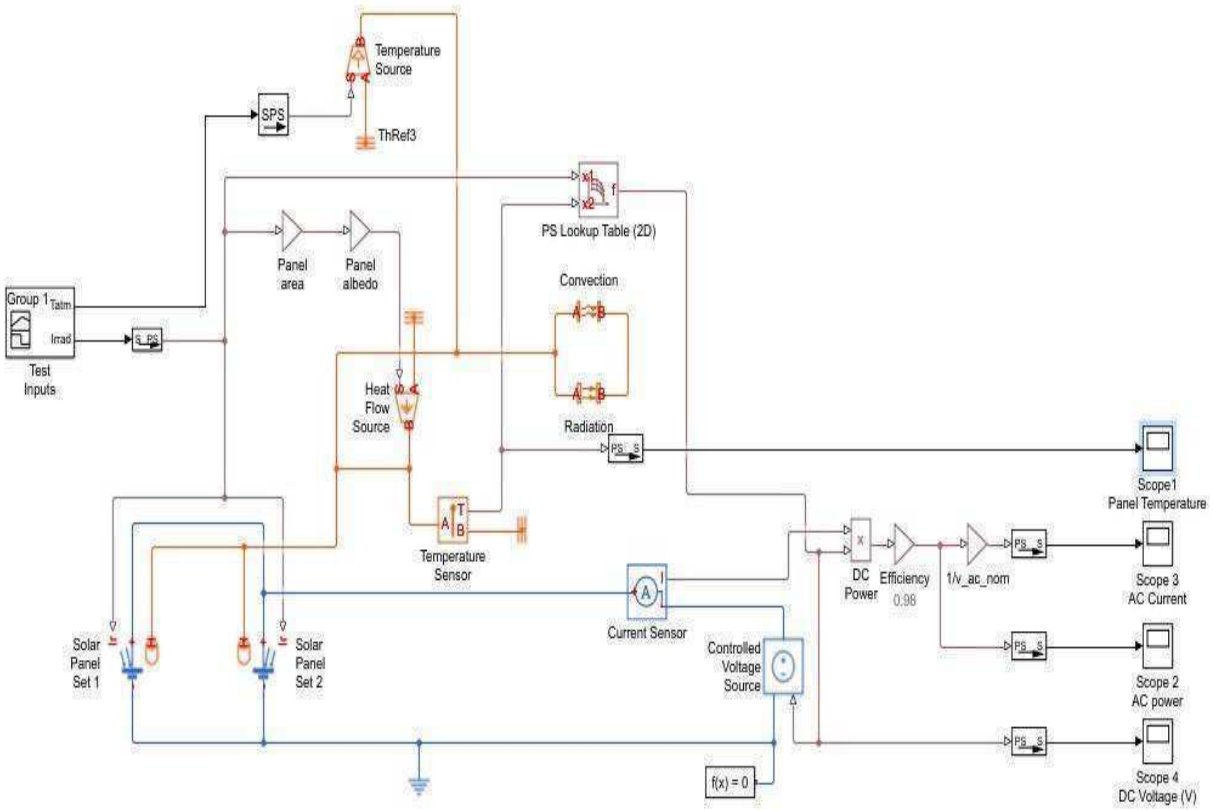


Fig 2 Photovoltaic Generator Model


ISSN 1737-9334

6. An Ideal Heat Flow Source- The block represents an ideal source of thermal energy that is powerful enough to maintain specified heat flow at its outlet regardless of the temperature difference across the source.

7. An Ideal Temperature Sensor - The block represents a device that determines the temperature differential measured between two points without drawing any heat

8. An Ideal Temperature Source - The block represents an ideal source of thermal energy that is powerful enough to maintain specified temperature at its outlet regardless of the heat flow consumed by the system. The temperature differential across the source is directly proportional to the control signal.

9. Thermal Reference - The block represents a thermal reference point, that is, a point with a zero or constant temperature, with respect to which all the temperatures in the system are determined.

10. PS Simulink Converters - Converts the unit less Simulink input signal to a Physical Signal, The unit expression in 'Input signal unit' parameter is associated with the unit less Simulink input signal and determines the unit assigned to the Physical Signal.

11. Scope - The Simulink Scope block displays the generated time domain signals with respect to simulation time.

## III. IMPLEMENT AND SIMULATE THE PHOTOVOLTAIC GENERATER

There are several things that effects the output power of the Photovoltaic generator and in this paper the focus would be on the effect of changing the DC-AC Converter gain which is the efficiency of the converter and how it effect on the output AC power of the system, and in another test will see what would happens to the output AC power of the system by adding more solar panels to the system.

The experiment duration time would be 30 min, so we will get a results for a period of 1800 seconds.

### A. *DC-AC Converter Efficiency*

The PV module was implemented using a Matlab program. The model parameters are evaluated duringexecution using the listed parameters:

1. DC-AC converter Efficiency 80%
2. DC-AC converter Efficiency 90%
3. DC-AC converter Efficiency 98%

By varying the PS gain which is the efficiency of the converter we can get three different results, while on the other hand the Solar panels would be fixed in two solar panels.

### B. *The number of solar pan*

The other test is to change the number of the solar cells of the PV model, by adding more panels and connecting them in parallel with the two panels that already in the model and see the change on the output AC power of the model.

At this experiment the efficiency of the DC-AC converter would be assumed to be a fixed 98 percent. And would get three results of the output AC power.

1. Two Solar Panels with DC-AC converter Efficiency 98%.
2. Three Solar Panels with DC-AC converter Efficiency 98%.
3. Four Solar Panels with DC-AC converter Efficiency 98%.

## IV. RESULTS OF MATLAB™ PHOTOVOLTAIC GENERATERMODEL

DC-AC Converter Efficiency

1. When the DC-AC converter Efficiency is 80% we would get the next result for the output AC power.

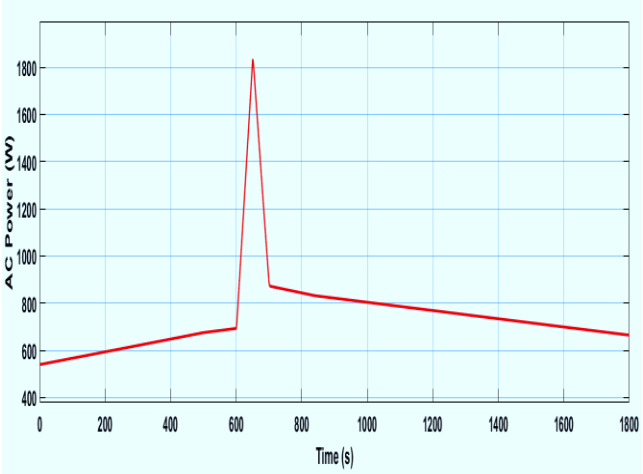


Fig 3 AC Power with DC-AC converter Efficiency is 80%

2. When the DC-AC converter Efficiency is 90% we would get the next result for the output AC power.




ISSN 1737-9334

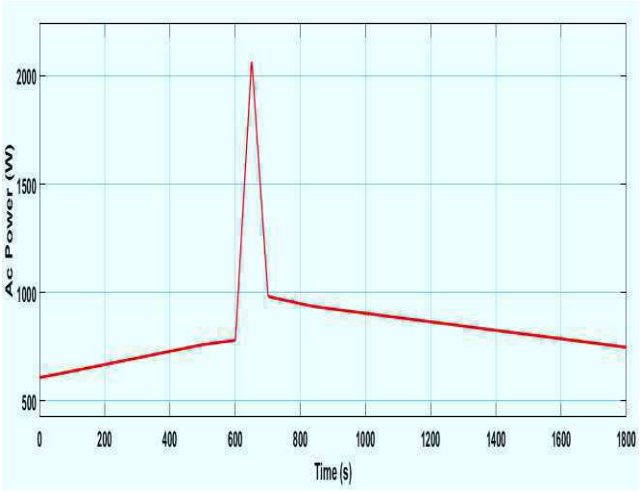


Fig 4 AC Power with DC-AC converter Efficiency is 90%

3. When the DC-AC converter Efficiency is 98% we would get the next result for the output AC power.

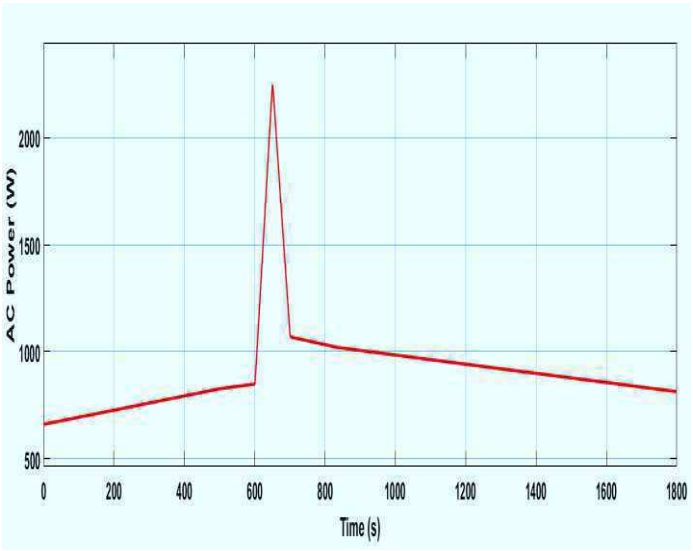


Fig 4 AC Power with DC-AC converter Efficiency is 98%

- The result of AC power of the model for the three DC-AC converter Efficiency can be shown in the figure 5.

B. The number of solar panels

1. Two Solar Panels with DC-AC converter Efficiency 98%.

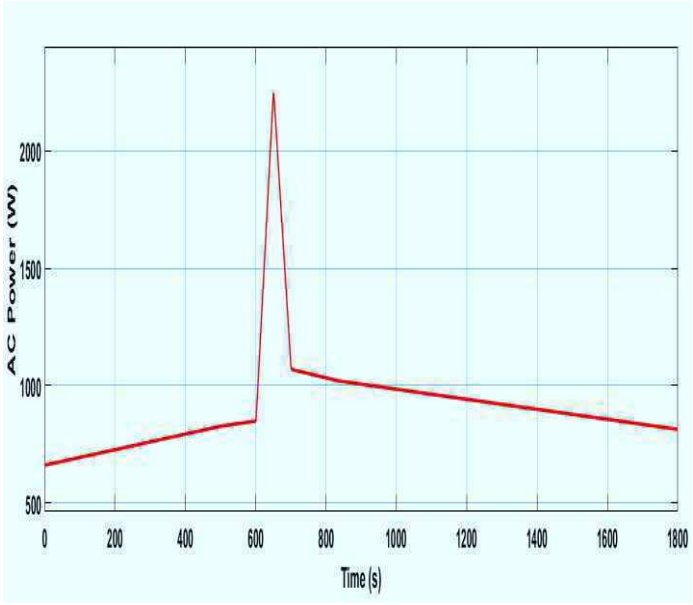


Fig 5 Two Solar Panels with DC-AC converter Efficiency 98%.

2. Three Solar Panels with DC-AC converter Efficiency 98%.

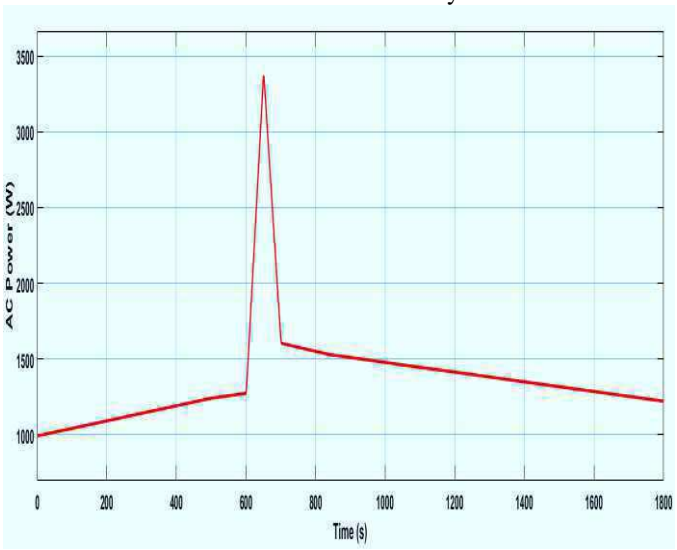


Fig 6 Three Solar Panels with DC-AC converter Efficiency 98%.

3. Four Solar Panels with DC-AC converter Efficiency 98%.




ISSN 1737-9334

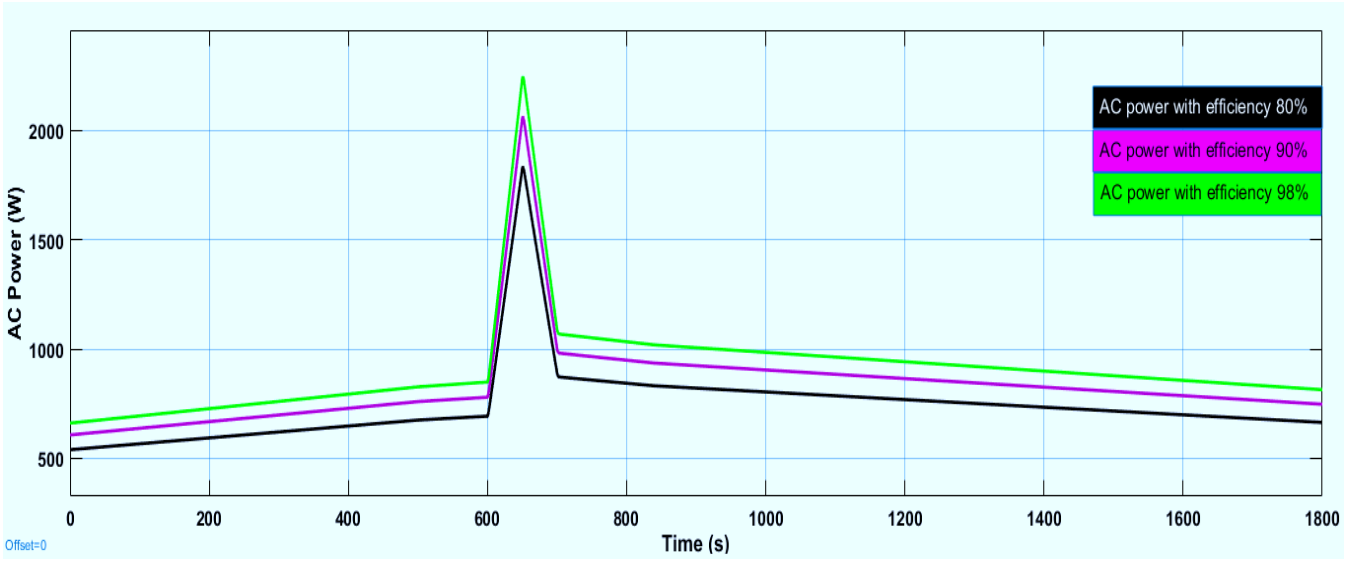


So the combined Final results for experiment for each DC-AC converter Efficiency, and the number of Solar panels can be shown as bellow on figure 8 and figure 9

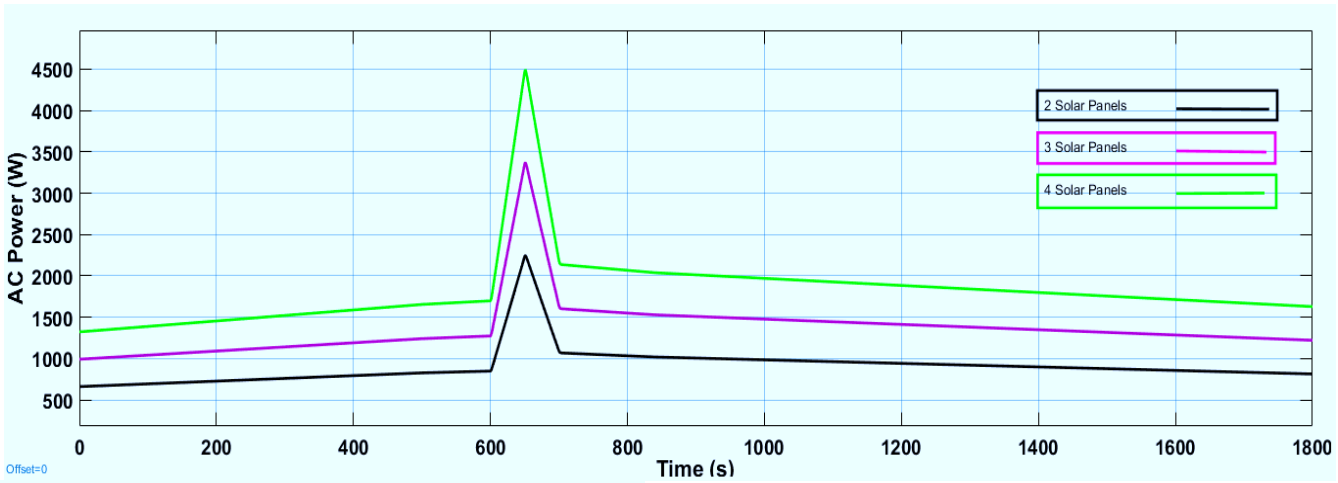


- Fig8 Matlab P-V curves for various DC-AC Efficiency
- Fig. 9 Matlab P-V curves for various Solar panels sets.

So, from the previous results we can summarize the following:

1) We can clearly see the effect of the efficiency of the DC-AC converter on the output power. A higher Converter efficiency will give us higher output power means a higher Photovoltaic Generator system efficiency.

2) More solar panels means more output power, when installing more solar panels the produced electric energy would rise and we will get more AC power at the output.

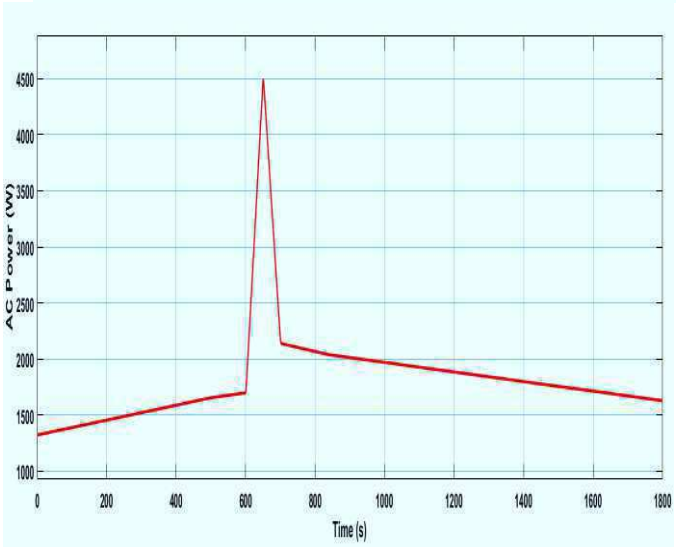


Fig 7 Four Solar Panels with DC-AC converter Efficiency 98%.




ISSN 1737-9334

## V. CONCLUSIONS

An accurate PV module electrical model is presented and demonstrated in Matlab for a typical solar panel, the model is tested by varying the irradiance which approximates the effect of varying cloud cover. Power generation steps immediately following the irradiance change. Environmental temperature also varies during the test. Finally the model development was used to show the effect of: DC-AC converter efficacy, number of solar panels.

This paper shows the effect of some parameters that effect the output power of the P-V system to develop a complete solar photovoltaic power electronic conversion with higher power.

## *References*

[1] L.D. Partain, Solar Cells and Their Applications, John Wiley & Sons, New York, 1995.

[2] M.R. Patel, Wind and Solar Power Systems, CRC Press, 1995.

[3] Eduardo Lorenzo (1994). Solar Electricity: Engineering of Photovoltaic Systems. Progensa. ISBN

[4] J. Clerk Maxwell, A Treatise on Electricity and Magnetism, 3rd ed., vol. 2. Oxford: Clarendon, 1892, pp.68-73.




ISSN 1737-9334

# Stabilization of Discrete Nonlinear Singularly Perturbed System with Time-Delay Represented by a Coupled Multimodel

R. Abdeljawad N. Bahri M. Ltaief
Research Unit: Numerical Control of Industrial Processes
National Engineering School of Gabes, University of Gabes, Tunisia
Email: abdeljawad_roukaya@hotmail.com, bahri.nesrine@gmail.com
majda.ltaief@enig.rnu.tn

***Abstract*—This paper investigates the problem of state feedback stabilisation for discrete nonlinear singularly perturbed system with time-delay which is represented by a coupled multimodel. Based on an appropriate Lyapunov function, new sufficient conditions are given as a set of Linear Matrix Inequalities (LMIs) that are used to get the gains of controllers. Numerical example is given to illustrate the effectiveness of the proposed method.**

## I. Introduction

In the past three decades, singularly perturbed system (SPS) have been intensively studied due to their ability to represent many industriel systems which are characterized by slow and fast dynamics and in the majority of cases these systems are also non-linear. This increases their complexity. Subsequently, traditional methods of analysis and synthesis become inefficient. In recent years, many techniques of simplification have been developed to reduce the complexity of modeling, control and analysis [4]. In most studies, the reduction of this complexity leads to a lack of information. This reduction is achieved either by neglecting certain phenomena (chemical reaction for example), or by elimination of certain parameters which do not have a significant importance on the dynamics of the system [[5], [4], [6], [7]]. Therefore, it is necessary to use another powerful technique to confront these problems. In this context, we will focus on the multimodel approach that is known by its power to handle with complex systems. In deed, this approach represents a powerful tool for modeling, observation and control of complex systems [8]. The basic idea of this approach is to decompose the global problem into a set of sub-problems that are simpler and easier to solve.
On the other hand, time-delay is commonly encountered in several industriel system. It can lead to instability or can degrade the performance of systems. Thus, it is important to design a controller that stabilize the closed loop system. Several research have studied the control problem for nonlinear singularly perturbed system [[9], [10], [11], [13], [12]]. In [[9], [10]], controller design for continuous-time nonlinear SPS with time-delay has been treated. However, these results can not handel with discrete-time cases. In [13], the problem of state feedback stabilization for fuzzy SPSs is treated. But, time-delay wasn't considered in this work. Chen et al. were investigated a control problem for discrete-time time-delay fuzzy SPS was described by fuzzy "IF-THEN" rules [11]. Liu et al. were considered the controller design for discrete-time fuzzy SPS under the fast-time version [15]. But this class of system does not always conserve the time scale character [14]. This paper present a new result on state feedback stabilization for discrete-time time-delay nonlinear SPS with slow rate which known by its preservation of time scale character. First, the discrete nonlinear SPS is represented by a discrete coupled multimodel by using Convex Polytopic Transformation (CPT). After that, based on an appropriate Lyapunov function, a new method for designing a controller is presented.
This paper is organized as follow. In section 2, nonlinear SPS with time-delay (NSPSD) and its representation with a coupled multimodel are represented. The main results are given in section 3, where the state feedback stabilization problem is treated. Simulation results for a discrete NSPSD show the effectiveness of the presented method in section 4. In section 5, a conclusion finishes this paper.

## II. Coupled Multimodel representation of Discrete Nonlinear Singularly Perturbed System with Time-delay

Consider a discrete non linear singularly perturbed system (NLSPS) with time-delay:

$$\begin{aligned} x_1(k+1) &= f_{NL}(x_1(k), x_2(k), x_1(k-d), x_2(k-d), u(k)) \\ x_2(k+1) &= \varepsilon g_{NL}(x_1(k), x_2(k), x_1(k-d), x_2(k-d), u(k)) \end{aligned} \quad (1)$$

where $x_1 \in R^n$, $x_2 \in R^m$ are system states and $u(k)$ is control input.
$d$: positif integer which is the time-delay.
$\varepsilon$: is a small positive parameter.
$f_{NL} : R^n \times R^m \to R^n$ and $g_{NL} : R^n \times R^m \to R^m$.
The discrete NLSPS with time-delay (1) can be represented by a coupled multimodel using Convex Polytopic Transformation (CPT). This method does not present an error of approximation and the choice of decision variable is realized in a systematic way [16]. It assumes that all non constant terms are bounded. If $r$ is the number of nonlinearity distincts existent in nonlinear




ISSN 1737-9334

system (1), then the obtained multimodel is composed of $2^r = N_m$ sub-models.
The following Lemma will be used to manipulate the nonlinear term.

**Lemma 1 [16]**
Let $H(x(t), u(t))$ a continuous and bounded function on the domain $D \subset \mathbb{R}^n \times \mathbb{R}^m \to \mathbb{R}$,
with $x \in \mathbb{R}^n$ and $u \in \mathbb{R}^m$.
Then there are two functions $G_i$ $(i = 1, 2)$

$$\begin{array}{l} G_i : D \mapsto [0, 1] \\ (x(t), u(t)) \mapsto G_i(x(t), u(t)) \end{array} \tag{2}$$

$G_1(x(t), u(t)) + G_2(x(t), u(t)) = 1$, with:

$$H(x(t), u(t)) = G_1(x(t), u(t)).H_1 + G_2(x(t), u(t)).H_2$$

For all $H_1 \geq maximum_{x,u\in D} H(x(t), u(t))$, $H_2 \leq minimum_{x,u\in D} H(x(t), u(t))$
The functions $G_1$ and $G_2$ are given as follow:

$$G_1(x(t), u(t)) = \frac{H(x(t), u(t)) - H_2}{H_1 - H_2} \tag{3}$$

$$G_2(x(t), u(t)) = \frac{H_1 - H(x(t), u(t))}{H_1 - H_2} \tag{4}$$

In particular: $H_1 = maximum_{x,u\in D} H(x(t), u(t))$ and $H_2 = minimum_{x,u\in D} H(x(t), u(t))$
The CPT can be summarized by the following steps.

**Step 1:** Write the system Eqn. (1) as a quasi linear parameter varying (quasi-LPV) form:

$$x(k+1) = A_\varepsilon(x_1(k), x_2(k))x(k) + D_\varepsilon(x_1(k), x_2(k))x(k-d) \tag{5}$$

where $A_\varepsilon(x_1(k), x_2(k)) \in \mathbb{R}^{n\times n}$ and $D_\varepsilon(x_1(k), x_2(k)) \in \mathbb{R}^{n\times n}$.
$r_1$ is the number of nonlinear terms in $A_\varepsilon(x_1(k), x_2(k))$.
$r_2$ is the number of nonlinear terms in $D_\varepsilon(x_1(k), x_2(k))$.
$r = r_1 + r_2$

**Step 2:** Set up the bound of each nonlinear term in $A_\varepsilon(x_1(k), x_2(k))$ and $D_\varepsilon(x_1(k), x_2(k))$.

**Step 3:** Let
$H_j(x_1(k), x_2(k))$, $j = 1, ..., r$ are the nonlinear term in $A_\varepsilon(x_1(k), x_2(k))$ and $D_\varepsilon(x_1(k), x_2(k))$.
Each nonlinear term $H_j(x_1(k), x_2(k))$, $j = 1, ..., r$ can be written according to its $G_1(x_1(k), x_2(k))$, its $G_2(x_1(k), x_2(k))$, its maximum $(H_1)$ and its munimum $(H_2)$ according to lemma 1.
To each sub-model $i$ corresponds a p-uplet $\sigma_i$ that codes the partitions of the decision variables existing in the corresponding weighting function.
The weighting function $\mu_i(x_1(k), x_2(k))$, $i = 1, .., N_m$ is obtained by multiplying the function $G_{j,\sigma_i^j}(x_1(k), x_2(k))$ that describe the partitions of the decision variable:

$$\mu_i(x_1(k), x_2(k)) = \prod_{j=1}^{r} G_{j,\sigma_i^j}(x_1(k), x_2(k)) \tag{6}$$

where $\sigma_i^j$ is the index in the $j^{th}$ position in the p-uplet $\sigma_i$.
$A_\varepsilon(x_1(k), x_2(k))$ can be written as a linear combination of constant matrix $A_j(\varepsilon)$:

$$A_\varepsilon(x_1(k), x_2(k)) = A_0(\varepsilon) + \sum_{j\in E_A} H_j(x_1(k), x_2(k))A_j(\varepsilon) \tag{7}$$

where $E_A$ includes all the indexes corresponding to the premises variables that exist in $A_\varepsilon(x_1(k), x_2(k))$.
$A_0(\varepsilon)$ and $A_j(\varepsilon)$ have the same dimension of the matrix $A_\varepsilon(x_1(k), x_2(k))$.
All the constant element of $A_\varepsilon(x_1(k), x_2(k))$ are found in $A_0(\varepsilon)$.
For the matrix $A_j(\varepsilon)$, at the position corresponding to $H_j(x_1(k), x_2(k))$, the constant element is equal to 1 and the other remaining positions are equal to zero.
Using the equation (7), the matrix $A_i(\varepsilon)$, $i = 1, ...N_m$ is given as follow:

$$A_i(\varepsilon) = A_0(\varepsilon) + \sum_{j\in E_A} z_{j,\sigma_i^j} A_j(\varepsilon) \tag{8}$$

$D_\varepsilon(x_1(k), x_2(k))$ can be found in the same way.

**Step 4:** Write the system in the form of multimodel and calculate the weighting functions $\mu_i(x)$, $i = 1...N_m$.
The coupled multimodel is given as follow:

$$\begin{array}{c} x(k+1) = \sum_{i=1}^{N_m} \mu_i(\xi(k))A_i(\varepsilon)x(k) + \sum_{i=1}^{N_m} \mu_i(\xi(k))D_i(\varepsilon) \\ x(k-d) + \sum_{i=1}^{N_m} \mu_i(\xi(k))B_i(\varepsilon)u(k) \end{array} \tag{9}$$

where

$$x(k) = \begin{bmatrix} x_1(k) \\ x_2(k) \end{bmatrix}, \quad B_i(\varepsilon) = \begin{bmatrix} B_{i1} \\ \varepsilon B_{i2} \end{bmatrix}$$

$$A_i(\varepsilon) = \begin{bmatrix} A_{i11} & A_{i12} \\ \varepsilon A_{i21} & \varepsilon A_{i22} \end{bmatrix}, \; D_i(\varepsilon) = \begin{bmatrix} D_{i11} & D_{i12} \\ \varepsilon D_{i21} & \varepsilon D_{i22} \end{bmatrix}$$

$N_m$ is the number of sub-models, $i = 1, 2, ...N_m$.

$A_{i11}$, $A_{i12}$, $A_{i21}$, $A_{22}$, $D_{i11}$, $D_{i12}$, $D_{i21}$, $D_{i22}$, $B_{i1}$ and $B_{i2}$ are appropriate dimension matrices.
$\mu_i(\xi(k))$ are the weighting functions that ensure the transition between the sub-models. They are characterized by the following properties:

$$\sum_{i=1}^{N_m} \mu_i(\xi(k)) = 1, \quad \forall k \tag{10}$$

$$0 \leq \mu_i(\xi(k)) \leq 1, \quad \forall k, \quad i = 1, 2, ...N_m \tag{11}$$

$\xi(k)$ is the decision variable. It can be signal input, signal output or system state.
The system (9) can be written as:

$$x(k+1) = \bar{A}(\varepsilon)x(k) + \bar{D}(\varepsilon)x(k-d) + \bar{B}(\varepsilon)u(k) \tag{12}$$


ISSN 1737-9334

where

$$\bar{A}(\varepsilon)=\sum_{i=1}^{N_m}\mu_i(\xi(k))A_i(\varepsilon),\ \bar{D}(\varepsilon)=\sum_{i=1}^{N_m}\mu_i(\xi(k))D_i(\varepsilon)$$
$$\bar{B}(\varepsilon)=\sum_{i=1}^{N_m}\mu_i(\xi(k))B_i(\varepsilon) \quad (13)$$

In the following, we propose to design a multimodel control law , which is given as follow:

$$u(k)=\bar{K}x(k),\bar{K}=\sum_{i=1}^{N_m}K_i \quad (14)$$

Then the resulting closed-loop system is given by:

$$x(k+1)=\bar{A}_{BF}(\varepsilon)x(k)+\bar{D}(\varepsilon)x(k-d) \quad (15)$$

where

$$\bar{A}_{BF}(\varepsilon)=\bar{A}(\varepsilon)+\bar{B}(\varepsilon)\bar{K}$$

We recall the following lemmas, in order to establish our main results.

**Lemma 2 [1]:**
For any positive scalar $\varepsilon^*$, if the following conditions are verified:

$$F_1\geq 0,$$
$$\varepsilon^{*2}F_1+\varepsilon^*F_2+F_3<0,$$
$$F_3<0,$$

then we get

$$\varepsilon^2F_1+\varepsilon F_2+F_3<0,\quad for\quad \varepsilon\in[0,\varepsilon^*]$$

**Lemma 3 [2]:**
Let $V\in\mathbb{R}^{n_1}$, $W\in\mathbb{R}^{n_2}$ and $N\in\mathbb{R}^{n_1*n_2}$.
Then for any matrices $M\in\mathbb{R}^{n_1*n_1}$, $S\in\mathbb{R}^{n_1*n_2}$ and $Z\in\mathbb{R}^{n_2*n_2}$ satisfying: $\begin{bmatrix} M & S \\ S^T & Z \end{bmatrix}\geq 0$, we have,

$$-2V^TNW\leq\begin{bmatrix} V \\ W \end{bmatrix}^T\begin{bmatrix} M & S-N \\ S^T-N^T & Z \end{bmatrix}\begin{bmatrix} V \\ W \end{bmatrix} \quad (16)$$

## III. Stabilisation of Nonlinear Singularly Perturbed System with Time-delay represented by a Coupled Multimodel

**Theorem 1**
Consider the system (9).
Let the positif real $\varepsilon^*>0$ and $d>0$ a positive integer, if there exist symmetric matrices define positif $X>0$, $\tilde{Q}>0$ and $\tilde{M}$, $\tilde{R}$ a symmetric matrix and matrices $\tilde{W}$, $\tilde{K}$ satisfying the following LMIs:

$$\tilde{\Omega}'_{ii}(\varepsilon^*)<0 \quad (17)$$

$$\tilde{\Omega}'_{ii}(0)<0 \quad (18)$$

$$\tilde{\Omega}'_{ij}(\varepsilon^*)+\tilde{\Omega}'_{ji}(\varepsilon^*)<0 \quad (19)$$

$$\tilde{\Omega}'_{ij}(0)+\tilde{\Omega}'_{ji}(0)<0 \quad (20)$$

$$\begin{bmatrix} \tilde{R} & \tilde{W} \\ \tilde{W}^T & \tilde{M} \end{bmatrix}\geq 0 \quad (21)$$

where

$$\tilde{\Omega}'_{ij}(\varepsilon)=\begin{bmatrix} (1,1) & * & * & * \\ (2,1) & (2,2) & * & * \\ (3,1) & (3,2) & (3,3) & * \\ (4,1) & (4,2) & (4,3) & (4,4) \end{bmatrix} \quad (22)$$

with
$(1,1)=-X+d\tilde{R}+\tilde{W}^T+\tilde{W}+\tilde{Q}$
$(2,1)=-\tilde{W}^T$
$(2,2)=-\tilde{Q}$
$(3,1)=A_i(\varepsilon)X+B_i(\varepsilon)\tilde{K}_j$
$(3,2)=D_i(\varepsilon)X$
$(3,3)=-X$
$(4,1)=\sqrt{d}A_i(\varepsilon)X+\sqrt{d}B_i(\varepsilon)\tilde{K}_j-\sqrt{d}X$
$(4,2)=\sqrt{d}D_i(\varepsilon)X$
$(4,3)=0$
$(4,4)=\tilde{M}-2X$

Then there exists a controller given by equation (23) such that the closed loop system is asymptotically stable $\forall\varepsilon\in[0,\varepsilon^*]$.

$$u(k)=\sum_{i=1}^{N_m}K_ix(k),\ avec,\ K_i=\tilde{K}_iX^{-1} \quad (23)$$

**Proof**
We consider the following Lyapunov-Krasovskii functional:

$$V(k)=V_1(k)+V_2(k)+V_3(k) \quad (24)$$

where
$V_1(k)=x^T(k)Px(k)$
$V_2(k)=\sum_{i=k-d}^{k-1}x^T(i)Qx(i)$
$V_3(k)=d\sum_{\theta=-d}^{(-1)}\sum_{i=k+\theta}^{k-1}\eta^T(i)M\eta(i),\quad \eta(i)=x(i+1)-x(i)$
with $P$, $Q$ and $M$ are symmetric and positive definite matrices.

$$Since\ \ \eta(i)=x(i+1)-x(i)$$

then we have:

$$x(k-d)=x(k)-\sum_{i=k-d}^{k-1}\eta(i) \quad (25)$$

Substituting (25) into (12), we obtain:

$$x(k+1)=A_{dd}(\varepsilon)x(k)-D(\varepsilon)\sum_{i=k-d}^{k-1}\eta(i) \quad (26)$$


ISSN 1737-9334

with $A_{dd}(\varepsilon) = \bar{A}(\varepsilon) + \bar{B}(\varepsilon)\bar{K} + \bar{D}(\varepsilon)$

$$\begin{aligned}\Delta V_1(k) &= V_1(k+1) - V_1(k)\\ &= x^T[\bar{A}_{dd}^T(\varepsilon)P\bar{A}_{dd}(\varepsilon) - P]x(k) - 2\sum_{i=k-d}^{k-1} x^T(k)\bar{A}_{dd}^T(\varepsilon)P\bar{D}(\varepsilon)\\ &\quad \eta(i) + N^T(k)\bar{D}^T(\varepsilon)P\bar{D}(\varepsilon)N(k)\end{aligned} \tag{27}$$

where $N(k) = \sum_{i=k-d}^{k-1}\eta^T(i)$
Posing $\theta = \bar{A}_{dd}^T(\varepsilon)P\bar{D}(\varepsilon)$ and using Lemma 3, we obtain:

$$\begin{aligned}\Delta V_1(k) &\le x^T[\bar{A}_{dd}^T(\varepsilon)P\bar{A}_{dd}(\varepsilon) - P + dR + W^T - \theta^T + W - \theta\\ &+ \bar{D}^T(\varepsilon)P\bar{D}(\varepsilon)]x(k) + x^T(k)[-W + \theta - \bar{D}^T(\varepsilon)P\bar{D}(\varepsilon)]x(k-d)\\ &+ x^T(k-d)[-W^T + \theta^T - \bar{D}^T(\varepsilon)P\bar{D}(\varepsilon)]x(k) + x^T(k-d)\\ &[\bar{D}^T(\varepsilon)P\bar{D}(\varepsilon)]x(k-d) + \sum_{i=k-d}^{k-1}\eta^T(i)M\eta(i)\end{aligned} \tag{28}$$

with $R$, $W$ and $M$ satisfying the following condition:

$$\begin{bmatrix} R & W \\ W^T & M \end{bmatrix} \ge 0 \tag{29}$$

$\Delta V_2(k)$ is given as:

$$\Delta V_2(k) = x^T(k)Qx(k) - x^T(k-d)Qx(k-d) \tag{30}$$

$\Delta V_3(k)$ can be written as follow:

$$\begin{aligned}\Delta V_3(k) &= dx^T(k)\bar{A}_{BF}^T(\varepsilon)M\bar{A}_{BF}(\varepsilon)x(k) + dx^T(k)\bar{A}_{BF}^T(\varepsilon)\\ &M\bar{D}(\varepsilon)x(k-d) + dx^T(k-d)\bar{D}^T(\varepsilon)M\bar{A}_{BF}(\varepsilon)x(k)\\ &+ dx^T(k-d)\bar{D}^T(\varepsilon)M\bar{D}(\varepsilon)x(k-d)\\ &- \sum_{i=k-d}^{k-1}\eta^(i)M\eta(i)\end{aligned} \tag{31}$$

with $\bar{A}_{BF}(\varepsilon) = \bar{A}(\varepsilon) + \bar{B}(\varepsilon)\bar{K} - I$
$\Delta V(k)$ is given as follow:

$$\begin{aligned}\Delta V(k) &= \Delta V_1(k) + \Delta V_2(k) + \Delta V_3(k)\\ &\le x^T(k)[\bar{A}_{dd}^T(\varepsilon)P\bar{A}_{dd}(\varepsilon) - P + dR + W^T - \theta^T + W - \theta\\ &- \bar{D}^T(\varepsilon)P\bar{D}(\varepsilon) + Q + d\bar{A}_{BF}^T(\varepsilon)M\bar{A}_{BF}(\varepsilon)]x(k) + x^T(k)[-W\\ &+ \theta - \bar{D}^T(\varepsilon)P\bar{D}(\varepsilon) + d\bar{A}_{BF}^T(\varepsilon)M\bar{D}(\varepsilon)]x(k-d) + x^T(k-d)\\ &[-W^T + \theta^T - \bar{D}^T(\varepsilon)P\bar{D}(\varepsilon) + d\bar{D}^T(\varepsilon)M\bar{A}_{BF}(\varepsilon)]x(k)\\ &+ x^T(k-d)[\bar{D}^T(\varepsilon)P\bar{D}(\varepsilon) - Q + d\bar{D}^T(\varepsilon)M\bar{D}(\varepsilon)]x(k-d)\\ &\le \xi^T(k)\Omega(\varepsilon)\xi(k)\end{aligned} \tag{32}$$

where

$$\xi(k)^T = \begin{bmatrix} x(k) \\ x(k-d) \end{bmatrix}^T$$

$$\Omega(\varepsilon) = \begin{bmatrix} \Omega_{11}(\varepsilon) & * \\ \Omega_{21}(\varepsilon) & \Omega_{22}(\varepsilon) \end{bmatrix}$$

with

$$\begin{aligned}\Omega_{11}(\varepsilon) &= [\bar{A}^T(\varepsilon) + \bar{K}^T\bar{B}^T(\varepsilon)]P[\bar{A}(\varepsilon) + \bar{B}(\varepsilon)\bar{K}] - P + dR\\ &\quad + W^T + W + Q + d\bar{A}_{BF}^T(\varepsilon)M\bar{A}_{BF}(\varepsilon)]\\ \Omega_{21}(\varepsilon) &= -W^T + \bar{D}^T(\varepsilon)P[\bar{A}(\varepsilon) + \bar{B}(\varepsilon)\bar{K}] + d\bar{D}^T(\varepsilon)M\bar{A}_{BF}(\varepsilon)\end{aligned}$$

$$\Omega_{22}(\varepsilon) = \bar{D}^T(\varepsilon)P\bar{D}(\varepsilon) - Q + d\bar{D}^T(\varepsilon)M\bar{D}(\varepsilon)$$

$\Delta V(k) < 0,\ \forall\varepsilon \in [0, \varepsilon^*]$ if and only if:

$$\Omega(\varepsilon) < 0,\ \forall\varepsilon \in [0, \varepsilon^*] \tag{33}$$

Applying the Schur Complement twice on (33), we get:

$$\Omega'(\varepsilon) = \begin{bmatrix} \Omega'_{11}(\varepsilon) & * & * & * \\ \Omega'_{21}(\varepsilon) & \Omega'_{22}(\varepsilon) & * & * \\ \Omega'_{31}(\varepsilon) & \Omega'_{32}(\varepsilon) & \Omega'_{33}(\varepsilon) & * \\ \Omega'_{41}(\varepsilon) & \Omega'_{42}(\varepsilon) & \Omega'_{43}(\varepsilon) & \Omega'_{44}(\varepsilon) \end{bmatrix} < 0 \tag{34}$$

with
$\Omega'_{11}(\varepsilon) = -P + dR + W^T + W + Q$
$\Omega'_{21}(\varepsilon) = -W^T$
$\Omega'_{22}(\varepsilon) = -Q$
$\Omega'_{31}(\varepsilon) = \bar{A}(\varepsilon) + \bar{B}(\varepsilon)\bar{K}$
$\Omega'_{32}(\varepsilon) = \bar{D}(\varepsilon)$
$\Omega'_{33}(\varepsilon) = -P^{-1}$
$\Omega'_{41}(\varepsilon) = \sqrt{d}\bar{A}(\varepsilon) + \sqrt{d}\bar{B}(\varepsilon)\bar{K} - \sqrt{d}I$
$\Omega'_{42}(\varepsilon) = \sqrt{d}\bar{D}(\varepsilon)$
$\Omega'_{43}(\varepsilon) = 0$
$\Omega'_{44}(\varepsilon) = -M^{-1}$
Multiplying equation (34) on the left and right by $diag = \{P^{-1}, P^{-1}, I, I\}$ and posing the following equalities:
$X = P^{-1},\ \tilde{R} = P^{-1}RP^{-1},\ \tilde{W} = P^{-1}WP^{-1},\ \tilde{Q} = P^{-1}QP^{-1},\ \tilde{K} = \bar{K}P^{-1}$
we get:

$$\tilde{\Omega}(\varepsilon) = \begin{bmatrix} \tilde{\Omega}_{11}(\varepsilon) & * & * & * \\ \tilde{\Omega}_{21}(\varepsilon) & \tilde{\Omega}_{22}(\varepsilon) & * & * \\ \tilde{\Omega}_{31}(\varepsilon) & \tilde{\Omega}_{32}(\varepsilon) & \tilde{\Omega}_{33}(\varepsilon) & * \\ \tilde{\Omega}_{41}(\varepsilon) & \tilde{\Omega}_{42}(\varepsilon) & \tilde{\Omega}_{43}(\varepsilon) & \tilde{\Omega}_{44}(\varepsilon) \end{bmatrix} < 0 \tag{35}$$

where
$\tilde{\Omega}_{11}(\varepsilon) = -X + d\tilde{R} + \tilde{W}^T + \tilde{W} + \tilde{Q}$
$\tilde{\Omega}_{21}(\varepsilon) = -\tilde{W}^T$
$\tilde{\Omega}_{22}(\varepsilon) = -\tilde{Q}$
$\tilde{\Omega}_{31}(\varepsilon) = \bar{A}(\varepsilon)X + \bar{B}(\varepsilon)\tilde{K}$
$\tilde{\Omega}_{32}(\varepsilon) = \bar{D}(\varepsilon)X$
$\tilde{\Omega}_{33}(\varepsilon) = -X$
$\tilde{\Omega}_{41}(\varepsilon) = \sqrt{d}\bar{A}(\varepsilon)X + \sqrt{d}\bar{B}(\varepsilon)\tilde{K} - \sqrt{d}X$
$\tilde{\Omega}_{42}(\varepsilon) = \sqrt{d}\bar{D}(\varepsilon)X$
$\tilde{\Omega}_{43}(\varepsilon) = 0$
$\tilde{\Omega}_{44}(\varepsilon) = -M^{-1}$
Since $M$ is a symmetric positive-definite matrix, we have:

$$(X - M^{-1})M(X - M^{-1}) > 0 \tag{36}$$




ISSN 1737-9334

Inequality (36) can be rewritten as:

$$XMX - 2X > -M^{-1} \tag{37}$$

According to (37), we know that the following inequality is sufficient to inequality (35):

$$\tilde{\Omega}^{'}(\varepsilon) = \begin{bmatrix} \tilde{\Omega}^{'}_{11}(\varepsilon) & * & * & * \\ \tilde{\Omega}^{'}_{21}(\varepsilon) & \tilde{\Omega}^{'}_{22}(\varepsilon) & * & * \\ \tilde{\Omega}^{'}_{31}(\varepsilon) & \tilde{\Omega}^{'}_{32}(\varepsilon) & \tilde{\Omega}^{'}_{33}(\varepsilon) & * \\ \tilde{\Omega}^{'}_{41}(\varepsilon) & \tilde{\Omega}^{'}_{42}(\varepsilon) & \tilde{\Omega}^{'}_{43}(\varepsilon) & \tilde{\Omega}^{'}_{44}(\varepsilon) \end{bmatrix} < 0 \tag{38}$$

where
$\tilde{\Omega}^{'}_{11}(\varepsilon) = -X + d\tilde{R} + \tilde{W}^T + \tilde{W} + \tilde{Q}$
$\tilde{\Omega}^{'}_{21}(\varepsilon) = -\tilde{W}^T$
$\tilde{\Omega}^{'}_{22}(\varepsilon) = -\tilde{Q}$
$\tilde{\Omega}^{'}_{31}(\varepsilon) = \bar{A}(\varepsilon)X + \bar{B}(\varepsilon)\tilde{K}$
$\tilde{\Omega}^{'}_{32}(\varepsilon) = \bar{D}(\varepsilon)X$
$\tilde{\Omega}^{'}_{33}(\varepsilon) = -X$
$\tilde{\Omega}^{'}_{41}(\varepsilon) = \sqrt{d}\bar{A}(\varepsilon)X + \sqrt{d}\bar{B}(\varepsilon)\tilde{K} - \sqrt{d}X$
$\tilde{\Omega}^{'}_{42}(\varepsilon) = \sqrt{d}\bar{D}(\varepsilon)X$
$\tilde{\Omega}^{'}_{43}(\varepsilon) = 0$
$\tilde{\Omega}^{'}_{44}(\varepsilon) = \tilde{M} - 2X$

with $\tilde{M} = XMX$.

Substituting (13) into (38), we get

$$\tilde{\Omega}^{'}(\varepsilon) = \sum_{i=1}^{Nm} \mu_i^2(\xi(k))\tilde{\Omega}^{'}_{ii}(\varepsilon) + \sum_{i<j}^{Nm} \mu_i(\xi(k))\mu_j(\xi(k))[\tilde{\Omega}^{'}_{ij}(\varepsilon) + \tilde{\Omega}^{'}_{ji}(\varepsilon)] < 0 \tag{39}$$

where $\tilde{\Omega}^{'}_{ij}(\varepsilon)$ is given by equation (22).

It is easy to know that inequalities (40) and (41) are sufficient to inequality (39)

$$\tilde{\Omega}^{'}_{ii}(\varepsilon) < 0, \ \forall \varepsilon \in [0, \varepsilon^*] \tag{40}$$

and

$$\tilde{\Omega}^{'}_{ij}(\varepsilon) + \tilde{\Omega}^{'}_{ji}(\varepsilon) < 0, \ \forall \varepsilon \in [0, \varepsilon^*] \tag{41}$$

By using Lemma 2, conditions (40) and (41) are satisfied if LMIs (17),(18), (19) and (20) are feasible.
where $R$, $W$ and $M$ satisfying the inequality (29).
Multiplying (29) on the left and on the right by $diag\{P^{-1}, P^{-1}\}$, we get:

$$\begin{bmatrix} \tilde{R} & \tilde{W} \\ \tilde{W}^T & \tilde{M} \end{bmatrix} \geq 0 \tag{42}$$

Therefore, the closed loop system is asymptotically stable $\forall \varepsilon \in [0, \varepsilon^*]$, if LMIs (17),(18), (19), (20) and (21) are feasible. This completes the proof.

## IV. Numerical Example

The considered discrete nonlinear singularly perturbed system with time delay is:

$$x(k+1) = \begin{bmatrix} 0.7 & 0.3x_2(k) \\ 0.8\varepsilon & \varepsilon \end{bmatrix} x(k) + \begin{bmatrix} 0.12 & 0.42 \\ \varepsilon sin(x_1(k)) & 0.37\varepsilon \end{bmatrix} x(k-d) + \begin{bmatrix} 1 \\ 0.9\varepsilon \end{bmatrix} u(k) \tag{43}$$

with $x(k) = \begin{bmatrix} x_1(k) & x_2(k) \end{bmatrix}^T$
Assume that $\mid x_2(k) \mid \leq 2$.
Non-constant terms are $x_2(k)$ and $sin(x_1(k))$.
By using the CPT, we get a multimodel composed of $2^2 = 4$ sub-models.
According to Lemma 1, $x_2(k)$ and $sin(x_1(k))$ can be written respectively as follow:

$$x_2(k) = F_{1,1}(x_2(k)).2 + F_{1,2}(x_2(k)).(-2) \tag{44}$$

$$sin(x_1(k)) = F_{2,1}(x_1(k)).1 + F_{2,2}(x_1(k)).(-1) \tag{45}$$

with
$F_{1,1}(x_2(k)) = 0.25(x_2(k) + 2)$
$F_{1,2}(x_2(k)) = 0.25(2 - x_2(k))$
$F_{2,1}(x_1(k)) = 0.5(sin(x_1(k)) + 1)$
$F_{2,2}(x_1(k)) = 0.5(1 - sin(x_1(k)))$
Considering the expression of $x_2(k)$, it can written as follow:

$$\begin{bmatrix} 0.7 & 0.3x_2(k) \\ 0.8\varepsilon & \varepsilon \end{bmatrix} = F_{1,1}(x_2(k)) \begin{bmatrix} 0.7 & 0.6 \\ 0.8\varepsilon & \varepsilon \end{bmatrix} + F_{1,2}(x_2(k)) \begin{bmatrix} 0.7 & -0.6 \\ 0.8\varepsilon & \varepsilon \end{bmatrix} \tag{46}$$

In order to make the partition functions appear $F_{2,1}(x_1(k))$ and $F_{2,2}(x_1(k))$, we multipy Eqn. (46), with the sum of these two function which is equal to 1. So, we get the following expression:

$$\begin{bmatrix} 0.7 & 0.3x_2(k) \\ 0.8\varepsilon & \varepsilon \end{bmatrix} = F_{1,1}(x_2(k))F_{2,1}(x_1(k)) \begin{bmatrix} 0.7 & 0.6 \\ 0.8\varepsilon & \varepsilon \end{bmatrix} + F_{1,1}(x_2(k))F_{2,2}(x_1(k)) \begin{bmatrix} 0.7 & 0.6 \\ 0.8\varepsilon & \varepsilon \end{bmatrix} + F_{1,2}(x_2(k))F_{2,1}(x_1(k)) \begin{bmatrix} 0.7 & -0.6 \\ 0.8\varepsilon & \varepsilon \end{bmatrix} + F_{1,2}(x_2(k))F_{2,1}(x_1(k)) \begin{bmatrix} 0.7 & -0.6 \\ 0.8\varepsilon & \varepsilon \end{bmatrix} \tag{47}$$

$\begin{bmatrix} 0.12 & 0.42 \\ \varepsilon sin(x_1(k)) & 0.37\varepsilon \end{bmatrix}$ can be found in the same way.
Then, we get the following coupled multimodel:

$$x(k+1) = \sum_{i=1}^{4} \mu_i(\xi(k)) \left[A_i(\varepsilon)x(k) + D_i(\varepsilon)x(k-d) + B_i(\varepsilon)u(k)\right] \tag{48}$$

with

$$A_1(\varepsilon) = A_3(\varepsilon) = \begin{bmatrix} 0.7 & -0.6 \\ 0.8\varepsilon & \varepsilon \end{bmatrix}$$




ISSN 1737-9334

$$A_2(\varepsilon) = A_4(\varepsilon) = \begin{bmatrix} 0.7 & -0.6 \\ 0.8\varepsilon & \varepsilon \end{bmatrix}$$

$$D_1(\varepsilon) = D_2(\varepsilon) = \begin{bmatrix} 0.12 & 0.42 \\ \varepsilon & 0.37\varepsilon \end{bmatrix}$$

$$D_3(\varepsilon) = D_4(\varepsilon) = \begin{bmatrix} 0.12 & 0.42 \\ -\varepsilon & 0.37\varepsilon \end{bmatrix}$$

$$B_1(\varepsilon) = B_2(\varepsilon) = B_3(\varepsilon) = B_4(\varepsilon) = \begin{bmatrix} 1 & 0.9\varepsilon \end{bmatrix}^T$$

$$\mu_1(k) = 0.125[x_2(k) + 2][sin(x_1(k)) + 1]$$
$$\mu_2(k) = 0.125[2 - x_2(k)][sin(x_1(k)) + 1]$$
$$\mu_3(k) = 0.125[x_2(k) + 2][1 - sin(x_1(k))]$$
$$\mu_4(k) = 0.125[2 - x_2(k)][1 - sin(x_1(k))]$$

By solving the LMIs of theorem 1 with $\varepsilon = 0.4215$ and $d = 1$ , we get:

$X = \begin{bmatrix} 10.2012 & -1.5983 \\ -1.5983 & 11.4832 \end{bmatrix}$, $\tilde{Q} = \begin{bmatrix} 5.9256 & -0.8860 \\ -0.8860 & 6.0323 \end{bmatrix}$, $\tilde{M} = \begin{bmatrix} 0.5210 & -0.3113 \\ -0.3113 & 4.9017 \end{bmatrix}$
$\tilde{R} = \begin{bmatrix} 0.1821 & -0.0700 \\ -0.0700 & 1.4834 \end{bmatrix}$, $\tilde{W} = \begin{bmatrix} -0.3052 & 0.0996 \\ 0.1944 & -2.6944 \end{bmatrix}$, $\tilde{K}_1 = \begin{bmatrix} -4.4144 & -7.2908 \end{bmatrix}$
$\tilde{K}_2 = \begin{bmatrix} -5.9895 & 4.8588 \end{bmatrix}$, $\tilde{K}_3 = \begin{bmatrix} -3.8300 & -7.2115 \end{bmatrix}$,
$\tilde{K}_4 = \begin{bmatrix} -5.9047 & 4.8004 \end{bmatrix}$
Then
$K_1 = \begin{bmatrix} -0.5441 & -0.7106 \end{bmatrix}$, $K_2 = \begin{bmatrix} -0.5325 & 0.3490 \end{bmatrix}$,
$K_3 = \begin{bmatrix} -0.4844 & -0.6954 \end{bmatrix}$
$K_4 = \begin{bmatrix} -0.5248 & 0.3450 \end{bmatrix}$
Then, the closed loop system is asymptotically stable $\forall \varepsilon \in [0, 0.4215]$ and $d \in ]0, 1]$ as shown in figure 2.

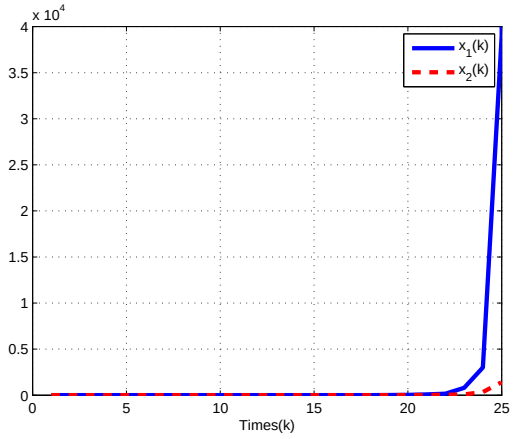


Fig. 1. Evolution des tats en boucle ouverte avec $\varepsilon = 0.4215$ et un retard $d = 1$

From the simulation results, it can be seen that the controller has been able to improve the bound stability of the closed-loop system.

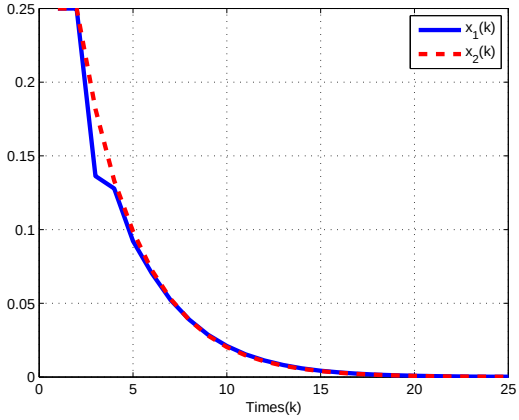


Fig. 2. Evolution des tats en boucle ferme avec $\varepsilon = 0.4215$ et un retard $d = 1$

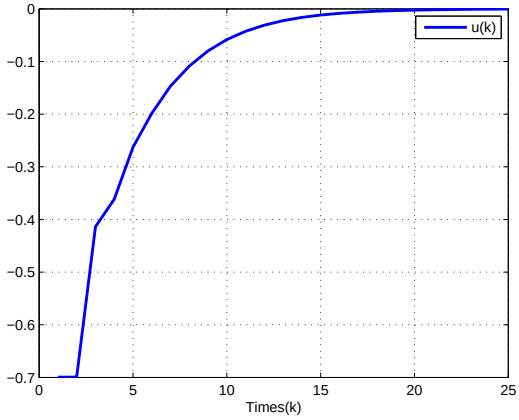


Fig. 3. Evolution de la commande du systme avec $\varepsilon = 0.4215$ et un retard $d = 1$

## V. Conclusion

State feedback stabilization is proposed for discrete nonlinear SPS with time-delay. The considered system is represented by a discrete coupled multimodel. Sufficient conditions for the existence of state feedback controller are obtained based on an appropriate Lyapunov function. Simulation example is given to illustrate the effectiveness of the presented method.

## Acknowledgment

This work was supported by the ministry of Higher Education and Scientific Research in Tunisia.

## References

[1] ABDELJAWAD, R., BAHRI, N., et LTAIEF, M. Stability bound analysis of slow sampling discrete-time singularly perturbed systems with time-delay. In : Sciences and Techniques of Automatic Control and Computer Engineering (STA), 2017 18th International Conference on. IEEE, 2017. p. 1-5.

[2] WU, Huai-Ning. Delay-dependent stability analysis and stabilization for discrete-time fuzzy systems with state delay: A fuzzy Lyapunov-Krasovskii functional approach. IEEE Transactions on Systems, Man, and Cybernetics, Part B (Cybernetics), 2006, vol. 36, no 4, p. 954-962.


ISSN 1737-9334

[3] CHEN, Jinxiang. Fuzzy singularly perturbed modeling and composite controller design for nonlinear multiple time-scale systems with time-delay. Fuzzy Sets and Systems, 2014, vol. 254, p. 142-156.
[4] NAGY, Anca Maria, MOUROT, Gilles, MARX, Benot, et al. Systematic multimodeling methodology applied to an activated sludge reactor model. Industrial & Engineering Chemistry Research, 2010, vol. 49, no 6, p. 2790-2799.
[5] MOORE, Bruce. Principal component analysis in linear systems: Controllability, observability, and model reduction. IEEE transactions on automatic control, 1981, vol. 26, no 1, p. 17-32.
[6] PETZOLD, Linda et ZHU, Wenjie. Model reduction for chemical kinetics: An optimization approach. AIChE journal, 1999, vol. 45, no 4, p. 869-886.
[7] SAYSEL, Ali Kerem et BARLAS, Yaman. Model simplification and validation with indirect structure validity tests. System Dynamics Review, 2006, vol. 22, no 3, p. 241-262.
[8] Ben Atia, Samah. Sur l'observation et la commande des systèmes non linéaires incertains et /ou à retard par l'approche. 2017. Thse de doctorat. Ecole Nationale d'Ingénieurs de Gabès.
[9] LIU, Huaping, SUN, Fuchun, HE, Kezhong, et al. Fuzzy control for nonlinear singularly perturbed systems with time-delay. In : Systems, Man and Cybernetics, 2003. IEEE International Conference on. IEEE, 2003. p. 798-803.
[10] SUN, Chao, WANG, Fuli, et HE, Xiqin. Delay-dependent stability and stabilization criteria for TS fuzzy singular systems with interval time-varying delay by improved delay partitioning approach. SpringerPlus, 2016, vol. 5, no 1, p. 349.
[11] CHEN, Jinxiang, ZHANG, Xiaoda, HUANG, Jian, et al. Fuzzy robust controller with time-delay design for discrete-time fuzzy singularly perturbed systems with time-delay. In : Control and Decision Conference (CCDC), 2015 27th Chinese. IEEE, 2015. p. 6533-6536.
[12] YANG, Zhigang et CHEN, Jinxiang. ROBUST STABILIZATION FOR DISCRETE-TIME FUZZY SINGULARLY PERTURBED SYSTEMS. Metalurgia International, 2013, vol. 18, no 5, p. 210.
[13] CHEN, J., SUN, F., YIN, Y., et al. State feedback robust stabilisation for discrete-time fuzzy singularly perturbed systems with parameter uncertainty. IET control theory & applications, 2011, vol. 5, no 10, p. 1195-1202.
[14] NAIDU, D. S., PRICE, D. B., et HIBEY, J. L. Singular perturbations and time scales (SPaTS) in discrete control systems-an overview. In : Decision and Control, 1987. 26th IEEE Conference on. IEEE, 1987. p. 2096-2103.
[15] LIU, Huaping, SUN, Fuchun, et SUN, Zengqi. Stability analysis and synthesis of fuzzy singularly perturbed systems. IEEE Transactions on Fuzzy Systems, 2005, vol. 13, no 2, p. 273-284
[16] NAGY, Anca Maria, MOUROT, Gilles, MARX, Benot, et al. Systematic multimodeling methodology applied to an activated sludge reactor model. Industrial & Engineering Chemistry Research, 2010, vol. 49, no 6, p. 2790-2799.




ISSN 1737-9334

# Hack the Bank and Best Practices for Secure Bank

Trust Tshepo Mapoka [#1], Keneilwe Zuva[*2], Tranos Zuva[#3]

[#]*Cyber Security Centre of Excellence (CSCE)*
*Cyber Intelligence Agency*
*Gaborone, Botswana*
[1]ttmapoka@ciabotswana.com

[*]*Department of Computer Science*
*University of Botswana*
*Gaborone, Botswana*
[2]zuvak@ub.ac.bw

[#]*Department of ICT*
*Vaal University of Technology*
*Vanderbijlpark, South Africa*
[3]tranosz@vut.ac.za

***Abstract*— Financial institutions are tremendous targets of opportunity for electronic thievery. Intermingled threats, improvements to man-in-the-middle or browser exploits, and advances in malware diversity has resulted in to easy hacks in to the banks by even less-skilled cybercriminals. The hacks usually targets target something that is of utmost value such as customer credentials and money in the Bank. Historically, banks have purchased various systems to manage threat risks, however their existing perimeter defense controls don't necessarily integrate well. Banks typically have had various fraud prevention controls with various tools for each type of exploit. Further, as these exploits continue to blossom, regulators have struggled to figure out best practice recommendations. Payment Card Initiatives and other banking regulations are a great start, but they haven't kept up with the online threat landscape. This paper addresses many ways of hacking the bank and recommend best practices to securing online banking transactions.**

***Keywords—financial crime, secure banking, fraud, cybersecurity***

## I. INTRODUCTION

The emergence of Internet over a decades has indorsed people to adopt an all connected attitude in expediting their daily tasks [1]. Above all, the usage of internet has attracted the banking sector at large by introducing internet or online banking. The emergence of internet banking has enabled financial institutions to offer their customers relatively convenient and flexible banking, also referred to e-banking. Basically, e-banking refers to bank customers utilising the internet to perform financial services such as online transactions [2]. Online transactions include but not limited to fund transfers, account management and bill payments. Furthermore, e-banking enables ubiquitous online access to the bank accounts without travelling to the bank branch [3]. Internet banking has also benefited both banks and customers because banks have diminished their operational costs by decreasing physical facilities involving human resources, paperwork, and supporting staff. Many countries have integrated the use of the internet into their traditional banking system.

Despite the benefits that the banks are offering through e-banking with faster access to various financial activities [4, 5], there are security concerns that accompany the e-banking systems. [6]. Threat actors widely known as hackers have emerged diversity of intangible techniques for hacking the bank. Though numerous rewards of utilizing e-banking, security issues discourage customers from accepting online usage. This has brought fear to many customers having discovered that online banking usage expose their financial information assets (private credentials, money) at risk [7, 8].

Meanwhile, most banks are widely accepting online usage through the internet, a cumulative number of hackers commit their time to conduct fraudulent activities by using online banking system. It has also emerged in recent research studies that banks can be hacked in so many ways that will be described fully in this paper [9, 10].

This paper is arranged as follows; Section II describes various ways of hacking the bank, Section III describes examples of recent hacking incidents along with the most common hacking types in banks, Section IV describes the true facts about SWIFT and how it correlates with banks from the security perspective. Section V gives the current recommendations that banks can adopt to enhance security. Finally the future strategic best practices for securing the bank are discussed in Section VI.

## II. HACKING THE BANK

There are various methods that can be exploited by the threat actor to hack the bank:

- Downloading malicious software in to the enterprise network.
- Social engineering tips to get in to the infrastructure (servers, systems).
- Use of affected peripheral devices such as external USBs.
- Use of Weak cipher suites (SSL/TLS) from web applications.
- Malicious account takeover (Command and Control) which has now increased by greater than 150%.




ISSN 1737-9334

- Use of weak perimeter controls to defend (Anti-virus.
- Connect to any network is undesirably.
- Total access and control to untrusted private bank sites.

Above ALL, the common weak point that the threat actors/hackers take advantage of is the internal staff or people who have interacted or have prior knowledge about the banking system.

### A. *Most Common Hacking Types*

The most common hacking types in financial institutions include:

- Online and Mobile fraud,
- Phishing scams (misleading emails, pop ups or messages) and malware.
- Distributed Denial of Service (DDoS),
- Money Mule scams ( triggers the use your own account to perform illegal money transactions),
- Social networking risks and identity theft..

## III. SIMILAR HACKING ATTEMPTS RECENTLY

A series of recent bank heists or attempted heist follows malware enabled SWIFT transfers where bank officials received through phishing attempt a malware disguised as the PDF reader.

This is what happens: Attackers conduct months' worth of reconnaissance (study the banks internal processes and controls) before attempting to submit fraudulent SWIFT messages and route bank funds to attacker controlled offshore accounts. In simple context, the hackers use the knowledge and access gained during reconnaissance to begin submitting fraudulent money orders to webs of offshore companies hence enabling them to siphon off millions of dollars. The hackers usually use banks publicly available information and tools to penetrate then commit the theft. The perpetrators gain access to the credentials of those authorized to create and approve messages. The perpetrators then have the capability to send fake messages via Bank computers/systems that interface with the SWIFT system, which enables financial institutions to exchange information on transaction details.

Recently, dozens of Banks mostly in Russia and Ukraine surfaced with unprecedented massive hit of fraudulent enabled SWIFT transfers which led to Hundreds of millions of Dollars being stolen and some salvaged.

### A. *Banco De Chile loses $10Million in SWIFT Related Attack.*

The bank in May 24 2018 surfaced a malware attack then lost about $10 million due to fraudulent SWIFT wire transfers. The compromise occurred while the bank was dealing hundreds of workstations and servers that suddenly ceased working. The malware targeted the bank work stations, affecting cashiers and hampering branch services and phone banking. Some funds were successfully transferred to Hong Kong [11].

### B. *Hackers siphon $100 Million from Bangladesh Central Bank's reserve Account in New York*

The incident follows a malware SWIFT related transfer heist at the BCB reserve Bank in New York. This took place in February 2016, when instructions to fraudulently withdraw US$ 1 billion from the account of Bangladesh Bank, the central bank of Bangladesh, at the Federal Reserve Bank of New York were issued via the SWIFT network. Five transactions issued by security hackers, worth $101 million and withdrawn from a Bangladesh Bank account at the Federal Reserve Bank of New York, succeeded, with $20 million traced to Sri Lanka (since recovered) and $81 million to the Philippines (about $18 million recovered).The Federal Reserve Bank of New York blocked the remaining thirty transactions, amounting to $850 million, at the request of Bangladesh Bank. It was identified later that Dridex malware was used for the attack. Basically, the attackers were able to move laterally within the banks' networks with direction from the attackers' command-and-control servers, compromise administrators' credentials and use those credentials to execute their attacks [12].

### C. *Ukraine: US$ 10 Million Stolen From Unnamed Bank via Swift*

It was revealed that revealed that cyber criminals exploited the SWIFT international banking system to steal US$ 10 million from a Ukrainian bank. The theft was conducted in a way similar to the one the Bangladesh central bank experienced earlier this year – when cyber criminals stole about US$ 81 million from the bank [13].

### D. *Tien Phong Bank in Vietnam in May*

In May 2016, such similar fake transfer requests were also used in an attempt to steal more than US$ 1.1 million from the Tien Phong Bank in Vietnam [14].

### E. *India's Cosmos bank raided for $13m by hackers*

Cosmos Bank in India says that hackers made off with $13.4m in stolen funds through Money mule and SWIFT related attacks. Multiple reports out of the country say that a group of attackers used cloned cards to withdraw cash from ATMs at a set time and perform a fraudulent SWIFT money transfer. Together, the efforts resulted in about $13.4m being stolen from the bank and its account holders. The attack was believed to have taken place in two phases. The first attacker was an international effort with money mules in 28 different countries, all extracting cash from their local ATMs. According to the Hindustan Times, 15,000 transactions were carried out over the seven-hour period. The second phase when a SWIFT transaction saw Cosmos move $1.93m to an account at a bank in Hong Kong [15].

## IV. TRUE FACTS ABOUT SWIFT

SWIFT is a Brussel based cooperative that interconnect about 11 000 banks worldwide, thus making it attractive and widespread target to the threat actor. However, attackers haven't yet exploited any specific vulnerabilities within the SWIFT system but rather sort to exploit the weak controls at the Enterprise networks for the Banks [16, 17]. The threat actor then compromise key accounts for bank officials in order to create fraudulent transfers. Since the breath taking


ISSN 1737-9334

attacks, Banks around the world have seen attempts to undermine the SWIFT infrastructures but to its credit, SWIFT has tripled its security team by launching a 24/7 Security Operation Centre (SOC) that performs real time monitoring of emanating cyber threats and vulnerabilities. In addition, the SWIFT raise continuous awareness to users and improve security by sharing attack related information. Therefore it is the responsibility of the Banks to up their game with proactive defensive controls to triple the impact of the existing security [18-20].

## V. RECOMMENDATIONS FOR NOW

To help protect your Bank from security breaches, you should adopt best practice internal controls [21] and guidelines like the following:

### *A. Enhance Identity verification during logon*

Bank MUST at all times adopt multi factor authentication such that during system logon attempt, the system interact with the actual entity attempting to login. E.g. utilize combination of factors such as Credentials plus OTP sent through text to the mobile phone. Geolocation, pattern based or face recognition factors can be incorporated if desired.

### *B. Implement Dual Custody during Transactions*

Adopt dual authorization and/or transaction-based authentication procedures during financial transfers. Identify verification should adopt real time interaction with the actual entity performing the transaction (Multi factor authentication must apply during transfers).

### *C. Creating and Protecting Credentials password.*

Adopt best practice when creating passwords such as use of combination of alphanumeric characters (./?!#@%*&), One upper case letter, 2 numbers. Bank users SHOULD never share login credentials with anyone and SHOULD never write it down. Use a secure password manager if you need help keeping track of many passwords.

### *D. Protect your Machines*

Place limits and controls on who has access to your computer systems. Users should avoid or cancel the remember passwords prompt on online banking login sites. Make sure the bank's computers are running the latest operating system and versions of software, web browser, and anti-virus protection. Automatic update with security fixes is key. Users should not do your online banking from a computer that has unknown perimeter control status.

### *E. Routine Risk and Vulnerability Assessment*

Since no risk and vulnerability assessment has been carried out before:

It is important for the Bank to know its security posture from the risk perspective. Threat actors take advantage of exploitable vulnerabilities that exist within enterprise (corporate) network points (endpoints, systems, servers) to penetrate deep in to something that is value (i.e. systems that does money transfers, user credentials for online, user privilege escalation procedures). Therefore, recommend the bank to perform routine vulnerability assessment for entire system in combination with Penetration test in the perspective of the hacker. The results will determine the vulnerabilities that can exploited and tested against the existing perimeter controls then report on remediation control measures (necessary patching) that should be in place to maintain protection.

From the risk assessment perspective, routine risk assessment screening must be performed in this context so that any employee contractor, or third party user termination or change of employment or responsibilities cannot result in to deliberate breach. Usually the ex-employees/contractors/third party users understand the banking system and have the credentials at termination. Therefore termination procedures between the Human resource and IT resource must be in place to ensure immediate disabled access of the terminated within the AD or any other related security access to the enterprise and disable access to the facility to avoid future disgruntled breaches. Risk assessment must be performed Prior to employment, during employment and after employment (termination) to maintain up to date records.

*1) Tools for Vulnerability Risk Management:* Majority of the Banks are now integrating real time vulnerability and risk management tools in to their Enterprises to ensure real time visibility and analytics of risk threats attempting to impact business systems, endpoints, servers etc. In this case you can proactively identify, prioritize, and remediate vulnerabilities before being breached.

Desired Tools in the market: InsightVM, Qualys Enterprise Suite

### *F. Routine Cyber fraud awareness*

Employees need routine awareness on current Cyber heist to be cautious and suspicious, and never take e-mail at face value – especially if it seems urgent or contains threats. These may be phishing attempts designed to trick people into opening a malicious link or attachment. They should know to always check any suspicious or unexpected communications by calling, e-mailing, or going to a website directly instead of clicking any links.

### *G. Compliance to Security Standards*

Banks should strictly to adhere to international best practice standards (e.g. ISO 17799 and 27001, PCI-DSS) to avoid unprecedented breaches. Proper information security policies and procedures should adopt international best practice. Failure to meet regulatory guidelines can result in severe penalties for financial institutions [22,23].

## VI. FUTURE STRATEGIC SECURITY INITIATIVES

Due to persistent cyber heists affecting Banks recently, I suggest the following:

- Proactive approach to Cyber security [24-26]: Establish Unified Security Operations and Analytics platform known as the Cyber Security Operation Centre (CSOC/CERT/CSIRT/CIRT) similar to the SWIFT SOC. The CSOC [27-29] shall integrate with the existing perimeter controls acting as perimeter wall that provides overall visibility and proactive real time monitoring over evolving (insider and outsider) threats and vulnerability exploits targeting the Bank enterprise network systems. Early detection and prevention is better than cure. The centralised platform consists of incident response management team that promote information sharing on current surfaced threats targeting the Bank. If you cannot afford the


ISSN 1737-9334

establishment then outsource through reputable Managed Security Service Provider (MSSP) so that you are monitored 24-7-365 days.

- Enhance strong information sharing capability of emanating security incidents with SWIFT.
- Eliminate single sign on factor and expand to multi-factor support to authenticate SWIFT messages
- Enhance security and audit risk baselines for participating banks,
- Increase integrity support for anomaly detection and stop-payment controls,
- Engage third-party consultants to assist with security assessments and implementation
- Adopt analytics technology that performs Darkweb monitoring [30] for threats that occur in the dark space such as Blockchain (Bitcoins).
- Carry out risk assessment by updating the employee credentials database such that terminated officials have disabled access to the VPN, ADs and disabled physical access to sensitive facility areas.
- Carry out vulnerability assessment to proactively identify, prioritize, and remediate vulnerabilities before being breached.

## REFERENCES

[1] Razak LT(2016). The Effect of Security and Privacy Perceptions on Customers' Trust to Accept Internet Banking Services: An Extension of TAM" Mohammed A. Al-Sharaf,"Ruzaini A. Arsha," Emad Abu-Shanab and "Nabil Elayah" Faculty of Computer Systems and Software Engineering, UMP. Journal of Engineering and Applied Sciences, 100, 545-552.

[2] Jolly V(2016). The Influence of Internet Banking on the Efficiency and Cost Savings for Banks' Customers. International Journal of Social Sciences and Management, 3, 163-170.

[3] Safeena R(2010). Customer perspectives on E-business value: case study on Internet banking. Journal of Internet Banking and Commerce. 15, 1-17.

[4] Sharma S(2016). A detail comparative study on e-banking VS traditional banking. International Journal of Advanced Research, 2, 302-307.

[5] Konoth RK, van der Veen V, Bos H(2016). How Anywhere Computing Just Killed Your Phone-Based Two-Factor Authentication. In Proceedings of the 20th International Conference on Financial Cryptography and Data Security.

[6] Vaciago G, Ramalho DS(2016). Online searches and online surveillance: the use of trojans and other types of malware as means of obtaining evidence in criminal proceedings. Digital Evidence & Elec. Signature L. Rev., 13, 88.

[7] Balk R, Yap BK, Loh C, Wong HD(2009). To trust or not to trust: the consumer's dilemma with e-banking. Journal of Internet Business, 6,1-27.

[8] Leukfeldt ER, Kleemans ER, Stol WP(2016). Cybercriminal Networks, Social Ties and Online Forums: Social Ties Versus Digital Ties within Phishing and Malware Networks. British Journal of Criminology, 9.

[9] Chiu CL, Chiu JL, Mansumitrchai S(2016). Privacy, security, infrastructure and cost issues in internet banking in the Philippines: initial trust formation. International Journal of Financial Services Management, 8, 240-271.

[10] Arachchilage NAG, Love S, Beznosov K(2016). Phishing threat avoidance behaviour: An empirical investigation. Computers in Human Behavior, 60, 185-197.

[11] Bank info Security News. J Kirk (2018, Jun. 13). Banco de Chile Loses $10 Million in SWIFT-Related Attack [Online]: https://www.bankinfosecurity.com/banco-de-chile-loses-10-million-in-swift-related-attack-a-11075.

[12] New York Post. K Dugan. (2016. Mar 7). Bangladesh bank says hackers stole $100M from its New York Fed account [Online]: https://nypost.com/2016/03/07/bangladesh-bank-says-hackers-stole-100m-from-its-new-york-fed-account/.

[13] Occrp News. I Spaic. (2016. Jun 28). Ukraine: US$ 10 Million Stolen From Unnamed Bank via Swift [Online]: https://www.occrp.org/en/27-ccwatch/cc-watch-briefs/5419-ukraine-us-10-million-stolen-from-unnamed-bank-via-swift.

[14] The Wall Street Journal. T Khanh Vu, K Burne (2016. May 16). Vietnam's Tien Phong Bank Targeted in Bangladesh-Like Cyberattack [Online]: https://www.wsj.com/articles/vietnamese-bank-says-it-was-target-of-attempted-cyber-heist-1463405095.

[15] Wn.com news. ZDnet (2018. Aug 27). How_hackers_managed_to_steal_135_million_in_Cosmos_bank_heis [Online]: https://article.wn.com/view/2018/08/27/How_hackers_managed_to_steal_135_million_in_Cosmos_bank_heis/

[16] Kumar Parekh, Society for Worldwide Inter bank Financial Telecommunication, 2006.

[17] SWIFT routing protocol, 2007, [online] Available: http://www.swift.com.

[18] Roberto Andrade, Jenny Torres, Pamela Flores, "Management of information security indicators under a cognitive security model", Computing and Communication Workshop and Conference (CCWC) 2018 IEEE 8th Annual, pp. 478-483, 2018.

[19] Shakeel Durrani, Imran Jattala, Junaid Farooqi, Naila Shakeel, Mohsin Murad, "Design and development of wireless RTU and cybersecurity framework for SCADA system", Information & Communication Technologies (ICICT) 2013 5th International Conference on, pp. 1-6, 2013.

[20] Jan M. Ahrend, Marina Jirotka, Kevin Jones, "On the collaborative practices of cyber threat intelligence analysts to develop and utilize tacit Threat and Defence Knowledge", Cyber Situational Awareness Data Analytics And Assessment (CyberSA) 2016 International Conference On, pp. 1-10, 2016. SOC

[21] Siddharth Mahajan, Mitesh Parekh, Hardik Patel, Sharvari Patil, "BRB dashboard: A web-based statistical dashboard", Innovations in Information Embedded and Communication Systems (ICIIECS) 2017 International Conference on, pp. 1-6, 2017.

[22] Rigon Alencar, E. Merkle, C. Westphall, Santos, D. Ricardo dos, C. Becker Westphall, "A cyclical evaluation model of information security maturity", Information Management & Computer Security, vol. 22, no. 3, pp. 265-278, 2014.

[23] 2. Y. Cherdantseva, J. Hilton, "A reference model of information assurance & security", Availability reliability and security (ares) 2013 eighth international conference on, pp. 546-555, 2013, Septembe

[24] Marina Danchovsky Ibrishimova, Advances on P2P, Parallel, Grid, Clou Andrea Dufkova, "National/governmental CERTs ENISA's recommendations on baseline capabilities" in , Enisa Publications.

[25] 2. Karen Kent, Suzanne Chevalier, Tim Grance, Hung Dang, "Recommendations of the National Institute of Standards and Technology", NIST.

[26] 3. Carnegie Mellon, "Creating and Managing Computer Security Incident Handling Teams", CERT Training and Education. d and Internet Computing, vol. 24, pp. 469, 2019.

[27] Zahra Zohrevand, Uwe Glasser, Hamed Yaghoubi Shahir, Mohammad A. Tayebi, Robert Costanzo, "Hidden Markov based anomaly detection for water supply systems", Big Data (Big Data) 2016 IEEE International Conference on, pp. 1551-1560, 2016.

[28] Boyeon Song, Sang-Soo Choi, Jangwon Choi, Jungsuk Song, Information Security, vol. 10599, pp. 437, 2017.

[29] Boyeon Song, Jangwon Choi, Sang-Soo Choi, Jungsuk Song, "Visualization of security event logs across multiple networks and its application to a CSOC", Cluster Computing, 2017.

[30] Eric Nunes, Paulo Shakarian, Gerardo I. Simari, "At-risk system identification via analysis of discussions on the darkweb", APWG Symposium on Electronic Crime Research (eCrime) 2018, pp. 1-12, 2018.




ISSN 1737-9334

**Dr. Trust T Mapoka** received BEng and MEng degrees in Telecommunications and Internet Engineering from University of Bradford, United Kingdom, in 2010 and 2011 respectively. He obtained PhD. Degree in Cybersecurity from university of Bradford, UK in 2016. He hold professional certifications such as Certified Ethical Hacker (CEH), Certified Network Defense Architect (CNDA), Certified Information Security Management Principles (CISMP). He is member of IEEE and IET. He is currently the Senior Cyber Security Expert and provide consultancy on various expertise of Cybersecurity that include Security Operations Analytics, Fraud Management, Ethical Hacking and Vulnerability Management, User Entity Behavioral Analytics (UEBA), Incident Dectection and Response, Network Forensics and Auditing, Identity Spoofing and Training and Awareness. Research interest include IoT Security analytics, Light Cryptography, Wearable devices security, Security Information and Event Management (SIEM) technologies for IoT security, Data Mining, Business Intelligence.

**Mrs. Keneilwe Zuva** is a Senior Lecturer in the Department of Computer Science at University of Botswana. She holds a Master of Engineering (Information Systems and Networks) from the University of Essex in United Kingdom. Her research interests are in Recommender Systems, Computer Networking and Cyber Security threat detection and Analytics, Network Forensics Auditing, Perimeter defenses, multi factor Authentication, Cryptography, IoT security.

**Prof. Tranos Zuva** is an Associate Prof in the Department of ICT in Vaal University of Technology, South Africa. He has published extensively in computer science field. His research areas include recommender systems, networking, Data mining, Business Intelligence and image processing. He is a IEEE member.




ISSN 1737-9334

# Simulation and Modeling of Uncertainties in the Calibration of an Fluorescence Chemical Spectrometer (FRX)

Samira. DJEMILI[1]; Djamel. BERDJANE[1]; Assia. HAMOUDA[1]; Badreddine. MAALEM[1]
[1.]Research Center in Industrial Technologies CRTI: P.O. Box 64, Cheraga 16014
Algiers - Algeria.
s.djemili@crti.dz

***Abstract*— Sensitivity analysis and uncertainty estimation are of major importance for the declaration of conformity of finished products. Models must be sought to analyze the test data. The main objective of this work is to establish reliable models to analyze our experimental data and validate them. So we have studied and used the Monte Carlo and Bootstrap simulation methods, we have been able to realize programs that calculate the uncertainty according to the ISO 8466 standard on X-ray fluorescence spectrometer samples from the URASM CRTI chemical analysis laboratory. Programs and interfaces are made with Matlab (GUI).**

***Keywords—simulation; uncertainties; Monte carlo; Bootstrap; calibration***

## I. INTRODUCTION

In test laboratories and chemical analyzes of the metallic materials, the quality control of the applications is essential. The analysis of sensibility and the estimation of the uncertainties are of major importance for the declaration of conformity of finished products. It is necessary to analyze the data. The main objective of this work is to establish reliable models to analyze our experimental data and validate them. Equipment calibration involves applying a known standard value to the input of the measurement system to verify that the output corresponds to the expected value. There are several models that are used to adjust the calibration curve. The linear regression model is the best known. During calibration, it is necessary to validate the model. Laboratories are obliged to respect the accuracy of the analysis result. We must look for methods that would allow us to predict the standard deviations of the coefficients from a single measure of the measurement, without repeating the measurements. Uncertainty modeling is a very broad field of study. This requires a good foundation in statistical analysis. A very simple case study is the modeling of a calibration curve with the simple linear regression model, but there are other more complicated ones namely the Monte Carlo method and the Bootstrap method.

Our purpose is to realize the simulation by specific programs, to make a comparison between these methods then apply them to real data outcome of the chemical analyses of steels.

## II. PRESENTATION OF THE SIMULATION

Numerical simulation is one of the tools for simulating real phenomena. It relies on the implementation of theoretical models often using mathematical techniques. As well as graphical interfaces allow the display (visualization) of the results (profits) of the calculations by computer generated images. The simulation is performed as follows:

- Generate data which are random variables according to specific models ·
- Execute the experience in a fast and economic way and the improvement of the forecasts.
- Solve the problems of probability and statistics.

To study the finite sample behavior of the test statistics, numerical simulation methods are used, taking advantage of the large computational capacity of the computers, which makes it possible to visualize the results graphically and numerically and thus to predict its behavior and its evolution [1]. Monte Carlo methods are certainly the most common simulation techniques and these are the ones we will use to study the numerical performances of the different tests.

Another alternative approach is developing today using bootstrap methods. The Bootrasp is a method of resampling. It is one of the revolutions of calculation method, it allows us to quantify uncertainties by calculating standard errors and confidence intervals as well as tests.

## III. SIMULATION METHODS

### *A. Algebraic method of distribution of the errors*

The purpose of curve fitting is to find the parameters of a mathematical model that describes a set of (usually noisy) data in a way that minimizes the difference between the model and the data. The most common approach is the "linear least squares" method, also called "polynomial least squares"[2].


ISSN 1737-9334

### B. *Monte Carlo*

The term Monte Carlo is used in many disciplines and refers to procedures where quantities of interest are approximated by generating many random realizations of any stochastic process and calculating any of their mean values [1] (Fig. 1).

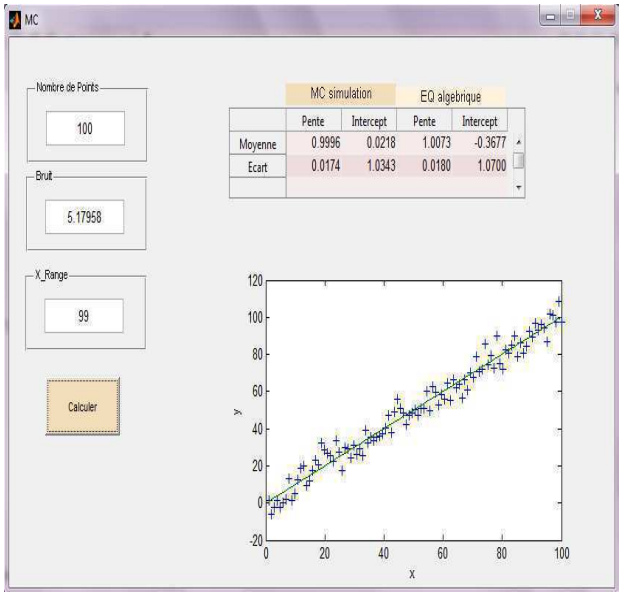


Fig. 1. MC method simulation

### C. *Bootstrap*

Bootstrap: is a technique for performing statistical inference, based on the simulation of data from a limited number of observations, it is intended to facilitate the inference in complex situations where the analytical methods are not enough not [3]. The bootstrap can therefore be applied to any estimator other than the mean such as the median, the correlation coefficient between two random variables or the main eigenvalue of a covariance variance matrix. The bootstrap makes no assumptions about the underlying statistical distribution; hence its generality and power. [4]

### D. *COMPARISON OF ERROR PREDICTION METHODS*

The compar.m program compares these three methods (Monte Carlo simulation, the algebraic method and the bootstrap method) for a linear adjustment of 100 first order points. Each method is repeated on different data sets with the same average slope, interception and random noise, then the SD (SDslope) and intercepts (SDint) were compiled and are shown in the following figure (Fig. 2).

On average, the average standard deviation ("mean SD") of the three methods is fine, but the algebraic and bootstrap methods fluctuate more than the Monte Carlo simulation each time this program is run because they are based on noise in a single 100-point data set, while Monte Carlo simulation reports the average of many data sets. Of course, the algebraic method is simpler and faster to compute than the other methods. However, an algebraic error propagation solution is not always possible, whereas the Monte Carlo and bootstrap methods do not depend on an algebraic solution and can easily be applied to more complicated curve situations, such as least squares non-linear iterative.

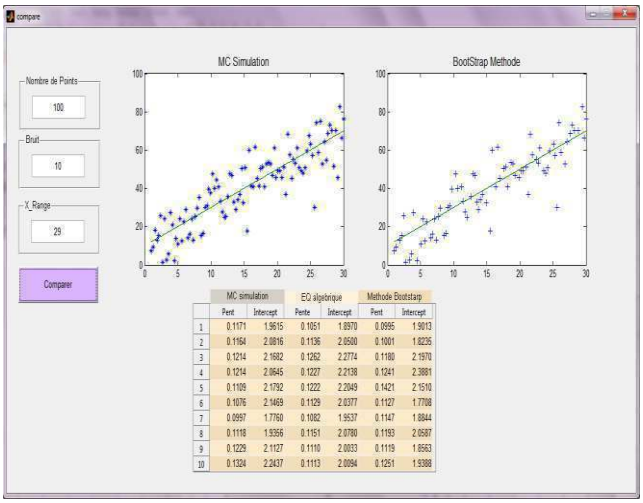


Fig. 2. Comparison of algebric, MC and Bootstrap methods

## IV. TOOL OF SIMULATION "GUIDE MATLAB"

The language used to perform the simulation programs is Matlab with its IDE tool dedicated to the creation of graphical interfaces (GUI). This tool, called GUIDE (Graphical User Interface Development Environment), allows to design these graphical interfaces. HMIs (Human Machine Interfaces) are called Graphical User Interfaces (GUIs) in MATLAB. They allow the user, through graphical objects (buttons, menus, check boxes, ...) to interact with a computer program [5]. These interfaces make it easier for users to use programs.

## V. APPLICATION ON REAL DATA

We applied the simulation on real data by considering standard samples of an X-ray fluorescence spectrometer from the URASM CRTI chemical analysis laboratory. The computer associated with the spectrometer is equipped with the SIEMENS SPECTRA3000 PC LEO 52X MAX chemical control and analysis software.

The quantitative analysis by X-ray fluorescence spectrometry is a basic analysis method, it allows to determine the quantitative composition of the various elements or combinations that enter the composition of the body to study. It consists of measuring the intensity of the element under study and positioning it on the calibration line drawn from the measurement of appropriate standards. The x-ray tube is powered by the x-ray generator. The x-ray tube's radiation excites the atoms of the sample and generates X-ray fluorescence radiation. The collimator selects a portion of this radiation and directs it onto a crystal. analyzer in the form of a parallel beam according to the BRAGG law:

$$\mathbf{n\lambda = 2d\ Sin\theta}$$


ISSN 1737-9334

The BRAGG equation is verified for some values of θ. The analyzer crystal disperses the corresponding radiation that a proportional or scintillation counter collects located exactly at the 2θ angular positions. The intensity of wavelength radiation is expressed by the number of wavelength photons emitted in one second. The meters convert these photons into electrical pulses with a certain efficiency. A counting scale integrates for a predetermined time the number of electrical pulses. The result expresses in KCPS, numbers the intensity of a radiation.

### *A. Statistical evaluation of the linear calibration function*

ISO 8466[6] is applicable to methods requiring calibration, it is specially designed for the evaluation of the analytical method and for the calculation of the performance characteristics of the calibration function. In order to obtain comparable analytical results and to serve as a basis for analytical quality control, the calibration and evaluation of analytical methods must be carried out in a uniform manner [7]. We represent some examples and windows of calculation of error with the Monte Carlo method of the program Tab_incert.m realized with Matlab (GUI) (Fig. 3, 4, 5).

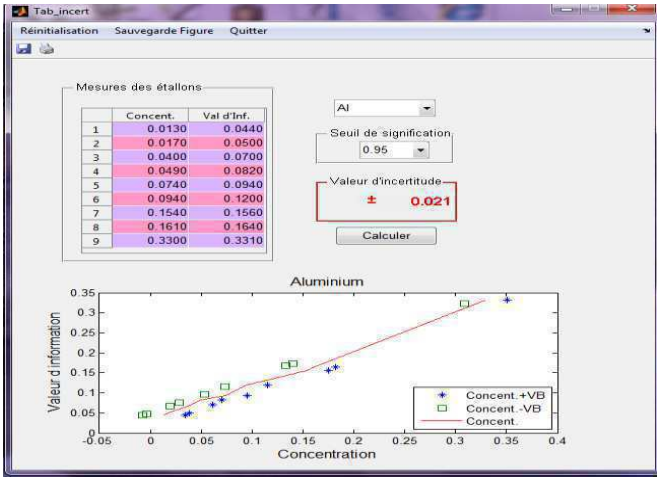


Fig. 3. Applying the simulation to real data from an aluminum standard

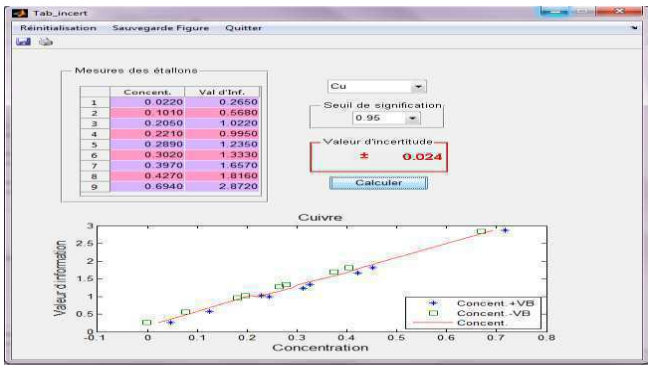


Fig. 4. Applying the simulation to real data from a Copper standard

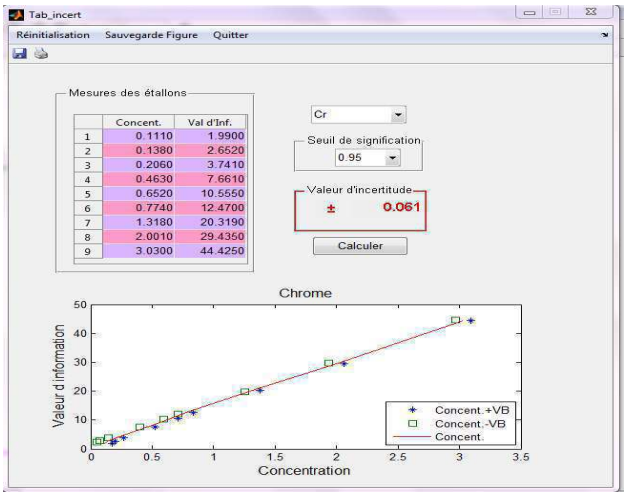


Fig. 5. Applying the simulation to real data from a Chrome standard

## VI. CONCLUSION

The Monte Carlo method is a pillar of numerical simulation in statistical physics, nuclear physics and many other fields for the following reasons: it simplifies the calculations of uncertainties when the adjustment by the models is too complex, its efficiency increases when the number of points generated n increases. This MC simulation method does not depend on an algebraic solution and can be easily applied to more complicated curve situations, such as non-linear iterative least squares. The Bootstrap method still needs to be developed and applied to other measuring equipment as well.

## *References*

[1] Emmanuel Flachaire, "Méthodes de Simulations", Université Paris I Panthéon-Sorbonne, 2003.

[2] David Boilley, "Eléments de métrologie : incertitudes et analyse des resultats de mesure", Université de Caen Basse-Normandie et GANIL, 2011

[3] Irène Buvat, "Introduction à l'approche bootstrap", 2000.

[4] Jean-Marc Martinez, " Apprentissage statistique et techniques de ré-échantillonnage", Centre d'Études de Saclay - Gif-sur-Yvette, France , 2003.

[5] Emmanuel Zenou, " Introduction à Matlab ", Institut Supérieur de l'aéronautique et de l'espace, 2013.

[6] Norme internationale ISO 8466- 1, " Méthodes d'étalonnages" :1990 (F).

[7] Metropol, " Méthode d'étalonnage pour la quantification des polluants ", INRS, 2015.


ISSN 1737-9334

# Effect of Adjacent and Co-Channel Interference on AWGN Channel Using 16-PSK Modulation for Data Communication

*Amaal Omar Althini* [1] , *Hend Hassan Ben-Hamed*[2] *and* Amer *M. Daeri*[3]

[1]*High Institute of Science and Technology, Sorman, Libya*
E-mail asial.mh2013@gmail.com
[2]*College of Electronic Technology, Communication Engineering Department*
*Tripoli, Libya*
E- mail hendayad1234@gmail.com
[3]Zawia University, Faculty of Engineering/ Computer Engineering Department,
Zawia, – Libya,
E-mail amer.daeri@zu.edu.ly

***Abstract*—Interference is a fundamental nature of wireless communication system that is multiple transmission often take place simultaneously over a common communication media. Interference is a major limiting factor in the performance of cellular radio. It limits capacity and increases the number of dropped calls. It has a direct correlation of quality of communication system. It is a prime issue, and has to be taken into consideration of design cellular wireless communication system. Sources of interference are another mobile in the same cell, a call in progress in neighboring cell, and other base station operating in the same frequency band. There are two major types of interference, co-channel interference (CCI), and adjacent channel interference. 16-PSK digital modulation technique has a good performance in wireless frequency band, and widely applications on wireless communication. Three interference signals are introduced on AWGN channel. The effect of this interference is analyzed, and simulated using Matlab.**

***Keywords—CCI; ACI; 16-PSK; AWGN.***

## I. INTRODUCTION

The core concept of the cellular communication is the frequency reuse. Frequency reuse is a technique of reusing channels, and frequencies within a communication channel to improve capacity and spectral efficiency, but interference is introduced due to the common use of the same channel may occur if the system is not properly planned. This type of interference is called co-channel interference (CCI), it is the most critical one, which occur in cellular radio, and it depends on the cellular traffic. At the busy hours of a cellular system, the greatest possibility of appearing of co-channel interference. [1].

The interference between two adjacent channels of the adjacent cells is known as adjacent channel interference (ACI). "Adjacent channel interference results from the equipment limitations, mainly from imperfect receiver filters, which allows near by frequencies to leak into the passband. This interference can be minimized through careful channel assignments by keeping the frequency separation between each channel in a given cell as large as possible". [2].

"Mary modulation technique is the most important technique in digital communication, where group of n-bits can be expressed into a symbol that again ismapped into one out of a set of $M=2^n$ waveforms". The main object of any modulation format of digital communication is to transmit as much information as possible with certain energy level in the transmitted signal. This modulation scheme provides low bit error rate at low received signal to noise ratios, and well performance under wireless fading environments, requires less bandwidth, and easy implementation. The existing modulation technique may not satisfy all the schemes together, but some of them depending on the application requirements. [3]

16-PSK technique is selected to represent the modulation scheme in the proposed communication system, which is simulated by using Matlab program; the interferences are modified to obtain best results.

## II. WIRELESS COMMUNICATION SYSTEM

Typical wireless communication system is represented in figure (1).[2].

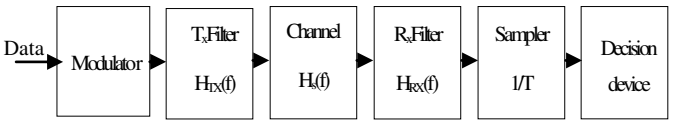


Fig. 1 typical wireless communication system

As seen in the figure the output of the modulator is filtered by the transmitter filter with frequency function $H_{TX}(f)$, which is band limiting filter, then the signal is transmitted over a radio channel, which can represented as filter with frequency function Hc(f), then the signal is filtered by the receiver filter with frequency function $H_{RX}(f)$. The target of this filter is to minimize the noise. Consider the extreme case the channel is AWGN channel. The receiver is followed by a sampler that


ISSN 1737-9334

provides estimates of signal once per symbol period T, then the task of the receiver filter is to maximize the signal to noise ratio (SNR) at the end of the symbol period t=T. This means the filter should maximize signal instantaneous power at time t=T and minimize noise average power. [4]

Raised cosine filter is the most common filtering technique, which is used in the most of communication applications, this filter is divided into two parts, one placed in the transmitter, and the other in the receiver, each one is called square root raised cosine filter. [5, 6].

## III. 16-PSK

16- Phase Shift Keying is Mary modulation technique, which is instead of sending one bit as in binary digital modulation technique, here n-bit can be sent at a time, where one symbol would represent n number of bits.

$M = 2^n$ (1)

Where M represent the number of symbols.

For 16-PSK four bits are combined to form 16 symbol, therefore phase shift is:

$$= \frac{2\pi}{16} = \frac{\pi}{8} = 22°$$

The duration of each symbol of 16-PSK will be $4T_b$, where $T_b$ The duration of each bit.

The transmitted signal in Mary is represented as:

$$s(t) = \sqrt{2P_s}\cos(2\pi f_0 t + \emptyset_m) \quad (2)$$

Symbol phase angle $\emptyset_m = (2m+1)\frac{\pi}{M}$ (3)

Where: m=0, 1, 2,…, M-1

$P_s$power of the symbol.

$F_o$ frequency of the transmitted signal.

The power spectral density is:

$$S_b(f) = 2P_S T_S \left[\frac{\sin(\pi f n T_b)}{\pi f n T_b}\right]^2 \quad (4)$$

Where: $T_S$symbol duration.[7].

## IV. CONSTELLATION DIAGRAM

The transmitted digital signal refers to a point in the vector, space that called constellation point. All these constellation points are shown in a diagram, known as constellation diagram. It provides a geometrical representation of all possible symbol states in amplitude and phase. The x-axis represent in phase components, while y-axis represents the quadrature-phase components."Different modulation schemes result in different magnitude of distance between the constellation points. The distance between the constellation points is a measure of how well a receiver can define a possible symbol when a signal is received. It implies how well a receiver can identify the correct symbol and differentiate from all other possible symbols. The distance between the constellation points refers to the degree of probability of error".

The constellation diagram of 16-PSK is shown in figure (2).

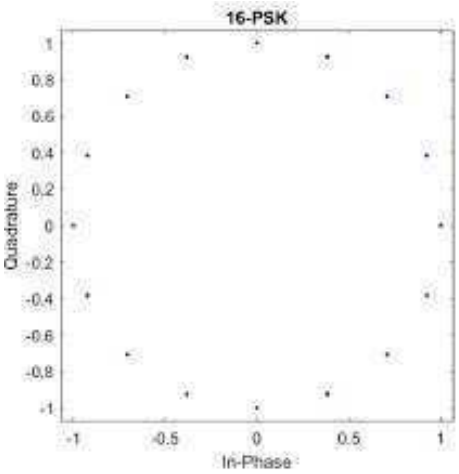


Fig.2 constellation diagram of 16-PSK

As shown in the above figure a 16-PSK would consist of 16 small bright dots that fall in the circle where the permitted phase are $\emptyset(t)=22^o$. But because of radio hardware, generally system imperfection, noise, and interference, the display actually may consist of 16 small clusters. [10,11].

## V.AWGN CHANNEL

Digital communication system's performance is quantified by the probability of bit detection errors in the presence thermal noise. The addition of random signal raising from the vibration of atoms in the receiver electrons is the main source of thermal noise in wireless communication. [8]

It is a basic noise model used in information theory to simulate the effect of many random processes, which is occur in nature. This noise is called additive white Gaussian noise (AWGN) due to the following reason:

- Additive: because it is added to any noise, which might be intrinsic to the information system.
- White: refers to the ideal that it has uniform power across the frequency band for the information system, it is analogy to the color white that has uniform emission at all frequencies in the visible spectrum.
- Gaussian: because it has a normal distribution in the time domain with an average time domain value of zero. [9]

## VI. SIMULATION MODEL

The system model can be built in simulink using its libraries of blocks that represent submodules and component. These libraries contain a wide variety of sources, sinks, connectors, and components. Blocks depending on the level of detail required by the design, modeling, or simulation problem. These models can be modified by changing their internal design. [12].

This communication system simulation model as shown in figure (3) includes the following parameter:

- Bernoulli Binary Generator block: generates random binary numbers using a Bernoulli distribution.


ISSN 1737-9334

- 16-PSK modulator: modulate the input signal using the phase shift keying method, when the input type parameter is set to bits, the input width must an integer multiple of the number of bits per symbol.
- Raised cosine transmit filter: up sample and filter the input signal using a square root raised cosine FIR filter.
- AWGN channel: Add white Gaussian noise to the input signal.
- Root Raised cosine receive filter: filter the input, and using the square root raised cosine FIR filter.
- Down sampler: use to decrease the sampling rate by an integer factor.
- 16-PSK demodulator: demodulate the input signal using the phase shift keying method.
- Three interference: each of them has a similar to the transmitted signal but has a modified frequency offset and power gain as indicated in thefigure.
- Constellation diagram: display constellation diagram of the received signal.

## VII. RESULT AND ANALYSIS

After running the matlab program the following results of the simulated model are accomplished, figure (4)shows the transmitted signal with three interference, includes the additive white Gaussian noise.

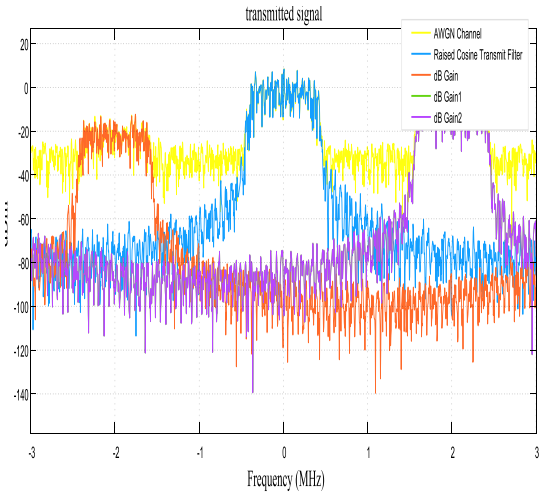


Fig. 4 Power spectrum of transmitted signal.

Figure (5) shows the received signal that the interferences is minimized in this model by using the root square raised cosine filter.

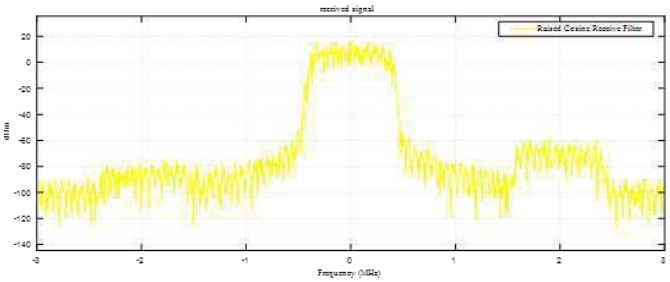


Fig. 5 Power spectrum of received signal

Figure (5) shows the received constellation diagram.

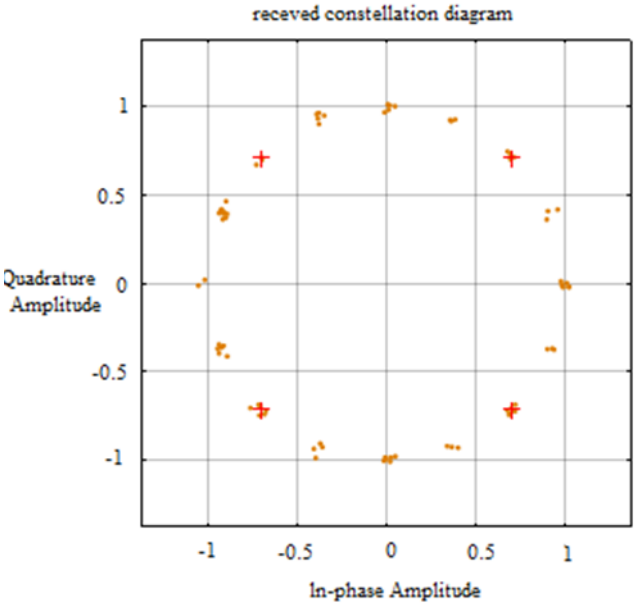


Fig. 6 constellation diagram

To decrease the frequency offset and the negative dB gain of the interference signals, the spectrum analyzer of the transmitted signal shows the interference signals moving from the adjacent channel into the frequency band of the original signal causing co-channel interference that is represented in figure (7)

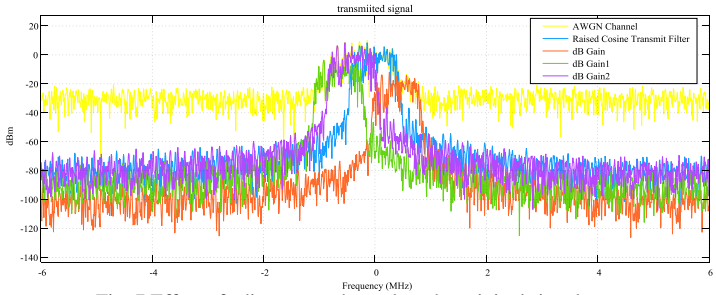


Fig. 7 Effect of adjacent co-channel on the original signal


ISSN 1737-9334

Figure (8) shows the constellation point of 16-PSK that becomes difficult to demodulate

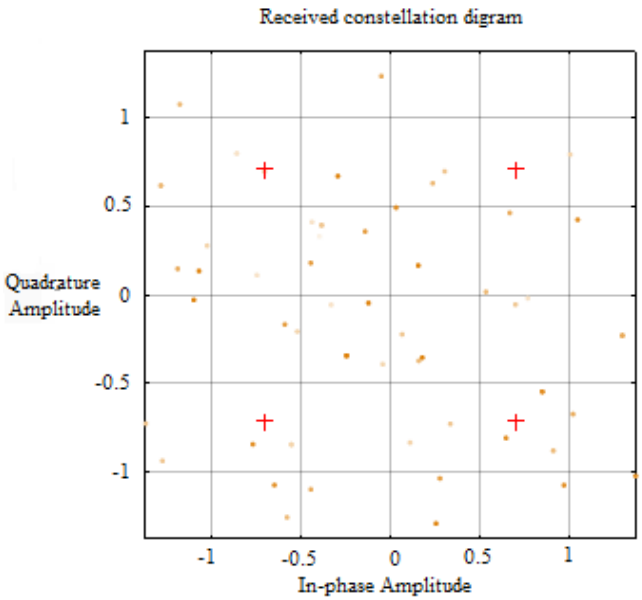


.Fig. 8 Constellation points of 16-PSK

## VIII. CONCLUSION

Effect of adjacent and co-channel interference on additive white Gaussian noise using 16-PSK modulation technique is analyzed, and has been mitigated by using a square root raised cosine filter, which is considered here as a part of the communication system, and by modifying the frequency offset, and the power gain of each interference. Since the received signal quality can analyzed by displaying the constellation diagram of the signal at the receiver, in this case the constellation diagram is uniform, which indicate of minimum effect of interference. While decreasing the offset frequency, and power gain the adjacent channel moving into the frequency band of the original signal causing co-channel interference. In this case, the constellation diagram has a random distribution that refers to the interference.

## REFERENCES

[1] T.L.Singal,“ Wireless communications,”, McGraw-Hill offices ,2010.

[2] Ivan Stojmenovic, “ Handbook of wireless Network and mobile computing,”, A Wiley-Interscince Publication, 2003.

[3] Iti Saha Misra, “Wireless communications and Networks:3G and beyond,”,McGraw-Hill Eduction offices, 2nd ED 2013.

[4] Evgenii Krouk, Sergei Semenov, “ Modulation and coding Techniques in wireless communication,”, wiley,2011.

[5] Dejan Markovic, Robert W. Broaerson, “DSP Architecture Desig Essentials,”, Springer, 2012..

[6] Xuejun Zhang, Lawrence E. Larson, Peter M.Asbeck “Design of linear RF outphasing power amplifier,”, Artech house, Boston . London,2003.

[7] Anokh Singh, A.K. Chhabra, “ Principle of communication engineering,” , S Chand & Company PVT.LTD, 2006.

[8] Kevian McClaning, Tom Vito,“ Radio Receiver design”, Nople publishing corporation, 2011.

[9] Qasim Chandhari, “ Wireless communication from the group up”, 2016.

[10] Saniay Kumar, “ Wireless communication the fundamental and advanced concepts,”, River Publishers, 2015.

[11] Chief Jeary, D. Gibeson, “ The mobile communications Hand Book,”CRC press, Taylor & Francis Group, 3td ED 1999.

[12] Khaled M. Gharaibe,“ Non linear distortion in wireless sysrem: Modeling & Simulation with Matlab”, IEEE press, Wiley, 2011.




ISSN 1737-9334

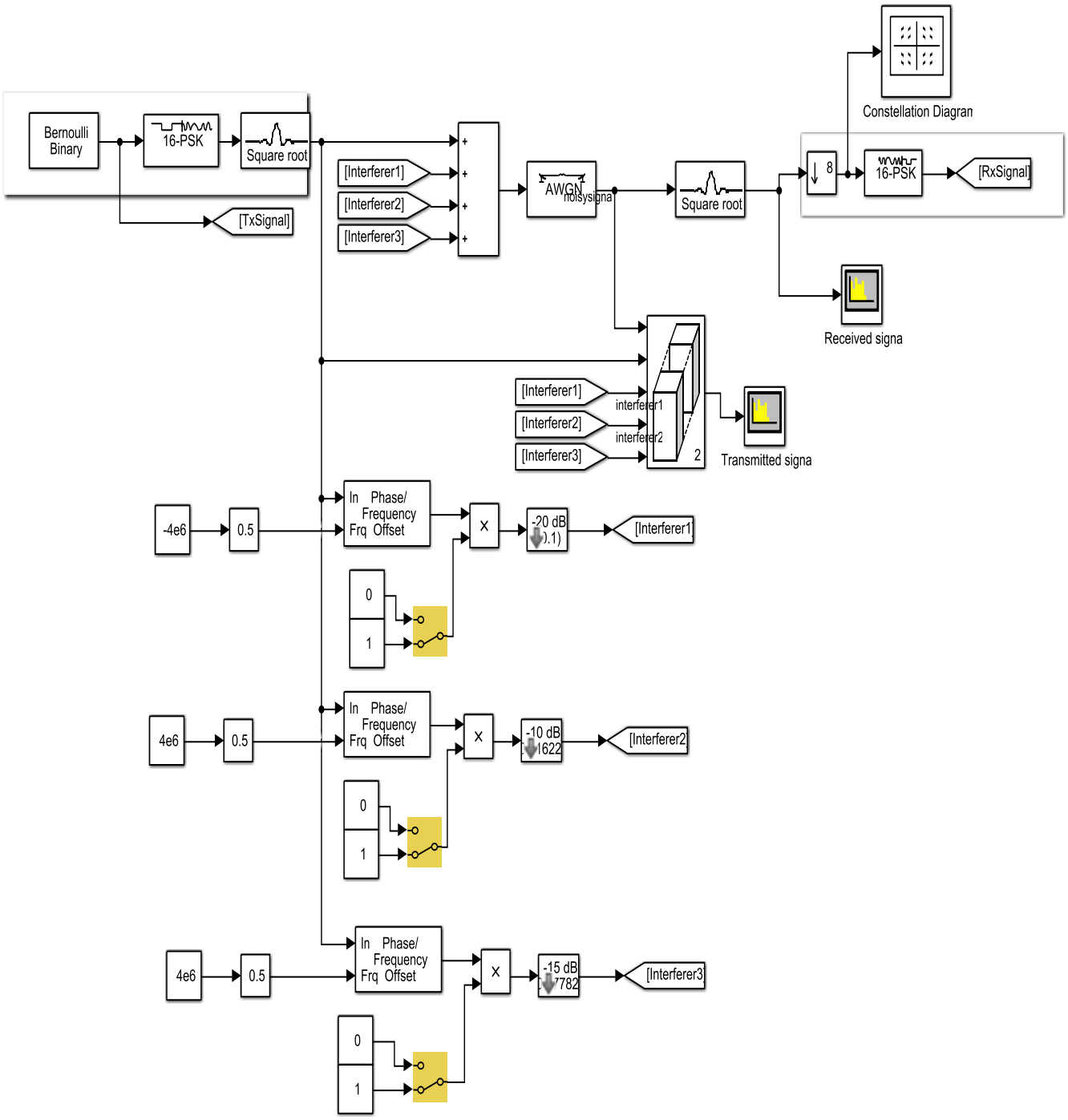


Fig.2 The proposed simulation model




ISSN 1737-9334

# The importance of Web 2.0 Tools for Foreign Language Teaching and their Security Issues

Sedieg A.Elatab[1] , [2]Lamia Gweder , [3]Karima M. Boges

[1] *Scientific Affairs Department , College Of Technical Engineering , Libya*

[2]*High institute of science and technology-Surman, Libya*

[3]*Sabratha University , college of arts ,Libya*

[1]It2017Cisco@gmail.com

[2]lamiagweder@yahoo.com

***Abstract*-Recently, there is no doubt that Information and Communication Technology (ICT) in education has been believe to improve learning and teaching environments , especially Web 2.0 tools, has shortened the distance between people and makes communication easier and faster than the past. Nowadays, the Web 2.0 is becoming the preferred environment for communication, collaboration and sharing especially among young generation population. Although Web 2.0 tools are handy, simpler to spread , free or not expensive and ready to be used in a diverse states, this encourages many actors in the world of education to study the possible ways for applying these technologies in the educational field. Many educators globally, among them an English language teachers, are now taking innovative elements to integrate technology into their teaching environments. In language teaching, language teachers have a wide variety of choices for integrating advancement into their classes. One of these is the use of Web 2.0 tools.The purpose of this abstract going to present some of the most powerful Web 2.0 tools for teaching English as a foreign language include blogs, wikis, Skype, podcasts, google drive ( forms, documents) and multiuser virtual environment. Many of these Web 2.0 tools have been integrated into foreign language classrooms to boost the way of learning for students, such an approach is more useful for language teachers to be knowledgeable about the possible usages of Web 2.0 tools which offers the learner with a variety of activities that enhance his learning and at the same time stimulates him to increase their teaching environments. What is more, it is aimed to discuss some challenges related to the security issues such as technical issues, privacy and Other Legal and Ethical issues when Web 2.0 is used in a foreign language teaching.**

**Keywords: Web 2.0; Learning; Security Issues.**

## I. INTRODUCTION

The Web2.0 is a set of web user-centered design applications . These popular new services implement innovative services designed to facilitate the use and to save time, effort and energy. They allow smooth communication and enhance knowledge sharing on global scale. Many of these services could provide a favourable environment for relevant educational scenarios if some warnings and limitations of use are respected. Selecting some of these services is a necessity to avoid excesses and abuses of potential use by learners if they use them as a mean of entertainment, amusement or loss of time in classroom activities[1].The use of technology in educational settings has certain benefits. It "can increase motivation, decrease anxiety, foster more student-centered activities, provide students with authentic materials and audiences" [2] .

English language teachers are now taking innovative steps to integrate technology into their teaching environments. Teachers have a wide variety of choices for integrating technology into their classes. One of these choices is the use of Web 2.0 tools. With these tools, if integrated properly into language lessons, teachers can create a more engaging, interactive and motivating learning environment in their lessons. However, there are hundreds of these tools on the Internet all of which are not promising for teaching and learning purposes. Therefore, it is important to determine appropriate ones for use in language teaching. Our aim in this paper is to introduce some of the most familiar and useful Web 2.0 tools for teaching English as a foreign language, determined after a rigorous selection based on practical experiment and experience. Such an approach is useful for language teachers to be knowledgeable about the possible uses of Web 2.0 tools to enrich their teaching environments. Moreover, it is aimed to give creative and practical ideas to language teachers on the use of these tools in English Language Teaching[3].


ISSN 1737-9334

This paper describes educational use of 2.0 tools such as blogs and wiki , were explored by pre-service teacher´s with different pedagogical goals: to build individual/group e-portfolios, to enhance cooperation and collaboration, to facilitate interaction and communication competencies. Additionally, It discusses the Possible challenges of Web 2.0 tool use in a foreign language classroom and best practices to avoid security risks.

## II. Web 2.0 IN EDUCATION

Web 2.0 covers a wide range of technologies. The most widely used are blogs, wikis, podcasts, information tagging, prediction markets, and social networks. A short description of these technologies potentialities is given in table 1.

TABLE 1. Web 2.0 TECHNOLOGIES

| Web2.0 Classification | Web2.0 tools | Specific technology examples |
|---|---|---|
| Communicative | Blogs (text, audio and video) | Blogger |
| | Instant messaging tools(text,audio and video based ) | Skype<br>Google talk |
| Collaborative | Wikis | Pb wiki |
| | Virtual communities of practice | Google docs<br>NING |
| Documentative | Blogs | blogger |
| | Electronic portfolios | NING |
| Generative | Immersive gaming environments | World of warcraft |
| | Virtual worlds | Second life |
| | Virtual communities of practice | NING |
| Interactive | Social networking | Facebook<br>Myspace<br>linkedIn |
| | Virtual communities of practice | NING |
| | Virtual worlds | Second life |

The idea of using Web 2.0 applications may be based on several learning theories. Dumitrescu (2015)[4] argued that, with the use of Web 2.0, learning and teaching approaches seemed to be based on the theories of connectivism of cognition and instruction. However, they cannot discard other learning theories such as traditional-behaviourist, cognitivist, and constructionist, on which technologies may rely to a lesser extent than connectivism. Farkas (2012)[5] argued that when teachers use Web 2.0 in the classroom learning environment, they need to understand social constructivist and connectivism pedagogy.

Web 2.0 applications have the potential benefit to establish effective teaching and learning environments. For example, Rogers-Estable (2014)[6] suggested that Web 2.0 tools offer opportunities for learning, whilst creating connection and interaction between teachers and students inside and outside of the classroom. These tools help students to create groups for sharing, collaborating, and growing together. Similarly, Wheeler (2010)[7] found that the use of Web2.0 helps students who are geographically separated to interact, communicate, and share the learning content of the courses. Students using Web 2.0 tools can create, produce, edit, and evaluate knowledge (Richardson, 2009)[8]. This can help teachers to create effective student-centred learning environments.

## III. WIKIS[9]

Wikis allow asynchronous communication and group collaboration across the Internet.Variously described as a composition system, a discussion medium, a repository, a mail system, and a tool for collaboration, wikis provide users with both author and editor privileges; the overall organization of contributions can be edited as well as the content itself. Wikis are able to incorporate sounds, movies, and pictures; they may prove to be a simple tool to create multimedia presentations and simple digital stories.

### *A.Benefits of wikis*

According to David Jakes (2006)[10] , wikis are extremely flexible tools that have many classroom, professional development, and administrative uses including the following:

*1)Classroom:* Students can use wikis as platforms for collaborative problem solving; group laboratory reports; classroom writing projects; and the creation of a class "textbook." The short, wikis can be used to support any type of collaborative student project.

*2)Professional Development:* Wikis are handy tools for planning workshops or conferences. Trainers can post documents and other resources at the wiki prior to the workshop and have participants create and post their own notes during the event. Later, participants can return to the wiki to further reflect on what they have learned.

*3)Administrative Uses:* Administrators can leverage wikis to allow teachers, technology staff, and others help create and edit policy documents.

### *B.Usage in teaching and learning*

Wikis are one of many Web 2.0 components that can be used to enhance the learning process. A wiki is a web communication and collaboration tool that can be used to engage students in learning with others within a collaborative environment (Kevin & Joseph, 2007)[11]. Collaboration using a wiki is not limited to students. Faculty can use wikis to collaborate on projects, whether editing a textbook, preparing a journal article, or assembling a syllabus or reading list. Wikis might also prove to be an ideal vehicle for soliciting ongoing input for research or projects where community input can help inform and direct subsequent investigation. The possibilities for using wikis as the platform for collaborative projects are limited only by one's imagination and time. Wiki-enabled projects can provide various levels of site access and control to team members, offering a fine-tuning element that enhances the teaching and learning experience (Educause 2009)[12].




ISSN 1737-9334

Duffy and Bruns (2006)[13] list several possible educational uses of wikis:

1) Students can use a wiki to develop research projects, with the wiki serving as ongoing documentation of their work.
2) Students can add summaries of their thoughts from the prescribed readings, building a collaborative annotated bibliography on a wiki.
3) A wiki can be used for publishing course resources like handouts, and students can edit and comment on these directly for all to see.
4) Teachers can use wikis as a knowledge base, enabling them to share reflections and thoughts regarding teaching practices, and allowing for versioning and documentation.
5) Wikis can be used to map concepts. They are useful for brainstorming, and editing a given wiki topic can produce a linked network of resources.
6) A wiki can be used as a presentation tool in place of conventional software, and students are able to directly comment on and revise the presentation content.
7) Wikis are tools for group authoring. Often group members collaborate on a document by emailing to each member of the group a file that each person edits on their computer, and some attempt is then made to coordinate the edits so that everyone's work is equally represented; using a wiki pulls the group members together and enables them to build and edit the document on a single, central wiki page.

## IV.BLOG

Generally, a weblog or blog is a personal diary, collaborative space, breaking-news outlet and a collection of links to your own private views memos to the world. In short, your blog is whatever you want it to be. There are so many of them, in various shapes and sizes, and there are no real rules. In simple terms, a blog is a website, where you write stuff on an ongoing basis. New stuff shows up at the top, so your visitors can read what is new. Then they comment on it or link to it or email you. In the field of education, blog or weblogs are being used to satisfy a variety of communication needs to favour e-learning practices (Susana & Sergio 2007)[14]

### *A.Advantages of weblogs or blogs :*

According to Susana and Sergio (2007), weblogs or blogs have several advantages:

1) They are easy to setup and administrate in contrast to other technologies.
2) They are easier to publish all types of resources (text, images, video, etc.) to the Web when compared to traditional web publishing.
3) They allow instant publishing with just one click and are easy to create and maintain, as opposed to traditional web pages that are labor-intensive and require at least some web design knowledge (HTML, CSS, JavaScript).
4) They can be updated easily, from anywhere without having to worry about FTP connections, web authoring software, etc.
5) They have the ability to reach a large audience without losing information quality and allowing for different levels of detail. They break the trade off between reach and richness of information.
6) The access to information posted in weblogs is 24/7 (anytime/anywhere).
7) No special blogging software is needed to create a weblog. Some bloggers use plain HTML to create their weblogs. However, most blogging software allows a person to create and maintain a weblog without knowing HTML. Instructor does not need to periodically request the learning logs to the students.
8) Other technologies can be applied jointly into a weblog. For example, using of Wikis as enablers for group writing and knowledge sharing (eg. Building glossaries).

### *B.Benefits of using a blogs*

The following are the benefits of using a blog listed by Anamaria (2010)[15] .

1) A blog allows web-savvy students to legitimately use their favorite source of information, the Internet, and makes use of their skills for the purposes of the program.
2) It increases the students' motivation to take an active part in the learning process, since blogging is fun and interesting.
3) It develops the communication skills of students that are less internet-savvy through peer-to-peer learning.
4) It keeps students informed with the most up-to-date information about of their object of study.
5) Through the use of comments and other forms of feedback, it develops critical thinking (and the appropriate ways to put it into writing).
6) It is a portal for creativity and personal initiative where good ideas are rewarded not only with good grades but also with direct responses from readers across the web.
7) It increases the visibility of our programs on the web and has the effect of giving it a more clearly defined positive image, which in turn may result in higher commitment of the students to the program and a sense of pride in their work.
8) It makes learning flat, not hierarchical, with the teacher as control point rather than unique source of information and interpretation.

### *C.Ways of using blogs*

According to Susana and Sergio (2007), weblogs can be used by instructors and students as follows:

- Instructor weblog: weblogs written by instructors are mainly used as an additional communication channel to share information with students. Instructor weblogs usually contain course content, course management information, general commentary to all students about their learning progress, etc.



ISSN 1737-9334

• Student weblog: weblogs written by students are basically learning weblogs or project weblogs. A learning weblog (Lowe 2006)[16] is a learning diary, created concurrently with the learning experience, and reporting on the learning content as wells as the process (including time taken, sources used, and so forth). A project weblog, often authored by a team of students, documents the project progress and findings.

## V. The Possible Challenges of Web 2.0 Tool Use in a Foreign language Classroom

Although there are great potentials for Web 2 .0 tools use in foreign language classrooms, there are numerous factors that must be taken into consideration when deciding to use Web 2.0 - examples include the effectiveness of the instructional activities conducted using these tools, the availability of these tools, potential technical difficulties of the tools, and their cost. Following three of the more serious challenges are discussed:

*1.Security threats* : The security concern is a specific obstacle to adoption and integration of social media in organizations. The top four perceived threats from employees' use of Web 2.0 are malicious software (35 percent), viruses (15 percent), overexposure of information (11 percent) and spyware (10 percent). To solve this issue , one may consider limiting the use of JavaScript in the browser to protect from malicious script4 attacks. In addition, the latest security patches recommended by the anti-virus product vendors should be applied. When writing and publishing blogs, care must be taken to protect one's own personal data, as well as sensitive or even confidential information about other persons or organisations. For example, personal information such as email addresses, mobile phone numbers, or even personal photos should not be disclosed without good reason. Figure1 illustrates the top concerns perceived by companies about the use of Web 2.0 technologies.

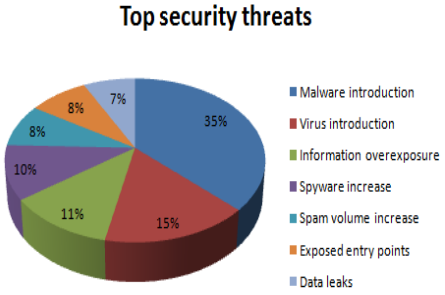


Fig 1: Top security threats of Web 2.0 usage.

*2.Technical Problems:* About sixty percent of the students in some studies mentioned technical difficulties associated with uploading their videos. The difficulties included the incompatibility of the video format and length of upload time. To solve the technical problems, instructors should test whether there are technical problems, such as how much time it needs to upload a video and compatibility issues, beforehand,. Moreover, the instructor's timely feedback in the study also helped to solve the technical difficulties.

*3. Privacy and Other Legal and Ethical Issues:* Of course, Web 2.0 users in this study could engage in inappropriate behavior, such as illegal file-sharing (copyright infringement), spamming, multiple identities, identity deception, and illicit materials (Kerbs 2005)[17] . Other inappropriate activities in the virtual world include breach of privacy, eavesdropping, exploitation, violating professional ethics, violating confidentiality, and sharing proprietary information.

## VI . PATHS AND BEST PRACTICES TO AVOID SECYRITY RISKS

Most enterprises already have a form of an acceptable use policy, which should govern the use of all resources in the enterprise computing environment. The Web 2.0 application evaluation should form part of the organization's risk management process. Organizations can implement policies restricting employees' use of Web 2.0 applications. The following guidelines should be followed when formulating the policy:

- The policy should be created after consultation with all stakeholders.
- The policy should be based on principles, but should be detailed enough to be enforceable.
- The policy must be effectively communicated.
- Policies should be aligned with those already in operation relating to, for example, e-mails.

Some best practices should be taken into account when implementing the policy. First, responsibility of implementing and enforcing the policy should be shared and delegated to the various departments. Second, a compliance officer should be made accountable for the oversight and co-ordination function. Finally, all users must acknowledge the policy in writing. We must always consider that a policy is only effective if it is known and understood by all users. The users should be aware and educated on the safeguards and policies. Therefore, users must be trained to identify Web 2.0 applications and understand the risks, as well as stay informed about the latest news on fraudulent Internet activities. Employees should understand and implement the security feature, which these websites provide.

## VII. CONCLUSION

Web 2.0 tools have transformed teaching and learning in the 21st century and they have a potential to offer new affordances for learning, creating, sharing and using




ISSN 1737-9334

information and knowledge.Web 2.0 can make learning more flexible and interesting.

As it was presented above, the contribution of Web 2.0 tools such as wikis and blogs is very important since this kind of tools keep getting more and more popular. In order to obtain the most efficient results using wikis and blogs, we need to explore a number of questions. Learners are familiar with regular written assignments but not with the different nature of wikis. Consequently, educationalists should provide sufficient help and instructions to learners in order for them to understand the demands of writing in a wiki. So a question to be explored is what the exact kind of guidance should be for the learners to achieve the best performance conducting this kind of assignments. Can blogging promote reflection and deep learning? We need to come up with activities empowering current excitement on blogs use and that is a field to explore.

Web2.0 brings new developments to the web and the internet. However, new security risks also need to be taken into account. In particular, attackers may shift their focus from the server side to the client side, which is usually considered the weakest link in the security chain. The fundamental tenets of application security should not be ignored and overlooked. Security should be built into web2.0 applications from the earliest stages of development. security processes, controls and management oversight should be in place before applications are deployed. Periodic and ongoing security risk assessments should be conducted to identify and fix vulnerabilities. management, application developers and end-users all need to work together to tackle these challenges in the new era of web2.0.

## REFRENCES

[1] The use of Web 2.0 Innovations on Education and Training, Mchichi Tarik*, Afdel Karim, Systems Laboratory Vision , Ibnou Zohr University Agadir, Morocco.
[2] Erben, T. (2013). Calling All Foreign Language Teachers. Hoboken: Taylor and Francis.
[3] Using Web 2.0 Tools in English Language Teaching, Ahmet Başal, Talat Aytan - Yildiz Technical University (Turkey).
[4] One step ahead: From Web 1.0 to web 2.0 technologies in higher education. Paper presented at the 4th International Scientific Conference: eLearning and Software for Education: eLSE, Bucharest. Romania: CAROLI, National Defence University Publishing House.
[5] Participatory technologies, pedagogy 2.0 and information literacy. Library Hi Tech,30 (1), 82 – 94.
[6] Web 2.0 use in higher education. European Journal of Open, Distance and eLearning,17(2):129-141.
[7] Open content, open learning 2.0: Using wikis and blogs in higher education. In U.-D. Ehlers & D. Schneckenberg (eds.), Changing cultures in higher education: Moving ahead to future learning, (pp. 103-114). New York, NY: Springer. doi:10.1007/978-3-642-03582-1_9.
[8] Blogs, wikis, podcasts, and other powerful web tools for classrooms (2nd ed). Thousand Oaks, CA: Corwin Press.
[9] WEB 2.0 TOOLS INOQUICK GUIDE , MOHAMED AMIN EMBI, Centre of Academic Advancement Universiti Kebangsaan Malaysia 2011.
[10] David Jakes. 2006. Wild about wikis. Retrieved from http://www.techlearning.com/article/6164 [25 March 2011].
[11] Kevin R.P. & Joseph T.C. 2007. Wiki as a Teaching Tool. Interdisciplinary Journal of Knowledge and Learning Objects. 3(2007):57-71.
[12] Educause. 2009. 7 things you should know about wikis.
[13] http://net.educause.edu/ir/library/pdf/ELI7004.pdf [25 March 2011].
[14] Duffy, P. & Bruns, A. (2006). The use of blogs, wikis and RSS in education: A conversation of possibilities. Proceedings of the Online Learning and Teaching Conference 2006, Brisbane: September 26. http://eprints.qut.edu.au/5398/1/5398.pdf [25 March 2011].
[15] Susana de Juana-Espinosa & Sergio Lujan-Mora. 2007. The use of weblogs in higher education: Benefits and barriers.
[16] Anamaria Dutceac Segesten. 2010. Blogs in higher education – some ideas about their benefits and downsides. http://uvenus.org/2010/06/07/blogs-in- ighereducation-% E2%80%93-some-ideas-about-their-benefits-and-ownsides/html [4 May 2011]. http://gplsi.dlsi.ua.es/proyectos/webeso/pdf/inted07.pdf [4 April 2011]
[17] Lowe, A.J. 2006. Blog use in teaching–Dragster activity. Internet: ttp://www.webducate.net/dragster2/examples/bloguse/. [4 May 2011].
[18] Kerbs, R. W. 2005. "Social and Ethical Considerations in Virtual Worlds." *The* Electronic Library 5 (23): 539-547.


ISSN 1737-9334

# License Plates Recognition System for Light Limited Conditions

Ali Ganoun, Faraj Farhat and Omar El Baruni

*University of Tripoli, Faculty of Engineering, Electrical and Electronic Engineering Department*
*Tripoli, Libya*
a.ganoun@uot.edu.ly, f.farhat@uot.edu.ly, O.Elbaruni@uot.edu.ly

*Abstract*—**A growing demand for traffic data concerning traffic flow and automatic car identification, motivates researchers around the world to adopt advanced computer vision techniques to monitor and control traffic flow.**
**This paper presents the application of License Plate Recognition (LPR) system for Libyan vehicles in light limited conditions. The proposed system based on captured image sequences with infrared camera.**
**Generally, LPR system consists of four main stages, in the first stage video frames was processed and analysed with some image processing techniques such as equalization and filtering. The second stage is the localization of license plates in the image. The next stage is the segmentation of plate characters. The last stage is the recognition stage where the plate characters recognized and identified.**
**The proposed system was implemented and tested using three videos sequences with different sizes. The overall system accuracy level was about 51% in its best cases, while for the localization and the segmentation stages the system provided an 80% percent accuracy.It is observed that results influenced by the quality of input images and distance between the camera and the vehicle.**

***Keywords*— LPR, localization, segmentation, recognition light limited conditions.**

## I. INTRODUCTION

LPR system is the ability to automatically extract and recognize of vehicle number plates from an image. In essence, it consists of a camera that can capture images and algorithm ms that can detect and recognize license plates.

LPR systems has been used in many applications such as security control, traffic management systems, border crossings, car parking and many other applications.

In general, vehicles in each country have a unique license number written on its license plate used to distinguish one vehicle from the other. An automated LPR system can be implemented to identify the license plate of a vehicle and extract the characters from the region containing a license plate. The license plate number can be used to retrieve more information about the vehicle and its owner, which can be used for further processing [1,2].

The main objective of this project was to develop an efficient LPR system that recognize the license plates in limited luminance conditions. and to Implement and test the proposed system. Other objective is implement, test and evaluate the performance of the proposed system.

## II. PRINCIPLES OF LICENSE PLATE RECOGNITION

As shown in Fig 1, a typical LPR system consist of the following stages:

- License plate Localization.
- License Plate Segmentation.
- License Plate Numbers Recognition.

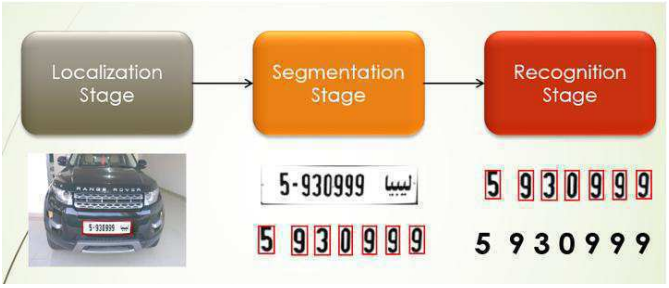


Fig. 1 The main stages of a typical LPR system

### A. License plate Localization

License plate Localizations the most important and the most difficult stage in the recognition process. Generally, it is based on license plate regional characteristics to determine the location of the license plate in the image. The accuracy of this stage directly influence the accuracy of the whole LPR system. There are many techniques can be used for localization stage such as Neural networks, Ad boost Algorithm.

Other methods use the structure of plate texture, edge, gray histogram, angular point, horizontal or vertical projection geometry characteristics combined with the image processing methods to determine the location of the license plate. There are also many techniques are based on the license plate's



ISSN 1737-9334

background color, color-space distance, and similarity calculation [3,4].

### B. License Plate Segmentation

After license plate localization, segmentation involves splitting characters and segment each character. Many techniques can be applied for character segmentation such as Thresholding which provides an easy and convenient way to perform image segmentation based on different intensities or colours in the foreground and background regions using a threshold value. The main challenge in this approach is selecting the optimum threshold value. Other techniques based on edge detection. Edges occur on the boundary between two different regions in an image. Based on this, edge detection is segmenting the image using the difference in pixel values. There are many techniques based Connected Component Analysis (CCA), which analyse and segment connected components in a binary image. The goal of the connected component analysis is to detect connected region or object. The set of connected components are used to partition an image into segments. [6,7]

### C. License Plate Recognition

Plate recognition refers to the process of assigning a given input data into one of a given number of categories. It is the process of identifying each character and assigning it to the correct character class. There are several recognition techniques can be used such template matching, neural networks, statistical approach, structural approach [7,8].

## III. INFRARED LIGHT

Infrared (IR) radiation was discovered in 1800 by astronomer William Herschel, who discovered a type of invisible radiation in the light spectrum beyond red light. Slightly more than half of the total energy from the Sun was eventually found to arrive on Earth in the form of infrared. Infrared light is emitted or absorbed by molecules when they change their rotational-vibrational movements. Infrared light is used in industrial, scientific, and many medical applications.

IR light is an electromagnetic radiation with longer wavelengths than those of visible light, extending from 700 nm to 1 mm. Which corresponds to a frequency range of approximately 430 THz down to 300 GHz. IR LPR based systems can capture plates in complete darkness where the plate's reflection will be very bright to the camera because of the illuminator, even though human beings see no light.

In this project IR photography is used, a technique that can capture on film or on a digital sensor where the IR radiation reflected by the scene. Both film and sensor are seriously limited in their capability to record IR radiation. Digital sensors can go as far as 1300nm. Commercial IR films are unable to record radiations below about 900nm.

## IV. PROPOSED LPR SYSTEM

This section discusses the proposed LPR system used in the identification of the Libyan licence plates in light limited conditions using Infrared illumination. All license plate images and videos are taken with an infrared static camera.

The flow chart in Fig2shows the main stages of the proposed license plate recognition.

### A. Pre-processing

Pre-processing for video frames is performed to extract images for the purpose of LP recognition. Pre-processing is done as following:

- Convert the image to gray scale, which can ease further processing.
- Apply an order static filter, to filter the noise on the image.
- Apply histogram equalization to adjust the contrast of the image. Histogram equalization accomplishes this by effectively spreading out the most frequent intensity values. Equalization can help in infrared LP images as the lights of the stop lamps makes the license plate vanish and unreadable, but with the equalization process the light in the image will be redistributed and the license plate can be recognized.
- The last step is to adjust the image to become darker so that the license plate area will become clearer.

Fig 3 shows the pre-processing stages.

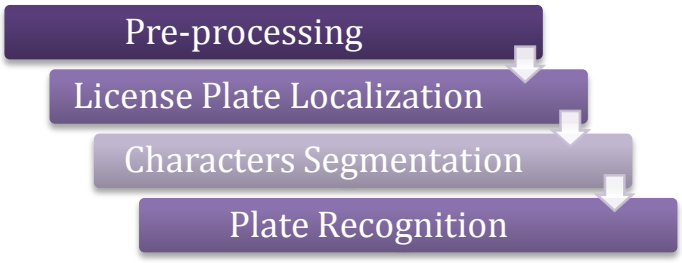


Fig. 2 Block Diagram of the Proposed License plate system.




ISSN 1737-9334

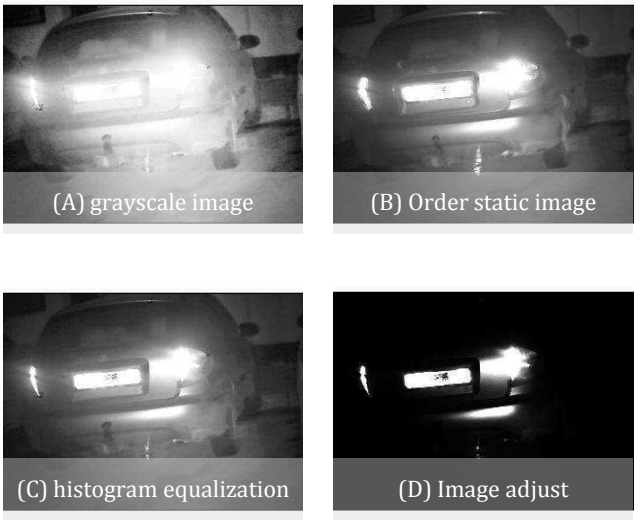


Fig. 3 The Pre-processing Stage

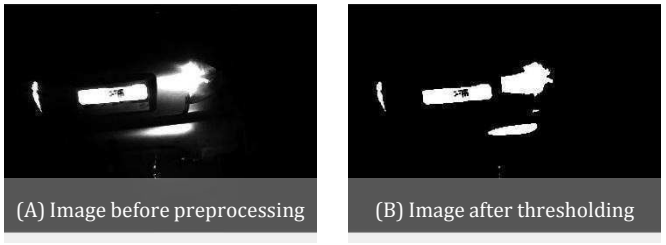


Fig. 4 Binary Thresholdingof IR Image.

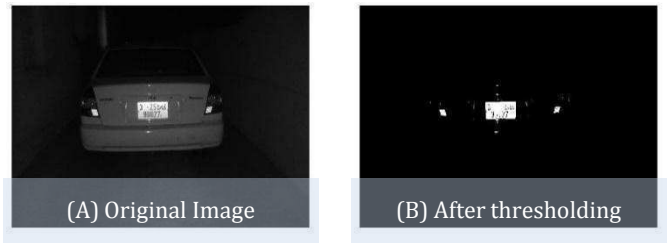


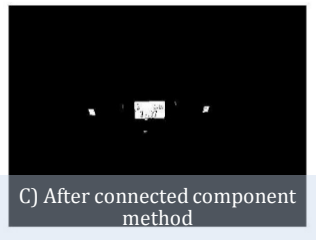


Fig. 5 Effect of Connected Component Elimination.

### *B. License Plate Localization*

In order to have a reliable localization of license plate in light limited conditions, several steps are required. which includes the following steps:

#### *1)Binary Thresholding*

This step used to detect regions and objects in a digital image that similar in properties, Fig. 4 shows demonstrates the binary thresholding for an Infrared image. As can be seen Thresholding can help in removing any non-white object in the image, which can minimize the plate candidates. Usually in infrared car plates images leaves only the plate and the rear lights, this is a good feature of infrared images because this can ease the localization process.

#### *2) Connected component elimination*

All objects that have a value which is fewer than P pixels would be eliminated in this step, which can be done by using a connected component filter. In general, connected component labelling is done by forming an algorithm that labelling the vertices based on the connectivity and relative values of their neighbours. Connectivity can be 4-connected or 8-connected. In the proposed system, the connected component elimination effect is performed after the original image is converted to binary, the use of connected component elimination is vital to remove small objects as shown in Fig. 5 [5].

#### *3) Rectangular ratio*

As all license plates have a rectangular shape, therefore in the proposed LPR a filter has been used to filter all non-rectangular shapes, which leaves only the License plate, and some accompanying noise.

#### *4) Euler Number Objects Elimination*

Euler number for the binary image is the total number of objects in the image minus the total number of holes in those objects. The proposed system make use of this feature given that objects in the license plate image have at least 7 or 8 holes because it represents the license characters. Generally, other objects in the image have a maximum of 2 or 3 holes so the Euler number can be used to discard these objects. Fig 6 shows the image after applying Euler elimination filter [5].

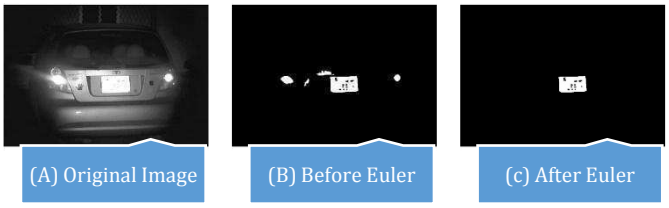


Fig6 Euler Number Effect.




ISSN 1737-9334

### C. License plate segmentation

After the detection of the license plate position in the image the next stageis the segmentation stage. The segmentation is one of main stages in all LPR systems. If the segmentation fails, a character can be improperly divided into two pieces, or two characters can be improperly merged together. Horizontal and vertical projection of a plate image has been used for the plate segmentation.

The input image to this stage is the localized license plate image. The first step is to convert the image to binary image as required for horizontal and vertical projection.

Next, the system applies horizontal projection where the image is processed row-wise. A histogram is prepared based on this processing. With the horizontal projection the image plate can be divided into two sub images ready for further processing as shown in Fig 7.

The last step in this stage is the vertical projection, which is an essential step in plate segmentation; the image is processed column wise and the operation of scanning the image from left to right column by column. By doing this operation the characters will be separated individually and are ready for recognition as shown in Fig. 8.

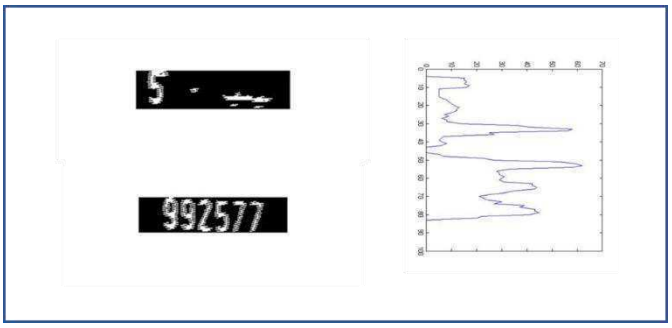


Fig. 7 Horizontal Projection of License Plate.

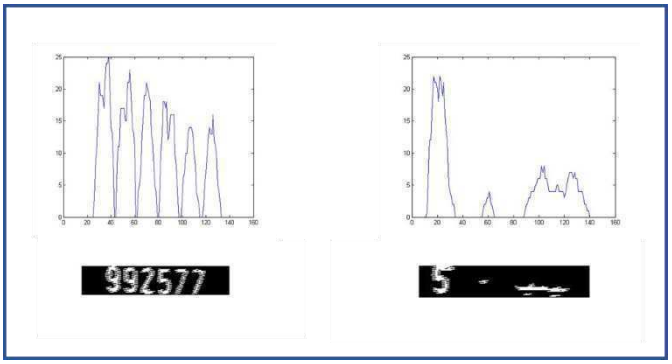


Fig. 8 Vertical projection of License Plate.

### D. License Plate Recognition

After the segmentation of plate characters, the next stage is to develop a technique to identify the plate characters. Template matching technique has been used for this stage, this method has fast recognition speed, especially for binary images, and it can meet the real-time requirements, this method can have a higher recognition rates when the license plate image is clear.

The method is quiet simple, it works on the principle of comparing the segments from the previous stage with the templates, a correlation is done with stored templates until the system find its match.

The implemented template matching includes the following steps:

- The system checks if the segment is a number or not, if so the operation proceeds, if the segment is a letter or any kind of noise its immediately discarded.
- Sometimes the segment has a blank space above or below the number, this can affect the matching process, the solution for this problem is removing this blank space using Horizontal projection.
- The system resizes the provided segment to the same size of the saved template so the process of correlation can take place.
- Before the matching operation can start, the system inverts the binary segment. Then it passes through an order static filter to reduce the black area to prepare the segment for matching as shown in Fig. 9.
- The matching is the done by XOR the segment with all stored templates, the highest correlation with the template is saved, this process continues for all sub-images as shown is Fig.10.

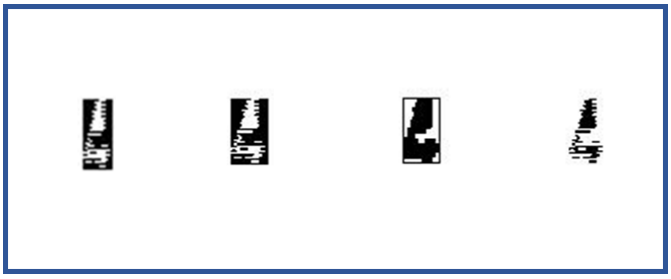

Fig. 9 (A) Segment after removing blank space - (B) Resizing segment - (C) negative Segment - (D) applying order static filter.




ISSN 1737-9334

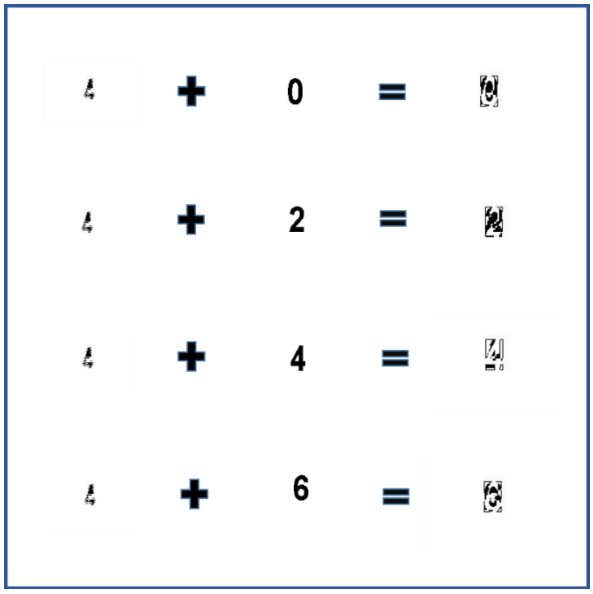


Fig. 10 Example of template matching of sub-image with some samples

## V. RESULTS AND PERFORMANCE ANALYSIS

The proposed LPR system deals with video frames as the input signal rather than static images, the performance of the system has been tested using 3 video sequences; these sequences were taken in light limitedconditions with an Infrared camera. Table 1 shows some properties of the test sequences.

The recognition result wasanalysed and the system performance accuracy was determined for each sequence where the percentage of success for every video sequence has been measured.The system compared the outputs of each stage with the actual plates information which had been inserted manually.

From the 258 frames that was tested the license plate was successfully located in 218 frames with a success percentage of 84.91 %, the reason for the 15.09 % error often comes from the source image. For the segmentation process, the characters of 210 frames were successfully separated. The success percentage was 81.39%. The recognition process is analysed by comparing between recognition with thinning or without thinning for each video sequence. Thinning is a step in the recognition stage performed used by using an order static filter.

The overall performance of the proposed system is summarized in Table 2 and Fig.11. The accuracy percentage of the result was calculated using the formula:

$$Accuracy = \frac{Total\ number\ of\ correctly\ detected\ plates}{Total\ number\ of\ plates}$$

TABLE 1
TEST SEQUENCES.

| Source | Video Sequence # 1 | Video Sequence # 2 | Video Sequence # 3 |
|---|---|---|---|
| Number of frames analysed | 258 | 362 | 534 |
| Frames size | 720x576 | 720x576 | 720x576 |

TABLE 2
TEST RESULTS FOR VIDEO FRAMES DETECTION AND RECOGNITION

| Source | Video Sequence # 1 | Video Sequence # 2 | Video Sequence # 3 |
|---|---|---|---|
| Localization stage success | 218 | 289 | 292 |
| Localization success percentage | 84.91 % | 80% | 54.8% |
| Segmentation stage success | 210 | 289 | 292 |
| Segmentation success percentage | 81.39% | 80% | 54.8% |
| Recognition stage success% (with thinning) | 51% | 31.8% | 13.7% |
| Recognition stage success % (without thinning) | 39% | 25% | 10.4% |

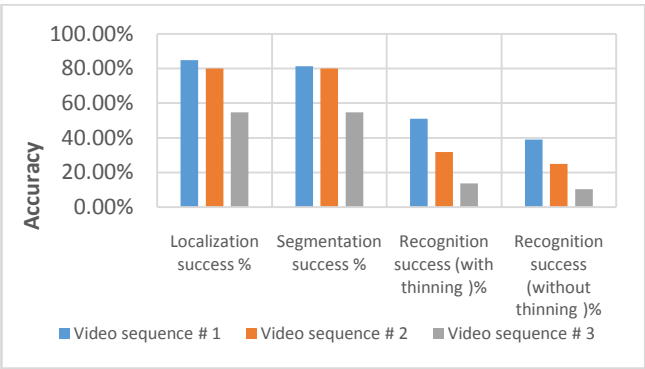


Fig. 11 The Performance of the proposed LPR system.

## VI. CONCLUSIONS

This project related to the design and implementation of License Plate Recognition system for Libyan license plates in light limitedconditions (e.g. at night time) using video sequences as input source.

Since the input to the system is a video sequence and not static images, pre-processing was needed before initiating the three major stages in any LPR system. The pre-processingneeded to prepare frame images for the localization




ISSN 1737-9334

stage by reducing noise, redistribution of the light in the image and adjusting the intensity values.

In the localization stage many image-processing techniques has been performed such as elimination of small objects using connected component analysis, then using Euler number to minimize the objects in the image .Finally, using structural properties, the correct plate region is identified and localized fromthe candidate regions.

After the selection of plate image, it is passed to the character segmentation stage.For segmenting the individual characters, Horizontal and vertical projection has been considered. In the final stage, a template matching technique has been used to classify and recognize the characters.

It has been noted that the main failure in car licence plate localization and segmentation caused by the low quality source images, also plate angle was a problem in some cases.

The failure in many licence plate segmentation and recognition caused by the variation in image illumination.

This work successfully implemented and tested with Libyan License plate sin light limited conditions; the system achieved an acceptable accuracy level with three sequence images.

The following notes has to considered to improve the performance of the LPR system:

- The used camera has a major effect on the performance to the LPR system, most of video frames that had been captured were in a very weak condition no matter what analysis or filters used to improve its quality, therefore a better quality camera is recommended for development of LPR systems.
- The proposed system did not perform well for high-speed vehicles, in fact any vehicle moving in a speed higher than 20 Km/h would not be analyzed by the system, improvement in this matter is recommended to make the system applicable as a real time system.
- The system efficiency can be improved by considering different techniques and filters.
- Some frames provided a skewed license plates, these frames could not be analyzed properly especially in segmentation stage, therefore a proper skewing technique can enhance the system performance.
- The distance between the camera and the vehicles did not exceed 5 meters because of the limited distance coverage of Infrared camera, so an infrared source with higher distance capability is recommended.

## ACKNOWLEDGMENT

This research was supported by the Libyan Authority of Natural Science Research and Technology.

## REFERENCES

[1] T. Duan et al. “Building an Automatic Vehicle License-Plate Recognition System”, Intl. Conf. in Computer Science – RIVF’05.

[2] V. Nguyen et. al, “A Fast Evolutionary Algorithm for Real-Time Vehicle Detection”, IEEE TRANSACTIONS ON VEHICULAR TECHNOLOGY, VOL.62, NO.6, JULY2013.

[3] Ali Ganoun, “Automatic localization system of Libyan license plates”, IEEE Vehicle Power and Propulsion Conference, 2015.

[4] W Algablawi et al. “Libyan Vehicle License Plate Recognition System” International Conference on Elecetrical and Computer Engineering, 2013.

[5] L. He, S. Member, and Y. Chao, “A Very Fast Algorithm for Simultaneously Performing Connected-Component Labeling and Euler Number Computing,” presented at IEEE TRANSACTIONS ON IMAGE PROCESSING, vol. 24, no. 9, pp. 2725–2735, 2015.

[6] O. Martinsky, "Algorithmic and Mathematical Principles of Automatic Number Plate Recognition Systems", B.Sc.Thesis, Brno University of Technology, Faculty of Information Technology, Department of Intelligent Systems, 2007.

[7] C. Rahman et al "A Real Time Vehicle's License Plate Recognition System", Proceedings of the IEEE Conference on Advanced Video and Signal Based Surveillance, 2003.

[8] K. JABAR, M. NASRUDIN, LIBYAN VEHICLE PLATE RECOGNITION USING REGIONBASED FEATURES AND PROBABILISTIC NEURAL NETWORK, Journal of Theoretical and Applied Information Technology, Vol.94. No.1, 2016.




ISSN 1737-9334

# *An Efficient Approach to Secure Cloud Computing*

Haddadi Mohamed[1,2,**]
[1] Département des sciences commerciales, Faculté des sciences économiques, commerciales, et sciences de gestion, Université de M'hamed Bougara de Boumerdes, Avenue de l'Indépendence, Boumerdes 35000, Algérie

Beghdad Rachid[2,*]
[2] Département d'informatique, Faculté des sciences exactes, Université de Bejaia, Bejaia 06000, Algérie

** haddadimohamed2013@gmail.com, m.haddadi@univ-boumerdes.dz *rachid.beghdad@gmail.com

***Abstract*— Cloud Computing is more and more used in the organizations because it can reduce the cost and complexity of applications. On the other hand, such complex and distributed architectures become an attractive target for attacks, such as flooding based Distributed Denial of Service (DDoS) attack, which represents a serious danger that can deny the legitimate users to access the service delivered by cloud. This paper proposed an Improved version of Hop Count Filtering (IHCF) technique to detect DDoS attacks, especially attackers that generally do not bother to spoof IP addresses. The proposed algorithm is implemented in cloud lab by using VMware, such as Virtual Machine Manager (VMM) and JAVA application. Compared to the original HCF technique and its variants, IHCF decreases the false negative and positive rates and consequently increases the detection rate of flooding attacks to 94% with low computation time.**

***Keywords—cloud computing; cloud computing security; VMware architecture; DDoS attack; IP spoofing; IHCF.***

## I. INTRODUCTION

Nowadays, Cloud computing is a long-held imagination of computing as a utility. Because of this, it becomes more and more used for its advantages, such as access on-demand resources which means that you can consume resources as a service anytime and from anywhere and pay only for resources that you use by only your personal computer and internet connection.

Currently, Cloud computing is a model to provision on-demand network access to a shared pool of computing resources that can accommodate varying end user demands with minimal service provider intervention [1]. The services provided by the cloud are categorized as Infrastructure as a Service (IaaS), Platform as a Service (PaaS), and Software as a Service (SaaS) [2]. Generally, these services become unavailable at significant time because of security issues.

In practice, there are many types of DDoS attacks such as SYN flood, UDP flood and ICMP flood. Indeed, these attacks can be a serious threat to the resources canters [3]. Mostly, they generate a huge amount of attack packets towards the target server by using generally IP spoofing technique. The main purpose of the attacks is to block the legitimate access during a long period of time.

In the last two decades, serveral researches on DDoS attacks have been worked and lots of new techniques have been put forward, but their detection methods are able to recognize packets that match a known signature database. So, these techniques are vulnerable to flooding attacks which needs new defense mechanisms that should be able to differentiate attack packets from legitimate ones.

Practically, it is crucial to detect accurately DDoS attacks. This is due to various issues in getting significant performance metrics. So, some techniques have been designed to limit the efficiency and the effectiveness of DDoS attacks. But, they have not been generally implemented. On the other hand, there are various performance issues, trade-offs in placing these defense techniques and so on.

In this paper, our proposed algorithm (IHCF) works in the IaaS layer of the cloud stack. So, It changes the alert state of HCF to include all the possible Hop Count (HC) values. On the other hand, instead of using <*IP, HC*> we use <*IP,* $HC_{list}$, *count*>. This is because of using multiple alternative paths to the same destination, which can yield a variety of allowed HC values. Moreover, we use a discarding threshold (*thd*) that depends on server's workload when the communications are correctly established. This discarding threshold is computed at the end of each slot time by using statistical properties, such as variance and standard deviation. The source IP addresses are extracted from IP and TCP headres. In addition, we utilize a blacklist which aims to reduce the computation time of each attack packet. This backlist includes two fields, namely, *srcIp and xtime*. The *srcIp* is the attack source IP. The *xtime* is an amount of time. We make the source IP in the blacklist when its number is greater than the *thd* during a slot-time.

The rest of this paper is organized as follows: section II introduces some related works cited recentely whereas Section III provides a design of the proposed Algorithm (IHCF). Experiments and evaluations are given Section IV. Finally, section V covers a brief conclusion of our work.

## II. LITERATURE RIVIEW

This section provides several techniques available in recent literature that detect flooding based DDoS attacks. Each of which comes with its benefits and limitations. We begin with the proposal of Wang et al. [4] who proposed the HCF algorithm to detect IP spoofing. The algorithm is based on the idea that although an attacker can spoof the source IP, the attacker cannot spoof the number of hops a packet traverses as it moves from sender to receiver. HC is not sent in the IP



ISSN 1737-9334

packet but is rather inferred from the TTL (Time To Live) field. The receiver can estimate the HC by subtracting the received TTL value from the closest initial TTL value bigger than the received packet's TTL. Usually, these initial TTL values are operating system dependent and are limited to few possibilities, which include: 30, 32, 60, 64, 128, and 255 [5]. Therefore, the algorithm first learns the IP to HC mapping and stores the mapping in an IP2HC table. Once a packet arrives, it is compared to the HC stored for this IP. If the HC values match, then the packet is legitimate. Otherwise, the packet is discarded. In general, the algorithm captures roughly 90% of spoofed packets. I believe improvements are needed to enhance the approach. One shortcoming is that this approach only works with attacks that involve IP spoofing. Another potential gap is that the author did not study the case where the packet uses multiple alternative paths to the same destination, which can yield a variety of allowed HC values. In that case, the detection rate (90%) may be systematically lower. Moreover, the high number of false positives identified through dropping of a large number of IP addresses belonging to legitimate users.

Another approach developed is by Karnwal et al. [6], who proposed a comber approach called filtering tree, to secure cloud against application layer attacks, such as HTTP-XML-DDoS attack. This proposed scheme includes five steps as follows: sensor filter, HC filter, IP frequency divergence filter, confirm legitimate user IP filter, and double signature filter. The proposed approach has a few shortcomings. The first being its vulnerability to attackers that generally do not bother to spoof IP addresses. A second shortcoming is that there is a negative impact, due to the additional processing to the network traffic. A third shortcoming is that the author did not study the case where the packet uses multiple alternative paths to the same destination, which can yield a variety of allowed HC values.

Vikas et al. proposed in [7] a filtering scheme which shares similar filtering ability as that mentioned in [4], but in addition to that, it extracts synflag to include four cases for each captured packet. The results show that the proposed scheme can save computation time, but it has a few limitations as [4]. Detection rate, false positive and negative rates were unreported in this paper.

Chapade et al. [8] proposed a classification scheme of network traffic into legitimate and malicous by using Mean Absolute Deviation (MAD) of TTL values. Their simulaton results show that the proposed scheme has a high detection rate with low false positive rate. MAD has some limitations. The first, it cannot recognize forged packets whose source IP addresses have the same HC value as that of a zombie. Moreover, an attacker may circumvent it entirely by not using spoofed traffic or partially by bombarding a victim with much more attacking traffic.

A framework called SBTA (SOA-Based Traceback Approach) [9] was proposed by Yang et al. It is a combination of SBTA and CF (Cloud Filter). The use of SOAP is to traceback the source of DDoS attacks and CF for filtering the attack traffic. The proposed scheme has a high efficiency and effectiveness for detecting and identifying the attack traffic, and high detection rate with low false positives. It has one shortcoming being its vulnerability to IP spoofing, i.e., an attacker can use a spoofed IP belonging to unreachable user that renders the path reconstruction undetermined during the attack.

Joshi et al. [10] proposed a method to traceback the source of attack traffic by using Cloud TraceBack (CTB) and employs neural network (Cloud Protector) to detect and filter the attack's bases on DDoS. The proposed scheme has one shortcoming being its vulnerability to IP spoofing, i.e., an attacker can use a spoofed IP address belonging to unreachable user which renders the path reconstruction undetermined during the attack.

Karnwal et al. [11] who proposed a filter Tree approach to protect cloud against HTTP-XML DDoS attacks. They present a Cloud Defender which uses IP addresses to recognize and traceback the illegitimate virtual machines (VMs). The Cloud Defender includes five steps as follows : sensor filtering, HC filtering, IP frequency divergence filter, confirm legitimate user IP filter, and double signature filter. The proposed approach has a few shortcomings. The first being its vulnerability to attackers that generally do not bother to spoof IP addresses. A second shortcoming is that the author did not study the case where the packet uses multiple alternative paths to the same destination, which can yield a variety of allowed HC values.

Doua et al. [12] proposed a Confidence Based Filtering method (CBF) to prevent DDoS attacks in cloud environment. This method monitors the transport and network layers and it based on few correlation characteristics of attributes in the IP and TCP headers during two periods, i.e., non-attack period and attack period. The simulation results showed that the model has a high efficiency and low storage requirement when working with high workload networks.I believe improvements are needed to enhance the approach. One shortcoming is that there is a negative impact, due to the high processing.

A framework called HCF-CBF (Hop-Count Filtering and Confidence Based Filtering ) [13] was proposed by Mamtesh et al. First, HCF is used to detect spoofed packets. After, CBF is used to detect attackers that do not bother to use IP spoofing and that they were not detected by HCF. The simulation results show that the scheme is efficient and effective against DDoS attacks. I believe improvements are needed to enhance the framework. One shortcoming is that there is a static discarding threshold issue.

A novel probabilistic packet marking scheme [14] was proposed by Abdullah et al. It infers forward paths from attacker sites to a victim site. The simulation results show that the technique can construct the forward path from an attacker site after receiving 20.23 packets on the average for DoS attacks. I believe improvements are needed to enhance the technique. One shortcoming is that the technique can consume more bandwidth because it utilizes the 40 bytes record route options field of the IP header.

The above DDoS detection techniques, which are recently discussed in this section, are summarized in TABLE I that provides a few limitations of them.



ISSN 1737-9334

TABLE I
DDOS DETECTION TECHNIQUES SUMMARY

| Approach | Prevention Technique | Limitations |
|---|---|---|
| HCF [4] | Packet Filtering | -Varied allowed HC values problem<br>-False positive problem<br>-Problem of attackers that do not bother to spoof IP |
| Filtering Tree [6] | Packet Filtering and variation | - Attackers that do not bother to spoofIP<br>-Varied allowed HC values problem |
| HCF [7] | Packet Filtering | -Detection rate, FN and FP were unreported<br>-Attackers that do not bother to spoof IP<br>-Varied allowed HC values problem |
| MAD [8] | Distance based | - Attackers that do not bother to spoofIP |
| SBTA & CF [9] | Traceback method | -IP spoofing problem |
| CTB&CP [10] | Traceback Method and Neural Network | -IP spoofing problem |
| Filtering Tree [11] | Packet Filtering and variation | -Varied allowed HC values problem<br>-Problem of attackers that do not bother to spoof IP |
| CBF [12] | Packet Filtering | -Negative impact, due to the processing |
| HCF-CBF[13] | Packet filtering & variation | -Static discarding threshold issue. |
| Probabilistic model [14] | Traceback method | -Consumes more bandwidth. |

## III. DESIGN OF THE PROPOSED ALGORITHM

A flow chart diagram of the proposed algorithm is shown in the Fig. 1. It consists of the following four levels as follows:

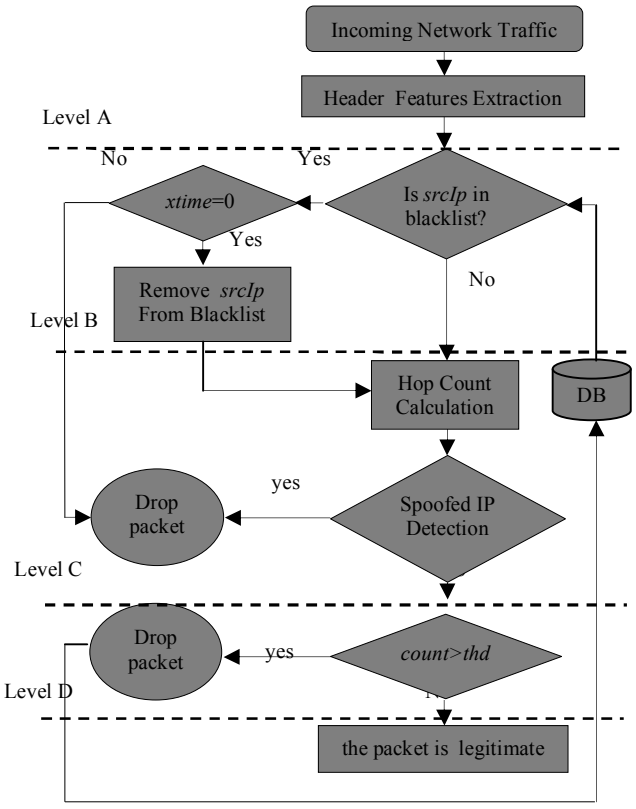


Fig. 1 Flow chart diagram of the proposed algorithm (IHCF).

### A. Level A

In his level, *srcIp*, $TTL_f$ value and *synflag* are extracted from each packet of incoming network traffic.

### B. Level B

This level can reduce the computation time of each attack packet by using the blacklist. the packet is forwarded to the level C, if *srcIp* is not in the blacklist or *xtime* = 0. Otherwise, the packet is droped, If *xtime*≠0. The *srcIp* is removed from the blacklist when *xtime=0*.

### C. Level C

In this level, $TTL_f$ value is used to compute the number of hops that the packet has travelled (*HC*). An attacker can spoof the packet header, but not able to manipulate the *HC* value. Then, itBy compares the *HC* value with the stored Hop Count (*HCs*) into the $IP2HC_{list}$ table that have the same *srcIp*. If no accurate matches are found, then the packet is spoofed so discard it directly, else the packet is forwarded to the level D.

### D. Level D

This level is used to verify the number of packets of the same *srcIP* during the same slot time into the the $IP2HC_{list}$ table, if the *count* > *thd*, the packet is spoofed, so delete *srcIp* from $IP2HC_{list}$ table and add it in the blacklist, else the packet is legitimate.

To help illustrate our proposed algorithm. TABLE II shows few parameters that have been used in the experiments.

TABLE II
IHCF ALGORITHM PARAMETERS

| IHCFitems | Utilization |
|---|---|
| **Nominal Profile** | - To include all the possible available Hop Count values <*srcIp, $HC_{list}$, count*>.<br>-To compute the first *thd*. |
| **Dynamic Threshold (*thd*)** | -To calculate before starting attack detection and after.<br>-To compute the number of packets during a slot time.<br>-Depends on server's workload when the connections are correctly established. |
| **Counter (*count*)** | -To compute the number of packet IP during a slot time in the $IP2HC_{list}$ table for detecting attackers that do not bother to use IP spoofing.<br>- We initialize all their counters (*count*)in the $IP2HC_{list}$ table by zero (0) in the end of the slot time for restarting the computation. |
| **Blacklist** | -Contains attackers that do not bother to use IP spoofing when its count greater than a threshold during a slot time.<br>-Minimizes the computation time and updates in $IP2HC_{list}$ table<br>-We remove from it every IP address that is not used by an attacker during X amount of time. |
| ***$HC_{list}$*** | -To contain a variety of allowed HC values |

## IV. PERFORMANCE EVALUATION

In this section, we will test the proposed algorithm (IHCF) in a cloud lab as shown in Fig. 2 in order to study its performance against DDoS attacks. We show and analyze the results obtained from experiments by taking into account the comparison with others like HCF [4], HCF [7], and CBF [12].


ISSN 1737-9334

### A. Experimental Environment

In this subsection, we build a cloud lab by deploying one server, namely, a target server, which is a container of cloud services hosted in the form of two virtual machines (Client VM1 and Client VM2) that have windows 7 and windows xp like OSs (Operating Systems ) respectively. These VMs were created by VMware ESXI 5.0.0 Hypervisor which is a Virtual Machine Manager (VMM).

Data Base (DB): The DB is implemented using MySQL and has two tables, namely, $IP2HC_{list}$ table and blacklist table. The $IP2HC_{list}$ table includes three fields, namely, *srcIip*, $HC_{list}$ and the *count*. The blacklist table includes two fields, namely, IP address and a default value (*xtime)* which decreases automatically.

Three legitimate users, namely, User1, User2 and User3 which are generating normal traffic, such as UDP traffic.

Two attackers: The attackers are using attack generation algorithm as shown in the Fig. 3**,** which is built by using a combination of java libraries like Jpcap and WinPcap. There are a few routers between attackers (users) and that specific router (R).

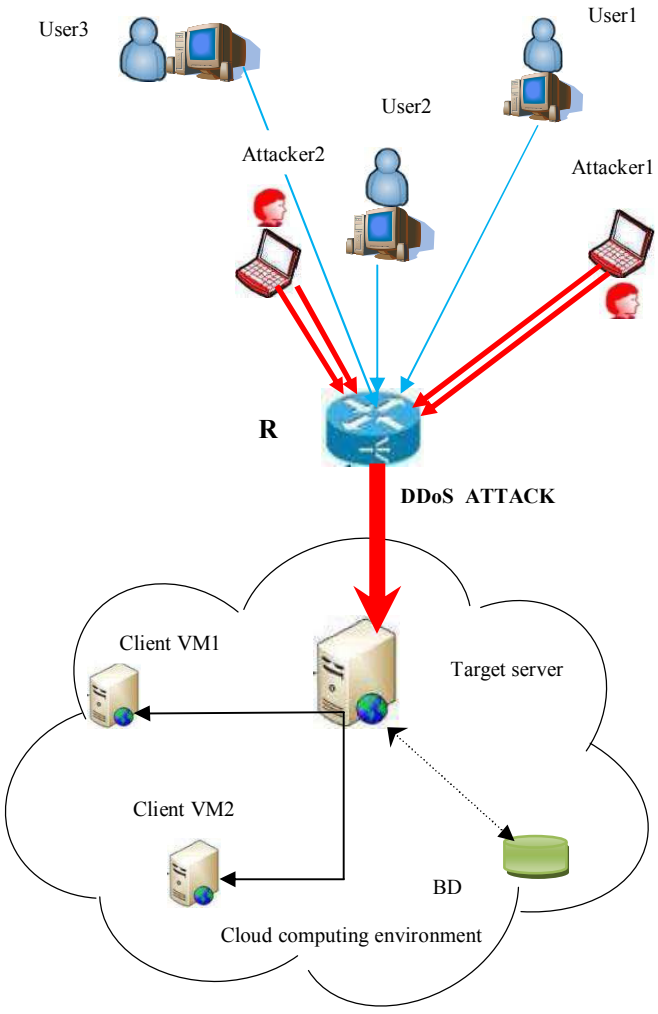


Fig. 2 Architecture of our experimentation with VMware ESXI 5.0.0

### B. Traffic generation

In this subsection, we use DDoS attack generation algorithm which is a combination of three types of flooding based DDoS attacks used in the experiments. Each one sends

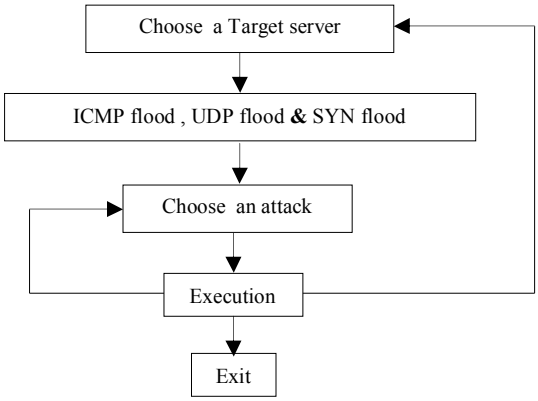


Fig. 3 DDoS attack generation algorithm

a huge number of packets to the target server. Haddadi at al. [15] summarized the following DDoS attacks.

*1) TCP syn flood attack :* It is an important form of DDoS attacks. It generates a huge number of SYN packets (connection requests) without ACK packet to the target server to consume all available TCP connection queues.

*2) UDP flood attack:* It continuously sends a large number of UDP packets to random ports on the target.

*3) ICMP flood attack :* It simply sends a large number of ICMP packets by broadcasting to the target.

To help generate these attacks, a combination java library like Jpcap based on WinPcap that interacts with the OS and NIC (Network Interface Card) to capture packets.

### C. Software configuration

The experiments were processed within a NetBeans IDE 8.0.1 environment where a combination of Jpcap and WinPcap java libraries were carried out. Jpcap (Java packet capturing) is an open source java library for transferring and capturing network packets to establish applications for capturing packets from a network interface and explore them in java. Over them, the proposed algorithm (IHCF) was installed for packet monitoring in the cloud environment by extracting only $TTL_f$ value, *synflag* and *srcIp* of each captured packet. At the beginning, all non spoofed packets are allowed in the learning period and all their headers (*srcIp,* $TTL_f$ value and *synflag*) are extracted to include all the possible available *HC* values for each *srcIp* and compute the *thd* to verify the frequency counter (*count*) of each captured packet, if it exceeds it or not during a slot time. The fixed discarding threshold is feasible if there is no variation in the server's workload level during a slot time, but the dynamic discarding threshold can be adopted because of a variation in the each server's workload level. Selecting an inaccurate value of *thd* may raise false alarms. If the value is too low or if it is too high, it can cause the legitimate traffic being considered as malicious traffic. All packets that do not respect the precedent *thd* are directly


ISSN 1737-9334

discarded in order to stop similar packets to bypass the cloud lab. This might decrease the amount of false positives and false negatives to a small extent and increase the detection rate (> 90% ) which means that the ability of the algorithm to detect attacks over the total amount of attacks.

### *D. Performance Metrics*

Performance indicators [16] for the flooding based DDoS attacks are: False Negative (FN), False Positive (FP), Detection rate (Dr), True Positive (TP), and Computation Time (CT).

- **CT:** Is factor for performance measurement of cloud network and it improves processing relevant power of cloud server and minimizes loss of available resources.
- **FN:** Is an anomalous behavior we failed to detect.
- **FP:** Is that the legitimate client IP address which is incorrectly identified as spoofed.
- **TN:** Represents that the normal behavior which is correctly predicted as normal.
- **Dr**=TP/(FN+TP).

### *E. Simulation Results and Analysis*

In the following, we simulate results between the proposed algorithm (IHCF) and a few previous algorithms that have been discussed in literature, such as HCF [4], HCF [7], and CBF [12] in term of the following performance metrics.

*1) Computation time :* The sample inputs are taken as an arrival rate in mseconds, various results have been analyzed and presented in Fig. 4.

For HCF [7], it has a very good performance, especially in samples 3, 4 and 5. This means that the sample 3 needs more time than sample 4 and 5 because it depends on receiving field of packets compared to the proposed algorithm (IHCF) which is continuously increasing. For CBF [12], it has a negative impact, due to the processing, i.e., examining the Packets for extracting header fields, such as $TTL_f$ value, computing the confidence values, and updating the nominal confidence, if the new confidences are used in each time interval which can add additional processing to the network traffic compared to the proposed algorithm which does only some verifications in the first slot time during the attack. In HCF [4], the computation time rests in continuous increasing because the author did not study the issue of updates of IP to HC by using packets from established TCP connections ( *synflag*) which ensures that an attacker cannot slowly pollute a $IP2HC_{list}$ table by spoofing source IP which can increase the processing time of each IP packet in comparison to the proposed algorithm (IHCF) which take into account this issue.

According to the Fig. 4 which shows that the proposed algorithm has better computation time in the high rate compared to other ones. In the other hand, It also obtained a desirable results that are surly adopted in the cloud computing environment. The usefulness of the proposed algorithm (IHCF) is that there is a bad performance in the beginning in comparison to other ones. This is because of several verifications, such as blacklist especially in the first slot time during the flooding attack. So, the proposed algorithm seems clearly to have a very good performance when there are several attackers that do not use IP spoofing technique.

*2) Detection rate :* Fig. 5 shows a few comparisons that have been done between the proposed algorithim (IHCF) and other ones in term of detection arte. So, they are mentioned as follows:

In the proposed algorithm (IHCF), it was approximately 94%: It means a very good detection rate.

In the HCF [7], it was approximately 86%: It means a bad detection rate. In the HCF [4], it was approximately 85%: It means a worse detection rate. In the CBF [12] algorithm, it was approximately 89%: it means a good detection rate.

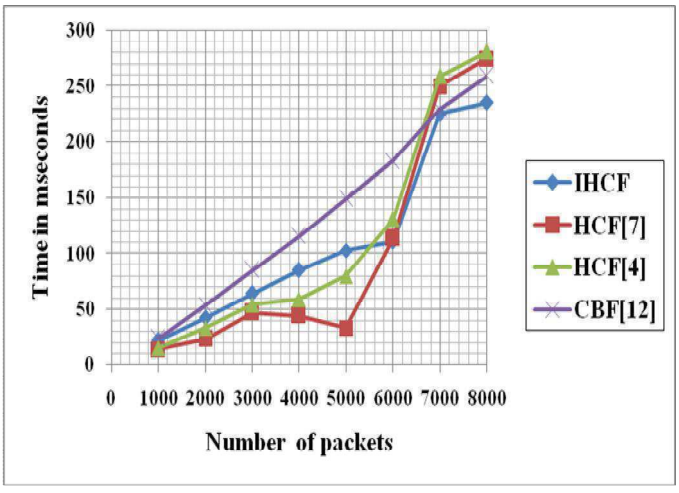


Fig. 4 Computation time comparison between the proposed algorithm ( IHCF) and other ones

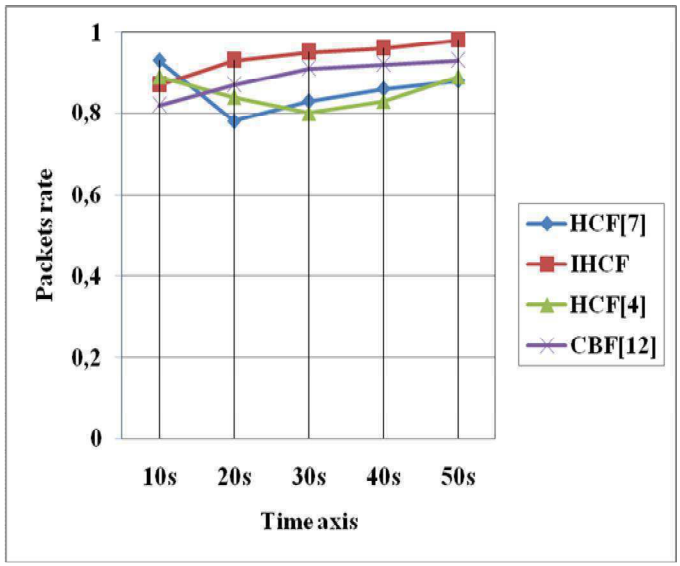


Fig. 5 The effect of TCP SYN flood attack in the proposed algorithm (IHCF) and other ones




ISSN 1737-9334

*3) False positive rate:*

In the proposed algorithm (IHCF), all packets are nearly identified correctly, so the false positive rate is approximately equal to zero (≈**0**). But in HCF [4] and HCF [7], they are approximately equal to 10%, so that they are very bad. In the CBF [12], it is equal to 7.7% so that it is bad.

In the beginning of the action state, HCF[4], HCF[7], and CBF[12] have better performance than our proposed algorithm (IHCF) in terms of detection rate which means that 0,93[7], 0,89 [4] and 0,93 [12] against 0,87(IHCF).

*4) False negative rate :*The proposed algorithm has only 6%. But in HCF[4] and HCF [7], they are equal to 5% and in CBF [12], it is equal to 7.7%.

According to this comparison, we clearly observed that the proposed algorithm (IHCF), in the detection rate and false positive rate, has better performance in comparison to the other ones (HCF [4], HCF [7], and CBF [12]). But in false negative rate, HCF [4] and HCF [7] have better performance in comparison to the proposed algorithm (IHCF). The results show that the proposed algorithm (IHCF) has one problem in terms of false negative rate.

The performance of flooding based DDoS attack detection schemes may be measured in terms of false positive and negative rates and detection rate as shown in Fig. 6.

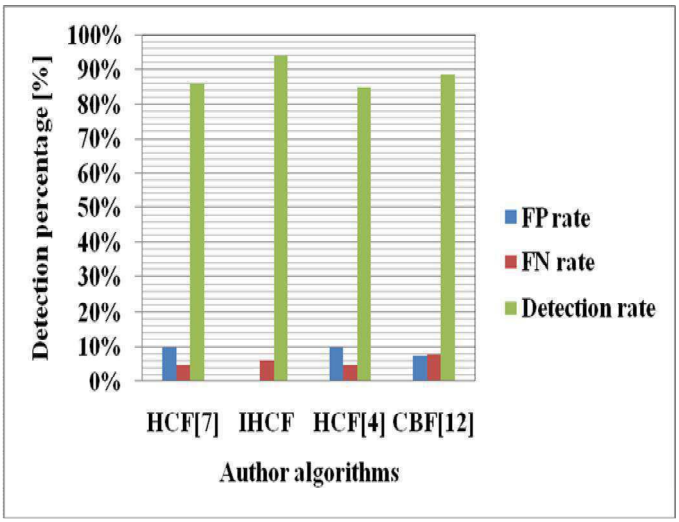


Fig. 6 Comparison between the proposed algorithm (IHCF) and other ones in terms of detection rate, false negative and false positive rates

## V. CONCLUSION

In cloud infrastructure service where several users can share the same infrastructure which can cause DDoS attacks. Because of this, IHCF was proposed in the purpose to detect DDoS attacks, especially attackers that generally do not bother to spoof IP addresses. Firstly the proposed algorithm changes the alert state of HCF technique to include all the possible available HC values. Another parameter is used, instead of using <*IP, HC*> we use <*IP,* $HC_{list}$*, count*> because of using multiple alternative paths to the same destination, which can yield a variety of allowed HC values. Moreover, we added a counter column (*count*) into the IP2HC table for computing the number of the each packet IP during a slot time. In addition to that, we use a blacklist where we make *srcIp* that is detected like legitimate and forwarded to target server. But its frequency counter (*count*) is greater than the *thd* during a slot time for facilitating the research of *srcIp* and *xtime* during the execution of the proposed algorithm (IHCF) levels. The *srcIp* has to be deleted from the $IP2HC_{list}$ table. Finally, we must initialize all their counters to zero (*count*=0) for restarting the research of attacker IP.

## REFRENCES

[1] P. Mell, and T. Grance, " The NIST definition of cloud computing, " Natl. Inst.Stand. Technol. Special Publication SP 800-145 , 2011.

[2] F. Sabahi, "Cloud computing security management," 2nd International Conference on Engineering Systems Management and Its Applications (ICESMA), pp. 1-7, 2010.

[3] Kumar, P. A. R., & Selvakumar, S, "$M_2$KMIX: Identifying the type of high rate flooding attacks using a mixture of expert systems," International journal of Computer Network and Information Security(IJCNIS), vol. 4, no. 1, pp. 1-16, 2012.

[4] H. Wang H, C. Jin , and K. G. Shang, " Defense against spoofed IP traffic using hop-count filtering, " IEEE/ACM Transactions on Networking (ToN), vol. 15, no. 1, pp. 40-53, 2007.

[5] Kravets D. (2011,March) "U.N. Report declares internet access a human right," (accessed April 28, 2012) Available: http://www.wired.com/threatlevel/2011/06/internet-a-human-right.

[6] T. Karnwal, T. Sivakumar, and G.Aghila, "A comber approach to protect cloud computing against XML DDoS and HTTP DDoS attack," in Proceedings of the IEEE students' Conference on Electrical, Electronics and Computer Science (SCEECS), Bhopal, pp. 1-5, 2012.

[7] C. Vikas and S. K. Peddoju, "Packet monitoring approach to prevent DDoS attack in cloud computing,"International Journal of Computer Science and Electrical Engineering (IJCSEE), vol. 1, no. 2315-4209, pp. 38-42, 2012.

[8] S. S. Chapade, K. U. Pandey and D. S. Bhade, "Securing Cloud Servers Against Flooding Based DDOS Attacks," *2013 International Conference on Communication Systems and Network Technologies*, Gwalior, pp. 524-528, 2013.

[9] L. Yang, T. Zhang, J. Song, J. S. Wang and P. Chen, "Defense of DDoS attack for cloud computing," *2012 IEEE International Conference on Computer Science and Automation Engineering (CSAE)*, Zhangjiajie, China, pp. 626-629, 2012.

[10] B. Joshi, A. S. Vijayan and B. K. Joshi, "Securing cloud computing environment against DDoS attacks," *2012 International Conference on Computer Communication and Informatics*, Coimbatore, pp. 1-5, 2012.

[11] T. Karnwal , S. Thandapanii, and A. Gnanasekaran , "A filter tree approach to protect cloud computing against XML DDoS and HTTP DDoS attack, " Intelligent Informatics, Springer Berlin Heidelberg, pp. 459-469, 2013.

[12] Doua, W., Chen, Q., Chen, J, " A confidence-based filtering method for DDoS attack defence in cloud environment," Future Generation Computer Systems(FGCS), vol. 29, no. 7, pp. 1838–1850, 2013.

[13] [1] R. Nath and M. T. Scholar, "An Improved Defense Mechanism Based on Packet Filtering to Mitigate DDOS Attack in Cloud Computing Environment," vol. 5, no. 4, pp. 239–243.

[14] A. Y. Nur and M. E. Tozal, "Record route IP traceback: Combating DoS attacks and the variants," *Comput. Secur.*, vol. 72, pp. 13–25, 2018.

[15] M. Haddadi and R. Beghdad, "DoS-DDoS: TAXONOMIES OF ATTACKS, COUNTERMEASURES, AND WELL-KNOWN DEFENSE MECHANISMS IN CLOUD ENVIRONMENT," *Edpacs*, vol. 57, no. 5, pp. 1–26, 2018.

[16] Pajouh, H. H., Dastghaibyfard, G., & Hashemi, S, "Two-tier network anomaly detection model: a machine learning approach," Journal of Intelligent Information Systems, Springer, pp. 1-14, 2015.


ISSN 1737-9334

# Image De-noising Signal Based on Discrete Wavelet Transforms

Kenz A. Bozed [#1] and Nahla L. M. Hweesa [*2]

[#1] *Benghazi University, Faculty of Information Technology Department of Computer System Design*
*Benghazi, Libya*
kenz.bozed@uob.edu.ly

[*2] *Zawia University, Faculty of Engineering, Electrical and Electronic Eng. Department*
*Zawia,Libya*
Nano_20202001@yahoo.com

***Abstract*— Removing noise from the original signals and images is still a difficult task for researchers, De-noising the image corrupted by noise is popular problem in image processing, and De-noising methods based on wavelet decomposition is one of the most significant applications of wavelets. This paper is the result of some noise reduction work, which means exploring noise reduction using some threshold methods. The wavelet threshold is a signal recognition technique that utilizes wavelet conversion capabilities to reduce noise and Image De-noising is achieved by Matlab.**

***Keywords*— Wavelet transform , Signal De-noising, Thresholding.**

## I. INTRODUCTION

In the real world signals always exist with noise. This noise adds high frequency components to the signal and may cause significant corrupt to it. Therefore, this noise must be removed and the process of removing the noise from data is named signal De-noising. One of methods to reduce noise is wavelet transform which useful in image compression, signal processing and computer graphics [1]. Wavelet transforms are based on small wavelets with limited duration. There are two main types of wavelet transform - continuous wavelet transform and discrete wavelet transform ,computer programs use discrete wavelet transform because the computer is discreet in its nature[2 ] .

Wavelet transform is important to solve problem of image corrupted by Gaussian noise. Therefore, the wavelets provide a framework for signal decomposition in the form of a sequence of signals known as approximation signals with decreasing resolution supplemented by a sequence of additional touches called details [3][4].

## II. WAVELET TRANSFORM

There are many transforms available: Hilbart Transform, Short Time Fourier Transform (STFT) as shown in Fig.1 (a), Wigner Distribution, Radon Transform, and Wavelet Transform as shown Fig.1(b). Every transformation has its own advantages disadvantages and application.

The wavelet transform is very useful tool of signal and image processing that used in signal processing, computer graphics, image compression, and pattern recognition, Wavelet Transform is suitable for the applications of non-stationary. The wavelet transform basis functions are finite in time, while the Fourier sine and cosine functions are not, so the wavelet transform can obtain time information about a signal in addition to frequency information [5].

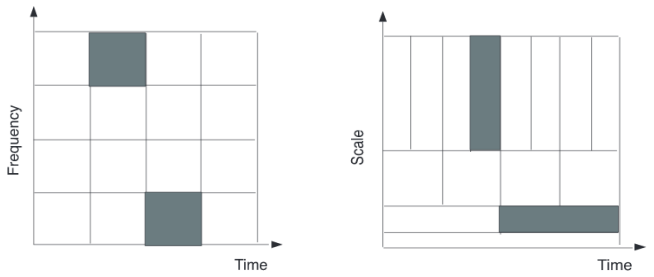


(a) (b)

Fig. 1 Wavelet Transform

Wavelet transform can give more reliable and detailed time-scale representation for it more than the short time Fourier transform.




ISSN 1737-9334

A wavelet is a wave-like oscillation with amplitude that starts from zero, increases, and then decreases return to zero. Signals which are not localized in frequency but also in space to deal with it needs to wavelet transform [6]. Wavelet domain is useful because Discreet Wavelet Transform make the signal energy concentrate in a small number of coefficients, noisy image Discreet Wavelet Transform consists of number of coefficients having high Signal to Noise Ratio and big number of coefficients having high Signal to Noise Ratio[7] . The image is reconstructed using inverse Discreet Wavelet Transform after removing the low Signal to Noise Ratio coefficients [8].

## III. DISCRET WAVELET TRANSFORM

For one dimensional signal, the signal split into two parts, low frequencies and high frequencies edge components are limited in high frequency. This process is continued until signal has been completely decomposed or the given application stops it [9].

By 1D transform can implement Two-dimensional discrete wavelet transform (DWT), where it is applied to rows and columns of 2D-signal separately and subsequently is same as hierarchical sub band system where the sub bands are logarithmically spaced in frequency and represent octave-band decomposition.

As a result of one-level 2D-DWT, we get the wavelet spectrum with four squared discrete sets called Sub bands: one with lower frequency components and three Sub bands with higher frequency components associated with horizontal, vertical and diagonals edge directions in discrete wavelet transform domain usually assumes thresholding (threshold zeroing) [9,10].

Wavelet coefficients and critically sampled by applying DWT as shown in Fig. 2(a). These sub bands are formed by separable applications of horizontal and vertical filters. Sub-bands with label LH1, HL1 and HH1 correspond to finest scale coefficient while sub-band LL1 represent coarse level coefficients .The LL1 sub band is further decomposed and critically sampled to find out the next coarse level of wavelet coefficients as shown in Fig. 2(b). It results in two levels wavelet decomposition [11].

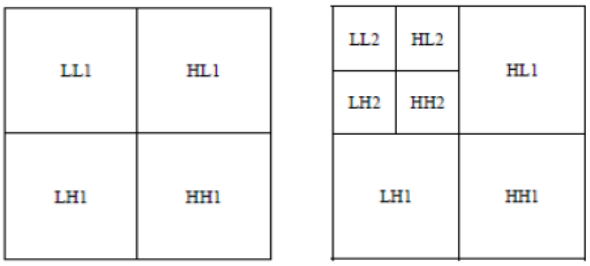


(a) One level (b) Two level

Fig. 2 Scheme of decomposition up to the second level

By using simple filter convolution the Discrete Wavelet Transform (DWT) is performed and the original signal can be reconstructed; the reconstruction of original signal from DWT coefficients is known as Inverse DWT (IDWT) [8,12].

The filtering steps of DWT are multiply and accumulate operations. A filter in the algorithmic discrete sense is a number of coefficient values. The number of these values referred to as the width of the signals and also these coefficients are referred to as taps. In each of data-word of the input the filter spans across that data-word and its neighbouring data-words as a window. Within this window the values are multiplied by their corresponding coefficient of filter and all the results are added together to provide the filtered result for this data-word. The filtering operation can extracts certain frequency information from the data depending on the characteristics of the filter. This operation of the filtering can be done also with a systolic array. It is easy to construct the systolic array for each level of the DWT but the arrays are poorly used because the decreasing data-rates of the levels. It is possible through some complex timing to use a single array to carry out all levels of the DWT. Fig. 3 is presented the DWT filtering process[5,8].




ISSN 1737-9334

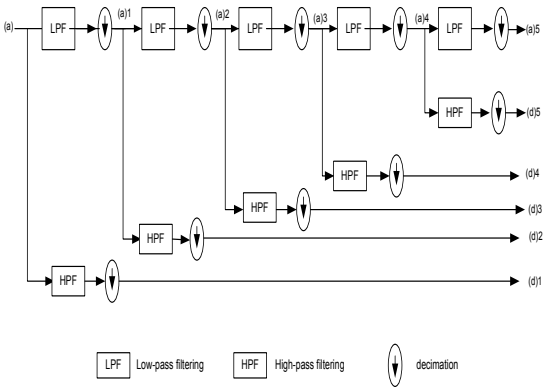


Fig. 1 filtering Process

The IDWT is the computational reverse as illustrated in Fig.4. The lowest low-pass and high-pass data-streams are up sampled (i.e. a zero is located between each data-word and then filtered by using filters related to the decomposition filters). The obtained two results of streams can be cleanly added together to form the low-pass result of the previous level of processing. This can be joint with the high-pass result in a similar fashion to create further levels the process continuing until the original data-stream is implemented [5 ,13].

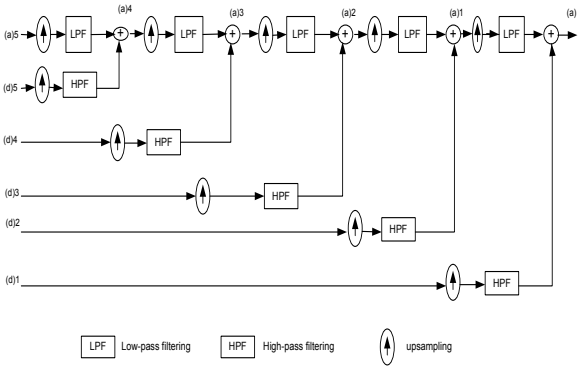


Fig. 4 The Inverse DWT filtering process

## IV. WAVELET THRESHOLDING

There are two steps of Wavelet thresholding for image De-noising. These two steps are summarized in the following points:

### A. *Step 1*

Calculating the wavelet coefficient carries more signal information than noise.

### B. *Step 2*

Setting to zero the coefficients with relatively small or insignificant magnitude by eliminating small coefficients. It is dominated by noise one gets rid of wavelet-based functions that contain coefficients below a certain threshold. Choosing an appropriate threshold is critical in any process to reduce noise. There are two thresholds, called the hard and soft threshold, respectively [14].

By selecting a significantly large threshold, and multiplying it with the standard deviation of random noise, most noise can be removed by thresholding the wavelets transform coefficients this is known as hard threshold [5, 13, 14].

$$T_\tau^{\text{hard}} = \begin{cases} Y[m,n], & |Y[m,n]| > 0 \\ 0, & |Y[m,n]| \le 0 \end{cases} \quad (1)$$

Where τ, is the threshold value.

With a slight adjustment to the hard threshold approach, a method known as soft threshold can be created [7, 14].

$$T_\tau^{\text{soft}} = \begin{cases} sgn(Y[m,n])(|Y[m,n]| - \tau, & |Y[m,n] > 0| \\ 0, & |Y[m,n] \le 0| \end{cases} \quad (2)$$

Given a threshold value T, the hard thresholding replaces a wavelet coefficient by zero if its absolute value is smaller than T; instead, the soft thresholding allows a wavelet coefficient to be shrunk by T if its absolute value is less than T [5, 8, 14].

## V. MATLAB ANALAYSIS & RESULTS

Matlab as a programming language is used to implement and discuss the problem of retrieving signals from noisy data .The general De-noising procedure involves three steps they are:

- Decompose Threshold detail coefficients and Reconstruct,
- Two points must be addressed in particular,
- How to choose the threshold and how to perform the thresholding.

Hard thresholding can be described as the usual process of setting to zero the elements whose absolute values are lower than the threshold hard threshold signal is *x* if $|x| > thr$ , and is *0* if $|x| <= thr$ ,


ISSN 1737-9334

Soft thresholding is an extension of hard thresholding, first setting to zero the elements whose absolute values are lower than the threshold ,and then shrinking the nonzero coefficients towards *0* The soft threshold signal is *sign(x)(|x|-thr)* if $|x| > thr$ and is *0* if $|x| <= thr$.

Four threshold selection rules are implemented in the function *THSELECT*.

*Rule-1:* Selection using principle of *Stein's Unbiased Risk Estimate (SURE).*

*Rule-2:* Fixed form threshold equal to *sqrt(2*log(length(y))).*

*Rule-3:* Selection using a mixture of the first two options.

*Rule-4:* Selection using minimax principle

*Min, Max* and *SURE* threshold selection rules are more conservative and would be more convenient when small details of the signal lie near the noise range. The two other rules remove the noise more efficiently.

Fig.5 is shown the original, noisy and de-noised images

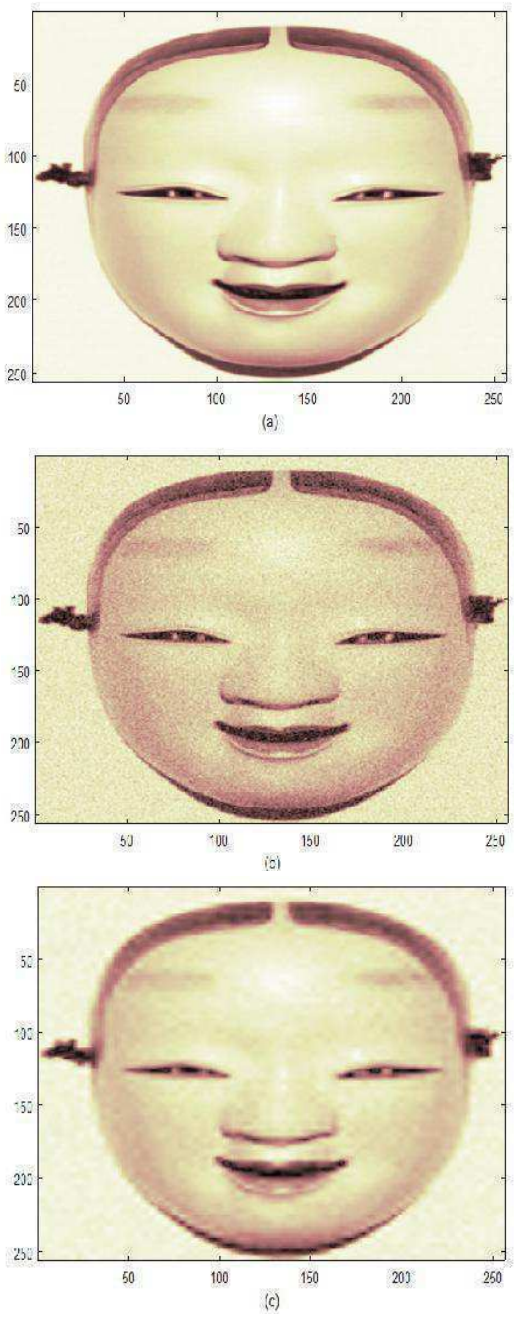


Fig.5 De-noising Image Using Wavelet (a)Original image, (b) Noisy image and (c) De-noised image

In this case, the fixed form threshold is used with an estimate of the noise level, the threshold mode is soft and the rounding coefficients are retained.

Fig.6 Illustrates original signal, hard threshold and soft threshold using of 0.8 thresholds.




ISSN 1737-9334

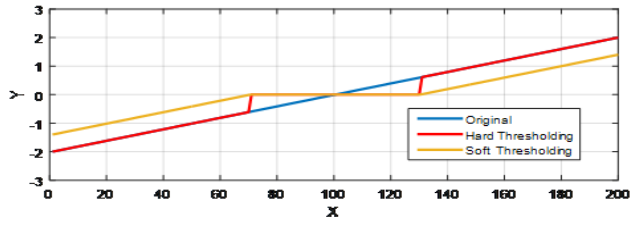


Fig. 6 Original, Hard and Soft Thresholds

Fig.7 used model assuming standard Gaussian white noise with Signal to Noise ratio = 20 db.

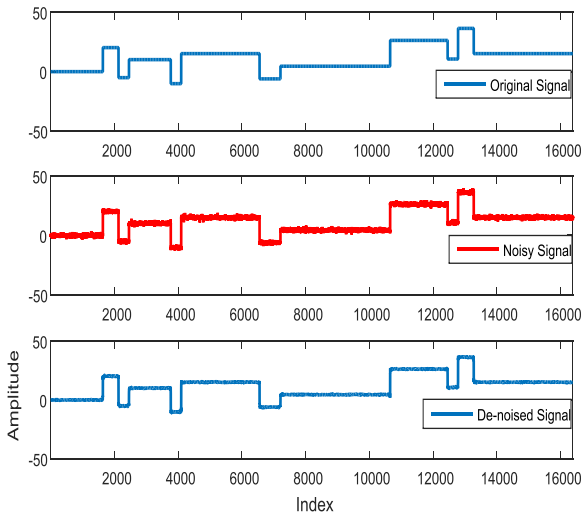


Fig. 7 Original, Noisy and De-noised Signals

Using a level-dependent estimation of the level noise is illustrated in Fig.8.

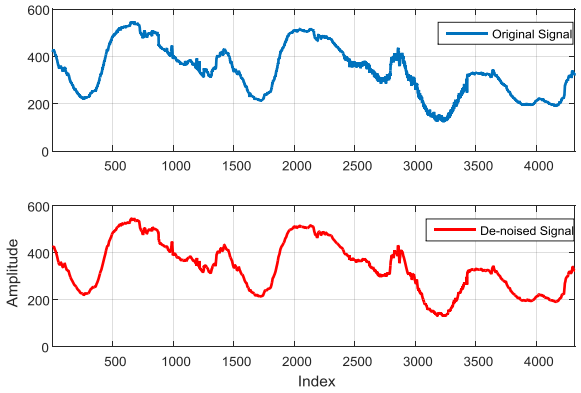


Fig. 8 Original Signal and De-noised Signals

## VI. Conclusions

This paper presents signal and image De-noising using soft and hard-threshold for the signal used 0.8 threshold and standard Gaussian white noise with Signal to noise ratio = 20 db and soft-threshold to De-noise image. The threshold is set to higher values for high frequency sub-bands and lower values for low frequency sub-bands. Threshold selection and rebuilt threshold function is the main point to indicate the reduction of the results in the reduced the wavelet threshold De-noising.

## References

[1] Y. Rajput, V. S. Rajput , A. Thakur and G. Vyas, “Advanced Image Enhancement Based on Wavelet & Histogram Equalization for Medical Images,” *IOSR Journal of Electronics and Communication Engineering.,* ISSN 2278-2834, Vol(2), No(6), Oct. 2012, PP 12-16 [online] Available: www.iosrjournals.org

[2] P. Singh and R. Shree “comparative study to Noise models and Image restoration Techniques, "International Journal of Computer Applications. , Sept.2016, Vol (149).

[3] S.D. Ruikar, and D. Doye, “Wavelet Based Image Denoising Technique,” *International Journal of Advanced Computer Science and Application (IJACSA).*, vol. 2, pp. 49–53, March 2011.

[4] A.K. Boyat, and B.K. Joshi, “A REVIEW PAPER: NOISE MODELS IN DIGITAL IMAGE PROCESSING,” *Signal & Image Processing: An International Journal (SIPIJ).*, vol. 6, No.2, pp. 63–775, April 2015 .

[5] K. Shivhare and G. Bhardwa, “Analysis of Wavelet Denoising with Different Types of Noises,” International Journal of Current Engineering and Technology., E-ISSN 2277 – 4106, P-ISSN 2347 – 5161, Dec. 2016. [online] Available: http://inpressco.com/category/ijcet

[6] M. Soni, A. Khare, and S. Jain, “Problem of De-noising in Digital Image Processing and Its Solving Techniques,” *International Journal of Emerging Technology and Advanced*., ISSN 2250-2459, ISO 9001:2008, Vol. 4, No. 4, April 2014.

[7] C. Pearson, "High Speed Digital to Analog Converters Basics", *Texas Instruments application report SLAA523A*, 2012, [online] Available: http://www.ti.com.

[8] C.P. Dautov and M.S,.Ozerdem, " Introduction to Wavelets and their applications in signal denoising," *JOURNAL OF SCIENCE AND TECHNOLOGY*, E-ISSN 2146-7706, Vol.8, No.1 , April 2018.

[9] H. ALZAQ and U B. Berk, “A comparative analysis of 1-level multiplier-free discrete wavelet transform implementations on FPGAs,” *Turkish Journal of Electrical Engineering & Computer Sciences.*, ISSN: 2194 – 2205, doi:10.3906/elk-1707-101, Vol. 26, Sept 2018.

[10] A. Rajni , “PERFORMANCE ANALYSIS OF IMAGE DENOISING WITH WAVELET THRESHOLDING METHODS FOR DIFFERENT LEVELS OF DECOMPOSITION,” *The International Journal of Multimedia & Its Applications*., DOI : 10.5121/ijma.2014.6303, Vol.6, No.3, June 2014.

[11] R. Sihagand , R. Sharma and V. Setia, “Wavelet Thresholding for Image De-noising,” *International Conference on VLSI, Communication & Instrumentation (ICVCI), Proceedings published by International Journal of Computer Applications® (IJCA).*, 2011

[12] Sharan V, Keshari N, Mondal T. Biomedical image denoising and compression in wavelet using MATLAB. International Journal of Innovative Science and Modern Engineering (IJISME) ISSN. 2014 May:2319-6386.

[13] Canty, Morton J. Image analysis, classification and change detection in remote sensing: with algorithms for ENVI/IDL and Python. Crc Press, 2014.

[14] Srivastava M, Anderson CL, Freed JH. A New Wavelet Denoising Method for Selecting Decomposition Levels and Noise Thresholds. *IEEE Access*. 2016;4:3862-3877




ISSN 1737-9334

# Arc Voltage Signals-Based Flicker Effect Analysis Using SampEn Multi-scale Entropy Algorithm

Salim AOUABDI[1]
[1]Research Center in Industrial Technologies CRTI,
P.O.Box 64, Cheraga-Algiers-ALGERIA.
s.aouabdi@crti.dz

Nadir BOUTASSETA[2] and Hocine BENDJAMA[3]
[2,3]Research Center in Industrial Technologies CRTI,
P.O.Box 64, Cheraga-Algiers-ALGERIA.
{n.boutasseta and h.bendjama}@crti.dz

**Abstract — Real-time monitoring in the steel and metallurgical production sector is of great importance. To ensure competitiveness, the industrial process will have to innovate and evolve towards better quality. Therefore, the monitoring of the voltage signal in Electric Arc Furnace (EAF) has a vital role in keeping a nominal operation of electrical components in order to achieve high performance. A new monitoring method based on multi-scale Sample Entropy (SampEn) (MSE) algorithm for EAF voltage flicker is proposed. In the proposed method, different percentages of flicker effect analysis are presented. The current voltage characteristic of the EAF in conjunction with MSE and comparison of observed values with those predicted from a Cassie and Mayr model built using nominally healthy data are analysed. In order to achieve the classification procedure, five extracted features are used to adapt the subtractive clustering network for each state of the flicker effect and the performance of the classifier during the training is given with success.**

**Keywords — Electric Arc Furnace (EAF), power quality, Voltage flicker, Voltage unbalance, SampEn Multi-scale entropy algorithm, subtractive clustering.**

## I. INTRODUCTION

Electrical network quality analysis is an important technical step to keep a nominal operation of an electrical installation [1]. In order to analyze the network, we use a new algorithm based on measurement acquisitions that allow a complete diagnosis of the state of health of the arc furnace. The system to be modeled is the AC arc furnace [2]; this work focuses on monitoring the arc furnace operating in both modes. An anomaly detection tool based on the combined approach, current voltage characteristic vectors of the electric arc and multi-scale entropy (MSE) [3] is presented. The studied flaw in the present work are the flicker effect and the voltage imbalance [4, 5]. The arc furnace behaves like a nonlinear load and creates energy quality problems such as unbalanced voltages and voltage flickers that were the subject of many research works [6-8]. Several arc furnace models have been developed to analyze the flicker effect caused by EAF according to needs and their application [9, 10]. The Mayr model is an appropriate representation of an arc for weak currents, while the Cassie model gives good results for high current arcs [11]. Under normal operating conditions, the power grid is subject to electrical stress [12]. The emphasis is increased during transients, such as load variations, which may lead to electrical failure and degradation of arc furnace operation [13]. Many of the advanced Flicker effect analysis techniques have been used; these techniques have their respective advantages and disadvantages [14, 15]. This study focuses on a robust method for the early analysis of flickers effect, where an anomaly is defined as a deviation from the expected behavior of the process dynamics. Signal processing techniques are used for flicker detection. The methodology is mainly guided by the data. The idea is first to understand the mechanisms of the flicker effect [16], then apply the data processing techniques to extract the information that gives the indication of the state of operation of studied system. The analysis of flicker signatures as well as the information on the different variations of the flicker percentage studied is not easily discernible directly from arc voltages, especially for the small percentage of flicker [17]. The multi-scale entropy strategy has been adopted to identify flicker signatures. Indeed, to improve the optimal operation of the arc furnace it is necessary to know at every moment the state of operation of this system and to be able to discriminate normal and abnormal states. The control of the arc furnace is determined by two parameters, the quality and quantity of the load introduced in addition to the wear and heating of the material [18]. The load is related to the scrap products, and the arc connected to the priming with or without liquid metal load. To achieve a minimum merge, it is necessary to place in the load the optimal power by making a compromise between the following criteria [19]:

- Monitoring the energy consumed according to the energy allocated by the distributor.
- Heating connections and in particular electrodes.
- Overload of the furnace transformer.

The following flow diagram shows the evolution of the system and possibility of successive failures with the taking into account the improvement of the driving of the system. The proposed diagnosis strategy shows the progress of different approaches:


ISSN 1737-9334

- Fault modeling,
- Generation of the database of arc currents and voltages,
- Diagnostic techniques,
- Extraction and selection of indicators,
- Classification method and statistical tests.

In order to achieve the best performance of the monitoring, a diagnostic strategy for analyzing flicker is desirable.

The ability of MSE to analyze the flicker caused by EAF depends on the optimization of the calculated parameters of the SampEn measure, by analyzing the voltage waveforms from obtained model of EAF [2, 8].

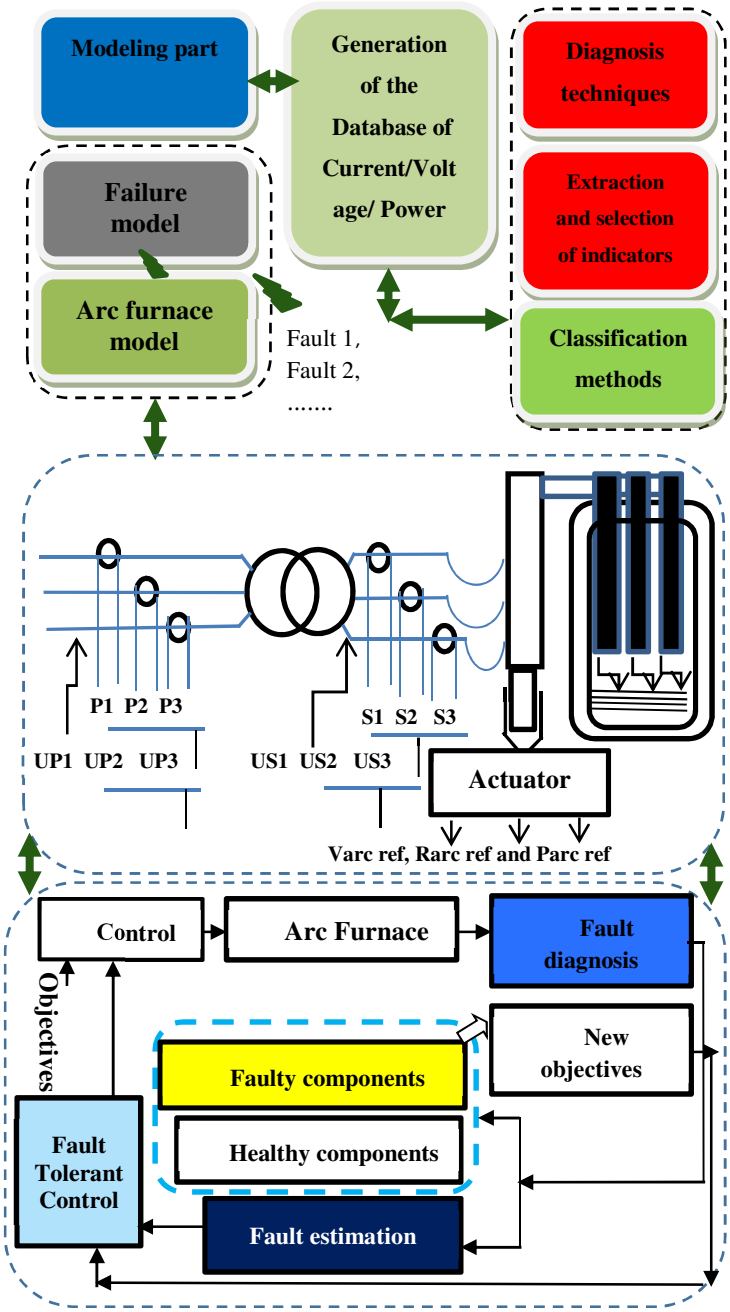


**Fig. 1.** Flow diagram of the proposed strategies and future work.

## II. EAF VOLTAGE FLICKER DETECTION VIA SAMPEN MULTI-SCALE ENTROPY ALGORITHM

The signal data acquisition issued from the EAF voltage in different cases is processed and then passed to inspect the presence of abrupt variation in the signal. We used the data provided by [2].

The use of the Multi-scale entropy (MSE) strategy for the monitoring and diagnosis of EAF voltage flicker effect is an advantage because this strategy makes possible the improvement of EAF voltage and take into account not only the dynamic non-linearity, but also the effects of interaction and coupling between the system components [3].

Via MSE analysis, a coarse time series is first constructed from the original time series $\{V_1, \dots, V_v, \dots, V_N\}$. Coarse consecutive time series $\{y^{(\tau)}\}$ are constructed with the scaling factor $\tau\,\{\tau = 1.2, \dots N\}$ according to equation:

$$y_j^{(\tau)} = 1/\tau \sum_{v=(j-1)\tau+1}^{j\tau} V_v \qquad (1)$$

Where $\tau$ represents the scale factor, and we have: $1 \le j \le N/\tau$. In order to adjust the values of the parameters for the arc voltage signal, we have simulated the SampEn algorithm for the optimal values of: $m = 2$ and $r = 0.15$.

The time series of N points is given by: $\{V(1), \dots, V(v), \dots, V(N)\}$, and the SampEn algorithm is defined as follows [20-26]:

Train $m$ length vectors $V'_m(v)$

$$V'_m(v) = \{V(v), V(v+1), \dots, V(v+m-1)\}$$
$$1 \le v \le N - m + 1 \qquad (2)$$

The distance between two vectors is defined as follows:

$$d[V'_m(v), V'_m(j)] = \max_{k\in[1,m-1]}(|V(v+k) - V(j+k)|) \qquad (3)$$

For each $V'_m(v)$ and the fixed tolerance $r$, leave $A_v$ the number of vectors satisfying $d[V'_m(v), V'_m(j)] \le r$, then $B_v^m(r)$ as follows:

$$B_v^m(r) = \frac{A_v}{N-m+1} \quad 1 \le v \le N\text{-}m \qquad (4)$$

The average $B_v^m(r)$ is designed as:

$$B^m(r) = \frac{1}{N-m} \sum_{v=1}^{N-m} B_v^m(r) \qquad (5)$$

By increasing the dimension of $m+1$ and repeating the previous steps to find $B^{m+1}(r)$, the SampEn is defined as follows:

$$\mathrm{SampEn}(m, r) = \sum_{N\to\infty} -\ln \frac{B^{m+1}(r)}{B^m(r)} \qquad (6)$$

For a finite number of data points $N$ we have:

$$\mathrm{SampEn}(m, r, N) = -\ln \frac{B^{m+1}(r)}{B^m(r)} \qquad (7)$$


ISSN 1737-9334

In order to reduce the number of the input signal and in the same time to achieve the classification performance, we use five statistics indicators over MSE of the EAF voltage signal (phase A). Five indicators are extracted from the SampEn algorithm and the results are given in the next section.

## III. ANALYSIS OF FLICKER SIGNATURES

Through the use of both approaches : current voltage characteristic of the EAF in conjunction with MSE and comparison of observed values with those predicted from a Cassie and Mayr model built using nominally healthy data, we can describe EAF voltage flicker phenomena. A suitable 2-D representation is based on the current voltage characteristic. The complete Arc model is given by [2]:

$$g_1 = g_{min} + \left( (1 - e^{-\left(\frac{i_f}{i_0}\right)^2}) \left(\frac{i_f}{E_1}\right)^2 \frac{1}{g_1} + e^{-\left(\frac{i_f}{i_0}\right)^2} \frac{{i_f}^2}{P_0} - \theta_a \frac{dg_1}{dt} \right) \quad (8)$$

With

$$\theta_a = \theta_0 + \theta_1 e^{-\alpha|i_f|} \quad (9)$$

Where $\alpha > 0$ and $\theta_1 \gg \theta_0$ and we can see that $\theta_a$ function of arc current from (9).

$$g_1 = g_{min} + \left( (1 - e^{-\left(\frac{i_f}{i_0}\right)^2}) \left(\frac{i_f}{E_1}\right)^2 \frac{1}{g_1} + e^{-\left(\frac{i_f}{i_0}\right)^2} \frac{{i_f}^2}{P_0} - \left(\theta_0 + \theta_1 e^{-\alpha|i_f|}\right) \frac{dg_1}{dt} \right)$$

$$= g_{min} + \left(\frac{i_f}{E_1}\right)^2 \frac{1}{g_1} - \left(\frac{i_f}{E_1}\right)^2 e^{-\left(\frac{i_f}{i_0}\right)^2} \frac{1}{g_1} + e^{-\left(\frac{i_f}{i_0}\right)^2} \frac{{i_f}^2}{P_0} - \theta_0 \frac{dg_1}{dt} - \theta_1 e^{-\alpha|i_f|} \frac{dg_1}{dt}$$

$$= g_{min} + {i_f}^2 \left[ \frac{1}{g_1 {E_1}^2} - \frac{1}{g_1 {E_1}^2} e^{-\left(\frac{i_f}{i_0}\right)^2} + \frac{1}{P_0} e^{-\left(\frac{i_f}{i_0}\right)^2} \right] - \theta_0 \frac{dg_1}{dt} - \theta_1 e^{-\alpha|i_f|} \frac{dg_1}{dt}$$

$$= g_{min} + {i_f}^2 \left[ \frac{1}{g_1 {E_1}^2} - \frac{1}{g_1 {E_1}^2} e^{-\left(\frac{i_f}{i_0}\right)^2} + \frac{1}{P_0} e^{-\left(\frac{i_f}{i_0}\right)^2} \right] - \theta_0 \frac{dg_1}{dt} - \theta_1 e^{-\alpha|i_f|} \frac{dg_1}{dt}$$

$$g_1 + \left(\theta_0 + \theta_1 e^{-\alpha|i_f|}\right) \frac{dg_1}{dt} = g_{min} + {i_f}^2 \left[ \frac{1}{g_1 {E_1}^2} - \left( \frac{1}{g_1 {E_1}^2} - \frac{1}{P_0} \right) e^{-\left(\frac{i_f}{i_0}\right)^2} \right]$$

$$\frac{dg_1}{dt} = -\frac{g_1}{\left(\theta_0 + \theta_1 e^{-\alpha|i_f|}\right)} + \frac{g_{min}}{\left(\theta_0 + \theta_1 e^{-\alpha|i_f|}\right)} + {i_f}^2 / \left(\theta_0 + \theta_1 e^{-\alpha|i_f|}\right) \left[ \frac{1}{g_1 {E_1}^2} - \left( \frac{1}{g_1 {E_1}^2} - \frac{1}{P_0} \right) e^{-\left(\frac{i_f}{i_0}\right)^2} \right] \quad (10)$$

We have

$$v = \frac{i}{g} \quad (11)$$

So

$$\frac{dg_1}{dt} = -\frac{g_1}{\left(\theta_0 + \theta_1 e^{-\alpha|i_f|}\right)} + \frac{g_{min}}{\left(\theta_0 + \theta_1 e^{-\alpha|i_f|}\right)} + i_f / \left(\theta_0 + \theta_1 e^{-\alpha|i_f|}\right) \left[ \frac{v}{{E_1}^2} - \left( \frac{v}{{E_1}^2} - \frac{i_f}{P_0} \right) e^{-\left(\frac{i_f}{i_0}\right)^2} \right]$$

$$\frac{dg_1}{dt} = -\frac{1}{\left(\theta_0 + \theta_1 e^{-\alpha|i_f|}\right)} \left[ g_1 - g_{min} - i_f \left( \frac{v}{{E_1}^2} - \frac{i_f}{P_0} \right) e^{-\left(\frac{i_f}{i_0}\right)^2} \right] \quad (12)$$

Equation (12) indicate the dynamic specification of EAF is affected by conditions of the furnace.

The sinusoidal variation can be expressed mathematically as:

$$E_1(t) = E_{01}\left(1 + m \sin(\omega_f t)\right) \quad (13)$$

Where $m$ and $\omega_f$ are modulation index and flicker frequency respectively.

## IV. RESULTS AND DISCUSSION

Reporting and analysis of waveforms in healthy case is presented by the figures (Fig 2-4), and the waveform report and analysis in faulty case is presented in the figures (Fig 5-7).

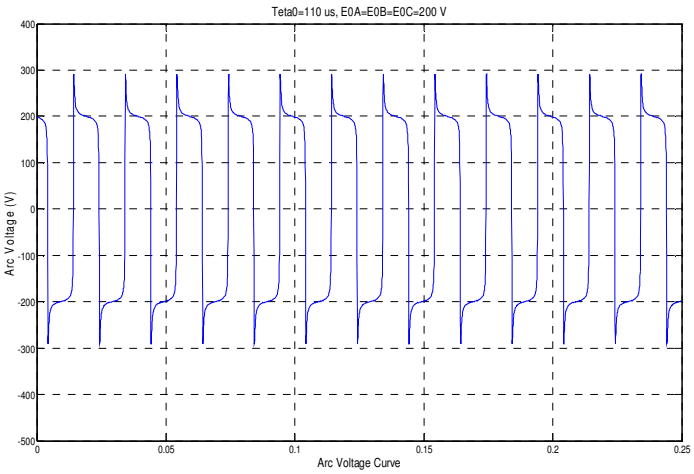


**Fig.2.** Arc voltage curve in healthy case.




ISSN 1737-9334

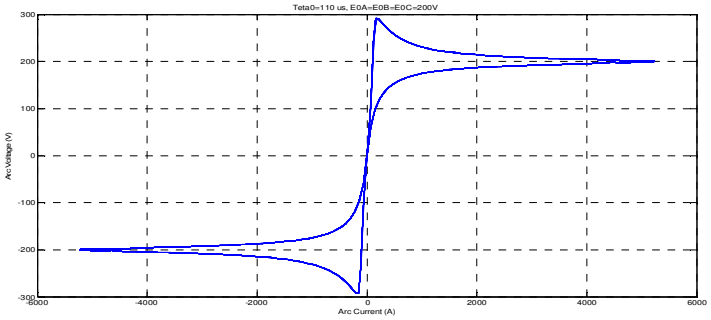


**Fig.3.** Arc Voltage Current voltage characteristic of the EAF.

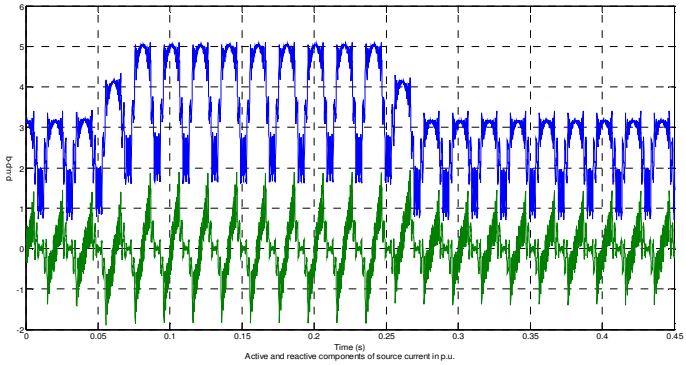


**Fig.4.** Active and reactive power in healthy case.

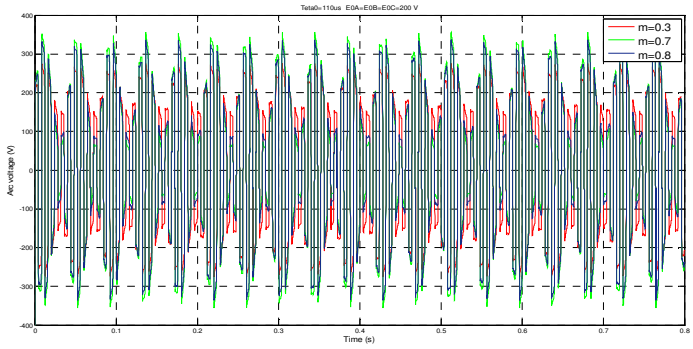


**Fig.5.** Arc Voltage with unflagging flicker percentage variation without unbalance conditions.

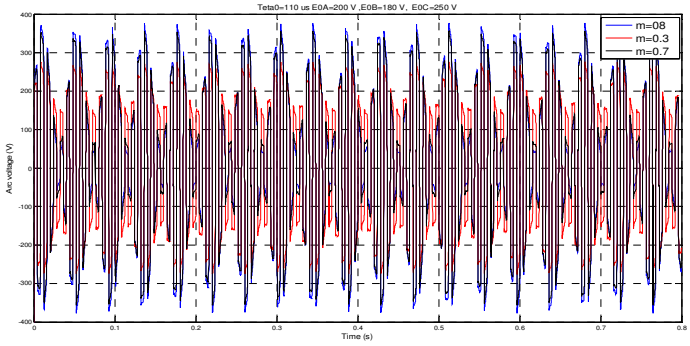


**Fig.6.** Arc Voltage with unflagging flicker percentage variation with unbalance conditions.

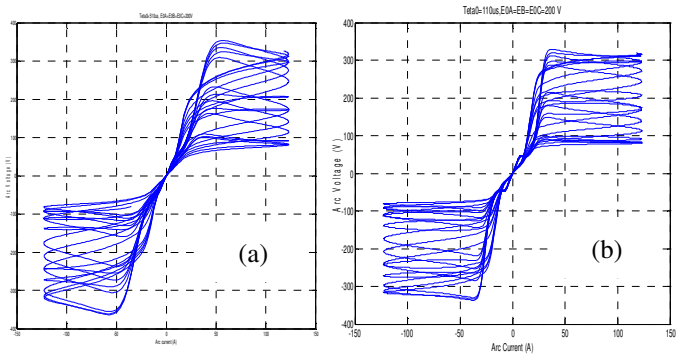


**Fig.7.** Current voltage characteristic of EAF (a) Teta=510 us (b): Teta =110 us.

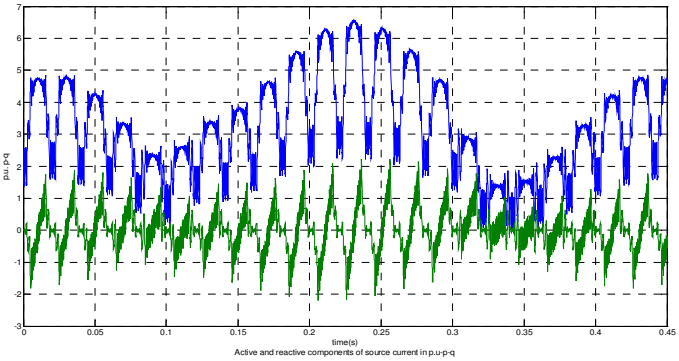


**Fig.8.** Active and reactive power in faulty case.

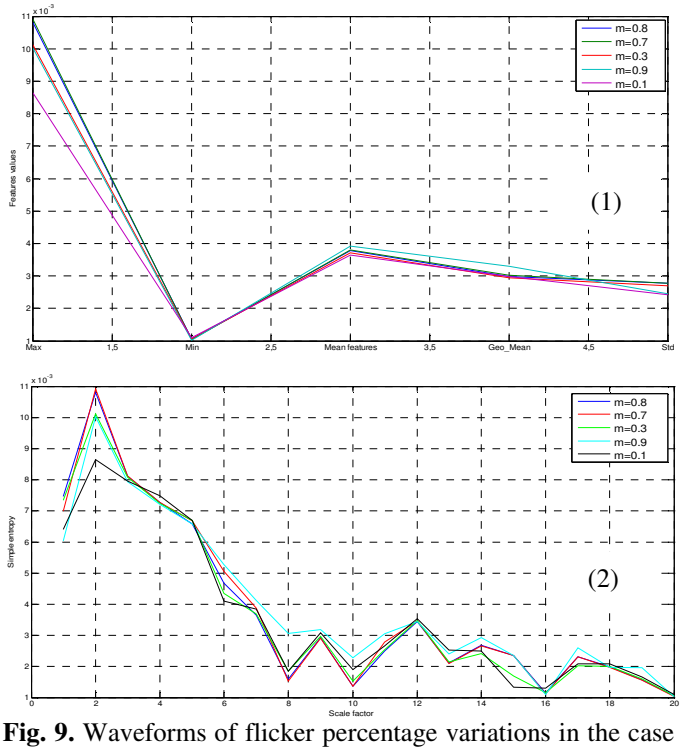


**Fig. 9.** Waveforms of flicker percentage variations in the case without unbalance conditions. (1): Teta=110us : Five statistics during MSE. (2) : MSE over 20 scales.


ISSN 1737-9334

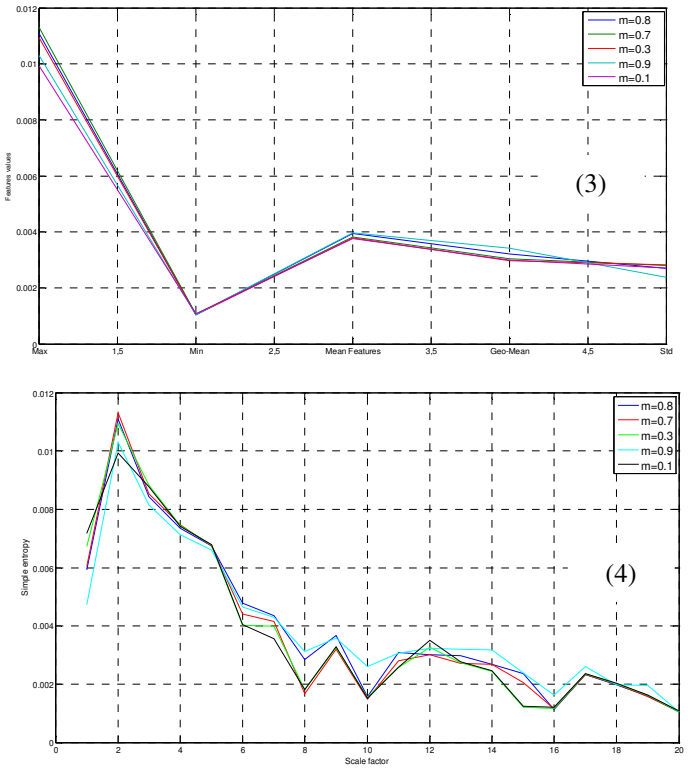


**Fig. 10.** Waveforms of flicker percentage variations in the case without unbalance conditions. (3): Teta=510 us : Five statistics during MSE. (4): MSE over 20 scales.

The dynamic I-V characteristic of the obtained electric Arc has been shown in Fig.3 and Fig.7 (a) and Fig. 7(b). The dynamic voltage variation, obtained by the simulation, is graphically shown in Fig. 2 and Fig. (5-6). In order to analyze the flicker effect caused by the electrical Arc, the simulation results obtained by using the different variation of the flicker percentage and the comparison of the data measured in both cased with Teta =110 us and with Teta =510 us as shown in Fig. 5 and Fig. 6. The dynamic characteristic of the electrical arc by flicker effect is observed as shown in Fig. 7 (a) and Fig. 7 (b). Multi-scale entropy is used to inspect the different variation of voltage flicker, MSE across 20 scales are computed from a set of features containing information about the state indicating evolution of different variations present in the Arc voltage Fig. 9 (b) and Fig. 10 (b). Five statistics are extracted from the set of original characteristics Fig. 9 (a) and Fig. 10 (a). The reduced feature vectors in the case of different percentage of flickers with Teta =110 us compose the database of the expert system for fault diagnosis (Figs .13-16). The global database is divided into a training data set (500 samples) and the local database is divided into training data set (100 samples) and the global testing data set (375 samples) and local testing data set (75 samples). The training data set is used to train the classifier model, in order to predict the expected outputs.

The figure 11 and 12 shows the performance of the classifier during the training procedure.

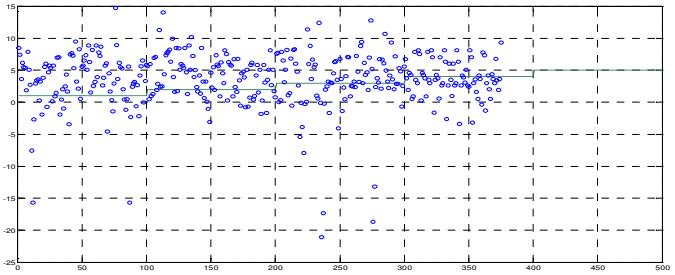

**Fig. 11.** The simulation of the model output against checking data.

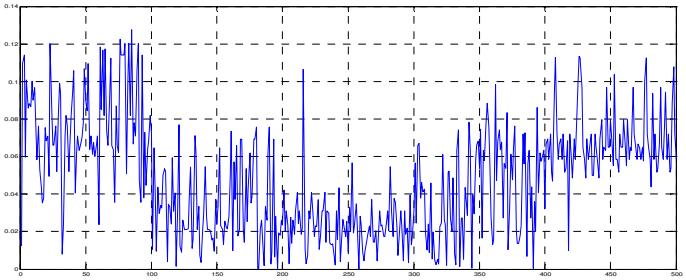

**Fig.12.** The root mean square error generated by the training data.

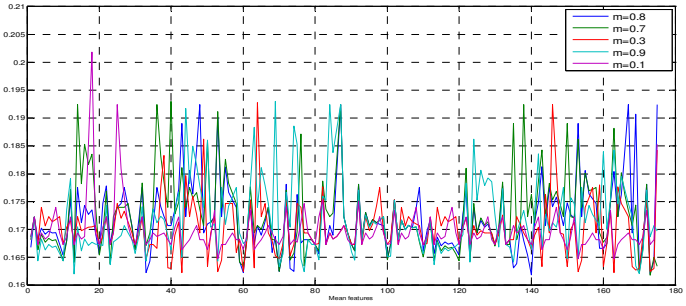


**Fig. 13.** Mean features of the expert system in the case of the teta=110 us.

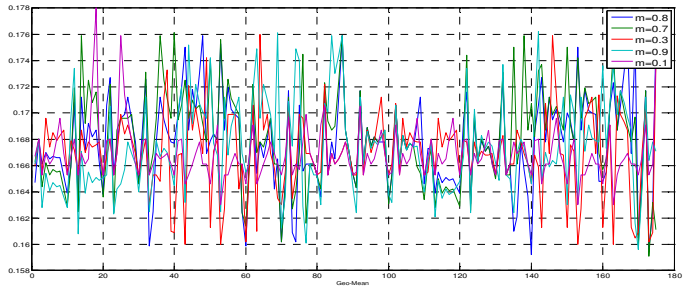


**Fig. 14.** Geometric-Mean of the expert system in the case of the teta=110 us.




ISSN 1737-9334

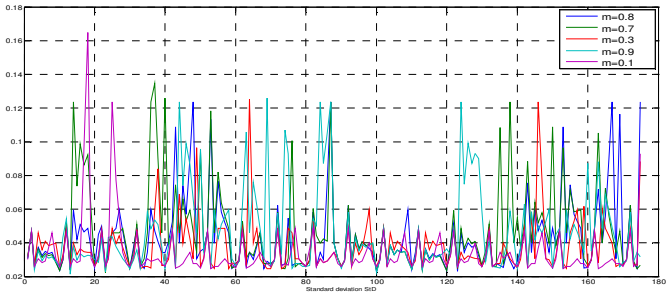


**Fig. 15.** Standard deviation of the expert system in the case of the teta=110 us.

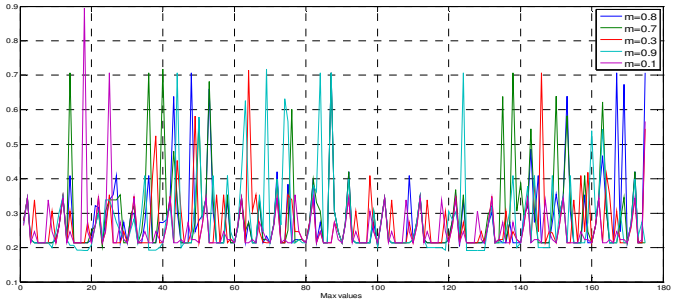


**Fig. 16.** Maximum values of the expert system in the case of the teta=110 us.

## V. CONCLUSION

A new approach for monitoring AC Arc furnace has been presented. A theoretical analysis was presented. This inspection was made for both conditions (healthy and faulty case). MSE across 20 scales is extracted to take into account for dynamic nonlinearity as well as coupling and interaction effects between process elements. In order to reduce the number of entries approaching training process, five statistics are used through MSE. The classification procedure is then executed to determine the state at which the system is operating using the features extracted from the arc voltage signal. The used approaches can be also effective for assessing the level of the abrupt change of Flicker.

## REFERENCES

[1] Mustafa Seker and Arif Memmedov.: Investigation of voltage quality in Electric Arc Furnace with Matlab/ Simulink. International Journal of Engineering and Technical Research (IJETR), Vol.2, N0. 11, pp. 274–284 (2014).

[2] H. Mokhtari, M.Hejri.: A new three phase time-domain model for electric arc furnaces using MATLAB. Transmission and distribution conference and exhibition, pp. 2078–2083. (2002).

[3] Salim Aouabdi, Mahmoud Taibi, Slimene Bouras and Nadir Boutasseta.: Using multi-scale entropy and principal component analysis to monitor gears degradation via the motor current signature analysis. Mechanical systems and signal processing, Vol. 90, pp. 298–316. (2017).

[4] Yacine Djeghader, Hocine Labar and Chelli Zoubir.: Mitigation of voltage Flicker in steel plant using STATCOM. 1 ST International conference on electrical engineering ICEEB'14. (2014).

[5] Y. Djeghader, H. Labar.: Investigation of voltage unbalance problems in Electric Arc Furnace operation mode. Leonardo Journal of sciences, Vol.22, pp. 37-48, (2013).

[6] Yu-Jen Liu, Gary W. Chang, Rong-Chin Hong.: Curve-fitting-based method for modeling voltage-current characteristic of an AC electric arc furnace. Electric power systems research, Vol.80, pp. 572–581. (2010).

[7] Arash Kiyoumarsi, Mohhamad Ataei, Rahmatollah Hooshmand and Arash Dehestani Kolagar.: Electric Arc Furnace voltage Flicker Mitigation by applying a predictive method with closed loop control of the TCR/FC compensator. Journal of electrical engineering & technology, Vol.5, N0. 1, pp. 116-128. (2010).

[8] A. Tavakkoli, M. Ehsan, S. M. T. Batahiee and M. Marzband.: A Simulink study of Electric Arc Furnace power quality improvement by using STATCOM. IEEE International conference on industrial technology, pp. 1–6. (2008).

[9] M. A. Golkar, S. Meschi.: MATLAB modeling of Arc furnace for Flicker study. IEEE International Conference on Industrial Technology. (2008).

[10] G. W. Chang, Y. J. Liu, C. I Chen.: Modeling voltage-current Characteristics of an Electric Arc Furnace based on actual recorded data: a comparison of classic and advanced models IEEE Power and energy society meeting-conversion and delivery of electrical energy in the 21 st century, pp.1-6, (2008).

[11] Antoni Sawicki, Maciej Haltof.: Spectral and integral methods of determining parameters in selected electric arc models with a forced sinusoid current circuit. Archives of electrical engineering, Vol. 65, N0. 1, pp. 87-103, (2016).

[12] Manuela Panoiu, Caius Panoiu and Sorin Deaconu.: Study about the possibility of elctrodes motion control in the EAF based on adaptive impedance control. 13 th International power electronics and motion control conference, pp. 1409-1415, (2008).

[13] V. S. Cherednichenko, R. A. Bikeev, V. A. Serikov, A. V. Rechkalov and A. V. Cherednichenko.: New algorithm for controlling Electric Arc Furnaces using their vibrational and acoustic characteristics. Russian Metallurgy (Metally), N0. 12, pp. 1183–1186. (2016).

[14] Yu-Jen Hsu, Kuan-Huang Chen, Po-Yi Huang, Chan-Nan Lu.: Electric Arc Furnace voltage flicker analysis and prediction. IEEE Transactions on instrumentation and measurement, Vol. 60, N0. 10, pp. 3360–3368. (2011).

[15] Arash Kiyoumarsi, Mohhamad ataei, Rahmatollah Hooshmand, Arash Dehestani Kolagar.: Electric Arc Furnace voltage flicker mitigation by applying a predictive method with closed loop control of the TCR/FC Compensator. Journal of electrical engineering & technology, Vol. 5, N0. 1, pp. 116–128. (2010).

[16] K. Anuradha, B.P. Muni, A.D.Raj Kumar.: Modeling of electric arc furnace & control algorithms for voltage flicker mitigation using DSTATCOM. IEEE, 6 th IPEMC, pp. 1123–1129. (2009).

[17] Chen-Wen Lu, Shyh-Jier Huang, Ching-Liien Huang.: Flicker characteristic estimation of an AC Electric Arc Furnace. Electric power systems research, Vol. 54, pp. 121-130,(2000).

[18] Y. Djeghader, H. Labar, K. Bounaya.: Modelling and parametrical approximation of an electric arc furnace of steelmaking. Journal of electrical engineering, pp. 1-6, (2009).


ISSN 1737-9334

[19] Blanca Rodriguez, Joaquin Santos, Miguel Strefezza, Leonardo Contreras.: Control and regulation of elctrodes in an electric furnace from a FMEA. IFAC Proceedings, pp. 1-6, (2009).
[20] Rainer Ansorge.: What does the entropy condition mean in traffic flow theory. Transpn. Res, Vol. 24, N0. 2, pp. 133–143. (1990).
[21] Jin Wang, Pengjian Shang, Jianan Xia, Wenbin Shi.: EMD based refined composite multi-scale entropy analysis of complex signals. Physica A, Vol. 421, pp. 583–593. (2015).
[22] Madalena Costa, Ary L. Goldberger, C. K. Peng.: Multiscale entropy analysis of complex physiologic time series. Physical review letters, Vol.89, N0. 6, pp. 68102–68105. (2002).
[23] Hong-Bo Xie, Wei-Xing He, Hui Liu.: Measuring time series regularity using nonlinear similarity-based sample entropy. Physics letters A, Vol. 371, pp. 7140–7146. (2008).
[24] J. S. Richman, J. R Moorman.: Physiological time-series analysis using approximate entropy and sample entropy. Am J Physiol Heart Circ Physiol, Vol. 278, H.2039. (2000).
[25] Lake De, Richman J. R, Moorman J. R.: Sample entropy analysis of neonatal heart rate variability. Am J Physiol Heart circ Physiol, Vol. 283, R789. (2002).
[26] K. Zhu, X. Song, D. Xue.: A roller bearing fault diagnosis method based on hierarchical entropy and support vector machine with particle swarm optimization algorithm. Measurement, Vol. 47, pp. 669-675. (2014).




ISSN 1737-9334

# Identification of Nonlinear Systems Using T-S Fuzzy tuned by Backtracking Search Optimization Algorithm

Mourad Turki[#1]

[#] *Higher Institute of Technological Studies of Mahdia , Tunisia*

[1] mouradessturki@yahoo.fr

***Abstract*— This paper proposes a novel metaheuristic optimization algorithm called Backtracking Search Optimization Algorithm BSA to extract T-S model. In this work, the structure and parameters of the fuzzy model are encoded into a particle. Thus, the optimal structure and parameters are achieved simultaneously. The proposed method was compared with others methods such as PSO and CS through a modelling problem.**

***Keywords*— Modeling, TS Fuzzy Systems, Backtracking Search Optimization Algorithm, nonlinear systems**

## I. INTRODUCTION

Takagi-Sugeno (T-S) fuzzy models have been used in many fields due to their ablility to handle the complex nonlinear problems and they are more interpretable than the black-box models. A fuzzy model is formed by several linguistic If-Then rules, which approximate the relationship between the input and output [1].

To optimize the Fuzzy models two tasks are needed: the identification of structure and parameters. Because of their global searching capability, evolutionary algorithms (EAs), such as genetic algorithm (GA), genetic programming (GP), evolutionary programming(EP) and evolution strategy (ES), have been employed to optimize the parameters of the fuzzy models [2] - [4]. The particle swarm optimization PSO is also used to extract fuzzy models such as in [5].

In [6] the cuckoo search algorithm CS is used to optimize both the structure and parameters of the fuzzy models.

In this paper a novel method of optimization called Backtracking Search Optimization BSA is proposed to extract fuzzy models and compared with CS and PSO methods.

This paper is organized as follows. Section II introduces the structure of T–S fuzzy model. Backtracking Search Optimization algorithm BSA is described in Section III. Section IV presents the simulation results. Conclusions are given in Section V.

## II. STRUCTURE OF T-S MODEL

The Takagi–Sugeno (T–S) fuzzy model was first presented in [7] and is described by the following fuzzy IF–THEN rules:

Rule i :If $x_1$ is $A_i^1$ and ... and $x_{N_I}$ is $A_i^{N_I}$ Then

$$y_i = \alpha_i^0 + \alpha_i^1 x_1 + ... + \alpha_i^{N_i} x_{N_i} \quad (1)$$

Where $i = 1,...,N_R$ , $N_R$ is the number of fuzzy rules ; $x = [x_1,...,x_{N_I}]$ is the input variable, $N_I$ is the dimension of input variable ; $\alpha_i^0, \alpha_i^1, ..., \alpha_i^{N_i}$ are the consequent parameters, $y_i$ is an output from the $i^{th}$ fuzzy rule, and $A_i^j$ is a fuzzy variable.

Given the input $x = [x_1,...,x_{N_I}]$ , the final output of the fuzzy model is inferred by a weighted mean defuzzification as follows:

$$\hat{y} = \frac{\sum_{i=1}^{N_R} \omega_i y_i}{\sum_{i=1}^{N_R} \omega_i} \quad (2)$$

Where the weight strength $\omega_i$ of the $i^{th}$ rule is calculated as:

$$\omega_i = \prod_{j=1}^{n} \mu(A_i^j) \quad (3)$$

Where $\mu(A_i^j)$ is the grade of the membership function (MF) of $A_i^j$ and is characterized by a Gaussian function as

$$\mu_{A_i^j}(x_j) = \exp\left( -\frac{1}{2}\left( \frac{x_j - c_i^j}{\sigma_i^j} \right)^2 \right) \quad (4)$$

Where $c_i^j$ and $\sigma_i^j$ represent the centre (or mean) and the width (or standard deviation) of the MF respectively. $c_i^j$ and $\sigma_i^j$ are adjustable parameters called the premise parameters [8].

## III. BACKTRACKING SEARCH OPTIMIZATION ALGORITHM

Backtracking Search Optimization Algorithm (BSA) is a newly developed stochastic search algorithm, which has been first proposed in [9] by Pinar Civicioglu. Unlike many swarm-intelligence optimization algorithms, BSA has a single


ISSN 1737-9334

control parameter which is not extremely sensitive to the initial value of this parameter. As a population-based iterative evolutionary algorithm (EA), the population generation strategy of BSA includes three operators: selection, mutation and crossover. The searching framework of BSA is described in Fig. 1 with corresponding details stated as follows.

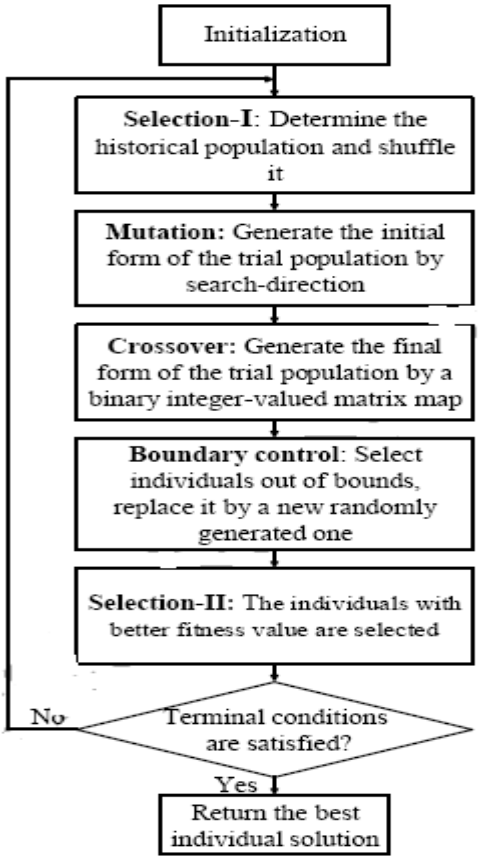


Fig. 1 The framework of BSA

At the first step, the BSA generates two randomly distributed initial populations P and initial historical population oldP according to Eq.(5):

$$\begin{cases} P_{ij} = U(low_j, up_i) \\ oldP_{ij} = U(low_j, up_i) \end{cases}, i=1,2,...N; \quad j=1,2,.....D \tag{5}$$

where $N$ , $D$ and $U$ are the population size, the individual dimensionality and the uniform distribution, respectively. Each $P_i$ is a target individual in the population $P$. Then the first selection determines the historical population *oldP* to be used for calculating the search direction. BSA has the option of redefining *oldP* at the beginning of each iteration through the „if-then" rule in Eq. (6):

$$if \ a<b \ \ then \ oldP := P|a,b \sim U(0,1) \tag{6}$$

where := is defined as the update operation. Eq. (6) ensures that BSA designates a population belonging to a randomly selected previous generation as the historical population, which is temporarily recorded until it is changed. After that, the order of the individuals in *oldP* needs to be randomly ordered by a shuffling function, as is illustrated below:

$$oldP := permuting(oldP) \tag{7}$$

In order to generate the initial form of the trial population *Mutant* , the mutation operation considers both $P$ and *oldP* , where (*oldP* - $P$) is the search-direction matrix. The process is described as:

$$Mutant = P + F.\ (oldP - P) \tag{8}$$

where the mutation coefficient $F = 3.rndn$ , $rndn \sim N(0,1)$ ( $N$ is the standard normal distribution), controls the amplitude of the search-direction.

The crossover process of BSA generates the final form of the trial population $T$ . Firstly, a binary integer-valued matrix **map** of size $N \times D$ is obtained by:

$$\begin{aligned} &Map(1:N,1:D)=0 \ //Initial\ map \\ &If\ a<b|\ a,b \sim U(0,1)\ then \\ &For\ I\ from\ 1\ to\ N\ do \\ &Map_{i,u(1:[mixrate.rnd.D])}=0|u=permuting(<1,2,.....,D>) \\ &End \\ &Else \\ &For\ I\ from\ 1\ to\ N\ do,\ map_{i,randi(D)}=0,\ end \\ &End \end{aligned} \tag{9}$$

where *mixrate* is the sole control parameter in BSA (the mix rate parameter), controls the number of elements of individuals that will mutate in a trial by using [*mixrate.rdn.D*]. Secondly, $T$ is updated with:

$$\begin{aligned} &if\ map_{nm}=1,\ (n=1,2,....,N, m=1,2,.....,D), \\ &Then \quad T_{nm}=P_{nm} \end{aligned} \tag{10}$$

Some individuals of the final trial population $T$ can overflow the allowed search space, so boundary control is rather necessary. Subsequently, the last step comes to the greedy selection. At this stage, the $T_i$ s that have better fitness values than the corresponding $P_i$ s are used to update the $P_i$ s. If the best individual $P_{best}$ has a better fitness value than the global minimum value obtained so far by BSA, the global minimize is updated to be $P_{best}$ , and the global minimum value is updated to be the fitness value of $P_{best}$ .

## IV. Simulation Results

In this section, the proposed BSA algorithm is used to extract T-S models in the aim to identify a nonlinear plant modelling problem and compared to PSO [10] and CS [6]. The parameters of CS and PSO algorithms are given respectively in Table I and Table II.


ISSN 1737-9334

TABLE I

PARAMETER VALUES

| Parameter | Value |
|---|---|
| Number of nests | 20 |
| $p_a$ | 0.25 |
| λ | 1.5 |
| Step size α | 1 |

TABLE III

PSO PARAMETER VALUES

| Parameter | Value |
|---|---|
| Population size | 20 |
| $c_1$ | 1.49 |
| $c_2$ | 1.49 |
| $w_{min}$ | 0.4 |
| $w_{max}$ | 0.9 |

For the BSA algorithm the mixrate=1.For the three methods the commonly used parameters are given as follows: population size = 20, maximum generation=500. Thus the number of evaluations is 10000.

The mean square error MSE is used to test the performance indices, and it is defined as follows:

$$MSE = \frac{1}{n}\sum_{k=1}^{n}(y_{ref}(k) - y(k))^2 \quad (11)$$

The structure and parameters are all encoded into a particle. As shown in Fig. 2, the particle is represented by a vector which includes the premise parameters, the consequent parameters and the labels. The fuzzy rules are selected as follows:

If $l_i > 0$ then the rule $i$ is active, $i \in [1 \ldots N]$, where N is the pre-defined maximum number of rules. In our work, N is set to 5. All the active rules compose the fuzzy inference system.

The nonlinear dynamic plant used is described by the difference equation [10] as follows:

$$y(k) = g\left(y(k-1), y(k-2)\right) + u(k) \quad (12)$$

where

$$g\left(y(k-1), y(k-2)\right) = \frac{y(k-1)y(k-2)(y(k-1)-0.5)}{1+y(k-1)^2+y(k-2)^2} \quad (13)$$

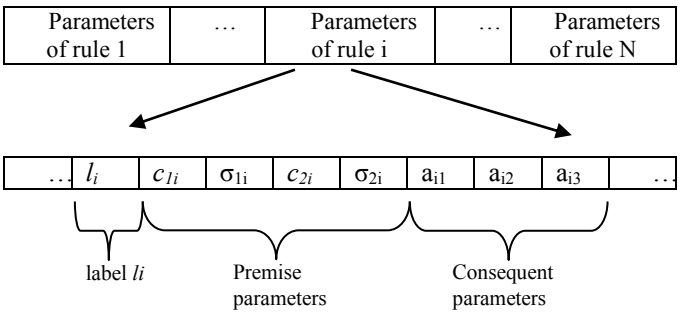


Fig. 2 Structure of a particle

The goal is to approximate the nonlinear part $g\left(y(k-1), y(k-2)\right)$ called the "unforced system" in control literature. It is a two input /single output model. The evolution process was repeated 50 times on a Pentium Core 2 Duo (1.8 GHz CPU) and 2GB of main memory in the same computing environment (MATLAB 2007a). All the coefficients of the consequent linear function are limited to [-10, 10] and the width of the Gaussian function is limited to [0, 5].

The 400 simulated data points were obtained from the nonlinear dynamic plant defined by (12) and (13). The 200 training data were generated using a random input signal u(k) that is distributed in [−1.5, 1.5], and 200 samples of testing data were generated using a sinusoidal input $u(k) = \sin\left(\frac{2\pi k}{25}\right)$.

The results of BSA method are compared with PSO and CS. The BSA method has the best MSE in both training and testing stages than PSO method. This demonstrates that BSA gives good results compared to PSO and CS.

Fig. 3 shows the target and CS model output in the training and testing stages. The errors between target output and model output can be seen in Fig. 4. As we can see in Fig. 3, the BSA method has good identification ability and it can predict the output with small errors.

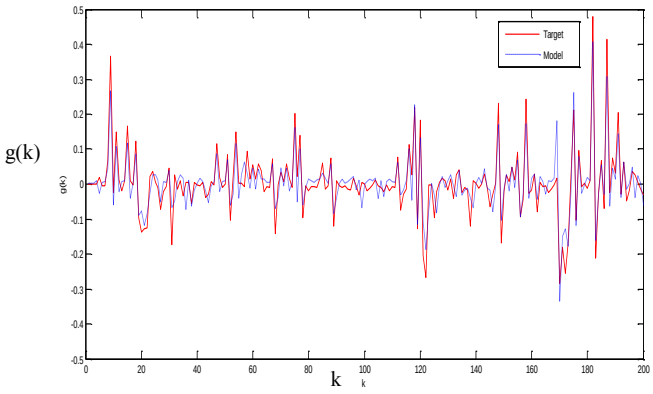


(a)




ISSN 1737-9334

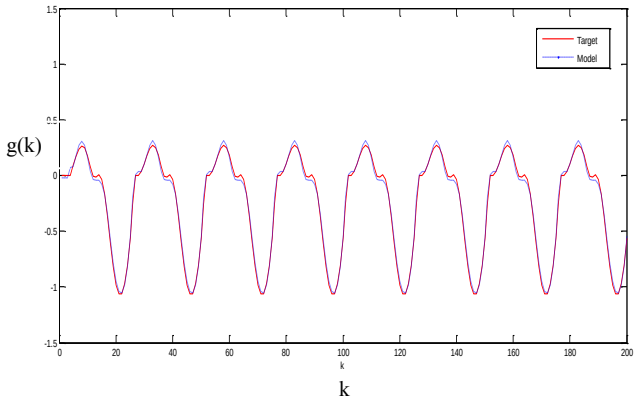


(b)

Fig. 3 The target output and model output for nonlinear plant modelling problem, (a) training stage and (b) testing stage

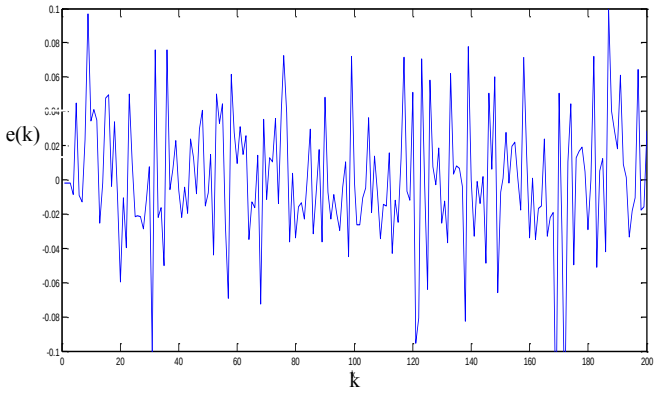


(a)

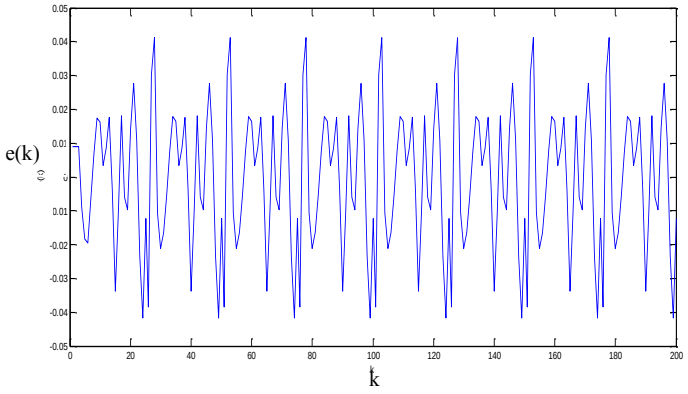


(b)

Fig. 4 The errors between target output and model output, (a) training stage and (b) testing stage

## V. CONCLUSION

In this paper, the extracting of T–S fuzzy model using Backtracking Search Optimization BSA is presented. The developed T–S fuzzy model has the advantage that the rules structures and both the premises and consequents parameters can be optimised simultaneously. The obtained T–S fuzzy model with BSA method has a smaller MSE than PSO and CS in modelling of nonlinear system. Thus we can conclude that BSA method has a better optimizing accuracy in modelling.

## REFERENCES

[1] M. S. Kim, C.H.Kim and J.J. Lee, "Evolving compact and interpretable Takagi-Sugeno Fuzzy models with a new encoding scheme," IEEE Trans. on Systems, Man, and Cybernetics. Part B: Cybernetics, 36(5), 2006, pp 1006-1023.

[2] O.Cordon and F. Herrera, "A Two-Stage Evolutionary Process for Designing TSK Fuzzy Rule-Based Systems, IEEE Trans. Systems., Man, and Cybernetics. Part B: Cybernetics, 29(6), 1999, pp 703-715.

[3] O. Cordon, F.Herrera ,F. Gomide, F. Hoffmann and L. Magdalena, "Ten years of genetic fuzzy systems: current framework and new trends," in Proc. IFSA and 20 th NAFIPS conference , 2001, pp 1241 - 1246

[4] S.J. Kang, C.H. Woo, H.S. Hwang and K.B. Woo, "Evolutionary Design of Fuzzy Rule Base for Nonlinear System Modeling and Control," IEEE Trans. Fuzzy Systems, 8(1), 2000, pp 37-45.

[5] A. Khosla, S. Kumar and K.K. Aggarwal, "A framework for identification of fuzzy Models through particle swarm optimization," in: IEEE Indicon Conference, Chennai, India, 2005, pp. 388–391.

[6] M. Turki and A. SAKLY, "Cuckoo search-based TS fuzzy identification of nonlinear systems," In : *Systems and Control (ICSC), 2015 4th International Conference on*. IEEE, 2015. p. 151-154.

[7] T.Takagi and M.Sugeno, "Fuzzy identification of systems and its application to modeling and control," IEEE Trans. On Systems, Man, and Cybernetics. Part B: Cybernetics, 15(1), 1985, pp 116-132.

[8] C.F. Juang, I.F. Chung and C.H. Hsu, "Automatic construction of feedforward/ recurrent fuzzy systems by clustering-aided simplex particle swarm optimization," Fuzzy Sets and Systems, 2007, pp 1979–1996.

[9] P. Civicioglu, Backtracking search optimization algorithm for numerical optimization problems, Applied Mathematics and Computation, 219 (2013) 8121-8144.

[10] L. Wang and J. Yen, "Extracting Fuzzy Rules for System Modeling Using a Hybrid of Genetic Algorithms and Kalman Filter," Fuzzy Sets and Systems , 101 (3), 1999, pp 353–362.




ISSN 1737-9334

# Pattern Design of 2D Antenna Arrays using Biogeography Based Optimization

Abdelmadjid Recioui, Nabil Arhab and Imadeddine Zeghad
Laboratory Signals and Systems, Institute of Electrical and Electronic Engineering
University M'hamed Bougara of Boumerdes, Avenue de l'indépendance, 35000
Boumerdes, Algeria.
e-mail: a_recioui@univ-boumerdes.dz

*Abstract*— **In this work, the design of two dimensional antenna arrays using the biogeography based optimization (BBO) is considered. The purpose is to match a desired pattern while preserving acceptable properties as compared to the conventional arrays. Three array geometries considered in this work are: the rectangular array, the circular array, the concentric circular array and the hexagonal array. The parameters that are varied are the element excitation amplitude and the variation is continuous from 0 to 1. Examples are included to demonstrate the effectiveness of the optimization technique in solving the antenna array design problem**

**Keywords-antenna arrays, BBO, optimization, directivity, sidelobe level**

## I. INTRODUCTION

An antenna array consists of more than one element. A single-element antenna is usually not enough to achieve some radiation characteristics needed for modern communication systems [1-3]. An antenna array acts as a spatial filter which permits signal from a certain direction while rejecting all other signals coming from other directions, impinging on the array. To attain this, an array must be designed with high gain at the desired look direction, and achieve maximum signal to noise plus interference ratio (SNIR) at the output. For linear array design, there are two important conventional types of arrays: the equi-spaced uniformly excited array and the Chebyshev excited array. The former is an array with high resolution but with a relatively high sidelobe, whereas the latter generally has a larger beam width as compared with the former, its sidelobes are controllable and of equi-height [4-6].

Array parameters such as output gain, input impedance and desired radiation pattern can be optimized by carefully choosing the design of antenna [7]. Optimized selection of these multiple parameters can be efficiently achieved. Pattern synthesis techniques are, in general, based on the variations of the array parameters such as the element excitations (amplitude and/or phase) and positions of array elements. The characteristics of the desired pattern can vary depending on the required application. Some synthesis methods are concerned with reducing the Sidelobe Level (SLL) while preserving the gain of the main beam [8]. Others deal with null control to eliminate the effects of interference and jamming. Other methods of controlling the array pattern use non-uniform excitation and phased arrays [9]

The Schelkunoff array polynomial method [10-12] has been used to synthesize the equispaced linear array pattern. In this method, the pattern synthesis problem is reduced to the determination of proper roots of the array polynomial for a desired pattern. From this the element excitations are determined. The works reported in literature considered large arrays based on various optimization techniques together with the Schelkunoff unit circle representation of the array polynomial for uniform linear array. A genetic algorithm has been used for the pattern synthesis by Monorchio et. al. [13]. Optimized low sidelobe levels have been presented by the F. Yu et al. in [14]. The optimization has been performed for different beamwidth values and the tradeoff between the sidelobe level and the main beam examined. Another genetic algorithm based optimizer has been proposed by A. Recioui et al and the results have been compared with other techniques [12].

Nature inspired evolutionary algorithms which have earned their place because of their simplicity, no mathematical analysis, larger solution space and faster convergence. In antenna array design problems, the evolutionary algorithms including Genetic Algorithm (GA) [15], Particle Swarm Optimization (PSO) [16], Ant-Colony-Optimization (ACO) [17] and Differential Evolution (DE) [18] have been deployed to find the optimum solutions. Haupt [15] has done a lot of research on the synthesis of antenna array using genetic algorithm. Recently more algorithms such as Invasive Weed Optimization algorithm [19], Tabu Search (TS) [20], Bees Algorithm (BA) [21], Bacteria Foraging Algorithm (BFA) [22], Taguchi's Algorithm [23] and Plant Growth Simulation Algorithm (PGSA) [12] have flourished to solve optimization problems. Guney et al. [22-24] proposed BFO, PGSA and Bees Algorithm to synthesize antenna pattern for reducing sidelobe levels with null control using the methods, amplitude-only and position control of elements.

In this work, the Biogeography Based Optimization is used as a technique to optimize the amplitude excitation, to get best reduction of SLL and the largest possible directivity. These two properties turn out to be conflicting as optimizing for one would automatically affect the other. In fact, optimizing for sidelobe level only means obtaining bad directivity and optimizing for directivity only would automatically worsen the sidelobe level. The indea of the


ISSN 1737-9334

present work is to use a mask to force the directivity and sidelobe levels to stay within the limits dictated by the user. The design concerns non-uniformly excited rectangular, circular, concentric circular and hexagonal antenna array geometries.

## II. PROBLEM FORMULATION

To provide very directive patterns, it is necessary that the fields from the elements of the array interfere constructively in the desired directions and interfere destructively in the remaining space. Depending on the array geometry, different array factor expressions exist.

### A. Rectangular arrays

If N linear arrays are placed at even intervals along the y direction, a rectangular array is formed. We assume again that they are equispaced at a distance and there is a progressive phase shift along each row. We also assume that the normalized current distribution along each of the x-directed arrays is the same but the absolute values correspond to a factor of $\mathbf{I_{1n}}$(n=1, …, N). Then, the Array Factor(AF) of the entire MN array is:

$$AF(\theta,\phi)=\sum_{n=1}^{N}\sum_{m=1}^{M} I_{nm}\exp(j(n-1)(kd_x\sin\theta\cos\phi+\beta_x \times \exp(j(m-1)(kd_y\sin\theta\sin\phi+\beta_y)) \quad (1)$$

### B. Circular arrays

The array factor of circular antenna arrays is given as [7];

$$AF(\theta,\varphi)=\sum_{n=1}^{N} I_n e^{j(ka\sin(\theta)\cos(\varphi-\varphi_n)+\alpha_n)} \quad (2)$$

Where, $I$ is the excitation amplitude of element n; $\varphi_n$ is its position and $\alpha_n$ is the excitation phase. k is the wave number and a is the circle radius.

### C. Concentric Circular Array

A concentric circular array antenna is an array that consists of many concentric rings of different radii and a number of elements on its circumference. For the concentric circular array with $M$ rings and $N_m$ elements in the corresponding $m^{th}$ ring, the array factor is given as:

$$AF(\theta,\varphi)=\sum_{m=1}^{M}\sum_{n=1}^{N_M} I_{nm}\exp\{jka_m\sin(\theta)\cos(\varphi-\varphi_{nm})+\alpha_{nm}\} \quad (3)$$

### D. The hexagonal array antenna

The hexagonal array (HA) can be treated as consisting of two concentric N -element circular arrays of different radii $r_1$, $r_2$ as the peripheral curve of its vertices is a circle [7]. The array factor of the hexagonal array is expressed by:

$$AF(\theta,\phi)=\sum_{n=1}^{N} A_n\exp(jr_1\sin\theta(\cos\phi_{1n}\cos\phi+\sin\phi_{1n}\sin\phi) + B_n\exp(jr_2\sin\theta(\cos\phi_{2n}\cos\phi+\sin\phi_{2n}\sin\phi) \quad (4)$$

With $$r_2=r_1\cos(\frac{\pi}{n}) \text{ and } r_1=\frac{d_e}{\sin(\frac{\pi}{n})} \quad (5)$$

Where $d_e$ is the inter-element spacing along any side of the hexagonal array.

### E. The objective function

The objective function to be optimized is the least squares sum of differences between the produced Array Factor and the desired mask. Fig. shows an example of a Mask, Noting that the values of $AF$ and $AFmin$ and the intervals of each one of them should be modified to adapt to the specific array factor of the 2D shape we want to optimize. For this, adjustment must be suitable to the sidelobes level (SLL) and the Directivity (Dir) of the uniform array factor of that specific shape.

The fitness function to be minimized is:

$$F=\frac{\sum_{n=1}^{N}\left|AF_d(\theta)-AF_p(\theta)\right|}{N} \quad (6)$$

$AF(\theta)_d$: The desired array factor which is represented by the mask shown above.

$AF(\theta)_p$: The produced array factor (using eqs 1 to 4).

$N$: Number of point. Throughout our work: $N$=36000.

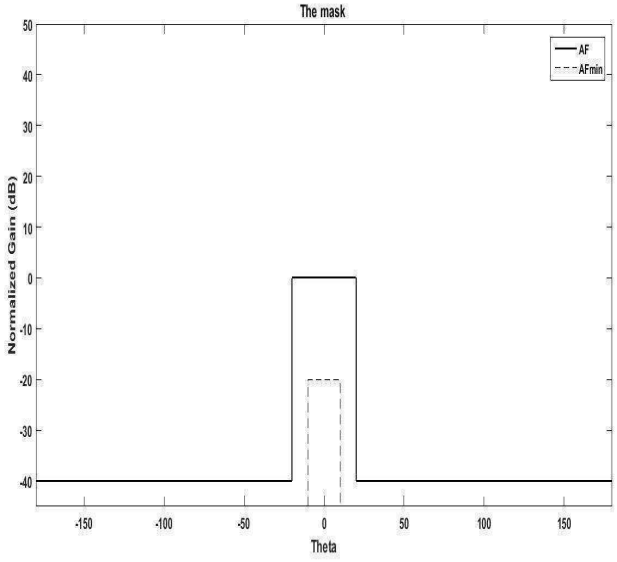


Fig. 1 The shape of the mask used in the optimization




ISSN 1737-9334

## III. THE BIOGEOGRAPHY BASED OPTIMIZATION

Biogeography based optimization (BBO) is an evolutionary algorithm (EA) that optimizes a function by stochastically and iteratively improving candidate solutions with regard to a given measure of quality or fitness function, since it does not make any assumptions about the problem, it can be applied to a wide class of problems [25]. It is typically used to optimize multidimensional real-valued functions and It does not require the function to be differentiable therefore it can be used on discontinuous functions.

Like many Evolutionary Algorithms, BBO was motivated by a natural processing particular, BBO was motivated by biogeography, which is the study of the distribution of biological species through time and space, it has been introduced by Dan Simon in 2008 [25]. Generally, Mathematical models of biogeography describe how species migrate from one island to another, how new species arise, and how species become extinct. The term "**island**" here is used descriptively rather than literally. That is, an island is any habitat that is geographically isolated from other habitats. So, Geographical areas that are well suited as residences for biological species are said to have a high **habitat suitability index** "HIS". and the variables that characterize habitability are called **suitability index variables** "SIVs", SIVs can be considered the independent variables of the habitat, and HSI can be considered the dependent variable [6]. Candidate solutions of a problem are represented by an array of integers as:

$$Habitat = [SIV_1, SIV_2, ..., SIV_N] \tag{7}$$

The Habitat suitability index (HSI) can be also referred to as the value of the fitness function since it is directly proportional to it [25,26], and it is found by evaluating the fitness function:

$$Fitness(habitat) = f([SIV_1, SIV_2, ..., SIV_N]) \tag{8}$$

### *A. BBO Main Operators*

The BBO algorithm is based on two main operators **Migration** and **Mutation**

- **Migration Operator**

In BBO algorithm each habitat ($H_i$) is a solution candidate for the optimization problem and the position of each habitat ($H_i$) is an n-dimensional search space represented by **(SIVs)** which is an n-dimensional vector, and the quality of each habitat is measured by the "HSI" which is directly proportional to the fitness function value. This algorithm uses **Migration** operator as a powerful tool to share information between habitats in the solution space. **The Migration operator** shares information between habitats based on **immigration and emigration rates**, probabilistically. Ea0ch habitat has its own immigration $\lambda_i$ and emigration rates $\mu_i$ which are the functions of species in the habitat.

For a given habitat, the immigration $\lambda_i$ rate is inversely proportional to the HSI (fitness) value, while the emigration $\mu_i$ rate is directly proportional to HSI value. The habitats with high immigration rates (poor solutions) are more likely to accept information from the other habitats with high HSI values, while the habitats with low immigration rates (good solutions) share their information with other poor habitats with a high probability [25,26]. The immigration and emigration rates are calculated for each habitat as follows:

$$\mu_i = E(\frac{K}{S_{\max}}) \tag{9}$$

$$\lambda_i = I(1 - \frac{K}{S_{\max}}) \tag{10}$$

$I$: Maximum possible immigration rate
$E$: Maximum possible emigration rate
$K$: Number of species in the ith habitat
$S_{max}$ : Maximum number of species

Habitats with a high HSI value tend to have a large number of species, while those with a low HSI have a small number of species. from Figure 1, it can be concluded that the habitat with few species (poor solution, low HSI) like $S_1$, has a low emigration rate and a high immigration rate. This means that the habitat with low HSI tends to take information about the good habitats with the high probability, while the probability of sharing its information for other habitats is relatively low. On the other hand, the habitat which has more species (good solution, high HSI) like $S_2$, has a low immigration rate and a high emigration rate. Such habitats with high HSI values share their information with the other habitats with a high probability. By utilizing this mechanism [25,26], the Migration Operator of the BBO algorithm can achieve adequate exploitation ability between the habitats in the search space. For each variable of a given solution ($H_i$), the immigration $\lambda_i$ rate decides whether or not to immigrate.

- **Mutation Operator**

In most cases, it is possible that a meta-heuristic algorithm is trapped to the local optimum by lapse of the iteration. In order to escape from the local traps in the search space, the BBO algorithm utilizes a **Mutation Operator**. Which is a probabilistic operator that modifies a habitat's SIV randomly based on mutation rate (*pMutate*) [25], which is related to the habitat's probability. The mutation rate (*pMutate*) for each habitat is calculated as follows:

$$pMutate = m_{\max}(\frac{1 - P_i}{P_{\max}}) \tag{11}$$

$m_{max}$: user-defined parameter.
$P_{max}$: max{ $P_i$ }
$P_i$ =probability of the number of each species


ISSN 1737-9334

Based on this equation a variable of each habitat mutates randomly in search space with a given probability.

Another feature of the BBO algorithm is that the elitehabitats with high HSI values are selected to keep and transfer from previous generation to the current one. Therefore, the ***"Keeprate"*** parameter is defined for this purpose. For Example, 20% of habitats with high HSI values are selected to keep in each generation. It means that the 20% of elite habitats from the previous population are transferred to the current generation and combined with new habitats (*Keeprate=0.2)*. Finally, the habitats with high HSI values are selected from the combined population of habitats to form a new population.

Fig. 2 shows the flowchart that describe the simplified algorithm of the BBO. The algorithm starts by generating random habitats and evaluating the cost function then the migration rates are calculated to be used in formulating the migration operator after that the mutation operator is applied to save the algorithm from trapping in a local minima, at the end the habitats with high HSI would be conserved to pass to the next generation. The same steps will be repeated until the termination criterion will be satisfied.

## IV. RESULTS AND DISCUSSIONS

The following BBO parameters has been used: Number of population: 60,KeepRate=0.2, Number of iterations =100, Maximum migration rates E=1 and I=1, Mutation probability = 0.04.

### *A. Rectangular Planar Array*

It is seen from figure 3 that the side lobes level and the Directivity of the uniform array are -12.65dB, 18.34dB respectively, and after optimizing the values obtained are SLL= -20.96dB , Directivity=17.14dB. From figure 4 by varying the amplitude, the side lobes level and the Directivity of the uniform array are -12.96dB to 21.70dB respectively, and after optimizing the values obtained are SLL= -20.82dB , Directivity=20.27dB.

When optimizing with 49 elements and 100 elements, for the 7 x 7 arraythe uniform one has a ratioDIR/SLLof 1.4498, we have optimized it to 0.8177,for the 10 x 10 array the uniform one has a ratioDIR/SLL1.6744, we have optimized it to 0.9736 and although we have obtained a better SLL for both cases but we had a decrease in directivity.

### *B. Concentric Circular array*

We have used a 92 elements concentric circular array consisting of 5 rings, each ring hold a specific number of element Nm= [6 12 18 2531]. The results obtained are shown in Fig. 7 for the uniform array we have got SLL = -15.10dB, and Directivity=16.23dB and after optimizing we have a got a reduction of sidelobes level to-34.2dB, and a decrease in Directivity to 15.29dB.

We have used also a 168 elements concentric circular array consisting of 7 rings, with: Nm= [8 16 24 32 40 48].

For the second case the results obtained are shown in Figure 6, for the uniform array we have got SLL = -15 dB, and Directivity=18.95dB and after optimizing we have a got a reduction of sidelobes level to-34.09dB, and a decrease in Directivity to 16.95dB.

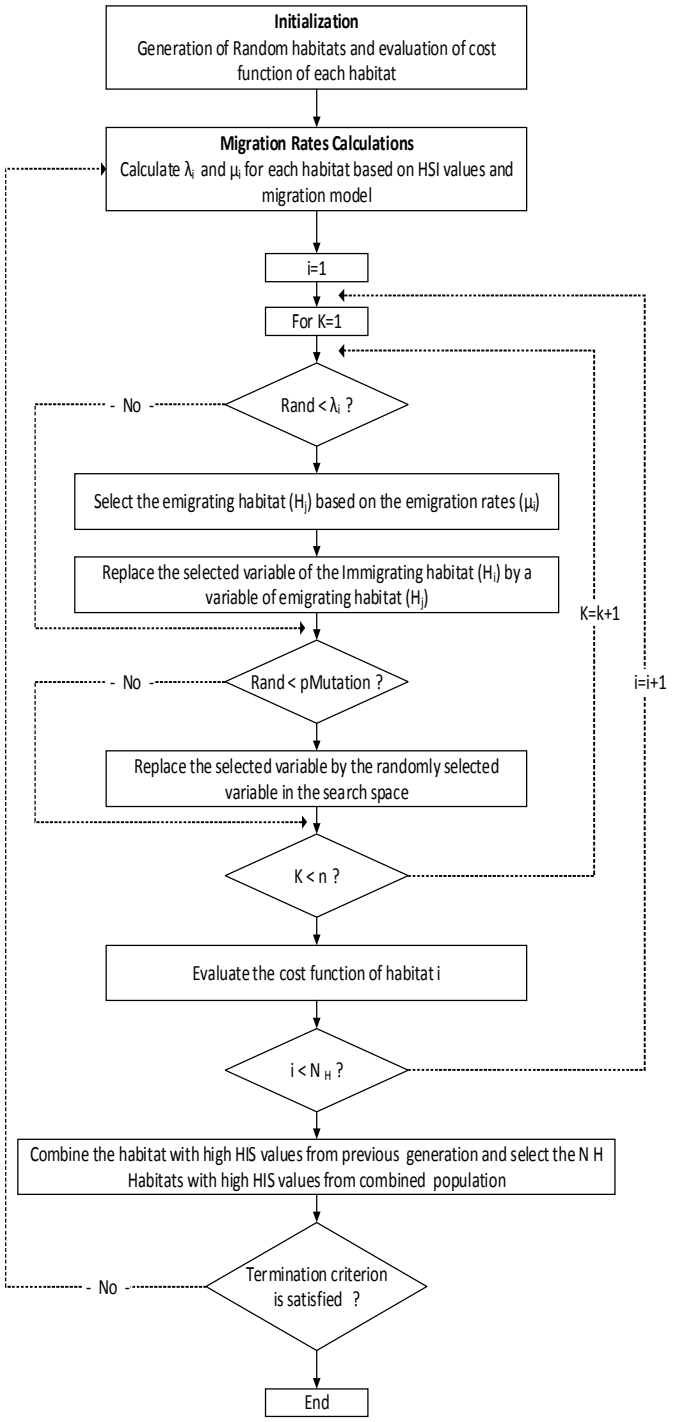


Fig. 2 the flowchart of the main BBO Algorithm




ISSN 1737-9334

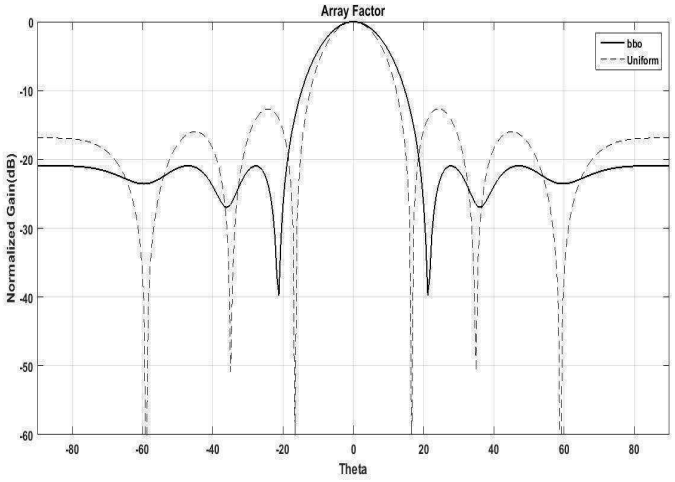


Fig. 3 Array factor of 7 x 7 Planar Rectangular Array optimization

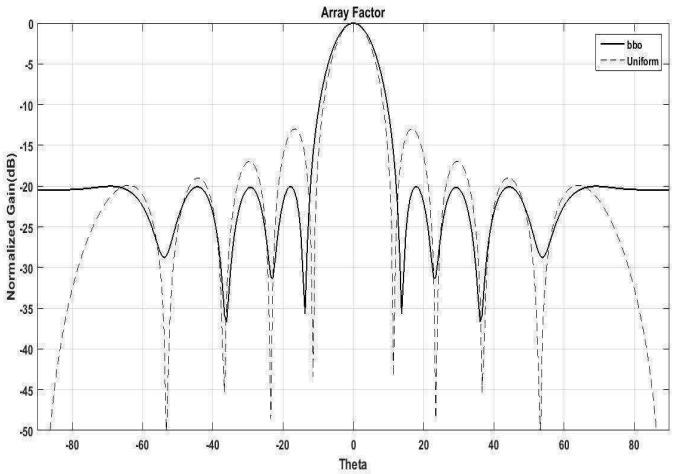


Fig. 4 Array factor of 10 x 10 Planar Rectangular Array optimization

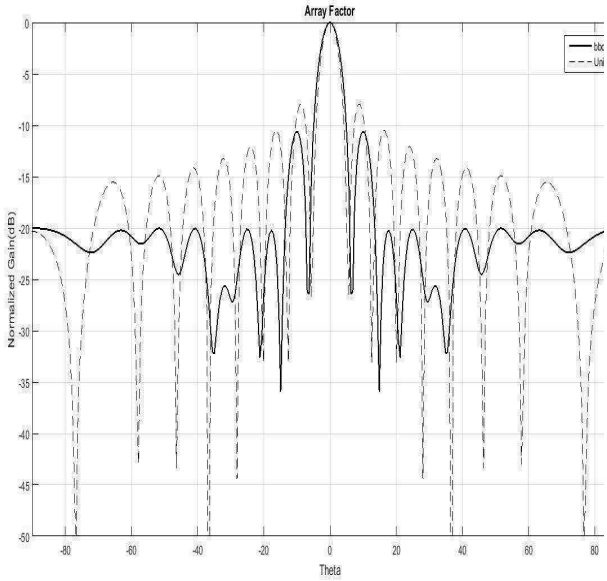


Fig. 5 Array factor of 92 element Concentric Circular array

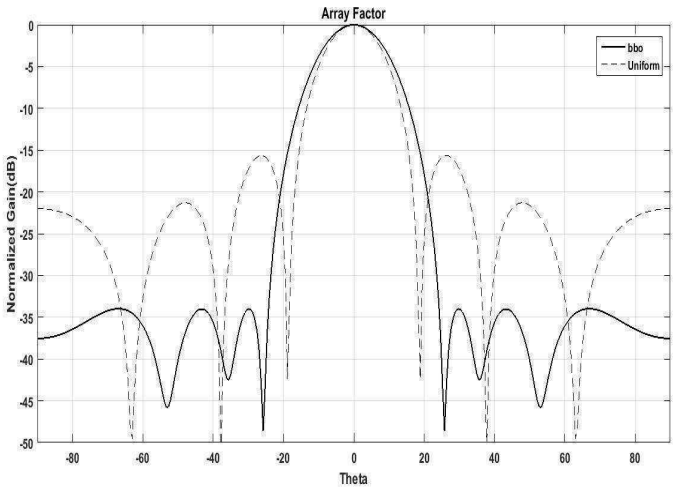


Fig. 6 Array factor of 168 element Concentric Circular array

### *C. The hexagonal array*

A 20 elements hexagonal array is used, in the figure 7 the uniform and a non-uniformly excited hexagonal array are shown, for the uniform array we have got SLL = -07.91dB, and Directivity=15.51dB and after optimizing we have a got a reduction of SLL to-20.48dB, and a decrease in Directivity to 13.53dB.

A 50 elements hexagonal array is used, the results obtained are shown in Figure 8, for the uniform array we have got SLL =-08.01dB, and Directivity=20.34dB and after optimizing we have a got a reduction of sidelobes level to=-13.99dB, and a decrease in Directivity to 18.31dB.

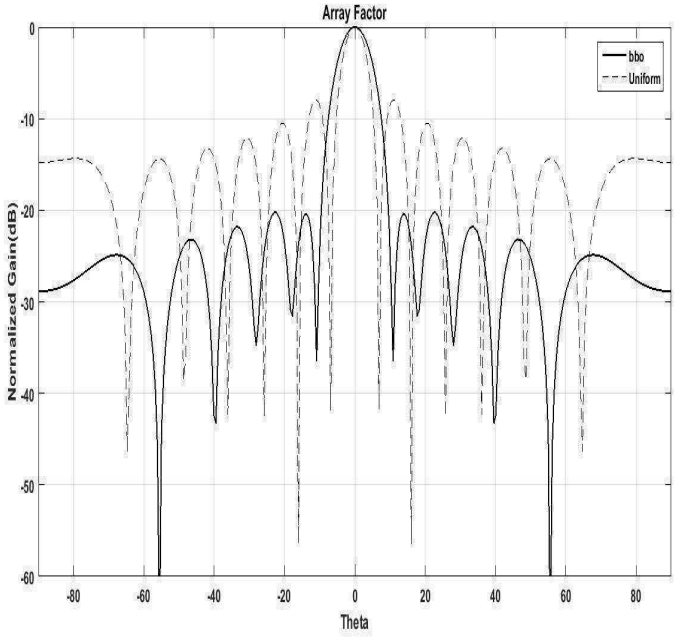


Fig. 7 Array factor of 20 element hexagonal array with optimization




ISSN 1737-9334

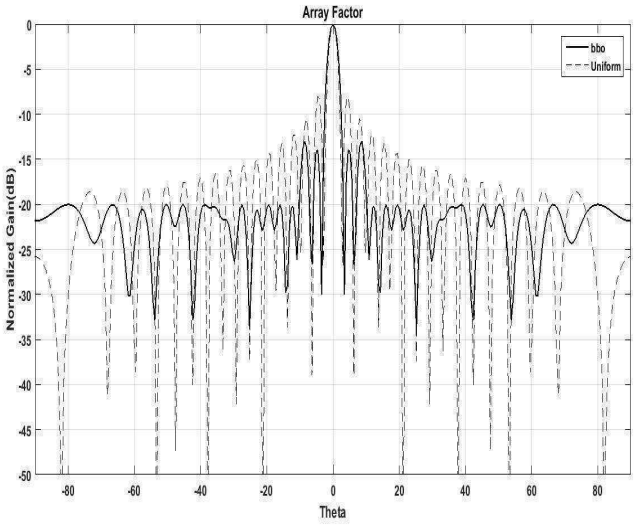


Fig. 8 Array factor of 50 element hexagonal array with optimization

## V. CONCLUSION

This paper presented the optimization of a planar rectangular array, Concentric Circular and the hexagonal antenna arrays through varying the excitation amplitudes. The optimization was handled using a new nature-inspired global optimization technique which is the Biogeography based algorithm (BBO). The objective was to minimize the SLL using a designed mask while the fitness function to be used in the optimizations is the sum of the differences between the array factor treated and a specific mask made for it.

The obtained results were fairly noticeable in terms of sidelobe levels reduction. However, we noticed a decrease in directivity in all the array shapes but in many cases it was negligible due to the considered uniform array which is known to possess high directivity already as it is a common property in array antennas. The proposed mask method was just as efficient as or better than SLL objective functions implemented in literature.

## References

[1] A. RECIOUI and H. BENTARZI, "Genetic Algorithm based MIMO capacity enhancement in spatially correlated channels including Mutual Coupling", *Wireless Personal communications, Springer*, Volume 63, Number 3, 2012, pages: 689-701. DOI: 10.1007/s11277-010-0159-5.

[2] Abdelmadjid Recioui and Hamid Bentarzi, Capacity Optimization of MIMO Wireless Communication Systems Using a Hybrid Genetic-Taguchi Algorithm, Wireless Personal Communications , Volume 71, Issue 2, 2013, pp 1003-1019 .

[3] ABDELMADJID RECIOUI, APPLICATION OF A GALAXY-BASED SEARCH ALGORITHM TO MIMO SYSTEM CAPACITY OPTIMIZATION, ARABIAN JOURNAL FOR SCIENCE AND ENGINEERING, (2015), DOI: 10.1007/s13369-015-1934-0

[4] A. RECIOUI and H. BENTARZI, "Pattern nulling in linear array antennas with mutual coupling effects using Taguchi method", AMSE transactions on modeling, measurement and control, Vol. 83, Issue 3, 2010.

[5] Abdelmadjid Recioui, Application of a Hybrid Taguchi-Genetic Algorithm to the Multiobjective Design Optimization of Yagi–Uda Antennas, Wireless Personal Communications , Volume 71, Issue 2, 2013, pp 1403-1420

[6] R. S. Elliott, "*Antenna Theory & Design*," IEEE Press, John Wiley & Sons, 2003.

[7] BALANIS, C. A. : Antenna Theory: Analysis and Design, Third Edition, John Wiley & Sons, New York, 2005.

[8] Abdelmadjid Recioui, Optimization of Antenna Arrays Using Different Strategies Based on Taguchi Method, Arabian Journal for Science and Engineering, Volume 39, Issue 2, 2014, pp 935-944.

[9] Abdelmadjid Recioui, Design and Thinning of Linear and Planar Antenna Arrays Using a Binary Teaching Learning Optimizer, ACTA PHYSICA POLONICA A, Vol. 130,n° 1, July 2016.

[10] S. A. Schelkunoff, "A mathematical theory of linear arrays," *Bell System Tech.* J.,22, 1943, p. 80-107.

[11] ABDELMADJID RECIOUI, PATTERN SYNTHESIS OF NONUNIFORMLY SPACED ARRAYS BASED ON UNIT CIRCLE REPRESENTATION AND TAGUCHI METHOD, WIRELESS PERSONAL COMMUNICATIONS, VOLUME 75, ISSUE 4,2014, PP 1969-1981.

[12] A. RECIOUI, A. AZRAR, "Use of Genetic Algorithms in Linear and Planar Array Synthesis using Schelkunoff Method", *Microwave and Optical Technology Letters*, Vol. 49, issue 7, July 2007.

[13] Monorchio, A., Genovesi, S., Bertini, S., & Brizzi, A., "An efficient interpolation scheme for the synthesis of linear arrays based on Schelkunoff polynomial method", *IEEE Antennas and Wireless Letters,* Vol. 6, 2007, pp. 484–487.

[14] F. YU J. Ronghong, W. Zhengyi, L. Bo and G. Junphig, "Pattern Synthesis of Linear Arrays Using a Hybrid Optimization Algorithm," *ICSP Proc. 2004*, Vol. 1, p. 428-30.

[15] R. L. Haupt, Thinned arrays using genetic algorithms, IEEE AP-S Trans. 42:993–999
(July 1994).

[16] M.M. Khdier and C.G. Christodoulou, Linear array geometry synthesis with minimum sidelobe level and null control using particle swarm optimization, IEEE Trans Antennas Propag 53 (2005), 2674–2679.

[17] Rajo-Iglesias, E. and O. Quevedo-Teruel, "Linear array synthesis using an ant-colony-optimization-based algorithm," IEEE Antennas and Propagation Magazine, Vol. 49, No. 2, 70–79, April 2007.

[18] Lin, C., A. Qing, and Q. Feng, "Synthesis of unequally spaced antenna arrays by using di□erential evolution," IEEE Transactions on Antennas and Propagation, Vol. 58, No. 8, 2553–2561, 2010.

[19] Siddharth Pal, Anniruddha Basak, Swagatam Das and Ajith Abraham, "Linear Antenna Array Synthesis with Invasive Weed Optimization Algorithm", 2009 International Conference of Soft Computing and Pattern Recognition 978-0-7695-3879-2/09© 2009 IEEE DOI 10.1109/SoCPaR.2009.42167.

[20] Fanni, A., A. Manunza, M. Marchesi, and F. Pilo, "Tabu search metaheuristics for electromagnetic problems optimization in continuous domains," IEEE Trans. Magnetics, Vol. 35, 1694–1697, 1999.

[21] Guney, K. and M. Onay, "Amplitude-only pattern nulling of linear antenna arrays with the use of bees algorithm," Progress In Electromagnetics Research, PIER 70, 21–36, 2007.

[22] Guney, K. and S. Basbug, "Interference suppression of linear antenna arrays by amplitude-only control using a bacterial foraging algorithm," Progress In Electromagnetics Research, PIER 79, 475–497, 2008.

[23] W. C. Weng, F. Yang, and A. Z. Elsherbeni, "Linear antenna array synthesis using Taguchi's method: a novel optimization technique in electromagnetics," IEEE Transactions on Antennas and Propagation, vol. 55, no. 3 I, pp. 723–730, 2007.

[24] K. Guney, A. Durmus and S. Basbug,, "a plant growth simulation algorithm for Pattern nulling of linear antenna arrays By amplitude control", Progress In Electromagnetics Research B, Vol. 17, 69–84, 2009.

[25] Simon, D: Biogeography Based Optimization, IEEE Transactions on Evolutionary computation, VOL.12, NO.6, DECEMBER 2008

[26] Ashraf Sharaqa,NihabDib,Design of Linear and Elliptical Antenna Arrays using Biogeography Based Optimization ,Arab J SciEng. DOI 10.1007/s13369-013-0794-8.


ISSN 1737-9334

# Existence of the solution of a quasilinear equation and its application to image denoising

Samira Lecheheb
Laboratoire LAMAHIS
Departement of mathematics
Reu El-Hadaiek P.O.Box 26
Université 20 août 1955 Skikda,
21000, Algeria
Email: lecheheb.samira24@gmail.com

Messaoud Maouni
Laboratoire LAMAHIS
Departement of mathematics
Reu El-Hadaiek P.O.Box 26
Université 20 août 1955 Skikda,
21000, Algeria
Email: m.maouni@univ-skikda.dz

Hakim Lakhal
Laboratoire LAMAHIS
Departement of mathematics
Reu El-Hadaiek P.O.Box 26
Université 20 août 1955 Skikda,
21000, Algeria
Email: H.lakhal@univ-skikda.dz

***Abstract*—We give in this paper a new method to show the existence of the solution for the proposed model is a combination of the Perona-Malik equation and the Heat equation. We also give numerical implementation details and show experimental results on examples images which prove the efficiency and effectiveness of our model.**

***Index Terms*—Perona-Malik equation, functional minimization, quasi-linear equation, image denoising, image decomposition**

## I. Introduction

The purpose of this article is to investigate the existence of solution for quasilinear equation, in a bounded domain of $\mathbb{R}^N$, with Neumann boundary conditions. The stady of this problem started with the use of Brouwer degree theory, then we pass to the limit when we do reach dimension approximation spaces to infinity to build a solution the starting problem. We also study the numerical of our problem and we prove that the limit problem coincides with the Perona-Malik model (see [2], [11]) in the some subregion where the proposed model is an interpolation of two classical models, Perona-Malik [1], [3], [7] and the Heat equation, as in [13] where they proposed a modified Perona-Malik model based on directional Laplacian, for alleviate the staircasing effect, preserve sharp discontinuities, and remove noise simultaneously. On the other hand there are several new works on the same field used the method of the total variation (see [8], [9], [10]). In this work we establish the existence of weak solution of the problem

$$\begin{cases} -\mathrm{div}\Big(g(|\nabla u|)\nabla u\Big) - \dfrac{1}{\lambda^2}\,\mathrm{div}(\nabla u) = f(x) - uk(x) \ \text{ in } \Omega, \\ \Big(g(|\nabla u|) + \dfrac{1}{\lambda^2}\Big)\nabla u \cdot \vec{\eta} = 0. \ \text{ on } \partial\Omega, \end{cases} \tag{1}$$

where $f$ is a given function, $\Omega \subseteq \mathbb{R}^N$ is the bounded domain with smooth boundary $\partial\Omega$, $\lambda > 1$ be a given contrast parameter, $k \in L^\infty(\Omega)$ and the function $g(\cdot)$ is defined by the following expression:

$$g(z) = \frac{1}{1 + (\frac{z}{\lambda})^2} \quad \text{or} \quad g(z) = \exp\big(-\frac{z^2}{2\lambda^2}\big).$$

It is clear, that the function $g(z)$ is a decreasing non-negative function satisfies the following conditions

$$\begin{cases} \lim\limits_{z\to 0} g(z) = 1, \\ \lim\limits_{z\to +\infty} g(z) = 0. \end{cases} \tag{2}$$

In the case where the Euler-Lagrange equation equal to $u - \mathrm{div}\Big(g(|\nabla u|)\nabla u\Big) - \dfrac{1}{\lambda^p}\,\mathrm{div}(|\nabla u|^{p-2}\nabla u) = f(x)$ was treated in [2].
The problem (1) is equivalent to solve the Perona-Malik problem in the region where the norm of the gradient is less than $\lambda$ and equivalent to solve the heat equation if not.

This paper is organized as follows. In the next section, we prove the existence of the solution of the problem (1). And the last section is devoted to numerical results and comments.

## II. Proposed model

Given $f \in L^2(\Omega)$ and $k \in L^\infty(\Omega)$, in the application $k$ is the probability density of noise (we speak here on the gaussian noise because the probability density of this variable is the gaussian law). We are interested in finding weak solutions of the problem (1) for a quasilinear equation, we need the following definition

**Definition II.1.** *We say $u \in H^1(\Omega)$ is a weak solution for the problem* (1) *if for any $\varphi \in H^1(\Omega)$ we have*

$$\int_\Omega \Big(g(|\nabla u|) + \frac{1}{\lambda^2}\Big)\nabla u \nabla\varphi \,\mathrm{d}x = \int_\Omega f(x)\varphi \,\mathrm{d}x - \int_\Omega uk(x)\varphi \,\mathrm{d}x. \tag{3}$$

We use the same notations as in the previous section.

**Theorem II.1.** *Under condition* (2)*, problem* (1) *has at least one solution.*

*Proof:* Let V be a finite-dimensional subspace of $H^1(\Omega)$ endowed with the $H^1$-norm, and $\mathrm{V}^*$ its dual. Define the




ISSN 1737-9334

mappings $H : V \times [0,1] \longrightarrow V^*$ by

$$\begin{aligned}&\langle H(u,t),\varphi\rangle_H\\&= \int_\Omega \Big(g(t|\nabla u|)+\frac{1}{\lambda^2}\Big)\nabla u\nabla\varphi\,\mathrm{d}x - \int_\Omega f(x)\varphi\,\mathrm{d}x\\&+\int_\Omega uk(x)\varphi\,\mathrm{d}x,\end{aligned} \tag{4}$$

for all $\varphi \in V$, $H$ is well defined. Let us show now that

$$\Big\{u \in V : H(u,t) = 0, \quad \text{for some } t \in [0,1]\Big\} \subset \bar{B}(0,\widetilde{\rho}).$$

such that

$$\widetilde{\rho} = \frac{1}{\min(\frac{1}{\lambda^2},k)}\|f\|_{L^2}$$

**Lemma II.1.** *Let the mappings $H$ defined by* (4)*, there exist $R > 0$, such that*

1)
$$\begin{cases} \forall t \in [0,1], \forall u \in V \\ H(t,u) = 0 \Rightarrow \|u\|_{H^1(\Omega)} \le R. \end{cases}$$
2) *$H$ is bounded.*
3) *$H$ is continuous on $\bar{B}^{\mathrm{V}}(R)\times[0,1]$.*

*Proof:*
Indeed, if $H(u,t) = 0$ for some $(u,t) \in V \times [0,1]$, then

$$\begin{aligned}\|f\|_{L^2}\|u\|_{H^1(\Omega)} &\ge \frac{1}{\lambda^2}\int_\Omega |\nabla u|^2\,\mathrm{d}x + \int_\Omega u^2k(x)\,\mathrm{d}x\\&\ge \min\Big(\frac{1}{\lambda^2},k\Big)\|u\|^2_{H^1(\Omega)},\end{aligned}$$

which implies that

$$\|u\|_{H^1(\Omega)} \le \frac{1}{\min\Big(\frac{1}{\lambda^2},k\Big)}\|f\|_{L^2}. \tag{5}$$

Consequently, for any $R > \Big(\min(\frac{1}{\lambda^2},k)\Big)^{-1}\|f\|_{L^2}$ we have

$$H(u,t) \neq 0 \quad \text{ if } (u,t) \in \partial B^V(R)\times[0,1].$$

We now show that the mapping $H$ is bounded, if $(u,t) \in \bar{B}^V \times [0,1]$, we have

$$\begin{aligned}&|\langle H(u,t),\varphi\rangle|\\&\le \Bigg(\underbrace{\max\Big(1+\frac{1}{\lambda^2},\|k\|_{L^\infty}\Big)R + \|f\|_{L^2}}_{\widetilde{R}}\Bigg)\|\varphi\|_{H^1(\Omega)},\end{aligned}$$

for all $\varphi \in H^1(\Omega)$, and hence

$$H\Big(\bar{B}^{\mathrm{V}}(R)\times[0,1]\Big) \subset \bar{B}^{\mathrm{V}^*}(\widetilde{R}). \tag{6}$$

We now show that $H$ is continuous on $\bar{B}^{\mathrm{V}}(R)\times[0,1]$. Let $(u_n,t_n) \in \bar{B}^{\mathrm{V}}(R)\times[0,1]$ converge to $(u,t)$ in $V\times[0,1]$, i.e in $H^1\times[0,1]$. Since $(H(u_n,t_n))$ is bounded because of (6), to prove that

$$H(u_n,t_n) \to H(u,t)$$

it is sufficient to show that $H(u,t)$ is the unique cluster point of $(H(u_n,t_n))$. Let $\widetilde{k} \in \mathrm{V}^*$ be such a cluster point, still denoted by $(t_n),(u_n)$ a subsequence of $(t_n),(u_n)$ respectively such that

$$H(u_n,t_n) \to \widetilde{k} \text{ in } \mathrm{V}^*.$$

Since $u_n \to u$ in $H^1(\Omega)$, it follows that $u_n \to u$ in $L^2(\Omega)$, and hence, going if necessary to a subsequence, we may assume that $u_n \to u$ a.e in $\Omega$ . On the other hand, $\partial_i u_n \to \partial_i u$ in $L^2(\Omega)$, therefor $\nabla u_n \to \nabla u$ a.e in $\Omega$. This implies that

$$g(t_n|\nabla u_n|) \to g(t|\nabla u|) \quad \text{ a.e in } \Omega, \tag{7}$$

and hence, for any $\varphi \in V$,

$$g(t_n|\nabla u_n|)\nabla\varphi \to g(t|\nabla u|)\nabla\varphi$$

in $L^2(\Omega)$. We conclude that

$$\begin{aligned}&\langle H(t_n,u_n),\varphi\rangle_H\\&= \int_\Omega u_nk(x)\varphi\,\mathrm{d}x + \int_\Omega \Big(g(t_n|\nabla u_n|)+\frac{1}{\lambda^2}\Big)\nabla u_n\nabla\varphi\,\mathrm{d}x\\&\to \int_\Omega uk(x)\varphi\,\mathrm{d}x + \int_\Omega \Big(g(t|\nabla u|)+\frac{1}{\lambda^2}\Big)\nabla u\nabla\varphi\,\mathrm{d}x\\&= \langle H(t,u),\varphi\rangle_H.\end{aligned}$$

Thus $\widetilde{k} = H(t,u)$. ■

It is clear that

$$H : V\times[0,1] \to V^*$$

is a continuous homotopy and the existence of at least one solution of the problem (1) would follow from

$$\deg_B\Big(H(\cdot,1),B(R),0\Big) \neq 0$$

All those proprieties allow us to apply the homotopy invariance propriety and obtain

$$\deg_B\Big(H(\cdot,1),B(R),0\Big) = \deg_B\Big(H(\cdot,0),B(R),0\Big). \tag{8}$$

But $H(u,0) = 0$ is equivalant to the linear problem

$$(1+\frac{1}{\lambda^2})\int_\Omega \nabla u\nabla\varphi\,\mathrm{d}x - \int_\Omega f(x)\varphi\,\mathrm{d}x + \int_\Omega uk(x)\varphi\,\mathrm{d}x = 0,$$

for all $\varphi \in \mathrm{V}$, whose solution is unique because of the bounededness of the set of its possible solutions. Consequently,

$$\deg_B\Big(H(\cdot,0),B(R),0\Big) = \pm 1$$


ISSN 1737-9334

and from (8) and the existence propriety of degree, there exists $u \in B^{\mathrm{V}}(R)$ wich satisfies

$$\begin{aligned} &\int_\Omega \Big(g(|\nabla u|) + \frac{1}{\lambda^2}\Big)\nabla u \nabla\varphi \,\mathrm{d}x \\ &= \int_\Omega f(x)\varphi \,\mathrm{d}x - \int_\Omega uk(x)\varphi \,\mathrm{d}x \text{ and} \\ &\|u\|_{H^1} \leq \frac{1}{\min\Big(\frac{1}{\lambda^2},k\Big)}\|f\|_{L^2} \end{aligned} \tag{9}$$

for all $\varphi \in V$. We now show the passage to the limit. Consider the function $a : \mathbb{R}^N \to \mathbb{R}^N$ defined by

$$a(\xi) = \Big(g(\xi) + \frac{1}{\lambda^2}\Big)\xi \quad \text{for any } \xi \in \mathbb{R}^N.$$

To prove the passage to the limit, we need the following two lemmas:

**Lemma II.2.** *Let $0 < \lambda \leq 1$, for any $\xi, \eta \in \mathbb{R}^N$ sush that $\xi \neq \eta$ we have*

$$\big(a(\xi) - a(\eta)\big) \cdot (\xi - \eta) > 0.$$

*Proof:* The proof of this lemma remains to prove that $F_\lambda$ is a nondecreasing function defined by

$$F_\lambda(s) = sg(s) + \frac{s}{\lambda^2} \quad \text{for } s > 0.$$

We compute for this the derivative of $F_\lambda(s)$, and then we find

$$F'_\lambda(s) = \widetilde{g}(s) + \frac{1}{\lambda^2},$$

where $\widetilde{g}(s) = \dfrac{\lambda^2 - s^2}{\lambda^2(1 + (\frac{s}{\lambda})^2)^2}$
or $\widetilde{g}(s) = \dfrac{\lambda^2 - s^2}{\lambda^2}\exp\Big(-\dfrac{s^2}{2\lambda^2}\Big)$.
For $s \leq \lambda$, we have $1 - \Big(\dfrac{s}{\lambda}\Big)^2 \geq 0$ and $\dfrac{\lambda^2 - s^2}{\lambda^2} \geq 0$ then $F'_\lambda(s) \geq 0$.
For $s \geq \lambda$, using the fact that $\lambda^2 \leq 1$, we have $\dfrac{s^4}{\lambda^6} \geq \dfrac{s^2}{\lambda^2}$, we deduce that $F'_\lambda(s) \geq 0$ and we find the desired result. ∎

**Lemma II.3.**

$$\begin{cases} \textit{If } a \in C(\mathbb{R}^N, \mathbb{R}^N),\ a(\xi) \leq (1 + \frac{1}{\lambda^2})\xi \quad \textit{for all } \xi \in \mathbb{R}^N \\ \textit{and} \\ \textit{if } u_n \to u \textit{ in } H^1(\Omega) \\ \textit{so} \\ a(\nabla u_n) \to a(\nabla u) \textit{ in } L^2(\Omega). \end{cases}$$

Lemma (II.3) is proved by the dominated convergence theorem of Lebesgue. Now, it is well known that one can write $H^1(\Omega) = \overline{\bigcup_{n\geq 1} V_n}$ where $V_n \subset V_{n+1} (n \geq 1)$ and $V_n$ has dimension $n$. Consequently, given any $\varphi \in H^1(\Omega)$, there exists a sequence $\varphi_n$ with $\varphi_n \in V_n$ which converges to $\varphi$. On the other hand, by (9) applied to $V = V_n$, there exists, for each $n \geq 1$, some $u_n \in V_n$ such that

$$\int_\Omega a(\nabla u_n)\nabla\psi \,\mathrm{d}x = \int_\Omega f(x)\psi \,\mathrm{d}x - \int_\Omega u_n k(x)\psi \,\mathrm{d}x,$$

for all $\psi \in V_n$. In particular, taking $\psi = \varphi_n$ introduced above,

$$\begin{aligned} &\int_\Omega a(\nabla u_n)\nabla\varphi_n \,\mathrm{d}x = \int_\Omega f(x)\varphi_n \,\mathrm{d}x - \int_\Omega u_n k(x)\varphi_n \,\mathrm{d}x, \\ &\|u_n\|_{H^1(\Omega)} \leq \frac{1}{\min\Big(\frac{1}{\lambda^2},k\Big)}\|f\|_{L^2} \end{aligned} \tag{10}$$

for all $n \geq 1$. The estimate in (10) implies that, going if necessary to subsequences, we can assume that there exists $u \in H^1(\Omega)$ such that

$$u_n \to u \text{ weakly in } H^1(\Omega),$$
$$u_n \to u \text{ strongly in } L^2(\Omega).$$

As $\big(a(\nabla u_n)\big)_{n\in\mathbb{N}}$ is bounded in $L^2(\Omega)$, then there exists $\zeta \in L^2(\Omega)$ such that

$$a(\nabla u_n) \to \zeta \text{ weakly in } L^2(\Omega),$$

and $\nabla\varphi_n \to \nabla\varphi$ strongly in $L^2(\Omega)$, one can let $n \to \infty$ in (10) to obtain

$$\int_\Omega \zeta\nabla\varphi \,\mathrm{d}x = \int_\Omega f(x)\varphi \,\mathrm{d}x - \int_\Omega uk(x)\varphi \,\mathrm{d}x \quad \text{for all } \varphi \in H^1(\Omega). \tag{11}$$

It remains to show that

$$\int_\Omega \zeta\nabla\varphi \,\mathrm{d}x = \int_\Omega a(\nabla u)\nabla\varphi \,\mathrm{d}x \quad \text{for all } \varphi \in H^1(\Omega),$$

for it using the tirck of Minty [6], we begin by studying the limit of $\int_\Omega a(\nabla u_n)\nabla u_n \,\mathrm{d}x$. Indeed

$$\begin{aligned} \int_\Omega a(\nabla u_n)\nabla u_n \,\mathrm{d}x &= \int_\Omega f(x)u_n \,\mathrm{d}x - \int_\Omega u_n^2 k(x) \,\mathrm{d}x \\ &\to \int_\Omega f(x)u \,\mathrm{d}x - \int_\Omega u^2 k(x) \,\mathrm{d}x, \end{aligned}$$

because $u_n \to u$ weakly in $H^1(\Omega)$. But we know that $u$ satisfied (11), and hence

$$\int_\Omega f(x)u \,\mathrm{d}x - \int_\Omega u^2 k(x) \,\mathrm{d}x = \int_\Omega \zeta\nabla u \,\mathrm{d}x.$$

Therefore

$$\begin{aligned} \lim_{n\to+\infty} \int_\Omega a(\nabla u_n)\nabla u_n \,\mathrm{d}x &= \int_\Omega f(x)u \,\mathrm{d}x - \int_\Omega u^2 k(x) \,\mathrm{d}x \\ &= \int_\Omega \zeta\nabla u \,\mathrm{d}x. \end{aligned} \tag{12}$$

Let $\varphi \in H^1(\Omega)$; it exists $(\varphi_n)_{n\in\mathbb{N}}$ such that $\varphi_n \in V_n$ for all $n \in \mathbb{N}$ and $\varphi_n \to \varphi$ in $H^1(\Omega)$ when $n \to +\infty$. We will




ISSN 1737-9334

pass to the limit in the term $\int_\Omega a(\nabla u_n)\nabla\varphi_n \,\mathrm{d}x$ through the monotony assumption.
Indeed,

$$0 \le \int_\Omega (a(\nabla u_n) - a(\nabla\varphi_n))(\nabla u_n - \nabla\varphi_n)\,\mathrm{d}x =$$
$$\int_\Omega a(\nabla u_n)\nabla u_n \,\mathrm{d}x - \int_\Omega a(\nabla u_n)\nabla\varphi_n \,\mathrm{d}x$$
$$- \int_\Omega a(\nabla\varphi_n)\nabla u_n \,\mathrm{d}x + \int_\Omega a(\nabla\varphi_n)\nabla\varphi_n \,\mathrm{d}x$$
$$= \quad L_{1,n} \quad - \quad L_{2,n} \quad - \quad L_{3,n} \quad + \quad L_{4,n}.$$

We saw in (12) that $L_{1,n} \to \int_\Omega \zeta\nabla u \,\mathrm{d}x$ when $n \to \infty$. We have

$$\lim_{n\to+\infty} L_{2,n} = \int_\Omega \zeta\nabla\varphi \,\mathrm{d}x.$$

Similarly,

$$\lim_{n\to+\infty} L_{3,n} = \int_\Omega a(\nabla\varphi)\nabla u \,\mathrm{d}x.$$

Finally, we also have

$$\lim_{n\to+\infty} L_{4,n} = \int_\Omega a(\nabla\varphi)\nabla\varphi \,\mathrm{d}x.$$

when $n \to +\infty$.
The passage to the limit into inequality therefore give:

$$\int_\Omega (\zeta - a(\nabla\varphi))\cdot(\nabla u - \nabla\varphi)\,\mathrm{d}x \ge 0 \text{ for all } \varphi \in H^1(\Omega).$$

We now choose astutely test function $\varphi$ . We take $\varphi = u + \frac{1}{n}v$, with $v \in H^1(\Omega)$ and $n \in \mathbb{N}^*$. We thus obtained:

$$-\frac{1}{n}\int_\Omega \big(\zeta - a(\nabla u + \frac{1}{n}\nabla v)\big)\nabla v \,\mathrm{d}x \ge 0,$$

and so

$$\int_\Omega \big(\zeta - a(\nabla u + \frac{1}{n}\nabla v)\big)\nabla v \,\mathrm{d}x \le 0.$$

But $u + \frac{1}{n}v \to u$ in $H^1(\Omega)$, therefore by lemma (II.3),

$$a\big(\nabla u + \frac{1}{n}\nabla v\big) \to a(\nabla u) \text{ in } L^2(\Omega)$$

. Passing to the limit when $n \to +\infty$, then we obtained

$$\int_\Omega (\zeta - a(\nabla u))\nabla v \,\mathrm{d}x \le 0 \quad \forall v \in H^1(\Omega).$$

By linearity (can be changed $v$ into $-v$), we have:

$$\int_\Omega (\zeta - a(\nabla u))\nabla v \,\mathrm{d}x = 0 \quad \forall v \in H^1(\Omega).$$

We deduce that

$$\int_\Omega \zeta\nabla v \,\mathrm{d}x = \int_\Omega a(\nabla u)\nabla v \,\mathrm{d}x \quad \forall v \in H^1(\Omega).$$

Hence we have to show that $u$ is a solution of (1). ■

## III. Numerical aspects and results

The artificial time discretisation associated with the functional (3) can be rewritten as follows:

$$\begin{cases} \dfrac{\partial u}{\partial t} - \operatorname{div}\big(\Psi(|\nabla u|)\nabla u\big) = f - ku \quad \text{in } \Omega\times(0,T) \\ \Psi(|\nabla u|)\nabla u\cdot\vec{\eta} = 0 \quad \text{on } \partial\Omega\times(0,T) \end{cases} \tag{13}$$

where $\Psi$ is defined by

$$\Psi(t) = \frac{1}{1+(\frac{t}{\lambda})^2} + \frac{1}{\lambda^2} \quad \text{or } \Psi(t) = \exp\Big(-\frac{t^2}{2\lambda^2}\Big) + \frac{1}{\lambda^2}.$$

We use a finite difference scheme (see. [4]). Let us denote the space step by $h$ supposed equal to one and the time step by $\Delta t$, we can write

$$(\nabla u)^1_{i,j} = \begin{cases} u_{i+1,j} - u_{i,j} & \text{si } i < N, \\ 0 & \text{si } i = N. \end{cases}$$

$$(\nabla u)^2_{i,j} = \begin{cases} u_{i,j+1} - u_{i,j} & \text{si } j < N, \\ 0 & \text{si } j = N. \end{cases}$$

$$|(\nabla u)_{i,j}| = \sqrt{((\nabla u)^1_{i,j})^2 + ((\nabla u)^2_{i,j})^2}.$$

For every field $p = (p_1, p_2) \in \mathbb{R}^2$, we define the discrete divergence as

$$(\operatorname{div}\mathbf{p})_{i,j} = \begin{cases} \mathbf{p}^1_{i,j} - \mathbf{p}^1_{i-1,j} & \text{si } 1 < i < N \\ \mathbf{p}^1_{i,j} & \text{si } i = 1 \\ -\mathbf{p}^1_{i-1,j} & \text{si } i = N \end{cases} + \begin{cases} \mathbf{p}^2_{i,j} - \mathbf{p}^2_{i,j-1} & \text{si } 1 < j < N \\ \mathbf{p}^2_{i,j} & \text{si } j = 1 \\ -\mathbf{p}^2_{i,j-1} & \text{si } j = N \end{cases}$$

Then we use the algorithm of chambolle that sets in [4] by

$$p^{n+1}_{i,j} = \frac{p^n_{i,j} + \tau(\nabla(\operatorname{div}p^n - f/\lambda))_{i,j}}{1 + \tau|(\nabla(\operatorname{div}p^n - f/\lambda))_{i,j}|}$$

As shown in the figures below for images 1 and 2 . The choice for our numerical tests are: for noise we use the gaussian noise ( the probability density of noise $k$ with zero mean and variance $\sigma^2 = 0,5$), the time step size $dt = 10^{-4}$ and the number of iterations is equal to $3.5 \times 10^3$. We start by the improvements tests (Fig. 3) in the restorations provided by our approach and we choose the parameter $\lambda = 1$. In the second experiment, we illustrate the difference between our proposed method and the method of the total variation and the Perona-Malik model (see Figs. 6-7) and we will show that our method is effective in reducing the staircasing effect and preserving fine details.




ISSN 1737-9334

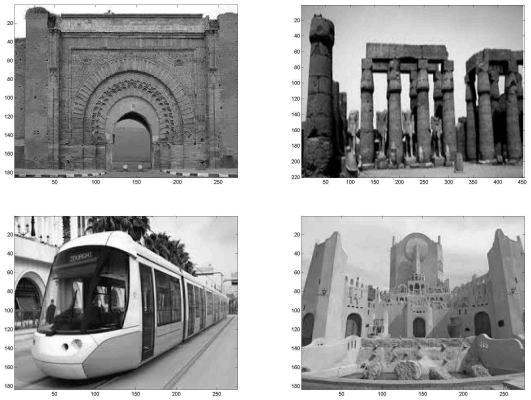

Fig. 1: Original image

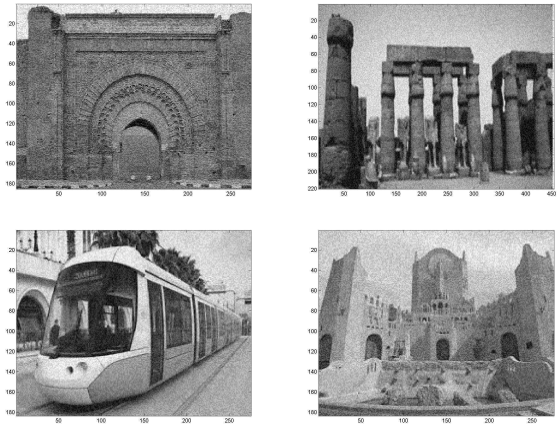

Fig. 2: Noisy image

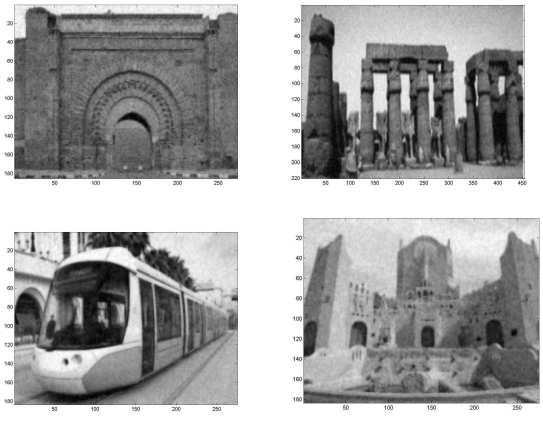

Fig. 3: Restored image by using our model

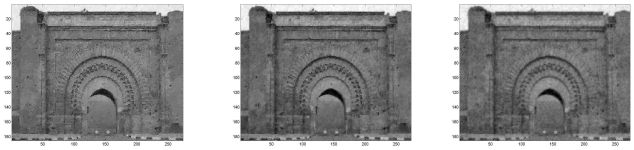

(a) (b) (c)

Fig. 4: (a) The image restored by using the Perona-Malik model (PSNR=17.9571), (b) the image restored by using the method of the total variation (PSNR=17.9714) and (c) is obtained by our model (PSNR=18.0285)

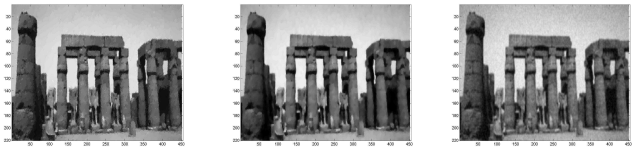

(a) (b) (c)

Fig. 5: (a) The image restored by using the Perona-Malik model (PSNR=18.2266), (b) the image restored by using the method of the total variation (PSNR=18.2295) and (c) is obtained by our model (PSNR=18,3190)

(a) (b) (c)

Fig. 6: (a) The image restored by using the Perona-Malik model (PSNR=19,6138), (b) the image restored by using the method of the total variation (PSNR=19.6166) and (c) is obtained by our model (PSNR=19,9261)

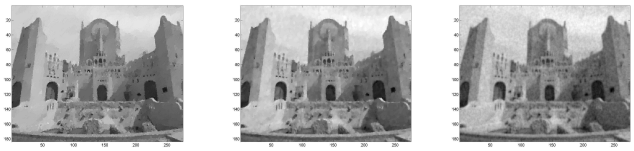

(a) (b) (c)

Fig. 7: (a) The image restored by using the Perona-Malik model (PSNR=19,8125), (b) the image restored by using the method of the total variation (PSNR=19,8469) and (c) is obtained by our model (PSNR=20,6295)




ISSN 1737-9334

| **Iteration** | $PSNR_{OM}$ | $PSNR_{TV}$ | $PSNR_{PM}$ |
|---|---|---|---|
| 1 | 17.4285 | 17.3714 | 17.3357 |
| 50 | 17.7285 | 17.6500 | 17.5642 |
| 100 | 17.9071 | 17.8142 | 17.74258 |
| 150 | 17.9892 | 17.9285 | 17.8928 |
| 200 | 18.0285 | 17.9714 | 17.9571 |

TABLE I: PSNR comparisons for the three models (for image 01)

| **Iteration** | $PSNR_{OM}$ | $PSNR_{TV}$ | $PSNR_{PM}$ |
|---|---|---|---|
| 1 | 17.4190 | 17.3523 | 17.3523 |
| 100 | 17.9952 | 17.8380 | 17.6285 |
| 200 | 18.2476 | 18.1619 | 17.8666 |
| 300 | 18.2904 | 18.2095 | 18.0666 |
| 400 | 18.3142 | 18.2285 | 18.1904 |
| 500 | 18.3190 | 18.2295 | 18.2266 |

TABLE II: PSNR comparisons for the three models (for image 02)

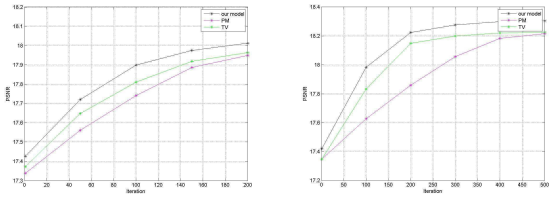


Fig. 8: The PSNR for different numbers of iterations for image 1,2

## IV. Conclusion

In this paper we present results on the existence of the solution for a equation (1). these results gives us a good numerical result with a better choice of parameters in (1). Therefor shows us that our model is the best when compared with the model of Perona-Malik and the method of the total variation since the proposed model not only preserves the edges but also removes staircase during the image denoising.

## References

[1] R. Aboulaich, D. Meskine, A. Souissi; *New diffusion models in image processing*, Comput. Math. Appl. 56(4)(2008)874-882.
[2] A. Atlas, F. Karami, D. Meskine; *The Perona-Malik inequality and application to image denoising*, Nonlinear Analysis: Real World Applications 18 (2014) 57-68
[3] H.F. Catte, P.L. Lions, J.M. Morel, T. Coll; *Image selective smoothing and edge detection by nonlinear diffusion*, SIAM J0 Numer. Anal. 29(1) (1992) 182-193.
[4] A. Chambolle; *An Algorithm for Total Variation Minimization and Applications*, J.Math. Imaging Vis., 20(2004), PP. 8997.
[5] Chun Pong Lau, Yu Hin Lai, Lok Ming Lui; *Variational models for joint subsampling and reconstruction of turbulence-degraded images*, CAM Report 18-21 April 2018
[6] A. Fattah, T. Gallouët , H. lakehal; *An Existence proof for the stationary compressible stokes problem*, Ann. Fac. Sci. de Toulouse Math. 6, 4 (2014), 847-875.
[7] P. Guidotti; *A bakward-forward regularization of the Perona-Malik equation*, J.Differential Equations 252(4)(2012) 3226-3244.
[8] Hubin Chang, Yifei Lou, and Yuping Duan; *Total Variation Based Phase Retrieval for Poisson Noise Removal*, CAM Report 16-76 October 2016
[9] Huibin Chang, Yifel Lou, Michael K. Ng, and Tieyong Zeng; *Phase Retrieval from Incomplete Magnitude Information Vsia Total Variation Regularization*, CAM Report 16-39, UCLA June 2016.
[10] Jun Liu and Xiaojun Zheng; *A Block Nonlocal TV Method for Image Restoration*, CAM Report 16-25 May 2016.
[11] V Kamalaveni, R Anitha Rajalakshmi, K A Narayanankutty; *Image Denoising using Variations of Perona-Malik Model with different Edge Stopping Functions*, Procedia Computer Science 58(2015) 673-682
[12] L. Rudin, S. Osher, E. Fatemi; *Nonlinear total variation based noise removal algorithms*, Physica D 60 (1992) 259-268.
[13] Y.Q. Wang, Jichang Guo, Wufan Chen, Wenxue Zhang; *Image denoising using Modified PeronaMalik Model based on Directional Laplacian*, Signal Processing 93 (2013) 25482558.


ISSN 1737-9334

# Smart Beds For Hospitals with Internet of Things Solutions

*Moeid M Elsokah* [1] , *Hend M. Farkash*[2] and Amer R. Zerek[3]

[1] *College of Electronic Technology, Communication Engineering Department*
*Tripoli, Libya*
E- mail moayedmohamedm@gmail.com
[2] College of Electrical & Electronic Technology
Benghazi Libya
E mail hend.mf_ceet@ceet.edu.ly
[3]*Zawia University, Faculty of Engineering/ EE Department,*
*Zawia, – Libya,*
E-mail anas_94az@yahoo.co.uk

***Abstract - Many industries depend on the technological development of the world. Medical industries need to be more advanced as Internet list things. With the help of Internet tools, doctors can monitor patients remotely and give medicines based on tracked information. This bed not only helps patients but will also help to advance the health system around the world and provide medical and health status studies and ability to perform statistical analysis, data collection and easy handling with the patient. Patients with special needs who need this have depended on their family on a daily basis. Recently, health care facilities have begun to use various specialized sensors in hospitals to improve health outcomes and overall construction efficiency. Provides independence for the patient and does not require the help of others as in the past if there has been a disorder then that makes it impossible to live independently in the home. Technological developments in smart homes and life-saving hospitals allow people to stay indoors in a comfortable, secure and independent way where they want to be. Internet solutions are options that can make living independently possible, easy, fun, less stressful and faster. It provides massage therapy and mobility, takes some heavy duty that nurses usually do, saves lives in the end, and provides greater independence for the elderly and the disabled. Energy used to feed is clean energy using solar energy. A hospital bed is a bed designed specifically for patients in hospitals or other people who need some forms of health care that can be used with voice commands and phone applications. Common features include adjustable height for the entire bed, head and feet, adjustable, adjustable, temperature, pressure, database, voice command and application to run both family using sensors and cameras. This family features are special features for both the ease and comfort of the patient and the comfort of health care workers.***

***Keywords- sensor, The Internet of Things (IoT), Smart Bed System, , Portable system, spherical joint, smart technology, information technology.***

## I. INTRODUCTION

Today's generation of hospital beds is much more than just a place for patients to rest. It's part of many tools used by hospitals to treat patients, especially hospitals interested in technological developments. It's part of keeping up with the development and research that brings smart technology to hospital beds to increase patient comfort and reduce the incidence of preventable problems, such as pressure ulcers.It's a system of interconnected computing devices, mechanical and digital machines, objects or people that are equipped with unique identifiers and the ability to transmit data over a high-speed network. Canada's Innovation, Science and Economic Development (ISED) works with Canadians in all areas of the economy and across the country to improve investment conditions, enhance Canada's innovation performance, increase Canada's share of global trade, and build fair, efficient and effective competitive market. We are a federal institution that leads the portfolio of innovation, science and economic development [2]."It's becoming a golden standard of care," said Dr. Donna Macricci, director of intensive care at the New York General Hospital. The most advanced hospital beds are used in the New York General Hospital intensive care unit, where most patients are treated. Ten of the 24 beds here are "smart beds," with computers that can do everything from patient weight to help prevent pneumonia and bed ulcers. It's estimated that 6.5 percent of Americans have an independent living disability, and 3.6 percent of Americans have self-care disabilities. For those suffering from such disabilities the challenges may range from being unable to dress themselves, to being unable to shop for groceries, running errands, or taking the same doctor. A special concern for older persons can be self-care disabilities with cognitive, mobile, hearing or vision impairments, which require more support for accommodations and devices that enable a person to live a more independent life at home for as long as possible. Objects or things that contain an attachment sensor for data exchange, and with the help of the Internet that is used to communicate for decision-making called "Internet objects". These objects measure and report data. This data can be simple numbers from a static or moving sensor (such as a temperature sensor). The results can also be more complex as devices that measure


ISSN 1737-9334

many data flows and reports each time. These advanced devices can operate or affect the data being measured. Your housing needs may change during your retirement period. For example, you may need more help doing work at home or you may need nursing care as you age. The growth of the number of older individuals in Canada is accelerating, with the total number of older individuals expected to reach about 10 million by 2036.Empowering and encouraging older people to share their knowledge, skills and experience with others in society, and to promote social well-being and community vitality for older people are the goals of the New Horizons Program for Older Persons (NHSPs)[3]. There are many types of accommodation options available to you. You can stay in your home and get help at home, or you may live in a retirement home with meals and care provided. The cost of housing depends on the level of service and care you need. For more services and care, it will be more expensive. Find out about the cost of housing for seniors in your county or territory in the Canadian Mortgage and Housing (CMHC) Housing Reports. [4]

## II. METHODOLOGY

The objective of this project was to design a smart bed in the hospital that can be relied on by running voice command, application or button so that it can be manufactured locally and developed. With the completion of this project we hope that our bedside design is widely used throughout hospitals in the world. The price of the bed is greatly reduced and allows affordable modern health care for a large part of the patients and the elderly. Once the research is completed successfully, a prototype of our bed is manufactured, and cross-sectional analyses of structural stability and other mechanical properties are performed to ensure the safety of the bed. The final goal of the team will be to design a reliable local hospital bed by completing the following objectives.

1. To analyse all existing bed products and select from the top quality in relation to price.
2. To manufacture a prototype of the bed and develop it.
3. To identify and support the overall quality of the hospital bed.
4. To provide movement by acoustic ultrasound.
5. To provide an application that can be used on the phone to increase the possibility of communication with the patient.

### A. *Bed frame*

The intelligent hospital bed frame is divided into two parts including the upper frame and support lifts. The upper frame of the smart bed consists of three parts of the head, thigh and foot parts. The linear stabilizers are responsible for adjusting the upper frame to different positions such as sitting position, leg height, back height, back and leg height.

### B. *National Standards*

The specific Curatorial Industry Standards recommendations can be seen below in Table 1. The parameters listed below in Table 1 are the design specifications on which they were worked.

TABLE1: Curatorial Industry Standards of Hospital Beds that have been applied

| | **Maximum Value** | **Minimum Value** |
|---|---|---|
| Bed length | 200 cm | 190 cm |
| Bed Width | 100 cm | 90 cm |
| Weight Capacity | N/A | 230 KG |

### C. *Food and Drug Administration Guidelines*

"The American Food and Drug Administration, or FDA, recently released a statement which discusses in extensive detail the many issues involving patient entrapment on Hospital Beds. The FDA performed extensive background research of their own and sought the information of such reputable organizations as the International Organization of Standards, Stryker International, Hill Rom, the American Red Cross and a number of top American hospitals to find out which areas of modern hospital beds are most dangerous for entrapment, ergonomic data, the number of entrapment occurrences over a number of years and the injuries that resulted. The FDA concluded that there were seven zones which were most dangerous and made size recommendations for those zones to reduce the rate of patient entrapment. Combined knowledge of danger zones, as concluded from the hospitals and bedmanufacturers, as well as the ergonomic data, the FDA determined the seven danger zones as can be seen in the following Figure 12: Seven potential entrapment areas in hospital beds determined by the FDA Figure 1.

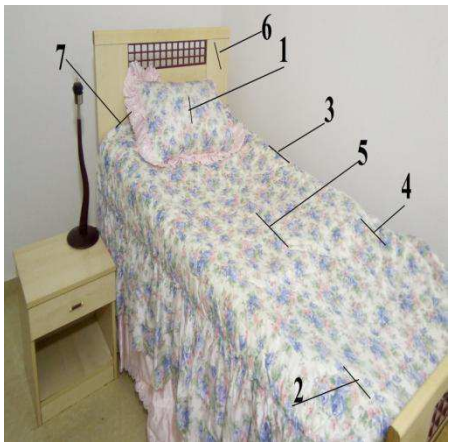


Fig 1: Seven potential entrapment areas in hospital beds determined by the FDA



ISSN 1737-9334

The seven sections can be defined as follows:
• Section 1 is the area of spacing within the rail
• Section 2 is representative of the area under the rail, between the rail supports or next to a single rail support
• Section 3 is the area between the rail and the mattress
• Section 4 distinguishes the area under the rail, at the ends of the rail
• Section 5 is defined as the area between split bed rails
• Section 6 between the end of the rail and the side edge of the head or foot board
• Section 7 clarifies the area between the head or footboard and the mattress end Upon determining the seven zones where entrapment was most likely to occur, the FDA used ergonomic data from the National Centre for Health Statistics to define the spatial limitations for four zones in bed design. Although the FDA recognizes seven potential sections of entrapment, only sections one through four have had dimensional limits recommended because they are the areas where entrapment is most likely to occur. A summary of the limitations imposed upon these zones is described in below Table2 “. [5]

TABLE 2: Summary of FDA Hospital Bed Dimensional Limit Recommendations

| Zone | Dimensional Limit Recommendation |
|---|---|
| 1<br>Within the rail | < 120 mm (< 4 3 /4 “) |
| 2<br>Under the rail, between rail supports or next to a single rail support | < 120 mm (< 4 3 /4 “) |
| 3<br>Between rail and mattress | < 120 mm (< 4 3 /4 “) |
| 4<br>Under the rail, at the ends of the rail | < 60 mm (< 2 3 /8 “)<br>AND<br>>60° angle |

### *D. Anthropometric Data*

Anthropometric data is a set of measurements to determine the length of the individual appendices based on the height of that person and the calculation of the ratio. This data is determined by conducting many measurements on a random sample of people and averaging the arithmetic mean for them. Anthropometric data is essential to the success of this project to determine the dimensions of the bed and its structural integrity. We need the right distance for the human body to make this bed reasonably comfortable for the patient. Anthropometric data are available in Figure 2 below.This data is all related to the overall height of the person.

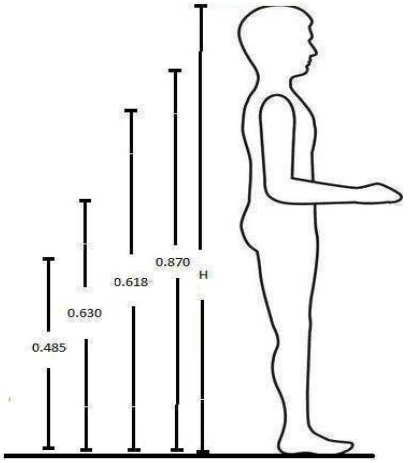


Fig 2: Anthropometric data of a standing person

The second type of anthropometric chart used was someone in the sitting position. Anthropometric data are available in Figure 3 below. In order to determine the lengths characteristic of each part of our hospital bed design, we used the person's data in the sitting position because it is very similar to the location that will be placed on a fully tilted hospital bed.

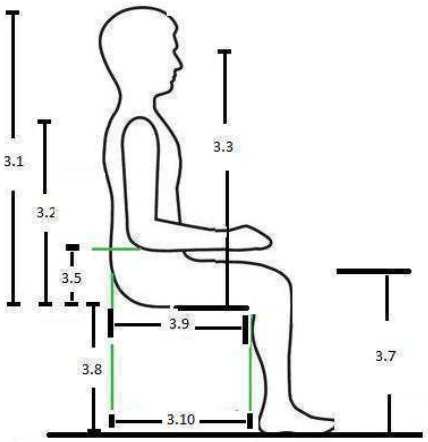


Fig 3: Anthropometric Data showing various human proportions

## III. Hardware

Motor, Linear actuator, Coupling, Relay, Spherical joint, Raspberry Pi, Sensors, Jumper cable, Sukam inverter and Battery.


ISSN 1737-9334

## IV. SPEECH RECOGNITION

Google Cloud Speech-to-Text enables developers and innovators to convert audio to text by implementing powerful neural network models in a simple-to-use API where the voice signal is intercepted by the microphone and converted to an analog signal from a digital signal and the API recognizes 120 languages and variants to support your global user base and take advantage of these features by connecting them with Raspberry Pi. It can enable commands and voice control in many applications and can handle real-time or pre-recorded audio and handle these commands using Google's automated learning technology. Figure 4 below shows the Raspberry Pi installation with the bed which receives the voice commands and turns them into signals and then perform the work required.

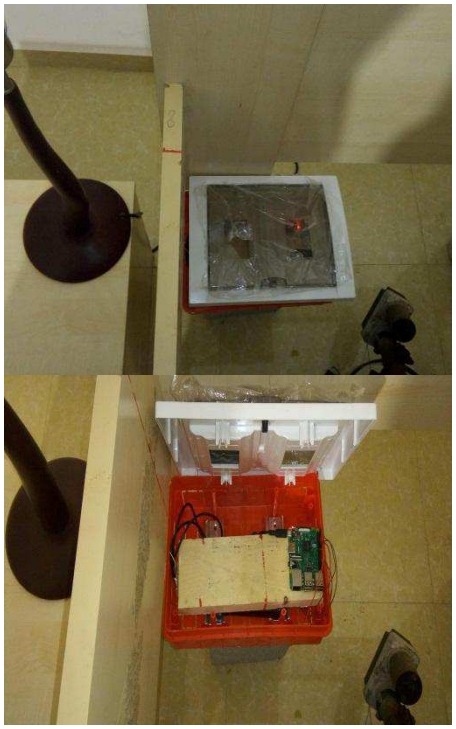

Fig4: Raspberry Pi installation with the bed

## V. SHAPING AND ADOPTING TECHNOLOGY

It is time to build the technology nurses want.Nurses do not want to be passive consumers of technology, but they want to be partners in the design and testing of new and innovative applications and devices that are patient friendly and affordable. Nurses have their needs for information systems, technology systems, devices that automate manual functions, speed the delivery of information, and add incremental measures of safety. Nurses unique needs should drive technology development, with better functionality and integration across systems. They want technology solutions that will not only improve delivery of care, but also reduce nursing demand, and reduce the physical burden of work, thus improving retention. It is important to remember nurses often have information and work process needs different from other healthcare providers, which call for unique solutions. Improved technologies can eliminate waste in nursing workflow resulting from inefficient work patterns, interruptions, inaccessible information, documentation, missing supplies, equipment and medications. Reducing the opportunity for error improves patient safety. Technology driving medication administration systems, improved communications, timely acquisition of equipment and supplies, and fool-proof patient identification are just some applications that improve safety. There is great value in point-of-care devices and systems that accomplish data entry or retrieval and documentation more quickly. Wireless systems that provide rapid efficient communication, free up the nurse to spend more time on patient interaction, as well as higher-level cognitive functions such as planning and analysing care which are needed. The added value and benefits of technology and automation in nursing, enable care to be delivered in a timely, compassionate manner. [6]

## VI. IMPACT

Nurses believe it is essential to have smart, portable, point-of-care solutions for capturing and transmitting data, as well as routine communication. They also want technology to reduce demand for nursing time and to facilitate patient life. The study demonstrated the greatest impact of technology is on written communication and data, followed by improvement in safe delivery of care, system integration and oral communications. Technology can also alleviate some employment and workload problems, help track staff, doctors and patients, facilitate the drug cycle, improve the efficiency of the physical environment and facilitate the work flow for the patient. Nurses are not technology averse. They need tools to help prevent errors, reduce them, improve the process and provide information to allow them to practice with confidence and efficiency and get the most accurate results. Technology should be everywhere, helpful and unobtrusive. If appropriately designed. The need to develop technology that will reduce the demand placed on nurses in today's fast-paced and labour-intensive environments.

## VII AIR MATTRESS

The hospital bed is equipped with an Alternating Pressure Therapy/Low Air Loss Mattress system developed by Lumex. The mattress system is not only efficient for preventing and treating stages 1 – 4 of pressure ulcers but also convenient for long-term bedridden patients. In order to provide the best therapy and comfort for each type of patient, the hospital bed staff can adjust the pressure and alternating cycle time of the mattress. Providing 6 options of mattress pressure and an optional static mode enables the mattress to meet all the requirements of the patient. Figure 5presents the air mattress integrated into the bed system.


ISSN 1737-9334

Fig 5: air mattress integrated into the bed system

It is recommended to use Smart mattresses. The first thing that Smart Ranker does is keep track of your sleep smoothly and record data, eliminating the need to wear a high-heeled bracelet to sleep or sleep with your phone. Smart family collects sleep data without having to do anything. To access the data, you can simply open the application and discover your personal sleep information. By helping you understand your sleep, smart mattresses will guide you to a better sleep and thus improve your health. There is no uniform definition of "smart mattress" but it is used informally to describe a ranking that contains sensors to analyse your sleep patterns, provide information about the quality of your sleep, and in some cases, actively improve your sleep. Smart mattresses in the market do so in a variety of ways. Some of them provide sleep tracking functions to measure sleep duration and sleep cycles by observing your body movement, heart rate and breathing. [7]

## VIII COMMUNICATION AND DATABASE

Online database: An online database with statistics and all patient data will be created in real time so that it can be accessed by doctors, health care carriers and close relatives. The screens will be visual and audio screens controlled by the user's privacy level and doctors will have full access to all medical data outputs and sensors. Automatic alerts will be sent via e-mail messages and phone calls.

## IX CONCLUSION

This bed not only helps patients but will also help supply a demand all over the world which will help all patients and the elderly. Hospitals and the world continue to focus on technological development to achieve the best results. It is not a new professional or medical intervention in health care. Hospital beds are medically necessary for many situations such as placing the body for example, to relieve pain, avoid respiratory infections, sores and prevent cramps or the need to raise the bed head due to congestive heart failure, suction and chronic lung disease. Hospitals are using a new resource in patient care. The family is designed to move and massage patients and receive voice commands for the user and to adjust different movement situations of the patient which reduces the risk of bed ulcers and lung infections. It takes some of the heavy lifting traditionally done by nurses, ultimately saves lives, and provides greater independence for older people and the disabled. Patients with special needs and need their family on a daily basis. The automatic bed can make life a bit easier for nurses, with 85 percent suffering from back injuries by having to deal with patients. We hope this will help keeping them in a better and healthier shape. One of the most important features of the smart bed is to receive voice commands and is connected to the Internet and this feature to connect to the network provides comfort, help and independence for the patient. Similarly, efficiency of resource utilization, nurses and medical staff with decreased human efforts, lower costs and bring productivity. Also it provides analytics and data collection with best customer experiences and high quality data.

## REFERENCES

1. [1] techtarget, IoMT " Internet of Medical Things", Available: in https://internetofthingsagenda.techtarget.com/definition/IoMT-Internet-of-Medical-Things ,Jul 4 ,2018 7:00 PM
[2] Public Health Agency of Canada Available:http://www.phac-aspc.gc.ca., Jul 13-14 ,2018 2:00 AM.
[3 ] Public Health Agency of Canada . Available in :https://www.canada.ca/en/employment-social development/programs/new-horizons-seniors.html, Jul 13-14 ,2018 1:00 PM.
[4] Public Health Agency of Canada , Housing options for seniors ,Available in :https://www.canada.ca/en/financial-consumer-agency/services/retirement-planning/cost-seniors-housing.html ,Aug 16,2018 6:00 PM.


ISSN 1737-9334

[5] U.S. Food and Drug Administration ,Available in :https://www.fda.gov/ForConsumers/ConsumerUpdates/ucm164366.htm . Feb 11, 2013 4:00 PM.

[6] Linda Burnes Bolton, Dr PH, RN, FAAN; Carole A. Gassert, PhD, RN, FACMI, FAAN; and Pamela F. Cipriano, PhD, RN, FAAN. "Smart Technology, Enduring Solutions" sep 2008. Available :https://aan.memberclicks.net/assets/docs/fall_jhim.pdf .

[7 ]H. Nguyen , "Advanced Assistive Control Strategies For Smart Hospital Beds ", University of Technology Sydney Faculty of Engineering and Information Technology, Sydney, Australia,2016,https://opus.lib.uts.edu.au/bitstream/10453/90266/2/02whole.pdf.




ISSN 1737-9334

# IMAGE RESTORATION USING NONLINEAR ELIPTIC EQUATION

Samira Lecheheb, Messaoud Maouni and Hakim Lakhal
Laboratoire LAMAHIS, Departement of mathematics, Reu El-Hadaiek P.O.Box 26,
Université 20 août 1955 Skikda, 21000, Algeria
Email: lecheheb.samira24@gmail.com
m.maouni@univ-skikda.dz
H.lakhal@univ-skikda.dz

***Abstract*—In this paper, we study the existence of solutions for nonlinear elliptic problem, in a bounded domain of $\mathbb{R}^N$, with zero Neumann boundary conditions, and give an existence theorem of weak solutions for the following equation**

$$A(u) = f(u),$$

**where** $A(u) = -\mathrm{div}\Big(g(|\nabla u|)\nabla u\Big) - \frac{1}{\lambda^2}\,\mathrm{div}(\nabla u)$, **and** $f \in L^2(\Omega)$**. We also give some numerical results on examples images of the application of this problème for restoration in image processing.**

***Index Terms*—Topological degree, elliptic problem, homotopy, image restoration**

## I. Introduction

Let $\Omega$ be a bounded domain in $\mathbb{R}^N$. In the classical Sobolev space $W^{1,p}(\Omega)$, A.Atlas, F.Karami, D.Meskine [1] studied the solution of the following problem:

$$u - \mathrm{div}\Big(g(|\nabla u|)\nabla u\Big) - \frac{1}{\lambda^p}\,\mathrm{div}(|\nabla u|^{p-2}\nabla u) = f.$$

where $g$ is a decreasing function defined by $g(k) = \dfrac{1}{1+(\frac{k}{\lambda})^2}$ or $g(k) = \exp\big(-\dfrac{k^2}{2\lambda^2}\big)$. We recover the linear diffusion if $g = 1$, and we remark that $g$ satisfies the following conditions.

$$\begin{cases} \lim\limits_{k\to 0} g(k) = 1, \\ \lim\limits_{k\to +\infty} g(k) = 0. \end{cases} \tag{1}$$

In this paper we study the existence of a solution for the following nonlinear problem:

$$\begin{cases} -\mathrm{div}\Big(g(|\nabla u|)\nabla u\Big) - \dfrac{1}{\lambda^2}\,\mathrm{div}(\nabla u) = f(u) \quad \text{in } \Omega, \\ \Big(g(|\nabla u|) + \dfrac{1}{\lambda^2}\Big)\nabla u \cdot \vec{\eta} = 0. \quad \text{on } \partial\Omega, \end{cases} \tag{2}$$

where $\Omega \subseteq \mathbb{R}^N$ is the bounded domain with smooth boundary $\partial\Omega$, $\lambda > 1$ be a given contrast parameter.

We assume that $f : \Omega \times \mathbb{R} \to \mathbb{R}$ is continuous function satisfying the caratheodory conditions, and verifying also the growth restriction defined below:

$$|f(x,s)| \le d(x) + \frac{1}{2\lambda^2}|s|, \tag{3}$$

where $d \in L^2(\Omega)$ and $\lambda > 0$ is real positive constants.

Many algorithms are proposed for image processing [6], [7], [9]–[11]. In this paper, we present a new model for image restoration. The existence of solution of our PDE model is given by the compacteness methode . On the other hand we aplly our theoretical result in a noisy images (see [1], [7], [9]).

This article is organized as follows. In the next section, we give the definition of weak solution, the theorem of main result and we prove the existence of the solution of the problèm (2). And the last section is devoted to numerical aspects and results.

## II. Proposed model

Given $f \in L^2(\Omega)$, we are interested in finding weak solution of the problem (2).

We give now a definition of weak solution.

**Definition II.1.** *We say $u \in H^1(\Omega)$ is a weak solution for the problem (2) if for any $v \in H^1(\Omega)$ we have*

$$\int_\Omega \Big(g(|\nabla u|) + \frac{1}{\lambda^2}\Big)\nabla u \nabla v \,\mathrm{d}x = \int_\Omega f(u)v \,\mathrm{d}x. \tag{4}$$

Our main result is formulated in the following theorem.

**Theorem II.1.** *Under condition (1) and (3), problem (2) has at least one solution.*

*Proof:* Let $W$ be a finite-dimensional subspace of $H^1(\Omega)$ endowed with the $H^1$-norm, and $W^*$ its dual. Define the mapping $H : W \times [0,1] \to W^*$ by

$$\langle H(u,t), v\rangle_H = \int_\Omega \Big(g(t|\nabla u|) + \frac{1}{\lambda^2}\Big)\nabla u \nabla v \,\mathrm{d}x - \int_\Omega f(tu)v \,\mathrm{d}x \tag{5}$$

for all $v \in W$. $H$ is well defined. Let us show now that $\Big\{u \in W : H(u,t) = 0, \text{ for same } t \in [0,1]\Big\} \subset \bar{B}\big(2\lambda^2\|d\|_{L^2}\big)$.


ISSN 1737-9334

**Lemma II.1.** *There exists $R > 0$, such that*

1)
$$\begin{cases} \forall t \in [0,1], \forall u \in V \\ H(t,u) = 0 \Rightarrow \|u\|_{H^1(\Omega)} \leq R. \end{cases}$$

2) *$H$ is bounded.*

*Proof:*
Indeed, if $H(u,t) = 0$ for same $(u,t) \in W \times [0,1]$, then

$$\begin{aligned} 0 = \langle H(u,t), u\rangle &\geq \frac{1}{\lambda^2}\|u\|_{H^1}^2 - \|f(u)\|_{L^2}\|u\|_{L^2} \\ &\geq \frac{1}{\lambda^2}\|u\|_{H^1} - \|d\|_{L^2} - \frac{1}{2\lambda^2}\|u\|_{H^1}, \end{aligned}$$

which implies that

$$\|u\|_{H^1} \leq 2\lambda^2\|d\|_{L^2}. \tag{6}$$

Consequently, for any $R > 2\lambda^2\|d\|_{L^2}$, we have

$$H(u,t) \neq 0 \text{ if } (u,t) \in \partial B^W(R) \times [0,1]. \tag{7}$$

Now, if $(u,t) \in \bar{B}^W(R) \times [0,1]$, we have

$$\begin{aligned} |\langle H(u,t), \varphi\rangle| &\leq \big(\max(1 + \frac{1}{\lambda^2}, \frac{1}{2\lambda^2})\|u\|_{H^1} + \|d\|_{L^2}\big)\|v\|_{H^1}, \\ &\leq (KR + \|d\|_{L^2})\|v\|_{H^1}, \end{aligned}$$

such that $K = \max(1 + \frac{1}{\lambda^2}, \frac{1}{2\lambda^2})$, for all $v \in H^1(\Omega)$, and hence

$$H\Big(\bar{B}^{\mathrm{W}}(R) \times [0,1]\Big) \subset \bar{B}^{\mathrm{W}^*}(KR + \|d\|_{L^2}). \tag{8}$$

■

We now show that H is continous.

**Proposition II.1.** *The mapping $H$ is continuous on*

$$\bar{B}^W(R) \times [0.1]$$

.

*Proof:* Let $(u_m, t_m) \in \bar{B}^{\mathrm{W}}(R) \times [0,1]$ converge to $(u,t)$ in $W \times [0,1]$, i.e. in $H^1 \times [0,1]$. Since $(H(u_m,t_m))$ is bounded because of (8), to prove that

$$H(u_m,t_m) \to H(u,t),$$

it is sufficient to show that $H(u,t)$ is the unique cluster point of $(H(u_m,t_m))$. Let $\ell \in \mathrm{W}^*$ be such a cluster point, still denoted by $(t_m), (u_m)$ a subsequence of $(t_m), (u_m)$ respectively such that

$$H(u_m,t_m) \to \ell \text{ in } \mathrm{W}^*.$$

Since $u_m \to u$ in $H^1(\Omega)$, it follows that $u_m \to u$ in $L^2(\Omega)$, and hence, going if necessary to a subsequence, we may assume that

$$u_m \to u \text{ a.e in } \Omega \text{ and } \exists\, H \in L^2(\Omega);\ |u_m| \leq H \text{ a.e.} \tag{9}$$

On the other hand, $\partial_i u_m \to \partial_i u$ in $L^2(\Omega)$. This implies that

$$g(t_m|\nabla u_m|) \to g(t|\nabla u|) \quad \text{a.e in } \Omega,$$

and hence, for any $v \in W$,

$$g(t_m|\nabla u_m|)\nabla v \to g(t|\nabla u|)\nabla v$$

in $L^2(\Omega)$. We conclude that

$$\begin{aligned} &\int_\Omega \Big(g(t_m|\nabla u_m|) + \frac{1}{\lambda^2}\Big)\nabla u_m \nabla v \,\mathrm{d}x \\ &\to \int_\Omega \Big(g(t|\nabla u|) + \frac{1}{\lambda^2}\Big)\nabla u \nabla v \,\mathrm{d}x. \end{aligned}$$

For the last term,

$$f(t_m u_m) \to f(tu) \text{ a.e.},$$

by dominated convergence (from (3) and (9)) we have

$$f(t_m u_m) \to f(tu) \text{ in } L^2(\Omega),$$

and consequently

$$\int_\Omega f(t_m u_m)v \,\mathrm{d}x \to \int_\Omega f(tu)v \,\mathrm{d}x.$$

We obtain

$$\begin{aligned} &\langle H(t_m,u_m), v\rangle_H \\ &= \int_\Omega \Big(g(t_m|\nabla u_m|) + \frac{1}{\lambda^2}\Big)\nabla u_m \nabla v \,\mathrm{d}x - \int_\Omega f(t_m u_m)v \,\mathrm{d}x \\ &\to \int_\Omega \Big(g(t|\nabla u|) + \frac{1}{\lambda^2}\Big)\nabla u \nabla v \,\mathrm{d}x - \int_\Omega f(tu)v \,\mathrm{d}x \\ &= \langle H(t,u), v\rangle_H. \end{aligned}$$

Thus $\ell = H(u,t)$. ■

It is clear that

$$H : W \times [0,1] \to W^*$$

is a continuous homotopy and the existence of at least one solution of the problem (2) would follow from

$$\deg_B\Big(H(\cdot,1), B(R), 0\Big) \neq 0$$

All those proprieties allow us to apply the homotopy invariance propriety and obtain

$$\deg_B\Big(H(\cdot,1), B(R), 0\Big) = \deg_B\Big(H(\cdot,0), B(R), 0\Big). \tag{10}$$

But $H(u,0) = 0$ is equivalant to the linear problem

$$(1 + \frac{1}{\lambda^2})\int_\Omega \nabla u \nabla v - \int_\Omega f(x,0)v = 0,$$

for all $v \in \mathrm{W}$, whose solution is unique because of the bounededness of the set of its possible solutions. Consequently,

$$\deg_B\Big(H(\cdot,0), B(R), 0\Big) = \pm 1,$$

and from (10) and the existence propriety of degree, there exists $u \in B^{\mathrm{W}}(R)$ wich satisfies

$$\begin{aligned} &\int_\Omega \Big(g(|\nabla u|) + \frac{1}{\lambda^2}\Big)\nabla u \nabla v = \int_\Omega f(u)v, \\ &\|u\|_{H^1} \leq 2\lambda^2\|d\|_{L^2}. \end{aligned} \tag{11}$$


ISSN 1737-9334

for all $v \in W$.

We now show the passage to the limit.
Consider the function $a : \mathbb{R}^N \to \mathbb{R}^N$ defined by

$$a(\xi) = \Big(g(\xi) + \frac{1}{\lambda^2}\Big)\xi \quad \text{for any } \xi \in \mathbb{R}^N.$$

To prove the passage to the limit, we need the following lemma:

**Lemma II.2.** *Let $0 < \lambda \leq 1$, for any $\xi, \eta \in \mathbb{R}^N$ sush that $\xi \neq \eta$ we have*

$$\big(a(\xi) - a(\eta)\big) \cdot (\xi - \eta) > 0.$$

The proof of the above lemma can be found in [**?**].

**Lemma II.3.** *[3]*

$$\begin{cases} \text{If } a \in C(\mathbb{R}^N, \mathbb{R}^N),\ a(\xi) \leq (1 + \frac{1}{\lambda^2})\xi \quad \text{for all } \xi \in \mathbb{R}^N \\ \text{and} \\ \text{if } u_n \to u \text{ in } H^1(\Omega) \\ \text{so} \\ a(\nabla u_n) \to a(\nabla u) \text{ in } L^2(\Omega). \end{cases}$$

Lemma II.3 is proved by the dominated convergence theorem of Lebesgue. Now, it is well known that one can write $H^1(\Omega) = \overline{\bigcup_{m\geq 1} W_m}$ where $W_m \subset W_{m+1} (m \geq 1)$ and $W_m$ has dimension $m$. Consequently, given any $v \in H^1(\Omega)$, there exists a sequence $v_m$ with $v_m \in W_m$ which converges to $v$. On the other hand, by (11) applied to $W = W_m$, there exists, for each $m \geq 1$, some $u_m \in W_m$ such that

$$\int_\Omega a(\nabla u_m)\nabla\psi \,\mathrm{d}x = \int_\Omega f(u_m)\psi \,\mathrm{d}x,$$

for all $\psi \in W_m$. In particular, taking $\psi = v_m$ introduced above,

$$\begin{aligned} &\int_\Omega a(\nabla u_m)\nabla v_m \,\mathrm{d}x = \int_\Omega f(u_m)v_m \,\mathrm{d}x, \\ &\|u_m\|_{H^1(\Omega)} < 2\lambda^2\|d\|_{L^2} \end{aligned} \tag{12}$$

for all $m \geq 1$. The estimate in (12) implies that, going if necessary to subsequences, we can assume that there exists $u \in H^1(\Omega)$ such that

$$u_m \to u \text{ weakly in } H^1(\Omega),$$

$$u_m \to u \text{ strongly in } L^2(\Omega).$$

As $\big(a(\nabla u_m)\big)_{m\in\mathbb{N}}$ is bounded in $L^2(\Omega)$, then there exists $\gamma \in L^2(\Omega)$ such that

$$a(\nabla u_m) \to \gamma \text{ weakly in } L^2(\Omega),$$

and $\nabla v_m \to \nabla v$ strongly in $L^2(\Omega)$. On the other hand, as $f(u_m) \to f(u)$ in $L^2(\Omega)$, one can let $m \to \infty$ in (12) to obtain

$$\int_\Omega \gamma\nabla v \,\mathrm{d}x = \int_\Omega f(u)v \,\mathrm{d}x \quad \text{for all } v \in H^1(\Omega). \tag{13}$$

It remains to show that

$$\int_\Omega \gamma\nabla v \,\mathrm{d}x = \int_\Omega a(\nabla u)\nabla v \,\mathrm{d}x \quad \text{for all } v \in H^1(\Omega),$$

for it using the tirck of Minty, we begin by studying the limit of $\int_\Omega a(\nabla u_m)\nabla u_m \,\mathrm{d}x$. Indeed

$$\int_\Omega a(\nabla u_m)\nabla u_m \,\mathrm{d}x = \int_\Omega f(u_m)u_m \,\mathrm{d}x \to \int_\Omega f(u)u \,\mathrm{d}x,$$

because $u_m \to u$ weakly in $H^1(\Omega)$. But we know that $u$ satisfied (13), and hence

$$\int_\Omega f(u)u \,\mathrm{d}x = \int_\Omega \gamma\nabla u \,\mathrm{d}x.$$

Therefore

$$\begin{aligned} \lim_{n\to+\infty} \int_\Omega a(\nabla u_m)\nabla u_m \,\mathrm{d}x &= \int_\Omega f(u)u \,\mathrm{d}x \\ &= \int_\Omega \gamma\nabla u \,\mathrm{d}x. \end{aligned} \tag{14}$$

Let $v \in H^1(\Omega)$; it exists $(v_m)_{m\in\mathbb{N}}$ such that $v_m \in W_m$ for all $m \in \mathbb{N}$ and $v_m \to v$ in $H^1(\Omega)$ when $m \to +\infty$. We will pass to the limit in the term $\int_\Omega a(\nabla u_m)\nabla v_m \,\mathrm{d}x$ through the monotony assumption.
Indeed,

$$\begin{aligned} 0 \leq &\int_\Omega \big(a(\nabla u_m) - a(\nabla v_m)\big)(\nabla u_m - \nabla v_m) \,\mathrm{d}x = \\ &\int_\Omega a(\nabla u_m)\nabla u_m \,\mathrm{d}x - \int_\Omega a(\nabla u_m)\nabla v_m \,\mathrm{d}x \\ &- \int_\Omega a(\nabla v_m)\nabla u_m \,\mathrm{d}x + \int_\Omega a(\nabla v_m)\nabla v_m \,\mathrm{d}x \\ = \quad &S_{1,m} \quad - \quad S_{2,m} \quad - \quad S_{3,m} \quad + \quad S_{4,m}. \end{aligned}$$

We saw in (14) that $S_{1,m} \to \int_\Omega \gamma\nabla u \,\mathrm{d}x$ when $m \to \infty$. We have

$$\lim_{m\to+\infty} S_{2,m} = \int_\Omega \gamma\nabla v \,\mathrm{d}x.$$

Similarly,

$$\lim_{m\to+\infty} S_{3,m} = \int_\Omega a(\nabla v)\nabla u \,\mathrm{d}x.$$

Finally, we also have

$$\lim_{n\to+\infty} S_{4,m} = \int_\Omega a(\nabla v)\cdot\nabla v \,\mathrm{d}x.$$

when $m \to +\infty$.
The passage to the limit into inequality therefore give:

$$\int_\Omega \big(\gamma - a(\nabla v)\big)(\nabla u - \nabla v) \,\mathrm{d}x \geq 0 \text{ for all } v \in H^1(\Omega).$$

We now choose astutely test function $v$ . We take $v = u + \frac{1}{m}\widetilde{v}$, with $\widetilde{v} \in H^1(\Omega)$ and $m \in \mathbb{N}^*$. We thus obtained:

$$-\frac{1}{m}\int_\Omega \big(\gamma - a(\nabla u + \frac{1}{m}\nabla\widetilde{v})\big)\nabla\widetilde{v} \,\mathrm{d}x \geq 0,$$

and so


ISSN 1737-9334

$$\int_\Omega \big(\gamma - a(\nabla u + \frac{1}{m}\nabla\widetilde{v})\big)\nabla\widetilde{v}\,\mathrm{d}x \le 0.$$

But $u + \frac{1}{m}\widetilde{v} \to u$ in $H^1(\Omega)$, therefore by lemma II.3,

$$a\big(\nabla u + \frac{1}{m}\nabla\widetilde{v}\big) \to a(\nabla u) \text{ in } L^2(\Omega)$$

.
Passing to the limit when $m \to +\infty$, then we obtained

$$\int_\Omega \big(\gamma - a(\nabla u)\big)\nabla\widetilde{v}\,\mathrm{d}x \le 0 \quad \forall\widetilde{v} \in H^1(\Omega).$$

By linearity (can be changed $\widetilde{v}$ into $-\widetilde{v}$), we have:

$$\int_\Omega \big(\gamma - a(\nabla u)\big)\nabla\widetilde{v}\,\mathrm{d}x = 0 \quad \forall\widetilde{v} \in H^1(\Omega).$$

We deduce that

$$\int_\Omega \gamma\cdot\nabla\widetilde{v}\,\mathrm{d}x = \int_\Omega a(\nabla u)\nabla\widetilde{v}\,\mathrm{d}x \quad \forall\widetilde{v} \in H^1(\Omega).$$

Hence we have to show that $u$ is a solution of (2). ■

## III. Numerical aspects and results

The artificial discretisation associated with the problem (2) can be rewritten as follows:

$$\begin{cases} \dfrac{\partial u}{\partial t} - \varepsilon\mathrm{div}(\Phi(|\nabla u|)\nabla u) = f(u) \text{ in } (0,T)\times\Omega \\ \Phi(|\nabla u|)\nabla u\cdot\vec{\eta} = 0 \text{ in } (0,T)\times\partial\Omega \end{cases} \tag{15}$$

where $f$ and $\Phi$ are defined respectively by

$$f(s) = \exp\Big(-\frac{s}{\lambda}\Big) \text{ and } \Phi(t) = \frac{1}{1+(\frac{t}{\lambda})^2} + \frac{1}{\lambda^2},$$

or $\Phi(t) = \exp\Big(-\dfrac{t^2}{2\lambda^2}\Big) + \dfrac{1}{\lambda^2}$

The discretization of the Problem (15) is given by the finite difference method (see [2]). Let us $h = 1$ the space step and $\Delta t$ the time step, we can write

$$(\nabla u)^1_{i,j} = \begin{cases} u_{i+1,j} - u_{i,j} & \text{si } i < N_1, \\ 0 & \text{si } i = N_1. \end{cases}$$

$$(\nabla u)^2_{i,j} = \begin{cases} u_{i,j+1} - u_{i,j} & \text{si } j < N_1, \\ 0 & \text{si } j = N_1. \end{cases}$$

$$|(\nabla u)_{i,j}| = \sqrt{((\nabla u)^1_{i,j})^2 + ((\nabla u)^2_{i,j})^2}.$$

We can also write for every field $\mathbf{p} = (\mathbf{p}_1, \mathbf{p}_2) \in \mathbb{R}^2$, the discrete divergence approximation:

$$(\mathrm{div}\ \mathbf{p})_{i,j} = \begin{cases} \mathbf{p}^1_{i,j} - \mathbf{p}^1_{i-1,j} & \text{si } 1 < i < N_1 \\ \mathbf{p}^1_{i,j} & \text{si } i = 1 \\ -\mathbf{p}^1_{i-1,j} & \text{si } i = N_1 \end{cases} + \begin{cases} \mathbf{p}^2_{i,j} - \mathbf{p}^2_{i,j-1} & \text{si } 1 < j < N_1 \\ \mathbf{p}^2_{i,j} & \text{si } j = 1 \\ -\mathbf{p}^2_{i,j-1} & \text{si } j = N_1, \end{cases}$$

where $N_1$ is an integer greater than 2. One can write the following scheme:

$$u^{k+1}(i,j) = u^k(i,j) + \Delta t\Big(\mathrm{div}(\Phi(|\nabla u^k(i,j)|)\nabla u^k(i,j))\Big) - f(i,j),$$

where $u^k(i,j) = u(x_i, y_j, t_k)$, $x_i = ih$, $y_j = jh$, $t_k = k\Delta t$ and $\Delta t = \dfrac{T}{M}$.
As shown in the figures below 1 and 2. Most algorithm parameters are chosen heuristically for the algorithms to problem their best. We choose the Gaussian noise 50%, $\Delta t = 0.3$, $\varepsilon = 2\times10^{-3}$ and the number of iterations is 700. We given firstly restore of noisy images (Figs. 2,3) by our approach and we choose the parameter $\lambda = 0.2$. In the second experiment, we give the difference between our results, the method of the total variation [2], [5]–[7] and the Perona-Malik model [1], [8], [10], [12] (see Fig 4, 6), and we give also zoom in these results (see Fig, 5, 7). We can notice from the results of PSNR in the figure 8 that our model is better then the model of Perona-Malik and the total variation method.

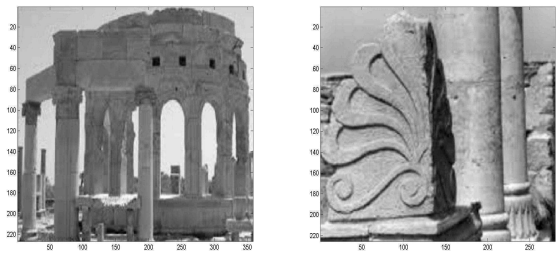

Fig. 1: Original image

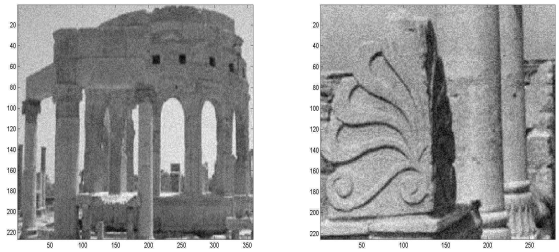

Fig. 2: Noisy image




ISSN 1737-9334

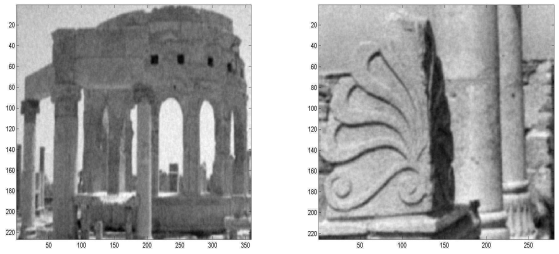

Fig. 3: Restored image by using our model with $g(k) = \dfrac{1}{1+(\frac{k}{\lambda})^2}$

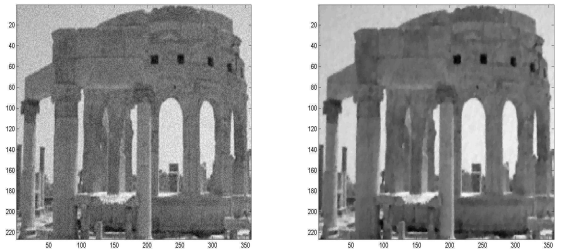

(a) (b)

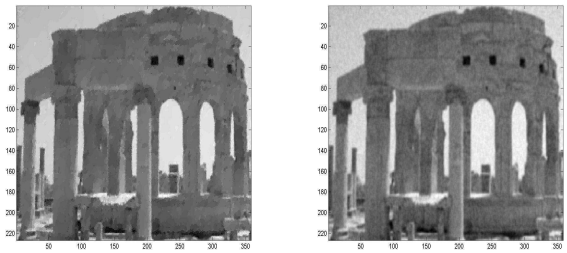

(c) (d)

Fig. 4: (a) The noisy image, (b) the image restored by using the method of the total variation, (c) the image restored by using the Perona-Malik model and (c) is obtained by our model

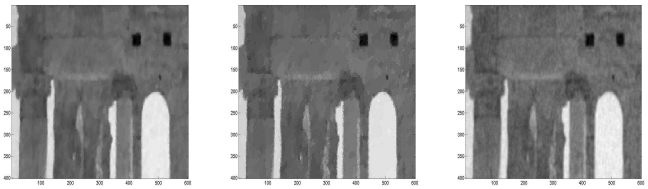

(a) (b) (c)

Fig. 5: (a) Zoom in of the image restored by TV, (b) zoom in of the image restored by PM and (c) zoom in of the our model

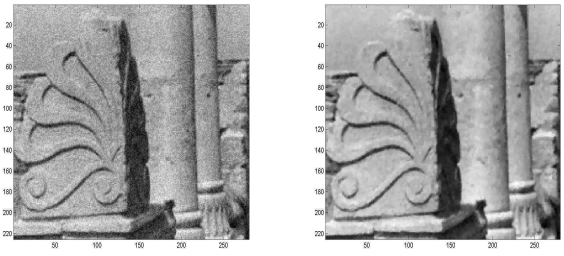

(a) (b)

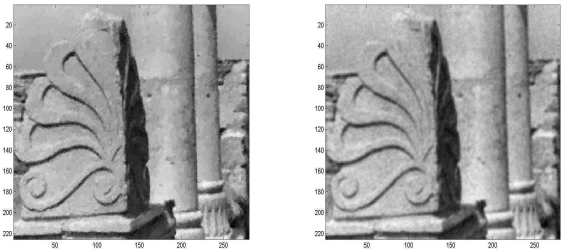

(c) (d)

Fig. 6: (a) The noisy image, (b) the image restored by using the method of the total variation, (c) the image restored by using the Perona-Malik model and (d) is obtained by our model

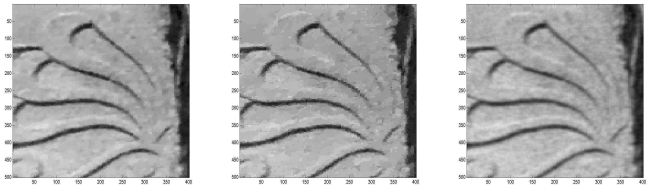

(a) (b) (c)

Fig. 7: (a) Zoom in of the image restored by TV, (b) zoom in of the image restored by PM and (c) zoom in of the our model

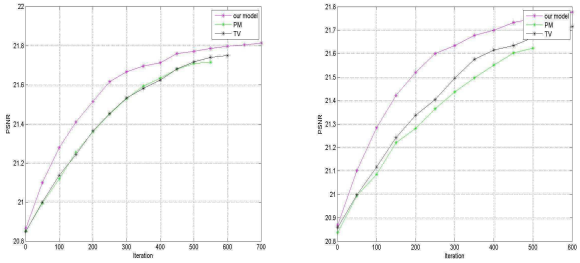


Fig. 8: The PSNR for different numbers of iterations for image 1,2




ISSN 1737-9334

| **Iteration** | $PSNR_{OM}$ | $PSNR_{TV}$ | $PSNR_{PM}$ |
|---|---|---|---|
| 1 | 20.8668 | 20.8529 | 20.8520 |
| 100 | 21.2799 | 21.1378 | 21.1190 |
| 200 | 21.5155 | 21.3650 | 21.3607 |
| 300 | 21.6672 | 21.5327 | 21.5300 |
| 400 | 21.7134 | 21.6251 | 21.6340 |
| 500 | 21.7720 | 21.7184 | 21.7105 |
| 600 | 21.7989 | 21.7502 | 21.6962 |

TABLE I: PSNR comparisons for the three models (for image 01)

| **Iteration** | $PSNR_{OM}$ | $PSNR_{TV}$ | $PSNR_{PM}$ |
|---|---|---|---|
| 1 | 20.8694 | 20.8591 | 20.8381 |
| 100 | 21.2846 | 21.1174 | 21.0856 |
| 200 | 21.5200 | 21.3370 | 21.2816 |
| 300 | 21.6341 | 21.4951 | 21.4376 |
| 400 | 21.6781 | 21.6149 | 21.5518 |
| 500 | 21.7456 | 21.6787 | 21.6234 |
| 600 | 21.7628 | 21.7153 | / |

TABLE II: PSNR comparisons for the three models (for image 02)

## IV. Conclusion

We present in this article a novel model for image denoising (see [1]) when we shown their theoretical results. These results give the best numerical outcome with a better choice of parametres ($\Delta t$, $\lambda$,...), and we also present that our model give a better PSNR when compared with the model of Perona-Malik and the method of the total variation. This model preserve the contours and removes staircase during the image denoising.

## References

[1] A.Atlas, F.Karami, D.Meskine; *The Perona-Malik inequality and application to image denoising*, Nonlinear Analysis: Real World Applications 18 (2014) 57-68

[2] A.Chambolle; *An Algorithm for Total Variation Minimization and Applications*, J.Math. Imaging Vis., 20(2004), PP. 8997.

[3] Th. Gallouet, O. Kavian; *Resonace for jumping non-linearities*, Journal of Partial Differential Equations. 7, 3 (1982), 325-342.

[4] Chun Pong Lau, Yu Hin Lai, Lok Ming Lui; *Variational models for joint subsampling and reconstruction of turbulence-degraded images*, CAM Report 18-21 April 2018.

[5] Hubin Chang, Yifei Lou, and Yuping Duan; *Total Variation Based Phase Retrieval for Poisson Noise Removal*, CAM Report 16-76 October 2016.

[6] Huibin Chang, Yifel Lou, Michael K. Ng, and Tieyong Zeng; *Phase Retrieval from Incomplete Magnitude Information Vsia Total Variation Regularization*,CAM Report 16-39, UCLA June 2016.

[7] Jun Liu and Xiaojun Zheng; *A Block Nonlocal TV Method for Image Restoration*, CAM Report 16-25 May 2016.

[8] V Kamalaveni, R Anitha Rajalakshmi, K A Narayanankutty; *Image Denoising using Variations of Perona-Malik Model with different Edge Stopping Functions*, Procedia Computer Science 58(2015) 673-682.

[9] S. Levins, Y. Chen and J. Stanich, *Image restoration via nonstandard diffusion*, Technical-Report 04-01, Dept of Mathematics and Computer Science, Duquesne University, 2004.

[10] P. Perona and J. Malik; *Scale-espace and edge detection using anisotropic diffusion*, IEEE Transactions on Pattern Analysis and Machine Intelligence, 12(1990), pp. 429-439.

[11] Stanley Osher, Zuoqiang Shi, and Wei Zhu; *Low Dimensional Manifold Model for Image Processing*,January 2016.

[12] Y.Q. Wang, Jichang Guo, Wufan Chen, Wenxue Zhang; *Image denoising using Modified PeronaâĂŞMalik Model based on Directional Laplacian*, Signal Processing 93 (2013) 2548âĂŞ2558.


ISSN 1737-9334

# A Correct-by-Design Role-Based Access Control Model for Healthcare Information Systems

Zoubeyr Farah*,1, Hania Gadouche*,2, Abdelkamel Tari*,3
*LIMED Laboratory, Department of Computer Science
Faculty of Exact Sciences
Abderrahmane Mira University, Bejaia, Algeria
Email: 1zoubeyr.farah@gmail.com 2gad.hania@gmail.com 3tarikamel59@gmail.com

***Abstract*—In this paper, a correcte-by-design approach is proposed to specify Role-Based Access Control (RBAC) for Healthcare Information Systems. The proposed approach is based on the Event-B formal method and its tool support RODIN plateform. To design a valid and multilevel access control model, a number of refinement operations are performed leading to a specification with several abstraction levels, each level implements selected properties according to the RBAC standard.**

***Index Terms*—Correct-by-Design, Event-B, Formal Methods, Healthcare Information System, Proof and Refinement, Role-Based Access Control, Specification and Validation.**

## I. Introduction

In Healthcare Information Systems (HIS), wrong access definitions can lead to the violation of patient privacy due to the sensitive nature of the handled data. Access Control (AC) is a solution that is commonly used for controlling access to resources. Role-Based Access Control (RBAC) is currently the most used model as the management of access control is simplified; because defined permissions are granted to roles. In fact, RBAC is an ANSI standard [1], [2] that is used principally in industry [3] and enterprise management systems. An access control policy specification must be validated before its deployment. The specification validation includes the validity of the declarative aspect (i.e. properties definition) and the correctness of the behavioral one. The declarative aspect of RBAC considers the typing and the definition of relations between its components. The correctness of the behavioral aspect implies the preservation of the specification consistency. For this purpose, many methods are defined in the literature and several specification models for RBAC have been proposed [4]. Among the different formalisms used to model access control: SPIN model checker [5], LTL (Linear Temporal Logic) formalism [6], Alloy [7] CPN-Tool for Colored Petri Nets [8] and EB3SEC [9]. Regardless of used formalism, validation methods are generally based on a-posteriori verification process [10]–[12], or on a combination of both a-posteriori and a-priori verification process [13]–[15]. However, the increasing complexity of systems makes the a-posteriori verification process more difficult. To overcome this limit, some works have used formal methods to define a full-based a-priori verification process [16], [17] . Specification approaches that are based on formal methods, such as Event-B [18], are widely used to validate faultless critical systems. The use of formal methods requires understanding the system behavior and the relations between its components. Several works in the literature have used the Event-B method to specify the RBAC standard. In [19], access control is modeled in many levels of abstraction where each level defines a class of properties, as well, a two-step refinement approach is proposed to generate the model. In [12], an Event-B formulation of an E-Marking System access control is proposed. The verification and validation of the proposed formulation are carried out using the ProB tool [20]. Authors in [17] propose to validate the 2012 RBAC standard using the B method [21]. Most existing formal validation approaches deal only with the declarative aspect of the model without covering the behavioral features. In this paper, we deal with both of the declarative and the behavioral aspects. We use the Event-B formal method, since it allows the specification of systems according to a correct-by-construction methodology, additionally, it provides a large selection of tools and techniques for specifying, validating and checking properties of systems. Our approach is suitable for healthcare information systems where the validation of the constructed specification is crucial. The proposed specification approach is based on refinement and gives a multilevel view of the access control model. The refinement starts from a high abstract level of specification to the most concrete one. The specification consistency is preserved through all its levels as the model properties are linked to the behavior. Indeed, defining properties of the model according to its behavior allows to get an a-priori verification of the specification correctness. Our approach is based on an a-priori formal verification process, similarly to the one proposed to validate communicating systems in [22], and the one applied on Attribute-based access




ISSN 1737-9334

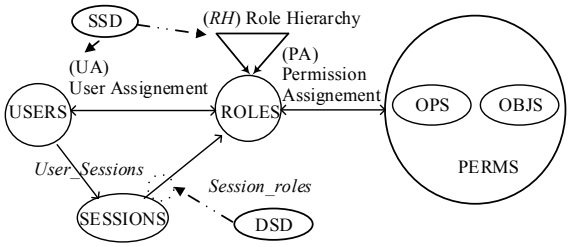


Fig. 1. RBAC model

control (ABAC) [23], [24] . RODIN platform [25] is used to develop and validate the model specification. The remainder of the paper is organized as follows: Section 2 gives a presentation of the RBAC standard. Section 3 describes the Event-B formal method. Section 4 gives a browse of each level of the proposed Event-B specification process. Proof obligations are mentioned in Section 5. Finally, the conclusion and some research perspectives are given in Section 6.

## II. Role-Based Access Control

In this section, an overview of the ANSI RBAC Standard (Institute, 2004; Institute, 2012) is given. This standard is defined by five sets: i) users (USERS); ii) roles (ROLES); iii) objects (OBJS); iv) actions or operations (OPS); v) sessions (SESSIONS).The RBAC concept is defined with permissions whom are granted to users through affected roles. Operations are applied on objects and sessions define the period of time when users can activate roles. An important aspect of RBAC is the definition of constraints on role activation. In term of these constraints, RBAC defines the notion of Separation of Duty (SoD). SoD relationships are used to apply conflict-of-interest management policies. Organizations employ these policies to prevent users from exceeding a reasonable level of authority for their positions. Two types of SoD are defined to avoid possible conflicts in the assignment of roles in RBAC: Static Separation of Duty (SSD) and Dynamic Separation of Duty (DSD).

- The SSD prevents the assignment of conflicted roles to the same user. Even in the hierarchy, a descendant role cannot be assigned to a user if its ascendant is in conflict of interest with another assigned role.
- The DSD prevents the assignment of conflicted roles to a user in the same time, during the allocation of a session. The solution of this problem can be resolved by assigning the conflicted roles to the user but in different sessions.

Figure 1 depicts the main RBAC entities and their associations [2]. In RBAC, user-to-role and permission-to-role assignments can be many-to-many. Thus, the same user can be assigned to many roles and a single role can be assigned to many users. Similarly, a single permission can be assigned to many roles and a single role can be assigned to many permissions.

TABLE I
The Event-B Development Structure

| | |
|---|---|
| Context ctxt_a<br>Extends ctxt_b<br>Sets s<br>Constants c<br>Axioms A(s,c)<br>Theorems T(s,c)<br>End | Machine mach_a<br>Refines mach_b<br>Sees ctxt_a<br>Variables v<br>Invariants I(s,c,v)<br>Theorems T(s,c,v)<br>Variants V(s,c,v)<br>Events evt= Any x<br>Where G(s,c,v,x)<br>Then v :\| BA(s,c,v,x,v')<br>End<br>End |

## III. Event-B Method

Event-B is a formal method used to model and analyze systems. The key features of Event-B are in the use of:

- Set theory as a modeling notation,
- Refinement, to represent systems at different abstraction levels,
- Mathematical proofs, to verify the consistency between refinement levels.

An Event-B development model [18] is based on components of two kinds: Contexts and Machines. Contexts contain the static parts (axiomatization and theories) of the model, whereas the Machines implement the dynamic parts (states and transitions). Machines and contexts have various relations: a machine can be refined by another one, and a context can be extended by another one. Moreover, a machine can see one or several contexts. A Context is defined by the following clauses : CONTEXT, EXTENDS, SETS, CONSTANTS, AXIOMS and THEOREMS. Similarly to Contexts, Machines are defined by a set of clauses : MACHINE, REFINES, SEES, VARIABLES, INVARIANTS, THEOREMS and VARIANT.

The general structure of an Event-B development is illustrated in the Table I, where $s$ denotes sets, $c$ denotes constants and $v$ denotes the declared variables of the machine. Axioms are denoted by $A(s,c)$ and theorems by $T(s,c)$ , whereas invariants are denoted by $I(s,c,v)$ and local theorems by $T(s,c,v)$. For an event $evt$, its guards are denoted by $G(s,c,v,x)$ and its actions by the before-after predicate $BA(s,c,v,x,v')$.

The $EVENTS$ clause defines a list of events (transitions) that can occur in a given model. Each event is characterized by its guards and is described by a set of actions (substitutions). Each machine must contain an initialization event. The events occurring in an Event-B model affect the state described in clause. An event consists of the following clauses:

- Refines : declares a list of events refined by the described event.
- Any : lists a set of the event parameters.
- Where : expresses a set of guards for the event. An event can be fired when its guard turns to true. If several guards of events become true, only a single event is fired.
- Then : contains a set of actions of the event that are used to modify variables.


ISSN 1737-9334

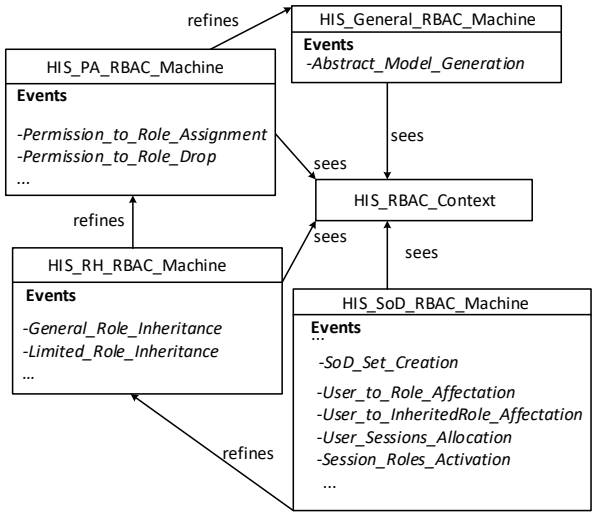


Fig. 2. The proposed Event-b specification

Event-B is based on a refinement methodology, it allows the system developer to start with an abstract model of the system considering its context, and gradually add details to the model. This process leads to a sequence of concrete models until the final implementation is reached. A number of proof obligations are generated through this process, which guarantees the correctness of the model as well as any desired invariants (properties) that the model should preserve.

## IV. Event-B Specification of RBAC for Healthcare Information Systems

The proposed RBAC specification is detailed in this section. In the suggested approach, properties of the model are given in conjunction with the behavior specification. The model is developed in a way to link up between behavior and properties of RBAC components. Following a correct-by-design approach, validity and correctness of the RBAC properties definition are guaranteed through the specification process. In order to simplify the construction of the model, accesses are defined only by PERMISSIONS without splitting them on OPERATIONS and OBJECTS. The developed Event-B model contains one context that forms the static part of the specification, and four machines which form the dynamic part. Each machine expresses a level of the model specification. Figure 2 gives the structure of the proposed specification.

- $HIS\_RBAC\_Context$ : The basic elements of RBAC are introduced in the static part of the specification. All the required static definitions to operate the dynamic part of the model are declared in this context (see Table II). In $HIS\_RBAC\_Context$ , the declared working sets are: $HIS\_PERMISSIONS$ ,$HIS\_ROLES$ , $HIS\_USERS$ and $HIS\_SESSIONS$ . The single condition on the definition of these sets is stated as an axiom: The sets must not be empty. The model is designed for a surgical clinic, where the medical staff is already organized into roles and the users achieve tasks (permissions) according to the roles granted to them. The process to be instantiated involves a Patient who has come to a surgical clinic to perform an operation. He possesses a file created by a Secretary, whom the Doctor can read or modify; the Patient must be operated by a Surgeon under anesthesia that the Anesthesiologist administered to him with the supervision of the ChiefDoctor. After this, the Nurse and the Doctor will take care of the postoperative follow-up of the Patient by checking and monitoring his condition but also treating his wounds. The process is divided into four sessions that users can allocate according to the involved roles.

TABLE II
The HIS RBAC Context

| | |
|---|---|
| CONTEXT | HIS_RBAC _Context |
| SETS | HIS_USERS, HIS_ROLES, HIS_PERMISSIONS, HIS_SESSIONS |
| CONSTANTS | |
| | check,operate, treat, create_files, read_files, modify_files, supervise. Anesthetize, ChiefDoctor, Doctor, Nurse, Surgeon, Anesthesiologist, Patient, Secretary. user1, user2, user3, user4, user5 registration, diagnosis, surgery, treatment |
| AXIOMS | |
| axm1 : | partition(HIS_PERMISSIONS, {check}, {operate}, {treat}, {anesthetize}, {create_files}, {read_files}, {modify_files}, {supervise}. |
| axm2 : | partition(HIS_ROLES, {ChiefDoctor}, {Doctor}, {Surgeon}, {Anesthesiologist}, {Nurse}, {Patient}, {Secretary}) |
| axm3 : | partition(HIS_USERS, {user1}, {user2}, {user3} , {user4}, {user5}) |
| axm4 : | partition(HIS_SESSIONS, {registration}, {diagnosis}, {surgery}, {treatment}) |
| Axm5 : | HIS_USERS $\neq \varnothing \wedge$ HIS_ROLES $\neq \varnothing \wedge$ HIS_PERMISSIONS $\neq \varnothing \wedge$ HIS_SESSIONS $\neq \varnothing$ |
| END | |

- $HIS\_General\_RBAC\_Machine$ : The dynamic specification starts with a level that gives a global and high view of RBAC. It is expressed by the machine $HIS\_General\_RBAC\_Machine$ as depicted in the Figure III.
In this level, details are not important; the RBAC structure has just to be in a brief and perceivable view, the considered properties are about the components typing and the definition of relations between them. The dynamic RBAC components are expressed by the variables: $PA$, $RH$, $UA$, $US$ and $RS$. $PA$ for permission to role assignment, $RH$ for the role hierarchy definition, $UA$ for the affectation of roles to users, $US$ for the allocation of sessions by users and $RS$ for the activation of roles during a session. These variables are manipulated by the event $Abstract\_Model\_Generation$ that generates


ISSN 1737-9334

TABLE III
THE HIS GENERAL RBAC MACHINE

**HIS_General_RBAC_Machine**
...
INVARIANTS
Inv1 : PA ⊆ HIS_PERMISSIONS × HIS_ROLES
Inv2 : RH ⊆ HIS_ROLES × HIS_ROLES
Inv3 : UA ⊆ HIS_USERS × HIS_ROLES
Inv4 : US ⊆ HIS_USERS × HIS_SESSIONS
Inv5 : RS ⊆ HIS_SESSIONS × HIS_ROLES
EVENTS
...
Abstract_Model_Generation
ANY
permissions, roles, users, sessions
WHERE
grd1: permissions ⊆ HIS_PERMISSIONS
grd2: roles ⊆ HIS_ROLES
grd3: users ⊆ HIS_USERS
grd4: sessions ⊆ HIS_SESSIONS
THEN
act1: PA :∈ ℙ(permissions×roles)
act2: RH :∈ ℙ(roles × roles)
act3: UA :∈ ℙ(users × roles)
act4: US :∈ ℙ(users × sessions)
act5: RS :∈ ℙ(sessions × roles)
End
End

TABLE IV
THE PERMISSION TO ROLES ASSIGNMENT MACHINE

**HIS_PA_RBAC_Machine**
...
INVARIANTS
...
Inv6 : PA1 ⊆ HIS_PERMISSIONS × HIS_ROLES
Inv7 : permissions1 ⊆ HIS_PERMISSIONS
Inv8 : roles1 ⊆ HIS_ROLES
EVENTS
...
Permissions_to_Roles_Assignment
ANY permission, role
WHERE
grd1: permission ∈ HIS_PERMISSIONS
grd2: role ∈ ROLES
THEN
act1: permissions1 := permissions1 ∪ { permission }
act2: roles1 := roles1 ∪ { role }
act3: PA1 := PA1 ∪ { permission ↦ role }
END

abstract views of the model. To preserve the abstraction, non-deterministic assignments are used. These affectations will gradually be determined in the refinement process.

- $HIS\_PA\_RBAC\_Machine$: This level provides more precision on the $PA$ relation. As illustrated in the Figure IV, the variable $PA1$ concretizes $PA$ by specifying roles and permissions that are involved in the relation. In order to preserve the typing properties of permissions and roles, witnesses are used in the refinement of the event $Abstract\_Model\_Generation$ as shown in the Figure V. The events where are handled the variables $PA$, $roles$ and $permissions$ ($Permissions\_to\_Roles\_Drop$, $Role\_Drop$,) are also declared in this machine.
- $HIS\_RH\_RBAC\_Machine$: This machine introduces the notion of hierarchy between roles. The event $General\_Role\_Inheritance$ allows a role who is hierarchically beyond another role to get all of his permissions. The principle guard of this event ($grd4$ )states that both of the two roles must have been assigned to permissions. The concrete variable $RH1$ contains the inheritance couples as illustrated in the Figure VI.
  Besides the general role hierarchy defined in the RBAC Standard, there is the limited role hierarchy. The event $Limited\_Role\_Inheritance$ detailed in the Figure VII, states that for any different two roles $role1$, $role2$: if $role1$ inherits $role2$; there is no other role $role3$ that is inherited by $role1$ in the relation $RH1$.
  The event $Abstract\_Model\_Generation$ is concretized by refinement in each machine of the specification.
- $HIS\_SoD\_RBAC\_Machine$: The event $SoD\_Set\_Creation$ (Figure VIII) generates the set $SOD$ that is composed of conflicted roles, sorted in couples $(rs, n)$ .Where $rs$ is the subset of conflicted roles and $n$ is the number of roles that can be assigned.
- $UA\_RBAC\_Machine$: Users are introduced in this level, and are affected to roles with the event: $Users\_to\_Roles\_Affectation$. The variable $UA$ is instantiated as $UA1$ after conditions have been defined

TABLE V
REFINEMENT OF THE EVENT ABSTRACT_MODEL_GENERATION

Abstract_Model_Generation
REFINES Abstract_Model_Generation
ANY users, sessions
WHERE
...
grd3: dom(PA1) ⊆ permissions1 ∧ ran(PA1)⊆roles1
WITH
permissions: permissions=permissions1
roles: roles=roles1
THEN
act1: PA :=PA1
...
End
...

TABLE VI
ROLE HIERARCHY MACHINE

**HIS_RH_RBAC_Machine**
...
EVENTS
...
General_Role_Inheritance
ANY role1, role2
WHERE
grd1: role1 ∈ HIS_ROLES ∧ role2 ∈ HIS_ROLES
grd2: role1 ∈ roles1 ∧ role2 ∈ roles1
grd3: role1 ≠ role2
grd4:(PA1 ▷ {role1} ≠ ∅ ) ∧ (PA1 ▷ {role2} ≠ ∅)
THEN
act1: RH1 := RH1 ∪ {role1 ↦ role2}
END
...




ISSN 1737-9334

TABLE VII
LIMITED ROLE INHERITANCE

```
...
Limited_Role_Inheritance
        ANY role1, role2
        WHERE
        grd1:role1 ∈ roles1 ∧ role2 ∈ roles1 ∧ role1≠role2
        grd2: {role1 ↦ role2} ⊆ RH1 ∧
        grd2: {role1 ↦ role2} ⊆ RH1 ∧
              ¬(∃ role3 · RH1▷{role1}={role3})
        THEN
        act1: RHL := RHL ∪ {role1}
END
...
```

TABLE VIII
HIS_SOD_RBAC_MACHINE

```
HIS_SoD_RBAC_Machine
...
INVARIANTS
              ...
              Inv10: SOD ⊆ ℙ(HIS_ROLES) × ℕ
              Inv11: users1 ⊆ HIS_USERS
...
EVENTS
...
SoD_Set_Creation
              ANY rs, n
              WHERE
              grd1: rs ⊆ HIS_ROLES ∧ n ∈ ℕ
              grd2: finite(rs) ∧ (n≥2 ∧ n ≤ card(rs))
              THEN
              act1: SOD := SOD ∪ {rs↦n}
END
...
```

when selecting the roles to assign. The guard $grd4$ of the Figure IX ensures that the roles that are (or must be) assigned to a user and those of the subset $t$ do not exceed $(n-1)$ . In other words, a user cannot be affected to more than $(n-1)$ conflicted roles of $rs$.
The event $User\_to\_InheritedRole\_Affectation$, depicted in the Figure IX, allows the assignment of a descendant role to a user if its' ascendant is assigned to this same user. Considering that the separation of duty is categorized according to abstraction levels in the proposed model, the $grd4$ shows that a user cannot be assigned to more than $(n-1)$ role of $rs$, the same way as in the preceding event. The difference is that the role from $rs$ has an inheritance link in $RH1$. Sessions are allocated with the event $User\_Sessions\_Allocation$ depicted by the Figure X. The assignment of sessions to a user $(user, session)$ is contained in the concrete variable $US1$.

## V. PROOF OBLIGATIONS OF THE MODEL

The entire Event-B model presented above has been developed within the Rodin platform. This latter generates automatically Proof Obligations in the form of sequences [18]. The automatic Prover of RODIN can discharge automatically many of the POs, the remainder of non-discharged POs can be tackled by the interactive Prover. The developed model led

TABLE IX
EVENTS FOR THE STATIC SEPARATION OF DUTY

```
...
User_to_Role_Affectation
ANY user, role, rs, n, t
WHERE
grd1: user ∈ HIS_USERS ∧ rs ∈ dom(SOD)
grd2: finite (rs) ∧ t⊆ rs ∧ n≥2 ∧ n ≤ card(rs)
grd3: finite(t) ∧ card(t)≥n ∧ role ∈ t
grd4: card(UA1[{ user }] ∩ t)≤ n−1
THEN
act1: users1 := users1 ∪ {user}
act2: UA1 := UA1 ∪ {user↦role}
END

User_to_InheritedRole_Affectation
ANY user, role, role1, rs, n, t
WHERE
grd1: user ∈ HIS_USERS ∧ user ∈ users1 ∧ n ∈ ℕ
grd2: finite(rs) ∧ rs ∈ dom(SOD) ∧finite(t) ∧
      t ⊆ rs ∧(n≥2 ∧ n≤card(rs) ∧ card(t)≥n)
grd3: user↦role⊆ UA1 ∧ {role↦role1}⊆ RH1
grd4: card(UA1[{user}] ∩ t) ≤ n−1
THEN
act1: UA1 := UA1 ∪ {user↦role1}
END
```

TABLE X
USER_SESSIONS_ALLOCATION EVENT

```
...
User_Sessions_Allocation
        ANY user, session
        WHERE
        grd1: user ∈ HIS_USERS ∧ session ∈ HIS_SESSIONS
        grd2: user ∈ users1
        THEN
        act1: sessions1:= sessions1 ∪ {session}
        act2: US1 := US1 ∪ {user↦session}
END
...
```

to 32 proof obligations. 31 were proved automatically and one needed few interactive proof steps. Table XI gives the details of these results. As can be seen, the adopted specification approach engendered a few number of POs since the properties were expressed in the events' guards. Accordingly, several POs were automatically guaranteed by construction.

## VI. CONCLUSION

In this work, an approach is presented to design an RBAC model for healthcare systems. Due to the limitation of approaches that are based on a-posteriori checking process and in order to deal with the validation of large-scale systems, a correct-by-design approach is proposed. Accordingly, we propose an Event-B specification of the RBAC model for a

TABLE XI
STATISTIC OF PROOFS

| Model components | PO | Automatic proof | Interactive proof |
|---|---|---|---|
| HIS_General_RBAC_Machine | 5 | 5 | 0 |
| HIS_PA_RBAC_Machine | 7 | 7 | 0 |
| HIS_RH_RBAC_Machine | 2 | 2 | 0 |
| HIS_SoD_RBAC_Machine | 18 | 17 | 1 |



ISSN 1737-9334

healthcare system where all the properties are validated and the correct behavior is proved. The main features of the solution are:

- The model is designed in stepwise manner, with refinements and proving-based specification.
- The approach generates specifications with different abstraction views which simplify the observation and analysis of the specified model.

As future work, the aim would be to:

- Extend the approach to allow model reconfiguration;
- Apply the approach to other access control paradigms [26].

## REFERENCES

[1] A. N. S. Institute, *Role Based Access Control, INCITS 359-2004*, ANSI, 1430 Broadway, New York, NY 10018, USA, 2004.

[2] ——, *Role Based Access Control, INCITS 359-2012*, ANSI, 1430 Broadway, New York, NY 10018, USA, 2012.

[3] A. C. OConnor and R. J. Loomis, "2010 economic analysis of role-based access control," *NIST, Gaithersburg, MD*, vol. 20899, 2010.

[4] E. Ferrari, "Guest editorial: Special issue on access control models and technologies," *ACM Transactions on Information and System Security (TISSEC)*, vol. 8, no. 4, pp. 349–350, 2005.

[5] T. Ahmed and A. R. Tripathi, "Static verification of security requirements in role based cscw systems," in *Proceedings of the eighth ACM symposium on Access control models and technologies*. ACM, 2003, pp. 196–203.

[6] M. Drouineaud, M. Bortin, P. Torrini, and K. Sohr, "A first step towards formal verification of security policy properties for rbac," in *Quality Software, 2004. QSIC 2004. Proceedings. Fourth International Conference on*. IEEE, 2004, pp. 60–67.

[7] G. Hughes and T. Bultan, "Automated verification of access control policies using a sat solver," *International journal on software tools for technology transfer*, vol. 10, no. 6, pp. 503–520, 2008.

[8] L. Kahloul, K. Djouani, W. Tfaili, A. Chaoui, and Y. Amirat, "Modeling and verification of rbac security policies using colored petri nets and cpntool," in *International Conference on Networked Digital Technologies*. Springer, 2010, pp. 604–618.

[9] P. Konopacki, M. Frappier, and R. Laleau, "Expressing access control policies with an event-based approach," in *International Conference on Advanced Information Systems Engineering*. Springer, 2011, pp. 607–621.

[10] M. Koch, L. V. Mancini, and F. Parisi-Presicce, "A graph-based formalism for rbac," *ACM Transactions on Information and System Security (TISSEC)*, vol. 5, no. 3, pp. 332–365, 2002.

[11] B. Shafiq, A. Masood, J. Joshi, and A. Ghafoor, "A role-based access control policy verification framework for real-time systems," in *Object-Oriented Real-Time Dependable Systems, 2005. WORDS 2005. 10th IEEE International Workshop on*. IEEE, 2005, pp. 13–20.

[12] N. Al-Hadhrami, B. Aziz, and L. ben Othmane, "An incremental b-model for rbac-controlled electronic marking system," *International Journal of Secure Software Engineering (IJSSE)*, vol. 7, no. 2, pp. 37–64, 2016.

[13] C. Yuan, Y. He, J. He, and Z. Zhou, "A verifiable formal specification for rbac model with constraints of separation of duty," in *International Conference on Information Security and Cryptology*. Springer, 2006, pp. 196–210.

[14] H. Hu and G. Ahn, "Enabling verification and conformance testing for access control model," in *Proceedings of the 13th ACM symposium on Access control models and technologies*. ACM, 2008, pp. 195–204.

[15] H. Ferrier-Belhaouari, P. Konopacki, R. Laleau, and M. Frappier, "A design by contract approach to verify access control policies," in *Engineering of Complex Computer Systems (ICECCS), 2012 17th International Conference on*. IEEE, 2012, pp. 263–272.

[16] N. Li, J.-W. Byun, and E. Bertino, "A critique of the ansi standard on role-based access control," *IEEE Security & Privacy*, vol. 5, no. 6, 2007.

[17] N. Huynh, M. Frappier, A. Mammar, R. Laleau, and J. Desharnais, "A formal validation of the rbac ansi 2012 standard using b," *Science of Computer Programming*, vol. 131, pp. 76–93, 2016.

[18] J. Abrial, "Modeling in event-b: System and software development," 2010.

[19] T. S. Hoang, D. Basin, and J.-R. Abrial, "Specifying access control in event-b," *Technical report*, vol. 624, 2009.

[20] M. Leuschel and M. Butler, "Prob: A model checker for b," in *International Symposium of Formal Methods Europe*. Springer, 2003, pp. 855–874.

[21] S. Schneider, *The B-method: An introduction*. Palgrave, 2001.

[22] Z. Farah, Y. Ait-Ameur, M. Ouederni, and K. Tari, "A correct-by-construction model for asynchronously communicating systems," *International Journal on Software Tools for Technology Transfer*, vol. 19, no. 4, pp. 465–485, 2017.

[23] V. C. Hu, D. R. Kuhn, D. F. Ferraiolo, and J. Voas, "Attribute-based access control," *Computer*, vol. 48, no. 2, pp. 85–88, 2015.

[24] H. Gadouche, F. Zoubeyr, and A. Tari, "A correct-by-construction model for attribute-based access control," in *MEDI*, 2018.

[25] J.-R. Abrial, M. Butler, S. Hallerstede, T. S. Hoang, F. Mehta, and L. Voisin, "Rodin: an open toolset for modelling and reasoning in event-b," *International journal on software tools for technology transfer*, vol. 12, no. 6, pp. 447–466, 2010.

[26] A. A. E. Kalam, S. Benferhat, A. Miège, R. E. Baida, F. Cuppens, C. Saurel, P. Balbiani, Y. Deswarte, and G. Trouessin, "Organization based access control," in *Proceedings of the 4th IEEE International Workshop on Policies for Distributed Systems and Networks*, ser. POLICY '03. Washington, DC, USA: IEEE Computer Society, 2003, pp. 120–. [Online]. Available: http://dl.acm.org/citation.cfm?id=826036.826869




ISSN 1737-9334

# Tuning of Fractional PI$^{\lambda}$D$^{\mu}$A Controllers by Using PSO

Khalfa Bettou, Abdelfatah Charef

*Département d'Electronique, Université des Frères Mentouri de Constantine, route Ain El-bey, Constantine 25000, Alegria*

Bettou_kh,afcharef@yahoo.com

***Abstract*— The paper presents the development of a new tuning method for fractional order PI$^{\lambda}$D$^{\mu}$A controller. The basic ideas of this new tuning method are based, in the first place, on the classical tuning methods for setting the parameters of the fractional order PI$^{\lambda}$D$^{\mu}$A controller for λ=μ=1, which means setting the parameters of the classical PIDA controller, and on the minimum of integral absolute error (IAE) criterion by using particle swarm optimisation (PSO) algorithm for setting the fractional integration action order λ and the fractional differentiation action order μ. It is clearly shown that the fractional order PI$^{\lambda}$D$^{\mu}$A controller, which the parameters obtained by the proposed tuning method, gives better response than the classical one for the same system.**

***Keywords*— Integer order PIDA controller, Fractional order PI$^{\lambda}$D$^{\mu}$A controller, PSO algorithm, IAE criterion, Induction motor.**

## I. INTRODUCTION

The most commonly and practically controller used in all industrial feedback control applications is the proportional-integral-derivative (PID) controller. Many techniques have been suggested for their parameters tuning [1]-[3]. In many control application, the systems are modelled as a third order. PID controllers are unsuitable, especially for third-order systems. This is the reason that a new structure of the controller becomes the necessity of such systems.

In 1996, Jung and Dorf have proposed a new structure of controller and termed as proportional-integral-derivative and acceleration (PIDA) controller [4]. A new analytical approach of the PIDA controller parameters design was proposed by Kitt's [5]. A comparative design and analysis of PIDA controller was presented in [6].

Fractional calculus is a mathematical topic with more than 300 years old history but its application in physics and engineering has been reported only in recent years. In the last decades, besides the theoretical research in the field of fractional integrals and derivatives [7],[8], there are growing numbers of applications of fractional calculus in different areas of control engineering [9]-[11]. The idea of using fractional calculus in feedback control systems dates back to the early sixties. Oustaloup was the one who really introduced a fractional order controller [9]. More recently, Podlubny proposed a generalisation of the PID controller, namely the fractional order PI$^{\lambda}$D$^{\mu}$ controller [10]. Many researchers have been interested in the use and tuning of this type of controller and more effort is being taken in order to define new effective tuning techniques for fractional order PI$^{\lambda}$D$^{\mu}$ controllers using classical control theory [12]-[14].

Therefore, a possible way to enhance the performances of a feedback control system with the classical PIDA controllers is to extend the orders of integration and differentiation actions of the classical PIDA controller to real numbers instead of both limited to one. In this paper, we propose the design of the fractional order PI$^{\lambda}$D$^{\mu}$A controller of a classical unity feedback control system whose plant's transfer function is considered to be a third order system. The controller is the fractional order PI$^{\lambda}$D$^{\mu}$A controller whose transfer function is given as:

$$C_F(s) = k_p + k_i \frac{1}{s^{\lambda}} + k_d s^{\mu} + k_a s^2 \qquad (1)$$

With $k_p$ is the proportional constant, $k_i$ is the integration constant, $k_d$ is the differentiation constant, $k_a$ is the acceleration constant, λ is the fractional integration action order such that $0<\lambda<1$ and μ is the fractional differentiation action order such that $0<\mu<1$.

The proposed tuning method is based, in the first place, on any existed tuning methods for setting the parameters $k_p$, $k_i$, $k_d$ and $k_a$ of the fractional order PI$^{\lambda}$D$^{\mu}$A controller for λ=μ=1 which means setting the parameters of the classical PIDA controller. In this work, we have used Kitti's and Jung-Dorf tuning methods [6]. Then using the parameters $k_p$, $k_i$, $k_d$ and $k_a$ obtained in the first step, the error function $e(t)=r(t)-y(t)$, where the input $r(t)$ is the unit step, is minimised through the IAE optimisation criterion to determine the optimum settings of the fractional integration action order λ and the fractional differentiation action order μ of the fractional PI$^{\lambda}$D$^{\mu}$A controller. The IAE minimisation criterion is obtained by using PSO algorithm [15]. To use this PSO algorithm, the irrational transfer functions of the fractional order PI$^{\lambda}$D$^{\mu}$A controller must be approximated by a rational function, in a given frequency band of practical interest using the singularity function method [16].

The proposed tuning method can also use any already tuned classical PIDA controller by any method for the four parameters $k_p$, $k_i$, $k_d$ and $k_a$ and then determine the optimum settings of the fractional order integration λ and the fractional differentiation μ. The optimum tuning of the parameters of the fractional order PI$^{\lambda}$D$^{\mu}$A controller is not the main objective of our proposed design method. Instead,


ISSN 1737-9334

our objective is to enhance the control performances of the feedback control system already using a classical PIDA controller by just adding the fractional order integration λ and the fractional order differentiation μ. The paper is organised as follows: Section 2 introduces the approximation of the fractional integrator, differentiator and the fractional order $PI^{\lambda}D^{\mu}A$ controller by a rational function in a limited frequency band of interest. In section 3, we introduce the proposed tuning method for the fractional order $PI^{\lambda}D^{\mu}A$ controller. In section 4, an illustrative example is presented to demonstrate the advantages of the proposed tuning method. Finally, section 5 draws the main conclusions.

## II. Approximation of Fractional Order PIDA Controller

When fractional order controllers have to be implemented or simulations using them have to be performed, fractional order transfer functions are usually replaced by integer order transfer functions whose behaviour is close enough to the desired ones. There are many different ways to get such approximations, in our work; the singularity function method of approximation of the fractional order operators by rational transfer function has been used [16].

### A. Fractional Order Integrator

In the frequency domain, the fractional order integrator, which is the integration action of the fractional order $PI^{\lambda}D^{\mu}A$ controller, is represented by the following irrational function:

$$C_I(s) = \frac{1}{s^{\lambda}} \tag{2}$$

Where λ is a positive real number such that $0<\lambda<1$.

In a given frequency band of practical interest, the fractional order integrator of (2) is approximated by a rational function as [16]:

$$C_I(s) = \left( \frac{1}{K_{II}} \frac{\prod_{i=0}^{N_I-1}\left(1+\frac{s}{z_{Ii}}\right)}{\prod_{i=0}^{N_I}\left(1+\frac{s}{p_{Ii}}\right)} \right) \tag{3}$$

The gain $K_{II}$, the poles $p_I$'s and the zeros $z_I$'s are given as in [16].

### B. Fractional Order Differentiator

In the frequency domain, the fractional order differentiator, which is the differentiation action of the fractional order PIDA controller, is represented by the following irrational function:

$$C_D(s) = s^{\mu} \tag{4}$$

Where μ is a positive real number such that $0<\mu<1$.

In a given frequency band of practical interest, the fractional order differentiator of (4) is approximated by a rational function as [16]:

$$C_D(s) = \left( K_{DD} \frac{\prod_{i=0}^{N_D}\left(1+\frac{s}{z_{Di}}\right)}{\prod_{i=0}^{N_D}\left(1+\frac{s}{p_{Di}}\right)} \right) \tag{5}$$

The gain $K_{DD}$, the poles $p_d$'s and the zeros $z_d$'s are given as in [16].

### C. Fractional Order $PI^{\lambda}D^{\mu}A$ Controller

In sections II.A and II.B, we showed how we can approximate the fractional order integrator and differentiator by rational functions, in a given frequency band of practical interest; so (1) becomes:

$$C_F(s) = k_p + k_i.C_I(s) + k_d.C_D(s) + k_a s^2 \tag{6}$$

## III. Fractional Order PIDA Controller Tuning

In this paper we propose the design of the fractional order $PI^{\lambda}D^{\mu}A$ controller of a classical unity feedback control system shown in Fig.1.

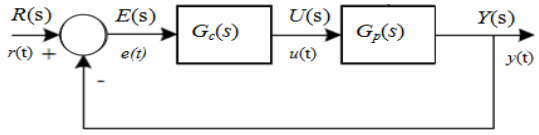


Fig. 1 Classical unity feedback control system

The proposed tuning method is based, in the first place, on any existed classical PIDA controller. In this work, we have used classical PIDA controllers tuned by using Kitti's and Jung-Dorf tuning methods [6]. The error function $e(t)=r(t)-y(t)$, where the input $r(t)$ is the unit step, is minimised through the IAE optimisation criterion to determine the optimum settings of the fractional integration action order λ and the fractional differentiation action order μ of the fractional $PI^{\lambda}D^{\mu}A$ controller. The IAE minimisation criterion is obtained by using PSO algorithm [15].

### A. Particle Swarm Optimization (PSO)

Our Particle Swarm Optimization algorithm is an intelligent optimization algorithm intimating the bird swarm behavior which was proposed by psychologist Kennedy and Dr. Eberhart in 1995 [15]. Compared to other optimization algorithms, the Particle Swarm Optimization is more objective, easy and performs well. It is applied in many fields such as the function optimization, the neural network training, the fuzzy system control, etc. In Particle Swarm Optimization algorithm, each individual is called "particle" which represents a potential solution. The algorithm achieves the best solution by the variability of some particles in the tracing space. The particles search in the solution space following the best particle by changing their positions and the fitness frequently; the flying direction and velocity are determined by the objective function.


ISSN 1737-9334

Assuming $X_i = (x_{i1}, x_{i2}, ..., x_{iD})$ is the position of *i*-th particle in *D*-dimension, $V_i = (v_{i1}, v_{i2}, ..., v_{iD})$ is its velocity which represents its direction of searching. In iteration process, each particle keeps the best position *pbest* found by itself, besides, it also knows the best position *gbest* searched by the group particles, and changes its velocity according two best positions. The standard formula of Particle Swarm Optimization is as follow:

$$v_{id}^{k+1} = wv_{id}^{k} + c_1 r_1 (p_{id} - x_{id}^{k}) + c_2 r_2 (p_{gd} - x_{id}^{k}) \quad (7)$$

$$x_{id}^{k+1} = x_{id}^{k} + v_{id}^{k+1} \quad (8)$$

In which: $i$=1,2,…$N$; $N$ the population of the group particles; $d$=1,2,…,$D$; $k$ the maximum number of iteration; $r_1$ and $r_2$ the random values in [0,1] used to keep the diversity of the group particles; $c_1$ and $c_2$ the learning coefficients, also they are called acceleration coefficients; $v_{id}^{k}$ the number $d$ component of the velocity of particle $i$ in $k$-th iteration; $x_{id}^{k}$ the number $d$ component of the position of particle $i$ in $k$-th iteration; $p_{id}$ the number $d$ component of the best position particle $i$ has ever found; $p_{gd}$ the number $d$ component of the best position the group particles have ever found; $w$ denotes the inertia weight factor.

The procedure of standard Particle Swarm Optimization is given as following:

Step1: Initialize the original position and velocity of particle swarm;

Step 2: Calculate the fitness value of each particle;

Step 3: For each particle, compare the fitness value with the fitness value of *pbest*, if current value is better, then renew the position with current position, and update the fitness value simultaneously;

Step 4: Determine the best particle of group with the best fitness value, if the fitness value is better than the fitness value of *gbest*, then update the *gbest* and its fitness value with the position;

Step 5: Check the finalizing criterion, if it is satisfied, quit the iteration; otherwise, return to step 2.

### *B. Tuning of the Parameters $K_p$, $K_i$, $K_d$ and $K_a$*

Our tuning strategy is based, in the first place, on Kitti's or Jung-Dorf tuning methods for setting the parameters $K_p$, $K_i$, $K_d$ and $K_a$ of the fractional $PI^{\lambda}D^{\mu}A$ controller for λ=μ=1 which means setting the parameters fo a simple classical PIDA controller.

### *C. Tuning of the parameters λ and μ*

With the parameters $k_p$, $k_i$, $k_d$ and $k_a$ obtained in the first step, we use the PSO algorithm [15] to determine the optimum settings of the fractional integration action order λ and the fractional differentiation action order μ of the fractional order $PI^{\lambda}D^{\mu}A$ controller. The PSO algorithm consists of finding, for a linear system, a controller minimising the IAE of a classical unity feedback control system for a unit step input. The IAE is given as:

$$Min\ J = Min\left[\int_0^{\infty} |e(t)|dt\right] \quad (9)$$

Where $e(t)$=[$r(t)$-$y(t)$] is the error signal.

## IV. ILLUSTRATIVE EXAMPLE

In this section, we will present two simulation examples for the same system by using two tuning methods of classical PIDA controller; this is to show the effectiveness of the proposed design method of the fractional PIDA controller in the performance enhancement of the feedback control system.

A simplified induction motor position control proposed in [6] is used. The transfer function of the induction motor is given as:

$$G(s) = \frac{168.0436}{s(s^2 + 25.921s + 168.0436)} \quad (10)$$

### *A. Case 1:*

In this case, first the parameters λ and μ are set to be λ=μ=1, which means the fractional order $PI^{\lambda}D^{\mu}A$ controller becomes a classical PIDA controller. Then using Jung-Dorf tuning method [6], the parameters $k_p$, $k_i$, $k_d$ and $k_a$ are found to be $k_p$=12.2383, $k_i$=21.8548, $k_d$=2.4601 and $k_a$=0.1268. For this case, the fractional order $PI^{\lambda}D^{\mu}A$ controller's transfer function becomes:

$$C_F(s) = 12.2383 + 21.8548\frac{1}{s^{\lambda}} + 2.4601 s^{\mu} + 0.1268 s^2 \quad (11)$$

To set the parameters λ and μ using our proposed method, $C_F(s)$ is approximated by a rational function using the method proposed in section II.

From the simulation results, the minimum IAE index $J(\lambda,\mu)$ obtained, using PSO algorithm, correspond to the couple (λ,μ)=(0.0750,0.2553). Then the fractional order $PI^{\lambda}D^{\mu}A$ controller's transfer function $C_F(s)$ required is given as:

$$C_F(s) = 12.2383 + 21.8548\frac{1}{s^{0.0750}} + 2.4601 s^{0.2553} + 0.1268 s^2 \quad (12)$$

Fig. 2 shows the step responses of the closed-loop control system with both the classical PIDA and the fractional order $PI^{\lambda}D^{\mu}A$ controllers in its rational form. Apparently, the fractional order $PI^{\lambda}D^{\mu}A$ controller shows a superior performance than the conventional PIDA controller, for the set-point response.

For feedback control performance enhancement comparison, we have summarised some performance characteristics in Table I for the feedback control system with both controllers. It can be noticed that the fractional order $PI^{\lambda}D^{\mu}A$ controller obtained from the proposed tuning method can provide very satisfactory response better than


ISSN 1737-9334

the classical PIDA controller in terms of overshoot (O%), settling time (St) and rise time (Rt).

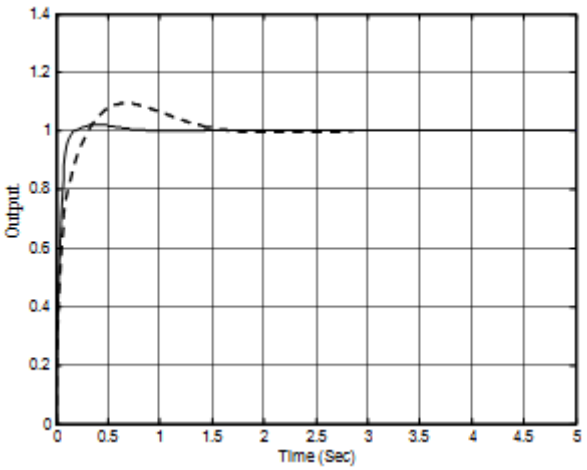


Fig. 2 Step responses of the closed-loop system with a classical PIDA controller (dashed line), and fractional $PI^{\lambda}D^{\mu}A$ controller (solid line)

TABLE I
TEMPORAL CHARACTERISTICS

| Controller | Rt(0.1:0.9) | St (2%) | O % | J |
|---|---|---|---|---|
| PIDA | 0.181 | 1.38 | 9.48 | 0.0714 |
| $PI^{0.075}D^{0.2553}A$ | 0.0791 | 0.486 | 2.29 | 0.0114 |

*B. Cas2:*

In this case, first the parameters λ and μ are set to be λ=μ=1, which means the fractional order $PI^{\lambda}D^{\mu}A$ controller becomes a classical PIDA controller. Then using Kitt's tuning method [6], the parameters $k_p$, $k_i$, $k_d$ and $k_a$ are found to be $k_p$=5.6672, $k_i$=9.3764, $k_d$=0.7027 and $k_a$=0.0248. For this case, the fractional order PIDA controller's transfer function becomes:

$$C_F(s) = 5.6672 + 9.3764\frac{1}{s^{\lambda}} + 0.7027 s^{\mu} + 0.0248 s^2 \qquad (13)$$

To set the parameters λ and μ using our proposed method, $C_F(s)$ is approximated by a rational function using the method proposed in section II.

From the simulation results, the minimum IAE index J(λ,μ) obtained, using PSO algorithm, correspond to the couple (λ,μ)=(0.0370,0.5663). Then the fractional order $PI^{\lambda}D^{\mu}A$ controller's transfer function $C_F(s)$ required is given as:

$$C_F(s) = 5.6672 + 9.3764\frac{1}{s^{0.037}} + 0.7027 s^{0.5663} + 0.0248 s^2 \qquad (14)$$

Fig. 3 shows the step responses of the closed-loop control system with both the classical PIDA controller and the fractional order $PI^{\lambda}D^{\mu}A$ controller in its rational form. The performance improvement of the proposed fractional order $PI^{\lambda}D^{\mu}A$ control structure for set point change is clear.

For feedback control performance enhancement comparison, we have summarised some performance characteristics in Table II for the feedback control system with both controllers. It can be noticed that the fractional order $PI^{\lambda}D^{\mu}A$ controller obtained from the proposed tuning method can provide very satisfactory response better than the classical PIDA controller in terms of smoothest and fastest response.

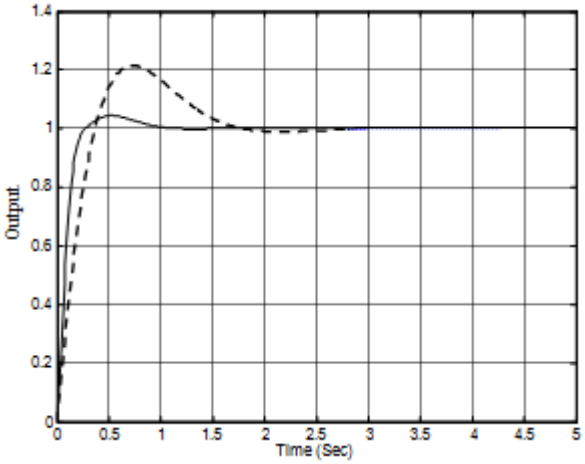


Fig. 3 Step responses of the closed-loop system with a classical PIDA controller (dashed line), and fractional $PI^{\lambda}D^{\mu}A$ controller (solid line)

TABLE III
TEMPORAL CHARACTERISTICS

| Controller | Rt(0.1:0.9) | St (2%) | O % | J |
|---|---|---|---|---|
| PIDA | 0.278 | 1.59 | 21 | 0.3234 |
| $PI^{0.037}D^{0.5663}A$ | 0.151 | 0.805 | 4.4 | 0.1107 |

## V. CONCLUSION

In this paper fractional order $PI^{\lambda}D^{\mu}A$ controller have been introduced. The novelty of the proposed controllers consists in the extension of integration and derivation order from integer to fractional numbers. This fact opens the way in the designing of more flexible class of controllers and therefore towards the solution of wider variety of control problems, such as, for example, the control of processes with resonances, integrators and unstable transfer functions.

Our proposed fractional order $PI^{\lambda}D^{\mu}A$ controller is a generalization of the classical PIDA controller. The presented tuning method of the proposed fractional order $PI^{\lambda}D^{\mu}A$ controller is based on the idea of using Jung-Dorf or Kitt's tuning methods and PSO algorithm. The parameters $k_p$, $k_i$, $k_d$ and $k_a$ of the fractional order $PI^{\lambda}D^{\mu}A$ controller for λ=μ=1, which means setting the parameters of the classical PIDA controller, have been computed from Jung-Dorf or Kitt's tuning methods and the remaining parameters λ and μ


ISSN 1737-9334

have been found from an optimization problem using PSO algorithm.

Values of the fractional order $PI^{\lambda}D^{\mu}A$ controller parameters are tuned to achieve better step response. The simulation results demonstrated that the fractional order $PI^{\lambda}D^{\mu}A$ controller has better response than the classical PIDA controller.

Our further research efforts include: testing on more type's criterions, experiment on real plants.

## REFERENCES

[1] J.G. Ziegler and N.B. Nichols, 'Optimum Settings for Automatic Controllers', Transactions of the ASME, 64,759–768. 1942.

[2] K.J. Astrom and T. Hagglund, *PID Controllers: theory, design and tuning*. Instrument Society of America, Research Triangle Park, North Carolina, U.S.A. 1995.

[3] A. Dwyer, *Handbook of PI and PID controller tuning rules*. Imperial College Press, London. 2003.

[4] S. Jung, and R.C. Dorf, Analytic PIDA controller design technique for a third order system. *Proceedings of the* 35*th IEEE Conference on Decision and Control*, Kobe, pp. 2513-2518. 1996.

[5] P. Ukakimaparn, P. Pannil, P. Boonchuay and T. Trisuwannawat, PIDA controller designed by kitti's method. In: ICCAS-SICE.pp.1547-1550. 2009.

[6] D.K. Sambariya and D. Paliwal, Comparative Design and Analysis of PIDA Controller Using Kitti's and Jung-Dorf Approach for Third Order Practical Systems. *British Journal of Mathematics & Computer Science* Vol.16, N° 5, pp.1-16. 2016.

[7] K.S. Miller and B. Ross, An Introduction to the Fractional Calculus and Fractional Differential Equations, New York: Wiley. 1993.

[8] K.B. Oldham, and J.Spanier, The Fractional Calculus, New York: Academic Press. 1 974.

[9] A. Oustaloup, La Commande CRONE, Paris: Herme`s (In French). 1991.

[10] I. Podlubny, 'Fractional Order Systems and $PI^{\lambda}D^{\mu}$ Controllers', IEEE Transactions on Automatic Control, 44(1), 208–214. 1999.

[11] I. Petras, and B.M. Vinagre, 'Practical Application of Digital Fractional-order Controller to Temperature Control', Acta Montanistica Slovaca, 7(2), 131–137. 2002.

[12] C.A. Monje, B.M. Vinagre, V. Feliu and Y.Q. Chen, Tuning and Autotuning of Fractional Order Controllers for Industry Applications. *Control Engineering Practice*, 16, pp. 798–812. 2008.

[13] F. Padula, and A. Visioli, Tuning rules for optimal PID and fractional order PID controllers. *Journal of Process Control.* Vol. 21, No.1, pp.69-81. 2011.

[14] A. Neçaibia, and S. Ladaci, Self-tuning fractional order $PI^{\lambda}D^{\mu}$ controller based on extremum seeking approach. *International Journal of Automation and Control* , Vol.8, N° 2 , pp. 99–121. 2014.

[15] J. Kennedy and R. C. Eberhart, Particle swarm optimization. *Proc. Of IEEE Int. Conf. on Neural Networks*, pp.1942-1948. 1995.

[16] A. Charef, H.H. Sun, Y.Y. Tsao and B.Onaral, Fractal system as represented by singularity function. *IEEE Tran. On Auto. Cont*. Vol. 37, N°9, pp. 1465-1470. 1992.




ISSN 1737-9334

# Design, Analysis and Evaluation of Results of Vivaldi Antenna for Millimeter Band Application

Nafaa M. Shebani [1], Feras A. Osman[2] and Amer R. Zerek[3]

[1]Electrical & Electronic Eng. Department, Sabratha University, Sabratha, Libya
E- mail nafah@yahoo.com
[2] College of Electronic Technology, Communication Engineering Department, Tripoli, Libya
E-mail Feras.Osman750@gmail.com
[3]Zawia University, Faculty of Engineering/ EE Department,, Zawia, – Libya,
E-mail anas_94az@yahoo.co.uk

***Abstract* - Characteristics of the antenna is one of the most important factors which should be considered in millimetre band. Extremely high frequency (EHF) has a number of applications that make it attractive for a variety of applications such as ground penetrating radars (GPR), remote sensing and phased arrays. This paper offered the design of a tapered slot Vivaldi antenna for millimetre wave application of which operates in GHz to achieve high performance in terms of bandwidth and directivity. Designed Vivaldi Antenna works in the frequency band of 42.2-50 GHz. All simulations are carried out by CST microwave studio software to obtain the voltage standing wave ratio (VSWR). Obtained VSWR Ranges from 1 to 2 and high directivity level ranges from 5.3 dBi at 45 GHz to 5.47 dBi at 48.5 - 50 GHz which shows the Progress in directivity and upper frequency range coverage. The Proposed Vivaldi antenna displays steady radiation pattern throughout the frequency band. The VSWR characteristic and Far-field radiation pattern are plotted to realize the antenna Mechanism.**

***Keywords* -**Vivaldi antenna, Exponentially, TSA, GPR, Radar, Bandwidth, Dielectric, Frequency , VSWR , Return loss , Radiation pattern , Directivity , Gain, Far-field.

## I. INTRODUCTION

The Vivaldi antenna is appropriate for a special category of Tapered slot antenna (TSA) which having exponential flares profile. In the area where the separation between conductors is lesser related to the free-space wavelength , the waves are strongly bound and if the separation rises, the bond turn out to be gradually weaker and the waves become radiated away from the antenna[2].It is economical to manufacture and can deal with high directivity and wideband Performance [3]. The Vivaldi antenna, initially presented by Gibson in 1979[4] contains of a tapered slot arrangement where the slot Boundary has an exponential profile. The Vivaldi antenna has the benefits of being a very simple and compact planar Configuration, which has a high directivity, wide bandwidth, and linear polarization. Vivaldi antenna delivers a flat Transition between the radiated plane wave and guided wave which is drifting in the slot transmission line. Desired impedance and pattern bandwidths have been realized by width, optimizing length and tapered shape of aperture. The detection of the buried object located near the ground surface as well as small and low-contrast landmines needs to use higher frequencies to achieve a better resolution. The TSA attracts much attention in GPR application due to its low cost, low weight, simple fabrication, compactness, wideband properties and end-fire radiation. A compact TSA for GPR applications, which has large bandwidth and small size, besides, more stable in the energy.

## II. ANTENNA GEOMETRY & DESIGN PARAMETERS

Taper of the slot line transmission line can be described as an exponential function, earning the antenna the name exponentially tapered slot antenna or Vivaldi antenna [5], the antenna utilizes a micro strip feed to excite the slot line. The micro strip feed uses one conductor of the slot line as a ground plane and connects to the other side via a shorting pin, which is done at the narrowest part of the slot. The gradualness of the taper is described by a constant referred to as taper rate. The taper rate dictates the beam width of the antenna [17]. The maximum separation between the slot line conductors is equivalent to a free space half wavelength of the lowest operating frequency. Vivaldi antenna is considered as Two dimensional exponential curve, can be better understand by given below Fig.1 and equation where 'S' is the distance between origin and y-intercept, but in antenna prospective view 'S' is the half Of the slot width of Vivaldi.

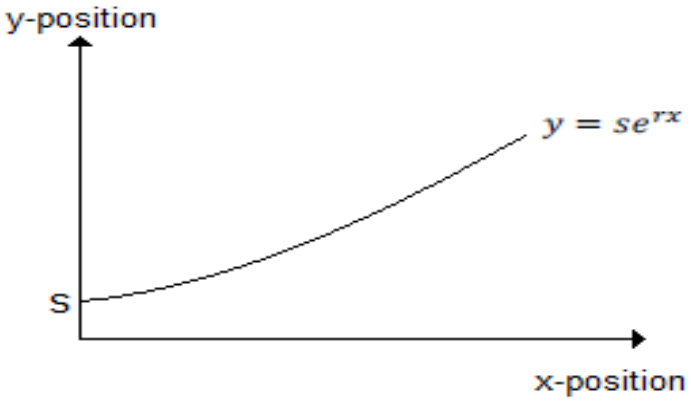


Fig.1: Two dimensional Cartesian plots for exponential curve

Now this equation ($y = se^{rx}$) converted into parametric


ISSN 1737-9334

Equation in three dimension with set up of this given equation (1), (2) and (3)

$$\upsilon(t) = t \quad (1)$$

$$\nu(t) = se^{rx} \quad (2)$$

$$\omega(t) = 0 \quad (3)$$

Where υ, ν and ω are the three positions.
Now keeping in mind above figure and equations it can be transformed into tapered exponential profile of Vivaldi Antenna which can be defined by equation (4)

$$f(x) = c_1 e^{Rx} + c_2 \quad (4)$$

Where Coefficient $c_1$ and $c_2$ is given by equation (5) and (6)

$$c_1 = \frac{y_2 - y_1}{e^{Rx_2} - e^{Rx_1}} \quad (5)$$

$$c_2 = \frac{y_1 e^{Rx_2} - y_2 e^{Rx_1}}{e^{Rx_2} - e^{Rx_1}} \quad (6)$$

As the electrical length of the antenna increases with frequency the gain increases. The length of antenna will be the addition of taper length, balun length, feed length, backwall offset and width must be equal to $\lambda_0$, where $\lambda_0$ is the free space wavelength at the low frequency. The exponential taper profile is determined by $(x_1, y_1)$ and $(x_2, y_2)$ Where R is the Rate of tapering, $(x_1, y_1)$ is the starting point of taper and $(x_2, y_2)$ is end point of Taper.

W is the width of tapered slot antenna which must satisfy the Given equation (7)

$$W < \frac{c}{f_H \sqrt{\varepsilon_e}} \quad (7)$$

Where $\varepsilon_e$ is the effective relative dielectric constant.
Now to transform the above equation into real Antenna we are using CST microwave studio [2] [6]. The Structure of the proposed Vivaldi Antenna is shown in Fig.2 and Fig.3 respectively. Fig.2 displays the front view of Proposed designed antenna and fig.3 displays the 3D view of proposed designed antenna.

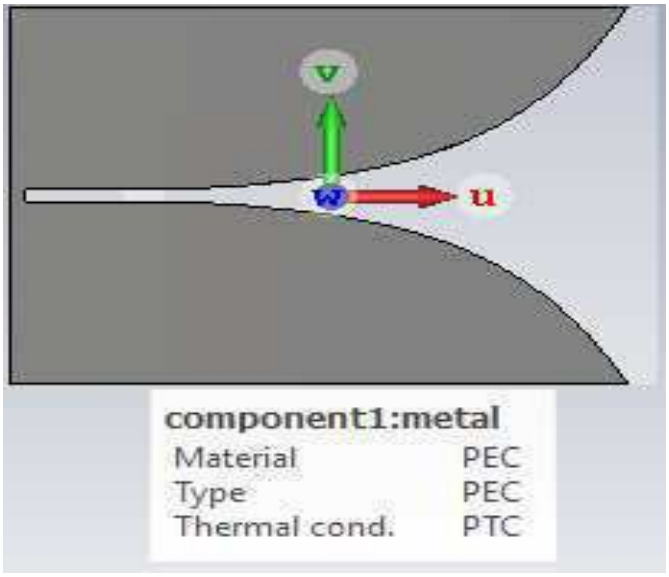

Fig.2: Front view of designed Vivaldi Antenna

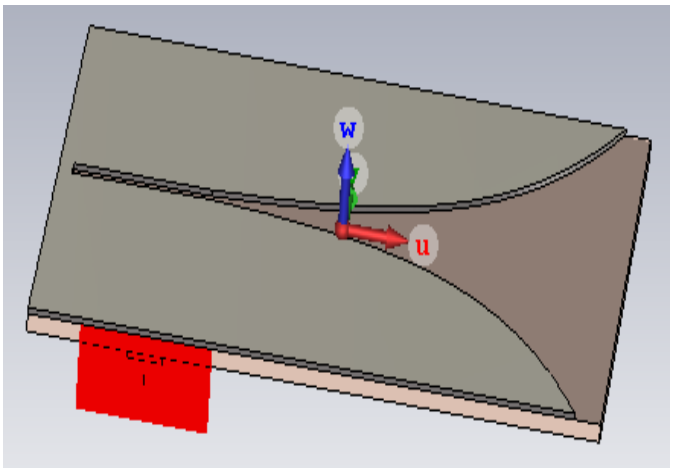

Fig.3: 3D view of designed Vivaldi Antenna

Geometry of Vivaldi antenna [7][8] A tapered slot patch dimensions with thickness 't' and substrate of dimensions with thicknesses 'h' are shown in below fig. 4. Permittivity value $\varepsilon_r$ is taken as 3.78 and loss tangent tanδ is considered as 0.001 for better performance of designed antenna. Thickness of micro-strip line and tapered slot patch is taken as 0.035 mm. The antenna was optimized In order to


ISSN 1737-9334

achieve a transition that has low return loss over a wide frequency band of 42.2-50 GHz, the impedances of the micro strip line and the slot line must be matched to each other to reduce the reflections. The characteristic impedance of a slot line increases with increasing slot width, so the width of slot line must be selected to be as small as possible to achieve an impedance value close to 40Ω. The width, characteristic impedance and guided wavelength of slot-line are calculated with procedures suggested in [9]. The strip-line feed used in a Vivaldi antenna is either connected directly to the transmitter/ receiver circuitry or is fed by a coaxial cable attached to a connector. The strip-line width and guided wavelength is calculated using formulas given in [10].

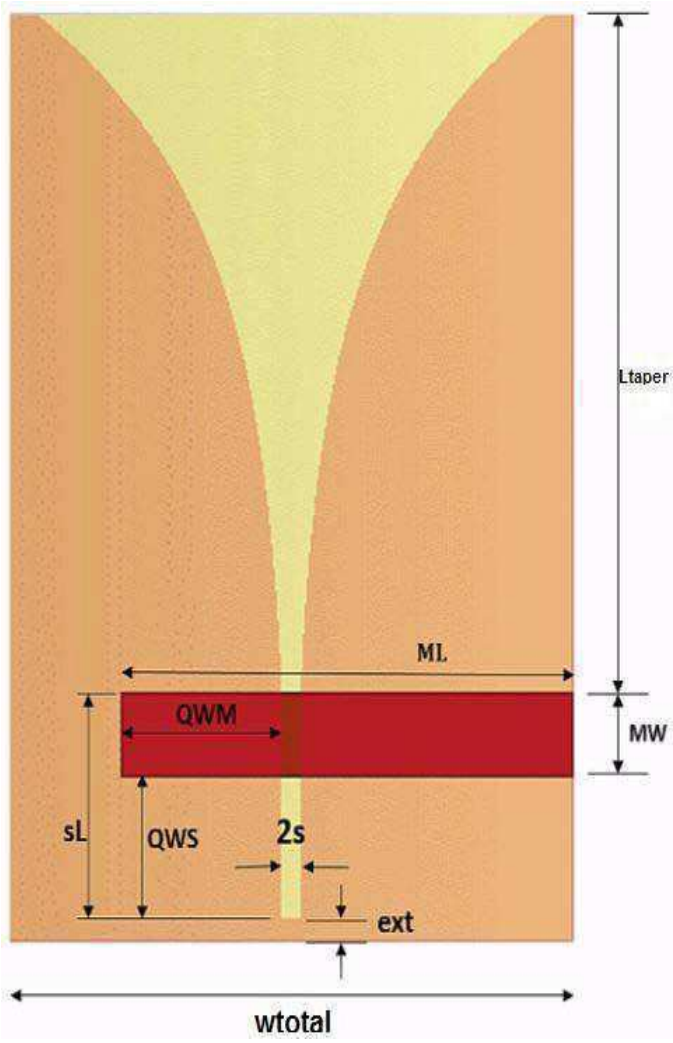


Fig.4: Geometry of the proposed antenna.

The material used in substrate is low cost PEC (Perfect electric conductor) material is used for exponential tapered section and for microstrip section.

The design parameters are given in Table1 shown below.

| Antenna Design Parameters | | |
|---|---|---|
| ***Index*** | ***Value*** | ***Unit*** |
| r | 1.1208 | mm |
| s | 0.05 | mm |
| sL | 1 | mm |
| TL | 3 | mm |
| subw | 3 | mm |
| ext | 0.1 | mm |
| s | 0.05 | mm |
| sL | 1 | mm |
| TL | 3 | mm |
| QWM | 0.9 | mm |
| h | 0.1 | mm |
| ML | *QWM + s + subw /2* | mm |
| MW | 0.25 | mm |
| QWS | 0.75 | mm |

## III. RESULTS AND DISCUSSIONS

The Vivaldi antenna is simulated mathematically with the CST software to examine VSWR, the return loss and far-field radiation characteristic over the frequency band of 42.2-50 GHz. The term VSWR is a quantity that defines how well an antenna is impedance matched to the transmission line it is associated to. Fig.5 shows the VSWR behaviour over the frequency range of 42.2 - 50 GHz. It is clearly seen that VSWR at frequencies 45 GHz, 43.378GHz, and at 48.407 GHz are found to be 1.0046, 1.4371, and 1.6641 respectively. All the obtained VSWR value is less than 2 which is required.

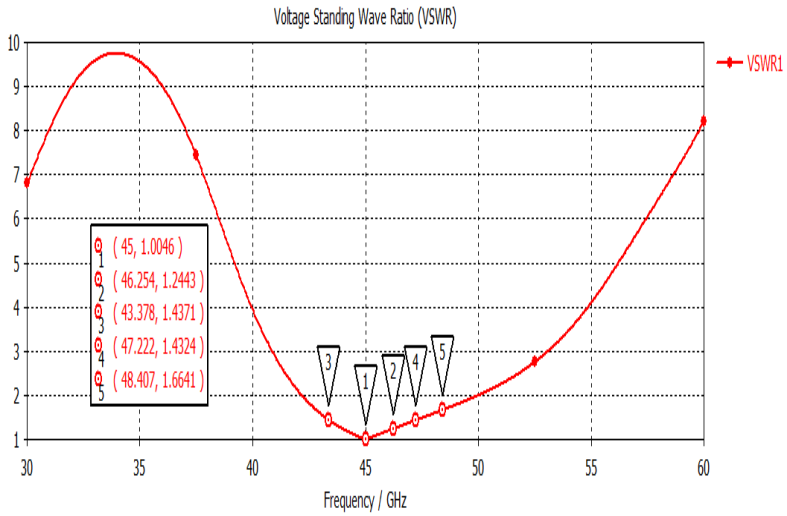


Fig.5: VSWR.




ISSN 1737-9334

The Fig.6 shows the S-parameter of the antenna. The return loss of the antenna is minimum at 45 GHz

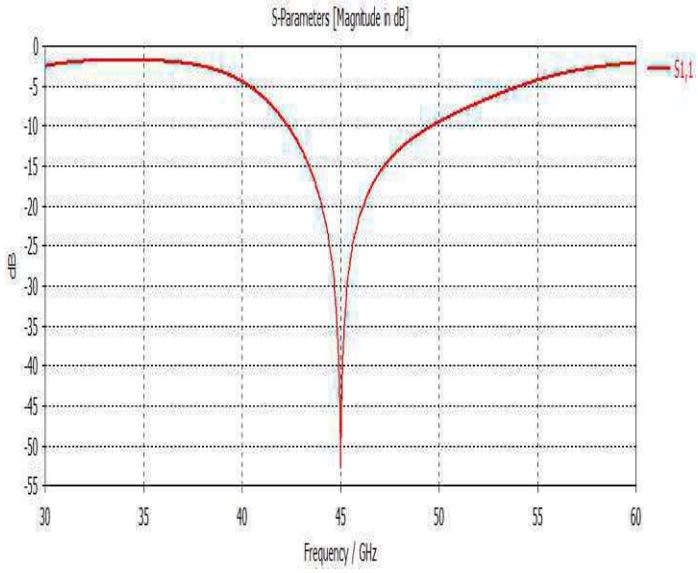


Fig.6: Return loss (S11) and steady state parameters.

Fig.7 shows the far field radiation pattern study at three different frequencies 45, 47, 48.5 GHz. 3-D view. Red color pattern in 3-D view shows the maximum directivity along the x-axis at three different frequencies. The directivity of these main lobes is different for the selected frequencies. It is maximum in case of 48.5 - 50 GHz (5.47 dBi) and minimum in case of 45 GHz (5.30 dBi) along both positive x-axis and negative x-axis. Also Directivity is found to be 5.44 dBi in case of 47 GHz frequency. Additionally it can be observed the radiation pattern is symmetric along the x-axis. The use of this outcome delivers us an extensive flexibility at the time of design of Vivaldi Antenna at Extremely high frequency. These simulated results will play important role in application where need particular directivity along the required direction.

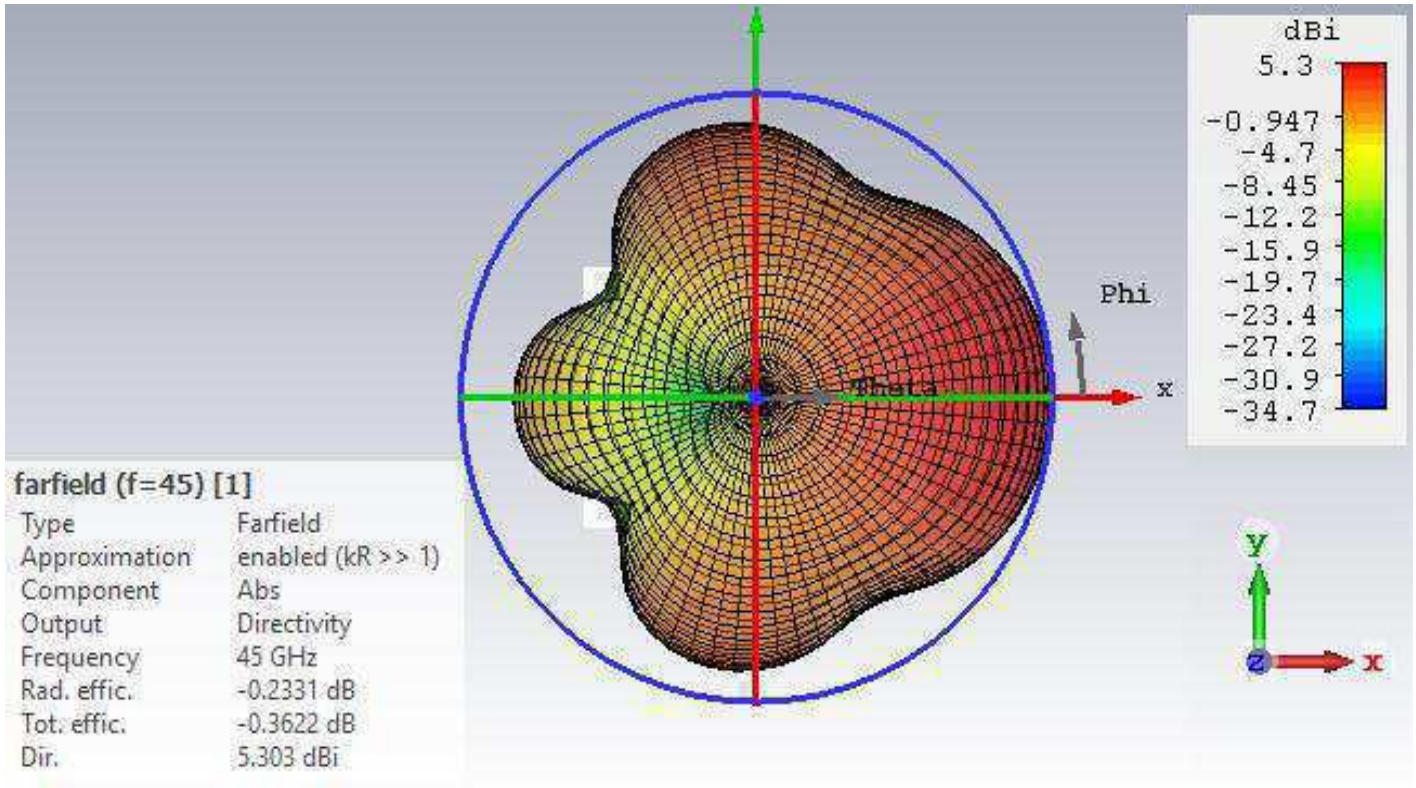


(a)




ISSN 1737-9334

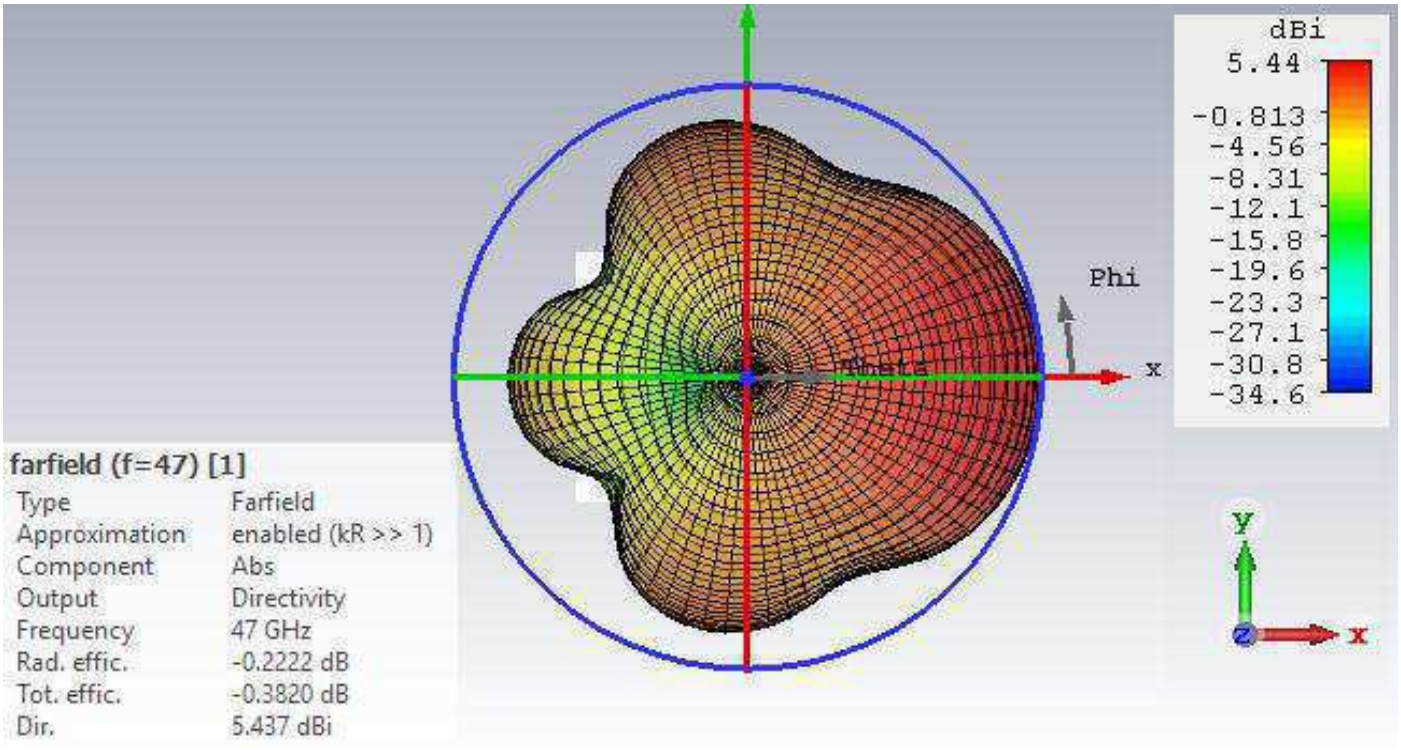


(b)

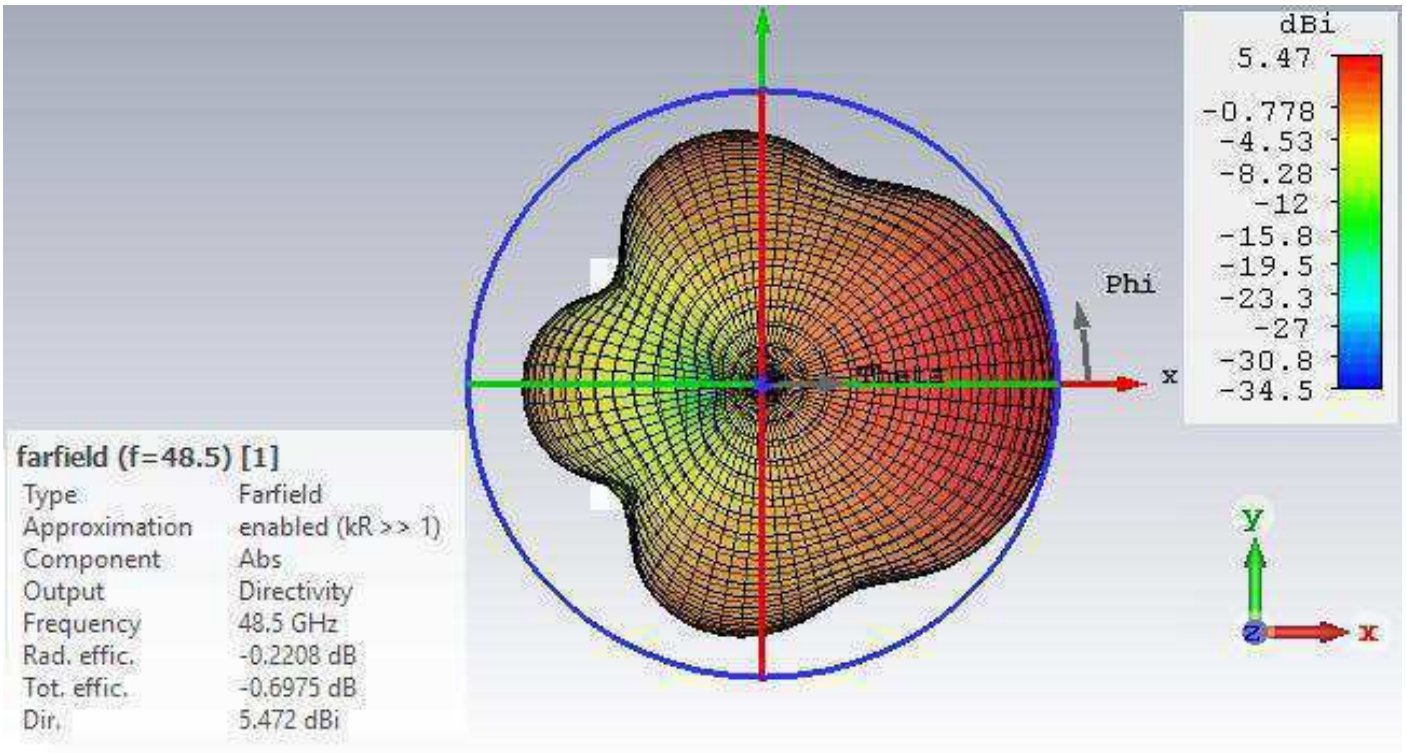


(c)

Fig.7: Simulated radiation patterns of the Vivaldi antenna. (a) 45 GHz. (b) 47GHz. (c) 48.5GHz.




ISSN 1737-9334

Fig.8 shows the realized gain of the proposed Vivaldi Antenna, it is observed that due to the loading of the corrugation on the edges of tapering and grating elements on the slot area, the realized gain of the antenna improved significantly throughout the operating frequency band of 42.2-50 GHz. radiation minimizes in the direction other than the bore sight direction which results in the improved realized gain and directivity of antenna in the bore sight direction. The realized Gain was achieved by three different frequencies at 45, 47, 48.5 GHz. the realized gain is maximum in case of 47 GHz (5.06 dB) and minimum in case of 48.5 GHz (4.77 dB) along both positive x-axis and negative x-axis. Also realized gain is found to be 4.94 dB in case of 45 GHz frequency.

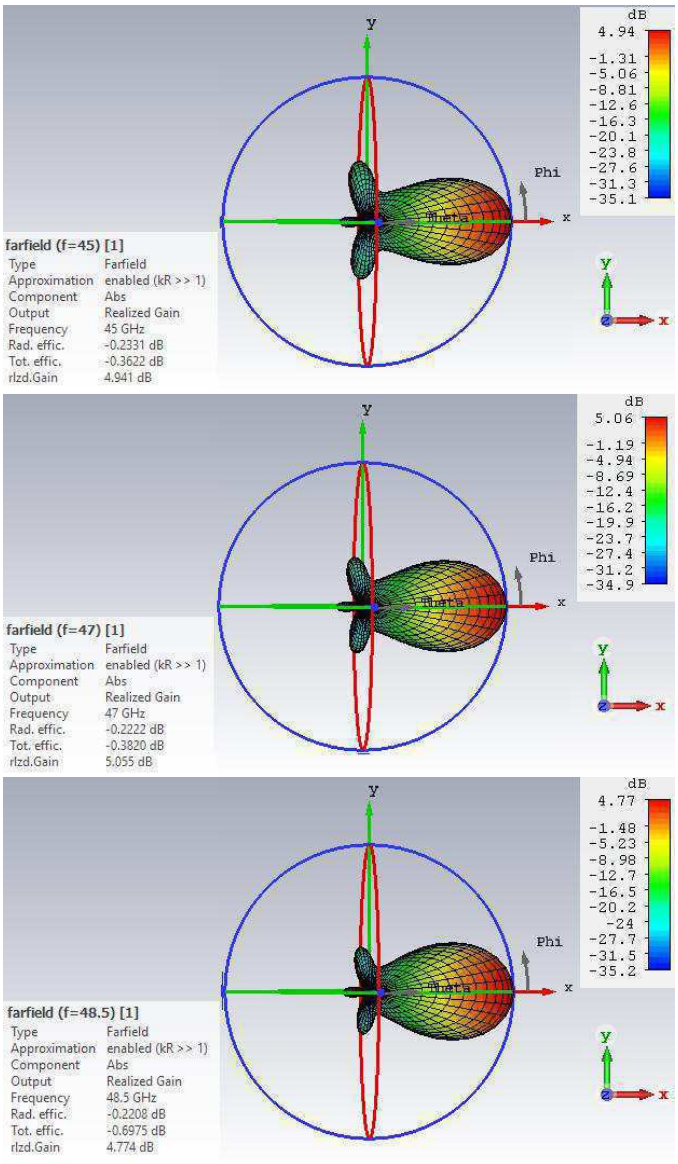


Fig.8: The realized gain for three different frequencies

## IV. CONCLUSION

In this paper, a Vivaldi antenna was simulated with at a-Extremely high frequency range from 42.2-50 GHz , so that can define how well is an antenna is impedance matched to the Transmission line it is associated with. Also far field radiation characteristics have been analyzed. The designed Vivaldi antenna has a wide bandwidth, impedance matching and relatively high directivity at the 45 GHz and the realized Gain of 4.9 dB, Additional enhancement are needed to increase the achieved low values of gain by transforming the antenna geometry structure and by means of new type of materials with lesser loss at high frequencies. VSWR and the radiation pattern of the antenna has been plotted to realize the antenna operating principles. The proposed antenna can be used not only in GPR "Imaging and Diagnosis" but also it can be used in various optical applications where need wave's generation at Extremely high frequency.

## REFERENCES

[1] N. V Venkatarayalu and G. Yeow-Beng, "Design of a tapered slot array antenna for UWB through-wall RADAR," Antennas Propag. Soc. Int. Symp. (APSURSI), 2010 IEEE, pp. 1–4, 2010.
[2] M. Moosazadeh and S. Kharkovsky, "Design of Ultra-Wideband Antipodal Vivaldi Antenna for Microwave Imaging Applications," in 2015 IEEE International Conference on Ubiquitous Wireless Broadband, ICUWB 2015, 2015.
[3] R. H. Johnston, "Efficiency simulations on a vivaldi antenna in a wheeler cap," in IEEE Antennas and Propagation Society, AP-S International Symposium (Digest), 2009.
[4] P. J. Gibson, "The Vivaldi Aerial," in 9th European Microwave Conference, 1979, 1979, pp. 101–105.
[5] N. Vignesh, G. A. Sathish, and K. R. Brindha, "Design and Development of a Tapered Slot Vivaldi Antenna for Ultra-Wide Band Application," Int. J. Adv. Res. Comput. Sci. Softw. Eng., vol. 4, no. 5, pp. 2277–128, 2014.
[6] W. Sorgel, C. Waldschmidt, and W. Wiesbeck, "Transient responses of a Vivaldi antenna and a logarithmic periodic dipole array for ultra wideband communication," IEEE Antennas Propag. Soc. Int. Symp. Dig. Held conjunction with Usn. North Am. Radio Sci. Meet. (Cat. No.03CH37450), vol. 3, no. 1, pp. 592–595, 2003.
[7] M. S. Nepote, D. R. Herrera, D. F. Tapia, S. Latif, and S. Pistorius, "A comparison study between horn and vivaldi antennas for 1.5-6
[8] GHz breast microwave radar imaging," in 8th European Conference on Antennas and Propagation, EuCAP 2014, 2014, pp. 59–62. Y. Yang, Y. Wang, and A. E. Fathy, "Design of Compact Vivaldi Antenna Arrays for Uwb See Through Wall Applications," Prog. Electromagn. Res., vol. 82, pp. 401–418, 2008.
[9] R. Janaswam, Student Member, D.H. Schaubert, Senior Member "Characteristic Impedance of a Wide Slot Line on Low Permittivity Substrates" Department of Electrical and Computer Engineering University of Massachusetts Amherst, MA 01003.
[10] David M Pozar, "Microwave Engineering", 3rd Edition, John Wiley & Sons: 2008.




ISSN 1737-9334

# *Role of Media Literacy in Teaching an d Learning English in Libya*

Youssif Zaghwani Omar (PhD)
Department of English
Faculty of Arts
University of Benghazi
Benghazi, Libya
Youssif.omar@uob.edu.ly

***Abstract*– We are living in the 21st century, the era of technology and the Internet, in which people share ideas, thoughts, and beliefs with moments through media. Media, nowadays, represent an integral part in our life and involve in all facets of life, including education. Media have changed the concept of literacy from knowing how to read and write into knowing how to read and write and use media for analyzing and responding to messages. Thus, this paper is focusing on the use of media literacy in education. The researcher, in this paper, uses qualitative research method, in which he bases on literature review as a secondary resource and interviewing ten Libyan teachers of English, who were teaching English language courses at English language center in Benghazi, Libya, as a primary resource. The paper has gained some findings regarding the topic of the study. Based on the findings obtained, the researcher presents some recommendations regarding the importance of involving media literacy in education.**

***Keywords– Media literacy; media; technology; Internet; literate***

## I. RATIONALE

It is a matter of fact that people in the 21st century live in an era of technology almost dominated by the Internet. Media have become indispensible in our life in this era in a way that they become an integral part of our culture. In this regard, Fox (2001) emphasizes that "media and technology make up two main ingredients of our culture" (p. 192). People all over the world, however, reach information fast via technologies in a form of a powerful combination of images and sounds. In this era, it is inevitable that people use and create a wider set of literacy skills for producing messages and benefiting from the technological devices for understanding and analyzing the received messages.

Media, in fact,not only affect on our perception, but also they shape our thinking and images to the reality in a way in which we organize our ideas and beliefs about that reality. Media, in fact, have changed the concept of a literal person from the one who is able to read and write to add being acquainted and deal with messages sent and received by media. Accordingly, media literacy, with no doubt, has become a main part in the field of education, namely in teaching and learning languages. In this regard, Neal (2011) said, "Whether it is widely implemented or not in educational contexts, hypermedia pervades our lives and that of our students. As such, many composition and other writing classes include everything from writing websites to podcasts, blogs, wikis, social networking, digital video, and social bookmarking" (p. 93).

## II. LITERATURE REVIEW

A lot of research and studies have emphasized the importance of involving media in education, namely learning foreign languages. Media literacy, nowadays, has become an integral part in the process of learning and teaching foreign languages. Thus, this part introduces the literature review regarding media literacy in education.

### *A. Introduction*

Marzano, Pichering, and Polloch (2001) believe that "one of the best ways to learn a new word is to associate an image with it" (p. 126). Fox (2000), also, confirms that "an important focus of faculty development must be on the use of media literacy to teach print literacy" (p. 163). Similarly, several studies and research on firm that students use language more effectively when they believe in what they are writing or speaking about. In contrast,




ISSN 1737-9334

students become helpless and ineffective users of language when they write or talk about something they do not believe in, are not interested in, or have no background about. Talking or writing about a wedding party in the English culture, for example, without seeing a film or attending a wedding party in reality seems challenging for international students even when they theoretically study about English wedding parties in the classroom. International students, who come from different cultures, find themselves helpless to talk or write about this experience because they are guided and controlled by their deeply-rooted beliefs about wedding parties in their own cultures.

In fact, it is not incapability of using English that hinders international students from talking or writing about that experience; rather, it is incapability of thinking of that experience without seeing it in reality or knowing about it through the media: TV, Internet, movies, and the like. In this regard, Mayer (2003) argues that students learn more effectively from media that present both words and pictures than the media that present only words. This indicates that learners process visual and verbal knowledge in their brain in different ways and create different representations to the same reality.

*B. Media*

Dictionary defines "medium" as "anointer vening means, instrument or agency". This definition indicates that a medium is a channel that carries or transmits information. So, a medium is an instrument people use to send or receive a message. The dictionary defines "media" as the plural form of "medium." Media, then, provide channels for transmitting representations and images about the reality in various versions. Thus, media have a great effect on shaping individuals' understanding to the reality. The word, in its wider sense, includes all channels of communication: television, radio, computer, internet, cinema, advertising, games, photography, video, recorded music, newspapers, books, magazines, and many others.

The concept "media", in its wider sense, indicates the process of collecting, carrying, and delivering information through transmission channels. "Media", in its narrower sense, indicates the process of transmitting messages through all electronic or digital devices, such as Internet, still images, animation, audio, mobile devices, interactive graphics, videos, software programs, and the like used to transmit messages. Media, in fact, have become indispensible in this era, namely for children because, asFox (2000) believes, media "influence what kids think about other types of people – how they imagine what others are like, how they respect differences in others, how they communicate with others, how they treat others" (p. 13).

Reid (1994) defines media as "all means of communication, whatever its format" (p. 51). So, media might include TV, video, movie, Internet, and the like. According to Masats, Dooly, and Costa (2009), media offer "learners the opportunity of observing the dynamics of interaction (discourse modes, gazes, gestures, registers, paralinguistic cues, etc.) in context" (p. 344). Gordon (2007) focuses on the role of media in learning foreign languages and finds out that students enjoy learning languages through video. Whereas, Fox (2000) believes that the use of media "is highly intertextual because it often borrows from other sources" (p. 181).

Yunus, Salehi, and John (2016) conduct a study on Malaysian students who learn English as a second language in Malaysia. They find out that using pictures and video projects are beneficial for learning English literature. They notice that using visual aids motivates students to read English texts with interest. Visual aids have proven to be a great tool for enriching and enhancing reading skills. Visual aids, in fact, provide authentic situations to students to live the English culture and understand the English texts, accordingly. They, hence, recommend involving media in teaching and learning English.

Similarly, Frau-Meigs (2006) believes that media "play an important part in the socialization of young people, a phenomenon which has been gaining in momentum. A large part of the cultural capital of the planet is passed on to them by many kinds of vehicles with which they are very familiar" (p. 7). For that reason it is recommended that teachers use different kinds of media in the classroom and change the classroom into a cross-cultural classroom through media. Teachers, for example, can make the classroom an interesting place and film adaptation, so students are given "an opportunity to study some of the best examples of fiction and film, see how fiction leads to film, and consider the sort of choices that contribute to excellence" (Slethaug, 2007, p. 142).

When we talk about media, we necessarily talk about audience, or mass media to be more precise. Mass media imply that large audiences can reach the messages transmitted. Out of this




ISSN 1737-9334

clarification of mass media, it indicates that mass media are directed to audience in non-academic situations. Mass media, according to Hooks (2010), seek to "simplify messages, so most of the complex academic issues involving diversity are never conveyed accurately or completely" (p. 106).

However, media, in the wider sense, include both digital and printed sources. So, a book is considered a kind of media as it transmits information to audience, yet it reaches a small number of audience. The Internet is another kind of media, and it reaches a large number of audiences. This implies that each kind of media has its own audience and language. Television, for instance, uses language of images and sounds, newspaper uses the language of pictures and written words, and radio uses language of sounds only.

Talking about kinds of media leads us to talk about what is called "multimedia", which involve "the use of media such as audio and video equipment (VCRs, video disk players, video cameras), computers and related software, and Internet sources to do research, publish, and make classroom presentations" (Herrell and Jordan, 2008, p. 148). Multimedia representations in the classroom, according to Herrell and Jordan, help students share ideas and information with their peers. The use of visuals of many types of media "helps students and teachers to connect vocabulary and meaning, particularly for English learners" (p. 153).

*C. Media Literacy*

The concept "literacy" was used traditionally to refer to the ability of reading and writing. Hence, one is considered literal if he or she can read and write. Nowadays, the concept "literacy" has changed to cover not only ability to read and write, but also the ability to communicate with people in the community. The concept "literacy", hence, covers all kinds of social relationships, which shift literacy from identifying and comprehending written messages into writing, reading, analyzing, inquiring, and evaluating all kinds of messages.

The concept "literacy", in fact, has gained a lot of debates and conflicts between enlightenment and critical scholarship. Those who are advocate of seeing literacy as critical relationship believe that literacy is a process of empowering and democratizing people. They believe that thanks to democratic and critical approach to media literacy, people have become selective for the messages they receive. This change in the nature of people has shifted them from passive users of message into active ones. They shift to be not only receivers of messages, but also analyzers and evaluators of messages through being participants in the messages received.

Literacy, nowadays, is associated with media. Thus, one is considered literate if he or she is able to understand, analyze, and evaluate the various languages of the messages transmitted either still or moving images, verbal sounds, or written codes. Media literacy, hence, empowers students to read not only printed materials, but also other symbolic codes of images and sounds. Media literacy, according to Frau-Meigs (2006), "aims to develop both critical understanding andactive participation. It enables young people to interpret and make informed judgments as consumers of media; but it also enables them to become producers of media in their own right" (p. 20).

Fox (2000) argues that "a key principle of media literacy is that one sign or symbol can stand for something else" (p. 184). Hobbs (2008) claims that media literacy indicates one's ability to access, analyze, evaluate, and communicate a variety of media messages through mass media. Accordingly, media literacy helps people to be both critical thinkers and creative producers of media messages for the sake of communicating ideas, thoughts, and emotions. Media literacy, hence, has expanded information and communication skill receptive to the changing nature of information in the community. Media literacy covers all facets of life; for example, it determines the skills students need in school, the competencies people need to use information at home, and the abilities workers need to be involved in the 21st century.

Abunowara (Cited in Omar, 2018) emphasizes the role of media in teaching English as "having a computer in the classroom is an asset for any teacher. With a computer in the classroom, teachers are able to demonstrate new lessons, present new materials, illustrate how to use new programs, and show new websites" (p. 204). Alharam (Cited in Omar, 2018), also, asserts that "technology can promote autonomy, but the content of technology should be purposefully selected to teach students how to set their learning goals and select their learning content using online technology" (p. 239). Similarly, Alvarado (1981) highlights the importance of using media in school, claiming that two strands run through every




ISSN 1737-9334

classroom situation. These two strands are (1) a recognition of the significance and power of the present social formation structures and how people work successfully within the frame of these structures, and (2) a recognition of the significance and latent power of all arrangements of oppositional knowledge and groupings.

Alvarado, in this context, puts the responsibility over teachers' should ersat school for providing students with specific skills to empower them not only to read and write, but also to be part of this multimedia cultural community. Of course, this requires teachers being media educators. In other words, teachers should be acquainted of how to use technology. In this regard, Shyamlee (2012) said, "With teachers' instructions leading students' thought patterns and motivating students' emotions, the multimedia technology seeks integration of teaching and learning and provides the students greater incentives" (p. 152).

Media literacy, in general, is concerning with encoding and decoding the symbols and signs transmitted through media devices, synthesizing, analyzing, and producing informed messages. The Aspen Media Literacy Leadership Institute defines media literacy as "the ability to access, analyze, evaluate and create media in a variety of forms." Of course, this definition indicates the use of critical thinking for analyzing and understanding the intended message stransmitted through media. This requires one being a media literate. The definition above, however, emphasizes the four components of media literacy, which are access, analysis, evaluation, and creation. These four components work equally in all media literacy channels. The four components might be presented as:

1. Access: Access works effectively through an active and social process, not a one-off act of facility. Establishing access permits users to develop their literacy and alert continuality of upgrading hardware and software programs.
2. Analysis: People's involvement in print and audiovisual channels are based on a range of analytic competencies. The audiovisual domain requires understanding of the technologies, languages, representations, and audiences of the media used.
3. Evaluation: To work well, access and analysis require evaluation of the use of media devices and the language used for transmitting and conveying messages.
4. Creation: People reach a full understanding of the conventions and qualities of the message submitted if they have a good background about the content of the message. Hence, media literacy provides people opportunities to create online content.

*D. History of Using Media Literacy in Education*

It is a matter of fact that we are living in the era of technology, which is characterized as 24/7 media. Youths, nowadays, spend much time in watching and using media in all their forms. A recent study estimates that children from age eight to 18 spend almost eight hours a day with entertaining media outside of school. The study concludes that media are useful not only in entertaining children, but also in providing them with information. Rideout, Vandewater, and Wartella (2003) conduct a study regarding the impact of electronic media on infants. The participants of the study were six-year old and under infants. They find out that these infants spend almost two hours per day watching TV and videos.

Kendall (2005) argues that "when overall electronic media consumption, including television and radio programs, televised sports events, movies, videotapes, audio tapes and CDs, video games, and computer website materials, is taken into account, the typical person spends over three thousand hours per year as a consumer of media products" (p. 4). This indicates the importance of media in our life.

During its long history, media literacy has had various definitions, perceptions, and names. In England, for instance, the term "media education" has been used for media literacy to include the process of teaching and learning about media. It seems that the use of the term "education" in this context indicates the importance of media as an educational technology through which people become able to understand media and be able to access, analyze, evaluate, and create messages in a wide variety of media, genres, and forms. The concept in this regard is concerned with developing people's critical and creative competencies regarding mass media, popular culture, and digital media. In 1994, The Center for Media Literacy's Beyond Blame curriculum was set up to include: knowledge literacy, copyright, Internet safety, digital knowledge, self-image, privacy, and security.

Media literacy, in fact, is old, dating back to the 1400s, the invention of printing. The Industrial Era witnessed the use of magazines and newspapers.


ISSN 1737-9334

Many educators believe that media literacy is the expansion form of literacy that results because of expansion of technology. The beginning of media literacy in education was in 1920s in former Russia. In 1930s, media literacy educators used Edgar Dale's movie in education, using the movie to help students learn how to analyze the content of the movie critically.

The end of 1950s and beginning of 1960s witnessed the use of media literacy through encouraging seminars and conferences at high schools and universities in Europe. Media literacy in education was developed in the United States in 1950s and 1960s through using "Film Grammar" approach in schools. Media literacy educators used commercial movies at schools to teach new vocabulary. Students were encouraged to understand the new vocabulary through understanding the mode, tone, plot, and characters of movies exposed.

The end of 1970s and beginning of 1980s witnessed a positive shift towards using media literacy in education. Media literacy educators evoked English language teachers to use types of media, such as TV, movies, and others in addition to print to teach English. Project Censored Program began in 1976 for providing a model of learning service to help students learn through media at high schools and universities in the United States. Later, media literacy educators used media in practical and theoretical educational work and PhD programs.

In 1980s, media literacy educators' awareness of the role of media literacy in education increased, focusing mainly on the influence of media for shaping children's behavior. They used new concepts related to media literacy in educations, such as desensitization, aiming at assisting students to understand, analyze, and critically evaluate the messages transmitted through media. By the beginning of 1990s, all states involved visual, digital, and electronic media in their curriculum framework. In 1993, a group of advocates of media literacy in the United States developed a definition of media literacy as "the ability to access, analyze, evaluate and create messages in a wide variety of forms."

The focus on role of media literacy in education continued, focusing mainly on movies due to their great effects on people in general and students in specific. A study was conducted by the British Film Institute showed the importance of media literacy in education and recommended European countries to allocate school curricula based on media. In 1997, a group of schools in the United Kingdom involved media arts, such as videogames, movies, animation, and comic scripts in their school curricula. In North America and Europe, media literacy is seen as an expanded conceptualization of literacy used for treating mass media, popular culture, and digital media as new shapes of texts that need analysis and evaluation.

In 2001, the UNESCO conducted a survey about involving media literacy in education. The survey was distributed on 72experts in the field of media literacy (teachers, educational advisors, and policy makers) in 52 countries. The questionnaire covered mainly three key areas: media education at schools, partnerships, and the development of media education. The survey shows that media literacy concepts are integrated across the curriculum in almost all developed countries: the United States, Australia, New Zealand, Mexico, and Canada. For example, high school English teachers in the United States started using movies in teaching English in 2000s for helping students improve their critical thinking and communicative skills. In Ontario, Canada, media literacy in education is mandatory from 1$^{st}$ grade till 12$^{th}$ grade. Media literacy is involved in English literature and constitutes a quarter of every course in 10$^{th}$, 11$^{th}$, and 12$^{th}$ grades

*E. Importance of Media Literacy in Education*

The discussion above shows that media literacy is a 21$^{st}$ century approach to education that provides a scaffold for accessing, analyzing, evaluating, creating, and participating with information in various forms through channels as print, video, Internet, and the like. Media literacy seeks to achieve the relationship among textuality, competence, and power. Media literacy in education is indispensible as it is used for teaching students the skills associated with media literacy and builds a comprehension of the role of media in the community to alert them from consumers of information into users of information.

Hobbs (2005) emphasizes that media literacy helps students be aware of the outside world. Media provide students with representation of the world by using specific skills to critically analyze the messages received. Hence, media literacy encourages students to comprehend and contribute in classroom discussions about various topics. Media literacy engages students in learning and motivates them to make their voices heard. Kist (2005) emphasizes that students become "excited and engaged with reading




ISSN 1737-9334

and writing after their experience with media literacy in the classroom" (p. 103).Goodman (2003) calls media literacy as "the cultural triangle of fashion, sports and music" (p. 27), which indicates that media literacy evokes students to analyze the representations of the references in the external world.

Information in this technological-cultural society is conveyed not only through printed materials, but also through sounds and images. So, media literacy has a significant role in this society as it helps students write and read audio/visual language fluently and easily, which provides them with power to be competitive in today's multimedia culture. In this vein, Buckingham (2003) claims that students nowadays "are increasingly participating in cultural and social worlds that are inaccessible, even incomprehensible to their parents" (p. 32).

Buckingham, in fact, highlights the importance of media literacy in education through involving students in the today's multimedia culture. Media literacy in education is not only a form of protection, but also it is a form of preparation for students to understand, analyze, and think critically to evaluate the message. Media literacy in this context, "aims to develop a more reflexive style of teaching and learning, in which students can reflect on their own activity both as 'readers' and as 'writers' of media texts, and understand the broader social and economic factors that are in play" (Buckingham, 2003, pp. 13-14).

Media literacy, also, is used in education for helping students become competent, critical thinkers, literate, and users of all forms of media in a way that they analyze and interpret the messages they receive from media channels. Teachers of foreign languages can benefit from media literacy in education through motivating students to ask questions about what they watch, hear, and read. Accordingly, student become critical thinkers with the ability to expand their knowledge of media and develop creative competencies in interpreting and creating messages. Teachers, also, can use media literacy in education to encourage students to be able to identify authors' purpose and point of view, examine construction techniques and genres, evaluate patterns of media representation, find out purpose of messages, and explore structural features of media ownership.

Kist (2005) conducted a study regarding the importance of media literacy in education, concluding that media literacy enhances social skills via providing students with opportunities to work collaboratively. Kist assigned 8$^{th}$ grade students in the Snow Lake School in Manitoba to complete an advertising project: a print ad, a radio ad, and an Internet ad. Thanks to media literacy, the students could complete their project assignment collaboratively and could transfer their in-school experience into out-school experience, revealingsocial interaction and ability to work collaboratively.

Goodman (2003) focuses on the role of media literacy in education through its role in changing the students' power of asking questions instead of answering. This, of course, enhances students' confidence in themselves to feel fully competent. Moreover, teachers build good relationships with their students through having information about their students' interests and trends.

*F. Critical Media Literacy Framework*

Scharrer (2003) inquires including media literacy in K-12 curriculum. She emphasizes the role of media literacy in developing strategies for students to know how to create, market, and distribute messages. This, of course, enhances students' confidence and abilities to participate in various kinds of media. Scharrer, in fact, encourages use of media literacy as a critical perspective that provides students good insights to be good users of different types of media. Scharrer gives highlights to what is called "critical media literacy", which includes building counter-hegemonic alternative media accessible to a large number of people.

Critical media literacy has been involved in education for the sake of finding the relationships between media and students from one side and knowledge and power from the other side. Through such relationships, students will be able not only to critically analyze the messages received, but also to create new messages themselves. Critical media literacy enables students to comprehend the power structures of media through analyzing the messages transmitted. Critical media, in fact, helps students critically analyze central readings and symbols that lay behind media in order to comprehend the reality. Students become able to analyze and understand the messages transmitted from the image and create various meanings.

Critical media literacy in education, however, is essential as it helps students interpret, analyze, and



ISSN 1737-9334

evaluate the messages transmitted by media. Students become critical visual analysts to the messages received. In this regard, Kellner (2011)said, "The gaining of critical media literacy is an important resource for individuals and citizens in learning how to cope with a seductive cultural environment. Learning how to read, criticize, and resist sociocultural manipulation can help one empower oneself in relation to dominant forms of media and culture" (p. 7)

Torres and Mercado (2006 ) claim that critical media literacy involves three main dimensions, which are: (1)closely examining how corporate for-profit mainstream media work, in terms ofeconomic, political, social, and cultural power; (2) developing abilities and consciousnessfor searching, creating, developing, and supporting alternative nonprofit independent public-interest media; and (3) understanding the educators' responsibility to help students become critical-media's literate and actively engaged in alternative media use and development. (p. 261)

Some scholars proposed theoretical frameworks for critical media literacy. Hobbs (2008), for instance, presented three frameworks for introducing media literacy to learners as: (1) authors and audiences (AA), (2) messages and meanings (MM), and (3) representation and reality (RR). Hobbs, also, identified basic ideas of theoretical frameworks of media literacy in synthesizing the literature from media literacy, information literacy, visual literacy, and new literacy.

Buckingham (2003), similarly, presented four theoretical frameworks of critical media literacy as: (1) Production, which indicates the texts made by individuals or working groups for themselves or others, (2) Language, which indicates the medium used for transmitting the message, (3) Representation, which indicates the representation or imaginary of the reality, and (4) Audience, which indicates the targeted demographic audiences that use, interpret, and respond to media.

Share (2002) classifies approaches to critical media literacy into four areas as:

1. The protectionist approach, in which the audiences of mass media are seen as victims of the media, defenseless to cultural, ideological, or moral influences. Thus, they need protection by education.
2. The media arts education, which emphasizes the importance of producing various types of media by learners themselves.
3. The media literacy movement, which seeks to apply the old aspects of literacy based to the new types of media.
4. Critical media literacy, which seeks to include new concepts of literacy as culture, mass communication, and technology in education.

*G. Conclusion*

The discussion above shows that media literacy has become an integral part in our life and an essential tool in education. Media literacy works to change students from passive consumers of useless messages into positive users of useful messages. In the 21st century, it has become a waste of time for families to turn off TV or Internet for protecting their childrenas there are a large number of tools nowadays that children use to contact the outside world. Media, in fact, are integrated in our culture, and they have a great effect on cultures to the extent that they become culture itself.

The literature review shows us that for one to be a media literate does not mean that one memorizes or consumes messages from media channels; rather, a media literate means that one raises inquiries, analyzes, and evaluates what is sent by media channels. For one to be a literate in the 21st century is to be part of the technological environment, in which media dominate all facets of life. Media literacy creates a new way of learning, in which students are armed with tools and strategies to think critically and be part of the process of learning and teaching.

## III. METHODOLOGY OF THE STUDY

To fulfill the purposes of this study, the researcher conducted Qualitative Research Method to understand the main questions of this study from the participants' perceptions and how they would see the world around them. In this study, the researcher used secondary resources based on literature review and primary resources based on interviewing ten Libyan teachers of English, who are teaching English at three English language centers in Benghazi: University of Benghazi English Language Center, Kingdom of Education English Language Center, and Al-Kimma Al-Alia Training Center.

*A. Problem of the Study*


ISSN 1737-9334

Studies and research reveal that both Libyan teachers of English and Libyan learners of English encounter challenges in using media in learning and teaching English. For example, Alharam (Cited in Omar, 2018) conducted a study regarding using technology in teaching English in Libya and concludes that "teacher's and student's literacy in technology and teacher's resistance to change their traditional method of teaching are the greatest challenges that EL teachers encounter in using online technology for promoting their adult learners autonomy" (p.240).

In fact, using media literacy in education has been a challenge for most developing countries, in which Libya is one of them. For the challenges of using media literacy in education, Neal (2011) said, "Perhaps one of the most challenging obstacles we face in implementing new writing and assessment technologies in our writing classes is ourselves, especially our lack of expertise and confidence in these new technologies that prevents us from allowing our students to explore new media literacy possibilities in their composing processes" (p. 126).

Neal refers to the challenges encountered by using media literacy in education, and Libya in no exception of this situation. In fact, use of media literacy in teaching and learning English as a foreign language is hardly used at Libyan schools and universities. Though some English language centers in Libya use media literacy in teaching and learning English ,the media used in classrooms are restricted to computers and records, in addition to books, as the participants of the study declare. Similarly, Rutledge (1994) said, "We lack curricula designed to help students understand media messages" (p. 209). Rutledge's quotation indicates explicitly that there is a problem represented in using media literacy in education. Studies and research regarding teaching and learning English in Libya show that one of the most challenges Libyan teachers and learners of English encounter is the use of media literacy in learning and teaching English.So, the researcher sees that there is a problem that needs more investigation.

*B. Questions of the Study*

To fulfill the objectives of this study, the researcher posed the following question as the main question of the study: What do Libyan teachers of English report about their experiences in using media literacy in teaching and learning English in Libya? To investigate and answer the main question of this study, the researcher posed other sub-questions that might be related directly or indirectly to the main question. These sub-questions are:

What kind of media Libyan teachers use in teaching English?

What challenges do Libyan teachers encounter while using media in teaching English in Libya?

What is the role of media in teaching English?

How do the participants learn English?

*C. Participants of the Study*

The participants of this study are ten Libyans–four males and six females–who are teaching English in English language centers in Benghazi. The participants were selected carefully to serve the objectives of this study as: (1) they use a kind of media in teaching English; (2) they teach English in different levels; (3) they learned English in Libya; and (4) they are voluntarily willing to do the interviews and present their experience of using media in teaching and learning English in Libya.

*D. Objectives of this Study*

The main objective of this study is to investigate about using media literacy in teaching and learning English in Libya. This study might be used as a good resource for Libyan authorities in the fields of English language learning and teaching. It might help these authorities to set up new strategies for using media literacy in teaching and learning English effectively at Libyan schools, universities, and English language centers.

*E. Scope of the Study*

The scope of this study is directed mainly to identifying the use of media literacy in teaching and learning English in Libya. The participants of the study comprise ten Libyan teachers, who are teaching English at English language centers in Benghazi. The study was conducted in Benghazi, Libya from the periods of April 1, 2018 toJuly25, 2018.

*E. Data Collection*

The researcher had had face-to-face interviews, using a camera for recording the interviews. The interviews were conducted at the participants' places of teaching. The researcher gave pseudo names to the participants for confidentiality. He, then, transcribed the participants' interviews and




ISSN 1737-9334

coded them into categories according to their relevance. Later, heanalyzed the coded data based on his own interpretation and perception to the topic of the study. He reached findings through analyzing the participants' interviews and presented implications and recommendations based on the findings obtained.

*F. Data Analysis*

Data analysis is a process for arranging the data according to specific arrangements to help researchers understand the data and present findings accordingly (Bogdan and Biklen, 1992, p. 153). To analyze the interviews, the researcher transcribed the interviews, read them thoroughly, and coded them according to their relevance to reach findings.

## IV. FINDINGS

Based on the questions of the study after analyzing the data obtained, there searcher reached several findings. Some of the them are:

- The term media literacy for the participants is still vague, and almost all the participants have had no idea about. This indicates the ignorance regarding using media literacy in education.
- The kind of media all participants use in classroom is restricted to books, and only three participants use computers for listening purposes only.
- The data analysis of the study show that most English language teachers encounter challenges in using media literacy in education, which results in gap between what is called 'in school' and 'out school." Nouha said, "I can't use the Internet in classroom though we have Internet signals in the center." Samia said, "We can't use Internet or computers as most of times the light is off." Zaid was so frank and said, "To be honest, I don't know how to use computer well."
- The participants reveal that most Libyan teachers lack use of media literacy in education due to their being unqualified for using technological devices in teaching.
- The participants in this study attribute teachers' lack of using technology to lack of training. Jamila, for example, said, "We don't have teacher's training in using technology in Libya. All we have is just simple information." Ziad thinks that "teachers lack training regarding how to use technology in school." Ayah believes that "teachers are not aware of importance of technology because of have no training."Amina said, "Most of teachers have little idea about use of technology because they have no training courses."
- The participants blame educational authorities for not encouraging media literacy in education. For instance, Shadi thinks that "Libyan teachers are not given facilities or opportunities to use technology in classroom" Ziad said, "Government does not like giving training courses to teachers to use technology in classroom."
- The data analysis emphasizes the importance of using media literacy in teaching and learning English in Libya. The participants see that Libyan learners of English should be aware of English culture, and this is done through media. In this study, the participants learned English through media. For example, Fouzi said, "I learned English through listening to music and watching TV." Ziad said, "I learned how to speak English through imitating native speakers through listening to movies and news." Nuria said, "I used to follow movies and listen to music, so I learned English." Ayah said, "I learned English by listening to music and watching movies." Also, Nuri said, "I learned English by using music and movies." Samiasaid, "I used to listen to CNN and BBC, so I leaned English."
- The participants of the study emphasize the need for media in teaching and learning English. They emphasize that media help learners understand the reality and create new knowledge. Media make learners educated and critical thinkers, which provide them more opportunities to be good users of English in communicative situations.

## V. RECOMMENDATIONS

Based to the findings obtained, the study presents the following recommendations:

- The Internet is used nowadays to shrink the gaps between school and reality. So, the researcher recommends that Libyan teachers of English be acquainted with how to use technology to teach English, and learners need to be acquainted with how to use technology to learn English. Technology, according to Means and Haertel (2004) "can support ways of learning that would otherwise be difficult to achieve" (p. 17).
- The researcher recommends that Libyan teachers of English should use multiple technological devices in teaching English in order to provide authentic situations to learners. Authentic situations provide learners with opportunities to use the language in reality and share with native speakers what they have already learned in the classroom. Using the language with native speakers enables learners to notice how language is used and notice the differences between


ISSN 1737-9334

their language and the language used by native speakers.

- The researcher recommends teachers to use the Internet or encourage learners to make functional conversations in different situations through chatting with native speakers. In this vein, Short, Harste, and Burke (1996) believe that to be effective users of a foreign language, "all learners need many opportunities to use language with other people for real purposes" (p. 458).
- The researcher recommends that teachers use media literacy in education to integrate language instruction with cultural settings.
- The researcher recommends that teachers shift from linguistic competence to sociocultural competence, in which English is used communicatively in the classroom, where students imitate native speakers, talk with them, and take native speakers' language proficiency as a target.
- The researcher recommends school system in Libya to change to accommodate changes in the globalized world. Using media literacy in education enhances students' learning and strengthens teachers' methods of teaching. Media literacy connects students' in-school experiences with their out-school ones. In this vein Buckingham (2003) emphasizes that "if media education is to help bridge the widening gap between the school and the world of children's out-of-school experience, it must surely begin with the knowledge children already possess" (p. 34).

## *References*

[1] Abunowara, A. M. (2018). Using technology in EFL/ESL classroom. In Y. Z. Omar (Ed.). *Pedagogy and theory in language, meaning, and cultural identity*. (199-221). Benghazi: Research and Consulting Center.

[2] Alharram, M. A. (2018). Using online technology for promoting adult English language learners' (ELLs') autonomy. In Y. Z. Omar (Ed.). *Pedagogy and theory in language, meaning, and cultural identity*. (222-249). Benghazi: Research and Consulting Center.

[3] Alvarado, M. (1981). Television studies and pedagogy. *Screen Education*, *38*, 191-206.

[4] Bogdan, R. C. & Biklen, S. K. (1992). *Qualitative research for education: An introduction to theory and methods*. Boston, MA: Allyn and Bacon.

[5] Buckingham, D. (2003). Media education and the end of the critical consumer. *Harvard Educational Review* 73 (3): 309–27.

[6] Gordon, T. (2007). *Teaching young children a second language*. Westport, Connecticut and London: Praeger.

[7] Fox, R. F. (2000). *Harvesting minds: How TV commercials control kids*. London: Westport, Connecticut.

[8] Fox, R. (2001). Voices entwined. In R. Fox. *MediaSpeak: Three American voices*. (pp. 191-198). Westport, CT: Greenwood Publishers.

[9] Frau-Meigs, D. (2006). *Media education: A kit for teachers, students, parents and professionals*. Paris: L'exprimeur.

[10] Goodman, S. (2003). *Teaching youth media: A critical guide to literacy, video production, and social change*. New York: Teachers College Press.

[11] Herrell, A. L. & Jordan, M. (2008). *50 strategies for teaching English language learners*. (3rded.). Upper Saddle River, New Jersey and Columbus, Ohio: Pearson

[12] Hobbs, J. (2005). Interactive lexical phrases in pair interview tasks. In C. Edwards & J. Willis(Eds.). *Teachers exploring tasks in English language teaching*. (pp. 143-156). New York: Palgrave Macmillan.

[13] Hobbs, R. (2008). Multiple visions of multimedia literacy: Emerging areas of synthesis. In R. D. Robinson & M. C. McKenna (Eds.). *Issues and trends in literacy education* (4th ed.). (pp. 238-252). Boston and others: Pearson.

[14] Hooks, B. (2010). *Teaching critical thinking: Practical wisdom.* New York and London: Routledge.

[15] Kellner, D. (2011). Cultural studies, multiculturalism, and media culture. In G. Dines and J. M. Humez (Eds.). *Gender, race, and class in media: Critical reader* (3rd ed.). (pp. 7 – 18). Thousand Oaks, California: SAGE Publications Inc.

[16] Kendall, D. (2005). *Framing class: Media representations of wealth and poverty in America*. London and other places: Rowman & Littlefield publishers, Inc.

[17] Kist, W. (2005). *New literacy's in action: Teaching and learning in multiple media*. New York: Teachers College Press.

[18] Marzano, R. J., Pichering, D. J., & Polloch, J. E. (2001). *Classroom instruction that works: Research-based strategies for increasing student achievement.* Upper Saddle River, New Jersey and Columbus, Ohio: Pearson.

[19] Masats, D., Dooly, M., & Costa, X. (2009). Exploring the potential of language learning through video making. Proceedings of the EDULEARN09 Conference. 6th-8th July 2009, Barcelona, Spain. Retrieved on Oct. 28, 2017 from http://divisproject.eu/attachments/083_EDULEARN_09_DIVIS.pdf

[20] Mayer, R. E. (2003). The promise of multimedia learning: Using the same instructional design methods across different media. *Learning and Instruction*, 13: 125–139.

[21] Means, B & Haertel, G. D. (Eds.). (2004). *Using technology evaluation to enhance student learning.* New York and London: Teachers College, Columbia University.

[22] Neal, M. R. (2011). *Writing assessment and the revolution in digital texts and technologies*. New York and London: Teachers College, Columbia University.

[23] Reid, R. L. (1994). Reading, using, and creating media: The development of a definition of media education and guidelines for media use. In B. Foundation (Ed.). *Media as a challenge: Education as a task.*(pp. 49-55). Gutersloh, Germany: Bertelsmann Foundation.

[24] Rideout, V., Vandewater, E., & Wartella, A. (2003). Zero to six: Electronic media in the lives of infants, toddlers and preschoolers. Menlo Park, CA: Kaiser Family Foundation.

[25] Rutledge, K. E. (1994). Analyzing visual persuasion: The art of duck hunting. In R. F. Fox (Ed.). Images in language, media, and mind. (pp. 204-218). Illinois: National Council of Teachers of English.

[26] Scharrer, E. (2003). Making a case for media literacy in the curriculum: Outcomes and assessment. *Journal of Adolescent & Adult Literacy* 46 (4): 354–358.

[27] Share, J. (2002). Media literacy. Retrieved on Oct. 12, 2017 from https://en.wikipedia.org/wiki/Media_literacy

[28] Short, K. G, Harste, J. C, & Burke, C. (1996). *Creating classrooms for authors and inquiries* (2nd ed.). Portsmouth, NH: Heinemann.

[29] Shyamlee, S. D. (2012). Use of technology in English language teaching and learning: An analysis. *IPEDR* 33: 150-156.


ISSN 1737-9334

[30] Slethaug, G. E. (2007). *Teaching abroad: International education and the cross-cultural classroom*. Hong Kong: Hong Kong University Press.
[31] Torres, M. & Mercado, M. (2006). The need for critical media literacy in teacher education core curricula. Educational Studies, 39 (3): 260-282.
[32] Yunus, M. M., Salehi, H., & John, D. S. A. (2016),Using visual aids as a motivational tool in enhancing students' interesting reading literary texts recent advances in educational technologies Retrieved on Dec. 18, 2017 from http://arxiv.org/ftp/arxiv/papers/1305/1305.6360.pdf




ISSN 1737-9334

# Robust MPC for fractional MIMO systems

Khaled HCHEICHI and Faouzi BOUANI
University Tunis EL Manar
National Engineering School of Tunis
Analysis, Conception and Control of Systems Laboratory, Tunis, Tunisia
Email: khaled.hcheichi@gmail.com, bouani.faouzi@yahoo.fr

***Abstract*—This paper deals with fractional multi-input, multi-output systems that guarantees a very small number of parameters that can reduce the computation time. It focuses in particular on the state-space representation of systems which highlights the state variables and allows to study the internal behavior of the system taking into account the initial state. It also discusses the discretization of this type of system to finally adapt the Robust Model Predictive Control to apply it and shows its efficiency and performance in these systems.**

## I. Introduction

The fractional systems proved their efficiency in the description of certain physical processes [1] [2]. It urged the researchers to study the behavior and the performances of the fractional systems [3] [4]. They also adapted several strategies of control for this type of system. The majority of the works which treat the fractional systems focus on SISO systems represented by transfer functions. Nevertheless, certain systems have several inputs or several outputs, that explains the necessity of studying the MIMO fractional systems. And in this case the state-space representation will be the best choice because it is easier to adapt to the systems MIMO. The rarity of searches and tools which treat the fractional MIMO systems represents one inconvenience of their use. For that reason this article focuses on the discrétisation and the control of this type of systems.

Model predictive control (MPC) strategy offers an effective way to tackle the problems in multivariable control system by including the process model in the computation of control actions [5]. For processes with strong interaction between different signals MPC can offer substantial performance improvement compared with traditional single-input single-output control strategies [6]. MPC has been used for several decades, and has been accepted as an important tool in many process industry applications. And from the control engineering viewpoint, MPC promises a great benefit to maintain the optimal economic operation of the plant and preserves the lifetime of the equipment. One of the main drawbacks of MPC is the difficulty to incorporate model uncertainties of plant explicitly, and for this reason, increasing attention has been placed on robust MPC problems.

This paper focuses on the state representation of MIMO fractional systems. It extends the discretization of fractional MIMO systems in the first section. In the second section it presents the robust predictive control that has been adapted for this type of systems. Simulation results are discussed in the third section.

## II. Discritization of fractional state-space model

In the case of non-commensurate fractional systems, discretization must take into account the plurality of derivations of state variables, contrary to the commensurate case.

To move from a continuous model to a discrete model it is necessary to use this approximation [7], [8], [9]:

$$D^{\gamma}x(t) = \frac{1}{T_s^{\gamma}}\sum_{j=0}^{p}(-1)^j\binom{\gamma}{j}x((k-j)T_s) \tag{1}$$

Let's assume that the vector of continuous model derivation $\gamma = \begin{bmatrix}\gamma_1 & \gamma_2 & \cdots & \gamma_{nr}\end{bmatrix}^T$, $T_s$ is the sampling time and $p \in \mathbb{N}$ is the number of samples with which the derivation was computed.

If $(i = 1, \cdots, nr)$, the term $\binom{\gamma}{j}$ can be written as follows:

$$\binom{\gamma}{j}^T = \left[\binom{\gamma_1}{j} \quad \binom{\gamma_2}{j} \quad \cdots \quad \binom{\gamma_{nr}}{j}\right] \tag{2}$$

$$\binom{\gamma_i}{j} = \begin{cases} 1 & for \quad j = 0 \\ \dfrac{\gamma_i(\gamma_i-1)...(\gamma_i-j+1)}{j!} & for \quad j > 0 \end{cases} \tag{3}$$

By multiplying (1) by $T_s^{\gamma}$ and developing the terms of $j = 0$ and $j = 1$ the found result is:

$$\begin{aligned} T_s^{\gamma}D^{\gamma}x(t) = {} & x(kT_s) - \gamma x((k-1)T_s) + \\ & + \sum_{j=2}^{p}(-1)^j\binom{\gamma}{j}x((k-j)T_s) \end{aligned} \tag{4}$$

Let consider the following continuous fractional MIMO state-space model [10]:

$$\begin{cases} D^{\gamma}x(t) &= A_c x(t) + B_c u(t) \\ y(t) &= C_c x(t) \end{cases} \tag{5}$$

With $A_c \in \mathbb{R}^{nr\times nr}$, $B_c \in \mathbb{R}^{nr\times ni}$ and $C_c \in \mathbb{R}^{no\times nr}$ are the state matrices of the continuous fractional model and $nr$ is the number of varibales in state-space model, $ni$ is number of inputs and $no$ is the number of outputs.

$$\begin{aligned} T_s^{\gamma}A_c x(kT_s) - x(kT_s) = {} & -\gamma x((k-1)T_s) + \\ & + \sum_{j=2}^{p}(-1)^j\binom{\gamma}{j}x((k-j)T_s) - B_c T_s u(kT_s) \end{aligned} \tag{6}$$




ISSN 1737-9334

note that $I_r \in \mathbb{R}^{nr\times nr}$ the identity matrix and $T_s^{\gamma}$ the diagonal matrix filled in by $(\ T_s^{\gamma_1} \cdots T_s^{\gamma_{nr}})$.

To facilitate writing, let's note

$$\mathbb{Z} = (T_s^{\gamma} A_c - I_{nr})^{-1} \tag{7}$$

$$\begin{aligned} x(kT_s) = &-\mathbb{Z}\gamma x((k-1)T_s) + \mathbb{Z}\sum_{j=2}^{p}(-1)^j \binom{\gamma}{j} x((k-j)T_s) \\ &-\mathbb{Z}B_c T_s^{\gamma} u(kT_s) \end{aligned} \tag{8}$$

and with $(i = 1, \cdots, nr)$

$$c_j = diag\{(-1)^j \binom{\gamma_i}{j} \tag{9}$$

Now we can write the above equation as:

$$x(k) = \mathbb{Z}\, c_1 x(k-1) + \mathbb{Z}\sum_{j=2}^{p} c_j x(k-j) - \mathbb{Z}\, B_c T_s^{\gamma} u(k) \tag{10}$$

To simplify the equation:

$$A_j = \mathbb{Z}\, c_j \tag{11}$$

By expanding all terms and simplifying, the new form of (10)

$$x(k) = A_1 x(k-1) + A_2 x(k-2) + \cdots + A_k x(0) - \mathbb{Z}B_c T_s^{\gamma} u(k) \tag{12}$$

The system can therefore be described by a discrete state-space representation [11]:

$$\begin{cases} X_d(k+1) = A_d X_d(k) + B_d u(k) \\ y(k) = C_d X_d(k) \end{cases} \tag{13}$$

With

$$X_d(k+1) = \begin{pmatrix} x(k+1) \\ x(k) \\ \vdots \\ x(k-p+1) \end{pmatrix} \quad , \quad X_d(k) = \begin{pmatrix} x(k) \\ x(k-1) \\ \vdots \\ x(k-p) \end{pmatrix}$$

$$A_d = \begin{pmatrix} A_1 & A_2 & \cdots & A_{p-1} \\ I & 0 & \cdots & 0 \\ 0 & I & \cdots & 0 \\ \vdots & \vdots & \ddots & \vdots \\ 0 & \cdots & I & 0 \end{pmatrix}, \quad B_d = \begin{pmatrix} -\mathbb{Z}B_c T_s^{\gamma} \\ 0_{ni} \\ \vdots \\ 0_{ni} \end{pmatrix}$$

$$\text{and } C_d = \begin{pmatrix} C & 0_{no} & \cdots & 0_{no} \end{pmatrix}$$

with $u$, $y$, $X_d$ are respectively the input, output and variables state of the process. $p$ is the number of past iterations which the system takes into account for calculating a variable, $0_{ni} \in \mathbb{R}^{1\times ni}$, $0_{no} \in \mathbb{R}^{no\times 1}$, $A_d \in \mathbb{R}^{(nr*p)\times(nr*p)}$, $B_d \in \mathbb{R}^{(nr*p)\times ni}$ , $C_d \in \mathbb{R}^{no\times(nr*p)}$ and $X_d \in \mathbb{R}^{(nr*p)\times 1}$ .

## III. Robust Fractional MPC

The principle of the predictive control is to create an anticipatory effect for the system with respecting the trajectory to follow known in advance, based on the prediction of the future behavior of the system and minimizing the gap of these predictions to the trajectory and by minimizing a certain cost function $J$, within respecting operating constraints [12], [13].

In this section we have developed a predictive control from the discrete fractional state-space model described in the previous section. For that we will make a variable change : $\Delta X_d(k) = X_d(k) - X_d(k-1)$ the input variable difference: $\Delta u(k) = u(k) - u(k-1)$, and using it in (13) this transformation is found:

$$\Delta X_d(k+1) = A_d \Delta X_d(k) + B_d \Delta u(k) \tag{14}$$

The new state variable vector is:

$$X(k) = [\Delta X_d(k)^T \; y(k)]^T$$

with $y(k)$ is the output and :

$$y(k+1) - y(k) = C_d A_d \Delta X_d(k) + C_d B_d \Delta u(k) \tag{15}$$

The system can be written in the form:

$$\begin{cases} X(k+1) = AX(k) + B\Delta u(k) \\ y(k) = CX(k) \end{cases} \tag{16}$$

$$A = \begin{pmatrix} A_d & 0_d^T \\ C_d A_d & I_{no} \end{pmatrix}; \; B = \begin{pmatrix} B_d \\ C_d B_d \end{pmatrix};$$

$$C = \begin{pmatrix} 0_d & I_{no} \end{pmatrix}; \; 0_d \in \mathbb{R}^{no\times(nr*p)}$$

Future state variables can be predicted and written in the form:

$$\begin{cases} X(k+1) &= AX(k) + B\Delta u(k) \\ X(k+2) &= AX(k+1) + B\Delta u(k+1) \\ &= A^2X(k) + AB\Delta u(k) + B\Delta u(k+1) \\ &\vdots \\ X(k+H_p) &= A^{H_p}X(k) + A^{H_p-1}B\Delta u(k) + \\ &\quad A^{H_p-2}B\Delta u(k+1) + \cdots \\ &\quad + A^{H_p-H_c}B\Delta u(k+H_c-1) \end{cases} \tag{17}$$

Based on (17) the future system outputs can be predicted:

$$\begin{cases} y(k+1) &= CAX(k) + CB\Delta u(k) \\ y(k+2) &= CAX(k+1) + CB\Delta u(k+1) \\ &= CA^2X(k) + CAB\Delta u(k) + \\ &\quad CB\Delta u(k+1) \\ &\vdots \\ y(k+H_p) &= CA^{H_p}X(k) + CA^{H_p-1}B\Delta u(k) + \\ &\quad CA^{H_p-2}B\Delta u(k+1) + \cdots \\ &\quad + CA^{H_p-H_c}B\Delta u(k+H_c-1) \end{cases} \tag{18}$$

$H_p$ and $H_c$ are respectively the prediction horizon and the control horizon with $H_p \geq H_c$. Assume the vector $Y$




ISSN 1737-9334

which contains $H_p$ system's predicted future outputs and $\Delta u$ contains $H_c$ future controls:

$$Y^T = [y(k+1)\ \ y(k+2)\cdots y(k+H_p)]$$

$$\Delta u^T = [\Delta u(k)\,\Delta u(k+1)\cdots\Delta u(k+H_c-1)]$$

The vector $Y$ can also be written as :

$$Y = FX(k) + \Phi\Delta u \tag{19}$$

$$F = \begin{pmatrix} CA \\ CA^2 \\ CA^3 \\ \vdots \\ CA^{H_p} \end{pmatrix} \tag{20}$$

$$\Phi^T = \begin{pmatrix} CB & CAB & CA^2B & \cdots & CA^{H_p-1}B \\ 0 & CB & CAB & \cdots & CA^{H_p-2}B \\ 0 & 0 & CB & \cdots & CA^{H_p-3}B \\ \vdots & \vdots & \vdots & \ddots & \vdots \\ 0 & 0 & 0 & & CA^{H_p-H_c}B \end{pmatrix} \tag{21}$$

The aim of predictive control is to find the control vector $\Delta u$ which forces the system's output $y$ to follow the setpoint $y_s$. In order to achieve this we must optimize a criterion $J$ which represents the control objective [14]:

$$J = \sum_{i=1}^{H_p}(y_s(k+i) - y(k+i))^2 + \lambda \sum_{i=0}^{H_c-1}\Delta u^2(k+i) \tag{22}$$

The criterion $J$ can be written in matrix form:

$$J = (Y_s - Y)^T(Y_s - Y) + \Delta u^T\lambda\Delta u \tag{23}$$

With $Y_s^T = [y_s(k+1)\ \ y_s(k+2)\cdots y_s(k+H_p)]$ is the vector filled by the future values of the set-points and $\lambda$ is weight coefficient on the control.

Let consider in the following, a state-space description of an uncertain system that can generally be written in the form [15] [16]:

$$\begin{cases} D^\gamma x(t) &= A_c(\theta)x(t) + B_c(\theta)u(t) \\ y(t) &= C_c(\theta)x(t) \end{cases} \tag{24}$$

With $A_c$, $B_c$ and $C_c$ are the state matrices of the continuous fractional model, the vector of continuous model derivation $\gamma = \begin{bmatrix}\gamma_1 & \gamma_2 & \cdots & \gamma_{nr}\end{bmatrix}^T$ and $nr$ is the number of varibales in state-space model.

$$A_c(\theta)) = A_{c0} + \Delta A_c \tag{25}$$

$$\Delta A_c = \sum_{i=1}^{N}\theta_i A_{ci} \tag{26}$$

with

$$\theta_i \in \left[\underline{\theta}_i, \overline{\theta}_i\right]$$

For this representation, matrices $A_{ci}$ distribute the uncertainty on the different elements of the matrix $A_c(\theta)$.

In RFMPC the control sequence represents the best solution to the worst case. Consequently, the optimal control law can be obtained by the resolution of the following min-max problem [17]

$$\min_{\Delta u}\ \max_{\theta}\ J(\Delta u, \theta) \tag{27}$$

The min-max problem is resolved in two steps. The first step consists to calculate the maximum of the performance criterion $J(\Delta u, \theta)$ compared to the uncertainties parameters of the set $\theta$ . Starting with an initial solution, RFMPC searches the solution of following function in taking into account constraints on the parameters model.

$$J^*(\Delta u) = \max_{\theta}\ J(\Delta u, \theta) \tag{28}$$

The second step concerns the minimization of the criterion $J^*(\Delta u, \theta^*)$ in taking into account the solution found in Eq. (28) and the control sequence constraints:

$$J_2 = \min_{\Delta u}\ J^*(\Delta u) \tag{29}$$

## IV. Simulation results

Consider a fractional MIMO system whose state-space representation is of the form:

$$A_c = \begin{pmatrix} 0 & 1 \\ -a_1 & -a_2 \end{pmatrix},$$

$$B_c = \begin{pmatrix} 1 & -1 \\ 0 & -1 \end{pmatrix}, \qquad C_c = \begin{pmatrix} 1.25 & 0 \\ 1 & 1 \end{pmatrix}$$

$$\gamma = \begin{pmatrix} 1.3 \\ 0.9 \end{pmatrix}$$

with $a_1 = 1.25$ and $a_2 = 0.625$

The step response of system is shown in Fig.1.

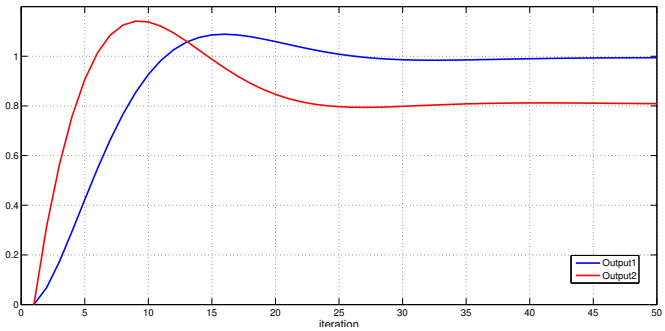


Fig. 1. The step responnse of system.

Let consider in this section that the system is represented by the Oustaloup model called $M$ equivalent to the previous state-space, during the simulation the variables $a_2$ will


ISSN 1737-9334

change to 0.425 and 0.825 to find respectively the models of Oustaloup $M_1$ and $M_2$.

For each simulation the real system will be represented as follows:

- for $1 \leq k \leq 50$ : the system is the model $M$.
- for $51 \leq k \leq 100$ : the system is the model $M_1$.
- for $101 \leq k \leq 160$ : the system is the model $M_2$.

The chosen predictive control parameters are: $H_p$=3, $H_c$=1, $\lambda$=1. The chosen sampling period for discretization is: $T_s = 0.3s$.

To ensure a better control for the system an uncertainty will be imposed on the values of $a_1 = 1.25$ and $a_2 = 0.625$ with :

$$a_1 \in [1, 1.5] \text{ and } a_2 \in [0.375, 0.875]$$

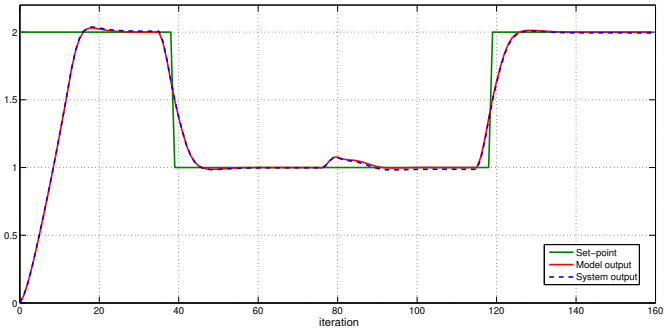


Fig. 2. First output.

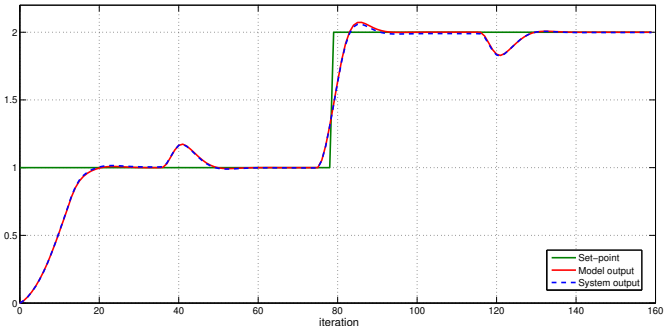


Fig. 3. Second output.

Fig.2 and Fig.3 show that RFMPC is able to force the system to follow the set-point. At each iteration RFMPC find the worst values of $a_1$ and $a_2$ for the system and then calculate the best value of control to satisfy the criterion $J$. The worst values of $\Delta a_1$ and $\Delta a_2$ are shown in Fig.4.

Fig.5 and Fig.6 represent the signals of control generated by RFMPC.

The choosen constraint on the control variables is $\| \Delta u(k) \| \leq 0.2$.

Assuming that the control variable $\Delta u(k)$ can only increases or decreases in a unit of magnitude less than 0.2 [18], the operational constraint is :

$$-0.2 \leq \Delta u(k) \leq 0.2$$

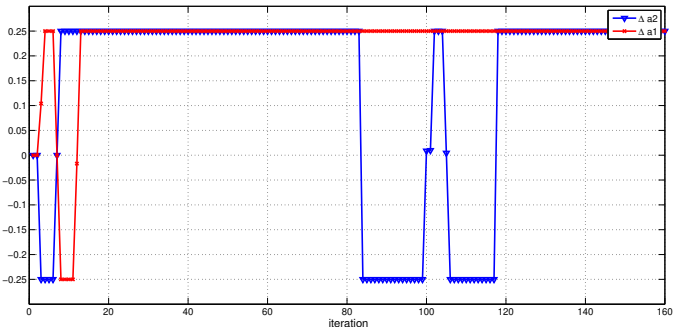


Fig. 4. The worst values of $\Delta a_1$ and $\Delta a_2$ in each iteration.

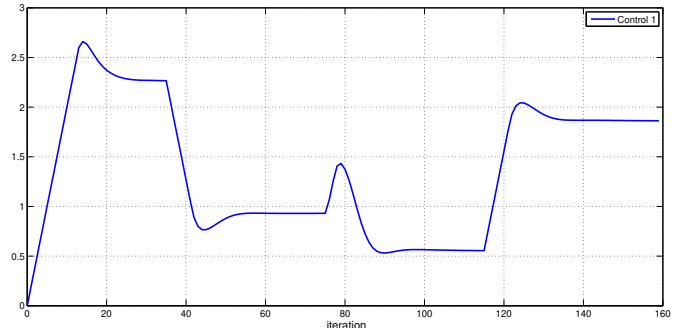


Fig. 5. First control .

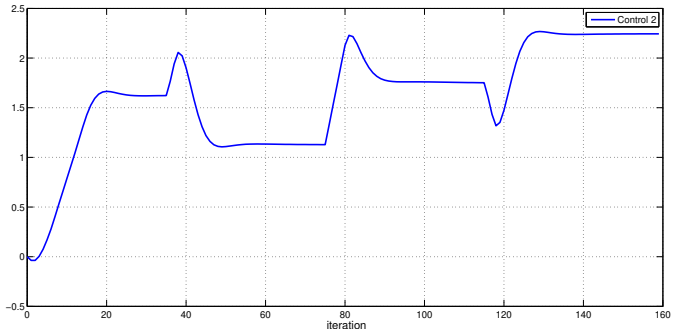


Fig. 6. Second control.

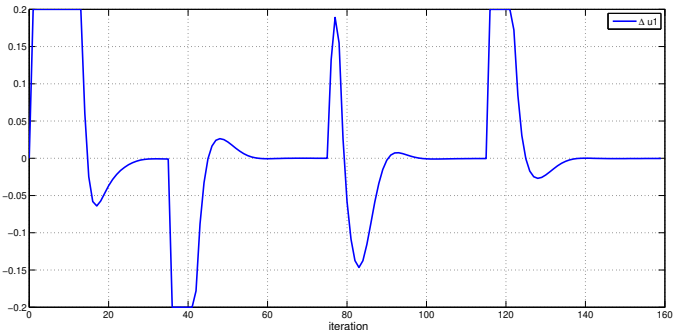


Fig. 7. Increment of first control.

Even under constraint the RFMPC can ensure that the outputs follow the set-point. Constrains on the control




ISSN 1737-9334

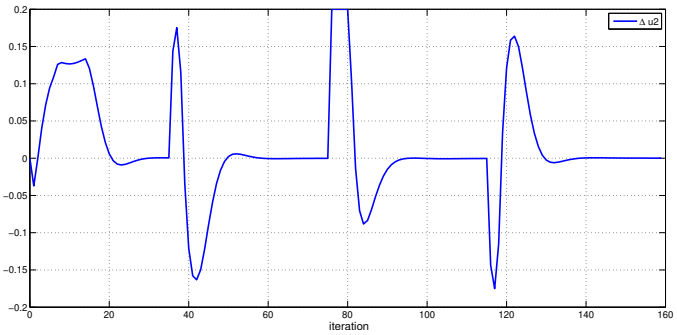


Fig. 8. Increment of second control.

increment represented in Fig.7 and Fig.8 guarantees that there is no peaks in the control signal. In return, the outputs porsuite becomes slower as shown in the Fig.2 and Fig.3. The choice of the the interval $\Delta u$ is very important, because if the interval is too wide the condition will not be taken into account when minimizing criterion J, and if the interval is too small the control will no longer be able to bring the outputs to follow the set-point, even if it happen the system will be too slow.

## V. Conclusion

The use of fractional models becomes more and more frequent given the efficiency they provide in the discription of certain physical systems. Nevertheless they remain a little difficult to handle. The majority of research [19], [20], [21] deals with SISO fractional models that have proved effective at describing several physical phenomena. This article has adapted predictive control to apply it to a MIMO fractional system. The importance of this work is that it deals with the state-space representation of MIMO fractional systems from discritization to control. It first introduced the dicritization of fractional MIMO state-space representation. Then for the same kind of system, it adapted the robust predictive control and applied it.

## References

[1] J.T. Machado, V. Kiryakova and F. Mainardi "Recent history of fractional calculus" *Communications in Nonlinear Science and Numerical Simulation*, March 2011, 16 (3) : 1140–1153

[2] H.G. Sun, Y. Zhang, D. Baleanu, W. Chen and Y.Q. Chen "A new collection of real world applications of fractional calculus in science and engineering" *Communications in Nonlinear Science and Numerical Simulation*, November 2018, 64 : 213–231

[3] B. Gao, R. Cao, Z. Hou and H. Zhou "Model-free adaptive MIMO control algorithm application in polishing robot" *6th Data Driven Control and Learning Systems (DDCLS)*, Chongqing, China, May 2017, pp. 135–140

[4] A. Noshadi, J. Shi, W. S. Lee, P. Shi and A. Kalam "System Identification and Robust Control of Multi-Input Multi-Output Active Magnetic Bearing Systems" *IEEE Transactions on Control Systems Technology*, July 2016, 24 (4) : 1227 – 1239

[5] S. Vrazhevsky, I. Furtat and A.Kremlev "Robust output control for nonlinear MIMO plants using modified backstepping algorithm" *IEEE Industrial Cyber-Physical Systems (ICPS)*, St. Petersburg, Russia, May 2018, pp. 187–192

[6] M.M. Joshi, V.A. Vyawahare and M.D. Patil "Model predictive control for fractional-order system a modeling and approximation based analysis." In: *International Conference on Simulation and Modeling Methodologies, Technologies and Applications (SIMULTECH)*, Vienna, Austria, August 2014, pp. 361–372

[7] Z. Belkhatir and T.M. Laleg-Kirati "Parameters and fractional differentiation orders estimation for linear continuous-time non-commensurate fractional order systems" *Systems and Control Letters* , 2018, 115: 26 – 33

[8] A. Dzieliǹski and D. Sierociuk "Adaptive Feedback Control of Fractional Order Discrete State-Space Systems." In: *International Conference on Computational Intelligence for Modelling, Control and Automation and International Conference on Intelligent Agents, Web Technologies and Internet Commerce (CIMCA-IAWTIC'06*, Vienna, Austria, December 2011, pp. 1–6

[9] P. Ostalczyki and D. Mozyrska "The second form of the variable-, fractional-order discrete-time integrator." In: *21st International Conference on Methods and Models in Automation and Robotics (MMAR)*, Miedzyzdroje, Poland, August 2016, pp. 859–864

[10] A. Dzieliǹski and D. Sierociuk "Ultracapacitor modelling and control using discrete fractional order state-space models and Fractional Kalman Filters." In: *European Control Conference (ECC)*, Kos, Greece, July 2007, pp. 2916–2922

[11] M. Abedini, M.A. Nojoumian, H.Salarieh and A. Meghdari "Model reference adaptive control in fractional order systems using discrete-time approximation methods" *Communications in Nonlinear Science and Numerical Simulation*, 2015, 25 (1-3): 27 – 40

[12] H. Aboukheir "Predictive Control of Fractional Order Systems" *IFAC Proceedings Volumes*, 2012, 45 (13): 622–626

[13] J.B. Rawlings "Tutorial overview of model predictive control" *IEEE Control Systems*, 2000, 20 (3): 38–52

[14] Q. Zou, Q. Jin and R. Zhang "Design of fractional order predictive functional control for fractional industrial processes" *Chemometrics and Intelligent Laboratory Systems*, 2016, 152: 34 – 41

[15] Li Li and Liao Fucheng (2018) Design of a robust $H_\infty$ preview controller for a class of uncertain discrete-time systems *Transactions of the Institute of Measurement and Control* 40 (8): 2639-2650

[16] Bayrak A, Gursoy H, Efe MO (2017) A novel robust fuzzy control of an uncertain system *Transactions of the Institute of Measurement and Control* 39 (3): 324


ISSN 1737-9334

- 333

[17] M. Zhao, Y. Wen, Y. Wang and Z. Chen "LPV based robust MPC for a multi-vectored airship" In: *Eighth International Conference on Intelligent Control and Information Processing (ICICIP)*, Hangzhou, China, Nov 2017, pp. 314–318

[18] B. Sikora and J. Klamka "Constrained controllability of fractional linear systems with delays in control" *Systems and Control Letters*, 2017, 106: 9 – 15

[19] Z. Belkhatir and T.M. Laleg-Kirati "High-order sliding mode observer for fractional commensurate linear systems with unknown input" *Automatica*, 2017, 82: 209 – 217

[20] R. Martìnez-Guerra, C.D. Cruz-Ancona and C.A. Pérez-Pinacho "Estimators for a class of commensurate fractional order systems with caputo derivative." In: *14th International Conference on Electrical Engineering, Computing Science and Automatic Control (CCE)*, Mexico City, Mexico, October 2017

[21] S. Saxena, V. Yogesh and P.P. "Arya Reduced-order modeling of commensurate fractional-order system." In: *14th International Conference on Control, Automation, Robotics and Vision (ICARCV)*, Porto, Portugal, Nov 2016, pp. 1–6




ISSN 1737-9334

# Control and Management of Residencial Load in Micro-Grid

Abderrahmane Djellouli[1], Fatiha Lakdja[2], Meziane Rachid[1]
[1]*Electro-Technical Engineering Laboratory*
[2] *ICEPS laboratory, University of Sidi-Bel-Abbes, Algeria*
*Faculty of Technology, University of Saida, Algeria*
djellouli7abderrahmane@gmail.com, flakdja@yahoo.fr, meziane22@yahoo.fr

***Abstract*— The importance of energy from renewable resources, such as wind and solar, is increasing and their penetration rate in power increases each year due to several factors. Firstly, the perpetual rise in demand, particularly because of population growth and economic development. Second, pledges made by many Governments to increase their reliance on renewable sources of energy, with a view to reducing the devastating consequences of climate change on the environment. The multiplication of decentralized production connected to the low-voltage power grid causes the appearance of a bidirectional energy flow. This is at the origin of many electrical phenomena that are increasingly difficult to manage it by distribution system operators. An innovative solution consists in controlling the integration of renewable energies and managed the flow of the powers for a different source. This work covers integration of renewable energy into the public grid for hybrid system. Or more precisely, a microgrid that contains two renewable energy sources (PV + wind), battery and public network all the system is connected in a residential charge. Furthermore, the control of all devices for this integration, management of load from renewable energy and public grid.**

***Keywords—Renewable energy; Wind; Solar; Management; Microgrid***

## I. INTRODUCTION

Today, in many countries, there is a sharp increase in decentralized generation sources (solar photovoltaic, wind, hydroelectric, heat-power coupling, etc.) with the addition of the storage system and the diesel generator that are connected to the utility grid. The multiple combination of these sources that are called hybrid power systems.

Although positive, the multiplication of these sources of energy connected to the low voltage (LW) electrical network also has limits. In fact, the decentralized injection of electricity into the grid (by fossil and /or renewable sources) is a factor of instability.

This is due to the presence of a final consumer who, having become both a producer and a user of electricity, causes the appearance of a bidirectional energy flow using an infrastructure that was not designed, at the same time, originally, to welcome him.

Paradoxically, a good coordination of these different sources of injection would better manage power flows and have better oversight of the quality of electricity [1]. The general trend is therefore to move towards the use of smart grid or namely micro-grid. Research in the field of microgrid system has been reviewed in the preview studies using the computer tool and control strategy [2].

This work aims to design a simple micro-grid that includes two renewable energy sources (PV + Wind) and a storage battery, this system is connected in a public grid and do not forget the control system. The study is done in MATLAB interface.

To carry out this work, this paper is divided into six sections. the first section is an introduction. Section 2 presents a generality on micro-grids. The operation of the photovoltaic system and the wind turbine was devoted in sections 3 and 4 successively. The model and the simulation results are presented in section 5. Finally, we conclude this work with a conclusion presented in section 6.

## II. MICRO-GRID

With the progress of human society, electric power has been the symbol of modern civilization. Power supply reliability and power quality have become more and more important. Facing pressures from traditional resource depletion and environmental pollution, power generation methods based on fossil fuel and the centralized power supply mode have been difficult to meet the requirements of economic and social development. So, to facilitate access to energy, local-scale power generating and consumption systems called microgrids are gradually being introduced [3].

Microgrid idea is generally developed in countries such as the United States, Canada, Japan and the United Kingdom. It has been investigated and implemented [4]. micro-grid is defined as a system that consisting of renewable sources integrate in the electrical grid, small in size, it comprises low voltage (LV) system with distributed energy resources (DERs) together with storage devices and flexible loads, which can be operated in either on-grid (grid connected) or off-grid (islanded) mode of operation [5][6].

Design of a microgrid can be differentiated according to the applications and expectations. Some microgrids are developed to achieve high end use reliability and stability. Reliability is a common property for a microgrid. Microgrids are able to use more reliable and controllable energy sources like diesel sets, natural energy sources etc. to ensure reliability and stability of the system. Most of these types are implemented as a backup system for large industries and


ISSN 1737-9334

military stations located in remote areas. Some others will integrate more renewable and waste energy resources. Overcoming limitations introduced by these kinds of resources is a challenging task. It is seen that there is no clear common architecture for microgrids. So, design, implementation and operation of a microgrid are differentiated according to the purpose [7].

A microgrid is typically made up of:

- Renewable energy sources (solar, wind or biomass).
- Fossil fuel energy sources to ensure grid stability.
- Energy storage solutions (batteries, hydrogen storage, mechanical storage, etc.).
- A low-voltage supply grid regulated by a smart control system.

"Fig. 1," represents the general design of a micro-grid system.

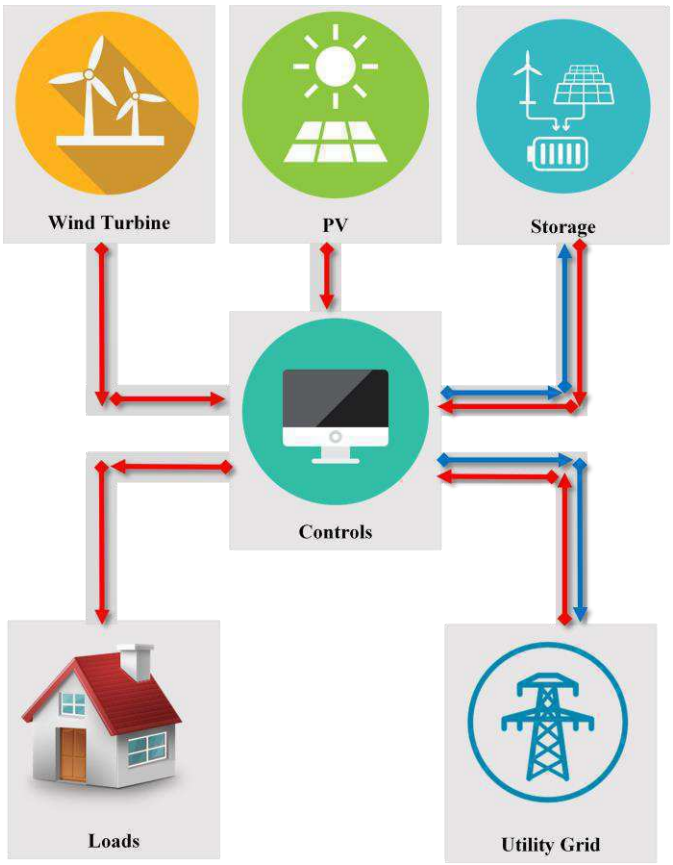


Fig. 1. General structure of a micro-grid.

## III. PHOTOVOLTAIC SYSTEM

Photovoltaic solar energy comes from the conversion of sunlight into electricity due to the photovoltaic effect [8][9]. When the photons of sunlight come into contact with the semiconductor materials, they are given the necessary energy for the electron to move from one band to another, this movement produces an electric current [10]. This continuous micropower current calculated in watt peak (Wc) can be converted into alternating current due to an inverter.

The equivalent circuit of a photovoltaic panel is shown in Fig. 2. It includes a current source, a diode, a series resistor and a shunt resistor [11].

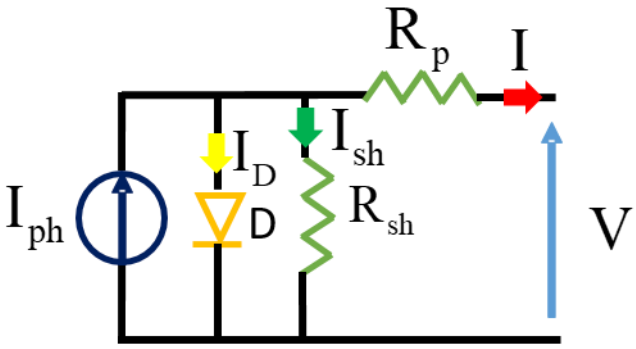


Fig. 2. Electrical model of a PV panel.

Based on the circuit Above and using Kirchhoff law, the current generated by the solar panel can be determined [12], as in (1).

$$I=I_{ph}-I_0\left(\exp\frac{q(V+R_SI)}{aKTN_S}-1\right)-\frac{(V+R_SI)}{R_P} \quad (1)$$

Where

$$I_{ph}=\left(I_{SC}+K_i\left(T-298.15\right)\right)-\frac{G}{1000} \quad (2)$$

$$I_0=\frac{I_{SC}+K_i\left(T-298.15\right)}{\exp\left(\frac{q(V_{oc}+K_V(T-298.15)}{aKTN_S}\right)-1} \quad (3)$$

Where $I_{pv}$ and $I_0$ are the photovoltaic and saturation currents of the array; $I_m$ and $V_m$ represent the voltage and the current at the terminals of the module; $R_s$ and $R_p$ are series and shunt resistance; T mean the ambient temperature in Kelvin; G [W/m²] is the irradiation on the device surface; q represents the charge of the electron; a is the factor of ideality.

## IV. WIND POWER SYSTEM

wind energy is a renewable source energy that transforms the wind's kinetic energy into electrical energy. "Fig. 3," shows the operation of this energy.




ISSN 1737-9334

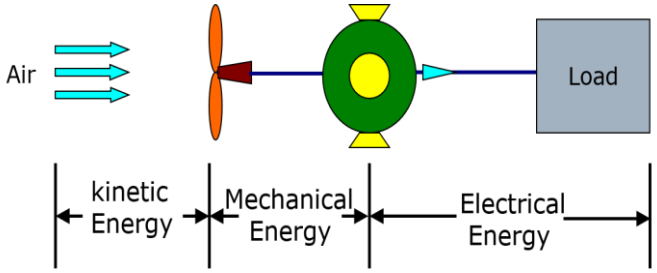


Fig. 3. The operation principle of wind energy.

The model is based on the steady-state power characteristics of the turbine. The output power of the turbine is given by the following (4) [13].

$$P_m = \frac{1}{2} C_p \times S \times \rho \times V^3 \quad (4)$$

Where

$P_m$: Mechanical output power of the turbine (W).

$C_p$: Performance coefficient of the turbine.

ρ: Air density (kg/m³).

S: The Total Blade Area swept by the rotor blades (m²).

V: The wind velocity (m/s).

## V. MODEL PROPOSED

The proposed model of this work using MATLAB is illustrated in Fig. 4. The micro-grid contains a photovoltaic system, wind, public grid and a battery that are connected to a load.

The photovoltaic system is characterized by a power of 4.5Kw and a voltage of 290V for a temperature of 25°C and an irradiance of 1000 W/m². The Maximum Power Point Tracking (MPPT) control takes maximum power from the solar panel using a unidirectional DC/DC converter.

The wind turbine in this model generates a power of 3 Kw and a voltage of 440V, this source is connected in an AC / DC rectifier.

A controller consisting of a power conditioning system and a battery control system is also connected directly to the system.

The power grid is connected to the system by a pole-mounted distribution transformer. It can absorb or demand energy from the system.

the previous three elements (PV + Wind + Battery) that are putting in cascade, they are connect to a bidirectional DC/AC inverter which connected in series with a public grid.

Three loads of 1.5 kW can be connected to the system. They consume a total of 6 kW of electrical power when All of them are connected.

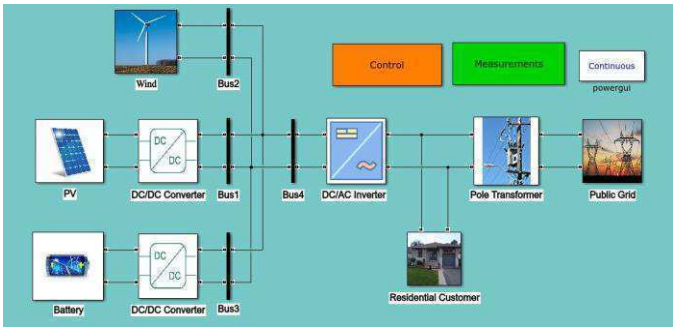


Fig. 4. Proposed micro-grid model.

## VI. RESULTS AND DISCUSSION

### A. RESULTS

After the execution of the proposed model shown in Fig. 4. We obtained the following results:

"Fig. 5," shows the operating time of each load, such that load 1 operates between {0.25-0.75 s and 1.25-1.75 s}, load 2 operates between {0.5-0.75 s and 1.5-1.75 s} and load 3 works between 0.75-1.25 s.

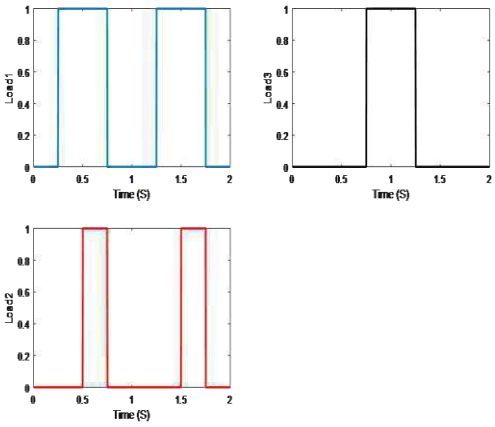


Fig. 5. the operation time for the three loads..

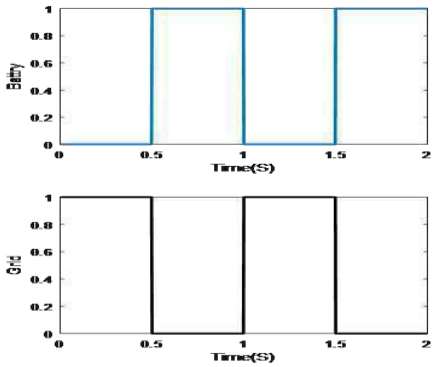


Fig. 6. The operation time for the battery (blue) and the grid (dark).




ISSN 1737-9334

"Fig. 5," shows the operating time of the grid and battery. we managed the time so that if the grid works, the battery is disconnected and vice versa. This management makes it possible to maintain the continuity of service.

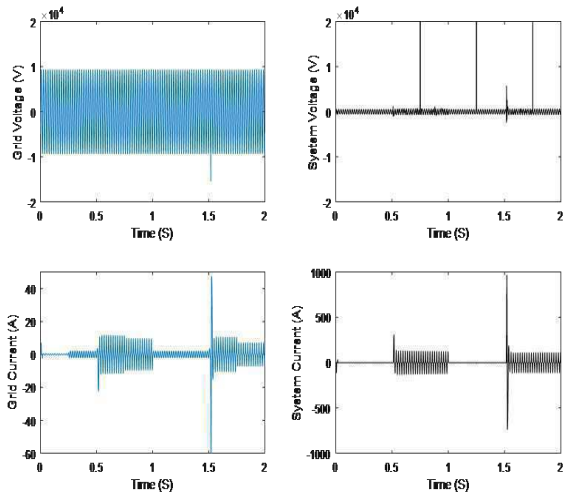


Fig. 7. The voltage and current profile for: the grid (blue), the hybrid system (dark).

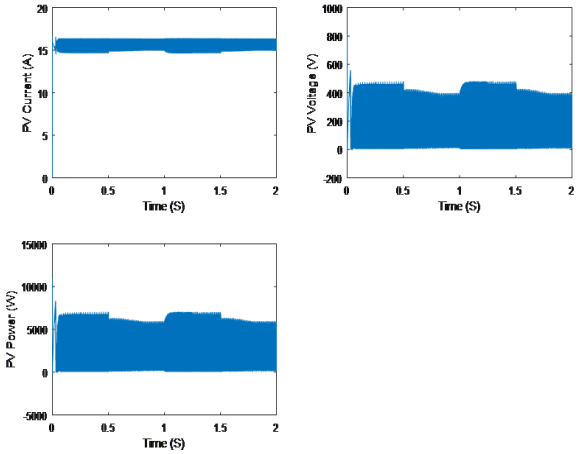


Fig. 8. The current, voltage and power profile of the PV.

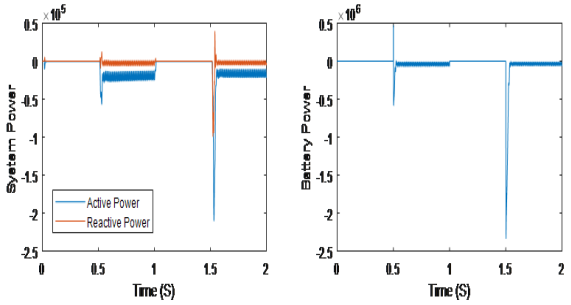


Fig. 9. The power profile of the battery (right) and the hybrid system (left).

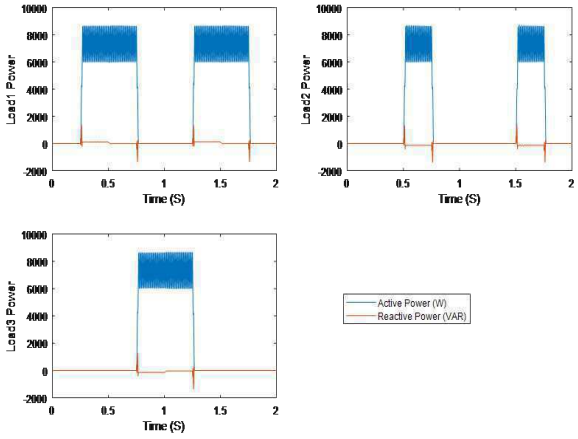


Fig. 10. The power profile of the three loads.

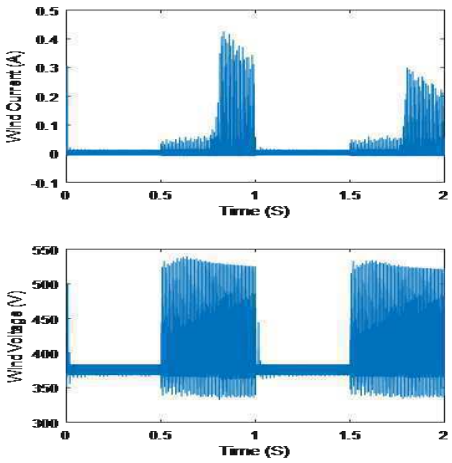


Fig. 11. The current and voltage profile of the wind.

## B. DISCUSSION

### 1) Grid connected

- The battery is not connected to the system and the charges are not activated.
- The power generated by the hybrid system is sent to the public grid.
- The power generated by the hybrid system is kept approximately constant at the nominal power due to the integration of the control system.

### 2) Battery connected

- The grid not yet connected.
- The power generated by the system is negative because all three loads are connected. The system requires an additional energy from the grid.


ISSN 1737-9334

- The power generated by the system hybrid rest constant.

Load 1 et 2 then disconnected, load 3 is disconnected at time (t=1.25 s). Then the battery is connected to the system. Therefore, we can disconnect the public grid management system because the hybrid system (PV + Wind + Battery) is sufficient to provide the total load.

## VII. CONCLUSION

In this article we started by giving a generality on the micro-grids system. Then we present the two renewable energy sources (PV + Wind) that we used in this work.

this system consists of a photovoltaic source, a small wind source, a storage unit that is the fuel cell and a load of 6kW, the whole is connected to a DC bus.

We realized this global system in MATLAB Simulink, with the setting of the initial variables of each component. In addition, we have installed a process to control all system variables, such as DC bus voltage control, MPPT control, control of the DC / AC converter for the synchronization of the AC output with the public grid. As we have installed a power

management system et de control from all sources that is in the charge, battery and public grid.

Finally, the simulation is launched in a duration of 2 s, the results obtained are satisfactory fact that, the following functions are provided:

- The control of system components and variables facilitates the integration of renewable energies in public grid and guarantees operation even in adverse cases.
- The installation of a power management system plays a very important role not only to promote the use of renewable energies but also the reduction of the use of the public network (consumer become both a producer and a user of electricity).

## REFERENCES

[1] J. Jaton, G. Besson, M. Carpita, and D. Ducommun, “Gestion intelligente et autonome du réseau électrique basse tension,” Electrosuisse, Technopark, Zürich, 17.Oktober 2013.

[2] M. H. Nehrir, C. Wang, K. Strunz, H. Aki, R. Ramakumar, J. Bing, Z. Miao, Z. Salameh, “A Review of Hybrid Renewable/ Alternative Energy Systems for Electric Power Generation: Configuration, Control, and Applications”. IEEE Transactions on Sustainable Energy, Vol. 2, No. 4, October 2011, pp. 392-403.

[3] Y. Xu, Z. Shi, J. Wang and P. Hou, "Discussion on the Factors Affecting the Stability of Microgrid Based on Distributed Power Supply," Energy and Power Engineering, Vol. 5 No. 4B, 2013, pp. 1344-1346.

[4] M. Moradian, F.M. Tabatabaei, and S. Moradian, “Modeling, Control & Fault Management of Microgrids,” Smart Grid and Renewable Energy, Vol. 4, No. 1, 2013, pp. 99-112.

[5] N.A LUU, “Control and management strategies for a microgrid,” Saint-Martin-d'Hères, Grenoble University, December,18, 2014.

[6] A. Vinayagam, K.S.V. Swarna, S.Y. Khoo, A.T. Oo, and A. Stojcevski, “PV Based Microgrid with Grid-Support Grid-Forming Inverter Control-(Simulation and Analysis),” Smart Grid and Renewable Energy, 8, 1-30, 2017.

[7] M. Ariyasinghe and K. Hemapala, "Microgrid Test-Beds and Its Control Strategies," Smart Grid and Renewable Energy, Vol. 4 No. 1, 2013, pp. 11-17.

[8] M. Venkateshkumar, R. Indumathi, and P. Poornima, “Photovoltaic cell power generation for stand-alone applications,” IEEE-International Conference On Advances In Engineering, Science And Management (ICAESM -2012), pp. 57-62.

[9] R. Indumathi, M. Venkateshkumar, and R. Raghavan, “Integration of D-Statcom Based Photovoltaic Cell Power in Low Voltage Power Distribution Grid,” IEEE-International Conference On Advances In Engineering, Science And Management (ICAESM -2012), pp. 460-465.

[10] M. Venkateshkumar, and R. Raghavan, “Hybrid Photovoltaic and Wind Power System with Battery Management System using Fuzzy Logic Controller,” Vol. 5, No. 2, August 2016, pp. 72-78.

[11] M. G. Villalva, J. R. Gazoli, and E.R. Filho, “Modeling and circuit-based simulation of photovoltaic arrays”, Power Electronics Conference, COBEP '09. Brazilian, 2009, pp. 1244-1254.

[12] H. Bellia, R. Youcef, and M. Fatima, “A detailed modeling of photovoltaic module using MATLAB,” NRIAG Journal of Astronomy and Geophysics, Vol. 3, No. 1, June 2014, pp. 53-61.

[13] K. K. M. S. Kariyawasam, K. K. N. P. Karunarathna, R. M. A. Karunarathne, M. P. D. S. C. Kularathne, and K. T. M. U. Hemapala, “Design and Development of a Wind Turbine Simulator Using a Separately Excited DC Motor,” Smart Grid and Renewable Energy, Vol. 4 No. 3, 2013, pp. 259-265.


ISSN 1737-9334

# A Review of Reconfigurable Antenna for Wireless Communication Systems

Nafaa M. Shebani[#1], *AbdalnaserF. kaeib*[*2], Amer R. Razek[*3]

[#]*Electrical & Electronic Eng. Department, Sabratha University*
*Sabratha, Libya*

[1]nafah@yahoo.com

[*]*Electrical & Electronic Eng. Department, Zawia University*
*Zawia, Libya*

[2]naser.kaeib@gmail.com

[3]anas_az94@yahoo.co.uk

***Abstract***— Reconfigurable antenna is an antenna that capable to reconfigure its characteristics such as frequency, pattern, bandwidth, and polarization to adapt to the environment. The reconfiguration is not limited to a single characteristic but can be a combination of different characteristics depending on the application. The purpose of a reconfigurable antenna is to reduce the complexity of an antenna system operating over a wide frequency band, and to reduce the need of multiple antennas to perform a specific task, providing a relatively large bandwidth and achieving a dynamical reconfiguration within a few microseconds to meet the requirements of the modern wireless communication systems. This paper presents the concept of reconfigurable antenna and details the emerging technologies that make reconfigurable antennas possible, how to achieve reconfigurability in terms of different parameters with switching mechanism and the different feeding techniques used are discussed.

***Keywords***— Reconfigurable antenna, reconfigurable frequency, reconfigurable radiation pattern, a reconfigurable polarization.

## I. INTRODUCTION

Modern wireless systems usually have multiple standards so that they require modern antenna systems with multiple capabilities and functions without enlarging occupied volume. The reconfigurable antenna becomes a popular solution because it provides variety in antenna performance to satisfy diverse communication requirements and decrease the interference [1]. Single antenna can be used for multipurpose application by changing their parameter such as frequency, pattern or polarization [2]. With multiband capability, reconfigurable antennas can utilize more efficiently radio frequency spectrum, facilitating a better access to wireless services in modern radio transceivers [3].

The ability to control the operating band of an antenna system can have many useful applications. Systems that operate in an acquire and track configuration would see a benefit from active bandwidth control. In such systems a wide band search mode is first employed to find a desired signal then a narrow band track mode is used to follow only that signal. Utilizing active antenna bandwidth control, a single antenna would function for both the wide band and narrow band configurations providing the rejection of unwanted signals with the antenna hardware. This ability to move a portion of the RF filtering out of the receiver and onto the antenna itself will also aid in reducing the complexity of the often expensive RF processing subsystems.

The radiation pattern and functionality of an antenna are related to the current distribution on its surface. Any slight change in the geometrical configuration of the structure will create new current paths and new radiation edges, which give the antenna new resonances and operational functionality, a lot of reconfigurable antennas make use of switches, rotating parts and many other components to vary the current distribution over the physical surface of the antenna. This constitutes a transformation or a translation from a physical activity into an electrical behaviour change. [4]

This paper aims to present a briefly survey on the different types of reconfigurable antennas and display the switching techniques that used to achieved the reconfigurability of the antenna.

## II. SWITCHING TECHNIQUES.

The techniques that can be used for reconfigurability in antennas are many such as by using active switches based on micro electro mechanical systems (MEMS), PIN diodes, varactor diodes or using a mechanical movement of different patches by using stepper motors, bending of one or more of its parts or even using a photo-conductive switches. Another way to achieve controllable antenna features is to bias different antenna parts at different times, appropriately feed antenna array and reconfigure feeding networks [5]. Varactor diodes for frequency tuning. These are normally accompanied by biasing lines and high biasing voltages. PIN diodes in reconfigurable antennas have also gained in popularity, as they require lower biasing voltages. MEMS are limited by low-power handling capabilities and mechanical failure due to moving parts. All these designs require metallic biasing lines to be attached to the antenna which can interfere with the radiation patterns. Using fibre optic cables instead to activate optical switches have the advantage of being electromagnetically transparent and so do not interfere with the radiation patterns of the antenna [6].

Based on some properties, the basic comparisons between the different types of switches such as MEMS, PIN diodes, Varactor, optical switches, physical technique, and smart materials are tabulated in Table 1.


ISSN 1737-9334

TABLE 1 COMPARISON OF DIFFERENT WITH SWITCHING TYPES.

| Tunable component | Advantages | Disadvantages |
|---|---|---|
| RF MEMS | Insertion loss is less, very high linearity, good isolation, low power loss and consumes no DC power used. | High control voltage is needed (50-100 V) poor reliability, switching speed is slow, discrete tuning, limited lifecycle. |
| PIN diodes | Driving voltage needed is less, tuning speed and power handling capabilities is high, very low cost, and very reliable as no rotating part. | In its ON state needs high DC bias voltage and consumes large amount of energy, on linear characteristics, poor quality factor and discrete tuning. |
| Varactor | It gives continuous tuning, and consumes less energy than others. | Highly nonlinear and have low dynamic range and require complex circuitry. |
| Optical switches | More reliable , linear characteristics , no biasing circuits | Lossy behavior, complex activation mechanism |
| Physical technique | Does not require bias circuits which eliminates interference , losses and radiation pattern distortion | Slow response, cost, power requirements, size, complex integration, |
| Smart materials | Size as it has high relative permittivity, permeability | Low efficiency[5] |

## III. TYPES OF RECONFIGURABLE ANTENNA.

The Ability to reconfigure any parameter of the antenna according to the requirement is defined as reconfigurability [7]. Antenna with reconfigurable feature can be of large variety and different shapes and sizes, there are four reconfiguration properties that a reconfigurable antenna can achieve. An antenna can exhibit a reconfigurable frequency of operation, a reconfigurable radiation pattern, a reconfigurable polarization behaviour, or a combination of any of these properties [8].

### *A. Frequency Reconfigurable Antenna.*

An antenna operating on multiple frequency bands has gained a lot of attention due to the proliferation of modern wireless technology and customer demand for multiple services in a single device. Conventionally, a frequency band is associated with a particular wireless service; therefore multi-band antenna is required to support multiple services in a single wireless device. Multi-band antennas can operate over different frequency bands exhibiting good gain and stable radiation pattern. Albeit, multiband antennas transmit electromagnetic waves simultaneously at all the supported frequencies in addition to the desired frequency [9].

Below are some of the papers that explain how to implement and design changeable antennas by frequency, and the techniques used to switch.

Frequency Reconfigurable antenna they planned circular patch with back coaxial feed instrument and the PIN diode is used as a switch and it is mounted on the arc shaped slot in paper [10]. Five PIN diodes as switches are symmetrically located in the slot by 20°, 32°, 90°, 148°, and 160°. The simulated and measured results show that the antenna can operate from 1.82GHz to 2.46GHz, which is located in DCS1800 (1.71–1.88GHz), UMTS (2.11–2.20GHz), WiBro (2.3–2.4GHz), and Bluetooth (2.4–2.48GHz) frequency bands and so forth The simulated design is shown in Figure 1, the experimental results indicate good agreement with the simulation results with little resonant frequency offset as displayed in Figure 2.

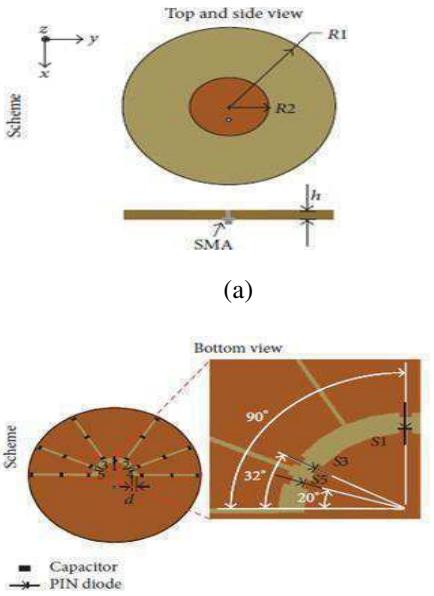


Figure 1. Simulated design, (a) Top view, (b) Side view

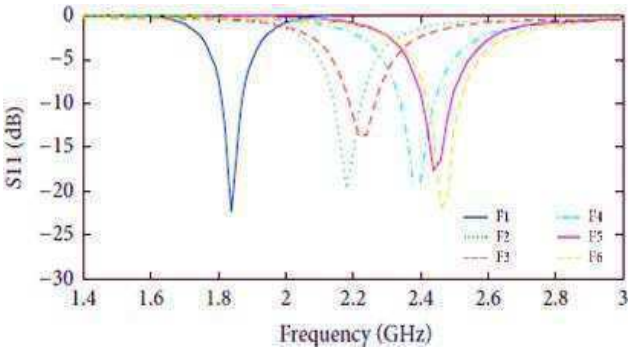


Figure 2. The experimental results vs simulation results

In [11], a reconfigurable printed patch (50 × 60 ×1.6mm3) antenna capable of communication over eight different 4G LTE bands is proposed. The reconfigurability in this patch antenna is achieved using three RF PIN diodes as switches. These switches are controlled by three separate DC lines. Figure 3 shows a top view and a fabricated prototype of the proposed antenna.




ISSN 1737-9334

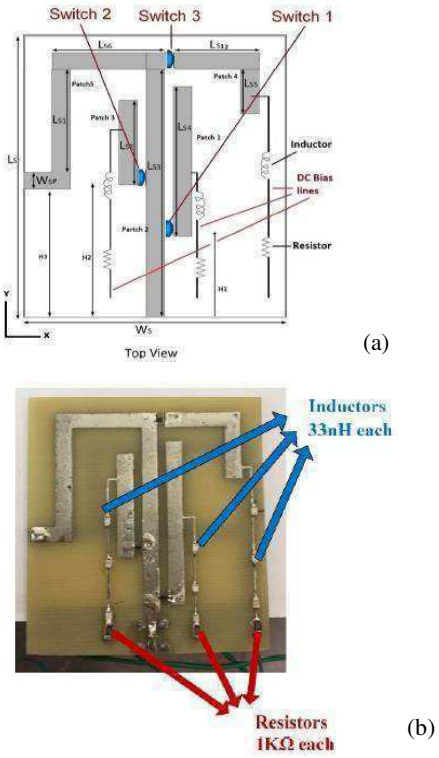


Figure 3. Proposed antenna. (a) Top view (b) A fabricated prototype

It is clear from the results for S11 < -10 dB that this reconfigurable antenna covers nine different LTE/WLAN frequency bands including 0.9 GHz, 1.4 GHz, 1.5 GHz, 1.6 GHz, 1.7 GHz, 1.8 GHz, 2.5 GHz, 2.6 GHz, and 3.5 GHz bands under different switching combinations/modes.

In paper [12], a frequency reconfigurable patch-slot antenna with directional radiation pattern has been designed and measured. Geometry of the antenna is shown in Figure 4.
It has been demonstrated that the frequency reconfigurability can be achieved by inserting switches in the slot of the antenna. The antenna is capable to reconfigure up to six different frequency bands from 1.7 GHz to 3.5 GHz.

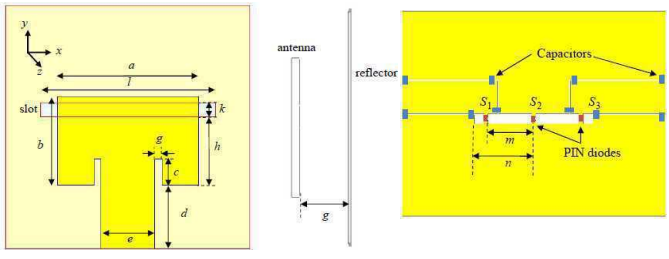


Figure 4. Geometry of the proposed antenna, (a) front view, (b) side view, and (c) back view of the proposed antenna.

The microstrip patch antenna produces three different frequency bands with directional radiation pattern while the microstrip slot antenna produces another three frequency bands with bidirectional radiation pattern. Due to the reflector placed at the back of the antenna, the radiation pattern is directional at all frequency bands.
Simulated and measured reflection coefficient of the proposed antenna is illustrated in Figure 5. Form the results, it is clear that the antenna has a different resonant frequencies such as 1.9 GHz, 2.4 GHz, 3 GHz, and 3.5 GHz.

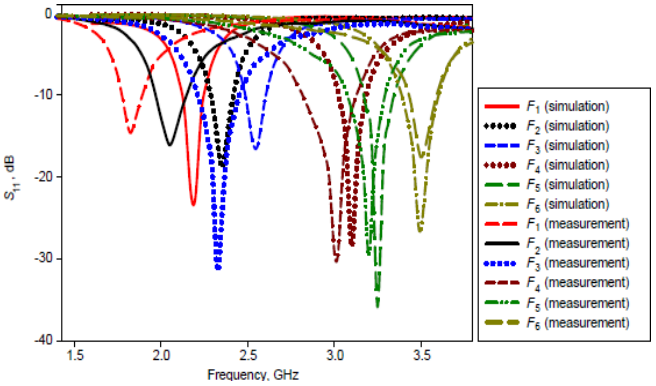


Figure 5. Simulated and measured reflection coefficient in dB of the proposed antenna.

In work [13], a reconfigurable antenna design is investigated. The antenna patch has a circular form that rotates to feed different shapes. Frequency reconfigurability is achieved while maintaining the same omni-directional radiation pattern in both the E and H planes. Four different rotations can be done making the antenna cover five different bands (from 2 GHz up to 7 GHz) correspondingly. A complete agreement was found between the simulated and the measured data. In this paper the photoconductive switch was used. Photoconductive switches usually require a high laser pumped power level to excite enough electrons from the valence band to the construction in order to make the switch conductive.
The corresponding antenna structure is shown in Figure 6. It consists of two layers. The bottom layer is a partial ground to allow radiation above and below the substrate, and the top layer is a rotating circular shape. The chosen substrate is Taconic TLY with a dielectric constant of 2.2 and a thickness of 1.6 mm.

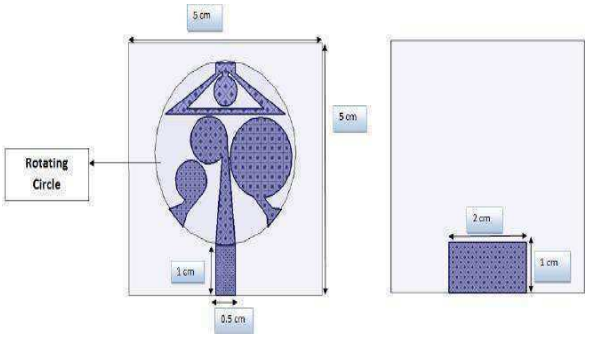


Figure. 6. Antenna structure (a) top layer (b) bottom layer.

A 4×4 frequency reconfigurable antenna array using periodic dumbbell slotted aperture is presented in [14], the antenna array with size 80×80 mm is designed and fabricated by considering


ISSN 1737-9334

the switching activities in ideal condition, meaning that without real PIN diode.

A corporate feed network is used as a power divider between antenna elements. The 50 Ω transmission line consists of 70.7 Ω λ/4 transformer with 100 Ω power divider is designed with two conditions by referring to the "OPEN" and "SHORT" condition of feeding network as shown in Figures 7 and 8, respectively.

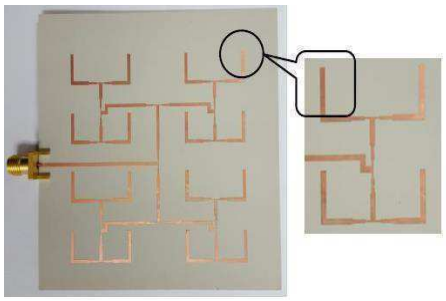

Figure 7. Feed line in "OPEN" condition.

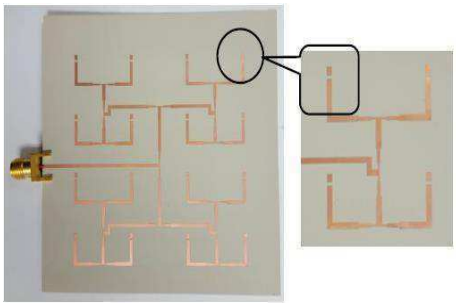

Figure 8. Feed line in "SHORT" condition.

The obtained results show the fabricated responses are slightly shifted compared with simulated response. Where in "OPEN" feeding line the antenna resonates at 7.39 GHz, while in "SHORT" feeding line the fabricated antenna resonate at 8.76 GHz. The directivity of the proposed antenna seems consistent where it is 15.26 dBi for "OFF" condition, and 17.78 dBi for "ON" condition for measured mode; and it provides very high values to support outdoor wireless communication systems.

*B. Reconfigurable Radiation Pattern.*

The pattern reconfigurable antenna in particular has received much attention because manipulation of the radiation pattern enables avoidance of noise sources, improved security by directing signals only toward intended users, sensibility of signal, intentional jamming, improved beam steering capability of phased array systems, and diversity systems [15]. Some of the papers that studied this type of antenna will be clarified.

In [16], a compact microstrip antenna with radiation pattern reconfigurability using MEMS switches is proposed and investigated. Six MEMS switches are used to respectively connect or disconnect the fan-shaped coupling cells and fan-shaped radiations cells of the proposed antenna, changing the current distribution and achieving radiation pattern diversity.

Twelve basic operation states (state 1 to state 12) are obtained for the proposed antenna. Sequentially switching operation states from state 1 to state 12 can rotate the main radiation beam by 30° from 0° to 330° in azimuth plane, maintaining 35° in elevation plane. Moreover, this novel pattern-reconfigurable antenna can operate around 4 GHz stably with all operation states. Figure 9 exposed Geometry of the proposed antenna.

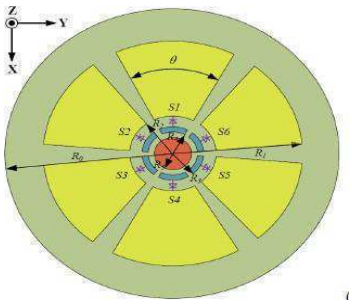


Figure 9. Geometry of the proposed pattern-reconfigurable antenna

Simulated and measured radiation patterns (azimuth plane) for different three operation states is shown in Figure 10, state 1when (S1=1, S2 ,S3, S4, S5 and S6=0), State 2 (S1=0, S2=1, S3, S4, S5, an S6 =0) and state 2 (S1, S2, S5, S6, =0 and S3, S4 =1).

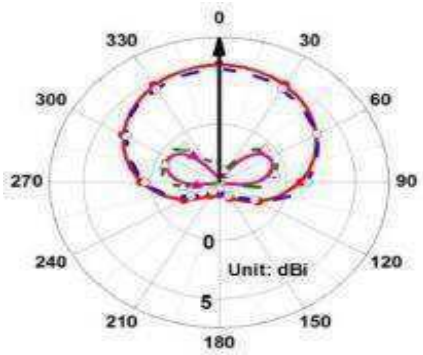


State 1

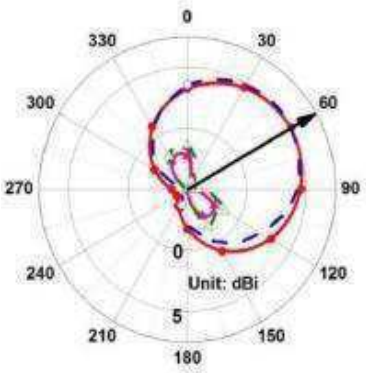


State 2

Figure 10 Simulated and measured radiation patterns (azimuth plane) for different operation states

In [17], a compact and multidirectional pattern-reconfigurable antenna is presented. The antenna design is based on the




ISSN 1737-9334

principles of the common Yagi–Uda antenna. The main driven circular patch is surrounded by several parasitic circular patches, and four pin diode switches are used to short/open the parasitic patches to ground. The proposed antenna was fabricated and evaluated experimentally, and measured results are in good agreement with the simulated. The operating bandwidth ranges from 2.36 to 2.39 GHz, and the antenna can provide beam control at nine different angular directions ($\phi$,$\theta$) = ($0^o$ , $0^o$) ($0^o$ , $23^o$ ), ($45^o$, $22^o$ ), ($90^o$ , $24^o$ ), ($135^o$ , $22^o$ ), ($180^o$ , $24^o$ ), ($225^o$ , $25^o$), ($270^o$ , $25^o$), and ($315^o$ , $22^o$) with realized gain levels greater than 7.0 dBi. In Figure 11. Geometry of the proposed antenna.

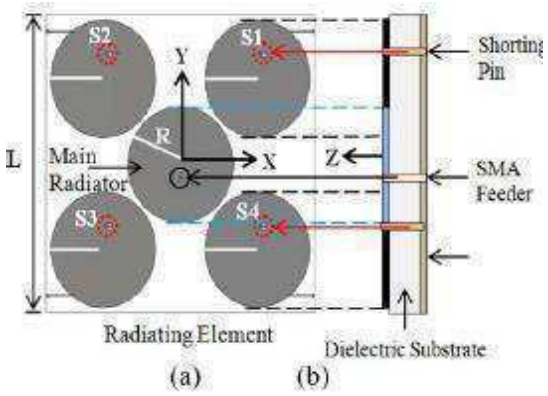


Figure 11. Geometry of the proposed antenna. (a) Top view. (b) Side view.

Simulated and measured radiation pattern at 2.38 GHz, for different states shown in Figure 12. (a) ALL PIN diodes are ON, Phi=0, (b) PIN diodes S1 and S4 are OFF, Phi=0.

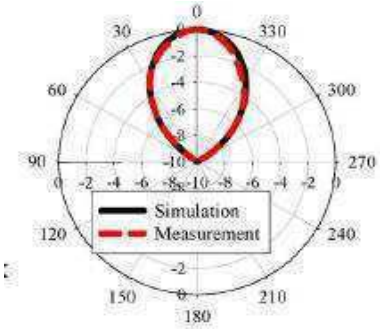


(a)

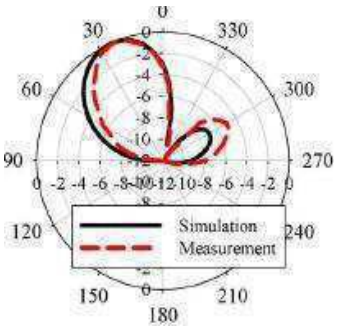


(b)

Figure 12. Simulated and measured radiation pattern at 2.38 GHz.

In [18], this paper presents the use of micro-electromechanical systems (MEMS) switches to realize the radiation pattern reconfiguration of microstrip antenna, which works in Ka band. The antenna was fabricated on a silicon substrate and designed to reconfigure radiation pattern at the operation frequency of 35 GHz. The simulation results show that by controlling the states of MEMS switches between the driven element and two parasitic elements, the antenna can achieve reconfiguring into three maximum radiation directions in the H-plane. The layout of the antenna is shown in Figure 13. The measured maximum radiation directions of modes 1, modes-2, modes-3 and modes-4 are $\phi$ = 17◦, -25.8◦, 3.5◦, 0.7◦ and gains of four modes at the maximum radiation direction are 5.78 dBi, 6.49 dBi, 7.24 dBi and 6.31 dBi, respectively. The measured results are closely consistent with the simulation ones.

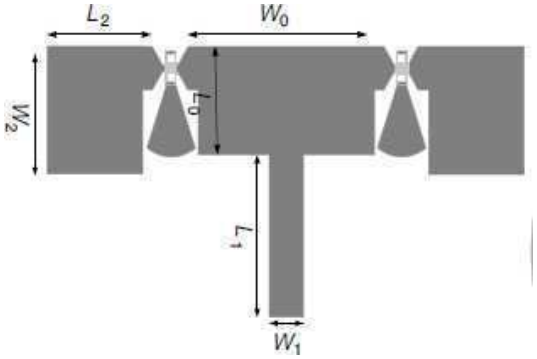


Figure. 13. Top view of proposed reconfigurable antenna

Figure 14 shown the simulation results of radiation pattern in H-plane for different modes.

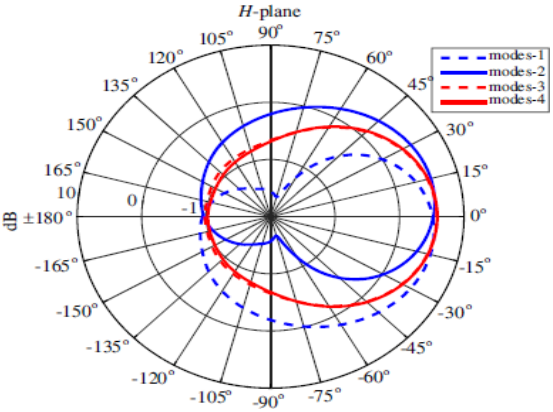


Figure 14. The simulation results of radiation pattern in H-plane for different modes.

A radiation pattern reconfigurable microstrip antenna is proposed in [19]. There is the presence of four PIN diodes as switches to control the main beam. Different possibilities of beam rotation is achieved by activating the switches; the antenna main beam rotates by 90° in every step in the azimuth planes, with 30° deflection in the elevation planes. Here the operating frequency attained is 3.44-3.6 GHz which is used for WiMAX systems. In Figure 15 proposed design and implemented antenna design is presented.




ISSN 1737-9334

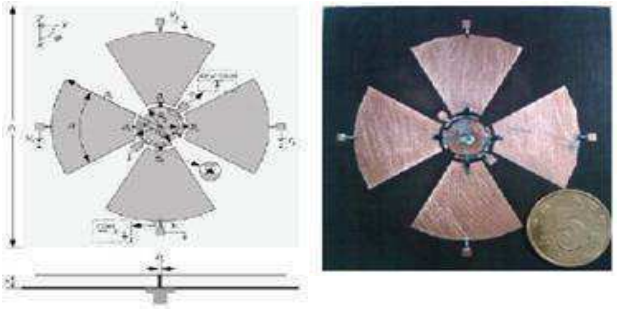

Figure 15. Geometry of proposed antenna

Measured radiation patterns at 3.5 GHz Elevation plane and Azimuth plane are given in Figure 16.

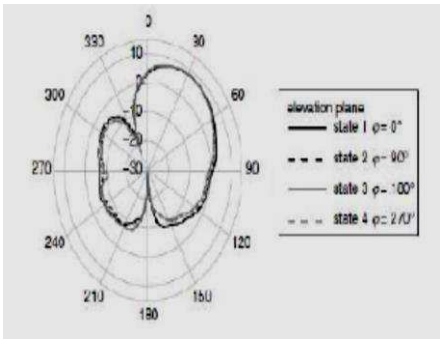


(a)

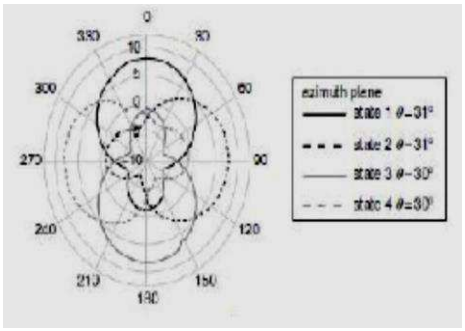


(b)

Fig 16.Measured radiation patterns at 3.5 GHz (a) Elevation plane , (b) Azimuth plane

In [20], The reconfigurable antenna consists of numerous metal cylinders arranged around the annular slot antenna. A shorting pin is inserted to allow the annular slot antenna to have an omnidirectional radiation pattern By controlling pin diodes associated with the metal cylinders, the antenna is capable of working up in different directions with a maximum working beam angle of 11.25° at a frequency of 1.05 GHz.

*C. Reconfigurable Polarization.*

The Polarization of Electromagnetic wave is defined as the orientation of electric field vector in space with respect to time. Polarization reconfiguration is the process of altering the orientation of the charges according to the requirement of the particular application. There are three types of EM wave polarizations Horizontal, Vertical and Circular (LHCP/RHCP) polarization.

In common horizontal and vertical polarization is termed as linear polarization and Reconfiguring the polarization among these three modes is said to be polarization reconfiguration. [8] Some related surveyed contents are listed.

In [21], this paper The antenna is capable of switching its polarization from right hand circular polarization (RHCP) to left hand circular polarization (LHCP) and vice versa. The design targets the WLAN IEEE 802.11 b/g frequency band (2.4–2.5 GHz) being used in various wireless communication systems. Good agreement is obtained between simulated and measured results. The antenna exhibits a 7% effective bandwidth from 2.4 GHz to 2.57 GHz with 8.7 dBic maximum gain. Figure 17 illustrates the geometry of a single-feed reconfigurable E-shaped patch antenna with integrated DC biasing circuit.

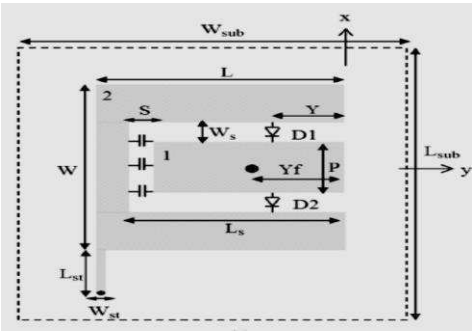


Fig 17 Geometry of a single-feed reconfigurable E-shaped patch antenna

Simulated and measured radiation pattern of the proposed antenna at 2.45 GHz shown in Figure 18: (a) x-z plane at state 3; (b) y-z plane at state 3; (c) x-z plane at state 4; and (d) y-z plane at state 4.

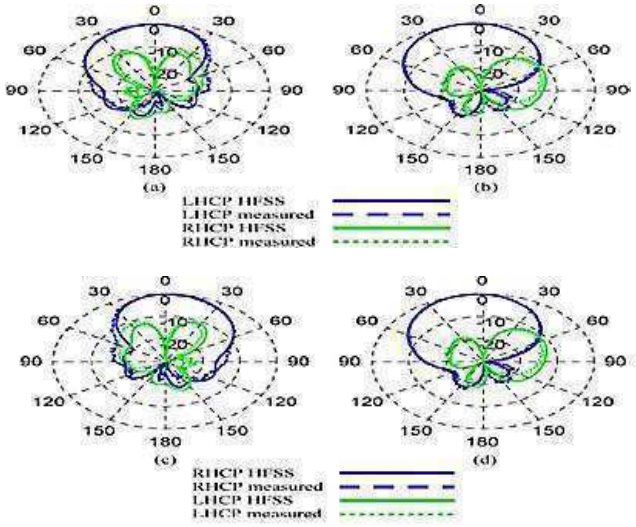


Figure 18. Simulated and measured radiation pattern of the proposed antenna at 2.45 GHz.

Paper [22] demonstrates a new microstrip dual-band polarization reconfigurable antenna for wireless local area network (WLAN) systems operating at 2.4 and 5.8 GHz. The antenna consists of a square microstrip patch that is aperture coupled to a microstrip line located along the diagonal line of


ISSN 1737-9334

the patch. By switching between the different states of PIN diodes, the proposed antenna can radiate either horizontal, vertical, or 45 linear polarization in the two frequency bands. Measured results on reflection coefficients and radiation patterns agree well with numerical simulations. The antenna consists of two substrate layers as shown in Figure 19 (a) and (b), respectively. A side view of the antenna structure is given in Figure 19 (c).

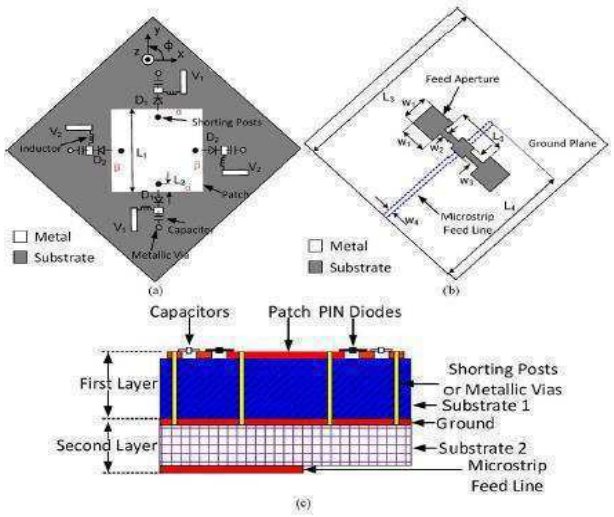


Figure 19. Schematics of the proposed antenna: (a) first layer, (b) second layer, (c) side view.

State 1, D1 is forward biased, D2 reversed biased and the polarization is oriented in x-direction. State 2, D1reversed biased, D2 forward biased and polarization y-oriented. And state 3 D1 and D2 is reversed biased, polarization is 45°-oriented. Figure 20 shown simulated and measured E-plane normalized radiation patterns at 2.45 GHz for state 1, state 2 and state 3.

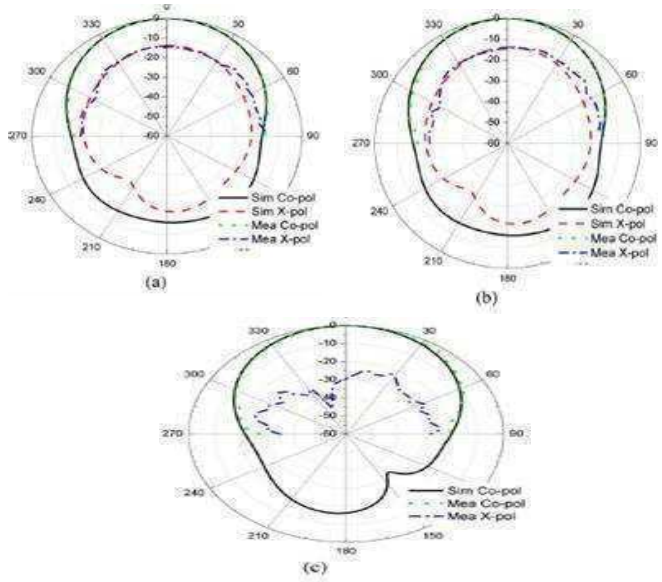


Figure 20. Simulated and measured E-plane normalized radiation patterns at 2.45 GHz: (a) State 1 (b) state 2 (c) state 3

A simple polarization and beam switching reconfigurable antenna is presented in [23]. The circular patch with annular slot is used as the radiating element. The circular metallic conductor positioned below the substrate with the air dielectric acts as the ground plane for the antenna. The proposed antenna is intended to operate at 2.4 GHz band with switchable polarization capability. Four PIN diodes have been placed diagonally covers the corresponding switch-ability, with good efficiency more than 80%. The detailed antenna geometry is shown in Figure 21.

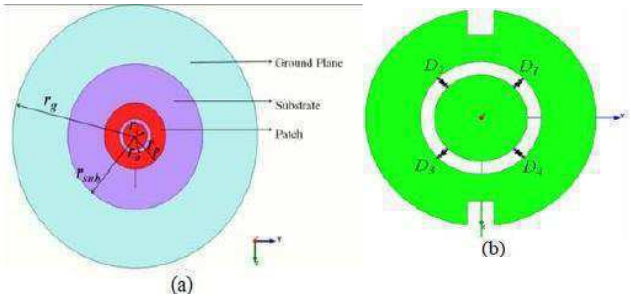


Figure 21. Geometry of Proposed Antenna (a) circular patch antenna with annular slot (LP Antenna) (b) with insertion of PIN diodes (CP Antenna)

The radiation patterns are obtained using EM simulations for E-plane is shown in Figure 22.

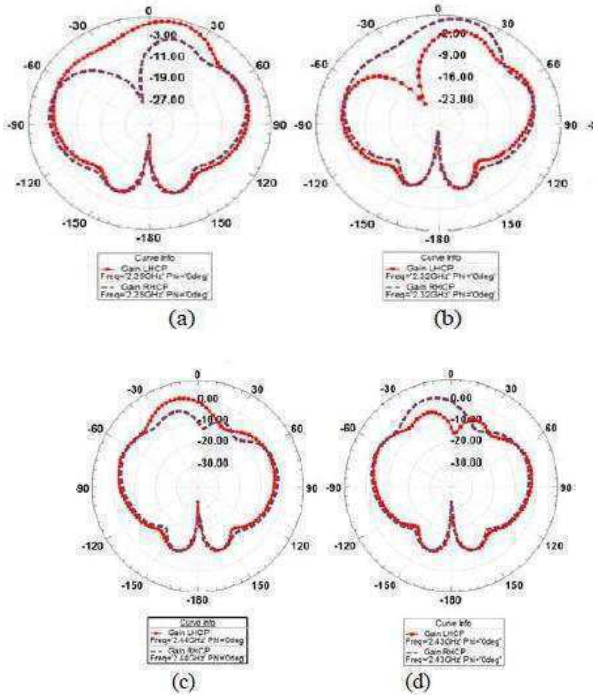


Figure 22. 2D-radiation patterns in E-plane for Antenna with four-diodes at resonant frequencies (a) D1 ON (b) D2 ON (c) D3 ON (d) D4 ON

In paper [24], a novel technique to design polarization reconfigurable antennas using two types of perturbations is presented. A square slotted ground plane and an L-shape microstrip segment are used simultaneously to obtain polarization reconfigurability. The square slot on the ground creates a negative perturbation. The negative perturbation can


ISSN 1737-9334

be eliminated by a positive perturbation that is made by adding an L-shape microstrip segment to the patch using a switching diode. The layout of the proposed reconfigurable antenna is illustrated in Figure 23. The polarization sense can be alternated between CP and LP at different frequencies by changing the state of a diode.

Moreover, the benefit of the this antenna is to use a single switching diode to achieve polarization and frequency diversities that helps to attain better gain than other conventional polarization reconfigurable antennas using multiple switching diodes.

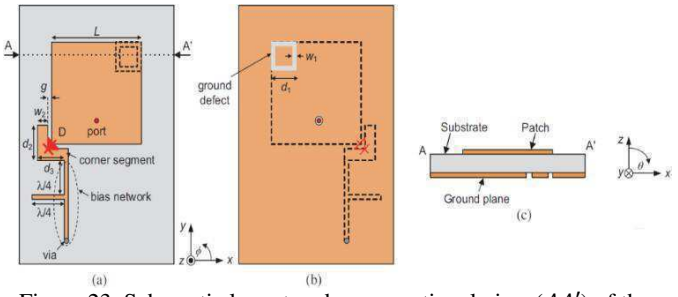


Figure 23. Schematic layout and cross sectional view ($AA'$) of the proposed antenna.

In addition, this antenna is suitable to enhance polarization reconfigurability by integrating active components on the ground slot with simple bias circuit arrangement on the ground plane as the polarization reconfigurability achieved by defected ground perturbation is free from radiation performance degradation that is caused in the case of the patch side perturbation segment and bias networks. The antenna structure is very simple and compact; and it is attractive for wireless and satellite communication applications such as terrestrial digital broadcasting.

A new circular polarization reconfigurable antenna for 5G wireless communications is presented in [ 25]. The antenna that shown in Figure 24, containing a semicircular slot, was compact in size and had a good axial ratio and frequency response.

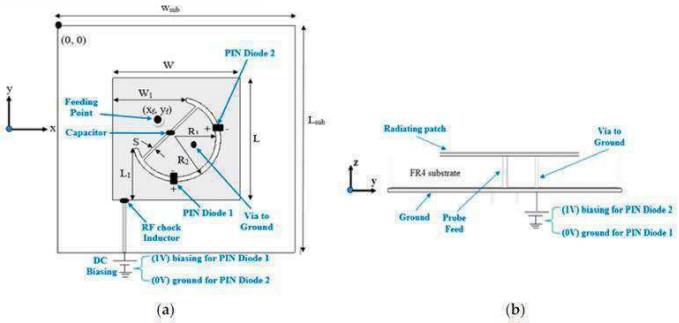


Figure 24. Proposed polarization-reconfigurable patch antenna: (a) Top view; (b) Side view.

Two PIN diode switches controlled the reconfiguration for both the right-hand and left-hand circular polarization. The proposed microstrip antenna was fabricated on an FR-4 substrate with a loss tangent of 0.02, and relative dielectric constant of 4.3. The radiating layer had a maximum size of $18.3 \times 18.3\ mm^2$ , with $50\ \Omega$ coaxial probe feeding.

Reconfigurable orthogonal polarizations were achieved by changing the states of the two PIN diode switches, and the reflection coefficient $|S11|$ was maintained, which is a strong benefit of this design.

The proposed antenna is reconfigurable for both RHCP and LHCP, by adjusting the DC biasing of two PIN diodes. The proposed design shows a 9.11% fractional bandwidth, with maximum realized gain of (3.1 to 4.8) dBi at 3.5 GHz, and a good axial ratio below 1.8 dB for both modes of operation.

Figure 25 shows the measured and simulated radiation patterns of the proposed structure for both configurations (RHCP and LHCP) at resonance frequencies.

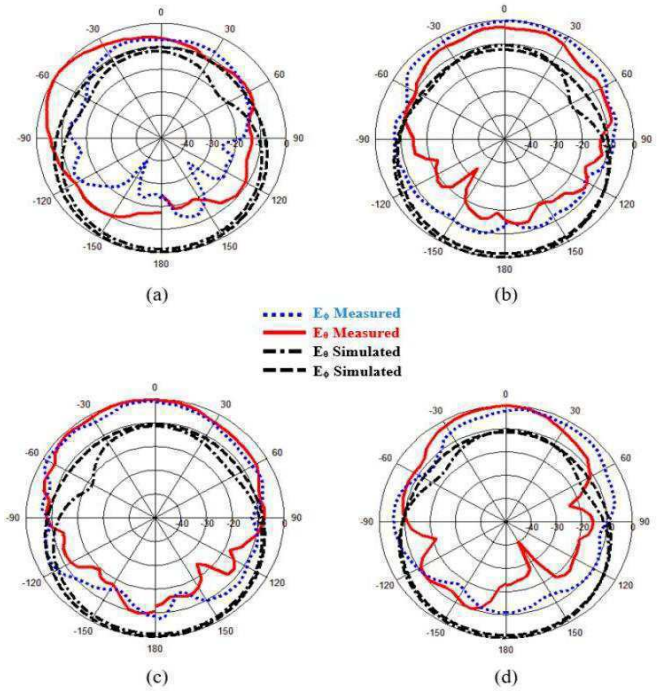


Figure 25. Simulated and measured radiation patterns of the proposed antenna: (a) ON-OFF state, xz plane; (b) ON-OFF state, yz plane; (c) OFF-ON state, xz plane; (d) OFF-ON state, yz plane.

### *D. Hybrid Reconfigurable Antenna*

A dual-notch polarization and beam reconfigurable microstrip antenna is illustrated in [26]. It uses parasitic which incorporate switches to steer its beam away from boresight and dual notches that incorporate switches to reconfigure between linear and circular polarization. The antenna is a low profile microstrip patch antenna, which only uses a single feed, allowing it to be compact and simple in terms of its structure.

CP can be preserved for some steering angles. The dual-notch microstrip patch antenna is fed using a coaxial feed. The notches are located on a line angled at 45° to the location of the feed. The antenna is designed for LHCP operation; the size of the notches controls the CP operation of the antenna.

Figure 26 shows the structure of the proposed antenna. It is important to note that the copper switches are used; when


ISSN 1737-9334

copper is present the switch is ON when copper is not present the switch is OFF. However, PIN diodes can be used in the notches to switch between CP and LP.

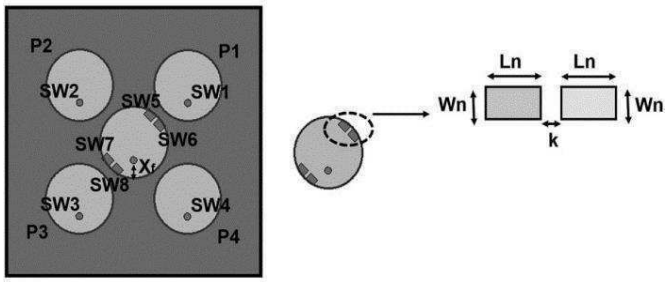


Figure 26. Structure of the dual-notch single element antenna

Form the results of mode 2 where the switches 1 and 4 are ON and other switches are OFF, it can be observed that the antenna supports CP over a range of steering angles at 10.3 GHz. More specifically, the AR is less than 3 dB from −55° up to 38°. This shows that the antenna is CP for several steering angles; and from the radiation pattern responses at mode 2, it can be observed that there is acceptable agreement between measurement and simulation. Measurement differs from simulation at the back lobe direction due to the presence of cables always affect the radiation performance of an antenna.
In [27] a novel flexible frequency and pattern reconfigurable antenna for wireless system is proposed. The antenna consists of two completely symmetrical radiating elements, a feedline and ground. Eight PIN diodes are loaded on the symmetric hexagonal split ring and monopole branches to select the radiation element. The geometry of the flexible reconfigurable antenna is presented in Figure 27.
The antenna with bias lines is fabricated on a Rogers5880 substrate. By controlling PIN diodes, the proposed antenna achieves frequency reconfiguration in the 1.9 GHz band with a bandwidth of 1.84–2.00 GHz and the 2.4 GHz band with a bandwidth of 2.27–2.49 GHz, and it is capable of steering the beam in two directions in each band.
When operating at 1.9 GHz band, the antenna can switch the pattern in the direction of φ = 60° and φ = 300°, and when operating at the 2.4 GHz band, the antenna can switch the pattern in the direction of φ = 34° and φ = 326°. Meanwhile, the antenna works at four states with omnidirectional radiation patterns.

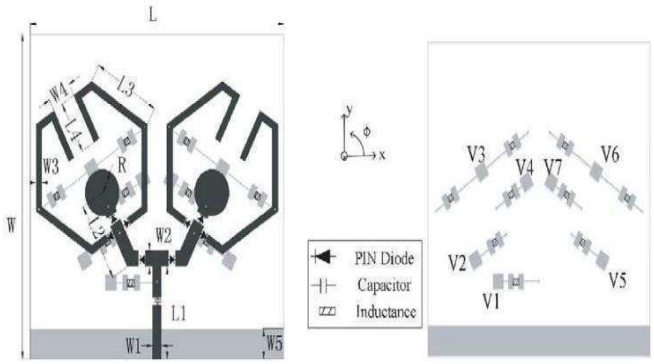


Figure 27. Geometry of the flexible reconfigurable antenna.

Simulated and measured radiation patterns of E plane at states ofS1 (P1, P2 and P3 are ON and other diodes are OFF) and S3 (P5, P6 and P7 are ON and other diodes are OFF) are shown in Figure 28 at 1.9 GHz; and at states of S2 (P1 and P4 are ON and other diodes are OFF) and S4 (P5 and P8 are ON and other diodes are OFF) are shown in Figure 29 at 2.4 GHz. The simulation and measurement of the two states are basically in agreement.

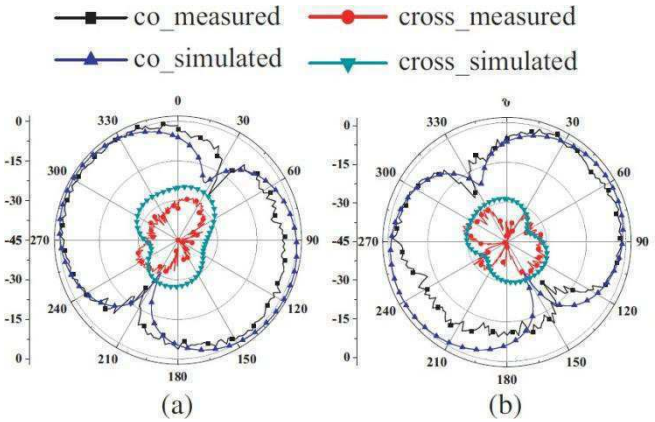


Figure 28. Radiation-patterns for different states of the proposed antenna at 1.9GHz. (a) E plane at S1. (b) E plane at S3.

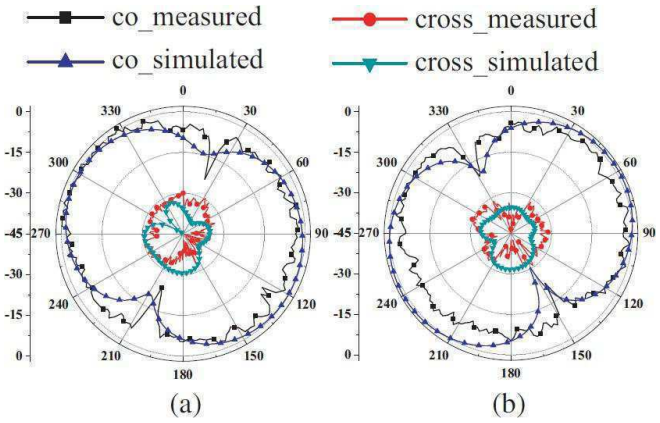


Figure 29. Radiation-patterns for different states of the proposed antenna at 2.4GHz. (a) E plane at S2. (b) E plane at S4.

## IV. Conclusions

In this paper, a concepts of four types of reconfigurable antenna and switching techniques are presented in details.
From the brief survey of the reconfigurable antenna, it can be concluded that
The single reconfigurable antenna can be operated with more efficient for different modes than other types of antenna, and it gives an effective communication with low cost and less complexities.
The switching techniques that used to achieve a reconfigurability of the antenna are choice based on some specifications such as complexity of fabrication, biasing network required, time of switching, and the cost of switches. Each of the switching techniques has its own advantages and limitations. Due to the advantages of PIN diode, where it has a




ISSN 1737-9334

low cost and a simple fabrication process, and possibility to avoid a complicated of the DC biasing circuit, it becomes a very common approach used to realize the reconfigurability of the antenna; and an important characteristic of PIN diode is it has a nearly pure resistance at microwave frequencies.

The good specifications of reconfigurable antennas make them a suitable choice to use in various communication applications such as radar systems, mobile and satellite communications.

## REFERENCES

[1] C.Sebastian, S. Thankachan2, A. George, G.Nath "A Survey On Frequency Reconfigurable Antenna T Echniques", Vol. 4, Issue 1, January 2016.

[2] Abirami .M, Rajasekar G, Puvaneshwar S," A Survey Of Different Reconfigurable Antennas For Various Wireless Applications ",Vol. 4, Issue 2, February 2016.

[3] S. Phadte " Reconfigurable Antenna Methodologies And Switch Technologies: A Review ", Vol 5 Issue 2, January, 2016.

[4] Sudhina H. K, Ravi M. Yadahalli, N. M. Shetti "Bandwidth Control Using Reconfigurable Antenna Elements "World Academy Of Science, Engineering And Technolog International Journal Of Electronics And Communication Engineering , Vol:7, No:12, 2013.

[5] N.Kumar " Design And Analysis Of Frequency Reconfigurable Microstrip Antennas", A Thesis Submitted In Partial Fulfillment Of The Requirements For The Degree Of Master Of Technology In Communication And Networks, May 2015.

[6] C.Panagamuwa, A.Chauraya, Member, J. Yiannis, C. Vardaxoglou, "Frequency And Beam Reconfigurable Antenna Using Photoconducting Switches" Ieee Transactions On Antennas And Propagation, Vol. 54, No. 2, February 2006.

[7] Uma Maheswari P, Manikandan , Sivakumar "Study Of Reconfigurable Antenna" International Journal Of Electronics, Electrical And Computational System, Volume 6, Issue 11, November 2017.

[8] J.Costantine, Y.Tawk, S.Barbin, C.Christodoulou "Reconfigurable Antennas: Design And Applications", Proceedings Of The Ieee | Vol. 103, No. 3, March 2015.

[9] M.Hassa , F. Arshad, Sy.Naqvi, Y.Amin, H.Tenhunen," A Compact Flexible And Frequency Reconfigurable Antenna For Quintuple Applications" Radioengineering, Vol. 26, No. 3, September 2017.

[10] Y. Chen, L.Ye, J.Zhuo, Y.Liu, L.Zhang, M.Zhang, Q.Liu " Frequency Reconfigurable Circular Patch Antenna With An Arc Shaped Slot Ground Controlled By Pin Diodes",International Journal Of Antennas And Propagation, 2017.

[11] H.Chattha, M.Hanif, X.Yang, I. Rana, Q.Abbasi "Frequency Recon_Gurable Patch Antenna For 4g Lte Applications ", Progress In Electromagnetics Research M, Vol. 69, 1-13, 2018.

[12] H.Majid, M.Rahim, M.Hamid, M.Ismail "Frequency Reconfigurable Microstrip Patch-Slot Antenna With Directional Radiation Pattern", Progress In Electromagnetics Research, Vol. 144, 319{328, 2014.

[13] Y. Tawk, J. Costantine, C.Christodoulou," A Frequency Reconfigurable Rotatable Microstrip Antenna Design" , Ieee 2010.

[14] M. Aris, M. T. Ali, N. Abd Rahman, and I. Pasya, " Frequency Reconfigurable Antenna Array Using Defected Ground Structure for Outdoor Wireless Communication Systems", International Journal Of Electrical And Electronic Systems Research, Vol. 9, DEC 2016.

[15] J.Baik, S.Pyo, T.Lee, Y.Kim." Switchable Printed Yagi-Uda Antenna With Pattern Reconfiguration" , Etri Journal, Volume 31, Number 3, June 2009.

[16] W.Ma, G.Wang, Y.Wang, B.Zong," Compact Microstrip Antenna With Pattern-Reconfigurable Characteristic", March 2, 2017.

[17] M. Jusoh, T. Aboufoul, T.Sabapathy, A.Alomainy, M. Kamarudin, "Pattern-Reconfigurable Microstrip Patch Antenna With Multidirectional Beam For Wimax Application" Ieee Antennas And Wireless Propagation Letters, Vol. 13, 2014.

[18] Z. Deng, J.Gan, H. Wei, H. Gong, X.Guo, "Ka-Band Radiation Pattern Reconfigurable Antenna Based On Microstrip Mems Switches", Progress In Electromagnetics Research Letters, Vol. 59, 93-99, 2016

[19] S.J. Shi And W.P. Ding, "Radiation Pattern Reconfigurable Microstripantenna For Wimaxapplication",Electronics Letters 30th April 2015 Vol. 51 No. 9 Pp. 662–664.

[20] N. Ab Aziz, A. Radhi, R.Nilavalan," A Reconfigurable Radiation Pattern Annular Slot Antenna".

[21] A. Khidre, K. Lee, F. Yang, A. Elsherbeni," Circular Polarization Reconfigurable Wideband E-Shaped Patch Antenna For Wireless Applications", Ieee Transactions On Antennas And Propagation, Vol. 61, No. 2, February 2013

[22] P.Qin, Y. Jayguo, C. Ding, "A Dual-Band Polarization Reconfigurable Antenna For Wlan Systems", Ieee Transactions On Antennas And Propagation, Vol. 61, No. 11, November 2013.

[23] M. Ajay Babu, B. Madhav, B. Mohan Reddy, R. Chaitanya, T. Satish, T. Anilkumar, "A Dual-Polarization Reconfigurable Antenna With Beam Switching Characteristics Fors-Band Applications", ARPN Journal of Engineering and Applied Sciences, VOL. 12, NO. 16, AUGUST 2017.

[24] M. Rahman, E. Nishiyama and I. Toyoda, "A Polarization Reconfigurable Microstrip Antenna Employing Dual-Perturbation Technique", Progress In Electromagnetics Research M, Vol. 69, pp.197–206, 2018.

[25] Y Al-Yasir and others, "A New Polarization-Reconfigurable Antenna for 5G Applications", Electronics (ISSN 2079-9292) open access journal on the science of electronics and its applications, 2018.

[26] M. Allayioti, J. Kelly and R. Mittra, "Beam and polarization reconfigurable microstrip antenna based on parasitics", Microwave and Optical Technology Letters,pp. 1460-1464, June 2018.

[27] Z. Zhu, P. Wang, S. You and P. Gao, "A Flexible Frequency and Pattern Reconfigurable Antenna for Wireless Systems", Progress In Electromagnetics Research Letters, Vol. 76, 63–70, 2018.


ISSN 1737-9334

# The E-Band as Future Candidate for Next Generation Networks

Abdussalam M. Ammar [1], Amira Y. Ellafi [2], Amer R. Zerek [3] and *Yousef Jaradat* [4]

[1, 2] College of Electronic Technology, Communication Engineering Department, Tripoli, Libya
[1] E- mail Slm2010ly@gmail.com and [2]E- mail Amoor85ly@yahoo.com
[3]Zawia University, Faculty of Engineering/ EE Department,, Zawia – Libya,
E-mail anas_94az@yahoo.co.uk
[4]Department of Electrical Engineering, Al-Zaytoonah University of Jordan ,Amman, Jordan
E- mail Y.Jaradat@zuj.edu.jo

***Abstract* - Millimeter-wave (mm-Wave) frequencies between 30 and 300 GHz are a new frontier for cellular communication and this band is considered as the potential candidate for high speed communication services in 4 and 5G networks due to its huge bandwidth.This paper discuss the potential applications of mm-Wave communications in the 4 and 5G networks, including the small cell access, the cellular access, and the wireless backhaul. However, mm-Wave does come with its challenges. Some of most prominent issues like rain attenuation and directivity of beam of antenna.**

***Index Terms – mm-Wave , E-band ,FSO, Pencil Beam ,FCC .***

## I. INTRODUCTION

With a 5th generation technology that is expected to be commercially launched during this year or next year, the new generation will offers 1000 times of current capacity and supports smart devices more than 100 times the current cellular networks. And of all data transfer rates that services requiring a high transmission rate, such as video streaming ,IPTV ,etc.[1].

Increased distribution of small cells produces a huge backhaul traffic in the core network, which decisively becomes an important, but somewhat less addressed bottleneck in the system. Using the fiber cable in dense small cell backhaul would result in prohibitively high cost and practical difficulty in deployment [2].

Wireless backhaul may offer an acceptable and cost-reduction solution. However, traditional microwave frequency bands, e.g., sub-5 GHz, may be limited in achievable gains due to the existing spectrum shortness. Despite emerging mechanisms to enhance spectrum efficiency it remains difficult to achieve data rates exceeding 1 Gbps or even 10 Gbps. Therefore, it is hard to meet the rapid increase of 5G traffic demands in such relatively low frequency bands.

Also for coverage issue the traditional broadband spectrum need to be more suitable for increased data rate demand even in 4G not to mention the upcoming 5G services .Here comes the need for old/new spectrum technique as an evolved solution and available resources that will reduces the cost of both Radio Frequency (RF) resources and the fiber cable installation .

The radio-frequency covering the range 30 to 300 GHz is known as millimeter-Wave frequency or very high-frequency. The mm-Wave frequency has drew a lot of attention due to multi-gigabit communication services including high definition multimedia interface, uncompressed high definition video streaming, high-speed internet, wireless gigabit Ethernet, and close-range automotive radar sensor [3].

Till last few years there was a huge "gap" between fiber and other wireless systems . Fig.1 shows the major higher capacity wireless technologies that available now, and how they fit together to produce the current broadband wireless landscape . For many years, optical fibers stayed the only way to realize medium and long distance communications at the diffuse GigE networking interface speed, but the cost of installing and maintaining made its accessibility limited to just a few numbers of users ,only two can reach fiber-like gigabit per second speeds.

These are both of the Free Space Optical systems (FSO) and 60 GHz system limited in distance of just a few hundred yards, significantly limiting their effectiveness as part of wide area networks. There numerous longer distance wireless alternatives, but these are limited in data rate to around 100 Mbps or so.

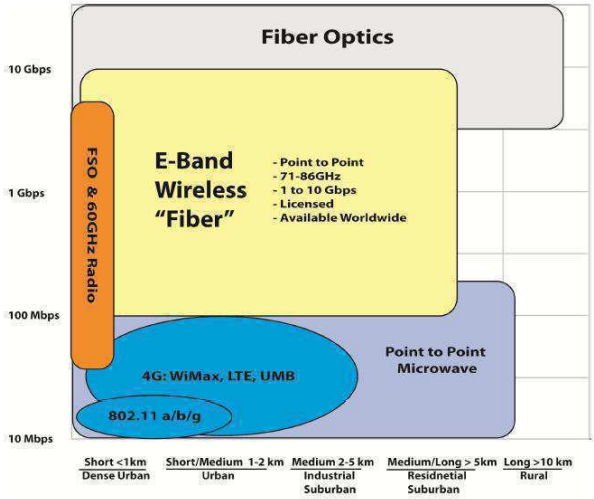


Fig. 1. The major higher capacity wireless technologies.




ISSN 1737-9334

For these reasons, the Federal Communications Commission (FCC) and many other regulators around the world have opened up the e-band 71-76 GHz and 81-86 GHz frequency bands. The availability of this spectrum enables fiber-like gigabit per second and up interconnection speeds, multiple mile transmission distance systems, and products with significantly lower cost and improved economics over buried fiber.

## II THE MM-WAVE

The current 4th generation (4G) systems including Long Term Evolution (LTE) and mobile Worldwide Interoperability for Microwave Access (WiMAX) already use advanced technologies such as Orthogonal Frequency Division Multiplexing (OFDM), Multiple Input Multiple Output (MIMO), multi-user diversity, link adaptation, turbo code, etc, to achieve the most spectral efficiencies close to theoretical limits in terms of bits per second per Hertz per cell [4]. With limitations for future spectral efficiency improvement, another possibility to increase capacity per geographic area is to install many smaller cells such as femtocells and heterogeneous networks. Anyway, because the capacity can only grow linearly with the number of cells, small cells alone will not be able to meet the increased capacity required to met the increases in mobile data traffic. As the mobile data demand grows, the sub 3 GHz spectrum is becoming increasingly crowded. On the other side , a huge amount of spectrum in the 3 to 300 GHz range remains underutilized. The 3 to 30 GHz spectrum is generally referred to as Super High Frequency (SHF) band, while 30 to 300 GHz is referred to as Extremely High Frequency (EHF) or millimeter- Wave band.

Since radio waves in the SHF and EHF bands share similar propagation characteristics, we refer to 30 to 300 GHz spectrum collectively as millimeter-wave bands with wavelengths ranging from 10 to 100 mm.

### *A. History Of mm-Wave.*

May be the reader thought this term (mm-Wave) could be new in the world of wireless communication, the history of mm-Wave technology goes back to the 1890's when J.C. Bose was experimenting with mm-Wave signals at just about the time when his colleagues at that time like Marconi were inventing radio communications. Following Bose's research, mm-wave technology remained within the limits of university and government laboratories for almost half a century.

The technology started so see its early applications in Radio Astronomy in the 1960's, followed by applications in the military in the 70's. In the 80's, the development of mm-Wave integrated circuits created opportunities for vast manufacturing of mm-Wave products for commercial applications. In the beginning of 90's, the existing of automotive collision avoidance radar at 77 GHz marked the first consumer oriented use of mm-Wave frequencies above 40 GHz. In 1995, the FCC opened the spectrum between 59 and 64 GHz for unlicensed wireless communication, resulting in the development of availability of broadband communication and radar equipment for commercial application.

On October 16, 2003 the FCC announced that the 71–76 GHz, 81–86 GHz, and 92–95 GHz frequency bands collectively referred as E-band had become available to very high-speed data communication including point-to-point wireless local area networks, mobile backhaul, and broadband Internet access. A total of 12.9 GHz bandwidth is available in the E-band as shown in Fig. 2, with a narrow 100 MHz exclusion band at 94.0–94.1 GHz. Highly directional beam signal characteristics in E-band permit systems in these bands to be engineered in close proximity to one another without causing interference. Therefore, the FCC and regulators in other countries have introduced "light licensing" schemes for managing this band. These innovative licenses keep the advantages of full interference protection.

### *B. mm-Wave Allocation Frequency.*

mm-Wave frequencies usually refer to the frequency range from 30GHz to 300GHz, the wavelength of which is between 10 mm to 100 mm. There are many Motivational points for desire to use E-Band frequencies in radio links:

1) The radio spectrum at mm-Wave frequencies is still rather undeveloped, and more bandwidth is available at these frequencies.
2) The same RF can be reused again at closest distances because of higher attenuation in free space and through walls.
3) The inherited security and privacy is much better at mm-Wave frequencies because of the limited range and the relatively narrow beam widths that can be achieved.
4) The physical size of antennas at mm-Wave frequencies becomes too small that it becomes practical to build complex antenna arrays.

Figure 2 shows the mm-wave band allocation in the United States. There is 5GHz bandwidth available at the 60GHz band (59–64GHz) for Industrial, Scientific and Medical (ISM) unlicensed applications. The 24GHz band (22–29GHz) band and 77GHz band (76–77GHz) are currently assigned to automotive radar. Fixed point-to-point communication links can use 71–76GHz, 81–86GHz and 92–96GHz that need a license in the USA from The FCC [5].

### *C. Mm-Wave Products*

The mm-Wave frequency bands offer many new products and services, for example:-


ISSN 1737-9334

1) The huge bandwidth at 60GHz can gives unlicensed short-range high-speed links for Wireless Personal Area Network (WPAN) (802.15.3c) and short-range super Wireless Fidelity (Wi-Fi) (802.11ad ) which providing data throughput speeds up to 7 Gbps for wireless high definition video streaming (Wireless HD.

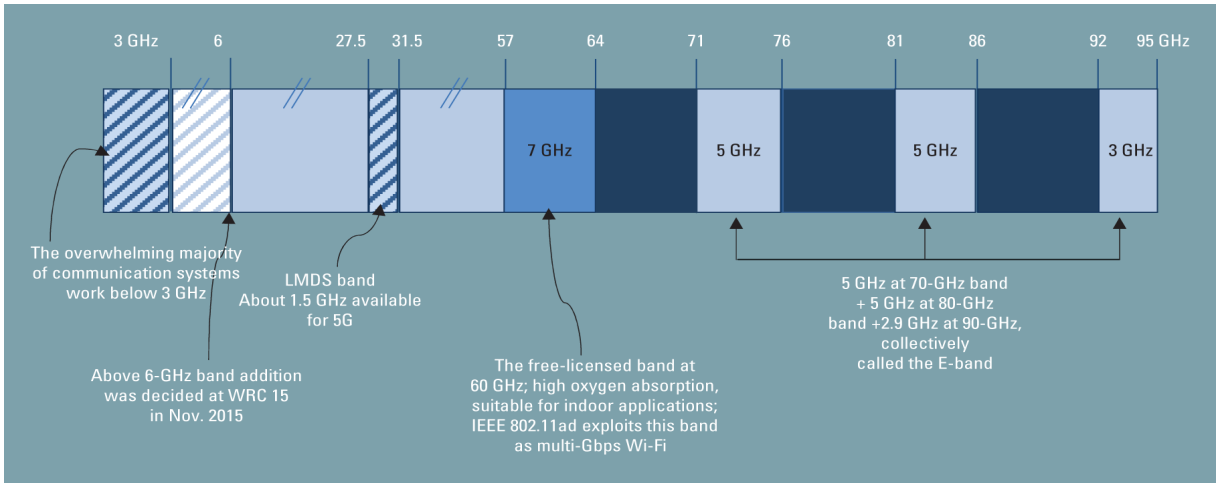


Fig. 2. mm-Wave Spectrum.

2) The 77GHz band is convenient for automotive long-range (100m) Autonomous Cruise Control (ACC) radar. The high carrier frequency allows small size antennas to have a small beam width and therefore a better angular resolution.
3) The 24GHz band can be used in automotive short-range radar, since the large bandwidth at 24GHz offers sufficient small distance resolution nearly 5cm.
4) The large bandwidth at 71–76GHz, 81–86GHz and 92–95GHz can provide licensed high-speed links with data throughput up to 10Gbps.
5) The natural thermal emission of objects in the 35GHz and 94GHz bands allows passive imaging to construct an image.

*D. mm-Wave Applications.*

The mm-Wave offer many applications that will be more efficient such as:-

1) Small Cell Sites.

High density of small cells has been suggested to get the 10,000 times increase in network capacity by 2030 [6,7,8]. mm-Wave small cells are able to provide the multi-gigabit rates, and wideband multimedia applications such as live streaming of both compressed and uncompressed High Definition TeleVision (HDTV), high-speed data transfer between devices, such as cameras, pads, smart phones, and personal computers, wireless gaming can be also supported , and wireless gigabit Ethernet .

2) Cellular Access sites.

The huge bandwidth in the mm-Wave bands supports the usage of mm-Wave communications in the 4G and 5G cellular access sites , The mm-Wave cellular networks have the possibility for huge coverage and capacity as long as the infrastructure is densely installed.

3) Wireless Backhaul.

With small cells densely deployed in the next generation of cellular systems (4G and 5G), it is expansively to connect the Base Stations (BSs) to the other BSs and to the network via fiber optics backhaul [9]. In other side, high speed wireless backhaul is better as cost-efficient, flexible, and easier to install. With large bandwidth available, wireless backhaul in mm-Wave bands, such as the 60 GHz band and E-band (71–76 GHz and 81–86 GHz), gives several-Gbps data rates and can be a promotes backhaul solution for small cells. As shown in Fig. 3, the E-band backhaul provides the high speed transmission between the small cell base stations (BSs) or between BSs and the gateway. And few of mm-Wave applications are illustrates in Table(1).

TABLE 1
APPLICATIONS OF MM-WAVE COMMUNICATIONS

| No | Frequency Band (GHz) | Scenario | Application |
|---|---|---|---|
| 1 | 60 | indoor Office | Internet Access |
| 2 | 60 | WPAN | transmission between devices flows with QoS requirements |
| 3 | 60 | WLANS | uplink channel access |
| 4 | 28,38.71-76,81-86,92-95 | urban street | access and backhaul |
| 5 | 60 | WPAN | HD video |
| 6 | 60,70 | indoor | multimedia |




ISSN 1737-9334

## III THE 60 GHz BAND.

The unlicensed 60 GHz frequency band has more bandwidth available than all of other unlicensed bands together. Even for the smallest allocation, there is more than 3 GHz of bandwidth available, and most regions around the world allow use of at least 7 GHz. In comparison, the 5 GHz unlicensed band has about 500 MHz of total valid bandwidth, and the 2.4 GHz band has less than 85 MHz of bandwidth in most regions. The additional bandwidth increases the channel capacity, but is not enough to enable high-speed communications for practical applications. Exchange operational systems that can use the wide bandwidth at low cost are necessary.

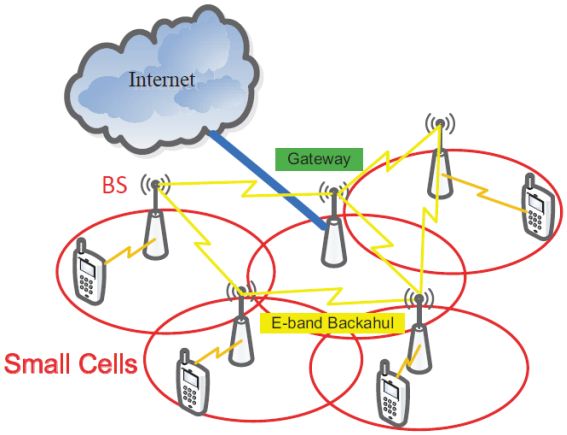


Fig. 3. E-band backhaul for small cells densely deployed [9].

A specific challenge for 60 GHz is get rid off the path loss from transmitter to receiver. The Friis equation is used to compute this effect:

$$P_r = \frac{P_t.G_t.G_r.\lambda^2}{(4\pi.R)^2}$$

Where is $P_r$ is the received power, $P_t$ is the transmitted power, $G_t$ is the transmitter antenna gain, $G_r$ is the receiver antenna gain, $\lambda$ is the wavelength, and R is the range from transmitter to receiver.

### *A. The 60 GHz Band Standardization .*

Due to the great possibilities of mm-Wave communications, many international organizations have emerged for the standardization, including European Computer Manufacturer's Association (ECMA) [10], Institute of Electrical and Electronics Engineers (IEEE) 802.15.3 Task Group 3c (TG3c) [11], IEEE 802.11ad standardization task group [12], the WirelessHD consortium [13], and the Wireless Gigabit Alliance (WiGig) [14]. two standards, IEEE 802.11ad and IEEE 802.15.3c,will be reviewed here briefly .

#### 1) IEEE 802.11ad.

In an effort to provide capacity requirements a very high frequency Wireless Local Area Network (WLAN) modification has been proposed (IEEE 802.11ad). IEEE 802.11ad, also referred to as Wireless Gigabit (WiGig), operates in the globally unlicensed 60 GHz band and offers channel bandwidths nearly 100 times as wide as 802.11n. The higher bandwidth Paves to multi-Gbps throughput .

IEEE 802.11ad specifies the physical layer and MAC layer in 60GHz band to support multi-gigabit wireless applications including instant wireless sync, wireless display of High Definition (HD) streams, wireless computing, and internet access [11]. In the physical layer, two operating modes are defined, the OFDM mode for high data rate applications , and the single carrier (SC) mode for low power and low complexity implementation. In IEEE 802.11ad, a Basic Service Set (BSS) consists of a designated device, called Access Point (AP), and N non-AP Devices (DEVs). AP provides the basic timing for the BSS, and coordinates medium access in the BSS to coordinates the traffic requests from the DEVs.

#### 2) IEEE 802.15.3c

IEEE 802.15.3c specifies the physical layer and MAC layer for indoor Wireless Personal Access Networks (WPANs) (also referred to as the Piconet) contains of several wireless Nodes (WNs) and a single PicoNet Controller (PNC). The PNC provides network synchronization and coordinates the transmission in the Piconet. In IEEE 802.15.3c, network time is divided into a sequence of super frames, each of it consists of three portions: the Beacon Period (BP), the Contention Access Period (CAP), and the Channel Time Allocation Period (CTAP). During BP, the network synchronization and control messages are broadcasted from the PNC. CAP is for devices to send transmission requests to the PNC by the Carrier-Sense Multiple Access with Collision Avoidance (CSMA/CA) access method, and CTAP is for data transmissions among devices. During CTAP, Time Division Multi-Access (TDMA) is applied, and each time slot is scheduled to a specific flow.

### *B. Oxygen Absorption and the 60 GHz Band*

For several years the intelligence authorities had been use P2P wireless systems operating at 60 GHz for high security communications such as the military satellite-to satellite communications. Their concerns in this band comes from a phenomenon of nature, Oxygen atoms (O2) absorb electromagnetic energy at 60 GHz. Fig. 4, shows the gaseous attenuation for both oxygen and water vapor absorption as a function of range, over and above the free-




ISSN 1737-9334

space loss. The resonances for frequencies below 100 GHz happens at 24 GHz for water vapor and 60 GHz for oxygen. Absorption occurs to a much higher degree at 60 GHz than at the lower frequencies typically used for wireless communications.

Absorption attenuates 60 GHz signals over distances, so that signals cannot pass far beyond their target. For this reason, 60 GHz is a perfect choice for hidden satellite-to-satellite communications because the Earth's atmosphere acts like a shield preventing Earth-based eavesdropping. Because of the huge number of applications in this band, a wide variety of components and subassemblies for 60 GHz products are available today

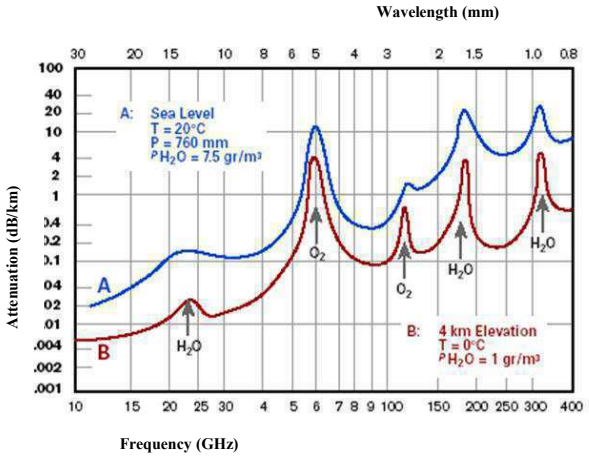


Fig 4: Gaseous Absorption at 60 GH.

Another benefit of O2 absorption is that radiation from one particular 60 GHz antenna is quickly decreased to a level that will not interfere with other 60 GHz links operating in the same area. This reduction enables higher frequency reuse, for example, the ability for more 60 GHz links to operate in the same geographic area than links with longer ranges [15].

### C. *Advantages of 60 GHz Band [16]*

There is many advantages of this band such as :-

1) Large spectrum.
2) Small Antenna Separation:
3) Easy Beamforming.
4) Low Interference.
5) Directional Antennas.
6) Inherent security.
7) Higher power transmission.

### D. *Disadvantages of 60 GHz Band [17]*

There is a few disadvantages like large attenuation, directional deafness ,easily blocked.

## IV THE 71-76 , 81-86 AND 92-95 GHz E-BAND FREQUENCIES.

In 2003 the FCC opened up 13 GHz of spectrum at frequencies much higher than had been available commercially before . This spectrum provides the means for economical broadband connectivity for the first time at true gigabit data rates and more.

Some of interest frequencies is the 10 GHz of bandwidth between 70 and 80 GHz. Designed to be exist, the 71-76 GHz and 81-86 GHz allocations allow 5 GHz of full duplex transmission bandwidth, enough to transmit a gigabit of data even with the simplest modulation schemes. With more spectrally efficient modulations, full duplex data rates of 10 Gbps via Optical Carrier interfaces (OC-192, STM-64 or 10 GigE) can be achieved.

This is will be possible by using the pencil beam as concept of operation, in which high level requirements are placed on the antenna radiation pattern of at least 50 dBi gain and no more than a 0.6-degree |Half Power Beam Width (HPBW) , in Fig .5 a comparison between the mm-Wave beam (pencil beam) and MicroWave (MW) beam.

The three spectrum segments of the E-band (71-76, 81-86, and 92-95 GHz) have been yet the highest frequency spectrum allocated to licensed operation, and it contains sufficient space for digital transmission speeds comparable to optical communication systems (1.25-5 Gbps).

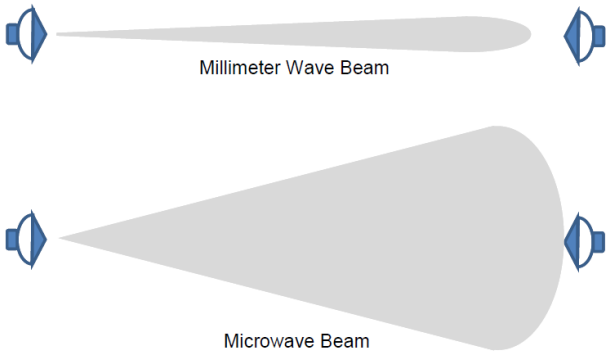


Fig. 5. Millimeter Wave Beam (Pencil Beam) vs MW Beam.

### A. *E-band Wireless Benefits.*

E-band wireless systems offer the most convincing alternative to fiber optics system. Of all the high capacity wireless technologies, the E-band systems offer numerous benefits including:-

1) Highest data rates : E-band offers the highest data rates of any available wireless technology, with systems available that offer 1 Gbps and above through full-duplex throughput.




ISSN 1737-9334

2) Guaranteed data rates : On the reverse of WiFi, WiMAX and other broad coverage technologies that has system performance depends strongly on the radio frequency environment, number of users, distance from Base Station (BS) and even installation quality, E-band systems guarantee data throughput performance, even under poor transmission conditions.

3) Guaranteed interference protection : Since the E-band is a licensed technology, all links has to be registered with national wireless regulators and coordinated with other links in the area. This gives links full interference protection from other nearby wireless sources.

4) Long distance transmissions : With the exception of lower data rate and more complex Microwave systems, the E-band wireless offers the longest transmission distances of the higher capacity wireless systems. Under any environmental condition, a 1 Gbps E-band system can transmit many times further than similar data rate 60 GHz

## V THE CHALLENGES OF MM-WAVE TECHNOLOGY

Even with the available bandwidth in the E-band is more than 50 times the entire cellular spectrum, radio signals in the E-band are more adversely affected by environmental factors [18]. The characteristics of E-band signals and systems can be summarized as follows:-

1) Due to the higher carrier frequencies, the antennas are need to be more directional, making E-band systems mainly convenient for line-of-sight (LOS) applications.

2) Rain and obstacles: Rain attenuation will form natural limits on link distances. As shown in fig.6, mm-Wave transmissions can experience significant rain attenuations during the rain [19]. “Heavy” rainfall at the rate of 25 mm/hour cause just over 10 dB/km attenuation at e-band frequencies. This increases to 30 dB/km for 100 mm/hour (which is not often present in Libya weather ) tropical rain. These values of attenuation are used in link planning to determine the maximum link length allowed to overcome rain events.

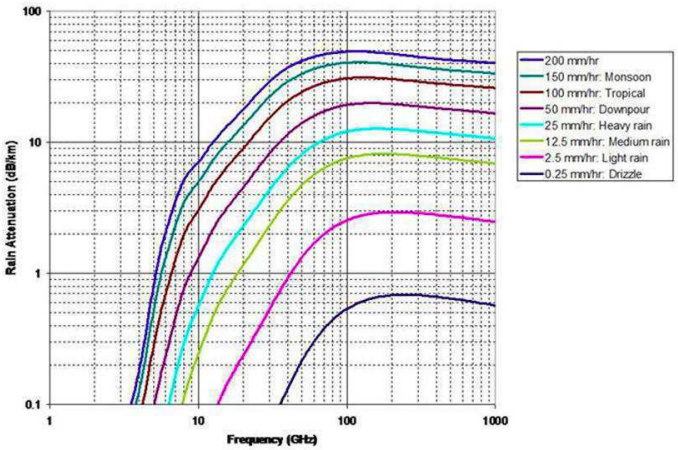


Fig. 6. Rain attenuation at microwave and mm-Wave frequencies.

## VI CONCLUTION

The mm-Wave technology is a promised technology that will improve the overall performance of the network to met the increased requirements of data rates in 4 and 5G systems . With the cost and geographical limitations of Fiber optics systems , the E-band systems will be The most appropriate alternative for both coverage cells and transmission backhaul .And even through the heavy rain which is not common in the Libya’s weather this technique will be more suitable and gives a significant flexibility for the growing networks .

## REFERENCES

[1] R. A. Alhalabi, Y.-C. Chiou, and G. M. Rebeiz, ―Self -shielded high-efficiency Yagi-Uda antennas for 60GHz communications,‖ IEEE Trans. on Antennas and Propagat., Vol. 59, No. 3, 742–750, 2011.

[2] O. Kramer, T. Djerafi, and K. Wu, ―Very small footprint 60 GHz stacked Yagi antenna array,‖ IEEE Trans. on Antennas and Propagat., Vol. 59, No. 9, 3204–3210, 2011.

*[3]* M. Sun, Y. P. Zhang, K. M. Chua, L. L. Wai, D. Liu, and B. P. Gauche, ―Integration of Yagi antenna in LTCC package for differential 60-GHz radio,‖ IEEE Trans. on Antennas and Propagat., Vol. 56, No. 8, 2008.

[4] F. Khan, *LTE for 4G Mobile Broadband: Air Interface Technologies and Performance*, Cambridge Univ. Press, 2009.

[5] Ning Wang and PengGao, ―A 60GHz End-Fire High- Gain Tapered Slot Antenna with Side-Lobe Suppression‖ Progress In Electromagnetics Research Letters, Vol. 55, 2015.

[6] A. Ghosh, T. A. Thomas, M. C. Cudak, R. Ratasuk, P. Moorut, F. W. Vook, T. S. Rappaport, G. R. MacCartney, S. Sun, and S. Nie, “Millimeter-Wave Enhanced Local Area Systems: A High-Data-Rate Approach for Future Wireless Networks,” IEEE Journal on Selected Areas in Communications, vol. 32, no. 6, pp. 1152–1163, June 2014.

[7] T. S. Rappaport et al., “Special session on mmWave communications,” in Proc. ICC, Budapest, Hungary, Jun. 2013.

[8] R. Baldemair, T. Irnich, K. Balachandran, E. Dahlman, G. Mildh, Y. Seln, S. Parkvall, M. Meyer, and A. Osseiran, “Ultra-dense networks in millimeter-wave frequencies,” IEEE Communications Magazine, vol. 53, no. 1, pp. 202–208, January 2015.

[9] R. Taori, A. Sridharan, “Point-to-multipoint in-band mmwave backhaul for 5G networks,” IEEE Communications Magazine, vol. 53, no. 1, pp. 195–201, January 2015.




ISSN 1737-9334

[10] ECMC TC48, ECMA standard 387, "High rate 60 GHz PHY, MAC and HDMI PAL," Dec. 2008.
[11] IEEE 802.15. WPAN Millimeter Wave Alternative PHY Task Group 3c (TG3c).Available:http://www.ieee802. org/15/pub/TG3c.html , Nov 2009.
[12] Draft Standard for Information Technology–Telecommunications and Information Exchange Between Systems–Local and Metropolitan Area Networks–Specific Requirements–Part 11: Wireless LAN Medium Access Control (MAC) and Physical Layer (PHY) Specifications–Amendment 4: Enhancements for Very High Throughput in the 60 Ghz Band, IEEE P802.11ad/D9.0, Oct. 2012.
[13] WirelessHD: WirelessHD specification overview, August 27, 2009.
[14] Wireless Gigabit Alliance. [online]. Available: http://wirelessgigabitalliance.org/ , January 3rd , 2013.
[15] "WiGig White Paper: Defining the Future of Multi-Gigabit Wireless Communications," July 2010, [Online] Available: http:// wirelessgigabitalliance.org/specifications/.
[16] Millimeter-Wave Radios in Backhaul Networks papre, Communication Infrastructure Corporation ,2008.
[17] S. Yong, P. Xia, A. Valdes-Garcia, "60 GHz Technology for Gbps WLAN and WPAN: From Theory to Practice," Wiley, Aug. 2011, pp 296.
[18] J. Wells, Multi-Gigabit Microwave and Millimeter-Wave Wireless Communications. Artech House, 2010.
[19] ITU-R P.838-3, "Specific attenuation model for rain for use in prediction methods," 2005.




ISSN 1737-9334

# Optimal Tuning of Fuzzy-PIDN Controller for Autonomous Microgrid Incorporating Various Renewable Energy Sources and Multiple Energy Storage Systems

Nour EL Yakine KOUBA, Slimane SADOUDI, Smail HAROUN and Mohamed BOUDOUR

Laboratory of Electrical and Industrial Systems, University of Sciences and Technology Houari Boumediene, Algiers, Algeria

E-mail: nkouba@usthb.dz; slimane.sadoudi@usthb.dz; haroun.smail@yahoo.com; mboudour@ieee.org

***Abstract*— In this paper, a new efficient Fuzzy-PID controller with Derivative Filter (Fuzzy-PIDN) optimized via Grasshopper Optimization Algorithm (GOA) was proposed for Load Frequency Control (LFC) of an interconnected microgrid. The GOA was employed to fine tune the scaling factors of fuzzy logic and PIDN controllers gains by generating their optimal settings. The investigated microgrid system includes two interconnected areas incorporating Diesel engine, Wind turbine, Solar Photovoltaic (PV), and Energy storage systems including Redox Flow Batteries (RFBs), Superconducting Magnetic Energy Storage (SMES), Fuel Cells (FCs) and Aqua Electrolyzers (AEs). The frequency control of the addressed autonomous microgrid was studied using a dynamic modeling of each unit. The power demand variation was considered as disturbance, where, the conventional controllers PID, Fuzzy-PID and Fuzzy-PIDN were implemented for comparative analysis of the LFC performance. The superiority of the proposed GOA strategy was demonstrated under various scenarios using four performance criteria functions, which are : Integral Square Error (ISE), Integral Absolute Error (IAE), Integral Time multiply Absolute Error (ITAE) and Integral Time multiply Square Error (ITSE). The behavior of the microgrid was analyzed in several case studies, and some control actions were suggested to improve the frequency control in presence of renewable energy. The obtained results were compared in view of peak undershoot / overshoot and settling time. The performed simulations prove the validity of the used GOA optimization tool, and shows that GOA optimized Fuzzy-PIDN controller was robust and can cope with system disturbance to solve frequency regulation problem.**

***Keywords*— *Microgrid, Photovoltaic, Wind turbine, Redox Flow Batteries (RFBs), Superconducting Magnetic Energy Storage (SMES), Fuel Cells (FCs), Aqua Electrolyzer (AE), Fuzzy-PIDN Controller, Grasshopper Optimization Algorithm (GOA).***

## I. INTRODUCTION

In a near future, modern electrical networks will contain many types of renewable energy sources (RESs) in large numbers. In small power system such as a microgrid, which majorly includes various kinds of RESs such as wind, solar, wave energy,...etc, the control actions such as frequency regulation need to be of high performance to avoid system instability [1-2]. Presently, the microgrid is considered as a new developing technology, which can be operated in two modes namely, the utility-grid-connected mode and the autonomous or isolated operation mode. The microgrid can be considered as a closed small network that consist of micro-turbines and diesel engine generators. The microgrid reliability can be improved using the Distributed Generation (DG) like wind and solar sources [3-5].

The DG units are mostly installed near to the load centers to satisfy the power demand locally. On one hand, the use of DG units is an attractive tool to deliver a clean power. On the other hand, power system control is required to enhance the quality of power supply in such system that includes several DG units, because the equilibrium between the power supply and consumption is of major concern. Basically, the microgrid includes mainly two kinds of power sources that can be classified as inertial or non-inertial in terms of power flow control. The inertia sources are that kind of units which their output power can be controlled to maintain the desired microgrid frequency at nominal value such as micro turbines, fuel cells and diesel generators. However, non-inertial sources like wind and PV, are used to supply only a portion of the total power demand. Whereas, the output power of this kind of sources depends on the environmental conditions. Thus, it is difficult to handle the large number of DGs during disturbances [6-10].

Regarding the problem of network instability, the microgrid system sometimes witness instability due to load change. According to the event of load disturbance, the system frequency gets affected due to unbalance between power supply and load. To ensure that, the frequency of the autonomous microgrid that is operated in isolated operation mode is maintained within scheduled limits, a secondary control action named Load Frequency Control (LFC) comes as an auxiliary control system to maintain the frequency at nominal value during load change using the Area Control Error (ACE). Moreover, to operate the microgrid as fast as possible, a robust regulation including the LFC in coordination with some rapid dynamic response devices such as the Energy Storage System (ESS) is required [10-11].




ISSN 1737-9334

Conventionally, the microgrid frequency fluctuation is handled using the droop control and power sharing method in the microgrid. In addition, the LFC loop can be associated with a PI controller to enhance the frequency regulation. In contrast, the integration of DG units like wind and solar PV makes the frequency control more difficult, which requires an efficient control strategy to mitigate the frequency fluctuation. Therefore, it is very important to contribute for enhancing the microgrid frequency regulation in presence of various renewable energy sources by the use of some strategies that can bring more robustness to the microgrid control.

Over the last years, several strategies have been published in the scope of the microgrid control employing Artificial Intelligence (AI) and nature-inspired optimization algorithms. Most of the developed techniques for microgrid regulation were based on PI or PID controller. Some interesting applications of fuzzy logic and neural networks have been also proposed. In reference [12], Leong Kit Gan et al., have proposed to study a hybrid power system in Scotland. In reference [13], S. Rehman and I. El-Amin, have proposed to study a hybrid power system in the Saudi Arabia, where, in reference [14], J. G. Mcgowan et al., have proposed to study a hybrid power system in the South American. In reference [15], Julius K. Tangka have proposed an intelligent electronic module for energy management of hybrid microgrid, whereas, M. Venkatesh and G. Sudheer have proposed an optimal LFC of microgrid using Dragonfly Algorithm [16].

Furthermore, some researchers have discussed the applications of energy storage system (ESS). In reference [17], Gayathri Nair S and Nilanjan Senroy have studied the dynamics of a Flywheel energy storage system. In [18], authors have studied the optimal sizing of ESS using GSA optimization algorithm. In [19], authors have proposed an optimal management of smart grid system using PSO algorithm. In [20], authors have studied the LFC control using the vehicle-to-grid (V2G) technique. In reference [21], authors have studied the dynamic frequency control support by ESS to reduce the impact of RESs integration, where, in reference [22], authors have proposed the use of an optimized fuzzy-cuckoo controller to enhance the control of the storage system in a hybrid microgrid.

Based on the above literature study, the key contributions of this paper are:

- A new optimized Fuzzy-PIDN controller was employed and optimized using the recently developed Grasshopper Optimization Algorithm (GOA).
- An effective LFC scheme support with multiple energy storage systems such as Redox Flow Batteries (RFBs), Superconducting Magnetic Energy Storage (SMES), Fuel Cells (FCs) and Aqua Electrolyzer (AE) was proposed.

The rest of the paper is organized as follows. Section II presents the dynamic model of the investigated microgrid. Section III describes the proposed optimized Fuzzy-PIDN controller, followed by a brief description of the employed GOA optimization algorithm. Section IV presents the simulation results with a detailed discussion of each case study. Finally, Section V concludes the paper.

## II. Autonomous Hybrid Microgrid Model

In recent years, the integration of decentralized generation units (DGs) in power systems is significantly increasing [23]. This results from the liberalization of the electricity market and the desire to promote renewable energies. As a consequence, new and stricter connection constraints are being developed to address the issues associated with the intermittent energy sources. Their dependence on climatic conditions will be a problem when participating in the power management. To deal with this situation, hardware and algorithmic solutions can be used to minimize this intermittent aspect, as a set of control strategy, support and control systems such as storage devices, frequency/voltage control systems and conventional generators. Fig.1 presents the investigated two-area interconnected microgrid. The used system contains Diesel engine, Solar Photovoltaic, Fuel Cells and Aqua Electrolyzers in Area-1, and comprise Diesel engine, wind turbine, Redox Flow Batteries and Superconducting Magnetic Energy Storage in Area-2.

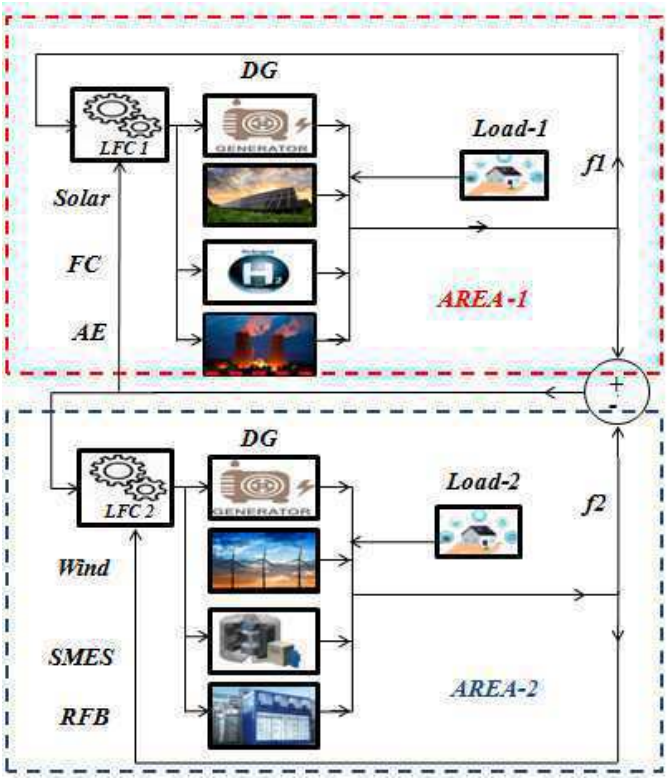


Fig. 1. Interconnected Two-area Hybrid Microgrid.

Focusing mainly on the frequency control (LFC), each area was modeled separately. The two-area system was modeled as shown in Fig. 2 and Fig. 3 respectively. The storage was used to compensate the LFC regulation capacity in presence of both wind and solar PV units. The dynamic modeling of each unit can be found in references [1, 2, 5 and 6]. In other hand, to improve the LFC loop, an optimal Fuzzy-PIDN controller with Derivative Filter was associated to each control area to handle the frequency fluctuation due to the wind and solar PV power variations. During this study, each area was analyzed independently as a hybrid microgrid, then an interconnection between the two areas was established and studied.




ISSN 1737-9334

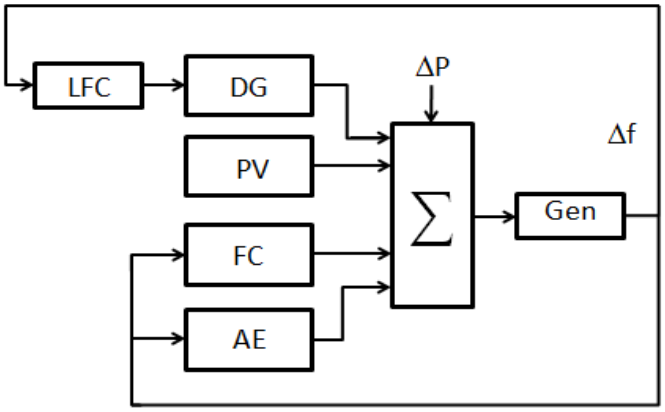


Fig. 2. Hybrid Solar PV-Diesel Microgrid with Storage System.

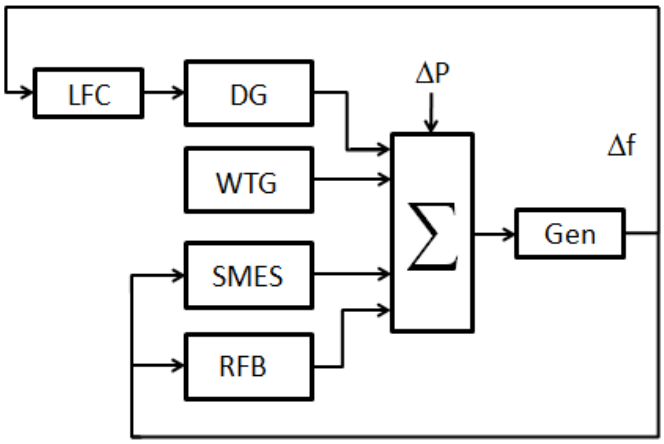


Fig. 3. Hybrid Wind-Diesel Microgrid with Storage System.

## III. Proposed Control Strategy

During the last decades, various LFC schemes have been proposed to enhance the frequency regulation. This work proposes the design of a new optimal LFC controller in coordination with storage system for interconnected hybrid microgrid. The proposed methodology involves the combination of both Fuzzy Logic controller and the PID controller with a Derivative Filter. In addition, the controller parameters where tuned using the recently developed Grasshopper Optimization Algorithm (GOA). During the optimization process, four objective functions were used to show the robustness of the applied control strategy, which are : ISE, IAE, ITAE and ITSE.

### *A. Fuzzy-PID Controller with Derivative Filter*

Conventionally, most of the regulation systems are based on the PI or PID controllers. Nowadays, such controllers are widely used in industry, where more than 90% are composed from the three actions: Proportional (*P*), Integral (*I*), and Derivative (*D*), since that present an efficient solution and has a simple construction. The PIDN is a classic PID controller associated with a Derivative Filter (*N*) [24]. The PIDN comprise a low pass first-order filter with a coefficient (*N*), that presents a solution for eliminating the undesirable noise caused by the Derivative (*D*) action.

On the other hand, a robust control technique developed by Pr. Lotfi A. Zadeh in 1965 called fuzzy logic have shown a high performance in the regulation area. Unlike binary logic, fuzzy logic allows an infinite number of degrees of truth to be taken into consideration. The first application of this technique go back to Professor Mamdani in 1975. The first industrial application of fuzzy logic was made later in 1978 by the Danish company F.L. Smidth.

This paper proposes a new controller based on combining both of fuzzy logic and PIDN controllers in order to enhance system regulation by assembling the advantages of both controllers. In Fig. 4 the structure of the used PIDN controller is presented [24-27], where, the PIDN controller transfer function is given by the Eq.1. The input of the PIDN controller is taken from the output of the Fuzzy Logic controller (FLC), where the input of the fuzzy controller is the Area Control Error (ACE) given in Eq. 2 as shown in Fig. 5.

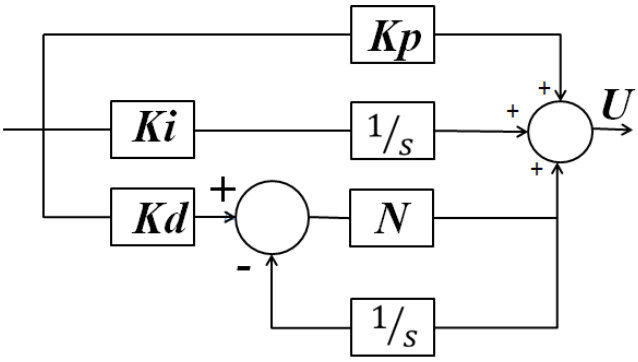


Fig. 4. *PIDN Controller Structure* [24].

$$TF_{PIDN} = Kp + K_i \frac{1}{s} + K_d \frac{N.s}{N} \quad (1)$$

$$ACE = \Delta P_{tie} + \beta_f \Delta f \quad (2)$$

The Mamdani fuzzy inference mechanism with a center of gravity method of defuzzification was used, where the triangular membership functions were selected for the inputs and outputs. Noting that *K*1e and *K*2e are scaling factors of the fuzzy logic controller. As shown in Fig. 6, the triangular membership functions have been chosen to represent the input linguistic variables ACE, the derivative of ACE, and the FLC output *uf*. Five linguistic terms have been considered, which are: Negative Big (NB), Negative Small (NS), Zero (ZE), Positive Small (PS), and Positive Big (PB), as cited in Tab.1.

Table.1. FLC Control Rules.

| *dACE* | *ACE* | | | | |
|---|---|---|---|---|---|
| | NB | NS | ZE | PS | PB |
| NB | NB | NB | NS | NS | ZE |
| NS | NB | NB | NS | ZE | ZE |
| ZE | NS | NS | ZE | PS | PS |
| PS | ZE | PS | PS | PB | PB |
| PB | ZE | ZE | PS | PB | PB |


ISSN 1737-9334

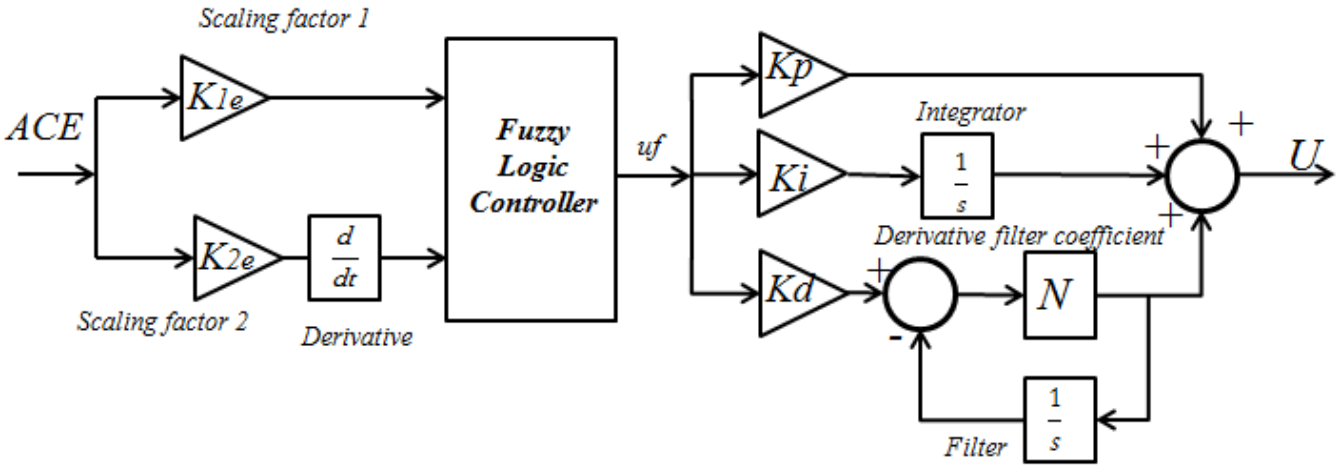


Fig. 5. Fuzzy-PIDN Structure [27].

The control signal is given by:

$$uf = A + (K1eP.ACE) + (K2eD.\frac{dACE}{dt}) \quad (3)$$

$$U = (Kp.uf) + (Ki\int_0^t uf(t)dt) + (\frac{duf(t)}{dt}) \quad (4)$$

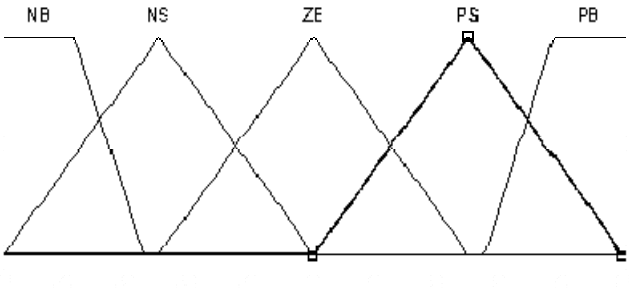


Fig. 6. Membership Functions for FLC Inputs and Outputs.

### B. Grasshopper Optimization Algorithm (GOA)

Grasshopper Optimization Algorithm (GOA) is a new developed meta-heuristic algorithm proposed by Shahrzad Saremi et al. in 2016 [28]. GOA was inspired from the social life and hunting behavior of Grasshopper in nature. The pseudo code of the GOA algorithm is shown in Fig.7.

### C. Objective Function

In order to solve the optimal LFC problem in the interconnected hybrid microgrid, four performance criteria functions (*Fit*) have been used as given in Eqs. 5 to 8:

- Integral Square Error (*ISE*).

$$ISE = \int_0^\infty \left(x(t) - y(t)\right)^2 .dt = \int_0^\infty \left(e(t)\right)^2 .dt \quad (5)$$

- Integral Absolute Error (*IAE*).

$$IAE = \int_0^\infty \left(\left|x(t) - y(t)\right|\right).dt = \int_0^\infty \left(\left|e(t)\right|\right).dt \quad (6)$$

- Integral Time multiply Square Error (*ITSE*).

$$ITSE = \int_0^\infty t.\left(x(t) - y(t)\right)^2 .dt = \int_0^\infty t.\left(e(t)\right)^2 .dt \quad (7)$$

- Integral Time multiply Absolute Error (*ITAE*).

$$ITAE = \int_0^\infty t.\left(\left|x(t) - y(t)\right|\right).dt = \int_0^\infty t.\left(\left|e(t)\right|\right).dt \quad (8)$$

*Initialize the swarm $X_i$ (i = 1, 2, ..., n)*
*Initialize cmax, cmin, and maximum number of iterations*
*Calculate the fitness of each search agent*
***T**=the best search agent*
***while** (1 < Max number of iterations)*
*Update c*
***for** each search agent*

*Normalize the distances between grasshoppers in [1,4]*

*Update the position of the current search agent*

*Bring the current search agent back if it goes outside the boundaries*
***end for***
*Update T if there is a better solution*
*l=l+1*
***end while***
*Return **T***

Fig. 7. Pseudo Code of the GOA Algorithm [28].

The frequency variation $\Delta f$ and the tie-line power flow exchange deviation $\Delta P_{tie}$ have been used as inputs for the above equations, where $t$ represents the simulation time. The optimization problem constraints are the fuzzy logic scaling factors and the PIDN controller parameters bounds. Therefore, the design problem can be formulated as the following optimization problem:

- Minimize the objective function *Fit* given in Eqs. (5-8) using GOA algorithm, subject to:




ISSN 1737-9334

$$\begin{Bmatrix} K_{p\,min} \le K_p \le K_{p\,max} \\ K_{i\,min} \le K_i \le K_{i\,max} \\ K_{d\,min} \le K_d \le K_{d\,max} \\ N_{min} \le N \le N_{max} \end{Bmatrix} \quad \begin{Bmatrix} K_{1emin} \le K_{1e} \le K_{1emax} \\ K_{2emin} \le K_{2e} \le K_{2emax} \end{Bmatrix}$$

## IV. Simulation Results

To evaluate the performance of the interconnected two-area microgrid, shown in Fig. 1, a series of simulation have been executed. The presented scenarios were updated concerning load variation in each area of the microgrid. Three scenarios have been analyzed and presented. In the first scenario, only the isolated hybrid solar PV-diesel system was simulated with and without storage system. In the second scenario, only the isolated hybrid wind-diesel system was simulated with and without storage system. Finally, in the third scenario, the interconnection between the two isolated hybrid systems was established, and the interconnected two-area microgrid was simulated. The simulation was performed in presence of 0.1 pu step load disturbance. A comparative study between the employed objective functions was carried out, then a comparative study between the classical PID, Fuzzy-PID, and Fuzzy-PIDN controllers based GOA was presented.

### A. Scenario 1 : Hybrid Solar PV-Diesel with Storage System

Fig.8 presents the frequency variation in the hybrid PV-diesel system with and without storage system.

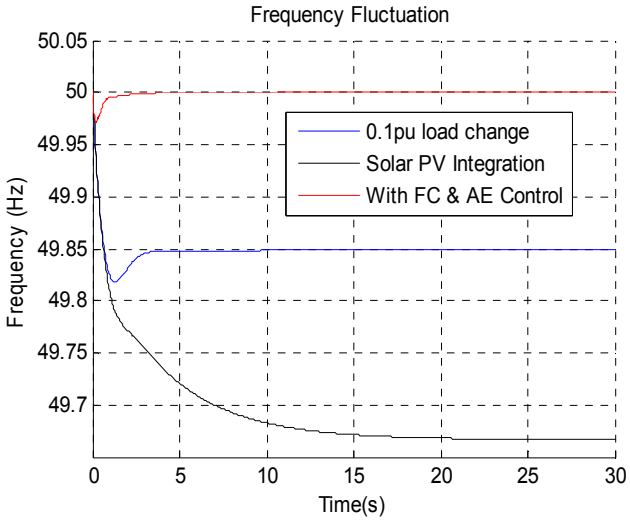


Fig. 8. Frequency Deviation in Area-1.

### B. Scenario 2: Hybrid Wind-Diesel with Storage System

Fig.9 presents the frequency variation in the hybrid wind-diesel system with and without storage system. The impact of both RFBs and SMES devices was analyzed in view of frequency deviation minimization in presence of load change and wind power fluctuations.

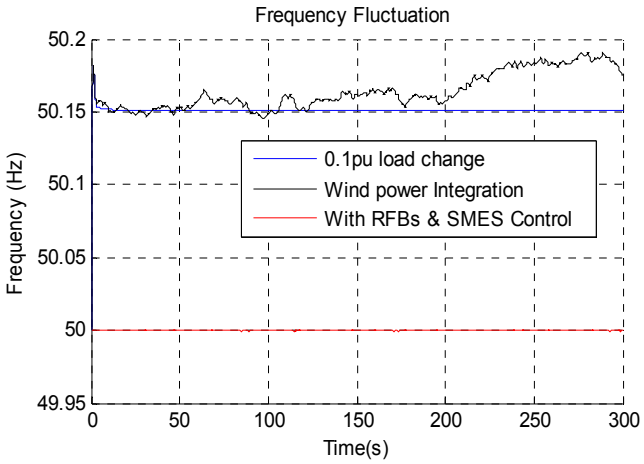


Fig. 9. Frequency Deviation in Area-2.

### C. Scenario 3 : Interconnected Two-Area Microgrid

In this scenario, an interconnection between the solar PV-diesel and the wind-diesel hybrid systems was established. The interconnected microgrid was simulated for 0.1 pu step load change in presence of both wind and solar fluctuations. A comparative study between four performance criteria (ISE, IAE, ITSE and ITAE) is presented in Fig.10, where a comparative analysis between the tested controller is presented in Fig.11. The ITAE was chosen as best objective function.

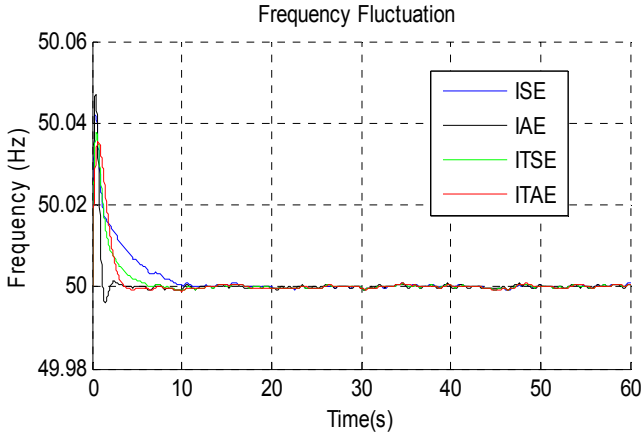


Fig. 10. Comparative Performance Analysis.

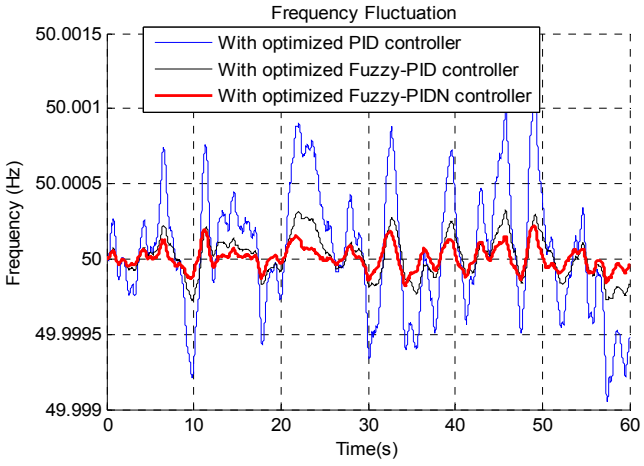


Fig. 11. Frequency Deviation with Optimal LFC.




ISSN 1737-9334

The microgrid was analyzed in presence of wind and solar PV units. The LFC was supported with storage system in each area of the microgrid. From the obtained results, it can be seen that the storage system (FC, AE, RFBs and SMES) can help the secondary LFC loop to handle the frequency fluctuation in presence of renewable energy sources. Several objective functions have been tested, where the ITAE presents the best performance in view of settling time, peak undershoot and overshoot. Furthermore, as seen from the presented Figures above, the optimized Fuzzy-PIDN controller quickly regulates the system frequency towards the nominal value, where the proposed controller improves the LFC performance further and outperforms all other controllers tested in this work.

## V. CONCLUSION

This paper has presented a novel optimal control strategy for microgrid frequency regulation involving a combined fuzzy-PID controller with derivative filter. A Recently developed optimization algorithm named Grasshopper Optimization Algorithm (GOA) was employed to fine tune the controller parameters. The developed controller was applied to a hybrid two-area microgrid including various renewable energy sources. The LFC loop was supported with multiple energy storage systems to enhance the microgrid stability. Several scenarios have been presented to demonstrate the effectiveness of the proposed approach. Finally, the obtained results confirm the effectiveness of the proposed strategy.

## REFERENCES

[1] N. E. Y. Kouba, A. Benseddik, Y. Amrane, M. Hasni, and M. Menaa, "Coordinated Control of Optimal LFC Method and Energy Storage System for Microgrid Frequency Regulation in Presence of Wind Farm," *International Journal of Electronic and Electrical Engineering Systems* 2018, vol. 0, no. 0, pp. 9-15.

[2] L. Wang, D.-J. Lee, W.-J. Lee, and Z. Chen, "Analysis of a novel autonomous marine hybrid power generation/energy storage system with a high-voltage direct current link," *Journal of Power Sources* 2008, vol. 185, no. 2, pp. 1284-1292.

[3] M. Vahedipour-Dahraie, H. R. Najafi, A. Anvari-Moghaddam, and J. M. Guerrero,"Study of the effect of time-based rate demand response programs on stochastic day-ahead energy and reserve scheduling in islanded residential microgrids,"*Applied Sciences* 2017,7(4),pp.378-397.

[4] M. Vahedipour-Dahraie, H. Rashidizaheh-Kermani, H. R. Najafi, A. Anvari-Moghaddam, and J. M. Guerrero, "Coordination of EVs participation for load frequency control in isolated microgrids," *Applied Sciences* 2017, vol. 7, no. 6, pp. 539-555.

[5] S. K. Pandey, S. R. Mohanty, N. Kishor, and J. P. Catalão, "Frequency regulation in hybrid power systems using particle swarm optimization and linear matrix inequalities based robust controller design," *International Journal of Electrical Power & Energy Systems* 2014, vol. 63, pp. 887-900.

[6] P. SANKI and M. BASU, "New approach in two-area interconnected AGC including various renewable energy sources using PSO," *Turkish Journal of Electrical Engineering & Computer Sciences* 2018, vol. 26, no. 3, pp. 1491-1504.

[7] L. Meng, E. R. Sanseverino, A. Luna, T. Dragicevic, J. C. Vasquez, and J. M. Guerrero, "Microgrid supervisory controllers and energy management systems: A literature review," *Renewable and Sustainable Energy Reviews* 2016, vol. 60, pp. 1263-1273.

[8] L. I. Minchala-Avila, L. E. Garza-Castañón, A. Vargas-Martínez, and Y. Zhang, "A review of optimal control techniques applied to the energy management and control of microgrids," *Procedia Computer Science* 2015, vol. 52, pp. 780-787.

[9] T. Ota, K. Mizuno, K. Yukita, H. Nakano, Y. Goto, and K. Ichiyanagi, "Study of load frequency control for a microgrid," in *Power Engineering Conference*, *AUPEC 2007*. Australasian Universities, pp. 1-6.

[10] Y. Sawle, S. Gupta, and A. Kumar Bohre, "PV-wind hybrid system: A review with case study," *Cogent Engineering* 2016, 3, (1), pp. 1-31.

[11] Y. Yoldaş, A. Önen, S. Muyeen, A. V. Vasilakos, and İ. Alan, "Enhancing smart grid with microgrids: Challenges and opportunities," *Renewable and Sustainable Energy Reviews 2017*, vol. 72, pp. 205-214.

[12] L. K. Gan, J. K. Shek, and M. A. Mueller, "Hybrid wind–photovoltaic–diesel–battery system sizing tool development using empirical approach, life-cycle cost and performance analysis: A case study in Scotland," *Energy conversion and management* 2015, vol. 106, pp. 479-494.

[13] S. Rehman and I. El-Amin, "Study of a solar PV/wind/diesel hybrid power system for a remotely located population near Arar, Saudi Arabia," *Energy Exploration & Exploitation* 2015, 33: (4), pp. 591-620.

[14] J. McGowan, J. Manwell, C. Avelar, and C. Warner, "Hybrid wind/PV/diesel hybrid power systems modeling and South American applications," *Renewable energy* 1996, vol. 9, no. 1-4, pp. 836-847.

[15] J. K. Tangka, P. Tchakoua, H. Fotsin, and A. Fomethe, "Development of an intelligent electronic module for energy management in wind/diesel or photovoltaic/diesel hybrid systems," *British Journal of Applied Science & Technology* 2012, vol. 2, no. 3, pp. 275-295.

[16] M. Venkatesh and G. Sudheer, "Optimal load frequency regulation of micro-grid using dragonfly algorithm," *International Research Journal of Engineering and Technology* 2017, vol. 4, no. 8, pp. 978-981.

[17] G. Nair and N. Senroy, "Dynamics of a flywheel energy storage system supporting a wind turbine generator in a microgrid," *International Journal of Emerging Electric Power Systems* 2016, 17:(1), pp. 15-26.

[18] A. Mahesh, K. S. Sandhu, and J. V. Rao, "Optimal Sizing of Battery Energy Storage System for Smoothing Power Fluctuations of a PV/Wind Hybrid System," *International Journal of Emerging Electric Power Systems* 2017, vol. 18, no. 1, pp.1-13.

[19] R. Shigenobu, A. S. Noorzad, C. Muarapaz, A. Yona, and T. Senjyu, "Optimal operation and management for smart grid subsumed high penetration of renewable energy, electric vehicle, and battery energy storage system," *International Journal of Emerging Electric Power Systems* 2016, vol. 17, no. 2, pp. 173-189.

[20] J. Yang, Z. Zeng, Y. Tang, J. Yan, H. He, and Y. Wu, "Load frequency control in isolated micro-grids with electrical vehicles based on multivariable generalized predictive theory," *Energies* 2015, vol. 8, no. 3, pp. 2145-2164.

[21] G. Delille, B. Francois, and G. Malarange, "Dynamic frequency control support by energy storage to reduce the impact of wind and solar generation on isolated power system's inertia," *IEEE Transactions on Sustainable Energy*, vol. 3, no. 4, pp. 931-939, 2012.

[22] M. Einan, H. Torkaman, and M. Pourgholi, "Optimized Fuzzy-Cuckoo Controller for Active Power Control of Battery Energy Storage System, Photovoltaic, Fuel Cell and Wind Turbine in an Isolated Micro-Grid," *Batteries* 2017, vol. 3, no. 3, pp. 23-41.

[23] M. Sechilariu, F. Locment, and I. Houssamo, "Multi-source power generation system in semi-isolated and safety grid configuration for buildings," in *15th IEEE Mediterranean Electrotechnical Conference MELECON*, 2010, pp. 967-972.

[24] S. J. Safi, S. S. Tezcan, I. Eke, and Z. Farhad, "Gravitational Search Algorithm (GSA) based PID Controller Design for Two Area Multi-Source Power System Load Frequency Control (LFC)," *Gazi University Journal of Science* 2018, vol. 31, no. 1, pp. 139-153.

[25] A. Kumar and S. Suhag, "GWO Algorithm Based Fuzzy-PID Controller with Derivative Filter for Load Frequency Control of Multi-Source Hydrothermal Power System," *The 5th International Conference on Control, Mechatronics and Automation*, 2017, pp. 50-55.

[26] R. K. Sahu, G. C. Sekhar, and S. Panda, "DE optimized fuzzy PID controller with derivative filter for LFC of multi source power system in deregulated environment," *Ain Shams Engineering Journal* 2015, vol. 6, no. 2, pp. 511-530.

[27] A. Kumar and S. Suhag, "Multiverse optimized fuzzy-PID controller with a derivative filter for load frequency control of multisource hydrothermal power system," *Turkish Journal of Electrical Engineering & Computer Sciences* 2017, vol. 25, no. 5, pp. 4187-4199.

[28] S. Saremi, S. Mirjalili, and A. Lewis, "Grasshopper optimisation algorithm: theory and application," *Advances in Engineering Software* 2017, vol. 105, pp. 30-47.




ISSN 1737-9334

# Rapid Prototyping using HIL, PID and Fuzzy Logic Controller

**Daw M. Alzentani**
.[1] (*Department of Electrical and Electronic Engineering*)
*Alzawia University,* Libya.
daw_425@yahoo.com .

**Almokhtar M. Alzhari**
.[2] (*Department of Computer Engineering*)
*Alzawia University,* Libya.
ali441@yahoo.com .

**Abstract**
Rapid Prototyping of embedded hardware/software systems is important, because it shortens the path from specification to the final product. Prototypes play a major role in decision making, concept and design validation, feature and limit exploration, as well as design verification in every phase of the product development cycle, including product planning, requirement engineering, and product development. Rapid prototyping of embedded systems can emulate different kind of processes, through the mathematical modelling that represent their dynamic characteristics. This make easier to emulate different control strategies, which can interact with the real signals of the embedded process, making a better approach of the real response than a simple simulation. This paper presents the results of the emulation of the dynamic behaviour in the study case to work, in order to validate control strategies like PID and Fuzzy, using the concepts of rapid prototyping and hardware-in-the-loop (HIL). To achieve this objective, two embedded systems were employed, the first one to emulate the dynamics of the process, and the second one to implement the control strategy. Both systems were interconnected using the Controller Area Network protocol (CAN). The principal contribution of this work is the methodological development in the application of the control strategies through HIL

**Keywords:** HIL, CAN bus, Fuzzy controller, PID controller.

## i. INTRODUCTION

Nowadays, one of the most useful strategies for such a technological product development is the communication platform between each devices and components of the whole system [1].
CAN protocol technology, uses in the interconnection task of the embedded system, allowing the distribution of the control process through different stages using a modular structure [3].
The CAN protocol facilitates the development of control systems based in the concept of rapid prototyping, which can emulate processes or control methods through the use of Hardware-in-the-loop techniques, as show in [4]. This help the product development, reducing the time and production costs, giving the possibility to experiment with the dynamic signals in an embedded system and test different control strategies, in order to obtain a final desired system that interacts through a communication protocol [5, 6].
As support of the HIL concept, exist tools of rapid prototyping which allow to generate the code to be implemented in embedded systems since process simulation [7]. An example of this kind of tools is the Waijung® Blockset developed by Math works [8].
This tool creates code for ARM® processors based in a MatLab-Simulink Package. An important work about rapid prototyping is presented in [9], where is shown the application of modern procedures to implement control methods to regulate climatic behaviours into a vehicle, which are complemented with HIL to emulate the control strategies using models of heating, ventilation and air conditioning elements, which finally provide an efficient tool to verify, validate and optimize the control algorithms in real time, that are implemented in interconnected platforms through communication interfaces, reducing costs and production times in the process.
An implementation of hardware in the loop to design a flexible architecture to control an electric hybrid vehicle platform, presented in [10]. is taking into account methods that guarantee the emulation in real time. Methods based on multi-thread technology, and implemented in development platforms which use the high speed CAN communication protocol, have as result the emulation of hardware and the control strategies which validate the process, removing errors automatically.
Hence, this paper describes a product development methodology using the rapid prototyping and HIL concepts, and based on the implementation of the Waijung® tool, to describe the dynamic process in the embedded systems, communicated through CAN protocol with the simulated models in MatLab-Simulink®. According to this, are obtained the results to apply this method to operation stages in a process with different control strategies in discrete time.
This document is organized as follows: In section I, the preliminary and introductory theoretical basis about the developed work is presented. In section II, is described the principal documentation of the software tool to use, as well as the main features of the CAN protocol and its implementation characteristics in the embedded system. In section III, is summarized the analysis of results. And finally, the conclusions of the work are presented.


ISSN 1737-9334

### ii. CAN protocol characteristics

For the development of this work, is proposed the CAN protocol to communicate two embedded systems of the ARM® family, to interconnect the signals between the embedded process in one board with the control system emulated in the second board. As control strategies a PID controller and a Fuzzy Control were tested. The plant to control consists of a PITTMAN direct current motor. In Figure 1, a diagram of this application is presented.

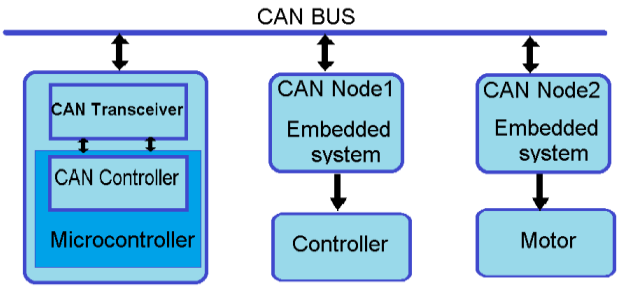


**Figure 1:** Connection CAN bus diagram

### iii. Mathematical Model of the DC Motor

To calculate the mathematical model of the DC motor, as a first step, must be defined if the motor is controlled by armature or by field, in this case, the motor is controlled by armature, so the electro-mechanical diagram of the motor is defined as is depicted in the Figure 2.

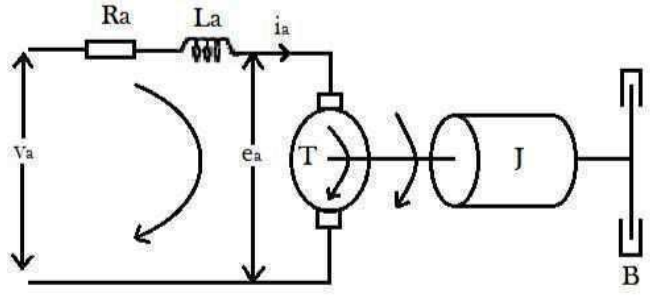


**Figure 2:** DC Motor armature Current controlled

From schematic Diagram figure 2, the dynamic behavior of the electrical part is presented [11].

$$v_a(t) = R_a * i_a(t) + L_a * \frac{di_a(t)}{dt} + e_a(t) \quad (1)$$

In the equation (2), is shown the mathematical model of the mechanical part [12].

$$T(t) = J * \frac{dw(t)}{dt} + B * w(t) \quad (2)$$

The relation between the mechanical and electrical part is given in the equation (3) and (4) respectively.

$$T(t) - T_L = K_m * i_a(t) \Rightarrow T_L = 0 \quad (3)$$

$$e_a(t) = K_e * w(t) \quad (4)$$

Substituting the equation (4) in (1) is obtained the equation (5).

$$v_a(t) = R_a * i_a(t) + L_a * \frac{di_a(t)}{dt} + K_e * w(t) \quad (5)$$

Then it is replaced the equation (3) in the equation (2), where is obtained the equation (6).

$$K_m * i_a(t) = J * \frac{dw(t)}{dt} + B * w(t)$$

$$i_a(t) = \frac{J}{K_m} * \frac{dw(t)}{dt} + \frac{B}{K_m} * w(t) \quad (6)$$

Finally, the equation (6) is replaced in the equation 5, where is obtained the equation (7) that represents the system behaviour.

$$v_a(t) = \frac{R_a * J}{K_m} * \frac{dw(t)}{dt} + \frac{R_a * B}{K_m} * w(t) + \frac{L_a * J}{K_m} * \frac{d^2w(t)}{dt} + \frac{L_a * B}{K_m} * \frac{dw(t)}{dt} + K_e * w(t) \quad (7)$$

Applying Laplace in equation (7) is obtained the equation (8)

$$v_a(s) = \left(\frac{R_a * J}{K_m} * s + \frac{R_a * B}{K_m} + \frac{L_a * J}{K_m} * s^2 + \frac{L_a * B}{K_m} * s + K_e\right) * w(s) \quad (8)$$

Resolving the equation (8), should be obtained the transfer function of the system which is shown in the equation (9).

$$\frac{w(s)}{v_a(s)} = \frac{\frac{K_m}{L_a J}}{s^2 + \left(\frac{R_a}{L_a} + \frac{B}{J}\right)s + \left(\frac{R_a B}{L_a J} + \frac{K_e K_m}{L_a J}\right)} \quad (9)$$

The variables values that characterize the 24 volts PITTMAN motor DC054B-2 (14202), are presented in table 1 [13], and are used to simulate the system.

**Table 1:** Features motor data [13]

| Parameters | Symbol | Value |
|---|---|---|
| Armour Resistance | $R_a$ | $1.73\ \Omega$ |
| Armour Inductance | $L_a$ | $2.54 * 10^{-3} H$ |
| Friction Coefficient | $B$ | $0.09\ Nm - s/rad$ |
| Electrical Constant | $K_e$ | $0.055\ Vs/rad$ |
| Mechanical Constant | $K_m$ | $0.042\ N - m/A$ |
| Inertial Moment | $J$ | $0.0023\ Kgm^2$ |

The values in table 1 should be replaced in the equation 9 to obtain the final equation (10), which describes the system behaviour.


ISSN 1737-9334

$$\frac{\omega(s)}{v_a(s)} = \frac{7189}{s^2 + 720.2s + 27050} = G(s)$$

( 10)

The DC Motor's transfer function is obtained, and then we have to calculate the PID and the Fuzzy controller.

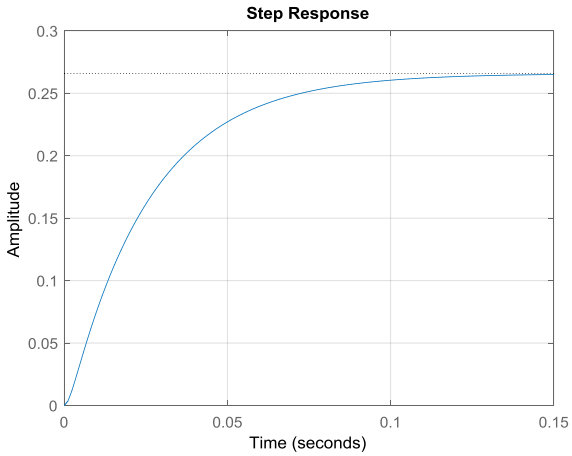


**Figure 3** DC Motor Time Response

### iv. Calculation of PID Controller

To calculate the PID controller, first a system discretization stage must be performed. For this case the discretization method to use, is the ZOH (Zero Order Hold), which executes the Z transformation using partial fractions of the continuous control signal [14].

$$G(z) = Z\{G_{ZOH}(s) * G(s)\} = (1 - z^{-1})\left\{\frac{G(s)}{s}\right\} \quad (11)$$

Then, T is defined as the sample time, used to perform the Discretization of the plant, which for this case is:

$$T = 0.0012789$$

Finally the discretized plant transfer function is represented by the equation (12).

$$G(z) = \frac{0.0044083z^{-1} + 0.0032477z^{-2}}{1 - 1.3693z^{-1} + 0.3981z^{-2}} \quad (12)$$

The discretized plant's transfer function obtained, then we have to calculate PID parameters, controller with filter in discrete time is conducted using the characteristic transfer function shown in equation (13) [15].

$$PID(z) = \frac{q_0 + q_1z^{-1} + q_2z^{-2}}{1 + (so - 1)z^{-1} - soz^{-2}} \quad (13)$$

With the definition of the characteristic equation of a PID controller with filter, the process is continued with the definition of the characteristic and the desired system polynomial. The characteristic polynomial is a representation that shows the current plant behaviour, and has as variables the four factors defined by equation (13).

the desired polynomial represents the wanted behavior for the plant. Keeping this in mind, will be defined the representative equation. The equation (14) defines the structure of the desire polynomial.

PC(z) = 1+

$$+\frac{q_0 + q_1z^{-1} + q_2z^{-2}}{1 + (so - 1)z^{-1} - soz^{-2}} \frac{0.0044083z^{-1} + 0.0032477z^{-2}}{1 - 1.3693z^{-1} + 0.3981z^{-2}}$$

14)

To complete the definition of the desire polynomial has to be Set the sample time value, in this case is the same value of Time used to discretize the plant. Also, the parameters that define the plant behaviour after the control application have to be set. So, is proposed the characteristics in table 2.

**Table 2:** Design parameters [13]

| Parameters | Value |
|---|---|
| Error | 2 % |
| Ts / open loop | 0.012789 |
| Desired Ts | 95 % \| open loop |
| Number of Samples | 10 samples |
| Overshoot | 10 % |

With the overshoot (Mp), is defined the value of zita $(\xi)$ to be used in the calculation of the controller. Using the equation (15) is obtained this value.

$$\xi = \sqrt{\frac{1}{1 + \frac{\pi^2}{\ln(Mp)^2}}} \quad (15)$$

Resolving the equation, the value of zita corresponds to:

$$\xi = 0.591155$$

The next variable to use is the natural system frequency, represented by equation (16).

$$Wn = \frac{-\ln(error)}{\xi * 0.95\ ts|_{open\ loop}} \quad (16)$$

$$Wn = 544.6780077\frac{rad}{s}$$

Obtaining the value of Wn, the next variable to calculate is Wd, for this is used the equations(17) and (18):

$$if\ 0 < \xi < 1\ then\ Wd = Wn\sqrt{1 + \xi^2} \quad (17)$$

$$if\ \xi \geq 1\ then\ Wd = \sqrt{Wn^2 + \xi^2} \quad (18)$$

$$Wd = 632.733064\frac{rad}{s}$$

When obtained these values, should be proceeded to determinate the magnitude and angle of the system in the Z domain, the values, are calculated using equation (19) and (20) respectively.

$$|Z| = e^{-T*\xi*Wn} \quad (19)$$

$$\angle Z = T * Wd \quad (20)$$

The desired polynomial is represented by the equation (21) and is calculated using the real and imaginary values obtained




ISSN 1737-9334

in (19) and (20).

$$Pd(k+t) = (1 - re + jim) \otimes (1 - re - jim) \otimes \left(1 - e^{-T*\xi*Wn}\right) \otimes \left(1 - e^{-T*\xi*Wn}\right) \quad (21)$$

Where $\left(1\_e^{-T*\xi*Wn}\right)$, is a non-dominant Z pole.

The next step is the equalization of the characteristic and the desired polynomial to finally determinate the values in the equation (13) which represent the PID controller with filter.

$$PID(z) = \frac{177.2707 - 190.3629 * z^{-1} + 53.23637 * z^{-2}}{1 - 0.56599 * z^{-1} - 0.43401 * z^{-2}}$$

### v. Calculation of the Fuzzy Controller

Nowadays a useful alternative to design the control of a system is using the fuzzy logic concepts, which allows through the expert understanding of the process to generate a knowledge base for the system, and provide it the ability to Make decisions about certain actions to rule its operation [16]. To implementing a fuzzy control, is necessary to define the fuzzy logic of the process, this allows to the systems to work with no accurate information and with qualitative values, such as low error, decrement control, among other variables, which are defined as linguistic values [17].

To develop a fuzzy controller, first starts defining the output variables of the system and the structure of the input variables. The control output in this case is given directly by the DC motor operation. To define the input, should be considered what kind of variable controls the output, thus is defined as input variable the error, calculated from the difference between the system reference and the feedback plant value. This process is depicted in the Figure 4.


**Figure 4:** fuzzy control structure

Considering the fuzzy sets, then is proceeded with the clusters structure that set up the input and output variables. For the input variable (Error), are defined five clusters, four of them are trapezoidal and one triangular, each one obeys to the error linguistic variables defined as: very low, low, none, high and very high. The shapes for the clusters were chosen in judgment of the developers. Finally that set includes a range of values from-4 to 4, because the error system values vary within this range, as it can be seen at Figure 5.

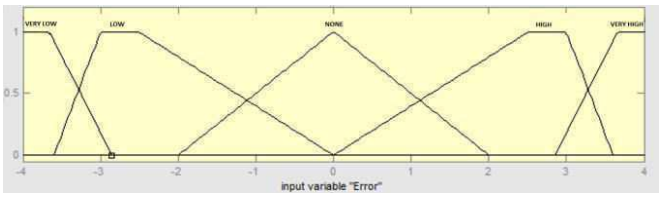


**Figure 5:** Input Fuzzy Control

In the output control variable case, it has five clusters, four of them are trapezoidal and the last one is triangular, each one corresponds to a linguistic control value defined as: Decrease, few decreases, none, few increase, and increase. In this case, the sets have a range of-300 to 300, to generate the sub-damped desire response, as shown in Figure 6.

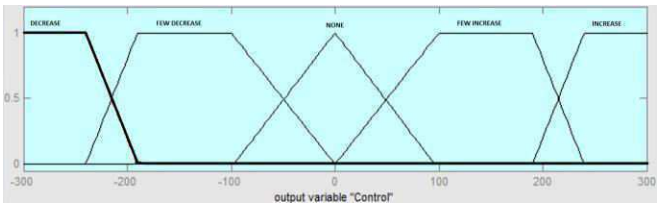


**Figure 6*:* Output Fuzzy Control**

To set the fuzzy rules that define the control operation, in this case is proposed that for an error input given as very low, the control must have a decrease value and for a very high error the control must increment, thus, are proposed intermediate cases to complete the set of rules to make the control work, as shown in table 3.

**Table 3:** Control Rules

| Rule | Case |
|---|---|
| 1. | If (Error is very low) then (Control is Decrease) |
| 2. | If (Error is none) then (Control is none) |
| 3. | If (Error is very high) then (Control is Increase) |
| 4. | If (Error is low) then (Control is Few Decrease) |
| 5. | If (Error is high) then (Control is Few Increase) |

After to define the input and output fuzzy sets, and the stipulated fuzzy rules, is proceeded with the inference process as shows in Figure 7, for this case was chosen the Mamdani process. This method is based on the calculation of membership values for different clusters in each input space

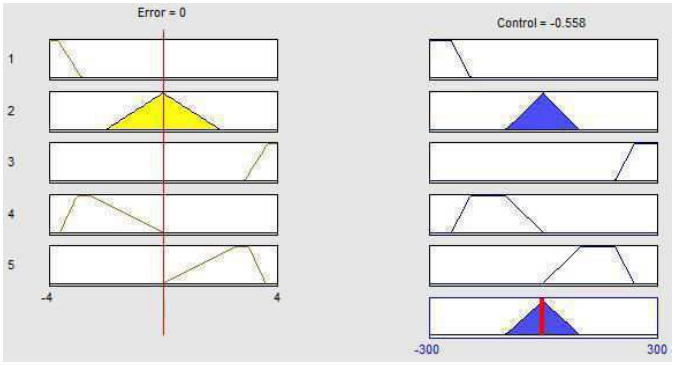


**Figure 7:** Inference Process to Zero Input Error

Finally, must be performed the defuzzification process, which for this case is used the centroid method, and consists in the calculation of the gravity centre from the resulting sets after the implementation of the controller rules. This defuzzification method is defined by the equation (22).




ISSN 1737-9334

$$y_{centroide} = \frac{\sum_{x \in X} x\mu_A(x)}{\sum_{x \in X} \mu_A(x)} \quad (22)$$

### vi. Embedded System Program

To program the embedded controllers, is used the Matlab® Simulink® tool, which allows to design the feedback control system. The first step is the implementation of the discretized plant, for this, is required the basic program configuration of the development board to use in the block Simulink Target Setup, then are configured the CAN and USB VCP communication protocols. The CAN protocol allows to perform the communication between the embedded control board and the discrete plant board. To configure this protocol PB8 and PB9 pins are set up to receive and transmit information respectively, also the baud rate is configured to a rate of 125Kb, and the line communication which the data transfer is performed, corresponds to CAN LOW.

Moreover the USB VCP protocol is used to display the system response from a pulse train input. The visualization can be performed in the setup of the reception blocks as shown in Figure 8.

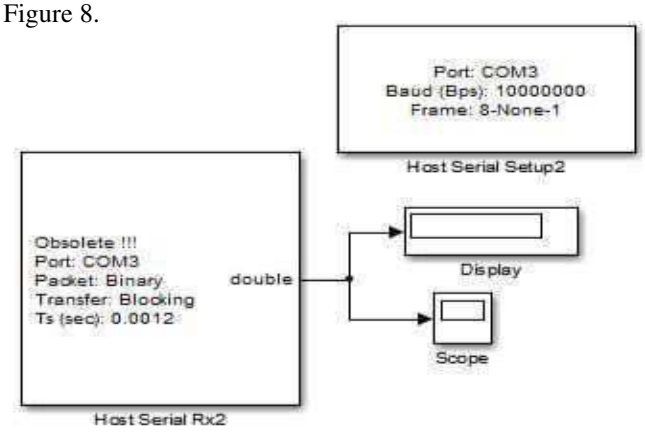


**Figure 8:** Block diagram for displaying the Plant Response

The program also offers the possibility to observe the system response in an oscilloscope through a DAC (Digital-to-Analog converter) output, programmed in the development board.

Continuing with the board configuration, is proceeded with the implementation of the plant to work and the integration of the previously mentioned blocks, to complete the programming task of the board, and emulate the behavior of a controlled by armature DC motor, as shown in the Figure 9.

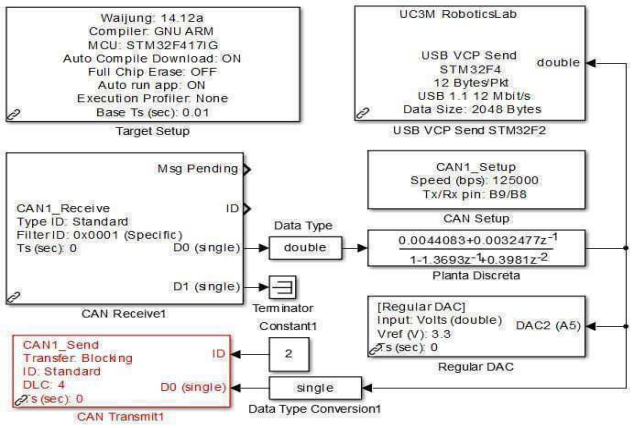


**Figure 9:** Block Diagram for Data Transfer and Emulation DC Motor

In Figure 9 can be observed, the data is received through the CAN module, then is converted to double data type and connected with the plant, next the output data is returned using the same CAN protocol line in order to feedback the plant response, and calculate the error to introduce it as control parameter and determinate the proper action for the plant to obtain the desire behavior.

### vii. Embedded Control Programming

After implement the plant in the embedded system, is continued with the programming of the control methods to handle the desired response of the system. The Figure 10 shows the block diagram of the programming of the development board that is responsible of the system emulation controller. There is shown some blocks are surrounded by coloured squares which will be explained in next section of this work

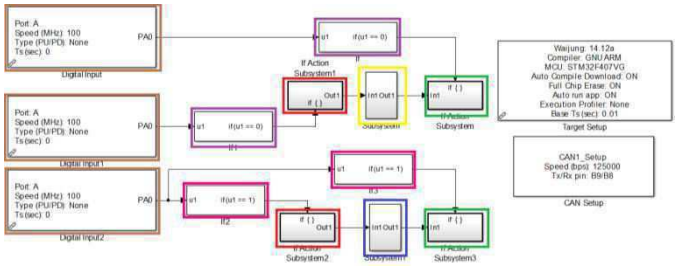

**Figure 10:** Block Diagram for Configuring the PID and Fuzzy Controllers

First, the program gets as parameter a value of zero or one given by the user, which determinates if the controller to use is PID or Fuzzy, this signal is acquired through the PA0 pin (brown Colored Square). If this signal is zero, the purple block is activated and allows performing the functions in the red, yellow and green subsystems within a loop until the signal gets the value of one. For this case the PID controller blocks are activated.

The red subsystem is responsible to receive the plant values from the CAN protocol this is used for both controllers to work. It consists of a reception CAN block that filters the data received with ID 2, with a sample time of 0.0008 seconds, then the data is sent to the following subsystems in the control line. The data flow is shown in Figure 11.

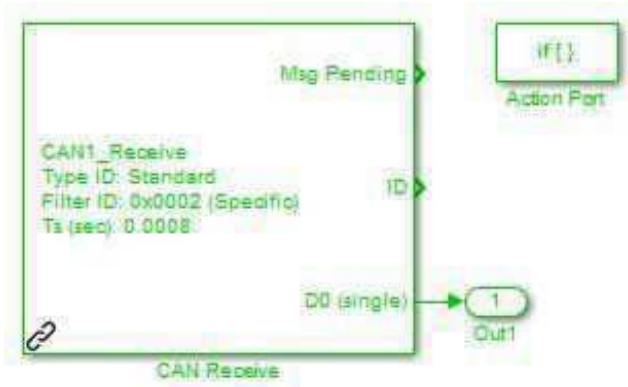


**Figure 11:** Reception Module Configuration through CAN Protocol




ISSN 1737-9334

The yellow subsystem contains the PID controller structure, which gets the data from the red subsystem to be processed. The received data comes from the plant feedback given and enters to a sub-process where is performed a subtraction with the reference signal. The result, enters to the controller which calculates the values that must be set on the plant to change and generate the desired behaviour. This subsystem is depicted in Figure 12, which shows how the error is calculated to enter in the green subsystem.

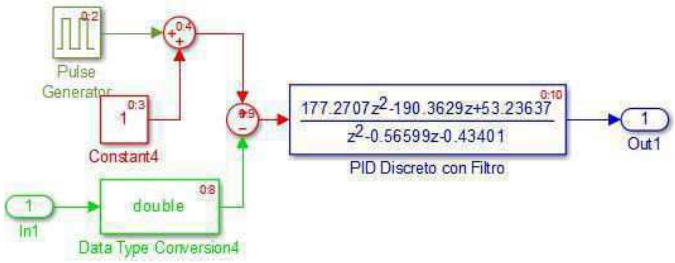


**Figure 12:** PID Controller Setup

From the yellow subsystem to the green subsystem is transferred the variable through CAN protocol, to change the system behaviour. In this case the CAN transmission module is configured with a sample time of 0.012 seconds to send the signal, because the sample time of the controller and the plant have the same value that is shown in Figure 13.

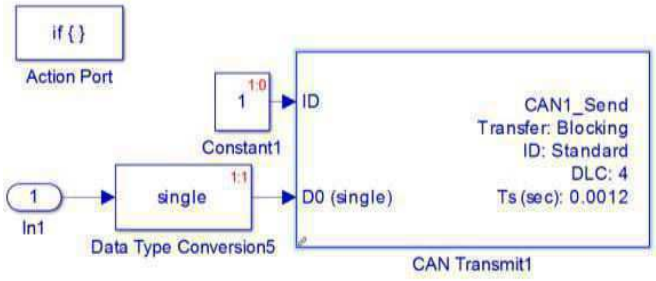


**Figure 13:** CAN Transmission module Setup

Now is analysed the behaviour of the program when the signal has a constant value of one and is entered to the brown block of the Figure 9. This action performs the activation of the pink blocks and deactivating the purple blocks.

When the pink blocks are activated the signal enters as parameter for the red subsystem, which as previously mentioned has the same function of the reception block subsystem for the PID controller.

Then the feedback value enters to the blue subsystem, where the subtraction between the reference system and the value generated by the plant is performed. Is observed that the value generated by the plant have a compensation of 0.955 to delete peaks in the control signals that cause a system destabilization, however as consequence the plant does not reach the desired reference. The used controller in this stage is a fuzzy controller whose input is the error and the output is the control signal, as shown in Figure 14.

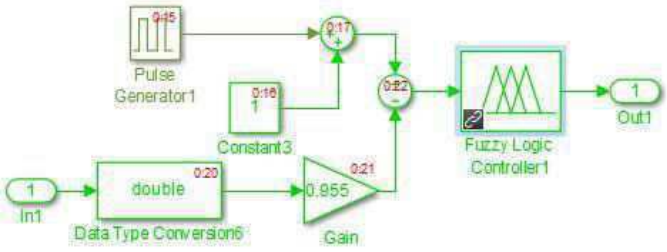


**Figure 14:** Fuzzy Controller Setup

This subsystem throws an output variable that enters to green subsystem, which transmits it by CAN protocol to the plant and achieve the desired effects in the system. As it is shows in this case, the sample time of the protocol handles a value of 0.0008, which mark a difference between the values of transmission between PID controller and the Fuzzy Controller as it is shown in Figure 15.

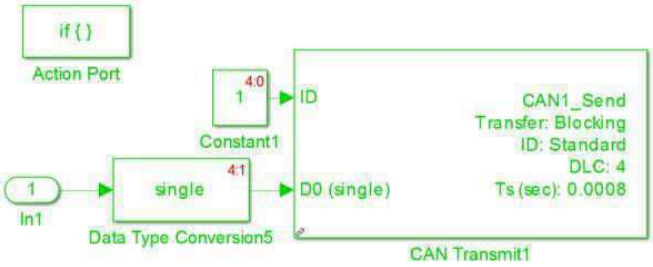


**Figure 15:** CAN Transmission Module Setup

### viii. Analysis of Results and Discussion

After assembling the system embedded controllers, in the Figure 16 the response of the system is obtained. There is shown that for stabilize adequately the system, has a strong control signal to keep the system in the desire point after a change in the reference, in this case the control generate a peak in the signal with a big overshoot (overshoot reached in the second step). This kind of behaviour is observed when the system have a settling time longer and it must force the plant to stabilize in short times.

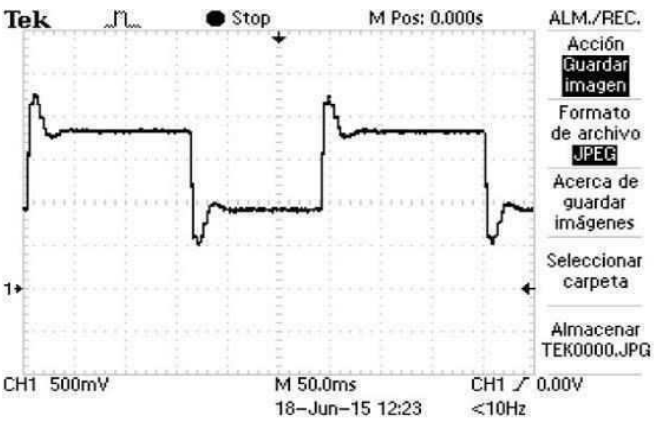


**Figure 16:** PID Controller Response




ISSN 1737-9334

In Figure17 is depicted the signal taken from the CAN module.

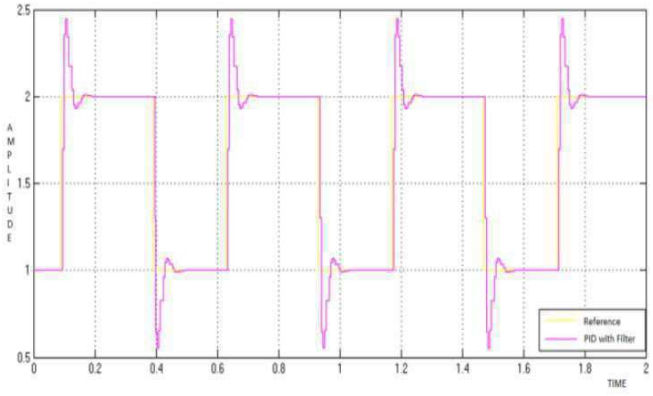


**Figure 17:** PID Controller Response Taken From HOST

Regarding to the stabilization of the system, is presented a reduced settling time and to achieve it are sufficient few samples.

For a Fuzzy controller is necessary more samples to stabilize the system in a desired reference, because is complicated to get a robust fuzzy control, for this case is due to the generation of the control rules which do not take into account settlings times or overshoots. So it generates a strong control signal if the error is maximum and a weak control signal if the error is minimum. Hence, the obtained control over the system is observed in the Figure 18.

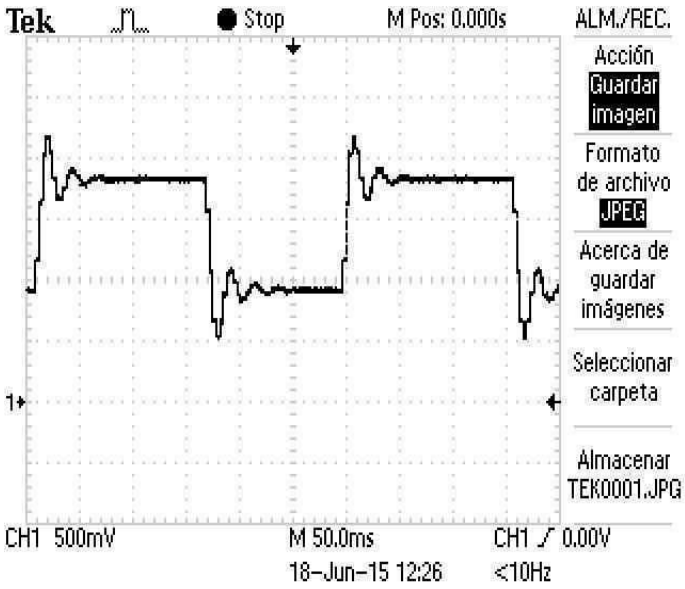


**Figure 18:** Fuzzy Controller Response

In Figure 19 is shown the signal that taken by the CAN module for the fuzzy controller.

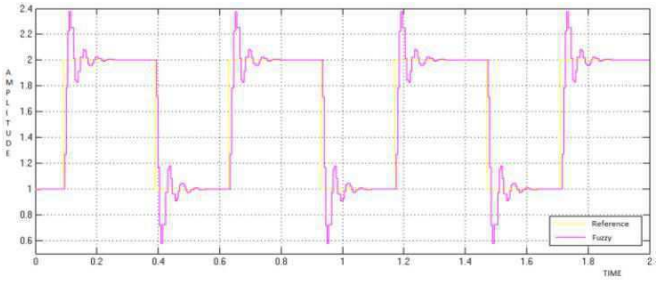


**Figure 19:** Fuzzy Controller Response Taken From HOST

Applying these two control methodologies, is necessary keep in mind that although the PID controller had a better response and stabilization with fewer samples than the fuzzy controller, can be observed that the last controller provides more robustness to system disturbances, or unwanted signals, due the rules and conditions of the clusters.

Another point to analyse into the development of this work, is the fact to have several transmission and reception CAN modules, instead of one for transmission and one for reception. This is because as shown previously, the reception and transmission has to be done with different sample times for each process. If the same sample times would have taken the control signal would distorted, having as a consequence an unstable system.

## ix. CONCLUSION

During the development of the work. It was observed that the sensitivity of the controllers in discrete time increases when are performed slight changes of the sample time, so is important to keep in mind that to perform the design of the control, first is necessary to define the time values to avoid interfere in the operation of the system when exist modifications by different control strategies.

Even though a conclusion may review the main results or contributions of the paper, do not duplicate the abstract or the introduction. For a conclusion, you might elaborate on the importance of the work or suggest the potential applications and extensions.

Moreover, the development of this work counted as advantage with the implementation of tools as Matlab® and its toolboxes, which allow the designer to focus in the knowledge on how to provide solutions to certain works, leaving as a second item, generating lines of C code, implemented in this type of development boards that intend emulate the behaviours of everyday life processes.

As future work, is proposed to perform the emulation of different parts of a vehicle and interconnect them through CAN communication protocol. As complement is planned to build a graphic interface to observe the behaviour of the emulated systems and apply possible control methods.


ISSN 1737-9334

## REFERENCES

[1] P.S. Kedareswar and V. Krishnamoorthy, "A CAN protocol based embedded system to avoid rear-end collision of vehicles," in Signal Processing, Informatics, Communication and Energy Systems (SPICES), 2015 IEEE International Conference on, Feb 2015, pp. 1-5.

[2] Xiaoyuan Z., Hui Z., Dongpu C., Zongde F., "Robust control of integrated motor-transmission powertrain system over controller area network for automotive Applications" Mechanical Systems and Signal Processing, Volumes 58-59, June 2015, Pages 15-28.

[3] T.R. Jena, A.K. Swain, and K. Mahapatra, "A novel bit stuffing technique for Controller Area Network (CAN) protocol," in Advances in Energy Conversion Technologies (ICAECT), 2014 International Conference on, Jan 2014, pp. 113-117.

[4] A.Devi, G. Gnanavel, and G. Antoni Gracy, "MCS-51 microcontroller based industrial automation and control system using CAN protocol," in Communications and Signal Processing (ICCSP), 2014 International Conference on, April 2014, pp. 61-65.

[5] Zhibin S.; Hui Z.; Junmin W.; Jianqiu L.; Minggao O.; "Combined AFS and DYC Control of Four-Wheel-Independent-Drive Electric Vehicles over CAN Network with Time-Varying Delays," in Vehicular Technology, IEEE Transactions on, vol.63, no.2, pp.591-602, Feb. 2014. doi: 10.1109/TVT.2013.2279843

[6] Richardson, P.; Elkateeb, A.; Sieh, L., "An adaptive real-time intravehicle network protocol for intelligent vehicle systems," in Vehicular Technology, IEEE Transactions on, vol.53, no.5, pp.1594-1606, Sept. 2004. doi: 10.1109/TVT.2004.833616.

[7] R. Subramanian, P. Venhovens, and B.P. Keane, "Accelerated design and optimization of battery management systems using HIL simulation and Rapid Control Prototyping," in Electric Vehicle Conference (IEVC), 2012 IEEE International, March 2012, pp. 1-5.

[8] Caballero A., Copaci D., Blanco M. Moreno L. Herrán J., Fernández I., Ochoteco E., Cabañero G., Grande H.; "Innovative Pressure Sensor Platform and Its Integration with an End-User Application"; Sensors 2014, Vol. 14 pp. 10273-10291; doi:10.3390/s140610273.

[9] D. Michalek, C. Gehsat, R. Trapp, and T. Bertram, "Hardware-in-the-loop-simulation of a vehicle climate controller with a combined HVAC and passenger compartment model," in Advanced Intelligent Mechatronics. Proceedings, 2005 IEEE/ASME International Conference on, July 2005, pp. 1065-1070.

[10] Heike B.; Florian R.; Toralf B.: Development and hardware-in-the-loop test of a guidance,navigation and control system for on-orbit servicing; Acta Astronautica; Vol. 44; 2014; pp. 67-80.

[11] Youngki K.; Ashwin S.; Jason B.; Zoran F.; Anna S.; Tulga r.; " Hardware-in-the-loop validation of a power management strategy for hybrid powertrains"; Control Engineering Practice; V 9; 2014; pp. 277-286.

[12] Zeina B.; Samih J.; Imad K.; "Modeling and Simulation of Series DC Motors in Electric Car"; Energy Procedia; Vol. 50; 2014; pp. 460-470.

[13] PITTMAN. (2015) PITTMAN DC054B-2 (14202) Brush DC Motor. [Online]. http://www.pittman-motors.com/Brush-DC-Motors/14202-Brush-DC-Motor.aspx

[14] Xie L.; Shieh L.; Tsai J.; Wu C.; Park J.; "Digital and analog integer delayed modeling and control for multivariable systems with multiple time delays in states, inputs and outputs"; Applied Mathematical Modelling; 2015. DOI: 10.1016/j.apm.2015.08.012.

[15] K. Benjamin C, Sistema de Control Automatico, cap 10, pag 708-714: Prentice Hall, Septima Edición.

[16] Cigánek J.; Filip N.; Štefan K.; "Modeling and Control of Mechatronic Systems Using Fuzzy Logic"; international review of automatic control; Vol 7, No 1, 2014. DOI: http://dx.doi.org/10.15866/ireaco.v7i1.1291.

[17] Ibrahim H., Mahmoud E.; "A Comparative Study of PID, Fuzzy, Fuzzy-PID, PSO-PID, PSO-Fuzzy, and PSO-Fuzzy-PID Controllers for Speed Control of DC Motor Drive"; International Review of Automatic Control; Vol 6, No 4, 2013.


ISSN 1737-9334

# *College Students' Active Involvement in Collaborative and Social Learning through Canvas Discussion Boards*

Rania A.K. Elmajdoubi

*English Language Department, University of Tripoli*
*College of Education*
*Tripoli, Libya*
ano901990@gmail.com

***Abstract*—this paper reports a study which supports e-learning by the incorporation of online collaborative and social learning into Canvas discussion boards which encourage small project groups of college-level students to interact, discuss, share ideas and reflect on their own research. This study aimed at establishing an online collaborative and social environment for providing EFL Libyan learners taking the graduation projects as groups in their last semester at a college of education with online learning experience through collaborative and social interactivity. Rich data were collected qualitatively and then were analysed to explore the matters being reflected upon by using a content analysis technique. The results revealed that collaborative and social space as a virtual learning community through Canvas discussion forums created richer collaborative and social dialogues and established stronger relationships among students themselves as well as with their supervisor.**

***Keywords*—***E-learning, Collaborative learning, Social Learning, Canvas Discussion boards, Interactivity.*

## I. INTRODUCTION

Higher education institutions in Libya replace teaching with lecturing, thus Libyan college students are passive and demotivated during their lectures. Their focus is commonly directed towards passing exams rather than involving them in the learning process. Students commonly feel responsible for collecting marks without worrying too much about being centred and achieving learning outcomes. Teacher-centred classes are considered as an obstacle that students encounter while they are learning English for both general and academic purposes. The reason behind teacher-centredness might be the result of the nature of our culture in which the teacher is always dominant and controlling, instead of being a facilitator, motivator, monitor and guide.

Therefore, the researcher seeks to establish a practical foundation for EFL Libyan learners to think holistically and practically about their learning skills, knowledge and performance as they relate to college-level courses. Furthermore, the current study puts expectations with regard to the master of their levels of interaction, involvement and motivation as much as online social and collaborative active learning is incorporated into the content, course objectives and teaching repertoire of college-based modules through online discussion forums which support written communication.

### *A. Problem Statement*

The current study addresses the challenges ofhow to promote an e-learning environment supported by online discussions which aim at achieving a high-level of collaboration for constructing and exchanging information, increasing learners' participation as individuals, and maximizing their social interactivity with their peers, course instructors and/or project supervisors.

### *B. Main Research objective*

More specifically, this individual action research is guided by the following main objective:

- To identify whether Canvas discussion boards provide EFL Libyan learners taking a college-level graduation project with online effective learning experience through collaborative and social interactivity with their peers and with their supervisor.

### *C. Importance of the Research*

The value of this research paper is derived from:

- The e-learning atmosphere will enhance the social and collaborative characteristics of the learning experience.




ISSN 1737-9334

- Departments at Libyan faculties are capable of using any free online discussion boards for different courses and supervised projects, which necessitate the regular collaboration between course instructors/supervisors and students in order to accelerate the progress of the learning process.
- EFL students' involvement in online discussion boards saves much time and encouragesthemcontinuously to contact with their instructors not only during the assigned lecture hours, but also anytime it is needed.

## II. Literature Review

### *A. Group E-learning*

Group e-learning or collaborative e-learning indicates to knowledge-construction from experience, meaning-negotiation and/or problem-solving achieved through mutual involvement of a group of learners in an organized step utilizing technological tools and online interaction (Salmons, 2008).

According to Siemens (2002, p. 8), peer to peer interactions in an e-learning environment can be considered from the perspective of four stage continuum as follows:

1. Communication: People 'talking,' and discussing.
2. Collaboration: People sharing ideas and working together (occasionally sharing resources) in a loose environment.
3. Cooperation: People doing things together, but each with his or her own purpose.
4. Community: People striving for a common purpose.

### *B. Social Learning*

From the perspective of the social learning theory, knowledge is socially constructed and experience is shared while learners are interacting with each other through activities, discussions and feedback (Henning 2004). Students' interactions within the social context promote understanding and knowledge is distributed among them. Creating a socializing spot for initiating and sustaining a social learning interaction can be carried over to the online educational atmosphere for the course requirements. As indicated by King (2002), greater social interaction is perceived by students, especially when detailed discussions are set up and shared within web-based learning environments (WBLEs). Students' social interaction through technology-mediated environment plays a crucial role in learning success (Hara, Bonk, and Angeli 2000; King 2002).

Most importantly, social learning as a group assists learners with gaining experience in collaboration and enhancing their critical thinking, self-reflection, and knowledge-building (Brindley et al., 2009).

### *C. Collaborative Learning*

Group collaboration maximizes meaningful learning interactions among students. It also results in facilitation of group structure, formation and dynamics. Through group work, community knowledge is obtained, besides effective peer communication (Northrup 2001). Collaborative learning can be effectively blended in virtual and in-class environments. Hiltz et al. (2000), for instance, conducted a field experiment on collaborative learning which revealed that students' group involvement in collaborative virtual learning was either as good as or better than that of learners in the traditional learning environment.

This study focuses on the impact of online learning environments on small groups of EFL learners' social and collaborative learning interactions through the use of Canvas synchronous/asynchronous discussion boards.

Palloff and Pratt (2005, p. 12) referred to particular pedagogical advantages of collaborative learning which include:

1. Development of critical thinking skills,
2. Co-creation of knowledge and meaning,
3. Reflection, and
4. Transformative learning**.**

### *D. Research question*

The main area of this research is summarized in the following question:

- Do Canvas discussion boards provide EFL Libyan learners taking a college-level graduation project with online effective learning experience through collaborative and social interactivity with their peers and with their supervisor?

## III. Methodology

### *A. Study Sample*

Data of this experimental research were collected from 10 fourth- year project students at a college of education in West Libya over one semester. The target students were females between the ages of 21 and 24. They took the group projects in their last semester before graduating. Their project supervisor engaged them in Canvas discussion boards for accelerating the completion of their project while working collaboratively either synchronously or asynchronously.

### *B. Research Methods and Design*

- ***Qualitative nature of the study***




ISSN 1737-9334

The present study was qualitative in nature, which means it "involved data collection procedures that result primarily in open-ended, non-numerical data which is then analysed primarily by non-statistical methods (Dörnyei, 2007, p. 24).
The choice of qualitative individual action research was suitable for obtaining data which provided information corresponding to the descriptive sorts of its research question. Rich qualitative data were analysed to explore the matters the students taught and reflected upon by using a content analysis approach. Such analysis necessitated the generation of categories, sub-categories and coding scheme deductively in order to connect the research results with the aforementioned theories for drawing inferences (Hsieh & Shannon, 2005).

- ***Canvas as a data collection instrument***

The qualitative data were obtained from Canvas as an online learning management system which facilitates virtual teaching and learning. Its tools (e.g. announcements, assignments, discussions, files, etc.) are designed to be accessed from various web browsers, mobile phones, and tablets. Canvas network, for instance, allows educators to start new courses where resources can be stored in an online space so that they can be imported and shared.

- ***Piloting Canvas***

In preparation for Canvas usage, the process of piloting was primarily required for the participants because the website was totally new to them. The piloting phase was a good opportunity to ensure the quality and sufficiency of the Canvas tools in order to apply changes, build rapport, avoid a great deal of difficulties and potential extra work later on.
As Gass and Mackey (2005, p. 57) explained, pilot testing "can help avoid costly and time-consuming problems during the data collection procedure… [as well as] the loss of valuable, potentially useful, and often irreplaceable data".
The pilot study was carried out with participants who resembled the target population: students were supervised by the researcher in the same environment of the research site. The researcher invited her targeted students to a workshop for introducing them to the different uses and functions of the website tools a step by step, especially its online discussion boards (see Appendix 1 for more details about the workshop and announcement).

- ***Canvas purposes for the current research***

Canvas was used in the current research for different purposes including:

a) Starting new courses and adding modules to Canvas Home Pages.
b) Adding EFL Libyan students and assigning them into group sets.
c) Adding online folders for uploading files as course repository so that students can download files for their courses prior to the meeting day without any financial costs.
d) Adding online pinned discussion groups opened for comments and replies (as presented in Appendix 2).

Canvas discussion boards were mainly the researcher's area of interest for promoting virtual social and collaborative interactions through group work and written communication. "Threaded" discussions as long-lived spaces were utilized to sustain longer with multiple posts referring to one specific topic.

### *C. Data Analysis Procedures*

Canvas data were analysed on the basis of structuring categories and subcategories so that they "make the research process more reliable and produces results that are comparable across classrooms and over time" (Dörnyei, 2007, p. 185).
More specifically, it was organized as Case A in which the categories were labelled on the basis of interaction moods (i.e. *student-supervisor, supervisor-student* and *peer to peer interactions),* deriving *purposes* and *outcomes* from them as sub-categories.

## IV. RESULTS/DISCUSSION

This chapter addresses the quality of learning experience provided to college-level Libyan learners through collaborative and social interactivity with their supervisor (the researcher) and their peers on Canvas discussion boards.
Interestingly, the results from the current research indicated that the target discussion groups with their first experience of being engaged in Canvas discussion boards had managed to use it to a satisfactory level.
During the faculty based and distance learning time, the researcher's small graduation project groups of 10 students for their bachelor's degree developed individual, social and collaborative learning aspects online. This provided evidence of progression, coherence and reflection as they progressed towards the writing of their project chapters.
For instance, one of the most productive learning behaviours, as listed in *Table 1*, was elicited from a project student's contribution to their Canvas discussion board.It was about asking the supervisor for online checking of their project introduction: (*I want to tell you i wrote the introduction but need from you to check it if u not mind ...*).
The student's request for checking their writing continued as a way of negotiating meaning in order to overcome a problem of confusion: (*When i check on almost previous projects and*



ISSN 1737-9334

*i found most of them they wrote problems of study after literature review and i face problem when i try to write it .. indeed im confused □□ So this is my problem of study, check it plz*).

**Table 1:***Learning experience gained from social and collaborative* ***student-supervisor interactions.***

| | |
|---|---|
| ***Student-Supervisor Interactions*** | **(Purpose)**<br>- Ask for checking their writing (e.g. of a project introduction).<br>- Negotiate meaning<br>- Problems of confusion. |
| | **(Outcomes)**<br>- Reduce confusion, anxiety, & nervousness.<br>- Solve a writing problem. |

The results in *Table 1* were supported by Salmons (2008) who claimed that collaborative e-learning did not only promote the construction of group's knowledge (e.g. knowledge of starting writing their project introduction following a coordinated structure), but also encouraged them to negotiate meaning with their supervisor as means of solving the problem of writing to overcome their confusion.

As soon as the course instructor initiated the online discussion by providing the group with online direct/indirect feedback: (*Introduction mainly includes a brief explanation of why your research topic is worthy of study…*), the collaborative teacher-student interaction succeeded to achieve the clarification of research objectives. As a consequence, the student restated her ideas of research objectives: (*Here's Aims and Objective…To explore the use and benefits of visual and audio aids, on Libyan college learners learning process*) (As stated in *Table 2*).

The project supervisor's online feedback promoted students'social learning with the provision of effective chances to construct knowledge, share experience and develop skills of group work(Henning 2004).

**Table 2:***Learning experience gained from social and collaborative* ***supervisor-student interactions.***

| | |
|---|---|
| ***Supervisor-Student Interactions*** | **(Purpose)**<br>- Promote online direct/indirect feedback on learning.<br>- Clarify research objectives.<br>- Facilitate group learning and respond to students' problems. |
| | **(outcomes)**<br>- Facilitate learners' continuous participation in a small project group.<br>- Restate ideas of research objectives.<br>- Foster a non-threatening collaborative learning environment.<br>- Build up students' self-esteem, critical-thinking and problem-solving skills to become more active, productive and involved in online learning. |

The findings of this study further revealed that the small collaborative learning group in the virtual environment had a positive impact on facilitating learners' continuous interactivity with their supervisor. In line with Brindley et al., cooperative learning makes a major contribution to the development of "sense of community, increased skill acquisition, and better learning outcomes) (2009, p. 1).

Furthermore, exposing the small project group of the present study to online communication created a non-threatening collaborative learning environment. This interesting outcome led to some psychological and academic benefits on the groups of learners from the perspective of reducing anxiety, building up their self-esteem, critical-thinking and problem-solving skillsto be more active, productive and involved (Laal &Ghodsi, 2012).

In order to achieve a positive outcome of the quality of the learning experience, engagement should not only be connected with teacher-student interaction or vice versa, but should also be extended torefer to "…peer-to-peer collaboration and active learning..." (Chen, Gonyea, &Kuh, 2008, para. 2). Thus, peer-to-peer engagement on Canvas was achievable here as they interacted with each other for the purposes and outcomes presented in *Table 3*). The purposes and outcomes outlined in *Table 3* were extracted from the following online interactivity among the group members:

*Girls, I want to emphasize that I put the full introduction on our online discussion. You will find it above in the comments with the objectives and research questions. Surely, the first objective has two questions which I surely took them. The second, third and fourth objectives have one research question each. Once you choose any of the listed questions, you should let us know directly so that no one of us exhausts herself with searching for information and it turns out to be the same point. Another advice, any question you take, answer it to facilitate your work on the project. Hopefully, it is clear now* ❤.

**Table 3:***Learning experience gained from social and collaborative* ***peer to peer interactions***


ISSN 1737-9334

| | |
|---|---|
| **Peer to Peer Interactions** | **(Purpose)**<br>- Confirm and clarify information.<br>- Monitor group work online. [6]<br>- Remind groups of ground rules for group interaction.<br>- Equalize participation among group members. [7]<br>- Give instructions/advice for facilitating project completion. |
| | **(Outcomes)**<br>- Improve skills of group work [8]<br>- Gain social learning experience<br>- Develop critical thinking, self-reflection and knowledge-building. [9] |

Student-student interactions on Canvas discussion forums reflected the importance of Siemens's (2002) four phase continuum of students' engagement as an effective framework for scaffolding progressively with their communication, collaboration, cooperation and the feeling of belonging to professional learning communities.

## V. Conclusions

Providing students with collaborative and social spaces as a virtual learning community through Canvas discussion boards gave them the chance to collaborate and communicate socially not only with their supervisor, but also with their peers. Canvas discussions also facilitated theiraccess to a rich learning environment that provided them with opportunities for interaction and connectedness. Moreover, the findings of this research revealed the extent to which the quality of learning experience became more effective with the variation in interactivity moods. As a further recommendation, learners and educators should be exposed to the adoption of online learning and integrate it into the culture of higher-education sectors with feasibility to promote the qualities of language teaching, learning, interactivity, feedback and assessment.

## *References*

[1] Brindley, J.E., Walti,C. &Blaschke,L.M. (2009) Creating Effective Collaborative Learning Groups in an Online Environment. *International Review of Research in Open and Distance Learning,vol. 10* (3): pp.1492-3831.

[2] Chen, P., Gonyea, R., &Kuh, G. (2008). Learning at a distance: Engaged or not? *Innovate, vol. 4*(3). Available online at http://www.innovateonline.info/index.php?view=article&id=438&action=article.

[3] Dörnyei, Z. (2007) Research Methods in Applied Linguistics: Quantitative, Qualitative, and Mixed Methodologies, OUP: Oxford.

[4] Hara, N., Bonk, C.J. &Angeli, C (2000) Content analysis of online discussion in an applied educational psychology course. *Instructional Science, vol. 28* (2): pp. 115–152.

[5] Hiltz, S., Coppola, N., Rotter, N., Turoff, M.&Benbunan-Fich, R. (2000) Measuring the importance of collaborative learning for the effectiveness of ALN: A multi-measure, multi-method approach. *Journal of Asynchronous Learning Networks, vol. 4* (2). Available online at: http://www.aln.org/publications/ jaln/v4n2/v4n2_ hiltz.asp.

Henning, W. (2004) Everyday cognition and situated learning. *Handbook of research on educational communications and technology* (2nd edition): pp. 143–168, edited by Jonassen,D.,Erlbaum: Mahwah, NJ.

Hsieh, H.-F. & Shannon, S.E. (2005) Three approaches to qualitative content analysis. *Qualitative Health Research, vol. 15* (9):pp.1277-1288. Available online at: http://qhr.sagepub.com/content/15/9/1277.short?rss=1&ssource=mfc.

King, K. P. (2002) Identifying success in online teacher education and professional development. *Internet and Higher Education, vol. 5* (3): pp. 231–246.

Laal, M. &Ghodsi, S.M. (2012) Benefits of collaborative learning. *Procedia-Social and Behavioral Sciences,vol. 31*: pp. 486-490.

[10] Mackey, A. &Gass, S.M. (2005) Second Language Research: Methodology and Design, Routledge: New Jersey.

[11] Northrup, P. T. (2001) A framework for designing interactivity into Web-based instruction. *Educational Technology, vol. 41* (2): pp. 31–39.

[12] Palloff, R. M., & Pratt, K. (2005) Collaborating online: Learning together in community, Jossey-Bass: San Francisco.

[13] Siemens, G. (2002) Interaction. E-Learning Course. Available online at: http://www.elearnspace.org/Articles/Interaction.htm.

[14] Salmons, J. E. (2008) Taxonomy of collaborative e-Learning.*Encyclopedia of Information Technology Curriculum Integration*: pp. 839-846.

## *Appendixes*

***Appendix 1:****The workshop details.*



ISSN 1737-9334

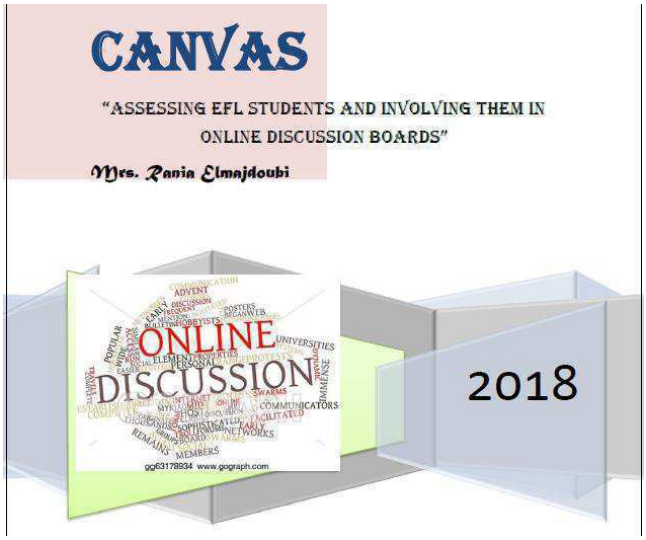


***Appendix 2:****Samples ofCanvas Discussion Boards*

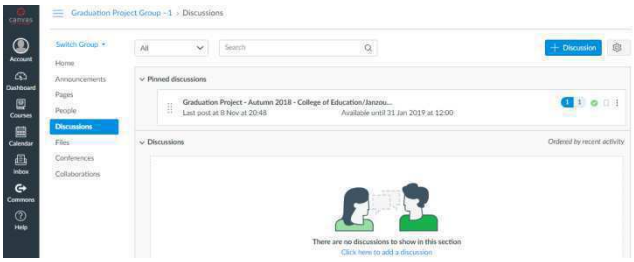


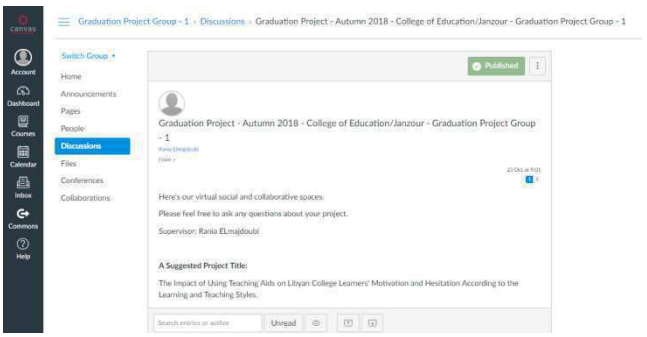


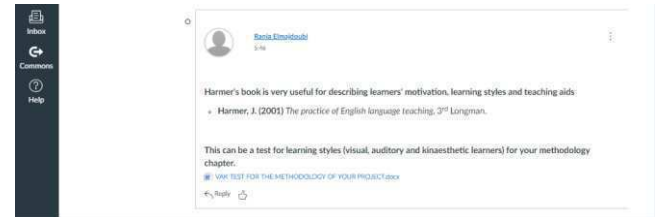



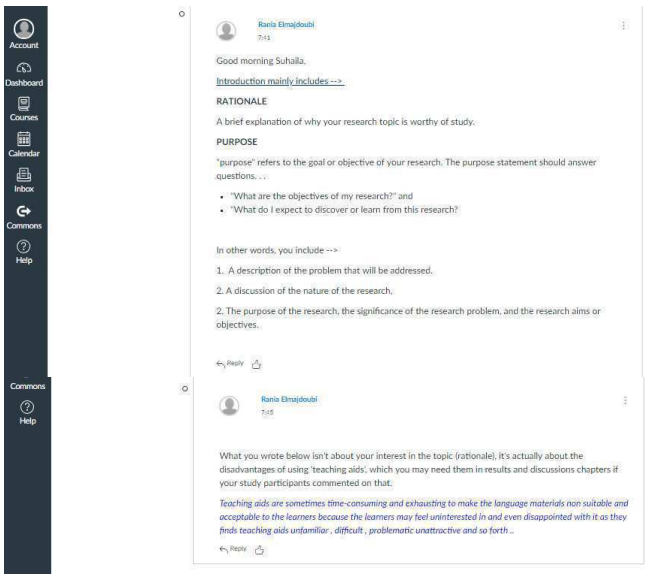



ISSN 1737-9334

# Comparison of Real-Time Performance Between ĆUK and SEPIC Converters for an MPPT Based on the P&O Method Using Xilinx System Generator

Rezki Tadrist[#1], Mountassar Maamoun[*2], Adnane Hassani[#3]

[#]*Laboratoire LSIC ENS de Kouba. B.P N°92 16308 Vieux-Kouba – Alger*
[1]rtadrist1959@gmail.com
[3]Adnhassani@yahoo.fr
[*]*Département d'Electronique, Université de Blida, Algérie*
[2]mountassar.maamoun@univ-blida.dz

***Abstract* - Today, the electrical energy extracted at the output of photovoltaic panels is still low despite the significant efforts made in the development and improvement of the converters in the photovoltaic field. In addition the maximum energy extraction is also achieved using a Maximum Power Point Tracking (MPPT) method that could increase the electrical power efficiency and also significantly reduce the overall cost of a photovoltaic system. However, this paper compares the performances of two main and popular converters, the ĆUK and the SEPIC which monitor the MPP of the photovoltaic (PV) system. As a result, the advantages and disadvantages between the two converters have been described and discussed. The results of the simulation showed that the ĆUK and SEPIC converters followed the MPP with a very small gap difference. The experimental simulation system was developed using Matlab/Xilinx System Generator (XSG) for the operation of the proposed algorithm and the architecture structure was developed in the XSG environmental tool for its implementation on an FPGA device with a minimal resource. Thus, the current research work was completed using a minimal resource and led to a simple and inexpensive system.**

***Keywords*: Maximum Power Point Tracking (MPPT), Photovoltaic (PV), Perturb and Observe, ĆUK and SEPIC converters, Xilinx System Generator.**

## I. INTRODUCTION

The sun is an inexhaustible source of energy, it is naturally regenerated in a short time, for this reason, it is called "renewable energy" or "sustainable energy". Due to the gravity of the global energy crisis and environmental pollution, the photovoltaic (PV) system has become a kind of important source of renewable energy. Solar energy has important advantages, a maximum reserve, inexhaustible, without geographical limits, it is thus the photovoltaic technology of our day becomes a vast subject of popular research. On the other hand the oil reserves would have been exhausted in 2040, the natural gas in 2060, and the coal in 2300 [1]. In Algeria, the authorities have become aware of this challenge, renewable energy objectives will be doubled (12-25) GW by 2030 [2], the country has about 350 MW of photovoltaic projects under development.

A tariff system offers surrender rates of approximately US $ 0.20 for (1-5 MW) projects and a slightly different rate for projects over (5 MW). Currently research work has focused on how to extract more efficient power from photovoltaic cells. The efficiency of PV systems is still low due to the influence of changes in insolation and temperature. To improve the efficiency of a PV system, monitoring of the maximum power point is essential in order to obtain maximum energy from the PV system. Since 1968, the date of the first publication of the control law on the MPPT algorithm, research work has continued to appear [3]. Different types of powerful algorithms on PPM research are cited in the literature [4] [5].

There are many MPPT algorithms such as Perturb and Observe (P&O), Incremental Conductance (IC), fraction of short-circuit current, fraction of open-circuit voltage, neural networks and fuzzy logic, ext ....

In [6] the concept of power monitoring for photovoltaic systems is highlighted and an overview of 40 old and recent maximum power point tracking (MPPT) methods, available in the literature, is presented and classified. The Perturb and Observe method presents a problem in determining the optimum operating point in rapid changes in sunlight, but is easier and more reliable under normal conditions [7] [8] [9] [10]. DC-DC converters act as interfaces between the load and the photovoltaic module. They are generally used as a means of MPPT research as needed. For example the Boost converter is used in the case of raising the output voltage. But in other cases the desired output voltage must be lower than the input voltage [11]. In [12], the comparative analysis between the SEPIC topology and the ĆUK topology is presented. The ĆUK and SEPIC converters operate on the principle of energy transfer using capacitors and inductors to reduce current ripple in the circuit. In this article, the comparison of real-time performances between two converters, ĆUK and SEPIC for a MPPT based on the P&O method is studied and implemented using Xilinx System Generator.

For integration on a single chip, FPGAs offer lower implementation costs than microcontrollers and DSPs. FPGAs can provide equivalent or better performance than ASICs. FPGAs also offer the advantage of being


ISSN 1737-9334

reprogrammed at any time while the system is running thus providing a high degree of robustness. In addition to robustness and reprogramming, FPGAs can also provide a high level of flexibility [13]. Therefore, to meet the required performance, FPGAs are desirable since their performance can easily outperform the performance of microcontrollers and DSPs.

## II. MODELING A PANEL (PHOTOVOLTAIC CELL)

A photovoltaic cell can be compared to the equivalent circuit shown in Fig. 1 [14].

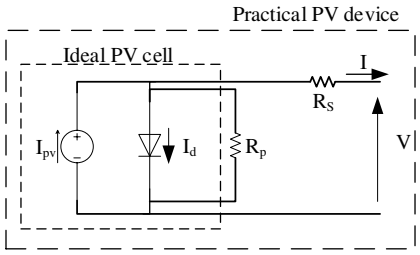


Fig. 1 Circuit equivalent to a single diode of a PV cell

To model the cell, the electrical quantities represented in the circuit above are expressed in the form of an equation, the current in the diode is expressed by:

$$I_D = I_0\left[exp\left\{\frac{V_D}{V_T}\right\} - 1\right] = I_0[exp\left\{\frac{(Vpv + Ipv * Rs)}{V_T}\right\} - 1] \quad (1)$$

$Io$ is the saturation current of the reverse polarization of the diode.

Avec:

$$V_D = (Vpv + Ipv * Rs) \quad (2)$$

And $V_T$ is the thermal tension defined by:

$$V_T = \frac{kT}{q} \quad (3)$$

With $k$ the Boltzman constant equal to 1.3806503x10$^{-23}$ J/K, $T$ is the operating temperature of the cell in Kelvin degree, and $q$ the charge of the electron. The voltage $Vpv$ is given by:

$$V_{pv} = (V_D - Ipv * Rs) \quad (4)$$

And:

$$I_p = \frac{V_D}{R_p} = \frac{Vpv}{R_p} + \frac{Rs}{R_p} I_{pv} \quad (5)$$

Finally, we obtain the expression of the current $I_{pv}$ of the cell:

$$I_{pv} = I_{sc} - I_D - I_p = I_{sc} - I_0[exp\left\{\frac{(Vpv + Ipv * Rs)}{V_T}\right\} - 1] - \frac{Vpv}{R_p} - \frac{Rs}{R_p} I_{pv} \quad (6)$$

Photovoltaic cell can not provide enough power to power a load or power grid. It is therefore necessary to assemble several cells in series and in parallel in order to obtain more power. A serial connection increases the output voltage of the solar panel, while a parallel combination increases the current supplied to the load. Then, it is necessary to introduce two new parameters $Np$ and $Ns$ respectively represent the number of cells in parallel and in series. The expression of the current $I_{pv}$ becomes:

$$I_{pv} = N_p I_{sc} - N_p I_0[exp\left\{\frac{(Vpv)}{N_s V_T} + \frac{(Ipv * Rs)}{N_p V_T}\right\} - 1] - \frac{Vpv}{R_p} - \frac{Rs}{R_p} I_{pv} \quad (7)$$

With:

- $Isc$: Short circuit current of the cell;
- $Rp$: The resistance characterizing the carrier recombination losses due to defects in the material;
- $Rs$: Characterizes the Joule losses in the semiconductor and the losses through the gate and the bad ohmic contact of the cell.

The amount of solar radiation directly affects the production of charge carriers in the solar panel, therefore affects the current produced by the latter, its expression is given by:

$$I_{os} = Irs\ [T/Tr]^3\ \exp\left[q * \frac{E_{G0}}{\beta * K}\left\{\frac{1}{Tr} - \frac{1}{T}\right\}\right] \quad (8)$$

And:

$$I_{sct} = [I_{sc} + K_I(T - 298.15)]\frac{G}{1000} \quad (9)$$

$Tr$ : is the reference temperature ($K$ = 298.18), ( $E_{G0}$ = 1.12 eV) is the width of the silicon band, ($\beta$ = 1.740) the ideality factor, $Irs$ is the reverse saturation current of the cell, $Ios$ is the saturation current of the cell.

In this comparison, we deliberately chose the monocrystalline photovoltaic solar panel Atersa A-250M. This is one of the modules used in the Ghardaia station in southern Algeria. It has a high efficiency, its value is highly competitive. In addition, these modules are covered by a 10-year guarantee [15].


ISSN 1737-9334

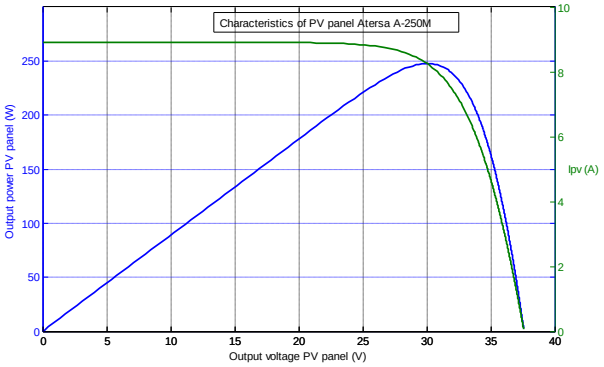


Fig. 2 Characteristics of PV panel

Table. I below summarizes the manufacturer's data. Based on the parameters of the table. I, the PV module is modeled in the Matlab/Simulink environment for standard test conditions (STC) of 25 ° C and 1000 W/m2. Fig. 2 above shows the characteristics of the Atersa-250M panel under standard conditions (G = 1000w / m2, T = 25 ° C).

TABLE. I ELECTRICAL AND THERMAL CHARACTERISTICS OF THE PANEL A-250M (STC: 1Kw/m2, 25 ° C ± 2 ° C)

| | |
|---|---|
| **Nominal power** | 250 W |
| **Module efficiency** | 15.35% |
| **Open circuit voltage** | 37.62 V |
| **Voltage at the point of maximum power (Vmp)** | 30.35 V |
| **Short circuit current** | 8.79 A |
| **Current at the point of maximum power (Imp)** | 8.24 A |
| **Coefficient of temperature voltage Voc (β)** | -0.34%/°C |
| **Current temperature coefficient Isc (α)** | -0.03%/°C |
| **Power temperature coefficient P (λ)** | -0.43%/°C |

## III. TRACKING MAXIMUM POWER POINT (MPPT)

### *A. MPPT charge regulator*

The technique (MPPT) is used to couple the inverters to power grids, solar battery chargers and similar devices in order to obtain the maximum possible power from one or more photovoltaic devices. The photovoltaic cell has a non-linear current/voltage characteristic as a function of the insolation and the temperature of the cell. The role of the MPPT is to ensure a coherent adaptation between the solar panel and the converter by generating an appropriate command to deliver the maximum power to the load whatever the climatic variations of the insolation and the temperature. MPPT devices are generally integrated into power conversion systems. In addition they ensure the regulation of the voltage and the current provided whatever the variation of the load or the network to feed [16] [17].

### *B. MPPT techniques*

Maximum Power Point (MPP) tracking is the automatic control algorithm to adjust the power interfaces and achieve the greatest possible power extraction, regardless of the changes in insolation and temperature or the effects the shading. This is therefore to ensure the operation of the system at the PPM point under varying atmospheric conditions. The MPPT then became an essential element for evaluating the performance of PV power system design [18]. There are different techniques used to track the maximum power point. Among the most widely used techniques are: disturbances and observations, incremental conductance, the fraction of the circuit current, the fraction of the open circuit voltage, the neural networks and the fuzzy logic. The choice of the algorithm depends on the complexity and execution time of the algorithm for monitoring the PPM, the cost of the algorithm and its implementation [19]. In this article the P & O technique (perturbe and observer) is used and implemented on FPGA target.

### *C. Description of the adopted algorithm*

The algorithm called "P & O" is an MPPT command whose operation is based on the disturbance of the voltage $V_{pv}$, by increasing or decreasing it by a small amplitude around its initial value [20][21]. This disturbance has the effect of acting directly on the duty cycle of the signal controlling the DC-DC converter. The disturbance is followed by the observation of its impact on the power output of the PV panel, with a view to a possible correction of this duty cycle. The figure. 3 shows the flowchart describing the algorithm providing this command called "P & O". The "P & O" method is widely used today because of its simplicity of implementation. However, this technique has some problems related to oscillations around the PPM it generates in steady state, because the search procedure of the PPM must be repeated periodically, forcing the system to oscillate permanently around the PPM. These oscillations can be minimized by reducing the value of the disturbance variable. However, a low increment value slowed down the search for the PPM, so you have to find a compromise between accuracy and speed. Which makes this order difficult to optimize.

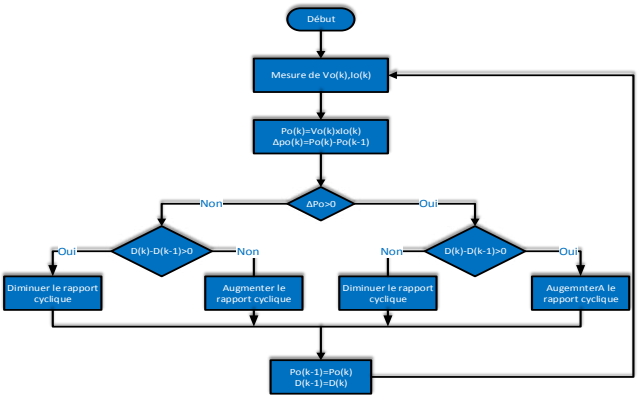


Fig. 3 Flowchart of P&O Algorithm for MPPT control




ISSN 1737-9334

*D- DC-DC converter design*

When proposing a PPM follower, the main task is to choose and design a very efficient converter, which is supposed to function as the main part of the MPPT. Most DC-DC converters are well designed to work with high efficiency.

1) *ĆUK CONVERTER*

The ĆUK converter has a special configuration. It is new compared to other converters. Originally, this converter was developed to generate a high output voltage. In addition, the setting of the output voltage is better than the buck converter and boost converter, as is the case with the Buck-Boost converter, and that's one of the reasons that makes it so popular. The second consideration is that in the continuous conduction mode, the input and output currents are not wavy and reduce electromagnetic interference (EMI). But the disadvantage of this circuit is that it provides, at the output, a voltage whose polarity is opposite to the input voltage [22]. The ĆUK converter has low switching losses and higher efficiency. It can provide better current efficiency due to the inductance of the output stage. Essentially, the ĆUK converter consists of two stages, an input stage and an output stage. Fig. 4 illustrates the circuit of the converter ĆUK.

2) *SEPIC CONVERTER*

The SEPIC converter is a DC-DC converter that converts a DC voltage into another DC voltage of different value (lower or higher). SEPIC is similar to buck-boost but has the advantage of having a non-inverted output (the output voltage is of the same polarity as the input voltage) [23]. This montage was developed by Slobodan ĆUK in the late 1970s. The basic diagram is illustrated in FIG. 5, it consists essentially of three capacitors (Cin, C1, and C2), two coupled inductances (L1 and L2), and a transistor (switch) and a diode. Both ĆUK and SEPIC converters operate at minimum values of their parameters as shown in the table. II below.

TABLE. II DESIGN PARAMETERS FOR BOTH CONVERTERS SEPIC AND ĆUK

| | values | |
|---|---|---|
| components | **SEPIC** | **ĆUK** |
| L1 | 293.8 µH | 450 µH |
| C1 | 300 µF | 0.21 µF |
| L2 | 293.8 µH | 925 µH |
| C2 | 150 µF | 0.88 µF |

## IV. COMBINED SYSTEM MODLING OF SEPIC AND ĆUK CONVERTER

Modeling of the system using Matlab/Simulink includes: the modeling of the photovoltaic system based on the equations (1) - (9), on the other hand the MPPT controller

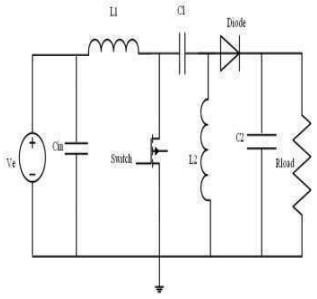


Fig. 5 Circuit diagram of SEPIC converter

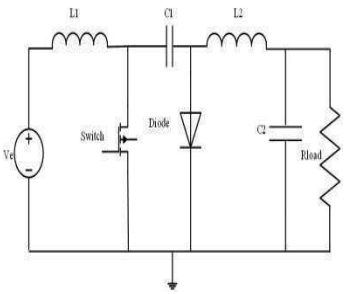


Fig. 4 Circuit diagram of ĆUK converter

based on the flowchart of Fig. 3 is modeled using the Xilinx System Generator environment. The adopted parameters of the two converters are summarized in the table. II. Figure 6 shows the combined system modeled to compare the two systems. Both systems are exposed to the same weather conditions (temperature and insolation) and also have the same PV parameters.

## V. RESULTS AND DISCUSSIONS

Fig. 6 below shows the schematic diagram of the principle of the entire photovoltaic generator system. The different blocks essentially constitute the PV panel, the MPPT algorithm, the two DC/DC converters connected to a resistive load. As we mentioned above in the previous section, the controller is designed in the Xilinx System

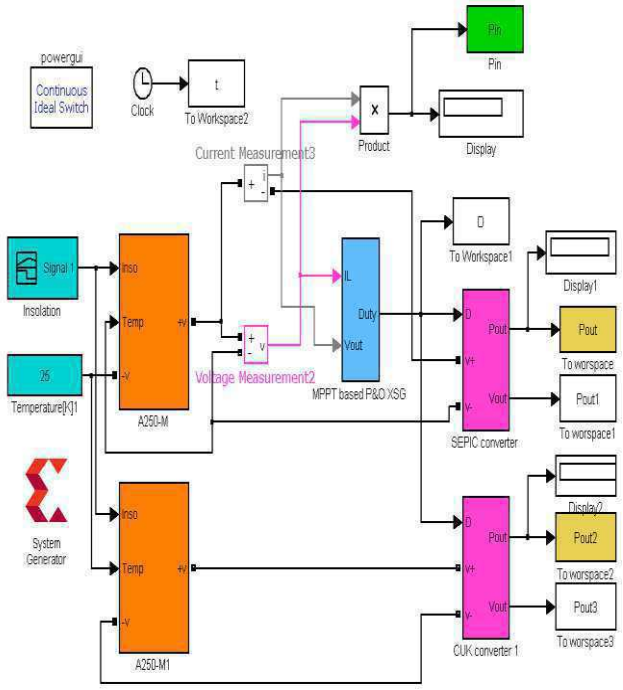


Fig. 6 General architecture of system simulation




ISSN 1737-9334

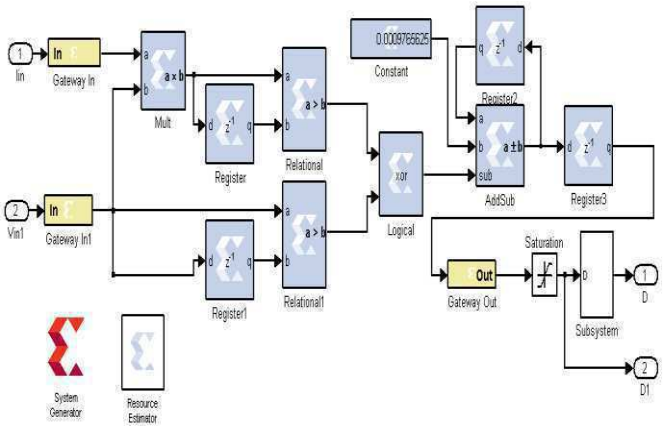


Fig. 7 Implementation of the P&O algorithm based XSG

Generator environment and the results are validated for both converters. Fig. 7 above shows the Xilinx System Generator architecture adopted for the implementation of the MPPT algorithm.

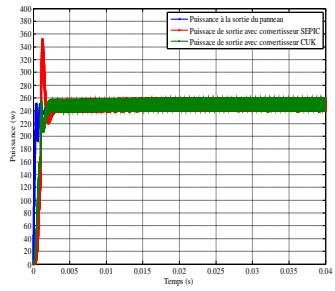


Fig. 8 Power output at constant temperature of 25°C and constant irradiance of 1 kW/m$^2$

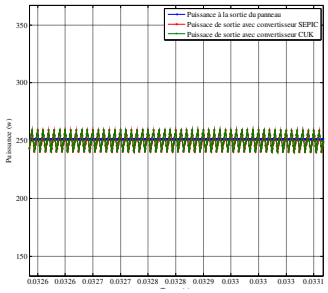


Fig. 9 Expanded time scale waveform at constant temperature of 25°C and constant irradiance of 1 kW/m$^2$

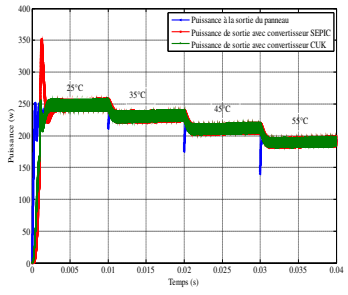


Fig .10 Output power at variation of temperature and constant irradiance of 1 kW/m$^2$

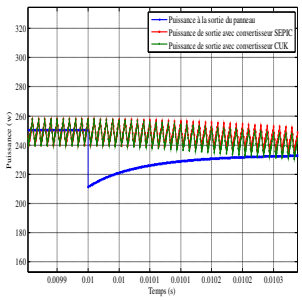


Fig .11 Expanded time scale waveform of output power for a step change of temperature from 25 ° C to 35 ° C and constant irradiance of 1 kW/m2

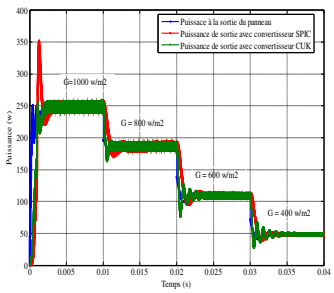


Fig .12 Output power at constant temperature of 25 ° C with step changes of irradiance

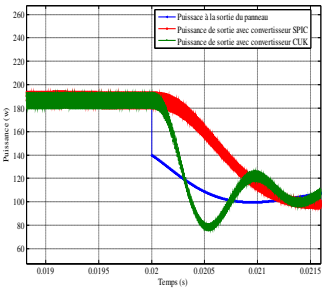


Fig .13. Expanded time scale waveform of output power at constant temperature 25 ° C with a step change of irradiance from 800 W/m2 to 600W/m$^2$

During implementation, the main problem encountered lies in the implementation of complex functions given the limited number of these functions that an FPGA contains. These functions increase the execution time and the space used on it. Nevertheless, there are practical approaches to bringing these functions together with simple FPGA designs. In [24], a simple and improved integral function model has been presented in which the equations of the SEPIC converter have been simplified to fit for FPGA implementation. In [25], the presence of the exponential function in the equation describing the current-voltage characteristic (I-V), making it difficult to locate the optimal point thanks to its first derivative, the Cubic Natural Spline Method is used.
Given the high speed of the FPGA for data processing on the one hand, and the maximum delays that can cause the analog/digital converters. So we have choose a CAN that ensures a good synchronization with the FPGA. In our circuit, an 8-bit ADC (TDA8703) is used which can sample the input signal at a rate of 4.43 MHz. Fig. 14 summarizes the system's circuit adopted with an integrated controller on an FPGA. The CANs are the link between the analog part and the digital part.

### *A used resources*

The use of FPGA resources is a key measure to materialize a system. Reducing the resources used is particularly important when the goal is to find the best behavioral performance of the system. The results are obtained using Xilinx Sysrem Genrator [26], the synthesis is ensured with the ISE 12.3 in the target SPARTAN3E xc3s500e-5fg320. The ISE environment, provides an implementation report in the form of tables containing useful information related to the following design: The table. III below counts all internal resources used in number and percentage of MPPT P&O controller.

### *B routing*

Routing is an Important Step in Developing an architecture for FPGA Target Implementation. It consists in creating physical connections between the logical elements of


ISSN 1737-9334

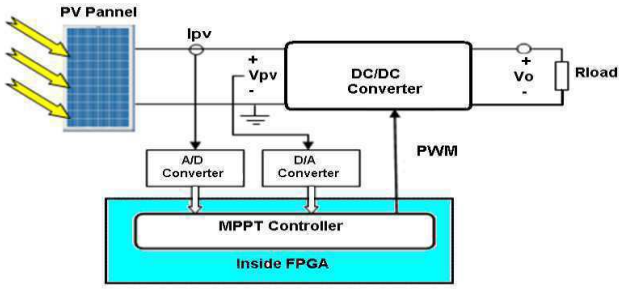


Fig.14 Diagram of the principle of the adopted PV system with integrated controller on FPGA

the FPGA by respecting the parameters of the architecture [27]. Each signal must therefore be connected to the FPGA routing resources. After these simulation results, the design was synthesized, a system-wide bitflow device was generated. It has been verified successfully by downloading it on the FPGA target mentioned above. The overall and internal diagram of the architecture of the proposed P&O algorithm is shown in FIG. 15 below. Fig. 16 shows the routing of the FPGA circuit for the "MPPT P&O" controller program.

Table. III Resources used for the P&O algorithm

| Logic Utilization | Used | Available | Utilization |
|---|---|---|---|
| Number of Slice Flip Flops | 52 | 9,312 | 1% |
| Number of 4 input LUTs | 53 | 9,312 | 1% |
| Number of occupied Slices | 44 | 4,656 | 1% |
| Number of Slices containing only related logic | 44 | 44 | 100% |
| Number of Slices containing unrelated logic | 0 | 44 | 0% |
| Total Number of 4 input LUTs | 53 | 9,312 | 1% |
| Number of bonded IOBs | 41 | 232 | 17% |
| IOB Flip Flops | 16 | | |
| Number of BUFGMUXs | 1 | 24 | 4% |
| Number of MULT18X18SIOs | 1 | 20 | 5% |
| Average Fan out of Non-Clock Nets | 1.45 | | |

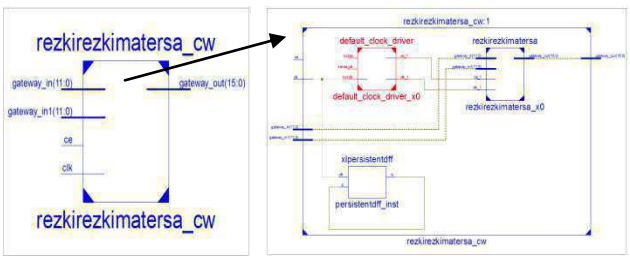


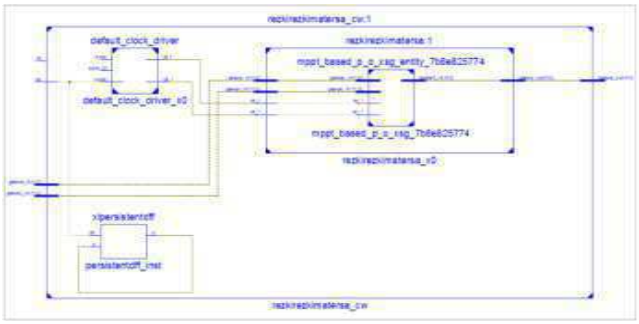

Fig. 15 Global RTL scheme of the P & O algorithm

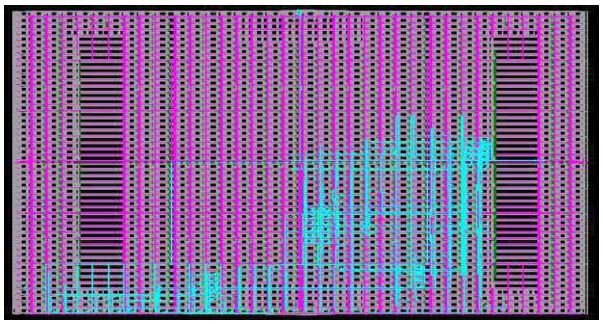

Fig. 16 FPGA circuit routing for the MPPT P&O controller program

We analyze the simulation results described in Figures 8 to 13, we can conclude that:

- The MPPT algorithm (Perturb and Observe) reaches the maximum power point (PPM) very fast for both converters ĆUK and SEPIC.
- Both systems respond to changes in temperature and irradiation.
- The output power of the system for the SEPIC converter has a 40% overshoot, but no overrun is recorded for the converter ĆUK.
- The rise time for both converters is almost the same, its value is 0.55ms.
- The output power of the system is more stable with the SEPIC converter at the point of maximum power compared to the system with the converter ĆUK.

## VI. Conclusion

This study compares the performance of two converters ĆUK and SEPIC used for the design of a MPPT using the P&O (Perturb and Observe) technique. The MATLAB/ Simulink software was used to simulate the system including the two converters and the photovoltaic module. On the other hand, the MPPT algorithm is executed in the XSG environment. The research work is carried out with minimal resources, making the system easy to implement on target FPGA and is therefore inexpensive. The results show that the output power of the ĆUK convertor is greater than the one of the SEPIC convertor within a short period of time. They also show that both systems easily detect the maximum power point in a period of time less than 0.005s. The ĆUK converter


ISSN 1737-9334

is much more stable with less power drive at the PPM position than the SEPIC converter.

## REFERENCES

[1] Nabil Karamia, Nazih Moubayedb, Rachid Outbib, "General review and classification of different MPPT Techniques'', Renewable and Sustainable Energy Reviews 68 (2017) 1–18. www.elsevier.com/locate/rser.

[2] MENA 2013, "The International Renewable Energy Agency (IRENA)'', www.irena.org.

[3] T. Esram ;P. L. Chapman, "Comparison of Photovoltaic Array Maximum Power Point Tracking Techniques'', IEEE TRANSACTIONS ON ENERGY CONVERSION, VOL. 22, NO. 2, JUNE 2007.

[4] Priety, Vijay Kumar Garg 1M. Tech Student(EE) "A Review Paper On Various Types Of Mppt Techniques For Pv System" e-ISSN 2277-2685, p-ISSN 2320-976 IJESR/May 2014/ Vol-4/Issue-5/320-330.

[5] Ali RezaReisi a,n, Mohammad HassanMoradi b, ShahriarJamasb, "Classification and comparison of maximum power point tracking techniques for photovoltaic system: A review'', Renewable and Sustainable Energy Reviews 19 (2013) 433–443.

[6] K. H. Hussein, I. Muta, T. Hoshino, and M. Osakada, "Maximum photovoltaic power tracking: An algorithm for rapidly changing atmospheric conditions", Proc. Inst. Elect. Eng., Generation, Transmission and Distribution, Vol. 142, No. 1, January 1995, pp. 59–64.

[7] S. Surawdhaniwar, R. Diwan "An Improved Approach of Perturb and Observe Method Over Other Maximum Power Point Tracking Methods ", International Journal of Recent Technology and Engineering (IJRTE) ISSN: 2277-3878, Volume-1, Issue-3, August 2012.

[8] D. P. Hohm and M. E. Ropp, "Comparative Study of Maximum Power Point Tracking Algorithms'', Published online 22 November 2002 Received 12 February 2002 Copyright # 2002 John Wiley & Sons, Ltd. Revised 2 June 2002.

[9] N. Femia, Member, IEEE, G. Petrone, G. Spagnuolo, Member, "Optimization of Perturb and Observe Maximum Power Point Tracking Method'', IEEE, and Massimo Vitelli IEEE TRANSACTIONS ON POWER ELECTRONICS, VOL. 20, NO. 4, JULY 2005.

[10] L. R. Shanmugasundaram , K. Sarbham . "Load Controlled Adaptive P&O MPPT Controller PV Energy Systems'', International Journal of Innovative Research in Science, Engineering and Technology; Vol. 4, Issue 5, May 2015.

[11] N. Mohan, T. M. Undeland, and W. P. Robbins, "Power Electronics: Converters, Applications and Design'', Third Edition, John Wiley, New York, 2003.

[12] Gayathri Deivanayaki.VP, Dhivyabharathi.R, Surabhi.R, Naveena.P, "comparative Analysis of Bridgeless CUK and SEPIC Converter'', International Journal of Innovative Computer Science & Engineering, Volume 3 Issue 1; January-February-2016; Page No. 15-19.

[13] A. Messai , A. Mellit, A. Guessoum, and S.A. Kalogirou, "Maximum power point tracking using a GA optimized fuzzy logic controller and its FPGA implementation", Solar energy, vol.85, pp.265–277, 2011.

[14] M. G. Villalva, J.R. Gazoli & E. Rupert. "Modeling and circuit based simulation of photovoltaic arrays'', Brazilian Journal of Power Electronics, Vol/Issue: 14(1). Pp. 35- 45, 2009.

[15] www.atersa.com.

[16] K. Kassmi, M. Hamdaoui and F. Olivié, "Caractérisation des Panneaux Photovoltaïques. Conception et Optimisation d'un Système Photovoltaïque pour une Meilleure Exploitation de l'Energie Solaire'', Energies Renouvelables, Organisation des Nations Unies pour l'Education, la Science et la Culture, Bureau de l'UNESCO à Rabat, Bureau Multi Pays pour le Maghreb, Les Energies Renouvelables au Maroc, Le débat est lancé. ISBN9954_8068_2_2, Rabat, Maroc, pp. 87 - 110, 2007.

[17] M. El Ouariachi, T. Mrabti, B. Tidahf, Ka. Kassmi and K. Kassmi, "Regulation of the Electric Power Provided by the Panels of the Photovoltaic System'', International Journal of Physical Sciences, Vol. 4, N°5, pp. 294 – 309, May 2009.

[18] H. Othmani, H. chaouali, D. Mezghani, A. Mami. "Optimisation de la Technique de Perturbation et Observation par la logique floue'', 3ème conférence Internationale des énergies renouvelables CIER-2015 International Journal of Scientific Research & Engineering Technology (IJSET).

[19] A. R. Saxena, S. M. Gupta, "Performance Analysis of P&O and Incremental Conductance MPPT Algorithms Under Rapidly Changing Weather Conditions'', J.Electrical systems, 10-3(2014):292-304.

[20] P .Bhatnagar, RK. Nema, "Maximum power point tracking control techniques: State-of the art in photovoltaic applications", Renewable and Sustainable Energy Reviews Sci Verse Science Direct, 2013; 224–241.

[21] N. Femia, G. Petrone, G. Spagnuolo and M. Vitelli, "Optimization of Perturb and Observe Maximum Power Point Tracking Method", IEEE Transactions On Power Electronics, Vol.20, No. 4, pp. 16-19, Mar. 2004

[22] P. de Souza , P. de Oliveira, R. Gules, E. F. R. Romaneli, A. A. Badin, "A high static gain CUK DC-DC converter ) '', 2015 IEEE 13th Brazilian Power Electronics Conference and 1st Southern Power Electronics Conference (COBEP/SPEC.

[23] M. Kaouane, A. Boukhelifa, A. Cheriti, "Design of a synchronous sepic DC-DC converter for a stand-alone photovoltaic system, Electrical and Computer Engineering (CCECE) '', 2015 IEEE 28th Canadian Conference on.

[24] R. Tadrist, A. Hassani, M. Maamoune, A. Nesba, "Nouvelle Approche d' Implémentation Sur FPGA d'un Modèle du Convertisseur Sepic Basé Sur Xilinx System Generator", 2ème conférence Internationale des énergies renouvelables CIER-2014 International Journal of Scientific Research & Engineering Technology (IJSET) Vol.3-pp.94-101, Copyright - IPCO 2015.

[25] R. Tadrist, A. Hassani, M. Maamoune, A. Nesba, I. Kebli, "Nouvelle Approche Temps-Réel de Modélisation des Panneaux Photovoltaïques basée sur FPGA", Revue des Energies Renouvelables Vol. 17 N°4 (2014) 611 – 622.

[26] Xilinx System Generator User's Guide, www.Xilin x.com.

[27] V. Betz and J. Rose, "How Much Logic Should Go in an FPGA Logic Block?", IEEE Design and Test Magazine, Spring 1998, pp. 10 - 15




ISSN 1737-9334

# *Using Internet Based Videos Lessons in Teaching English Word Stress to Libyan EFL University Students*

Ahmed Maher
Department of English. Faculty of Education-Janzour
University of Tripoli
Tripoli, Libya
a.maher@uot.edu.ly

Nadia Nsir
Department of English. Faculty of Education-Janzour
University of Tripoli
Tripoli, Libya
nuseirn@hotmail.com

***Abstract*—This study aims to investigate the impact of using Internet-Based Pronunciation Video lessons on improving the quality of teaching the production of English word stress patterns correctly to Libyan EFL University students. The participants of the study consisted of forty female students whose major is English at the Faculty of Education-Janzour. Due to the nature of the study as experimental, the participants were divided into two groups, control group and experimental group. It took four weeks to collect the data using the same pre-test and post-test as research instruments. The obtained data were analysed using the 0.23 version of the Statistical Package for Social Sciences (SPSS) in order to reach accurate results.The findings of the study indicate that there were statistically significant differences between the two examined groups. The privilege was given the experimental group that received intensive Internet based videos through showing more accurate use of English word stress of the examined word list comparing with the control group that received a traditional lectures.**

***Keywords—English phonetics; word stress; instructional technology; English word stress teaching.***

## I. INTRODUCTION

Educational technology is a sub-discipline which is relevant to Computer-application in Second Language Acquisition (CASLA). It is a specialization within the study of education by which researchers try to find out the best and the most appropriate methods of using computer technology for instruction, as well as examining its effectiveness. Educational technology has many applications across subject areas that has steered a number of researchers to announce that computer-assisted language learning (CALL) has its root in educational technology (Chapelle, 2005).By using Internet-based video lessons over the last two decades, educators have enhanced the deployment of videos in the classroom. Unlike printed or audio material, video presents a powerful source of information. This fact is supported by Norton and Wiburg (2003) who stated that videos help students to learn new contents by observing their context. Videos enable students to better comprehend the social, cultural, or emotional aspects of contents and their consequences. If English is not their mother tongue, videos can assist prospective EFL teachers in mastering new words or expressions, as well as suitable intonation patterns and non-verbal aspects of communication. Further, visual learning contributes to increasing learners' motivation and promoting retention of information (Weyers, 1999). It can be stressed that language found in videos could help NNSs to comprehend stress patterns. This is based on the fact that videos can provide the learner with the opportunity to view both rhythm and speech rhythm in second language discourse via the employment of authentic language and speed of speech in a variety of situations. Additionally, videos enable contextual clues to be presented. Furthermore, videos can arouse students interests (Canning-Wilson, 2000). For modern EFL teachers, it is usually a struggle to utilize potentially useful teaching methods and bring more instructional technology tools into the EFL classroom to endorse their students' autonomy, and present exciting lectures. One of these methods is the use of online audiovisual resource such as www.youtube.com which is considered as a tremendous resource for teachers and students, (Kabooha&Elyas, 2018; Heriyanto, 2015). These online video resources can also present a good opportunity to expose the EFL learners to more authentic materials and native-live environment, particularly, for those who live in non-native countries which corresponds with the sample of the present study.

### *A. The statement of the problem*

As a matter of fact most of the Arab countries including Libya still away from integrating technology and of utilizing multimedia when teaching a foreign language. This fact was also confirmed by Al-Shamayleh (2014) who explained the identical situation in Jordon. Apart from the problematic phenomena of using technology and multimedia in the classroom, most of EFL learners face different problems when




ISSN 1737-9334

learning a foreign language. This is due to the fact that learning how to speak a new language is more than just learning words, sentences and know the grammar of the language. The process of learning includes other factors such as varying the utterances with accurate pronunciation. In this regard, Gilakjani (2012) highlights the important role played by this integral part of foreign language learning which affects learners' communicative competence as well as performance. He mentioned that limited skills of pronunciation can lead to reducing learners' self-confidence and in turn limiting their interaction resulting in lowering estimations of a speaker's credibility and abilities.

In order to have accurate pronunciation, Gilakjani (2012) stated that most of former ESL approaches' focus was on segmental features such as emphasizing the differences between the minimal pairs ship/sheep. Bearing this importance in mind, there are many researches such as (Jenkins, 2002 and Burns, 2003) that proved that when teaching focuses on supra-segmental features, learners' intelligibility is greatly enhanced. Besides, these researches emphasize that improving supra-segmental production can lead to effective communicative pronunciation competence in preference to segmental ones. Supportingly, Hismanoglu (2012) mentioned that the lack of adequate knowledge about supra-segmental aspects in general and English stress in particular could lead to major problems in placing and using the English stress.

Based on the researcher's observation, English words stress has been found to be one of the challenging issues to be learned and used accurately by Libyan EFL students. In consequence, this paper seeks to find out if the use of Internet based videos has an impact on enhancing the students' awareness of placing the English stress correctly.

### *B. Significance of the Study*

The present research is of two significances; the first, it examines the benefits of using online video-streaming website (www.youtube.com) for the Libyan EFL community as recommended by (Watkins & Wilkins, 2011). The second significance is to investigate the impact of using internet based videos lessons on teaching a particular language area which is English word stress to Libyan EFL university students.

Hismanoglu (2012) confirmed that the accurate placement of stress on a particular syllable is the key to communicating the intended meaning of a word in English, due to the fact that English employs stress distinctively. Nevertheless, and in spite of its importance, some researchers do believe that teaching English pronunciation in general and stress in particular will not lead to native like pronunciation; however, in the researcher's opinion, making the students aware of the importance and the effectiveness of using English stress in addition to using instructional technology to achieve this goal could lead to native-like pronunciation. The above opinion is supported by Dale and Poms (2005) and Underhill (1994) cited in Kucukoglu (2012) who asserted the importance of mastering and using the English stress accurately in order to avoid difficulty in comprehension as a result of using the wrong stress patterns.

In consequence, the researcher in the present paper aims to target the attention to the effectiveness of integrating technology into the classroom and to examine the impact of using Internet based video lessons on enhancing the use of English word stress accurately.

## II. LITERATURE REVIEW

### *A. Definition of English stress*

In English, stress is one of the supra-segmental features that can occur at different point in the word, nevertheless; it is fixed for each individual word. There are four phonetic variables that are used as the most significant indicators of stress; they are intensity, pitch variation, vowel quality and vowel duration (Colins&Mees, 2013). In other words, stress is used to describe the point in a word or phrase where pitch changes, vowels is lengthened and volume is increased. It is vitally important in conveying meaning in phrases and sentences. However, a word with more than one syllable is more complex especially those word that could be used as verb and noun, for example 'export' is a noun if the primary stress is placed on the first syllable while it is a verb if the primary stress is moved to the second syllable (Harmar, 2007). In terms of function, there are many functions of using stress; they include: giving special emphasis to a word or contrasting a word with another;indicating the syntactic relationships between words or parts of words, and distinguishing between a compound noun and an adjective followed by a noun (Ladefoged, 1993).

### *B. The Importance of teaching supra-segmental features*

Hismanoglu(2012) stated that during the past 20 years, pronunciation specialists have stressed on the importance of supra-segmentals rather than segmentals to enhance oral communication. This fact has been also stated by (Morley, 1991) who referred to the importance of changing the methodologies of teaching from emphasizing segmental elements of pronunciation to supra-segmental elements of pronunciation in one hand in addition to changing the attention from linguistic competence to communicative competence in the other hand. Hismanoglu (ibid) cited Cutler's (1984) view, who stated that "not only ungrammatical sentences or articulation of individual sounds, but also inaccurate placement of primary stress in L2 words may give rise to miscommunication in that the misplacement of lexical stress can precipitate false recognition, often in defiance of segmental evidence" (p. 27).

### *C. Using YouTube Video-based lessons to teaching English stress*

In the researcher's opinion, using videos as a teaching tool


ISSN 1737-9334

changes the classroom environment and makes it more interesting and attractive and then stimulates learner autonomy. This opinion is supported by (Watkins & Wilkins, 2011). They stated the Internet access availability could help both students and teachers to use YouTube as a valuable tool through teaching multiple foreign language skills. They further confirmed that the use of YouTube both inside and outside the classroom can enhance conversation, listening, and pronunciation skills. Besides, they mentioned that any lesson activities could be structured around YouTube videos. Another fact concerning using the YouTube as an assisted tool is that it helps educational endeavors throughout the vast varieties of content it has. In terms of validity, many recent studies such as Kabooha&Elyas, 2018; Heriyanto, 2015; and Watkins & Wilkins, 2011) ensured thatYouTube is a valid resource for teachers who seek to enhance their lessons with lively and topical content. In addition, a study conducted by Kasper (1997) illustrated that teaching English to students using multimedia such as print, film, video and Internet encourage students. Kasper's findings reflected the significant role of using multimedia on increasing the achievement of his participants. Another study conducted by Al-Shamayleh (2014) to examine the impact of using multimedia on enhancing the quality of teaching English stress and intonation. In his study, he referred to the tendency of accepting multimedia as a viable means of teaching language by many modern language teachers. He also emphasized the positive role of using multimedia due to its efficiency instead of using the teacher center model solely, particularly, when teaching phonetics. He attributed this to the fact that using multimedia to teach phonetics motivates students to learn as theyenjoythe process of learning. Generally, no one can ignore the extraordinary and positive impact of using a wide variety of English media on enhancing and gaining more features of the target language in general and English phonetics in particular. .

## III. METHODOLOGY

### A. *Research design*

This study used a quantitative design to collect students' scores and analyze them using SPSS program, and the procedures included giving the pre-test and the post-test to all the participants at the same time to avoid variations of additional preparation for the test.

### B. *The participants and setting of the study*

The participants are forty Libyan EFL female studentsstudying in their fifth semester at the Faculty of Education-Janzour, Tripoli University, in Libya during the Autumnsemester of 2017, of the academic year 2017-2018.It is important to mention here that the majority of the students at the Faculty are female.The participants are enrolled in a program leading to a bachelor degree in English and they are all 22 years of age, since they had been enrolled as intake of the same university year when they first joined the department. It is worth noting that they were all taking the phonetics (2) course during this period. The forty participants were equally and arbitrary divided and then assigned to two sub groups; named, control and experimental as shown in Table1.

Table 1 the demographic properties of the participants

| Group Name | Experiential (Group 1) | Control (Group 2) |
|---|---|---|
| Students' Number | 20 | 20 |

### C. *Procedures and instruments*

The two selected groups were subjected to the same pre-test and post-test items. The post-test included the same English words with which the students were tested in the pre-test. As for the purpose of the pre-test, it was designed to assess the general language proficiency of the participants and to determine their level in pronunciation. Both tests consisted of the same word list that was made up of 45 English words. They were all of different word patterns i.e. two syllable words, three syllable words and words with more than three syllables. It is worth mentioning that the word list was collected from the book of "English phonetics and phonology" by Peter Roach (2009). In order to have a reliable test, the word list was reviewed by two language experts. It is important to highlight that the purpose of using this mixed word list is to find out if the participants will manage to produce the given words correctly using the correct place of stress or not. The experimental group was to learn the use of the correct word stress through the use of multimedia (short videos) in the classroom using data show, personal laptop and high quality speakers. Whereas, the control group was to learn the same rules through the traditional method using a while board and a board maker classroom.

### D. *Data Collection*

The pre-test was given to the students during the third week of the Autumnsemester of 2017. The students were asked to place the stress on the correct syllables of the given word list. It is important to mention here that during the first three weeks of the semester, the students were introduced the syllable structure of English words and they all have basic ideas about the English stress. The students were given 45 minutes to place the stress on the correct syllable under the supervision of the researcher. After finishing the written part of the test, the students were invited individually to another quiet room to record their voices while pronouncing the list of words. The students were asked to produce the words and orally place the stress on the correct syllable. They were also asked to produce the words clearly and pause a second before pronouncing the next word. It took two minutes for each student to pronounce the whole words in the list. After four weeks of instruction, the researcher repeated the same procedures using the same test i.e. post-test. Each participant



ISSN 1737-9334

was assigned a number during the data analysis procedure due to ethical considerations and they were reminded that the data gathered would not be utilized for any assessment purposes and that their personal details would be kept confidential.

### *E. Ethical issues*

The participants were introduced to the study procedures by briefing them about the purpose of the study and inviting them to participate. Those who agreed to participate were told that participation is voluntary and they have the right to withdraw from the study at any time without being held responsible for any commitments. Further, the head of the department was informed about the study and her consent letter was obtained before starting the research procedures. All the materials, pre-test and post-test sheets, participants scores, assessment forms were saved on a CD and will bedamagedonce the study is published. The scores were anonymously recorded on assessment forms using number codes of the participant students.

### *F. Analytical approach*

For the analytical approaches, statistical t-test was used to answer the research question of this study. The t-test was applied to investigate the differences between students' scores in both tests i.e. the pre-tests and the post-tests and among both groups. The sample was divided into experimental and control groups. The *t*-test model was run by means of IBM SPSS statistics software program version 0.23. Descriptive analysis was obtained through assessing statistical results from SPSS. Mean, median, and mode were used to describe the general information about the sample of the study. In addition, inferential analysis was carried out to get statistical values that can be used in answering the research question, and so to address the research question, a two-paired *t*-test was used.

## IV. Results and Discussions

This section describes the research findings using both descriptive and inferential statistics. This study aimed to investigate the impact of using Internet-based videos on enhancing the students' ability in placing stress on English words correctly.

### *A. Descriptive Statistics*

A total of 40 participants in both groups responded to the test questions and that there were no missing values in the out-put of the *t*-test.Table 2 shows the percentage of (100%) of the students attending both the pre-test and post-test of the experiment.

Table 2 shows full attendance of both study groups indicating no missing values in both tests.

| | Valid | | Cases Missing | | Total | |
|---|---|---|---|---|---|---|
| | N | Percent | N | Percent | N | Percent |
| **Pre-Test Experimental Group** | 20 | 100.0% | 0 | 0.0% | 20 | 100.0% |
| **Post-test Experimental Group** | 20 | 100.0% | 0 | 0.0% | 20 | 100.0% |
| **Pre-Test Control Group** | 20 | 100.0% | 0 | 0.0% | 20 | 100.0% |
| **Post-test Control Group** | 20 | 100.0% | 0 | 0.0% | 20 | 100.0% |

### *B. Inferential Statistics*

The first independent paired sample *t* test was performed to ensure the equality of the two examined groups and to prove that there is no significant differences that might affect the findings of the research. By looking at the following table 3, it is clear that there are not any statistically significant differences between the scores of the two groups in the pre-tests. The *t* value is 1.636) at the level of significance (0.11) which is higher than the level of significance (0.05). These results prove that both groups are of the same level concerning using the correct place of stress on the English words.

Table3 shows the paired sample *t* test of the pre-test of the two groups

| Group | N | Means | SD | df | T | Sig |
|---|---|---|---|---|---|---|
| **Pre-Test Experimental Group** | 20 | 13.9 | 3.4 | 38 | 1.636 | 0.11 |
| **Pre-test Control Group** | 20 | 11.9 | 4.3 | | | |

To answer the research question, Paired Sample t-test was carried out using SPSS software. By looking at Table 4 there were statistically significant differences between students' scores of the post-tests, as the students in experimental group scored ($M$=33.9, $SD$=3.9) and students' scores in the controlled group ($M$=25.5, $SD$=5.2), where t=5.779 $p$ = 0.01.

Table4 shows the paired sample test of the post test of the two groups

| Group | N | Means | SD | df | T | Sig |
|---|---|---|---|---|---|---|
| **Post-Test Experimental Group** | 20 | 33.9 | 3.9 | 38 | 5.779 | 0.01 |
| **Post-test Control Group** | 20 | 25.2 | 5.2 | | | |

Table 4 shows the results of paired sample t-test reflecting the significant differences between the scores of the two posttests in the case of experimental and controlled groups. This statistical significance is in the favor of the experimental group and thus the intervention of using internet based videos does impact the scores of the experimental group leading to a change in increasing their ability to place the stress on the English words correctly.

In order to verify the validity of the previous findings, another independent paired sample test was performed to find out if there is a significant differences between the scores of the pre-


ISSN 1737-9334

test and post-test in case of the experimental group as shown in the following table.

Table 5 shows the means and standard deviation of the pre and post-test of the experimental group.

| Group | Means | SD | df | T | Sig |
|---|---|---|---|---|---|
| **Pre-Test of the Experimental** | 11.9 | 4.2 | 19 | -14.532 | 0.01 |
| **Post-test Experimental Group** | 25.5 | 5.1 | | | |

Table 5 shows mean and standard deviation as compared in each test (i.e. pre-test/post-test) in the case of experimental group. There are statistically significant differences between the scores of the experimental group in the pre and post-tests where the value of t= (-14.532) at the level of significance (0.01) which is smaller than the level of significance (0.05). These results prove the effectiveness and the more positive impact of using internet based videos on enhancing the students' performance in place the stress on English words correctly.

## V. Conclusion

By having a look at the results, it is obvious that using Internet-based videos such as YouTube videos would have a great impact on enhancing the students' ability to place stress on English words correctly comparing with only following the traditional methods of teaching pronunciation to Libyan EFL students. The students' scores were increased after being exposed to different Internet-based pronunciation video lessons. These findings are consistent with many previous studies such (Hismanoglu, 2012 and Al-shamayleh, 2014; Watkins & Wilkins, 2011 and Kasper, 1997), who all confirmed the effectiveness of using multimedia when teaching any language skills in general and phonetics and word stress in particular.

## VI. Implication of the Research

The findings reveal the fact that using Internet based videos has impact on the participants'performance in mastering English word stress. Therefore, it is highly recommended that all EFL classes should be equipped with instructional technology tools to help instructors to achieve their targets in more professional ways. In addition, EFL instructors should have access to the necessary technology and make good use of YouTube and other trusted online video-streaming sites due to its salient roles in facilitating the learning processes, changing the classroom autonomy, and motivating learners. Furthermore, EFL instructors should utilize modern techniques and effective materials especially multimedia and computer-based designs of instructional materials. In addition, they ought to encourage their students to access these materials both inside and outside the classroom for the sake of learning and practicing the phonetic features in particular.

## VII. Recommendations for Further Research

This study was not without limitations and one limitation was the fact that the sample in this study was of small size and that it only included female students due to course enrollment facts of the study setting, i.e. the Faculty of Education-Janzour. Therefore, researchers who are concerned with second language education are invited to further study this area of interest, and research should be conducted to focus on the relationships between gender and the use of instructional technology inside the classroom and the new methods of teaching English in general and pronunciation in particular.

## *References*

Al-shamayleh, T. S. (2014). Improving the Quality of Teaching English Stress and Intonation To University Students Who Are Learning English As a Foreign Language Using Multimedia, *10*(25), 207–228.

Colins, B. & Mees,I.M. (2013). Pr*actical Phonetics and Phonology*. (3rd ed.)Routledge: London.

Gilakjani, A. P. (2012). A Study on the Situation of Pronunciation Instruction in ESL/EFL Classrooms. *Journal of Studies in Education*, *1*(1), 1–15. https://doi.org/10.5296/jse.v1i1.924

Hismanoglu, M. (2012). Teaching word stress to Turkish EFL (english as a foreign language) learners through internet-based video lessons. *Online Submission*, *1*, 26–40. Retrieved from http://www.eric.ed.gov/PDFS/ED530678.pdf

Heriyanto, D. (2015). The Effectiveness of Using Youtube for Vocabulary Mastery. Volume 6, Number 1, Februari 2015

Kabooha, R., & Elyas, T. (2018). The Effects of YouTube in Multimedia Instruction for Vocabulary Learning: Perceptions of EFL Students and Teachers. *English Language Teaching*, *11*(2), 72. https://doi.org/10.5539/elt.v11n2p72

Kucukoglu, H. (2012). Sentence Stress and Learning Difficulties of ELT Teachers: A Case Study. *Procedia - Social and Behavioral Sciences*, *46*, 4065–4069. https://doi.org/10.1016/j.sbspro.2012.06.198

Kasper, L. F. (1997). The impact of content-based instructional programs on the academic progress of ESL


ISSN 1737-9334

students. *English for Specific Purposes*, *16*(4), 309–320. https://doi.org/10.1016/S0889-4906(97)00035-5

Ladefoged, Peter. (1993). *A Course in Phonetics*. (3rd ed.). University of California: Los Angeles.

Roach, P. (2009). *English phonetics and phonology: A practical course*. (4th ed.). Cambridge, England: Cambridge University Press.

Watkins, J., & Wilkins, M. (2011). Using YouTube in the EFL Classroom. *Language Education in Asia*, *2*(1), 113–119. https://doi.org/10.5746/LEiA/11/V2/I1/A09/Watkins_Wilkins


ISSN 1737-9334

# Modeling and Analyzing the BER and SER Performances of MIMO System using Multi Level - DPSK Modulation Technique Under Rayleigh Fading Channel

Nsreen Hawisa [1] and Amer R. Zerek[2]

[1, 2]Zawia University, Faculty of Engineering, Electrical and Electronic Eng. Department
Zawia, Libya
[1]E-mail hawisansreen@gmail.com
[2]E-mail anas_az94@yahoo.co.uk

*Abstract*—**Nowadays wireless communication system is improving for the new generation of data communication technology, since it has to facilitates the user to communicate and share information or data through different wirelessly connected equipment. These techniques improve and examine the existing technologies to make technology easier for the subscribers in order to provide several features.**
**One of most important M-ary carrier digital modulation schemes is M- ary Differential Phase Shift Keying (MDPSK) which is very important part of the implementation of modern wireless communications systems .**
**In this paper investigation and simulation of the multi-level ( M-ary) DPSK modulation using Matlab with Simulink 2017 for M=16, 32, 64 and 128,so that theproposed system implements multi antenna diversity of 2x4 ,where the number of transmitter antennas is 2 and the receiver antennas is 4. This investigationanalysis and compares the BER and SER performanceover Rayleigh channel. The obtained results showed that as the level of modulation increases the BER and SER increases at the same $E_o/N_o$ value. This means the lower the M value the better the performance.**

**Keywords— wireless communication, M-aryDPSK, BER , SER and MIMO**

## I. INTRODUCATION

Modulation plays an important role in transmission of signals from transmitter to receiver in all communication systems and the performance of digital modulation systems is the most important key factor to achieve the best results without interference, for example; mobility, better productivity, low cost, easy installation facility and scalability, modulation to increase efficiency of radiation.....etc.
The digital modulation is categorized into two main schemes such as pulse digital modulation and carrier digital modulation. Carrier digital modulation can be classified into two main types that are binary carrier digital modulation and multi-level or M-ary carrier digital modulation . In both types of carrier digital modulation techniques there are three main parameters of a sinusoidal signal that are modulated,which are amplitude, phase, and frequency. According to this concept of these types of parameters binary and multi-level (M-ary) . A binary carrier digital modulation include Binary Amplitude Shift Keying (BASK) , Binary Phase Shift Keying (BPSK) and Binary Frequency Shift Keying (BFSK) . Also an M-ary or multi-levelcarrier digital modulation includes three main types: M-ary FSK, M-ary PSK and M-ary ASK. The M-ary ASK called Quadrature Amplitude Modulation (QAM)) .For an M-ary PSK where M=4 this type of modulation is calledquadrature phase shift keying (QPSK). When that scheme of modulation uses differential encoding is usually called DQPSK which can be extended to an M-ary DPSK. In M-ary DPSK modulations $\log_2 M$ (= $L$) bits per symbol transmission is achieved providing powerand bandwidth-efficient communication. [1].
This paper will investigate and analyzes the BER and SER performances of MIMO system using multi-Level DPSK modulation technique Rayleigh fading channel.

## II. MIMO SYSTEM

Multi input multi output (MIMO) system uses $n_T$ antennas at transmitter and $n_R$at receiver i.e ($n_T$,$n_R$) and there is a communication channel between each of the transmit and receive antennas . Figure 1 illustrated the MIMO system with transmit and receive n antennas. This MIMO system is used to improve overall throughput of the wireless link.In addition to that MIMO channels offer a several benefits over conventional single input single output (SISO), single input multi output (SIMO), and multi input single output (MISO), communication channels such as the array gain, the diversity gain, and the multiplexing gain. While the array and diversity gains are not exclusive of MIMO channels and also exist in single-input multiple-output (SIMO) and multiple-input single-output (MISO) channels, the multiplexing gain is a unique characteristic of MIMO channels.
MIMO system is significantly used in a number of wireless technologies like Wireless Fidelity( Wi-Fi) , 4G, Long Term Evolution (LTE) and Worldwide Interoperability for Microwave Access (WiMAX), IEEE 802.16e to name some few important ones.[ 2, 3, 4].

In this work a MIMO system along with two transmit antennas and four receive antennas (2x4) is considered as shown in figure (1)




ISSN 1737-9334

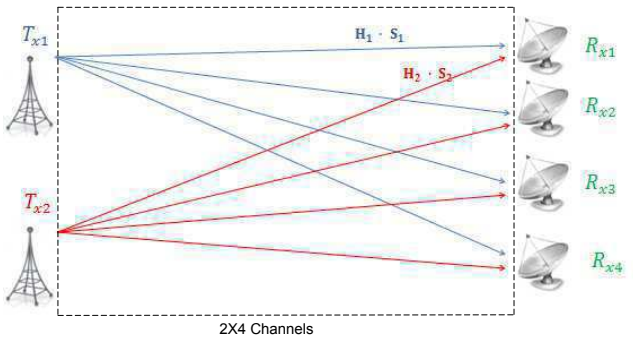


Figure 1.2x4 MIMO System

The received signal on the first receive antenna is

$$R_1 = H_{11}S_1 + H_{12}S_2 + N_1 \qquad (1)$$

The received signal on the second receive antenna is

$$R_2 = H_{21}S_1 + H_{22}S_2 + N_2 \qquad (2)$$

The received signal on the third receive antenna is

$$R_3 = H_{31}S_1 + H_{32}S_2 + N_3 \qquad (3)$$

The received signal on the fourth receive antenna is

$$R_4 = H_{41}S_1 + H_{42}S_2 + N_4 \qquad (4)$$

Where

$R_1, R_2, R_3 and R_4$ are the received symbol on the first , second, third and fourth antennas respectively .
$H_{11}$ is the channel from $1^{st}$ transmit antenna to $1^{st}$ receive antenna

$H_{12}$ is the channel from $2^{nd}$ transmit antenna to $1^{st}$ receive antenna

$H_{21}$ is the channel from $1^{st}$ transmit antenna to $2^{nd}$ receive antenna

$H_{22}$ is the channel from $2^{st}$ transmit antenna to $2^{nd}$ receive antenna

$H_{31}$ is the channel from $1^{st}$ transmit antenna to $3^{rd}$ receive antenna

$H_{32}$ is the channel from $2^{nd}$ transmit antenna to $3^{rd}$ receive antenna

$H_{41}$ is the channel from $1^{st}$ transmit antenna to $4^{td}$ receive antenna

$H_{42}$ is the channel from $2^{nd}$ transmit antenna to $4^{td}$ receive antenna

$S_1 and\ S_2$ are the transmitted symbols and $N_1$,$N_2$, $N_3$ and $N_4$ is the noise on the $1^{st}$,$2^{nd}$,$3^{rd}$ and $4^{th}$ receive antennas respectively.

Equation 1 to 4 can be illustrated in matrix form as follows:

$$\begin{bmatrix} R_1 \\ R_2 \\ R_3 \\ R_4 \end{bmatrix} = \begin{bmatrix} H_{11} & H_{12} \\ H_{21} & H_{22} \\ H_{31} & H_{32} \\ H_{41} & H_{42} \end{bmatrix} \cdot \begin{bmatrix} S_1 \\ S_2 \end{bmatrix} + \begin{bmatrix} N_1 \\ N_2 \\ N_3 \\ N_4 \end{bmatrix} \qquad (5)$$

Hence

Received signal vector = $\begin{bmatrix} R_1 \\ R_2 \\ R_3 \\ R_4 \end{bmatrix}$

Channel matrix = $\begin{bmatrix} H_{11} & H_{12} \\ H_{21} & H_{22} \\ H_{31} & H_{32} \\ H_{41} & H_{42} \end{bmatrix}$

Transmitted signal vector = $\begin{bmatrix} S_1 \\ S_2 \end{bmatrix}$

Noise signal vector = $\begin{bmatrix} N_1 \\ N_2 \\ N_3 \\ N_4 \end{bmatrix}$

Then received vector can be expressed as

$$R = H.S + N \qquad (6)$$

## III FADING

One of the more intriguing features of wireless communication channels is fading. Different path-loss or shadowing, which are large-scale attenuation effects owing to distance or obstacles.Fading is caused by the reception of multiple versions of the same signal. The multiple received versions are caused by reflections that are referred to as multipath. The reflections may arrive nearly simultaneously, for example, if there is local scattering around the receiver or at relatively longer intervals,owing to multiple paths between the transmitter and the receiver. [5].

When some of the reflections arrive at nearly the same time, their combined effect is depending on the phase difference between the arriving signals, the interference can be either constructive or destructive, which causes a very large observed difference in the amplitude of the received signal even over very short distances. In other words, moving the transmitter or the receiver even a very short distance can have a dramatic effect on the received amplitude, even though the path-loss and shadowing effects may not have changed at all.

The time-varying tapped-delay-line communication channel model of Equation 3. This channel h(t) response can be thought of as having two dimensions: a delay dimension τ and a time-dimension t, as illustrated in Figure 2. Since the channel changes over distance and hence time, the values of $h_0, h_1, h_2 \ldots h_n$, may be totally different at time $t$ versus time $t + \Delta t$ Because the channel is highly variant in both the τ and $t$ dimensions, it must use statistical methods to discuss what the channel response is. [6].

$$h(k,t) = h_0\,\delta(k,t) + h_1\delta(k-1,t) + \ldots + h_n(k-n,t) \qquad (3)$$




ISSN 1737-9334

The use of an overall model describing the channel in discrete time is a simple Tap-Delay-Line (TDL). Here, the discrete-time channel is time varying so it changes with respect to and has non-negligible values over a span of *n+1* channel taps.

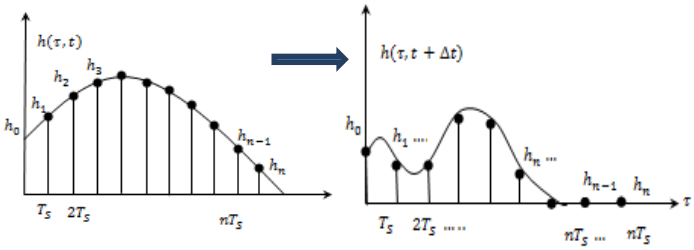


Figure 2 Channel h(t) Response Delay τ and Time t

A good way to understand wireless fading channel, is by considering its key physical parameters and modeling issues, the characteristic of wireless channel is the variation of the channel strength over time and frequency, the variations can be roughly divided into two types:the first type is fast fading whichrefers to changes in signal strength between a transmitter and receiver as the distance between the two changes by a small distance of about one-half a wavelength. The second type is a slow fading which refers to changes in signal strength between a transmitter and receiver as the distance between the two changes by a larger distance, well in excess of a wavelength.

The fading also can be classified intoflat fading or nonselective and selective fading.The flat fading, is that type of fading in which all frequencycomponents of the received signal fluctuate in the same proportions simultaneously. While the selective fading affects unequally the different spectral components of a radio signal.

## IV RAYLEIGH FADING

The path between the transmitter and receiver can vary from simple line-of-sight to one that is severely obstructed by buildings, mountains, and foliage, non- line-of-sight. Unlike wire channels that are stationary and predictable, fading channels are extremely random and do not offer easy analysis. There are two main types of fading channels models such as Rican and Rayleigh. The Rayleigh fading channel model will be used in this work.

The Rayleigh channel is also known as a non-line of sight (NLOS) channel; , generally in wireless communications, the envelope of the carrier signal is Rayleigh distributed; and that distribution is caused by multipath with or without the Doppler effect. In the multipath case, when the main signal becomes weaker, such as in the NLOS case, the received signal is the sum of several components that are reflected from the adjacent obstacles building, … etc . In this scheme of channel , there are many other paths by which the signal may reach the receiver. When the signals reach the receiver, the overall signal is acombination of all the signals that have reached the receiver via the multitude of different paths that are available.

In that Rayleigh channel combines line of sight (LOS) and NLOS transmission components and because of that some of reflections that happens to the signal could have a positive factor and improves performance of the communication system. [7].

## V MULTI-LEVEL DPSK MODULATION TECHNIQUE

Differential Phase Shift Keying (DPSK) is a common form of phase shift keying modulation in which there is no reference phase signal required , the transmitted signal itself can be used as a reference signal. The DPSK is used in analog modems, does not needcomplex demodulation circuitry and is less susceptible to random phase changes in the transmitted signal . In this scheme of modulation the phase of the DPSK modulated signal is shifted relative to the previous signal element. No reference signal is deemed here. The phase of the modulated signal follows the 1 or 0 state of the previous element. This DPSK technique doesn't need a reference signal oscillator.[8]

The DPSK modulation technique has several advantages over the binary phase shift keying such as It has a better performance, it needs smaller bandwidth and does not need coherent detection,DPSK receiver is very simple to implement also carrier recovery circuitry is not required i.e. has a non-coherent demodulation. While PSK typically does not support this function. [9, 10].

M-ary- DPSK modulation is widely used in satellites and space telemetry. A more efficient use of bandwidth is achieved when eachsignaling element represents more than one bit. Although DPSK can be extended to an M-ary DPSK modulation which achieve the transmission of n= $\log_2 M$ or $M=2^n$ bits per symbol, In this paper bit error rate ( BER) for DPSK modulation schemes has been analyzed for different values of M= 16, 32 , 64 and 128 over Rayleigh fading channel.

## VI PERFORMANCE ANALYSIS OF MULTI LEVEL DPSK USING MATLAB SIMULINK

Simulink is an extension to MATLAB, It is a software package for modeling, simulating and analyzing dynamic and embedded system It gives a graphical environment and a set of block libraries that let researcher design, implement , simulate, and test a variety of linear and non-linear systems, including a variety of fields e.g. communication, control, digital signal processing, networks, image processing … etc. The baseband simulation models of 16, 32, 64 and 128 DPSK under Rayleigh fading channel is illustrated in figure (3).The simulation of multi-level DPSK model consists of three main parts;the transmitter, Rayleigh fading channel and the receiver. These parts include the following elements.

A) Transmitter Side
- The *Random Integer Generator block* generates uniformly distributed random integers in the range [0, *M*-1], where *M* is the **Set size** defined in the dialog box.


ISSN 1737-9334

- The *Integer to Bit Converter* block maps each integer (or fixed-point value) in the input vector to a group of bits in the output vector.
- The *M-DPSK Modulator Baseband block* modulates using the M-ary differential phase shift keying method. The output is a baseband representation of the modulated signal. The **M-ary number** parameter, M, is the number of possible output symbols that can immediately follow a given output symbol.
- The *Goto block* passes its input to its corresponding From blocks. The input can be a real- or complex-valued signal or vector of any data type. From and Goto blocks allow you to pass a signal from one block to another without actually connecting them.
- The Constellation Diagram block plots constellation diagrams, signal trajectory, and provides the ability to perform EVM and MER measurements. The symbols that the Constellation Diagram scope displays are always the most recently available symbols from the time buffer.

B) Communication Channel

- The *OSTBC Encoder block(Alamouti)* encodes an input symbol sequence using orthogonal space-time block code (OSTBC). The block maps the input symbols block-wise and concatenates the output codeword matrices in the time domain..
- Themulti-input/multi-output(*MIMO)*Rayleigh *Fading Channel block* filters an input signal using a MIMO multipath fading channel. This block model Rayleigh and employs the Kronecker model for modeling the spatial correlation between the links.
- The *Squeeze block* removes singleton dimensions from its multidimensional input signal. A singleton dimension is any dimension whose size is one. The Squeeze block operates only on signals whose number of dimensions is greater than two.
- The *OSTBC Combiner b*
- *lock* (Almaouti Code $4R_x$) combines the input signal (from all of the receive antennas) and the channel estimate signal to extract the soft information of the symbols that were encoded using an OSTBC. The input channel estimate may not be constant during each codeword block transmission and the combining algorithm uses only the estimate for the first symbol period per codeword block. A symbol demodulator or decoder would follow the Combiner block in a MIMO communications system.

C) Receiver Side

- The *M-DPSK demodulator baseband block* demodulates a signal that was modulated using the multi-level DPSK method. The input is a baseband representation of the modulated signal. The input and output for this block are discrete-time signals. This block accepts a scalar-valued or column vector input signal.
- The *Bit to Integer Converter block* maps groups of bits in the input vector to integers in the output vector. *M* defines how many bits are mapped for each output integer.
- The ***Error Rate Calculation block*** compares input data from a transmitter with input data from a receiver. It calculates the error rate as a running statistic, by dividing the total number of unequal pairs of data elements by the total number of input data elements from one source.
- The ***To Workspace block*** inputs a signal and writes the signal data to a workspace. During the simulation, the block writes data to an internal buffer. When the simulation is completed or paused, that data is written to the workspace. Data is not available until the simulation is stopped or paused.

**Display**

- The Spectrum Analyzer block, referred to here as the scope, displays the frequency spectra of signals.

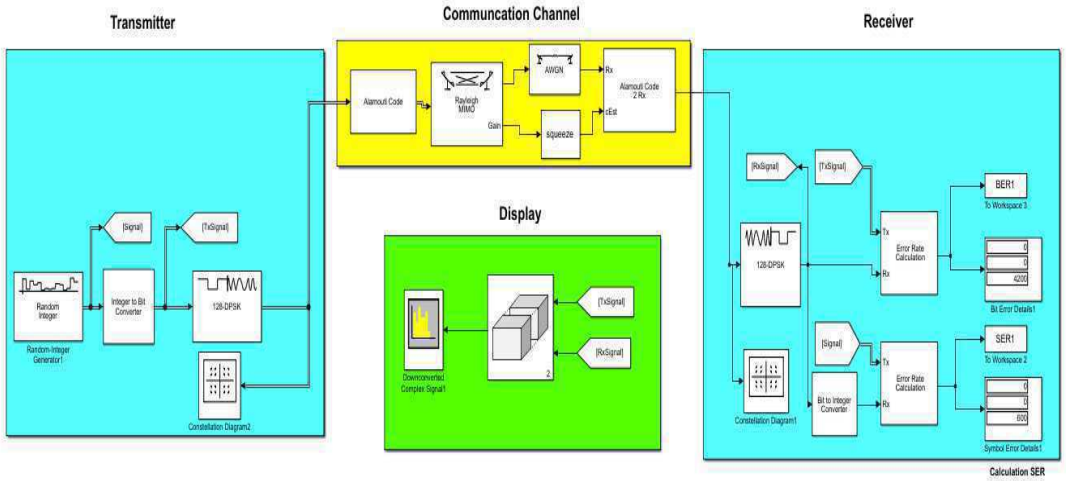


Figure . 3 .*Simulation model for Multi-Level DPSK*




ISSN 1737-9334

## VII PERFORMANCE ANALYSIS OF MULTI LEVEL DPSK USING MATLAB SIMULINK

The results of bit error rate (BER) and symbol error rate (SER) performances of multi-level (M-ary) differential phase shift keying for M=16, 32, 64 and 128 obtained using Matlab Simulink communication toolbox are shown in figures4 and 5.

The comparative analysis of simulated results for BER vs $E_b/N_o$ and for SER vs $E_b/N_o$for 16, 32, 64 and 128 DPSK overRayleigh fading channels are summarized in the tables 1 and 2 respectively.

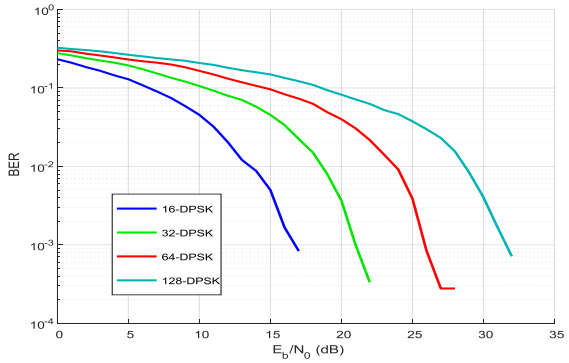


Figure 4. Bit Error Rate vs. $E_b/N_o$ Performance of 16-32-64-128 DPSK Over Rayleigh Channel

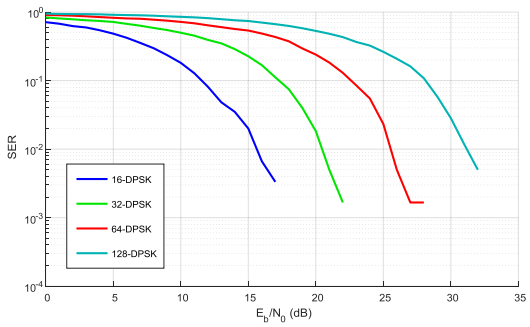


Figure 5. Symbol Error Rate vs. $E_b/N_o$ Performance of 16-32-64-128DPSK Over Rayleigh Channel

Table 1 Bit Error Rate vs. Eb/No Comparison of Rayleigh Channel for 16-32-64 and 128 DPSK

| Channel | 16-DPSK | | 32-DPSK | | 64-DPSK | | 128-DPSK | |
|---|---|---|---|---|---|---|---|---|
| | $E_b/N_0$ | BER | $E_b/N_0$ | BER | $E_b/N_0$ | BER | $E_b/N_0$ | BER |
| Rayleigh | 17 | 0.0008333 | 22 | 0.0003333 | 27 | 0.0002778 | 32 | 0.0007143 |

Table 2 Symbol Error Rate vs. Eb/No Comparison ofRayleigh Channel for 16-32-64 and 128 DPSK.

| Channel | 16-DPSK | | 32-DPSK | | 64-DPSK | | 128-DPSK | |
|---|---|---|---|---|---|---|---|---|
| | $E_b/N_0$ | SER | $E_b/N_0$ | SER | $E_b/N_0$ | SER | $E_b/N_0$ | SER |
| Rayleigh | 17 | 0.003333 | 22 | 0.001667 | 27 | 0.001667 | 32 | 0.005 |

Examining the plots in figures (4) and (5) for BER and SER performances under various levels of DPSK modulation i.e. 16, 32, 64 and 128 DPSK , when considering the fading model Rayleigh channel the following can be noted:

- It is quite clear that as the level increases the BER and SER increases i.e. a more signal energy is needed to get a better BER and SER.
- It can be noted also theRayleigh model has improved the performance in terms of BER and SER and that can be explained in that Rayleigh model combines line of sight and non-line of sight transmission components and because of that some of reflections that happens to the signal could have a positive factor and enhances performance. .

## VIII CONCLUSION

In this paper the simulations using Matlab Simulink shows that the bit error rate (BER) and symbol error rate (SER) for the multi-level DPSK modulation techniques decrease monotonically with increasing values of $E_b/N_0$ for MIMO (2x4) under Rayleigh channel. Also it is conclude that the using Rayleigh model has enhanced the performance in terms of both BER and SER and that can be clarified in that Rayleigh model combines line of sight (LOS) and non-line of sight (NLOS) transmission components and hence some of reflections that happens to the signal could have a positive impact and improves performance.

Simulation of multi-level DPSK using Matlab Simulink gives the better results. This scientific tool also simplifies the process of passing from simulation to implementation, without the necessity of being a specialized hardware engineer.

## REFERNCES

[1] P. H. Hwei , “Analog and Digital Communications-Schaum`s Outlines”, McGraw-Hill, 2003..

[2] S. Kumari and R. Bera, Sourav Dhar, “Modeling and Analyzing the BER Performance of MIMO System using Different Modulation Technique”, International Journal of Engineering Research & Technology (IJERT) , Vol. 4 Issue 05, May-2015

[3] A.J.Paulraj, D.A.Gore, R.U.Nabar, H.Bölcskei, An overview of MIMO communications- A key to gigabit wireless, IEEE proceedings, vol.92, pp 198-218, Feb.2004

[4] M. Assaad, D. Zeghlache, Comparison between MIMO techniques in UMTS-HSDPA system, IEEE Conferences, 2004, Page(s): 874-878.

[5] A. Sudhir Babu and Dr. K.V Sambasiva Rao,” Evaluation of BER for AWGN, Rayleigh and Rician Fading Channels underVarious Modulation Schemes”, International Journal ofComputer Applications (0975 – 8887) Volume 26– No.9, July2011

[6] A. Sudhir Babu and Dr. K.V Sambasiva Rao,” Evaluation of BER for AWGN, Rayleigh and Rician Fading Channels under Various Modulation Schemes”, International Journal of Computer Applications (0975 – 8887) Volume 26– No.9, July2011.

[7] T. Tokle, M. Serbay, Y. Geng, J. B. Jensen, W. Rosenkranz, and P. Jeppesen, “Penalty-free transmission of multilevel 240 Gbit/s RZ-DQPSK-ASK using only 40 Gbit/s equipment,” in Proc. Eur. Conf. Opt. Commun., Gasglow, U.K., 2005, Paper Th.4.1.6..

[8] M. Riaz Ahmed, Md.Rumen Ahmed , Md.Ruhul Amin Robin, Md. Asaduzzaman, Md. Mahbub Hossain, Md. Abdul Awal, “Performance Analysis of Different M-Ary Modulation Techniques in Fading


ISSN 1737-9334

Channels using Different Diversity", Journal of Theoretical and Applied Information Technology, Vol. 15. No.1, pp 23-28, May 2010..

[9] T. Tokle, M. Serbay, Y. Geng, J. B. Jensen, W. Rosenkranz, and P. Jeppesen, "Penalty-free transmission of multilevel 240 Gbit/s RZ-DQPSK-ASK using only 40 Gbit/s equipment," in Proc. Eur. Conf. Opt. Commun., Gasglow, U.K., 2005.

[10] C. Behrens, R. I. Killey, S. J. Savory, M. Chen, and P. Bayvel, "Nonlinear distortion in transmission of higher order modulation formats,"IEEE Photon. Technol. Lett., vol. 22, no. 15, pp. 1111–1113, 2010.

.


ISSN 1737-9334

# Effect of interface states on CdS/CGS solar cells

Benslimane Hassane
Laboratory of semiconductors devices physics,
Materials science Department,
Tahri Mohammed University, Bechar, Algeria
hassane_ben@Yahoo.fr

Mebarki Redouane
Materials science Department,
Tahri Mohammed University, Bechar, Algeria

***Abstract*—The aim of this research is to investigate the effect of interface state density on the performance of the CGS solar cell structure. The simulations for this work were done by giving the diode equations and varying interface state density of CdS/CGS . The interface recombination leads to lower values of the open-circuit voltage, short-circuit current density, and fill factor**

***Keywords— Solar cells; interface state; CdS-CGS; efficiency***

## I. INTRODUCTION

A solar cell is an electronic device which directly converts sunlight into electricity. Light shining on the solar cell produces both a current and a voltage to generate electric power. Thin-film ZnO/CdS/CGS solar cells are especially outstanding due to their low cost [1], radiation hardness [2], long-term stability [3]. CGS is one of most promising materials for thin film photovoltaic devices because of its appropriate band gap and high absorption coefficient for solar radiation.
ZnO/CdS/CuGaSe2 cells, have gained a great deal of interest both in high voltage modules
(as single cells) and in tandem systems (as top cells) [4–7]
The interfaces occur between the different layers, generally play an important role in this film solar cells devices, can cause stresses, defects ,interface states, and surface recombination centers. In this study, we will investigate the effect of the interface states concentration on CGS efficiency. A model is presented for p–n hetero-junction CdS/CuInGaSe2 solar cells in which interface recombination is the dominant diode current transport mechanism.

.

## II. MODEL

The band gap diagram of d p–n hetero-junction with interface states is shown in figure (1).
The interface states $N_s$ are assumed to be in the n-region close to the interface.$V_{d1}$; $V_{d2}$ are the diffusion voltage components in the n- and p-region, respectively.$W_1$and$W_2$ are the depletion layer width values in the n- and p-region, respectively. The recombination path way through the interface states is also shown in figure 1

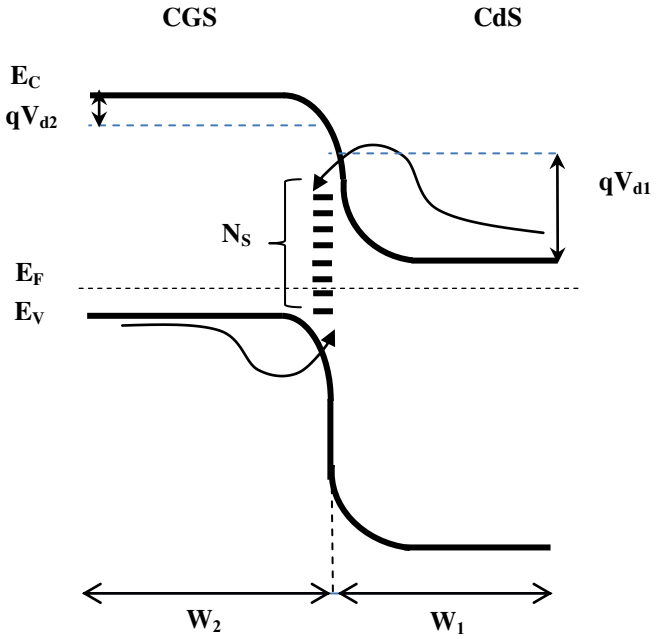


Figure 1 p–n hetero-junction with interface states.

The ideality factor reflects the influence presence of interface states it will be calculated as functions of absorber CIGS doping $N_2$.

$$n = \frac{V_d}{V_{d2}} \qquad (1)$$

Where Vd diffusion voltage is related to energy band gap by

$$V_d = E_{g2} - \delta_n - \delta_p - \Delta E_c \qquad (2)$$

Where

$$\delta_n = E_c - E_F \text{ and } E_F - E_c = KT\ln\frac{N_1}{N_{c1}} \quad \text{for n type}$$

$$\delta_p = E_F - E_v \text{ an } E_v - E_F = KT\ln\frac{N_2}{N_{v2}} \quad \text{for p type}$$

The neutrality of the junction implies between window CdS and absorber CIGS layers with interface state

$$N_1W_1 = N_S + N_2W_2 \qquad (3)$$




ISSN 1737-9334

Where $N_1$ the donor concentration, $N_2$ the acceptor concentration, $W_1$the depletion layer width in the CdS region,$W_2$ the depletion layer width in the absorber layer and Ns is the interface states.

Solving the Poisson equation for this system the individual built-in diffusion voltages $Vd_1$and $Vd_2$ in the n-region and p-region of the junction, respectively

$$V_{d1} = \frac{q}{2\varepsilon_{r1}\varepsilon_0} N_1 W_1^2 \quad (4)$$

$$V_{d2} = \frac{q}{2\varepsilon_{r2}\varepsilon_0} N_2 W_2^2 \quad (5)$$

$\varepsilon_{r1}$ and $\varepsilon_{r2}$ are dielectrics constants of CdS and CIGS respectively, $\varepsilon_0$ is vacum dielectric constant.

The factor n >2 in this case interface recombination becomes the dominant diode current transportmechanism.and the diode parameters will be calculated as functions of $N_S$ (n) [8].
Using the equations (4) and (5), $W_1$and $W_2$can be given by

$$W_1 = \sqrt{\frac{2\varepsilon_{r1}\varepsilon_0 V_d (n-1)}{qN_1 n}} \quad (6)$$

$$W_2 = \sqrt{\frac{2\varepsilon_{r2}\varepsilon_0 V_d}{qN_2 n}} \quad (7)$$

Where $V_d = V_{d1}+V_{d2}$

Using (3), (6) , (7) to find the following equation of $N_S$

$$N_S = \sqrt{\frac{2\varepsilon_{r1}\varepsilon_0 N_1 V_d}{q}\frac{(n-1)}{n}} - \sqrt{\frac{2\varepsilon_{r2}\varepsilon_0 N_2 V_d}{qn}} \quad (8)$$

The interface recombination of holes is the dominant diode current, the saturation and current–voltage for a diode can be given respectively [9]

$$j_0 = qv_{th}\sigma_p N_S N_2 \exp\left(\frac{-qV_d}{nKT}\right) \quad (9)$$

$$j = j_0\left(e^{\frac{qv}{nkT}} - 1\right) \quad (10)$$

Where $V_{th}$ is the thermal velocity, $\sigma_p$ cross section of hole, KBoltzmann constant, T is the absolute temperature.
The short-circuit current density *Jsc* and open-circuit voltage $V_{oc}$ can be written as [9]

$$j_{sc} = \frac{j_L}{1+\frac{\sigma_p v_{th} N_S \varepsilon_{r1}\varepsilon_0}{q u_1 N_1 W_1}} \quad (11)$$

$$V_{oc} = \frac{nKT}{q}\ln\left(\frac{J_{sc}}{J_0}+1\right) \quad (12)$$

## III. RESULTS

Under AM1.5 illumination the photovoltaic characteristics is shown in following figures. We draw the these characteristics for different values of $N_S$ corresponding to various value of ideality factor n.
The influence of $N_S$ on the short-circuit current density (Fig.2) is small. However, because of the strong increase of $J_0$ (eq. 11) the open-circuit voltage decreases with increasing $N_S$

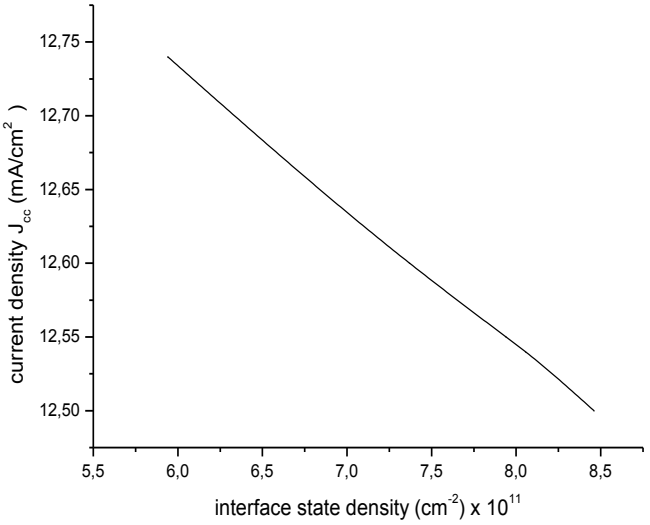


Figure. 2. Open circuit current vs interface state density $N_S$

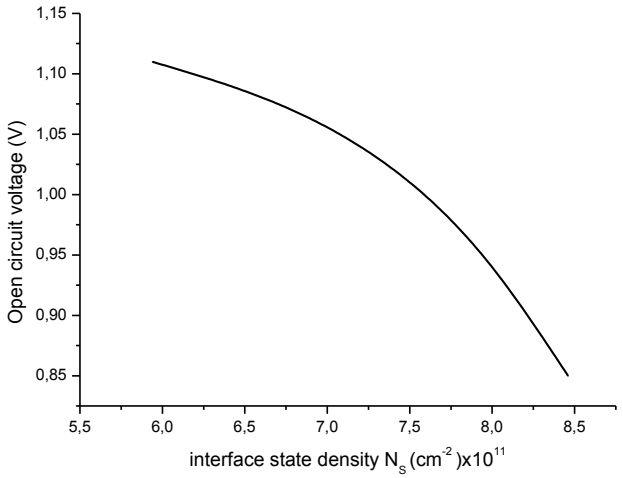


Figure. 3. Photocurrent vs interface state density $N_S$

Fig.4 shows the dependence of the fill factor on the interface state density. It can be seen that the interface recombination leads to a decrease in the fill factor


ISSN 1737-9334

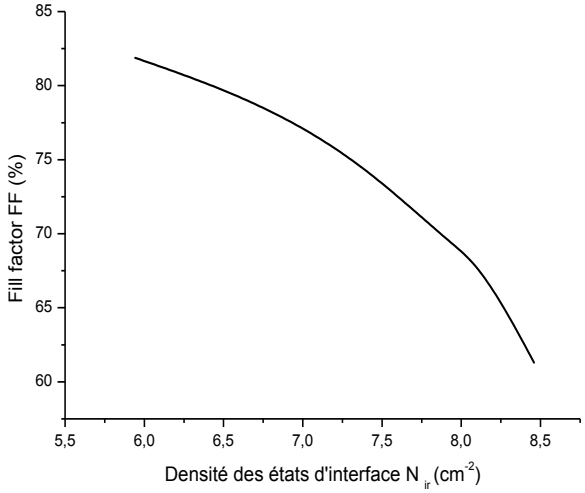


Figure. 4. Fill factor vs. interface state density $N_S$

Fig.5 shows the variation of the efficiency as a function of interface state density Note that the efficiency decreases with increasing $N_S$

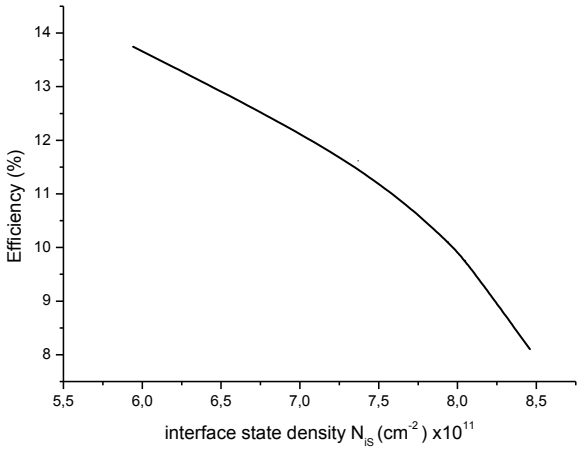


Figure. 5. Efficiency vs interface state density $N_S$

## CONCLUSION

We have used a simple model to investigate the dependence of interface state of CdS/CGS heterojunction. We have seen that energy conversion efficiency increases with decreasing interface state density. Because the diode ideality factor exceeds 2 and interface recombination becomes the dominant diode current transport mechanism. This can lead to a decrease in the open-circuit voltage, the short-circuit current density and the fill factor.

.

## REFERENCES

[1] Dimmler, B, Schock, H.W. “Scalability and pilot operation in solar cells of CuInSe2 and their alloys”. Prog.Photovolt.Res.Appl.6, 193–199 (1998).

[2] Jasenek, A. Rau, U. “Defect generation in Cu(In,Ga)Se2 heterojunctionsolarcells by high energy electron and proton irradiation”. J.Appl.Phys. 90, 650–658(2001).

[3] Guillemoles, J. F. “Stability of Cu(In,Ga)Se2 solar cells a thermodynamic approach” .Thin Solid Films 361–362, 338–345 (2000).

[4] V. Nadenau, U.Rau, A.Jasenek, H.W.Schock, “Electronic properties of CuGaSe 2 -based heterojunction solar cells. Part I. Transport analysis” J.Appl.Phys.87 (1) (2000) 584.

[5] A.Jasenek, U.Rau, V.Nadenau, H.W.Schock, “Electronic properties of CuGaSe 2 -based heterojunction solar cells. Part II. Defect spectroscopy” J.Appl.Phys.87 (1) (2000) 594.

[6] J.H. Sch. on, M.Klenk, O.Schenker, E.Bucher, “Photovoltaic properties of CuGaSe 2 homodiodes” Appl.Phys.Lett.77 (22) (2000) 3657.

[7] V. Nadenau, D.Hariskos, H.W.Schock, M.Krejci, F.-J.Haug, A.N.Tiwari, H.Zogg, G.Kostorz, “ Microstructural study of the CdS/CuGaSe2 interfacial region in CuGaSe2 thin film solar cells ” J.Appl.Phys.85 (1) (1999) 534.

[8] M. Saad, A.Kassis “Effect of interface recombination on solar cell parameters” journal of Solar Energy Materials & Solar Cells 79 (2003) 507–517.

[9] A. Rothwarf, “CuInSe2/Cd(Zn)S Solar cell modelling and analysis” Solar cells 16 (1986) 567–590.




ISSN 1737-9334

# IMAGE PROCESSING BY A FRACTIONAL PARTIAL DIFFERENTIAL EQUATION

ZEGHBIB FATIMA ZOHRA and Messaoud Maouni
Laboratoire LAMAHIS, Departement of mathematics, Reu El-Hadaiek P.O.Box 26,
Université 20 août 1955 Skikda, 21000, Algeria
Email: zeghbib49@gmail.com
m.maouni@univ-skikda.dz

***Abstract*—Many fractional-order based methods have been used in image processing field, and many methods are developed to solve the problem of fractional systems. The traditional integer-order partial differential equation-based image denoising approaches often blur the edge and complex texture detail; thus, their denoising effects for texture image are not very good. To solve the problem, a fractional partial differential equation-based denoising model for texture image is proposed, which applies a novel mathematical method—fractional calculus to image processing from the view of system evolution. We know from previous studies that fractional-order calculus has some unique properties comparing to integer-order differential calculus that it can nonlinearly enhance complex texture detail during the digital image processing.**

***Index Terms*—Topological degree, elliptic problem, homotopy, image restoration**

## I. Introduction

Removing noise while preserving fine details is a challenging issue in image processing. One classical partial differential equation (PDE) based technique is the total variation (TV) minimization, which was inaugurated in [1] by Rudin and al. depicted as

$$\min_{u\in BV(\Omega)\cap L^2(\Omega)} \int_\Omega |Du| + \frac{\gamma}{2}\int_\Omega |u-u_0|^2\,dx, \qquad (1)$$

where $\Omega$ denotes a bounded open domain with a Lipschitzian boundary, $u$ and $u_0$ represent the original image and the observed image respectively. Furthermore, to improve the edge-preserving capability, T. CHAN and Chan [2,3] presented the adaptive TV approach to image restoration.

The PM model has good performance in flat regions with uniform intensity distribution,and the TV model works better inpreserving edges X.Zhang et al.[5] proposed anovel model (i.e., PMTV model) by weighted combinations of PM model and TV model A. Yahya et al.[6] proposed a new denoising technique by blending isotropic diffusion, PM model, and TV model. Although the above second-order PDEs can reduce noise level while preserving the image features, they tend to make the processed image look "blocky", because the images used by second-order PDEs to approximate an observed image are often piecewise constant. In order to reduce blocky effect, a class of four-order PDEs were introduced by You and Kaveh in 2000 [7], but these methods often lead to speckle effect.

To overcome those aforementioned limitations, fractionalorder PDEs have recently been researched and applied to the field of image processing and computer vision. For example, Bai and Feng [8] proposed a class of FPM models for image denoising, in which the energy function is defined as:

The main goal of this work is to apply an adaptive fractional order regularization term for the restoration of textured images corrupted by additive noise and blur. To achieve this aim, we use a 2-phase approach. First we apply a suitable texture detection method on the observed image to obtain a texture map. Then a fractional order regularization is applied to the parts of the image which are characterized to be texture regions by the map and the classical TV regularization ($\ell^1 - TV$) is applied elsewhere. In particular, we propose to replace the TV regularization term $\|u\|_{TV}$ in 1 with a spatially adaptive fractional order TV regularization term, thus integrating the following four ingredients:

- use of the fractional order $\alpha$ of derivatives to better preserve textures,
- spatial adaptivity of $\alpha$ in order to allow flexibility in choosing the correct regularizing operator,
- spatial adaptivity of $\gamma$ in order to locally control the extent of restoration over image regions according to their content,
- an effective texture detection methodology based on the noise auto-correlation energy which makes no assumption about the noise level of the image. This inspired part of the work [5].

## II. The proposed adaptive model

We propose to modify the functional in 1 to the following adaptive fractional variational model:


ISSN 1737-9334

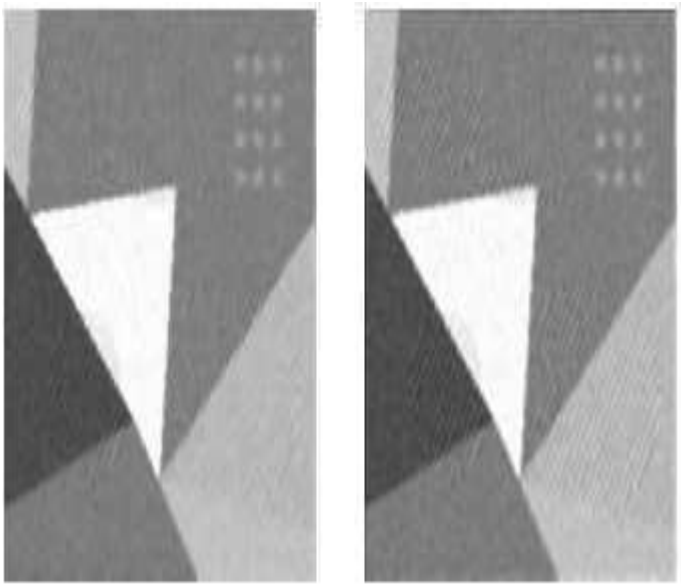

Fig. 1: $\alpha = 1.0 and 1.5$

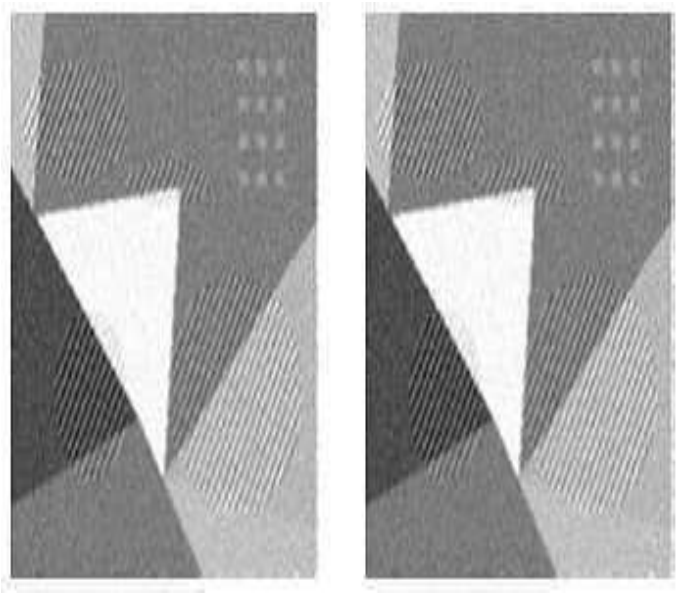

Fig. 2: $\alpha = 1.8,\ \alpha = 2$

$$\min_{u \in BV(\Omega) \cap L^2(\Omega)} \int_{\Omega} \left| D^{\alpha} \left( G_{\sigma} * u \right) \right| + \frac{\gamma}{2} \int_{\Omega} |u - u_0| \, dx, \quad (2)$$

where $\gamma$ representing the regularization parameter for the $i$th pixel, where $\alpha$ represents the fractional order of differentiation for the $i$th pixel and $G_{\sigma}$ is a Gaussian function of standard deviation $\sigma$, and

$$D^{\alpha} u = \left( D_x^{\alpha} u, D_y^{\alpha} u \right)^t$$

is the fractional-order discrete gradient operator, with components representing the $x$ and $y$-directional fractional finite difference operators.

Let us motivate our model by analyzing the high-pass filtering character of the fractional order derivative operator. In Fig. 1 we show the restored images of the blurred and noisy test image in Fig. 2 and Fig.3 by applying model (1) while keeping $\gamma = 1.0$.

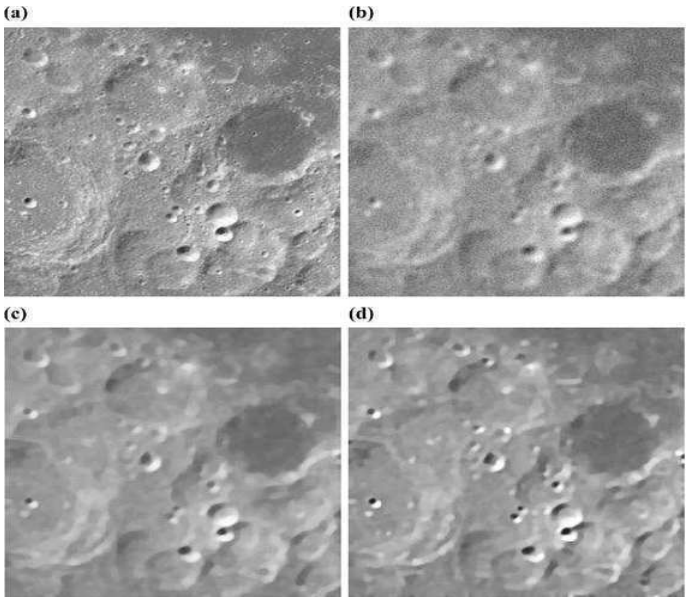


Fig. 3: (a) true image, (b) $\alpha = 1.5$ $(c)\alpha = 1.8$, $(d)\alpha = 2$

## III. Texture detection method

Our idea is to use the auto-correlation function to detect non-whiteness in data. Inspired by [1], starting from the observed degraded image, i.e., $u(0) = u_0$ , we apply a simple TV-flow with Neumann homogeneous boundary conditions

$$u^{(k+1)} = u^{(k)} + t \nabla \left( \frac{\nabla^{\alpha} u^{(k)}}{\left| \nabla G_{\sigma} * u^{(k)} \right|} \right) \quad (3)$$

which approaches a piecewise constant image, so-called "cartoon model", that we denote by $u^{(k)}$.

Under this decomposition, the residual can be represented as

$$r^{(k)} = f - u^{(k)} = u_{nc} + e,$$

we propose to consider the auto-correlation of the residue $r^{(k)}$ and to choose $\tilde{k}$ accordingly.

To describe the details of the approach, we briefly introduce some required statistical concepts. Let $\epsilon = \{E_{i,j} : i, j = 1, \cdots, n\}$ be an $n \times n$ discrete random field with $E_{i,j}$ denoting the scalar random variable modeling noise at pixel $(i, j)$. The auto-correlation of $\epsilon$ is a function


ISSN 1737-9334

$\rho_\epsilon$ mapping pairs of pixel locations $(i_1, j_1)$, $(i_2, j_2)$ into a scalar value that must lie in the range $[-1, 1]$, which represents the Pearson's correlation coefficient between the two corresponding random variables $E_{i_1,j_1}$, $E_{i_2,j_2}$, i.e.,

$$\rho_\epsilon [i_1, j_1, i_2, j_2] = \frac{E\left[\left(E_{i_1,j_1} - \mu_{i_1,j_1}\right)\left(E_{i_2,j_2} - \mu_{i_2,j_2}\right)\right]}{\sigma_{i_1,j_1}\sigma_{i_2,j_2}} \tag{4}$$

where $E$ is the expected value operator, $\mu_{i,j}$ and $\sigma_{i,j}$ are the mean and standard deviation of the random variable $E_{i,j}$.

Since we assume that noise is white, i.e., wide-sense stationary, zero-mean, uncorrelated, the auto-correlation of $E$ depends only on the lag between the two pixel locations $[l, m] = (i_2 - i_1, j_2 - j_1)$ and (4) can be rewritten as follows

$$\rho_\epsilon [l, m] = \frac{1}{\sigma^2} E [E_{i,j} E_{i+l,j+m}] = \begin{cases} 1 & if \quad (l, m) = (0, 0) \\ 0 & otherwise, \end{cases} \quad l, m = 0, \cdots, n-1 \tag{5}$$

independently on $i, j$. That is, a white noise is characterized by zero values of the autocorrelation function at all non-vanishing lags.

Moreover, assuming that the noise process is also ergodic, provided that the observed realization e of the noise random field $\epsilon$ is "sufficiently long", implies that $\rho_\epsilon$ in (5) is well estimated by the sample auto-correlation function of $e$ defined as

$$\widehat{\rho}_\epsilon [l, m] = \frac{1}{n^2 \widehat{\sigma}^2} \sum_{i,j=1}^{n} e_{i,j} e_{i+l,j+m}, \tag{6}$$

where $\widehat{\sigma}^2$ is the sample variance of the observed noise realization $e$. We remark that, for a generic observed realization $x$, the sample auto-correlation $\widehat{\rho}_x[l, m] \in [-1, 1]$, with 1 indicating perfect correlation and $-1$ indicating perfect anti-correlation.

In order to find a characteristic scale $\tilde{k}$ to detect textures, we propose to minimize the following residual auto-correlation energy

$$J_{r^{(k)}} = \max_{[l,m] \neq [0,0]} \left| \widehat{\rho_{r^{(k)}}} [l, m] \right|, \tag{7}$$

that, according to 6, for a cartoon image corrupted by white noise should be zero. For a cartoon image without textures, the energy $J_{r^{(k)}}$ monotonically decreases and vanishes. In the presence of textures, initially, the TV-flow makes the residual image be essentially given by noise, so that the auto-correlation energy $J_{r^{(k)}}$ decreases. As soon as the texture part $u_{nc}$ initiates to contaminate the residual, the energy $J_{r^{(k)}}$ starts increasing since textures are typically correlated.

Our proposal is based on the idea to find the characteristic scale $\tilde{k}$ which makes the auto-correlation energy of the residual image $J_{r^{(k)}}$ minimal.

## IV. The numerical algorithm

The fidelity and regularization terms in 1 are not differentiable, therefore in the following we use a smoothed version of them. To this end, let us define $|v|_\varepsilon = \sqrt{v^2 + \varepsilon}$ for any $v \in \mathbb{R}$ and $\varepsilon > 0$, let $\beta$ and $\gamma$ be two small regularization parameters. Hence, we want to minimize the functional

**Algorithm 1.1: Texture Detetion (TD) Algorithm**

**Input**: degraded image $u_0$ , number of texture classes $C$ ;

**Output:** texture-adaptive parameters $\gamma_i$ , $\alpha_i$ , $i = 1,\cdots, n^2$ ;

1) Initialize the iterative process by setting $u(0) = u_0$ ;
2) Repeat
3) perform one step of the $TV$ flow $u^{(k+1)} = TV(u^{(k)})$ by 3
4) compute the residue image $r^{(k+1)} = u_0 - u^{(k+1)}$
5) compute the residue auto-orrelation $3c1_{r^{(k+1)}}$ by 6
6) compute the residue auto-orrelation energy $J_{r^{(k+1)}}$ by 7
7) until $J_{r^{(k+1)}} > J_{r^{(k)}}$
8) $\tilde{k} := k$ harateristi sale found at the rst lo al minimum;
9) $T =$ ComputeTexture Measure $(u^{(\tilde{k})})$ with $T$ taking values in $[0, 1]$;
10) partition $T$ into $C$ classes $T_1, T_2, \cdots, T_C$;
11) assign $(\lambda_i, \alpha_i)$ a ording to $T_i$ for $i = 1, \cdots, C$ .

## V. CONCLUSION

This work proposes new applications of fractional-order partial differential equations in image processing. Our studies led to proposing a general reconstruction algorithm that incorporates the fractional derivative implementation from [1]. Concerning denoising, better results are obtained with an order $\alpha$ which is fractional rather than integer. The interesting values for the fractional order $\alpha$ seem to be around 1.5 and 1.75. It corroborates previous results [1]. Contrary to existing iterative processes with a fractional order, the algorithm presented here is non iterative. It gives similar results for a shorter computer time and can be used to solve texture problems. The comparison with state-of-the-art methods involving partial differential equations showed better results in terms of quality.

## References

[1] T. CHAN AND S. ESEDOGLU, *Aspects of total variation regularized L1 function approximation*, SIAM J. Appl. Math., 65 (2005), pp. 1817–1837.

[2] R. H. CHAN AND H. X. LIANG, *A fast and efficient half-quadratic algorithm for TV-L1 image restoration*, CHKU research report 370, 2010, submitted; available at ftp://ftp.math.u hk.edu.hk/report/2010-03.ps.Z.


ISSN 1737-9334

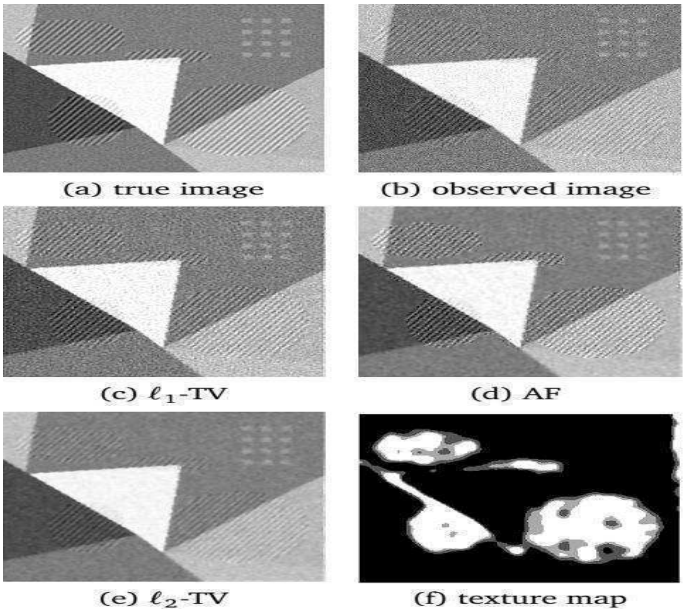


Fig. 4: (a) blur- and noise-free image;
(b) the corrupted image produced by Gaussian blur, defined by the parameters $band = 3$ and $sigma = 1.5$ and by 0.1 of Gaussian noise;
(c) restoration with $\ell^1$ -TV with $\lambda_1 = 0.1$;
(d) restored image determined by AF algorithm;
(e) restoration with $\ell^2-$ TV with $\lambda_1 = 0.1$;
(f ) texture classes computed on (b)

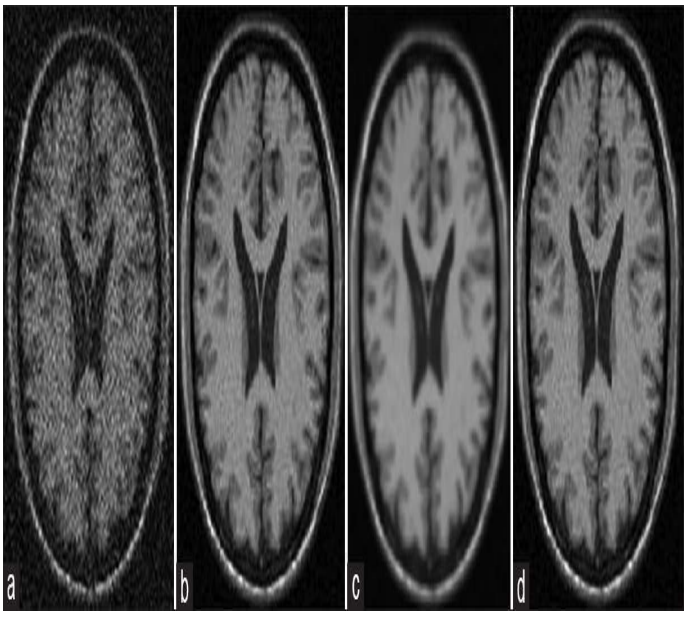


Fig. 5: (a) blur- and noise-free image;
(b) the corrupted image produced by Gaussian blur, defined by the parameters $band = 3$ and $sigma = 1.5$ and by 0.1 of Gaussian noise;
(c) restoration with $\ell^1$ -TV with $\lambda_1 = 0.1$;
(d) restored image by our model;

| **Iteration** | $PSNR_{OM}$ | $PSNR_{TV}$ | $PSNR_{PM}$ |
|---|---|---|---|
| 1 | 20.8668 | 20.8529 | 20.8520 |
| 100 | 21.2799 | 21.1378 | 21.1190 |
| 200 | 21.5155 | 21.3650 | 21.3607 |
| 300 | 21.6672 | 21.5327 | 21.5300 |
| 400 | 21.7134 | 21.6251 | 21.6340 |
| 500 | 21.7720 | 21.7184 | 21.7105 |
| 600 | 21.7989 | 21.7502 | 21.6962 |

TABLE I: PSNR comparisons for the three models (for image 01)

| **Iteration** | $PSNR_{OM}$ | $PSNR_{TV}$ | $PSNR_{PM}$ |
|---|---|---|---|
| 1 | 20.8694 | 20.8591 | 20.8381 |
| 100 | 21.2846 | 21.1174 | 21.0856 |
| 200 | 21.5200 | 21.3370 | 21.2816 |
| 300 | 21.6341 | 21.4951 | 21.4376 |
| 400 | 21.6781 | 21.6149 | 21.5518 |
| 500 | 21.7456 | 21.6787 | 21.6234 |
| 600 | 21.7628 | 21.7153 | / |

TABLE II: PSNR comparisons for the three models (for image 02)

[3] T. F. CHAN, S. OSHER AND J. SHEN, *The digital TV filter and nonlinear denoising*, IEEE Trans. Image Process., 10(2) (2001) pp. 231–241.
[4] Chun Pong Lau, Yu Hin Lai, Lok Ming Lui; *Variational models for joint subsampling and reconstruction of turbulence-degraded images*, CAM Report 18-21 April 2018.
[5] R. H. Chan, A. Lanza, S. Morigi and F. Sgallari,.*An Adaptive Strategy for the Restoration of Textured Images using Fractional Order Regularization.* Numer. Math. Theor. Meth. Appl. Vol. 6, No. 1, (2013)pp. 276-296.
[6] H. FARID, *Discrete-Time Fractional Differentiation from Integer Derivatives* , TR2004-528, Department of Computer Science, Dartmouth College, 2004.
[7] Hubin Chang, Yifei Lou, and Yuping Duan; *Total Variation Based Phase Retrieval for Poisson Noise Removal*, CAM Report 16-76 October 2016.
[8] X. Zhang, R. Wang, and L. C. Jiao, *Partial differential equation model method based on image feature for denoising,* in Proc. M2RSM, Jan. 2011, pp. 1Ű4.
[9] A. A. Yahya, J. Tan, and M. Hu, *A blending method based on partial differential equations for image denoising,* Multimedia Tools Appl., vol. 73, no. 3, pp. 1843Ű1862, 2014.
[10] Y.-L. You and M. Kaveh, *Fourth-order partial differential equations for noise removal*, IEEE Trans. Image Process., vol. 9, no. 10, pp. 1723Ű1730, Oct. 2000.
[11] J. Bai and X. C. Feng, *Fractional-Order anisotropic diffusion for image denoising*, IEEE Trans. Image Process., vol. 16, no. 10, pp. 2492Ű2502, Oct. 2007.




ISSN 1737-9334

# Simulation and Analysis of Surface Wave Loss on Dielectric Substrate Materials at 94GHz Band

Adel Saad Emhemmed (1), Daw Ali Mohamed(2) , Abdulbast Kriama (3)
[1]Electrical and Electrronic Engineering Department, University of Tripoli, Tripoli, Libya, dr. adel. elec@gmail. com
[2]Electrical and Computer Engineering Department, The Libyan Academy, Tripoli, Libya, Daw. Ali. Mohamed@gmail. com
[3] Faculaty Of Engineering , University Of Zawia, Zawia, Libya, kriama@zu. edu. ly.

***Abstract*** **– Abstract- In this paper surface wave loss in two grounded dielectric substrates has been analyzed and simulated at 94GHz band using HFSS simulation software. The first material was Duroid (εr=2.2) since it has lower dielectric constant. The second material was Gallium Arsenide (εr=12.9) which is has high dielectric constant and it is used for integrated circuits. In order to study the effect of surface wave, two grounded dielectric substrates are simulated for different thickness. The thickness of substrate and size is same for valid comparison of surface wave level. The grounded Gallium Arsenide substrate with 0.2mm thickness gives high insertion loss of 5dB and surface wave level of 2.1x$10^5$V/m , therefore substrate type and thickness must be chosen to avoid coupling to the first higher surface wave mode.**

***Keywords*** **– Surface wave loss, high order mode, grounded dielectric substrate, HFSS software.**

## I. INTRODUCTION

There are wide variety of substrate materials have been found for microstrip patch antenna design with mechanical, thermal and electrical properties which are attractive for use in both planar and conformal antenna configurations. The material used for substrate can be dielectric constant in the range of 2.2 ≤ r ≤ 12.9. If we change the material of substrate and the thickness of substrate of a microstrip antenna, it changes the system performance by changing the dielectric constant ($\varepsilon_r$). Cost, power loss and performance are trade-off considerations in choosing the substrate material. The patch size reduces for higher dielectric constant and it also reduces bandwidth and radiation efficiency [1].

The purpose of an antenna is of course to radiate space waves. These waves move towards the free space where they do not find any further interfaces. However, there are also other types of waves such as surface waves and leaky waves can be excited in the microstrip antenna substrate depending on its thickness, and angles of reflection at the substrate metallic boundaries [2]. The excitation of surface wave is often considered to be a disadvantage in all microstrip patch antennas application. The reason for this is that most surface waves are generally difficult to control and are not radiated in the main-beam direction, but in the direction parallel to the air-dielectric interface, distorting the main beam radiation pattern and increasing the level of the side lobes as well as the back lobes. Hence, the surface wave power is treated as a loss mechanism when calculating the radiation efficiency [3].

Surface waves in the substrate can be existed in the form of Transversal Electric (TE) and Transversal Magnetic (TM) modes, because ground dielectric cannot support TEM wave. The phase velocity of these modes is a function of dielectric constant ($\epsilon_r$) and substrate thickness (h). If a quasi-TEM wave is present under the antenna radiator with a phase velocity close to the phase velocity of a surface wave mode, strong mode coupling can occur. For higher order TE and TM modes, the cut-off frequency is given by [1]-[3]:

$$F_c = \frac{nc}{4h\sqrt{\epsilon_r - 1}} \quad \ldots\ldots\ldots\ldots\ldots\ldots\ldots\ldots\ldots\ldots\ldots\ldots\ldots\ldots (1)$$

For $TE_n$ modes n = 1, 3, 5,… , n = 0, 2, 4,... for $TM_n$ modes and c equal the speed of light in vacuum $(c = 3\times10^8 m/s)$. $TM_0$ mode has zero cut off frequency, the power coupled into this mode can be reduced by choosing small (h) and ($\epsilon_r$).If dielectric has finite thickness and dielectric constant slightly large than one, there is always at least one propagating (TM) mode, designated as: ($TM_0$) mode, which has zero cut off frequency. ($TM_0$)mode can have some field lines aligned with field line of (QTEM) mode of microstrip line, which are often used to construct feeding structures of integrated antennas on dielectric [4]- [8].

Therefore, reducing surface-wave excitation from microstrip antennas can be beneficial for various reasons. First, the reduction of surface-wave excitation will increase the radiation efficiency of the antenna. Second, the reduction of surface-wave excitation will result in less diffraction from the edges of the substrate or ground plane supporting the antenna, resulting in less back radiation and interference with the main pattern in the forward region. Also, reduced surface-wave excitation usually results in reduced coupling between antenna elements [6]- [10].

In this paper two different substrates with different dielectric constant and different thickness have been analyzed the surface wave effect using HFSS simulation software

## II. HIGHER ORDER MODES EFFECT IN DIELECTRIC

surface wave losses are always present in the case of a grounded substrate, even if the amount of lost power can be considered negligible for thickness $d<0.01\lambda_0$ of the dielectric. Generally, the power lost in substrate modes increases significantly as higher order modes appear.



ISSN 1737-9334

Fig. 1 and Fig. 2 show the relation between cut off frequencies of surface waves and the thickness of substrate (h) by using Matlab software for gallium arsenide and Duroid substrates. From the results, we note that the surface wave modes increase by increasing the thickness (h) and dielectric constant substrate($\varepsilon_r$). When we using Gallium Arsenide material value cut off frequency increasing compared with Duroid, this will reduce the efficiency

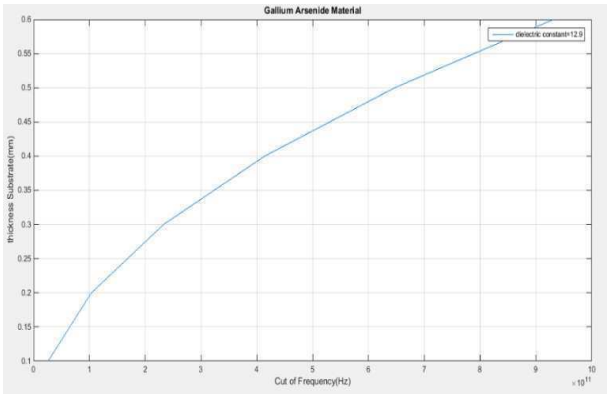


Fig. 1: Relation between cut of frequency and thickness of the Gallium Arsenide material

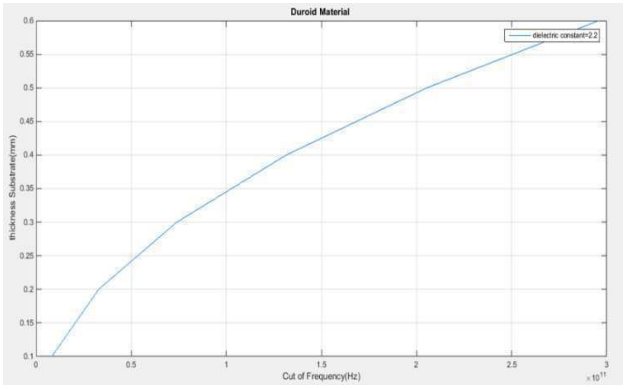


Fig. 2 Relation between cut of frequency thickness of the Duroid material

## III. ANALYSIES SURFACE WAVES

In order to study the effect of surface wave, two grounded dielectric substrates are simulated for different thickness. The thickness of substrate and size is same for valid comparison of surface wave level. The first material was Duroid ($\varepsilon_r$=*2.2*) since it has lower dielectric constant. The second material was Gallium Arsenide ($\varepsilon_r$=*12.9*) which is has high dielectric constant and it is used for integrated circuits. The simulation was done by using HFSS software for two different thickness (*h=0.1mm, h=0.2mm*) to study the effect of surface wave loss by measuring insertion losses ($S_{21}$).

*a) Surface Waves in Two Different Material at h=0.1mm*

The 3D surface wave level for two different materials is shown in Fig. 3. The maximum value of surface wave was $5.1x10^4$ V/m at 94GHz for Gallium Arsenide material, while the maximum value at the same frequency was $4.7x10^4$ V/m for Duriod.

The insertion loss in two materials at 94GHz band is shown in Fig. 4. The insertion loss of grounded dielectric increase by increasing the frequency. The loss of Gallium Arsenide material has 1.07dB at 110GHz and 0.42 dB for Duroid at the same frequency.

Table (I) shows the comparison between two materials. From the comparison table, it has been concluded that with the decrease in relative permittivity of substrate material the effect of surface wave can be ignored. This will enhance the efficiency of the devices.

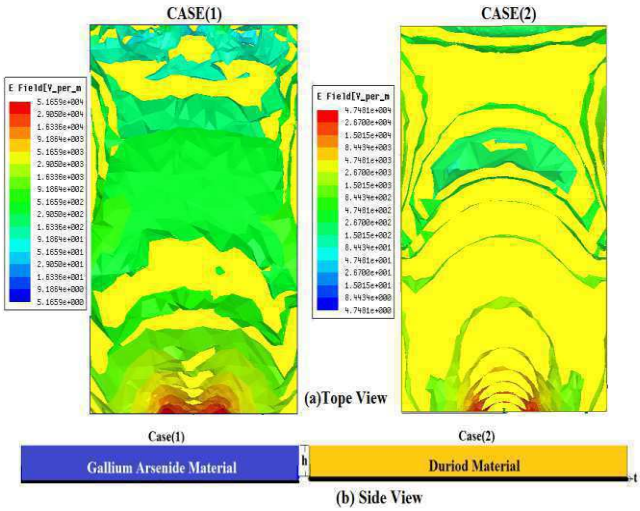


Fig. 3 Surface Waves in Two Different Material at h=0.1mm

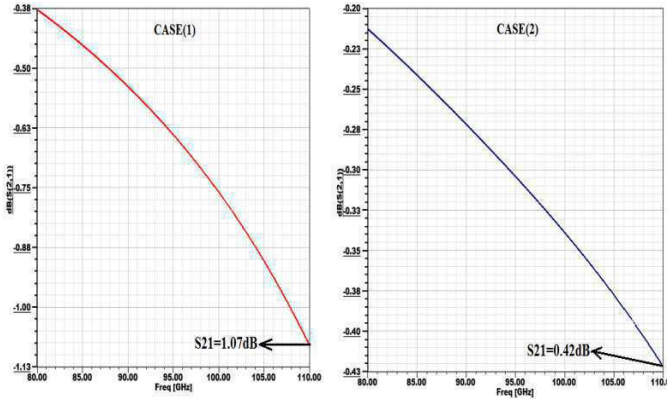


Fig.4 Insertion Loss in Two Different Material at h=0.1mm

Table(I): Comparing Gallium Arsenide with Duroid Materials at(h=0.1mm)




ISSN 1737-9334

| Parameters with Thickness Substrate=0.1mm | Gallium Arsenide Material | Duroid Material |
|---|---|---|
| Wave Length of Cut-off frequency | 1.38mm | 0.438mm |
| Insertion Loss | 1.07dB | 0.42dB |
| Elevation angle (θ) | 90°≤θ≤163.8° | 90°≤θ≤137.6° |
| Surface waves level | High | Low |

*b) Surface Waves in Two Different Material at h=0.2mm*

From Fig. 5 and Fig 6 we can see that the surface waves level inside Gallium Arsenide material more than Duriod material. Gallium Arsenide material has maximum value of surface wave is $2.1x10^5$ V/m and insertion loss is 5dB while Duroid material has $1.04x10^5$ V/m of insertion loss and insertion loss is 0.56 dB. Table II shows the comparison between two materials.

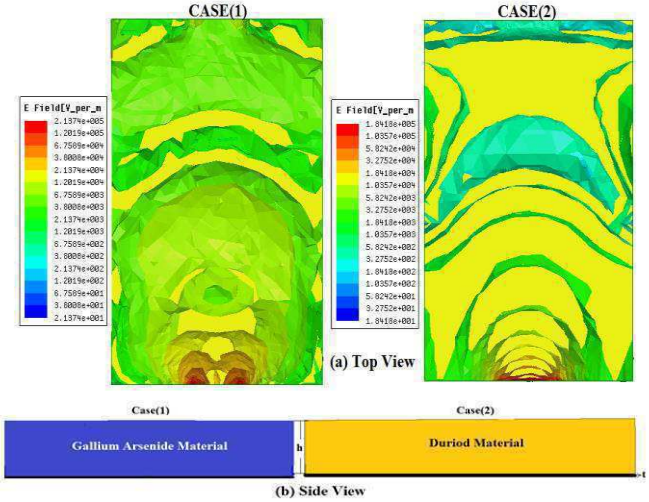


Fig.5 Surface Waves in Two Different Material at h=0.2mm

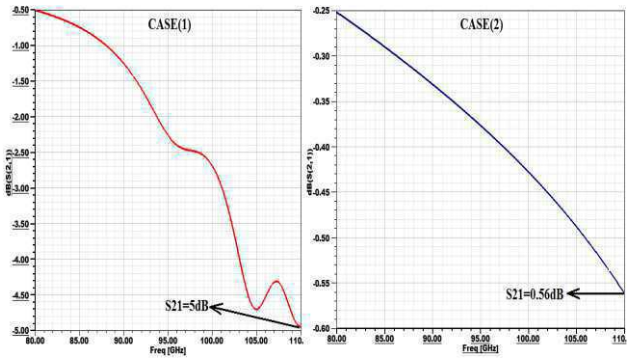


Fig.6 Insertion Loss in Two Different Material at h=0.2mm

Table(II): Comparing Gallium Arsenide with Duroid Materials at (h=0.2mm)

| Parameters with Thickness Substrate=0.2mm | Gallium Arsenide Material | Duroid Material |
|---|---|---|
| Wave Length of Cut-off frequency | 5.55mm | 1.75mm |
| Insertion Loss | 5dB | 0.56dB |
| Elevation angle (θ) | 90°≤θ≤163.8° | 90°≤θ≤137.6° |
| Surface waves level | High | Low |

## IV. CHARACTERIZATION AND DISCUSSIONS

The phase velocity of the surface waves is strongly dependent on the substrate parameters (h , $\varepsilon_r$). From equation (1) we can calculate ($TE_1$) mode at n=1 with Gallium Arsenide material has $\epsilon_r = 12.9$ , Hence the value of $(\frac{h}{\lambda c})^1$ will be :

$$(\frac{h}{\lambda c})^1 = \frac{n}{4\sqrt{\varepsilon_r - 1}} = \frac{1}{4\sqrt{12.9 - 1}} = 0.072$$

where $\lambda c^1 = (\frac{c}{F_c})^1$

Can calculate ($TE_1$) mode at n=1 with Duroid material has dielectric constant ($\epsilon_r = 2.2$)

$$(\frac{h}{\lambda c})^1 = \frac{n}{4\sqrt{\varepsilon_r - 1}} = \frac{1}{4\sqrt{2.2 - 1}} = 0.228$$

Since $TM_0$ mode has no cutoff frequency then, the lowest order $TM_0$ mode will excited at all grounded dielectric materials. At 94GHz frequency the lowest order ($TE_1$) mode is excited at h=0.22mm in grounded Gallium Arsenide material and with Dourid material ($TE_1$) mode is excited at h=0.72mm.

If we decreasing the frequency to 10GHz the lowest order ($TE_1$) mode is excited at h=2.17mm with Gallium Arsenide material and at h=6.8mm for Dourid material.

From this comparison we can conclud that with the decrease in relative permittivity and thickness of substrate material surface wave loss will be decreasing.

## V. CONCLUSION

This paper introduces effect surface waves in two different grounded dielectric substrates. The grounded Gallium Arsenide substrate with 0.2mm thickness gives high insertion loss of 5dB and surface wave level of $2.1x10^5$ V/m, therefore substrate type and thickness must be chosen to decrease the surface wave level.

It has been concluded that RF circuits on high dielectric substrate at mm-wave frequencies suffer greatly from surface wave losses because typical substrates become electrically thick at these frequencies. The excitation of surface wave


ISSN 1737-9334

modes is often considered to be a disadvantage in all RF circuits. The reason for this is that most surface waves are generally difficult to control and are not flow the main field. Hence, the surface wave power is treated as a loss mechanism when calculating the efficiency of the system

## REFERENCES

[1]. David M- Pozar,"microwave engineering" , fourth edition ,2012
[2]. Adel Saad Emhemmed, Abdulmagid A. Aburwein, "Surface Waves Reduction in Microstrip" IEEE ,2013
[3]. Ankit S. Solanki , Ayush Agarwal **,** "Millimeret-w-Wave integrated circuits preview or an overview on monolithic microwave integrated circuits (MMIC)" , International Journal of Industrial Electronics and Electrical Engineering, Dec.-2014
[4]. Varadarajan Komanduri, David R. Jackson," Reducing surface wave Excitation from MSA by using a Cavity Filling", Institute of Electrical and Electronics Engineers (IEEE) ,2007
[5]. Shruti Dhamankar, Snehal Lopes- "MUTUAL COUPLING REDUCTION TECHNIQUES IN MSA", International research journal of engineering and technology(IRJET), Mar-2016.
[6]. Hyung Suk Lee, Jeong-Geun Kim, Songcheol Hong, "Micromachined CPW-Fed Suspended Patch Antenna For 77 GHz Automotive Radar Applications", IEEE Transactions on Antenna and Propagation, Vol. **45,** No. **6,** March 2008
[7]. D. M. Pozer, ''Consideration for Millimetre Wave Printed Antennas'', IEEE Transactions on Antennas and Propagation, Vol. AP-31, NO. 5, pp. 740-747, Sep 2005.
[8]. Adel Emhemmed, I. McGregor, K. Elgaid, " Elevated conductor coplanar waveguide-fed three-level proximity-coupled antenna for G-band applications'', IEEE Microwaves, Antennas & Propagation Journal, Vol. 4, No. 11, pp 1910-1915, Oct 2010.
[9]. Adel Saad Emhemmed**,** Daw Ali Mohamed **"** High Performance 94GHz Holes-backed Integrated Antennas Fed by Inset Tapered Microstrip Line**",** 5th International Conference on Control & Signal Processing (CSP-2017) - Kairouan . Tunisia
[10]. Punita Mane, S.A Patil and P.C.Dhanawade, "Comparative Study of Microstrip Antenna for Different Subsrtate Material at Different Frequencies", International Journal of Emerging Engineering Research and Technology Volume 2, Issue 9, PP 18-23,December 2014.


ISSN 1737-9334

# Security Issues for Cloud Computing

Sedieg A.Elatab[1] , Rabeah H.Ghareb [2]
[1] *Scientific Affairs Department , College Of Technical Engineering , Libya*
[2]*Sabratha University , Economy College , Libya*
[1]It2017Cisco@gmail.com
[2]Rabee7878@gmail.com

***Abstract*— Cloud computing is becoming an adoptable technology for many of the organizations with its dynamic scalability and usage of virtualized resources an a services as a service through the Internet. It represents a shift a way from computing as a product that is purchased , to computing as a service that is delivered to consumers over the internet from large –scale data centers or "clouds" . Whilst cloud computing is gaining growing popularity in the academia appeared to be lagging behind the rapid developments in this field [1] .**

**The main features of cloud computing is that the user does not have any setup of expensive computing infrastructure and the cost of its services is less. The cloud provider provides its services through the Internet and uses many web technologies that arise new security issues. In the recent years, cloud computing integrates with the industry and many other areas, which has been encouraging the researcher to research on new related technologies.**

**The biggest challenge in cloud computing is the security and privacy problems caused by its multi-tenancy nature and the outsourcing of infrastructure, sensitive data and critical applications .**

**This paper discussed about the basic features of the cloud computing. Moreover, the paper describes several key topics related to the cloud, namely cloud architecture framework, service and deployment model, cloud technologies, cloud security concepts, security issues, threats and attacks and their solutions.**

***Keywords*— Cloud computing ;security issues; cloud technology** .

## I. INTRODUCTION

Nowadays , the term "cloud computing" has been an important term in the world of Information Technology(IT).Cloud computing is a kind of computing which is highly scalable and use virtualized resources that can be shared by the users. Users do not need any background knowledge of the services. A user on the internet can communicate with many servers at the same time and these servers exchange information among themselves (Hayes , 2008)[2]. Cloud computing is currently one of the new technology trends(virtualization, fast connection and broadband internet ).Cloud computing encompasses elements from grid computing, utility computing and autonomic computing, into an innovative deployment architecture. This rapid transition towards the clouds, has fuelled concerns on a critical issue for the success of information systems, communication and information security. The major security challenge with clouds is that the owner of the data may not have control of where the data is placed. This is because if one wants to exploit the benefits of using cloud computing , one must also utilize the resource allocation and scheduling provided by clouds. There are numerous security issues for cloud computing as it encompasses many technologies including networks, databases, operating systems, resource scheduling, virtualization, transaction management, load balancing, concurrency control and memory management. Therefore, security issues for many of these systems and technologies are applicable to cloud computing. For example, the network that interconnects the systems in a cloud has to be secure[3]. This paper is designed as following, Section I illustrates the cloud computing architectural framework. Section II essential characteristics of cloud computing . Cloud services models are presented in Section III . Finally conclusion is given in

## II.CLOUD COMPUTING ARCHITECTURAL FRAMEWORK[4]

The National Institute of Standard and Technology(NIST) defines cloud computing by describing five essential characteristics , three cloud service models, and four cloud deployment models. They are summarized in visual form in figure1 and explained in detail below .




ISSN 1737-9334

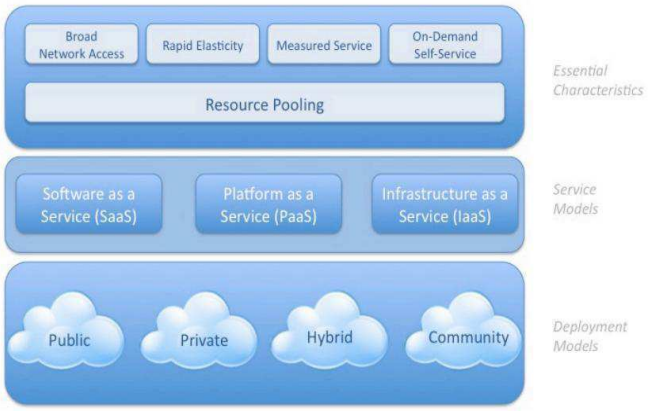


Fig. 1. NIST Visual Model of Cloud Computing Definition

In the researcher point of view the cloud computing is a model for enabling ubiquitous, convenient , on-demand network access to a shared pool of configurable computing resources (e.g, networks , servers , storage , applications , and services ) that can be rapidly provisioned and released with minimal management effort or service provider interaction .

## III.ESSENTIAL CHARACTERISTICS OF CLOUD COMPUTING

There are five essential characteristics associated to the cloud services which demonstrate their relation to , and their differences from , traditional computing approaches:

### A. On-Demand Self-Service

A consumer can unilaterally provision computing capabilities such as server time and network storage as needed automatically , without requiring human interaction with a service provider.

### B. Broad Network Access

Capabilities are available over the network and accessed through standard mechanisms that promote use by heterogeneous thin or thick client platforms(e.g., mobile phones , laptops , and PDAs) as well as other traditional or cloud based software services.

### C. Resource Pooling

The provider 's computing resources are pooled to serve multiple consumers using a multi-tenant model , with different physical and virtual resources dynamically assigned and reassigned according to consumer demand . Examples of resources include storage , processing , memory , network bandwidth , and virtual machine .

### D. Measured Service

Cloud systems automatically control and optimize resource usage by leveraging a metering capability at some level of abstraction appropriate to the type of service (e.g., storage , processing , bandwidth , or active user accounts). Resource usage can be monitored , controlled , and reported-providing transparency for both the provider and consumer of the service.

### E. Rapid Elasticity

Capabilities can be rapidly and elastically provisioned-in some cases automatically – to quickly scale out ; and rapidly released to quickly scale in . To the consumer , the Capabilities available for provisioning often appear to be unlimited and can be purchased in any quantity at any time.

## IV.CLOUD SERVICES MODELS

Cloud service delivery is divided among three archetypal models and various derivative combinations. The three fundamental classifications are often referred to as the "SPI Model" where "SPI" refers to Software ,Platform or Infrastructure (as a Service), respectively – defined thus

### *D. Cloud Software as a Service (SaaS)*

The capability provided to the consumer is to use the provider's applications running on a cloud infrastructure.

The applications running are accessible from various client devices through a thin client interface such as a web browser (e.g. , web-based email ). The consumer does not manage or control the underlying cloud infrastructure including network , servers , operating systems , storage , or even individual application capabilities , with the possible exception of limited user-specific application configuration setting.

### *E. Cloud Platform as a Service (PaaS)*

The capability provided to the consumer is to deploy onto the cloud infrastructure consumer-created or acquired applications created using programming languages and tools supported by the provider. The consumer does not manage or control the underlying cloud infrastructure including network , servers , operating systems , or storage , but has control over the deployed applications and possibly application hosting environment configurations.

### *F. Cloud Infrastructure as a Service (IaaS)*

The capability provided to the consumer is to provision processing , storage , network , and other fundamental computing resources where the consumer is able to deploy and run arbitrary software , which can include operating systems and applications. The consumer does not manage or control the underlying cloud infrastructure but has control over operating systems , storage , deployed applications , and possibly limited control of select networking components (e.g., host firewall).

## V.CLOUD DEPLOYMENT MODELS

Regardless of the service model utilized (SaaS,PaaS , or IaaS) there are four deployment models for cloud services , with derivative variations that address specific requirements.

### *G. Public cloud*

The cloud infrastructure is made available to the general public or a large industry group and is owned by an organization selling cloud services .




ISSN 1737-9334

*H. Private cloud*

The cloud infrastructure is operated solely for a single organization . It may be managed by the organization or a third party , and may exist on –premises or off-premises.

*I. Community cloud*

The cloud infrastructure is shared by several organizations and supports a specific community that has shared concerns ( e.g., mission , security requirements , policy , or compliance considerations) . It may be managed by the organizations or a third party and may exist on-premises or off-premises.

*J. Hybrid cloud*

The cloud infrastructure is a composition of two or more clouds (private , community , or public ) that remain unique entities but are bound together by standardized or proprietary technology that enables data and application portability (e.g., cloud bursting for load – balancing between clouds ) .

## VI. Cloud security concepts

The cloud security covers various security issues and threats. The paper identifies the source of the vulnerability and threats to understand the concept of cloud security. This section discusses some cloud specific concepts like virtualization, multi-tenancy, cloud platforms, data outsourcing, data storage standardization and trust management, to understand the security issues present in the cloud.

*K. Virtualization aspect*

Virtualization is a conceptual process of extracting the services, applications, computing resources and operating system from the hardware on which they run. The Virtual Machine (VMs) and Virtual Machine Manager (VMMs) are referred as a component of the virtualization. A VM is an image of large size contents per-image of the operating system (OS) called guest OS content memory and storage. The guest OS is responsible for running multiple programs on it.

The main feature of VM image is, it can easily move to another place, easily copied and make clones. Cloud delivers high available and scalable services to their customer. In case of machinery cloud which have a lack of resources, but due to the VM it can not be realized that the resources are limited.

*L. Multi-tenancy*

Multi-tenancy is a feature of cloud computing environment, that introduce the sharing concept, in which each running instances can be shared by one or more users called tenants. It provides capability to share single cloud platform among multiple users. Consider an IaaS provider, VMMs is referred to a multi-tenancy sharing platform while VMs refers to the instances. In a PaaS provider, Virtual Platform (VP) enables user to run multiple applications such as Java Virtual Machine (JVM) and .NET in multi-tenancy environment. Resulting from them, attacker can access neighbour VMs or running applications. Denial of Service (DoS) attack is another issue that can happen by consuming much resources.

*M. Security controls*

Security controls are countermeasure used to reduce or avoid risk. The countermeasures also prevent or respond to security threats. A list of security countermeasures, how to use them and all related information about countermeasures is given in the security policy. It contains a set of rules and practices used for implementation of security controls in a system, service or security plans. The security controls help us to achieve maximum security of sensitive data and critical resources.

*N. Security policies*

Security policy is a mechanism to establish set of security rules and regulations. This security policy further defines how these rules and regulations are implemented in a security system. For example, security policies can be helpful to know positioning and usage of security controls and mechanisms.

*O. Cloud security services*

The cloud security service is a complex service, technique, regulation and behaviour that is composed to protect IT assets. IT security measures aim to define security services for the cloud. This security service helps us to understand the need for security. The four fundamental cloud security services are defined as follow:

- **First main security service is confidentiality**, that refers to only authorized parties or system having permission to access the IT resources.
- **A key term of integrity** in the information security refers the characteristic in which data have not been modified by an unauthorized party. This security service is achieved by protecting assets from unauthorized deletion, modification or fabrication.
- **The authentication** is a process of verifying of an entity that a subject made to act on behalf of a given principal. The authentication attack aim is to verify own identity as a legitimate user. For restriction of unauthorized access and maintain the privacy of user accounts on a cloud required a strong authentication. The weak password, easy recovery method, and insecure registration process can break the authentication.
- **The high availability feature** of cloud computing aim is to minimizing application downtime and preventing business disruption. It refers the characteristic that having ability to every IT resource is accessible and usable during a specified period of time. In the cloud computing environment, the cloud provider and the cloud carrier are responsible for the availability of cloud IT resources.

*P. Security identification of the threats*

The most challenging issues at the time of implementation of suitable countermeasure in an IS, is identifying the unique security threats. In the standard security system designing process, first aim is to identify security threats associated with them, then find the security requirements then apply selected


ISSN 1737-9334

security controls to achieve the high reliability, maintainability and supportability. The confidentiality, integrity, availability is the building block of designing any security system. These important security aspects necessary applied to be made a secure cloud. The cloud architectural design provides a number of security advantages, which included the high availability, centralization of security, redundancy, and data process segmentation.

*Q. Cloud platforms*

Cloud users want to deploy their application and services to the cloud, it required some workable frames those are helpful to deploy their application. For example, VMM (a virtualized layer) is used as a cloud platform for IaaS services. In case of PaaS, .NET, and JVM platform is used as a development platform. These platform provides the tools that are required to build SaaS applications. The platform provides APIs, and IDE for development of the cloud applications. All the tools depend upon the underlying infrastructure of the platform and the programming language.

## VII. CLOUD COMPUTING SECURITY CHALLENGES

Cloud security is a part of computer security. It describes set of policies, technology, and control that is helpful to protect the data and services. The threats and attacks directly or indirectly affect the cloud system. Integrity, availability and confidentiality of the cloud resources as well as service of different layers are breach, that may be raised new security concern[5].

The benefits introduced by cloud computing are legion. The most beneficial aspects of using cloud include fast and easy deployment, the pay-per-use model, and reduction of in-house IT costs. However, they also point out that security is the most important issue to be addressed in order to promote the widespread use of cloud computing.

Cloud computing providers need to solve the common security challenges of traditional communication systems. At the same time, they also have to deal with other issues inherently introduced by the cloud computing paradigm itself. In this section, we have categorized the main cloud security issues as traditional and new cloud security challenges.

*R. Traditional security challenges*

Although the security concerns in traditional communication systems also apply to the cloud, the use of cloud computing introduces new attack vectors that will make attacks either possible or simply easier to carry out.

The authentication and authorization applications for enterprise environments may need to be changed to work with a cloud environment. Such vulnerabilities represent an even more serious problem in multi-tenant environments, where the compromise of a virtual machine can affect all users on the same physical server. Cloud providers, therefore, might need to reconsider traditional security concerns from different angles.

*S. Cloud security challenges*

As end-users utilize the cloud services and store their data in the provider's infrastructure, the most critical security concern is about privacy and user data confidentiality. End-users want to know where their information is stored, and who is in control of that information in addition to the owners. They also want to be guaranteed that the critical information is not accessed and used illegally, even by the cloud providers.

## VIII. THREATS TO CLOUD COMPUTING

In computer security, threat is defined as anything which is capable of causing serious harm to a computer system. Threats can lead to potential attacks on the computer system or network infrastructure. The paper (Hubbard and Sutton, 2010)[6] presented the top threats that are related to the security architecture of the cloud services. This paper exhibits several potential threats that are harmful to the cloud is shown in Table 1.

Table 1. Exhibits several potential threats

| A comprehensive study on cloud threats described by the CSA in 2013 and its solutions | | | |
|---|---|---|---|
| Threats | Effects | Affected Cloud Services | Solutions |
| Malicious insiders | Penetrate organization recourses, damage assets, affect an operation | PaaS,SaaS,and IaaS | Use agreement reporting and breach notifications. |
| Shared technology issues | Interfere one user services to other user services by compromising hypervisor | IaaS | Audit configuration and vulnerability, for administration task use strong authentication and access control |
| Data loss and leakage | Personal sensitive data can be deleted , destructed, corrupted or modified | PaaS,SaaS,and IaaS | Provide data storage and backup mechanisms |
| Service/Account hijacking | Stolen user account credentials, access the critical area of the cloud. | PaaS,SaaS,and IaaS | Adoption of strong authentication mechanisms,security polices , and secure communication channel |
| Risk profiling | Internal security operations, security policies, auditing and | PaaS,SaaS,and | Acknowledge partial logs,data and infrastructure aspect, to secure data use monitoring and altering |


ISSN 1737-9334

When cloud adopted new technology in cloud infrastructure, definitely new attacks have come.
There are some attacks those are launch when cloud adopt new cloud technology.

The survey is summarized in Fig. 2. The Fig. 2 creates a building block in the reader's mind that is helping to understand the current security issues. The presented data storage and computing issues, virtualization and platform related issues are coming under the cloud delivery models. Additionally, the survey going on Internet related issues. Finally, the survey cover security issues related to trust and legal issues.

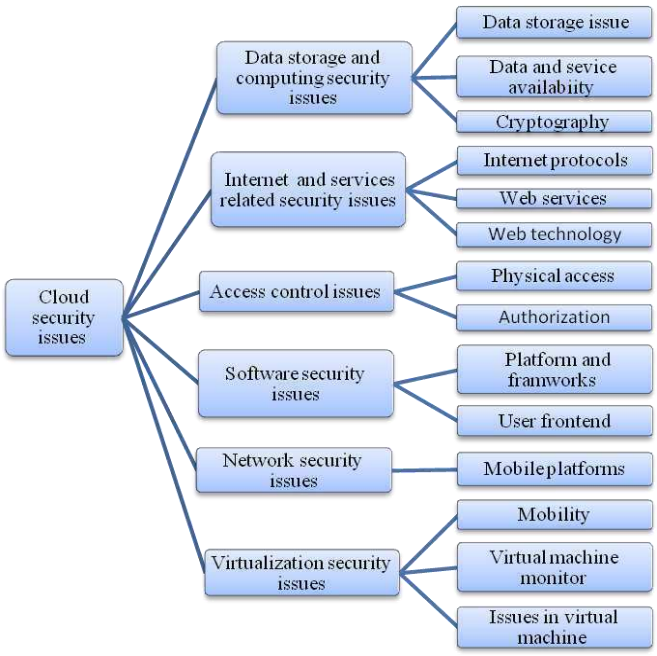


Fig. 2.A summary of the computing security issues

## IX.Issues Of Security To Clarify Before Adopting Cloud Computing

The world's important information technology, advisory company, research and has identified seven security apprehensions that an enterprise cloud computing user should discourse with cloud computing providers (Edwards, 2009)[7] before approving.

- **User Access.** Ask providers for unambiguous information on the hiring and oversight of privileged administrators and the controls concluded their access to information. Major Companies should demand and enforce their own hiring principles for personnel that will operate their cloud computing environments.
- **Data location**: Enterprises should necessitate that the cloud computing provider store and process data in specific jurisdictions and should follow the privacy rules of those Jurisdictions.
- **Data Segregation:** Realize what is done to segregate your data, and probe for proof that encryption schemes are deployed and are effective.
- **Disaster Recovery.** Ask the provider for a contractual commitment to sustenance specific types of investigations, such as the research involved in the discovery phase of litigation, and verify that the provider has successfully supported such activities in the past. Deprived of evidence, don't assume that it can do so.
- **Regulatory Compliance**. Create sure your provider is willing to submit to external Audits and security certifications.
- **Disaster Recovery Verification**. Know what will happen if adversity strikes by asking whether your provider will be capable of utterly restore your data and service, and find out how long it will take.
- **Long-term Viability**. Ask forthcoming providers how you would get your data back if they were to fail or be assimilated, and find out if the data would be in a arrangement that you could easily import into a replacement application.

## X.Countermeasures and Controls

The vulnerabilities and threats in the cloud are well documented. Each cloud service provider and cloud consumer have to devise countermeasures and controls to mitigate the risks based on their assessment. However, the following are some of the best practices in countermeasures and controls that can be considered[8] .

- **End-to-end encryption.** the data in a cloud delivery model might traverse through many geographical locations; it is imperative to encrypt the data end-to-end.
- **Scanning for malicious activities.** end-to-end encryption while highly recommended, induces new risks, as encrypted data cannot be read by the Firewall or IDS. Therefore, it is important to have appropriate controls and countermeasures to mitigate risks from malicious software passing through encryption.
- **Validation of cloud consumer**. the cloud provider has to take adequate precautions to screen the cloud consumer to prevent important features of cloud being used for malicious attack purposes.
- **Insider attacks.** cloud providers should take precaution to screening employee and contractors, along with strengthening internal security systems to prevent any insider attacks.
- **Secure leveraged resources.** in a shared/multi-tenancy model, the cloud provider has secure shared resources such as hypervisor, orchestration, and monitoring tools.

## XI.Conclusion

Cloud computing provides the benefit of quick deployment, cost efficiency, large storage space and easy access to the system anytime and anywhere. So, the cloud computing is very much evident rapidly emerged technology and widely accepted computing environment around the world. However, there are many security and privacy concerns that obstacle to adoption of the cloud computing. All the cloud users should be well aware of the vulnerabilities, threats and


ISSN 1737-9334

attacks existing in the cloud. The awareness of security threats and attacks will help the organizations to carry out fast rate adoption of the cloud.

Cloud computing is a model to provide convenient, on-demand access to a shared pool configurable computing resources. In cloud computing, IT-related capabilities are provided as services, accessible without requiring detailed knowledge of the underlying technologies, and with minimal management effort. The great savings promised by the cloud are however offset by the perceived security threats feared by users. Cloud Computing is a rapidly revolution with IT and will become the default method of IT delivery moving into the future-organizations would be advised to consider their approach towards beginning a move to the Clouds sooner, rather than later [9] .

The researcher summaries the three operational domains of concern for cloud computing which can be applied to any combination of cloud service and deployment model as explained in the following points

- ***Application Security***. Securing application software that is running on or being developed in the cloud . This includes items such as whether it's appropriate to migrate or design an application to run in the cloud, and if so, what type of cloud platform is most appropriate (SaaS, PaaS, or IaaS).
- ***Encryption and Key Management***. Identifying proper encryption usage and scalable key management This section is not prescriptive, but is more informational is discussing *why* they are needed and identifying issues that arise in use, both for protecting access to resources as well as for protecting data.
- ***Identity and Access Management***. Managing identities and leveraging directory services to provide access control . The focus is on issues encountered when extending an organization's identity into the cloud. This section provides insight into assessing an organization's readiness to conduct cloud-based Identity and Access Management(IAM).

There are numerous security issues for cloud computing as it encompasses many technologies including networks, databases, operating systems, virtualization, resource scheduling, transaction management, load balancing, concurrency control and memory management. Therefore, security issues for many of these systems and technologies are applicable to cloud computing. For example, the network that interconnects the systems in a cloud has to be secure. Furthermore, virtualization paradigm in cloud computing results in several security concerns. For example, mapping the virtual machines to the physician machines has to be carried out securely. Data security involves encrypting the data as well as ensuring that appropriate policies are enforced for data sharing. In addition, resource allocation and memory management algorithms have to be secure. Finally, data mining techniques may be applicable to malware detection in clouds.

## REFERENCES

[1] Ahmed E.Youssef and Manal Alageel , A Framework for Secure Cloud Computing , Dept.of Information System , King Saud University Riyadh, 1154,KSA , IJCSI International Journal of Computing Science Issues, Vol.9, Issue4, No3, July 2012 , ISSN(Online): 1694-0814, www.IJSI.org.

[2] Peter Mell,Timothy Grance , The NIST Definition of Cloud Computing ,The National Institute of Standard and Technology, U.S.Department of Commerce ,Special Publication 800-145

[3] Security Issues for Cloud Computing , Technical Report UTDCS-02-10, Department of Computer Science, The University of Texas at Dallas, February 2010, (*Kevin Hamlen, Murat Kantarcioglu, Latifur and Bhavani Thuraisingham*).

[4] Security Guidance for Critical Area of Focus in Cloud Computing V2.1, Prepared by the Cloud Security Alliance December 2009.

[5] Ashish Singh, Kakali Chatterjee ,Cloud security issues and challenges: A survey - Department of Computer Science & Engineering, National Institute of Technology Patna 800005, Bihar, India.

[6] Hubbard and Sutton, 2010: Hubbard, D., Sutton, M., 2010. Top threats to cloud computing v1.0 Cloud Security Agency.

[7] Gururaj Ramachandra, Mohsin Iftikhar, Farrukh Aslam Khan, A Comprehensive Survey on Security in Cloud Computing , The 3rd International Workshop on Cyber Security and Digital Investigation (CSDI 2017).

[8] Edwards, 2009- Buyya R, Chee Shin Y, Venugopal S, Broberg J, Brandic I. Cloud computing and emerging IT platforms: vision, hype, and reality for delivering computing as the 5th utility. Future Generation Computer Systems; 2009; 25(6):599–616.

[9] Understanding the Cloud Computing Stack SaaS , PaaS , IaaS , At site : www.rackspaceclouduniversity.com.


ISSN 1737-9334

# Intelligent System Design for Early Warning and Cooling From Very High Temperatures in Voltage 30 Kv Transformers

Salem Aboalkasem [*1], marad balkasm [#2], faraj fetouri [*1], Nasar Aldian Ambark Shashoa [#3]
[#2] *University of South Wales*
[#3]*Department of Electrical and Electronic Engineering, Azzaytuna University, Libya*
[2]muradbalkasm@gmail.com
[3]dr.naser.elec@gmail.com
[*1] *General Electric Company Libya, Libya*
[1]salem.aboalkasem@academy.edu.ly
[1]faraj.a.fetouri@gmail.com

***Abstract*— The East Asian and North African countries, especially the Libyan state, rely on 30kv oil-cooled medium voltage transformers that require constant monitoring by engineers especially in the summer because of high temperature, affects the ability of transformers. The temperature of these transformers are sensed by the mechanical sensor (Albokhalz) which famous for its failures due to several factors impede its movement. therefore, necessitated the presence of human supervision, and if the supervisor is not in the station " whose is doing the manual separation" during the occurrence the emergency situation of the mechanical sensor, the heat Will cause the damage of this transformer, which will lead to the interruption of feeding on lines that feeding from it including vital lines which can be affected by power outages such as (intensive care rooms in hospitals, educational institutions and other vital institutions). In this paper, Intelligent System for Early Warning and Cooling from Very High Temperatures in Voltage 30 Kv transformers is designed. This design keeps the transformers from the unwanted rise in temperature. Also, another solution exists in this design if the temperature has risen to the level of danger. Here, the system will turn off the transformer to save it from the explosion and then, the all lines loaded on the transformer will be separated including vital lines. Then, the signal is sent to AVR device for putting it on automatic mode to raise the capacity of the second transformer. at the same time, two signals are sent, the first signal is sent to the" Fractionator" connection line which makes the vital line ready to connect to the second transformer , and second signal is sent to the conduction circuit device Siemens so as to connect the vital line (Previously separated) with the second transformer located inside the station.**

***Keywords*— transformer; buchholz relay; GSM SIM800; Microcontroller;**

## I. INTRODUCTION

Transformers are considered the devices that helped people meet their energy needs. A transformer is a static device consisting of a winding, or two or more coupled windings, with or without a magnetic core [1], for inducing mutual coupling between circuits; Transformers are exclusively used in electric power systems to transfer power between circuits with electromagnetic induction [2]. Power transformers used at each of the points where is a transition between voltage levels and for step-down operation, mainly used to feed distribution circuits the construction of a transformer depends upon the application. For instance, transformers intended for indoor use are primarily of the dry type but can also be liquid immersed for outdoor usage [3]. Most countries especially North African countries including Libya depends on the oil-cooled transformers especially the 30 kV transformers for their high efficiency to reach the highest conversion rate designed for it, where increasing the cooling rate of a transformer from increases its capacity. Cooling methods must not only maintain a sufficiently low average temperature but must prevent an excessive temperature rise in any portion of the transformer (i.e., it must prevent hot spots). For this reason, working parts of large transformers usually submerged in high-grade insulating oil [4]. However, transformers oil-cooled need constant monitoring is divided into self-monitoring which is a protective device designed to deal with the events of emergency on the transformers and be installed inside the operating room of the transformer. It can be divided into special protection devices transformers into two types, first Prevention mounted on body transformer. The second is the protection on the transformer circuit that deals with the problems of the transformer with the electrical network, Gas Relay, Oil Level Gauges, Lightning Arrestors, Protective Relay, Differential Protection, Over Current Protection, Bochholtz Relay and a Buchholz relay [5]. It is commonly known as the gas accumulation relay is constructed so that it accumulates all or a fixed portion of the gas released by the protected equipment. It operates when the volume of gas reaches a certain level [6]. In addition, human monitoring of manual handling of emergency events on transformers, which determines the type of control is the key next to the converter be either automatic or manual, where Libyan state has adopted a control management to manual monitoring oil-cooled transformers called operating management and monitoring. Its mission is to employ engineers who supervise the operation of transformers in alternating groups throughout the 24-hour to Follow-up the distribution of the required load efforts as well as the control of transformers from an emergency occurs to it as coolant Low oil level in the transformer tank. It increase load signals, and converter oil pressure signal Using Buchholz




ISSN 1737-9334

that consists of 2 Relays. The first to determine the level of transformer oil, and the second to sense the pressure of gases inside the transformer body pressed as the oil temperature rises send the sensor A signal that the heat of the transformer has risen to a protective or monitoring device for self- separating transformer. This increase in temperature usually caused by increased load, precisely at peak times during hotter or cooler weather, and human monitoring of manual handling of emergency events on transformers , which determines the type of control is the key next to the converter either be automatic or manual , especially During summer season, many power transformers are exposed to intensive, direct insolation. On the other hand, in recent years, the use of increasing number of air conditioning systems during summer caused growing trend of electrical load. As the consequence, blackouts of power transformers occurred during summer [7] often the gas pressure sensor often consumed mechanically because it contains mechanical movement. Consumption by reasons of loss of oil properties which prevents the movement of the mechanical sensor, and becomes compressed gas inside the adapter is unable to move the sensor mechanical to feel that the protection device that the temperature has risen. Then the monitoring will not disconnect the converter and then will cause serious damage if the engineer cannot turn off the converter because of his increasing voice, which indicates the increase of load [8]. If the engineer outside the power station severe damage to the transformer will cause damage and fire, and out of all the lines loaded on this converter, including vital lines for ex "such as sudden separation of electricity to the hospital care room " This is the most common problems which can be solved by solving the problem in installing the intelligent cooling system on the body of the transformer when reading the temperature in an instant manner by a sensor installed inside the poles off. The paper is structured in the following manner: in the section 2, system description is discussed. The installation and operation of the system is explained in section III. In section IV, the Simulation results is presented. Section V contains the conclusion.

## II. SYSTEM DESCRIPTION

The cooling problem in the transformers mentioned previously are common especially in 30 kv transformer in Libya. To prevent fires, increase periodic maintenance and preventing the development of calcifications in these types of transformers, a smart cooling system is designed in this paper. This system separates between control of transformer oil and temperature control heat the transformer electrodes and it is composed of 10 components.

### 1. Microcontroller (arduino)

This electronic circuit provides ports for connecting electronic components, The Arduino circuit also contains a 16-megahertz (Crystal Oscillator) with a USB port for connection to the computer, and a separate power input. Also, it contains a small atmega 328 chip [9], which is used in controlled programming by atmel. This electronic circuit is shown in Fig. 1.

Fig.1 A microcontroller

### 2. liquid crystal screen

In our work, this screen was used to display letters and numbers which is a 2x 16 screen [10] as shown in next figure.

Fig 2. Display

### 3. Sensors DS18B20

The way this sensor works is that when we give it in its 5 volts, the output exceeds 1 mV [11], per Celsius degree i.e. that at 1 ° C the output will be 1 mV. This sensor can read the temperature between 50 to 150 ° C [12]. Fig. 3 shows this type.

Fig. 3 DS18B20 sensor

### 4. Resistors

Fig.4 shows the resistors which their values among (560 ohms 10 K. ohms). These resistors are considered as the protection of micro-controller and they are placed on the entrances and exits of controlling.

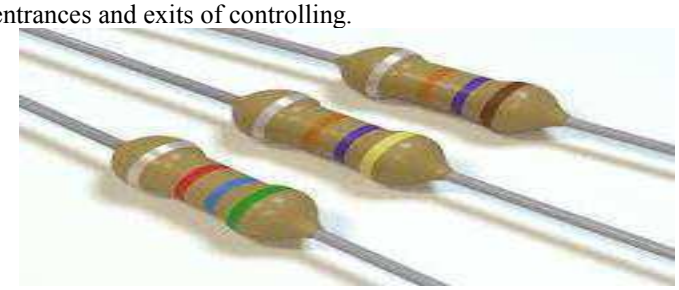

Fig5. Resistors

### 5. Relays

Fig. 5 shows the relay which works to relay a voltage and a small current to carry a large load and it advantages to lies in




ISSN 1737-9334

its ability to completely isolation between the source and load circuit.


Fig. 5 Relay

### 6. Light diodes

Some photovoltaic diodes are shown in Fig. 6.

Fig. 6 Light diodes (lamp)

### 7. Bipolar Digital Integrated Circuit ULN2803

Fig. 7 shows bipolar digital integrated circuit ULN2803. This integrated circuit operates when receiving signal from the Arduino connections [13].

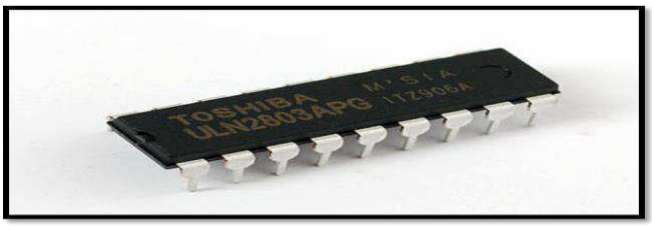


Fig. 7 ULN2803 piece full of transistors

### 8. Buzzer

Buzzer is shown in fig. 8.

Fig. 8 Siren

### 9. Fan

The type of the fan that using in our work is shown in the following figure.

Fig. 9 Fan

### 10. GSM SIM800

GSM SIM800 is in Fig. 10, and this device send a message sent by the controller.

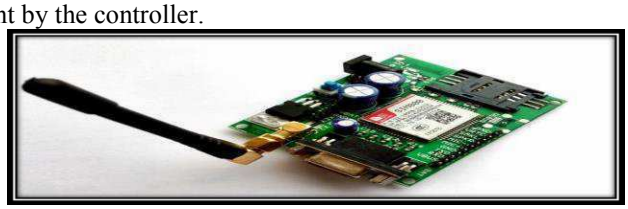

Fig. 10 GSM SIM800

## III. Installation and Operation of the System

First, the heat sensor is installed inside the transformer and the input of the transformer is installed and the fan is installed on the transformer oil cooling panels, outside the operating station. Then, the LCD display, red and green alarms and the alarm are all installed inside the operating station. Next, the signal cables are connected to the AVR to increase the capacity of the second transformer inside the station as well as the signal cable to connect the operating circuit to the vital line to load it on the second transformer after separating it from the first transformer. Finally, all the components will be connected to the control panel. The final form of this circuit is shown in Fig. 11. This system was programmed to include reference numbers for temperature. L was sent to the system by temperature sensor and was compared with reference numbers that were divided into four stages from 0 to 100 ° C, where these stages are less than 40 ° C of the hot spots that cause the transformers to collapse, which Will be at 140 ° C.


ISSN 1737-9334

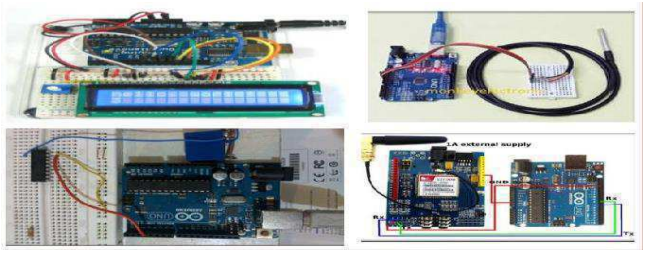

Fig. 11 Final assembly of a circle

When temperature inside the transformer is high, the sensor sends the temperature to the microcontroller, which compares it with the reference stages (Normal heat mode, High temperature, Very high temperature, Full closure for transformer for service) and this temperature is displayed on the screen LCD. On the basis of comparison results, the microcontroller selects function of the system, either by sending a signal to activate the fan on level the first or second, or Sends the signal to turn the lamp red or green, or Sends the signal to activate the siren to inform the supervising engineer that the transformer is at a critical stage, or Sends the signal to disconnect the transformer from service. Then, sends a message to a phone of the supervisor engineer of the operating station as a text message (the transformer temperature is very high and the transformer will be disconnected now from the service) to inform him about the situation of the transformer if the supervisor engineer outside the operating station. Thereafter, the system sends a signal to putting AVR device on automatic mode to raise capacity the second transformer that located at the same station. Then, the system sending two signals at the same time, first signal is sent to the" Fractionator" connection line which makes the vital line ready to connect to the second transformer that located on the same station, and the second signal is sent to connect the circuit device Siemens to the cutter of the vital line to be officially linked with the second transformer that located inside the station. The connection between the system and the transformer body is shown in Fig. 12 and Fig .13 is an illustrative scheme of the system's entrances and exits and finally, this system is considered as early warning and cooling system.

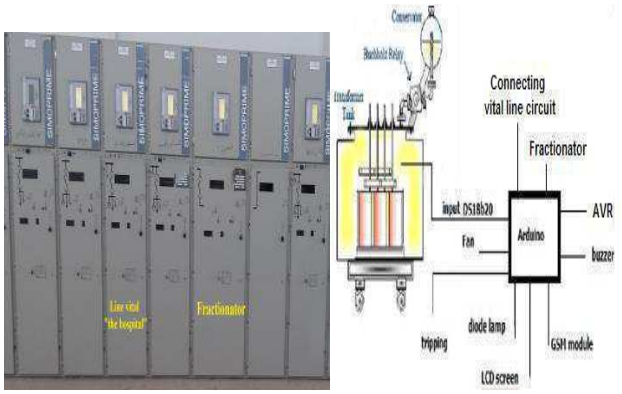


Fig .12 the connection between the system and the transformer.

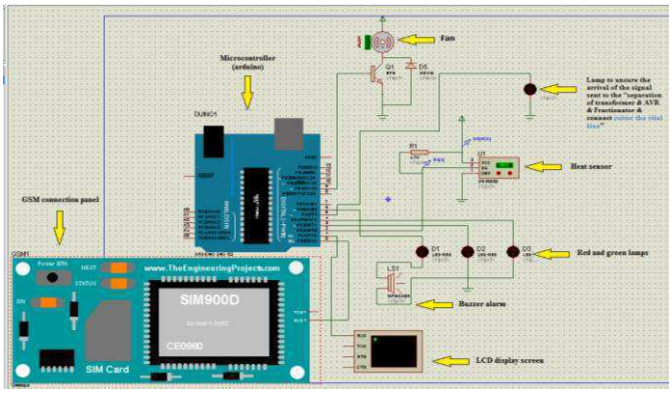


Fig .13 illustrative scheme of the system's entrances and exits

## IV. SIMULATION RESULTS

This intelligent system will be validate using the Proteus program, and all the pieces mentioned above will be selected. The most important component is the Arduino Plate and Fig. 14 shows the connection of all the components with each other.

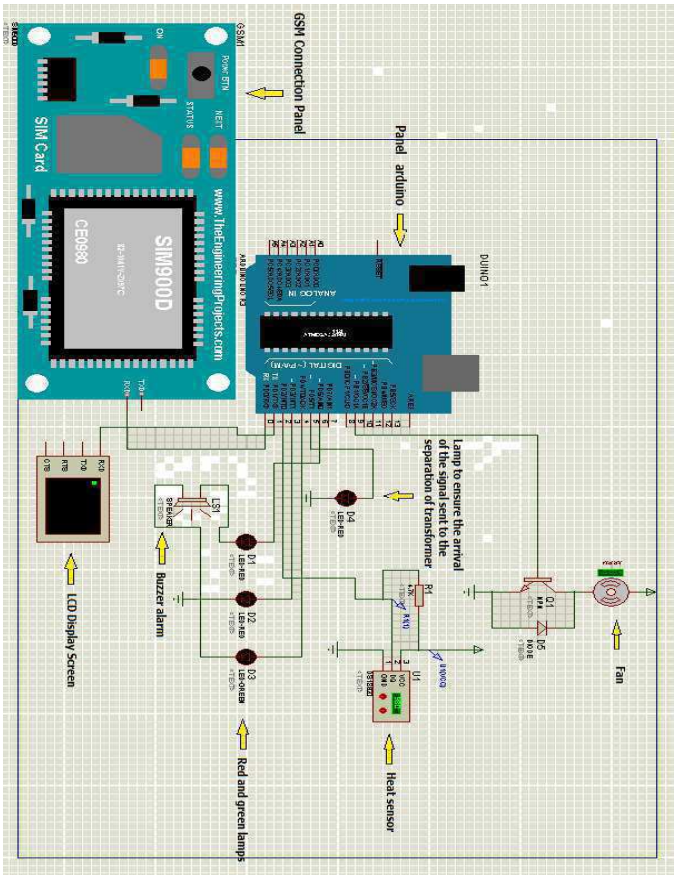


Fig.14 the Circuit Components Connection

First, the program is run and heat sensor readings is changed. On the basis of comparisons, a microcontroller defines the type of outputs (Display, green light, red light, alarm clock, signal wire connected to the separation circuit of a transformer and fan). The heat sensor measurement is




ISSN 1737-9334

considered as the input and it is displayed on the display screen and there are four comparison stages:

**1.** Normal stage: here, the temperature degree will be between (0-70) °C. In this stage, the microcontroller function is to run green lighting with momentary display on-screen of the temperature degrees that coming from the sensor. This stage is shown in fig. 15.

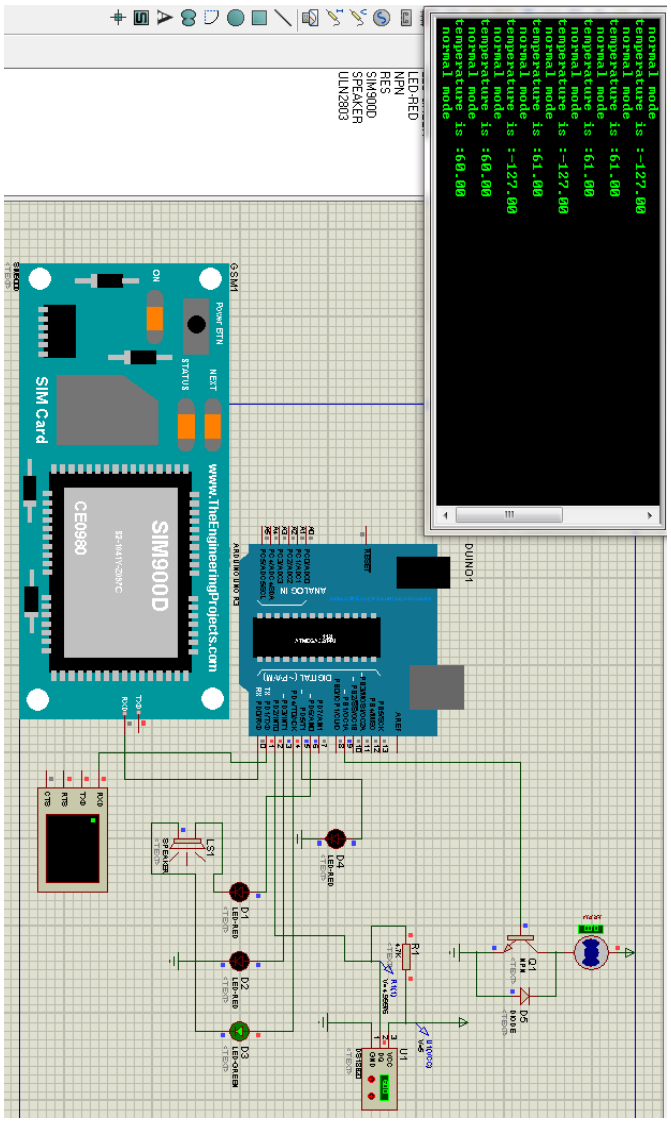


Fig.16 Normal Stage Mode

**2.** High temperature stage: In this part, a temperature will be between (70-80) °C. In this stage, the microcontroller function is to turn off the green light and replace it with red light as well as running the fan on the first level with an instantaneous display of temperature on the screen. The representation this stage is shown in Fig. 16.

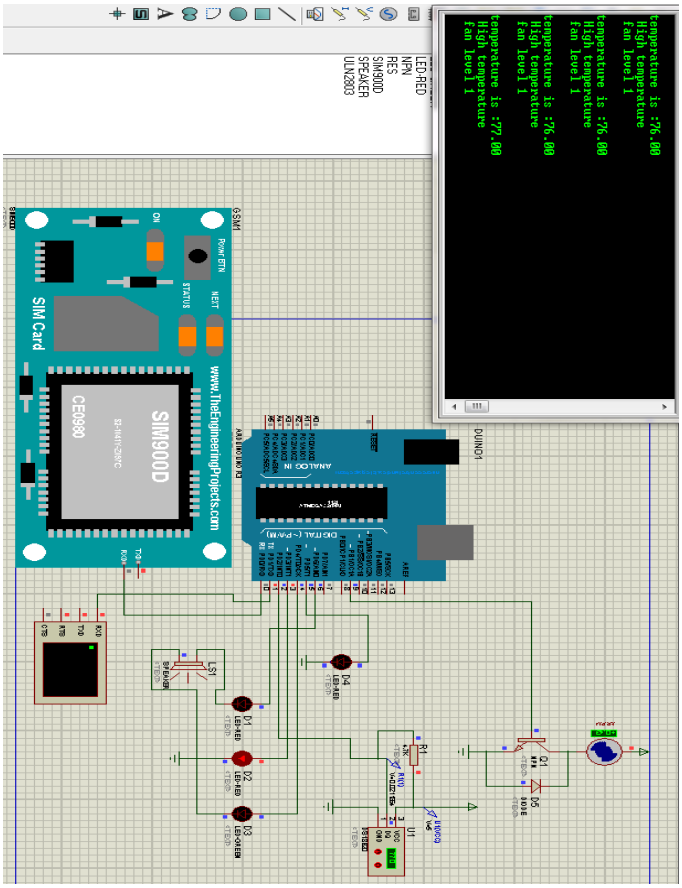


Fig. 16 High Temperature Stage

**3.** Very high temperature stage: In this part, a temperature will be between (80-90) °C. In this stage, the microcontroller function is to continue the red lighting as well as running the alarm clock. Also, the fan will be run on the second level. Fig. 17 shows this stage.




ISSN 1737-9334

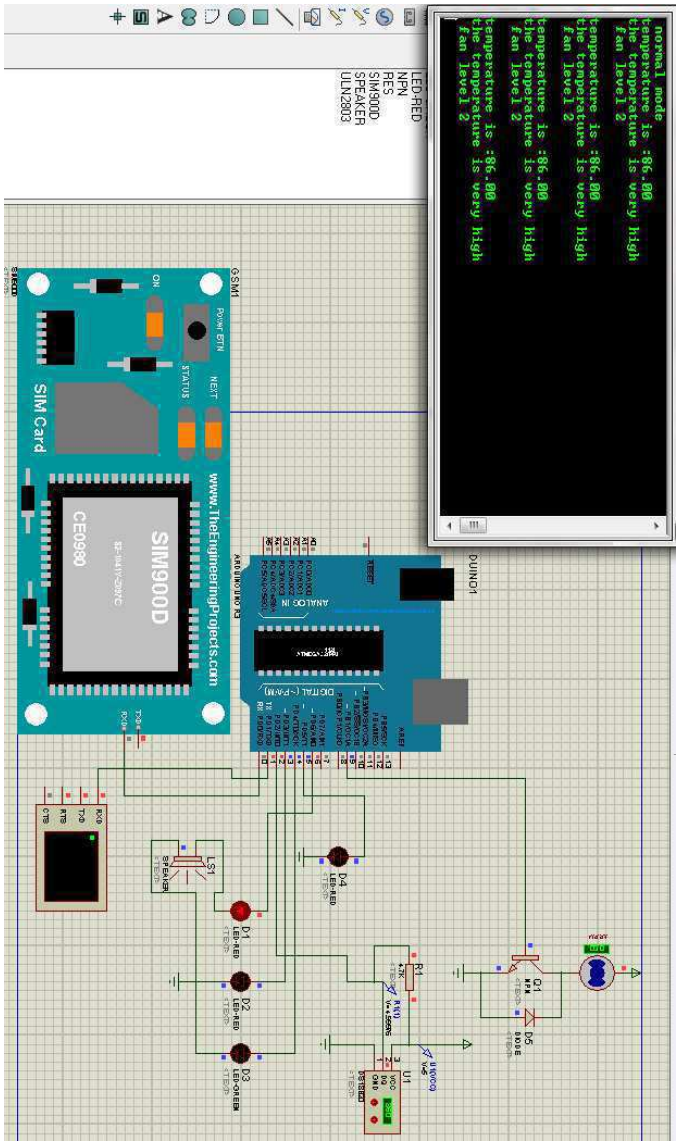


Fig. 17 Very High Temperature Stage

**4.** Full closure for transformer for service: Here, a temperature will be between (90, 100) °C. In this stage, the microcontroller function is continue to turn on the red light as well as the alarm clock and the fan on the second level until the temperature reaches 95 °C. Thereupon microcontroller will send a signal pulse to the line which will be linked to the separation circuit of a transformer (Off-duty). Also, the microcontroller works on extinguish the fan and the alarm will work continuously. Finally, a message will be sent by GSM. Then, the system will send a signal for putting AVR device on automatic mode to raise the capacity of the second transformer that located at the same station. Also, the system sends two signals at the same time, the system sends the first signal to the" Fractionator" connection line which makes the vital line ready to connect to the second transformer that located on the same station, and the system sends the second signal to the conduction circuit device Siemens. So as to connect the vital line (Previously separated) with the second transformer located inside the station. This stage is shown in fig. 18.

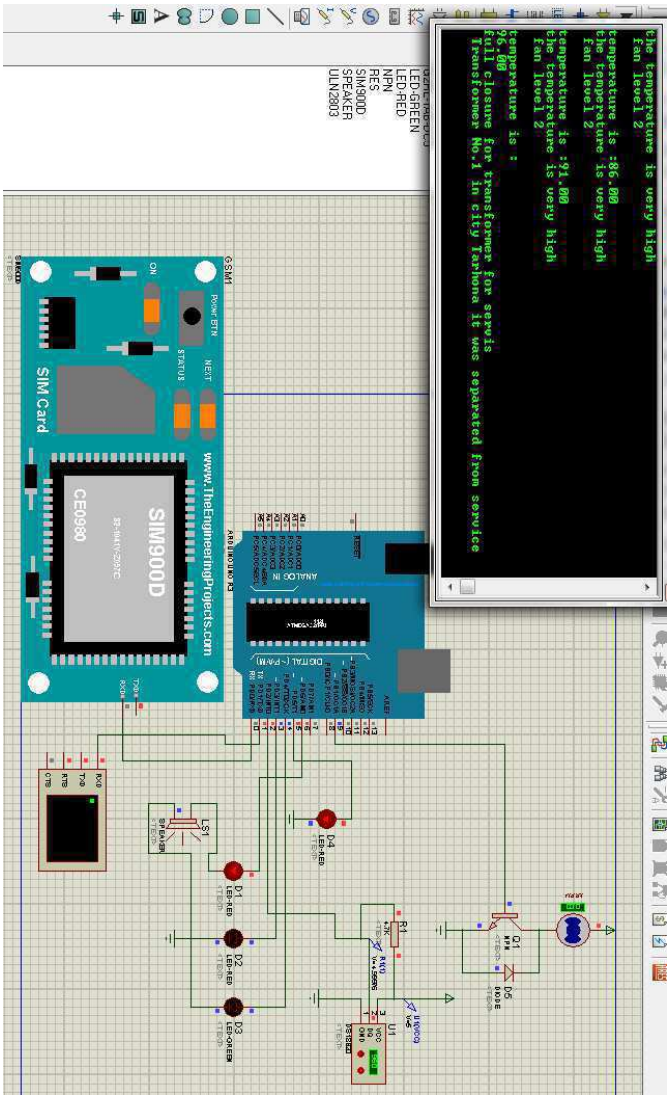


Fig. 20 Full closure of transformer

## V. CONCLUSIONS

The large error rate in the mechanic sensor Balbakhluz caused a combustion of several transformers in power grid, which commissioned the General Electricity Company in Libya huge amounts of money. In this paper, Intelligent System for Early Warning and Cooling from Very High Temperatures in Voltage 30 Kv transformers has been designed. Depending on this design, the transformers was kept from the unwanted rise in temperature and If the temperature is not controlled by this cooling system and the temperature has risen to the level of danger, the system will turn off the transformer to save it from the explosion. Then, the all lines loaded on the transformer will be separated including vital lines that cannot withstand the interruption of electricity "hospitals, educational institutions and other vital institutions. Then, this system sends a signal for putting AVR device on


ISSN 1737-9334

automatic mode to raise the capacity of the second transformer that located at the same station. Also, the system sends two signals at the same time, the system sends the first signal to the" Fractionator" connection line which makes the vital line ready to connect to the second transformer that located at the same station, and the system sends the second signal to the conduction circuit device Siemens so as to connect the vital line (Previously separated) with the second transformer located inside the station.

## REFERENCES

[1] S. V. Kulkarni and S. A. Khaparde. "Transformer engineering: design and practice,"Marcel Dekker, Inc, 2004.

[2] J. J. Winders, "Power Transformers Principles and Applications," Marcel Dekker, 2002.

[3] L. L. Grigsby, "Electric power Transformer Engineering," CRC Press LLC, 2004.

[4] "Transformers :Basics ,Maintenance, and Diagnostics ," Hydroelectric Research and Technical Services Group, April 2005,

[5] S. Sudipta, A. Chatterjee, and D. Sarkar. "Design of 132/33KV Substation," International Journal of Computational Engineering Research (IJCER) Vol, 03, |Issue, 7, July 2013.

[6] M. S. Sachdev and B. D. Nelson, "Terms Used by Power System Protection Engineers," IEEE Power System Relaying Committee, 1997.

[7] S. Maksimovich. S. Radojevich and V. M. Shiljkut, "The Influence of Direct Insolation on Outdoor Power Transformers Loadability," 21st International Conference on Electricity Distribution, June 2011.

[8] S. Aboalkasem, M. Alafram, H. Abdussallam, and A. Salem "Smart Cooling System for High Transformer," 5th International Conference on Green Energy and Environmental Engineering (GEEE-2018) Proceedings of Engineering and Technology, April 28–30, 2018, Sousse-Tunisia.

[9] J. Nussey, "Arduino for dummies," John Wiley & Sons, 2013.

[10] I, Volosyak, C. Hubert, and A. Gräser. "Impact of frequency selection on LCD screens for SSVEP based brain-computer interfaces," International Work-Conference on Artificial Neural Networks. Springer, Berlin, Heidelberg, 2009.

[11] X-F. Zhao, Q. Ba, L. Li, P. Gong and J-P. Ou, "A three-index estimator based on active thermometry and a novel monitoring system of scour under submarine pipelines," Sensors and Actuators, p.p 115-122. August 2012.

[12] M. Shahrestani, R.Yao, E. Essah, L. Shao, A. C., Oliveira, A. Hepbasli, E. Biyik, T. d. Caño, E. Rico and J. L. Lechón, "Experimental and numerical studies to assess the energy performance of naturally ventilated PV façade systems,". Solar Energy, p.p 37-51, 147, 2017.

[13] C. Hernández, R. Poot, L. Narváez, E. Llanes and V. Chi "Design and Implementation of a System for Wireless Control of a Robot," International Journal of Computer Science (IJCSI), Vol. 7, Issue 5, September 2010




ISSN 1737-9334

# A Novel Double Blumlein-Line Nitrogen Laser Circuit Analysis Based Distributed Parameters Model: Laser Source and Laser Amplifier

Mohamed O. Twati[#1], Mohammed N. Dorar[#2]

[#] *Electrical and Electronic Engineering Department, University of Tripoli*

[1]m.twati@uot.edu.ly

[2]M.Dorar@outlook.com

***Abstract*— In this paper, the analysis of a double Blumlein-line circuit that forms the oscillator – amplifier nitrogen laser system with one spark gap and based on a full-distributed parameter model is presented. The voltage, current and power waveforms outputs of the model are reported. The effect of the transmission line lengths, laser gap and spark gap parameters of the laser system on the output waveforms are studied and discussed. The simulation results presented here indicated that this analysis could be very useful and relatively more accurate than other models and techniques used for synchronization of the laser pulses between the laser oscillator and laser amplifier circuits. In addition this analysis is general and could be easily applied to study other laser systems such as metal vapour and carbon dioxide laser systems.**

***Keywords*— Blumlein-line; Fast discharge laser; Nitrogen laser; Laser amplifier; Pulse forming network.**

## I. INTRODUCTION

Although extensive studies and investigations that have been made on oscillator-amplifier (OSC-AMP) nitrogen lasers, operating on the 337.1 nm transition of the second positive band system, aimed at determining the optimum synchronization time between the laser oscillator pulses and the laser amplifier [1]-[3], still a lot of work has to be made concerning this issue. This include the selection of more adequate system design, accurate circuit models for simulating the laser system and the effects of the electrical parameters on the overall laser performance. The double Blumlein-line $N_2$ laser circuit (DBL) consists of two Blumlein-line pulse forming networks with one spark gap. One of them is working as an oscillator whereas the other as an amplifier. The pulse forming network consists of two parallel plate transmission lines (or coaxial cables) acting as energy storage capacitors, located at both sides of the cavity charged to high voltage Vo. When one side is short circuited, for instance using a spark gap, a transient voltage occurs across the laser cavity creating a gas discharge between the electrodes. The spark gap and the laser gap are usually represented by resistances and inductances. For the DBL, first, the light pulses is injected from the OSC to the amplifier via a set of reflecting mirrors and the synchronization between the laser oscillator pulses and the laser amplifier could be accomplished experimentally by varying the AMP gas pressure appropriately to reach the synchronization time condition between OSC and AMP sections and /or using the modeling and simulation results of the laser system to estimate the synchronization time [3]. Also, the synchronization could be achieved by using two park gaps, one for the oscillator and the other for the amplifier, and using a precise triggering circuits to synchronize the oscillator output with the peak amplifier discharge current [2]. Using two spark gaps and trigger circuits for synchronization purpose could make the system more complex and might reduce the accuracy in obtaining the synchronization time. Two concepts can be used in the analysis and modeling of the double Blumlein-line circuit, the lumped parameter model (LPM) and the distributed parameter model (DPM). However, LPM has the disadvantage of being valid only when the transit time on the transmission line is much smaller than the relative time constants of the spark gap and laser gaps [4].

This paper presents the theoretical analysis, electrical and optical output waveforms and the effect of some circuit parameters on the laser system performance of the double Blumlein-line




ISSN 1737-9334

$N_2$laser circuit that based on the DPM and using only one spark gap.

## II. The Double Blumlein-Line Differential Equations and Initial And Boundary Conditions

The schematic diagram and the mathematical configuration of the double Blumlein-line are shown in figures 1 and 2 respectively. For reasons of computational comfortability and simplifying the treatment with the mathematical model, the DBL is divided into four sections with three different zero coordinates. Two sections for each of the OSC and the AMP as shown in figure 2.

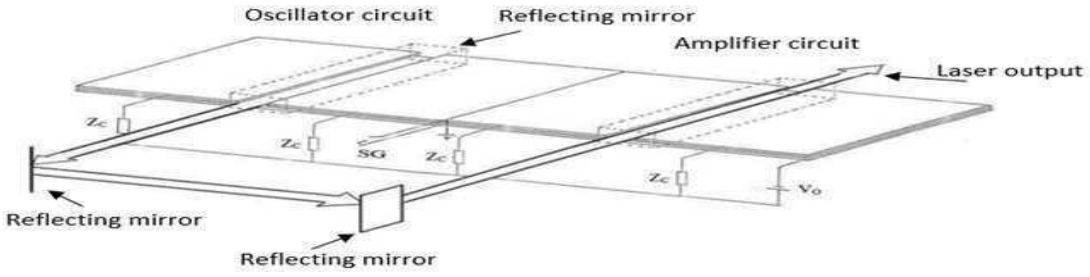


**Figure 1**. Schematic diagram of a transversely excited Blumlein circuit. Zc charging resistance; Vo: high voltage power supply; SG: spark gap.

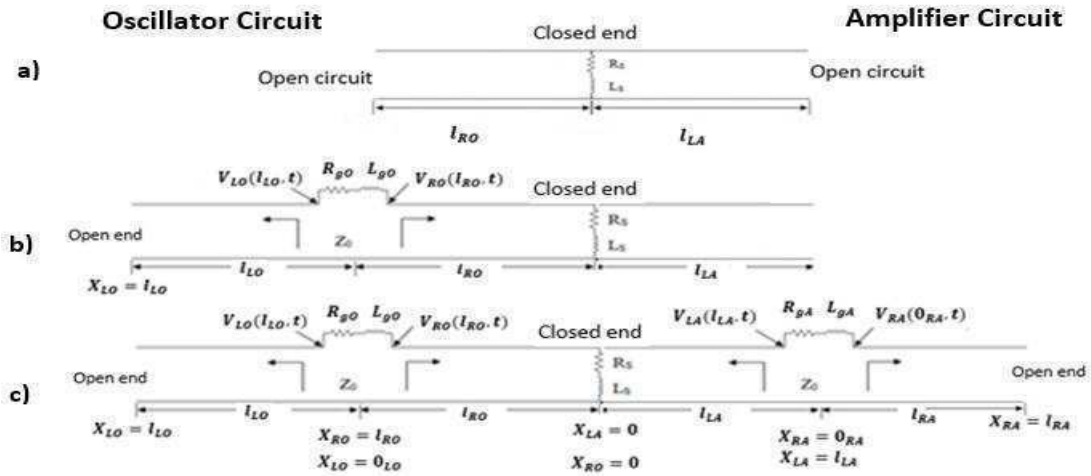


**Figure 2**. Mathematical configuration of the double Blumlein circuit. a): before breakdown of both OSC&AMP, b): after breakdown of OSC, c): after breakdown of both OSC& AMP; Zo: characteristic impedance.

For reasons of computational comfortability and simplifying the treatment with the mathematical model, the DBL is divided into four sections with three different zero coordinates. Two sections for




ISSN 1737-9334

each of the OSC and the AMP as shown in figure 2. The applicable partial differential equations for voltage V and current I on a section of transmission line of dx at any time t are given by,

$$\partial V_{ij}(x_{ij},t)/\partial x = -\bar{L}\,\partial I_{ij}(x_{ij},t)/\partial t \quad (1)$$

$$\partial I_{ij}(x_{ij},t)/\partial x = -\bar{C}\,\partial V_{ij}(x_{ij},t)/\partial t \quad (2)$$

where, $0_{ij} \le x_{ij} \le l_{ij}$, i = left (L) and right (R), and j = oscillator (O) and amplifier (A). $\bar{L}$ and $\bar{C}$ are the distributed inductance and capacitance per unit length respectively, and l is the total length of line section, where $Z_o$ ($Z_o = \sqrt{\bar{L}/\bar{C}}$) is the characteristic impedance of the line. The initial conditions are:

$$V_{ij}(x_{ij},0) = Vo \quad (3)$$

$$I_{ij}(x_{ij},0) = 0 \quad (4)$$

At the spark gap side $x_{RO} = x_{LA} = 0_{Sp}$, where $0_{Sp}$ is the spark-gap zero coordinate. Hence, the voltage boundary conditions at the end of the spark-gap can be written as:

$$V_{LA}(x_{LA},t) = V_{RO}(x_{RO},t) = V_{Sp}(0_{Sp},t) \quad (5)$$

$$V_{Sp}(0_{Sp},t) = -R_S[I_{Sp}(0_{Sp},t) + \tfrac{L_S}{R_S}\partial I_{Sp}(0_{Sp},t)/\partial t\,] \quad (6)$$

And the current boundary conditions as well can be written as:

$$I_{LA}(x_{LA},t) + I_{RO}(x_{RO},t) = I_{Sp}(0_{Sp},t) \quad (7)$$

The boundary conditions at the oscillator channel are:

$$V_{RO}(l_{RO},t) - V_{LO}(0_{LO},t) = L_{go}\partial I_{LO}(0_{LO},t)/\partial t + R_{go}I_{LO}(0_{LO},t) \quad (8)$$

$$I_{RO}(l_{RO},t) = I_{LO}(0_{LO},t) \quad (9)$$

The boundary condition at the open end of the oscillator is:

$$I_{LO}(l_{LO},t) = 0 \quad (10)$$

($L_S$ and $R_S$) and ($L_{go}$ and $R_{go}$) stand for inductances and resistors of the spark gap and laser gap of the oscillator, respectively.

Similarly, the boundary conditions for the amplifier section (amplifier channel & open end of the amplifier section) can be obtained just by interchanging the subscripts in the voltage and current equations of the oscillator by the amplifier subscripts. Therefore, the boundary conditions at the amplifier channel can be written as:

$$V_{LA}(l_{LA},t) - V_{RA}(0_{RA},t) = L_{gA}\partial I_{RA}(0_{RA},t)/\partial t + R_{gA}I_{RA}(0_{RA},t) \quad (11)$$

$$I_{RA}(0_{RA},t) = I_{LA}(l_{LO},t) \quad (12)$$

The boundary condition at the open end of the amplifier is:

$$I_{RA}(l_{RA},t) = 0 \quad (13)$$

where, $L_{gA}$ and $R_{gA}$ stand for the inductance and resistor of the amplifier laser gap respectively. The laser gap impedances in both the Oscillator and amplifier are not linear and must be treated as voltage dependent: as an open circuit before laser gaps breakdown and represented by a combination of ($L_{go}$& $R_{go}$) and ($L_{gA}$& $R_{gA}$) after laser gap breakdown. $I_{Sp}$ is the current passed through the spark gap inductance and resistance. $I_{RO}(l_{RO},t)$ and $I_{RA}(0_{RA},t)$ are the currents passed in the channel inductances of the oscillator and the amplifier respectively after laser gaps breakdown. This nonlinear behavior of the channel impedances, makes it necessary, in the time development of solution of the partial differential equations (8) and (11) to distinguish between three time intervals: the first one is before laser gaps breakdown, during which the state of only the right-hand side of the oscillator circuit and the left-hand side of amplifier circuit subject to the dynamical changes, whereas the left-hand side of the oscillator and the right-hand side of the amplifier remain in their initial state. The second time interval is after oscillator laser gap breakdown, in which the states of both sides of the oscillator and the left-hand side of the amplifier are time varying whereas the right-hand side of the amplifier remains in its initial state. The third time interval is after amplifier laser gap breakdown, in which the states of all sides are time varying.

## III. System of Equations for Optical Power Computation




ISSN 1737-9334

Equations for calculating the electrical waveforms behaviour (voltages and currents) of DBL have been derived and outlined in section 2. To obtain the equations that governing the temporal behaviour of the optical output power waveform of the DBL, two approaches can be utilized, the saturation approximation assumption and the general laser power assumption [5]. Here, the general laser power assumption is considered in calculating the output optical power.

According to Fitzsimmons' expression for relationship among the electron temperature, the instantaneous electric field E and the pressure P inside the laser channel [6], the electron density equation and the laser rate equations of the molecular nitrogen can be derived in term of (E/P). These equations are needed and will be used in obtaining the states densities and the optical output laser power. The Fitzsimmons' expression for the electron temperature, is given by [6]:

$$KT_e = 0.11(\mathrm{E/P})^{0.8} \tag{14}$$

The parameter *K* represents the Boltzmann's constant. The electron density equation can then be written as:

$$dn_e/dt = 4.06(10^{-3})n_e(\mathrm{E/P})^{4.7}\mathrm{P} \tag{15}$$

The laser rate equations are given by:

$$dN_C/dt = n_e N_o \sigma_{OC}(0.88/m\pi)^{0.5}(\mathrm{E/P})^{0.4} - \sigma_{Ostim}\, n_{ph} C(N_C - N_B) - N_C/\tau_C \tag{16}$$

$$dN_B/dt = n_e N_o \sigma_{OC}(0.88/m\pi)^{0.5}(E/P)^{0.4} + n_{ph} C(N_C - N_B) - N_B/\tau_B + N_C/\tau_C \tag{17}$$

$$dn_{ph}/dt = \sigma_{Ostim}\, n_{ph} C(N_C - N_B) - n_{ph}/\tau_{ph} + N_C/\tau_C \tag{18}$$

The electric field E is obtained from the voltage difference at the laser channels divided by channel electrodes separation *d* and can be written as:

$$[V_{RO}(l_{RO}, t) - V_{LO}(0_{LO}, t)]/d \tag{19}$$

All the above equations are applicable for both the oscillator and the amplifier sections, however, the subscripts in equation (19) should be changed for the amplifier section. $n_e$ is the electron density, $N_o$ ($\cong 3.2 \times 10^{16} P$) is the ground-state density which is assumed constant, $\tau_C$ is the radiative lifetime of the C-state (40ns) and $\tau_B$ is the radiative lifetime of the B-state (10$\mu$s). $\sigma_{OC}$ is the electron impact cross section of the state C and equals to $11.1 \times 10^{-18} cm^2$, whereas $\sigma_{OB}$ is the electron impact cross sections of the state B and equals $9.2 \times 10^{-18} cm^2$. $N_C$, $N_B$ and $n_{ph}$ are the number density of the C-state, the B-state, and the photons, respectively. $\tau_{ph}$ is the photon lifetime inside the laser tube. m is the electron mass ($9.2 \times 10^{-28}$g) and C is the speed of light. $\sigma_{Ostim}$ is the stimulated emission cross section ( $4.5 \times 10^{-15} cm^2$ ). Upon obtaining the electron density $n_e$ from equation (15), the above laser rate equations (16), (17) and (18) can then be solved.

## IV. Selection Of The Finite Difference Schemes And Computational Procedure

The voltages and currents solutions across the laser channels of the oscillator and the amplifier of the DBL can be obtained by using numerical schemes that based on the finite difference method. These are the forward, backward and central difference schemes along-with the" Lax-wendroff scheme". The schemes are applied to the partial differential equations and the boundary conditions of the DBL [4]. Standard numerical techniques were also used in solving the laser rate equations and the electron density equation to obtain the optical power output waveforms.

In order to apply the above mentioned schemes to the coupled partial equations (1) & (2) and to the boundary conditions of the DBL, it is convenient to decouple and normalize them first. The normalized and decoupled equations can be written as [7].

$$U_t = SBU_x \tag{20}$$

where, *S* is the phase velocity in the transmission line, and

$U_t = \begin{pmatrix} \partial u_1/\partial t \\ \partial u_2/\partial t \end{pmatrix}, U_x = \begin{pmatrix} \partial u_1/\partial x \\ \partial u_2/\partial x \end{pmatrix}, B = \begin{pmatrix} -1 & 0 \\ 0 & 1 \end{pmatrix}, \quad u_1 = u + i,$ $u_2 = u - i, u = V(x_{ij}, t)\sqrt{C}$ and $i = I(x_{ij}, t)\sqrt{L}$.

Now, discretization procedure in time and space should be applied to the problem equations before the application of the Lax-Wendroff and other finite difference schemes. The notations for an approximate value of u( $x_{ij,k}$ , $t_n$ ) at each point




ISSN 1737-9334

$(x_{ij,k}, t_n)$ in space and time, of the discretized problem is usually written as:

$$u(x_{ij,k}, t_n) = U^n_{ij,k} \quad (21)$$

where, $\Delta x = x_{ij,k+1} - x_{ij,k}$ is the increment in space and $\Delta t = t_{n+1} - t_n$ is the increment in tine. The system of equations (1) & (2) under the application of the Lax-Wendroff scheme becomes:

$$U^{n+1} = U^n + \lambda B D^1_0(U^n) + 0.5\lambda^2 B^2 D^1_+ D^1_-(U^n) \quad (22)$$

$U^n = \begin{pmatrix} U^n_{1,ij,k} \\ U^n_{2,ij,k} \end{pmatrix}$, $\lambda = S\,\Delta x/\Delta t$ and the different operators $D^1_0$, $D^1_+$ and $D^1_-$ are defined as follows:

$D^1_0(U^n_{ij,k}) = 0.5(U^n_{ij,k+1} - U^n_{ij,k-1})$, $D^1_+(U^n_{ij,k}) = (U^n_{ij,k+1} - U^n_{ij,k})$ and $D^1_-(U^n_{ij,k}) = (U^n_{ij,k} - U^n_{ij,k-1})$. The detailed process of the application of the Lax-Wendroff scheme can be found in previous work [3].

## V. Computational Results And Discussions

Upon completion of the application of the numerical schemes mentioned in the previous section and simulation of the DBL laser system, useful results were obtained. The effect of the spark gap inductance are simulated and illustrated. The 3D-plot of the output waveforms of the voltage variation for (OSC-AMP) is presented to clarify the operation dynamics. The values of the circuit parameters used in the simulation (shown in Fig. 2) that used in the simulation are: $\bar{C}$ =128.88nF/m, $\bar{L}$= 0.288nH/m, $R_{gO} = R_{gA}$ = 0.1Ω, $R_S$ = 0.0366Ω, $L_s = 13nH, l_{RO} = 0.2m, l_{LO} = 0.45m, l_{RA} = 0.45m,$ and $l_{LA} = 0.8m$. The parameter $Z_o$ is obtained from the expression $Z_o = \sqrt{\bar{L}/\bar{C}}$. The chosen value of $L_{gO}$ and $L_{gA}$ for the simulation is 3.2nH. The electrodes separation used in the simulation is 0.015m whereas their lengths and widths are 0.3m and 0.005m respectively. The pressure inside the laser tube is considered to be about 82Torr. The peak value of (E/P) across the laser channels is taken to be in the range of 100 to 140V/cm.torr. The electrical power is obtained from the expression $(I^2 R_{gA})$ and $(I^2 R_{gO})$ whereas the optical power is estimated from (18). In the waveform figures, the time is normalized by the propagation time on the spark-gap side transmission-line of the oscillator $T_r = l_{RO}\sqrt{\bar{L}\,\bar{C}}$.
Figure 3 shows the voltage waveforms variations of the oscillator and the amplifier, whereas figure 4 shows the current waveform variations.

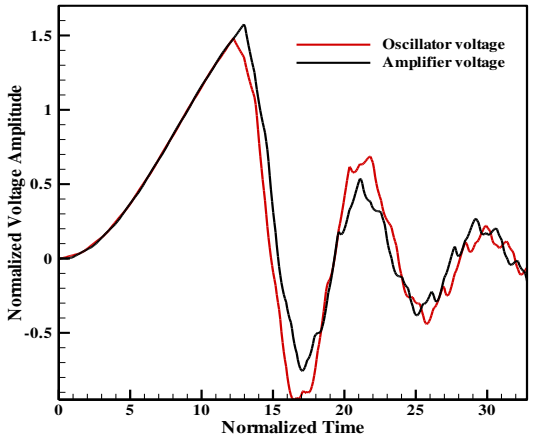


Figure 3. The laser channel voltages waveforms variations (OSC & AMP) with $L_s$ = 13nH, $l_{RO} = 0.2m$ and $l_{LA} = 0.8m$.

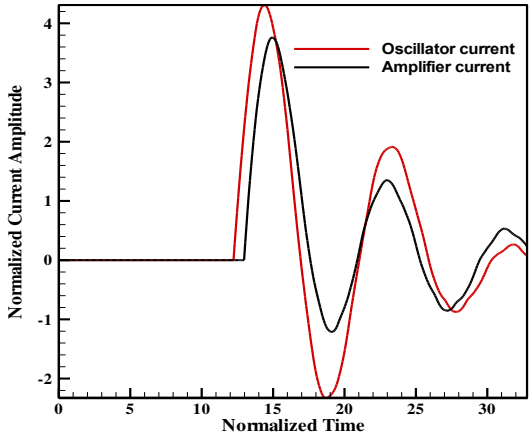


Figure 4. The laser channel currents waveforms variations (OSC & AMP) with $L_s$ = 13nH, $l_{RO} = 0.2m$ and $l_{LA} = 0.8m$.

The effect of the transmission-line lengths on the current waveforms variations as well as to the time of the peak currents occurrences is shown in figure 5. It is clear that the increase of $(l_{RO} = 0.4m)$ and the decrease of $(l_{LA} = 0.6m)$ reduces the time difference between the peak currents occurrences of the oscillator and the amplifier. Also the transmission-line lengths has an effect on the time of starting current peaks. Hence, the synchronization time between (OSC-AMP) will be affected. The effect of the spark gap inductance and laser gaps inductance are shown in figures 6 and 7 respectively.




ISSN 1737-9334

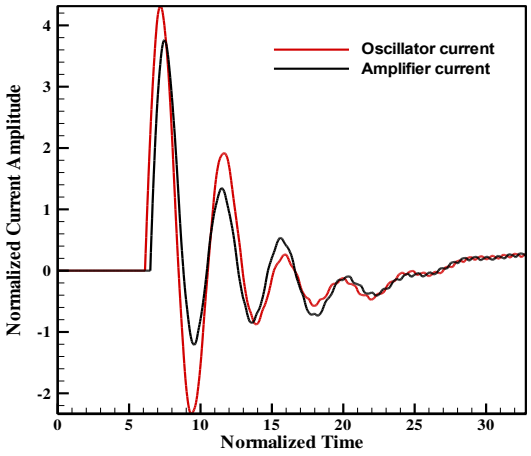


Figure 5. The laser channel currents waveforms variations (OSC & AMP) with $L_s$ = 13nH, $l_{RO} = 0.4m$ and $l_{LA} = 0.6m$.

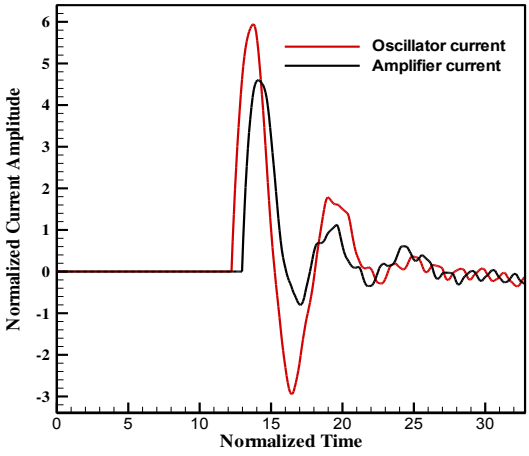


Figure 7. The laser channel currents waveforms variations (OSC & AMP) with $L_g$ = 1.2nH, $l_{RO} = 0.2m$ and $l_{LA} = 0.8m$.

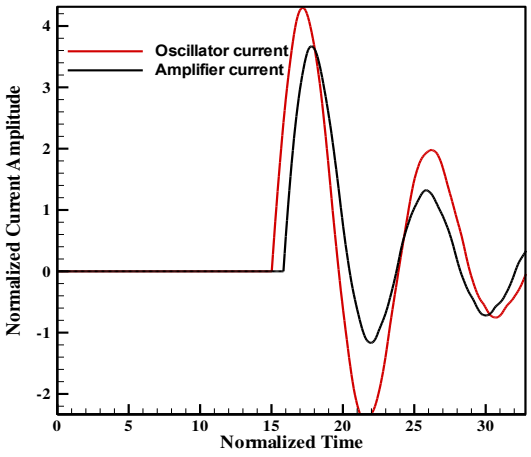


Figure 6. The laser channel currents waveforms variations (OSC & AMP) with $L_s$ = 20nH, $l_{RO} = 0.2m$ and $l_{LA} = 0.8m$.

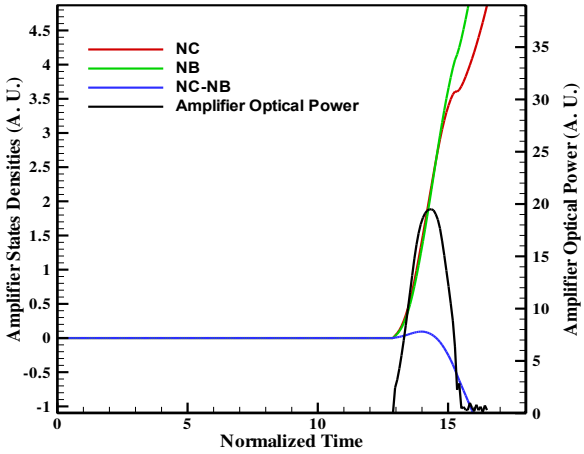


Figure 8. Shows $N_C, N_B, N_C - N_B$ and amplifier optical power waveforms.

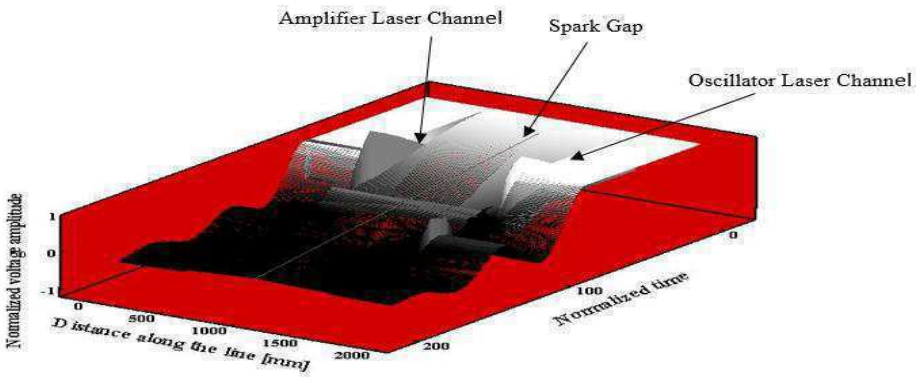



ISSN 1737-9334

Figure 9. A 3-D voltage waveform variations at all points and at any time along the DBL Line $N_2$ laser.

Figure 8 shows the waveforms of the density of the C-state, the B-state, and the optical power, as well as the density difference between the C and B states in the amplifier laser channel. The density of the C-state is appeared to be higher than that of the B-state for the first time span after the breakdown (~2.5Tr), then the density of the B-sates becomes higher for the rest of the time. This behaviour, however, is due to both the short lifetime of the C-state and the long lifetime of the B-state, and the density difference curves show this behaviour. The optical waveform of the amplifier shown in figure 8 represents the output as if the amplifier were not synchronized with the oscillator, however, the output would be increased if the reflecting mirror were arranged according to the computed synchronization time between the channel peak currents of the (OSC-AMP). For example, if the time difference between the two current peaks is 8ns, and since the transmission line length between the laser channels is 1m, and the phase velocity of the free space is $3x10^8$ m/s, the pulse will take 3.3333ns to travel from the OSC laser channel to the AMP laser channel, leaving 4.6670ns for reflector mirrors, which means 0.7m separation from the double Blumlein circuit for each mirror. That's the required time to align the output oscillator pulse with the peak value of the amplifier laser channel current. If the time between the current peaks changed, it would be better to change the mirror arrangements to make sure that the oscillator optical output reaches the amplifier channel while all the N2 molecules are excited and occupy the higher energy C state. The 3D voltage waveform variations at all points and at any time along the DBL circuit (OSC-AMP) using the DPM model is shown in figure 9.

## VI. CONCLUSIONS

In this paper we present a full distributed parameter model of the Double-Blumlein-line N2 laser with the use of decoupling approach of the laser rate equations from the electrical circuit equations that make the optical waveforms computations more simple. The electrical equations were first simulated in separate to obtain the voltages, currents waveforms variations. The effect of the transmission-line lengths, the spark gap inductance and the laser gap inductance on the output waveforms variations were carried out. The investigation results showed that the synchronization time between the OSC and AMP was highly affected by those parameters variations. Second, the optical power waveform of the amplifier was obtained by simulating the laser rate equations under the generalized condition in conjunction with the use of (E/P) values resulting from the simulation of electrical equations without using the reflected mirrors arrangements for synchronization. However, it is clear that the peak value of the amplifier optical power would be enhanced and amplified if the reflected mirrors arrangements for synchronization were considered.

Perhaps one of the most important result of this paper is that the mathematical model and the approach developed here could be used to optimize the (OSC-AMP) nitrogen laser system synchronization time, and to improve its performance over a wide range of parametric variations, since the computations here are based on the DPM, and the DPM was proved to be more accurate than convenient LPM. Also, in this model of the DBL, the synchronization could be achieved by using only one spark gap without the need of adding another spark gap with a precise triggering circuits to synchronize the oscillator output with the peak amplifier discharge current, and/or by varying the AMP gas-pressure appropriately to reach the synchronization time condition between OSC and AMP. I think the analysis presented here is quite general and could be applied to many other DBL (OSC-AMP) gas laser systems such as Cu-vapor, TEA CO2 laser, etc. Further experimental research will be pursued aimed at verifying the theoretical results experimentally and determining the optimum operating condition of the DBL (OSC-AMP) circuit.

## REFERENCES

[1] S. Panahibakhsh, S. Sarikhani, and A. Hariri, "Experimental and theoretical investigations for describing pressure dependence of amplified spontaneous emission output energy, small signal gain and electrical conductivity in nitrogen lasers," *Optik*, vol. 168, pp. 541–552, Sep. 2018.

[2] A.W. DeSilva, J.D. Sethian, and J. D. Sethiana, "A pulsed nitrogen laser for optical plasma diagnostics," Naval Research Laboratory, NRL Memorandum Report 6893, 1991.

[3] A. Hariri, M. Jaberi, and S. Ghoreyshi, "Nitrogen lasers: Optical devices of variable gain coefficient," *Opt. Commun*., vol. 281, pp. 3841–3852, Mar. 2008.

[4] Mohamed O. Twati, A. Ben Otman, "Distributed parameter analysis of a Blumlein-Line N2 Laser," *Opt. Commun.*, vol. 99, pp. 405-412, Jun. 1993.




ISSN 1737-9334

[5] Mohamed O. Twati, A. Ben Otman, "A Modified Approach for the Blumlein-line Laser Power Calculations: Electrical and Optical Power Waveforms," *Journal of Wireless Communications*, vol. 2, pp.1-6, Feb. 2017.

[6] Fitzsimmons W A, Anderson L W, Riedhauser C E and Vrtilek J M, "Experimental and Theoretical Investigation of the Nitrogen Laser," *IEEE J. Quantum Electron.*, vol. QE-12, pp. 624-633, New York Oct. 1976.

[7] C. R. Chester, *Technique in partial differential equations*, New York, USA: McGraw-Hill, 1971.




ISSN 1737-9334

# Blood Cells Segmentation by Using Thresholding Techniques

[1] Abdellatif BOUZID-DAHO
Department of Electronics
Faculty of Sciences of engineers
Laboratory LERICA, Badji Mokhtar University, Annaba, Algeria
E-mail: daholion@live.fr

[2] Nassim BOUKARI
Department of Electrical Engineering
Faculty of Technology
20 Août 1955 University, Skikda, Algeria

Mehdi BOUKROUH
Department of Electrical Engineering
Faculty of Technology
20 Août 1955 University, Skikda, Algeria

***Abstract*- In this paper, we present a segmentation method by thresholding for automated leukemia detection. This paper deals with the segmentation and threshold of blood cells for the purpose of detecting leukemia (abnormal blood cells). After the image acquisition and the preprocessing step, we proceeded to the application of the segmentation implemented in ImageJ. In order to show the interest of the proposed approach, we present the different cancerous regions identified with their characteristics for biomedical diagnostic aid. The proposed system is tested on image dataset and 96,63 % accuracy is achieved. The proposed system is successfully implemented in ImageJ, with the obtained experimental results are very encouraging.**

***Keywords : segmentation; thresholding; leukemia; abnormal blood cells.***

## I. INTRODUCTION

One of the fundamental processes in the chain of image processing is the segmentation. The segmentation is a difficult problem because we do not know a priori the type of textures present in the image to be analyzed, how many different textures are present and with which the region associate what texture or color. In fact, it is not necessary to know what exactly the existing textures are and what are the relevant colors ?

Automatic white blood cell segmentation which plays an important role in automatic blood cell morphology analysis remains a challenging issue because of the morphological diversity of WBCs and the complex background of blood microscopic images. In this paper, our focus is the leukemia detection using segmentation method by thresholding.

This study showed us all the problems that can be encountered in the field of medical imaging. And this especially when dealing with textured images as our research based on whole blood cells downloads [1]. This work allowed us to reflect on thresholding segmentation algorithms.

Segmentation is the process by which we determine the most important regions of an image. Here again, this process is extremely difficult to implement on highly textured images [2] for example microscopic WBC.

Some work on microscopic WBC image segmentation is available in the literature [3-5]. Treshold-based methods include Otsu's method [6].

Our paper is structured as follows. In section 1 we have described problematic of our work. In section 2 we discuss details the main steps of the proposed approach and in section 3 give experimental results and discussion. Finally, section 4 contains reference.

## II. PROBLEMATIC

A point of view the Medical blood cancer or leukemia with its different types remains a problem among hematologists for the detection of abnormal cells in the first stage of the patient. And a point of view technical, since, efforts of research Enormous have been carried out to develop new algorithms for clustering for the analysis by cluster.


ISSN 1737-9334

## III. METHODOLOGY

### A. *Medical context*

The type of microscopic medical images using on your work is the blood cells, which represents pathology [7]. Cancer of the blood, also known as leukemia, results from an excessive production of abnormal white blood cells [8]. They then fight infections more effectively and can interfere with the production of platelets and red blood cells, where the risks of anemia and bleeding disorders. There are many different types of leukemia. They are first classified by type of stem cell blood from which they develop.

### B. *Proposed system*

Our proposed system in this paper (Fig.1), contains two essential steps are, pretreatment of microscopic medical images after segmentation to identify abnormal blood cells based on the relevant element color.

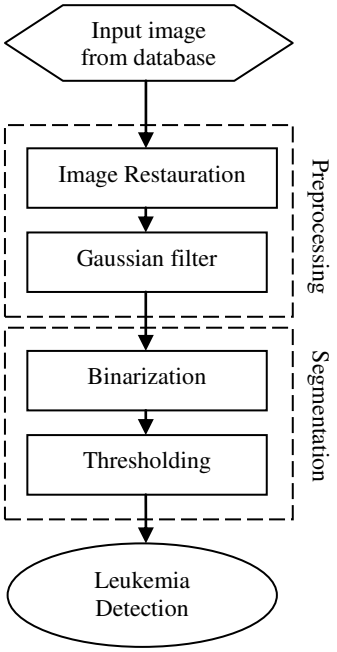


Fig. 1. Block diagram of the proposed algorithm

#### 1) *Database*

The proposed method was tested on 122 images taken from [9], a public and free, specifically designed for the evaluation and comparison of algorithms for segmentation and image classification. The images of the dataset have all been captured with an optical laboratory microscope coupled with camera with dimension 720*540.

The purpose of this step is to make all images to treat to a same size 256*256 for what is easy to manipulate by our method of segmentation.

#### 2) *Filtering*

In order to improve the visual effects of the image test filtering is necessary, which mainly includes the eliminate the noise and improve the quality of the image.

#### 3) *Testing procedure*

The threshold segmentation was implemented using (ImageJ) and tested the segment techniques on the image illustrated in the Fig 2.

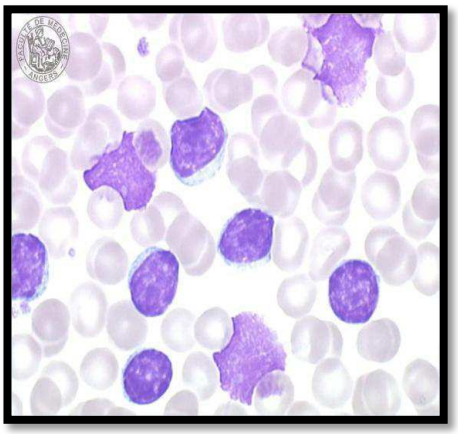

Fig. 2. Medical microscopic image (Blood Cell)

### C. *Segmentation by Thresholding technique*

This Threshold technique is one of the important techniques in image segmentation [10]. This technique can be expressed as:

$$T=T[x, y, p(x, y), f(x, y)] \quad (1)$$


ISSN 1737-9334

Where: T is the threshold value. x, y are the coordinates of the threshold value point. P (x, y) f(x, y) are points the gray level image pixels. Threshold image $g(x, y)$ can be define :

$$g(x,y) = \begin{cases} 1 & if\ f(x,y) > T \\ 0 & if\ f(x,y) \leq T \end{cases} \qquad (2)$$

## IV. RESULTS AND DISCUSSION

In this section we present the results of images segmentation that we have obtained. We have implemented the programs using ImageJ. The experimental results presented in this section show the efficiency of the thresholding segmentation method for the purpose [10]. environment and tested on a common PC Pentium (R) Dual-Core CPU Processor 2.20 GHz with 4 GB RAM.

### *A. Preprocessing*

In this step, we apply a Gaussian filter to reduce noise and improve image quality. (Fig.3)

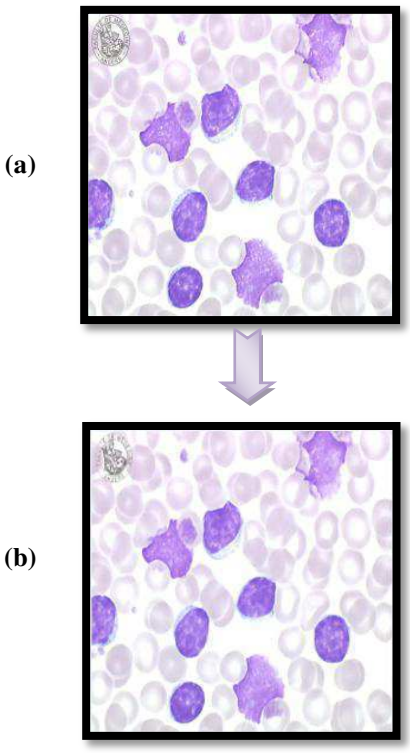


Fig. 3. Preprocessing: (a) Resizing initial image, (b) Image filter

### *B. Binarization*

Fig.4 shows the binarization that will enable to produce an image binarized matrix that is to say that a matrix containing values to 0 or 255 if we think on the whole [0..255], or 0 1 or when working across [0..1].




ISSN 1737-9334

Fig. 4. Binary image

### C. *Segmentation by thresholding*

Thresholding [12], as we have said, can produce an image in two classes. The object is represented by the color blue and the bottom of the green. The algorithm that results is very simple, just assign to all pixel having a gray level greater than the threshold value the green (bottom). If they are given the blue (leukemia) [13].

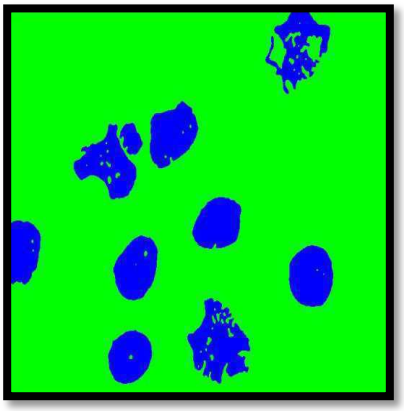

Fig. 5. Segmentation by thresholding

The histogram of our segmented image is shown in the following Fig. 6:

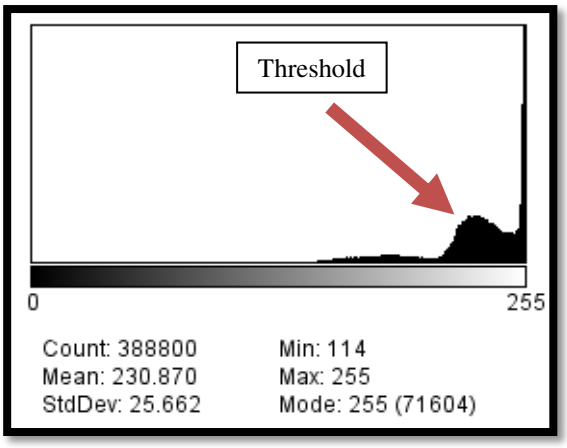


Fig. 6. Thresholding histogram

This histogram allows us to visualize the threshold of our segmentation, we tested on several image with this value of threshold = 205.

## V. CONCLUSION

In this paper, we have proposed a method to extract the cancerous regions of blood cells (leukemia). We have performed kinds of preprocessing the image restoration and Median filter before applying thresholding approach to Segment the image. This method is reasonably faster than manual approach and it helps in cancerous regions detection. Testing with blood cells datasets provided from the hematology service of the CHU Hospital. Finally, we will try to apply this approach on FPGA to test the algorithm in real time. This will make the object of our future work.

## *References*

[1] http://hematocell.univ-angers.fr/index.php/banque-dimages. (cons 2018)

[2] Bouzid-Daho, A., Boughazi, M., Tanougast, C., and Benali Medjahed, O.: ''Textural Analysis of Bio-Images for Aid in the Detection of Abnormal Blood Cells'', In International Journal of Biomedical Engineering and Technology, Vol. 25, N°. 1, pp. 1-13, (2017)

[3] C. Fatichah, M. L. Tangel, M. R. Widyanto, F. Dong, and K. Hirota, "Interest-based ordering for fuzzy morphology on white blood cell image segmentation," Journal of Advanced Computational Intelligence and Intelligent Informatics, Vol. 16, N°. 1, pp. 76-86. (2012)

[4] L. B. Dorini, R. Minetto, and N. J. Leite, "Semiautomatic white blood cell segmentation based on multiscale analysis," IEEE Journal of Biomedical and Health Informatics, Vol. 17, N°. 1, pp. 250-256. (2013)


ISSN 1737-9334

[5] M. Saraswat and K. V. Arya, “Automated microscopic image analysis for leukocytes identifcation: a survey,” Micron, Vol. 65, pp. 20-33 (2014)

[6] N. Otsu, “A threshold selection method from gray-level histograms,” Automatica, Vol. 11, N°. 285-296, pp. 23-27. (1975)

[7] Joshi, M.D., Karode, A.H., Suralkar, S. R.: White Blood Cells Segmentation and Classification to Detect Acute Leukemia. International Journal of Emerging Trends & Technology in Computer Science, vol. 2, N°. 3, pp. 147-151. (2013)

[8] Bouzid-Daho, A., Boughazi, M., Tanougast, C.: Segmentation of Abnormal Blood Cells to Aid Leukaemia Detection. Acta HealthMedica Journal, vol. 1 N°. 4, pp.12-17. (2016)

[9] Wei Zhu, Ruizhen Hu and Ligang Liu, "Grey conversion via perceived-contrast", The Visual Computer , Vol. 30, N°. 3, pp. 299-309 (2014)

[10] K. A. ElDahshan, M. I. Youssef, E. H. Masameer, and M. A. Hassan, “Comparison of segmentation framework on digital microscope images for acute lymphoblastic leukemia diagnosis using RGB and HSV color spaces,” Journal of Biomedical Engineering and Medical Imaging, Vol. 2, N°. 2, pp. 26-34. (2015)

[11] Purohit, P., Joshi, R.: A New Efficient Approach towards k-means Clustering Algorithm. International Journal of Computer Applications, vol. 65, N°. 11. (2013)

[12] Saleh Al-amri, S., Kalyankar, N.V, Khamitkar, S.D.; Image Segmentation by Using Thershod Techniques. Journal of Computing, vol. 2, N°. 5, pp. 83—86. (2010)

[13] Mishra, S.J., Deshmukh, A.P.: Detection of leukemia using matlab. International Journal of Advanced Research in Electronics and Communication Engineering, vol. 4, N°. 2, pp. 394-398. ( 2015)




ISSN 1737-9334

# The conventional commands for the robotic system

Amani Ayeb[#1], Abderrazak Chatti[#2]

[#]*Physical and Instrumentation Department, National Institute of applied sciences and Technology INSAT North urban center, BP 676, 1080 Tunis Cedex, Tunisia*

[1]ayeb.amani@gmail.com

[2]abderrazak_chatti@yahoo.fr

*Abstract*— **Many researches were realized for the robotics command in order to ensure the tracking of a desired reference trajectory. This current work concentrates on computed torque controller for robotic manipulator system by applying the linear and nonlinear control to ensure the position tracking. Indeed, the approach conventional control was applied to control a nonlinear dynamic system in order to displace the terminal organ of manipulator arm of an initial position towards any desired destination. The linear control allow us to linearize our system around a fixed point so-called an equilibrium point. Then, the application of the nonlinear control allows widening the application field. Simulations are presented to show the performance of the conventional control to guarantee the boundedness of the outputs robotic systems.**

***Keywords: Nonlinear systems, computed torque control, nonlinear control, position control***

## I. INTRODUCTION

In the last decades, the factories have been working faster than ever with the manipulator robots. The Manipulator arms have been widely used in industrial applications. Thanks to an adequate control, they accomplish the same task several times a remove day without errors and with great precision. As the manipulator arms are complex and non-linear systems, a number of theoretical and experimental studies attempt to develop robust commands based on new methods and algorithms. [1] [2] [3] [4]. By giving the complexity and nonlinearity of articulated systems, the use of mathematical tools becomes less effective in modelling and controlling such a process. However, several conventional control approaches [1] have been established to control these non-linear systems.

The question of the position control for robot manipulators is the choice of the appropriate torques so that the manipulator can follow the desired trajectory. Among these controls, there is linear control and nonlinear control. Indeed, this work proposes the realisation of a high-speed control of the robotic system. In order to have an accurate simulated model, the modelling of the robotic mechanical system 6 axis Staubli RX-60 has been done [5]. The dynamic model of three first links of six-axis Staubli RX60 robot has been developed according to the Lagrange-Euler formalism [6] [7] which translates the movement of the various articulations of the manipulator arm in order to validate the proposed controls. The linear approach will be used on the linearization of the equations of the robot's motion around an arbitrary chosen point of equilibrium. Then we implement the nonlinear control approach to extend the application field of our Robot Staubli RX-60. The present paper is organized as following. In section 2, we give a dynamic model of an industrial Staubli RX-60 wich has been done in the reference [5]. Then, the linear control is applied in section 3. Next, the nonlinear computed torque controller is designed in section 4. The conclusions are given in section 5

## II. DYNAMIC MODEL FOR CONTROL OF A ROBOTIC SYSTEM

The robot RX-60 is an articulated with 6 degrees of freedom. Staubli RX-60 is an anthropomorphous industrial non redundant robot with simple open structure (serial structure).

In this section, the dynamical model of the robot arm considers a relation between the joint torques/forces used by the actuators and the position, velocity and acceleration of the robot arm with respect to the time. The parameters of a dynamic model introduced here of a manipulator arm were estimated on experiments [5].

As reported Lagrange theory, a robot manipulator is described by the following equations:

$$J(\theta)\ddot{\theta} + H(\theta,\dot{\theta})\dot{\theta}+G(\theta)=U \quad (1)$$

$\theta, \dot{\theta}, \ddot{\theta}$ :Vector dimension nx1, respectively, positions, velocities and accelerations joint

$J(\theta) \in \mathbb{R}^{n\times n}$: Inertia matrix, positive definite symmetric matrix

$H(\theta,\dot{\theta}) \in \mathbb{R}^{n\times 1}$: Coriolis and centripetal forces vector

$G(\theta) \in \mathbb{R}^{n\times 1}$ : Gravity torques

$U \in \mathbb{R}^{n\times 1}$: Input torques

The last three joints of this manipulator which constitute the wrist are fixed at the zero(the positions $\theta_4 = \theta_5 = \theta_6 = 0$).The dynamic model for the first three joints of the Staubli RX60 robot arm is taken from [5] as follows in the relation :

$$\begin{bmatrix} U_1 \\ U_2 \\ U_3 \end{bmatrix} = \begin{bmatrix} J_{11} & J_{12} & J_{13} \\ J_{21} & J_{22} & J_{23} \\ J_{13} & J_{23} & J_{33} \end{bmatrix} \begin{bmatrix} \ddot{\theta}_1 \\ \ddot{\theta}_2 \\ \ddot{\theta}_3 \end{bmatrix} + \begin{bmatrix} H_1(\theta,\dot{\theta}) \\ H_2(\theta,\dot{\theta}) \\ H_3(\theta,\dot{\theta}) \end{bmatrix} + \begin{bmatrix} G_1(\theta) \\ G_2(\theta) \\ G_3(\theta) \end{bmatrix} \quad (2)$$

The expressions of the elements of the matrices J, H and the vector G are taken from the reference [5].

The demonstration and the calculation of elements of the matrix of the dynamic model is presented in the reference [5].

As of Staubli RX-60 manipulator dynamic formulation, this system is nonlinear, multi-input multi-output and uncertainly


ISSN 1737-9334

## III. LINEAR CONTROL :

The aim of modelling any process is to get the adequate command. First, we will implement a linear control based on the technique of linearization of the system's matrix writing around an equilibrium point fixed according to our choice.

The linear command is defined by the relation (3):

$$u = U_{eq} + V \quad (3)$$

The equilibrium state is represented by the following relations (4) and (5):

$$U_{eq} = G(\theta_{eq}) \quad (4)$$

$$\theta_{eq} = \theta - \varphi \quad (5)$$

With:

$U_{eq}$ : The torque required to maintain the robot to the equilibrium position

$\theta_{eq}$ : The static equilibrium position

$\varphi$ : The variation around equilibrium point

The linearization of the equation of motion around a chosen equilibrium point $\theta_{eq}$using the first order Taylor series approximation and substituting (5) into (1), we obtain the following relation (6):

$$J(\theta_{eq})\ddot{\varphi} + G(\theta_{eq}) + \left(\frac{\partial G}{\partial \theta}\right)_{eq} \varphi = U_{eq} + V \quad (6)$$

Substituting by (4) we obtain the matrix relation (7):

$$J(\theta_{eq})\ddot{\varphi} + \left(\frac{\partial G}{\partial \theta}\right)_{eq} \varphi = V \quad (7)$$

The matrix writing of the second order equation is rewritten by the following representation (8):

$$\dot{X} = A.X + B.V \quad (8)$$

with

$$X = \begin{bmatrix} \varphi \\ \dot{\varphi} \end{bmatrix}_{6\times 1} \text{ : System state vector} \quad (9)$$

$$\dot{X} = \begin{bmatrix} \dot{\varphi} \\ \ddot{\varphi} \end{bmatrix}_{6\times 1} \quad (10)$$

$$A = \begin{bmatrix} \mathbb{O}_{3\times 3} & \mathbb{I}_{3\times 3} \\ -J^{-1}(\theta_{eq})\left(\frac{\partial G}{\partial \theta}\right)_{eq} & \mathbb{O}_{3\times 3} \end{bmatrix}_{6\times 6} \text{ : State Matrix} \quad (11)$$

$$B = \begin{bmatrix} \mathbb{O}_{3\times 3} \\ J^{-1}(\theta_{eq}) \end{bmatrix}_{6\times 3} \text{ : order Matrix} \quad (12)$$

➢ *Stability and controllability of the robotic system*

In order to develop a control of a system, we study the stability of dynamical system by calculating the eigenvalues of matrix A. The condition of stability is explained by all eigenvalues of state matrix A have negative real parts. These eigenvalues are only the roots of the characteristic polynomial showed by the relation (13):

$$\det(\lambda I - A) = \lambda^2 I + J^{-1}(\theta_{eq})\left(\frac{\partial G}{\partial \theta}\right)_{eq} = 0 \quad (13)$$

According to the above equation, the robotic system is always unstable in open loop. In order to ensure local stability around a point of equilibrium and to design a feedback controller so that the process goes from any initial state $X_0$, to a specified desired state $X_T$, in some finite time. , the controllability of the system must be verified. . We proceed to calculate the matrix Q:

$Q = (B, AB, \ldots., A^5B)$. A necessary and sufficient condition for the complete controllability is that matrix Q is full rank.

$$Q = \begin{bmatrix} \mathbb{O}_{3\times 3} & J^{-1}(\theta_{eq}) \\ J^{-1}(\theta_{eq}) & \mathbb{O}_{3\times 3} \end{bmatrix}_{6\times 6} \quad (14)$$

The matrix Q is full rank so our system is controllable. This leads to the possibility of controlling our robotic system.

➢ *Linear control law synthesis*

We focus mainly on the design of a torque control U which ensures the displacement of our manipulator arm from an initial position $\theta_0, \dot{\theta}_0$ and $\ddot{\theta}_0$ to an equilibrium position $\theta_{eq}, \dot{\theta}_{eq}$ and $\ddot{\theta}_{eq}$.

We will ensure the stability in closed loop by the state feedback V.

$V = K.X = K_1.\varphi + K_2\dot{\varphi}$ Avec $K \in \Re^{3\times 3}$ : the position feedback gains $K_1$ and the velocity feedback gain $K_2$ are defined by the following differential equation:

$\ddot{\theta} + \Lambda_1\dot{\theta} + \Lambda_2\varphi = \mathbb{O}_{6\times 6}$ Avec $\Lambda_1$ et $\Lambda_2 \in \Re^{3\times 3}$ which present the poles imposed on the robotic system.

These are two diagonal matrices that represent respectively the sum matrix poles and the product matrix poles. So our system is written as follows in the relation (15):

$$J(\theta_{eq})\ddot{\varphi} + \left(\frac{\partial G}{\partial \theta}\right)_{eq} \varphi = K_1.\varphi + K_2\dot{\varphi} \quad (15)$$

Finally, the linear control applied to our robotic system as following (16):

$$U = U_{eq} + V = G(\theta_{eq}) + K_1.\varphi + K_2\dot{\varphi} \quad (16)$$

With:

$$K_1 = -J(\theta_{eq}).\Lambda_2 + \left(\frac{\partial G}{\partial \theta}\right)_{eq} \text{ and } K_2 = -J(\theta_{eq}).\Lambda_1 \quad (17)$$

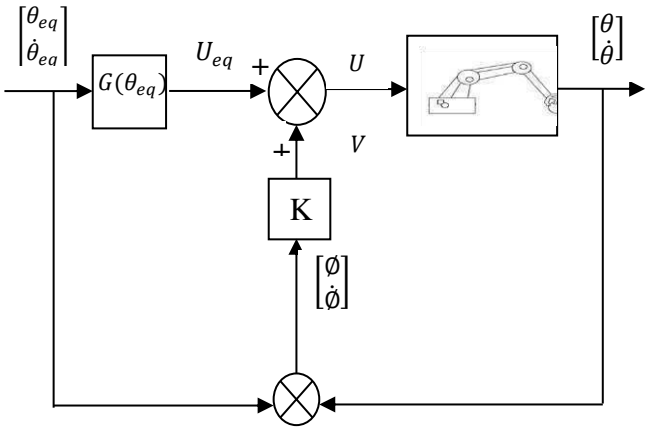


Fig. 1 Block diagram of linear control


ISSN 1737-9334

➢ *Simulation of the linear control*

To begin we choose the vector of the initial position in degrees $\theta_0 = [\theta_{01} \quad \theta_{02} \quad \theta_{03} \quad \dot{\theta}_{01} \quad \dot{\theta}_{02} \quad \dot{\theta}_{03}]^T = [0 \quad 0 \quad 0 \quad 0 \quad 0 \quad 0]^T$ and the vector equilibrium position in degrees $\theta_{eq} = [45 \quad 45 \quad 45 \quad 0 \quad 0 \quad 0]^T$.

Next, the angular position gain matrix K1 and the angular velocity gain matrix K2 are calculated by placing the poles of the system at (-8). Hence the values $\Lambda_1 = 16 \times \mathbb{I}_{3\times3}$ and $\Lambda_2 = 64 \times \mathbb{I}_{3\times3}$.

The simulation results:

$$A = \begin{bmatrix} 0 & 0 & 0 & 1 & 0 & 0 \\ 0 & 0 & 0 & 0 & 1 & 0 \\ 0 & 0 & 0 & 0 & 0 & 1 \\ 0 & 0.0215 & 0 & 0 & 0 & 0 \\ 0 & 4.3308 & 0 & 0 & 0 & 0 \\ 0 & -3.9458 & 0 & 0 & 0 & 0 \end{bmatrix};$$

$$B = \begin{bmatrix} 0 & 0 & 0 \\ 0 & 0 & 0 \\ 0 & 0 & 0 \\ 0.1289 & 0.0009 & -0.0004 \\ 0.00030 & 0.1748 & -0.1593 \\ 0.0002 & -0.1593 & 1.8098 \end{bmatrix};$$

$$K_1 = \begin{bmatrix} -496.5120 & 2.5812 & 0.1257 \\ 0.8304 & -422.8159 & -35.0276 \\ 0.1257 & -35.0276 & -38.4448 \end{bmatrix};$$

$$K_2 = \begin{bmatrix} -124.1280 & 0.6453 & 0.0314 \\ 0.2076 & -99.5102 & -8.7569 \\ 0.0314 & -8.7569 & -9.6112 \end{bmatrix}$$

The curves obtained at the angular positions are showed by the figure 2 as follows:

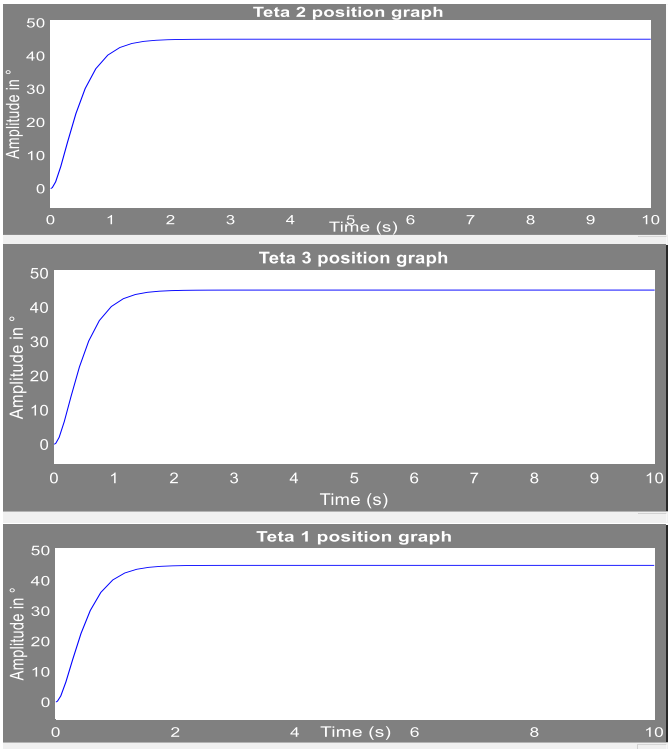


Fig. 2 Angular positions of the Staubli RX60 robot at the linear control case

The angular positions converge towards the desired values of equilibrium point. So the linear control ensures the local stability of the system. But, it does not present the adequate control for the robotic system. It has limitations.

## IV. NONLINEAR COMPUTED TORQUE CONTROLLER :

In this research, we focus on design nonlinear robust controller that guarantee stability, little tracking error and superb perturbation rejection.

This work is interested in the dynamics of the first three joints of the articulated mechanical system. The last three joints of this manipulator which constitute the wrist are fixed at the zero that is the angular positions $\theta_4 = \theta_5 = \theta_6 = 0$ the angular velocities $\dot{\theta}_4 = \dot{\theta}_5 = \dot{\theta}_6 = 0$ and the angular accelerations $\ddot{\theta}_4 = \ddot{\theta}_5 = \ddot{\theta}_6 = 0$.

We concentrate mainly to design a torque control U that ensures the displacement of our manipulator arm from an initial position $\theta_0, \dot{\theta}_0$ and $\ddot{\theta}_0$ to desired position $\theta_{des}, \dot{\theta}_{des}$ and $\ddot{\theta}_{des}$. The nonlinear computed torque control guarantees the global stability while compensating the non-linear part of the robotic system and imposing a stable dynamic loop.

The dynamics imposed by the following reference model presented by the relation (18):

$$\ddot{\theta} + \Lambda_1\dot{\theta} + \Lambda_2(\theta - \theta_{des}) = \Theta_{3x3} \quad (18)$$

Once the reference model is imposed, the nonlinear control by position and velocity feedback is developed using the dynamics of our robotic system and the dynamics of the reference model.

$$J(\theta)\ddot{\theta} + H(\theta, \dot{\theta}) + G(\theta) = U \quad (19)$$

The equation of the reference model can be put in the following form showed by (20):

$$\ddot{\theta} = -\Lambda_1\dot{\theta} - \Lambda_2(\theta - \theta_{des}) \quad (20)$$

By substituting equation (20) into equation (19), we obtain the nonlinear control law presented by equation (21).

$$U = J(\theta)\left(-\Lambda_1\dot{\theta} - \Lambda_2(\theta - \theta_{des})\right) + H(\theta, \dot{\theta}) + G(\theta) \quad (21)$$

The figure 3 shows the block diagram of the nonlinear control of the robot. It's about two feedback loops which a tracking error loop is an outer loop and a compensate loop is an inner loop

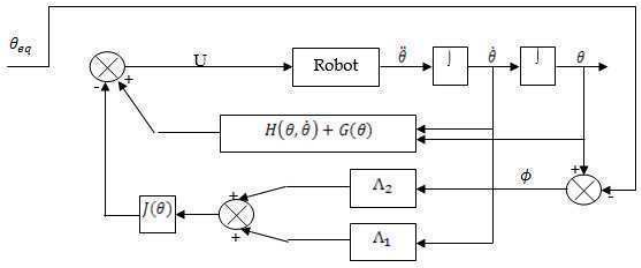


Fig. 3 Block diagram of nonlinear control

In this part we will apply the nonlinear feedback position and velocity robot arm control in order to move the terminal

organ of the manipulator arm from an initial position $\theta_0$ towards a final position $\theta_{des}$.

➢ *Simulation of the nonlinear control*

We will validate these results by simulations on Matlab Simulink environment. First, we choose the initial positions vector in degrees $\theta_0 = [0\ 0\ 0\ 0\ 0\ 0]^T$ and the Final positions vector in degrees $\theta_{des} = [10\ 10\ 10\ 0\ 0\ 0]^T$

Then, we proceed to calculate the angular position gain matrix $\Lambda_1$ and the angular velocity gain matrix $\Lambda_2$ by placing the poles of the system to -4. Hence the values $\Lambda_1 = 8 \times \mathbb{I}_{3\times3}$ and $\Lambda_2 = 16 \times \mathbb{I}_{3\times3}$.

The simulation of the evolution of positions and angular velocities was carried out over a period of 10 seconds.

The simulation of the angular positions are showed by the figures 4 and 5.

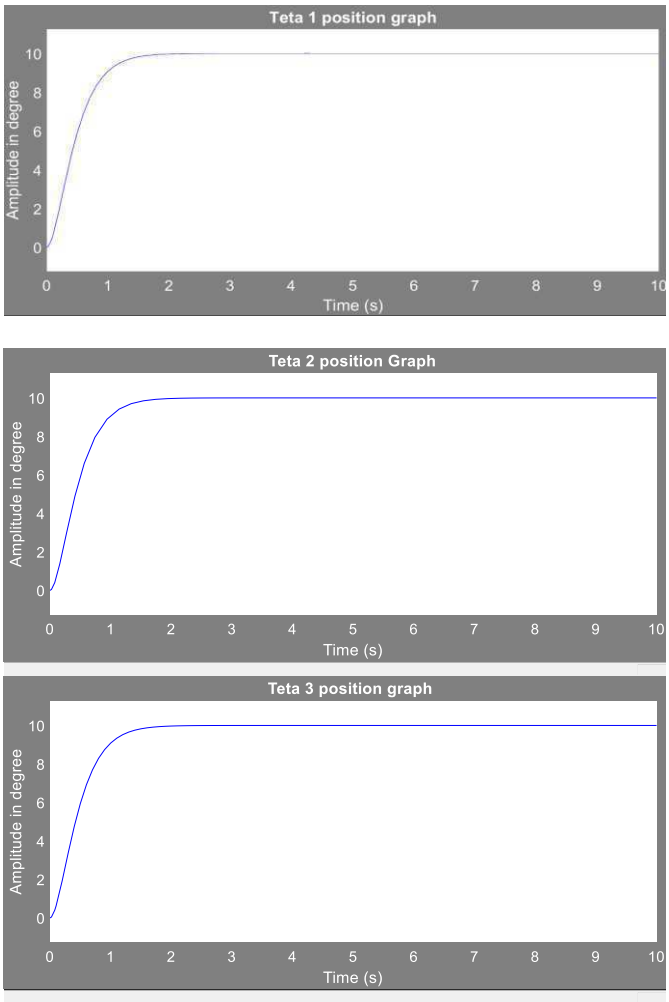


Fig. 4: Angular positions of the Staubli RX60 robot at the nonlinear control case

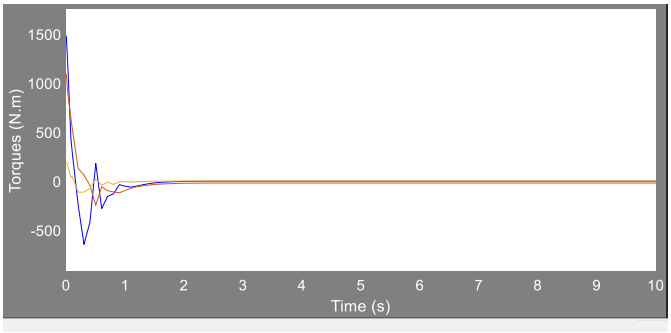


Fig. 5: Variation of the torques applied to the Staubli RX-60 provided with the nonlinear control by position and velocity feedback

To confirm the pertinence of the nonlinear control, it is proposed to attain a target in presence of uncertainty in unstructured input (e.g. disturbance). The simulation results in the presence of disturbance are given in the figures 6 and 7. The measurement noise is used the Simulink block diagram as white noise.

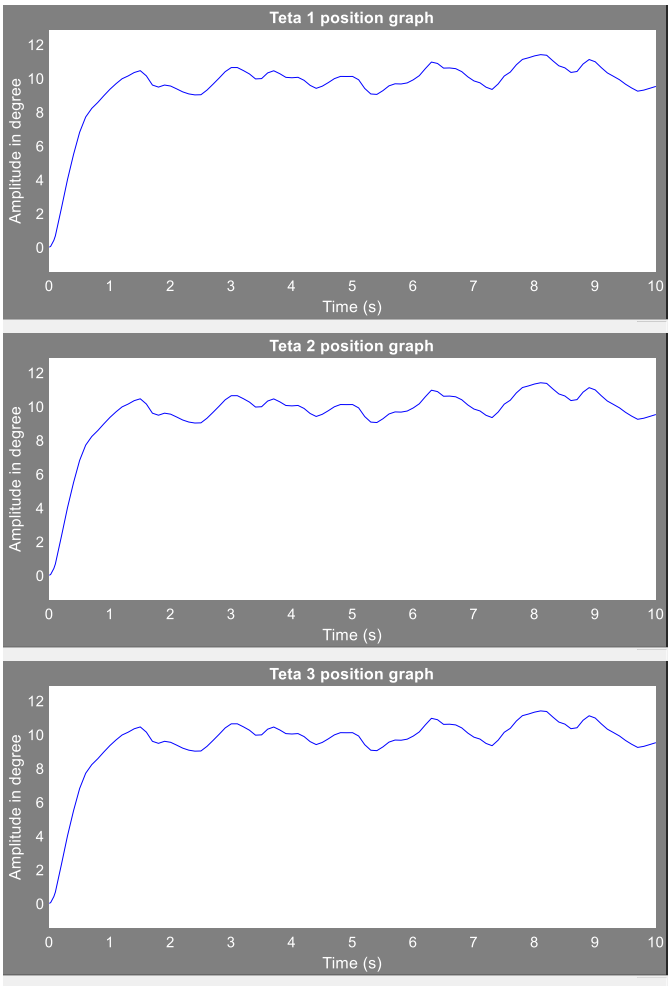


Fig. 6 ***Angular positions of the Staubli RX60 robot at the nonlinear control case in the presence of external disturbance***




ISSN 1737-9334

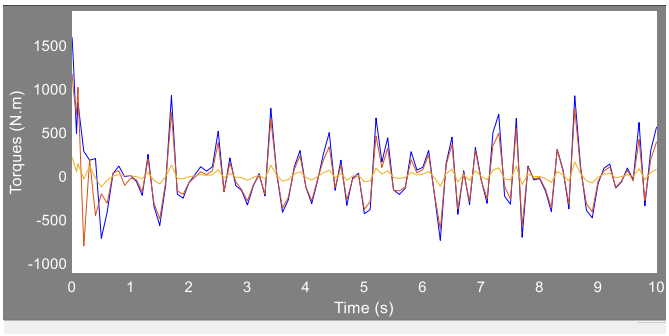


Fig. 7: Variation of the torques applied to the Staubli RX-60 in the presence of external disturbance

This command ensures the global asymptotic stability system. But the disadvantage of such control is the sensitivity against the uncertainties and disturbances. On the other hand, the modelling of a complex system is not always precise. So, we design the nonlinear feedback control of position, velocity and acceleration to improve the performance the behaviour of the robot in different circumstances.

Substitution of the equation's the reference model (18) in the equation of the dynamics of the robot (1), we get the control law:

$$U = (J(\theta) + I)\ddot{\theta} + H(\theta,\dot{\theta}) + G(\theta) + \Lambda_1\dot{\theta} + \Lambda_2(\theta - \theta_{des}) \qquad (22)$$

The figure 8 shows the control loop of the nonlinear control by position, velocity and acceleration feedback:

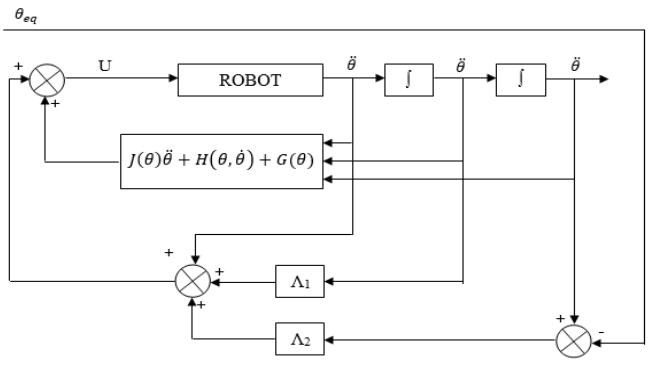


Fig. 8 Block diagram of nonlinear control by position, velocity and acceleration feedback

The same curves as the nonlinear feedback control of position and speed are obtained with and without incorporating external disturbance. So, the computed torque controller is able to hold each link at a particular angle but it is so sensible against unmodeled dynamics.

## V. CONCLUSIONS

We studied nonlinear controller applied to control of robot manipulator to achieve the specified joint acceleration, velocity and position state. This strategy guarantees accurate tracking in joint space and stability. We implemented the PD-computed torque controller on a dynamic modeling in MATLAB/SIMULINK environment. This designed controller is tested by band limited white noise with a predefined 40% of relative to the input signal amplitude which the sample time is equal to 0.1. These tools become less effective and less robust against disturbances and uncertainties and / or inaccuracy. Faced with this problem, the use of unconventional learning approaches has become a necessity in order to develop a command able to tolerate the uncertainties and neutralize the effect of external disturbances.

## REFERENCES

[1] Wisama Khalil, Etienne Dombre (1999), " *Modélisation, Identification et Commande des Roobots"*, Hermes Science Publications, Paris.

[2] M. Spong, M. Vidyasagar, "Introduction to robotics. Robot dynamics and control", MIT Press, Cambridge, 1989.

[3] Freeman, R et P. Kokotovix (1995) " Optimal Nonlinear controllers for feedback linearizable system" In Proc. The Amer Contr ConfSeattle, Washington, pp2722-2726

[4] Ali Hamlili (1993) " contribution to the dynamic modelling of articulated systems" doctoral thesis, Ecole Nationale des Ponts et Chaussées

[5] O. KARAHAN, Z. BINGUL, "*Modelling and Identification of STAUBLI RX-60*", IEEE, 2008

[6] R. Sepulchre, M. Jankovic et P.V . KOKOTOVIC (1997) " constructive nonlinear control" Springer-Verlag

[7] The zodiag ( collective work) (1996) " Theory of robot control" C.Canudas de Wit, B. Siciliano, G.Bastin Eds, Springer-Verlag, Berlin

[8] Lyapunov, "*The general problem of the stability of Motion*", Taylor and Francis, 1982.

[9] A Dayal Udai, S. Kumar Saha, "*Dynamic simulation of serial robots under force control*", int.J.Intelligent Machines and Robotics, Vol1, No.1,2018.

[10] F. Piltan1, A. Taghizadegan1 and N.B Sulaiman C, "*Modeling and Control of Four Degrees of Freedom Surgical Robot Manipulator Using MATLAB/SIMULINK", International Journal of Hybrid Information Technology Vol.8, No.11 (2015), pp.47-78*

[11] R. Freeman, P. Kokotovic,"*Optimal Nonlinear Controllers for feedback – Linearizable systems*", In Proc. the Amer. Contr Conf, Seattle, Washington, pp. 2722-2726, 1995.

[12] N. Bouzid, "*Neuronal control of the robotics systems*", Research Master, National Institute of Applied Sciences and Technology,

[13] Robot Manipulator Control Theory and Practice, Second Edition, Revised and Expended, 2011

[14] Jolly Shah1, Prof S.S.Rattan2, Prof B.C.Nakra3 "Dynamic analysis of two link robot manipulator for control design using computed torque control", International Journal of Research in Computer Applications and Robotics Vol.3 Issue.1, Pg:52-59 January 2015

[15] Luis Garcia-Valdovinos, Jesus Carlos Pedraza Ortega " 5DOF manipulator simulation based on MATLAB-Simulink methodology", IEEE, February 2010

[16] Shuyou Yu, Yu Zhou, Ting Qu, Fang Xu, and Yan Ma, « Control Invariant Sets of Linear Systems with Bounded Disturbances », International Journal of Control, Automation and Systems 16(X) (2018) pp.1-8


ISSN 1737-9334

# Simple and Efficient Recurrent Neural Network to Evaluate Classified Surgery Tasks

Malik Benmansour[#1], Abed Malti[#2]

[#]*GEE-GEE Department, Tlemcen-Tlemcen University*
*13000,Tlemcen, Algeria*

[1]malik.benmansour@gmail.com

[2]abed.malti@gmail.com

***Abstract*— In this work, we propose to use recurrent neural network (RNN) architecture to provide a dynamic evaluation of performing surgery tasks. The task is considered to be known and is represented by a sequence of kinematic data recorded from DaVinci Robot. The sequence of output represents a dynamic evaluation which gets updated while the sequence of input is feeded to the RNN. To train the RNN we use three levels of skills: expert, intermediate and novice to which we associate three scores: 1, 0.7 and 0.4 respectively. We test the performance of the proposed method on three different surgical gestures: knot tying, needle passing and suturing. We use one RNN per-gesture which we train with the corresponding data from JIGSAWS; a publicly available dataset of surgery tasks. We compare this approach with a static method that uses Deep Neural Network which provides a global score of the whole surgery task.**

***Keywords—surgery task, skill assessment, recurrent neural network.***

## I. INTRODUCTION

During the past few years, many classification approaches have been used to sort out surgical skills in both coarse or fine grained details [1, 2, 3]. Most of this approaches rely on Recurrent Neural Network (RNN) architectures because of the sequential nature of the data. In general, these data are video sequences containing the surgery intervention within organs and surgery tools. When the procedure is executed with a surgical robot, these data can be also kinematic trajectories containing positions, velocities and accelerations of articulated joints: joystick and robotic arm. Despite the importance of surgery task classification, few efforts have been made to automate the evaluation by providing numerical scores on how good or bad a surgery task is achieved.

An automatic and thus objective numerical evaluation of surgery tasks is crucial to help surgereon trainees improving their performance. Moreover it is scalable for continuous evaluation of multiple trainees. It provides the trainees with reliable feedback to improve their surgical skills.

In this paper, we propose to use a simple RNN to provide numerical scores to evaluate the performance of a given surgery task. The input are kinematic trajectories of positions, velocities and accelerations. They correspond to joystick and robotic arm motions from the DaVinci Robot. The provided scores are shaped as a time series of equal length as the input kinematic sequence. With this approach we are able to provide sequential scores with which we compute an average score for the whole task. We are also able to address different input sequence lengths without being obliged to downsample or upsample the sequence to fit a constant input length as it is the case when we used Deep Neural Networks [14, 15]. Our experiment runs on three different surgery tasks: suturing, knot tying and needle passing using the kinematic data and three levels of evaluation: expert, medium and novice.

This paper is organized as follows. First, we present an overview of the state-of-the-art of surgicall skills assessment. Second, we present the proposed setup with the RNN architecture and the training approach. Third, we show our experimental results with discussions and comments. Finally, we draw conclusions and future works on the basis of the obtained results.

## II. RELATED WORK

The state-of-the-art of surgical skills assessment relies mostly on publicly available dataset. The widely used one is JIGSAWS [1, 5] which contains both kinematic and video data of surgery gestures. During the past five years, artificial neural networks architectures have proven to be more efficient above other machine learning approaches [9]. Most of the proposed approaches addressed mainly classification approaches either for coarse tasks or fine grained sub-tasks. They also differ by relying on surgery videos or on kinematic data. [2] proposed a spatiotemporal RNN-CNN architecture for Fine-grained surgical skills segmentation based on image sequences. [3] utilized a labeled data from real surgery videos to train an accurate and efficient robotic instrument tracker based on the state-of-the- art Hourglass Networks. They evaluated the movement of the robotic instruments and automatically classified the technical level of a surgeon with a linear classifier, using peer evaluations of skill as the reference standard. [4] proposed both tool detection and operative skill assessment using region-based Convolutional Neural Networks. [7] proposed to use both videos and kinematic data




ISSN 1737-9334

to classify surgical gestures. [8] suggested to recognize both gestures and longer, higher-level maneuvers with a model of the mapping from kinematics to gestures/maneuvers with recurrent neural networks.

In real surgery applications, several deep network framerworks have been proposed. A. Twinanda et al. [10] used CNN for surgery phase recognition from cholecystectomy videos. The approach carried out both phase recognition and tool presence detection. A similar method was recently used for cataract surgery [11]. Rafii-Tari et al. [12] used catheter-tissue interaction and motion patterns across different skill levels to deliver an automated and objective assessment of performance. [6] proposed to assess skill and provide effective feedback to trainees for unstructured surgical tasks in the operating room, such as tissue dissection in septoplasty.

## III. METHODOLOGY

RNNs have been widely used into several sequence modeling of dynamic systems. Speech, text, handwriting are the main contexts where RNNs were originally applied.

**Structure:** an RNN is composed of a set of inputs $\{x_t\}$, hidden states $\{h_t\}$, outputs $\{m_t\}$ and a nonlinear block. A non-linear block in the RNN takes an input $x_t$ and a hidden state $h_{(t-1)}$ to produce an output $m_t$ and a hidden state $h_t$ which feeds the next nonlinear block with an input $x_{(t+1)}$ and so forth (see figure 1). In the case of RNN with feedback, which our case, the output $m_t$ is back connected to the nonlinear block.

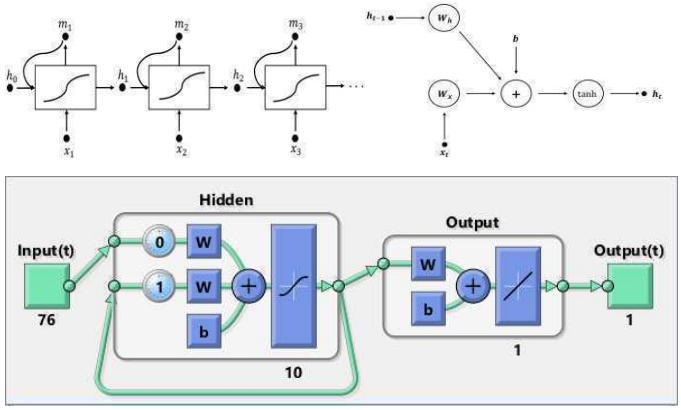


Fig. 1. A single Recurrent Neural Network (RNN) per given surgery task.

The relation involved by the nonlinear block can be written as

$$h_t = tanh(W_x \,.\, x_t \;\; + W_h \,.\, h_{\{t-1\}} + W_m \,.\, m_t \; + \; b) \quad (1)$$

$W_x$, $W_h$ and $W_m$ are weights to be learnt. $b$ is the bias. To obtain the output score $y_t$, we use a linear layer

$$y_t \;\; = W_y \,.\, m_t \; + \; b_y \quad (2)$$

$W_y$ and $b_y$ being also scalars to be learnt.

**Inputs:** the inputs are kinematic sequences from the JIGSAWS dataset [11]. Each sequence length represents the duration of the task completed by the surgeon. The input is a 76 vector of kinematic data containing positions, velocities and accelerations from the joytsticks and robotic arms of the DaVinci robot [7].

**Outputs:** The RNN is a single output scalar rating the task between 0 and 1. For every 76 kinematic input, the RNN delivers a score given that the input is part of a sequence of known surgery task.

**One RNN per-surgery-task:**

In our work we train three different RNNs with the same structure. They are described as follows :

**KT-RNN:** is dedicated to provide sequences of scores related to the Knot-Tying gesture. It has 76 input vector of kinematic data of Knot-Tying task from any level of knowledge: expert, intermediate and novice subjects. In the learning step three trials from each subject are taken. Two trials of the novice and intermediate subjects are left to for the test step. We refer to this model as "KT-RNN". Figure 2 displays a sample frame from the Knot-Tying.

Fig. 2. A sample frame of the Knot-Tying task.

**NP-RNN:** is dedicated to provide sequences of scores related to the Needle-Passing gesture. It has 76 input vector of kinematic data of Needle-Passing task from any level of knowledge: expert, intermediate and novice subjects. In the learning step three trials from each subject are taken. Two trials of the novice and intermediate subjects are left to for the test step. We refer to this model as "NP-RNN". Figure 3 displays a sample frame from the Needle-Passing.

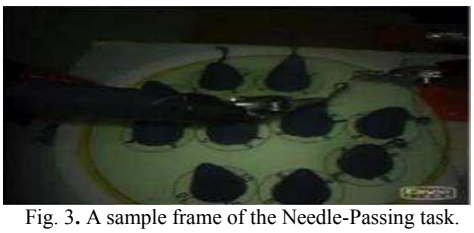

Fig. 3. A sample frame of the Needle-Passing task.




ISSN 1737-9334

**ST-RNN:** this third follows the same principle as the two previous onesand is related to Suturing. We refere to this model as ST-RNN. Figure 4 displays a sample frame from the Suturing gesture.

Fig. 4. A sample frame of the Suturing task.

## IV. Experimental Results

In the following section, we will present the setup of this paper but also, we will present shortly two others setups we presented in papers that we established for previous conferences [14, 15]. In these two setups, we used deep neural networks instead of recurrent neural networks to assess performance of the JIGSAWS subjects on the three tasks. Details are shown in the following subsection.

### *A. Experimental setup and compared methods*

**RNNs setup:** We used three independent recurrent neural networks. Each one is intended to assess all subjects of the JIGSAWS dataset on one task only. Therefore, each network takes as input, learning kinematic data of one of the three tasks. Each RNN contains 10 hidden layers. The training finishes after 50 epochs. The Levenberg-Marqaurdt algorithm is employed for the training process and the performance is calculated through the Mean Squared Error. The following figures depict the architecture of our three RNNs.

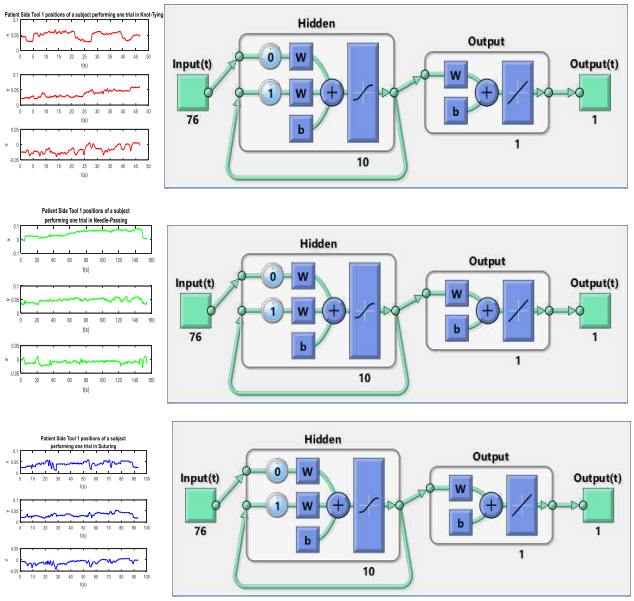


Fig. 5. Architechture of the proposed RNNs for specific task evaluation.

**Remark :** On the previous figure, each row represents the architecture of a RNN intended to assess one of the three tasks. On the left of each row is shown the evolution of the spatial positions of one Patient Side Tool (which is a component of the DaVinci surgery robot) while the task is performed by a surgeon.

**Compared methods:** The setups established in [14, 15] use deep neural networks. In [14], the goal was to design a deep neural network containing three hidden layers with 20 nodes per hidden layer. This network was trained with kinematic data of expert subjects of the JIGSAWS dataset performing the three tasks and next, kinematic data of intermediate and novice subjects were chosen to test the network. This network was intended to assess objectively the subjects on the three tasks at once. On the other hand, in [15], we established three independent neural networks and each one is responsible to assess subjects on one task only. Thus, each network is trained with kinematic data of some trials of all subjects of the JIGSAWS dataset, which means novice, intermediate and exepert subject and the test is completed using kinematic data of the remaining trials. Please refer to [1] for more details about the JIGSAWS content. Each of the three networks is composed of three hidden layers with 20 nodes per hidden layer. As it can be noticed through its description, the model of this setup is globally similar to the RNNs setup but we have used deep neural networks instead of recurrent networks.

### *B. Surgical skill assessment and disscussion*

We run the assessment procedure on the test data. It contains two intermediates and four novices. The intermediate subjects are labeled with the letters C and F and the novice subjects are labeled with the letters B, G, H and I. For the setup of [15] and for the RNNs, we give for each network,as


ISSN 1737-9334

test data, one trial of each subject performing the task the network is responsible to assess. For the model of the setup in [14], the test data contains one trial of each intermediate and novice subject performing each task.

The following tables show the scores of each novice and intermediate subject after performing the three tasks. For more convenience, we abbreviate the names of the tasks Knot-Tying, Needle-Passing and Suturing respectively by KT, NP and ST. We labeled any task performed by any subject by the abbreviation of the task concatenated with the label representing the subject followed by the number of the trial. For example, KTB4 stands for "novice subject B performing Knot-Tying task, trial 4".For the 1st table, in the "Rate" rows, the green colored cells show the test results of the model of the setup used in [14] while the yellow colored cells show the test results of the three independent models of the setup used in [15]. In the 2nd table are shown the results of RNNs setup.

The results prove that the RNNs yielded the best performance evaluation. Indeed, we can see that particularly, the two intermediate subjects C and F got better ratings than all the novice subjects B,G,H and I with the recurrent neural networks than with the deep neural networks. These results are plausible since intermediate subjects have more time experience in the domain than the novice subjects.

TABLE I
SCORES OF NOVICE AND INTERMEDIATE SUBJECTS AFTER ASSESSING THEIR PERFORMANCE THROUGH THE SETUPS USING DEEP NEURAL NETWORKS [14, 15]

| **Subject and task** | **KTB4** | | **KTG4** | | **KTH4** | | **KTI5** | | **KTC4** | | **KTF4** | |
|---|---|---|---|---|---|---|---|---|---|---|---|---|
| **Rate** | 60.8% | 39.00% | 98.6% | 36.5% | 58.2% | 39.9% | 0.8% | 50.8% | 98.9% | 87.7% | 85.2% | 50.9% |
| **Subject and task** | **NPB4** | | **NPG4** | | **NPH4** | | **NPI4** | | **NPC4** | | **NPF4** | |
| **Rate** | 99.7% | 43.58% | 32.9% | 50.0% | 99.9% | 31.1% | 99.8% | 33.7% | 32.5% | 100% | 60.3% | 64.4% |
| **Subject and task** | **STB4** | | **STG4** | | **STH4** | | **STI4** | | **STC4** | | **STF4** | |
| **Rate** | 0.05% | 26.93% | 0.01% | 46.8% | 0.00% | 27.3% | 3.8% | 34.5% | 0.02% | 78.2% | 27.3% | 45.2% |

TABLE III
SCORES OF NOVICE AND INTERMEDIATE SUBJECTS AFTER ASSESSING THEIR PERFORMANCE THROUGH THE RNNS.

| **Subject and task** | **KTB4** | **KTG4** | **KTH4** | **KTI5** | **KTC4** | **KTF4** |
|---|---|---|---|---|---|---|
| **Rate** | 40.1% | 39.9% | 40.2% | 39.7% | 99.2% | 69.7% |
| **Subject and task** | **NPB4** | **NPG4** | **NPH4** | **NPI4** | **NPC4** | **NPF4** |
| **Rate** | 40.1% | 40.0% | 39.9% | 40.5% | 70.3% | 66.5% |
| **Subject and task** | **STB4** | **STG4** | **STH4** | **STI4** | **STC4** | **STF4** |
| **Rate** | 39.9% | 40.0% | 40.7% | 40.0% | 69.3% | 59.6% |

As additional results, here are some figures representing the score evolution of the intermediate subject F performing each task. The "x" axis represents the duration (in frames) of the trial while the "y" axis represents the score at each frame.




ISSN 1737-9334

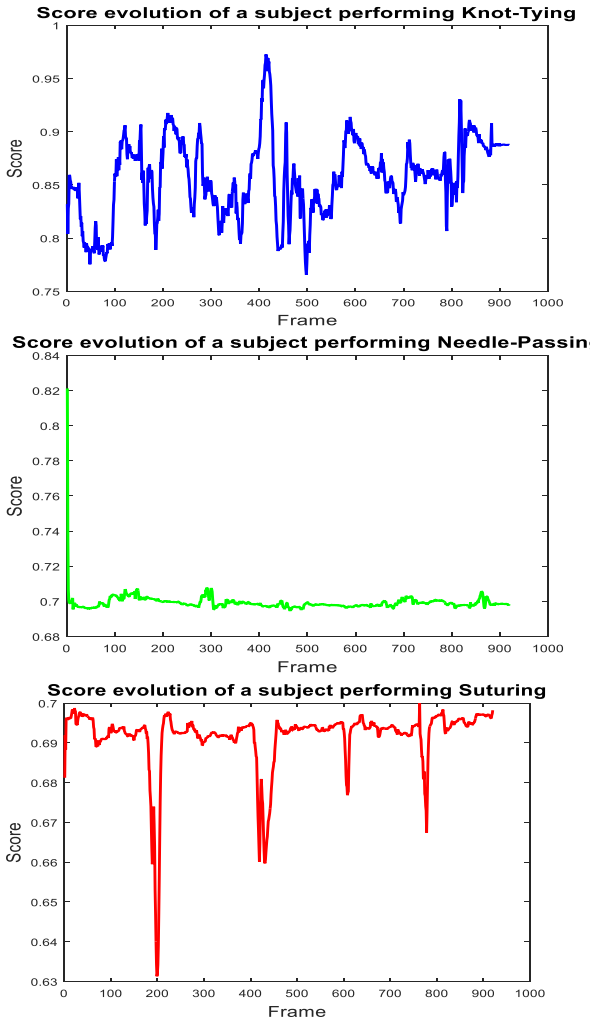


## V. CONCLUSION

In this paper, we presented an approach with the purpose of surgical skills evaluation. This method consists on assigning three independent recurrent neural networks that were trained on all subjects performing three corresponding gestures. The training scores for assessment were assigned according to the subject experience. Thus, each network is responsible on rating the performance of one task. We compared this approach with other approches that use deep neural netwroks We have experimentally shown that the proposed approach yields better and more logical assessment scores based in the fact that intermediate subjects have more experience than the novice subjects in the surgery domain. As future work, we aim to design Long Short Term Memory networks that will be able to learn from sequences of images that show the gestures composing each task and see if we will get any better results.

## REFERENCES

[1] Yixin Gao, S. Swaroop Vedula, Carol E. Reiley, and Narges Ahmidi, "JIGSAWS: The JHU-ISI Gesture and Skill Assessment Working Set," *CIRL*, 04-Sep-2014. [Online]. Available: https://cirl.lcsr.jhu.edu/research/hmm/datasets/jigsaws_release/.

[2] C. Lea, A. Reiter, R. Vidal, and G. D. Hager, "Segmental Spatiotemporal CNNs for Fine-grained Action Segmentation," *ArXiv160202995 Cs*, Feb. 2016.

[3] H. Law, K. Ghani, and J. Deng, "Surgeon Technical Skill Assessment using Computer Vision based Analysis," in *Machine Learning for Healthcare Conference*, 2017, pp. 88–99.

[4] A. Jin *et al.*, "Tool Detection and Operative Skill Assessment in Surgical Videos Using Region-Based Convolutional Neural Networks," *ArXiv180208774 Cs*, Feb. 2018.

[5] N. Ahmidi *et al.*, "A Dataset and Benchmarks for Segmentation and Recognition of Gestures in Robotic Surgery," *IEEE Trans. Biomed. Eng.*, vol. 64, no. 9, pp. 2025–2041, 2017.

[6] H. Doughty, D. Damen, and W. Mayol-Cuevas, "Who's Better? Who's Best? Pairwise Deep Ranking for Skill Determination," *ArXiv170309913 Cs*, Mar. 2017.

[7] N. Ahmidi *et al.*, "Automated objective surgical skill assessment in the operating room from unstructured tool motion in septoplasty," *Int. J. Comput. Assist. Radiol. Surg.*, vol. 10, no. 6, pp. 981–991, Jun. 2015.

[8] L. Zappella, B. Béjar, G. Hager, and R. Vidal, "Surgical gesture classification from video and kinematic data," *Med. Image Anal.*, vol. 17, no. 7, pp. 732–745, Oct. 2013.

[9] R. DiPietro *et al.*, "Recognizing Surgical Activities with Recurrent Neural Networks," in *Medical Image Computing and Computer-Assisted Intervention – MICCAI 2016*, 2016, pp. 551–558.

[10] L. Sbernini, L. R. Quitadamo, F. Riillo, N. D. Lorenzo, A. L. Gaspari, and G. Saggio, "Sensory-Glove-Based Open Surgery Skill Evaluation," *IEEE Trans. Hum.-Mach. Syst.*, vol. 48, no. 2, pp. 213–218, Apr. 2018.

[11] A. P. Twinanda, S. Shehata, D. Mutter, J. Marescaux, M. Mathelin and N. Padoy, "EndoNet: A Deep Architecture for Recognition Tasks on Laparoscopic Videos " *IEEE Trans. on medical imaging*, vol. 36, no. 1, pp. 86-97.

[12] K. Charrière, G. Quellec, M. Lamard, D. Martiano, G. Cazuguel, G. Coatrix and B. Cochener, "Real-time analysis of cataract surgery videos using statistical models " *Multimedia tools and application*", vol. 76, no. 21, pp. 22473-22491.

[13] H. Rafii-Tari, C. J. Payne, J. Liu, C. Riga, C. Bicknell and G-Z. Yang, "Towards automated surgical skill evaluation of endovascular catheterization tasks based on force and motion signatures", IEEE International Conference of Robotics and Automation – *ICRA 2015*, 2015, pp. 1789-1794.

[14] Malik Benmansour, Wahida Handouzi, Abed Malti, "A neural network architecture for automatic and objective surgical skill assessment", IEEE, The International Conference on Electrical Sciences and Technologies in Maghreb – *CISTEM 2018.*

[15] Malik Benmansour, Wahida Handouzi, Abed Malti, "Task-Specific Surgical Skill Assessment With Neural Networks", Advanced Intelligent Systems for Sustainable Development – *AI2SD'2018.*


ISSN 1737-9334

# Control in Stand-alone Wind Energy Conversion System Using Vector Control of DSIG

Samira Aitouaret Chekkal, Narimen Aouzellag Lahaçani, Djamal Aouzellag, Kaci Ghedamsi

*Département Génie Electrique, Université de Bejaia*
*Bejaia 06000, Algeria*
samirachekkal@yahoo.fr
nlahacani@yahoo.fr
aouzellag@hotmail.com
kghedamsi@yahoo.fr

***Abstract*— This paper presents the operation of a stand-alone wind energy conversion system using a Dual-Stator Induction Generator (DSIG) as well as the contribution they can make to its application in an energy production chain for dedicated operation for isolated sites. The role of stand-alone systems is to supply one or more consumers located in an isolated area of the electricity grid. The proposed system is modeled and simulated using Matlab / Simulink software to examine the dynamic characteristics of the system with the proposed control strategy. A controller is specifically designed to maintain constant dc bus voltage under wind speed and electrical load variations. The results of the modeling and simulations show that most of the isolated sites can be supplied with clean energy. Dynamic control of the dc-bus voltage has also been successfully demonstrated under varying load. A ramp dc-bus voltage reference is chosen and it is shown that the ramp slope is a deciding factor for successful current build-up. The simulation results ensure good dynamic control of the dc bus voltage with very small changes around its reference value.**

***Keywords*— Wind turbine, Dual-stator induction generator, Vector control, Stand-alone mode**

## I. INTRODUCTION

The next exhaustion of fossil fuels has contributed to the development of renewable energy in general and wind energy in particular [1]. For wind energy conversion system, recent research has been focused chiefly on squirrel-cage induction generators because they are the most robust rugged and economic reasons would dictate their deployment in remote wind-farms [2].

Shunt capacitors were traditionally used to supply reactive power but back-to-back voltage source converters were necessary to ensure maximal power extraction under variable wind speed. Initial voltage in the dc bus is derived from the terminal voltage of the unexcited machine, derived from remanent magnetism of the magnetic core. Machine flux was ramped up from this small initial voltage using scalar control although no analytical justification of the ramp slope was provided [3-4]. For voltage build-up, a ramp reference of defined slope is used for the dc voltage and the selection of slope is explained analytically.

The present work is inserted in this context, which consists of control in stand-alone wind energy conversion system using vector control of Dual-Stator Induction Generator (DSIG). This last shows, in addition to the advantages of cage induction motors, other benefits, such as conventional segmentation power, high reliability [5]. The mathematical model of the turbine and the DSIG, vector control, sharing of powers between the wind system and the stand-alone network will be studied and detailed. The simulation results are presented to shown the performance of the proposed system fig.1. The above study offer various possibilities of power generation in isolated system.

## II. SYSTEM CONFIGURATION AND MODELING

The basic device to be studied is that of Figure 1. This device is made up of a double stator induction generator, converter and a capacitor is connected on the power supply side of controlled converter, this makes it possible to obtain a standalone operation.

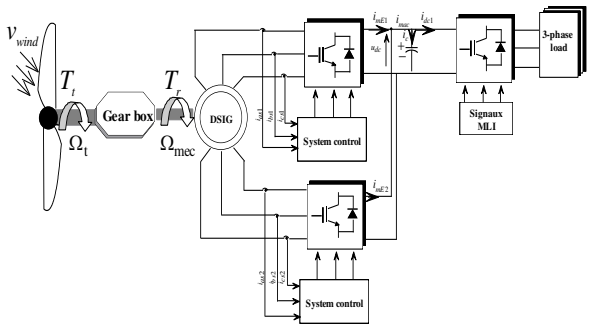


Fig 1. Scheme of the studied device

## III. SYSTEM MODELLING

### A. Wind turbine model

A wind turbine can only convert a certain percentage of the captured wind power. This percentage is represented by $C_p$ which is a function of the wind speed, the turbine speed and the pitch angle of any specific wind turbine blades [6-7]. The mechanical power ($P_t$) extracted from the wind is mainly governed by three quantities namely: the area swept by rotor


ISSN 1737-9334

blades ($S$), the upstream wind velocity ($v_{wind}$) and the rotor power coefficient ($C_p$) by following equation:

$$P_t = \frac{1}{2} C_p(\lambda) S v_{wind}^3 \quad (1)$$

Where $\rho$ is the air density, $C_P$ is the turbine power coefficient that is a function of tip speed ration $\lambda$ defined by Eq. (2).

$$\lambda = \frac{R\Omega_t}{v_{wind}} \quad (2)$$

The rotor efficiency curve $C_P(\lambda)$ is a nonlinear function of the tip speed ratio (TSR), $\lambda$, which is determined by the blade design, and the pitch angle [8].

From Fig.2, it is clear that there is a value of $\lambda$ for which $C_P$ is maximized, thus maximizing the power for a given wind speed. Because of the relationship between $C_P$ and $\lambda$, for each wind velocity, there is a turbine speed that gives a maximum output power.

The turbine torque is the ration of the output power to the shaft speed $\Omega_t$:

$$T_t = \frac{P_t}{\Omega_t} = C_P(\lambda) \frac{\rho}{2} S v_{wind}^3 \frac{1}{\Omega_t} \quad (3)$$

The torque and shaft speed of the wind turbine, referred to the generator side of the gearbox are given by following equations:

$$\Omega_t = \frac{\Omega_{me}}{G} \quad (4)$$

$$T_r = \frac{T_t}{G} \quad (5)$$

With: G: Gear box ratio

In this paper, a functional block diagram model of the turbine and power coefficient for the wind turbine model reported in [9] is used.

### *B. Modeling of dual-stator induction generator (DSIG)*

DSIG depends on the rotational speed of the rotor. If the latter is slightly greater than that of the magnetic field of the stator, it then develops an electromagnetic force similar to that obtained with a synchronous generator. On the other hand, the machine does not generate its own excitation energy. For that, it will be necessary to bring this energy either by a battery of capacitors, or by a static converter control, which will stabilize its output voltage and frequency through capacitors connected across the stator. The model of dual-stator induction machine (DSIM) is composed of a two-phase electrical phase windings shifted by an electric angle α = 30 °, and a rotor cage squirre. [9-10].

$$\begin{cases} v_{ds1} = R_{s1} i_{ds1} + \frac{d}{dt}\varphi_{ds1} - \omega_s \varphi_{qs1} \\ v_{qs1} = R_{s1} i_{qs1} + \frac{d}{dt}\varphi_{qs1} + \omega_s \varphi_{ds1} \\ v_{ds2} = R_{s2} i_{ds2} + \frac{d}{dt}\varphi_{ds2} - \omega_s \varphi_{qs2} \\ v_{qs2} = R_{s2} i_{qs2} + \frac{d}{dt}\varphi_{qs2} + \omega_s \varphi_{ds2} \\ v_{dr} = R_r i_{dr} + \frac{d}{dt}\varphi_{dr} - (\omega_s - \omega_r)\varphi_{qr} \\ v_{qr} = R_r i_{qr} + \frac{d}{dt}\varphi_{qr} + (\omega_s - \omega_r)\varphi_{dr} \end{cases} \quad (6)$$

The expressions for stator and rotor flux linkages are

$$\begin{cases} \varphi_{ds1} = L_{s1} i_{ds1} + L_m (i_{ds1} + i_{ds2} + i_{dr}) \\ \varphi_{qs1} = L_{s1} i_{qs1} + L_m (i_{qs1} + i_{qs2} + i_{qr}) \\ \varphi_{ds2} = L_{s2} i_{ds2} + L_m (i_{ds1} + i_{ds2} + i_{dr}) \\ \varphi_{qs2} = L_{s2} i_{qs2} + L_m (i_{qs1} + i_{qs2} + i_{qr}) \\ \varphi_{dr} = L_r i_{dr} + L_m (i_{ds1} + i_{ds2} + i_{dr}) \\ \varphi_{qr} = L_r i_{qr} + L_m (i_{qs1} + i_{qs2} + i_{qr}) \end{cases} \quad (7)$$

The electrical model is completed by this mechanical equation:

$$T_{em} - T_r = J \frac{d\Omega_{mec}}{dt} + k_f \Omega_{mec} \quad (8)$$

The electromagnetic torque expression as a function of stator currents and rotor flux is as follows:

$$T_{em} = p \frac{L_m}{L_m + L_r} \left[ (i_{qs1} + i_{qs2}) \varphi_{dr} - (i_{ds1} + i_{ds2}) \varphi_{qr} \right] \quad (9)$$

## IV. MODELING OF DSIM FIELD-ORIENTED CONTROL OF THE DUAL-STATOR INDUCTION GENERATOR

The main objective of the vector control of induction motors is, as in DC machines, to independently control the torque and the flux [9]. In this order, we propose to study the FOC of the DSIM. The control strategy used consists to maintain the quadrate component of the flux null ($\varphi_{qr}=0$) and the direct flux equals to the reference ($\varphi_{dr}=\varphi_r^*$):
$\varphi_r^*$ and the torque $T_{em}^*$ as well as:

$$\begin{cases} \varphi_{dr} = \varphi_r^* \\ \varphi_{qr} = 0 \\ \frac{d}{dt}\varphi_r^* = 0 \end{cases} \quad (10)$$

Substituting (10) into (6) yields




ISSN 1737-9334

$$i_{dr} = 0 \tag{11}$$

$$i_{qr} = -\frac{\omega_{gl}^{*}\varphi_r^{*}}{R_r} \tag{12}$$

With: $\omega_{gl}$*=$\omega_s$*-$\omega_r$ ($\omega_{gl}$*is the slip speed).

After calculation and rearrangement of the electromagnetic torque and stator voltages equations, following expressions are obtained

$$i_{dr} = \frac{\varphi_r^{*}}{L_m + L_r} - \frac{L_m}{L_m + L_r}\left(i_{ds1} + i_{ds2}\right) \tag{13}$$

$$i_{qr} = -\frac{L_m}{L_m + L_r}\left(i_{qs1} + i_{qs2}\right) \tag{14}$$

Substituting (14) into (12), obtain

$$\omega_{gl}^{*} = \frac{R_r L_m}{\left(L_m + L_r\right)}\frac{\left(i_{qs1} + i_{qs2}\right)}{\varphi_r^{*}} \tag{15}$$

The final expression of the electromagnetic torque is

$$T_{em}^{*} = p\frac{L_m}{L_m + L_r}\left(i_{qs1} + i_{qs2}\right)\varphi_r^{*} \tag{16}$$

With taking into the rotor field orientation, the stator voltage equations (6) can be rewritten as

$$\begin{cases} v_{ds1}^{*} = R_{s1}i_{ds1} + L_{s1}\dfrac{d}{dt}i_{ds1} - \omega_s^{*}\left(L_{s1}i_{qs1} + \tau_r\varphi_r^{*}\left(\omega_s^{*} - \omega_r^{*}\right)\right) \\ v_{qs1}^{*} = R_{s1}i_{qs1} + L_{s1}\dfrac{d}{dt}i_{qs1} + \omega_s^{*}\left(L_{s1}i_{ds1} + \varphi_r^{*}\right) \\ v_{ds2}^{*} = R_{s2}i_{ds2} + L_{s2}\dfrac{d}{dt}i_{ds2} - \omega_s^{*}\left(L_{s2}i_{qs2} + \tau_r\varphi_r^{*}\left(\omega_s^{*} - \omega_r^{*}\right)\right) \\ v_{qs2}^{*} = R_{s2}i_{qs2} + L_{s2}\dfrac{d}{dt}i_{qs2} + \omega_s^{*}\left(L_{s2}i_{ds2} + \varphi_r^{*}\right) \end{cases} \tag{17}$$

$$\tau_r = \frac{L_r}{R_r}$$

Where

Consequently, the electrical and mechanical equations for the system after these transformations in the space control may be written as follows:

$$\begin{cases} \dfrac{d}{dt}i_{ds1} = \dfrac{1}{L_{s1}}\left(v_{ds1}^{*} - R_{s1}i_{ds1} + \omega_s^{*}\left(L_{s1}i_{qs1} + \tau_r\varphi_r^{*}\left(\omega_s^{*} - \omega_r^{*}\right)\right)\right) \\ \dfrac{d}{dt}i_{qs1} = \dfrac{1}{L_{s1}}\left(v_{qs1}^{*} - R_{s1}i_{qs1} - \omega_s^{*}\left(L_{s1}i_{ds1} + \varphi_r^{*}\right)\right) \\ \dfrac{d}{dt}i_{ds2} = \dfrac{1}{L_{s2}}\left(v_{ds2}^{*} - R_{s2}i_{ds2} + \omega_s^{*}\left(L_{s2}i_{qs2} + \tau_r\varphi_r^{*}\left(\omega_s^{*} - \omega_r^{*}\right)\right)\right) \\ \dfrac{d}{dt}i_{qs2} = \dfrac{1}{L_{s2}}\left(v_{qs2}^{*} - R_{s2}i_{qs2} - \omega_s^{*}\left(L_{s2}i_{ds2} + \varphi_r^{*}\right)\right) \end{cases} \tag{18}$$

$$\frac{d}{dt}\varphi_r = -\frac{R_r}{\left(L_r + L_m\right)}\left(\varphi_r + L_m\left(i_{ds1} + i_{ds2}\right)\right) \tag{19}$$

$$\frac{d}{dt}\Omega_{mec} = \frac{1}{J}\left(\frac{pL_m\left(i_{qs1} + i_{qs2}\right)\varphi_r^{*}}{\left(L_r + L_m\right)} - T_g - f\,\Omega_{mec}\right) \tag{20}$$

For perfect decoupling, stator current control loops $\left(i_{ds1}, i_{qs1}, i_{ds2}, i_{qs2}\right)$ are added and at their outputs the voltage $\left(v_{ds1}, v_{qs1}, v_{ds2}, v_{qs2}\right)$ are obtained. The block control diagram is shown in Figure 2.

Dynamic equation for the dc bus voltage, shown in Figure 1, is derived as follows. Equating currents at the dc bus voltage, the following governing equation is obtained:

$$i_{dc} = C_{dc}\frac{d}{dt}v_{dc} \tag{21}$$

*Block diagram of current control*

The current control scheme is given in Figure 3. The references $i_d$* and $i_q$* are the outputs of the PI used in the external loop of voltage regulation $v_{ld}$ et $v_{lq}$. This regulation loop allows to set the amplitude of the voltage is $v_{ld}^{*}$ and void $i_{lq.}$

$$i_d^{*} = (PI)(v_d^{*} - v_d) \tag{22}$$

$$i_q^{*} = (PI)(v_q^{*} - v_q) \tag{23}$$

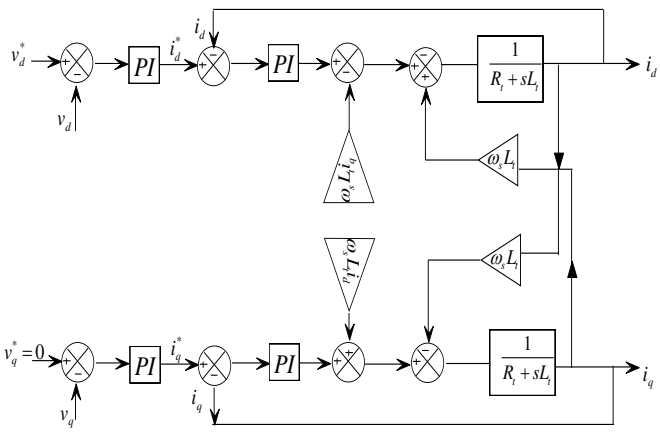


Fig 2 Current control scheme




ISSN 1737-9334

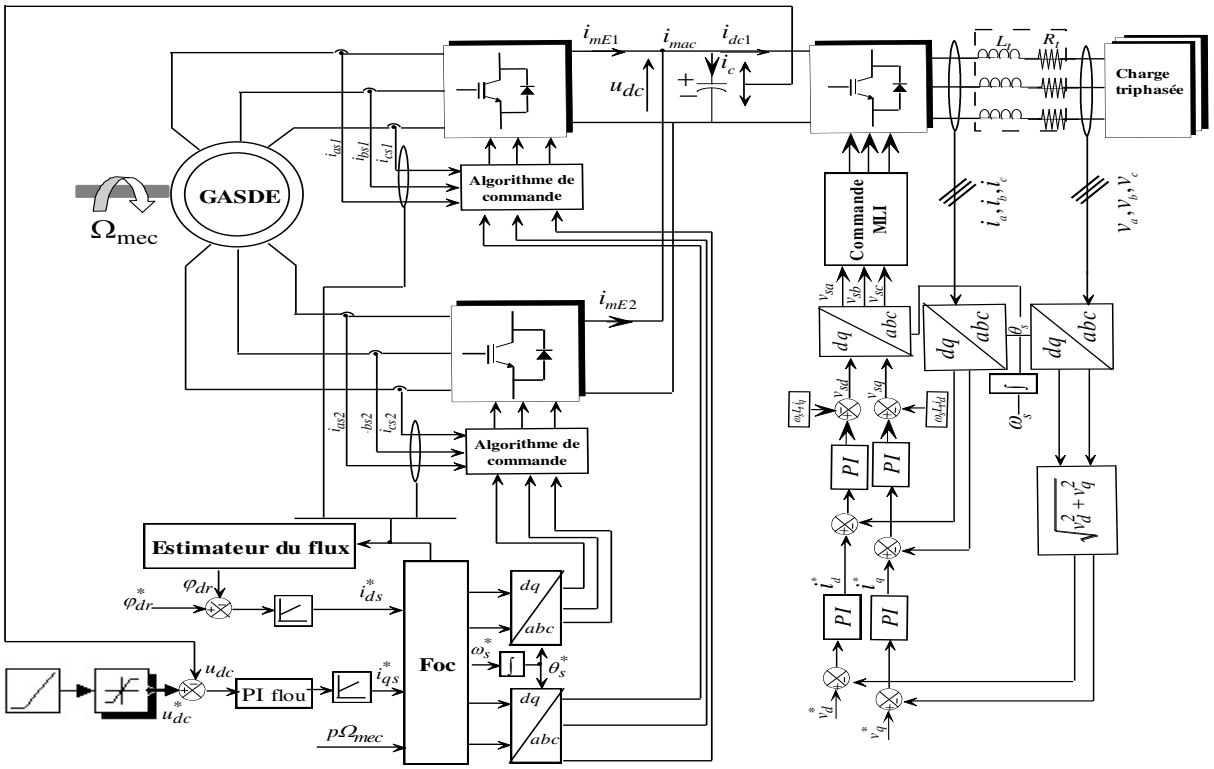


Fig 3 Control Scheme for the proposed stand-alone system

## V. RESULTS AND DISCUSSION

### A. *ESULTS AND DISCUSSION*

The overall system to be studied consists of a DSIG connected to a rectifier / inverter and controlled according to the control strategy presented above. In what follows, two simulation tests are performed are performed to analyze the performance of the control: The first test is dedicated to the control behavior at fixed speed control and purely resistive variable loads, the second is intended for the study of the control in the presence of an inductive load. The generator is driven at a speed of 314 rad/s with a value of voltage straightened reference $u_{dc}$*=622V throughout the entire duration of the simulation. The priming of the generator has taken place an empty, the presence of a remanent magnetic flux is essential or else loaded up the capacity at an initial value. In order to do this, we opted to loaded up initially the capacity an value 10 µF to 12V, to provide the reactive energy needed for priming, The q-axis current reference, generated from the voltage controller is kept at small value during starting by using the ramp voltage reference figure 4 (a and b). At the moment $t = 2s$, a balanced pure resistive three-phase load is inserted at 50% of its nominal value ($64\Omega$). At the moment $t = 4s$, another load of the same characteristic as the first one is inserted at 100% of its nominal value (64Ω). The DC- link voltage follows the reference as shown in Figure 4. Figure 5 illustrates the pace of the active power that reaches almost its nominal value which is the main advantage of the studied structure.

The analysis of the figures (6-11) made it possible to see the behavior of the current, the voltage and the electromagnetic torque according to the variation of the load, where we notice that the voltage is insensitive to this variation, unlike the current and the electromagnetic torque. We notice that the torque is still in the nominal operating range.

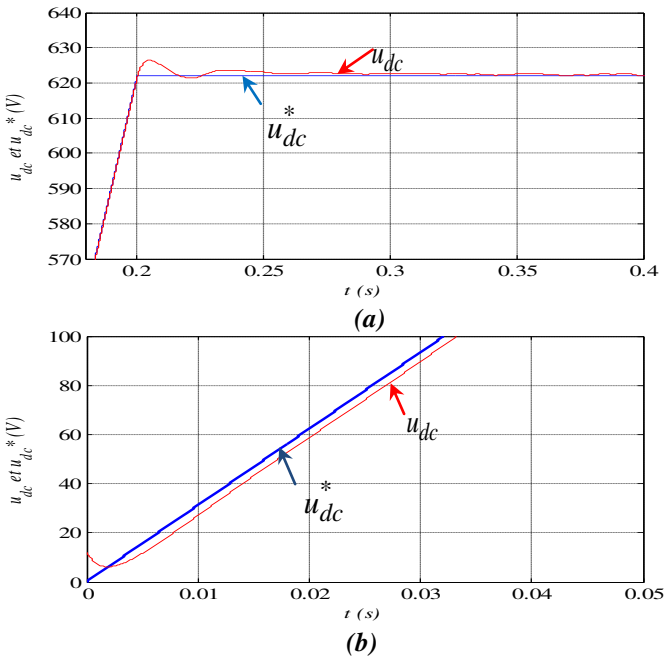


*Figure 4..DC-link voltage*




ISSN 1737-9334

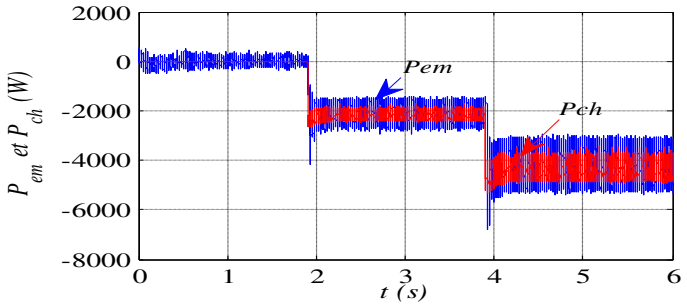


*Fig5.Electromagnetic and load powers*

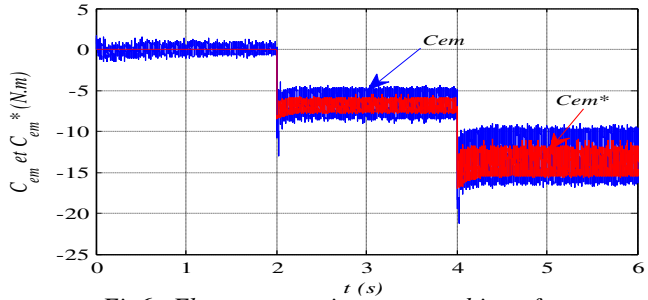


*Fig6. Electromagnetic torque and its reference.*

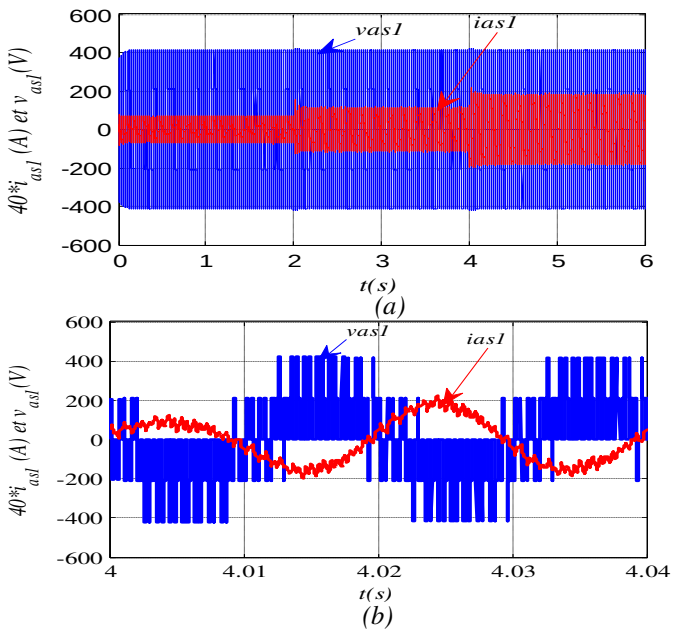


*Fig7 (a) Stator voltage and current for star 1.*
*(b) Zoom of the stator voltage and current for star 1.*

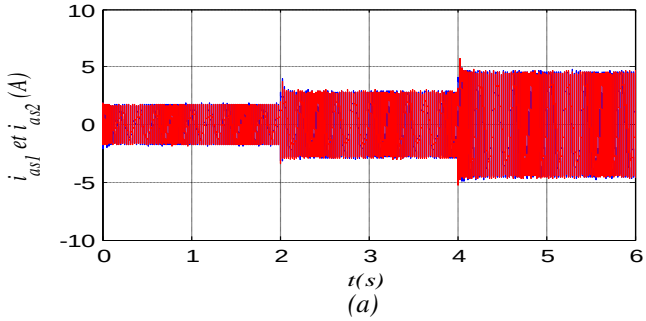


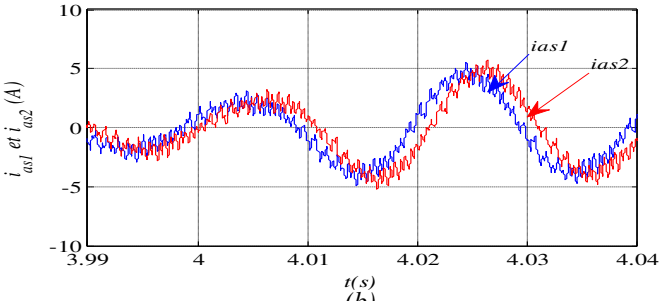


*Fig 8 (a) Stator current for star 1 and 2.*
*(b) Zoom of the stator current for star 1and 2.*

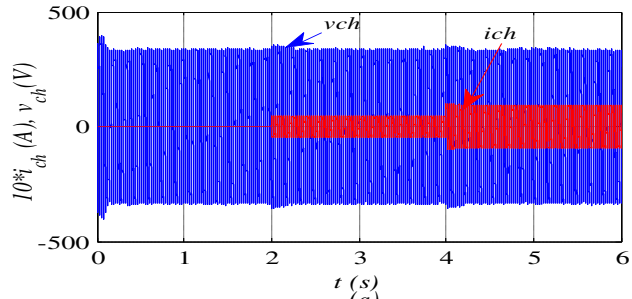


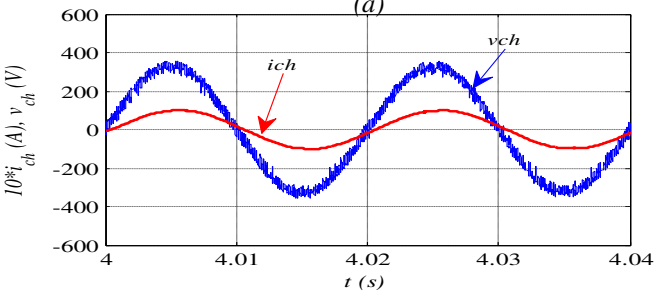


*Fig 9 Voltage and current for load*

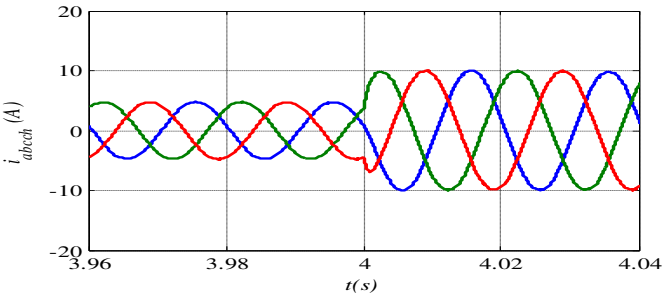


*Fig10. Three-phase Load current*

*B.* Influence of the variation of the inductive load

In this section, the performance of the GASDE is tested for an inductive load mainly consisting from the resistor (28Ω) and an inductance (50mH) per phase, while setting the drive speed at 314 rad/s. The vector control has given outstanding performance. The DC-link voltage schown in figure 11, it follows the reference. Figures [12-15] shown that active power, electromagnetic torque, voltages and stator currents are insensitive to the variation of the inductive load. Figure 16 shows the evolution of the load current and voltage, this last shown that the current in behind phase relative to voltage. In that event, we say that the stator provides active power.




ISSN 1737-9334

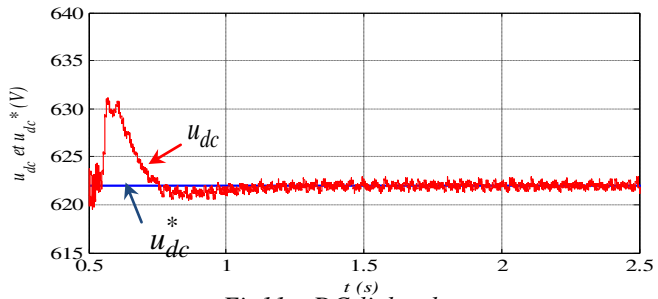


*Fig11. DC-link voltage*

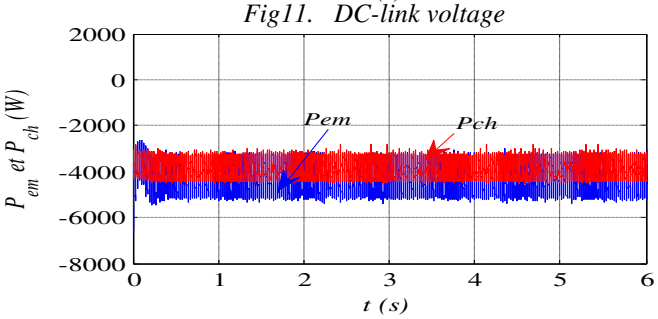


*Fig12. Electromagnetic and load powers*

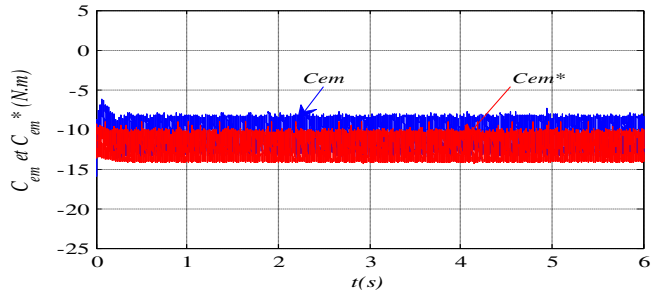


*Fig13. Electromagnetic torque and its reference.*

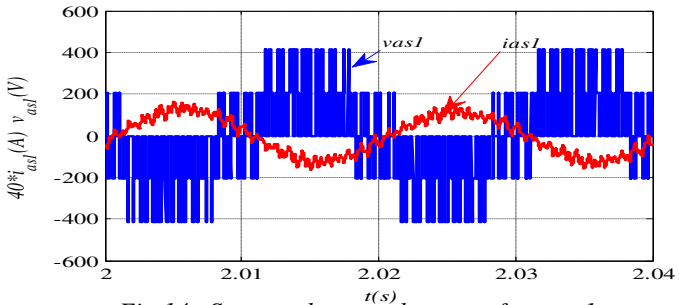


*Fig 14. Stator voltage and current for star 1.*

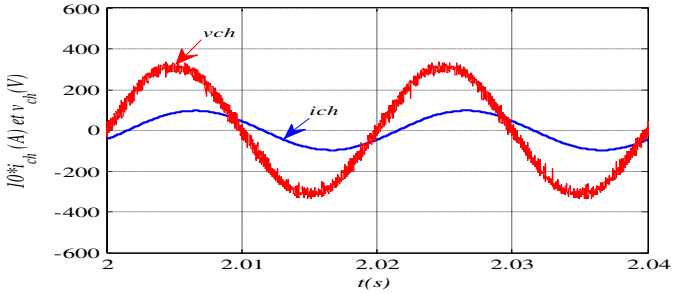


*Fig15. Voltage and current for load*

## VI. CONCLUSION

In this paper, the subject consists of improving the performance of wind turbines based on double-star asynchronous machines operating on isolated load.

A control structure of DSIG operating in autonomous sites is presented. The description of the latter is presented, adopting a mathematical model that defines the different equations describing the operation of the machine.

The generator is connected to the converter for the control of the voltage in the presence of the variations of the load.

Dynamic control of the dc-bus voltage has also been successfully demonstrated under varying load. A ramp dc-bus voltage reference is chosen and it is shown that the ramp slope is a deciding factor for successful current build-up. The simulation results ensure good dynamic control of the dc bus voltage with very small changes around its reference value.

## VII. REFERENCES

[1] Seyoum, D, Grantham ,C, Rahman, M. F. The dynamic characteristics of an isolated self-excited induction generator driven by a wind turbine. IEEE Trans on Indus Appl. 2003;39: 936–944.

[2] [Cardenas, R, Pena, R.. Sensorless vector control of induction machines for variable-speed wind energy applications IEEE Trans Energy Convers 2004; 19:196–205.

[3] Hazra, S, Sensarma, P. Vector approach for self-excitation and control of induction machine in stand-alone wind power generation IET Renew. Power Generation 2011: 5:397–405.

[4] Hazra, S, Sensarma, P.S. Self-excitation and control of an induction generator in a stand-alone wind energy conversion system IET Renew. Power Gener 2010; 4: 383–393.

[5] Hadiouche, D, Razik, H , Rezzoug, A. On the Modeling and Design of Dual-Stator Windings to Minimize Circulating Harmonic Currents for VSI fed AC Machines IEEE Trans. Ind. Appl 2004; 40.

[6] Ghedamsi K, Aouzellag D. Improvement of the performances for wind energy conversions systems. Int J Electr Power Energy Syst 2010;32(9):936–45.

[7] Aouzellag D, Ghedamsi K, Berkouk EM. Network power flux control of a wind generator. J Renewable Energy 2009;34:615–22.

[8] Poitiers F, Bouaouiche T, Machmoum M. Advanced control of a doubly-fed induction generator for wind energy conversion. Electric Power Syst Res 2009;79:1085–96.

[9] Chekkal, S, Aouzellag Lahaçani, N, Aouzellag, D , Ghedamsi K. Fuzzy logic control strategy of wind generator based on the dual-stator induction generator, International Journal of Electrical Power and Energy Systems IJEPES 2014: 59:166–175.

[10] Chekkal S, Aouzellag D, Ghedamsi K, Amimeur H. New control strategy of wind generator based on the dual-stator induction generator. In: 10th International Conference on Environment and Electrical Engineering (EEEIC), Italy; 2011. p.268–71.

[11] Singh, GK. Modeling and experimental analysis of a self-excited six-phase induction generator for stand-alone. International Journal of Research and Engineering Science direct, Renewable Energy Generation 2008 ;33:1605–21.

[12] Singh, G.K, Senthil Kumar,A, Saini, R.P. Performance evaluation of series compensated self-excited six-phase induction generator for stand-alone renewable energy generation Science direct, Energy 2010; 35 288–297.

[13] Singh, G, Senthil, A, Saini, R. Performance analysis of a simple shunt and series compensated six-phase self-excited induction generator for stand-alone renewable energy generation Science direct, Energy Conversion and Management 2011;52: 1688–1699.


ISSN 1737-9334

# Hybrid color MRI image compression by level set method and quincunx wavelet

Imane Haouam#1, Mohammed Beladgham*2,, Abdelmalik Taleb-Ahmed*3

[1,2]*Department of Electrical Engineering,*

[1,2]*TIT Laboratory, Tahri Mohammed University of Bechar, Bechar, Algeria*

[3]*Laboratoire IEMN DOAE. UMR CNRS 852, Valenciennes France*

1imahaouam@gmail.com

2beladgham.tlm@gmail.com

3Abdelmalik.Taleb-Ahmed@univ-valenciennes.fr

*Abstract*— **In recent years, researchers have increasingly targeted the development of hybrid systems to improve the quality of the compressed image. Hybrid methods are combinations of several techniques that take into account the advantages and disadvantages of it, in order to obtain a better image quality with a high compression ratio in a minimal calculation time. In this article, we are interested in geometric active contours techniques using the level-set method and the quincunx wavelet , so we proposed an hybrid algorithm for color medical image compression based on the level set method and the quincunx wavelet transform coupled with the set partitioning in hierarchical trees (SPIHT) algorithm. Experimental results show that the proposed algorithm gives better results compared to various methods, where it provides very important PSNR and MSSIM values.**

*Keywords*— **Color Medical image, Compression, level set, quincunx wavelet, SPIHT, PSNR**

## I. INTRODUCTION

The compression of medical images becomes a necessity to reduce their size, in order to ensure their archiving and facilitate their transmission. Currently hybrid methods acquired a huge popularity by aiming to match the advantages of each one, in order to obtain a powerful method with a high compression ratio, by giving a better image quality. It should be noted that magnetic resonance imaging has quickly become a critical study technique for the skull and brain.

The segmentation of the medical image gives an accurate analysis of the pathology while basing on the essential part of the image that contains the disease for a better diagnosis. Among the methods that have been proven in medical imaging segmentation, active contours, and in particular those based on "region", remain among the most adapted because they offer the possibility of taking into account a statistical aspect of the target region and therefore of integrate the specificities of the physical principle of acquisition into the segmentation process.

The segmentation by active contours aims to partition an image into different regions of interest, by means of an iterative process that allows an initiative curve to evolve towards the regions of interest, this deformation of contour is moved by image driven forces. Various medical image segmentation methods have been explored and widely presented in the literature [1]-[4]

This article aims to develop a method for better color medical image compression using quincunx wavelets which are better adapted to the image representation and was the subject of various research

The quincunx wavelet offers an optimal representation for image geometric. This structure of decomposition allows the construction of a non separable transform. Non separable wavelets, by contrast, offer more freedom and can be better tuned to the characteristics of images. Their less attractive side is that they require more computations. The quincunx wavelets are especially interesting because they are nearly isotropic. In contrast with the separable case, there is a single wavelet and the scale reduction is more progressive: one factor instead of 2[5]

Including to these two methods and their advantages, in this work we propose the quincunx algorithm coupled with the level set method for MRI color image compression. We enhance the image compression by our algorithm, by a comparison of the PSNR, MSSIM and MSE results obtained with the existing techniques




ISSN 1737-9334

## II. THE METHODS.

### A. Level set method

A large number of technique and methods have been proposed and used [6]-[8]

It was first introduced by Osher and Sethian [9] who proposed an effective implicit representation for evolving curves and surfaces, it allows for automatic change of topology, such as merging and breaking, and the calculations are made on a fixed rectangular grid, where The basic idea is to represent the curves or surfaces as the zero level set of a higher dimensional hyper-surface. The level set method proposed in [10] is used to solve the minimization problem of [11]

In the level set method, an interface C is represented implicitly as a level set of a function φ, called level set function, of higher dimension. The geometric characteristics and the motion of the front are computed with this level set function. The interface is now represented implicitly as the zero-th level set (or contour) of this scalar function. Specifically, given a closed curve C, the function is zero if the pixel lies on the curve itself, otherwise, it is the signed minimum distance from the pixel to the curve.

This method makes it possible to evolve a closed parametric curve C (p) according to an equation of the type $\frac{\partial c}{\partial t} = FN$ [12]:

Where t is time, F is the rate of evolution and N is the unit normal to the curve. Each point of the curve C evaluates in the normal direction to the curve with a speed F as shown in Fig.1

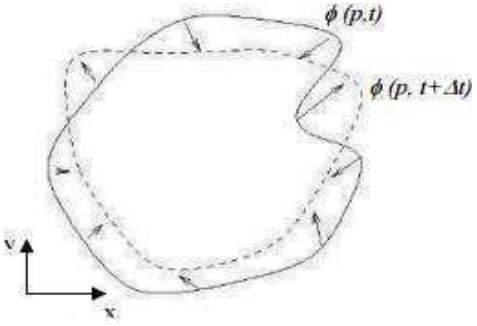


Fig. 1 The curve C evolved according to $\frac{\partial c}{\partial t} = FN$

Level set function $\phi(x, y)$, considering that $\phi(x, y) > 0$ if the point (x, y) inside c, $\phi(x, y) < 0$ if the point (x, y) is outside c $\phi(x, y) = 0$ if the point (x, y) is on c. Thus, the energy functional F(c1, c2, C) can be reformulated in terms of the level set function (x, y) as follows [13]:

$$F(c1, c2, \phi) = \lambda_1 \int_{\Omega} / I(x, y) - c1 /^2 H\varepsilon(\phi(x, y))dxdy + \lambda_2 \int_{\Omega} / I(x, y) - c2 /^2 (1 - H\varepsilon((\phi(x, y)))dxdy + \mu \int_{\Omega} \delta(\phi(x, y)) / \nabla\phi(x, y) / dxdy \quad (1)$$

Where H(Z) and $\delta\varepsilon(z)$ are, respectively, the regularized approximation of Heaviside function H and delta function $\delta$ as follows :

$$H(Z) = \begin{cases} 1 \vec{if} \bar{z} \geq 0 \\ 0 \bar{if} \bar{z} \prec 0 \end{cases} \qquad \delta(z) = \frac{d}{dz} H(z) \quad (2)$$

Using the Euler-Lagrange equations to solve the minimization problem of (1), the level set function (x, y) can be updated by the following gradient descent method:

$$\frac{\partial\phi}{\partial t} = \delta\varepsilon(\phi)\left[ \mu div(\frac{\nabla\phi}{|\nabla\phi|}) - \lambda_1 (I - c1)^2 + \lambda_2 (I - c2)^2 \right] \quad (3)$$

Where c1 and c2 can be expressed, respectively, as follows:

$$c1(\phi) = \frac{\int_{\Omega} I(x, y) H\varepsilon(\phi(x, y))dxdy}{\int_{\Omega} H\varepsilon(\phi(x, y))dxdy}$$

$$c2(\phi) = \frac{\int_{\Omega} I(x, y)(1 - H\varepsilon(\phi(x, y)))dxdy}{\int_{\Omega} (1 - H\varepsilon(\phi(x, y)))dxdy} \quad (4)$$

This technique not only provides more accurate numerical implementations but also handle topological change very easily. The main advantage of this method is the ability to automatically manage the change in topology of the evolving curve. The curve C can be divided into two or three curves; conversely several curves can merge and become a single curve

In image processing the level set method is most frequently used as a segmentation tool through propagation of a contour by using the properties of the image

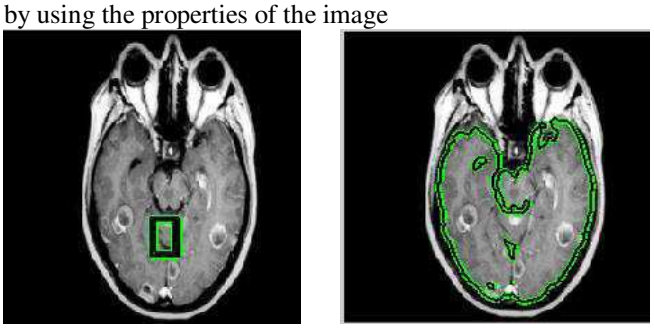

(a) (b)


ISSN 1737-9334

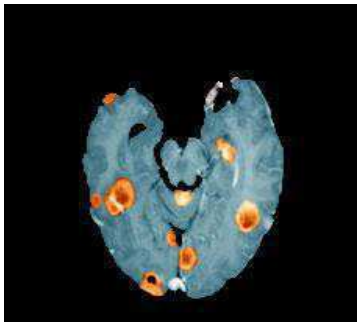

(c)

Fig.2 level set segmentation steps (a) Curve initialization, (b) level set segmentation, (c) foreground extraction

### *B. Quincunx wavelet*

The separable dyadic analysis require three families of wavelets, which is sometimes regarded as a disadvantage, in addition the factor of addition between two successive scales is 4 which may seem high. It is possible to solve these two problems, but at the cost of the loss of filter separability and therefore a slightly higher computational complexity. An analysis has been particularly well studied to find a practical application, known as "quincunx" [14]. Quincunx decomposition results in fewer subbands than most other wavelet decompositions, a feature that may lead to reconstructed images with slightly lower visual quality. The method is not used much in practice, but [15] presents results that suggest that quincunx decomposition performs extremely well and may be the best performer in many practical situations. Fig. 3 illustrates this type of decomposition. [16]

We notice that the dilation factor is not more than 2 between two successive resolutions, and that only one wavelet family is necessary [17, 18]. In this case the

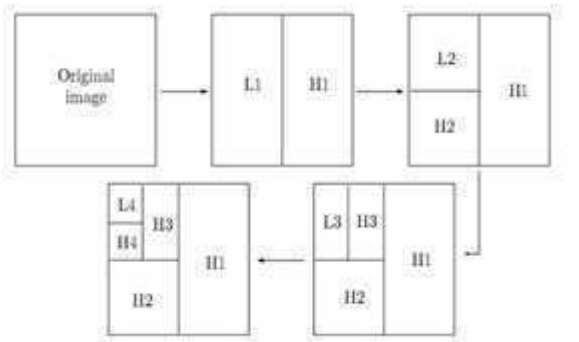


Fig. 3. Quincunx wavelet decomposition

In this case the Dilatation matrice will be :

$$M=\begin{bmatrix}1 & 1\\ 1 & -1\end{bmatrix}$$

The Grid transformation (lattice) is done according to $y_{i+1}[n]$ the following diagram:

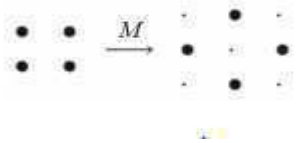


This matrix generates a quincunx lattice in 2D. The column vectors of this matrix form a basis to this lattice. The volume of the unit cell associated equals 2. The same lattice Fig. 4 is also emanating from the matrix below [14]

$$M'=\begin{bmatrix}1 & -1\\ 1 & 1\end{bmatrix}$$

It is noticed that the dilatation step is $\sqrt{2}$ on each direction and the geometry of the grid obtained justifies the name given to this multiresolution analysis

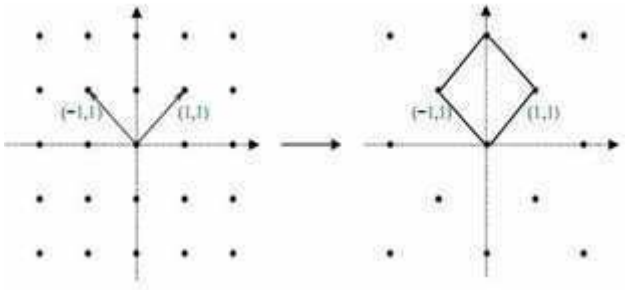


(a) (b)

Fig. 4. Examples of a lattice quincunx and unit cell (a) Lattice quincunx (b) Unit cell

#### *1) Quincunx Sampling and Filter*

First, we recall some basic results on quincunx sampling and perfect reconstruction filterbanks [19, 20]. The quincunx sampling lattice is shown in Fig. 4. Let $x[\vec{n}]$ with $\vec{n}=(n_1,n_2) \in Z^2$ denote the discrete signal on the initial grid. The two-dimensional (2-D) z-transform of $x[\vec{n}]$ is denoted by:

$$X(\vec{z})=\sum_{\vec{n}\in Z^2} x[\vec{n}]\vec{z}^{-\vec{n}} \quad \text{, where} \quad \vec{z}^{\vec{n}}=\vec{z}^{n_1}\vec{z}^{n_2} \tag{5}$$

The continuous 2-D Fourier transform is then given by

$$X(e^{j\vec{\omega}})=\sum_{\vec{n}\in Z^2} x[\vec{n}]e^{-j(\vec{w},\vec{n})} \quad \text{with } \overrightarrow{w=(w_1,w_2)} \tag{6}$$

and finally, the discret 2-D Fourier transform for $x[\vec{n}]$ given on an N x N grid (n1, n2= 0,1,…,N-1) by




ISSN 1737-9334

$$X\left(\vec{k}\right)=\sum_{n\in z^2} x\left[\vec{n}\right]e^{-j2\pi(\vec{k},\vec{n})/N},$$

With (k1,k2=0,1,…, N-1)

Now, we write the quincunx sampled version of x[$\vec{n}$] as:

$$\left[x\right]_{\downarrow M}\left[\vec{n}\right]=x\left[M\vec{n}\right] \quad \text{where} \quad M=\begin{pmatrix}1 & 1\\ 1 & -1\end{pmatrix} \tag{7}$$

Our down-sampling matrix M is such that $M^2 = 2$ I. where I is identity matrix.

The Fourier domain version of (2) is

$$\left[x\right]_{\downarrow M}\left[\vec{n}\right]=\leftrightarrow\frac{1}{2}\left[X\left(e^{jM^{-T}\vec{\omega}}\right)+X\left(e^{j\left(M^{-T}\overrightarrow{\omega+\pi}\right)}\right)\right] \tag{8}$$

Where $\vec{\pi}$ =(π , π) .

The up-sampling is defined by

$$\left[x\right]_{\uparrow M}\left[\vec{n}\right]=\begin{cases}x\left[M^{-1}\vec{n}\right], when n_1+n_2\\ 0 elsewhere\end{cases} \tag{9}$$

and its effect in the Fourier domain is as follows:

$$\left[x\right]_{\uparrow M}\left[\vec{n}\right]=\leftrightarrow X\left(e^{jM^T\vec{\omega}}\right) \tag{10}$$

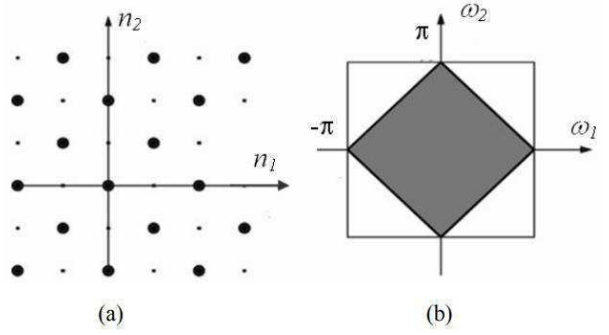


Fig. 5. (a) Quincunx lattice; (b) the corresponding Nyquist area in the frequency domain

If we now chain the down-sampling and up-sampling operators, we get

$$\left[x\right]_{\downarrow M\uparrow M}\left[\vec{n}\right]=\begin{cases}x\left[\vec{n}\right], when n_1+n_2 is even\\ 0 elsewhere\end{cases} \tag{11}$$

$$\left[x\right]_{\downarrow M\uparrow M}\left[\vec{n}\right]=\frac{1}{2}\left[X(e^{j\vec{\omega}})+X(e^{j(\vec{\omega}+\vec{\pi})}\right] \tag{12}$$

Since quincunx sampling reduces the number of image samples by a factor of two, the corresponding reconstruction filterbank has two channels Fig. 6. The low-pass filter $\tilde{H}$ reduces the resolution by a factor of $\sqrt{2}$ ; the wavelet coefficients correspond to the output of the high-pass filter $\tilde{G}$ [18]-[20].

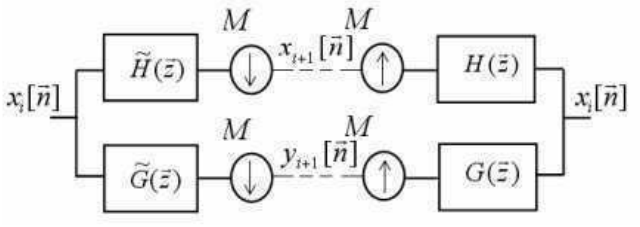


Fig. 6. Perfect reconstruction filter bank on a quincunx lattice

*2) Fractional Quincunx Filters*

As starting point for our construction, we introduce a new 1-D family of orthogonal filters

$$H_a(\omega)=\frac{\sqrt{2}(2+2\cos\omega)^{\frac{a}{2}}}{\sqrt{(2+2\cos\omega)^a+(2-2\cos\omega)^a}} \tag{13}$$

Which is indexed by the continuously-varying order parameter α.

Applying the diamond McClellan transform to the filter above is straightforward; it amounts to replacing cos ω by 1 2 (1/ 2)(cos $\omega_1+\cos\omega_2$ ) in (13). Thus, our quincunx refinement filter is given by

$$H_a(e^{j\omega})=\frac{\sqrt{2}(2+\cos\omega_1+\cos\omega_2)^{\frac{a}{2}}}{\sqrt{(2+\cos\omega_1+\cos\omega_2)^a+(2-\cos\omega_1-\cos\omega_2)^a}} \tag{14}$$

This filter is guaranteed to be orthogonal because the McClellan transform has the property of preserving biorthogonality. Also, by construction, the α th order zero at ω =π gets mapped into a corresponding zero at $(\omega_1,\omega_2)=(\pi,\pi)$ ; this is precisely the condition that is required to get a 2-D wavelet transform of orderα . Also, note the isotropic behavior and the flatness of $H_a(e^{j\omega})$ around the origin; i.e, $H_a(e^{j\omega})/\sqrt{2}=1+O(\|\vec{\omega}\|^a)$ for $\vec{\omega}\to 0$ . The orthogonal wavelet filter is obtained by modulation

$$G_a(\vec{z})=z_1H_a(-\vec{z}^{-1}) \tag{15}$$

The corresponding orthogonal scaling function is defined implicitly as the solution of the quincunx two-scale relation

$$\varphi_a(\vec{x})=\sqrt{2}\sum_{n\in z^2}h_a\left[\vec{n}\right]\varphi_a\left(M\vec{x}-\vec{n}\right) \tag{16}$$

Since the refinement filter is orthogonal with respect to the quincunx lattice, it follows that $\varphi_a(\vec{x})\in L_2\left(R^2\right)$ and that it is orthogonal to its integer translates. Moreover, for α >0 , it will satisfy the partition of unity condition, which comes as a direct consequence of the vanishing of the filter at


ISSN 1737-9334

$(\omega_1,\omega_2)=(\pi,\pi)$Thus, we have the guarantee that our scheme will yield orthogonal wavelet bases of $L_2(R^2)$. The underlying orthogonal quincunx wavelet is simply

$$\psi_a(\vec{x}) = \sqrt{2}\sum_{n\in z^2} g_a\left[\vec{n}\right]\varphi_a\left(M\vec{x}-\vec{n}\right) \quad (17)$$

### C. SPHT Coding scheme

SPIHT algorithm is an improved version of EZW algorithm proposed by A. Said and Pearlman [18] SPIHT performs a recursive partitioning of the tree in order to determine the position of the significant coefficients in the progeny of the considered coefficient

The success of SPIHT is due to the organisation of wavelet coefficients into the spatial orientation trees.

The following sets of coordinates are used to present the new coding method:

O (i, j) : set of coordinates of all offspring of node (i, j);

D (i, j) : set of coordinates of all descendants of the node (i, j);

H: set of coordinates of all spatial orientation tree roots (nodes in the highest pyramid level);

L (i, j) = D(i, j) - O(i, j).

In a practical implementation the significance information is stored in three ordered lists, called list of insignificant sets (LIS), list of insignificant pixels (LIP), and list of significant pixels (LSP). In all lists each entry is identified by a coordinate (i, j), which in the LIP and LSP represents individual pixels, and in the LIS represents either the set D (i, j) or L (i, j).

The first idea is always the same: if there is a coefficient in the highest level of transform in a particular subband considered insignificant against a particular threshold, it is very probable that its descendants in lower levels will be insignificant too, so we can code quite a large group of coefficients with one symbol. Fig.7 shows how a spatial orientation tree is defined in a pyramid constructed with recursive four subbands splitting. The coefficients are ordered in hierarchies [21]

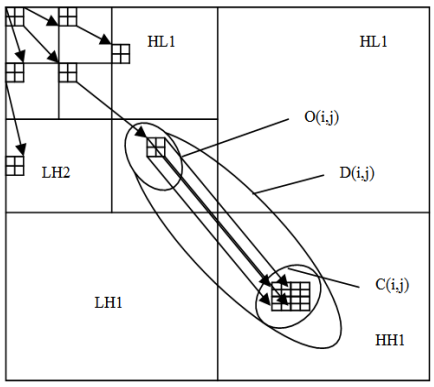


Fig. 7 Parent-child relationship

### D. Quality evaluation parameter

*3) The peak signal to noise ratio (PSNR).*

The peak signal to noise ratio (PSNR) used to measure the quality of reconstruction in image compression. It refers to the ratio between signal and reconstruction error variance in Decibel scale. It can be represented as [22]:

$$MSE = \frac{1}{M\,x\,N}\sum_{1=1}^{i=M}\sum_{j=1}^{j=N}\left(I(i,j) - \hat{I}(i,j)\right)^2 \quad (18)$$

Where

MSE: mean squar error between two images

Mean Square Error (MSE) which requires two MxN grayscale images I and $\hat{I}$ where one of the images is considered as a compression of the other

The PSNR is defined as:

$$PSNR = 10\log_{10}\left(\frac{(Dynamics\quad of\quad image)^2}{MSE}\right) \quad (19)$$

*4) The Structural Similarity Index(SSIM).*

This parameter compares the similarity the brightness, contrast and structure between each pair of vectors, the structural similarity index between two signals x and y is given by the following expression [23,24]:

$$SSIM(x,y) = l(x,y).c(x,y).s(x,y) \quad (20)$$

The MSSIM is used to measure the quality of the local image, which provides more information on the degradation of image quality, which is useful in medical imaging applications. It values exhibit greater consistency with the visual quality.

$$MSSIM(I,\hat{I}) = \frac{1}{M}\sum_{i=1}^{M} SSIM(I_i,\hat{I}_i) \quad (21)$$

Where

I and Î are respectively the reference and degraded images, $I_i$ and $\hat{I}_i$ are the contents of images at the i-th local window.

M: the total number of local windows in image.

Finally the quality measurement can provide a spatial map of the local image quality, which provides more information on the image quality degradation, which is useful in medical imaging applications.

## III. RESULTS AND DISCUSSION

The aim of our work lies in the possibility of reducing the rates, for which the image quality remains acceptable, which we are interested in hybrid compression methods based on activ contour segmentation and 2D wavelet transforms because of their interesting properties, applied to medical images. For this reasons the PSNR evaluation parameters and the MSSIM similarity index are used to estimate and judge the quality of the compressed image.

In order to verify the efficiency of our hybrid algorithm, we applied, (level set +CDF 9/7 (lifting scheme) + SPIHT)




ISSN 1737-9334

and (level set +quincunx + SPIHT) on color MRI medical images of size 512x512 encoded by 8 bits per pixel. This image is taken from the GE Medical System database [25].

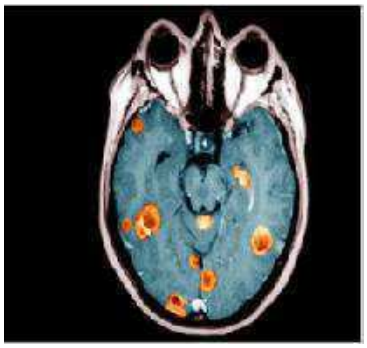

Fig. 8 MRI brain original image

Fig.9 shown below illustrates the steps of the compressed image (region of interest image) by the quincunx wavelet

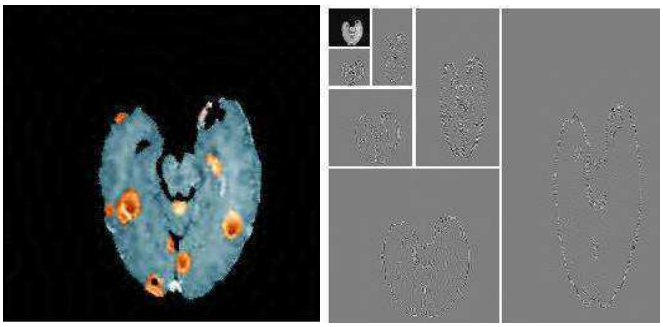

(a) (b)

Fig. 9 image compression (a) the region of interest (b) quincunx wavelet decomposition

The compressed image quality for different bit-rate values (number of bits per pixel) by the proposed algorithm is presented in the Fig .10

From the results of the PSNR, MSSIM and MSE values obtained, we note that from 0.5bpp, the reconstructed image becomes almost perfect.

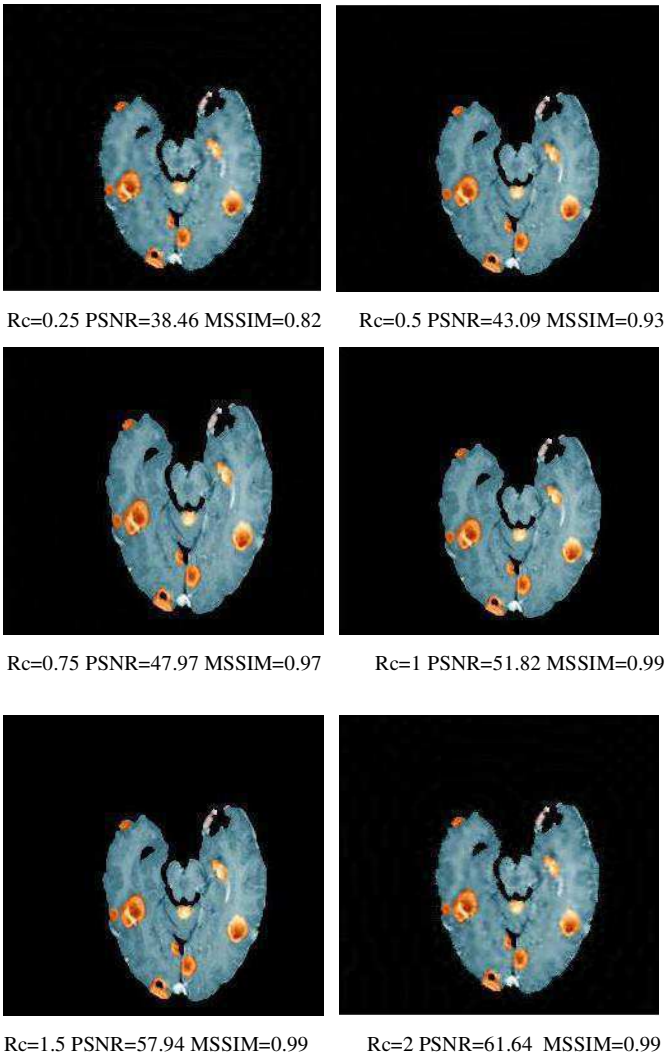

Rc=0.25 PSNR=38.46 MSSIM=0.82 Rc=0.5 PSNR=43.09 MSSIM=0.93

Rc=0.75 PSNR=47.97 MSSIM=0.97 Rc=1 PSNR=51.82 MSSIM=0.99

Rc=1.5 PSNR=57.94 MSSIM=0.99 Rc=2 PSNR=61.64 MSSIM=0.99

Fig..10 Compressing of an MRI brain image with level set coupled with quincunx wavelet and SPIHT coding

To ensure the performance of our proposed method, we compared between these different types of transform CDF9/7 (Lifting scheme)) coupled with level set method and SPIHT coding and CDF9/7 (Lifting scheme)) coupled with SPIHT coding without applied the level set segmentation applied to the same medical image. The table (1) and (2) given bellow represent these results




ISSN 1737-9334

TABLE I
PSNR AND MSSIM VARIATION USING DIFFERENT METHODS PROPOSED

| Typed'image | RC (bpp) | Level set + quincunx + SPIHT | | | Level set + CDF9/7 (lifting) + SPIHT | | |
|---|---|---|---|---|---|---|---|
| | | PSNR | MSSIM | MSE | PSNR | MSSIM | MSE |
| IRM | 0.25 | 38.46 | 0.82 | 9.27 | 36.12 | 0.47 | 16.03 |
| | 0.5 | 43.09 | 0.93 | 3.2 | 39.71 | 0.62 | 7.01 |
| | 0.75 | 47.97 | 0.97 | 1.04 | 44.19 | 0.79 | 2.5 |
| | 1 | 51.82 | 0.99 | 0.43 | 49.19 | 0.93 | 0.79 |
| | 1.5 | 57.94 | 0.99 | 0.11 | 57.77 | 0,99 | 0.11 |
| | 2 | 61.64 | 0.99 | 0.05 | 61.43 | 0.99 | 0.05 |

TABLE III
PSNR AND MSSIM VARIATION USING DIFFERENT METHODS PROPOSED

| RC (bpp) | Quincunx +SPIHT | | | CDF9/7 (lifting)+ SPIHT | | |
|---|---|---|---|---|---|---|
| | PSNR | MSSIM | MSE | PSNR | MSSIM | MSE |
| 0.25 | 38.98 | 0.91 | 8.23 | 36.35 | 0.64 | 15.22 |
| 0.5 | 44.33 | 0.96 | 2.4 | 41.51 | 0.79 | 4.63 |
| 0.75 | 47.91 | 0.98 | 1.06 | 45.88 | 0.94 | 1.7 |
| 1 | 50.75 | 0.99 | 0.56 | 48.15 | 0.96 | 1.01 |
| 1.5 | 54.12 | 0.99 | 0.26 | 53.04 | 0.99 | 0.33 |
| 2 | 56.45 | 0.99 | 0.16 | 55.80 | 0.99 | 0.18 |

Comparing the different values of PSNR,MSSIM, and MSE we ensure the efficiency of our algorithm in terms of compressed image quality for the low bit-rate

The fig.11 shown bellow, represent the results of the comparison obtained after application of different algorithms applied on an MRI brain, given by the PSNR curve

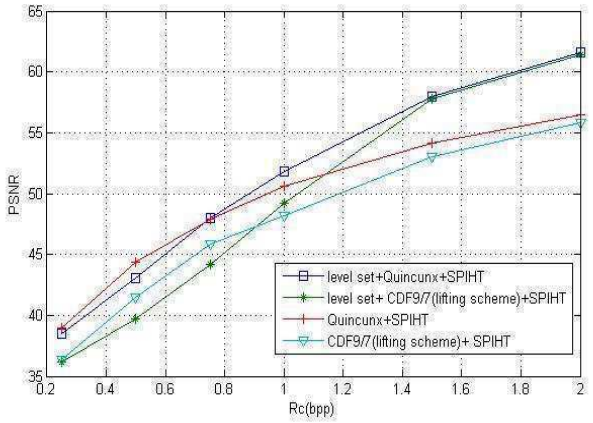


Fig. 11 PSNR variation using different proposed methods

According to the different results obtained for the several application of our hybrid method on color MRI medical image, we ensure that our proposed algorithm gives better quality and it is an efficient method compared with other technique, more precisely when compressed the region of interest image after applying the level set segmentation with quincunx algorithm coupled with SPIHT coding, which gives a better performance and image quality.

## IV. CONCLUSIONS

The work in this paper is to enhance medical images quality after the compression step.

We used an hybrid method composed of the level set method and the quincunx wavelet transform applied on MRI color medical image. We compared the founding results with the level set coupled with CDF9/7 lifting algorithm and SPIHT, we notice that the proposed algorithm gives better results than the other compression technique for the MRI color image. Generally the results obtained are very satisfactory in terms of compression ratio and compressed image quality.

## V. REFERENCES

[1] Kumar SN , Lenin Fred A, and Muthukumar S, '' A voyage on medical image segmentation algorithms'', *biomedical research, Special Section: Computational Life Sciences and Smarter Technological Advancement*,2018

[2] Abdelaziz E, Elhoussaine O and Abdenbi B,'' Medical Image Segmentation by Active Contour Improvement '', *American Journal of Software Engineering and Applications*, 6, (2), 2017, pp. 13-17

[3] Sanping Z , Jinjun W, Shun Z, '' Active Contour Model Based on Local and Global Intensity Information for Medical Image Segmentation'', *Preprint submitted to Journal of Neurocomputing, september* 2016.

[4] Adegoke, B. O , Olawale, B. ., Olabisi, N.I, '' Overview of Medical Image Segmentation'', *International Journal of Engineering Research and Development*, 8, (9), September 2013

[5] M. Beladgham, A. Bessaid, A. Taleb-Ahmed and I. Boucli Hacene, "Medical Image Compression Using Quincunx Wavelets and SPIHT Coding", Journal of Electrical Engineering & Technology Vol. 7, No. 2, pp. 264~272, 2012

[6] Daniel J. Withey and Z.J. Koles, "A Review of Medical Image Segmentation: Methods and Available Software", International Journal of Bioelectromagnetism, Vol. 10, No.3, pp.125-148, 2008

[7] R. Loganathan and Y. Kumaraswamy, "Active contour based medical image segmentation and compression using biorthogonal wavelet and embedded zerotree," Indian Journal of Science and Technology, vol. 6, pp. 4390-4395, 2013.

[8] P.nagaswara Reddy and C.P.V.N.J Mohan Rao, "BRAIN MR IMAGE SEGMENTATION BY MODIFIED ACTIVE CONTOURS AND CONTOURLET TRANSFORM", ICTACT journal on image and video processing, vol.08, novembre 2017

[9] J. A. Sethian, level set Methods and Fast Marching Methods, second ed., Cambridge University Press, 1999.

[10] S. Osher and J. A. Sethian, "Fronts propagating with curvature dependent speed: algorithms based on Hamilton-Jacobi formulations," Journal of Computational Physics, vol. 79, no. 1, pp. 12– 49, 1988.

[11] T. Chan and L. Vese, "Active contours without edges," IEEE Trans. Image Process. 10, 266–277 2001.


ISSN 1737-9334

[12] M. Beladgham, F. Derraz, '' Segmentation d'images médicales IRM par la méthode d'ensembles de niveaux (Level_Sets)'', Abou- Bekr Belkaid university –Tlemcen, january,2005
[13] L. Tingting Xu. Haiyong Xu, "Medical Image Segmentation Based on a Hybrid Region-Based Active Contour Model", Hindawi Publishing Corporation,Computational and Mathematical Methods in Medicine, vol14, juin 2014
[14] Dimitri VD., Thierry B. and Michael U. "On the Multidimensional Extension of the Quincunx Subsampling Matrix'', IEEE Signal Processing Letters, Vol. 12, No. 2, FEBRUARY 2005.
[15] Chen Y. Michael AD. and Wu-Sheng L. "Design of Optimal Quincunx Filter Banks for Image Coding'', EURASIP Journal on Advances in Signal Processing, Vol. 2007.
[16] Lee L., Oppenheir V.A., "Proprerties of approximate parks-McClellan filters'', IEEE, pp.2165-2168; 1997;
[17] Miaou S.G., Chen S.T. and Chao S.N., "Waveletbased lossy-to-lossless medical image compression using dynamic VQ and SPIHTcoding'', Biomedical engineering-applications, basis & communications, Vol. 15 No3, p 235-242, December 2003.
[18] Said A. and Pearlman W. A., "A new fast and efficient image codec based on set partitioning in hierarchical trees'', IEEE Trans. Circuits and Systems for Video Technology, Vol. 6, p243 – 250, June 1996.
[19] Vetterli M. and Kovacevé J., "Wavelets and Subband Coding'', Upper Saddle River, NJ: Prentice-Hall, 1995.
[20] Manuela F., Dimitri VD. and Michael U., "An Orthogonal Family of Quincunx Wavelets With Continuously Adjustable Order'', IEEE Transactions On Image Processing, Vol. 14, No. 4, APRIL 2005
[21] Yen-Yu C. and Shen-Chuan T., "Embedded medical image compression Using DCT based subband decomposition and modified SPIHT data organization'', Proceedings of the Fourth IEEE, (BIBE'04), 2004.
[22] M. Beladgham , A. Bessaid,' ' MRI IMAGE COMPRESSION USING
BIORTHOGONAL CDF WAVELET BASED ON LIFTING SCHEME AND SPIHT CODING' ', Quatrième Conférence Internationale sur le Génie Electrique CIGE' 10, 03-04 Novembre 2010, Université de Bechar, Algérie, Journal of Scientific Research vol. 2 (2010)
[23] Wang Z., Bovik A. C., Sheikh H. R. and Simoncelli E.P, "Image quality assessment: From error visibility to structural similarity'', IEEE Transactions on Image Processing, Vol. 13, No. 4, APRIL 2004.
[24] Wang Z. and Bovik A. C, "A universal image quality index'', IEEE Signal Processing Letters, Vol. 9, pp.81–84, Mar. 2002
[25] www.GE Medical System.com (database).




ISSN 1737-9334

# A Comparative Analysis Of Different Photovoltaic Cells Models Based On Fundamental Modeling Approaches

M. Aidoud [#1], C-E. Feraga [*2], M. Bechouat [#3], M. Sedraoui [#4], S. Kahla [#5],

[1]Laboratory of Automatic and Informatics of Guelma (LAIG) University 8 Mai 1945 Guelma, Algeria.

[2]Laboratory of Electrical Engineering LGEG. Department of Electrical Engineering and Automatic, University 8 Mai 1945 Guelma, Algeria.

[3,4]Laboratoires des Télécommunications LT, Department of Electronic and Telecommunication, University 8 Mai 1945 Guelma, Algeria.

[5] Research Center in Industrial Technologies, CRTI, Algiers, Algeria.

aidoudm@gmail.com

chferaga@yahoo.fr

mohcene.oui@gmail.com

msedraoui@gmail.com

samikahla40@yahoo.com

*Abstract*—**This work focuses on multiple fundamental approaches used for modeling photovoltaic (PV) cells behavior and PV arrays one. Indeed, the PV cells models are generally designed using conventional mathematical equations. Afterward, the obtained PV model is simulated in Matlab/Simulink software using fundamental mathematical blocks and Simulink advanced library. In this paper, three PV model types are discussed. The first one is designed through the SimElectronics, in which a solar cell that is available in its library is used for modeling the PV cell behavior. The second PV model is performed using the Simscape library where physical components are adopted to describe the PV cell behavior. The last PV model is designed through some conventional mathematic equations describing a single PV cell behavior, in which some mathematical operator library and functions are used. Furthermore, all previous PV models allow predicting the PV cell behavior under different physical and environmental parameters. They allow also highlighting the flexibility of Simulink and the advantages of using the physical modeling libraries. Finally, the simulation results which validate the proposed models are presented.**

***Keywords***— **PV cell, Simulink, Simscape, Simelectronics, PV model.**

## I. INTRODUCTION

The growing energy demand with the possibility of reduced supply of conventional fuels, proved by high petroleum prices, along with growing concerns about polluting effects on environment, has driven researchers and their developments to alternative energy sources which are cleaner, renewable and produce less environmental impact. Among the alternative sources, solar energy is one of the most used and readily available renewable energy sources. Solar energy supplied by the sun in one hour is equal to the energy required by the human population in one year. Power generated by PV module depends upon the solar irradiation.

It is observed from various studies, that mathematical models of few individual components of PV system are modeled and simulated for better understanding of their performances. Indeed, the most important component that affects the precision of the simulation is the PV cell modeling. With this model, we can estimate of the I-V and P-V characteristics. However, no specific mathematical models of PV module exist for all applications. The development of PV system has required simulation tools able to control the mathematical model. Simulations have facilitated the process of developing and estimation of new systems using PV energy, by reducing cost and time. In this context, during these last years, many research laboratories focused on the modeling methods for solar PV, and important renovations have been achieved on this theme [1-6]. It may be clear from the literature there have been a number of modeling options starting from equivalent circuit equations which have been researched for PV cells, trading off accuracy with complexity. The single diode model is the most popular PV cell model used by researchers due to its simplicity and flexibility during parameter estimation [7-8]. Matlab simulink provide many ways of modeling devices or components or modeling complex systems. This paper presents a comparative study between multiple fundamental approaches that can be used for modeling photovoltaic cells. The studied methods used for comparison in this paper include Simulink implementation using mathematical blocks, Simscape and Simelectronics libraries. This paper has basically three sections. The first section presents a description of modeling single–diode solar cell. In the second section are described how the PV solar array are modeled using the methods cited above. The results and discussions regarding simulation of PV system are also




ISSN 1737-9334

presented. Finally, in the last section of paper are presented the main conclusions of this study.

## II. PV CELL MODEL

PV systems are broadly characterized by circuit-based approaches. For modeling a PV system under the illumination, the simplest way is to consider a current source in parallel to a diode. Consequently, three unknown parameters, namely, photo generated current ($I_{ph}$), diode saturation current ($I_{sd}$) and diode ideality factor ($n$), make the parameters of the equivalent circuit model. For considering the PV cell metal contacts, an improved model, takes into account a series resistance ($R_s$) to the model. Though $R_s$-model is more accurate, it shows serious deficiencies under high temperature variations since it does not account for the open circuit voltage coefficient. Another modification was suggested by adding a shunt resistance ($R_{sh}$) to the diode to consider the partial short circuit current path near the cell's edges resulted from the semiconductor impurities and non-idealities. This type of the model is known as the single diode model. In the single diode model, shown in Fig. 1, the terminal current can be formulated as follows [1-4]:

$$\boldsymbol{I_{pv} = I_{ph} - I_d - I_{sh}} \qquad \textbf{(1)}$$

Where $I_d$ is the diode current and $I_{sh}$ denotes the shunt resistor current. By use of Shockley equation for the diode current and substituting the shunt resistor current, Eq. (1) is rewritten as given in the following equation:

$$\boldsymbol{I_{pv} = I_{ph} - I_{sd}\left[e^{\left(\frac{q(V_t+R_S\,I_{pv})}{nkT}\right)} - 1\right] - \frac{(V_t+R_S\,I_{pv})}{R_{sh}}} \qquad \textbf{(2)}$$

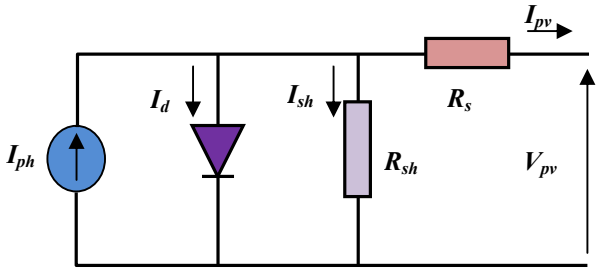


Fig 1. The single diode model of PV cell

Where $I_{sd}$ is the diode saturation current, $V_t$ is the terminal voltage, $q$ is the electronic charge, $k$ denotes the Boltzmann constant, $n$ is the diode ideality factor and $T$ ($°K$) is the cell temperature. When insolation drops, short-circuit current of cell drops in direction proportion. A PV module consists of series and parallel PV cell combinations.

In practice photocurrent $I_{ph}$ is dependent on actual and standard irradiance ($G$ and $G_{ref}$) and solar cell operating and standard temperature ($T$ and $T_{ref}$) according to the following relation:

$$I_{ph} = \frac{G}{G_{ref}}\left[I_{sc,ref} + K_i(T - T_{ref})\right] \qquad (3)$$

With $I_{sc,ref}$ is the cells short-circuit current provided by manufacturer at standard temperature ($25°C$), $K_i$ is temperature coefficient of the short circuit current.

## III. SIMELECTRONICS SIMULATION MODEL FOR A SOLAR CELL

SimElectronics is part of the Simulink Physical Modeling family, providing component libraries that include semiconductors, motors, drives, sensors, and actuators. To build electromechanical and electrical models, a combination of SimElectronics blocks and other Simscape and Simulink blocks can be used. These blocks are used to optimize system-level performance and to create installation templates for control design. Fig.2 shows the symbol of solar cell in SimElectronics. In its library, this block represents a single solar cell as a parallel current source $I_{ph}$, an exponential diode D and a shunt resistance $R_{sh}$, that are connected in series with a resistance $R_s$.

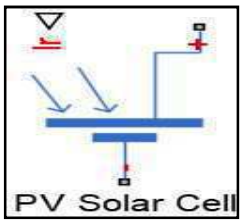


Fig. 2.Symbol of a Solar cell under SimElectronics environment

The SimElectronics model used for simple solar cell simulation is shown in Figure 3. The block of the PV cell (see Fig. 2) uses the five-parameter model with the impedance of parallel resistance being infinite. The model chosen makes it possible to optimize this block according to the parameters of the equivalent circuit model or the short-circuit current and the open-circuit voltage [8-13].

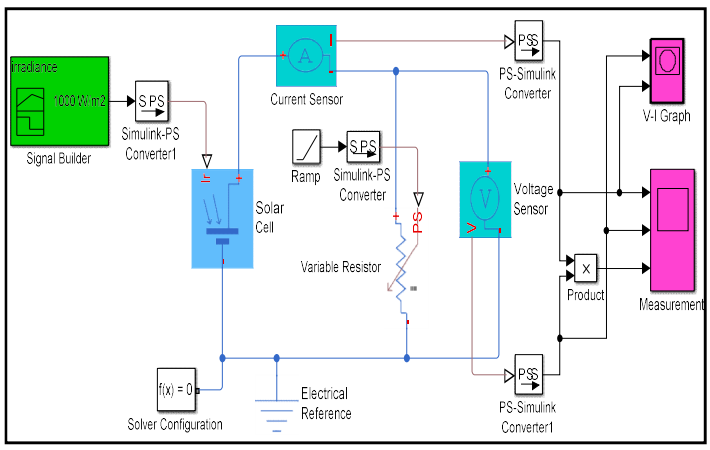


Fig. 3.SimElectronics Simulation Model for a single Cell




ISSN 1737-9334

The model shown in fig.3 was developed using blocks of SimElectronics and Simulink. In fact, the solar cell is connected to the current and voltage sensor blocks to measure current and voltage in the solar cell. In addition, an irradiance block is also connected in the above model. The other blocks formed the interface between the main blocks and were used to plot the I-V characteristics.

The solar cell was parameterized by equivalent circuit parameters. Diode reverse saturation current, $I_s$, was taken as *0.1nA*, measurement temperature was kept as *25°C*. Solar-generated current, $I_{ph0}$, and Irradiance used for measurements, $G_0$, were kept at their default values of *7.34A* and *1000 W/m²* respectively. The photovoltaic cell model is validated by simulating at a value of irradiance of *1000W/m²* and a temperature of *25°C*.

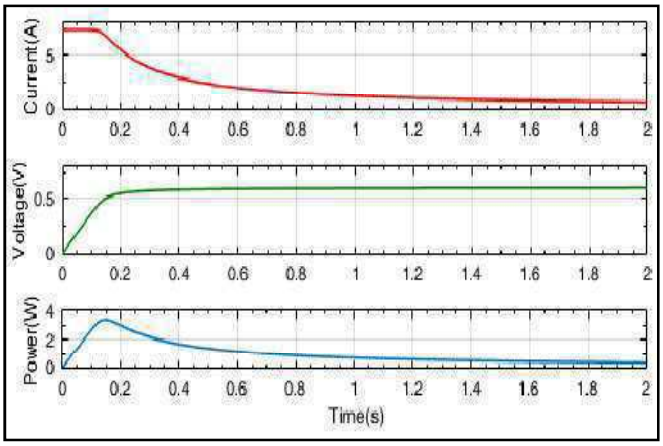


Fig. 4 Current, voltage and power curves for PV cell

Figure 4 shows the current, voltage and power curves of the photovoltaic cell. When the resistance of the load varies, the current, voltage and power faithfully describe the behavior of the PV generator

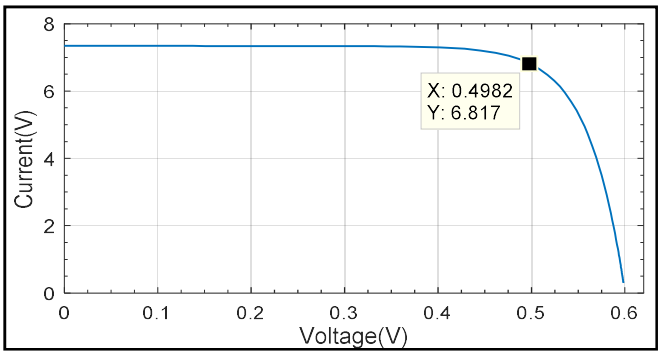


Fig. 5.The I-V characteristics of the photovoltaic cell.

The I-V characteristics of the photovoltaic cell is given in Figure 5. It represents the standard behavior of the photovoltaic cell. In the middle of this characteristic is the maximum power point. This point is very critical for this kind of system for maximum power extraction from the photovoltaic system. This result that, the main objective is to try operating around of this maximum point in order to make the photovoltaic cells to work at maximum efficiency.

### *A. Variation in irradiance*

Fig.6 shows the I-V and P-V characteristics .The simulation was performed for Irradiance which vary in steps of 300W/m² from 400 W/m² to 1000 W/m². The Circuit temperature (SimElectronics Environment Parameter) was kept at 25°C.

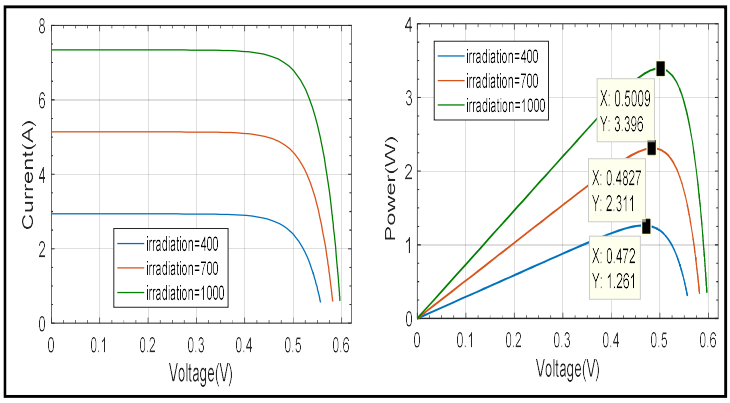


Fig.6. Characteristic: Current, Power = f (Voltage) for different illuminations

It is observed that the photocurrent varies with irradiance and the percentage change in short circuit current *($I_{sc}$)* is much more than the percentage change in open circuit voltage *($V_{oc}$)*.The current changes from 7.3A to 2.9A and power from 3.39W to 1.26W. The output power is higher for high irradiance value.

TABLE I

IRRADIANCE VARIATION

| **Irradiance(W/m²)** | 400 | 700 | 1000 |
|---|---|---|---|
| **$V_m$(V)** | 0.472 | 0.4827 | 0.5009 |
| **$P_m$(W)** | 1.261 | 2.311 | 3.396 |

## IV. MODEL USING PHYSICAL ELEMENTS

This model is developed using the Simscape library where physical components are adopted to describe the PV cell behavior. The circuit contains (a current source, two resistors and a diode); the equivalent circuit diagram of the solar cell is represented by the fig.7.


ISSN 1737-9334

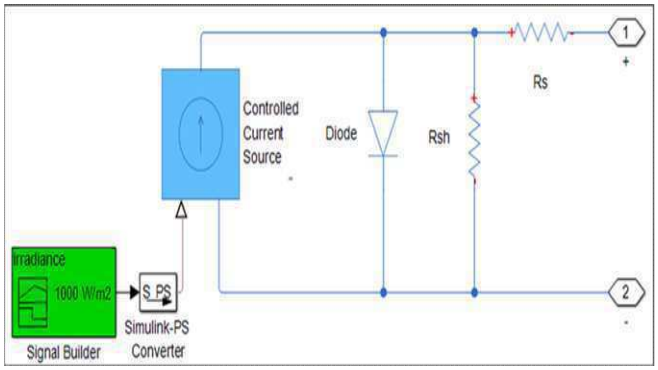


Fig.7. Equivalent circuit of a cell in Simscape environment

The complete simulation model of solar PV cell is shown in Fig.8. It consists of three main blocks, namely: PV cell block, sensors block and load block.

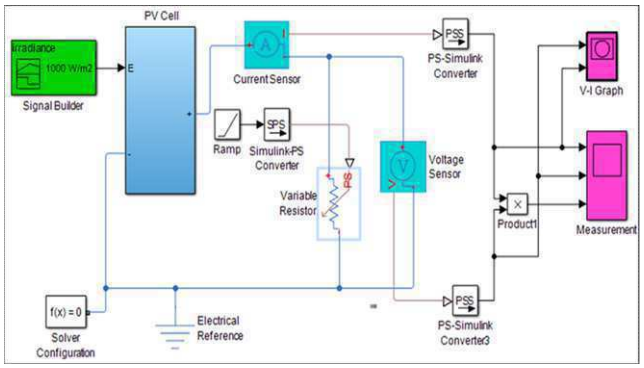


Fig.8. Modeling of the PV cell under the environment Simscape

Figure 9 shows the current, voltage and power which are obtained at output of PV cell. These curves are gives versus time. As soon as the resistance varies, the current and voltage vary depending on the voltage-time relationship which gives the power curve.

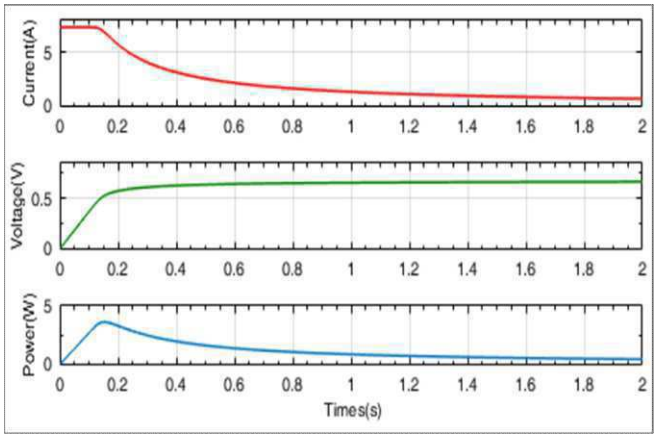


Fig. 9. Current, voltage and power curves for PV cell

Fig.10 shows the I–V characteristic of a PV cell under STC conditions of 25°C temperature and 1000 W/m$^2$ of irradiance.

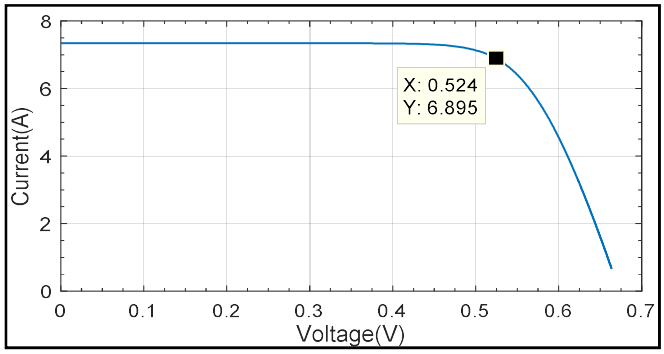


Fig. 10.The I-V characteristics of the photovoltaic cell.

In fig.11 the PV cell output current and power are greatly influenced by the change in radiation, whereas the output voltage stays approximately constant. There is a unique point in which the solar module is said to operate at maximum efficiency and produces its maximum output power $(P_m)$ corresponds to a specific current $(I_m)$ and voltage $(V_m)$. This point also changes with environmental conditions.

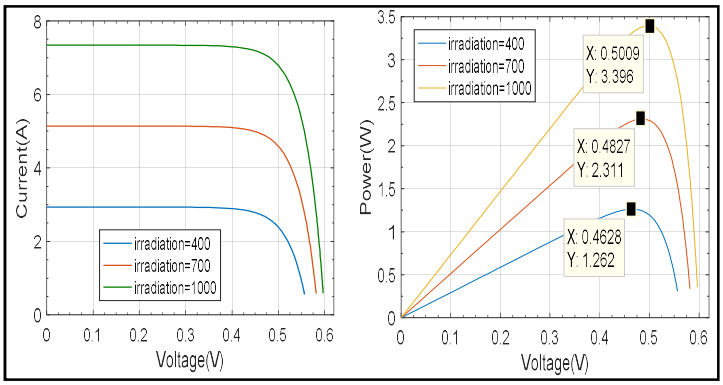


Fig.11. Characteristic: Current, Power = f (Voltage) for different illuminations

## B. *Variation in irradiance*

From Fig. 11 and Table 2, it can be observed that the irradiance value impacted the short-circuit current $(I_{sc})$ as well as open-circuit voltage $(V_{oc})$ but more affected was the value of $(I_{sc})$. As irradiance value increased, the short -circuit increased and the maximum power $P_m$ also increased.

TABLE II

IRRADIANCE VARIATION

| **Irradiance(W/m$^2$)** | 400 | 700 | 1000 |
|---|---|---|---|
| **$V_m$(V)** | 0.4628 | 0.4827 | 0.5009 |
| **$P_m$(W)** | 1.262 | 2.311 | 3. 396 |

## V. MODEL USING FUNCTION IN SIMULINK

By using general model (see fig.1) and applied equations (1) and (2), we have established the block of the PV generator in SimPowerSystems/ Simulink which is represented in fig.12.


ISSN 1737-9334

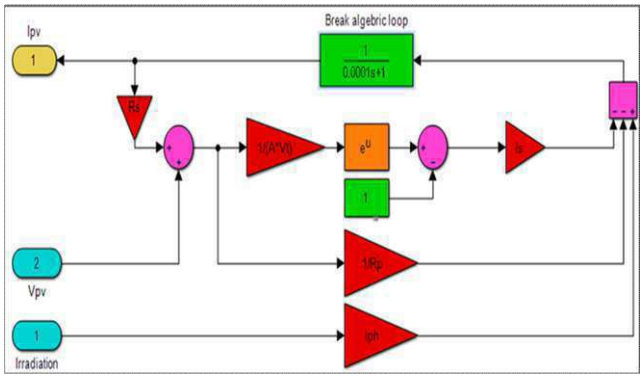


Fig. 12. Model of PV solar cell using Simulink /SimPower System.

The Simulink Simulation Model for a single Cell using SimPower System is represented by Fig.13. It contains a Solar cell which is connected to the variable resistor through current sensor and voltage sensor. The Simulink converter blocks provide the current and voltage of solar cell to the measurement blocks.

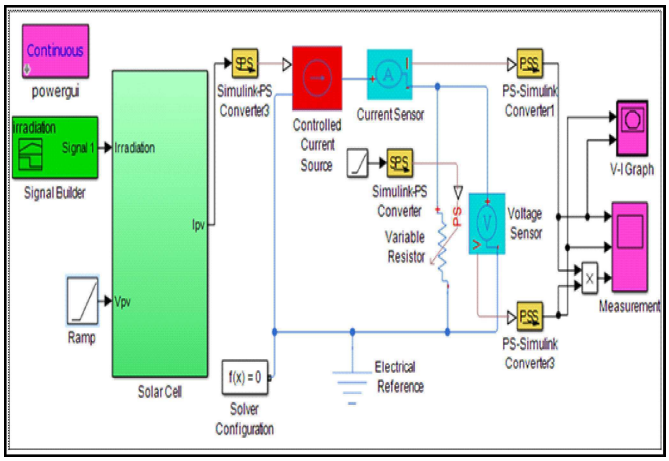


Fig. 13.Simulink Simulation Model for a single Cell

Fig. 14 also confirms the behavior expected from a solar cell: its current and voltage vary depending on the voltage-time relationship which gives the power curve.

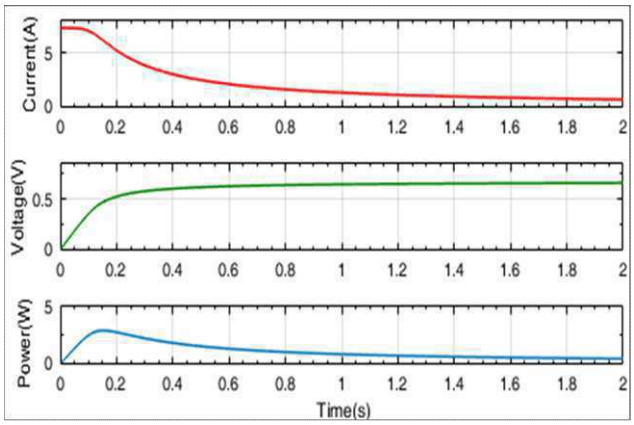


Fig. 14. Current, voltage and power curves for PV cell

The I-V characteristic is shown in fig.15. The curve indicates the solar cell maximum voltage and maximum output current at 25°C temperature and for an irradiation of 1000 W/m$^2$.

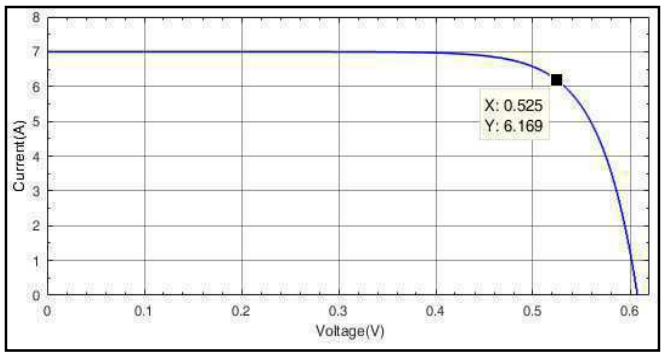


Fig. 15.The V-P characteristics of the photovoltaic cell.

## C. *Variation in irradiance*

In Figure 16 are given the P-V characteristics for different levels of solar radiation at the temperature of 25°C. From this Figure, it is observed that for an irradiance of 700 W/m$^2$, which corresponds to red curve is obtained a maximum power of 2.233W and for an irradiation of 1000 W/m$^2$ which corresponds to green curve, the PV cell provide a maximum power of 3.283 W. That gives an idea of measure in the power produced by a photovoltaic cell is affected by changing irradiance.

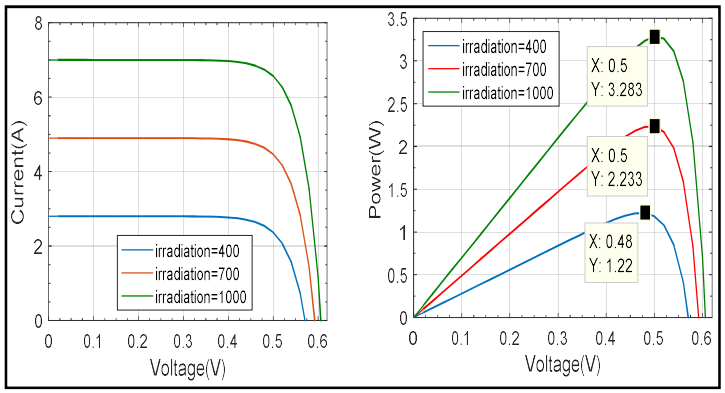


Fig.16. Characteristic: Current, Power = f (Voltage) for different illuminations

TABLE III

IRRADIANCE VARIATION

| **Irradiance(W/m$^2$)** | 400 | 700 | 1000 |
|---|---|---|---|
| **$V_m$(V)** | 0.48 | 0.5 | 0.5 |
| **$P_m$(W)** | 1.22 | 2.233 | 3.283 |

## VI. CONCLUSION

In this paper model for simulation of a solar cell has been developed in Simelectronics, simscape and mathematical


ISSN 1737-9334

blocks in MATLAB/Simulink environment using solar cell block and other interfacing blocks. In all the simulations, it could be observed that the power produced by a photovoltaic cell is affected by changing irradiance. So, it can be said that MATLAB with integrated library, can be used to simulate photovoltaic solar cells under different conditions and can substitute for expensive experiments on actual solar cells. The simulation results validate the proposed model. This developed model can also be used for modeling of large PV power system.

## REFERENCES

[1] E.Kiran, D. Inan, "An approximation to solar cell equation for determination of solar cell parameters," Renewable Energy, vol. 17, pp.235–241, 1999.

[2] W. De Soto, Klein, S.A. Beckman, W.A, "Improvement and validation of a model for photovoltaic array Performance," Solar Energy, vol. 80, pp. 78-88, 2006.

[3] M.G. Villalva, J.R. Gazoli, and E.R. Filho, "Comprehensive approach to modeling and simulation of photovoltaic arrays," IEEE Trans. on Power Electronics, vol. 24 (5), pp.1198-1208, 2009.

[4] F. Ghani, G. Rosengarten, M. Duke and J.K. Carson, "The numerical calculation of single-diode solar-cell modelling parameters,". Renewable Energy, vol. 72, 109-112. 2014.

[5] P. Huang, W. Xiao, J. Peng and J. Kirtley, "Comprehensive Parametrization of solar cell: Improved Accuracy with simulation efficiency,". IEEE Transactions On Industrial Electronics, vol.63, pp. 1549-1560,2016,

[6] A. Mellit, M. Benghanem, S.A. Kalogirou, "Modeling and simulation of a stand-alone photovoltaic system using an adaptive artificial neural network: Proposition for a new sizing procedure," Renewable energy 32 (2), pp.285-313, 2007.

[7] C. Carrero, J. Amador, S. Arnaltes, "A single procedure for helping PVdesigners to select silicon PV module and evaluate the loss resistances,". Renew.Energy, vol. 32 (15), 2579–2589, 2007.

[8] V.J. Chin, Z. Salam, K. Ishaque, "Cell modelling and model parametersestimation techniques for photovoltaic simulator application,": a review. Appl.Energy, vol.154, 500–519, 2015.

[9] W. De Soto, S.A. Klein, W.A. Beckman, "Improvement and validation of a model for photovoltaic array performance,", Sol. Energy, vol.80, pp.78-88, 2006

[10] R. Overstraeten, R. Mertens, "Characterisation and Testing of Solar Cells and Modules,", Hilger, Bristol, Engl, 1986.

[11] Verma, Deepak, et al. "Maximum power point tracking (MPPT) techniques: Recapitulation in solar photovoltaic systems." *Renewable and Sustainable Energy Reviews* 54 (2016): 1018-1034.

[12] Tomar, Rahul, and Prasenjit Guide Basak. Comparison between Perturb & Observe Method and Incremental Conductance Method for Maximum Power Point Tracking of PV Module. Diss. Thapar University, 2016.

[13] Priyadarshi, Neeraj, et al. "An Experimental Study on Zeta Buck–Boost Converter for Application in PV System." *Handbook of Distributed Generation*. Springer, Cham, 2017. 393-406.




ISSN 1737-9334

# A Service-Oriented Data Mining Platform: System of Assistance to Epidemiological Research and Monitoring of the Diseases

SABRI Mohammed[#1], RAHAL Sidi Ahmed[*2]

[#]*Computer Sciences Department,*
*National Polytechnic School of Oran, Algeria*
[1]mohammed.sabri.u@gmail.com

[*]*Computer Sciences Department*
*University of Sciences and Technology-Mohamed Boudiaf, Oran, Algeria*
[2]rahalsa2001@yahoo.fr

***Abstract*— This article relates our contribution in the field of public health and epidemiology through the design of a System of Assistance to Epidemiologic Research and Monitoring of Diseases (SARESM). SARESM provides to epidemiologists assistance for the definition of medical policies, and more specifically the planning of acquisition of pharmaceutical products for a given disease according to different factors including for example the period of the year and the geographical distribution of their use. Our contribution in this field is to provide prediction models for chronic diseases such as diabetes and asthma. These models are based on Service-Oriented Data Mining techniques, and an approach of Boolean modeling of the induction graphs. The proposed platform is a flexible and scalable system for aid in decision-making by trades' experts after extracting the epidemiologic prediction rules.**

***Keywords*— Data Mining, Services Oriented Architecture (SOA), Data Warehouse, Epidemiology**

## I. Introduction

The development of information systems and computer technologies has enabled the automation of the activities in every field of the real-world; this has induced a fast increase in the information availability, the development of high volume data ware-houses and finally, the emergence of Data Mining. The latter enables the extraction of available knowledge, until now hidden within the data, to be used in various fields such as trade, banking, public health, etc. Public health is the main concern for the world population and calls upon several disciplines, for the well-being of all.

However, the growing market draws attention to distributed Data Mining [8]; on the one hand, data and software are geographically distributed over a network instead of being located in a single site, and on the other hand, the cost is another reason for the distribution. In addition, thanks to the arrival of Web and Grid computing, distributed data is now much easier to access and distributed computing in heterogeneous environments became much more feasible [9]. At the same time, service-oriented architectures (SOA) are becoming one of the main paradigms for distributed computing [13]. Through an approach based on services, especially service-oriented architecture (SOA), integrated services can be defined to support the distributed data mining and knowledge discovery in databases (KDD) tasks in grids and the Web. The most important SOA implementation is represented by web services [6].

Let us recall that data mining has attracted a great deal of attention in the epidemiological information processing, as well as in area medical and public health as a whole. An important issue in the field is to relate a specific disease, for example asthma or diabetes, with physiological (e.g. age, gender) and environmental factors (temporal attributes such as period in the year, or spatial attributes such geographical locations). The available data in the field are complex, heterogeneous and uncertain, and it is not easy for medical doctors in the field to generate predictive rules linking a particular disease with these physiological and environmental factors. The main aim of our study will be to provide to experts in the field a platform that will enable them to generate such rules using data mining tools, and answer question related to the prevalence of a particular disease as a function of multiple factors such age or even geographical location.

Therefore, we propose here a platform for predicting models for the monitoring of chronic diseases (asthma and diabetes in the present case) guided by the service-oriented data mining which applied on real data related to drug sales in private pharmacies (that includes both physiological attributes such as age and gender, and environmental attributes). A new service-oriented data mining platform for the System of Assistance to Epidemiologic Research and Monitoring of Diseases (SARESM) [23] is thus proposed. This latter is part of an approach based on both (i) the storage and pre-processing of data and, and (ii) extraction of epidemiological prediction rules guided by the service-oriented data mining with the approach of Boolean modeling of the induction graphs [3].

The objective of our approach is to build a system that enables (i) extracting prediction rules, flexible and scalable for aid in decision-making by trades' experts, and (ii)




ISSN 1737-9334

reducing the knowledge management complexity and the response time.

## II. Related Work

For our approach, we have performed researches simultaneously in the field of pharmaceutical sales and study oriented-service data mining platforms.

Data mining in the pharmaceutical field, thanks to the information collected (Data coming from the direct sales to customers and other sources such as hospitals and medical reports) from the data records, has targeted two potential entities to obtain data mining models answering various aspects: the first entity is related to the patient's behavior (or customer) and the second one is related to the study of the product. The various models, obtained from the application of various data mining techniques, can be classified according to the objectives of each approach:

- Public health: Often faced with the marketing pressures, it tries to follow the medical prescription, using the retail data obtained from pharmacies purchasing records and health insurance companies, to determine which drugs the doctors prefer for specific diagnoses. This will allow creating detailed portraits for prescription of each doctor [14].
- Management and monitoring of some pathologies: Several studies have been conducted to understand and monitor certain diseases. These studies are aimed at both (i) understanding the sale of certain products for selected patients (e.g. asthma [4]) and (ii) determining the long-term effects of the intervention program [5]. Moreover, the development of new pharmaceuticals and the advancement in cancer therapies [28], and finally, the development of the bio-monitoring systems that can be used to identify normal manifestations of the disease and events resulting from the bio-attacks [22] are also considered.
- Assistance system to the medical prescription: The objective is to improve the medical prescription among practitioners, based on the results of data mining on medical records and data from pharmacies. The contribution of this prescription assistance system is multiple: first, it helps medical doctors in setting up recommendations; second, it encourages the prescription of the products that can be cheaper and more efficient [19]; third it provides exploration of reactions for unfavourable drug to alert physicians about the potential adverse effects [7].
- Optimal management of stock and its modeling: Managing a multi-product stock means getting the right product, in terms of quantity and availability when needed, taking into account customer behavior. Several models are obtained, cited in [2] to examine the dependence of purchase in the sale.
- Profit making in the sales of drugs: Finally, the commercial side is a field that uses data mining techniques to make financial profits. The important business entities in the pharmaceutical field used data mining techniques to increase their turnover significantly and thus achieve remarkable profits [15].

There have been many studies published aimed at adopting data mining platforms to service-oriented architecture paradigm.

FAEHIM (Federated Analysis Environment for Heterogeneous Intelligent Mining) based on Web services-based toolkit for supporting distributed data [25]. Dynamic data mining process (DDMP) system based on service-oriented architecture (SOA) introduced in [10], where each Web service represents an activity in data mining process. Xu et al. [30] proposed a service-based architecture for data mining applications, including a set of services (configuration, engine, monitor...). Weka4WS described (design and implementation) in [29] uses the WSRF libraries and services provided by Globus Toolkit. SINDBAD SAILS (Service Architecture for Inductive Learning Schemes) is a web service interface implemented in PHP and dedicated to the SINDBAD platform; this interface allows a user to access SINDBAD data mining techniques [16]. Anteater: a service-oriented architecture for data mining was developed by Ferreira et al. [13]. This platform relies on Web services to achieve extensibility and interoperability. It offers simple abstractions for users, and supports computationally intensive processing on large amounts of data through massive parallelism. Latha et al. [18] proposed a novel method to develop service oriented architecture for a weather information system and forecast weather using data mining techniques. These authors mentioned that this method aims at developing a weather information system as a web service that can be used by any type of application and uses the prediction techniques of data mining for weather forecasting. In a different work [17], other authors present the design and realization of a new open source platform, WS4KDM: Web Services for Knowledge Discovery and Management. This platform regroups several web services dedicated to the extraction and knowledge management. Data mining techniques, implemented in the WS4KDM platform are based on induction graph and use a named Boolean modeling technique BML (Boolean Modeling Language), which is based on the cellular principle CASI. SOMiner proposed by Birant D. [6] is a flexible service-oriented data mining architecture that incorporates the main phases of knowledge discovery process. Overall, this architecture provides a large collection of machine learning algorithms written for knowledge discovery tasks. Zorrilla and Garcia-Saiz [33] proposed a model which joins both facets: data mining and SOA. It describes a data mining service addressed to non-expert data miners which can be delivered as Software-as-a-Service. Shelke et al. [26] have proposed an architecture to improve mobile data mining techniques so that data retrieval for mobile devices is faster and mobility management efficient using proper web services.

In this context, the SARESM platform's concept proposed in this paper focuses on service-oriented data mining applied to both Epidemiologic Research and Disease Monitoring, a field of investigation that necessitates important resources in




ISSN 1737-9334

terms of algorithm definition, life cycle management, and visualization reporting.

## III. Approach

The approach that has been taken in the design and the implementation of SARESM (Fig. 1) results from the overall process of knowledge discovery from databases.

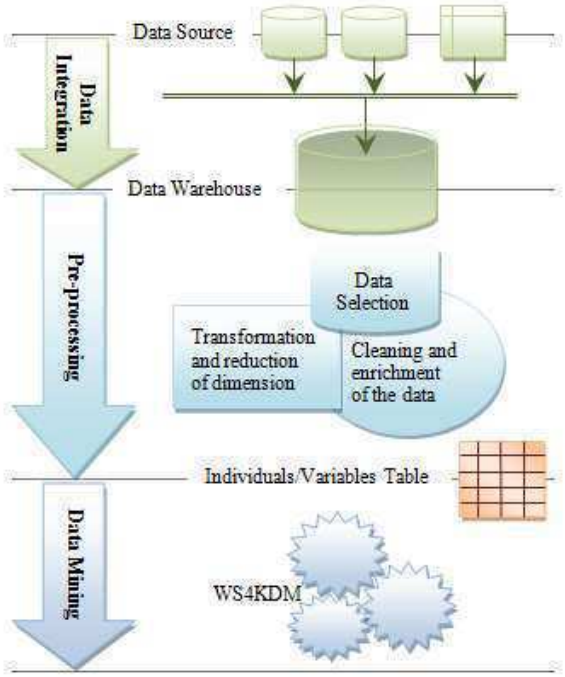


Fig. 1. Illustrating the selected approach for SARESM

### A. Data warehousing

The first phase of our approach is the design of the data warehousing, with the objective of obtaining a unique source of data to carry out the data mining tasks.

Our data sources are based on records of sales from private Algerian pharmacies. The architecture of the SARESM data warehouse (Fig. 2) is articulated around three axes:

- Integration: This first step consists of extracting and gathering the data coming from the various databases of private pharmacies and the external sources [20]. These databases are supported by the same relational DBMS (Data Base Management System), they are identical in terms of structures, and are installed in different sites (where no connection exists between these sites). The source databases (files) are coded and stored in the file system.
- Building: It consists of extracting the relevant data and copying it in the warehouse [20]. Consequently, the SARESM warehouse will constitute a centralized collection of materialized and historical data, available for data mining. Whereas the data related to the drug sales and the characteristics related to the sold products are taken into account in our study, the other data such as the purchases are not considered.
- Structuring: This step consists in reorganizing the data, in data marts, to support the data mining [24]; a specific data mart is created, in relation to the information concerning the chronic diseases selected out of all the retail sales and the characteristics of the patients belonging to the essential variables for the data mining.

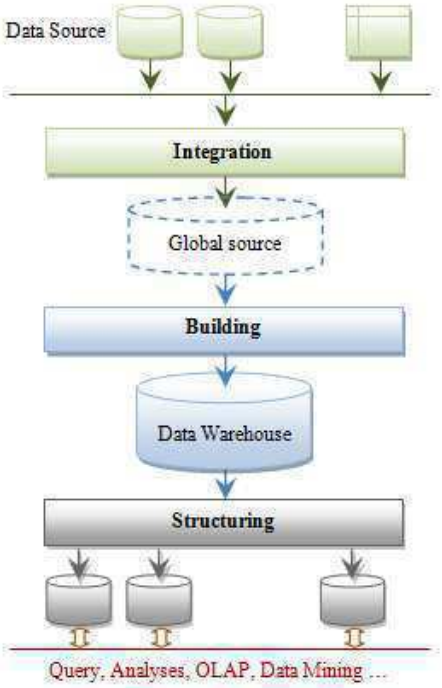


Fig. 2. Architecture of SARESM data warehouse.

SARESM data warehouse is based on the star model (Fig. 3) and contains all the information about retail sales, products and places where the pharmacies are located. The source data available is commercial data (basic sales records) to carry out medical research (epidemiologic), and according to the studies carried out by F. Ravat and al. [21], we chose a traditional multidimensional modeling for the SARESM data warehouse. The data of the warehouse are as follow:

The fact table “VENTES”; contains sold quantity (gross), selling price, etc.

The dimension tables:

- Localization of selected pharmacies “LOC_OFFI”.
- Dimension date “DATES”.
- Table of the handled products “PRODUITS” includes commercial name, etc.
- Specialties of the various existing products in database “SPECI_PDT”.
- “DCI” and corresponding diseases.
- Laboratories manufacturers’ products “LABORAT”.
- Patients “ASSURES”. Confidential details NOT downloaded in data warehouse.


ISSN 1737-9334

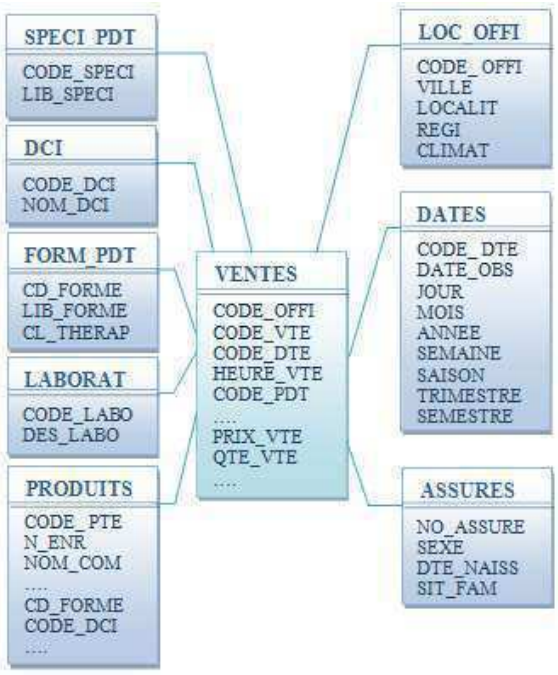


Fig. 3. The star model of SARESM.

### B. The pre-processing

Data from the warehouse is very varied and is not necessarily all exploitable by the data mining techniques [27]. Most of the used techniques process only data tables in the traditional lines/columns. The objective is to prepare lines/columns tables, in other words, tables of individuals/variables (Table I), obtained by the following stages:

TABLE I
EXAMPLE OF A TABLE OF INDIVIDUALS/VARIABLES.

| | Town | Season | Age | Gender | Diseases |
|---|---|---|---|---|---|
| ω1 | Oran | Winter | Young | Male | Asthma |
| ω2 | Oran | Winter | Young | Female | Asthma |
| ω3 | Tlemcen | Winter | Young | Male | Diabetes |
| … | … | … | … | … | … |

1) *Data selection*: It is carried out on the data which already exist in the data warehouse and which are in tabular form. Filters are then applied to select a subset of lines or columns [12]. Data selection is based on the following information:

- From the fact table "VENTES", we will take the sold quantity, taken first in its "gross" state and aggregated according to the selected dimensions.
- From table "LOC_OFFI", the attribute "LOCATION".
- The date dimension "DATES" in order to carry out the data mining on a time interval. In our case, we proceed by the period "MONTH".
- From the table "DCI", we take information about present diseases. A filter is then applied to keep the records related to the selected diseases only.
- Finally, the patients, present in the table "ASSURES" and from which we take the gender and age attributes (recommendations of the experts).

2) *Cleaning and enrichment of the data:* A stage of cleaning of the data is essential in order to process the missing data (suppression of records). Besides, enrichment by external sources was carried out during the creation of the data warehouse [12].

3) *Transformation and reduction of dimension:* This is about transforming an attribute A into another A' which would be more relevant to match the objectives of the study [12]. For example, patients' dates of birth have been transformed to obtain age within intervals (see various discretization methods in [11]).

### C. Service-Oriented Data Mining (WS4KDM)

After data storage and pre-processing, the phase of data mining may start. For producing epidemiological prediction rules, we chose WS4KDM [17] as the service-oriented data mining module. WS4KDM was developed in order to regroup several web services dedicated to the extraction and knowledge management. Data mining techniques, implemented in the WS4KDM platform are based on induction graph and use a named Boolean modeling which is based on the cellular principle [3] (Fig. 4). This approach is named CASI [1] and is based on the induction graphs (IG) methods produced by the SIPINA algorithm [31] [32].

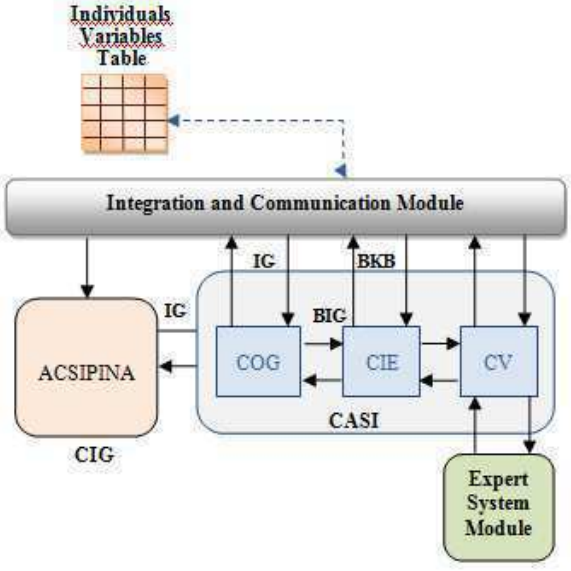


Fig. 4. Architecture of WS4KDM platform.

The architecture of WS4KDM is articulated around:

1) *CIG (Cellular Induction Graph) Module:* this module uses the SIPINA method that produces induction graphs.

2) *CASI Machine Module:* CASI [1] is a cellular automata which simulates the basic operating principle of an inference engine. It ensures the optimization of the induction graph (IG), the generation of the conjunctive rules ("If cond1 [AND cond2]…[AND condn] Then conclusion"), and the validation




ISSN 1737-9334

of the obtained model. Starting from a training sample, a symbolic processing starts for the IG building (e.g. ACSIPINA, ACID3, and ACJ48 algorithms). CASI module is composed by three sub-modules:

- COG (Cellular Optimization and Generation) consists of assisting the processing made by the ACSIPINA algorithm (or ACID3, or ACJ48) to generate the Boolean Induction Graph (BIG).
- CIE (Cellular Inference Engine) can, from the BIG, generate a Boolean Knowledge Base (BKB). This module simulates the operation of the basic cycle of an inference engine by using two finite layers of finite automata: CELFACT, for the fact base and CELRULE for the rule base.
- CV (Cellular Validation) is devoted to the validation process of the proposed model.

*3) Integration and Communication Module:* it ensures the communication between the various modules proposed in the WS4KDM platform. It presents the Input/Out layer of different operations proposed by the platform as web services.

4) *Expert System Module:* it operates the CASI machine principle and uses the CIE module as cellular inference engine to set off inferences in forward and backward. This module can be used for validation by the deduction of rules extracted from data, and it can be used independently of the KDD process to develop dedicated expert systems.

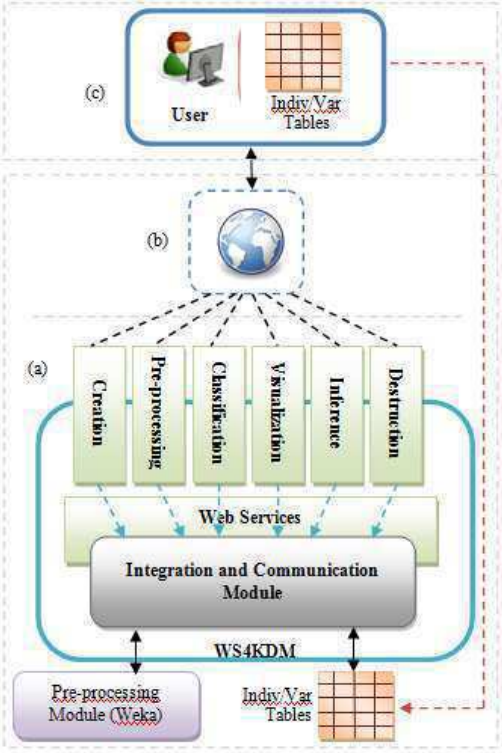


Fig. 5. Web services of WS4KDM platform.

Fig. 5 illustrates the implementation of the WS4KDM platform and the operating mode of its different web services (a). These latter are:

- Creation: This service allows a customer to create a session (account) or to access at its session via a login, to create its resources to ensure the services performance coherence.
- Pre-processing: This service is designed to make available to the customer various methods of filtering and discretization provided by the module pre-processing.
- Classification: A specification service of the desired method by the client to generate the model. It is characterized by the name and settings of the algorithm (the classification method), the learning base and the test database.
- Visualization: This service allows visualizing the generated model graphically (vertices and arcs). The graph is a Boolean matrix.
- Inference: This service renders available for the clients an inference engine and knowledge management. The service receives a set of rules and a test database (classification and class assignment) to validate the client model or affect the class for the individuals in the base.
- Destruction: Service for liberate the resources used by the client in the WS4KDM platform and to log out.

Via a network connection (local, Internet) (b), users can access to WS4KDM platform through an interface developed (c).

## IV. Experiments

Before giving the results of the experimental phase, we want to highlight the fact that the data warehousing has represented a major task in the implementation of the project, especially the data collection. Data records of sales, spread out between 2003 and 2010, related to 4 departments in the west of Algeria. It should be noted that these records represent raw data of sales on which no form of aggregation was carried out. Therefore, in a first step, data were pre-processed by identifying diseases (Asthma and Diabetes), patients' characteristics (Gender and Age) and environmental attributes.

Moreover, after a second step of investigation, we realized that there was a significant number of redundant sales transactions. Because the presence of combinations of several products for the same disease exist in the same prescription (e.g. insulin and Glucophage in the same prescription to care diabetes), it was decided in collaboration with experts to analyse the data by medical prescription rather than by sale detail. Therefore, the generation of data in the DataMart has been improved, which allowed us to have a total of about 122,000 acts of prescriptions (combination of sales acts).

We then tested the service-oriented data mining platform SARESM with five different bases resulting from the chronic disease DataMart. We first applied service-oriented data mining on the entire database for the western region of Algeria (called BRO). Second, we passed to the other four departmental bases called TLM, SBA, ORN, and ATM referring, respectively, to the departments of Tlemcen,



ISSN 1737-9334

Belabbes, Oran and Temouchent. These bases are described by the same common attributes.

In order to carry out our experimentation, we imported the data in WS4KDM, and then selected the attributes and the variable to predict (Table II) (as stated above, induction was launched using SIPINA).

Fig. 6 presents the individual numbers of learning samples of the experimental bases.

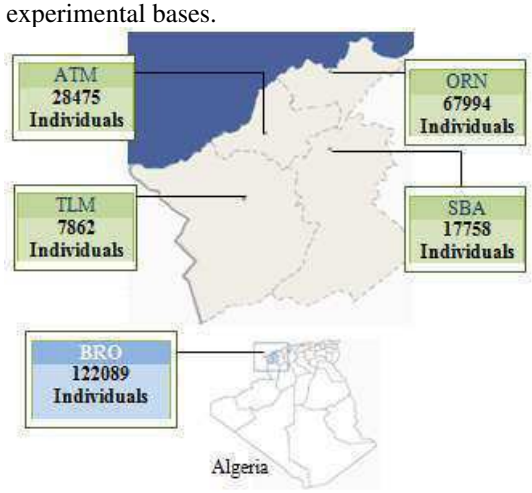


Fig. 6. Characteristics of the five bases of experimentation.

For the five selected bases, we used the same attributes mentioned in Table II (excluding the department attribute).

Note that we have added a diabetes-high blood pressure combination class since it was important for experts to dissociate between diabetes alone and diabetes accompany by high blood pressure.

TABLE III
REPRESENTATION OF ATTRIBUTES AND CLASS

| **Attributes** | **Signification** | **Possible Values** |
|---|---|---|
| X1 : MONTH | The selected period is the calendar month | 01 (January), .., 12 (December). |
| X2 : WILAYA | Department number | 13, 22, 31, and 46 |
| X3 : LOCATION | The locality or city relating to the chosen pharmacy | TLEMCEN, SENIA, ARZEW… |
| X4 : CLIMAT | The climate versus humidity mainly | High, Average, and Low. |
| X5 : PROXIM | Proximity of the location in relation to the sea | Inside, Coastal |
| X6 : GENDER | Patient's gender | M and F |
| X7 : AGE | Patient's age - Age intervals | Chi (<=16), Adt1 (16 - 40), Adt2 (41-65), and Old (>65). |
| Y : CLASS_THRP | Class of disease to be predicted | ast (Asthma), dbt (Diabetes) et dbt-hta (Diab-High blood pressure). |

- "BRO" experimentation: firstly (case 1), we have used all attributes (Table II) and we can visualize 34 epidemiological prediction rules (conjunctive rules) produced by SARESM platform. In a second experiment (case 2), we did not select the attribute "LOCATION", and obtained 13 epidemiological prediction rules (Table III). In this case, the success rate was 86.7989% (105,972 correct instances for 122,089 acts).

TABLE IIIII
CONJUNCTIVE RULES PRODUCED IN THE EXPERIMENT OF BRO – CASE 2

| | |
|---|---|
| 1 | if (age = old) then dbt-hta |
| 2 | if (age = adt1) then ast |
| 3 | if (age = chi) then ast |
| 4 | if (climat = high and age = adt2) then ast |
| 5 | if (wilaya = 46 and climat = aver and age = adt2) then ast |
| 6 | if (wilaya = 31 and climat = aver and gender = m and age = adt2) then dbt |
| 7 | if (wilaya = 31 and climat = aver and proxim = coastal and gender = f and age = adt2) then dbt |
| 8 | if (wilaya = 13 and climat = low and age = adt2) then dbt |
| 9 | if (wilaya = 46 and climat = low and age = adt2) then dbt |
| 10 | if (wilaya = 31 and climat = aver and proxim = inside and gender = f and age = adt2) then dbt |
| 11 | if (wilaya = 22 and climat = low and age = adt2) then dbt |
| 12 | if (wilaya = 31 and climat = low and proxim = inside and age = adt2) then ast |
| 13 | if (wilaya = 31 and climat = low and proxim = coastal and age = adt2) then dbt |

## V. CONCLUSIONS

In this article, we have used a service-oriented data mining approach applied to the field of epidemiology. Experts in the field are faced with the issue of relating a specific disease (asthma or diabetes in our case), with physiological and environmental factors (age, gender, period in the year, geographical locations). We provide here prediction models of such chronic diseases (asthma and diabetes), using Boolean modeling of the epidemiologic prediction rules. In the context of the analysis of the chronic diseases, the generated cellular induction graph enables us to determine the relations between the disease and the people exposed to it versus the physiognomic characteristics and the environment. These generated models will facilitate the identification of the diseases by experts so that the patients are better taken care of. In addition, it is worth noting that our platform is flexible at various levels. First, the user can decide which parameters are of interest in their analysis. For example, the "BRO" experiment (entire base) provided different classification rates (92.8% vs. 86.8%) and different number of predictive rules (34 vs. 13) as a function of including or not the variable "LOCATION". In sum, the user can opt between a very highly accurate but complex model (92.8% associate to 34 rules) and a highly accurate but simpler model (86.8% associated to 13 rules). Second, another form of flexibility is the possibility of enriching the bases with additional data



ISSN 1737-9334

resources (updating, new pharmacies, new patients, and new characteristics).

## REFERENCES

[1] B. Atmani and B. Beldjilali, "Knowledge Discovery in Database: Induction Graph and Cellular Automaton," Computing and Informatics Journal, vol. 26, no. 2, pp. 171-197, 2007.

[2] P.K. Bala, "Data Mining for Retail Inventory Management," Advances in Electrical Engineering and Computational Science, Sio-Iong Ao, Len Gelman, Springer Science & Business Media, pp. 587-598, 2009.

[3] M. Benamina and B. Atmani, "WCSS: un système cellulaire d'extraction et de gestion des connaissances," Troisième atelier sur les systèmes décisionnels, 10 et 11 octobre 2008, Mohammadia, Maroc, pp. 223-234, 2008.

[4] B.J. Bereznicki, G.M. Peterson, S.L. Jackson, H. Walters, K. Fitzmaurice, and P. Gee, "Pharmacist-initiated general practitioner referral of patients with suboptimal asthma management," Pharm World Sci, 2008.

[5] B.J. Bereznicki, G.M. Peterson, S.L. Jackson, H. Walters, and P. Gee, "The sustainability of a community pharmacy intervention to improve the quality use of asthma medication," Journal of Clinical Pharmacy and Therapeutics, vol. 36, no. 2, pp. 144-151, 2011.

[6] D. Birant, "Service-Oriented Data Mining," New Fundamental Technologies in Data Mining, K. Funatsu and K. Hasegawa, Published by InTech, Croatia, pp.3-18, 2011.

[7] J. Chen, H. He, J. Li, H. Jin, D. McAullay, G. Williams, R. Sparks, and C. Kelman, "Representing Association Classification Rules Mined from Health Data," International Conference on Knowledge-Based Intelligent Information and Engineering Systems, 9th , KES 2005, Melbourne, Australia, Lecture Notes in Computer Science, Volume 3683, 2005, pp. 1225-1231, 2005.

[8] N. Chen, N.C. Marques, and N. Bolloju, "A Web Service-based approach for data mining in distributed environments," in Proceeding of the 1th International Workshop on Web Services: Modeling, Architecture and Infrastructure (WSMAI-2003), Angers, France, pp. 74-81, 2003.

[9] W.K. Cheung, "Scalable and privacy preserving distributed data analysis over a service-oriented platform," Data Mining Techniques in Grid Computing Environments, W. Dubitzky, University of Ulster, UK, pp. 105-118, 2008.

[10] C.C. Chiu and M.H. Tsai, "A Dynamic Web Service based Data Mining Process System," in Proceeding of the 5th International Conference on Computer and Information Technology (CIT 2005), Shanghai, China, pp.1033-1039, 2005.

[11] J. Dougherty, R. Kohavi, and M. Sahami, "Supervised and unsupervised discretization of continuous attributes," Machine Learning: Proceedings of the 12th International Conference (ICML-95), Morgan Kaufmann, pp. 194-202, 1995.

[12] U.M. Fayyad, G. Piatetsky-Shapiro, P. Smyth, and R. Uthurusamy, Advances in Knowledge Discovery and Data Mining, American Association for Artificial Intelligence Menlo Park, 1996.

[13] R.A. Ferreira, O.G. Dorgival, and W.Jr. Meira, "Anteater: A Service-Oriented Data Mining," Data Mining Techniques in Grid Computing Environments, W. Dubitzky, University of Ulster, UK, pp. 179-198, 2008.

[14] A. Fugh-Berman, "Prescription Tracking and Public Health," Journal of General Internal Medicine, vol. 23, no. 8, pp. 1277-1280, 2008.

[15] Y. Hamuro, N. Katoh, Y. Matsuda, and K. Yada, "Mining Pharmacy Data Helps to Make Profits," Data Mining and Knowledge Discovery, vol. 2, no. 4, pp. 391-398, 1998.

[16] W. Jörg, C. Brosdau, L. Richter, and S. Kramer, "SINDBAD SAILS: A Service Architecture for Inductive Learning Schemes," In Proceedings of the 1st Workshop on Third Generation Data Mining: Towards Service-oriented Knowledge Discovery, 2008.

[17] H. Kadem and B. Atmani, "Conception d'une Plateforme Cellulaire Open Source d'Extraction et de Gestion des Connaissances : WS4KDM," 7ème Séminaire National en Informatique BISKRA (SNIB'2010), Université Mohamed Khider-Biskra, Algérie, 2010.

[18] C.B.C. Latha, P. Sujni, E. Kirubakaran, and S. Narayanan, "A Service Oriented Architecture for Weather Forecasting Using Data Mining," The International Journal of Advanced Networking and Applications (IJANA), vol. 02, no. 02, pp. 608-613, 2010.

[19] K. Melley and K. Petersen, "Prescription Data Mining," Fact Sheet, Pew Prescription Project, http://www.prescriptionproject.org, 2008.

[20] F. Ravat, O. Teste, and G. Zurfluh, "Modélisation et extraction de données pour un entrepôt objet," Université Paul Sabatier (Toulouse III), IRIT, équipe SIG, 2000.

[21] F. Ravat, O. Teste, and G. Zurfluh, "Modélisation multidimensionnelle des systèmes décisionnels," Extraction des connaissances et apprentissage, vol 1, no. 1, pp. 201-212, 2001.

[22] M.R. Sabhnani, D.B. Neill, and A.W. Moore, "Detecting Anomalous Patterns in Pharmacy Retail Data," Proceedings of the KDD 2005 Workshop on Data Mining Methods for Anomaly Detection, Chicago, Illinois, USA, pp. 132-137, 2005.

[23] M. Sabri and B. Atmani, "Système d'assistance aux recherches épidémiologiques et de surveillance des maladies : Modélisation Booléenne," Colloque International "Veille Stratégique Scientifique et Technologique (VSST)", VSST'10, Toulouse, France, 2010.

[24] N. Selmoune, S. Boukhedouma, and Z. Alimazighi, "Conception d'un outil décisionnel pour la gestion de la relation client dans un site de e-commerce," SETIT 3rd International Conference, Tunisia, 2005.

[25] A.A. Shaikh, O.F. Rana, and I.J. Taylor, "Web services composition for distributed data mining," in Proceeding of the 34th International Conference on Parallel Processing Workshops (ICPP 2005 Workshops), Oslo, Norway, pp. 11-18, 2005.

[26] R.R. Shelke, R.V. Dharaskar, and V.M. Thakare, "Data mining for mobile devices using web services," in Proceeding of the International Conference on Industrial Automation And Computing (ICIAC), Lonara, Nagpur, 2014, Published in : International Journal of Engineering Research and Applications (IJERA), vol. 8, no. 2, pp. 7-9, 2014.

[27] L. Soibelman, M. Asce, and K. Hyunjoo, "Data Preparation Process for Construction Knowledge Generation through Knowledge Discovery in Databases," Journal Of Computing In Civil Engineering, vol. 16, no. 1, pp. 39-48, 2002.

[28] S. Sumathi and S.N. Sivanandam, "Data Mining in Biomedicine and Science," Introduction to Data Mining and its Applications, Springer, pp. 499-543, 2006.

[29] D. Talia, P. Trunfioy, and O. Verta, "The Weka4WS framework for distributed data mining in service-oriented Grids," Concurrency and Computation: Practice and Experience, vol. 20, no. 16, pp.1933–1951, 2008.

[30] L. Xu, Y. Wang, G. Geng, X. Zhao, and N. Du, "SDMA: A Service based Architecture for Data Mining Applications," IEEE International Conference on Services Computing, pp. 473-474, 2008.

[31] Zighed D.A., "Méthodes et outils pour les processus d'interrogation non arborescents," PhD Thesis, Université Lyon 1, 1985.

[32] D.A. Zighed, J.P. Auray, and G. Duru, "SIPINA: Méthode et Logiciel," Lacassagne, 1992.

[33] M. Zorrilla and D. García-Saiz, "A service oriented architecture to provide data mining services for non-expert data miners," Decision Support Systems, Elsevier, vol. 55, no. 1, pp. 399-411, 2013.


ISSN 1737-9334

# A Discontinuous PWM Techniques Evaluation by Analysis of Voltage and Current Waveforms

Fares Zaamouche[#1], Salah Saad[*2] and Larbi Hamiche[*3]

[#] *Mining Institute, Electromechanical Department, Larbi Tebessi University, Tebessa 12000, Algeria*

[1]f.zaamouche@univ-tebessa.dz

* *Laboratory LSELM, Badji-Mokhtar University, BP 12, Annaba 23000, Algeria*

[2]saadsalah2006@yahoo.fr

[3]hamiche_larbi@yahoo.fr

***Abstract* – In this paper experimental and simulation results of three phase voltage source inverter (3P-VSI) controlled by a discontinuous pulse width modulation technique (DPWM) are presented. This technique is proposed to overcome the disadvantages of the space vector pulse width modulation (SVPWM) mainly high modulation frequency and increased inverter switching losses. This control strategy is a simple and an easy technique generating the same switching pattern as space vector modulation with less switching losses and reduced total harmonic distortion. The main motivation of the present paper is that the DPWM is not largely and deeply investigated and can present a serious alternative to other PWM techniques. The obtained results have showed that with DPWM technique, switching losses and total harmonic distortion (THD) are reduced. Furthermore, the implementations of this technique in a dSPACE (DS1104) controller are discussed and analyzed.**

***Keywords* – Discontinuous modulation, PWM Inverter, DPWM, Harmonics, switching losses**

## I. INTRODUCTION

The main disadvantage of the PWM voltage source inverter is the non-sinusoidal currents and voltages produced at its output, affecting greatly the motor (harmonic currents and pulsating torques). Many works have investigated the methods to solve this problem by introducing several control techniques such as sinusoidal pulse width modulation SPWM [1], space vector pulse width modulation SVPWM [2] and recently discontinuous pulse width modulation DPWM. The purpose of these PWMs is to achieve minimum switching losses, less total harmonic distortion (THD), reduced torque fluctuation and short time response to speed regulation [3-7].
The use of PWM inverters in variable speed AC drives [8-13] is mainly due to development in both fast switching power semiconductors and microprocessors technology. An alternative modulation technique known as discontinuous PWM (DPWM) is becoming very popular and important PWM technique for three phase voltage source inverter controlling AC motors especially induction motor. With this technique, the output voltage can reach the desired high values and it can be realized digitally. Therefore, it can be implemented easily in a DSP or a microcontroller [2]. In the literature several papers have studied different PWM techniques to compare their performances [14-18] in order to choose the best inverter control technique.
In the present work, the proposed discontinuous PWM technique for the control of three-phase voltage source inverter fed induction motor was simulated in the Matlab/Simulink environment and tested experimentally in a dSPACE board. In addition, testing this technique in open loop V/f control of three phase induction motor supplied by voltage source inverter has showed that this technique have many advantages over other techniques. As a result, the numbers of commutations and the switching losses are reduced and consequently the electromagnetic torque ripples are minimised and the speed becomes stable rapidly for DPWM which means better speed regulation. This paper is a contribution to the discontinuous pulse width modulation using the zero sequence signals to achieve less switching losses and reduced torque ripples. This work includes the description of SVPWM and DPWM modulations theories and the implementation of the proposed scheme experimentally using a dSPACE DS1104 board. The obtained results are discussed and analyzed and compared.

## II. INVERTER CONTROL TECHNIQUES

Recently, several pulse width modulation (PWM) techniques were developed, studied and applied to ac motors control. Two techniques were given a great deal of interest mainly, space vector modulation (SVPWM) and discontinuous pulse width modulation (DPWM).

### A. *Theory of SV-PWM technique*

The SVM technique was firstly developed for space vector electrical machines control. Its principle is to rebuild the reference vector from different voltage vectors. Each vector corresponds to a combination of a three phase inverter switches states. The SVPWM technique processes the signals directly on the diphase frame of the Concordia transformer. Thus, the line to neutral voltages are represented in the (α, β) frame. From the combination of the three state variables, the inverter has eight switching states. It can generate eight different vectors of voltage output. These eight space vectors define the limits of the six sectors in the (α, β) and two of these vectors equal to zero. Theoretical developments of this technique are described and studied elsewhere [2-6].


ISSN 1737-9334

It can be observed that in this technique the periods of use of zero vectors $T_0$ et $T_7$ are equal, therefore a factor corresponding to a distribution of these periods is defined as follows:

$$K = \frac{T_7}{(T_0+T_7)} \quad (1)$$

In this case K=0.5 for SVPWM technique, and always this factor is in the interval $0 \leq K \leq 1$

### B. *Theory of DPWM technique*

The basic principle of this technique is to saturate the reference for 120° of a period of 360°, keeping one of the three legs of the inverter without commutation. Therefore a switching discontinuity is obtained during this period of time. This will reduce considerably the number of commutations therefore the switching losses will be reduced as for each 120 ° there is a leg without commutation [19].

There are numerous strategies of discontinuous PWM based on the choice of the saturation position of the corresponding modulating at +1 is OFF upper state or at -1 is OFF at lower state.

- *Only one saturation of 120°:* this corresponds to the strategies denoted by **DPWMMIN** in the literature (modulating saturation at -1 during 120°) or DPWMMAX (saturation at +1 during 120°).
- *Two saturations of 60°: this corresponds to the strategies DPWM0, DPWM1 and DPWM2. It will be observed that it is possible to provide other intermediate placements of saturations to favor certain operating points.*
- *Four saturation of 30°: this corresponds to the strategy called DPWM3.*

It can be noted from the curves presented in Fig.1 that each modulating is saturated for 60°, i.e. each half period at different angles in relation to the initial sinusoidal reference. The values of these angles are as follows:

φ = -π/6 pour DPWM0
φ = 0 pour DPWM1
φ = π/6 pour DPWM2

*Modulation index:* the modulation index M is defined by the relation between the magnitude of the reference vector and the fundamental peak voltage of a square wave ($2*V_{dc}/\pi$).

Calculation principle of these PWM strategies is based on the injection of the zero sequence components $U_0$ in reference waveforms ($V_{aref}$, $V_{bref}$ and $V_{cref}$), [20-21].

With:

$$V_{max} = Max(V_{aref}, V_{bref}, V_{cref}) \quad (2)$$

$$V_{min} = Min(V_{aref}, V_{bref}, V_{cref}) \quad (3)$$

According to the previous chronogram the difference between DPWM and SVPWM is in the distribution factor K, regarding this factor many strategies can be determined:

a) With K =0.5, this factor results in the technical SVPWM, because the time of use of the zero vector $T_z$ is also distributed at the beginning and at the end of the timing

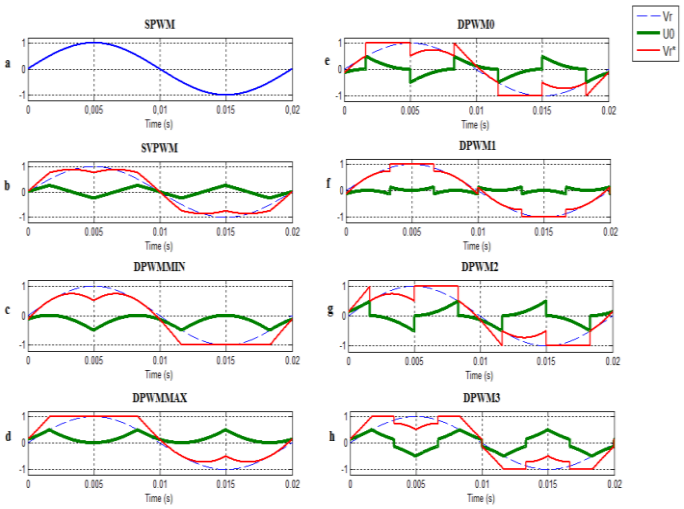


Fig.1. The reference waveforms $V_r$, $V_r^*$ and the zero-sequence components $U_0$ injected width different strategies

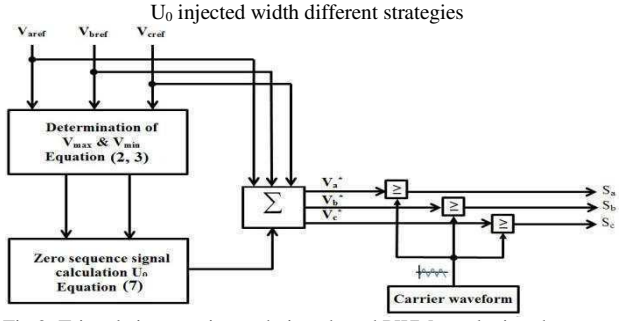


Fig.2. Triangle intersection technique based PWM employing the zero-sequence injection principle

As stated previously, the main idea is to keep the state of an arm of the inverter unchanged during each switching period.

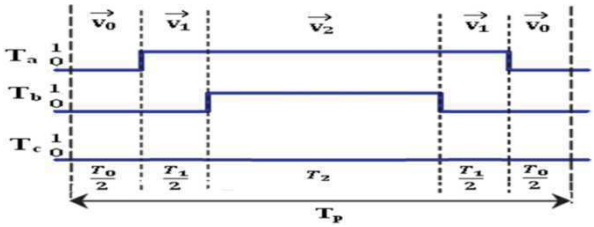


Fig.3. Chronogram of pulses based on two phase PWM (DPWM)

($T_0$=$T_7$). So the zero sequence components is given by (Fig.1(b)).

$$U_0 = -(V_{max} + V_{min})/2 \quad (4)$$

b) With K = 0, in this case, $T_7$ =0 and $T_0$=$T_z$, one of the pole voltage is connected to the negative DC-bus clamping the pole voltage during 120° while the other two phases modulate. So the zero sequence components is given by (Fig.1(c)).

$$U_0 = -(V_{min} + E/2) \quad (5)$$

c) With K= 1, in this case, $T_0$ =0 and $T_7$=$T_z$, one of the pole voltage is connected to the positive DC-bus clamping the pole voltage during 120° while the other two phases modulate. So the zero sequence components is given by (see Fig.1(d))


ISSN 1737-9334

$$U_0 = -(V_{max} - E/2) \quad (6)$$

d) With k = 0 →1, there are four possibilities as shown in Fig.1(e) and (h) and are referred as discontinuous pulse width modulation (DPWM0, DPWM1, DPWM2 and DPWM3).

A general relation that enables constructing the zero-sequence component, $U_0$, as a function of K, $V_{max}$ and $V_{min}$ inside each sector is given by [22-23]:

$$U_0 = -\left(KV_{max} + (1-K)V_{min} + (1-2K)\frac{E}{2}\right) \quad (7)$$

## III. COMPUTER SIMULATION

In order to validate and compare the developed algorithms computer simulations were conducted on a two level inverter feeding induction motor.

Motor parameters are given in Table 2, the tests are carried out for two modulation index is M= 0.9 and M = 1.2, and a commutation frequency is 6 KHz.

TABLE II
INDUCTION MOTOR PARAMETERS

| | |
|---|---|
| MOTOR PARAMETERS | P=1.5 Kw, $V_{ab}$= 380 V, f=50 Hz, $I_n$= 3.6 A and n=1400 tr.mn$^{-1}$.$R_s$=4.85Ω, $R_r$=3.085 Ω, $L_s$= $L_r$=0.274H, M=0.258 H, $f$=0.00114Nm.rad$^{-1}$.s$^{-1}$, J=0.031 Kgm$^2$ and $T_r$=3N.m |

The obtained waveforms are presented in Fig.4 and Fig.5 for modulation index M=0.9 and M =1.2 (presenting an over modulation) respectively.

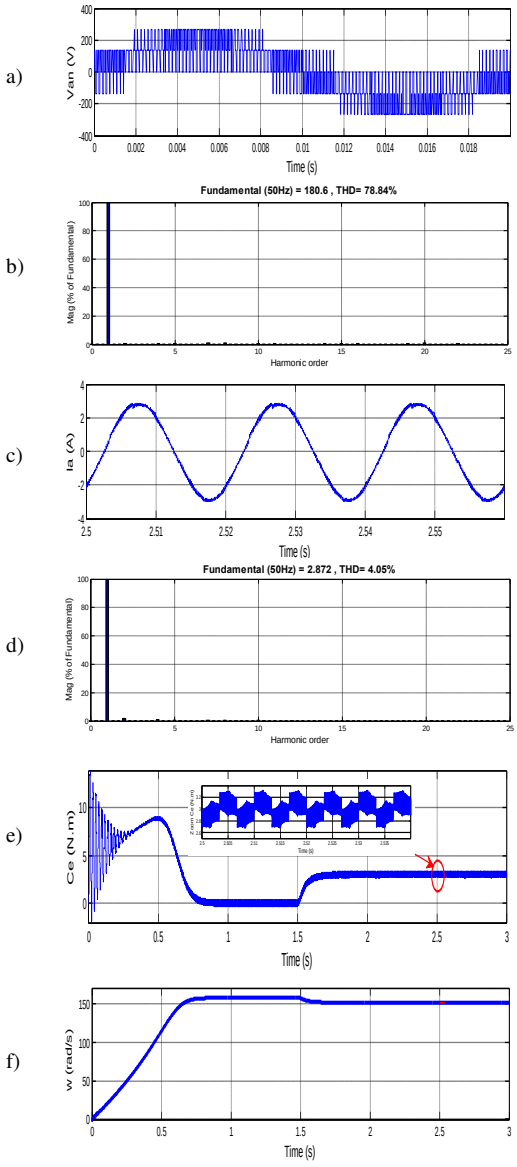


Fig.4. Discontinuous Pulse Width Modulation (DPWM_3), **M = 0.9**, a)Line to neutral voltage $V_{an}$(v), b)Voltage frequency spectrum THD (%), c) Phase current $I_a$(A), d) Current frequency spectrum THD (%), e) Torque ripples (N.m) and f) Motor speed (rad/s)

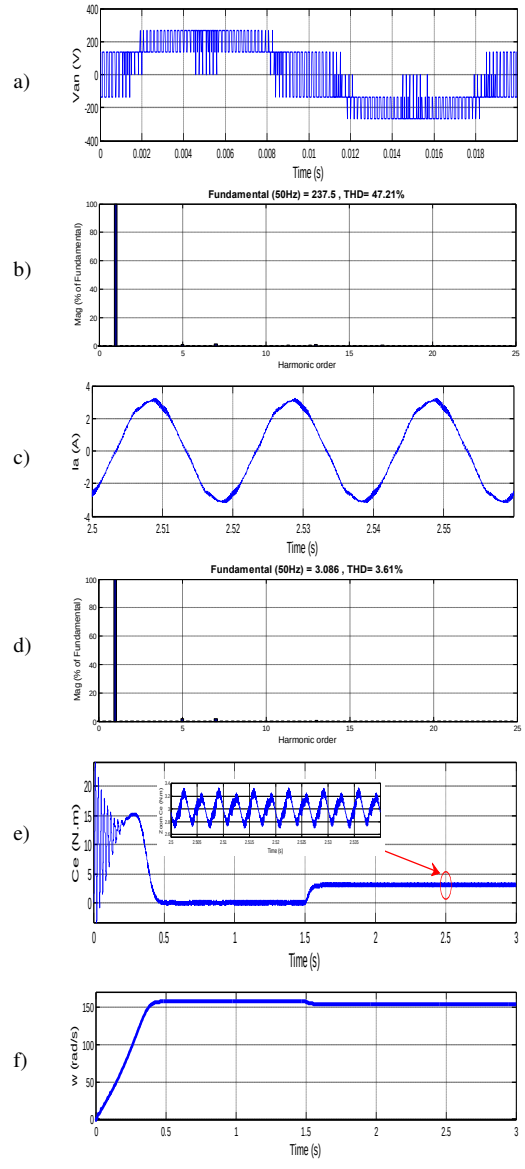


Fig.5. Discontinuous Pulse Width Modulation (DPWM_3), **M = 1.2**, , a)Line to neutral voltage $V_{an}$(v), b)Voltage frequency spectrum THD (%), c) Phase current $I_a$(A), d) Current frequency spectrum THD (%), e) Torque ripples (N.m) and f) Motor speed (rad/s)


ISSN 1737-9334

## IV. IMPLEMENTATION AND EXPERIMENTS

An experimental rig Fig.6 is designed to validate and confirm the results obtained by computer simulation and evaluate at the same time the performances of DPWM and SVPWM control techniques. The real-time applications on the dSPACE DS1104 are carried out using Real-Time Interface in MATLAB/Simulink environment. This test rig is composed from the following elements:

- IGBTs voltage source inverter commercialized by SEMIKRON with a DC source of 400 V,
- A 1.5 KW induction motor,
- Powder brake used as load,
- A dSPACE 1104 card (controller Board) was integrated in a PC enabling to generate the required pulses to control the inverter switches,
- Current and voltage sensors.
- Harmonics analyzer (QualiStar C.A 8335)

The visualization of system waveforms is realized through CONTROL DESK software, enabling to control the signals from Simulink dSPACE schemes.

Fig.6. the rig of the experimental set up used in this work. The modulation frequency is 6 KHz and the torque applied to the motor shaft is 3 N.m.

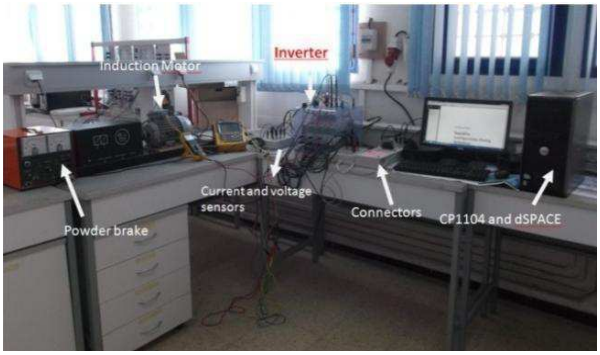


Fig.6. Experimental test rig

The waveforms obtained by experimental tests are presented in Fig.8 and Fig.9 for a modulation index M=0.9 and M=1.2 (over modulation) respectively.

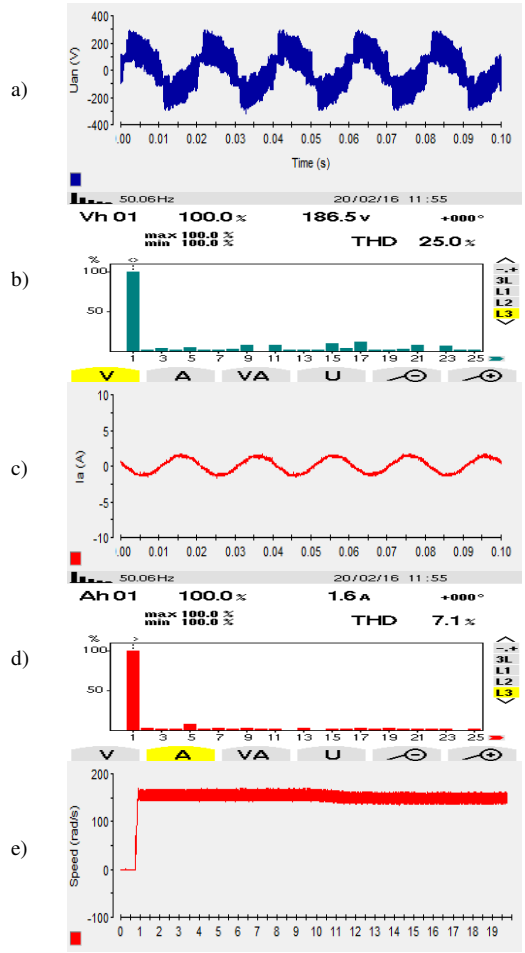


Fig.7. Discontinuous Pulse Width Modulation DPWM_3, **M = 0.9**, a)Line to neutral voltage $V_{an}$(v), b)Voltage frequency spectrum THD (%), c) Phase current $I_a$(A), d) Current frequency spectrum THD (%) and e) Motor speed (rad/s)

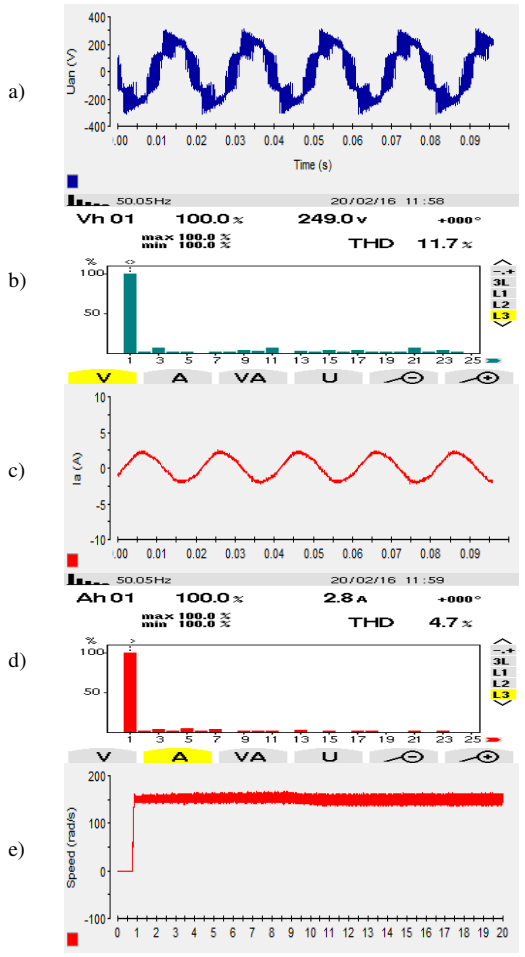


Fig.8. Discontinuous Pulse Width Modulation DPWM_3, **M = 1.2**, a)Line to neutral voltage $V_{an}$(v), b)Voltage frequency spectrum THD (%), c) Phase current $I_a$(A), d) Current frequency spectrum THD (%) and e) Motor speed (rad/s)


ISSN 1737-9334

## V. RESULTS AND DISCUSSIONS

The simulation obtained waveforms when DPWM is applied are presented in Fig.4 and Fig.5 for modulation index M=0.9, and M =1.2 (over modulation) respectively. The following table summarizes the obtained simulation results.

TABLE III
SIMULATION RESULTS

| Techniques | M=0.9 | | | M=1.2 | | |
|---|---|---|---|---|---|---|
| | $THD_U$ (%) | $THD_I$ (%) | P | $THD_U$ (%) | $THD_I$ (%) | P |
| **DPWM_MIN** | 77.38 | 03.13 | 79 | 48.35 | 04.49 | 51 |
| **DPWM_MAX** | 77.28 | 03.15 | 78 | 47.06 | 04.48 | 54 |
| **SVPWM** | **76.70** | **02.23** | **120** | **46.45** | **04.00** | **57** |
| **DPWM_1** | 77.60 | 04.29 | 81 | 48.81 | 03.78 | 53 |
| **DPWM_2** | 77.55 | 05.45 | 80 | 47.23 | 03.87 | 54 |
| **DPWM_3** | **78.84** | **04.05** | **78** | **47.21** | **03.61** | **53** |
| **DPWM_4** | 77.08 | 05.29 | 80 | 47.10 | 04.14 | 54 |

Width, P: is the Number of commutation in 1 cycle

The waveforms present the details of simulated and measured waveforms of the line to neutral voltage $V_{an}$(V) Fig.4.a and Fig.5.a, the voltage frequency spectrum THD (%) Fig.4.b and Fig.5.b, phase current $I_a$(A) Fig.4.c and Fig.5.c, current frequency spectrum THD (%) Fig.4.d and Fig.5.d, torque ripples (N.m) Fig.4.e and Fig.5.e, and motor speed curve Fig.4.f and Fig.5.f respectively. These waveforms are presented for evaluation and comparison.

It can be observed from the line to neutral voltage waveforms that the number of commutations is higher (120 commutation in one cycle) than the number of commutations (78 commutations in one cycle) when DPWM_3 is used. THD of voltage total harmonic distortion is 76.70 % and 78.84 % (Fig.4.b) for SVPWM and DPWM_3 respectively. It can be noticed that the voltage THD of DPWM_3 is higher than voltage THD of SVPWM. Current total harmonic distortion ($THD_I$) is 2.23% and 4.05% (Fig.4.d) for SVPWM and DPWM_3 respectively. Current harmonic distortion is higher when DPWM_3 is used. Torque fluctuations are more pronounced when DPWM is used as illustrated in Fig.5.e whereas speed curves are the same showing acceptable speed regulation for both strategies as presented in Fig.4.f.
The simulation results of SVPWM and DPWM are shown in the table III for a modulation index M=1.2, representing the over-modulation.

It can be observed from the line to neutral voltage waveforms that the number of commutations is higher (57 commutation in one cycle) when SVPWM is used than the number of commutations (53 commutations in one cycle) when DPWM_3 is used. $THD_v$ (voltage total harmonic distortion)) is 46.45 % and 47.21 % (Fig.5.b) for SVPWM and DPWM_3 respectively. It can be noticed that the voltage THD of DPWM_3 is slightly higher than voltage THD of SVPWM. Current total harmonic distortion ($THD_I$) is 4.00% and 3.61% (Fig.5.d) for SVPWM and DPWM_3 respectively. Current harmonic distortion is lower when DPWM_3 is used. Torque fluctuations are less when DPWM_3 is used as illustrated in Fig.5.e whereas speed curve is smooth when DPWM is used as illustrated in Fig.5.f. showing a better speed regulation when discrete pulse width modulation is employed.

- With modulation indexes less than 1(M=0.9):
  - It can be observed that SVPWM has a better spectrum quality ($THD_U$=76.70% and $THD_I$=2.23%) regarding other techniques (DPWM_3 ($THD_U$=78.84% and $THD_I$=4.05%),
  - According to switching losses, it can be remarked that DPWM_3 have reduced switching compared to SVPWM, thus a reduction by 1/3 of switching losses is obtained. Torque fluctuations are more when DPWM but speed curves are the same showing acceptable speed regulation for both strategies.
- With modulation indexes superior to 1 (over-modulation with M=1.2):
  - DPWM_3 has a better current spectrum quality ($THD_I$=03.61%) compared to other techniques (SVPWM, $THD_I$=4.00%),
  - The switching losses, are also reduced when DPWM_3 is used compared to SVPWM.
- With modulation indexes less than 0.5 (under-modulation with M=0.5): it can be noted that the transient state period is very long.
  - Torque fluctuations are less and speed curve is smooth when DPWM is used showing a better speed regulation.

The obtained experimental waveforms when DPWM_3 is applied are presented in Fig.7 and Fig.8 for a modulation index M=0.9 M =1.2 (over modulation) respectively. The obtained experimental results are summarized in the table IV.

TABLE IV
EXPERIMENTAL RESULTS

| Techniques | M | $THD_U$ (%) | $THD_I$ (%) |
|---|---|---|---|
| **SVPWM** | 0.9 | 27.10 | 03.70 |
| | 1.2 | 11.00 | 04.90 |
| **DPWM_3** | 0.9 | 25.00 | 07.10 |
| | 1.2 | 11.70 | 04.70 |

The waveforms present measured waveforms of the line to neutral voltage $V_{an}$(V) Fig.7.a and Fig.8.a, the voltage frequency spectrum THD is equal to 27.1% and 25% Fig.7.b Whereas phase current $I_a$(A) presented in Fig.7.c giving a current frequency spectrum THD equal to 3.7% and 7.1%. The motor speed curves shown in Fig.7.e is smooth when DPWM is applied showing better speed regulation.
The experimental results of SVPWM and DPWM are shown in the table IV for a modulation index M=1.2, representing the over-modulation.
It can be observed from THD (voltage total harmonic distortion) is 11.00 % and 11.70 % (Fig.8.b) for SVPWM and DPWM_3 respectively. It can be noticed that the voltage THD of DPWM_3 is slightly higher than voltage THD of SVPWM. Current total harmonic distortion ($THD_I$) is 4.90% and 4.70% (Fig.8.d) for SVPWM and DPWM_3 respectively. Current harmonic distortion is lower when DPWM_3 is used. The speed curve is smooth when DPWM is used as illustrated in Fig.8.e. showing a better speed regulation for DPWM.


ISSN 1737-9334

- With modulation indexes less than 1(M=0.9):
  - It can be observed that SVPWM has a better voltage spectrum quality ($THD_U$=11.00%) regarding other techniques (DPWM_3 ($THD_U$=11.70%) but a relatively lower current $THD_I$=4.70% compared to SVPWM ( $THD_I$ = 4.90%)
- With modulation indexes superior to 1 (over modulation M=1.2):
  - DPWM_3 has a better current spectrum quality ($THD_I$=4.70%) compared to other techniques (SVPWM, $THD_I$=4.90%).
  - The switching losses, are reduced when DPWM_3 is used compared to SVPWM
- With modulation indexes less than 0.5 (under-modulation with M=0.5): it can be noted that the transient state period is very long.
  - Speed curve is smooth when DPWM is applied showing a better speed regulation.

The experimental results are in good agreement with the simulation results in harmonics and switching losses reductions as stated and noticed previously.

## VI. CONCLUSIONS

In this paper the evaluation of DPWM performances as inverter control technique is conducted and compared to SVPWM technique. The implementation of both techniques is carried out by simulation in Matlab environment and real time implementation in dSPACE DS1104 experimental platform. It has been demonstrated by both tests that DPWM_3 technique has better performances over SVPWM in switching losses (reduced number of commutations) especially for over modulation achieving at the same time an acceptable level of harmonic distortion. Therefore, DPWM_3 technique is more appropriate to AC variable speed drives and system controllers with a high switching frequency. In the future works, real time implementation of DPWM_3 technique to control a three phase multilevel inverter will be conducted.

## ACKNOWLEDGEMENTS

The authors gratefully acknowledge the Algerian General Direction of Research for providing the facilities and the financial funding of this project.

## REFERENCES

[1] - A. C. Hernandez, G. V. Gaytán and J. L. M. Morales, “A new switching time calculation algorithm for SPWM three-phase voltaje source inverter”, IEEE International Autumn Meeting on Power, Electronics and Computing (ROPEC), pp. 1-6, 2017, Ixtapa, Mexico.

[2] - J. G. Guemez, D. S. Laila and S. M. Sharkh, ”State-space approach for modelling and control of a single-phase three-level NPC inverter with SVPWM”, IEEE Power and Energy Society General Meeting (PESGM), pp. 1-5, 2016, Boston, MA, USA.

[3] - G. Ramya and R. Ramaprabha, “Switching loss and THD analysis of modular multilevel converter with different switching frequency”, IEEE 11th International Conference on Power Electronics and Drive Systems, pp. 336-340, 2015, Sydney, NSW, Australia.

[4] - B. Alamri, S. Alshahrani and M. Darwish, “Losses investigation in SPWM-controlled cascaded H-bridge multilevel inverters”, 50th International Universities Power Engineering Conference , pp. 1-5, 2015, Stoke, UK.

[5] - P.S. Shete, R.G. Kanojiya and N.S. Maurya, “Performance of sinusoidal pulse width modulation based three phase inverter”, IJCA Proc. on Inter. Conf on Emerging Frontiers in Technology for Rural Area (EFITRA), pp. 22-26, 2012.

[6] - B. Lang, M. Miao, W. Liu and G. Luo, “Simulation and experiment study of space vector pulse width modulation”, presented at the 9th Inter. Conf. on electronic measurement and Instruments,pp.408-412,2009, Beijing.

[7] - R. Gregor, F. Barrero, S.L. Toral and M.J. Dura “Predictive-space vector PWM current control method for asymmetrical dual three-phase induction motor drives”IET Electr. Power App, Vol.4, Iss.1, pp.26-34, 2010.

[8] - N. Ravisankar Reddy, T. Brahmananda Reddy, J. Amarnath and D. SubbaRayudu, “ Family of space vector based hybrid PWM methods for induction motor drives without angle estimation for reduced ripple”, International Journal of Distributed Energy Resources, Vol. 6, no. 4, pp. 295-310, 2010.

[9 ] - T. Abhiram, P. S. Reddy and P.V.N. Prasad, “Integrated dead-time SVPWM algorithm for indirect vector controlled two-level inverter fed induction motor drive”, International Conference on Information, Communication, Instrumentation and Control, pp. 1-6, 2017, Indore, India.

[10 ] - N. R. Reddy, T. B. Reddy, J. Amarnath and D. S. Rayudu, “Simplified Space Vector Based Hybrid PWM Algorithm for Reduced Current Ripple”, International Journal of Recent Trends in Engineering, Vol. 2, no. 5, pp. 292-297, November 2009.

[11] – H. J. Lee, A. Yoo, C. Hong and J. Lee, “A Carrier-based Adjustable Discontinuous PWM for Three-Phase Voltage Source Inverter”, Energy Conversion Congress and Exposition, pp. 2870-2875, 2015, Canada.

[12] – A. Rahnamaee, H. Riazmontazer, A. Mojab, S. K. Mazumder and M. Zefran, “A Discontinuous PWM Strategy Optimized for High-Frequency Pulsating-DC Link Inverters”, Applied Power Electronics Conference and Exposition (APEC), IEEE, pp. 849-853, March 2015, Charlotte, USA.

[13] – S. An, X. Sun, Y. Zhong and M. Matsui, “Research on a New and Generalized Method of Discontinuous PWM Strategies to Minimize the Switching Loss”, Innovative Smart Grid Technologies (ISGT Asia), IEEE, pp. 1-6, May 2012, Tianjin, China.

[14] - G. N. Goyal and M. V. Aware, “A comparative performance of six-phase nine switch inverter operation with SPWM and SVPWM”, IEEE International Conference on Power Electronics, Drives and Energy Systems (PEDES), pp. 1-6, 2012, Bengaluru, India.

[15] - K. M. Siddiqui; S. Kuldeep and V. K. Giri, “Simulation Analysis and Performance Comparison of SPWM and SVPWM Inverter Fed Induction Motor Drives”, i-Manager's Journal on Future Engineering and Technology, Nagercoil, Vol. 13, No. 2, pp. 28-36, (Nov 2017-Jan 2018).

[16] - Y.R. Manjunatha and M.Y. Sanavullah, “Comparative study of PWM inverters fed 3-phase induction motor”, Asian power electronics journal, vol. 2, no. 2, pp. 98-102, Oct 2008.

[17] - S. Tunyasrirut, S. Srilad and T. Suksri, “Comparison power quality of the voltage source inverter type SVPWM and SPWM technique for induction motor drive”, SICE Annual Conf., the University Electro-communications, pp. 241-246, Aug 2008, Japan.

[18] - R. Cordero and J. O. P. Pinto, “Relationship between SPWM and SVPWM for under-modulation and over-modulation modes based on modified carrier signal”, presented at the 9th IEEE/IAS Inter. Conf. on industry applications, Nov 2010, Sao Paulo.

[19] - F. Liu, K. Xin and Y. Liu, “An adaptive Discontinuous Pulse Width Modulation (DPWM) method for three phase inverter”, IEEE Applied Power Electronics Conference and Exposition, pp. 1467-1472, 2017, Tampa, USA.

[20] - A. Anuchin, M. Gulyaeva, F. Briz and I. Gulyaev, “Modeling of AC voltage source inverter with dead-time and voltage drop compensation for DPWM with switching losses minimization”, International Conference on Modern Power Systems (MPS), pp. 1-6, 2017, Cluj-Napoca, Romania.

[21] – A. Pevere and R. Petrella, “Discontinuous Hybrid Modulation Technique for Three-Phase Three-Level Neutral Point Clamped Inverters”, Energy Conversion Congress and Exposition (ECCE), IEEE, pp. 3992-3999, September 2013, Denver, USA.

[22] - S. Yoo ; J. S. Lee and K. B. Lee, “A new discontinuous PWM method of three-level inverter for neutral-point voltage ripple reduction”, 9th International Conference on Power Electronics and ECCE Asia (ICPE-ECCE Asia), pp. 521-526, 2015, Seoul, South Korea.

[23] – F. Zaamouche, S. Saad, L. Hamiche and F. Chouaf, “Simulation and experimental tests of a real-time DPWM technique for the control of VSI-IM Drive”, Revue des Sciences et de la Technologie (Synthèse), Vol. 34, No. 1, pp. 177 -187, 2017.


ISSN 1737-9334

# Asynchronous HVDC System -based on Three Level NPC Converter

M. Flitti[#1], M. Khatir[*2], M.K. Fellah[*2], K. Mendez[#1]

*Intelligent Control and Electrical Power System Laboratory*

[1]*Djillali Liabes University of Sidi Bel-Abbes, Algeria*

[2]*Belhadj Bouchaib Center University of Ain Témouchent , Algeria*

flitti_med@yahoo.fr

***Abstract*— Voltage Source Converter High Voltage Direct Current (VSC-HVDC) systems have the ability to rapidly control the transmitted active power and independently exchange reactive power with transmissions systems. The present work investigates the modeling and control design of a high-voltage direct current (HVDC) transmission system based on three-level NPC multilevel converters with Subharmonic PWM modulation technique (SH-PWM), and a feed-forward decoupled current control strategy. By using this control strategy, not only the active and reactive power of HVDC can be controlled independently but also the dynamic responded time can be shortened. Simulation studies of a 200MW/ ±100 kV back to back VSC-HVDC system connecting two asynchronous ac networks are presented to confirm the satisfactory performance of the proposed system under active and reactive power variations from single phase to ground and three phases to ground fault conditions.**

***Keywords*— NPC multilevel converter, VSC based HVDC, SH-PWM**

## I. INTRODUCTION

Voltage Source Converter (VSC)-based High-Voltage Direct Current (HVDC) schemes using insulated-gate bipolar transistors (IGBTs) (known as VSC transmission) has attracted increasing attention. The main advantage of VSC power transmission is the high controllability, the ability to control independently active and reactive power at each terminal and the possibility for linking with dead networks. These characteristics make VSC transmission attractive in many applications like the emerging interconnection with renewable energy sources. The disadvantages are known as higher power losses and higher capital cost compared with conventional HVDC [1-2]. In order to maximize the potential of VSC transmission systems, a number of technology breakthroughs are required. One requirement is the reduction of the power losses and the harmonic distortion generated by the converters. This will allow the reduction of cooling needs and space requirements as well as increasing the system's operating efficiency and reliability. The other one is to ensure that the system operates satisfactorily during abnormal conditions, such as during severe network unbalances.

Theoretically, one promising way forward could be the adoption of a multilevel converter as a building block for the system. There are a number of distinct multilevel converter topologies which have been used or proposed for the VSC transmission system, namely, the neutral-point clamped (NPC), the flying-capacitor (FC) converter, and the cascaded Converters. While these multilevel converters have their respective merits and shortcomings, the selection of the converter topology is a detailed engineering design exercise. It needs to take into account a number of parameters, including the system design and control, power loss, cost, etc… [3]. Due to these characteristics this paper present the element of an asynchronous back-to-back VSC-HVDC system which uses three level neutral point clamped inverter topology with (SH-PWM) technique and a current-control strategy in rotation frame that the ac current is feedforward decoupled made the active and reactive power exchange controlled independently. The simulation results got from MATLAB software confirm that the control strategy provides satisfactory response and strong stability.

## II. INVERTER TOPOLOGY

Fig 1 illustrates the fundamental building block of a diode -clamped inverter. In this circuit, the dc-bus voltage is split into three levels by two series-connected bulk capacitors, $C_1$ and $C_2$ . The middle point of the two capacitors n can be defined as the neutral point. The inverter in Fig. 1 provides a three-level output across a and n.

$$V_{an} = \left( V_{dc}/2 \right), 0, \left( -V_{dc}/2 \right)$$

For voltage level $\left( V_{dc}/2 \right)$, switches $S_{11}$ and $S_{21}$ need to be turned 'ON'.

For $\left( -V_{dc}/2 \right)$ switches $S_{11}^{'}$ and $S_{21}^{'}$ need to be turned 'ON'; and for the '0' level, either pair $\left( S_{21}, S_{11}^{'} \right)$ needs to be turned 'ON'.

The same switching pattern applies across the phase 'b' leg (if 'a' is replaced by 'b') but phase shifted by 180° for




ISSN 1737-9334

the single phase configuration (in the three-phase configuration the shifts between the phases will be 120˚) [3].

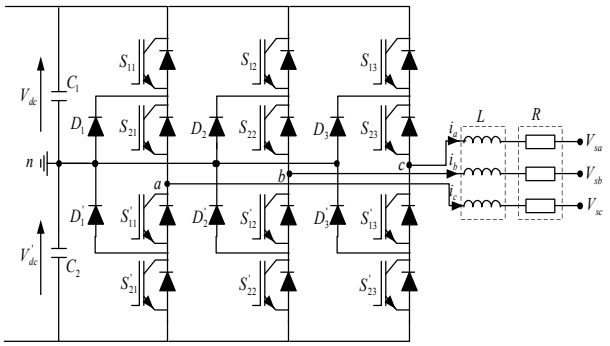


Fig. 1. Basic Model of VSC (Three-Level Neutral Point Clamped inverter circuit topology).

The control strategies are based on reducing harmonic distortion, power losses and speeding transient response. In which, the fundamental frequency switching method and PWM techniques show great advantages. Many different approaches of PWM techniques for multilevel inverters have been published. This paper proposes the Sub-Harmonic PWM (SH-PWM) technique [4], [5], [6].

The control principle of the SH-PWM method is to use several triangular carrier signals keeping only one modulating sinusoidal signal. For the three level inverter, two triangular carriers are needed (generally speaking, if a N-level inverter is employed, N-1 carriers will be needed). The carriers have the same frequency and the same peak-to-peak amplitude, and are disposed so that the bands they occupy are contiguous. The zero reference is placed in the middle of the carrier set.

Fig 2 show an example of the SH-PWM method used for three level inverter.

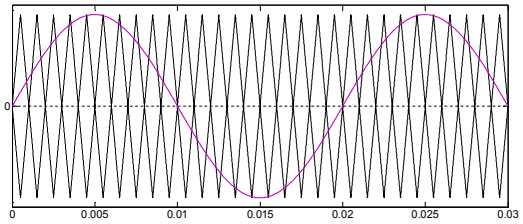


Fig. 2.a. Carrier and modulation waveforms using SH-PWM.Clamped inverter circuit topology).

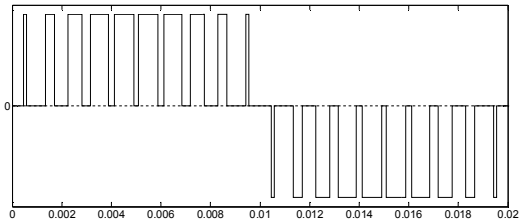


Fig. 2.b. Output voltage waveform using SH-PWM.

## III. VSC Transmission Analysis And Control

An equivalent system model for the back- to- back HVDC based on VSC converter is given in Fig. 3. There are two converter stations in the system. Each station shown in Fig. 1 is coupled with ac network via equivalent impedances $Z_1 = Z_{ac1} + Z_{T1}$ and $Z_2 = Z_{ac2} + Z_{T2}$, where $Z_{ac1}$ and $Z_{ac2}$ are the impedances of ac lines, respectively. $Z_{T1}$ and $Z_{T2}$ are the impedances of transformers. dc capacitor $C = C_1 = C_2 = C_1' = C_2'$ is used across dc side of the VSC-HVDC system.

The sending and the receiving VSC stations have same topology structure; we can establish the same model for both. To describe the mathematical models of converter it is assumed that the switches at the converter bridge should not be turn-on at the same time. We define the switch function $S_a, S_b$ and $S_c$, with $S_i$ the switching function defined by :

$$S_i = \begin{cases} 1 \; upper\ switch\ ON \\ 0 \; bottom\ switch\ ON \end{cases}$$

The mathematical model for the VSC used switch function is [7], [8]:

$$\begin{cases} L\dfrac{di_a}{dt} = -Ri_a + V_{sa} - \left(\dfrac{2S_a - (S_b + S_c)}{3}\right)V_{dc} \\ L\dfrac{di_b}{dt} = -Ri_b + V_{sb} - \left(\dfrac{2S_b - (S_a + S_c)}{3}\right)V_{dc} \\ L\dfrac{di_c}{dt} = -Ri_c + V_{sc} - \left(\dfrac{2S_c - (S_a + S_b)}{3}\right)V_{dc} \\ C\dfrac{dV_{dc}}{dt} = S_a i_a + S_b i_b + S_c i_c - i_{dc} \end{cases} \quad (1)$$

$S_a, S_b, S_c$ are discrete functions. It is difficult to directly analyse the control model. Omitting the high-frequency proportion, we get the steady fundamental frequency component $V_{ra}, V_{rb}, V_{rc}$ to present the VSC output voltage.

The voltage vector equation is:

$$L\frac{di_{abc}}{dt} = -Ri_{abc} + V_{sabc} - V_{rabc} \quad (2)$$

$$\begin{cases} L\dfrac{di_q}{dt} = -Ri_q - \omega Li_d + V_{sq} - V_{rq} \\ L\dfrac{di_d}{dt} = -Ri_d + \omega Li_q + V_{sd} - V_{rd} \end{cases} \quad (3)$$

The current equation of the VSC station is given by:

$$C\frac{dV_{dc}}{dt} = S_q i_q + S_d i_d - i_{load} \quad (4)$$

### A. Decoupled system

Formula (4) show that there exist coupling between two axis components, However, the PI current controllers have




ISSN 1737-9334

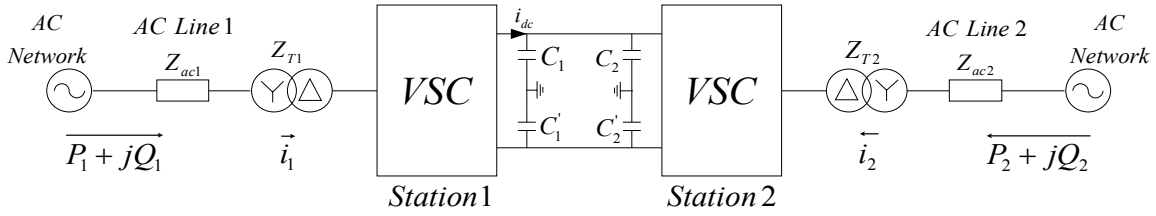


Fig. 3. A physical model for the VSC-HVDC system.

no satisfactory tracking performances when they have to regulate coupled systems. Therefore, in order to improve the performances of the PI current controllers in such systems, cross-coupling terms and voltage feed forward is usually used [9]. Now, assume that the VSC output voltage is determined by the following PI controller:

$$\begin{cases} V_{rq} = -\left(K_{pq} + \dfrac{K_{iq}}{s}\right)\left(i_q^* - i_q\right) - \omega L i_d + V_{sq} \\ V_{rd} = -\left(K_{pd} + \dfrac{K_{id}}{s}\right)\left(i_d^* - i_d\right) + \omega L i_q + V_{sd} \end{cases} \quad (5)$$

Substituting (6) into (4) the control variable equations given by:

$$\begin{cases} L\dfrac{di_q}{dt} = -\left[R - \left(K_{pq} + \dfrac{K_{iq}}{s}\right)\right] i_q - \left(K_{pq} + \dfrac{K_{iq}}{s}\right) i_q^* \\ L\dfrac{di_d}{dt} = -\left[R - \left(K_{pd} + \dfrac{K_{id}}{s}\right)\right] i_d - \left(K_{pd} + \dfrac{K_{id}}{s}\right) i_d^* \end{cases} \quad (6)$$

The structure of the VSC output voltage implemented in the synchronous reference frame is presented in Figure 4:

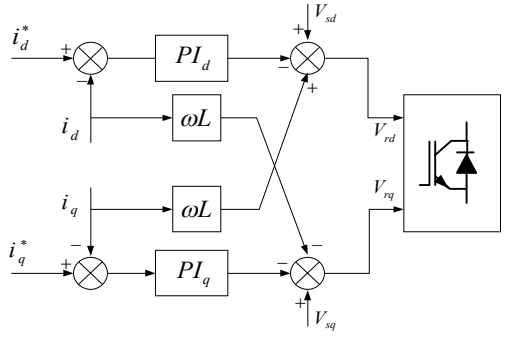


Fig. 4. Decoupled Controller

In dq frame, equation (8) will be:

$$V_{sq} = V_{moy} \quad V_{sd} = 0 \quad (7)$$

So, the active and reactive powers are given by:

$$\begin{cases} P_s = \dfrac{3}{2} V_{sq} i_q + \dfrac{3}{2} V_{sd} i_d = \dfrac{3}{2} V_{sd} i_q \\ Q_s = \dfrac{3}{2} V_{sq} i_d - \dfrac{3}{2} V_{sd} i_q = -\dfrac{3}{2} V_{sd} i_d \end{cases} \quad (8)$$

*B. Capacitor voltage and current control*

The goal of the dc voltage controller is to regulate the dc-link voltage to its reference and outputs the appointed reactive power to grid. At the dc side, the capacitance holds out the dc bus voltage and the dc cable or line is the channel to flow active power. The exchange of active power between the ac system and the VSC will result in variation of dc-link voltage of the converters. If the ac system provides more real power than the load demand and the converter losses, the excess power will be absorbed by the VSC resulting in the dc-link capacitor voltage to increase. If this real power is less than the load demand and the converter losses, the dc-link capacitor voltage will decrease. It is important to maintain the voltage across the capacitor to ensure continuous power flow. The ac active power current, used for controlling the balance of the dc power, consists of two parts: one is the steady portion, the other is variable portion to compensate the dc voltage fluctuation. This, of course, yields a stationary error in the dc bus voltage, proportional plus integral PI controllers are employed to control the ac side current, and generate references for the ac active power current in the rotation (dq) frames. In these control schemes, the output dc voltage is controlled by an outside voltage loop. The inside feedforward decoupled PI current regulators ensure that the input ac currents track these reference. The dc bus voltage controller is represented in figure (5).

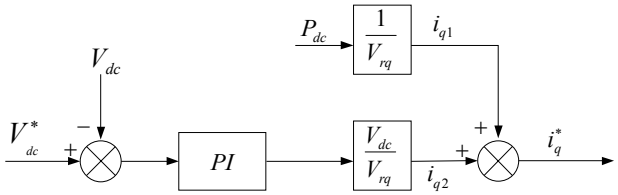


FIG. 5. DC BUS VOLTAGE CONTROLLER FOR VSC-HVDC

When the dc voltage is fixed, the fixed dc current control mode actually controls the active power transmission direction and quantity. The fixed dc bus current controller for the converter is show in figure (6).

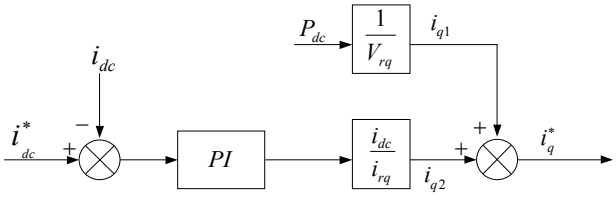


Fig. 6. dc bus Current Controller for VSC-HVDC




ISSN 1737-9334

It has the similar control structure to the fixed dc voltage control. PI regulators are also employed to control the ac side active power current. The output dc current is controlled by an outside current loop. The inside feedforward decoupled PI current regulators ensure that the input ac currents track these references [9].

The other aim of the fixed dc voltage and current control is to output the exact reactive power to ac grid as it's needed.

### C. *Fixed AC bus Voltage Control*

In the VSC-based HVDC transmission systems, another variable which can be subject to control is the AC voltage, the control scheme aim to keep the ac bus voltage at the appointed voltage through controlling the VSC station reactive power output. To passive ac net, the ac bus voltage is key to load normal working, the VSC station provide the active power and the reactive power according to the load to hold the ac bus voltage needed.

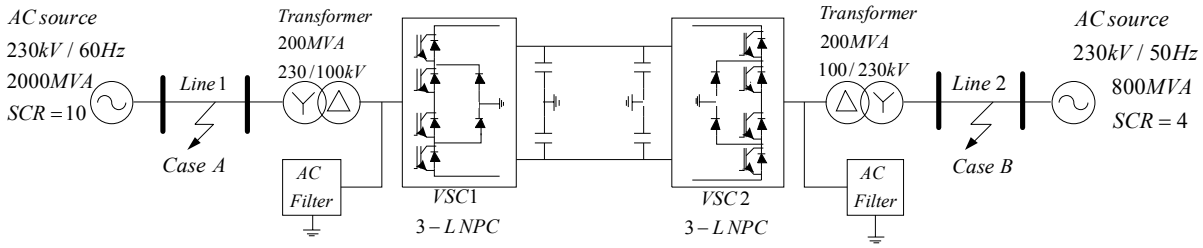


Fig. 7. dc bus Current Controller for VSC-HVDC

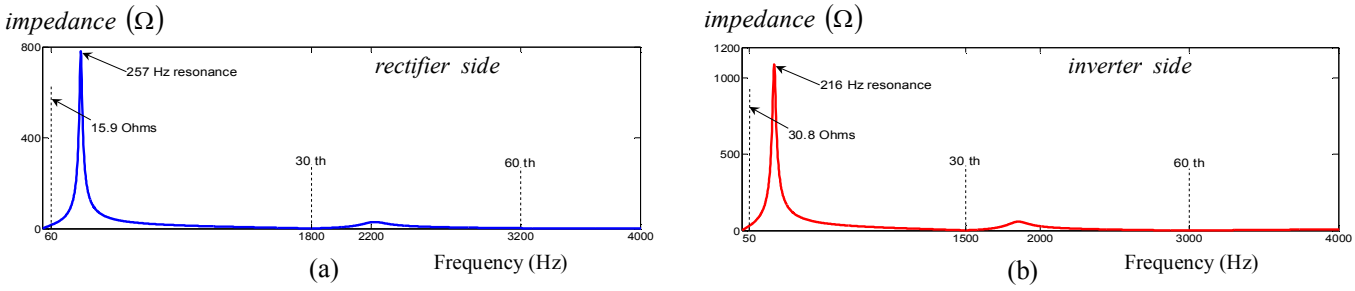


Fig. 8.1. Impedances of the two ac networks

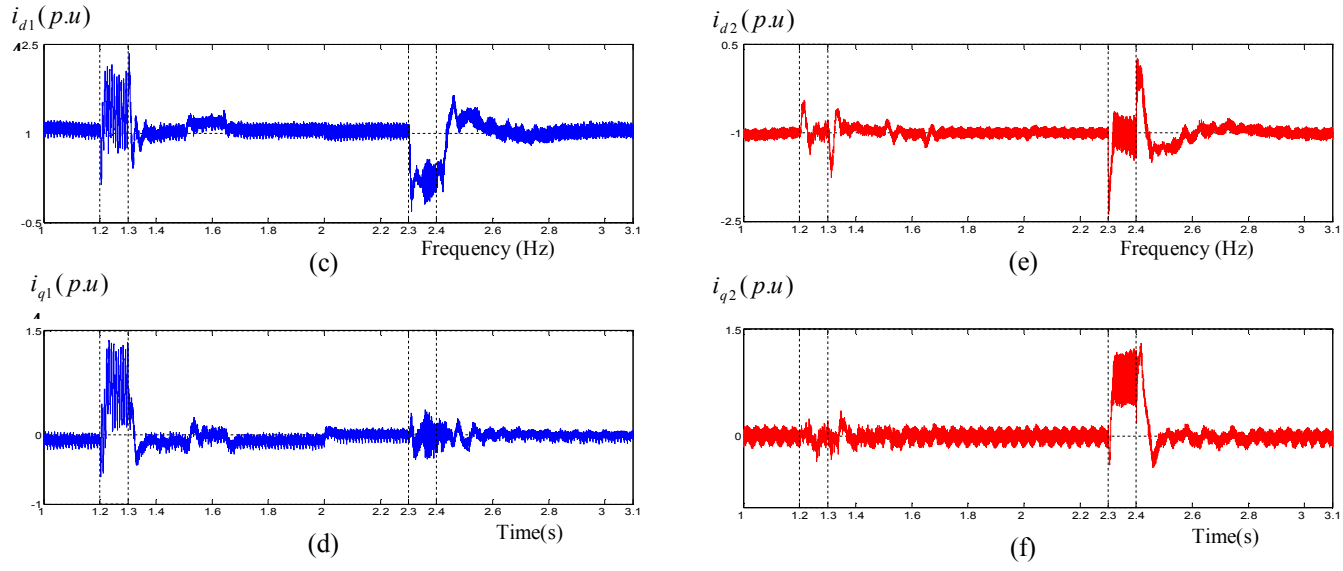


Fig. 8.2. Current control results: (c)-(d) Converter current control responses in dq frame reference (Rectifier side) . (e)-(f) Converter current control responses in dq frame reference (inverter side).

### D. *System Under Study*

An Asynchronous back-to-back HVDC link based on VSC converters rated at 200 MVA (+/- 100 kV) employing three-level NPC converters using close IGBT/Diodes used to transmit power from AC system 1 to AC system 2: AC system 1 is a 230 kV, 2000 MVA, 60 Hz system, having a Short Circuit Ratio (SCR) of 10 and consists of one source with an equivalent impedance $Z_{ac1} = 0.072 + j40.974\,\Omega$, length of ac cable is 50 km. AC system 2 is a 230 kV, 800


ISSN 1737-9334

MVA, 50 Hz system, having a SCR of 4 and consists of one source with an equivalent impedance $Z_{ac2} = 0.085 + j26.766\,\Omega$, length of AC cable is 50 km.

To simulate the system behaviour under parameters uncertainty conditions, faults are applied in cases A and B separately [10], as shown in Fig. 7. The Sinusoidal Pulse Width Modulation (SH-PWM) switching uses a two several triangular carrier signals with a frequency of 30 times fundamental frequency.

Case A:

t < 1.2 s, the system operates in normal conditions.

At t = 1.2 s, a single-phase to ground fault occurs at the transmission line 1.

At t = 1.3 s, line 1 is de-energized to clear the fault.

Case B:

t < 2.3 s, the system operates in normal conditions.

At t = 2.3 s, a three phase fault to ground occurs at the transmission line 2.

At t = 2.4 s, line 2 is de-energized to clear the fault.

Simulation results of system responses are shown in Figs. 8. First, figures 8.1. (a), (b) shows the magnitude seen from the bus bar where the filter is connected of the combined filter and AC network impedance as a function of frequency.

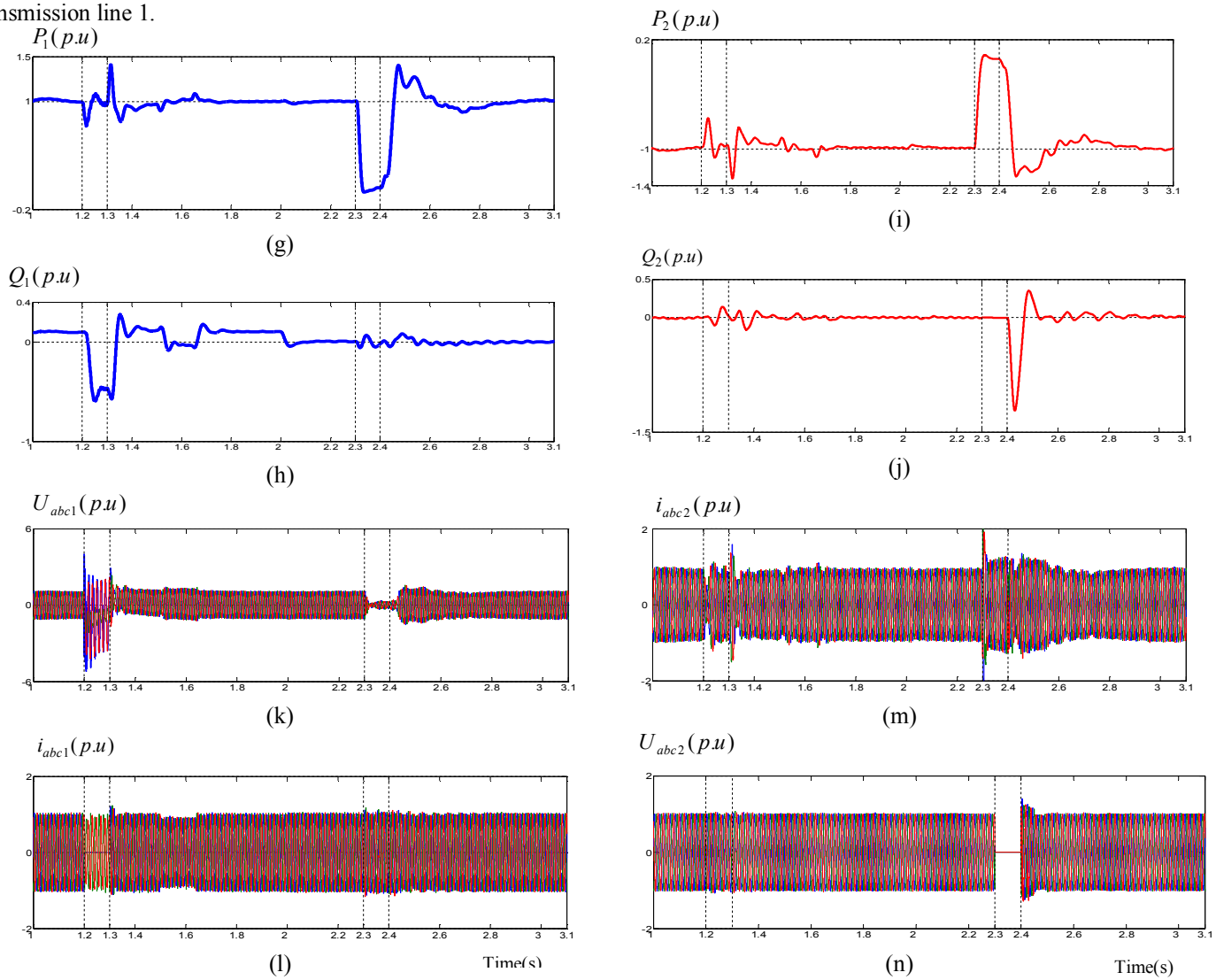


Fig. 8.3. ac side perturbations: (g)-(h) the transmitted active and reactive power at the Rectifier side.

(k)-(l)The transmitted active and reactive powers at the Inverter side (i)-(j) Rectifier ac phase current and Voltage. (m)-(n) Inverter ac phase current and Voltage.

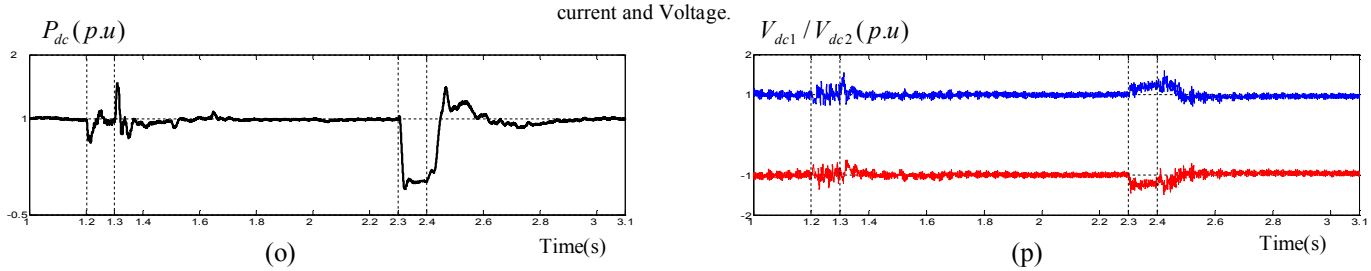


Fig. 8.4. (o) Active Power measured at the dc side. (p) dc voltages.




ISSN 1737-9334

Notice the two minimum impedances on the Z magnitudes of the ac systems: these series resonances are created by the 30th and 60th harmonic filters. They occur at 1800 Hz and 3200 Hz on the 60 Hz system (1500 Hz and 3000 Hz on the 50 Hz). The low principal natural frequency, coinciding with the parallel resonance at 257 Hz on the rectifier side and 216 Hz on the inverter side, is a determining factor in the development of the over voltages and interaction with the dc voltage [19].

is occurred at 1.2 s and 2.3 s that the current responses can quickly track the references. From fig 8.3.(g), (n) it can be seen that, when fault line 1 is de-energized in case A, the active power flow is 1 p.u, transmitted from VSC 1 to VSC 2 with same oscillation during the fault in case A. However, when faults occur at 2.3 s (case B), the transmitted power is reduced to 0 p.u and the values can return to the reference value after clearing the fault at 2.3 s after 0.5 s. the reactive power of VSC 1 decreased to 0.6 p.u during the fault at 1.2 s, with some oscillations at 2.3 s, when the reactive power of VSC 2 can track the reference in all operations, but we can see some oscillations after the severely fault at 2.3 s. Finally, the main dc and flying-capacitor voltages shows in fig 8.4 is maintained at the stable value 1 p.u with some oscillations during the fault in case A. During the fault in case B, the value progress about 1.1 pu, he recovers to the reference after 0.1s when the fault is cleared.

## IV. Conclusion

A control system for an HVDC link with voltage sourced converters has been established in this paper. A mathematical model was developed in the synchronous reference frame. The mathematical model was then used to analyze and synthesize the voltage and current control loops for the VSC. The performance of the VSC-HVDC system was verified by balanced and unbalanced fault conditions. Simulation results show that with the proposed control strategy, rapid response and desirable stability have been reached for steady-state and dynamic conditions. In addition, it is also confirmed that the active and the reactive power can be controlled with no mutual interference.

## References

[1] D. Jovcic, L. Lamont, K. Abbott « Control system design for VSC transmission » Electric Power Systems Research 77 (2007) 721–729.

[2] D. Velasco, C.L. Trujillo, R.A. Pena « Power transmission in direct current. Future expectations for Colombia» Renewable and Sustainable Energy Reviews 15 (2011) 759–765.

[3] J. Arrillaga, Y.H. Liu, N.R. Watson « Flexible power transmission, The HVDC options ». John Wiley & Sons, Ltd, 2007.

[4] J. Rodríguez, J.S. Lai, and F.Z. Peng « Multilevel Inverters: A survey of topologies, controls, and applications » IEEE Transactions On Industrial Electronics, vol. 49, no. 4, pp 724-738. August 2002.

[5] R.W. Menzies, Y. Zhung « Advanced static compensation using a multilevel GTO thyristor inverter » IEEE Transactions On Power Delivery. vol. 10, no. 2, pp 732-738, April 1995.

[6] L. M. Tolbert, T. G. Habetler« Novel Multilevel Inverter Carrier-Based PWM Methods » IEEE IAS 1998 Annual Meeting, St. Louis, Missouri, October 10-15, 1998, pp. 1424-1431.

[7] K. R. Padiyar, N. Prabhu « Modelling, control design and analysis of VSC based HVDC transmission system» International Conference on Power System Technology, 21-24 November 2004, pp 774-779.

[8] S.Akkari, J.Dai, M.Petit, X.Guillaud, "Interaction between the voltage-droop and the frequency-droop control for multi-terminal HVDC systems", Generation Transmission & Distribution IET, vol. 10, no. 6, pp. 1345-1352, 2016.

[9] N. A. Belda, C. A. Plet, R. P. P. Smeets , « Analysis of Faults in Multiterminal HVDC Grid for Definition of Test Requirements of HVDC Circuit Breakers », IEEE Transactions on Power Delivery , vol. 33, no.1, pp. 403-411, 2018.

[10] L.A. Lamont, D. Jovcic , K .Abbott, « VSC transmission control under faults » Universities Power Engineering Conference, 2004. UPEC 2004, PP 739 - 743.

[11] M. Khatir, S.A. Zidi, S. Hadjeri, M.K. Fellah «Dynamic performance of back-to-back HVDC station based on voltage source converters» Journal of electrical engineering vol. 61, no. 1, 2010, pp 29-36.

FLITTI Mohamed was born in Oran, Algeria, in 1982. He received the Eng. degree in electrical engineering, and the Master's degrees from the Djillali Liabes University of Sidi Bel-Abbes (Algeria), in 2005 and 2008 respectively. He is now a PhD Candidate in the Electrical Engineering Department of Djillali Liabes University. His main field of interest includes HVDC and FACTS.

FELLAH Mohammed-Karim was born in Oran, Algeria, in 1963. He received the Eng. degree in Electrical Engineering from University of Sciences and Technology, Oran, Algeria, in 1986, and The Ph.D. degree from National Polytechnic Institute of Lorraine (Nancy, France) in 1991. Since 1992, he is Professor at the university of Sidi Bel Abbes (Algeria) and Director of the Intelligent Control and Electrical Power

KHATIR Mohamed was born in Ain Temouchent, Algeria, in 1977. He received the Eng. degree in electro technical engineering, the Master's and the PhD degrees from the Djillali Liabes University of Sidi Bel Abbes (Algeria), in 2002, 2006 and 2010 respectively. Since 2010 he is a teaching member at the department of Electrical Engineering of Djillali Liabes University. His main field of interest includes HVDC and FACTS.

Mendez Kheira was born in Ain Témouchent, Algeria, in 1976. He received the engineer in electrical engineering from Djillali Liabes University, Sidi Bel Abes, Algeria, in 2005, and the M.S degrees in electrical engineering from Sidi Bel Abbes University, Algeria, in 2008; His research interests include high-frequency power conversion, magnetic design, EMI reduction techniques, power electronics and EMC in power converter), and research member at IRECOM Laboratory.




ISSN 1737-9334

# Design of Fuzzy Controller rule base using Bat Algorithm

Nesrine TALBI
Department of electronic, LAJ Research Laboratory
Faculty of sciences and Technology, Jijel University
Jijel, ALGERIA
t_nesrine2003@yahoo.fr

***Abstract*—** The work in this paper revolves fundamentally around the main axes of fuzzy control of the type Takagi-Sugeno (T-S) zero order for dynamic, complex nonlinear systems. In this paper, we present method for designing Fuzzy controller rule base using a new swarm intelligence algorithm, which is based on the Bat algorithm. The Bat algorithm is one of the most recent swarm intelligence based algorithms that simulates the intelligent hunting behavior of the bats found in nature. The main objective is to design the fuzzy rule base of fuzzy controller respecting the desired performance. To demonstrate the efficiency of the suggested approach, a control of a Magnetic Ball Suspension System is selected. Simulation results shows that the proposed approach could be employed as a simple and effective optimization method for achieving optimum determination of fuzzy rule base parameters.

***Keywords- Fuzzy rule base, Bat algorithm, Fuzzy controller, Magnetic Ball Suspension System.***

## I. INTRODUCTION

Fuzzy logic is an important research topic on which focus many scientists. Its theoretical basis was formulated in 1965 by Professor Lotfi A. Zadeh, of the University of California, Berkeley [1]. He introduced the notion of a fuzzy subset to provide a means of representing and manipulating imperfectly described, vague or inaccurate knowledge.

At that time, the theory of fuzzy logic was not taken seriously except by some experts. As early as 1975, Mamdani and Assilian published the first results allowing this theory to be used in control systems [2]. By using a relatively simple controller structure, they have obtained better results when controlling certain processes than those provided by a standard PID controller.

Shortly after, in 1977, the Danish Ostergaard [3] applied fuzzy logic to the control of grinding tubes for the manufacture of cement. At that time, most studies of fuzzy logic control systems were conducted in Europe [4]. From around 1985, it was the Japanese [5] who began to make extensive use of fuzzy logic in industrial and consumer products to solve control and adjustment problems.

The fuzzy controllers make it possible to control complex systems or difficult to model them using a reasoning method of "if *condition* then *action*". Fuzzy controller (FC) depends mainly on the characteristics of three subsystems: fuzzification, fuzzy rules and defuzzification [6]. The fuzzification phase is perfectly specified when the membership functions of the linguistic terms describing the inputs are defined.

The Design of a fuzzy rule base is the process that led to the formalization in the form of rules and/or learned relations, from a set of examples between the inputs and outputs of a process. In many cases, the structure is determined empirically by choosing a priori the type of relational approximate reasoning, the number of fuzzy sets for each input variable, and taking all possible combinations to build the fuzzy rule base. So, it is important to mention the difficulty of ensuring consistency & interpretability of fuzzy rules, in particular for multivariable systems where the number of rules becomes very high [7].

The adjustment by successive trial of fuzzy controller parameters is quite long and tedious. Various techniques of optimization and learning fuzzy controllers have been developed. They are mostly based on a learning that makes it possible to iteratively define the best set of parameters for a given controller structure. For now, researchers are mainly focused on the following approaches:

- Optimization of membership functions,

- Optimization of fuzzy rules,

- Simultaneous optimization of membership functions and fuzzy rules.

several researches have been established to optimize the membership functions of a fuzzy controller using genetic algorithms [8]-[12], Thrift is the first to describe a method for optimizing fuzzy rules by genetic algorithm, using three bits to encode each rule [13], Lee and Takagi propose, in 1993, an optimization method that simultaneously takes into account the membership functions of fuzzification and the fuzzy rules [14]. several methods using the same concept were published [15][16]. Another technique of tuning fuzzy systems was the use of swarm intelligence [17]-[20].

The vast majority metaheuristic algorithms have been derived from the behavior of biological systems and/or physical systems in nature. For example, particle swarm


ISSN 1737-9334

optimization is inspired by social behavior of animals moving in swarm [21], while simulated annealing is based on the annealing process of metals [22]. New algorithms are also emerging recently, including harmony search [23], the firefly algorithm [24], and the Bat algorithm (BA) [25], [26]. The BA technique is introduced by Yang in 2010. It is based on the echolocation behavior of bats. The capability of echolocation of micro-bats is fascinating as these bats can find their prey and discriminate different types of insects even in complete darkness [27]. Bat algorithm was successfully applied to a number of very different problems [28]-[31]. BA is simple to implement and produces good results [31].

This paper presents a simple and effective method using Bat algorithm for designing a fuzzy controller of type Takagi-Sugeno zero order by optimizing the centers of membership functions and the fuzzy rule base. The remaining of this paper is organized as follows: The structure of fuzzy controller to be optimized is described in the next section. After, the standard BA algorithm is briefly presented in the section III. Section IV explained the method of designing the fuzzy controller by BA. The test of the effectiveness of the proposed method is made in section V. Finally, the paper is ended by a conclusion.

## II. FUZZY CONTROLLER STRUCTURE

This section describes the fuzzy controller (FC) to be designed in this study. The FC is of type Takagi–Sugeno zero order. The $i^{th}$ rule, which is denoted as $R_i$ , is represented in the following form:

$$R_i: If\ e(k) is\ A_{i1}\ and\ \Delta e(k)\ is\ A_{in}$$
$$Then\ u(k)\ is\ o_i \quad (1)$$

where $k$ is the time step, $e(k), \Delta e(k)$ are the input variables, $u(k)$ is the fuzzy controller output variable, $A_{ij}$ is a fuzzy set, and $o_i$ is a crisp value. $A_{ij}$ is a fuzzy set which uses a triangular membership function defined by following equation:

$$\mu(x) = \max(min\left(\frac{x-a}{b-a}, \frac{c-x}{c-b}\right), 0) \quad (2)$$

where $a, b$ and $c$ represent respectively the locations of starting point, peak point and the ending point, for a triangle shaped membership function.

About the fuzzy rule base, the decision on the number of fuzzy rules is a very important issue because it plays a very important role in fuzzy control systems. Unfortunately, there is no systematic and effective procedure for selecting the number of the most appropriate rules, except for some proposals. A reasonable number of fuzzy rules, without losing too much information about the system to be controlled must be carefully obtained.

For flexibility of the implementation of fuzzy controller, the universe of discourse of inputs and output is limited to a range of [-1, 1], determined by the normalization of inputs and output [32]. To do this, the scale factors are used to have the desired dynamics.

This paper proposes a fuzzy rule base composed of only three enabled rules, extracted from analysis expressed as follows:

$\boldsymbol{R_1}: If\ e(k)\ is\ N(-1, a_1, a_2)\ and\ \Delta e(k)\ is\ N\ (-1, b_1, b_2)$
$then\ u(k) = o_1.$

$\boldsymbol{R_2}: If\ e(k)\ is\ Z(a_1, a_2, a_3)\ and\ \Delta e(k)\ is\ Z(b_1, b_2, b_3)$
$then\ u(k) = o_2.$

$\boldsymbol{R_3}: If\ e(k)\ is\ P(a_2, a_3, 1)\ and\ \Delta e(k)\ is\ P(b_2, b_3, 1)$
$then\ u(k) = o_3.$

where $e(k)$ is the difference between the desired output and the measured output of the controlled system. $N, Z$ and $P$ are fuzzy sets of input variables, and $o_1, o_2, o_3$ are real values of fuzzy controller output.

In the inference mechanism, the AND in the fuzzy rule is implemented by the algebraic product in the theory of fuzzy logic (according to Larsen) .Thus, given a set of input data $\vec{x} = (e, \Delta e)$, the degree of activation $\gamma_i(\vec{x})$ of Rule $i$ is calculated by:

$$\gamma_i(\vec{x}) = \mu_{A_i}(e(k)) \cdot \mu_{B_i}(\Delta e(k)) \quad (3)$$

If there are $n_r$ rules in fuzzy controller, the resulting output of the set of rules is given by the average of weighted individual outputs as follows:

$$u = \frac{\sum_{i=1}^{n_r} \gamma_i(\vec{x}).\, o_i}{\sum_{i=1}^{n_r} \gamma_i(\vec{x})} \quad (4)$$

where $o_i$ is the value of the conclusion of the $i^{th}$ rule.

In this paper, the optimization of the fuzzy controller includes the determination of all parameters of each fuzzy rule.

## III. BAT ALGORITHM

Bat algorithm is a metaheuristic optimization algorithm developed by Xin-She Yang in 2010 [25]. The algorithm is based on echolocation of micro-bats with varying pulse rates of emission and loudness. Bats use sonar echoes to detect and avoid obstacles: they determine the size of an object, how far away they are, how fast they are travelling and even their texture, all in split in a second. After hitting and reflecting, bats transform their own pulse to useful information to gauge how far away the prey is. Bats are using wavelengths, that vary from range [0.7, 17] mm or inbound frequencies [20,500] kHz. By implementation, pulse frequency and rate has to be defined. Pulse rate can be simply determined from range 0 to 1, where 0 means there is no emission and by 1, bats are emitting maximum [33]- [35].

In order to transform these behaviors of bats to algorithm, Yang used three generalized rules [25]:

1) All bats use echolocation to sense distance, and they also guess the difference between food/prey and background barriers in some magical way.
2) Bats fly randomly with velocity $v_i$ at position $x_i$ with a fixed frequency $f_{min}$, varying wavelength $\lambda$ and loudness $A_0$ to search for prey. They can automatically adjust the wavelength of their emitted pulses and adjust the rate of pulse emission $r$ from [0, 1], depending on the proximity of their target.



ISSN 1737-9334

3) Although the loudness can vary in many ways, we assume that the loudness varies from a positive large value $A_0$ to a minimum constant value $A_{min}$.

The initial position $x_i$, velocity $v_i$ and frequency $f_i$ are initialized for each bat. For each time step $t$ , the movement of the virtual bats is given by updating their velocity and position using the following equations:

$$f_i = f_{min} + (f_{max} - f_{min}).\rho \quad (5)$$

$$v_i^j(t) = v_i^j(t-1) + \left[x_{gbest}^j - x_i^j(t-1)\right].f_i \quad (6)$$

$$x_i^j(t) = x_i^j(t-1) + v_i^j(t) \quad (7)$$

where $\rho \in [0,1]$ indicates randomly generated number, and $x_{gbest}^j$ represents current global best solutions.

For the local search part, once a solution is selected among the current best solutions, a new solution for each bat is generated locally using random walk:

$$x_i^{new} = x_i^{old} + \sigma.A_{mean}^{old} \quad (8)$$

Where, $\sigma \in [0,1]$ is a random number and represents direction and intensity of random-walk. $A_{mean}^{old}$ is the average loudness of all the bats.

Based on these approximations and idealization, the basic steps of the Bat Algorithm (BA) can be summarized as the following pseudo code [26]:

Objective function $f(x)$, $x = (x_1, \dots, x_d)^T$
Initialize the bat population $x_i$ and $v_i$ for $i = 1, n$
Define pulse frequency $Q_i \in [Q_{min}, Q_{max}]$
Initialize pulse rates $r_i$ and the loudness $A_i$
while $(t < T_{max})$ // number of iterations
  Generate new solutions by adjusting frequency, and updating velocities and locations/solutions
  if $(rand(0,1) > r_i)$
    Select a solution among the best solutions
    Generate a local solution around the best solution
  end if
  Generate a new solution by flying randomly
  If $(rand(0,1) < A_i$ and $f(x_i) < f(x))$
    Accept the new solutions
    Increase $r_i$ and reduce $A_i$
  end if
  Rank the bats and find the current best
end while
Post process results and visualization

## IV. Designing Fuzzy Rule Base of Fuzzy Controller using Bat Algorithm

In this section, we propose to use Bat algorithm for designing a reduced fuzzy rule base of a fuzzy controller of type Takagi-Sugeno zero order, in order to obtain better performances of the system to control.

### A. Optimization Procedure

The diagram of the closed loop control is shown schematically in Fig. 1. We can summarize the optimization procedure of the fuzzy controller using Bat algorithm through the following steps:

1. Generation of an initial population of solutions characterizing the controller settings.
2. For all solutions:
   - Evaluate the objective function.
   - Classify obtained solutions according to their fitness.
   - Construction of a new population by updating process of frequencies, velocities and solutions.

The step 2 is repeated until a maximum number of iterations is performed. After the process of evolution, the final iteration of the algorithm consists of the well-adjusted solution who provide best solution.

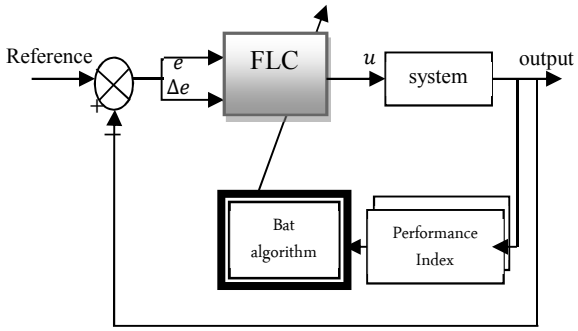


Fig.1. control structure and optimization

The inclusion of design constraints in the optimization process helps to preserve the semantics of fuzzy rules. For that, the constraints on the limits of the parameter vector to be identified, and limits on the control variables are imposed.

### B. Parameters's Vector Representation of Fuzzy Controller

The parameter vector (solution) $x$ of the fuzzy controller has nine parameters. These parameters represent the starting point locations, the pic point, and end point, for a triangular membership function belonging to the inputs of a fuzzy controller and fuzzy singleton for its release.

So $x = [\, a_1\ a_2\ a_3\ b_1\ b_2\ b_3\ o_1\ o_2\ o_3\,]$ (9)

While respecting the following constraint:




ISSN 1737-9334

$$\begin{cases} a_1 < a_2 < a_3 \\ b_1 < b_2 < b_3 \\ o_1 < o_2 < o_3 \end{cases} \quad (10)$$

### C. Generation of Initial Population of solutions

Initial population is randomly generated from real-valued vectors with dimension $d$ and number of bats $n$, by taking into account lower and upper boundaries. In this study, $d = 9$.

$$x_i^j = x_{min}^j + rand(0,1) * (x_{max}^j - x_{min}^j) \quad (11)$$

where $i = 1, n; j = 1, d$ and $x_{min}^j$ and $x_{max}^j$ are lower and upper boundaries for dimension $j$ respectively.

## V. APPLICATION

The test of effectiveness of the Bat algorithm is illustrated to designing fuzzy controllers of type Takagi-Sugeno zero order for control Magnetic Ball Suspension System.

The Bat algorithm parameters used in this section are given in Table I.

TABLE I
BA Control parameters values

| Parameter | Designation | value |
|---|---|---|
| $n$ | Population size | 20 |
| $ng$ | Number of generation | 100 |
| $f_{min}$ | Minimum frequency | 0 |
| $f_{max}$ | Maximum frequency | 1 |
| $A$ | Loudness | 0.5 |
| $r$ | Pulse rate | 0.5 |

### A. Magnetic Ball Suspension System

The model of the magnetic ball suspension system shown in Fig. 6 is given by [36] :

$$M * \frac{d^2y(t)}{dt^2} = M.g - \frac{i^2(t)}{y(t)}$$

$$v(t) = R * i(t) + L * \frac{di(t)}{dt} \quad (12)$$

where $y(t)$ is the ball position, $M = 0.1$ kg is the ball mass, $g = 9.8$ m/s$^2$ is the gravitational acceleration, $R = 50\ \Omega$ is the winding resistance, $L = 0.5$ Henrys is the winding inductance, $v(t)$ is the input voltage, and $i(t)$ is the winding current. The position of the ball is detected by a position sensor (e.g., an infrared, microwave, or photo resistive sensor) and is assumed to be fully detectable over the entire range between the magnetic coil and the ground level. The ball will stay between the coil and the ground level [37]:

$$\begin{cases} \frac{dx_1(t)}{dt} = x_2(t) \\ \frac{dx_2(t)}{dt} = g - \frac{x_3^2(t)}{Mx_1(t)} \\ \frac{dx_3(t)}{dt} = -\frac{R}{L}\, x_3(t) + \frac{1}{L}\, v(t) \end{cases} \quad (13)$$

where $[x_1(t),\ x_2(t),\ x_3(t)] = [y(t), \frac{dy(t)}{dt},\ i(t)]$. Notice that the nonlinearities are induced by the $x_3^2(t)$ and $\frac{1}{x_1(t)}$ terms in the $\frac{dx_2(t)}{dt}$ equation. By linearizing the plant model in Equation (13), assuming that the ball is initially located at $x_1(t) = y(0)$, we can find a linear system by calculating the Jacobian matrix at $y(0)$. The linear state-space form of the magnetic ball suspension system is given as [37]:

$$\begin{cases} \frac{dx_1}{dt} = x_2(t) \\ \frac{dx_2(t)}{dt} = \frac{g}{y(0)} x_1(t) - 2\sqrt{\frac{g}{My(0)}}\ x_3(t) \\ \frac{dx_3(t)}{dt} = -\frac{R}{L}\, x_3(t) + \frac{1}{L}\, v(t) \end{cases} \quad (14)$$

The objective of this section is to control the position of magnetic levitation magnetic ball. The controller used is of fuzzy controller where its output is the command $u(t)$.

We consider a fuzzy controller of the type Takagi-Sugeno zero order, its inputs are the error $e(t)$ and its variation $\Delta e(t)$and an output $u(t)$ (the command applied to the system).

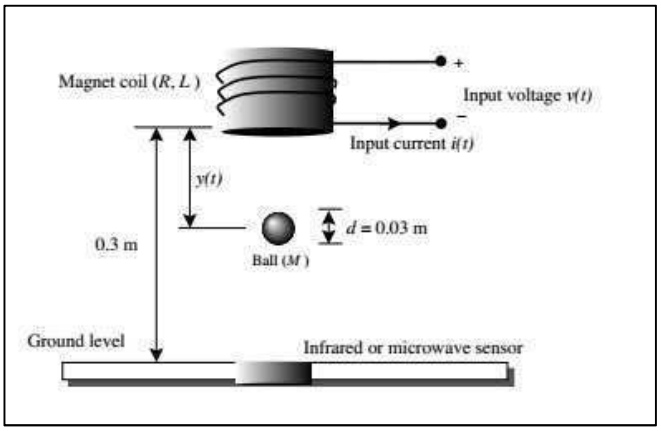


Fig.2. Magnetic ball suspension system [37]

The cost function is the mean square error calculated by the following equation:




ISSN 1737-9334

$$MSE = \frac{1}{nT}\sum_{k=1}^{n} e^2(k) \qquad (15)$$

Where: $n$ is the total number of samples and $T$ the sampling time, $e(t)$ is the difference between the value of the desired output and the value of the measured output process under control.

After 100 generations, we obtain the best parameter vector which gives best performance of the system with only three rules extracted for analysis. Figure 7 shows the evolution of the cost function. At the end of program execution, the evaluation function (mean square error ) is equal to $2.66 \times 10^{-6}$ and the fuzzy rules obtained are as follows:

$Rule\ 1: if\ e\ is\ N\ (-1, -0.99, 0.69)\ and\ \Delta e\ is\ N\ (-1, -0.72, 0.16)\ then\ u = -1.04$

$Rule\ 2: if\ e\ is\ Z\ (-0.99, 0.69, 0.99)\ and\ \Delta e\ is\ Z\ (-0.72, 0.16, 0.79)\ then\ u = -0.08$

$Rule\ 3: if\ e\ is\ P(0.69, 0.99, 1.00)\ and\ \Delta e\ is\ P\ (0.16, 0.79, 1.00)\ then\ u = 1.02$

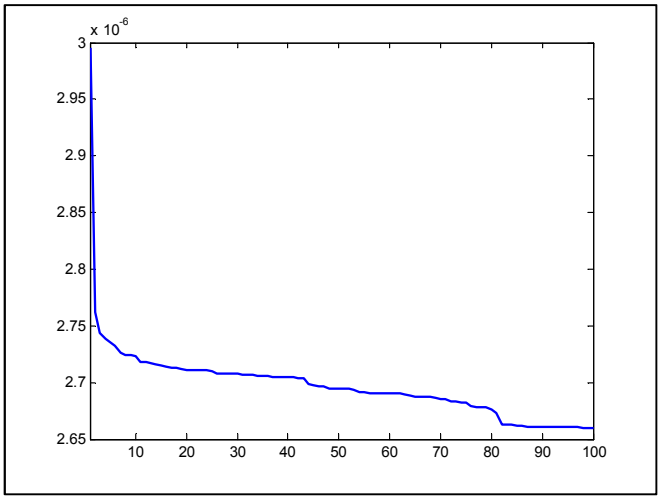


Fig.3. Evolution of fitness function

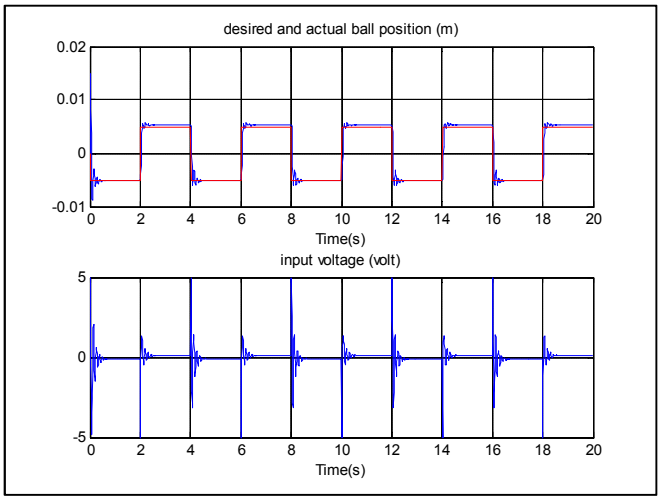


Fig.4 Responses of the system via nominal parameters

The results shows that the optimized fuzzy controller of electromagnetic voltage can stabilize the disturbance that would cause the metal sphere (ball) to fall or attach it to the electromagnet..

## VI. Conclusion

In this paper, BAT algorithm is used to design a fuzzy controller for Takagi-Sugeno zero-order, The difficulty of obtaining the rule base and membership functions is indeed very disadvantageous when using fuzzy techniques. the BAT algorithm optimizes simultaneously:

- The membership functions of the input and output variables of the controller,
- The conclusions of fuzzy rules which are the base of rules itself, since the fuzzy controller is type of T-S zero order. The fuzzy rule base is composed of three rules extracted from analysis.

To demonstrate the effectiveness of the presented approach, a control of a magnetic ball levitation system is selected. Simulation results show that the proposed approach presented here is a powerful tool for the control of nonlinear systems. We can say that the BAT algorithm present a very powerful tool for the design of intelligent controllers.

## References

[1] Zadeh, L. A. Soft computing and fuzzy logic. *IEEE Software*, 11(6), pp 48-56, 1994.

[2] Mamdani, E.H., Assilian, S. An experiment in linguistic synthesis with a fuzzy logic controller. *Int. J. Man Mach. Studies*, 7(1) : 1–13, 1975.

[3] Ostergaad, J.J. Fuzzy logic control of a heat exchange process. *in Fuzzy Automata and Decision Processes, M.M. Gupta, G.N. Saridis, and B.R. Gaines,Eds*., pages 285–320, 1977.

[4] Willaeys, D., Malvache, N. Use of fuzzy model for process control. *IEEE International Conference on Cybernetics and Society*, 1978.

[5] Tamakawa, T. High speed fuzzy controller hardware system. *Proc. 2nd Fuzzy System Symp*., pages 122–130, 1986.

[6] Jantzen, J. Foundations of Fuzzy Control. *John Wiley & Sons*, 2007

[7] M.S. Ju, D.L. Yang, "Design of adaptive fuzzy control based on natural control laws", Fuzzy Sets and Systems, Vol. 81, 1996, pp. 191-204.

[8] Karr, C.L. Design of an adaptive fuzzy linguistic controller using a genetic algorithm, *Proc. of the Fourth Int. Conf. Genetic Algorithms*, pages 450–457, 1991.

[9] Karr, C.L., Gentry, E.J. Fuzzy control of pH using genetic algorithms. *IEEE Trans. On Fuzzy Systems*, 1(1) : 46–53, 1993.

[10] Herrera, F., Lozano, M., Verdegay, J.L. Turning fuzzy logic controllers by genetic algorithms. *International Journal of Approximate Reasoning*, 12 : 299–315, 1995

[11] Shimojima, K., Fukuda, T., Hasegawa, Y. Self-turning fuzzy modeling with adaptive membership function, rules, and hierarchical structure based on genetic algorithm. *Fuzzy Sets and Systems*, 71 : 295–309, 1995.

[12] Liska, J., Melsheimer, S.S. Complete design of fuzzy logic systems using genetic algorithms. *Proceedings of the Third IEEE International Conference on Fuzzy Systems*, pages 1377–1382, 1994.


ISSN 1737-9334

[13] Thrift, P. Fuzzy logic synthesis with genetic algorithms. *Proc. of the Fourth Int. Conf.Genetic Algorithms*, pages 509–513, 1991

[14] Lee, M.A., Takagi, H. Dynamic control of genetic algorithms using fuzzy logic techniques. *Proceedings of the 5th Int'l Conf. on Genetic Algorithms*, pages 76–83, 1993.

[15] C.C. Chen and C.C. Wong, "Self-generating rule-mapping fuzzy controller design using a genetic algorithm", *In IEE Proceedings on Control Theory and Applications,* vol. 49, 2002, pp. 143–148.

[16] K. Belarbi, F. Titeli, W. Bourebia et K. Benmahammed, "Design of mamdani fuzzy logic controllers with rule base minimisation using genetic algorithm", *Engineering applications of artificial intelligence*, vol. 18, 2005, pp. 875–880.

[17] N. Talbi and K. Belarbi, "Optimization of Fuzzy Controller using Hybrid Tabu Search and Particle Swarm Optimization", *in Proc. IEEE, 11th International Conference on Hybrid Intelligent Systems (HIS)*, Malaysia, 2011, pp. 561-565.

[18] V. Mukherjee., .P. Ghoshal, "Intelligent particle swarm optimized fuzzy PID controller for AVR system". Electric Power Systems Research, Vol. 77, 2007, pp. 1689-1698.

[19] N. Talbi and K. Belarbi, "Designing Fuzzy Controllers for a Class of MIMO Systems using Hybrid Particle Swarm Optimization and Tabu Search", *International Journal of Hybrid Intelligent Systems, IOS Press,* vol. 10, n°1, 2013, pp. 1–9.

[20] C. F. Juang, P. H. Chang, "Designing fuzzy-rule-based systems using continuous Ant colony optimization", IEEE trans., *Fuzzy Syst.*, vol. 18, no. 1, 2010, pp. 138-149.

[21] J. Kennedy et R.C. Eberhart, " Particle swarm optimization", *IEEE International Conference on Neural Networks,* Piscataway*,* 1995, pp. 1942-1948.

[22] S. Kirkpatrick, C.D. Gelatt, and M.P. Vecchi, "Optimization by simulated annealing", Science, vol. 220,1983, pp. 671-680.

[23] Z.W. Geem, J. Kim, G.V Loganathan, "A new heuristic optimization algorithm: Harmony search", Simulation, vol. 76,2001, pp. 60-68.

[24] X.S. Yang, "Nature-inspired Metaheuristic Algorithms", Luniver Press, 2008.

[25] X.S. Yang, "A New Metaheuristic Bat-Inspired Algorithm", Nature Inspired Cooperative Strategies for Optimization (NISCO 2010) (Eds. J. R. Gonzalez et al.), Studies in Computational Intelligence, Springer Berlin,Springer,vol.284, 2010, pp. 65-74.

[26] X.S.Yang and A. H. Gandomi, "Bat Algorithm: A Novel Approach for Global Engineering Optimization", Engineering Computations, Vol. 29, Issue 5, 2012, pp. 464--483.

[27] K. Khan, A. Nikov,A. Sahai, "A fuzzy bat clustering method for ergonomic screening of office workplaces", *Advances in Intelligent and Soft Computin,* Springer , Vol. 101, 2011.; pp. 59–66.

[28] G.Q. Huang,W-J Zhao, Q.Q Lu, "Bat algorithm with global convergence for solving large-scale optimization problem", *Application Research of Computers*, 30(5), 2013, pp. 1323–1328.

[29] J. Zhang, G. Wang. "Image matching using a bat algorithm with mutation", *Applied Mechanics and Materials*, 203(1), 2012, pp.88–93.

[30] A. Alihodzic, M. Tuba, " Improved Hybridized Bat Algorithm for Global Numerical Optimization", *in Proc. IEEE, 16th International Conference on Computer Modelling and Simulation, 2014, pp.57-62.*

[31] K. Premkumar , B.V. Manikandan, « Bat algorithm optimized fuzzy PD based speed controller for brushless direct current motor », Engineering Science and Technology, an International Journal, vol. 19 , 2016, pp . 818–840

[32] C. C. Lee, "Fuzzy logic in control systems: fuzzy logic controller. Part 1", *IEEE Transactions on systems Man and Cybernetics*, Vol. 20, 1990, pp. 404-418.

[33] A.H. Gandomi, X.S. Yang, A.H. Alavi, and S. Talatahari, "Bat algorithm for constrained optimization tasks", *Neural Computing & Applications*, pages 1–17, 2012.

[34] P.W. Tsai, J.S. Pan, B.Y. Liao, M.J. Tsai, and V. Istanda. "Bat algorithm inspired algorithm for solving numerical optimization problems", *Applied Mechanics and Materials*, 148:134–137,2012.

[35] X.S. Yang, "Review of meta-heuristics and generalised evolutionary walk algorithm", *International Journal of Bio-Inspired Computation*, 3(2):77–84, 2011.

[36] J.T. Spooner, R. Ordonez, and K. M. Passino, "Direct adaptive fuzzy control for a class of discrete time systems", In *Proceedings of the American Control Conf.*, pages 1814–1818, Albuquerque, NM, June 4-6, 1997.

[37] K.M. Passino, S. Yurkovich, "Fuzzy Control", Wesley Longman, 1998.


ISSN 1737-9334

# Output waveforms of Blumlein-line Nitrogen Laser Circuit Based on the Distributed Parameter Model: Theoretical and Experimental Results

Mohamed O. Twati

*Electrical and Electronic Engineering Department, University of Tripoli*
*Tripoli, Libya*
m.twati@uot.edu.ly

***Abstract*— Optical power calculation of the Blumlein-line nitrogen laser circuit based on the distributed parameter model and the decoupling approach of the laser rate equation from the electrical circuit equations is developed and investigated. The dependence of both the electrical and optical power waveforms on the spark gap inductance is performed and discussed. The saturated laser power approach is assumed in calculating the optical power. The measured laser output waveform obtained is fairly equivalent to the calculated laser power waveform based the distributed model. The theoretical work suggested here could be used to estimate some of the system parameters and help in optimization of the circuit for better system performance.**

***Keywords*— Blumlein-line; Fast discharge laser; Nitrogen laser; Power calculations; optical waveform.**

## I. INTRODUCTION

Nitrogen lasers are important because they can provide high-power short-duration pulses of ultraviolet radiation (λ = 337.1 nm). These lasers are widely used in spectroscopy and fluorescence studies, pumping of dye lasers and other research and industrial applications [1]–[6].

The performance of the nitrogen laser is basically determined by the type of electrical system used to create the discharge in the gas. Many excitation schemes were employed for pumping nitrogen lasers, however, the Blumlein transverse excitation method has become very popular, because of its low cost and ease of construction [2]–[8].

The Blumlein-line pulse forming network consists of two parallel plate transmission lines (or coaxial cables) acting as energy storage capacitors, located at both sides of the cavity charged to high voltage Vo. When one side is short-circuited, for instance using a spark gap, a transient voltage occurs across the laser cavity creating a gas discharge between the electrodes. The spark gap and the laser gap are usually represented by resistances and inductances.

Depending on the relevant time constants of the spark gap and laser gap along with the wave propagation time on the transmission line, two concepts can be used in the analysis of the Blumlein-line circuit, the lumped parameter model (LPM) and the distributed parameter model (DPM). From a theoretical point of view, the LPM offers the advantage of a much simpler analysis over the DPM., however, it has the disadvantage of being valid only when the relevant time constants of the spark and laser gap are much larger than the wave propagation time on the transmission line [9].

In spite of extensive studies and investigations that have been made so far for understanding the performance of $N_2$ lasers based Blumlein-line pulse forming network, still extra research work has to be made that include the selection of more accurate circuit models for simulating the laser system and also the effects of the electrical parameters on the overall laser performance.

The $N_2$ Laser is a highly integrated electro-optical system and the prediction of the behaviour of $N_2$ laser requires a complicated theory that must include the electric circuit parameters, the gas kinetic parameters and detailed mechanism of energy transfer of the three laser levels of the molecular nitrogen. A significant simplification of the calculation has been brought about by Fitzsimmons [10]. Instead of estimating the electron temperature by solving the energy balance equation as a part of the coupled system, they used, in a decoupled procedure, another alternative approach to predict the electron temperature. Within this framework of the assumptions, the


ISSN 1737-9334

electron temperature is determined in terms of the instantaneous value of ratio of the electric field between the laser channel electrodes divided by the pressure inside the laser channel. Hence this procedure makes it possible to handle the laser rate equations in separate way. This can be done after getting the required time development of the electric field from the solution of the electric circuit equations. In the previous work, the general laser power assumption was used in calculating the output optical power, and the influence of the laser gap inductance (laser channel inductance) on the laser output power waveforms were investigated and studied [11].

This paper reports the theoretical analysis, power calculations and the effect of the spark gap inductance on the output waveforms of the Blumlein-line $N_2$ laser circuit. Here, the simplified saturated laser power approach was used in calculating the output optical power. A homemade Blumlein-line circuit was constructed and built with a free running spark gap. The measured current waveform was obtained by using a homemade current probe.

## II. Transmission Line Equations Of The Blumlein Line And The Boundary Conditions

A mathematical configuration of the Blumlein circuit is shown in Fig.1. The Blumlein line is divided into two sections, the right hand section and the left hand section with different zero coordinates. The applicable Transmission line equations for the voltage V and current I on a section of the transmission line of dx at any time t are given by [9],

$$\partial V_i(x_i,t)/\partial x = -\bar{L}\,\partial I_i(x_i,t)/\partial t \quad (1)$$

$$\partial I_i(x_i,t)/\delta x = -\bar{C}\,\partial V_i(x_i,t)/\partial t \quad (2)$$

i = left and right, $0_i \le x_i \le l_i$, $\bar{L}$ and $\bar{C}$ are the distributed inductance and capacitance per unit length respectively, and l is the total length of line section, $Z_o$ ( $Z_o = \sqrt{\bar{L}/\bar{C}}$ ) is the characteristic impedance of the line. The initial conditions are:

$$V_i(x_i,0) = Vo \quad (3)$$

$$I_i(x_i,0) = 0 \quad (4)$$

The boundary condition at the end of the spark-gap is:

$$V_R(0_R,t) = -R_S[I_R(0_R,t) + \frac{L_S}{R_S}\partial I_R(0_R,t)/\partial t\,] \quad (5)$$

The boundary conditions at the end of the channel are:

$$V_R(l_R,t) - V_L(0_L,t) = L_g\partial I_L(0_L,t)/\partial t + R_g I_L(0_L,t) \quad (6)$$

$$I_R(l_R,t) = I_L(0_L,t) \quad (7)$$

The boundary condition at the open end is:

$$I_L(l_L,t) = 0 \quad (8)$$

where ($L_S$ and $R_S$) and ($L_g$ and $R_g$) stand for inductances and resistors of the spark gap and laser gap, respectively. The laser gap impedance is not linear and must be treated as voltage dependent: as an open circuit before laser gap breakdown and represented by a combination of ($L_g$ and $R_g$) after laser gap breakdown. $I_R$ is the current passed in the spark gap inductance and. $I_L$ is the current passed in the channel inductance after laser gap breakdown. This nonlinear behavior of the channel impedance, makes it necessary, in the time development of solution of the partial differential equation (6) to distinguish between two time intervals: the first one is before laser gap breakdown, during which the state of only the right-hand section is subject to the dynamical changes, whereas the left-hand section remains in its initial state, and the second time interval is after laser gap breakdown, in which the states of both sides are time varying. The subscripts L and R in the current, voltage and lengths denoting for the left hand and the right hand sides of the Blumlein-line.

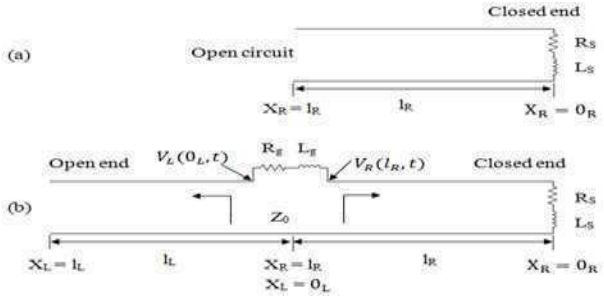


Fig. 1. Representation of Blumlein N2 Laser circuit. (a). Before breakdown (b). After breakdown.

## III. System Of Equations For Optical Power Computation

Calculation of the optical power is performed under the saturation approximation assumption. This method assumed that the laser transition is saturated; i.e., the laser power, $P_o$ is strong enough to equalize the densities $N_C$ and $N_B$ in the C and B states energy laser levels of the molecular nitrogen respectively. We can then let $N_C - N_B \ll N_C$and set $N_C = N_B = N$ and then calculate $P_o$. These equations can be easily derived in term of the instantaneous


ISSN 1737-9334

electric field E and the pressure P inside the laser tube and written as:

$$\frac{dN}{dt}+\frac{N}{2\tau_B}=\frac{1}{2}\left[n_e N_o(\sigma_{OB}+\sigma_{OC})\left(\frac{0.88}{m\pi}\right)^{\frac{1}{2}}\left(\frac{E}{P}\right)^{\frac{2}{5}}\right] \quad (9)$$

$$P_o=\frac{1}{2}\left[n_e N_o(\sigma_{OC}-\sigma_{OB})\left(\frac{0.88}{m\pi}\right)^{\frac{1}{2}}\left(\frac{E}{P}\right)^{\frac{2}{5}}-\frac{2-\left(\frac{\tau_C}{\tau_B}\right)}{\tau_C}N\right] \quad (10)$$

$E$ is given by $[V_R(l_R,t)-V_L(0_L,t)]/d$. $d$ is the electrodes separation. $n_e$ is the electron density, $N_o$ ($\cong 3.2\times10^{16}P$) is the ground-state density which is assumed constant, $\tau_C$ is the radiative lifetime of the C-state (40ns) and $\tau_B$ is the radiative lifetime of the B-state (10$\mu$s). $\sigma_{OC}$ and $\sigma_{OB}$ are the electron impact cross sections of the C and B states ( $11.1\times10^{-18}cm^2$ *and* $9.2\times10^{-18}cm^2$ respectively). $m$ is the electron mass ($9.2\times10^{-28}$g). The above equations can be solved after deriving the electron density equation in terms of (E/P) to obtain $n_e$ inside the laser channel as a function of time. The electron density equation can also be derived and written as:

$$\frac{dn_e}{dt}=4.06(10^{-3})\left(\frac{E}{P}\right)^{4.7}P.n_e \quad (11)$$

## IV. Selection Of The Schemes And Computational Procedure

To obtain voltage and current solutions across the laser channel, we applied numerical schemes that based on the finite difference method, the forward, backward and central difference schemes along-with the" Lax-wendroff scheme" to the partial differential equations of the Blumlein-line and the boundary conditions. The method and the schemes used were presented in detail in the previous work [9]. Standard numerical techniques were used in solving the excitation rate equation and the electron density equation.

## V. Computational Results And Discussions

Following the application of the numerical schemes mentioned in (III) and simulation of the laser system, useful results were obtained. Fig. 2 shows the waveform of the instantaneous (E/P) a cross the laser channel and influence of the spark-gap inductance on ∂(E/P)/∂t, whereas the electrical current, electrical power and optical power waveforms along-with the effect of the spark-gap inductance on them are shown in Figs. 3-5.

The values of circuit elements used in the simulation are: $\bar{C}$ =128.88nF/m, $\bar{L}$= 0.288nH/m, $R_g$= 0.1Ω, $R_S$ = 0.0366Ω, $L_g$= 0.2nH, $l_L = 55cm$ (open end side) and $l_R = 50cm$ (spark gap side). The chosen values of $L_s$ for the simulation are 14nH and 28nH. The electrodes separation used in the simulation is 1.5cm whereas their lengths and widths are 30cm and 0.5cm respectively. The pressure inside the laser tube is 67Torr. The electrical power is obtained from the expression ($I^2R_g$) whereas the optical power is obtained from (10). It is clear from Figs. 2-5 that the laser gap breakdown is a highly dependent on the spark gap inductance. Therefore, in order to obtain a smaller breakdown time in the gas, a smaller value of the spark-gap inductance must be maintained.

In the waveform figures, the time is normalized by $T_{normalized}=\frac{time}{l_R\sqrt{LC}}$.

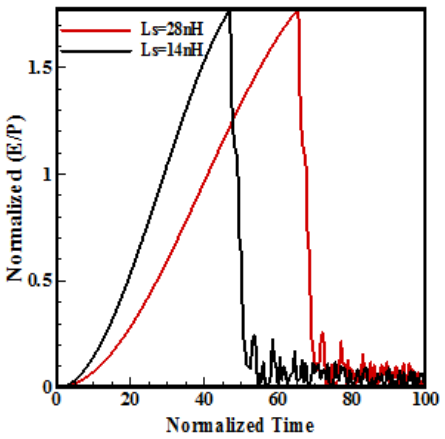


Fig. 2. Instantaneous E/P waveform and the influence of the spark-gap inductance on ∂(E/P)/∂t a cross the laser channel.

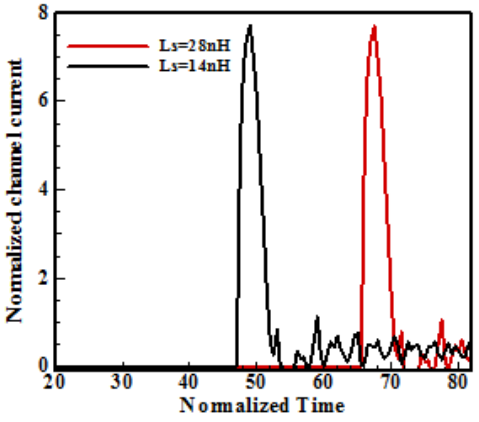


Fig. 3. Influence of the spark-gap inductance on the laser channel current




ISSN 1737-9334

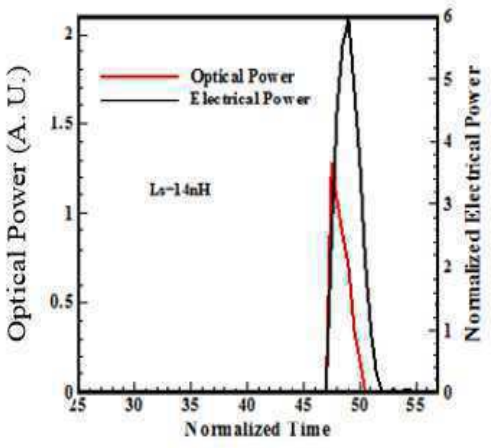


Fig. 4. Influence of the spark-gap inductance on the electrical and optical power waveforms of the laser channel at $Ls$ =14nH.

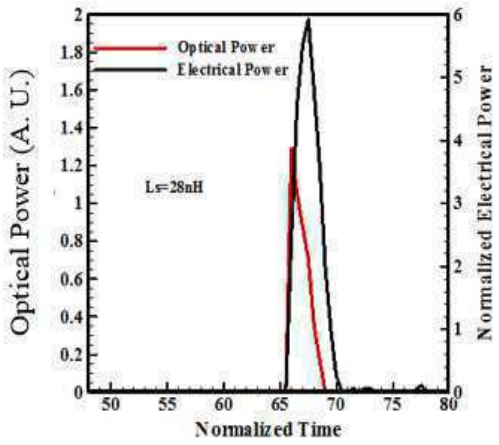


Fig. 5. Influence of the spark-gap inductance on the electrical and optical power waveforms of the laser channel at $Ls$=28nH.

(a)

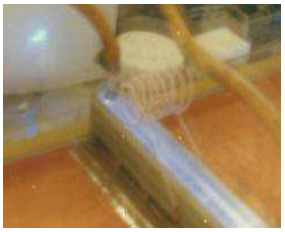

(b)

Fig. 6. (a) Physical construction of the Blumlein N2 laser (b). The laser tube along-with the output of a nitrogen laser is in the ultraviolet range

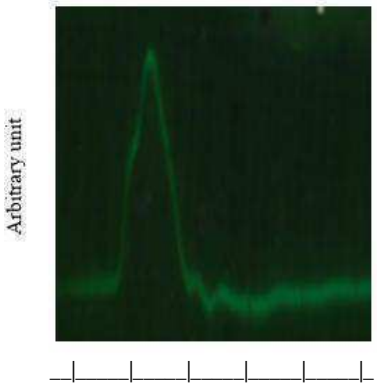


Fig. 7. Oscilloscope trace of photodiode signal. Time base is 10ns/div.

## VI. Temporal Measurement Of The Laser Output Waveform

Fig. 6(a) shows the physical construction of the Blumlein $N_2$ laser system showing the locations of the spark gap and laser tube relative to the copper parallel plates that comprise the energy storage capacitors and Blumlein transmission line.

The parallel plate transmission line are formed from a double sided copper coated printed board 104 x 34 cm, and of 0.1cm thick with relative permittivity of 5.03. Both surfaces of the board were etched away in 2cm wide border to prevent conduction between the plates. The aluminium laser channel electrodes are 30cm in length with a thickness of 0.1cm where they are separated by 1.2cm. The spark gap used was a free running two electrodes spark gap. The spark gap electrodes formed from two aluminium half spheres of 2cm in diameter. The spark gap is designed such that the distance between the electrodes can be controlled. Fig. 6(b) shows the laser tube along-with the output of a nitrogen laser is in the ultraviolet range, at a wavelength of 337.1nm, thus invisible. However, its beam can be observed as a light blue spot with a




ISSN 1737-9334

fluorescent material such a pieces of paper or cardboard placed at distance along the laser channel. The pulse shape of the laser output was detected by using OR-7184 photo diode together with a Teck.475 Oscilloscope. The pulse shape is shown in Fig7. The measured pulse width (FWHM) is 11nsec and it is supposed to be around 6nsec (typical values of such lasers), because we used a photodiode with limited rise time of 6.8nsec. It is clear that the measured and simulated optical power waveforms almost have the same form. This could help in estimating the laser channel parameters.

## VII. Conclusions

A full distributed parameter model of the Blumlein-line $N_2$ laser with the decoupling approach of the laser rate equations from the electrical circuit equations has been developed and investigated. The effect of the spark-gap inductance on the instantaneous (E/P), laser channel current, electrical power and optical power waveforms were carried out. The investigation results show that the time of ignition (the gas breakdown) depends on the spark gap inductance, i.e., the less the value of the spark-gap inductance the faster gas breakdown will occur, which is also very clear in the shift occurred in the current waveforms. With the use of this modified analysis, the $N_2$laser system may easily be optimized over a wide range of parametric variations that could assist in optimization efforts. This is because the distributed parameter model used here were proved to be more accurate than the other lumped parameter models in the previous work, which will provide a better predictions for the behavior of $N_2$ laser that are needed for better system performance and optimization. The analysis presented here is quite general and could be applied to many other gas laser systems. The experimental measurement of the laser output waveform presented here along-with the theoretical simulations might help in estimating the laser channel parameters that could help, in system optimization and design verification. Further experimental and theoretical work will be pursued for extra experimental verifications.

## References

[1] S. Panahibakhsh, S. Sarikhani, and A. Hariri, "Experimental and theoretical investigations for describing pressure dependence of amplified spontaneous emission output energy, small signal gain and electrical conductivity in nitrogen lasers," *Optik*, vol. 168, pp. 541–552, Sep. 2018.

[2] S. B. Han and S. H. Park, "Evaluation of Discharge Characteristics Followed by the Development of Blumlein pulsed power source," *Journal of the Korean Institute of Illuminating and Electrical Installation Engineers,* vol. 24, issue 10, pp. 99-105, 2010.

[3] Z. Liu, K. Yan, G. J. J. Winands, E. J. M. Van Heesch, and A. J. M. Pemen, "Novel multiple-switch Blumlein generator," *Rev. Sci. Instrum.* vol. 77, pp. 033502-1- 033502-5, Jan. 2006.

[4] Mohamed O. Twati, "A Novel Distributed Parameter Model of a Blumlein-line Laser Circuit Including the Effect of Time Varying Spark-Gap Inductance and Resistance," in *UKSim 16th Int. Conf. on Computer Modelling and Simulation*, vol. 76, 2014, pp. 586-589.

[5] A. Hariri, M. Jaberi, and S. Ghoreyshi, "Nitrogen lasers: Optical devices of variable gain coefficient," *Opt. Commun*., vol. 281, pp. 3841-3852, Mar. 2008.

[6] E. T. Gerry, "Pulsed-molecular-nitrogen laser theory," *Appl. Phys. Lett.,* vol. 7, pp. 6-8, Jul. 1965.

[7] Adolf J. Schawb, "Compact High-Power N2 laser: Circuit Theory and Design," *IEEE, J. Quantum Electronics*, vol. QE-12, pp. 183-188, Mar. 1976.

[8] Young-Su Roh† and Yun-Sik Jin, "Analysis of Output Pulse of High Voltage and Nanosecond Blumlein Pulse Generator," *J Electr Eng Tec-chnol.,* vol. 8, pp. 150-155, Jan. 2013.

[9] Mohamed O. Twati, and A. Ben Otman, "Distributed parameter analysis of a Blumlein-Line N2 Laser," *Opt. Commun*., vol. 99, pp. 405-412, Jun. 1993.

[10] Fitzsimmons W A, Anderson L W, Riedhauser C E and Vrtilek J M, "Experimental and Theoretical Investigation of the Nitrogen Laser," *IEEE J. Quantum Electron.*, vol. QE-12, pp. 624-633, Oct. 1976.

[11] Mohamed O. Twati, and A. Ben Otman, "A Modified Approach for the Blumlein-line Laser Power Calculations: Electrical and Optical Power Waveforms," *Journal of Wireless Communications*, vol. 2, pp.1-6, Feb. 2017.


ISSN 1737-9334

# *Investigation of EMF Radiation From GSM Base Stations and Mobile Antenna Towers in Different Locations–Libya*

Amer R. Zerek[1], Saleh Alahimer[2] and Mohamed M. M. Elfituri[3]

[1]Zawia University, Faculty of Engineering/ EE Department,, Zawia, – Libya,
E-mail anas_94az@yahoo.co.uk
[2] College of Electronic Technology, Communication Engineering Department, Tripoli, Libya
E-mail salahahimer@yahoo.com
[3] Authority of Natural Science Research and Technology. Tripoli, Libya
E mail *melfituri@yahoo.com*

***Abstract*— Cellular and wireless technology have high growing and demand worldwide. Some countries regulate the exposure and installation of radio frequency RF transmission stations. The purpose of this paper to assess the exposure of RF radiation from a selected cellular tower and mobile base stations antennas. Technology develops continuously, so the characteristics of radiation from electromagnetic field EMF sources expect to change in the power level and frequency of operation, which indicate of change of Human exposed level. This undertakes EMF surveys to investigate the levels of the power density of the global system for mobile communication GSM within some school buildings and compare the results with international standards for human exposure compliance.**

***Keywords***- *BTS, EMF Waves,* GSM*, Mobile Phones, Radiation.*

## I. INTRODUCTION

Biological effect of EMF radiation depends on both the power level and frequency [1]. As the RF energy is directly proportional to the frequency, the shorter wavelengths of waves the more energy produces, that why level exposure varies depending frequency.

People are exposed every day to RF Radiation from both natural and man-made EMF sources. Exposure to RF radiation and its potential biological effects is becoming the subject of concern. The EMF levels continue to increase as technology growth. Libya has now fast growth in the telecommunication industry with no clear guidelines. Most of the providers are more concern about profits and deliver their service by increasing the coverage areas regardless of RF radiation concern. Accordingly, it becomes necessary to manage and monitor the levels of transmitted energy by such sources.

This study discusses measurements and survey of RF radiation that produced by GSM system in some locations in the city of Tripoli.

## II. BIOLOGICAL EFFECTS

The biological effects of RF radiation can be classified as *thermal* and *non-thermal* Effects. Thermal impact are generally associated with the heat produced by EMF sources in a specific area. The thermal effect has sufficient energy to make an increase in the temperature of the human body (e.g. exceeding 1 °C ) in a level above 4w/kg "watts per kilogram". Non-thermal effects are associated with the amount of energy absorbed by a biological system that may cause changes in the system properties. Many studies and researches show that the maximum increase in temperature of the body exposed to GSM with 0.25 Watt power level antenna at 900 MHz and 1800 MHz were less than 0.1°.

## III. INTERNATIONAL STANDARDS

Various international guidelines and recommendations are implemented for protecting people from RF exposure. The safety limit is not an exact line between safe and risk; it provides a means of protection. The expected effect occur at levels of exposure results in significant heating of part or whole body.

The International Commission on Non-Ionizing Radiation Protection ICNIRP develops international guidelines and scientific advice on limiting exposure to non- ionizing radiation. ICNIRP limits are used in this study as a reference for comparison of the power measurements. Table I shows ICNIRP limits for potential exposure to EMF from high-frequency sources such as mobile phone System.


ISSN 1737-9334

TABLE I
ICNIRP REFERENCE LEVELS FOR GENERAL PUBLIC EXPOSURE FOR FREQUENCY UP TO 300 GHZ INCLUDING GSM BAND

| Frequency Range MHz | Equivalent Plane Wave Density ($W/m^{-2}$) |
|---|---|
| 400-2000 | *f*/200 |
| 2000-300000 | 50 |

Notes: *f* is frequency *of* the EMF signal

The equivalent power density is considered the maximum allowable power level that ICNIRP recommends not to be exceeded.

Table II shows Specific absorption rate SAR limitations given by ICNIRP. The limit values where established based on the increase of temperature by about 0.1 °C and the limit is depending on frequency of the RF source.

TABLE II
SAR LIMITS RECOMMENDED BY ICNIRP

| Exposure Characteristics | Frequency Range | Whole-Body Average SAR (W/Kg) |
|---|---|---|
| 400-2000 | *f*/200 | 0.4 |
| 2000-300000 | 50 | 0.08 |

Note: All SAR limits are averaged over six minutes period.

Note that allowable maximum estimated SAR value in relation to power density is about 45 $W/m^2$ for GSM-1800. According to ICNIRP and most of the reliable researches "it is very unlikely that a person could be exposed to RF levels from mobile stations in excess of standards limits. The purpose of this paper to evaluate RF radiation from GSM system against the international standard.

## IV. GLOBAL SYSTEM FOR MOBILE COMMUNICATION GSM OVERVIWE

Cellular systems usually use a number of low power transmitters to create mobile cells site, these cells sized in the area according to the power level, which based on the number of mobile subscribers and area to be covered. The most common mobile station MS systems use transmission power level range of about 5-20 W, while base transceiver station BTS systems have a power range of 20-320 W.

The most commonly used GSM systems operate in frequency ranges of 900 MHz and 1800 MHz bands. GSM-1800 provide more bandwidth and fewer power requirements than GSM-900 systems. Normally GSM antenna has gain about 15 dBi led to an increase in the total radiated power. The GSM 900 and GSM 1800 specification are shown in Table III [4].

TABLE III
GSM POWER AND FREQUENCY SPECIFICATIONS [4]

| System | GSM 900 | GSM 1800 |
|---|---|---|
| Downlink Frequency | 935-960 MHz | 1710-1785 MHz |
| Uplink Frequency | 890-915 MHz | 1805-1880 MHz |
| Modulation | GMSK | GMSK |
| Typical Mobile Transmit Power | 2 W | 1 W |
| Maximum Base Station Transmit Power | 320 W | 20 W |
| Maximum Distance | 35 Km | 8 km |

Note: GMSK IS Gaussian Minimum Shift Keying

GSM phones can emit more than twenty times more radiation compared to Code division multiplexing access CDMA phone systems and accordingly the use of CDMA of a better choice for reducing the average RF radiation [5].

## V. RFI AND MIDICAL DEVICES

Using cellular communication near medical devices can increase the risks of electromagnetic interference EMI on the devices, which can become a potential problem. Many studies report that medical devices, such as pacemakers and other medical devices have failed to operate properly because of interference from other RF sources. The powered wheelchair is an example of sensitive equipment's to RF interfering. One study shows radiofrequency interference RFI from two-way police radios 'walkie talkies' or even mobile phones causing the electronic wheelchair to drive itself into traffic put the patient at high risk [6]. Another example of RFI happened in Patient Monitoring System PMS: In 1987, PMS failed to produce sound alarms notifications because of RF interference, patients are reported to have died because of late response [7].
IEEE Committee on Man Radiation COMAR recommends that medical devices be properly shielded and increasing electromagnetic capabilities in EMF environments.

## VI. EMF RADIATION TYPES

EMF radiation is classified according to its energy into two types: Ionizing and non-ionizing, Ionizing radiation has sufficient energy to remove electrons from atoms resulting in tissue damage, includes X-rays and gamma rays where frequency above $10^{15}$ HZ. Non-ionizing radiation does not have sufficient energy to cause ionization. It includes radio waves, microwaves, infrared, ultraviolet, and visible radiation.

## VII. EXPERIMENTAL PART

EMCO 3115 Ridged Waveguide Horn Antenna and spectrum analyzer were used to collect measurements of power emitted by RF sources. The EMCO 3115 Antenna is a linearly polarized broadband antenna with excellent characteristics within the frequency range of 1 GHz to 18 GHz. It is designed especially for RF measurements and in evaluating high-frequency RF sources. The 3115 has features




ISSN 1737-9334

low VSWR, high power handling 500 W and broadband operation spectrum. This antenna used with the spectrum analyzer for site survey and measurements. Frequency scanned through the BST electromagnetic frequency range 800-1800 MHZ at a different distance from BTS. The double-ridged waveguide horn antenna showed in figure 1 which typically used by the universal mobile telecommunications System and has antenna gain shown in figure 1 with the spectrum analyzer.

Figure 1. Double- ridged waveguide horn antenna with spectrum analyzer

The antennae are connected to the spectrum analyzer through a 10-meter length RG 213 cable which has attenuation is evaluated from 0.5to 1 dB according to operating frequency. The spectrum analyzer allows displaying a graphic of the measurement results. The frequency range covered during measurements was from 800 MHz to 2.2 GHz. The amplitude displayed by the analyzer in *Root Mean Square* RMS value.

### A. *Calculation of Power Density:*

The spectrum analyzer measure amplitude in millivolts (mV). The following equation used to convert the received voltages into electric field strengths.

$$E = VrxAf\,10^{L/20} \tag{1}$$

Where E is the received electrical field, $V_{rx}$ is the voltage received by the antenna, *Af* is the antenna factor which is defined as the ratio of the electric field at the antenna to the voltage generated by the antenna, and L is the cable loss in dB.

$$Af = \frac{\text{field strength at antenna} \quad (\text{V/m})}{\text{Voltage produced by antenna} \quad (\text{V})} \tag{2}$$

Figure 2 shows the EMCO 3115 the antenna factor over the operating frequency range, while the antenna gain is in figure 3.

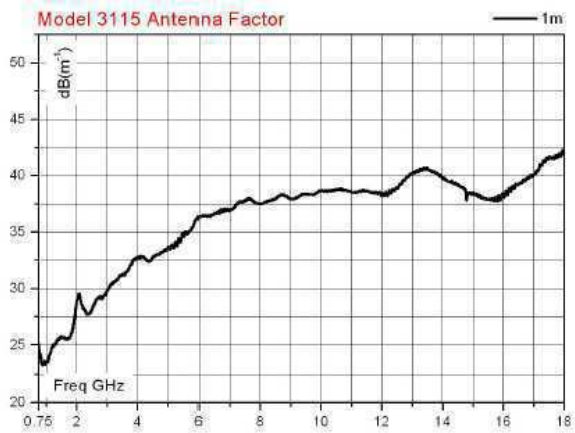


Figure 2. Model 3115 Typical Antenna Factor


Figure 3. Model 3115 Typical Antenna Gain

For the power density, it is simply calculated using the following equation

$$Pd = \frac{E^2}{\eta} \tag{3}$$

Where $\eta$ is the intrinsic impedance of free space equal to about 377 ohms and P*d* is the received power density.
Many factors to be considered while measuring the power emitted from the antenna including time average, polarization , and frequency of the transmitted power. This study aims to measure the maximum power at a different distance from BTS antenna.

### B. *Exposure Assessment:*

For exposure to radio waves, *exposure quotient* needs to be calculated it is the ration of power density measured $Pd_{ms}$ to the power density of standard limit $P_{dst.}$

$$\text{Exposure quotient} = \frac{Pdms}{Pdst} \tag{4}$$




ISSN 1737-9334

Where $P_{dms}$ is measured power density and $P_{dst}$ is the maximum allowable power density defined by the international standard.
If exposure quotient is less than unity, compliance with ICNIRP guidelines is demonstrated and power level to be considered acceptable.

### C. Site Selection

In this study, we choose the Site of measurement based on the following conditions.

- Direct and long-term exposure.
- Antenna mounted on top of School, hospitals, and buildings.
- Densely populated areas near to BTS.

We selected the school building because of some studies consider children absorb energy differently than adults because of differences in their anatomies and tissue composition, and because their bodies are still developing, children may be more susceptible to EMF radiations [8].

### D. Devices Calibration and Measurement Accuracy

The accuracy constitutes the biggest problem in EMF measurements. Accordingly, the calibration of equipment's is the most important part before any measurement procedure.
Power density measurements performed with an Advantest spectrum analyzer and calibrated with the directional antenna as a reference. EMCO 3115 Antenna shows great performance and accuracy and has been used because of it is superior specification over a wide frequency band.

### E. Sites Measurement

Sites location details: 1- Alfateh University.2- Elfernaj Secondary school, 3- Alittihad school for basics education 4- Tripoli clinic airport road: all sites located in Tripoli the capital city of Libya.
Note: In some locations, different sources of RF radiation observed including TV broadcast station and telecommunication towers, also some of the microwave transmitter which will be included in the receiving signal in the frequency range of 700 MHz to 2 GHz.
The power density measurements were conducted under daylight in real-life. The antenna was directed in various positions in order to receive maximum power densities. For interest (GSM900, GSM1800) frequency band measurements conducted for 6 min scanning time. The power density levels are given in $\mu W/m^2$ (microwatt per square meter). In addition, results were calculated in consideration of antenna factor and gain as well as cable and connector losses.
Final measurements were compared with other international measurements of same RF sources shows that all measurements were satisfied the comparison.

In these selected sites a large number of students are living and stays for a long time near to BTS mainly GSM antennas and it is expected to have long time exposure to EMF Radiated from Antenna cellular towers.
Distance from the RF source was taken for selected locations at different antenna heights and orientations from RF source.

### F. Measurement Results

The results of power measurements were processed and maximum value in each frequency range has been selected to compare against the international standard limitations.
The results translated to charts of power against frequency which is showed in figure 4 indicates to the final result in comparing the standard power limit.
The power density levels are given in μW/m², values are displayed in table III with respect to the *line of sight* in the proximity of the antenna (<100 m).

The measured power density ranged between 400 μW/m² to 1200 μW/m² "maximum obtained value at each measured frequency".
The highest power density levels were found is about 12900 μW/m² were recorded very close to the antenna on the upper floors of the building. Although these maximum recorded value considered the special case where not common to have people at this location.

The maximum power level in the area of interest was found to be ranged of 2500 μW/m² to 5000 μW/m² which is more considered for concern as people exposed to RFR for a long time daily.
The power density was noticed to be increased with height from ground level in the main beam of antenna radiation and reached its maximum value approximately 1300 μW/m² at the window ( about 9 m height) of the building with the line of sight from the antenna.
This measurement confirms that the exposure level is not only depending on the distance from RF source but it should depend on the location of the exposed person compared with antenna properties including the main beam of the radiation, and the characterizations of EMF waves like frequency and polarization. Some samples of power density are listed in Table IV.

TABLE IV
SAMPLES OF MAXIMUM MEASUREMENT

| Frequency *f* (MHz) | Measured Power Density μW/m² | ICNIRP Power Density Level ( *f*/200) μW/m² | Exposure Quotient |
|---|---|---|---|
| 850 | 1550 | 4250000 | 3.65E-09 |
| 900 | 8450 | 4500000 | 1.88E-08 |
| 910 | 12950 | 4550000 | 3.41E-10 |
| 920 | 8400 | 4600000 | 1.84E-09 |
| 930 | 8500 | 4650000 | 2.78E-09 |
| 1750 | 1350 | 8750000 | 9.71E-11 |
| 1800 | 9680 | 9000000 | 1.44E-10 |
| 1820 | 7680 | 9100000 | 1.48E-10 |
| 1830 | 2410 | 9150000 | 5.11E-10 |

*Note: The Exposure quotient values shows that the measured power level is found to be Orders of magnitude lower compared with the maximum exposure levels established by ICNIRP.*



ISSN 1737-9334

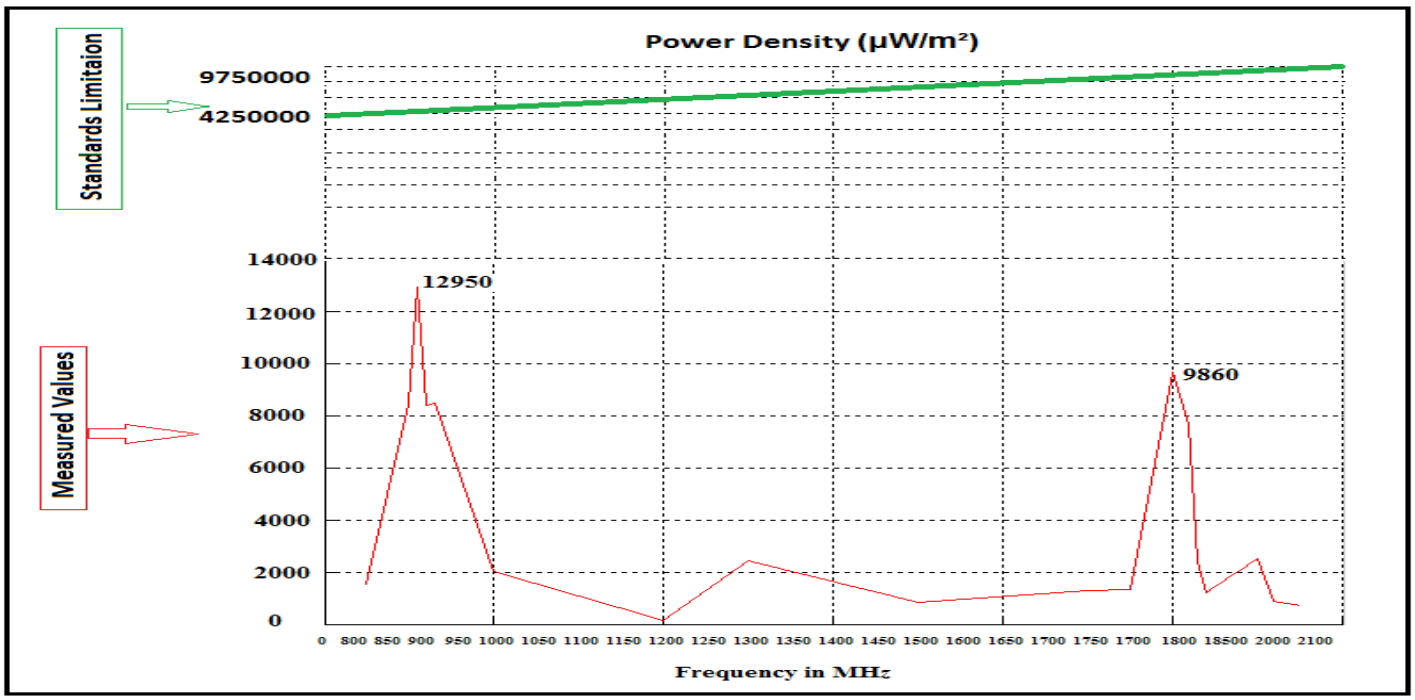


Figure 4. Measures results of all sites VS standard level

## VIII. CONCLUSION

The highest RF power levels in all locations were found the line of sight and according to antenna setup where main radiation beam concentrated. The power reduced as the meet of obstacles indoor measurements. Figure 4 Shows the final measurements compared to the allowable standard level.
The measured RF power density was much below the international standard recommended limit values. Accordingly, the cellular phone tower and BTS station under this investigation is to be considered safe in compliance with protection standards.

The results were compared with ICNIRP standards and show that the value of power density at general people exposure areas is about a thousand times smaller than the ICNIRP guidelines and hence the average values of the SAR estimated to be much lower than the Standards limitation.

## REFERENCES

[1] Electromagnetic fields and public health: mobile phones". WHO. Retrieved 19 January2018.

[2] Ben Greenebaum ،Frank S. Barnes "Bioengineering and Biophysical Aspects of Electromagnetic Fields" , ISBN-13: 978-0849395390, 3rd edition (October 20, 2006).

[3] B. Jon Klauenberg ،Martino Grandolfo ،David N. Erwin "Radiofrequency Radiation Standards: Biological Effects, Dosimetry, Epidemiology, and Public Health Policy". ISBN: 9780306449192 1999 5th Edition.

[4] Dr. S. A. Mawjoud, " Evaluation of Power Budget and Cell Coverage Range in Cellular GSM System, Almosol University of Baagdad, Iraq Oct. 2006.

[5] Cell Phone Radiation and Health Recommendations, Joel M. Moskowitz, Ph.D., Director Center for Family and Community Health, School of Public Health University of California, Berkeley, May 11, 2011.

[6] Healthcare engineering , International Conference on Healthcare Engineering - Latest Developments and Applications (November 2003 : IMechE Headquarters, London, UK).

[7] Jeffrey L Silberberg, 'Performance degradation of electronic medical devices due to electromagnetic interference', Compliance Engineering vol. 10 p. Oct 1993.

[8] Comments about the NTP Cell Phone Radiation Studies Joel M. Moskowitz, Ph.D. School of Public Health University of California, Berkeley March 12, 2018.

[9] Lapinsky, Stephen E, and Anthony C Easty. "Electromagnetic interference in critical care." Journal of critical care 21.3 (2006): 267-270.may 2006.

[10] Double-Ridged Waveguide Horn antenna, model 3115, EMCO manufacturers manual at :

http://www.ets-lindgren.com/products/antennas/double-ridged-guide/4002/400203


ISSN 1737-9334

# *The Role of Fixed &Timed Teaching Pulses in Enhancing Learners' Creative Productivity by Computer Assisted Language Learning*

Shaiban Harith Ahmed

English Department

Tripoli University-College of Languages

Tripoli-Libya

Sh2000_harith@yahoo.com

***Abstract I have created a new teaching technique depending on what I have called "time-fixed teaching pulses". This means using no more than 1 to 2 minutes to explain or present any new piece of knowledge or information. It is a ground theory research and data was collected and analyzed through three stages. This proposal covers the second stage of this methodology which is 1-2 minutes for each teaching pulse covering the time frame of language courses which I set here for 60 hours for CALL classes.***

***The classes vary from general English courses up to academic subject specialists ones. In this new methodology, I have taught them using fixed time teaching pulses during the whole process. This continuous teaching and timing consistency has resulted, in most of classes, in what I have noticed a whole and an enormous fast change in the students' productivity and receptivity of their targeted language goals and the most significant noticeable change was creative thinking in addition to problem solving. All the sessions were governed by specific and consistent timed teaching "pulses".***

***This new approach has proved its significance in speeding up the ability of acquiring and learning the language skills and exams requirements. Although some of these changes happened as a result of many known pedagogical and methodological techniques, it is still unknown what neurological factors that had led to such vast changes in a very short and fixed time. There is also this magnificent change that always happens to my students' productivity and creativity after exactly after 36 hours after starting their sixty hour courses.***

***Keywords— Ground theory approach, teaching pulses, fixed time teaching pulses, computer assisted language learning (CALL), neurology, neurolinguistcs, Self-Access Learning(SALL).***

## I. Introduction

Teaching theories and approaches have been under intense practice and investigation in the last 100 years. Scientists, scholars and teachers shared this magnificent quest for learning teaching methodologies and developing them since the 19th century till now. During these times methodologies started to emerge and develop rapidly and changed the way people learn and live as well. This has affected almost all the glob; according to Richards (1994) almost sixty percent of the world is multilingual. Of course this trend has increased rapidly due to the huge technological changes in social media and socio political variations as well. Computer Assisted Language Learning (CALL) is developing rapidly due to the fast changes and enhances in the computer technologies and social media. These projects were born out of the audio-lingual, behaviorist, and structuralists methods of language learning, which are associated with the behaviorist theories of B.F. Skinner (1957). The introduction of the microcomputer not only influenced the general field of educational technology, but prompted a "flourishing" in CALL research. Through this flood of research, CALL developed into a unique discipline within the academic world (Levy 1997). Teaching methods vary in their procedures and success but all have participated not only in education and learning but also to open the horizon of research and teaching development. So from grammar translation to self-access and computer assisted learning the route is long and very challenging. There are many procedures to be fulfilled during the learning processes, some have succeeded and some have not but they all shared the same good will of exploring language

acquisition and learning pedagogies. This leads to very important questions which are:

1- What are the outcomes of this new methodology if it is applied more thoroughly in e-learning like Computer assisted Language Learning(CALL) ,Self Access Learning(SALL) or social media learning?

2 -Is possible to shorten the time needed for students to finish their entire studies?

3-What are the neurological changes that have led to these enormous changes?

4- What is the hormone that led to such changes in the students' brains within this fixed period of time?

## II. Hypothesis

Short timed-fixed pulsatory teaching presents some serious questions concerning the innate mechanisms that are used and governed by human brains to acquire or learn languages and skills in such fast and fixed period of time. Also, it encourages exploring the future possibilities of developing such an approach and its possible impacts on other intelligence and cognitive learning and their applications in all other scientific learning methodologies and technologies. Finally, if the neural-elements responsible for these magnificent changes in the students' performance are uncovered, this would enormously change our insight and knowledge concerning learning concepts and methodologies of all sciences in the world no matter which language is used in teaching.

## III. Literature Review

Computer Assisted Language Learning (CALL) has three main phases where teaching methodologies and learning approaches developed and merged in the since 1960s till now.


ISSN 1737-9334

A. Structural (Behavioristic) CALL

This phase was considered in the 1950s and applied in the 1960s and 1970s. In that time, three main factors affected the use of CALL: (a) the use of programmed instruction based on behaviorism, (b) the improved complexity of data processing, and (c) the use of time sharing system for CALL purposes (Atkinson & Wilson, 1969). As the psychological basis of this phase declared, behaviorism theory, activities should be entailed "drill and practice". The computer was used as a transportation device to deliver learning materials and instructions to language learners. Taylor (1980) indicated that" The role of the computer was the same as tutor, and the delivered materials were repetitive language drills, vocabulary, and grammar and translation tests". The most famous tutorial system was PLATO which was based on a behavioristic learning pattern.

B. Communicative CALL

The second phase of the CALL was based on the communication approach where it came as a reaction to behavioral approach. It was the prominent approach between 1970s and 1980s. The advocators of this approach argued that "all CALL courseware and activities should build on intrinsic motivation and should foster interactivity of both learner-computer and learner-learner" (Han, 2009, p. 41). They also put the focus on using forms rather than on the forms themselves. Taylor and Perez (1989) defined the role of the computer as stimulus. This CALL approach was used for activities that involved communication such as conversations, written tasks, critical thinking, etc. Some activities such as spelling, grammar checks and text reconstruction programs were another model of computers in communicative phase which refer to the computer as a tool. They helped learners to learn and use the language easier. Moreover, Higgins and Johns (1984) declared that the courseware, which were based on text reconstruction and consisted of variations on cloze exercises, were communicative.

C. Integrative CALL

Moving from cognitive view of communicative language learning and teaching to socio-cognitive approach where tutors integrated different language skills like listening, speaking, reading and writing into language learning. This objective became possible by incorporating technology into language teaching and learning. The aim of the last phase of the CALL was to overcome the obstacles of language learning and teaching, and therefore to enhance the opportunities for integrating new technologies in the language classrooms. Different instructors and scholars tried to find more integrate manner of teaching instead of structure-based one, therefore, task-based approaches tried to integrate leaners in more authentic environments. From mid 1990s till now multimedia computers, smart phones and the internet were the base of the integrative CALL. Network-based technologies made the ultimate impact by which learners can share knowledge and communicate with each other globally.

## IV. Materials and Methods

This study is investigated empirically using the methodology of ground theory where continuous data collection and analysis go simultaneously throughout the period of the study. The subjects are the students of Tripoli University College of Languages-English Department 5$^{th}$ semester language learners who study English in order to pass exams. Sixty students have been chosen randomly out of a population of 160 candidates for this paper. A speaking pretest which is based on language skills (fluency, grammar, vocabulary and pronunciation) is taken to determine the candidates' level according to the Common European Framework of Reference for Languages (CEFR). The students' level is between B1 and B2 according to the Common European Framework of Reference for Languages. Then the experiment started by fully controlled timing processes where students used language- based interactive learning materials (Oxford University Press Interactive Learning) that have been installed on 20 computers. The experiment program included mainly 2 levels of interactive materials (Pre-intermediate & Intermediate). Also there were audio materials that cover daily life topics like work, TV, shopping, charity work and many other global topics. A desktop dictionary also used to facilitate learning new vocabulary. All skill-based learning procedures were governed by fixed timing (1-2 minutes) per each learning point. These learning points or units covered grammar, vocabulary, reading, listening and videos for15 classes (60 hours). The pulsatory teaching techniques included three highly controlled time phases:

1- The first stage included 40 -50 minutes that was dedicated for language tasks to check and develop the students' language skills, especially grammar and vocabulary. This was done by practicing some interactive self- corrected materials. This stage started usually from a bit lower language level of the candidates (The students' level was decided according to the results of the electronic evaluation tests included in the interactive learning materials). In this stage students were urged to finish 2 language- based tests (30 questions per test). Finishing the whole sets was non-mandatory but the tasks' time was highly controlled (40-50 minutes).

2- The second stage (40-50 minutes) was dedicated for 2 types of scripted videos. The first one described people's daily life activities and relationships and the second video was dedicated for a discussion point women' work or charity organizations and many other topics that cover people's daily life activities. Each video lasted for 8-10 minutes and the students watched them twice. The first watch (unscripted) was devoted for general understanding of the discourse used in the videos. The second time watch (scripted) was dedicated for better language comprehension and reading the scripts enabled the students to understand better and to enable them to link between spoken language and written scripts. This stage was extremely important because these videos enabled the learners to integrate the language skills they studied in the first part of the class together. This skills-integration helped them to develop language competence and consequently their language performance progressed as well.

3- The third stage (30-40 minutes) included oral discussions and topic development related questions that were written


ISSN 1737-9334

on the board. The students worked in pairs or groups of three to express their personal views concerning the topics on videos. This phase was a completely student- centered activity and the researcher just monitored the discussions and provided help when it was needed.

After finishing the 60 hour induction classes, a speaking posttest was given to the students to check their practical developments. As in the pre-test, all the tests were recorded to enable the researcher to measure precisely the changes in performance (Fluency, Vocabulary, Grammar and Pronunciation) and creative thinking that lead to such noticeable changes students' performances according to the European Framework of Reference for Languages (CEFR). In this post-test, each candidate was given a piece of paper with a question that he/ she should think about for about a minute then should speak about for 1-2 minutes. The questions covered a variety of topics that dealt with daily routine activities, hobbies and interests, free time activities, personal present and past experiences, schools and study, everyday problems, ecological issues, future plans and projections.

## V. Data collection

The following data has been obtained from the candidates who took the speaking course (Oral 1) in the English Department-College of Languages-Tripoli University. Table V.1 shows this data that covers 60 students who have been selected randomly out of the total groups of Oral 1 students (160 students).It can be seen that more than two thirds of the total candidates were females (70%) while males only presented 30% present of the total candidates' number.

| GENDER | FREQUENCY | PERCENT |
|---|---|---|
| Female | 42 | 70 |
| Male | 18 | 30 |
| Total | 60 | 100 |

Figure V.1. Gender

Table V.2 presents the percentage of attendance of the students who participated the 30 class (60 hours) CALL experiment. The highest percentage (50%) was for the students who attended less than 10 classes. This high percentage was because most of the candidates were females and could not attend the classes due to the some security issues happened during this research in the city.
On the other hand, the candidates who attended all or most of the classes(26%) got the highest scores in the post-test (see table V.4).

| ATTENDANCE | FREQUENCY | PERCENT |
|---|---|---|
| 0 >= 10 | 30 | 50.00 |
| 11 >= 20 | 14 | 23.33 |
| 21 >= 30 | 16 | 26.67 |
| Total | 60 | 100 |

Table V. 2 Attendance (out of 30 classes)

Figure V.3 shows that the average of marks of the pre test scores. The highest percentages were between 21-30 marks out of 40 (45%). While the second highest scores were gained by 18 students and were between 31-40 marks (30%). This percentage shows that the language level of these (18 ) students was between B1 and B2 according to the CEFR(**Common European Framework of Reference for Languages) See index.**

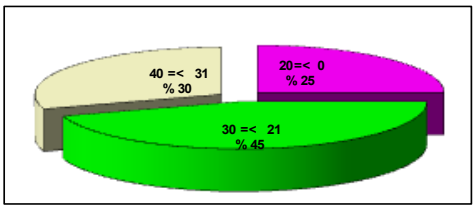


Figure V.3.a Pre-Test Marks (out of 40)

Table V.4 shows the average post-test scoring of the 60 candidates who participated in experiment. It can be seen that the highest percentage (56%) was for the students who got the highest scores (from 31-40).This significant increase was due to their regular attendance to the classes .While the lowest scores were gained by 11 students who were out of the total 60 candidates and (Their scores were between 0-20 out of 40). This low scoring was due to either their partial or total absenteeism. The majority of the students who got the highest scoring rates (from 31 to 40) have achieved level B2 in the post-test according to CEFR (see index).This development in the speaking level shows a significant improvement in a very short time (60 hours), if compared to the CEFR approximate development level (100 -200 hours per level).

| POST-TEST MARK | FREQUENCY | PERCENT |
|---|---|---|
| 0 >= 20 | 11 | 18.33 |
| 21 >= 30 | 15 | 25.00 |
| 31 >= 40 | 34 | 56.67 |
| Total | 60 | 100 |

Table V.4 Post Test Marks (out of 40)

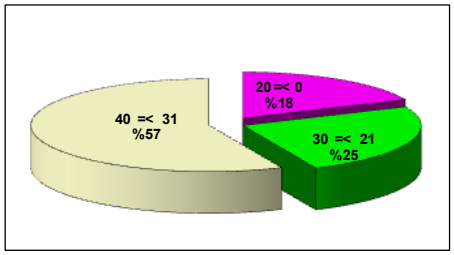


Figure V.4.a Post Test Marks (out of 40)

Hypothesis: There are statistically significant differences between the results of students in PRE-TEST and POST-TEST of the method of teaching English.


ISSN 1737-9334

Whereas :Naked Hypothesis: There are no statistically significant differences in the new teaching method that affect the results of the PRE-TEST and POST-TEST.

Alternative hypothesis: There are statistically significant differences in the new teaching method that affect the results of the PRE-TEST and POST-TEST of the study sample.

Table (V.5) shows the statistical significance of the differences between the arithmetic mean of the pre-test and the post-test of the sample. The statistical value of the "T" test for the differences amounted to (-7.992) in a significant value (0.00), which is below the level of morale (0.01). This indicates that there are significant statistical differences between the two tests. This statistical indication in favor of the post-test confirms the success of the new teaching method (fixed time teaching pulses).
Table V.5 shows the arithmetical averages and the value of "T-test" of the respondents' responses

| PAIRED SAMPLES TEST | PRE-TEST | | POST-TEST | | MEAN DIFFERENCE | T-TEST VALUE | SIGNIFICANT |
|---|---|---|---|---|---|---|---|
| | Average | S.D | Average | S.D | | | |
| Pre-Test-Mark (out of 40) - Post-test Mark ( out of 40) | 26.350 | 8.378 | 30.550 | 9.707 | -4.200 | -7.992** | 0.000 |

## VI. Discussion and results

From the previous data analyses, it is undoubtedly proven that the technique of using fixed timed pulses in learning language skills has made a significant change in the students' speaking performance. Also, it is clear that the more the students are exposed to this methodology the better their performance gets. According to the CEFR guide book, "**As a rough guide, Cambridge exams estimate that each level is reached with the following guided learning hours: A2, 180–200; B1, 350–400; B2, 500–600; C1, 700–800, and C2, 1,000–1,200".** So, the students who attended almost all the 60 hours had significant improvements in their oral performance in the post test. The candidates who attended regularly the classes and attended almost all the sessions (25-30 classes) , succeeded to move from B1 level to B2 level in around 60 hours of learning. This progress in their level, if compared to the above Cambridge exams estimated time for each level, shows a significant improvement in less than half the time designated to each level of language (150-200 hours needed to transfer from B1 level to B2 level).

## VII. Limitations

There are some issues and factors that affected negatively this research which are:
1- Almost 50% of the candidates missed the classes due to their absence. More than two thirds of the candidates of study were females and of course they could not attend the classes because of lack of security in Tripoli where the experiment took place.
2- Some students used to arrive late to the class and did not go through the three phases designed for this methodology precisely and accurately.

## VIII. Future Research

This is a new methodology and as researcher I am following a ground theory approach. This new trend needs further investigations to explore the learners' brain activities in more detail. This, of course, needs more sophisticated equipment and a team of specialists in neurology, biochemistry and psychology. Moreover, it is highly recommended that other areas of knowledge learning to be explored using time fixed learning pulses to see what new outcomes might be discovered. Finally, to uncover the inner brain chemical and physical changes that can lead to speed up the students' learning and creative thinking which happen as result of this new methodology in order to cure some uncured brain disorder due to ageing or diseases.

## IX. Conclusion and Justification

Fixed timed teaching pulses explored some new and unseen or previously discovered areas in the way that learners' brains deal with learning and creative thinking and problem solving. This teaching methodology has shortened the time needed for learning and developing creative thinking and problem solving. The human brain deals reacts with any piece of information or knowledge and processes it as same as all the other billions of inner operations that happen in every second. So if learning processes were designed and directed to the brain in the way that have been done in this new method, highly noticeable progresses will be gained. These teaching pulses go a long smoothly with the brains' inner mechanisms which, as a result, lead to having such a noticeable improvements which were almost the half the time needed for learning which are used in other conventional teaching and learning methodologies. The human brain is still and will always be a mysterious phenomenon where billions of its neurological reactions and responses are yet to be explored. Also integrating this new teaching methodology with computers enhanced the learning processes significantly. Moreover, CALL enabled the language learners to develop without paper course books and the learning environment was open and very flexible for any new learning sources. It is very easy to design and provide new materials to the students who needed further help or support without affecting other students. It is also possible that learning programs can be designed accordingly with each student's level within the whole group to achieve the target goals of the course within the same time limits of the course. Learning in this way can provide more challenging knowledge with fun and enjoyment. In addition, shorter time is needed to study and to get a degree. It would be also possible to achieve the maximum level of knowledge in just few years. Teaching & learning will be an easy and a pleasure experience with no sophistications. I think this would immensely affect all sorts of life and businesses around the world and makes learning and acquiring knowledge as easy as a child learns his mother tongue language in his first 4 years. Finally, this approach aims to make learning as natural and smooth as the brain's daily routine processes to gain excel in life.

## References

1- Atkinson, R.C., & Wilson, H.A. (1969). Computer-assisted instruction. In R.C. Atkinson & H.A. Wilson (Eds.), Computer-assisted instruction: A book of readings
2- Chapelle, C.A. (2001). Computer applications in second language acquisition: Foundations for teaching, testing, and research. Cambridge: Cambridge University Press.
3- Han, W. (2009). Benefits and barriers of computer assisted language learning and teaching. US-China Foreign Language, 6 (9), 40-43.


ISSN 1737-9334

4- Higgins, J., & Johns, T. (1984). Computers in language learning, London: Collins.
5- Taylor, M.B., & Perez, L.M. (1989). Something to do on a Monday. La Jolla, CA: Athelstan.
6- Taylor, R. (1980). The computer in the school: tutor, tool, tutee. New York: Teachers College Press.
7- Levy, Michael, and Allison Green. CALL Bibliography for Postgraduate Study. System 23.1 (1995): 87-106.
8- Levy, Michael. Design Processes in CALL: Integrating Theory, Research and Evaluation. CALL: Media, Design, and Applications. Ed. Keith Cameron. Lisse: Swets & Zeitlinger, 1999. Computer -Assisted Language Learning. Oxford: Clarendon, 1997.
9- Richards, J. C. and T.S. Rodgers. Approaches and Methods in Language Teaching: a description and analysis. Cambridge University Press. 1994.
10- Skinner, B. F. Verbal behavior. New York: Appleton-Century-Crofts. 1957.

INDEX

## 1 Common Reference Levels

### 1.1 Global scale

| | | |
|---|---|---|
| **Basic User** | **A2** | Can understand sentences and frequently used expressions related to areas of most immediate relevance (e.g. very basic personal and family information, shopping, local geography, employment). Can communicate in simple and routine tasks requiring a simple and direct exchange of information on familiar and routine matters. Can describe in simple terms aspects of his/her background, immediate environment and matters in areas of immediate need. |
| | **A1** | Can understand and use familiar everyday expressions and very basic phrases aimed at the satisfaction of needs of a concrete type. Can introduce him/herself and others and can ask and answer questions about personal details such as where he/she lives, people he/she knows and things he/she has. Can interact in a simple way provided the other person talks slowly and clearly and is prepared to help. |
| **Independent User** | **B2** | Can understand the main ideas of complex text on both concrete and abstract topics, including technical discussions in his/her field of specialization. Can interact with a degree of fluency and spontaneity that makes regular interaction with native speakers quite possible without strain for either party. Can produce clear, detailed text on a wide range of subjects and explain a viewpoint on a topical issue giving the advantages and disadvantages of various options. |
| | **B1** | Can understand the main points of clear standard input on familiar matters regularly encountered in work, school, leisure, etc. Can deal with most situations likely to arise whilst travelling in an area where the language is spoken. Can produce simple connected text on topics, which are familiar, or of personal interest. Can describe experiences and events, dreams, hopes & ambitions and briefly give reasons and explanations for opinions and plans. |
| **Proficient User** | **C2** | Can understand with ease virtually everything heard or read. Can summarize information from different spoken and written sources, reconstructing arguments and accounts in a coherent presentation. Can express him/herself spontaneously, very fluently and precisely, differentiating finer shades of meaning even in more complex situations. |
| | **C1** | Can understand a wide range of demanding, longer texts, and recognize implicit meaning. Can express himself/herself fluently and spontaneously without much obvious searching for expressions. Can use language flexibly and effectively for social, academic and professional purposes. Can produce clear, well-structured, detailed text on complex subjects, showing controlled use of organisational patterns, connectors and cohesive devices. |


ISSN 1737-9334

# Survey on FTTA and FTTB to Improve Performance of Mobile Networks

Amira Y. Ellafi[1] , Abdussalam M. Ammar[2] and Amer *M. Daeri*[3]

[1, 2] College of Electronic Technology, Communication Engineering Department
Tripoli, Libya
[1] E- mail Amoor85ly@yahoo.com and [2]E- mail Slm2010ly@gmail.com
[3]Zawia University, Faculty of Engineering/ Computer Engineering Department,
Zawia, – Libya,
*E-mail* E-mail amer.daeri@zu.edu.ly

***Abstract*** **- The continuous pursuit to improve the cellular communication networks lead to fit the huge demand of high data rates for the users. This paper reviews the Fiber To The Antenna (FTTA) and Fiber To The Base Station (FTTB) techniques as the ideal and best solutions in the world of modern communications. These techniques characterized by several features that gives a very positive addition to the existing networks, that is because the fiber optic technology has very wide bandwidth , higher data rates , very low power loss, and it is the main component of FTTA and FTTB solutions as well as it's avoid many defects which causing several prospective problems such as complexities in installation, limited development and costly consumption. When the comparison had done between the traditional system and the developed system , the differences was clear and large among them in favor of the developed system, here is also the explanation why and how fiber optic technologies are used efficiently in 4G networks, through reviews the advantages , challenges and the ways to overcome it in the FTTA and FTTB solutions.**

***Index Terms*** **- FTTA, FTTB, Integrated Optical and Wireless Network.**

## I. INTRODUCTION

The technical developments in the recent telecommunication world have been rapid, where communications have permeated in most of the daily life applications, which cause increasing demand on the huge capacity and higher data rate in order to have high efficiency and quality of services for all users around the world.

Originally the mobile systems have been designed for Circuit Switched (CS) voice traffic. Then after that it is developed and modernized towards the Packet Switched (PS) domain, to cover the continues demand for mobile data services such as mobile Internet access ,video streaming, gaming, navigation, banking, or IPTV. Fig.1 shows the trend of huge increase of user data rates in communication systems during one decade [1].

Here came the trend to introduce highly efficient a new elements in terms of data transfer speed with less interference, less noise , lower power consumption and lower cost. In addition to flexibility and high scalability according to the needs of the network.

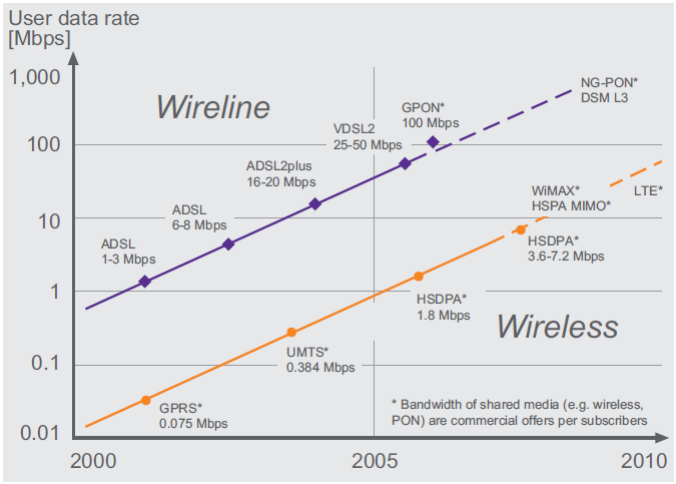


Figure.1. Increasing data rates in fixed and mobile services[1].

The optical fiber system currently considered the most suitable compared to the systems used recently. Fiber optics play an important role as ideal alternatives to traditional modes of data transport with limited potential , as it can easily be integrated into existing systems without complications. Therefore it is the first and best solution among all the available solutions so far.

## II- CLASICAL ARCHITECTURE OF MOBILE NETWORK SYSTEM.

In traditional method, coaxial cables are the medium, connecting the base station on the ground to an antenna on the tower, and used for transmitting high-frequency radio signals. Generally, almost 35% of the signal power is lost in coaxial cables (7/8 ") having a length of 30m and around 50 % of the


ISSN 1737-9334

signal can be degraded before the signal is even transmitted by the antenna [2]. As result of these losses, a deterioration of the transmission power occurs, which cause a reduction of the reception signal quality due to increased signal noise.

The radio communication system is mainly related to the Radio Frequency (RF) component, and is relied upon as a means of transferring data through the carrier air medium. That is why it has been still present during all successive developments. As they operate in a traditional composition based on coaxial cables as means of transport which leads to significant energy consumption that should be minimized as much as possible. The Radio Base Station (RBS) transmit the RF signals from the Base Station (BS) to the antenna through the coaxial cables mounted on a mast 30 to 100 meters above the base station [3].

The RBS architecture consist of several components such as Base Band Unit (BBU), signal power amplifier, RF filter, radio signal modulator as well as transmitter and receiver antenna as in Fig. 2 .

The whole control operations and base band signal processing are executed here. Before transmitting the signal to the antenna, the RBS modulates the data signals into allocated high-frequency band and consequently amplify the power of the modulated signals

Then , the output signals are transmitted via coaxial cables to the Tower Mounted Amplifier (TMA) from where the re-amplified signals are sent to antenna through coaxial jumper cables ,then the signals are radiated into free space.

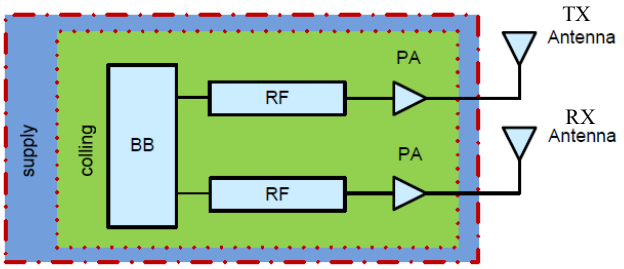


Figure.2. The classical architecture of RBS.

On the other hand, RBS is connected to the Base Stations Controller (BSC) via the microwave system, which have problems with limited capacity and distance that leads to less of flexibility and scalability infrastructure as illustrates in Fig. 3 .

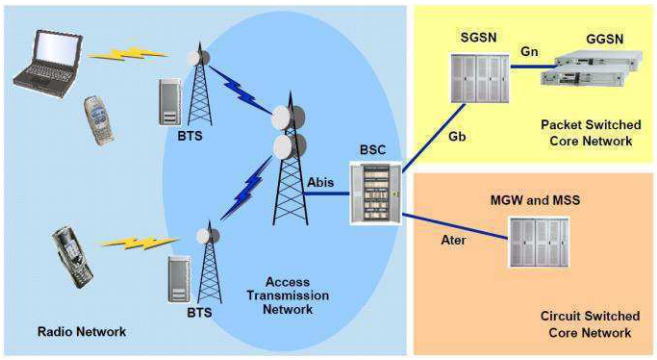


Figure.3. the classical architecture of mobile network system

## III- FIBER TO THE ANTENNA SOLUTION.

To get huge enhancements to the network performance , flexibility , speed and mobility, while reducing infrastructure and operating costs , will resort to FTTA as integrated solution for optical and wireless networks, furthermore, it can be easily eliminates the requirement of massive feeder cables from the Base Transceiver Station (BTS) to the antenna, and within the antenna itself, by replacing them with an optical feeds.

This solution is evolving, as continue increase of requirements of the data content and speed in the 4$^{th}$ generation (4G) communication systems. FTTA has served as an enabling architecture for the deployment of 4G mobile communications systems and later 5G.

In this part, will be review FTTA architecture, physical components, benefits and challenges.

### *A. Architecture of FTTA*

The evolved idea of new architecture of FTTA is based on insertion a new separated units as Remote Radio Unit (RRU) and BBU, where it is instead of one BS unit which performing all functions and interfacing to both the backhaul network and the antennas via coaxial cables . The separation of power and signal components from the BS to a smaller BBU at the bottom of the tower and multiple fiber feed RRUs at the top of the tower , as shown in Fig. 4. Fiber cables replace coaxial feeders running up the tower and their relocation to the top of the tower mast in RRU's.




ISSN 1737-9334

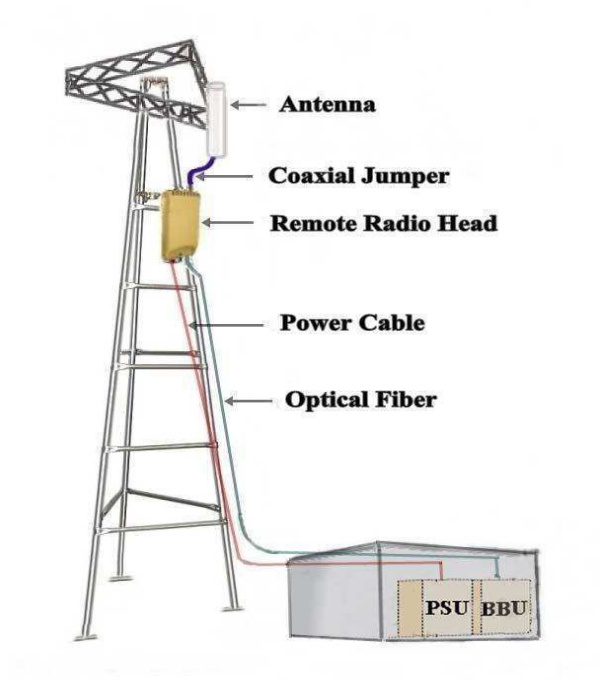


Figure.4. the architecture of FTTA.

This separation has allowed cell tower operators to comply with the performance requirements of 4G systems, created a smaller and greener footprint for the reconfigured BS, led to a reduced power, cost, and paradigm weight for the overall tower structure. The main component of this architecture are BBU, RRU, Hyper Cables , and coaxial jumper cables .

1)The Base Band Unit.

BBU is the common and fundamental unit that related between the FTTA and FTTB technologies where the BBU performs first step of digital processing of the baseband signals and delivered to RRU as part of FTTA architecture along with performing all functions of other side BSC as part of FTTB architecture.

2)The Remote Radio Unit.

The RRU consist of number of digital interfacing and processing functions as well as analog functions, all components collects into one device with low-weight (9.0 to 15 Kg) .The RRU is considered as the most important change in the evolved architecture of the cell site. The idea of RRU is the goal of development which is represented in shifts the whole high frequency and power electronic parts from the base station to a location adjacent to the antenna.

The characteristics of these changes include keep the control and base band signaling components in the BBU ,the small Form-Factor Pluggable (SFP) transceiver is the last signal generation unit in the BBU which converts the electrical signal to an optical signal. The optical signal is then transmitted via fiber optic cable from the BBU to one or more RRU's located close to antenna.

In the other side another SFP transceiver receive the optical signal at the input of RRU and converted it back into an electrical signal, where it is amplified and converted into a carrier frequency and fed to the antenna via a short coaxial cable jumper[2] .

Additionally, RRU is supplied with -24V or -48V DC through heavily shielded cables from the Power Supply Unit (PSU) at the bottom of the tower as shown in Fig.4. The existing coaxial feeders in the traditional system can be used for this purpose. Solar panel system also can be used to supply the power to RRU.

3)Hyper Cable Technology.

Advanced technology permits us to use hybrid cables where there is ability to combine power and optical fiber elements in a single cable cross section. There may also exists separate optical and power cables, reusable feeders that reuse coaxial cables that already exist to carry the power while a new fiber optic data cable is fed through the existing central duct.

Cases where involves upgrading the existing site reusable feeder cable solution is the most effective. The low friction design of the optical fiber means that the site engineer simply has to feed it in from the top connection of the antenna or RRU, usually at a height of 50 to 100 meters above ground. As a short length is inserted, the cable continues to fall under its own weight.

4)Coaxial Jumper Cable.

Later on, the optical signal is transmitted over the optical fiber to the RRU that converts the optical signal back into an electrical signal with the help of another SFP module, prior to high-frequency modulation and final power amplification. Then using short coaxial cables(Jumber 1/2”), RF signal is transmitted to the antenna for broadcasting.

*B. Advantages of FTTA.*

The FTTA technique has a several advantages such as :-

1) Eliminate The Energy Loss in the Transmission Medium.

Concerns about signal loss can be overcome by generating signal near to the antenna. By replacing the coaxial cables with fiber optics and new modifications to the positions of RRUs and antennas , due to the light weight of optical fibers, which reduces the load on the tower [4].


ISSN 1737-9334

2) High Speed Of Data Rate.

The speed obtained using optical fiber during the transmission to the antenna in the FTTA system is in femto second domain, this is a great achievement compared to the traditional system, where the coaxial cables has an electric speed for transmitting data which operating in micro or nano second domain. The coaxial transfer speed is 10 Mbps [5].

Alcatel-Lucent and BT have successfully tested data speeds of up to 1.4 terabytes per second via the current commercial fiber optic cable and the data transfer speed of 31 terabytes per second via 7200 km long long-range fiber optic [6].

3) Offers Wide Range Coverage and Huge Capacity.

Since the coaxial cables are greatly susceptible to be damaged, the transmission distance via coaxial cable in legacy system is limited to less than 50m. In case of larger distances, to eliminate the problem and extend the radio cell coverage by using low-loss but expensive coaxial cables which are also time-consuming to install due to their large external diameter. On the contrary, Single Mode Fiber optic (SMF) gives the opportunity to extend the transmission distance limits up to 15 or even 20 km [4].

In addition to that, most of the time, advanced antenna techniques like Multiple In Multiple Out (MIMO) and Remote Electrical Tilt (RET) are supported by RRUs that offer major increase in data throughput and link range without additional bandwidth or increased transmitting power [7].

4) Reduce Installation Time.

Installation is faster by fiber solution compared to coaxial solution . A team of four technicians would complete a coaxial tower work in four days while in FTTA is only three experts technicians and two days are needed. New upgrades are coming, such as Corning Inc. has developed a technology where installation is possible within one day using three labor hands [8].

5) Power Reduced.

The installation of FTTA in terms of replacing the coaxial cable with the optical cable and the presence of power amplifiers in the RRU reduces the loss of signal strength. The RRU power amplifiers allow the use of 48V DC instead of 110V AC and thus reduce the transport power cost taking into account frequency of the radio signal.

6) Reduced Cooling System.

The RF amplifier in the RRU tower is naturally cooled by air, which in turn reduces the need for a cooling system compared to conventional radio frequency amplifiers used in BS's. The cooling system conserves approximately 25% of the site energy which used in RRU's, also previously the most of the power is used in the amplifiers are results as heat. The continuous active cooling systems is needed and increases the cost of energy.

7) Lower Cost.

Already we have found that reduced cooling system along with use of hybrid cables greatly reduce the cost for the FTTA solution. Also, due to lower rental costs of telecoms facilities and antenna sites, operating costs are reduced. For instance, reinstalled fiber optics infrastructure in city networks or in buildings can be used to establish the connection between the BS and the RRU. Again, network operators have to spend huge amount of money to rental and licensing issues for BS and antenna sites.

As a solution, FTTA can be used, which permits BS to be installed at greater distances from the RRUs. Fiber feeds RRU can save around 50-60% on total maintenance and installation costs compared to coaxial cables deployments [8]. This makes things easier for the operators to acquire new sites to optimize network coverage when it is needed.

*C. Challenges of FTTA.*

This new technical developments as any other new technique isn't free from facing some of potential or unexpected obstacles during its installation and operation, which led to the some challenges that have a negative impact on the quality and efficiency of system performance. These challenges must be analyzed and solved to minimize or eliminate the consequences , those challenges including :-

1) The Water and Moisture.

Since the FTTA architecture make it vulnerable to external environmental factors such as rain and humidity as the coaxial cable and its connections are heavily affected by water leakage which directly affects the high frequency of the signal and damage it [9].

This challenge has been overcome in several ways by companies specialized in addressing these problems through methods like using tapes and mastic to wrap around connectors. As well as other methods more developed to avoid the disadvantages of the previous traditional method, including pre- stretched pipes (Hot pipe and cold pipe), also The sealing gel around the edges forms an effective barrier surrounding the connection. All those methods are easy in installation without tools, where is normally one person can installed in a minute or less[10].



ISSN 1737-9334

2) The Surge And Lightning Strike.

In the new FTTA structure ,The RRU is located at the top of the tower's mast and exposed. There are also power cables coming from low-voltage power supply (-48 V DC) and coaxial jumpers (copper wire) This structure is permanently, so the problem of surge and lightning cannot be avoided during planning, this challenge must be taken into account to protect the entire architecture from surge and lightning that which electrical components are exposed in the environment (without any convincing protection)[11].

Also elements that aren't directly affected by lightning , will experience some effects of the electromagnetic field due to the excessive flow of current which resulted from a high voltage on the elements around the exposed area of lightning strike.

In this case the solution to this challenge will be protect the system with various Surge Protection Devices (SPD) and must be included on the output side of the power source to protect the sensitive components of the power source.

3) The Human Labor Skills.

This is a type of technology that needs highly skilled workers and experience in dealing with optical cables and RRU's in terms of installation of other components at high altitudes above ground. Fiber optic is more susceptible to damage caused by crimping, bending or tension during pulling compared to pulling cable trunks or feeders, which significantly reduces fiber performance.

The solution for this challenge is by training the workers properly and rehabilitate them well and provide a suitable tools for the repair and installation processes.

## IV- FIBER TO THE BASE STATIONS SOLUTION .

This solution is Associate in integration of Microwave (MW) and optical networks, it's a potential candidate for increasing capability and quality as well as decreasing prices within the broadband access network .

FTTB makes it possible to centralize the RF signal processing functions in one shared location called Main Switch Room, and then to use optical fiber to distribute the RF signals to RBS's.

FTTB is a new system for feeding RF signals from either the BSC to RBS directly or from RBS to the antenna elements at the air interface. RF system designers are familiar with the few major limiting characteristics of coaxial cables as the increase in RF loss with frequency and length.

This type of system has lower transmission loss and greater power efficiency than the current systems. Other advantages including antenna main beam steering ,reduces antenna weight , reduced susceptibility to RF interference on the feeder network and simplified site installation. By using the MW technique, the data rates for communicating between the BSC and the RBS directly ,or through node site have been relatively low.

As the need for higher densities of RBS's develop and as wireless networks increases, also the need for higher data rates and higher data bandwidth between the RBS and the BSC has become apparent, here is comes the fiber optics as evolved solution.

### *A. Architecture of FTTB .*

Subcarrier Multiplexing (SCM) is multiple RF carrying signal to transmit through optical fiber using single wavelength. The SCM has ability to place different optical carriers together closely as in Fig. 5. Wavelength Division Multiplexing (WDM) is a multiplexer at the transmitter to join the signals together, and a de-multiplexer at the receiver to split them apart again [12].

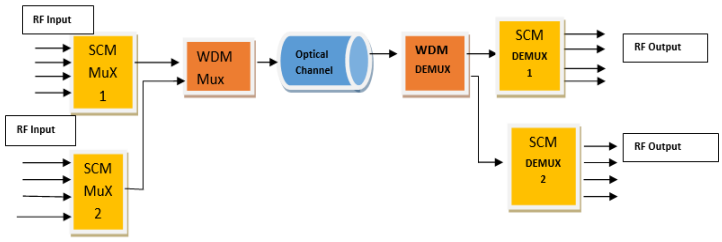


Figure.5. the architecture of SCM/WDM

SCM used in conjunction with WDM to utilize any significant fraction of the fiber bandwidth. The results is present higher bandwidth for long distance communication system. For example in SMF the distance could be reach to 150 km by using SCM/WDM for Radio over Fiber.

### *B. Benefits of FTTB.*

The FTTB techniques has many benefits including :-

1) Low Attenuation loss .
2) Large bandwidth .
3) Low RF power of RRU.
4) Dynamic resource allocation .
5) Line Of Sight (LOS) operation (multipath fading effects are minimized) .
6) Immunity to radio frequency interference .


ISSN 1737-9334

### *C. Challenges of FTTB.*

One challenge from the perspective of FTTB is the location of radio head and fiber optic transceiver in a harsh outdoor environment - especially severe weather at elevated, exposed heights. The components must operate over extreme environmental conditions, over a wider temperature range. The typical BTS application requires a fiber transceiver to operate over a range of 40 degree Celsius to 85 degree Celsius temperature.

The other challenge is The power supply to the Transceivers must be stable and noise free in order to maintain error free performance for the data passing through fiber optic link.

## V- CONCLUSION

the FTTA and FTTB as technical solutions offers increasing in the data flow rates as the main requirement in future applications , and those solutions has a lower loss of coverage and greater energy efficiency, where it is using 30% less energy than current traditional systems . This survey shows analysis of the current obstacles in the running systems and that barrier the deployment of 4 and 5G networks (as Smart City Needs) in the future. The solution to overcome those problems by using the fiber optic in transmission media as alternative system and get rid of MW and coaxial cables.

## REFERENCES

[1] Attila Hilt and László Pozsonyi , Application Of Fiber Optic Techniques In The Transport And Access Transmission Networks Of Mobile Systems.6th oct 2011.

[2] P. Skandakumaran, V. Khanikar, M. Smalc, J. Norley and B. Reis, Passive, lightweight thermal solutions for remote radio head (RRH) electronics,in 11th Intersociety Conf. on Thermal and Thermo mechanical Phenomena in Electron. Syst., Orlando, FL, 2008.

[3] M. Denker, Remote radio head systems -- requirements and concept of lightning and overvoltage protection, in Proc. 2013 35th Int. Telecommun. Energy Conf. 'Smart Power and Efficiency' (INTELEC), Hamburg, HBR, 2013.

[4] M. Strasser, FTTA Fiber to the antenna ,technology change in mobile communications, 17 February 2016.

[5] Fahimul Haque and others ,Fiber to the Antenna: Solution in Integrated Optical and Wireless Networks, 978-1-4799-6399-7/14/$31.00,2014, IEEE.

[6] M. Jackson. (2014, Jan 21). BT and Alcatel-Lucent claim fastest real world fiber optic speed of 1.4Tbps [Online]. Available: http://www.ispreview.co.uk/index.php/2014/01/bt-alcatel-lucent-claim-fastestreal- world-fibre-optic-speed-1-4tbps.html , 21 sep, 2014 (1:22 pm).

[7] S. King, Challenges -to-the- and solutions for fiber antenna networks, 3M Company, Austin, TX, White Paper, 80-6113-8623-8, 2011.

[8] HICKORY, N.C. Fiber to the antenna (FTTA): Corning cable systems solutions for wireless networks, Corning Incorporated, Rep. EVO-1040-EN, Apr. 2012.

[9] S. C. King, Evolution of weatherproofing solutions for the cell site, 3M Company, Austin, TX, 2012.

[10] N. Cannon, Troubleshooting passive intermodulation problems in the field, Anritsu, Atsugi-shy, KN, Rep. 11410-00586A, Dec 21, 2010.

[11] P. McClusky and J. L. Schroeder III PE, Fiber-to-the-antenna: benefits and protection requirements, in 2012 IEEE 34th Int. Telecommun. Energy Conf. (INTELEC), Scottsdale, AZ, 2012.

[12] JDSU, Milpitas, CA A quick start guide to fiber-to-the-antenna (FTTA) installation and maintenance testing, White Paper, Vol. 2, Oct. 2013.




ISSN 1737-9334

# Design and Comparison of Two-Loop and Three-Loop Autopilot with PI for Static Unstable Missile

**Daw M. Alzentani**
.[1] (*Department of Electrical and Electronic Engineering*)
*Alzawia University,* Libya.
daw_425@yahoo.com .

**Almokhtar M. Alzhari…….**
.[2] (*Department of Computer Engineering*)
*Alzawia University,* Libya.
ali441@yahoo.com .

***Abstract***

*The characteristics of non-minimum phase and static unstable of a tail controlled tactical missile are presented firstly. Then, in order to eliminate the static error, a cascade PI compensator was introduced to the classic two loop autopilot. Due to the slow tracking for command acceleration, the longitudinal three-loop autopilot design is driven based on LTI model of missile plant to stabilize the non-minimum phase static unstably missile airframe. The focus is to explain the performance and the control effect at different values of velocity and stability derivative ($M\alpha$) of two algorithms on missile plant. The analysis is executed by establishing a standard algorithm in virtue of MATLAB/Simulink for autopilot design.*

*The simulation results indicated that three-loop topology gives better tracking than two-loop with a cascade PI compensator at different value of stability derivative $M\alpha$. On the other hand, two-loop has a better*
*response and less control effort at different velocities. fin angle and fin angle rate are less than the three loop for static unstable and stable missile.*

**Keywords***: PI compensator, two loop autopilot, three loop autopilot, flight control system, and missile.*

## i. INTRODUCTION

An autopilot is a closed loop system, and it is the minor loop of the main guidance loop. The two- or three-loop autopilots have been introduced in tactical missiles in recent years [1], [2]. The lateral autopilots control missiles body by controlling surfaces to generate the required acceleration according to the guidance demand, such as; proportional navigation, augmented proportional navigation, line of sight, etc.

In some Russia missile design, one accelerometer and one angular acceleration gyro are used and the accelerometer has to be positioned in the rear section of the missile for structure reasons. Nevertheless, the lateral autopilots with
One accelerometer and one rate gyro are more commonly used in homing guidance tactical missiles [3].

The three-loop Raytheon has been designed especially for radar seeker missile to eliminate the coupling effect of radome and parasitic loop [4].

The classical two-loop autopilot consists of rate-damping loop which is used to act as damper and accelerometer loop
which provides control of the lateral acceleration of the missile. But when adding a synthetic stability loop, it is called three-loop autopilot [5], [6]. Lateral autopilot acts as an inner loop of the guidance loop which is used to control the pitch and yaw motions. When the missile has two planes of symmetry, so we need consider one channel only, the pitch autopilot say.

The structured autopilot design algorithm of flight path rate for tactical guided missile lateral autopilot has been presented [7], [8], where a design methodology has been developed by relevant analysis for a class of tactical guided missiles.

The flight dynamic characteristics of the missile depend on its aerodynamic coefficients which vary significantly with flight condition such as altitude and Mach number. The problem is to design a pitch plane autopilot to track the normal acceleration commanded from the guidance system. The autopilot generates fin angle commands which are sent to the tail surface servos. By deflecting the tail fins, they generate aerodynamic forces and moments that maneuver the missile. Rate gyro and accelerometer measurements are processed by the flight control system to close the feedback control loop.

This paper is an elaborated comparison between two-loop with a cascade PI compensator and three loop autopilot. This paper is organized as follows. Section 2 describes the longitudinal autopilot model of a tailed controlled guided homing missile with one accelerometers and one rate gyro whereas the accelerometer is putted coincidence with center of gravity of the missile [9].

Section 3 presents two-loop autopilot design with a cascade PI compensator. A derivation of missile model needed for the three-loop autopilot design is given in Section 4. Section 5 presents the performance of the two algorithms. Section 6 introduces the conclusion of this paper.

## ii. Autopilot and Missile Dynamic

The longitudinal (vertical plane) flight control system for a bank to turn missile form a single input multi-output design model. The autopilot that will be designed will command normal body acceleration using tail fin deflection control. The plant outputs are normal acceleration $Az(ft/s2)$, and pitch rate $q$ (rad/s), and the plant states are $\alpha$, $q$, $\delta$, and $\dot{\delta}$ (angle of attack, pitch rate, fin deflection, and fin rate respectively). The nominal longitudinal airframe dynamics is represented by $(s)$. The deferential equation used to describe these open loop dynamic as in [10] are:

$$\dot{\alpha} = Z_\alpha \alpha + q + Z_\delta \delta_e \qquad (1)$$
$$\dot{q} = M_\alpha \alpha + M_\delta \delta_e$$

$$A_z = VZ_\alpha \alpha + VZ_\delta \delta \qquad (2)$$

Assuming that the actuator is second order system as

$$\ddot{\delta_e} = -2\,\zeta\omega\dot{\delta_e} - \omega 2(\delta_e - \delta_c) \qquad (3)$$


ISSN 1737-9334

In the state space form, the airframe dynamics are represented by the following state space triple $(A, B, C)$:

$$\dot{X} = AX + BU \quad (4.a)$$
$$Y = CX + DU \quad (4.b)$$

$$A = \begin{bmatrix} Z\alpha & 1 & Z\delta & 0 \\ M\alpha & 0 & M\delta & 1 \\ 0 & 0 & 0 & 1 \\ 0 & 0 & -\omega^2 & -2\zeta\omega^2 \end{bmatrix}; \; B = \begin{bmatrix} 0 \\ 0 \\ 0 \\ \omega^2 \end{bmatrix}$$

$$C = \begin{bmatrix} VZ\alpha & 0 & VZ\delta & 0 \\ 0 & 1 & 0 & 0 \end{bmatrix}$$

The transfer function matrix is $(s) = (sI - A)^{-1} B$. The longitudinal missile dynamics form a single input multioutput design model. From equation 4, the transfer function matrix from the elevon fin deflection command $\delta c$ to the normal acceleration $Az$ and pitch rate $q$ is:

$$G(s) = \begin{bmatrix} \frac{\omega 2V(Z\delta s2 + Z\alpha M\delta - Z\delta M\alpha)}{(s2 - Z\alpha\, s - M\alpha)(s2 + 2\zeta\omega\, s + \omega 2)} \\ \frac{\omega 2(M\delta s2 + M\alpha Z\delta - M\delta Z\alpha)}{(s2 - Z\alpha\, s - M\alpha)(s2 + 2\zeta\omega\, s + \omega 2)} \end{bmatrix} = \begin{bmatrix} \frac{Az(s)}{\delta c(s)} \\ \frac{q(s)}{\delta c(s)} \end{bmatrix} \quad (5)$$

where $Z\alpha$ , $Z\delta$ , $M\alpha$ , $M\delta$ , and $Mq$ are the aerodynamic stability derivatives. The measurements that are available are normal acceleration $Az = VZ\alpha\ \alpha + VZ\delta\ \delta$ *(ft/s2),* $q$ pitch rate (rad/s). The scalar control input $u=\delta c$ (rad) is the fin angle command.

The above aerodynamics have been linearized and represented a trim $\alpha$ angle of attack of 16 degrees, Mach number=0.8, $V$=886.78 (ft/s), an altitude of 4000 (ft.), actuator damping $\zeta$=0.6, and actuator natural frequency $\omega$=113 (rad/s). The following parameters are the nominal values of the dimensional aerodynamic stability derivatives; $Z\alpha = -1.3046$ (1/s); $Z\delta = -0.2142$(1/s); $M\alpha = 47.7109 \pm$ (1/s2) which were taken from [6]. The sign of $M\alpha$ determines the stability of the open loop airframe.

When the $M\alpha$ is negative the airframe is stable, and when it is positive the airframe is unstable, which occurs when the aerodynamic center of pressure is forward of the center of gravity [5].

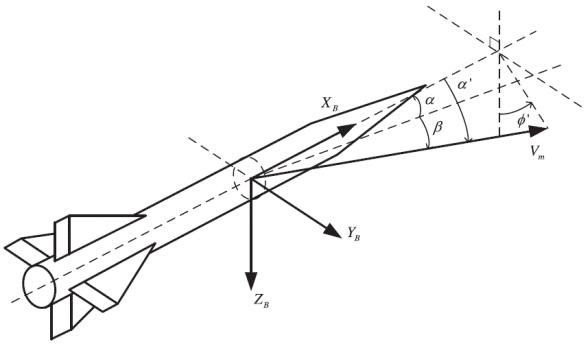


Fig. 1 Aeroballistics coordinates systems.

## iii. Two-loop autopilot

The two-loop autopilot system uses two loops to feedback information of the missile motion to the forward path of the autopilot.

One loop is involved with body rate information which is fed back using one rate gyro.

The other is the missile acceleration, sensed using accelerometer that considered the main feedback loop. So, modeling of missile airframe dynamics is an important part of configuring an autopilot system. Missile dynamics is of nonlinear type. The two-loop autopilot structure and the missile dynamics Transfer functions are displayed in Fig. 2. Equation (5) is used to design the normal acceleration command autopilot. In order to eliminate the static error, there are two controller blocks contained in the acceleration command autopilot.

The control input is fin deflection command $\delta c$ and the measured outputs are normal acceleration $Az$ and pitch rate $q$. The longitudinal autopilot controller blocks $(s)$ and $(s)$ are designed to give a good acceleration command tracking and to ensure missile stability.

The controller blocks $Ka(s)$, and $Kq(s)$ consist of proportional-plus-integral (PI) control elements.

The acceleration feedback loop controller block $Ka(s)$ has the structure

$$KAz\ (s) = \frac{kz(s + az)}{s}$$

Where the $kz$ is the proportional gain and $kzaz$ is the integral control gain. The pitch rate loop controller block $(s)$ has the structure

$$Kq(s) = \frac{kq(s + aq)}{s}$$

The longitudinal autopilot design process is automated to vary acceleration feedback loop and pitch rate loop gains and evaluate longitudinal autopilot performance and robustness properties.

The performance values examined are the normal acceleration command settling time, the percent undershoot, the percent Overshoot and the steady state error.

The two-loop autopilot feedback gains $kq = -0.3$, $kz = -0.00$, $aq$ =6, $az$ = 2, and $az$ = 2. The contribution of the controller blocks $KAz\ (s)$, and $K\ q\ (s)$ are analyzed in Section 4.

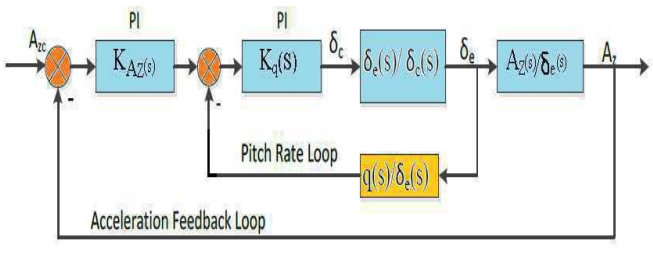


Fig. 2 Standard two-loop autopilot.




ISSN 1737-9334

### iv. Three-loop autopilot

The three loop autopilot is a new kind of autopilot developed recently years by one feedback loop (it is called synthetic loop) based on the traditional two loop autopilot.

Also a pure integrator is contained in the forward path of the autopilot loop.

The three loop pitch/yaw autopilot is used to most guide tactical missiles today as shown in Fig.3. It has four gains, $KA$, $K$ , and $\omega I$ ; which are used to control the third order dynamics of the autopilot.

These dynamics are due to second order dynamics and an integrator that allows the flight control system to control unstable airframe. The airframe transfer functions for a tailed homing tactical missile are driven referring to (1), and (2) as following:

$$\begin{aligned}
Az &= VZ\alpha\,\alpha + VZ\delta\delta e \\
&= V(\tfrac{Z\alpha}{S}\,\dot{\alpha} + Z\delta\,\delta e) \\
&= V(Z\delta\delta e + \tfrac{Z\alpha}{S}(Z\alpha\,\alpha + \tfrac{1}{S}\,\dot{q} + Z\delta\delta e)) \\
&= V(Z\delta\delta e + \tfrac{Z\alpha}{S}(Z\alpha\,\alpha + \tfrac{1}{S}\,(M\alpha\,\alpha + M\delta\delta_e) + Z\delta\delta e)) \\
&= V(\,\delta_e\left(Z\delta + \frac{Z\alpha Z\delta}{S} + \frac{Z\alpha M\delta}{S^2}\right) + \frac{1}{S}\left(\frac{Az}{V} - Z\delta\delta\right)\left(\frac{M\alpha}{S} + Z\alpha\right)) \\
&= V(\,\delta_e\left(Z\delta + \frac{Z\alpha Z\delta}{S} + \frac{Z\alpha M\delta}{S^2} + \frac{Z\delta}{S}\left(\frac{M\alpha}{S} + Z\alpha\right)\right) - \frac{1}{S}\,\frac{Az}{V}\left(\frac{M\alpha}{S} + Z\alpha\right)) \\
&= \left(\left(Z\delta + \frac{Z\alpha M\delta}{S^2} - \frac{Z\delta M\alpha}{S^2}\right) + \frac{1}{S}\,\frac{Az}{V}\left(\frac{M\alpha}{S} + Z\alpha\right)\right. \qquad (6)
\end{aligned}$$

Collecting terms gives

$$\frac{Az}{\delta e} = \frac{V\left(Z\delta S^2 + Z\alpha M\delta - Z\delta M\alpha\right)}{(S^2 - Z\alpha S - M\alpha)}$$

$$\frac{Az}{\delta e} = \frac{V(Z\delta M\alpha - Z\alpha M\delta)}{M\alpha}\left(\frac{1 - \frac{Z\delta S^2}{Z\delta M\alpha - Z\alpha M\delta}}{1 + \frac{Z\alpha}{M\alpha}S - \frac{S^2}{M\alpha}}\right) \qquad (7)$$

For $\Omega AF = \sqrt{-M\alpha}$, $\zeta AF = Z\alpha\Omega AF/2M\alpha$

$K1 = -(Z\delta M\alpha - Z\alpha M\delta)/M\alpha$

$\Omega z^2 = [Z\delta M\alpha - Z\alpha M\delta]/Z\delta.$

And for $Az = nL$, $q = \theta$. Then, the airframe relationship between the fin angle and missile acceleration is given by

$$\frac{Az}{\delta e} = \frac{nL}{\delta} = \left(\frac{K1\left[1 - \frac{S^2}{\Omega_Z^2}\right]}{1 + \frac{2\zeta_{AF}}{\Omega_{AF}}S - \frac{S^2}{\Omega_{AF}^2}}\right) \qquad (8)$$

After then, it should be driven the transfer function between body rate $q$ and missile acceleration $Az$.

Refer to (1) and (2)

$$\begin{aligned}
q &= \frac{1}{S}\,(M\alpha\,\alpha + M\delta\,\delta e) \\
&= \frac{1}{S}\,(M\alpha\,\alpha + \frac{M\delta}{Z\delta}\left(\frac{Az}{V} - Z\alpha\,\alpha\right)) \\
&= \frac{1}{S}\left(\left(M\alpha\,\alpha - \frac{M\delta Z\alpha}{Z\delta}\right)\alpha - \frac{M\delta}{Z\delta}\,\frac{Az}{V}\right) \\
&= \frac{1}{S}\left(\left(\frac{\left[M\alpha - \frac{M\delta Z\alpha}{Z\delta}\right]\left[1 + \frac{Z\delta}{M\delta}S\right]}{S - Z\alpha + \frac{Z\delta M\alpha}{M\delta}}\right)q - \frac{M\delta}{Z\delta}\,\frac{Az}{V}\right)
\end{aligned}$$

Rearrange terms gives

$$\begin{aligned}
\frac{q}{Az} &= -\left(\frac{\frac{1}{S}\left(\frac{M\delta}{Z\delta}\right)V}{1 - \frac{1}{S}\left[\frac{\left(M\alpha - \frac{M\delta}{Z\delta}Z\alpha\right)\left(1 + \frac{Z\delta}{M\delta}S\right)}{S - Z\alpha + \frac{Z\delta M\alpha}{M\delta}}\right]}\right) \\
&= -\frac{M\delta}{Z\delta V}\left(\frac{S - Z\alpha + \frac{Z\delta M\alpha}{M\delta}}{S^2 + S\left(\frac{Z\delta M\alpha}{M\delta} - Z\alpha\right) - \left(M\alpha - \frac{M\delta}{Z\delta}Z\alpha\right)\left(1 + \frac{Z\delta}{M\delta}S\right)}\right) \\
&= -\frac{M\delta}{Z\delta V}\left(\frac{S - Z\alpha + \frac{Z\delta M\alpha}{M\delta}}{S^2 + S\left(\frac{Z\delta M\alpha}{M\delta} - (Z\alpha)\right) - (M\alpha Z\delta - M\delta Z\alpha)\frac{1}{M\delta} - \left(M\alpha + \frac{M\delta}{Z\delta}Z\alpha S\right)}\right) \\
&= -\frac{M\delta}{Z\delta V}\left(\frac{S + \frac{(M\alpha Z\delta - M\delta Z\alpha)}{M\delta}}{S^2 - \frac{(M\alpha Z\delta - M\delta Z\alpha)}{Z\delta}}\right)
\end{aligned}$$

$$\frac{q}{Az} = \frac{1}{V}\left(\frac{1 + \frac{(M\delta).S}{M\alpha Z\delta - M\delta Z\alpha}}{1 - \frac{Z\delta.S^2}{M\alpha Z\delta - M\delta Z\alpha}}\right) \qquad (10)$$

By introducing a new variable $T\alpha = \frac{M\delta}{M\alpha Z\delta - M\delta Z\alpha}$ Then

$$\frac{q}{Az} = \frac{\dot{\theta}}{\eta_L} = \frac{1}{V}\left(\frac{1 + T\alpha.S}{1 - \frac{S^2}{\Omega_Z^2}}\right) \qquad (11)$$

And the transfer function that relating between missile body rate $q$ to the fin angle $\delta e$ is given by:

$$\frac{q}{\delta e} = \frac{Az}{\delta e}\frac{q}{Az} = K1\,\frac{\left(1 - \frac{S^2}{\Omega_Z^2}\right)}{1 + \frac{2\zeta AF}{\Omega_{AF}}.S - \frac{S^2}{\Omega_{AF}^2}}\,\frac{1}{V}\left(\frac{1 + T\alpha.S}{1 - \frac{S^2}{\Omega_Z^2}}\right)$$

$$\frac{q}{\delta e} = \frac{k3(1 + T\alpha.S)}{1 + \frac{2\zeta AF}{\Omega_{AF}}S - \frac{S^2}{\Omega_{AF}^2}} \qquad (12)$$

Where $3 = K1/V$ for the three loop autopilot, it includes an integrator for body rate in order to reduce the steady state error. It should be clear from Fig.2 that the acceleration feedback loop is a proportional controller acting on the acceleration error. The inner loops form a proportional plus integral (PI) for pitch rate to stabilize the missile body. The outer loop relationship is given by

$$e = A_{ZC}K_{DC} - Az \qquad (13)$$

Where $A_z$ is the measured output acceleration and $A_{zc}$ is the input acceleration command.




ISSN 1737-9334

$$\frac{Az}{Azc} = K_{DC}\frac{k3G(s)G1(s)}{1+G(s)G1(s)} \qquad (14)$$

Where $\text{?}1(s) = \frac{Az}{\delta e}$, $G2(s) = \frac{q}{\delta e}$, and

$$(s) = \frac{\delta e}{e} K_R\left(\frac{\omega_I}{S}(G2(S)\,\delta - eK_A) + G2(S)\,\delta\right)$$

$$= \frac{1}{S}\frac{K_A\omega_I K_R G_{M(s)}}{K_R G_{M(s)}\,G2(S)\left(\frac{\omega_I}{S}+1\right)-1} \qquad (15)$$

With substitution from (8) and (12) into equation (14), the final result is

$$\frac{Az}{Azc} = K_{DC}\frac{GM(s)KK_1\left(1-\frac{s^2}{\Omega_Z^2}\right)}{\{GM(s)K_0+[KRGM(s)(1+\omega_i T\alpha)-1]s + \left[GM(s)\left(\left(K_R K_3 T\alpha - \frac{KK_1}{\Omega_Z^2}\right)\right)\frac{2\zeta AF}{\Omega_{AF}}\right]s^2 - \frac{s^3}{\Omega_{AF}^2}\}} \qquad (16)$$

Where $K = K_R\omega_i K_A$, $K_0 = K\left[\left(\frac{K_3}{K_A}\right)+1\right]$.

For common practice it is assume that the actuator dynamic are very fast relative to the system response $(s) \cong 1$.
The closed loop transfer function after approximation is

$$\frac{Az}{Azc} = K_{DC}\frac{KK_1\left(1-\frac{s^2}{\Omega_Z^2}\right)/K_0}{\{1+[K_R G_M(s)(1+\omega_i T\alpha)-1]s/K_0 + \left[G_M(s)\left(\left(K_R K_3 T\alpha - \frac{KK_1}{\Omega_Z^2}\right)\right)\frac{2\zeta AF}{\Omega_{AF}}\right]s^2/K_0 - \frac{s^3}{K_0\Omega_{AF}^2}\}} \qquad (17)$$

Finally, for zero steady state error to a step input, it is required that the closed loop gain is

$$\frac{K_{DC}KK_1}{K_0} = 1 \qquad (18)$$

The longitudinal autopilot design process is automated to vary the acceleration feedback loop and the pitch rate loop gains and evaluate longitudinal autopilot performance and robustness properties.

The performance values examined are the normal acceleration command settling time, the percent undershoot, the percent overshoot and the steady state error.

It found that the three-loop autopilot feedback gains are $k_{DC} = 1.061,\ k_A = -0.007, \omega_I = 18.8, k_R = -0.7$.

The contribution of the three loop gains as shown in Fig.3, Fig.5, and Fig.6 but it gives a nonzero error as shown in Fig.4 at different velocity because $K1$ is dependent on the missile velocity $V$.

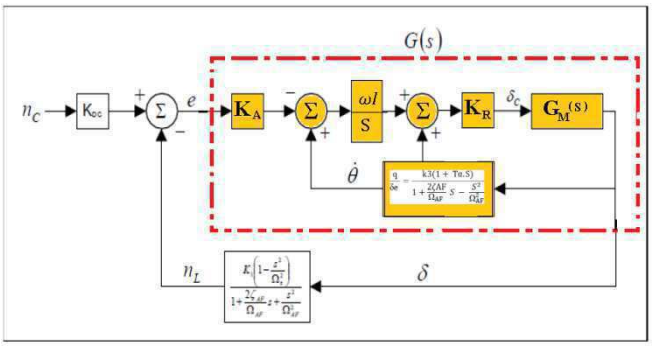


Fig. 3. Standard three-loop autopilot

## v. Results and Discussion

The aerodynamics acceleration transfer function contains a right half plane (RHP) zero. This no minimum phase relationship results from the missile fin deflection initially producing a lift force in the direction opposite to the command. The moment due to fin force, cause the airframe to pitch, creating an acceleration command.

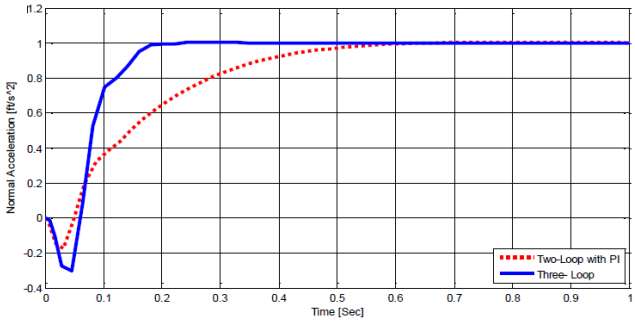


Fig. 4.a

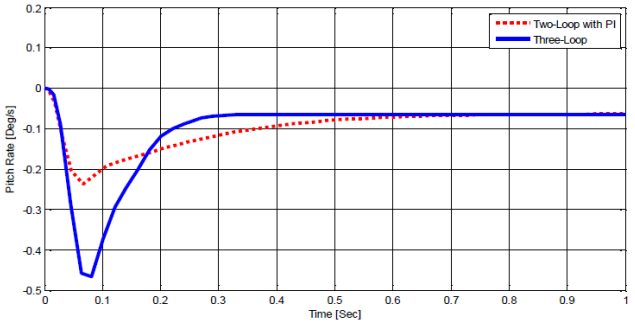


Fig. 4.b

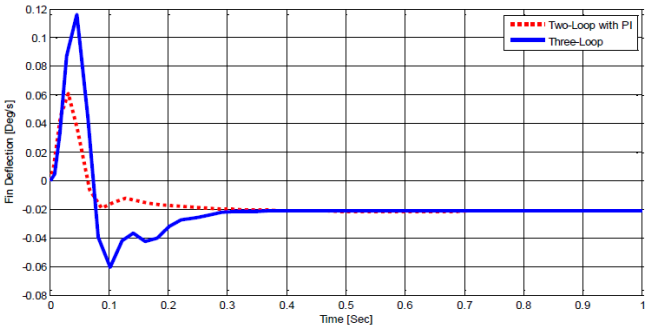


Fig. 4.c




ISSN 1737-9334

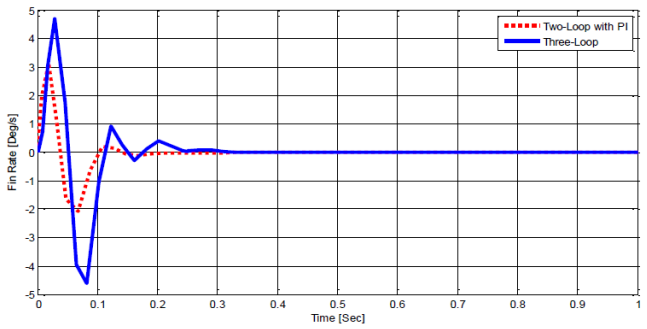


Fig. 4.d

Fig. 4. a.b.c.d Unit step response history of two topologies.

This phenomena is observed in the normal acceleration response as shown in Fig.3-5 as an initial undershoot in the time history of normal acceleration, because the initial value of step response is

$$\lim_{s \to \infty} s\left[\frac{1}{s}\frac{Az(s)}{\delta e\,(s)}\right] = Z\delta < 0$$

But the final value of the step response is

$$\lim_{s \to 0} s\left[\frac{1}{s}\frac{Az(s)}{\delta e\,(s)}\right] = \frac{Z\alpha M\delta - Z\delta M\alpha}{-M\alpha} > 0$$

And the stability of the airframe is governed by the value of the stability derivative $M\alpha$. When $M\alpha$ is negative, the airframe is stable and when $M\alpha$ is positive the airframe is unstable.

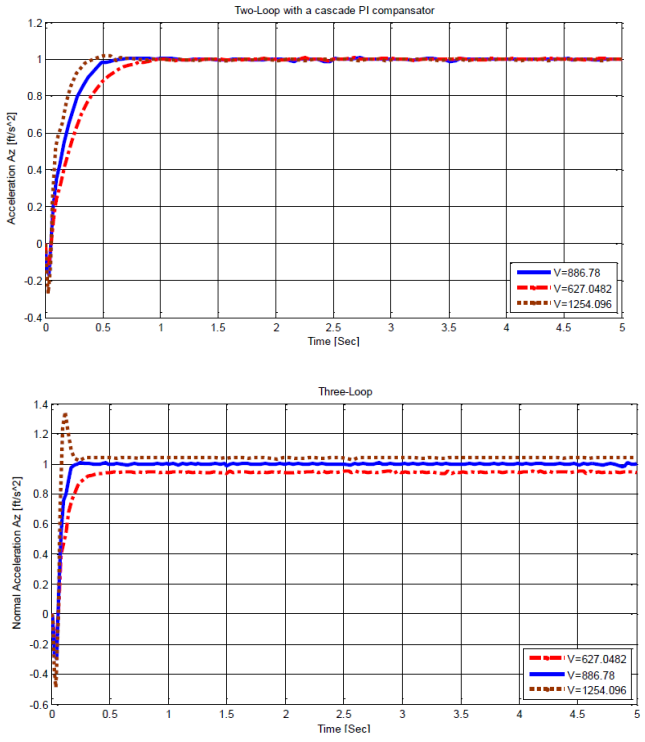


Fig. 5. Normal Acceleration $A_z$ of two-loop and three-loop at different value of velocity.

It is seen from Fig.5 that for different value of velocity $886.78\sqrt{2}$, $886.78$ *and* $886.78/\sqrt{2}$ (ft/s) respectively, two-loop has better response than three-loop that it has a steady state error and big overshoot when the velocity is changed. The analysis results as shown in Fig.6 at different value of $M\alpha$ show that the three-loop classic autopilot has the best robustness properties. In Fig.7 it is clear that the control input of two-loop with a cascade PI compensator is half value for all different value of $M\alpha$compared with the control Input of three-loop topology.

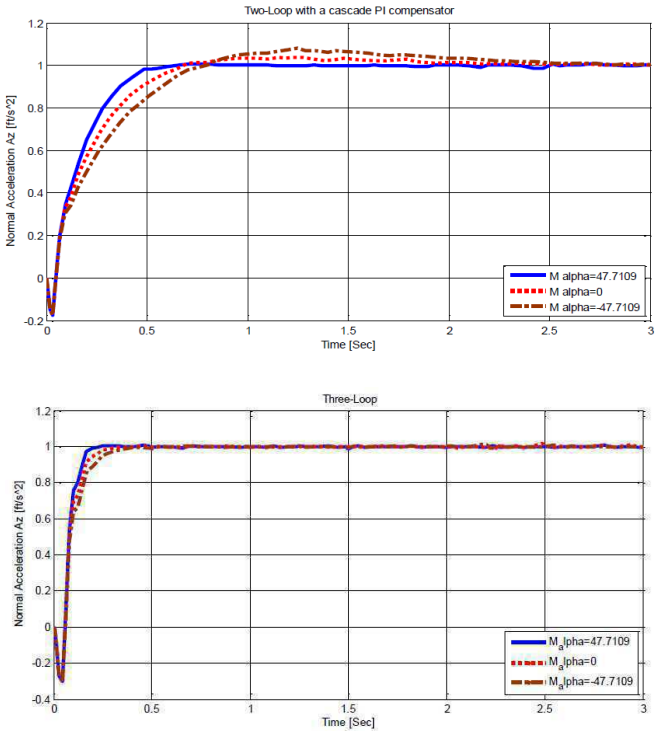


Fig. 6. Normal acceleration $A_z$ of two-loop and three-loop at different value of $M_\alpha$.

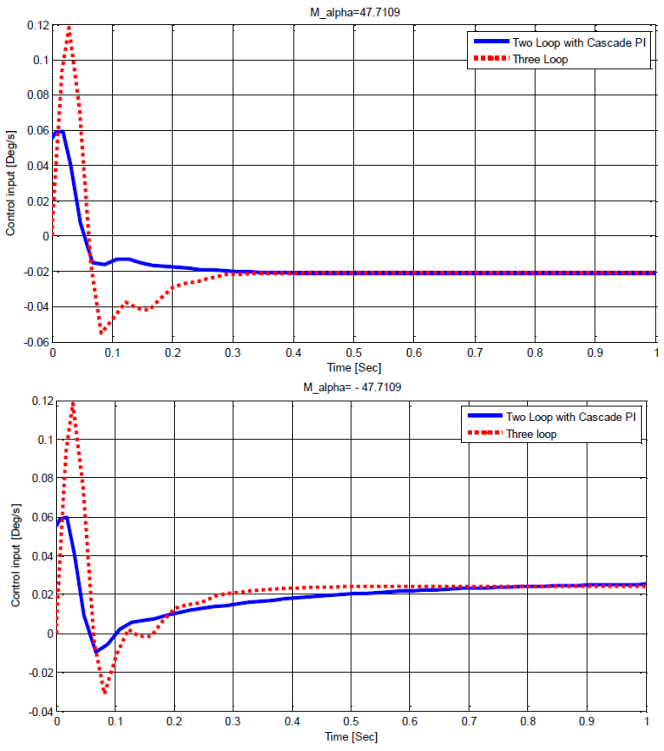


Fig. 7. Control input step response of two topology at different value of $M_\alpha$.




ISSN 1737-9334

## vi. Conclusion

Three-loop topology is faster than two loops for tracking normal acceleration. In addition, it is more robustly than two-loop for different value of aerodynamic stability derivative $M\alpha$ which it occurs due to movement of the center of gravity because of fuel burn during boost and changes in the aerodynamic conditions during glide flight. However, two-loop with a cascade PI controller has three advantages better Than three loop as follows: firstly, it has better response at different velocities because the PI compensator eliminates the static error of the system. Secondly, the control input and the fin deflection have half values compared to three loop at different values of stability derivative ($M\alpha$) which introduces negative value for stable missile and positive value for unstable missile. Finally, it has a small value of the fin deflection, fin rate, and pitch rate which could produce moderate actuator rates without rate saturation for sudden pitch rate demands. In future, to design a high-performance autopilot for the whole entire missile flight envelop, it is convenient to use a robust or adaptive control techniques.

**References**

[1] Paul, Z. (2002). *Tactical and Strategic Missile Guidance*. Virginia: AIAA Inc., 70-73.

[2] Arrow, A., & Williams, D. E. (1987). Comparison of classical and modern autopilot design and analysis techniques for a tactical air-to-air bank-to-turn missile.

[3] Devaud, E., & Siguerddidjane, H. F. S. (2000). Some control strategies for high-angle-of-attack missile autopilot. *Control Engineering practice*, *8*, 885-892.

[4] Garnel, P. (2003). Guided Weapon control systems. Beijing Institute of Technology.

[5] Nesline, F. W., & Nesline, M. L. (1984). How autopilot requirements constrain the aerodynamic design of homing missiles. *Proceedings of the Conference on American Control*.

[6] Fan, L. F., Chen, Y., & Lin, P. (2014). Control analysis for a non-minimum phase static unstably missile. *Proceedings of the 14th International Conference on Control, Automation and Systems* (pp. 947-952).

[7] Das, G., Datta, K., Ghoshal, T. K., & Goswami, S. K. (1996). Structured designed methodology of missile autopilot. *Journal of the Institution of Engineers (India)*, *76*, 49-59.

[8] Das, G., Datta, K., Ghoshal, T. K., & Goswami, S. K. (1998). Structured designed methodology of missile autopilot — II. *Journal of the Institution of Engineers (India*), *79*, 28-34.

[9] Wise, K. A. (2008). Robust stability analysis of adaptive missile autopilots. *Proceedings of the AIAA*




ISSN 1737-9334

# New *In Silico* Approach for the Determination of the Genetic Factors Associated with the Virulence of HxNy Influenza-A Family

Rima Soli[#1], Safa Berraies[#], Belhassen Kaabi[#2], Chokri Maktoof[*], Mourad Barhoumi[**],

and Sami Ben-Hadj Ahmed[***]

[#]*Pasteur Institute of Tunis, Tunisia.*
*13 Place Pasteur, BP 74, 1002 Belvedere-Tunis, Tunisia.*
[1]souli.rima@gmail.com

[3]belhassen.kaabi@gmail.com

**Laboratory of Biophysics and Nuclear Medicine*
*Pasteur Institute of Tunis, Tunisia*

***Laboratory of Molecular Epidemiology and Experimental Pathology,*
*Pasteur Institute of Tunis, Tunisia.*

****National Institute of Applied Sciences and Technology (INSAT), Tunis, Tunisia.*

***Abstract*— Capabilities of infiltration, replication and transmission of influenza-A virus to and from humans pose an imminent epidemic to pandemic threat to the world population and a major human healthcare burden. The viral genomic determinants, which facilitate these processes, are not well understood. Using Meta-data on influenza-A virus sequences and their respective estimated of basic reproductive number (R0) of different sub-types, we identified several genomic regions i.e. conserved patterns (using MEME) and SSR (using MiSA), by regressing R0 values against motif numbers and SSR repeats. Thus, we were able to detect genomic regions associated with virulence of the virus. A docking study showed also the association of the docking energy of HA and the sialic acid receptor and the number of repeats of some of these predetermined motifs (regions). Ninety-six (96) sequences of Influenza-A virus and their estimated R0 values covering H1N1, H3N2, H7N7, and H7N1 subtypes were acquired from the NCBI database. Using statistical linear regression, we identified several genomic regions in segments encoding the internal proteins (PB2, PB1, PA, M, NS) that are implicated in the virulence of VIAs, and these are correlated with the literature where they are already described.**

***Keywords*— Influenza-A, R0, MEME, MISA, virulence**

## I. INTRODUCTION

Influenza A virus (IAV) is an influential pathogen causative of frequent epidemics and occasional pandemics in human. IAV pandemics remain the greatest infectious disease outbreaks in the past century.

Three main factors sway the diffusion potential of an influenza virus: (i) the ability to cause human disease, (ii) the herd immunity of the population to the virus, (iii) the replication and the transmission potential of the virus (virulence) [1]. At the virus level, the abilities to enter, and to replicate within the host cell, amplifying viral numbers, and thus, the potential for host-to-host transmission are the main determinant of virulence. This process requires multiple rounds of entering the cells, replications, virion assembly, and release. The assembly of IAV involves packaging of several host and viral proteins from an eight distinct segmented genome. Even though, the selective assembly of the eight-segment core remains one of the most interestingly unresolved problems in virology, the interaction between the IAV viral ribonucleo-protein (vRNP) complex and other host factors are major determinants of viral pathogenicity [2]. Type A viruses that affect mammals and birds are further classified into subtypes based on their 18 hemagglutinin (HA) and 11 neuraminidase (NA), which gives theoretically 198 (18x11) possible subtypes [3]. Not all subtypes of IAV infect humans and cause disease, however, many of them do.

Pandemics have been caused by subtypes H1N1 (1918, 2009), H2N2 (1957) and H3N2 (1968), and currently H1N1 and H3N2 are the circulating seasonal influenza A subtypes [4], [5]. H5N1 avian influenza viruses have caused the deaths of nearly 60% of humans that they have infected since 1997 and clearly represent a threat to public health [6]. H9N2 virus circulates widely in poultry, and has been responsible for sporadic human infections, in several regions. Few studies have been conducted on the pathogenicity of H9N2 isolates, that have different genomic features [7].

In addition, many laboratories have-confirmed H7N9 virus human infection cases have been recorded, with a case fatality rate of more than 30%. Clinical research has shown that cytokine and chemokine dysregulation contributes to the pathogenicity of the H7N9 virus [8]. Poultry exposure is a major risk factor for human H7N9 zoonotic infections, for which the mode of transmission is unclear [1].


ISSN 1737-9334

HA and NA proteins are used in the nomenclature of the virus subtypes. The HA protein complex mediates virus entry by binding to cell surface receptors and fusing the viral and endosomal membranes following uptake by endocytosis.

This poly- cleavage site of the HA proteins is considered one of the most important determinant contributing to the virulence of the IAVes.

On the other hand, viral NA is a surface protein of influenza virus that enables the virus to be released from the host cell surface. NAs are enzymes that cleave sialic acid groups from glycoprotein's and are also required for the IAV replication. However, evidence is now accumulating that these sites alone are not sufficient to establish the high virulence (pathogenicity), and that other sites located outside the HA protein cleavage spot, which are expressed by IAV that contribute to its pathogenicity.

As virulence is also in most part is determined by the host response, understanding the key host molecular driver(s) of virus-mediated disease, in relation to the viral genes, is also, a promising approach to host-oriented drug efforts in preventing disease.

On the population level, when an outbreak occurs, such as epidemic or pandemic influenza, it is necessary to provide criteria to characterize the dynamics of the disease within the population as well as its severity and virulence [9]. The basic reproduction number R0 is the main epidemiological parameter characterizing disease severity and virulence.

The basic reproductive number, R0is defined as the expected number of secondary cases produced by a single infection in a completely vulnerable population [10].

Based on the assumption that any genetic region influencing the virulence will be associated (correlated) with the estimated R0, the aim of this work is to identify, motifs (genetic regions) that are responsible for the virulence of the IAV' subtypes. This can be done, by regressing the number of repeats of these conserved regions (determined using software of pattern and motif detection), while assuming certain genetic homogeneity in the human population. Understanding of the genetic basis of virulence determinants will provide important insights for antiviral drug and live attenuated vaccine development.

## II. METHODS

### A. Acquiring of Biological (Sequences) Data

The sequence data were chosen according to the following criteria: availability of the genomic sequences, an estimated basic reproductive number ($R_0$), and that the IAV subtype can infect human.

Based on these criteria, 96 sequences of IAV were found. The data cover several countries (Boston, Bochum, Honk-Kong, Italy, Johannesburg, Mexico, Netherlands, Sydney, Toronto, Warsaw, and several subtypes, which are H1N1, H3N2, H7N7, and H7N1.

To highlight the local and global similarities among the sequences since our objectives are; among others are elicitation of-conserved regions, detection of simple sequence repeats (SSR), and recognition of motifs (patterns). To do this, raw IAV sequences in fasta-format, served as input for multiple sequence alignment, motifs and repeats by the software T-coffee [11], MEME [12], and MiSA [13] respectively.

### B. SSR and Motifs Search

#### 1) Detection of SSRs

To detect SSRs in the EST sequence data sets, we used exact matching algorithms, implemented in a slightly modified version of the Perl script MIcroSAtellite identification tool (MISA). This program take a FASTA formatted sequence file containing multiple sequences, as an input, and search each sequence (contig or singlet) for all possible combination of mono-, di-, tri-, tetra-, and penta- as well as complex repeats with the default criteria of minimum numbers of repeats are set to 9 for di-nucleotides, 6 for tri-nucleotides, 5 for tetra-nucleotides, and 4 for penta-nucleotides.

Two output files are generated by MISA, one file reports the sequence description (including sequence ID and descriptive title), the number of SSR motifs in each sequence, the length and composition of SSR, the number of repeats, the SSR's start and end position, and the total length of the sequence containing the SSR. All identified sequences were then stored in FASTA-format files. Single (mono) nucleotide repeats were not selected because they were generally not considered as useful polymorphic markers.

The results of the MISA runs were transferred to an Excel style worksheet for further analyses.

### C. Motif Mining with MEME and Associated Programs

For a set of closely related sequences, often-shared motifs can be discovered using methods based on multiple alignments. Often, distantly related sequences that share common grounds cannot be easily aligned, leading to unsatisfactory results. To detect such subtle patterns, more sophisticated algorithms such as expectation-maximization (EM) are used.

The purpose of MEME (Multiple EM for Motif Elicitation) [14] is to allow users to discover patterns in the DNA or protein quasi-unrelated sequences [12], [15].

#### 1) Rfam

Non-coding RNA genes (ncRNAs) that are not translated into protein, but they may produce as final product functional RNA molecules. Among these functional RNAs are the transfer RNA and ribosomal RNA.

Like the genes encoding proteins, ncRNAs fall into families that have evolved from a common ancestor. By alignments of these gene families ncRNA we can learn about their structure and function. The basic objectives of RFAM RNA database [16] are:

To integrate as many of the existing structural RNA alignments (as well as new alignments) in a common structure annotated format Provide a system for analyzing and automatically annotate sequences (including complete


ISSN 1737-9334

genomic sequences) for detecting the presence of homologous known structural RNA [17].

*2) FIMO*

FIMO (Find Individual Pattern Occurrences) [18] is a tool that looks for sequences present in a specific database, which share similarities with the patterns obtained by the tool MEME, serving as a template.

The operation of this tool is based on the calculation of the score of the log report (likelihood) of each pattern with the position of the region, and then the score will be converted to p value using dynamic programming methods [19].

### *D. Blast Search of SSR and Multilevel Motifs*

BLASTx (https://blast.ncbi.nlm.nih.gov/Blast.cgi) was performed on translated SSR and multilevel motifs to search proteins with significant match to translated SSR nucleotide sequence. BLASTx was performed against non-redundant (nr) database. For this study, a significant match was defined as a sequence with expected value (E-value) <=1e-3 and identity>=70%.

### *E. 3D Modeling and Docking*

The challenge in developing vaccines against influenza is the ability of the virus to mutate rapidly to evade selective immune pressure. Hemagglutin is the predominant surface glycoprotein and the major determinant of antigenicity. Mutations leading to changes in the HA protein coding sites are often reported. However, genetic sequencing studies predict at best the disruption or creation of new sequence or motifs at this site (HA coding region) or other regions; but they rarely reflect actual phenotypic changes in HA structure, and most importantly the docking energy between HA complex and the sialic receptor. This energy reflects somehow the viral bioactivity. Therefore, combined analysis of evolution (mutation in active site), the distribution of the motifs (found by MEME) repeats in the original IAV sequences and docking (viral bioactivity) to better define the relationships among mutation and motif repeat distribution and actual virulence as reflected by structural change in the HA protein and its docking energy to the human receptor. We combined this information with structural change with binding data to correlate the phenotypic changes with biological activity. To understand the structural basis for site-specific mutation, we performed structural modeling (when needed) and evaluation of docking energy. We investigated the motifs distribution and reduced or increased docking energy.

### *F. Prediction of 3D Protein Structure:*

To model the 3D structure of mutated or original HA proteins we used the approach of modeling by similarity or comparative homology as commonly known. For this purpose the software Modeller [22], [23] is used. Once the 3D model is determined using Modeller, visualization and analysis is made using the software Chimera [22] and Pymol [23]. Models checking are assured by the software for Protein Structure Analysis: Prosa [24], [25] and Rampage [26], [27] for molecular energy and Ramachandran principals.

*1) The Receptors*

In the docking section, we intended to analyze the interactions between HA sequences and specific receptors. These receptors are located on epithelial cells of the human respiratory tract. The receivers used are of two types (LSTc, and 6'-SLN) in PDB format taken directly from the base RCSB [28]. All paragraphs must be indented. All paragraphs must be justified, i.e. both left-justified and right-justified.

### *G. Docking*

The ability to attach to and enter the cell is the first phase of the infection, this assured by docking of the HA protein to the cell receptor. To evaluate the quality of this attachment the docking energy of the Crystal, MNRI or computed 3D model protein with the sialic-acid needs to be evaluated, the lower this energy the better the attachment of the virus to the cell receptor

### *H. Statistical Analysis*

A simple statistical linear model (regression test) [29] was used to test for association (correlation) between the R0 and the number of repeats of each SSR type and motifs.

Holm's correction for multiple testing was applied when necessary [30]. Principal components analysis (PCA) [31] was performed, and associated biplot [32] was drawn. We visualized the distribution of the SSR and motifs with the IVA subtype, as reported in the principal components dimensions, energy values were reported as auxiliary variable.

All analysis was performed using the R software for statistical computing version 3.0, and associated packages: FactoMiner and SensoMiner, which are freely available from web [33].

## III. RESULTS

Using two criteria; availability of published $R_0$ in the scientific literature and that the IAV subtype infects humans: 96 sequences have been retrieved with their respective $R_0$s, covering H1N1, H3N2, H7N7, and H7N1. These sequences in fasta format were used as input for the software T-coffee, MEME and Misa, in order to detect conserved regions, motifs, and SSrs among these sequences.

### *Alignment, Conserved Motif, and SSR*

Global alignment is performed between the segments of the viral genomes, segment by segment. We obtained for each alignment a high score of about 900, this puts into consideration the relationship between subtypes of the virus so these viruses are probably counterparts and they derive from the same common ancestor. However, for the overall multiple alignments with T-coffee, we did not find any conserved alignment-block for most of the sequences through all viral segments.

Using Misa with various parameters, we found 16 complex SSRs of interest. Using regression analysis while adjusting for human population density (Fig.1) only SSR16: (TA)3 was found to be positively associate with $R_0$, i.e. the number of


ISSN 1737-9334

repeats of SSR16 is correlated with the $R_0$ values (p-value<0.05).

Using MEME, we were able to detect 4 multilevel motifs of interest. Only three (3) of them: motif-1, motif-2 and motif-3, (their number of repeats) were found to be associated with $R_0$. While motif-1, and motif2, and, are positively correlated with $R_0$, motif-3 is negatively correlated with $R_0$.

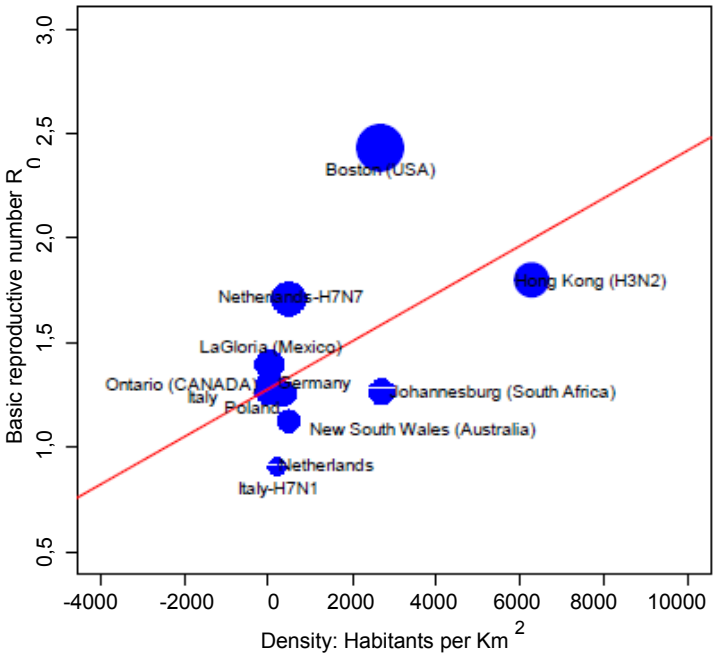


Fig. 1 Regression plot of the basic reproductive number $R_0$ against the population density in towns and country-wide. The IAV subtype is mentioned when it is different of H1N1.

*Searching for Significance and Biological Meaning of the Patterns (motifs) and SSRs*

Analysis of patterns and SSRs via Rfam revealed no sequence similarity; this can explained by the small size of the patterns and the SSRs analyzed. To overcome this difficulty, the FIMO tool is used, which plays the same role as Rfam. Each pattern (motif) and each SSR is matched to and positioned on sequences sharing similarity. These sequences are subsequently scanned on the database of "ssRNA negative strand virus" in NCBI. These patterns and SSRs were searched for in other sequences having their PDB format in the PDB database.

Positioning the SSR sand motifs on the DNA sequence retrieved by MAST (MEME suit) shows that these sequences are actually overlapping and they do fall in region coding for functional proteins such as: HA, M1-M2, NA, NP, PA, NS1-NEP (NS2), PB1, PB2. Indeed, Motif -1 overlaps with M1-M2, where matrix protein 1 (M1), is a major structural protein, and the dominant protein in determining virus morphology and also plays an important role in virus assembly and budding [34]. Matrix protein 2 (M2), on the other hand, is the ion channel that regulates the pH, and is responsible for virus uncoating, after virus entry into the cell [35], [36] Motif-1 covers also region coding for NA (neutralizing antibodies), NP, and PA. Motif-2 forms a part of the nucleic sequences, which codes for the proteins M1-M2, NS1-NEP, PA, and PB1. Motif-3 besides coding for M1-M2 and NA, PA, overlaps with region coding for PB1 and PB2. Motif-4 and besides overlapping with region coding for M1-M2, and PA, it codes for PB1. The SSR12 is in the sequence which codes for the protein NP and the SSR16 in the sequence that encodes for the HA (binding and fusion activities), PB2 and PB1 are ribonucleoproteins (RNPs), with NP, PB2 and PB1 are responsible for replication of the viral genome (Table 1).

Thus, the software MEME suite and MiSA allowed us to determine the patterns (common motifs) and SSRs that are involved either in virulence (Fixation or in viral replication).

As multilevel motifs are more comprehensive then SSRs (sequences found by exact matching algorithm), we will be using only multilevel motifs in the subsequent analysis. For all HA protein sequences, with pdb format corresponding to the 11 virus sequences used above (acquired from the NCBI database) (Table 2), a docking analysis with the sialic receptor was performed, and the docking energy evaluated.

The distribution of the 4 motifs and SSRs with respect to these HA proteins was also determined. From the data-table displaying these information and since there are a hefty number of variables, and because their representation is not feasible using the traditional approach, the principal component analysis (PCA) was used. The resulting biplot is drawn (Fig.2a, 2b). Note that motifs 1, and 3 and SSR-10 are in association with docking energy suggesting that these motifs and SSR are involved in the virulence of the virus, through attachment of HA to its sialic receiver. On the other hand, we found that the motif-2, motif-4 and the SSR-12, SSR-16 are independent of the docking energy and therefore they may not be involved in the fixation of the HA on the receptor. These results do not contradict the previously concluded ones (that these regions contribute to virulence). This suggests that motif-2 and SSRs 12 and 16 are rather involved in viral replication. Combining finding of the regression analysis and the principal components analysis shows that motifs and SSRs that are overlapping with genomic regions responsible for viral replication is the most significant. This means that the virus entry in the cell is not the whole story, although it is a necessary and crucial step. Replication and assembly, thus their rate is rather the major determinants of virulence and infectiousness.


ISSN 1737-9334

TABLE I
POSITION OF SSRS AND MOTIFS IN DNA SEQUENCES

| Motif/ SSRs | Protein Encoded & Overlapping SSR | Sequence in Logo-format |
|---|---|---|
| Motif1 | M1-M2 (SSR4) | 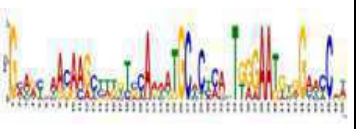 |
| | NA (SSR7/SSR11) | |
| | NP(SSR3/SSR12/ SSR13) | |
| | PA (SSR5) | |
| Motif2 | M1-M2(SSR4) |  |
| | NS1-NEP | |
| | PA (SSR2/SSR5 | |
| | /SSR9/SSR16) | |
| Motif3 | M1-M2 (SSR4) | 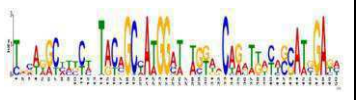 |
| | NA (SSR7) | |
| | PA(SSR5) | |
| | PB1 (SSR4/SSR8) | |
| | PB2 (SSR16) | |
| Motif4 | M1-M2 (SSR4) | 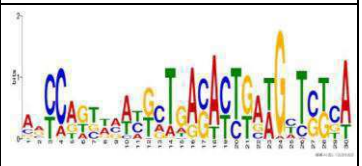 |
| | PA (SSR2/SSR5/SSR 9/SSR16) | |
| | PB1 (SSR4/SSR8) | |
| SSR16 | PB2 | (TA)3 |
| | PB1 (SSR4/SSR8) | |
| | NP(SSR3/SSR12 /SSR13) | |
| | NA (SSR7/SSR11) | |
| | HA (SSR10) | |

TABLE III
HA SEQUENCES (WILD AND MUTATED), MUTATIONS AND THEIR POSITIONS.

| Mutated Sequence | Subt-ype | Wild Sequence | Mutation | Position given "target sequence" |
|---|---|---|---|---|
| 4CR0.pdb | H5N1 | 3FKU.pdb | N182K | N186K |
| | | | G139R | G143R |
| 3KU6.pdb | H2N2 | 3QQI_A.pdb | Q226L | Q176L |
| A/Netherlands/33/03 | H7N7 | 4dj6 | A143T | A143T |
| 4GXX.pdb | H1N1 (1918) | 1RD8.pdb | D190E | D191E |
| | | | D225G | D226G |

## IV. DISCUSSION & CONCLUSION

The viral genome consists of eight molecules of RNA of negative polarity found in the form of ribonucleic complex (RNPv). RNA segments mutations are frequently the cause of epidemics and pandemics because the variability of their genomes makes them evolve very rapidly. This can be achieved by two mechanisms: antigenic drift and re-assortment.

We presented here a new *in silico* approach for the determination of the genetic regions responsible for the virulence of IAV based on $R_0$ values and whole genetic data of this microorganism. In fact, this method can be applied to other infectious micro-organism with data on $R_0$ and genome is available. Candidate regions were actually determined using programs like MEME and MISA, however, other bioinformatics tools, for pattern recognition, and sequence repeats that may can be used. The question which program is the best for a particular situation is open, and beyond the scope of this work.

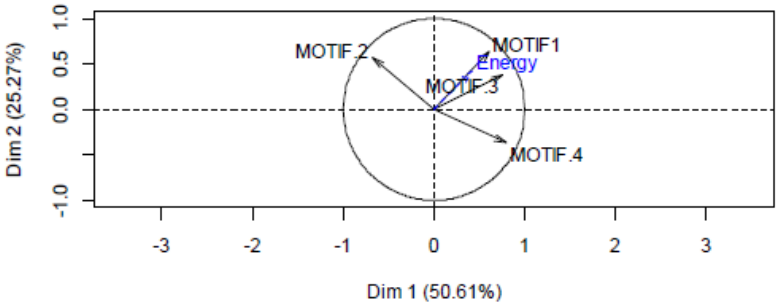


(Fig.2a)Variable Factor Map

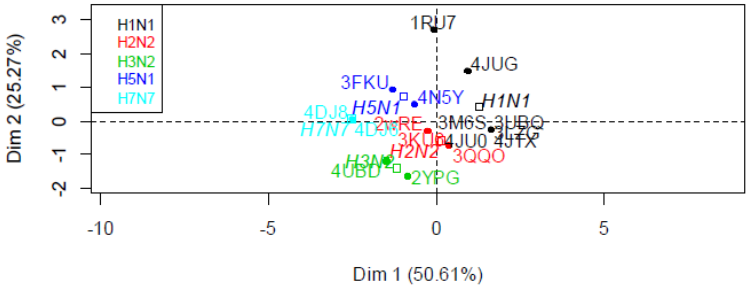


(Fig.2b) Individual Factor Map

Fig. 2 Biplot analysis: Motifs and SSR distribution

Two statistical approaches have been used to test for association (correlation) between candidates genetic regions motifs and SSRs found by MEME and MISA and measures quantifying the virulence, which are the $R_0$ and the docking energy between the HA and the sialic acid.

The first approach consists in regression of the number of repeats against $R_0$, which yields to the identification of motif-1, motif2, motif3, and SSR16, these regions overlap with those coding for the proteins: M1-M2, NS1-NS2, PA, PB1, and PB2. In fact, M1 is major surface component of the virus and it is responsible for virus budding, nuclear export and assembly [34]. M2 is an ion channel and a ph regulator for HA synthesis [36]. NS1-NS2 are responsible for control of gene expression and export of RNP from the nucleus during viral replication. Moreover, the polymerase complex responsible for viral transcription and replication is formed by PB1, PB2, and PA [37]. Most of these proteins are responsible for virus replication. Residues in the protein PA have identified as contributing to H7N3 virus virulence when infecting mice [38].

PB1-F2 protein is a factor of virulence of influenza A viruses which increases the mortality and morbidity associated


ISSN 1737-9334

with infection [39]. Most seasonal H1N1 Influenza A viruses express a truncated form of PB1-F2 [40].

The second approach consists in the study of the distribution of the motifs and SSRs with the docking energy-of HA and human receptor, this led to association between motif1, and motif3, which code for M1-M2, NA, and PA. SSR16 is also associated with the docking energy, and is situated in part of the region coding for HA.

The results from the first approach seems to more consistent as the ability and rate of the virus replication is more determinant to the virulence. The ability of docking and entry is also crucial but the virus either gets in the cell or not. While, the severity of influenza infection is not only influenced by viral virulence factors but also by individual differences in the host response, we adjusted in this analysis only for the density of human population, adjusting for the human genetic background is very difficult and requires identification of specific genetic region, and may even requires controlled experimentations.

## ACKNOWLEDGMENT

This study received financial support from the Secretariat of the State for Scientific Research, Technology, and Competencies Development in Tunisia, through funding of Research Program Contract for Institute Pasteur of Tunis (2011-2015).

## REFERENCES

[1] W. D. Tanner, D. J. Toth, A.V. Gundlapalli, "The pandemic potential of avian influenza A(H7N9) virus: a review," *Epidemiol Infect,* vol.143(16), pp. 3359-3374, Dec. 2015.

[2] T. Chen et R. Zhang, "Symptoms seem to be mild in children infected with avian influenza A (H5N6) and other subtypes," *J Infect,* vol. 71(6), pp.702-703, 2015.

[3] S. J. Gamblin, J. J. Skehel, "Influenza hemagglutinin and neuraminidase membrane glycoproteins," *J Biol Chem,* vol. 285(37), pp. 28403-28409, Sep. 2010.

[4] T. Bedford, S. Cobey, P. Beerli, M. Pascual, "Global migration dynamics underlie evolution and persistence of human influenza A (H3N2)," *Plos Pathog,* vol. 6(5), 2010.

[5] P. Wright G. Neumann, Y. Kawaoka. Orthomyxoviruses. *In Fields Virology* 2013. 6th Edition, Knipe DM et Howley P : Lippincott Williams & Wilkins; Chapter: 411186-411243.

[6] X. Feng, Z. Wang, J. Shi, G. Deng, H. Kong, S. Tao, C. Li, L. Liu, Y. Guan, H. Chen, "Glycine at Position 622 in PB1 Contributes to the Virulence of H5N1 Avian Influenza Virus in Mice," *J Virol,* vol. 90 (4), pp. 1872-1879, Dec. 9, 2015.

[7] H. Li, B.Cao, "Pandemic and Avian Influenza A Viruses in Humans: Epidemiology, Virology, Clinical Characteristics, and Treatment Strategy," *Clin Chest Med,* vol. 38(1), pp. 3859-3870, Mar. 2017.

[8] K. K. To, J. F. Chan, K. Y. Yuen, " Viral lung infections: epidemiology, virology, clinical features, and management of avian influenza A(H7N9)," *Curr Opin Pulm Me,* vol. 20(3), pp. 225-232, May. 2014.

[9] K. J. Taubenberger and D. M. Morens, "The Pathology of Influenza Virus Infections," *PMC Annu Rev Pathol*, vol. 3, pp. 499-522, 2008.

[10] S. Heffernam, Smith, J. R. Wahl, "Perspectives on the basic reproductive ratio,"*Soc Interface,* vol. 2(4), pp. 281-293, Sep. 22, 2005

[11] C. Notredame, D.G. Higgins, " T-Coffee: A novel method for fast and accurate multiple sequence alignment,"*J Mol Biol,* vol. 302(1), pp. 205-217, Sep. 8, 2000.

[12] L. Bailey, J. Johnson, G.E. CGrant, and W. S. Noble, " The MEME Suite," *Nucleic Acids Res*, vol 43, w39-w49, Jul. 2015.

[13] T. Thiel, W. Michalek, R. K. Varshney, A. Graner, "Exploiting EST databases for the development and characterization of gene-derived SSR-markers in barley (*Hordeum vulgare L.*),"*Theor Appl Gene,* vol. 106(3), pp. 411-422, 2003.

[14] The MEME website. [Online]. Available:http://meme.nbcr.net.

[15] L. T. Bailey, N. Williams, C. Misleh, and W. Li, "MEME: discovering and analyzing DNA and protein sequence motifs," *Nucleic Acids Res*, vol. 34, w369-w373, Jul. 2006.

[16] The rfam website. [Online]. Available: http://rfam.xfam.org/

[17] S. Griffiths-Jones, A. Bateman, M. Marshall, A. Khanna, R. Eddy, "Rfam: an RNA family database,"*Nucleic Acids Res*, vol.31(1), pp 439-441, Jan. 1, 2003 .

[18] The FIMO website. [Online].Available http://meme-suite.org/tools/fimo

[19] C. E. Grant, T. L. Bailey, W. S. Noble, "FIMO: scanning for occurrences of a given motif,"*Bioinformatics*, vol. 27(7), pp. 1017-1018, Apr. 1, 2011.

[20] The modeller website. [Online]. Available: https://salilab.org/modeller; version 9.15.

[21] B. Webb, A. Sali, " Protein Structure Modeling with MODELLER," *Methods Mol Biol*, vol.1654, pp. 39-54, 2017

[22] The chimera website. [Online]. Available: https://www.cgl.ucsf.edu/chimera/; version v1.10.2.

[23] N. Matthews, R. Easdon, A. Kitao, S. Hayward, S. Laycock, "High quality rendering of protein dynamics in space filling mode", *J Mol Graph Model,* vol. 78, pp. 158-167, Nov. 2017.

[24] The prosa website. [Online]. Available: https://prosa.services.came.sbg.ac.at; web version.

[25] F. Nazmi, M. A. Moosavi, M. Rahmati, Hoessinpour-Feizi MA4. "Modeling and structural analysis of human Guanine nucleotide-binding protein-like 3, nucleostemin," *Bioinformation*, vol. 11(7), pp. 353-358, Jul. 31, 2015.

[26] The rampage website. [Online]. Available: http://mordred.bioc.cam.ac.uk/~rapper/rampage.php

[27] M .Wiederstein and J. Sippl, "ProSA-web: interactive web service for the recognition of errors in three-dimensional structures of proteins," *Nucleic Acids Res*, vol. 35(2), pp. 407-410, Jul. 2007.

[28] The RCSB website. [Online]. Available: http://www.rcsb.org/pdb/home/home.do

[29] J. M. Chambers, *Linear models,* Chapter 4 of Statistical Models in S eds J. M. Chambers and T. J. Hastie, Wadsworth & Brooks/Cole, *J Pacif Gro,* 1992.

[30] S. Holm, "A simple sequentially rejective multiple test procedure," *Scandinavian Journal of Statistics*, vol. 6, pp. 65-70, 1979.

[31] W. N. Venables, and B. D. Ripley. *Modern Applied Statistics with S*, Springer-Verlag, 2002.

[32] K. R. Gabriel. "The biplot graphical display of matrices with application to principal component analysis," *Biometrika*, vol. 58, pp. 453-467, 1971.

[33] R Development Core Team. R: A language and environment for statistical computing. R Foundation for Statistical Computing, Vienna, Austria. ISBN 3-900051-07-0. Available: http://www.R-project.org. 2008.

[34] J. S. Rossman, R. A. Lamb. "Influenza virus assembly and budding", *Virology*, vol. 411(2), pp. 229-36, Mar. 15, 2011.

[35] A. Helenius, "Unpacking the incoming influenza virus", *Cell*, vol. 69(4), pp. 577-578, May. 15, 1992 .

[36] L .J. Holsinger, D. Nichani , L. H. Pinto , R. A. Lamb," Influenza A virus M2 ion channel protein: a structure-function analysis", *J Virol,* vol. 68(3), pp. 1551-1563, Mar. 1994 .

[37] B. W. Jagger , H. M. Wise, J. C. Kash , K. A. Walters , N. M. Wills, Y. L. Xiao , R.L. Dunfee , L. M. Schwartzman , A. Ozinsky , G. L. Bell et al , "An overlapping protein-coding region in influenza A virus segment 3 modulates the host response," *Science,* vol. 337(6091), pp.199-204, Jul. 13, 2012.

[38] B. L. DesRochers BL, R.E. Chen, A.P. Gounder, A. K. Pinto, T. Bricker, C. N. Linton, C. D. Rogers, G. D. Williams, R. J. Webby, A. C. Boon, "Residues in the PB2 and PA genes contribute to the pathogenicity of avian H7N3 influenza A virus in DBA/2 mice," *Virology,* vol. 494, pp. 89-99, Jul. 2016.

[39] H. Sediri, S. Thiele, F. Schwalm, G. Gabriel, H. D. Klenk, "PB2 subunit of avian influenza virus subtype H9N2: a pandemic risk factor," *J Gen Virol* , vol. 97(1), pp. 39-48, Jan. 2016 .


ISSN 1737-9334

[40] D. Ajjaji, C. A. Richard, S. Mazerat, C. Chevalier, J. Vidic, "N-terminal domain of PB1-F2 protein of influenza A virus can fold into amyloid-like oligomers and damage cholesterol and cardiolipid containing membranes," *Biochem Biophys Res Commun,* vol. 477(1), pp.27-32, Aug. 12, 2016.


ISSN 1737-9334

# *Roll Control of a Tail-Sitter VTOL UAV*

*Helmi Abrougui*
helmiabrougui@yahoo.fr

*Samir Nejim*
samir.nejim@centraliens.net

*Habib Dallagi*
habib.dallagi@ept.rnu.tn

Automatic Control & Marine Robotics Research Unit
Naval Academy, Tunisia

***Abstract*** **:—This paper deals with the development of a flight controller in order to stabilize the roll motion of a vertical take-off and landing unmanned air vehicle (VTOL-UAV) during hover flight. Using Newton Euler approach, a dynamic model is firstly described then a Proportional-Integral and Derivative regulator for the stabilization of the VTOL aircraft in the vertical plan is synthesized. Next, simulations are carried out in order to test the regulator performances. Finally, the proposed control law is executed in real time by an AtMega2560 micro-controller which is built in an Arduino module in order to stabilize the roll motion of a balance platform.**

**Keywords—VTOL aircraft; roll control; digital PID techniques.**

## 1-Introduction:

The use of planes onboard a naval vessel is very important for the projection of the naval forces and the increase of the action range. Hence, the necessity of deploying big ships equipped with long runways that could exceeds the ship's length in order to be able to embark fixed wings planes. A remedy for this issue, is the use of vertical take-off and landing aircrafts.
Due to the transition mechanism and airframe VITOL aircrafts can be generally classified into two main types [9]: Convertiplanes and Tail-Sitters.

A convertiplane is an aerial vehicle that takes off, cruises, hovers and lands with remaining horizontal, it means that the main body configuration does not change during flight as Tilt-Rotors [10] and Tilt-Wings [11].
A Tail-sitter is an aircraft that takes off and lands vertically and the aircraft main body tilts forward using differential thrust or control surfaces to flight horizontally; as Control Surface Transitioning Tail-sitters (CSTT) [12] and Differential Thrust
Transitioning Tail-sitters (DTTT) [13].

In addition to the operability onboard small platforms, VTOL aircraft offers several advantages such as high energy autonomy in comparison with multirotor aircraft.

The development of unmanned aerial vehicles (UAVs) has increased during the last few years, due to their wide range applications in both military and civilian. One of the latest trends in the UAV's technology is the development of mini aerial vehicles with vertical take-off and landing capabilities that are deployable even when no landing runway is available.
Also, many autopilot systems are designed based on classical control techniques. These control methods can be found in many flight controls studies such as [4,5]. Modern control techniques are also used in UAVs autopilot applications [6]. Fuzzy logic control was used too in order to control aircraft in [7]. Besides, in his project, Octavio Garcia [8] has presented a nonlinear control strategy based on Saturated-Proportional-Integral and Derivative technique.

The tail-sitter VTOL aircraft shows a natural unstable behavior in vertical flight according to previous projects so, the manual control is a difficult task. Therefore, this paper aims to design a regulator in order to stabilize the roll position of the tail-sitter VTOL aircraft during hover flight.

The paper is organized as follows. Section 2 presents the dynamic model obtained using the Newton-Euler approach. The roll control strategy is developed in section 3. The simulation results of the proposed roll control strategy applied to the system are given in section 4. Finally, the experimental platform and the embedded system were described and the real-time experimental results of an autonomous stabilized flight of the two-rotor mini UAV were discussed.

Figure 1: VTOL mini aircraft

## 2- Dynamic model of the tail-sitter VTOL aircraft:

In this section, a modeling approach of a VTOL aircraft will be presented. The VTOL aircraft is considered to be a solid plane moving in aerospace, it is submitted to torques


ISSN 1737-9334

and forces applied to its body depending on the type of flying object considered [3].

The VTOL aircraft requires high accuracy during landing and take-off maneuvers so these flying objects must be designed to control their roll, pitch and yaw motion in small area, the objective of this paper is to design a regulator that can stabilize the VTOL aircraft during hover flight by controlling its rolling motion. Firstly, the dynamic model for the VTOL system is described. This model is inspired from [1], and it was derived under the following approximations:

- The aircraft is assumed to be operated over a small local region on earth which justifies the utilization of the Flat-Earth model equations [2].
- The blade mass is neglected.

(Fig.2) shows the VTOL aircraft to be modeled using Newton's classic motion equations.

Let the north-east-down NED coordinate system $(x, y, z)$ be the inertial reference frame $(n-frame)$ and let the $(X, Y, Z)$ be the body fixed frame$(b-frame)$.

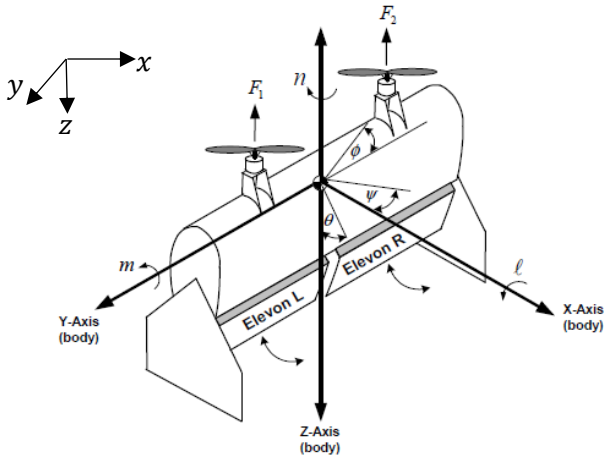


Figure 2: Studied VTOL aircraft and coordinate system

The orientation of the VTOL aircraft in the (n-frame) is given by the three Euler angles $\eta = (\phi\ \theta\ \psi)^T$ which are the classic yaw, pitch and roll Euler angles commonly used in aerodynamic applications.

The position of the center of mass of the rigid body relative to the (n-frame) is $\xi = (x, y, z)$.

Using Newton's classic equations of motion, the dynamic model of a rigid object evolving in aerospace is:

$$\dot{\xi} = RV \quad (1)$$

$$\dot{\eta} = W_\eta \Omega \quad (2)$$

$$m\dot{V} = -\Omega \times mV + F \quad (3)$$

$$J\dot{\Omega} = -\Omega \times JV + \tau \quad (4)$$

With

$R = \begin{pmatrix} c_\theta c_\psi & s_\phi s_\theta c_\psi - c_\phi s_\psi & c_\phi c_\theta c_\psi + s_\phi s_\psi \\ c_\theta s_\psi & s_\phi s_\theta s_\psi + c_\phi c_\psi & c_\phi s_\theta s_\psi - s_\phi c_\psi \\ -s_\theta & c_\theta s_\phi & c_\theta c_\phi \end{pmatrix}$: the orientation of the airframe relative to the fixed inertial frame where $c_a$ (respectively $s_a$) denote *cos(a)* (respectively *sin(a)*).

$\dot{\eta} = (\dot{\phi}\quad \dot{\theta}\quad \dot{\psi})^T$: The angular velocity in the local inertial system (n-frame).

$W_\eta = \begin{pmatrix} 1 & t_\theta s_\phi & t_\theta c_\phi \\ 0 & c_\phi & -s_\phi \\ 0 & s_\phi / c_\theta & c_\phi / c_\theta \end{pmatrix}$: The transformation of the angular velocity generated by a sequence of Euler rotations from the body to the local reference system during hover flight where $t_a$ denote *tan(a)*.

$m$: Total mass of the VTOL aircraft.

$V = (u\quad v\quad w)^T$: The speed vector of rigid body center of mass relative to body frame (b-frame).

$\Omega = (P\quad Q\quad R)^T$ :The angular velocity in the body frame.

$J$ : The inertia matrix of the flying body.

$F$ : The external thrust applied to the VTOL aircraft center of mass in the body frame.

$\tau = (L\quad M\quad N)^T$ :The torques applied to the VTOL aircraft center of mass in the body frame.

The set of attitude equations can be obtained using equations (2) and (4).

According to equation (2) we have: [1]

$$\dot{\eta} = \begin{pmatrix} P + \tan\theta\,(Q\sin\theta + R\cos\phi) \\ (Q\cos\phi - R\sin\phi) \\ (Q\sin\phi + R\cos\phi)/\cos\theta \end{pmatrix} \quad (5)$$

The inertia matrix is defined by

$$J = \begin{pmatrix} J_x & 0 & 0 \\ 0 & J_y & 0 \\ 0 & 0 & J_z \end{pmatrix} \quad (6)$$

The equation (4) can be written as:

$$\dot{\Omega} = \begin{pmatrix} \frac{(J_y - J_z)QR}{J_x} + \frac{L}{J_x} \\ \frac{(J_z - J_x)RP}{J_y} + \frac{M}{J_y} \\ \frac{(J_x - J_y)PQ}{J_z} + \frac{N}{J_z} \end{pmatrix} \quad (7)$$

Then the dynamic model is used to express and represent the behavior of the system over time, a regulation of the roll angle will be presented in the following section.

## 3 - roll control

This section presents the roll control of the VTOL aircraft during hover flight. The pitch and yaw motion would be stabilized with adequate control laws:

$$Q = R = 0 \quad (8)$$

Therefore, using the equations (7) and (8), the rotational dynamics for the roll angle can be represented by:

$$\ddot{\phi} = L/J_x \quad (9)$$


ISSN 1737-9334

where, the sum of moments $L$ can be calculated as follows:

$$L = u_c(t)d - C_L\,\dot{\phi} \tag{10}$$

With

$u_c(t)$ = F = $f_1 - f_2$ the force difference between the right and left rotor.
$d$ : the distance from the center of mass to each rotor.
The roll rate products an aerodynamic moment $-C_L\,\dot{\phi}$ opposing to the roll moment with a roll damping derivative $C_L$.
Equations (9) and (10) give us:

$$\ddot{\phi} = (u_c(t)d - C_L\,\dot{\phi})/J_x \tag{11}$$

Using (10) and applying the Laplace transform, the following transfer function for the roll angle is obtained:

$$H(s) = \frac{\phi(s)}{U_c(s)} = \frac{d/J_x}{s^2+(C_L/J_x)s} \tag{12}$$

Then, using the transfer function expressed in (11), the control loop system shown in the following Figure (Fig.3) is proposed to stabilize the roll angle.

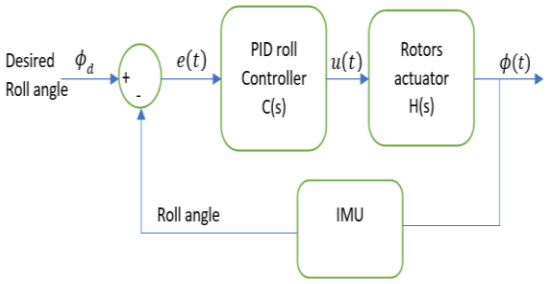


Figure 3: Roll Control Loop.

The transfer function of the control loop system is given by:

$$\frac{\phi(s)}{\phi_d(s)} = \frac{C(s)H(s)}{1+C(s)H(s)} \tag{13}$$

With
$C(s) = K_p + K_i\frac{1}{s} + K_d s$ : Transfer function of the PID regulator.

**4 – Simulation**

To show the behavior of the system control roll stabilization, a simulation of the model has been run using Matlab and Simulink (Fig.4).
During this simulation, the $K_p$, $K_d$and $K_i$ values are chosen by pole placement method (all poles are equal to -10):
We found that:

$$K_p = \frac{300J_x}{\mathrm{d}}\ ;\ K_i = 1000\frac{J_x}{\mathrm{d}}\ ;\ K_d = J_x\frac{30 - C_L}{d}$$

The desired roll angle was equal to 0 degrees and the initial roll angle of the system was chosen equal to $-5$ degrees.

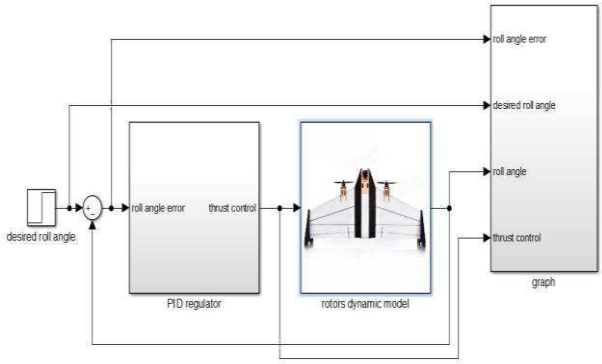


Figure 4: Block diagram

From Fig.6, the roll angle error shows a rapid convergence toward zero, hence the roll control which is based on the PID is performant.

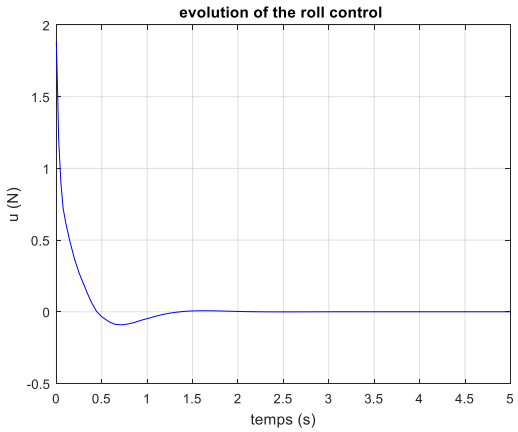


Figure 5: Evolution of the roll control

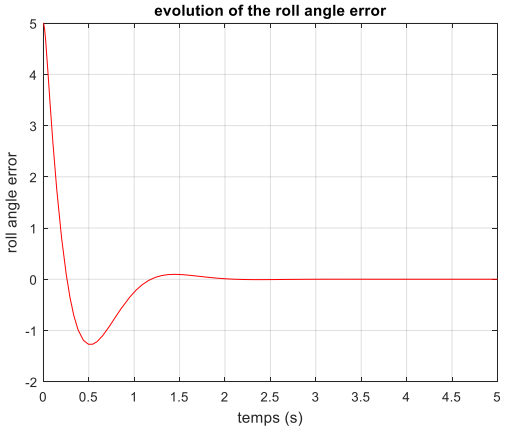


Figure 6: Evolution of the roll angle error

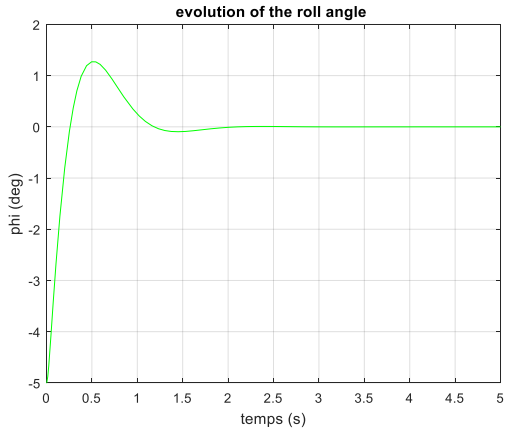


Figure 7: Evolution of the roll angle

## 5 - Experimental test

In this section, qualitative results of a roll stabilization test of the VTOL aircraft are discussed.

### 5-1- Description of used platform

A platform which is represented in (Fig.8) by a balance system with two contra-rotating brushless electric AC motors is fabricated and connected to microcontroller in order to implement and test our regulator.

Today's flight control systems have many hardware sensors like gyroscope, accelerometer modules, GPS, barometric pressure sensors and airspeed sensors which are connected on micro-controller. The gyroscope and accelerometer sensors are used together to detect any movement (roll and pitch) on each of the 3 axes, usually it gives back rotation velocity and acceleration values of the drone, using those values, the roll and pitch angle are calculated in each moment.

Our goal is to regulate the balance roll angle. In this project we will use an inertial movement unit IMU module like the MPU6050 which is a device capable of measuring the acceleration and rotation velocity. Generally, it consists of an accelerometer and gyroscope. Therefore, an IMU does not measure directly angles. However, it requires some calculations in order to obtain these angles.

Then, the use of a filter is very important to eliminate noise and error. The filter that we are going to use is known as complementary filter. It is ideal to implement with Arduino; easy to use, with low processing cost and good precision. This filter is actually a union of two different filters: a high-pass filter for the gyroscope and a low-pass filter for the accelerometer. In our case we will take just 98% of the angle obtained with the gyro data and 2% of the angle obtained with the acceleration data.

So, to get the best setting of the two motors velocity, an adequate value of P, I and D constants should be chosen. Each of these three constants will affect the PID control. The process of finding the perfect values of P, I and D is subsection below.

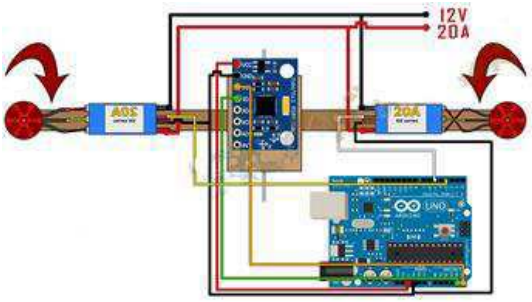


Figure 8: Platform top view

To obtain a more flexible system, the balance system architecture is controlled within only one processing unit. The control decisions that should be executed in real time are performed by a dedicated micro-controller, an AtMega2560, which is built in an Arduino module. This Arduino module is used to link actuators (two-rotors) to the sensor (IMU) through control laws (PID).

### 5-2- Digital PID design

A proportional-integral-derivative controller (PID controller) is a control law mechanism commonly used in industrial control systems. A PID controller continuously calculates an error $e(t)$ as the difference between a desired setpoint and a measured process variable (roll angle given by IMU) and it applies a correction based on proportional, integral, and derivative terms.

In this project we will use this mechanism to control the two-rotors in order to stabilize our mini UAV. We will control the inclination angle of the balance (the desired roll angle will be equal to zero), which means that the drone will be perfectly horizontal.

By using data from IMU, the real inclination angle of the balance was calculated. After that, we have to compare the calculated angle with the desired one which is equal to zero.

The two rotors controller is responsible for adjusting the balance inclination with respect to the desired angle. For this raison, the actual angle $\theta$ given by the IMU and the desired inclination $\theta_d$ are compared. The last one is given by radio transmitter (desired inclination). This generates an error that should be reduced at each iteration (14) of the algorithm due to the action of a PID controller. The control action $u_k$ is calculated with the following equations:

$$\begin{aligned} e_K &= \phi_d - \phi_k \\ P &= k_p e_K \\ I_k &= I_{k-1} + k_i T e_K \\ D &= k_d (e_K - e_{K-1}) \end{aligned} \tag{14}$$


ISSN 1737-9334

$$u_k = p + I_k + D$$
$$e_{K-1} = e_K$$

where P, I, D, $k_p$, $k_i$ and $k_d$ are respectively the proportional action, integral action, derivative action, proportional gain, integral gain and derivative gain. $e_K$ is the error between the desired roll angle $\phi_d$ and the actual roll angle $\phi_k$ and T is the sample time of the system, $e_{K-1}$ is the previous error.
We could observe that the PID controller works well in the balance system and a fine tuning is performed in order to get the final values of $k_p$, $k_i$ and $k_d$, such that the balance behaves as desired performance. After some tests, we found the values of $k_p$= 5, $k_i$ = 0.01 and $k_d$ = 2.6.
The left rotor controller is given by:

$$V_{left} = V_0 + u_k \quad (15)$$

Where $V_0$ is the initial rotors throttle and $V_{left}$ is the left rotor throttle.
The right rotor controller is given by:

$$V_{right} = V_0 - u_k \quad (16)$$

With $V_{right}$ the right rotor throttles.
The following figure (Fig.9) shows a real time response of the balance platform after a disturbance application.

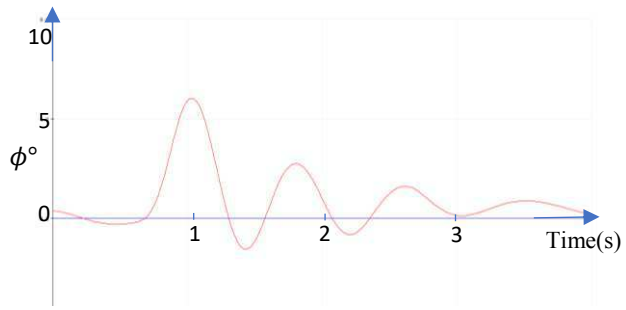


Figure 9: Real time response of the balance platform

## CONCLUSION

In this paper, a mathematical model describing the dynamic motion of a tail-sitter VTOL aircraft was presented using Newton Euler formulation. This model is an adequate mathematical presentation in order to apprehend the VTOL aircraft dynamic motion during hover flight. The PID controller is employed to perform roll control for the system.

The simulation results show that the used control technique gives good results in terms of regulation. After the validation of the proposed control law through simulation, the results are supported by experimental tests. Future work in this area includes a stabilization of the pitch and yaw angle in addition to the test of the aerospace stabilization position of the mini aircraft.

## *References*

[1] Wong, K. C., Guerrero, J. A., Lara, D., & Lozano, R. (2007, October). Attitude stabilization in hover flight of a mini tail-sitter UAV with variable pitch propeller. In Intelligent Robots and Systems, 2007. IROS 2007.

[2] B.L. Stevens and F.L. Lewis, Aircraft Control and Simulation, John Wiley and Sons, New Jersey USA; 2003. IEEE/RSJ International Conference on (pp. 2642-2647). IEEE.

[3] CASTILLO P., LOZANO R. and DZUL A., Modelling and Control of Mini-Flying Machines, Springer-Verlag, London, 2005

[4] MCLEAN, Donald. Automatic flight control systems(Book). Englewood Cliffs, NJ, Prentice Hall, 1990, 606, 1990.

[5] NELSON, Robert C. Flight stability and automatic control. New York : WCB/McGraw Hill, 1998.

[6] MAGNI, Jean-François, BENNANI, Samir, et TERLOUW, Jan (ed.). Robust flight control: a design challenge. Berlin : Springer, 1997.

[7] BOSSERT, David et COHEN, Kelly. Fuzzy logic non-minimum phase autopilot design. In : 2003 AIAA Guidance, Navigation, and Control Conference and Exhibit. 2003.

[8] GARCIA, Octavio, CASTILLO, Pedro, WONG, K. C., et al. Attitude stabilization with real-time experiments of a tail-sitter aircraft in horizontal flight. Journal of Intelligent & Robotic Systems, 2012, vol. 65, no 1-4, p. 123-136.

[9] SAEED, Adnan S., YOUNES, Ahmad Bani, ISLAM, Shafiqul, et al. A review on the platform design, dynamic modeling and control of hybrid UAVs. In : Unmanned Aircraft Systems (ICUAS), 2015 International Conference on. IEEE, 2015. p. 806-815.

[10] STREETLY, Martin (ed.). IHS Jane's All the World's Aircraft: Unmanned: 2013-2014. IHS Global, 2013.

[11] MURAOKA, Koji, OKADA, Noriaki, et KUBO, Daisuke. Quad tilt wing vtol uav: Aerodynamic characteristics and prototype flight. In: AIAA Infotech@ Aerospace Conference and AIAA Unmanned... Unlimited Conference. 2009. p. 1834.

[12] STONE, R. H. et CLARKE, G. The T-wing: a VTOL UAV for defense and civilian applications. University of Sydney, 2001.


ISSN 1737-9334

[13] SAEED, Adnan S., YOUNES, Ahmad Bani, ISLAM, Shafiqul, et al. A review on the platform design, dynamic modeling and control of hybrid UAVs. In: Unmanned Aircraft Systems (ICUAS), 2015 International Conference on. IEEE, 2015. p. 806-815.

Appendix A. VARIABLE DESCRIPTION

| **Notation** | **value** | **Description** |
|---|---|---|
| $J_x$ | 0.0144 kg.m$^2$ | - x-axis moment of inertia |
| $C_L$ | 0.36 | - roll damping derivative. |
| $d$ | 0.2 m | - Rotor distance from the center of mass. |

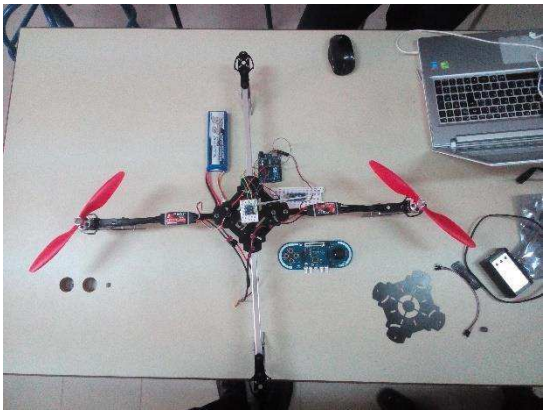


ISSN 1737-9334

Editors biographies :

Prof.Sundarapandian Vaidyanathanobtained his D.Sc. degree in Electrical and Systems Engineering from Washington University, St. Louis, USA in May 1996. He has specialized in the areas –Control Systems, Chaos Theory, Intelligent Control, Systems Modelling, Computational Science and Engineering Applications. Prof. Sundarapandian is working as Research Professor at Vel Tech University, Chennai from Sept. 2009. He has over 20 years of teaching and research experience. He has authored 3 subject books with Indian Publishers and 15 books with International Publishers. He has guided several doctorate students in Mathematics, Computer Science and Electrical Engineering. He has over 450 research publications indexed by Scopus.He has delivered many Keynote talks on Control Systems and Chaos Theory. He is in the Editorial Boards of many Scopus-indexed International Journals on Computer Science, Control Systems and Computational Science. He has conducted several workshops on Control Systems, Chaos, Mathematical Modelling and Computational Science using SCILAB and MATLAB.

Dr. Ahmed Rhif (Tunisia) is a Researcher & Engineer (PhD, Eng). He has more than 11 years of experience on Scientific Research, Teaching and industrial projects. He is actually the Dean of the International Centre for Innovation & Development (ICID). Ahmed Rhif has worked as a Technical Responsible Chief in LEONI (International Leader of Wiring Fibers Companies) and has occuped also the task of Project Manager and Method Engineer in both SMSI (electronic development industry) and CABLITEC (Engineering automobile company). Then he was a Lecturer at both the Private University of Sousah (UPS) and the High Institute of Applied Sciences and Technologies of Sousah (ISSATso) and now he is working as Lecturer in the High Institute of Applied Sciences and Technologies of Al Qayrawan (ISSATk). His research interests include Modelling, Control Systems and Engineering as well as the implantation of the international standard of quality (ISO-TS 16949). He has published a book with a German Publisher as well as several papers in International Conferences and International Journals. He is currently serving as an editorial board member and reviewer of several Scientific Journals (Elsevier - Springer - Inderscience - Taylor & Francis...). He is the founder/ Organizer of several international conferences where he served as a Keynote speaker.Ahmed Rhif is also the Founder and Advisor of the International Publisher & CO (IPCO).

The International Publisher & C.O (IPCO) is an organization that promotes science & engineering research worldwide without any discrimination. It acts as a bridge between young and experienced professionals through scientific journals. IPCO depends on researchers, academicians and corporate support for bridging relationships with existing scientific & engineering organizations and customizing relationships with standard bodies. The main purpose of this organization is to promote new research and scientific applications in the field of Control, Energy, Engineering, Computer Science and allied fields. IPCO provides high quality and flexible information solutions to researchers. We currently publish international journals and we provide online solutions to help researchers to achieve better results. Active Peer Review: All our journals, which are run by a group of experienced professional editors, are subject to an efficient, fair, and constructive peer review process. Maximum Global Distribution: Our website guarantees visibility, including social bookmarking services, so that your article reaches those people who need to read and cite it. High Quality, Reliable Rapid Production: Our production teams work together to continuously improve and enhance our services, building issues online and our new, even quicker production workflows. We deliver these innovations without compromising our high quality standards.

International Publisher & C.O (IPCO), in its new aspect, represents a new contribution between North African & International researchers and institutions and cover a wide range of academic disciplines. IPCO serves the world's research and scholarly communities, and aims to be one of the largest publishers for professional and scholarly societies. IPCO's journals maintain the highest standards of peer review, with some internationally-recognized editors serving on the editorial boards of IPCO's journals.

Maghreb Arab Street
Khzema East Sousse - Tunisia
Email : ipco.direction@gmail.com
Phone: (+216) 31 121 155
www.ipco-co.com
**ISSN: 1737-9334**

## Editors biographies :

Prof.Sundarapandian Vaidyanathanobtained his D.Sc. degree in Electrical and Systems Engineering from Washington University, St. Louis,USA in May 1996. He has specialized in the areas – Control Systems, Chaos Theory, Intelligent Control, Systems Modelling, Computational Science and Engineering Applications. Prof.Sundarapandian is working as Research Professor at Vel Tech University, Chennai from Sept. 2009. He has over 20 years of teaching and research experience. He has authored 3 subject books with Indian Publishers and 15 books with International Publishers. He has guided several doctorate students in Mathematics, Computer Science and Electrical Engineering. He has over 450 research publications indexed by Scopus. He has delivered many Keynote talks on Control Systems and Chaos Theory.
He is in the Editorial Boards of many Scopus-indexed International Journals on Computer Science, Control Systems and Computational Science. He has conducted several workshops on Control Systems, Chaos, Mathematical Modelling and Computational Science using SCILAB and MATLAB.

Dr.Ahmed Rhif (Tunisia) is a Researcher & Engineer(PhD, Eng).He has more than 11 years of experience on Scientific Research, Teaching and industrial projects. He is actually the Dean of the International Centre for Innovation & Development (ICID). Ahmed Rhif has worked as a Technical Responsible Chief in LEONI (International Leader of Wiring Fibers Companies) and has occuped also the task of Project Manager and Method Engineer in both SMSI (electronic development industry) and CABLITEC (Engineering automobile company). Then he was a Lecturer at both the Private University of Sousah (UPS) and the High Institute of Applied Sciences and Technologies of Sousah (ISSATso) and now he is working as Lecturer in the High Institute of Applied Sciences and Technologies of Al Qayrawan (ISSATk). His research interests include Modelling, Control Systems and Engineering as well as the implantation of the international standard of quality (ISO-TS 16949). He has published a book with a German Publisher as well as several papers in International Conferences and International Journals. He is currently serving as an editorialboard member and reviewer of several Scientific Journals (Elsevier - Springer - Inderscience - Taylor & Francis...). He is the founder/ Organizer of several international conferences where he served as a Keynote speaker.Ahmed Rhif is also the Founder and Advisor of the International Publisher & CO (IPCO).

ISSN: 1737-9334